Final Report

Reactive Capping Mat Development and Evaluation for Sequestering Contaminants in Sediments

SERDP Project ER-1493

August 2011

Amy Hawkins
Naval Facilities Engineering Command Engineering Service Center

Jesse Swanko
Gregory Tracey
Science Applications International Corporation

Kevin Gardner
Jeffery Melton
University of New Hampshire

SERDP
DOD ▪ EPA ▪ DOE

This page is intentionally left blank

REPORT DOCUMENTATION PAGE (SF 298)	Form Approved OMB No. 0704-0811

1. REPORT DATE *(DD-MM-YYYY)*	2. REPORT TYPE	3. DATES COVERED *(From – To)*
20-07-2010	Final Report	

4. TITLE AND SUBTITLE

Reactive Capping Mat Development and Evaluation for Sequestering Contaminants in Sediment

5a. CONTRACT NUMBER

5b. GRANT NUMBER

5c. PROGRAM ELEMENT NUMBER

6. AUTHOR(S)

Amy L. Hawkins, NAVFAC
Gregory A. Tracy, Ph.D., SAIC
Jesse J. Swanko, SAIC
Kevin H. Gardner, Ph.D., UNH
Jeffrey S. Melton, Ph.D., UNH

5d. PROJECT NUMBER

ER-1493

5e. TASK NUMBER

5f. WORK UNIT NUMBER

7. PERFORMING ORGANIZATION NAME(S) AND ADDRESSES

Naval Facilities Engineering Service Center
1100 23rd Avenue, Port Hueneme, CA 93043

8. PERFORMING ORGANIZATION REPORT NUMBER

9. SPONSORING/MONITORING AGENCY NAME(S) AND ADDRESS(ES)

Strategic Environmental Research and Development Program (SERDP)

10. SPONSOR/MONITORS ACRONYM(S)

11. SPONSOR/MONITOR'S REPORT NUMBER(S)

12. DISTRIBUTION/AVAILABILITY STATEMENT

13. SUPPLEMENTARY NOTES

14. ABSTRACT

Strategic Environmental Research and Development Program (SERDP) Project Number ER-1493 (Reactive Capping Mat Development and Evaluation for Sequestering Contaminants in Sediment) was implemented by a collaborative team from the NAVFAC Engineering Service Center (NAVFAC ESC), Science Applications International Corporation (SAIC) and the University of New Hampshire (UNH). The project consisted of developing a reactive geotextile mat system to serve as a chemically effective, mechanically stable, and cost efficient technology for reducing ecological risks by sequestering contaminants in sediment. Use of reactive mat systems could provide an alternative to costly dredging and offsite disposal, and a more stable solution for standard capping approaches. The mat system, if deemed successful, would be deployed in a wide variety of environmental settings to prevent both metals and organic contaminants from entering overlying surface waters while simultaneously allowing both groundwater flux and surficial biological colonization.

15. SUBJECT TERMS

16. SECURITY CLASSIFICATION OF:			17. LIMITATION OF ABSTRACT	18. NUMBER OF PAGES	19a. NAME OF RESPONSIBLE PERSON
a. REPORT	b. ABSTRACT	c. THIS PAGE			19b. TELEPHONE NUMBER *(include area code)*
U	U	U			

This page is intentionally left blank.

EXECUTIVE SUMMARY

Strategic Environmental Research and Development Program (SERDP) Project Number ER-1493 (Reactive Capping Mat Development and Evaluation for Sequestering Contaminants in Sediment) was implemented by a collaborative team from the NAVFAC Engineering Service Center (NAVFAC ESC), Science Applications International Corporation (SAIC) and the University of New Hampshire (UNH). The project consisted of developing a reactive geotextile mat system to serve as a chemically effective, mechanically stable, and cost efficient technology for reducing ecological risks by sequestering contaminants in sediment. Use of reactive mat systems could provide an alternative to costly dredging and offsite disposal, and a more stable solution for standard capping approaches. The mat system, if deemed successful, would be deployed in a wide variety of environmental settings to prevent both metals and organic contaminants from entering overlying surface waters while simultaneously allowing both groundwater flux and surficial biological colonization.

Laboratory Studies. Various mixtures of reactive amendments to potentially adsorb sediment contamination were evaluated in a laboratory setting to determine the optimal combination of reactive core materials (activated carbon, apatite, and organoclay) to be placed within prototype mats with woven geotextile tops and non-woven geotextile backs to be positioned on top of sediments of concern. Laboratory data from amendment isotherm experiments and kinetics studies identified CETCO Sediment Remediation Technologies organoclay containing bentonite as the base clay and coconut shell activated carbon as the optimal amendments for achieving maximum contaminant sequestration (as compared to other types of organoclay and activated carbon). Preloading studies with humic acid on activated carbon generally indicated negligible effects, but similar tests on organoclay showed that preloading with humic acid did change the relative adsorption capacity of individual PAHs and that the long term exposure of organoclay to natural organic matter might also affect mat performance by causing increased desorption of target compounds.

Gradient ratio testing and finite element modeling were conducted in a laboratory setting using both clean geotextiles and field weathered small-scale (6 ft x 6 ft) test mats to identify the non-woven geotextile most resistant to biofouling (8 oz/yd^2 polypropylene with 80 apparent opening size) for construction of the prototype mat system. These results along with numerical modeling showed that the coarser geotextiles (AOS 70 and 80) did not clog and did not lose amendment under controlled laboratory conditions while also experiencing relatively little sediment transport into the cap. Gas permeability testing also showed that these coarser geotextiles would allow the maximum methane levels produced in a freshwater environment to pass through the reactive mat without creating uplift as long as additional weight was supplied by an overlying sand cap. Based on these cumulative laboratory results, a reactive mat featuring a 0.28 lb/ft^2 activated carbon, 0.23 lb/ft^2 apatite, 0.28 lb/ft^2 organoclay amendment mixture and an AOS 80 geotextile was recommended for the treatment of metals and organics in aquatic environments of low to moderate dissolved organic matter levels.

Site Selection. Following an extensive desktop site selection process, Cottonwood Bay in Grand Prairie, Texas was selected as the most suitable project test site based on a variety of chemical, physical, biological and logistical factors. A comprehensive geophysical investigation, including

bathymetry, side-scan sonar, sediment profile imaging and groundwater seep surveys was conducted to characterize the site and identify a specific target area with a substantial groundwater plume for mat system placement. These surveys confirmed that the site was free of obstacles that would impede mat performance and provided baseline topography information for comparison to the sediment landscape following mat deployment. Groundwater seepage results identified an area of relatively high groundwater flow potential in the center of the bay as defined by average subsurface porewater temperatures 1.61ºC cooler and average subsurface porewater conductivity 0.71 mS/cm greater than corresponding surface water; known groundwater plumes were integral to the site selection process.

Prototype Testing. A prototype mat system was deployed in Cottonwood Bay in April 2008, featuring four 25 ft x 25 ft test arrangements (bare single layer geotextile, single layer geotextile with sand cap, bare double layer geotextile, sand cap only) and an undisturbed control. In fall 2008, following five months of soak time, the effectiveness of the various test arrangements for contaminant sequestration was monitored with passive samplers (peepers, semi-permeable membrane devices). The passive samplers were strategically placed at specific interfaces of interest in the various mat system treatments and allowed to soak for 50 days. Concurrent with the passive sampler recovery in December 2008, a post-construction geophysical investigation of the full scale mat system was conducted to evaluate the geophysical properties (*e.g.*, acoustic signature, sand cap placement, microorganism activity) of the various treatments. In summer 2009, approximately one year after deployment of the full scale mat system (six months after deployment of the passive samplers), Ultraseep and Trident Probe porewater measurements were collected to quantify water flux from sediments through the various treatments and identify any change in contaminant concentration with respect to potential overlying sources (*e.g.*, groundwater fluxing out of the mat versus overlying water penetrating the mat). Passive contaminant sampling at the prototype mat system was repeated in fall 2009 to provide comparative second year contaminant sequestration results. Sediment cores were also collected from each treatment area at that time to characterize the sediment from which previous porewater samples had been extracted and to establish the vertical chemical gradient in the natural sediments for confirmation of previous porewater sampler results.

Overall prototype field data indicated that below treatment porewater chemistry correlated to surface sediment trends across treatments, thus providing a reliable indicator of localized contaminant partitioning below the mat interfaces. Porewater flux (*i.e.*, Ultraseep) results showed that metals concentrations passing through the mats were comparable to above treatment peeper results, thus indicating that the mats are sequestering deep metal porewater concentrations observed in the Trident Probe dataset. In general the geophysical data revealed changes within the range of modeled expectations and exhibited sufficient sensitivity to be a useful tool for monitoring mat conditions. Mat uplift due to gas buildup beneath the geotextile was observed in the summer months for the mat only treatments, but these conditions were not found in the mat treatment with an additional sand cap providing sufficient weight, thus confirming the predicted results of the gas permeability testing.

Finally, the passive sampler (*i.e.*, peeper, SPMD) data showed generally consistent and statistically significant (at 90-95% confidence) two- to four-fold below/above reductions in primarily two treatments (mat/sand and double mat) between years for certain metals (nickel,

zinc, barium, silver, vanadium) and several polycyclic aromatic hydrocarbons (benzo[b]fluoranthene, indeno[1,2,3-c,d]pyrene, benzo[g,h,i]perylene, anthracene, benzo[a]anthracene), thus demonstrating that contaminant sequestration had occurred. Performance for other metals (*e.g.*, copper) was less robust and limited by overall low environmental concentrations relative to detection limits.

Conclusions and Recommendations. The selected implementation method including mat with sand cover is recommended as an effective technology to sequester contaminants in sediments while preventing uplift due to gas accumulation. Unlike the low level concentrations observed in surface sediments of the present study, the future candidate site sediments should contain contamination in the ecological effects range and be confirmed by an advance site chemical characterization study of the specific placement area (not performed in the present study). Laboratory verification via chemical testing and geotechnical modeling using methods developed in the present study should also be performed to predict mat performance metrics. These data will ensure that field passive sampler measurements (with an appropriate degree of sample replication) can reliably confirm/refute whether a broad suite of chemical gradients (as opposed to the limited metals and PAHs of the present study) are being better controlled by the mat treatment as opposed to a traditional capping approach (*i.e.*, sand/mix only covers). Based on the results of the present study, the project goal of further evaluating the reactive capping mat technology via a large-scale (~10,000 ft^2) implementation at a selected remediation site is recommended.

This page is intentionally left blank.

ACRONYMS AND ABBREVIATIONS

AldHA	Aldrich Humic Acid
AOS	Apparent Opening Size
AUS	American Underwater Services, Inc.
BET	Brunauer, Emmett and Teller
CMA	Coastal Monitoring Associates, Inc.
CoC	Contaminant of Concern
DOC	Dissolved Organic Carbon
DoD	Department of Defense
ESTCP	Environmental Security Technology Certification Program
FA	Fulvic Acid
FEA	Finite Element Analysis
FS	Feasibility Study
GC/MS	Gas Chromatograph/Mass Spectrometer
GR	Gradient Ratio
HOC	Hydrophobic Organic Contaminant
ICP-MS	Inductively Coupled Plasma-Mass Spectrometry
LCL	Lower Confidence Limit
LL	Liquid Limit
MDL	Method Detection Limit
MNA	Monitored Natural Attenuation
NAS	Naval Air Station
NAVFAC	Naval Facilities Engineering Command
NFESC	Naval Facilities Engineering Service Center
NOM	Natural Organic Matter
NWIRP	Naval Weapons Industrial Reserve Plant
PAH	Polycyclic Aromatic Hydrocarbons
PCB	Polychlorinated Biphenyls
PED	Polyethylene Device
PI	Plasticity Index
PMDS	Polydimethylsiloxan
QA/QC	Quality Assurance/Quality Control
SAIC	Science Applications International Corporation
SDI	Specialty Devices, Inc.
SEC	Size Exclusion Chromatography
SERDP	Strategic Environmental Research and Development Program
SPI	Sediment Profile Imaging
SPME	Solid Phase Micro-Extraction
SPMD	Semi-Permeable Membrane Device
SRHA	Suwannee River Humic Acid
SRFA	Suwannee River Fulvic Acid
SRNOM	Suwannee River Natural Organic Matter
TCMX	Tetrachlorometaxylene
TNRCC	Texas Natural Resource Conservation Commission

LIST OF ACRONYMS AND ABBREVIATIONS
(Continued)

TOC	Total Organic Carbon
TRRP	Texas Risk Reduction Program
UCL	Upper Confidence Limit
UNH	University of New Hampshire
USEPA	United States Environmental Protection Agency
USGS	United States Geological Survey
WAAS	Wide Area Augmentation System

TABLE OF CONTENTS

Page

TABLE OF CONTENTS
(Continued)

Page

LIST OF APPENDICES

LIST OF ATTACHMENTS

LIST OF TABLES

LIST OF FIGURES

1.0 INTRODUCTION

Strategic Environmental Research and Development Program (SERDP) Project Number ER-1493 (Reactive Capping Mat Development and Evaluation for Sequestering Contaminants in Sediment) was implemented by a collaborative team from the NAVFAC Engineering Service Center (NAVFAC ESC), Science Applications International Corporation (SAIC) and the University of New Hampshire (UNH). The project consisted of developing a reactive geotextile mat system to serve as a chemically effective, mechanically stable, and cost efficient technology for reducing ecological risks by sequestering contaminants in sediment. Use of reactive mat systems could provide an alternative to costly dredging and offsite disposal, and a more stable solution for standard capping approaches. The mat system, if deemed successful, would be deployed in a wide variety of environmental settings to prevent both metals and organic contaminants from entering overlying surface waters while simultaneously allowing both groundwater flux and surficial biological colonization.

2.0 OBJECTIVE

The objective of SERDP Project Number ER-1493 is to develop and test a mixture of chemically reactive materials suitable for incorporation within an engineered geotextile mat to create a composite active capping system capable of deployment in a wide variety of environmental settings in order to effectively sequester both metal and organic contaminants in sediments.

3.0 BACKGROUND

In situ capping has frequently been used to physically separate contaminated sediments from the aquatic environment above the cap and, in some cases, to act as an impermeable barrier to groundwater flux. Sequestration based on physical separation alone, however, is not always desirable because it does not ensure that dissolved phase contaminant flux is eliminated as a transport pathway either through or around the cap. More recently, *in situ* capping with chemically reactive materials has been explored as an option to provide a physical barrier to remobilization of sediment-bound contaminants while at the same time sequestering dissolved contaminants as they flow through the cap via groundwater flux (Knox *et al*. 2008, McDonough *et al*. 2007, Zhao *et al*. 2007, Reible *et al*. 2006). To date, studies of these reactive capping methods have largely focused on applying one type of reactive material to treat one particular class of contaminant and have typically involved deploying relatively thick layers of unconsolidated material (6 to 12 inches) over the bottom to accomplish this goal. Such an approach may not be effective at many sites with physically challenging conditions, multiple classes of contaminants or concerns with cap stability due to erosive forces. Loosely applied amendment caps may also be prohibitively expensive due to the increased costs associated with broadcasting larger amounts of coarsely applied reactive materials to achieve the desired cap thickness.

In contrast to thick layers of reactive material, *in situ* capping with a reactive geotextile mat may be a more practical means of sequestering sediment contaminants at many sites by preventing physical contact between biota and sediment and retarding leaching of chemicals into overlying waters while simultaneously allowing natural groundwater flow. The mixed reactive capping

materials developed in this project will satisfy these conditions when incorporated into a functional mat system. Overall, the reactive mats would be non-intrusive, would simultaneously address multiple contaminant classes, would be easily deployed and would offer greater permeability to natural groundwater flow than a thick layer of unconsolidated reactive material. These benefits also expand the utility of the reactive mat system to intertidal and sloped environments where the stability and effectiveness of either a traditional sand cap or unconstrained reactive materials would be diminished due to dynamic conditions. Finally, reactive mats can be fabricated on land to control mat thickness (0.5 inch) and amendment proportions, thus minimizing the amount and cost of composite material as compared to the current practice of placing large amounts of unconsolidated substrate cap material through the water column which can result in uncertain and variable layers.

Year One activities for SERDP Project Number ER-1493 were described in the First Year Annual Progress Report prepared in December 2006 (NAVFAC 2006). The first year actions involved separating the project into four separate tasks, performing composite material testing, identifying a primary pilot site, and fabricating small-scale test mats. Year Two activities were described in the Second Year Annual Progress Report prepared in December 2007 (NAVFAC 2007), including continued composite material testing, final pilot site selection, geophysical surveys for target area establishment and small-scale test mat deployment. This final report summarizes these results, describes additional year three and year four monitoring activities and provides final conclusions regarding the overall mat system effectiveness in achieving project goals. A final summary is also provided to outline the potential transition of this technology to future full-scale ESTCP remediation efforts. The Year One and Year Two Progress Reports are provided as Appendix A and Appendix B, respectively.

4.0 MATERIALS AND METHODS

This section provides a comprehensive description of how scientific questions were approached and addressed for each of four tasks established in the technical proposal. Based on the overall goal of developing a chemically effective, mechanically stable and cost efficient technology that could be deployed in a wide variety of environmental settings, the laboratory and field studies were designed to increase understanding of the practical effectiveness and limitations of this technology. The following sections summarize the experimental design of each investigation as well as associated desktop audits, field work, and laboratory analyses; detailed descriptions are referenced in appropriate Appendices. The considerable and important steps discussed in these sections include the following.

- ***Composite Material Testing***. Laboratory tests were designed and performed to identify the mixture of amendment materials to be incorporated into the reactive mats that most effectively sequesters contaminants of interest. The results of these experiments were used to design various small-scale test mats used for preliminary evaluation as well as to construct the prototype mats used for long-term monitoring and evaluation.
- ***Pilot Site Establishment.*** Desktop audits were performed to identify a project location (water body) that could be used as a pilot site for in-situ testing of various reactive mat and amendment arrangements. A subsequent geophysical investigation was then performed at this pilot site to select a particular area within the water body to serve as the

target location for long-term field testing of the prototype mat system constructed to the specifications of the composite material testing results. All field efforts for this project were performed at the selected pilot site.

- ***Geotextile Testing.*** Small-scale test mats featuring different types of geotextile materials were tested under controlled laboratory conditions as well as deployed at the selected pilot site and recovered after two predetermined soak times to assess the potential effects of biofouling, biofilm formation and weathering on final mat design and efficacy. The geotextile type found to be most resistant to biofouling while still maintaining proper integrity and porosity as determined from these tests was ultimately used to construct the prototype mat system used for long-term monitoring and evaluation.
- ***Prototype Mat Testing.*** Variations on a prototype mat system were constructed at the selected pilot site to include various treatments (*e.g.*, single mat, double mat, mat with sand cap) of a reactive mat featuring the most resistant geotextile as recommended by the results of the geotextile testing as well as the optimum amendment mixture as determined by the results of the composite material testing. This mat system was monitored and evaluated over a period of two years to determine the effectiveness of the proposed technology in achieving project goals.

4.1 Task 1: Composite Material Testing

The purpose of composite material testing for this project was to determine the optimal mixture of reactive sequestering materials to be incorporated in the final geotextile mat design. To accomplish this goal, many laboratory studies were required to empirically assess the adsorption behavior of various amendments primarily on different classes of organic compounds.

The first year effort for Task 1 primarily involved testing coconut shell-based activated carbon and three different formulations of brand name organoclays as potential sorbents for organic compounds; additional studies with apatite were conducted as the default sorbent for metals. The sorbent materials were exposed to several common contaminants of interest including five coplanar and non-coplanar polychlorinated biphenyls (PCBs), three polycyclic aromatic hydrocarbons (PAHs) of different ring structures and water solubilities and two heavy metals. Batch studies were performed as both single contaminant systems and multi-contaminant competitive systems. The methods for these initial experiments are discussed in detail in the First Year Annual Progress Report for this project (NAVFAC 2006).

Year two composite material testing investigated the interference caused by humic acid on the adsorption of coplanar and non-coplanar PCBs and PAHs onto activated carbons and organoclays, the two types of sorbents considered for incorporation into the final reactive mat design. To accomplish this goal, several additional kinetic and isotherm studies were conducted using various formulations of activated carbon and organoclay. The methods for these follow-up experiments are discussed in detail in the Second Year Annual Progress Report for this project (NAVFAC 2007).

Early in the third year of the project, laboratory studies were completed to determine the optimal mixture of reactive sequestering materials to be incorporated in the final geotextile mat design.

The results of previous investigations had already identified CETCO Sediment Remediation Technologies organoclay containing bentonite as the base clay and coconut shell activated carbon as the optimal amendments for achieving maximum contaminant sequestration (as compared to other types of organoclay and activated carbon).

Complete methods for the composite material testing activities are provided in the dissertation "Evaluation of Reactive Cap Sorbents for In-Situ Remediation of Contaminated Sediments" submitted to the University of New Hampshire by doctoral candidate Bhawana Sharma in 2008 (Sharma 2008, attached). Summaries of these methods as they pertain to SERDP Project Number ER-1493 are presented in the following sections.

4.1.1 Amendment Adsorption Capacity

Isotherm Experiments. Isotherm experiments for the characterization of the adsorption capacities of CETCO organoclay and coconut shell activated carbon were conducted in separate 125 mL batches with select concentrations of naphthalene, phenanthrene and pyrene, respectively, in contact with the sorbent phase. All the batch experiments were conducted using methanol and deionized water and were carried out at different loading rates of the select contaminants with both bare amendment and amendment preloaded with humic acid to obtain adsorption isotherms. The studies were conducted with an adsorption equilibration time of 48 hours for organoclay and 72 hours for activated carbon; previous experiments conducted as part of this project had shown these durations represented reasonable equilibration periods for adsorption of the select contaminants onto these types of amendments.

Batch adsorption experiments were also conducted with the field-conditioned sorbent mixture (0.28 lb/ft^2 activated carbon, 0.23 lb/ft^2 apatite, 0.28 lb/ft^2 organoclay) obtained from the small-scale test mat recovered from Cottonwood Bay (the selected mat system pilot site) after six months of soak time. These experiments were conducted for a duration of one week at five loadings of a contaminant mixture containing both 2,2',5,5'-tetrachlorobiphenyl and phenanthrene.

As the most favorable mixture of amendment materials was still uncertain after year two, additional batch isotherm experiments were conducted to evaluate the performance of CETCO organoclay and coconut shell activated carbon regarding the adsorption capacity of select PCBs (2-chlorobiphenyl, 2,2',5,5'-tetrachlorobiphenyl, 2,2',4,4',5,5'-hexachlorobiphenyl) and PAHs (naphthalene, phenanthrene, and pyrene) in the presence and absence of humic acid. Kinetics experiments were also conducted to determine the adsorption equilibration time for pyrene and phenanthrene on CETCO organoclay and coconut shell activated carbon. Finally, based on the adsorption equilibration time obtained for pyrene, additional isotherm studies were conducted to determine the desorption properties of naphthalene, phenanthrene and pyrene on CETCO organoclay and activated carbon when these amendments are treated as bare sorbents and preloaded with humic acid.

In addition to these adsorption studies, structural analyses for activated carbon and organoclay were conducted using scanning electron microscopy and x-ray diffractometry, atomic force microscopy and scanning electron microscopy, respectively. The purpose of the structural

analyses was to observe physical differences caused by humic acid on the surfaces of the sorbent material molecules. The Brunauer, Emmett and Teller (BET) surface area analysis was also conducted to determine the surface area of activated carbon and organoclay particles. These structural analyses were conducted as part of standard laboratory QA/QC practices defined for the study and the resulting characterization could serve to explain unexpected behavior in the amendment test experiments. As unexpected amendment behavior was not observed during the laboratory tests, the structural results were not pivotal to the conclusions of this report. Thermogravimetric analyses of organoclays were also performed to determine the percent organic content that increases the hydrophobicity, and thus adsorption capacity, of this type of material.

***Humic Acid Preloading*.** The preloading of both organoclay and activated carbon for the batch isotherm experiments was done with 1 g/L of humic acid solution prepared in deionized water. A sodium azide solution was added to the humic acid solution and the sorbent samples were equilibrated for 48 hours at 150 rpm on a rotary shaker to ensure thorough mixing. In the preloaded amendment samples, humic acid was present in two forms: (i) humic acid adsorbed due to preloading and (ii) humic acid in dissolved form in a deionized water matrix.

Sample Extraction. When the equilibrium time was reached for each batch experiment, the supernatant was extracted into hexane by the vial liquid-liquid extraction method with tetrachlorometaxylene (TCMX) as a surrogate standard. Twenty mL of sample and 10 mL of hexane were transferred into a 40 mL vial. The vials were sealed with Teflon®-lined screw caps and shaken vigorously for 30 seconds on three separate occasions. The vials were then stored for 24 hours at 4˚C, at which point the extracts were passed through sodium sulfate to remove any chemically bound water prior to analysis with gas chromatograph columns.

Gas Chromatographic Analysis. All sample extracts were analyzed for naphthalene, phenanthrene, pyrene and 2,2',5,5'-tetrachlorobiphenyl adsorption using a Varian CP3800 Gas Chromatograph (GC)/Saturn 2200 Ion Trap Mass Spectrometer (MS) with a CP8400 Auto Sampler. The GC column used was a DB-5 type capillary column (Varian Factor Four VF-5ms), 30 m long, 0.25 mm internal diameter and 0.5 µm thick. The ion-trap was operated in selected scan mode (MS/MS) for each PCB congener. The column oven temperature was programmed to hold at 40˚C for two minutes followed by a temperature ramp up to 184˚C at the rate of 12˚C per minute and then up to 280˚C at the rate of 4˚C per minute with the final hold time of two minutes.

Desorption Studies. When the kinetic (adsorption) experiments were completed for the CETCO organoclay and coconut shell activated carbon amendments, additional isotherm studies were conducted to determine the desorption properties of the same organic contaminants of concern (naphthalene, phenanthrene and pyrene). For these studies, humic acid was spiked into previously equilibrated samples of amendment-contaminant mixtures to determine whether continued exposure to high concentrations of organic acids would result in contaminant desorption into porewater.

4.1.2 Amendment Adsorption Kinetics

Kinetic Studies. In addition to the amendment adsorption studies (Section 4.1.1), batch kinetic experiments were conducted to evaluate the adsorption equilibrium times of pyrene and phenanthrene onto CETCO organoclay and coconut shell activated carbon. The experiment was conducted for 15 day durations in both the presence and absence of humic acid. Samples were spiked with the selected PAHs after preloading with humic acid (including a non-loaded control sample) and continuously mixed on a rotary shaker at 150 rpm for the duration of the experiment. The concentrations of the experimental PAH solutions were 0.16 mg/L for pyrene and 1.6 mg/L for phenanthrene. Humic acid preloading, sample extraction and GC analysis were accomplished in the same manner as described above for the batch isotherm experiments.

4.1.3 Combined Effects of Humic Acid, Fulvic Acid and Natural Organic Matter

Batch Experiments. Supplemental experiments were conducted to determine the effects on chemical adsorption of fulvic acid (FA) and natural organic matter (NOM) isolated from sediment pore water. These results supported the understanding of the influence that different fractions of dissolved organic carbon (DOC) would be expected to have on the sorbent properties of potential reactive mat amendments under real site conditions. Batch experiments were conducted to evaluate the adsorption of phenanthrene and 2,2',5,5'-tetrachlorobiphenyl on CETCO organoclay and coconut shell activated carbon in the presence and absence of two humic acids (Aldrich humic acid, Suwannee River (Georgia) humic acid), a fulvic acid (Suwannee River) and natural organic matter (Suwannee River) in a solution at neutral pH in order to assess the combined effects of these substances on overall amendment performance. All organic acid sources were purchased from appropriate vendors. Experiments were conducted in 40 ml vials with varying loading rates of 2,2',5,5'-tetrachlorobiphenyl and phenanthrene, and remaining free-phase concentrations were measured at 72 hours (determined in previous experiments to be sufficient to approximate equilibrium) in order to obtain the data for determination of adsorption isotherms. All batch experiments were conducted using methanol and deionized water as the stock solution for organoclay and acetone and deionized water as the stock solution for activated carbon.

Preloading Process. The preloading of organoclay and activated carbon was achieved by soaking these materials within varying solutions (1, 100 and 1000 mg/L) containing two natural organic matter (NOM) types (humic acid and fulvic acid). A 10% sodium azide was then added to the organic acid solutions to prevent bacterial degradation of the material. Finally, the sorbent samples were mixed for 48 hours at 150 rpm on a rotary shaker to ensure homogeneity.

4.1.4 Column Testing

Column Testing. During year three, project personnel designed and fabricated a stainless steel column specific to mat technology in order to better understand the treatment capabilities of reactive mats deployed in the field (Figure 4.1-1). In these studies, a solution containing select PAHs (naphthalene and phenanthrene) and PCBs (2-chlorobiphenyl and 2,2',5,5'-tetrachlorobiphenyl) was pumped upward through a reactive mat specimen at a flow rate similar to potential hydraulic flux expected under field conditions. Selected concentrations

were scaled to the solubility of each test contaminant (naphthalene: 31 mg/L, phenanthrene: 1.26 mg/L, 2-chlorobiphenyl: 3.35 mg/L, 2,2',5,5'-tetrachlorobiphenyl: 0.06 mg/L), and all contaminants were present as a mixture. Upflow velocity through the columns was 7.9 cm/day, which was higher than measured at the pilot site. The experiment duration was 7 days, and samples were taken once per day. Samples were extracted and analyzed for dissolved phase PCB and PAH as described in Section 4.1.1.

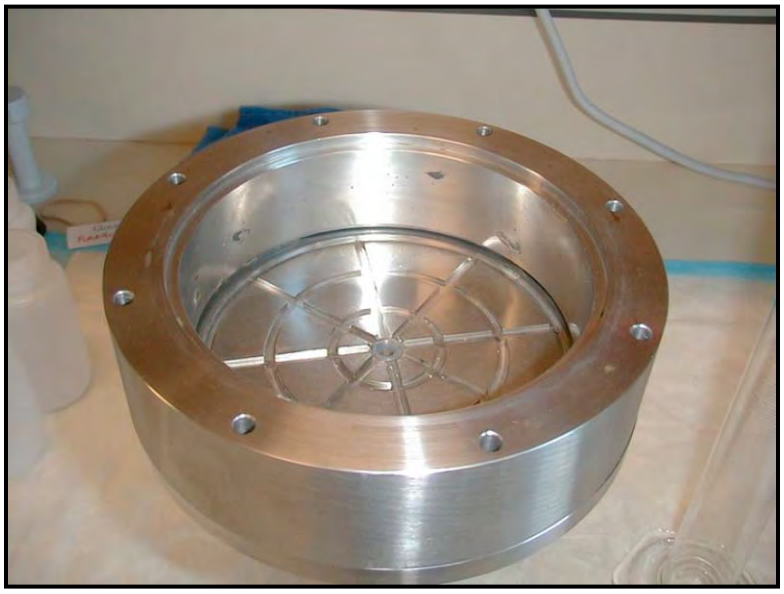

Figure 4.1-1. Experimental column for reactive mat flow-through testing.

4.2 Task 2: Pilot Site Selection

The purpose of selecting a pilot site for this project was to identify a location for the field testing of small-scale geotextile mats The site selection process consisted of screening a number of possible sites based on chemical, biological, and logistical factors, followed by focused geophysical surveys at the selected site to determine a specific area within the site that would serve as the location for prototype mat system deployment.

4.2.1 Strategy Overview

Pilot site selection was initiated in year one by conducting a review of data on potential sites to assess compatibility with expected mat performance characteristics. The pilot site selection process was two-phased, with the first objective being the identification of the most advantageous location from a "long list" of prospective Navy sites. Two sites, Cottonwood Bay in Grand Prairie, Texas and Pearl Harbor in Honolulu, Hawaii, were identified as potential pilot sites based on the criteria described in the First Year Annual Progress Report (NAVFAC 2006). Based on a comprehensive review of chemical, biological and logistical factors, Cottonwood Bay was ultimately chosen as the primary pilot site.

The second objective of the site selection process was to further characterize the geophysical properties of the primary pilot site (Cottonwood Bay) with the goal of defining a specific target

area for deployment of the prototype test mat system. The geophysical investigation included bathymetry, sub-bottom, side-scan sonar, sediment profile imaging (SPI) and groundwater seepage surveys completed during Year Two as described in the Second Year Annual Progress Report (NAVFAC 2007).

4.2.2 Primary Site Selection Criteria

During the Year One effort, a series of criteria were generated in order to screen many prospective sites for characteristics that would allow for the most comprehensive understanding of the field dynamics of the reactive mats. The criteria for phase one site selection included an evaluation of chemical, physical, and biological data as well as site management and logistical considerations. The desirable characteristics for each of these parameters were provided in a series of tables in the First Year Annual Progress Report (NAVFAC 2006).

While these criteria were not quantitatively weighted, priority was given to the presence of both metals and organics in sediment, and groundwater flux and biological colonization conditions suitable for comparing pre- and post-mat deployment conditions. Other practical criteria for initial screening included the chronology and direction of risk assessment remedial management plans. The ideal location would be a near-term candidate for remedial dredging or traditional capping for which it would be possible to evaluate a reactive mat as a more effective, stable and economically advantageous alternative. Additional logistic considerations included accessibility of the site, availability of information to characterize existing conditions and cooperation of site/program management staff with at least some minimal availability to support project planning and execution.

When the two most suitable pilot sites were established (Cottonwood Bay and Pearl Harbor), a comprehensive review of the literature for each location was performed to determine if remediation was planned and if contaminants of potential concern (CoPCs) had been established for metals and organics. Other site factors that were sought in the literature included the absence of major obstructions such as rocks and/or debris that would make deployment of the mats in direct contact with the sediments difficult. Also, it was deemed desirable to have a site with active groundwater seepage and associated contaminant transport to surface waters, wherein the mats would provide active contaminant sequestration while allowing the natural advective flow conditions to occur unimpeded. Additionally, a site with an energetic hydrodynamic environment, such as an intertidal zone or a shoal environment, would be an advantageous site because of the challenges of designing a traditional stable sand cap in such a setting. Other salient characteristics of the prospective pilot site included factors that would affect the bioavailability of contaminants and/or the reactive capacity of the apatite, organic carbon and organoclay to bind the contaminants. Findings from the Task 1 laboratory studies were considered in the evaluation of pilot site suitability because elevated organic carbon and humic acid in sediments could reduce contaminant bioavailability. Therefore, suitable pilot sites would not have high concentrations of these constituents for an optimal demonstration of reactive mat effectiveness. Finally, the availability of transportation facilities and shoreside infrastructure were also evaluated for each site in order to assess the ability to accommodate mat deployment and monitoring.

The results of this comprehensive review indicated that Cottonwood Bay would be the primary pilot site for future activities. A detailed description of Cottonwood Bay is provided in Section 5.2.2. This water body is situated between Routes I-30 and I-20 in Dallas County and is adjacent to the Vought Aircraft Industries plant (formerly the Naval Weapons Industrial Reserve Plant) and Naval Air Station Dallas (NAS). It is connected to the larger Mountain Creek Lake by a man-made diversion channel that transects NAS property, running underneath the entrance bridge and alongside the former base airstrip. Cottonwood Bay is divided into two main portions (East and West) by a causeway running from Vought property to NAS property. These two portions are hereafter referred to as "Cottonwood Bay East" and "Cottonwood Bay West" (Figure 4.2-1). Recent data for this site were provided by the USGS and included a computer model analysis of groundwater flow and the simulated effects of contaminant remediation (Barker and Braun 2000). In summary, concentrations of chromium and PCBs were generally higher adjacent to the current Vought shoreline while concentrations of PAHs (*e.g.*, fluoranthene) increased with proximity to the NAS. Concentrations of metals and organics were found to be generally lower by a factor of five in Cottonwood Bay West compared to stations in Cottonwood Bay East on the opposite side of the causeway. A series of wells and trenches were installed on the NWIRP (now Vought) property with the goal of removing groundwater from the local aquifer before it reaches Cottonwood Bay. Remedial action planning for Cottonwood Bay by NAVFAC Southeast on behalf of the Texas Natural Resource Conservation Commission (TNRCC) is ongoing.

4.2.3 Geophysical Surveys

An extensive geophysical investigation was conducted in Year Two to characterize Cottonwood Bay site conditions including water depth, habitat characteristics and lake sediment properties with the goal of selecting a specific location for future prototype mat system deployment. The evaluation consisted of bathymetry, sub-bottom profiling, side-scan sonar and sediment profile imaging (SPI) surveys conducted by SAIC. Coastal Monitoring Associates, Inc. (CMA) conducted a follow-up groundwater seepage survey to define the extent of sub-surface groundwater plumes that may be radiating from adjacent Vought property and serving as contaminant transport pathways into the bay.

All aspects of the Cottonwood Bay geophysical investigation were completed from July-September 2007 following the detailed methodology described in the Second Year Annual Progress Report (NAVFAC 2007). All pilot site selection activities for this project were completed by Year Two and no additional methodologies for this task are included in this final report.

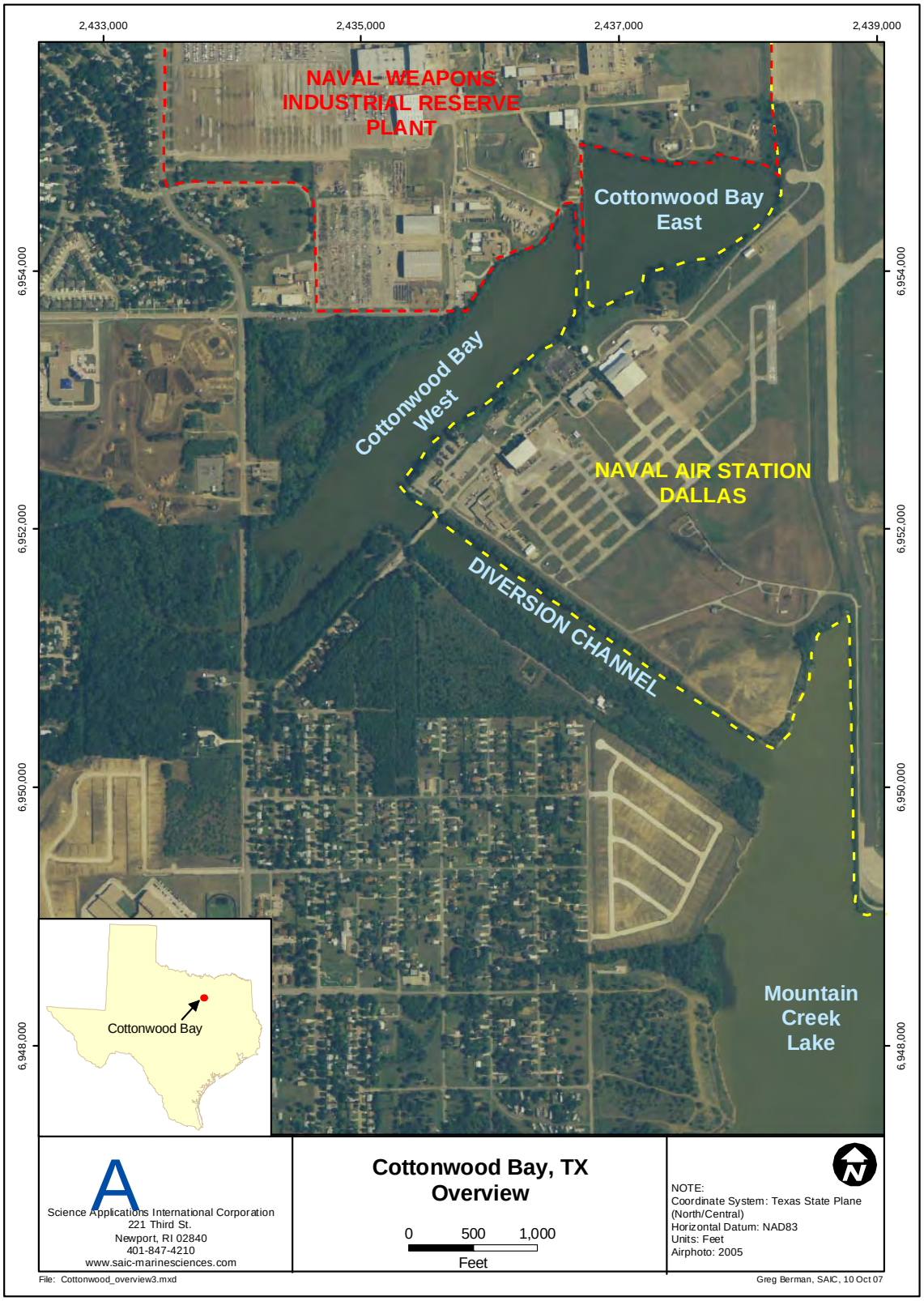

Figure 4.2-1. Overview of the Cottonwood Bay site.

4.3 Task 3: Geotextile Testing

The purpose of the geotextile testing task for this project was to field test different types of geotextile material at the selected pilot site in order to assess: (i) whether sediment clogging, biofouling and biofilm formation will adversely affect the ability of the fabric to allow water to pass through the final mat design, (ii) whether environmental weathering compromises the ability of the mat to retain the amendment material and (iii) whether environmental weathering compromises the reactivity of the sequestration agents. The geotextile found to be most resistant to biofouling after a specified soak period as determined from this small-scale field test was ultimately used for construction of the prototype mat system.

The geotextile testing task included the construction and deployment of small-scale test mats of different compositions (July 2007), six-month retrieval (December 2007), initial laboratory study (January-March 2008), one-year retrieval (October 2008), two-year retrieval (June 2009) and final laboratory study. While the test mats were soaking, laboratory gradient ratio testing and finite element analyses were conducted for clean, non-fouled mats to develop initial results regarding stability, clogging potential and prospective sediment deformation leading to excess pore water pressure as described in the Second Year Annual Progress Report (NAVFAC 2007). These laboratory testing and modeling procedures were continued in year three to incorporate field data from the recovered test mats. Results from the composite material testing and gradient ratio testing performed on these weathered mats were used to determine and confirm both the amendment mixture and the geotextile type most unaffected by biofouling to be used for prototype mat system testing.

4.3.1 Field Evaluation

Fabrication. During Year One of this project, the project team worked with the CETCO company of Arlington Heights, Illinois, to fabricate a total of 14 small-scale test mats of properties, each measuring 6 ft x 6 ft (Figure 4.3-1). These mats were designed and constructed by CETCO such that the amendment material was bound within a high loft core "sandwich" between a woven backing geotextile (silt curtain) and a non-woven top geotextile (fabric). This arrangement was chosen to allow the principal investigators the ability to assess how material type and apparent opening size affect biofouling and sediment clogging. Twelve of the mats contained a mixed core composite consisting of apatite (0.23 lb/ft^2), activated carbon (0.28 lb/ft^2) and organoclay (0.28 lb/ft^2). The maximum achievable loading rate for this mixture was ~0.8 lb/ft^2 due to the light density of activated carbon and associated volume limitations. The remaining two mats contained an Ottawa sand core to serve as a replicated control.

Table 4.3-1 below summarizes the properties of the small-scale test mats. Design variables for these mats included non-woven geotextile material (polyester or polypropylene), amendment core density (expressed as mass per unit area; oz/yd^2) and geotextile apparent opening size (AOS). The AOS for a particular geotextile (expressed as a US Sieve Number) reflects the approximate largest opening dimension available for soil/sediment to pass through as determined by dry sieving uniform sized glass beads of a known standard sieve size through the geotextile until the weight of beads passing through the geotextile is 5% or less. Because sieve numbers are inversely proportional to opening size, a geotextile with a larger AOS value will theoretically be

more susceptible to long-term clogging or blinding. The AOS values of 70, 80 and 170 used for construction of the small-scale test mats represent specified sieve opening sizes of 210, 177 and 88 microns, respectively.

Geotextile material was included as a test variable because different fabric types were expected to show different breakdown and clogging properties when exposed to field conditions. Core density was a test variable in order to evaluate the precise amount of amendment material needed per unit area of a reactive mat to achieve the most efficient chemical sequestration while minimizing clogging. Finally, AOS was a test variable in order to determine the relationship between mat porosity and performance and to evaluate the potential effects of clogging.

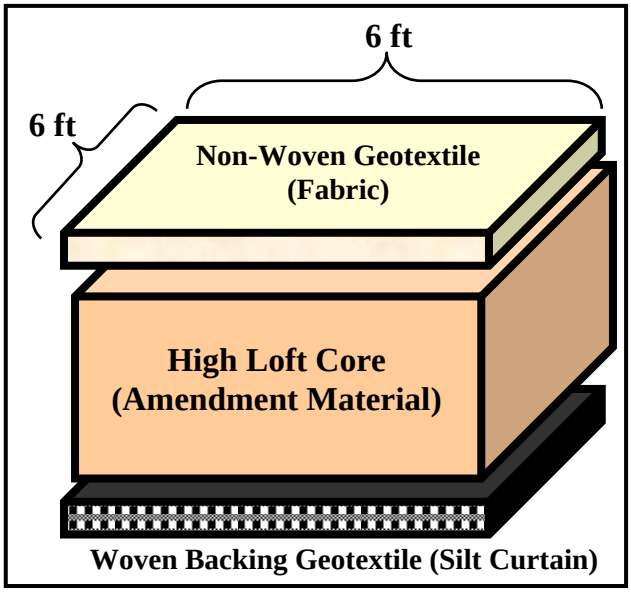

Figure 4.3-1. Construction diagram of small-scale geotextile test mats.

Table 4.3-1. Material design summary of small-scale geotextile test mats.

Total of 14 Test Mats Constructed			
Material	**Core / Mass Per Area**	**AOS**	**Quantity**
Polyester	Mixed - 5 oz/yd^2	170	4
Polypropylene	Mixed - 6 oz/yd^2	70	4
Polypropylene	Mixed - 8 oz/yd^2	80	4
Polypropylene	Ottawa Sand - 6 oz/yd^2	70	2

Deployment. In June 2007, the 14 small-scale mats were placed in Cottonwood Bay East in two rows of seven near the northern shore of the bay adjacent to the Vought property. Each of these rows consisted of two polyester test mats with a 170 apparent opening size and mixed core, two polypropylene test mats with a 70 apparent opening size and mixed core, two polypropylene test mats with an 80 apparent opening size and mixed core and one polypropylene control mat with a 70 apparent opening size and sand core.

All of the test mats contained the same amendment core mixture featuring a combination of apatite, activated carbon and organoclay. For the similar mats in each row, one replicate was deployed with the woven backing geotextile (silt curtain) face down and the other replicate was deployed with the woven backing geotextile face up. This arrangement was selected to investigate how the different geotextiles behave under direct contact with the sediment surface. The control mats were deployed with the woven backing geotextile face down in both rows.

All mats were weighted to the sediment surface with ceramic bricks tethered to each corner with plastic zip ties and the location of the southwest corner of each mat was marked with an aluminum stake. Each mat was also tagged with a colored zip tie to aid in differentiating each replicate during the evaluation process. Approximately five feet of space was left between each mat to reduce possible interference associated with edge effects (*e.g.*, suppression of groundwater flux by nearby mats). Field photographs of the small-scale test mat deployment process are shown in Figure 4.3-2.

Figure 4.3-2. Small-scale geotextile test mat deployment.

Monitoring. A preliminary field evaluation of the small-scale mat deployments was conducted in July 2007 (approximately one month after initial placement) by wading near the mats and observing whether any had substantially shifted position or become subject to any unexpected deterioration. It was noted at this time that Mat 1 in Row 1 (the westernmost mat in the row closer to shore) had accumulated gas underneath that was causing the mat to float off the lake floor. Similar conditions were also noted in Mat 2 and Mat 3 in Row 2 (the second and third westernmost mats in the row further from shore). The source of the gas was most likely a build-up of methane moving up through the sediments beneath the mat or gas being produced by biological activity taking place beneath the mat. Because the westernmost mats in each row featured the smallest apparent opening size (either 5 oz/yd^2 or 6 oz/yd^2), it was postulated that these gaseous accumulations were not able to pass through the small AOS. Whether the mat was deployed with the woven backing geotextile up or down did not appear to affect gas accumulation. Prior to concluding the field evaluation, field personnel released the bubbles from the mats in question by lightly stepping on them to force all gas accumulation out the side until they were again laying flat against the sediment.

Retrieval. The small-scale test mats were recovered after predetermined soak times to assess potential hydraulic conductivity changes due to biofouling and potential reactivity changes due to biofilm growth. Field personnel returned to Cottonwood Bay in December 2007 to conduct the six-month retrieval of the first set of the small-scale (6 ft x 6 ft) geotextile test mats that had been soaking in the eastern portion of the bay since June 2007. At this time, the first row of seven mats (six test mats and one control mat) were lifted from the lake floor and hoisted as flat as possible onto the deck of a dual Jon-boat shallow draft vessel. In contrast to the previous monitoring event, all seven mats were found to be laying flat on the lake floor with no noticeable gas buildup.

The mats were transported to shore and placed flat on a sheet of clear plastic and photographed. Colored zip ties were attached to the mats to identify the different test treatments in terms of geotextile material, apparent opening size and whether the mat was placed with the non-woven geotextile facing up or down. All mats were then covered on both sides with clear plastic, rolled around a 5 ft long 2 in x 3 in piece of wood, sealed in commercial grade garbage bags and encased in 12 in diameter cardboard sonotubes for shipping. This packing process was intended to preserve, to the greatest extent possible, any biofilm and sediment accumulation that had accumulated on each side of the mat during the six month soak time. All seven mats were then shipped at room temperature to UNH for controlled laboratory testing. Preliminary observations of the small-scale test mats following recovery indicated a moderate level of biofouling and the presence of several small red worms that appeared to have burrowed into the non-woven geotextile.

A similar retrieval event for the second set of small-scale test mats was conducted in October 2008 concurrently with deployment of passive contaminant samplers at the prototype mat system (see Section 4.4.4). At this time, two of the original four replicates of the 170 AOS, 5 oz/yd^2 non-woven geotextile test mats, (one each placed with woven geotextile up and down) were retrieved from Row 2 (further from shore) for repeat laboratory testing. These replicates were recovered after only one year of soak time because previous laboratory testing on similar test mats recovered after six-months of soak time had already indicated that this type of non-woven geotextile exhibited increased clogging and was unlikely to be used for full-scale implementation (see Section 5.3.2). The five remaining small-scale mats were left in place for an additional year in accordance with the project work plan. Small-scale test mats were packaged and shipped during all subsequent recovery efforts in the same manner as described above for the initial recovery effort. At the time of the second recovery effort, all remaining small-scale test mats were observed for gas buildup and none were found to be affected as evidenced by their laying flat on the lake floor with minimal floating.

The retrieval event for the five remaining small-scale test mats was conducted in June 2009 concurrent with the Ultraseep and Trident Probe surveys of the prototype mat system (see Section 4.4.5). At the time of this final recovery effort, a moderate level of gas buildup, lifting approximately 25% of each mat off the substrate, was observed immediately prior to test mat retrieval. Although the presence of this gas buildup was unlikely to effect the properties of the small-scale test mats, it did serve as an indicator of a proportional amount of buildup that could be expected below the larger prototype test mats at that time of year, which could in turn effect contaminant sequestration performance by reducing direct contact between the mat and the

sediment-water interface unless a corrective action was taken. This issue was addressed further during the placement and monitoring of full scale mats, discussed in Section 4.4.2.

Performance Evaluation. Following the initial test mat retrieval event, laboratory performance evaluations were conducted to investigate whether biofouling and/or surficial material accumulation which had occurred in the field resulted in changes in mat permeability and hydraulic conductivity. Parallel laboratory testing was also conducted to assess the effects of biofouling on amendment reactivity to determine if the presence of natural organic matter affects adsorption properties (see Section 5.1.3). The ultimate goal of these performance evaluations was to select the geotextile that offered the best balance between fouling resistance and amendment material effectiveness for design of the prototype mat system.

For geotechnical performance testing, a test column system was utilized following American Society of Testing and Materials (ASTM) method 5101 (Figure 4.3-4). Method 5101 is typically used to directly measure the clogging potential of a soil/geotextile system *(i.e.*, a layer of soil in contact with a geotextile such as in a landfill cap situation) and was adopted here to assess the impacts of sediment settlement/biofouling found to cover the reactive mats in the field. Accordingly, adoption of ASTM 5101 for this purpose was assumed to provide a realistic estimate of the actual cap performance with regard to clogging and sediment infiltration.

Figure 4.3-4. Geotextile sediment gradient ratio column experimental setup.

When the small-scale test mats were received at the UNH laboratory, initial observations were made regarding relative percent fouling of the geotextile material. Gradient ratio tests were then performed by placing a section of mat sample into the column and measuring the time required for static head pressure of an underlying water column to flux through the mat surface. The elapsed time was compared to the flux time of a clean, non-fouled mat.

Another concern for the mat performance evaluation was the growth of biofilms on the surface of the reactive materials themselves, regardless of specific type of amendment used in the mat.

These colonies may not be sufficient to cause biofouling by clogging geotextile pore spaces, but could influence the chemistry at the surface of the amendments and thus impact contaminant uptake. To investigate the potential for such interference, samples of biofilm coated materials were collected from the recovered mat segments and tested with the same column testing techniques described in Section 4.1.5 to quantify how biofilms may enhance or diminish amendment effectiveness (Mariah Arias-Thode, SERDP ER-1551); little influence of biofilms was observed.

4.3.2 Gradient Ratio Testing

General Procedure. The purpose of gradient ratio testing is to evaluate the stability and clogging potential of a sediment-geotextile filter system. Different flow rates are tested to determine whether the geotextile is likely to become impermeable to flow under a range of natural field conditions. Using the geotextile permeability column shown in Figure 4.3-4, water was pumped downward through the sediment perpendicular to the plane of the geotextile. The test scenario was inverted from field conditions (i.e., tested using downward flow) because initial experiments showed that pumping water up through the sediment into the cap led to sediment instability and collapse before any meaningful data could be collected. When evaluating the cap samples, the system was allowed to equilibrate under no flow conditions for 24 hours. Then an initial gradient (hydraulic head over the height of the sample) of 1 was applied. After 24 hours, the gradient was increased to 4, and then to 8 after another 24 hours. The onset of clogging can be determined by comparing the ratio of the hydraulic gradient in the geotextile-sediment system to the gradient in the sediment alone. In addition, the gradient ratio test was done in a closed, transparent system, so sediment transported through the geotextile could be observed and also collected when the test was completed. A detailed picture of the gradient ratio column showing geotextile-sediment contact and reactive mat-sediment contact is provided in Figure 4.3-5. Comparative images of a geotextile sample before and after a gradient ratio test are shown in Figure 4.3-6 and accumulated sediment that has passed through the geotextile during a test is shown in Figure 4.3-7.

The gradient ratio value is defined as the ratio of hydraulic gradient in the sediment-geotextile section of the test column to the hydraulic gradient in the sediment-only section of the test column as shown in the following equation:

$$GR = \frac{i_{\text{sediment-geotextile}}}{i_{\text{sediment}}} \begin{matrix} >1 \\ <1 \end{matrix} \begin{matrix} \text{Clogging} \\ \text{Piping} \end{matrix}$$

Values lower than unity (<1) indicate piping conditions along the walls of the chamber, or possibly at the geotextile-sediment interface, while values larger than unity (>1) indicate increased hydraulic pressure across the geotextile. A value greater than or equal to three is defined as a clogged geotextile. Values slightly less than one are generally preferred for a reactive mat system since they show a stable system allowing low flow without clogging. When evaluating the effectiveness of a geotextile, the stability of the gradient ratio value might be as important as the value itself because it denotes a stable filter system without further particle transport.

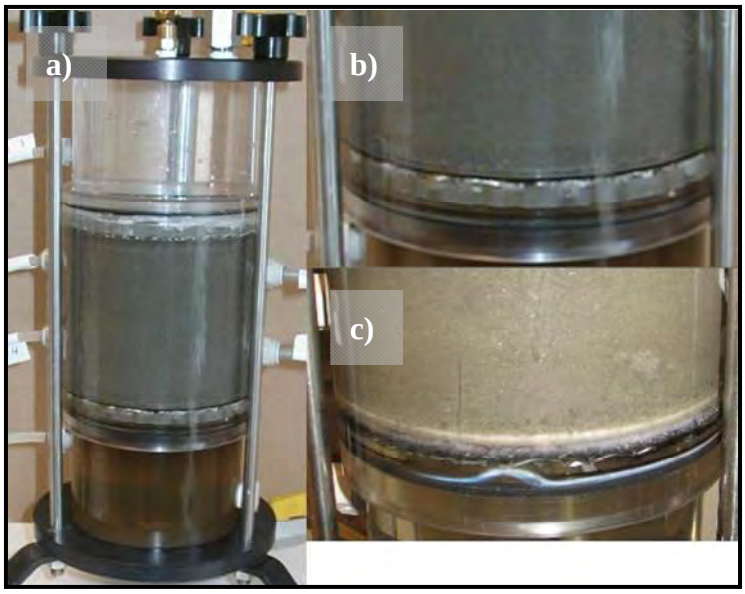

Figure 4.3-5. Detailed photograph of geotextile gradient ratio test column showing (a) permeameter for gradient ratio tests, (b) geotextile-sediment contact and (c) mat-sediment contact.

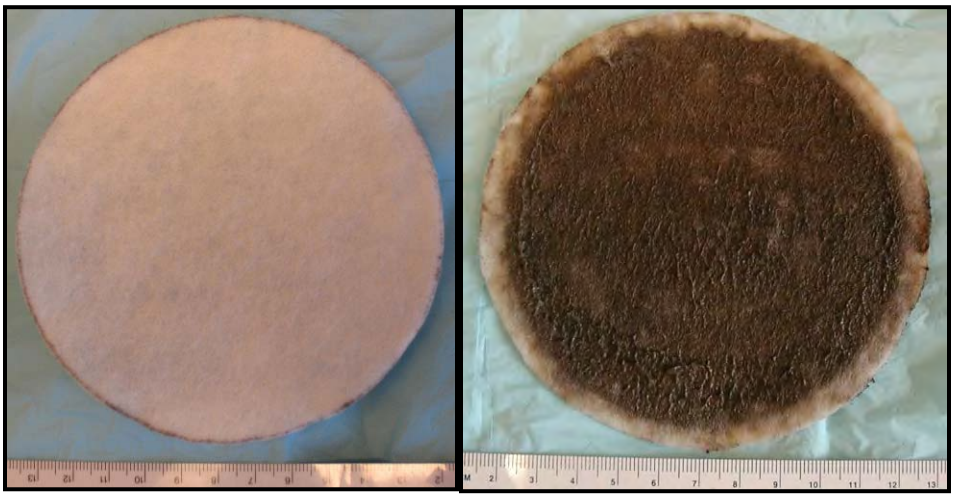

Figure 4.3-6. Comparative images of a geotextile sample before (left) and after (right) a gradient ratio test.

Figure 4.3-7. Sediment that has passed through the geotextile during a gradient ratio test.

Stock Geotextile Evaluation. Preliminary gradient ratio testing conducted on various stock geotextiles during Year One showed that bubbles trapped in the sediment matrix and under the geotextile sample are an impediment to groundwater flux through the system in a fine grained matrix such as the sediment expected to be encountered in Cottonwood Bay. Experiments were conducted to determine if sample preparation in a nitrogen atmosphere would help eliminate bubbles being trapped in the test column, but results indicated that such a process had negligible effects. The bubble trapping problem was ultimately corrected by refining sample preparation techniques to remove bubbles from the sediment prior to sealing the test column.

In Year Two, gradient ratio testing was continued on stock geotextiles as well as on clean, non-fouled mats in order to establish baseline stability and clogging conditions to which results from similar tests on field weathered geotextile mats would ultimately be compared. As mentioned earlier, vertical upward flow through the sediment-mat interface was planned for the testing process to provide consistency between the experimental conditions and the natural field conditions, but hydraulic consolidation occurred due to the effective stress variation with time and a separation between the sediment and the geotextile eventually developed. Thus downward water flow was used instead for all subsequent tests. Due to the low permeability of the sediment in the test column, it was not possible to measure the flow rate of the entire system according to the ASTM-D 5101 standard. Instead, clogging potential was evaluated using the gradient ratio value only. This procedure was repeated in year three using segments of the field-weathered small-scale test mats to determine whether biofouling increases the likelihood of clogging compared to a clean mat under similar hydraulic conditions.

The stock geotextiles used in the Year Two gradient ratio tests were the same three CETCO geotextiles (in terms of material, mass per area and AOS) used to construct the small-scale test mats (Table 4.3-1). These CETCO geotextiles were selected to cover a wide range of AOS and mass per area for practical applications as well as to mimic the arrangements being tested in the field, which was necessary to collect baseline data on the unweathered condition.

In addition to geotextiles, complete bare reactive mats were also subjected to gradient ratio testing for baseline clogging potential evaluation. The characteristics of the clean, non-fouled reactive mats used in these experiments are presented in Table 4.3-2. These representative mats contained various mixtures of the amendment materials that were considered for the final reactive mat design. As expected, preliminary results indicated that the reactive mats let less material pass through than the single sheet geotextiles.

Table 4.3-2. Characteristics of clean representative mats used in gradient ratio experiments.

Sample ID	Mass Per Area [kg/m^2]	Thickness [cm]	Reactive Material
RCM-1	4.0	~0.10	Organoclay
RCM-3	4.6	~0.10	Organoclay/Apatite
RCM-5	0.4	~0.10	Activated Carbon

Test Mat Performance Evaluation. Upon receipt at the UNH laboratory, the weathered small-scale test mats were cut into manageable pieces to be used for flow-through column gradient ratio testing following the same procedures described above. The goal of these laboratory tests was to assess whether biofouling and biofilm formation on weathered mats would adversely affect the ability of the fabric to allow water to pass through the final mat design and whether environmental weathering compromises the ability of the mat to retain the amendment material. Baseline data for these parameters to which the field data would ultimately be compared were previously established by gradient ratio tests performed on unweathered single sheet geotextiles and bare reactive mats similar to the small-scale test mats that were deployed in the field.

4.3.3 Finite Element Analysis

General Procedure. The main goal of finite element analysis (FEA) was to understand the potential sediment deformation (consolidation) that would be caused by the weight of the reactive mat as well as the resulting pressure increase that would force porewater out of the underlying sediment, potentially altering natural seepage and contamination patterns. Consolidation of the sediment would also change the ground water flow through the affected sediment. The use of FEA allows for a modeling evaluation of two-dimensional transport with regard to flow through the consolidated sediment and around the mat edges. A groundwater component was added to see how this edge flow affects advective transport.

Preliminary finite element models were constructed in Year One with Plaxis (v. 8.0) software using a simulated symmetrical half-sand cap 5 m in length placed over sediment that was treated as an elastic-plastic material with no creep. This elastic-plastic (or Mohr-Coulomb) model was a simple representation of soil/sediment behavior under loading in which the stress-strain behavior is treated as reversible (elastic) until the stress from loading reaches the failure point, at which time the soil/sediment cannot support any further load and the deformation is permanent (plastic behavior). The “no creep” condition requires that the soil/sediment does not undergo any time-dependent deformation in this model. After initial data were collected under this basic sand cap

model, a more complex sediment model was generated that considered both consolidation and secondary creep.

The simulated sand cap (protective layer) for the elastic-plastic model had a thickness of 30 cm (~1 ft). Because PLAXIS (v. 8.0) does not allow for changes in the permeability of geotextile elements, water was assumed to flow freely through the geotextile. To adjust for this deficiency and allow for the goal of evaluating varying permeability, the model was manipulated by adding a thin layer of low weight sand over the geotextile. The permeability of this thin sand layer was then adjusted to effectively change the permeability of the geotextile.

In Year Two, various geotextile mat components were added to the finite element model runs to assess increasingly sophisticated scenarios. These geotextile-inclusive models started with a hypothetical clean mat with the goal of investigating if and how flow patterns would be substantially affected by the level of clogging anticipated to occur under field conditions.

In year three, biofouling data obtained from the recovered small-scale test mats and sediment properties observed at the Cottonwood Bay pilot site were used to modify the finite element models with actual permeability values. Sediment samples were sent to a standardized laboratory for Atterberg limits and organic content testing. Results for Cottonwood Bay sediment indicated a liquid limit (LL) of 155-164 and a plasticity index (PI) of 121-125. These values were relatively high in comparison to an estuarine site (Piscataqua River, NH) where similar analyses indicated a LL of 33-34 and PI of 6-10. This difference may be related to the higher organic matter content observed for Cottonwood Bay sediments (4.3-5.8%) vs. Piscataqua sediment (4.1-4.2%). These data were ultimately applied to the FEA process to generate comparative finite element models for each site and therefore help define the operational range of the mat technology in both freshwater and estuarine conditions.

Geometry and Boundary Conditions. Geometry and boundary conditions were defined to constrain general field conditions and to promote applicability to different circumstances for the reactive mat finite element model. Field information obtained on a similar cap test project on the Anacostia River in Washington D.C. was used to develop the typical geometry for the initial model as shown in Figure 4.3-8.

This model was symmetrical with respect to the vertical left axis. The sediment region was 45 m long by 10 m deep and the reactive mat was defined as an overlying layer of sandy material 15 m long by 0.3 m thick. The mat permeability was used to simulate its clogged state, while the unit weight was used to simulate the weight of the mat's protective layer. The depth of water was set at 4.21 m, which was equivalent to the average depth observed at Cottonwood Bay.

The boundary conditions for the model included the displacement (flux rate) conditions as shown in Figure 4.3-9. The displacement boundary conditions fix any displacement at the base and the horizontal displacement on both sides of the model. The flux boundary conditions control the pressure head at the top of the sediment-mat regions based on the water level (static or tide variation). Flux was prohibited on both vertical sides of the model. The average flux rate (3.3 cm/day) observed on one of the evaluation mats of the Anacostia River was used to produce the groundwater flow for this seepage analysis. Because all the boundary conditions can only

coexist in a fully coupled analysis, they are not all required on each step of the uncoupled solutions.

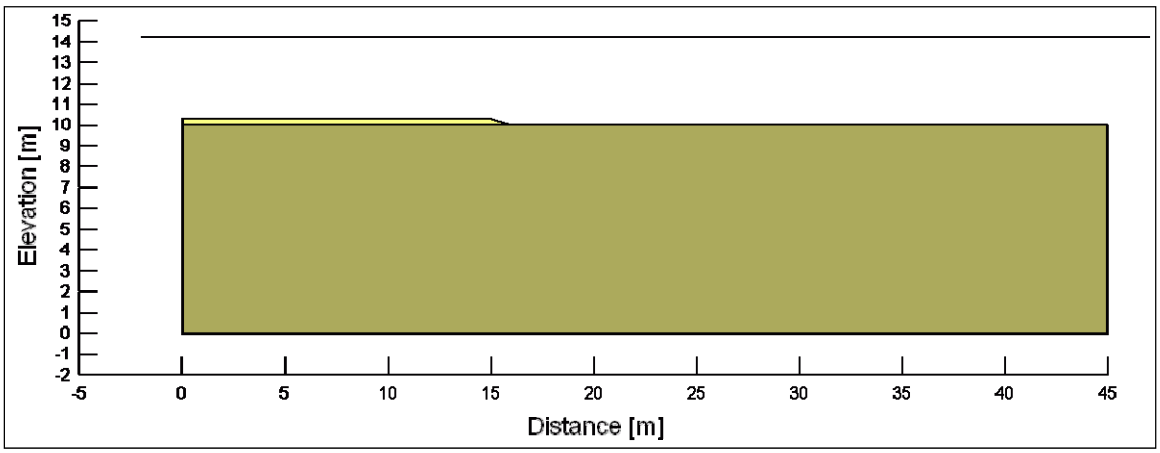

Figure 4.3-8. Geometry of a typical reactive mat application for finite element modeling.

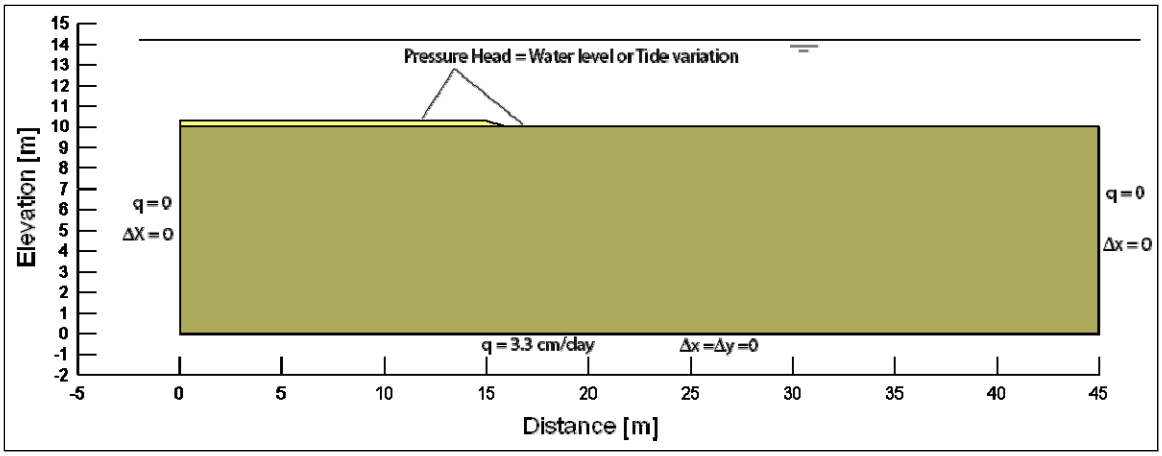

Figure 4.3-9. Summary of the boundary conditions for finite element modeling.

Geotechnical Parameters. For the initial finite element model, reliable estimates of soft sediment geotechnical properties were initially used for qualitative analyses in the absence of field data from the Cottonwood Bay pilot site. Table 4.3-3 shows a summary of the geotechnical property estimates.

The Young's modulus had a constant value from the sediment surface to a depth of 1 m to avoid numerical complications due to small or zero stiffness values. The high Young's modulus of sand was used to avoid numerical complications at the sloped end of the mat. A linear elastic model was used for a first approximation to the final configuration.

Consolidation and triaxial tests were simulated using various constitutive soil models which allowed for the calibration of geotechnical parameters and the definition of the best modeling procedure to simulate a reactive core mat deployment over soft sediment. Additional models

were also developed to calibrate contaminant transport during both soft sediment consolidation and potential geotextile permeability reduction.

Table 4.3-3. Summary of average geotechnical property estimates for finite element modeling.

Property	Sediment	Reactive Mat
Permeability, *k* [cm/s]	1.5×10^{-5}	1.0×10^{-3}
Initial void ratio, e	1.6	0.7
Unsaturated unit weight, γ_{unsat} [kN/m^3]	11	15
Saturated unit weight, γ_{sat} [kN/m^3]	14	17
Poisson's ratio, ν	0.3	0.25
Young's modulus at 1 m, E_{ref}[kN/m^2]	163.41	10000
Increment of Eper meter depth [kN/m^2]	163.41	0

Numerical solutions for the individual analyses of consolidation, seepage, and contaminant transport cases were available in the technical literature. Some finite element software includes these individual solutions but the fully coupled analysis is not available in the literature and is part of ongoing research. Consequently, the uncoupled solutions were employed in the initial model since they have been proven to be useful in understanding the individual contributions to the overall final configuration. They can also produce computationally more efficient results similar to those obtained using the coupled solution. The following sub-sections present uncoupled and coupled solutions to the consolidation-seepage problem.

Uncoupled Consolidation Model. The uncoupled consolidation model shows potential sediment deformation following mat placement independent of groundwater flow. This model was solved in two stages with the first stage computing the *in-situ* stress state of the sediment including the pore pressure distribution. The model assumed no steady state or transient groundwater flow and only the hydrostatic pressure was included. The geometry and boundary conditions of the model were the same as those shown in Figure 4.3-8 and Figure 4.3-9 above, but the flux rate at the base was q = 0 m^3/s to avoid groundwater flow through the sediment.

Consolidation time is the time required to dissipate the excess pore pressure induced by the weight of the mat. For practical purposes, 90-95% of the dissipation was defined as the end point of consolidation. A point was selected at mid-depth of the sediment layer to verify the excess pore pressure dissipation.

Uncoupled Seepage Model. The uncoupled seepage model shows potential changes in pore water properties and groundwater flow following mat placement independent of sediment consolidation. Two models were generated to assess post-mat groundwater seepage. The first model assumed the same permeability for the mat and the sediment. This scenario represented the case of an unclogged mat since the water drains freely from the sediment into the mat and out to the bay. The second model assumed a mat permeability one order of magnitude less than the sediment in order to simulate a clogged mat through which groundwater would not move freely.

Coupled Model. The coupled solution of the consolidation-seepage case is defined in three stages:

- Stage 1. Initial *in-situ* stress state without groundwater flow.
- Stage 2. Groundwater flow is applied by defining a flux rate at the base of the model and the total head at the sediment surface. A new initial stress state is achieved.
- Stage 3. Mat deployment and consolidation under groundwater flow conditions. Coupled solution.

The stages of the coupled modeling process were solved in sequence to simulate the real field conditions expected following mat deployment. No information was available from the consolidation tests to simulate the change of the sediment permeability during consolidation. Therefore, the time required to dissipate the excess pore pressure due to the mat deployment may be higher than the value estimated here. If a longer time is truly required to consolidate the sediment, that means that the lower permeability layer (filter cake) expected to develop beneath the mat will also take longer to develop. Again, a linear stress-strain relationship was used to simulate soil behavior. Field displacements were thus generally overestimated.

Oedometer Consolidation Testing. The geotechnical properties of soft sediment typical of that needed to calibrate the finite element model as appropriate for the Cottonwood Bay pilot site were determined by oedometer and seepage consolidation tests. During year three, two preliminary oedometer consolidation tests were carried out on sediment samples of similar properties collected from the Piscataqua River in New Hampshire. Loading, unloading, and reloading stages were fully completed and the results provide information about the primary consolidation and change of permeability of the sediment, as well as the secondary compression coefficient required for the numerical simulations. Given the soft nature of the sediment, and that information about the secondary compression is required for the reactive mat project, each consolidation test lasted 13 to 14 days. These results were used to guide oedometer testing on a sediment sample collected from Cottonwood Bay.

Seepage Consolidation Testing. Continued low stress sediment consolidation tests were performed during year three on unweathered geotextiles in order to provide compression curves (e vs. σ') that indicate a reduction of the void ratio as effective stress increases. The seepage consolidation test provided information about the behavior of sediment from Cottonwood Bay at 0.64, 1.1 and 2.1 kPa of effective stress which is not possible to obtain on oedometer consolidation tests. The results of the seepage consolidation were used to help calibrate the finite element models depicting a coupled solution featuring consolidation and advective flow contaminant transport.

Sediment Seepage Comparison. Test samples were extracted from the small-scale test mats recovered from Cottonwood Bay after approximately one year of soak time to investigate the amount of material that was able to seep into the mat under field conditions. This material was characterized and the results compared to the seepage properties of stock geotextiles as determined by the previous gradient ratio tests.

Consolidation Modeling. A detailed two-dimensional model was developed to simulate sediment consolidation beneath a reactive mat using the geotechnical properties of fine grained sediment as identified from the Cottonwood Bay sediment sample. The model assumed a sediment bed 8 m thick and 25 m wide where only 5 m of the sediment surface were capped using a 0.3 m layer of sand. The Modified Cam-Clay constitutive model was used to simulate soil behavior.

Groundwater Flow Modeling. A detailed two-dimensional model was developed to simulate groundwater flow through fine grained sediment. Similar to the sediment consolidation model, the groundwater flow model assumed a sediment bed 8 m thick and 25 m wide where only 5 m of the sediment surface was capped using a 0.3 m layer of sand. The reactive mat was simulated as a 1 cm thick layer of material with variable permeability to simulate clogging of the geotextile.

4.3.4 Gas Permeability Testing

As described during the test mat monitoring and retrieval phases, the buildup of methane gas beneath the reactive mats was observed during the field evaluation. The potential impacts of this gas buildup on reactive mat performance thus became an important parameter in further mat testing. Following prototype mat system observations in Cottonwood Bay that indicated potential gas buildup beneath the mats during the summer months that could be detrimental to mat performance, the SERDP review board requested additional laboratory testing to investigate the possible effects of gas accumulation under a reactive cap.

That bacterial activity in sediment can lead to the generation of significant volumes of gas, generally a mixture of methane and carbon dioxide with some other gases such as hydrogen sulfide in smaller amounts, has been well documented. The accumulation of gas underneath geotextile caps has the potential to cause cap instability if the buoyant force of the gas exceeds the submerged weight of the cap. These conditions have occurred in some caps where the geotextile layer was not covered with sand or armored with sufficient weight to offset the buoyancy of the gas. Gas production depends on the temperature of the site, water type and characteristics of the organic matter in the sediment. An upper estimate of biogenic methane gas production in marine sediments has been reported as 4.25 x 10-15 mol/day per gram (8.963 x 10-5 cm^3/day per square meter) of sediment (Colwell *et al*. 2008). However, a literature review showed reported gas production rates from wetland sediments, paddy soil, and other freshwater sediments in the range of 0.3 to 2640 cm^3/day per square meter of sediment surface, which is more than five orders of magnitude greater than production in marine sediments. Gas production rates in freshwater sediment also vary significantly with temperature from 0.3, to 341 to 917 cm^3/day, at 4, 22 and 35°C respectively (Qingzhong *et al*. 2007).

Gas does not exit the sediment in a uniform, steady flow, but rather typically builds up in the sediment and then escapes in large bubbles through a preferential path. Thus gas loading underneath a cap is in the form of sudden bubbles trapped at the geotextile layer. An important question for mat performance then becomes whether these gas bubbles have time to pass through the geotextile or do they continue to build until the cap becomes unstable. In order to address this question, an apparatus and test technique was designed to simulate a gas bubble trapped

under the geotextile and investigate how easily this bubble would migrate through the geotextile under a given hydraulic gradient simulating the rate of gas generation in natural sediment.

The gas permeability test was constructed using the same permeameter/geotextile setup as the gradient ratio test, but without the sediment sample. Water pressure and temperature alone influenced the gas dissolution in water. The purified deionized water used for the experiments remained at room temperature (20-22°C) to minimize variations of its influence on the results. In order to minimize the influence of water pressure on the gas dissipation rate, the water pressure on the gas bubble was held constant at 1" and no water flow was induced through the geotextile.

The geotextile samples were prepared by submerging the geotextile for a period of 24 hr in purified deionized water prior to assembling the permeameter. The fully saturated geotextile was then placed in the permeameter and the system was filled with purified deionized water from the bottom up to prevent trapping of gas bubbles in the system. The permeameter used to carry out the gas permeability test is shown in Figure 4.3-10, including the port used to inject the gas bubble and the location of the geotextile.

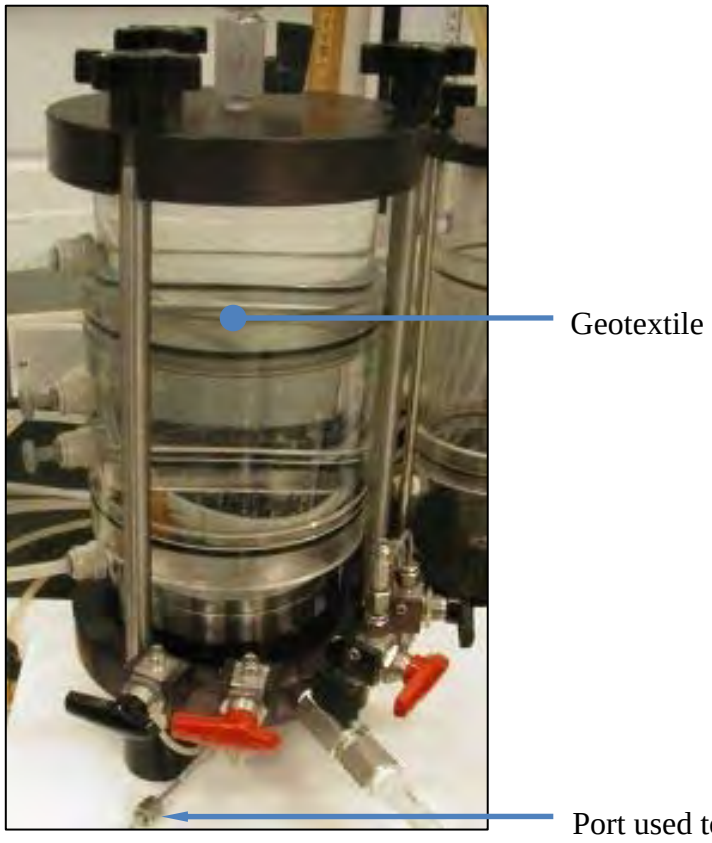

Figure 4.3-10. Permeameter setup for gas permeability testing.

After complete assembly of the permeameter, a 1 cm^3 gas bubble was injected beneath the geotextile and left to pass through the geotextile without any water flow in the permeameter. The gas bubble was monitored daily until it passed through and/or was dissolved in the water. Biogas collected from the Turnkey landfill in Rochester, NH was used for these tests since its

composition is typical of the gas produced by bacterial activity in freshwater sediment (methane, carbon dioxide, nitrogen, oxygen, hydrogen sulfide, and hydrogen). The gas permeability test was carried out using a fine geotextile of greater weight (AOS 170, 8 oz/yd^2) because if the gas flow/dissipation rate for this material was found sufficient to prevent significant gas accumulation beneath the geotextile, then no additional tests would be required on coarser and lighter geotextiles which would be assumed to have greater permeability. The geotextile used in these permeability tests corresponded to samples of the GT-4 geotextile used in the gradient ratio tests.

4.4 Task 4: Prototype Mat System Testing

The purpose of this task was to field test a prototype mat system constructed of different arrangements of the most effective amendment (identified in Task 1) and the geotextile most resistant to fouling (identified in Task 3) in order to assess *in-situ* chemical sequestration effectiveness and flux properties. To accomplish this task, larger prototype mats were constructed per proposed specifications and deployed at the target area in Cottonwood Bay. The Task 4 effort occurred entirely during years three and four of the project. Construction and deployment of the prototype mat system was completed in April 2008 and, the mat arrangements were monitored for contaminant adsorption and flux properties by various techniques through December 2009.

4.4.1 Prototype Mat System Design

Laboratory data from the ongoing composite material testing and gradient ratio testing were used to identify the most adsorbent amendment and the geotextile most unaffected by biofouling for construction of a prototype mat system to be deployed at the selected pilot site and used for long-term monitoring and evaluation of this technology. These design element results are discussed in detail in subsequent sections of this report as outlined in the following table.

Table 4.4-1. Report outline for design element experimental results used to guide construction of the final prototype mat system.

Design Element	Report Section
Amendment Core Mixture	5.1.1. Amendment Adsorption Capacity; 5.1.2. Amendment Adsorption Kinetics
Geotextile Material	5.3.2. Gradient Ratio Testing
Geotextile Apparent Opening Size	5.3.2. Gradient Ratio Testing
Geotextile Mass Per Area	5.3.2. Gradient Ratio Testing
Hydraulic Conductivity	5.3.2. Gradient Ratio Testing
Biofouling/Clogging Resistance	5.3.2. Gradient Ration Testing
Sediment Deformation	5.3.3. Consolidation Testing

The final mats created by CETCO for prototype testing were comprised of an 80 AOS and 8 oz/yd^2 polypropylene non-woven geotextile, a woven backing geotextile and a mixed amendment core made up of 0.23 lb/ft^2 crushed apatite, 0.28 lb/ft^2 coconut shell activated carbon and 0.28 lb/ft^2 CETCO organoclay. Each individual mat was made up of two 25 ft x 15 ft panels

to be placed with a five foot overlap for an overall footprint of 25 ft x 25 ft (Figure 4.4-1). The entire mat system was designed to consist of four test treatments including a single layer mat (T1), a single layer mat with sand cover (T2), a double layer mat (T3) and an area of sand cover only (T4), as well as a similar sized area of undisturbed lake floor (T5, not shown) to serve as a control for the test data (Figure 4.4-2). Where applicable, the sand cover component consisted of an approximately three-inch layer of clean material of moderate grain size to provide a substrate for recolonization of the benthos while at the same time protecting the mat from bioturbation.

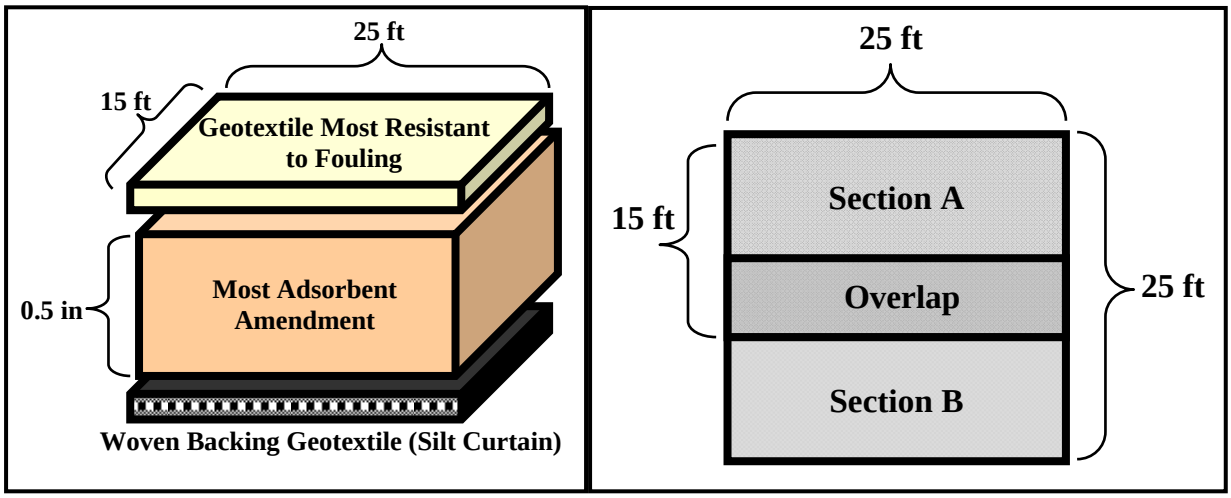

Figure 4.4-1. Construction and layout diagrams of prototype geotextile test mats.

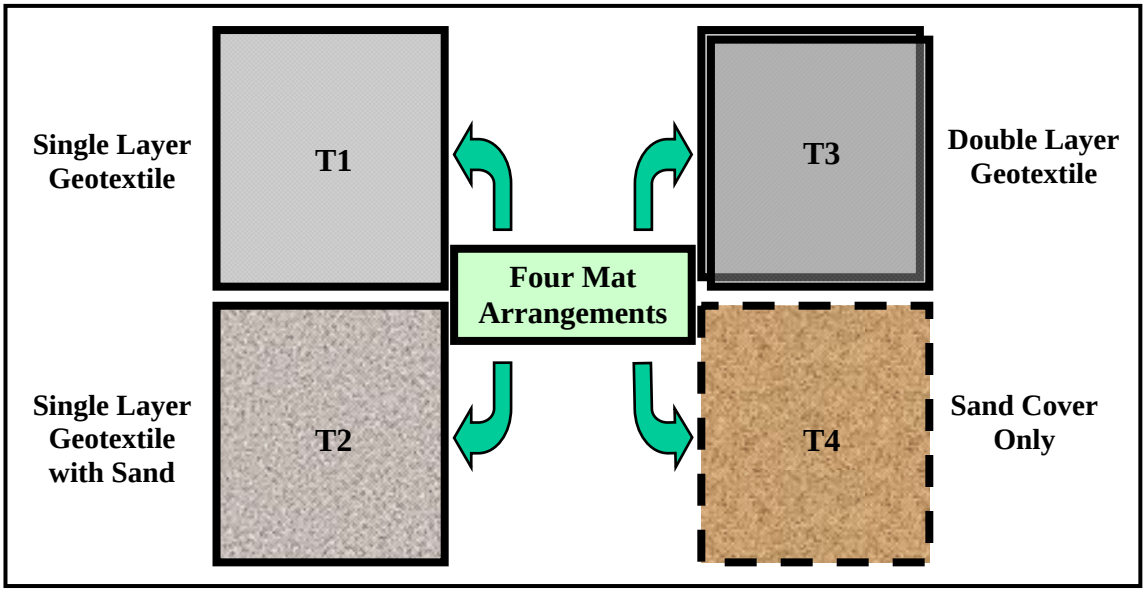

Figure 4.4-2. Various arrangements for prototype mat system testing.

4.4.2 Mat System Deployment

Mobilization. Deployment of the prototype mat system occurred during April 2008, with assistance from personnel from SAIC, UNH, and subcontractors American Underwater Services, Inc. (AUS) and Specialty Devices, Inc. (SDI). Equipment used for deployment included a dive platform, portable work platform, roll-off box, Bobcat loader, dredge pumps and a 12' dual Jon-boat vessel. The dive platform and work platform were delivered on trailers and lowered into the water from the shoreline staging area with a Sky-Trac telescoping forklift capable of extending 30 ft. The roll-off box was delivered and positioned using a dedicated flatbed truck and the dredge pumps were delivered on "gooseneck" trailers towed by heavy-duty pickup trucks. The Sky-Trac forklift and a smaller Bobcat loader were delivered to the site by a local rental company. The dual Jon-boat vessel was delivered on a dedicated trailer and assembled and launched by hand from the staging area shoreline.

Target Area Layout. Prior to mat deployment, personnel used the dual Jon-boat vessel and Hypack software interfaced with a laptop computer and DGPS antenna to mark off the precise target mat deployment area as well as a separate control area for baseline monitoring. The perimeter of the circular target area was marked with temporary open-cell orange foam floats attached to bricks by approximately 12 ft of line. The corners of the control area were marked to the east of the target area using higher grade permanent closed-cell orange foam floats also attached to bricks by approximately 12 ft of line. The temporary floats were intended to be removed when the different mat treatments had been deployed and the permanent floats were intended to remain throughout the course of the long-term monitoring process.

Mat Deployment. The entire prototype mat system was made up of four test areas and an undisturbed control area as discussed above and depicted in Figure 4.4-2. Approximately 25 ft of undisturbed sediment (*i.e.*, the length of one mat) was left between each test area to minimize interference and potential edge effects. The single layer mats were both placed with the non-woven geotextile side facing up (in contact with the water column). The double layer area, however, featured the non-woven geotextile side facing down (in contact with the sediment) on the bottom layer and the non-woven geotextile side facing up (in contact with the water column) on the top layer.

During mat deployment, AUS personnel towed the dive platform into the target area and anchored it in place with several Danforth-style anchors. High winds (20-40 kt) throughout the duration of the project necessitated the use of multiple anchors and spud poles to keep all vessels and barges in place while working. Reactive mat panels were transported to the target area on the portable work platform, which was then tied up alongside the dive platform. Two AUS divers attached to a surface supply airline system entered the water to place the mats while two AUS dive monitors remained on the dive barge to observe the compressor and communicate to the divers via the relay system in their helmets. Project personnel provided support and instruction from the dual Jon-boat vessel anchored nearby in the target area.

While the large mats were rolled up on the portable work platform, small lengths of polypropylene line were attached to the four corners of the individual 25 ft x 15 ft reactive mat panels to attach to the mats to the anchoring mechanism. One diver then screwed 36-inch screw

anchors into the sediment within the target area and the first mat panel was dropped in the water and floated into place. Based on previous work with small-scale test mats, the original anticipation was that the individual mat rolls would sink and they could be unrolled by divers while on the lake floor. However, air trapped in the roll prevented the mats from sinking until they were fully unfurled on the surface. Thus the polypropylene lines on one end of the mat were lashed by one diver to the screw anchors already in place while the other diver pushed the fabric on the surface, receiving assistance from personnel on the dual Jon-boat. The mats were unrolled, allowed to sink, and the divers smoothed the mats and secured the corners to the screw anchors.

Once the first 25 ft x 15 ft mat panel was secured in each test area, the process was repeated for the second 25 ft x 15 ft mat panel with polypropylene lines being positioned approximately four feet from the edge to account for the planned overlap and then lashed to the same screw anchors already under the water. Polypropylene lines attached to the far corners and the overlapping corners of the second panel were then fed through four additional screw anchors in order to pull the overlapping panel tight. For the test area featuring the double layer mat, the four individual panels were placed with an alternating overlap (*i.e.*, like a deck of cards). The upper layer was secured to the same screw anchors as the lower layer to limit both the dive time and the amount of anchors left at the site. When pulled tight to the screw anchors, the mat panels were brought into alignment with 100% overlap and no gaps in mat coverage present along the middle seam of the mat area.

The two single layer mat areas (T1, T2) and the double layer mat area (T3) were marked with a closed-cell orange foam float attached by a diver to the northwest screw anchor. In addition, the divers placed a screw anchor with a fourth float in the center of the sand only test area. These floats were color-coded to differentiate the test areas in the field log and were intended to remain in the water for the duration of long-term monitoring. All PVC pipes and other packing material used to transport the mat rolls were removed from the project site and discarded.

Sand Placement. Following the placement of the mats, AUS personnel assembled a sand slurry system to move capping material from the staging area on the NAS shoreline to two of the test areas in Cottonwood Bay. This slurry system consisted of a steel roll-off box serving as a hopper for the sand/water mix, one 6-inch hydraulic pump to move water from the lake into the roll-off box, a second 6-inch hydraulic pump to move slurry discharge from the roll-off box to the target area and a smaller submersible pump placed in the lake to provide a second water intake with a more concentrated stream for stirring the slurry. The hydraulic pumps used were both Holland Model H6TMS-D8 with a Perkins 1104.44 standard diesel engine power unit capable of moving up to 730 gal/min with a 50-ft head. The pumps used vegetable oil rather than typical hydraulic fluid to turn the impellers in order to minimize environmental impact and cleanup requirements should there be a breach in the line. The submersible pump used to stir the slurry was a 4-inch Honda gas-powered trash pump with a 16 hp engine capable of moving up to 705 gal/min. The approximately 600 ft discharge line consisted of 20-ft lengths of 6-inch diameter rigid pipe connected with buckle clamps and floated at the surface using 30 air-filled plastic barrels. The discharge impeller weighed several hundred pounds and was moved around the roll-off box using the Sky-Trac forklift to capture all available slurry material.

Fourteen cubic yards of "Cushion #1" screened fine sand was purchased from a local dealer to provide approximately three inches of cover on two 25 ft x 25 ft test areas (single layer mat, sand cover only). This material was delivered to the project site in a dump truck and unloaded on top of plastic sheeting to minimize impact on the local environment. During active slurry operations, the sand was transferred from the pile into the roll-off box using the Bobcat loader. The mixture was then stirred with the concentrated stream intake hose to ensure an adequate amount of material was discharged through the hose. The initial sand placement attempt was unsuccessful due to a prevalence of fine-grained material that was dispersed rather than deposited in the target area due to wind wave action. The decision was made to cease slurry operations with the "Cushion #1" sand and purchase a coarser grained material that would have a faster settling rate and be easier to control under the water.

To correct this problem, an additional ten cubic yards of coarser grained masonry sand was obtained from a second local dealer. This material would be left in the roll-off box and mixed with the remainder of the "Cushion #1" sand to achieve the planned three inches of cover on the two test areas. Rather than have a diver attempt to maneuver the discharge hose under the water, the decision was also made to shorten the pipeline by 20 ft, add a 45° angle spigot on the end facing down and hold the end in place using lines tied to the dive platform and the dual Jon-boats anchored nearby. By pulling on the lines, personnel on the dive platform and the Jon-boats could sweep the discharge pipe back and forth to ensure coverage of the entire test area.

The second sand placement attempt involved water being pumped into the roll-off box at 600 psi hydraulic pressure and slurry being discharged at 900 psi hydraulic pressure (corresponding to flow rates of approximately 400 gal/min and 600 gal/min, respectively, at 20-ft head according to Holland manufacturer specifications) over the T2 test area to feature a single layer mat with sand cap. These values were determined by trial and error to be the optimal pump settings for moving masonry sand slurry through 600 ft of pipeline without particles settling out in the hose or water overflowing the roll-off box while still being able to predict and control the discharge plume. Once discharged, the masonry sand settled much more quickly than the "Cushion #1" sand and produced only a small plume at the surface. Divers monitored the pumping effort periodically to ensure sand was being contained over the test area, but extremely poor visibility precluded the use of underwater video to document the sand placement and final site conditions. After 78 minutes of continuous pumping, diver measurements confirmed the presence of a uniform layer of sand approximately 2-3 inches thick over approximately 80% of the single layer mat. The remaining areas of the mat, encompassing the southernmost six feet (approximately 15% of the total) and the extreme southeastern corner (6 ft x 6 ft; approximately 5% of the total), were covered by ½ inch sand and a thin layer of rubble, respectively. There was also an approximately two foot overcast area covered by 2-3 inches of sand beyond the northern edge of the mat and a one foot undercast area covered by ¼ inch of the finest sand particles. This deviation from the planned three inch overall coverage with no overcast resulted both from an inability to gauge how far sand would settle from the end of the pipeline at the chosen discharge rate. The general bottom topography on which the mat was resting also contributed to variable sand thickness as some particles tended to accumulate in natural sinks.

With the single layer mat area (T2) covered, the discharge spigot was positioned over the T4 area (marked by a screw anchor and single float in the center) to receive sand cover only (no mat).

Again, water was pumped into the roll-off box at 600 psi (400 gal/min) and slurry was discharged at 900 psi (600 gal/min) and divers monitored the effort periodically. After 88 minutes of continuous pumping, divers confirmed that a 3-4 inch layer of sand extended approximately 10 ft to the east and west of the screw anchor and approximately 20 ft to the north and south. This layer tapered off to approximately once inch at the northernmost boundary of the test area. Samples of capping material were obtained from both test areas by the divers after placement as well as from the sand pile on shore for grain size analysis.

Demobilization. Following completion of the sand placement process, GPS locations of the permanent floats used to mark the four test areas were recorded, and all temporary floats were removed. Following project completion, the only visible materials left at the project site were four color-coded floats attached to screw anchors marking the four test areas and four additional floats attached to brick anchors marking the corners of the control area.

4.4.3 Geophysical Investigation

Geophysical Investigation. In December 2008, following approximately eight months of soak time, a small-scale geophysical investigation including bathymetry, sub-bottom, side-scan sonar and SPI surveys was conducted over the prototype mat system test area to record properties such as surface roughness and benthic colonization that could not otherwise be observed from above the water. The bathymetry and sub-bottom surveys were conducted with a single-beam echo-sounder interfaced with a BSS+3 survey computer featuring HYPACK v.4.3 software. The side-scan survey was conducted with an IMAGINEX dual frequency digital side-scan sonar transducer ("fish") also interfaced with a BSS+3 survey computer featuring HYPACK v.4.3 software. Both transducers were deployed from a small dual Jon-boat survey craft and several passes were made over the prototype mat system to ensure complete coverage of the study area. The highest resolution side-scan results were achieved with a start gain of 30 dB and a pulse link of 150 µs. Raw bathymetry, sub-bottom and side-scan data were processed to identify the post-impoundment and pre-impoundment surfaces and provide a pictorial view of the prototype mat system area. The final side-scan mosaic produced a clear image of the prototype mat layout and the distribution of sand capping material, which previously had been confirmed only by diver observations.

Sediment profile imaging technology utilizes an underwater still camera-mirror system to take cross-sectional pictures of the sediment-water interface and the upper six inches of sediment (or 3" in cases of sand over mats) in order to assess biological conditions at the sediment water interface. Several replicate SPI photographs were taken over the five test areas (including control) to analyze benthic habitat conditions that had developed after approximately six months of soak time. Cursory analyses of these images were performed to provide an evaluation of sediment buildup on the mats, confirmation of sand capping thickness in appropriate areas and a description of control area conditions.

4.4.4 Passive Contaminant Sampling

Monitoring Device Deployment – Year 1. In October 2008, after approximately six months of soak time, divers installed three types of in-situ passive diffusion samplers at the prototype mat

system to measure the sequestration of contaminants by each test treatment. The passive contaminant sampling devices included dialysis samplers ("peepers"), semi-permeable membrane devices (SPMDs) and solid phase micro-extraction (SPME) fibers. Peepers are expression samplers constructed of polyethylene plastic casing fitted with a nucleopore membrane used to evaluate metals in pore water. In contrast, SPMDs are permeable tube-like bags containing a high molecular weight lipid (triolein) attached to an aluminum deployment device that are used to simulate accumulation of organic contaminants in fish organs. The SPME fibers are coated with a liquid polymer that allows organic contaminants to establish equilibria between the fiber and the sample matrix. Because the utility of SPME devices in aquatic environments is still in the research and developmental phase, the data from these samplers were intended to provide a side-by-side comparison with similar data obtained from the SPMDs through more established techniques.

To install the peepers, SPMDs and SPMEs, divers peeled back a section of mat and placed the devices at least three feet from the edge in predetermined sampling locations. All samplers were attached to aluminum deployment rods that were custom fabricated to meet the specific needs of this project. These rods were then tethered to the screw-anchors that were already holding the mats in place. Precise sampler locations (*i.e.*, which specific corners of the treatment) were carefully selected to maximize interaction with the desired interface (*i.e.*, presence of sand cap) and avoid any anomalous features such as the sand cap overcast and undercast areas adjacent to the single layer mat area covered with sand, T2 (see Section 4.4.2).

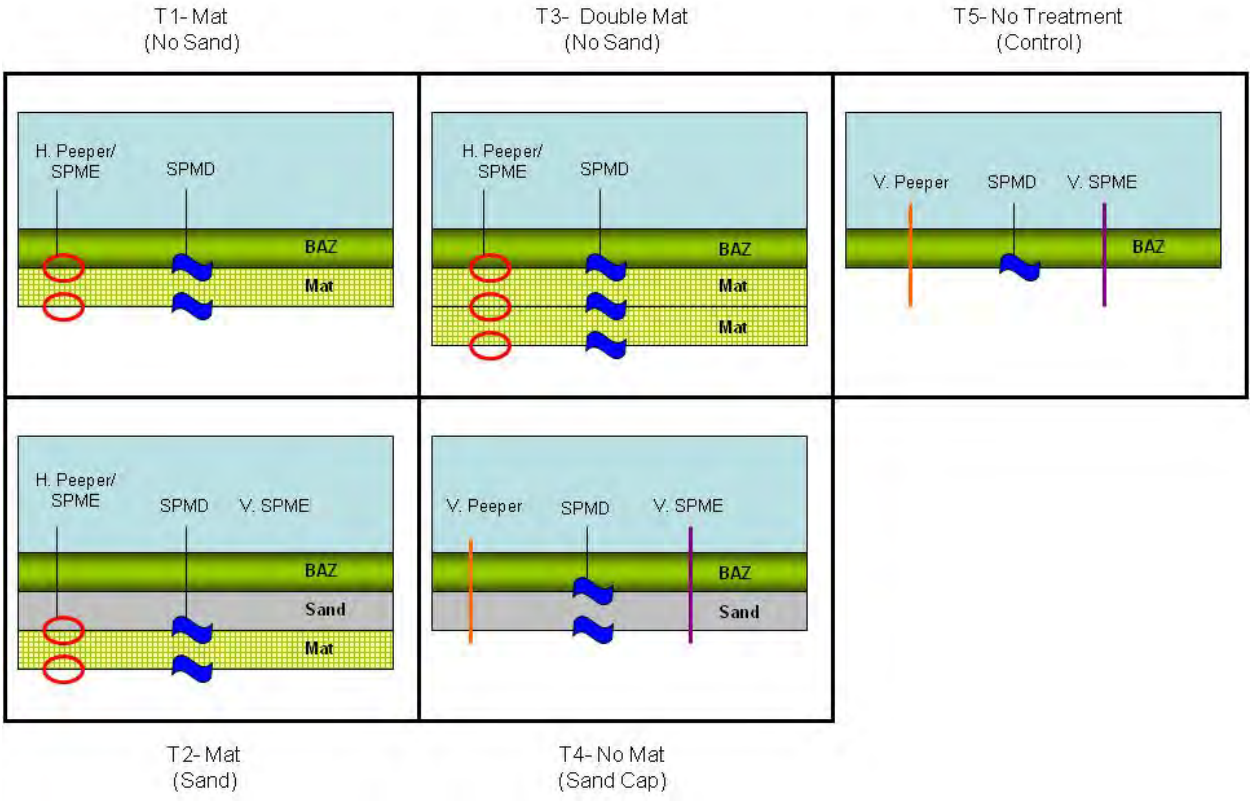

Figure 4.4-3. Vertical passive sampler layout in Cottonwood Bay.

A total of 21 horizontal peeper/SPME combination devices, 30 SPMDs, four vertical peepers and four vertical SPMEs were deployed at unique mat-water, sediment-mat, mat-sand, mat-mat, sand-water, sediment-sand and sediment-water interfaces across the five test areas (including control). The T4 area (sand cap only) and the T5 area (no treatment) received vertical peepers and SPMEs to evaluate conditions over multiple horizons in the absence of a mat. A graphical representation of the final vertical passive sampler layout as deployed in Cottonwood Bay is presented in Figure 4.4-3.

Monitoring Device Deployment – Year 2. In October 2009, after approximately 18 months of soak time, divers again installed three types of in-situ passive diffusion samplers at the prototype mat system to provide a comparative second year contaminant sequestration dataset. The same general sampling design, methods and sampler configuration were followed as in the previous investigation. One exception was that SPMEs were excluded from the second year sampling (based on ubiquitous non-detect results from the first round of sampling); these were replaced with horizontal and vertical polyethylene devices (PEDs) as an alternate experimental form of sampling for organics. The PEDs consist of a strip of low density polyethylene that measures the activity of hydrophobic organic compounds (*e.g.*, PAHs, PCBs, DDT) in the environment based on the partitioning of these compounds between polyethylene and water. The PED is deployed in the same manner as the SPMD such that freely dissolved hydrophobic organic compounds can passively adsorb onto the membrane. As with the SPMEs and SPMDs, equilibrium is reached on the order of days to weeks.

In a new approach, vertical peeper arrays were installed through small slits made into the mats in areas T1 and T2 to provide data over multiple horizons in these treatment areas that were not obtainable during the first round of sampling. A separate peeper and PED were also suspended in the water column using an independent anchor-float system to provide background information on contaminants present in the Cottonwood Bay.

The custom deployment rods holding the peepers, SPMDs and PEDs were modified following the first round of sampling to include a second cross-member designed to keep the SPMD taught on the sediment surface and eliminate some of the folding and tearing that was previously experienced. A total of 21 horizontal peepers, 30 SPMD/horizontal PED combinations, 8 vertical peepers (2 through mats) and 6 vertical PEDs were installed throughout the overall mat system in Year Two.

While installing the samplers, divers also inspected the mats for the presence of sand in the capping areas as well as any slumping affects due to wave and current action or potential air pockets caused by gas buildup below the mats. An air pocket measuring approximately 1-1.5 ft high and 3 ft in diameter was observed below the mat in area T1 (mat only); divers were able to remove the air by applying pressure to the mat until it escaped out the edge. In contrast, only minor air pockets were observed for T2 (mat with sand cap) and T3 (double mat) and if present, were also removed by the divers. Multiple ridges were also observed in area T3 likely caused by the weight of the double mat distorting the underlying soft sediment. The presence of 2-3 inches of coarse sand was observed in both capping areas (T2 and T3), which was consistent with the findings of the sediment cores (see Section 4.4.6).

Monitoring Device Retrieval – Year 1. In December 2008, divers retrieved the peepers, SPMDs and SPMEs from Cottonwood Bay after exactly 50 days of soak/sampling time by extracting the aluminum bars via the polypropylene lines and carefully bringing each array of samplers to the surface. Working from the dive platform/small survey vessel, project personnel extracted porewater from the individual peeper chambers using small syringes and placed the test material in vials for shipment to the analytical laboratory. All vertical peepers were recovered by the divers and processed on the dive platform/small survey vessel in the same manner as the horizontal peepers, with a separate sterile syringe used for extracting porewater from each discrete vertical chamber. The SPME deployment devices were encased in aluminum foil for processing and extraction at a later time.

Recovered SPMDs were carefully sealed in pre-labeled tin cans for shipment to the processing laboratory and the conditions of each sample were recorded on designated SPMD logs. One SPMD was not recovered (*i.e.*, lost) and several other SPMDs contained visible tears and creases upon first inspection. The extent of this damage and the potential effects on sample data quality were later quantified during the extraction process (see below).

During the sampler recovery effort, water quality measurements were also collected from the surface water at the mat system area using a handheld YSI 556 Multi-Probe water analyzer. . The probe was then lowered into Cottonwood Bay approximately one foot below the surface at the mat system area. Readings for temperature, conductivity, dissolved oxygen concentration, pH and oxidation-reduction potential stabilized, were recorded in the field logbook. The process was repeated with the probe lowered into Cottonwood Bay approximately one foot above the mats. Water temperature values were to be used to complete SPMD concentration calculations.

Monitoring Device Retrieval – Year 2. In December 2009, divers returned to retrieve the peepers, SPMDs and PEDs from Cottonwood Bay after 47 days of soak/sampling time following the same procedures used during the Year One recovery (discussed in the previous section). As for the vertical peepers, the vertical PEDs embedded in the sediment were recovered by the divers and processed in the same manner as the horizontal PEDs. Finally, the peeper and PED membranes suspended in the water column to analyze ambient surface water conditions were recovered directly from the survey vessel and processed in the same manner as the horizontal samplers.

All 30 test SPMDs were recovered (*i.e.*, none were lost) and all were found to be taught on the aluminum bars and appeared in good condition upon first inspection. The additional cross-member added to the deployment bars for the second year sampling appeared to have eliminated the tearing and folding that was experienced in Year One (discussed in previous section). While onsite, water temperature measurements were made using a submersible thermometer. At the time of sampler recovery in December, the water temperature in Cottonwood Bay was 7°C (45°F), as compared to 19°C (66°F) at the time of sampler deployment in October.

Finally, divers again inspected the mats for the presence of air pockets below the surface. In contrast to the observations made during passive sampler deployment, when multiple small air pockets (< 3 ft diameter) were observed in areas T1, T2 and T3, no air pockets were found under

any of the mats at this time. These findings were consistent with previous observations of the small-scale test mats that indicated potential gas buildup beneath the mats in the summer, minimal to no buildup in the fall, and no buildup in the winter.

Peeper Extraction and Analysis. Horizontal peepers were deployed in replicates of three at specific target interfaces (sediment-mat, mat-water, mat-sand, mat-mat) in areas T1 (mat only), T2 (mat with sand cap) and T3 (double mat). In contrast, vertical peepers were deployed in replicates of four (Year One) or three (Year Two) spanning specific target interfaces (sediment-sand, sand-water, sediment-water) in areas T4 (sand cap only) and T5 (no treatment/control). In Year Two, a peeper was also suspended in the water column in the middle of the treatments to provide background data on the ambient water column.

Each replicate peeper featured several membrane-bound chambers at each depth containing distilled water into which site porewater contaminants were allowed to equilibrate at that specific horizon. During the sampler recovery process, the peepers were removed from the water and a sterile syringe was used to puncture the membrane for each chamber and extract the contaminant enriched water. The extracted water was then placed directly into a chamber-specific vial for transport and analysis as a typical water sample. All vials containing water extracted from the peepers were sent with wet ice (4°C) to UNH and analyzed for metals by inductively coupled plasma-mass spectrometry (ICP-MS).

SPMD Extraction and Analysis. Semi-permeable membrane devices (SPMDs) consist of a dialysis bag filled with oil (triolein) which essentially mimics the tissue/lipid matrix of aquatic organisms. By measurement of the organic contaminants that accumulate in the oil, the environmental concentration and bioavailability of the contaminant can be determined. Additionally, because the oil will accumulate contaminants at very low concentrations, the method is much more sensitive than traditional surface water or direct porewater analyses.

Extraction of the triolein test material from the recovered SPMD tubes was performed at the processing laboratory (EST Labs, St. Joseph, Missouri). The SPMD extraction process generally involves (1) removal of exterior surficial periphyton and debris; (2) organic solvent dialysis; (3) size-exclusion chromatography (SEC); and (4) chemical class specific fractionation using Florisil, silica gel and/or alumina sorption chromatography (Petty et al. 2000). Cleaned SPMDs were dialyzed in hexane (125 mL of hexane per standard SPMD) for 18 hours at 18°C, followed by a second dialytic period (with 125 mL of fresh hexane) of 6 hours also at 18°C. The two dialysates were then combined and reduced in volume to about 1 ml for SEC cleanup (or an equivalent process) and GC/MS analysis (Petty et al. 2000).

During the extraction process, laboratory personnel observed the conditions of each SPMD tube in terms of the number of holes/tears, site water infiltration, apparent triolein loss and apparent distension. Both triolein loss and site water infiltration would increase uncertainty in SPMD analytical results as true representations of site porewater concentrations by diluting or altering the composition of the internal solvent prior to analysis. All SPMDs holes were sealed prior to extraction to limit the effects of any holes present. During the first round of SPMD sampling, 12 of 30 samplers exhibited at least one hole, with 7 of these samplers also experiencing measurable oil loss or water infiltration. During the second round of SPMD sampling, only 2 of

30 samplers exhibited holes and neither of these samplers experienced measurable oil loss or water infiltration. The data usability for these compromised SPMDs is discussed in the study results (Section 5.4.2).

Following the extraction process, the ampoules containing the resulting hexane dialysates were sent to the analytical laboratory (EnviroSystems, Inc., Hampton, New Hampshire) and analyzed for PAHs by EPA method PAH680. The subsequent analytical results were then entered into an "Estimated Water Concentration Calculator" provided by the SPMD processing laboratory, which converts the concentration of a measured PAH analyte in the SPMD extract (in units of ng/mL hexane) to an estimated porewater concentration at the deployment site (in units of pg/L). The calculation is based on mathematical models developed by the USGS Columbia Environmental Research Center (Version 4.1) as a function of days deployed (~50 days), water temperature (~10°C), mass of SPMD (4.5 g), volume of lipid (0.001 L), volume of membrane (0.0037 L) and volume of SPMD (0.0047 L).

SPME Extraction and Analysis. The SPME process for monitoring PAHs in Cottonwood Bay porewater was consistent with previously established protocol presented in Reible 2008. This sampling technique employed between 10 and 20 cm of 300/200 µm polydimethylsiloxan (PMDS) fiber (Fiberguide) per replicate sample. Fibers were deployed at 10 cm lengths in a protective stainless steel sheath which was slotted on three sides to allow adequate porewater/SPME interaction. Upon recovery, all SPME fibers were kept in their sheaths, immediately cooled below 0°C using dry ice and shipped overnight to the UNH analytical laboratory.

Within 48 hours of field recovery, the SPME fibers were removed from their protective casing, rinsed free of sediment with deionized water and cut to 1 cm increments which were placed in 300 µL of methylene chloride and allowed to desorb PAH analytes into the solvent for seven days. Following desorption, the contaminant-enriched solvent was stored below 0°C until analysis via GC/MS using a Varian 3800GC in line with a Saturn 2200 MS.

During chemical analysis, an external calibration for the 12 PAH compounds of interest for Cottonwood Bay indicated that all concentrations in the SPME solvents were below the reporting limit of the analytical instrument. Using the equation presented below, all porewater concentrations for the various interfaces in the prototype mat system were thus determined to be < 5 ng/mL.

$$C_{PW} = \frac{(C_{Solvent})*(V_{Solvent})}{(V_{SPME})}*K_f$$

Where:
C_{PW} = Porewater Concentration
$C_{Solvent}$ = Solvent Concentration (determined by GC/MS)
$V_{Solvent}$ = Volume of Solvent analyzed in GC/MS method
V_{SPME} = Volume of PDMS on SPME fiber analyzed
K_f = Partition Coefficient between Porewater and SPME fiber

4.4.5 Chemical Flux Survey

After one year of soak time, groundwater seepage measurements through the prototype mat system were made using Ultraseep groundwater seepage meters in order to quantify water flux through the mats from underlying sediments as well as to identify any changes in contaminant concentration with respect to the source (*e.g.*, groundwater flux out of the mat versus overlying water penetration into the mat). The Ultraseep is a modular, state-of-the-art seepage meter designed for direct measurement of groundwater plumes at the sediment-water interface. This unit was invented out of the need to accurately quantify contaminant flux into surface waters in a time-transient manner, as previous methods were not able to locate and quantify these measurements in a reliable way (Chadwick et al. 2003). Not only does the Ultraseep record flow parameters, but it also collects passive samples of groundwater passing through the selected interface to be used for chemical analysis.

Mobilization. Personnel from subcontractor Coastal Monitoring Associates (CMA) arrived at the mat test site on the weekend of 12-14 June to mobilize a portable on demand storage (PODS) unit containing all survey equipment and assemble an approximately 20 ft pontoon barge powered by a small electric trolling motor. Personnel from Specialty Devices, Inc. (SDI) then arrived on the morning of 15 June to launch the pontoon barge and assemble and launch a second 12' dual Jon-boat vessel powered by a small gasoline engine as well as a third single Jon-boat powered by another small electric trolling motor. The survey effort required three Ultraseep units and one Trident Probe unit modified for use in the reactive mat setting.

Ultraseep Groundwater Flow Modeling. Ultraseep meters were deployed at the different treatments within the prototype mat system (T1-single mat only, T2-single mat with sand cap, T3-double mat, T4- sand cap only, T5-no treatment/control) from 15-19 June 2009. During the deployment process, the units were lowered from the pontoon barge using a davit and hand-powered winch. Scuba divers provided underwater support for guiding the Ultraseep to the bottom and ensuring it was resting in place with a tight seal at the desired interface (*e.g.*, mat-water, sand-water, etc.). The Ultraseep meters were allowed to soak for approximately 24 hours to record groundwater flux data as well as collect a passive groundwater plume sample. Following this soak time, the Ultraseep meters were recovered from each treatment area with the aid of scuba divers and brought aboard the pontoon barge using the hand-powered winch. While being raised from the surface but still in the water, divers cleaned the units to remove any sediment or detritus. The units were then brought to shore and fully decontaminated following standard operating procedures. The internal bag containing the groundwater plume sample was removed from the unit and weighed. A small portion of the sample was then extracted and used to test water quality parameters (*e.g.*, temperature, conductivity, pH) using a handheld water quality meter. The remainder of the sample was then transferred to a pre-labeled jar containing 70% HCl as a preservative to be shipped to the UNH analytical laboratory for chemical analysis.

Over the course of the week, Ultraseep meters were deployed twice at each mat-system area (T1, T2, T3, T4) and once at the control area (T5). Sequencing, soak times and sample volume for each Ultraseep replicate are provided in Table 4.4-1. During each sampling event, a single Ultraseep unit was deployed at the treatment area and recovered the following day, with all three units typically being recovered, decontaminated and re-deployed during a full working day.

During the initial deployment attempt at the control area (T5), the native sediment proved too soft to support the Ultraseep unit without it sinking too far into the mud or tipping over. Thus the unit had to be retro-fitted with a thin plywood skirt to provide additional surface area for deployment on the following day. Electronic groundwater flow data were recorded successfully during all nine deployments. However, the second Ultraseep deployment at area T1 failed to produce a groundwater plume sample, which may have resulted from the mat folding over onto the unit, the unit being placed in an area where an air bubble had developed under the mat and prevented contact with the sediment below or the unit being placed in an area where groundwater flow was not percolating upwards into the overlying sediment.

Table 4.4-2. Ultraseep sampling summary for the Cottonwood Bay prototype mat system.

Treatment Area	Deployment (Date; Time)	Recovery (Date; Time)	Soak Time (~hours)	Sample Volume (mL)	Discharge Water in Sample (mL)	Discharge Fraction (%)	Surface Water Fraction (%)	Sample Type
T1 - Deployment 1	06/15/09; 1445	06/16/09; 1425	24	671	113.06	17	83	Composite
T1 - Deployment 2	06/18/09; 1030	06/19/09; 0859	22	2	-	-	-	No Sample
T2 - Deployment 1	06/15/09; 1400	06/16/09; 1412	24	215	13.39	6	94	Composite
T2 - Deployment 2	06/17/09; 1052	06/18/09; 0855	22	10	-	-	-	No Sample
T3 - Deployment 1	06/16/09; 1349	06/17/09; 1124	22	72	-	-	-	No Data Provided
T3 - Deployment 2	06/17/09; 1435	06/18/09; 1125	21	103	18.04	18	82	Composite
T4 - Deployment 1	06/17/09; 0938	06/18/09; 0840	23	868	172.65	20	80	Composite
T4 - Deployment 2	06/18/09; 0950	06/19/09; 0920	24	722	111.85	15	85	Composite
T5 - Deployment 1	06/18/09; 1418	06/19/09; 1306	23	344	34.09	10	90	Composite

Trident Probe Porewater Collection. Concurrent with the Ultraseep deployments, active surface and porewater samples were collected from various depths in each mat-system area using the Trident Probe. The Trident Probe unit is a flexible, multi-sensor water sampling probe used for screening and mapping groundwater plumes discharging from surfaces sediments into the overlying water column. The probe records real-time measurements of porewater temperature and conductivity, which can then be compared to the overlying surface water to find areas of probable groundwater flow (as evidenced by lower temperature and higher conductivity). The probe also features three screened and sand-packed arms through which porewater can be drawn into flexible hoses using a low-flow peristaltic pump. For the present study, the tips of these arms were set at 3.5 in, 11 in and 24 in, respectively, below the base plate to sample various depths within the test areas. A fourth hose (without a screen) was also set 2 inches above the base plate to sample surface water at the treatment-water interface. These sampling horizons were selected to mirror the same interfaces targeted previously by the passive contaminant samplers (*i.e.*, peepers, SPMDs) in order to analyze synoptic vertical chemical gradients.

During each Trident Probe event, the sampler was lowered from the dual Jon-boat vessel by hand and pushed upright into the underlying sediment. In test areas containing a mat, modified cutting tips were attached to each arm of the probe which were able to penetrate the geotextile layers with minimal use of force. Prior to initiating sampling, scuba divers provided visual confirmation that the probe was indeed in a desirable area (*i.e.*, penetrating the mat or sand cap where appropriate, particularly in areas where methane gas bubbles under the mats were problematic) and that the base plate of the probe was flat against the selected interface. A GPS

fix of the exact probe location was obtained and temperature and conductivity data from each arm, as well as a reference sensor in the surface water, were collected.

Active sampling was then initiated by attaching each hose from the various probe arms to a low-flow peristaltic pump and drawing water out of the target matrix (*i.e.*, surface water, sand cap, sediment). Approximately 250 mL of water were immediately purged from the sampling lines in order to eliminate potential contamination. A small sample was then extracted from each line and used to test water quality parameters (*e.g.*, temperature, conductivity, pH) using a handheld water quality meter. An additional 250 mL was then purged and a second water quality measurement was taken. Finally, the analytical sample was collected directly from the line into a pre-labeled jar containing 70% HCl as a preservative to be shipped to the analytical laboratory for chemical analysis. Following each Trident Probe sampling event, the unit was returned to shore and decontaminated following appropriate procedures (*i.e.*, Alconox scrub, nitric acid rinse, and distilled water rinse) prior to occupying a new sampling area.

Sampling from the surface line and the shallow arm (3.5 inches) took less than 10 minutes to fill the 125 mL sample jar. In contrast, sampling from the deeper arms (11" and 24", respectively) took over one hour due to fine sediment at depth and a very slow recharge rate. In the interest of time, sampling from these depths was stopped following collection of approximately 30 mL of porewater, which was the minimum volume identified by the analytical laboratory to successfully conduct the desired metals analyses. Due to extremely long sampling times, the deepest samples (24") were only collected from areas T3, T4 and T5. When attempting to sample the control area (T5), the probe base plate sunk into the very soft native sediment and the surface water sampling line became clogged in the absence of a screen. Here, scuba diver assistance was required to collect a surface water sample directly into a jar at the sediment-water interface. During each Trident Probe sampling event at the double mat area (T3) an additional water sample was taken from between the individual mat layers. In order to accomplish this task, a scuba diver placed a separate probe between the mats that was not attached to the main Trident Probe unit. This additional probe contained its own hose and was sampled in the same manner as the other lines.

Over the course of the week, Trident Probe measurements and samples were collected twice at each mat-system area (T1, T2, T3, T4) and once at the control area (T5). Sequencing and depths for each Trident Probe replicate are provided in the table below.

Chemical Analysis. In total, 8 analytical Ultraseep samples from the treatment-water interface and 32 analytical Trident Probe samples from various depths were collected from the Cottonwood Bay prototype mat system. Single equipment blank samples were also collected from the Ultraseep and Trident Probe units, respectively. These samples were shipped to the UNH analytical laboratory and analyzed for metals by inductively coupled plasma-mass spectrometry (ICP-MS).

Flow Data Processing. Specific discharge, temperature and conductivity data were downloaded from the Ultraseep instrumentation for each individual deployment and plotted as a function of time. These data allowed for determination of the volume of active flow discharge in the Ultraseep sample compared to the amount of instrument purge water also present in the sample.

The results were used to quantify the groundwater flow for each treatment as well as calculate the "discharge fraction" for each analytical sample (Table 4.4-1). This de facto dilution factor was applied to the raw chemistry results from the Ultraseep analytical samples to calculate the concentration of a specific analyte reflective only of the active flow sample (*i.e.*, the discharge; typically 0.1-1.0 L) and not the required volume of deionized water inside the instrument (~0.5L) with which the environmental sample is mixed when sampling is initiated. The following proportion was used to perform the desired calculation:

Equation: $[C_D] = ([C_S]*[V_S]) / [V_D]$

Where: C_D = Discharge water concentration (mg/L)
C_S = Analytical sample concentration (mg/L)
V_S = Analytical sample volume (mL)
V_D = Discharge volume (mL)

4.4.6 Sediment Coring

Core Collection. Concurrent with the second year passive sampler deployment effort, sediment cores were collected from the study site in order to help establish the vertical chemical gradient in the sediment from which previous porewater samples had been extracted. In areas without a mat (T4-sand cap only, T5-control), the sediment core was collected from the center of the treatment. In areas with a mat (T1-single mat only, T2-single mat with sand cap, T3-double mat), the sediment core was collected as close to the edge of the mat as possible without penetrating the mat with the corer barrel. The GPS coordinates of all coring locations were recorded in the field logbook using a handheld Garmin GPSMAP76 navigator with wide area augmentation system (WAAS) enabled.

Sediment coring was conducted using a WILDCO® hand corer consisting of an approximately 4-ft by 2.5-in internal diameter stainless steel tube with an 8-ft extension T-handle. Prior to sampling, a chemically clean 4-ft by 2-in internal diameter transparent butyrate core liner was inserted into the corer barrel and capped with a 2-in internal diameter core cutter at the end. The corer was pushed into the sediment from the sampling vessel by hand using fully leveraged body weight. Upon reaching the maximum possible penetration depth, the corer was recovered by slowly pulling the barrel out of the sediment by hand. The resulting vacuum created by the polyurethane flutter valve on the head assembly retained the material in the butyrate liner. The end of the corer was then covered with a sterile gloved hand, the core cutter removed from the barrel, the liner extracted and the core inspected for integrity. Each successful core, as determined by the presence of a continuous solid sample greater than eight inches in length with no washout (*i.e.*, intact sedimentary material and overlying water without loss due to drainage), was then immediately capped and sealed with electrical tape and stored upright in an ice chest to allow suspended particles to settle prior to processing. Prior to use at each station the core cutter was decontaminated by scrubbing with a solution of distilled water and phosphate-free detergent (Alconox) followed by distilled water and site water rinses.

Core Processing and Subsampling. Following settlement as described above, cores were visually observed with preliminary notes on various sediment layers recorded in the field

logbook. A designated core processing area was established on shore consisting of a small table with clean cover. During processing, the core liner was pierced with a razor knife above the sample to allow drainage of the overlying water. Excess core liner above the drainage point was cut off using a hacksaw and discarded, with special care given to prevent liner shavings from contacting the sample. The core liner was split length-wise into two halves to expose the sediment for observation and sub-sampling. The exposed core was measured and photographed and the physical properties (*e.g.*, color, grain size, and odor) of the core were characterized and recorded in the field logbook.

During sediment core sub-sampling, a stainless steel spoon was used to transfer the top four inches of the core directly into the pre-labeled jar for the surface (0-4") sample and the next four inches directly into the pre-labeled jar for the sub-surface (4-8") sample. The stainless steel spoon was decontaminated between each sub-sample by scrubbing with a solution of distilled water and phosphate-free detergent (Alconox) followed by a distilled water rinse.

All sediment sample jars were immediately sealed with rubber tape, wrapped in bubble-wrap and stored inside a cooler with wet ice at 4°C until overnight shipment to the analytical laboratory. Overall, 12 sediment sample jars from the 6 stations (2 depths per station) were shipped to the analytical laboratory (EnviroSystems, Hampton, New Hampshire) for chemical analysis.

Chemical Analysis. In total, 12 analytical sediment core sub-samples were collected from the Cottonwood Bay prototype mat system. These samples were analyzed for metals following USEPA Method SW6020B, PAHs following USEPA Method SW8270/SIM and TOC following USEPA Method SW9060.

5.0 RESULTS AND DISCUSSION

This section provides results of the tasks described in Section 4 and discussion of how the objectives for SERDP Project Number ER-1493 were met. Figures and tables are provided that highlight the results obtained for each task and support the final conclusions of the overall project. All final project data including raw data tables and intermediate results are provided in the designated appendices or referenced to the appropriate source document.

5.1 Task 1: Composite Material Testing

The purpose of Task 1 was to identify the mixture of amendment materials that would most effectively sequester contaminants as part of a reactive mat when also considering potential interference and complexation caused by interactions with natural organic acids. The reactive mats being developed in this project would be deployed directly over sediment beds, and would therefore be expected to be affected by high concentrations of natural organic matter. Thus the potential presence of organic acids (*e.g.*, humic acid, fulvic acid) originating from natural microbial activity and organic decay was considered a major factor in the design of the reactive mat system and the performance of sorbents to be used in the final amendment mixture.

To identify a suitable amendment, project personnel conducted laboratory tests to characterize different types of activated carbon and organoclay in terms of adsorption and desorption of PCBs

and PAHs in the presence and absence of humic acid. Additional experiments were also conducted to assess the combined effects of humic acid, fulvic acid and NOM on the adsorption properties of these materials. Following the evaluation of different sorbents individually, the preferred amendment mixture was prepared from stock materials and then similarly tested. The results were compared to the performance of a weathered mixture recovered from the small-scale test mats deployed at the Cottonwood Bay pilot site for six months.

Complete results of these experiments, including figures, graphs and tables, are presented in Sharma 2008. A summary of the results as they pertain to SERDP Project Number ER-1493 are presented in the following sections.

5.1.1 Amendment Adsorption Capacity

Preliminary amendment adsorption capacity results presented in the Second Year Annual Progress Report (NAVFAC 2007) showed that CETCO organoclay containing bentonite as the base clay and coconut shell activated carbon were the optimal amendments for achieving maximum contaminant sequestration as compared to other types of organoclay and activated carbon. Final adsorption capacity results in the presence and absence of humic acid, including all relevant plots and tables, after years three and four of laboratory investigation for PCBs on coconut shell activated carbon, PCBs on CETCO organoclay and PAHs on both coconut shell activated carbon and CETCO organoclay are presented in the "isotherm" subsections of Chapters 2, 3 and 4, respectively, in Sharma 2008.

The overall characterization of activated carbon showed that adsorption capacity was greater for higher chlorinated PCB congeners than for lower chlorinated PCB congeners and are affected by the preloading of humic acid. There was minimal desorption of these congeners as well as co-planar PCB congeners when exposed to humic acid over prolonged periods.

The characterization of different organoclays was similar to that of activated carbon, although with the CETCO organoclay the humic acid preloading effect was more pronounced for lower chlorinated congeners. The desorption from organoclays in the presence of humic acid was more pronounced than for activated carbon, however, the effect was not uniform and varied depending on specific contaminant.

Additional testing involving exposure of activated carbon and organoclay to humic acid, fulvic acid, NOM and porewaters from other sites (Passaic River, Hudson River) showed that preloading effects were more pronounced for humic acid than other compounds and that organic acids in sediment porewater have a significant impact on the effectiveness of potential reactive mat amendments in sequestering contaminants. The data showed that the humic fraction of NOM was the primary determinant of adsorption affinity reduction. This factor should be included in the final design and performance estimate of potential reactive mats under typical site conditions.

With regards to PAHs, laboratory results showed that the adsorption capacity of bare activated carbon was found to be higher than that of bare CETCO organoclay for three select PAHs. Within each bare amendment, the adsorption capacities for the three selected PAHs were

naphthalene > phenanthrene > pyrene. Similar to the bare sorbent tests, results when preloading with humic acid were significant and showed that the adsorption capacity of preloaded activated carbon was higher than the adsorption capacity of preloaded CETCO organoclay. Similar preloading studies with humic acid on activated carbon generally indicated negligible effects compared to the bare amendment. For CETCO organoclay, however, preloading with humic acid did change the relative adsorption capacity of the individual PAHs (pyrene > phenanthrene > naphthalene). This contrast shows that if the sorbents are exposed to very high concentrations of natural organics (*e.g.*, >1 g/L), the resulting interactions can affect the performance of the reactive core mat. Additionally, long term exposure of organoclay to natural organic matter might also affect mat performance by causing increased desorption of target compounds.

5.1.2 Amendment Adsorption Kinetics

Kinetic studies were an important laboratory component of this project in order to characterize adsorption equilibrium times for the different sorbents to be used in subsequent equilibrium isotherm experiments as well to assess the potential effectiveness of a thin reactive mat where contaminant residence time may be significantly less than 24 hours. Amendment adsorption equilibrium results after the first two years of work were presented in the Second Year Annual Progress Report (NAVFAC 2007). Final adsorption kinetic results in the presence and absence of humic acid, including all relevant plots and tables, after years three and four of laboratory investigation for PCBs on coconut shell activated carbon, PCBs on CETCO organoclay and PAHs on both coconut shell activated carbon and CETCO organoclay are presented in the "kinetics" subsections of Chapters 2, 3 and 4, respectively, in Sharma 2008.

For PCBs adsorbed on coconut shell activated carbon, preloading with humic acid was found to significantly increase the time required for 2,2',5,5'-tetrachlorobiphenyl to reach equilibrium over the course of the experiment, although these effects gradually decreased over time. Preloading with humic acid also appeared to increase the time required to reach equilibrium for 2,2',4,4',5,5'-hexachlorobiphenyl, but unlike 2,2',5,5'-tetrachlorobiphenyl these effects were found to be very low (due to the very low concentration of hexachlorobiphenyl used in the experiment) and remained consistent over time. These retardation effects could be due to the pore blockage effect and greater complexation of highly chlorinated congeners to humic acid as compared to mono-chloro-congeners. Greater complexation with humic acid is expected for more highly chlorinated congeners as shown by K_{DOC} complexation constants that increase with the increase in hydrophobicity of the compound (Pirbazari *et al*. 1989).

For PCBs adsorbed on organoclay, kinetics experiments showed that the adsorption equilibrium for 2-chlorobiphenyl was reached at approximately 48 hours for the bare amendment, but the presence of humic acid was found to slow the sorption kinetics. This increase in equilibrium time may have been due to the slow diffusivity of 2-chlorobiphenyl into the interlayer spacing of organoclays in the presence of humic acid molecules that can block the path of the contaminants via hydrophobic interactions with organophilic outer layers of the sorbent.

For PAHs, kinetics experiments showed that the effects of preloading with humic acid were less significant compared to that of activated carbon. The adsorption equilibrium times for phenanthrene were found to be approximately 72 hours on both bare sorbents, remained at

72 hours for organoclay preloaded with humic acid, but increased to approximately 120 hours for activated carbon preloaded with humic acid. The adsorption equilibrium times for pyrene were also found to be approximately 72 hours on both bare sorbents, but increased to approximately 100 hours on organoclay and 200 hours on activated carbon following preloading with humic acid.

The equilibrium delaying effects for PAHs caused by preloading the sorbents with humic acid can be attributed to the pore blockage effect on activated carbon and the blocking of interlayer spacing of organoclay resulting from the high loading of humic acid. Because humic acid molecules are $\leq$ 25 Å, they are capable of making bigger aggregates of about 400-500 Å (Osterberg *et al*. 1992 in Sharma 2008). These structures can in turn block the porous structure of activated carbon (<4-250 Å given by Henning and Schafer) and the interlayer spacing (35.74 Å) between the silica layers of organoclay, thus making the internal pore structure of activated carbon and the hydrophobic zone of organoclay less available to the target contaminants. The target compounds then diffuse more slowly through a reduced pore area into the available adsorption sites depending on their diffusivity, availability of sites and partition coefficients for humic acid.

5.1.3 Combined Effects of Humic Acid, Fulvic Acid and Natural Organic Material

Natural organic matter present in sediment porewater can be fractioned into humic acids, fulvic acids, proteins and peptides having both hydrophilic and hydrophobic properties, the ratios of which may affect the solubility, transport and bioavailability of hydrophobic organic contaminants (HOCs) such as PCBs and PAHs (Wu *et al.* 2003 in Sharma 2008). The chemical characteristics of these NOM fractions, including acid/base properties, elemental composition and aromaticity, depend on their origin and are different for freshwater, marine or terrestrial environments (Niederer *et al.* 2007 in Sharma 2008). Because NOM including fulvic acid and humic acid is present in the porewater of a sediment system, these substances will compete with HOCs for amendment sorption sites.

Following the selection of the preferred sorbent types, studies were conducted to evaluate the performance of coconut shell activated carbon and CETCO organoclay in the presence of different fractions of NOM. Additionally, the effects of NOM present in the Cottonwood Bay field site on the performance of the preferred amendment mixture (35% activated carbon, 35% organoclay, 30% apatite) in terms of sequestering two select organic contaminants (2,2',5,5'-tetrachlorobiphenyl and phenanthrene) was assessed.

In these studies, different concentrations of Aldrich humic acid (AldHA), Suwannee River humic acid (SRHA), Suwannee River fulvic acid (SRFA) and Suwannee River NOM (SRNOM), as well as porewater extracted from different locations (Hudson River, Passaic River), were used to assess a range of effects that may be encountered under different site conditions with the goal of quantifying the impact of different fractions of NOM from different origins on the performance of activated carbon, organoclay and an amendment mixture in sequestering organic contaminants. Weathered amendment mixture samples obtained from the reactive mats deployed in a non-contaminated area of Cottonwood Bay for six months were also evaluated to determine the effect of longer term exposure to NOM concentrations present at the pilot site on overall

reactive mat performance. The general results of this experiment indicated that organic acids, which are quite concentrated in sediment porewater, have a significant impact on the efficacy of reactive mat components and should be an essential factor in the final design and ultimate performance evaluation of the reactive mat technology.

Complete results of these experiments through Year Two of the project, including relevant plots and tables, were previously presented in the Second Year Annual Progress Report (NAVFAC 2007). In summary, the adsorption capacity of organoclay was found to be consistently higher than that of activated carbon for 2,2',5,5'-tPCB and phenanthrene. The effects of humic acid were more pronounced than the effects of fulvic acid and NOM, the latter of which were both found to have a negligible influence on the adsorption capacity of both sorbents. The preloading effect of extracted Hudson River porewater on adsorption was found to be important and was attributed to the high humic content of the sample. In contrast, Passaic River pore water (low in humics) had little effect on adsorption (Figure 5.1-1).

Batch adsorption experiments were also conducted at five loadings of a contaminant mixture of 2,2',5,5'-tPCB and phenanthrene on a virgin sorbent mixture, the weathered sorbent mixture recovered from the small-scale reactive mats deployed in Cottonwood Bay for six months, and a virgin sorbent mixture placed in Cottonwood Bay sediment porewater. The weathered sorbent mixture that was obtained from the mats represented the realistic scenario of having sorbents deployed in a geotextile mat over a natural sediment bed for a relatively long period of time. Results showed that there was a negligible effect of natural organics present at the Cottonwood Bay site on the adsorption of 2,2',5,5'-tetrachlorobiphenyl and a slight reducing effect on the adsorption of phenanthrene that was also found to be statistically negligible. Figure 5.1-2 shows the adsorption isotherms for 2,2',5,5'-tetrachlorobiphenyl on virgin sorbent mixture and on the sorbent mixture deployed in Cottonwood Bay for six months. Dotted lines in this figure are spline fits to show data point progressions whereas solid and dashed lines show Freundlich Isotherm fits.

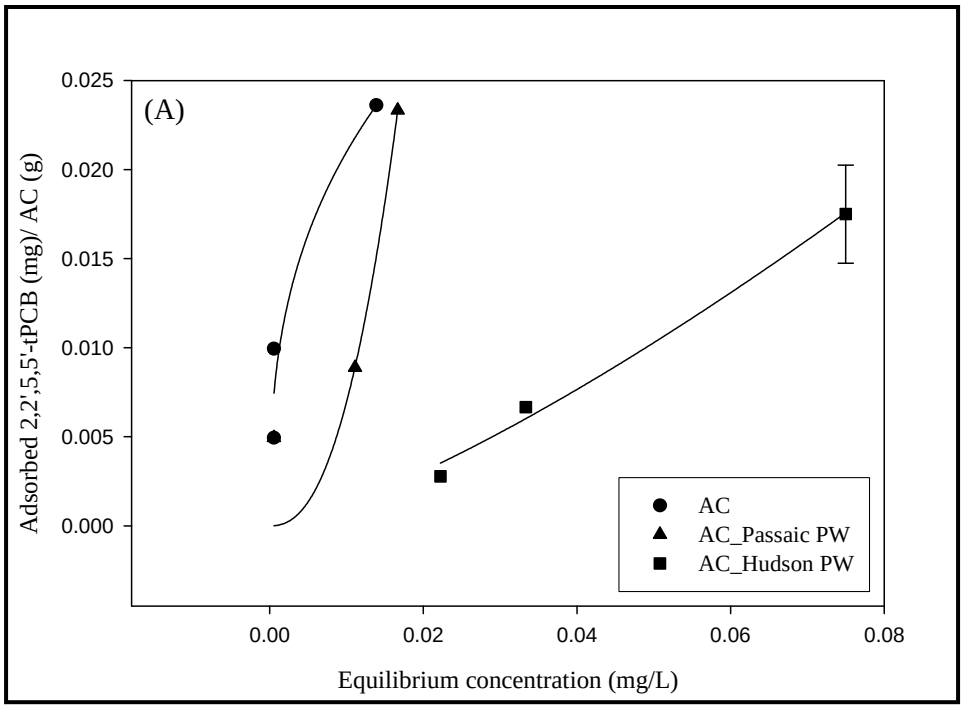

Figure 5.1-1. Adsorption of 2,2',5,5'-tetrachlorobiphenyl on bare activated carbon in the presence of Passaic River and Hudson River porewaters.

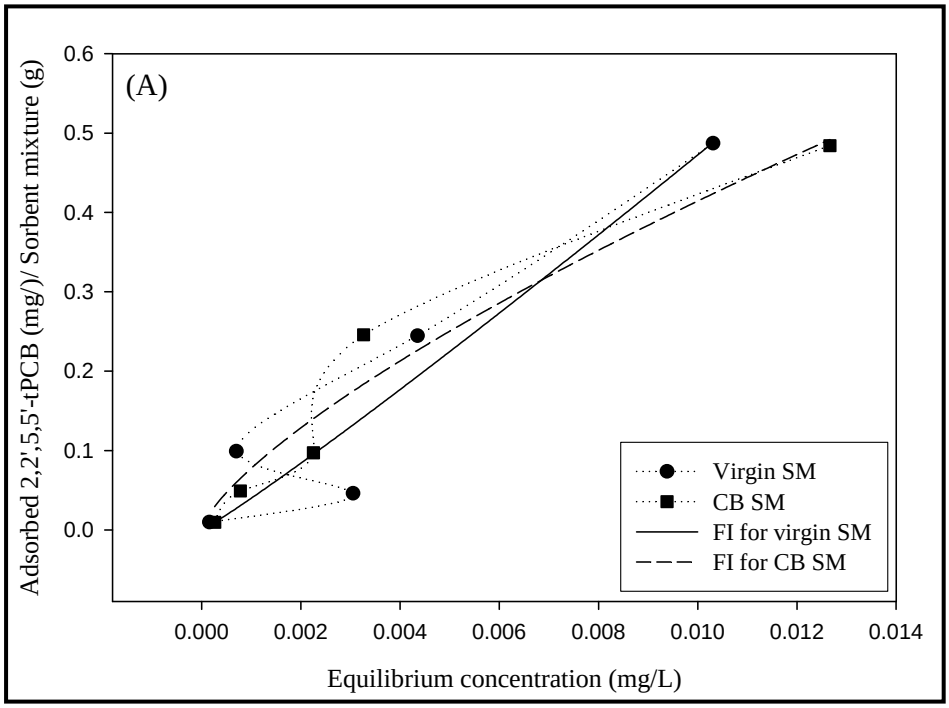

Figure 5.1-2. Adsorption of 2,2',5,5'-tetrachlorobiphenyl on virgin sorbent mixture (virgin SM) and weathered sorbent mixture after six months in Cottonwood Bay (CB SM).

5.2 Task 2: Pilot Site Selection

The purpose of selecting a pilot site for this project was to identify a suitable location for the small-scale field testing of geotextile mats as well as a specific target area for deployment of a prototype mat system. As described in Section 4.2, the pilot site selection process consisted of two phases that involved first narrowing a "long list" of potential Navy sites down to two primary sites. The decision was based on a series of chemical, physical, biological and logistical factors that would provide a suitable environment for geotextile testing and a focused comparison of two candidate sites in terms of history, surficial hydrology, hydrogeologic properties, nature and extent of contamination and past remediation efforts as documented in existing literature. This lead to selection of the primary site, Cottonwood Bay, which was then subjected to phase two of the pilot site selection process which involved conducting geophysical investigations to determine a specific area for prototype mat system deployment based on bottom topography, habitat characteristics and groundwater seepage properties.

5.2.1 Site Selection Overview

Phase One Site Selection. A detailed description of Phase I of the pilot site selection process was provided in the First Year Annual Progress Report for Project Number ER-1493 (NAVFAC 2006). Based on these criteria, Cottonwood Bay in Grand Prairie, Texas (adjacent to the NWIRP and NAS Dallas) and Pearl Harbor in Honolulu, Hawaii (adjacent to the Honolulu Naval Facilities) were identified as the most suitable locations for small-scale geotextile testing and prototype mat deployment.

Phase Two Primary Site Comparisons. The focused literature review for the selected primary sites focused on two reports each for Cottonwood Bay and Pearl Harbor. These documents were *Chemical Quality of Water, Sediment, and Fish in Mountain Creek Lake, Dallas, Texas, 1994-97* (VanMetre *et al*. 2003) provided by the U.S. Geological Survey (USGS), *Texas Natural Resource Conservation Commission Affected Property Assessment Report* (EnSafe 2001) provided by the Navy as part of the requirements of the Texas Risk Reduction Program (TRRP), *Remedial Investigation Report for Pearl Harbor Sediment* (NAVFAC 2006), and *Baseline Ecological Risk Assessment for Pearl Harbor Sediment Remedial Investigation* (NAVFAC 2006). Correspondence and phone conferences with site managers also contributed to the understanding of the conditions and management at each location as well as logistical considerations that would be important for further site assessment.

Detailed results of the focused site comparison between Cottonwood Bay and Pearl Harbor, including several tables and figures, are provided in the First Year Annual Progress Report (NAVFAC 2006). In summary, both sites were found to have sufficiently elevated concentrations of metals and organics to provide a representative test of reactive mat performance, although principal metals of concern at Cottonwood Bay were chromium and lead while principal metals of concern at Pearl Harbor were copper and zinc. At the time of the initial focused comparison, sediments had been more thoroughly and recently characterized at Pearl Harbor. Available data for Cottonwood Bay were all found to be greater than ten years old, thus introducing some uncertainty with regard to current site conditions. More current Cottonwood Bay data was obtained during Year Two to fill existing data gaps which included the document

Computer-model analysis of ground-water flow and simulated effects of contaminant remediation at Naval Weapons Industrial Reserve Plant, Dallas, Texas provided by the USGS (Barker and Braun 2000).

Regarding flow parameters, Cottonwood Bay appeared to have significant groundwater influence while Pearl Harbor is subject to tidal flow and limited groundwater movement. At both sites there is a likelihood of measurable biologically-driven deposition, although Cottonwood Bay was deemed more likely to have a higher accretion rate relative to Pearl Harbor, where turbidity and nutrient loading is expected to be lower. In terms of management planning, both sites have identified needs for remediation and groundwater control measures are currently in place at Cottonwood Bay. Pearl Harbor has been investigated following USEPA guidance for risk assessment and remedial investigations but a Feasibility Study (FS) for remediation alternatives had yet to be completed by the time of this project. Logistically, both Cottonwood Bay and Pearl Harbor were deemed accessible and found to possess the necessary infrastructure to support mobilization and field activities. Security limitations were identified for both sites, however, with water access to the eastern portion of Cottonwood Bay restricted by NAS security and entrance into Pearl Harbor near the Naval Facility berthing areas also restricted.

Final Site Selection. Cottonwood Bay was ultimately deemed more suitable for geotextile testing than Pearl Harbor and thus selected as the final pilot site for this project. Although contaminant conditions at both sites are generally similar, Cottonwood Bay was found to have more thorough mixtures of both metals and organics that would correspond well to overall adsorption goals. Cottonwood Bay was also found to have a significantly greater groundwater flow potential, which made it a more attractive location for evaluating potential groundwater flux through the reactive mats. Although an energetic environment such as the intertidal zones within Pearl Harbor was originally sought in order to provide conditions where a traditional sand cap would be insufficiently stable to provide a permanent form of remediation, the relatively constant conditions and groundwater flow parameter described by USGS for Cottonwood Bay were considered more important in evaluating mat performance than a dynamic setting. Logistical and travel considerations also contributed heavily to the selection of Cottonwood Bay since its location within the contiguous United States would make it more cost effective in terms of transporting equipment and field personnel. Finally, the location of Cottonwood Bay was within the general Mountain Creek Lake area already scheduled for remediation under the TRRP made it an attractive site for further investigation, with results of the proposed geophysical surveys not only applicable to SERDP goals but also to the overall Mountain Creek Lake remedial investigation and FS. Previously established contacts within NAVFAC and EnSafe, Inc. familiar with the Cottonwood Bay site were also able to assist with site access logistics as well as mitigating security concerns with the relevant landowner parties. In general, the criteria initially established for site selection proved effective and therefore applicable to other sites where this technology would be applied.

5.2.2 Selected Site Background Assessment

As discussed above, the majority of information regarding the background conditions at Cottonwood Bay was obtained from a USGS sampling effort (VanMetre *et al*. 2003), a TRRP analysis (EnSafe 2001) and subsequent groundwater modeling (Barker and Braun 2000). Details

about the site that were provided in these documents and compiled during both the Year One and Year Two efforts are described in the following sub-sections.

Site Description and History. Cottonwood Bay is located in northeastern Texas within Dallas County approximately four miles southeast of Grand Prairie between routes I-30 and I-20. The site is adjacent to the Vought Aircraft Industries, Inc. facility (former Naval Weapons Industrial Reserve Plant) and NAS Dallas and was created by fill placement that took place during the original construction of the NAS airstrip. Recreational fishing is popular in the connected Mountain Creek Lake, which is connected to Cottonwood Bay, but consumption of catch is banned due to documented PCB contamination. An overview of the entire Cottonwood Bay site was provided previously in Figure 4.2-1.

***Surficial Hydrology*.** Cottonwood Bay is an artificially constructed stream and groundwater-fed freshwater body that is connected to Mountain Creek Lake by a narrow channel (Figure 4.2-1). The Cottonwood Creek diversion channel feeds directly into the bay and, along with surface runoff, constitutes the main surface water input into the bay (Figure 5.2-1). The east and west lagoons on Vought property to the north of the bay were constructed to contain stormwater runoff but also receive input from groundwater. Cottonwood Bay has relatively consistent water elevations throughout the year (+/- 2 ft) and is not a very dynamic environment given both lack of wind fetch and wave action (i.e., boat wash).

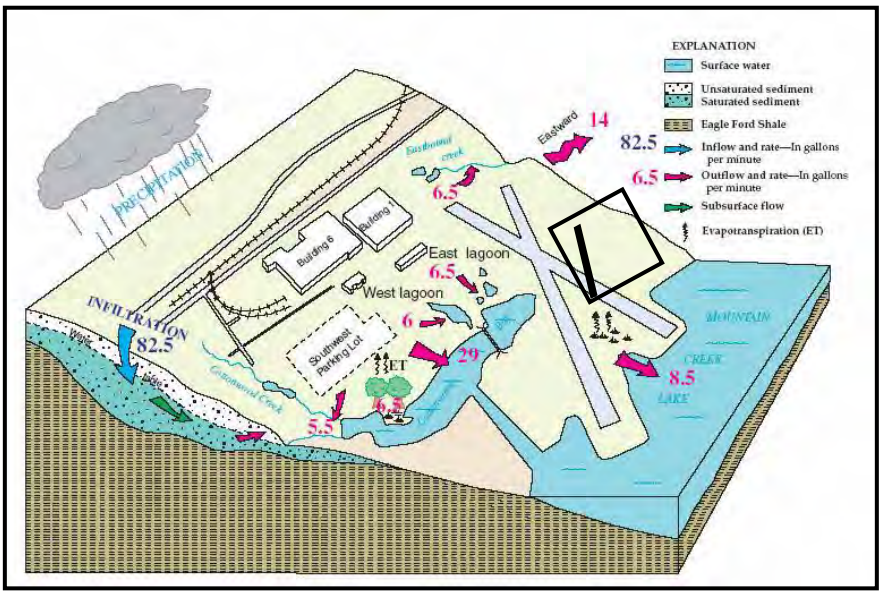

Figure 5.2-1. Conceptual model of the hydrogeologic setting of the Cottonwood Bay site (modified from Barker and Braun 2000).

Hydrogeologic Properties. The source of most groundwater is precipitation which averages about 36 in/yr in Grand Prairie (Owenby and Ezell 1992). Precipitation readily infiltrates the porous higher-altitude areas around the northern limits of the Cottonwood Bay site, while the buildings and impervious surfaces which characterize the lower elevations create runoff instead of infiltration.

As shown in Figure 5.2-1, the water table slopes toward Cottonwood Bay and Mountain Creek Lake. The aquifer is unconfined and composed mostly of silty sand and silty clay, which thins to the south and eventually becomes level with the site's water bodies (EnSafe 1994). Most of the groundwater discharges to Cottonwood Bay and Mountain Creek Lake which maintains the surface water levels of those water bodies. The rest of the ground water either discharges to the east and west retention lagoons, flows out of the site area to the east, or is evapo-transpired back into the atmosphere (Barker and Braun 2000).

Nature and Extent of Contamination. The concentrations of select contaminants of concern (CoCs) in Cottonwood Bay sediments, including three metals (chromium, copper and zinc), PCBs and fluoranthene (representing the highest measured PAH) as determined from previous site investigations are presented in Table 5.2-1. The locations of the historic samples from which these data were generated are shown in Figure 5.2-2. The red markers on this figure indicate previous sampling stations of interest with high concentrations of mixed contaminants that are included in the table below. Two of these stations are in the southwest end of the bay near the terminus of Cottonwood Creek diversion channel, while eight represent stations in the northeastern quadrant in the vicinity of the former NWIRP and current NAS.

Table 5.2-1. Select sediment data available from historic Cottonwood Bay samples showing elevated concentrations of contaminants of interest for the site selection process.

		Historic Cottonwood Bay Sediment Sampling Stations									
Parameter	**Units**	**BG1-01**	**MCL-5**	**OF4-01**	**M2.3**	**M2.4**	**M2.5**	**M2.7**	**Bay 7**	**Bay 11**	**Bay 16**
Metals											
Chromium	mg/Kg	15	83	473	240	255	256	329	349	350	350
Copper	mg/Kg	16	33	71	59	64	61	69	55	53	52
Lead	mg/Kg	25	26	95	95	90	89	96	84	82	61
Nickel	mg/Kg	19	56	34	49	50	51	325	64	NA	46
Zinc	mg/Kg	64	130	502	358	354	364	383	314	NA	280
PAHs											
Anthracene	ug/Kg	62	44	270	226	245	233	143	190	NS	410
Fluoranthene	ug/Kg	960	740	2400	2630	1940	1770	1820	3600	NS	4800
Benzo[a]anthracene	ug/Kg	480	350	1020	1500	1450	1370	996	1220	NS	2100
Other											
PCBs	ug/Kg	NS	6.0	4350*	NS	NS	NS	NS	210	NS	190

* = Sum of 3 Arochlors
NS = Not Sampled
NA = Not Available; Information is forthcoming

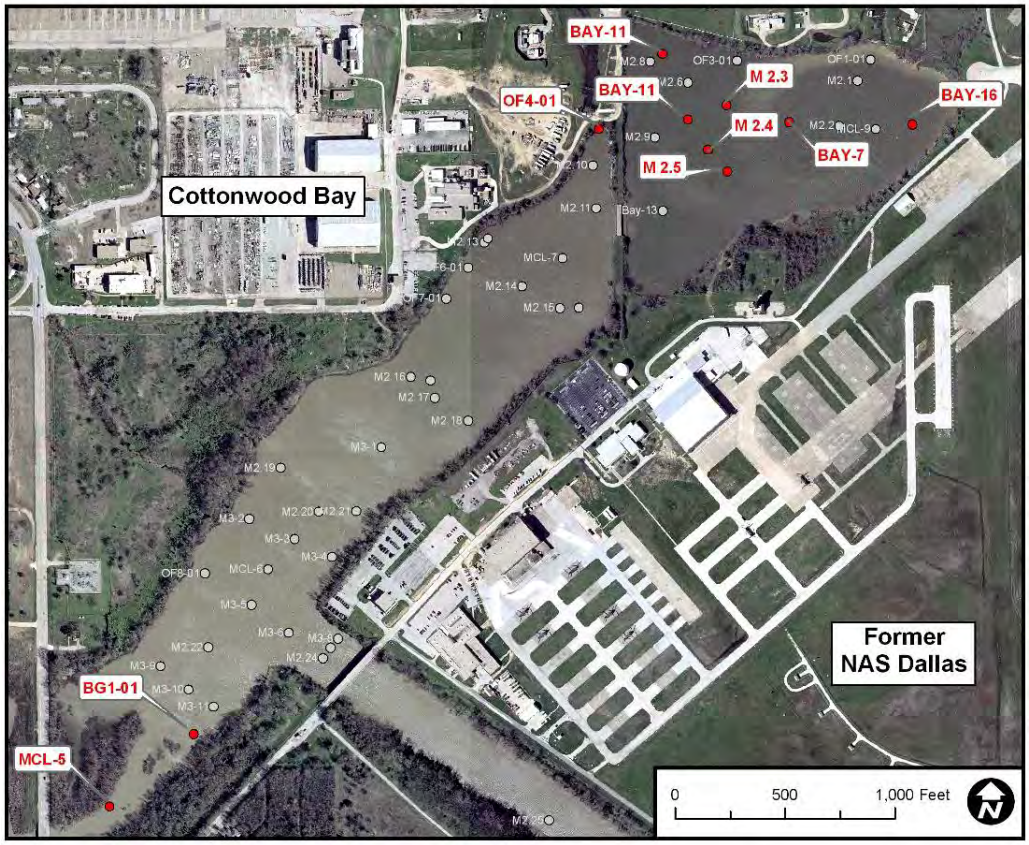

Figure 5.2-2. Historic Cottonwood Bay sampling stations used in the site background assessment (modified from EnSafe 2001).

The highest metals concentrations in the historic Cottonwood Bay sediment samples were found for total chromium and zinc while the greatest organic contaminant loads were found for PAHs. Concentrations of chromium and PCBs were generally higher at Station OF4-01 adjacent to the former NWIRP shoreline while concentrations of PAHs (*e.g.*, fluoranthene) increased with proximity to the NAS. Concentrations of metals and organics were found to be generally lower by a factor of five at the southwestern stations in Cottonwood Bay West where a diversion channel enters the bay as compared to stations in Cottonwood Bay East on the opposite side of the causeway. Groundwater intrusion may also be contributing to lake water and sediment risks because trichloroethene (TCE), dichloroethene (DCE), vinyl chloride (VC), chromium, lead, and other metallic contaminants have been measured in the shallow unconfined aquifer underlying the former NWIRP property (EnSafe 1996).

Remediation Efforts. A series of wells and trenches were installed at the Cottonwood Bay site as early as 1996 with the goal of controlling the flow of groundwater and surface runoff on the NWIRP (now Vought) property (Figure 5.2-3). The specific purpose of these remedial activities was to treat groundwater from the aquifer before it reaches Cottonwood Bay to mitigate VOC contamination. Modeling indicates that the trenches adjacent to Cottonwood Bay East intercept about 827 ft^3/day of groundwater that otherwise would enter the bay. While the trenches intercept groundwater before it can reach Cottonwood Bay, the wells (when actively pumping)

create a depression that reverses the direction of groundwater flow in order to draw contaminated water away from the bay.

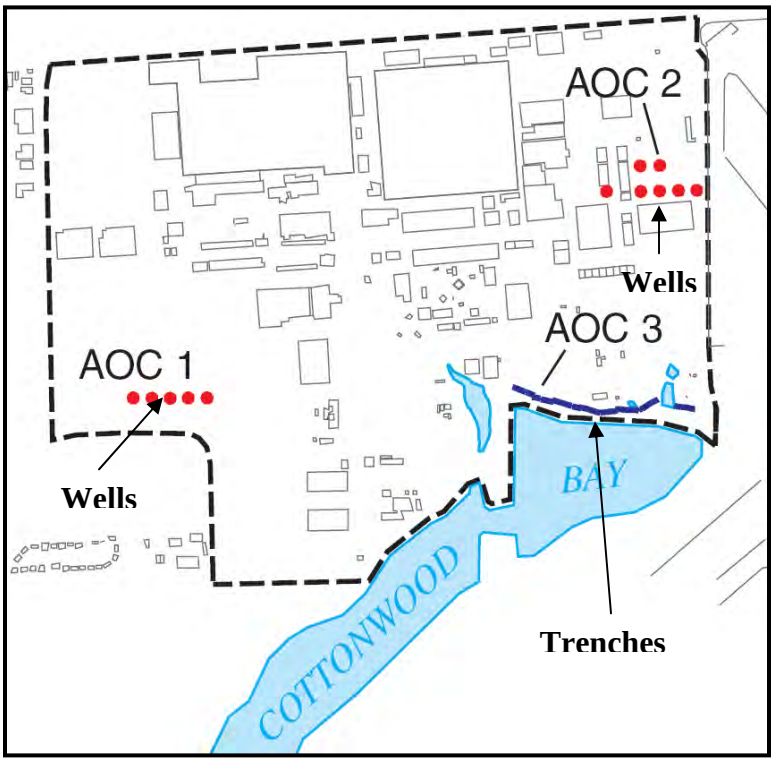

Figure 5.2-3. Locations of remedial wells and trenches at the Cottonwood Bay site (modified from Barker and Braun 2000).

Additional Cottonwood Bay remedial studies were conducted primarily by the USGS and can be characterized as "nature and extent" evaluations that provided data for a Screening Level Risk Assessment (EnSafe 2000). This report was not finalized when the Affected Property Assessment Report was submitted in 2001, but at that time the Texas Natural Resource Conservation Commission (TNRCC) determined that additional studies would be required before additional action could take place at the site.

5.2.3 Geophysical Surveys

The Cottonwood Bay geophysical investigation provided data on water depth, habitat characteristics and lake sediment properties with the goal of selecting a specific location for future prototype mat system deployment. Detailed results of this Phase II evaluation, including all relevant figures, were presented in the Second Year Annual Progress Report (NAVFAC 2007). A summary of the geophysical results is provided in the following sub-sections.

Bathymetry. Bottom topography in the eastern portion of Cottonwood bay ranged from zero along the shorelines to approximately 6.6 ft in the center at the time of the geophysical survey. Depth increases were found to be relatively steep with a majority of the area constituting the

deeper topography. Overall, water depths and gradients were substantially greater in Cottonwood Bay East compared to Cottonwood Bay West. Overall water depths (independent of topography) were found to fluctuate approximately 2 ft based on seasonal rain and drought conditions in northern Texas.

Sub-Bottom Profiling. In the eastern portion of Cottonwood Bay, sub-bottom profiling results showed that sediment thickness ranged from zero along the shorelines to approximately 2.5 ft in the center. Seismic profile cross-sections generated from these data along two select transects in Cottonwood Bay East showed a thin lens of material above the main sediment-water interface. The composition of this lens was unknown at the time, and may represent either a sediment deposit or a layer of leaf detritus. This lens was not confirmed in subsequent sediment vibracores.

Side-Scan Sonar. Side-scan sonar mosaic results for Cottonwood Bay East showed the presence of multiple linear features in the northwest portion of the study area near the Vought shoreline. These features may represent logs or man-made debris that could interfere with potential dredging or mat placement. In addition to these side-scan observations, visual observations indicated the presence of several stumps (approximately six inches in diameter) sticking out of the water and other submerged natural structures (*e.g.*, fallen trees) in both portions of Cottonwood Bay.

Sediment Profile Imaging. Sediment profile images for Cottonwood Bay showed a consistent grain size major mode of >4 phi for all images, which indicates predominantly fine-grained material such as silt or clay according to the Udden-Wentworth size class scale. Mean boundary roughness ranged from 0.00 cm (flat surface) to 2.94 cm, which signifies an uneven surface at some stations. For benthic habitat types, all but one of the 13 stations in Cottonwood Bay East were classified as "Unconsolidated Soft Bottom" (UN). These soft bottom stations were then further classified as either "Silty" (UN.SI) or "Very Soft Mud" (UN.SF). The one station that was not classified as unconsolidated soft bottom (CW-E-12) was considered indeterminate due to low camera penetration caused by the presence of localized debris.

Successional stage could only be determined at three stations in Cottonwood Bay East (CW-E-8, CW-E-9, CW-E-10). Each of these areas was considered a "Stage I" (ST I) infaunal habitat, which in a marine environment often includes the presence of opportunistic, pioneering species with rapid population growth rates that quickly colonize a site following disturbance and generally include smaller species that inhabit the uppermost portion of the substrate, feeding on surface sediments or from the water column (Rhoads and Germano 1982, 1986). Despite being a freshwater site, similar general principals are likely applicable for Cottonwood Bay.

Mean apparent oxygen penetration depth (RPD) depth in Cottonwood Bay East ranged from 1.40 cm to 3.04 cm. These values are generally indicative of moderately well-oxygenated surface sediments. The presence of bubbles was observed in most images, thus signifying gas formation (possibly methane) at depth across the entire study area.

Due to indeterminate data for some of the other parameters, the mean organism-sediment index OSI value, an indicator of macroinvertebrate population health, could only be calculated for

three stations in Cottonwood Bay East (CW-E-8, CW-E-9, CW-E-10). These values ranged from +1.00 to +3.00. In a marine environment, index values in this range would indicate highly degraded or disturbed overall habitat conditions. From the OSI data, the benthic habitat quality (BHQ) index based on a combination of surface and subsurface biogenic features was calculated. Because Cottonwood Bay is a freshwater habitat, the typical interpretation of OSI values based on marine sites are limited since the organic enrichment and disturbance paradigms used to assign benthic successional stage has not been developed. Allowing this uncertainty for consideration of site-specific variation, results in Cottonwood Bay East were similar and ranged from +2.00 to +4.00; these values are typical of pioneering communities in moderately stressed habitats (Iocco *et al*. 2000).

Overall, the SPI photographs collected from Cottonwood Bay revealed a generally consistent soft bottom with degraded habitat conditions. There was some variability between stations in terms of sediment color and amount of gas bubbles present, but this variability was not as substantial as in the adjacent Mountain Creek Lake where a similar SPI survey revealed soft bottom at some stations and shell bottom at other stations within the same cove. The fact that bottom conditions were consistent in Cottonwood Bay put less emphasis on the use of SPI results in determining a specific target area for geotextile testing as compared to other survey parameters.

Sediment Vibracoring. All confirmatory sediment vibracores taken during the original Cottonwood Bay geophysical survey were collected from Cottonwood Bay West due to site access restrictions on the vibracoring vessel. The locations of the Cottonwood Bay West vibracore stations corresponded to previously occupied SPI stations CW-8 and CW-17. Station CW-8 was targeted due to its location in the mouth of the diversion channel, thus making it likely to show historic sedimentation patterns due to potential influx into the bay. Station CW-17 was targeted due to its proximity to the causeway, thus making it more likely to be representative of conditions in Cottonwood Bay East. Core CW-8-C and Core CW-17-C are characterized in Table 5.2-2.

Table 5.2-2. Sediment core characteristics at two stations in Cottonwood Bay West.

Core ID: CW-8-C		**Core ID: CW-17-C**	
Total Length: 38”		Total Length: 36”	
0-16”	Soft reduced silt with clay faction.	0-16”	Soft reduced silt; organic odor.
16-32”	Reduced silty clay.	16-22”	Soft reduced silt with clay faction.
32-34”	Hard yellow clay with pebbles and coarse sand.	22-32”	Reduced silty clay.
34-38”	Hard yellow clay with silt.	32-36”	Hard yellow clay plug.

These characterizations were ultimately used to calibrate and confirm the sub-bottom profiling dataset for Cottonwood Bay. Sediment thickness results from the vibracores were consistent with the soft surface and hard underlying layers identified in the sub-bottom survey. In addition,

the vibracore characterizations were also used to confirm the grain size and habitat conditions identified in the SPI photographs.

Groundwater Seepage Survey. A Cottonwood Bay groundwater seepage survey was conducted by Groundwater Seepage, Inc. in 2007 with results provided in the *Final Data Report, Groundwater Upwelling Survey, Naval Weapons Industrial Reserve Plant, Cottonwood Bay, Dallas, Texas*. For this survey, horizontal mapping of elevated groundwater conductivity and decreased temperature data at the groundwater-surface water interface were used to identify likely areas of groundwater discharge and the potential relationship to increased contaminant loads being transported from upland properties within the groundwater flow. The seepage survey was designed to cover areas of suspected elevated sediment contamination as determined by the historic sampling dataset (Figure 5.2-2). Final Trident Probe stations for the Cottonwood Bay groundwater seepage survey are shown in Figure 5.2-4.

During the summer (2007) when the Cottonwood Bay seepage survey was conducted, groundwater in this region was expected to be cooler than the surface water. Groundwater temperatures in a monitoring well along the shore averaged 23°C during the course of the survey while Cottonwood Bay surface water temperatures as determined with the Trident Probe ranged from 27.8-29.8°C with an average 28.5°C across stations. Subsurface temperatures as determined by the Trident Probe ranged from 24.8-28.2°C and averaged 26.9°C across stations. Accordingly, areas with subsurface water temperatures less than the surface water minimum (27.8°C) were considered zones of potential groundwater upwelling.

Surface water conductivity as determined with the Trident Probe ranged from 0-0.5 mS/cm and averaged 0.39 mS/cm across stations. Subsurface water conductivity as determined with the Trident Probe ranged from 0-3.1 mS/cm and averaged 1.09 mS/cm across stations. All areas with subsurface conductivity measurements greater than the surface water maximum were considered zones of potential groundwater upwelling. Complete Trident Probe temperature and conductivity statistics for Cottonwood Bay are summarized in Table 5.2-3.

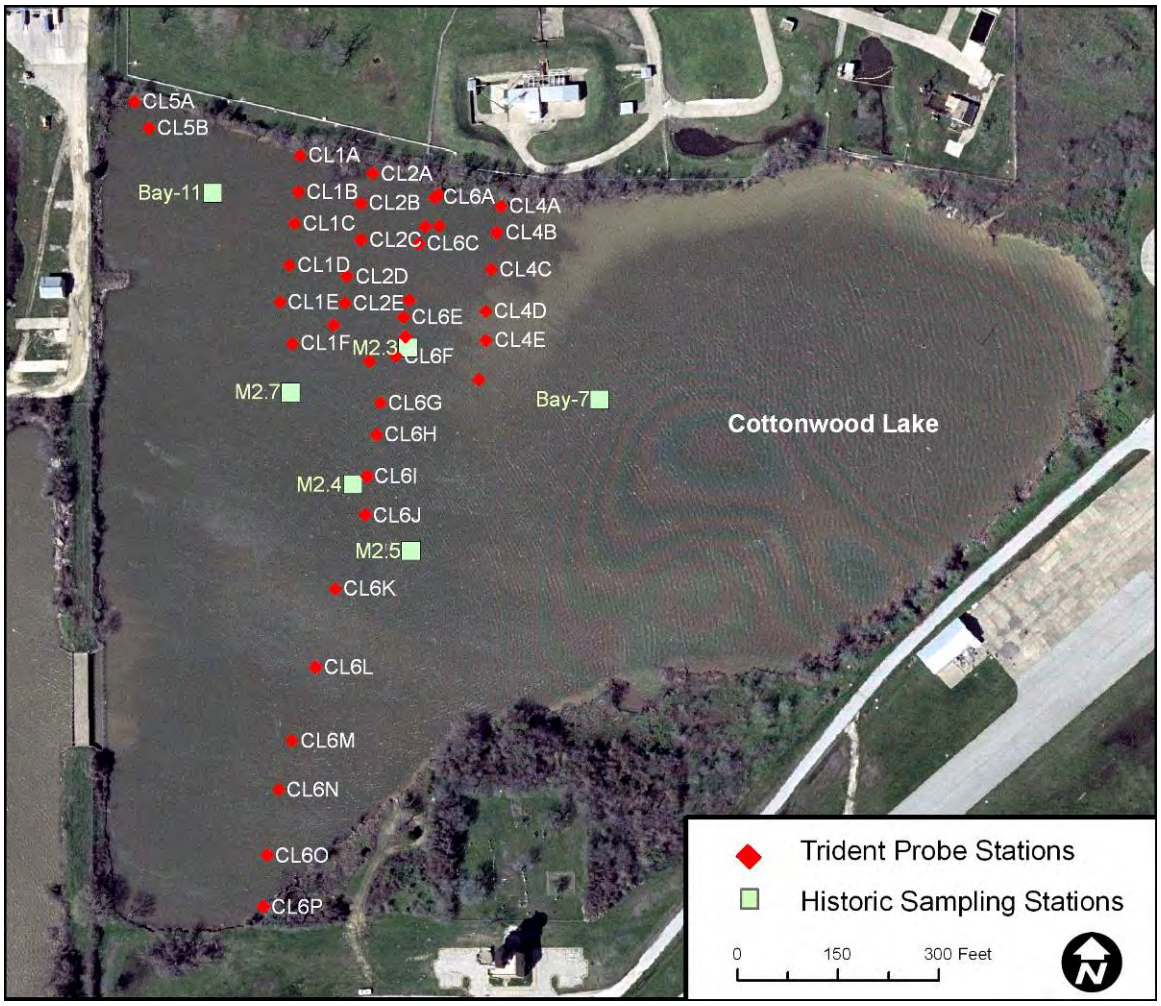

Figure 5.2-4. Trident Probe stations for the Cottonwood Bay groundwater seepage survey.

Table 5.2-3. Trident Probe subsurface temperature and conductivity results for Cottonwood Bay.

	Subsurface Temperature (°C)	Subsurface Conductivity (mS/cm)	Surface Temperature (°C)	Subsurface Conductivity (mS/cm)
Minimum	24.82	0.6	27.81	0.38
Maximum	28.23	2.1	29.84	0.5
Average	26.88	1.1	28.49	0.39
St. Dev.	1.15	0.39	0.51	0.02

Spatial results from the relative subsurface temperature and conductivity mapping process were used to define three zones of increasing groundwater discharge potential as shown in Figure 5.2-5. In general, cooler subsurface temperatures were observed in association with higher subsurface conductivity for several of the outer transect stations (E,F,G,H; Figure 5.2-4). The majority of these areas were found to be located approximately 200 feet from the northern shoreline, but similar conditions were also observed in one area near the southern shoreline. The zone with the highest potential for groundwater seepage (blue) begins approximately 200 feet

offshore. Lithology of an upland monitoring well coupled with observed resistance to Trident Probe penetration at some of the inshore stations seemed to indicate the presence of a clay layer deflecting terrestrial groundwater flow further offshore.

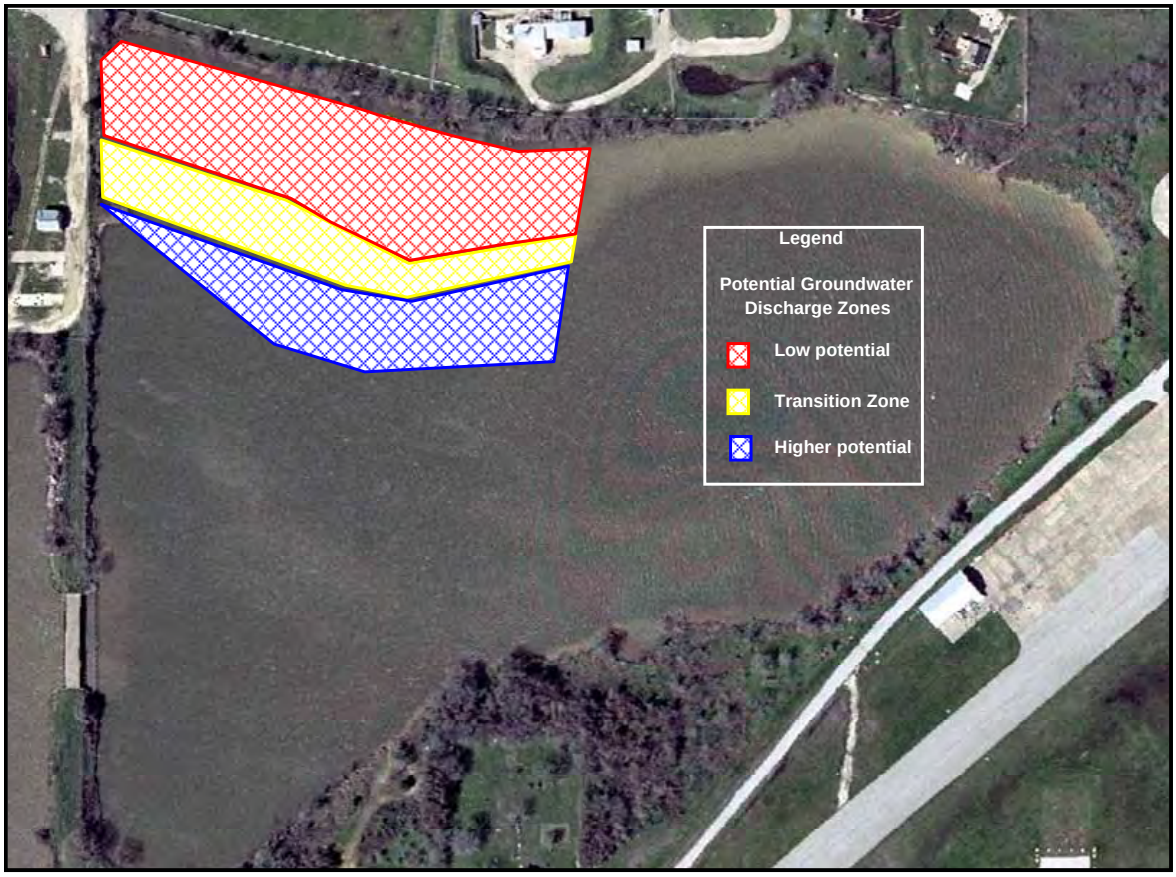

Figure 5.2-5. Potential groundwater discharge zones for Cottonwood Bay.

5.2.4 Target Area Establishment

Based on the overall results of the Cottonwood Bay geophysical investigation completed in summer 2007, the eastern portion of the bay was selected as the general area of focus for further prototype geotextile testing due to greater water depths, increased sediment layer thickness, consistent bottom characteristics and the presence of confirmed groundwater plumes that would allow for accurate assessment of flux through the various test mat arrangements. These parameters were then considered both individually and in combination to select a specific target area within Cottonwood Bay East to serve as the deployment for Task 4. The side-scan sonar survey did not generally identify any major obstacles in Cottonwood Bay East such as debris or hard bottom, save for some linear features of note nearby (possibly submerged logs) which should be avoided. The SPI photographs showed a consistently unconsolidated soft bottom environment with generally degraded habitat conditions, and therefore did not provide any site discriminators. Therefore, groundwater seepage results and sediment chemistry data from previous sampling events were the key factors for selecting a target area compatible with project goals.

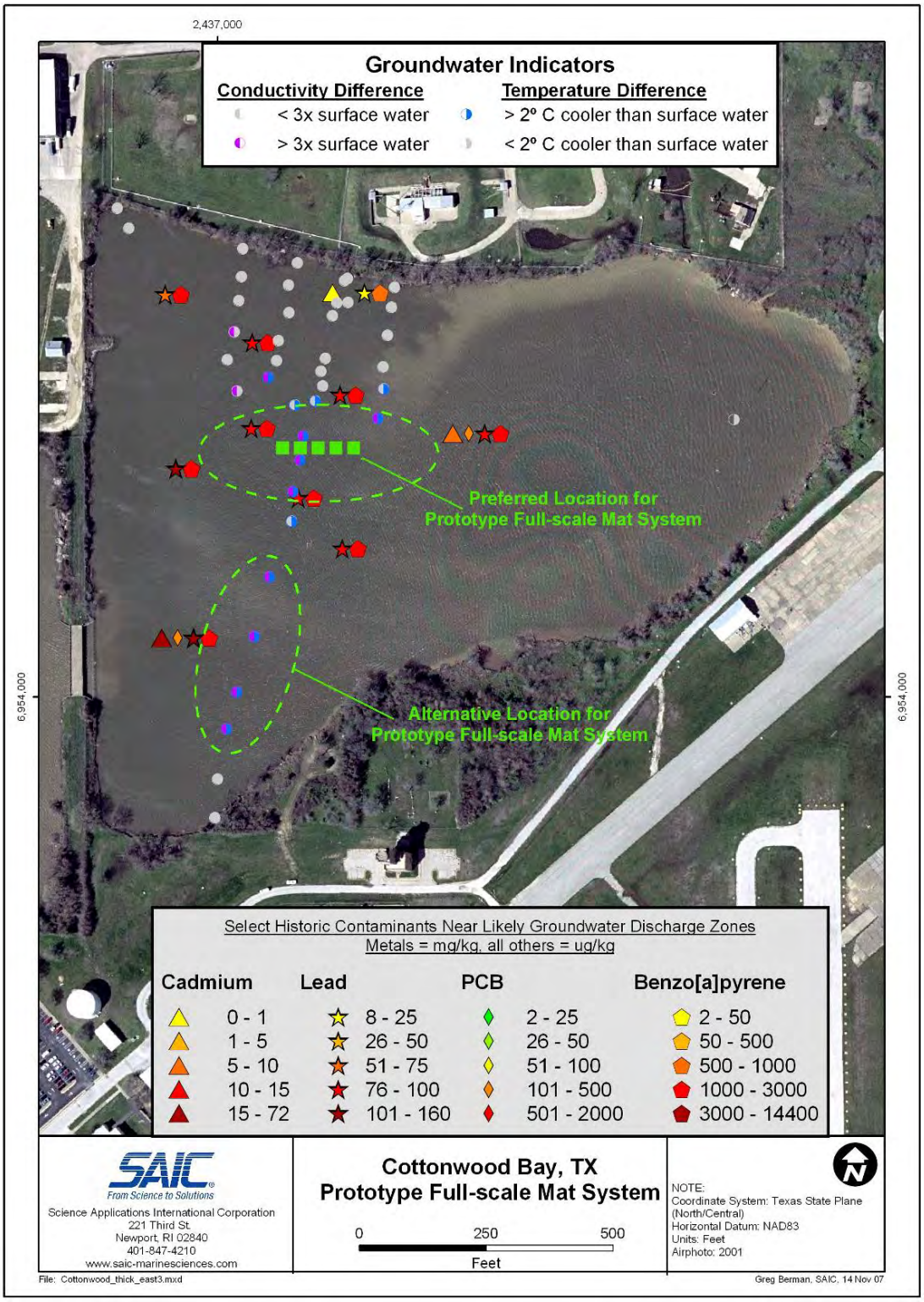

Figure 5.2-6. Preferred target areas for prototype mat system deployment based on the results of the Cottonwood Bay geophysical surveys.

The preferred target area determined from the geophysical investigation is located in the western portion of Cottonwood Bay East approximately 200 feet south of the Vought shoreline (Figure 5.2-6) and corresponds to a region of high potential groundwater discharge (Figure 5.2-5). Historical chemistry results for this area indicated consistently elevated concentrations of lead (>75 mg/kg) and benzo[a]pyrene (>1000 µg/kg) as well as indications of relatively high and consistent groundwater seepage based on temperature and conductivity data. Sub-bottom profiling and SPI results did not show any major obstructions that could impede groundwater flow or contaminant transport in this area. Challenges inherent in use of this location included water depths of approximately six feet at the time of the bathymetry survey, which would necessitate use of divers for mat system deployment and monitoring as opposed to wading. The location of this target area was also in the middle of the bay and therefore posed additional logistical challenges related to deploying the sand cap from the NAS shoreline staging area. On balance, the identified mat placement target was selected for meeting technical requirements despite the logistical challenges presented.

5.3 Task 3: Geotextile Testing

The purpose of the geotextile testing task for this project was to field test different types of geotextile material at the selected pilot site to assess (a) whether sediment clogging, and biofouling and biofilm formation would adversely affect the ability of the fabric to allow water to pass through the final mat design, (b) whether environmental weathering compromises the ability of the mat to retain the amendment material, and (c) whether environmental weathering compromises the reactivity of the sequestration agents. This task also included laboratory gradient ratio testing and finite element analysis to assess stability, clogging potential and prospective sediment deformation for clean, non-fouled mats before the weathered test mats are retrieved. A summary of the accomplishments for each component of this task are provided in the following sections.

5.3.1 Field Evaluation

Fourteen test mats of various compositions were deployed for field testing in Cottonwood Bay East in June 2007 as described in Section 4.3. The first group of mats were collected in December 2007 and shipped to UNH for performance testing with a geotechnical test column system via the ASTMD 5101 method. The mats were shipped wet in sealed tubes to maintain the surface conditions as well as possible. The second group of mats were retrieved in December 2008 and June 2009, but based on column testing results from the first group of mats the second group has not been tested and will be held indefinitely pending further instruction.

5.3.2 Gradient Ratio Testing

Preliminary laboratory gradient ratio testing conducted during Year One showed that trapped bubbles are a significant impediment to groundwater flux through a fine grained matrix. Purging the systems with carbon dioxide gas is the standard procedure for eliminating bubbles as the CO_2 forces the air from the system and then dissolves into solution. However, the fine-grained nature of the sediment made it impossible to pass CO_2 through the column, necessitating the attempt of different approaches. The most successful approach involved soaking the geotextiles under a

light vacuum to minimize air trapped in the fabric. In addition, the sediment was slurried for placement in the column, and a light vacuum was used to remove air bubbles prior to placement.

Gradient ratio testing was conducted on three stock CETCO geotextile fabrics (GT-1, GT-2 and GT-3) and a fourth geotextile (GT-4) chosen to represent an extreme case for clogging (thick fabric and small opening size). Two clean mats (one with organoclay, one with activated carbon) and three weathered mats were also tested. All tests followed the methods described in Section 4.3.2.

Single Geotextiles. Table 5.3-1 presents the physical properties of the four single layer geotextile fabrics used for gradient ratio testing. Gradient ratio tests were carried out on these geotextiles using three hydraulic gradients, i = 1, 4 and 8. The gradient ratio (GR) was measured over time for each geotextile and the results are shown in Figures 5.3-1 to 5.3-4, respectively. Each of these figures includes the results for the three hydraulic gradients; the first two curves are replicates of the same test and the last curve corresponds to a test starting at i = 0.5 for one day, followed by the i = 1, 4 and 8 tests. The objective of this later test was to study the effect of very low hydraulic gradients on the clogging potential of geotextiles.

Table 5.3-1. List of non-woven geotextiles used for reactive core gradient ratio testing applications.

Geotextile ID	Mass per unit area [g/m^2] (oz/yd^2)	Apparent Opening Size	Polymer Type
GT-1	170 (5)	170	Polyester – White
GT-2	203 (6)	70	Polypropylene – White
GT-3	271 (8)	80	Polypropylene – Black
GT-4	265 (7.8)*	170	Polypropylene – Grey

The GR was relatively stable for any hydraulic gradient after only one day, which falls into the recommendation of the ASTM standard for "some recognizable equilibrium or stabilization of the system." Although in some cases (Figure 5.3-1 and Figure 5.3-2) the GR was not fully stable after 24 hours at a constant hydraulic gradient, it is clear the system was not prone to clogging because the GR was less than 3 as recommended by the USACE. In general, all gradient ratio tests showed that no clogging potential of the four geotextiles would be expected in the field when used with similar fine-grained sediment.

The gradient ratio tests carried out on the finer geotextiles AOS 170 (Figure 5.3-1 and Figure 5.3-4, for GT-1 and GT-4, respectively) reached GR-values in the range of 1.2 to 2.2. The lower range of GR values were measured with the less dense geotextiles, which can be interpreted to be of lower tortuosity (degree of pathway meandering). In addition, piping conditions were also measured on lighter geotextiles. Under piping conditions some fine sediment particles move towards the geotextile, leaving small voids that eventually will interconnect to each other, forming small preferential flow paths for the water to pass through. This behavior can improve the performance of the reactive mat because it accelerates the flow of contaminated water from the sediment to the reactive material. Moreover, the transport of fine sediment particles is controlled so a stable filter system can develop.

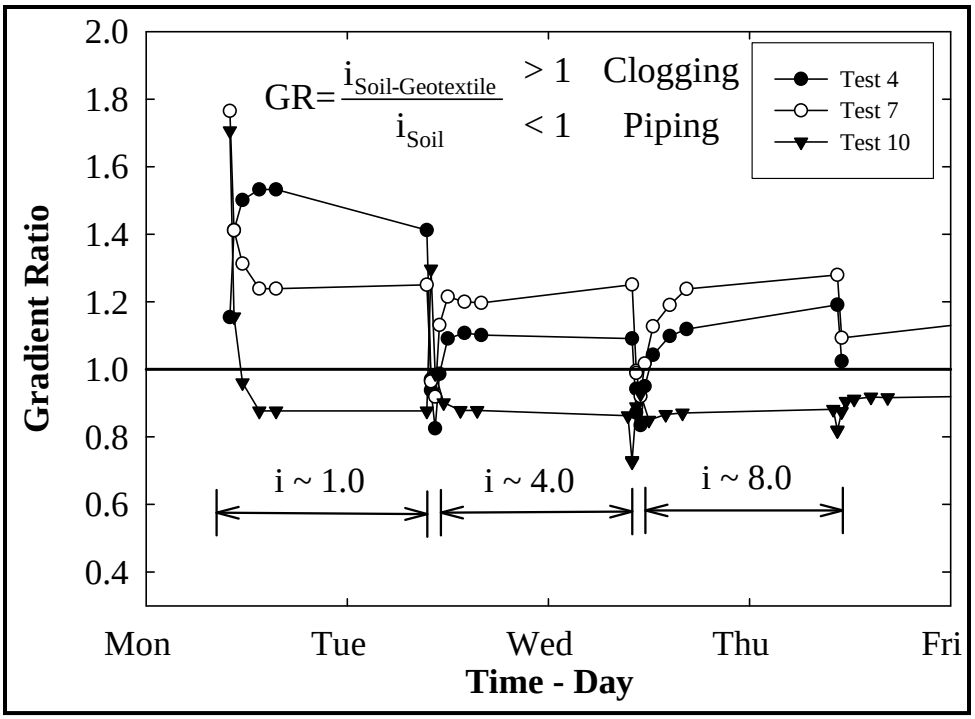

Figure 5.3-1. Gradient ratio test results for geotextile GT-1 (AOS 170).

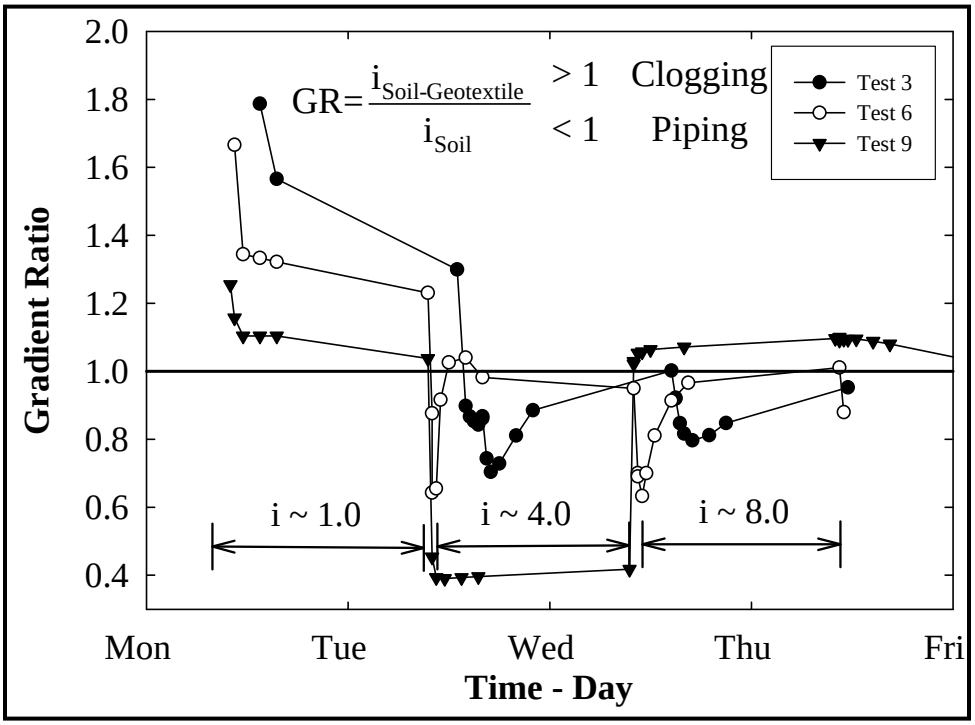

Figure 5.3-2. Gradient ratio test results for geotextile GT-2 (AOS 70).

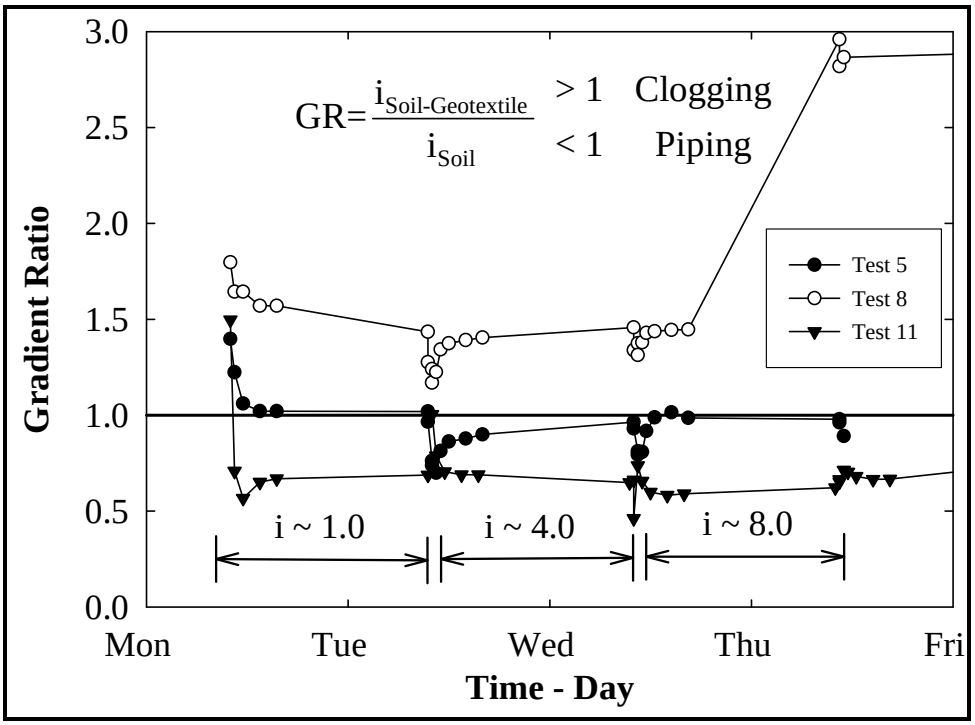

Figure 5.3-3. Gradient ratio test results for geotextile GT-3 (AOS 80).

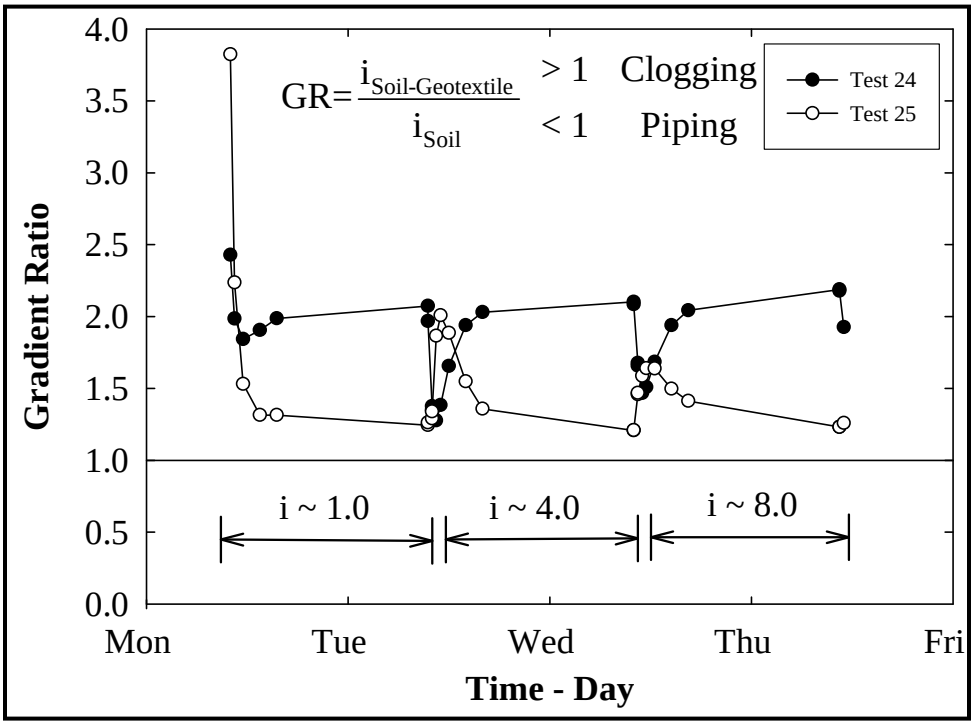

Figure 5.3-4. Gradient ratio test results for geotextile GT-4 (AOS 170).

The results on geotextiles with coarse AOS (70-80) (Figure 5.3-2 and Figure 5.3-3, for GT-2 and GT-3, respectively) showed smaller GR values than the finer geotextiles. In general, the final GR-values for coarse geotextiles ranged from 0.6 to 1.1, with the majority of values at the lower end of the range. These values indicate the geotextiles performed under piping conditions, with a GR value close to one or slightly less as recommended by the ASTM standard. Reactive core mats are typically constructed by CETCO using the geotextile GT-2 (AOS 70) as listed in Table 5.3-1.

Geotextile Mats. The clogging potentials of two clean reactive core mats, one containing organoclay as the reactive material and the other containing activated carbon, were also measured using the gradient ratio test. This process provided verification of the influence of swelling of the clay on the clogging potential of the reactive core mat.

Each mat has one non-woven and one woven side. The mats are typically deployed over the contaminated sediment with the woven geotextile facing the sediment; therefore, the reactive mats were placed in the test chamber with the woven geotextile facing the sediment to represent the most likely field conditions. Figure 5.3-5 shows the results of the GR tests on the clean reactive core mats featuring the GT-2 (AOS 70) geotextile.

The results showed no clogging potential for the reactive core mats under the test conditions. In addition, the overall tendency of the GR-value for the double geotextile mat arrangement was similar to the behavior exhibited by the single geotextiles discussed above. This result indicates that the presence of the second geotextile in the mat does not significantly affect the filtration behavior of the system. Finally, the GR-value stabilized at slightly less than unity as recommended by the USACE for slight piping conditions.

The first group of small-scale reactive test mats listed on Table 4.3-1 was deployed in Cottonwood Bay for a period of six months. Only the mats deployed with the woven geotextile in contact with the sediment were evaluated using the gradient ratio test (RCM-1, RCM-3 and RCM-5), because installation procedures for commercial applications prevent deployment with the non-woven geotextile facing the sediment. The results of the gradient ratio tests with duplicates for the reactive core mat RCM-1, RCM-3 and RCM-5 are shown in Figure 5.3-6 to 5.3-8, respectively.

These results showed no clogging potential on any of the weathered reactive core mats under the tests conditions. The mat with the finer geotextile (RCM-1, AOS 170) showed strong piping conditions (GR-value = 0.5), but eventually stabilized at a GR-value close to unity. The mats with coarser geotextiles (RCM-3, AOS 70 and RCM-5, AOS 80) showed stable gradient ratio values close to unity, ranging from 0.9 to 1.2, which is in agreement with the recommendations of the ASTM standard and the USACE.

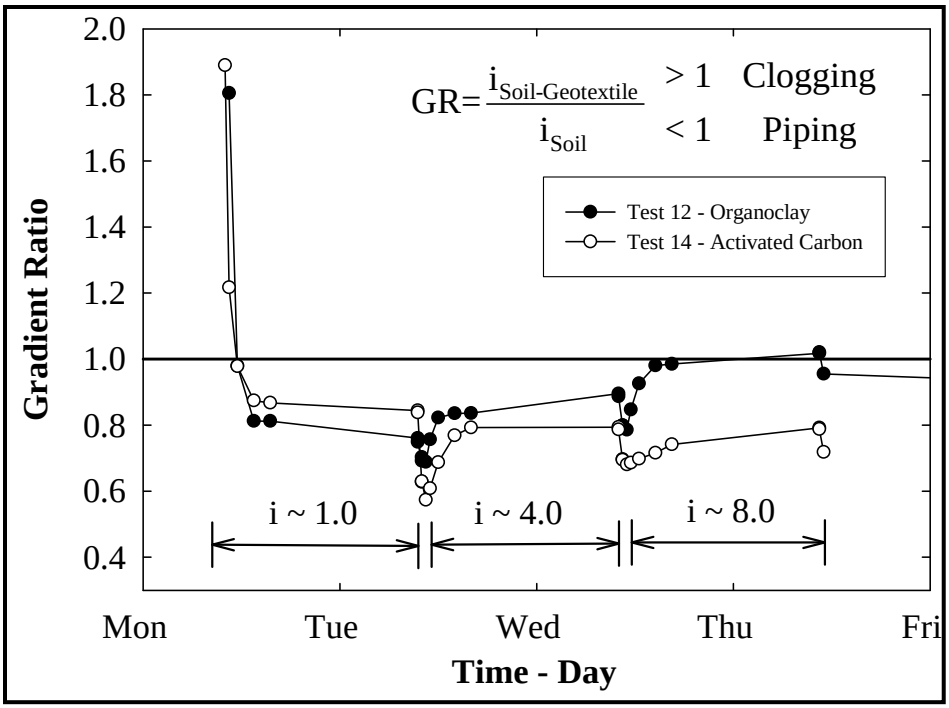

Figure 5.3-5. Gradient ratio test results for clean mats featuring the GT-2 (AOS 70) geotextile and containing organoclay and activated carbon as the reactive material.

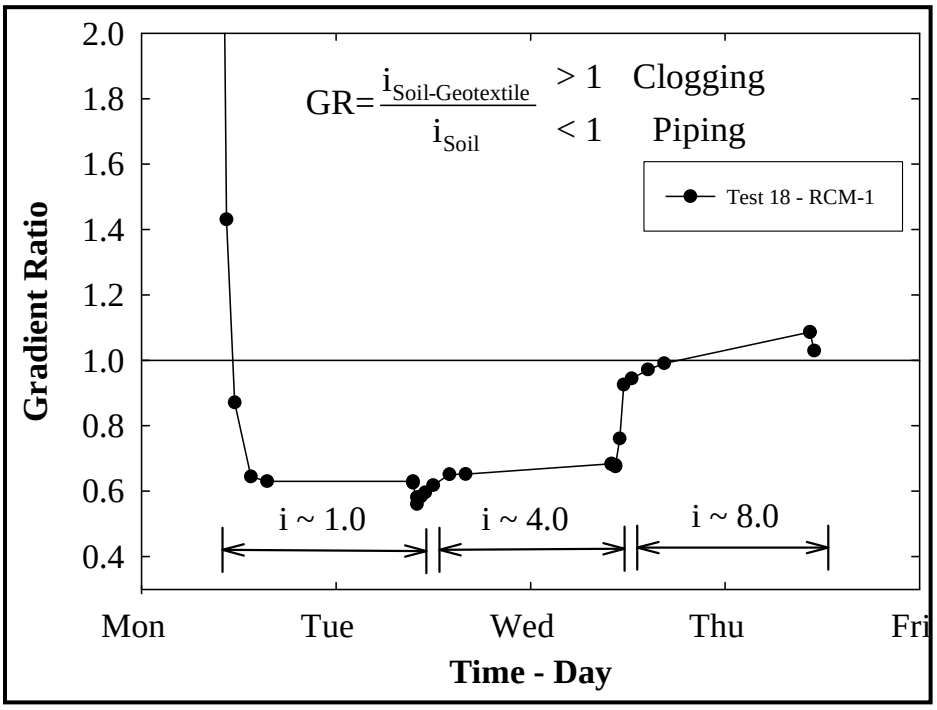

Figure 5.3-6. Gradient ratio test results for weathered geotextile mat RCM-1 after six months of soak time in Cottonwood Bay.

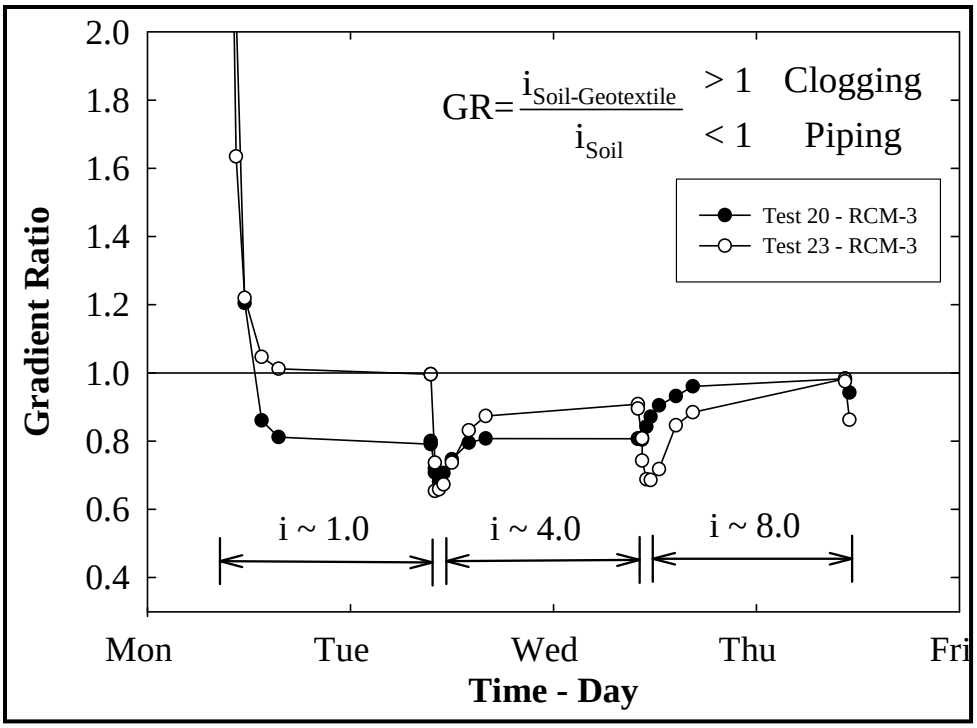

Figure 5.3-7. Gradient ratio test results for weathered geotextile mat RCM-3 after six months of soak time in Cottonwood Bay.

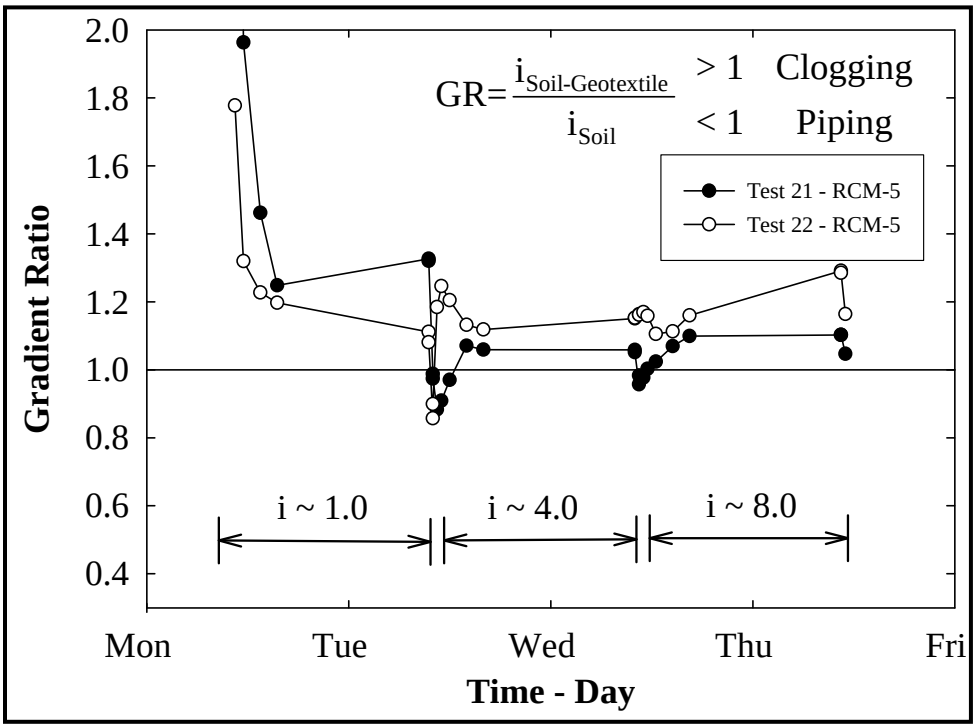

Figure 5.3-8. Gradient ratio test results for weathered geotextile mat RCM-5 after six months of soak time in Cottonwood Bay.

Long-Term Clogging Behavior of Geotextiles. Additional long-term gradient ratio tests were also carried out to evaluate the long-term performance of sediment-geotextile systems under expected field conditions. This type of extended gradient ratio test is initiated at a hydraulic gradient of $i = 1$ that is gradually increased to cover the hydraulic gradients expected in field applications. General site characteristics and seepage measurements from a previous pilot reactive capping project conducted in the Anacostia River (Melton *et al*. 2005) indicated maximum hydraulic gradients in the range of $i = 4$ to 5 for the type of sediment encountered in Cottonwood Bay. In addition, a hydraulic gradient of $i = 5$ represents a conservative condition for the modeling of most geotextile filter applications (Fischer *et al.* 1999). Two long term gradient ratio tests were conducted at $i = 4$ to 6 for nearly 30 days on geotextiles GT-2 and GT-3, with AOS 70 and 80, respectively. The results are shown in Figure 5.3-9.

The results of the long-term test on the geotextile GT-3 show a strong disturbance in the system after 25 days ($i = 6$), which results in a sudden jump of the GR-value from 1.01 to 1.18 followed by a gradual increase to 1.6. The GR-value step increment followed by a gradual increase was caused by the disturbance of the soil near the manometer ports, which promoted seepage along of the wall of the permeameter (Figure 5.3-10).

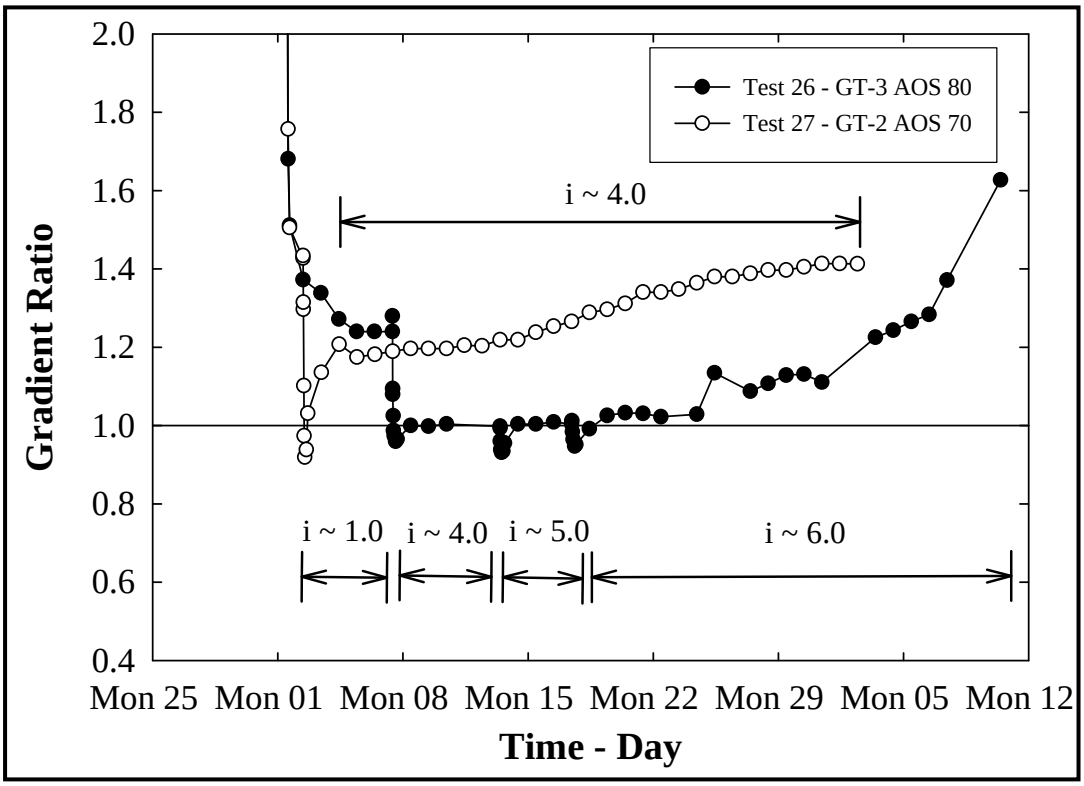

Figure 5.3-9. Long-term gradient ratio test results for geotextiles GT-2 and GT-3.

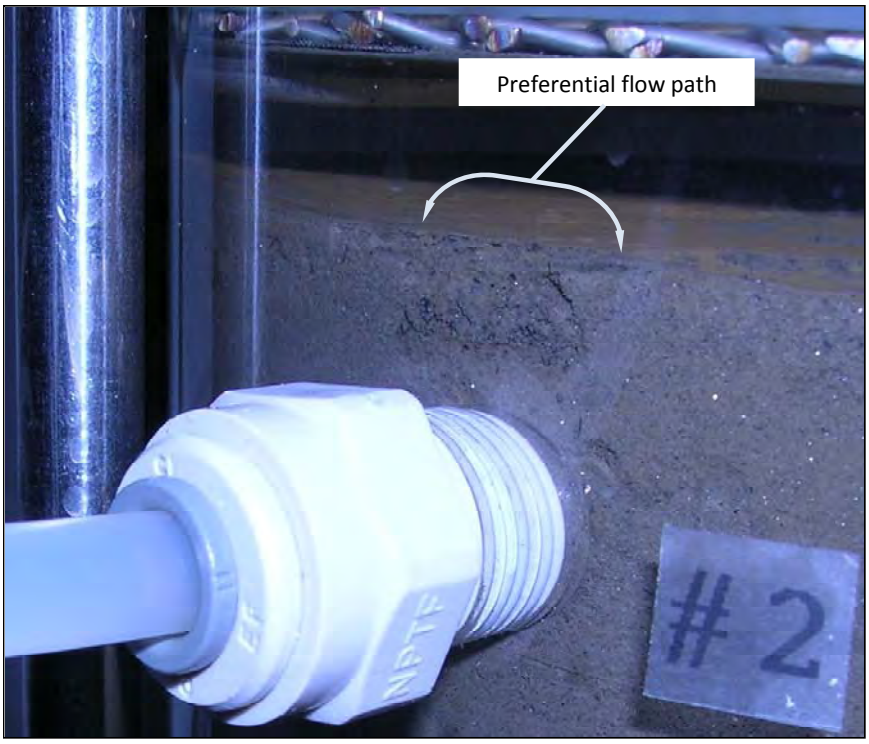

Figure 5.3-10. Evidence of wall seepage near the manometer port during the long-term gradient ratio test for single geotextile GT-3.

The long term GR test on the geotextile GT-2 (AOS 70) showed a GR-value of 1.2 after 24 hours at $i = 4.0$. This test was carried out for 30 days and the GR-value slowly leveled at 1.4, thus indicating that geotextile GT-2 is not prone to clogging according to the USACE recommendations (GR-value < 3.0). In addition, the difference in the results from running the test for 30 days versus only 1 day does not appear to be significant.

Numerical Modeling. The gradient ratio tests carried out on single geotextiles as well as on both clean and weathered reactive core mats did not show evidence of significant clogging that would adversely affect the filtration behavior of the system. However, given the uncertainty of the reactive mat installation process and the actual compatibility between the sediment and the reactive core mats at a given site, it was necessary to develop a numerical model to simulate the eventual clogging of the mat.

Gradient ratio testing results indicated that a significant hydraulic head would be required to force sediment particles into any of the test geotextiles to the extent that they would become clogged and thus impermeable to groundwater flow. Because such drastic hydraulic conditions are not expected to occur in the field, the use of geotextiles as planned to contain reactive material should be appropriate for achieving project goals. Overall results from the finite element modeling process (to be discussed below) indicated that soft underlying sediment will undergo some compression directly beneath a reactive mat following deployment, but this compression will not extend greatly beyond the mat edges. Porewater displacement caused by this consolidation will be confined mainly to the sediment directly below the mat. When using a fully permeable geotextile as the starting point for the models, results indicated that a

permeability decrease of several orders of magnitude would be required to greatly impact groundwater flow around the reactive mat. This level of clogging is not expected to occur under field conditions based on the results of the gradient ratio testing. Biofouling data from weathered test mats can ultimately be used to refine the finite element models with actual permeability values.

Given the fact that the sediment particles are contaminated and that it takes some time for the filter structure to develop at the interface between the sediment and the geotextile, it is important to control and verify that the amount of piped sediment does not compromise the retention efficiency of the system. As previously discussed, the gradient ratio test requires the flow of water through the sediment-geotextile system for several days. Also, the gradient ratio test column was modified to run water from top to bottom of the permeameter, while the geocomposite was placed beneath the sediment. Laboratory observations indicated that the water flow transported a measurable amount of fine particles of sediment through the geocomposite within the first day of the test but by the second day of the test only water passed through. Figure 5.3-11 shows an example of the sediment collected on the bottom plate of the permeameter at the end of a typical gradient ratio test.

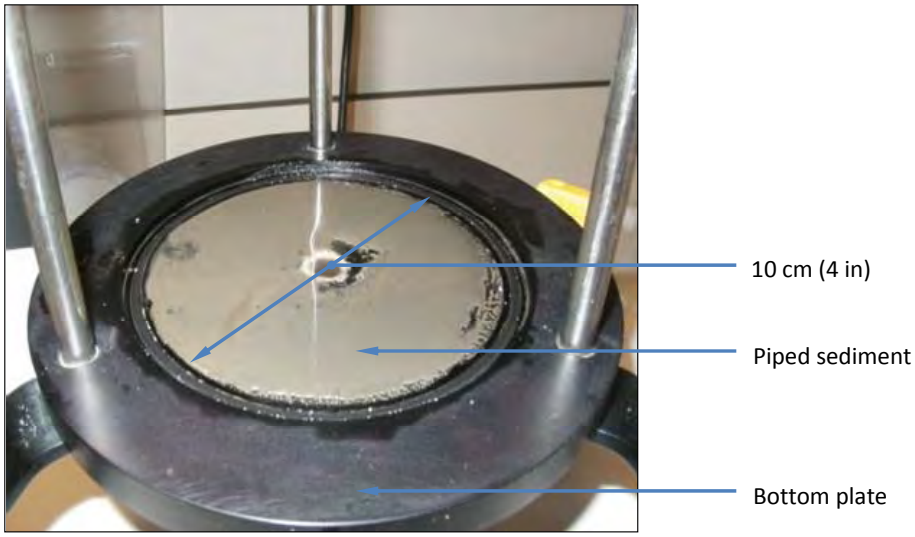

Figure 5.3-11. Example of sediment passing through the geotextile during a typical gradient ratio test.

A stable geotextile/soil system limits the amount of fine soil particles able to pass through the geotextile. The recommended limit for a stable system is 2500 g/m^2 (Lafleur *et al*. 1989), which for the area of a gradient ratio test permeameter amounts to 20 g. In order to determine whether the different geocomposites for this project met such goals, all sediment passing through the geotextile or reactive core mats during the gradient ratio tests was collected, weighed and analyzed in terms of the physical properties of the geocomposite. Figure 5.3-12 shows the weight of the piped sediment versus the mass per area and AOS of each geotextile for gradient ratio tests starting at a hydraulic gradient of $i = 5$. These results indicate that the geocomposite-

sediment filter system is stable in terms of its retention capabilities, and that all geocomposites tested for this project allow less than 2500 g/m^2 to move through the geotextiles.

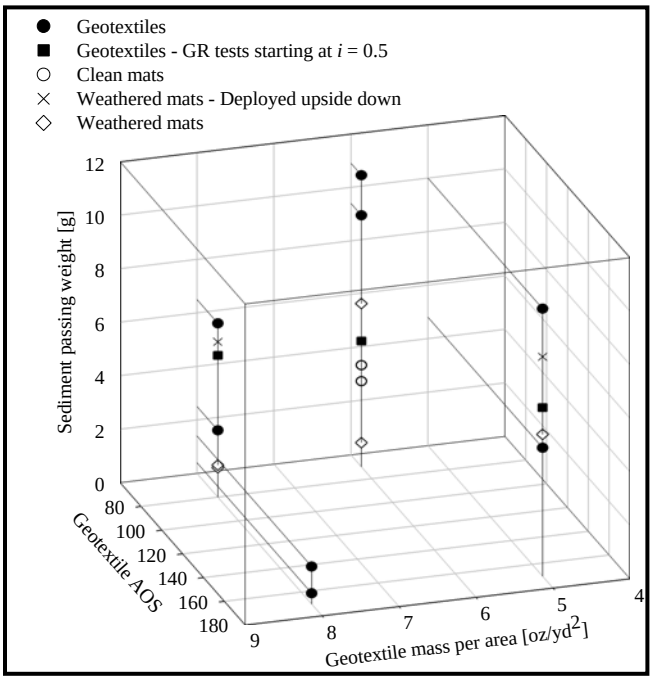

Figure 5.3-12. Sediment mass passing through different geotextiles and reactive core mats during gradient ratio tests starting at hydraulic gradient of *i* = 5.

These results also show that the use of a finer AOS (180) or a heavier geotextile (8 oz/yd^2), or a combination of both, drastically reduces the amount of sediment that is able to pass through the geocomposite. Furthermore, the model proves that reactive mats allow less material to pass through than single geotextiles, mainly because the flow path in reactive core mats is longer and expectedly more tortuous than in single geotextiles.

Conclusion. The main questions about mat design to be addressed by the gradient ratio testing and numerical modeling were how to balance the choice of the geotextile fabric such that the clogging potential was minimized while also preventing the loss of reactive amendment materials and sediment transport into the mat. Results of the numerical modeling influenced the prototype mat design by showing that clogging would have to be severe, with the permeability reduced to two orders of magnitude less than the sediment, before there would be significant adverse impacts on mat performance, thus providing a lower limit for success. The gradient ratio testing was then specifically designed to determine how the geotextile/sediment system and reactive mat/sediment system would actually behave under controlled conditions. Results showed that the coarser geotextiles (AOS 70 and 80) did not clog and did not lose amendment while also experiencing relatively little sediment transport into the cap. Based on these results, the AOS 80 geotextile was chosen for the cap. Subsequent testing on weathered tests mats confirmed that this geotextile size was resistant to clogging and would not reach the lower limit predicted by the model. The variability of the consolidation (*i.e.*, bathymetry) and groundwater

flow (*i.e.*, Trident Probe) field data made it difficult to draw conclusions about how the laboratory data and modeling compare to the field.

5.3.3 Consolidation Testing

In order to model the sediment deformation to be caused by the weight of an overlying geotextile mat system as accurately as possible, a series of consolidation tests were carried out on reference sediment from the Cottonwood Bay pilot site. The consolidation curves for this sediment were obtained from one dimensional and seepage consolidation tests. However, it is important to mention that only one seepage consolidation step was possible on the Cottonwood Bay sediment due to its low permeability, which promoted water flow alongside the permeameter wall instead of through the sediment sample after 30 days of test time. Though only one step was carried out, the results still followed the observed trends for one dimensional tests. Inspection of the results showed that the pressure caused by the porous stone, loading plate and bearing ball (2.457 kPa) induces 33% of strain on the sample.

The results of the consolidation tests performed on the Cottonwood Bay sediments are presented in the series of figures below. Figures 5.3-13 and 5.3-14 presents these results in terms of strain and void ratio as a function of effective stress, respectively.

Figure 5.3-15 shows the variation of the coefficient of consolidation with effective stress for this sediment, and Figure 5.3-16 presents the variation of the coefficient of volumetric compressibility. The inflexion point in the compressibility of the sediment occurs at 6-7 kN/m^2. Moreover, the coefficient of volumetric compressibility indicates stiffening of the sample.

The variation of the coefficient of consolidation with the void ratio is shown in Figure 5.3-17 and the variation of the coefficient of volumetric compressibility is shown in Figure 5.3-18. The variation of the permeability with effective stress is presented in Figure 5.3-19 and in terms of void ratio in Figure 5.3-20.

Overall, consolidation testing results for Cottonwood Bay sediment show a critical void ratio of 5.8 where the rate of permeability change has an inflexion point. Furthermore, this critical void ratio corresponds to an effective stress of 6-7 kN/m^2 and matches the results shown on Figure 5.3-15. In geotechnical engineering practice, the compression index (*Cc*) and recompression index (*Cr*) is commonly used to estimate the settlement and the rate of consolidation of soils. The corresponding parameters of both sediments are calculated from the *Log(σ') vs. e* curves obtained from the consolidation tests.

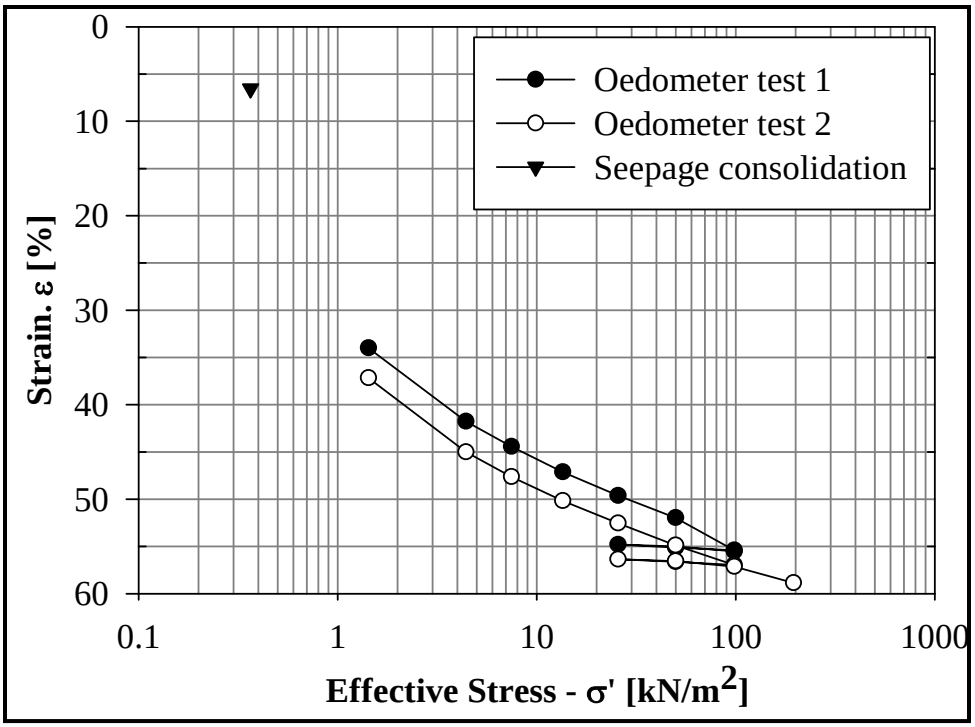

Figure 5.3-13. Consolidation of Cottonwood Bay sediment; strain versus effective stress.

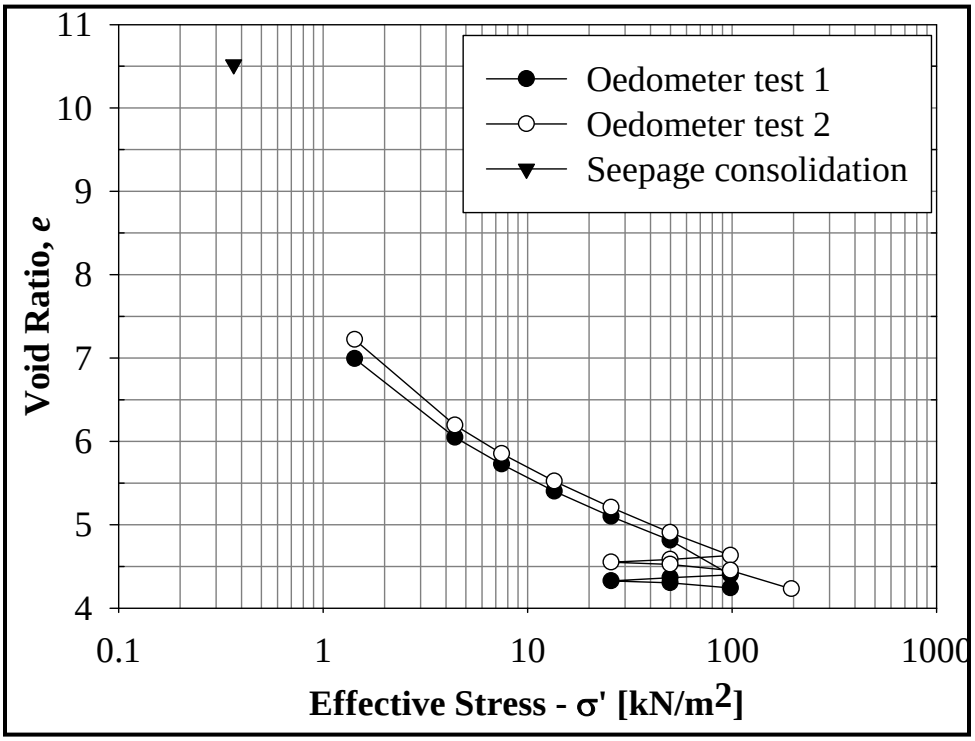

Figure 5.3-14. Consolidation of Cottonwood Bay sediment; void ratio versus effective stress.

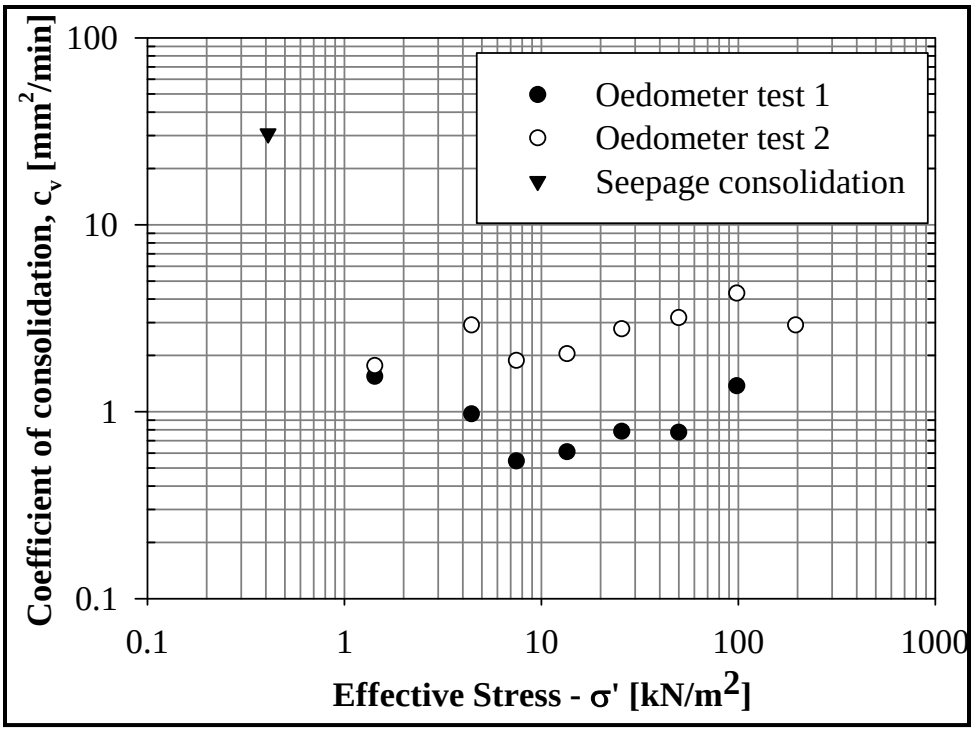

Figure 5.3-15. Coefficient of consolidation of Cottonwood Bay sediment.

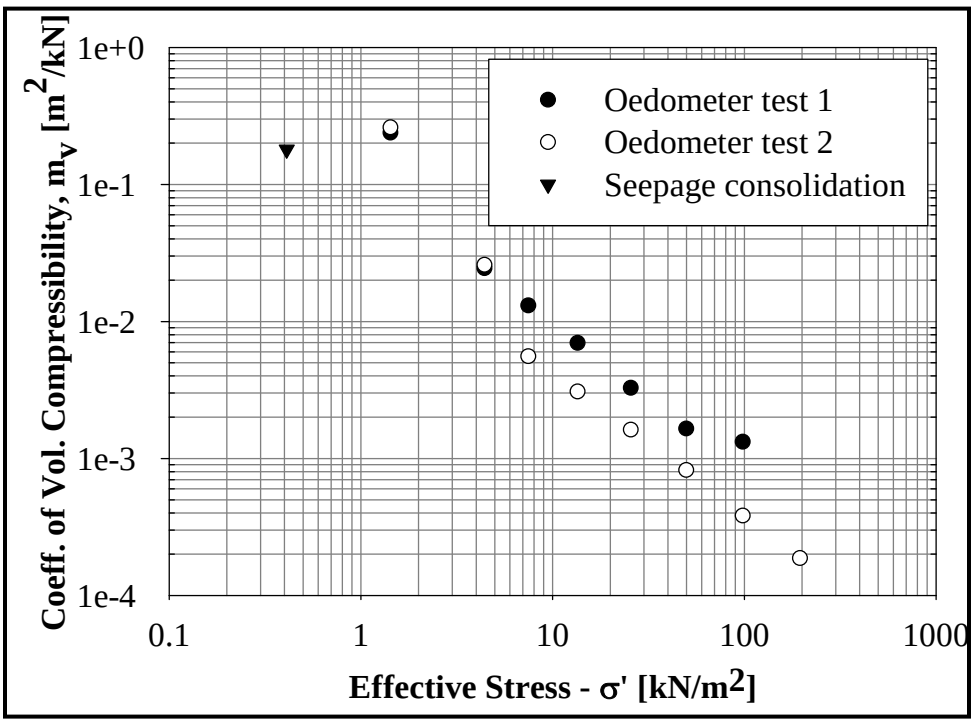

Figure 5.3-16. Coefficient of volumetric compressibility of Cottonwood Bay sediment.

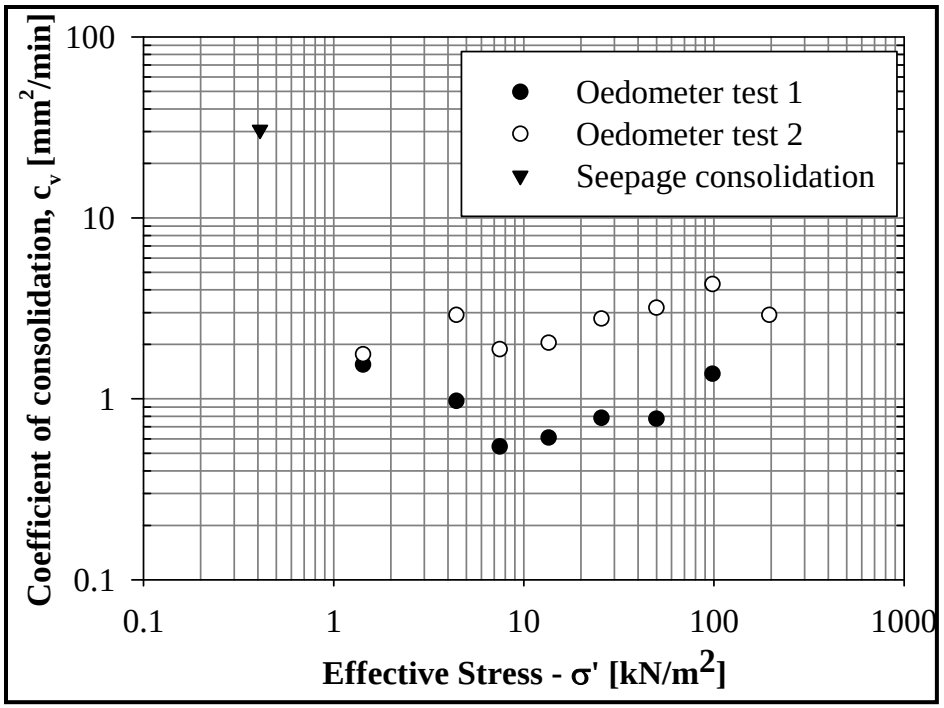

Figure 5.3-17. Variation in coefficient of consolidation with void ratio for Cottonwood Bay sediment.

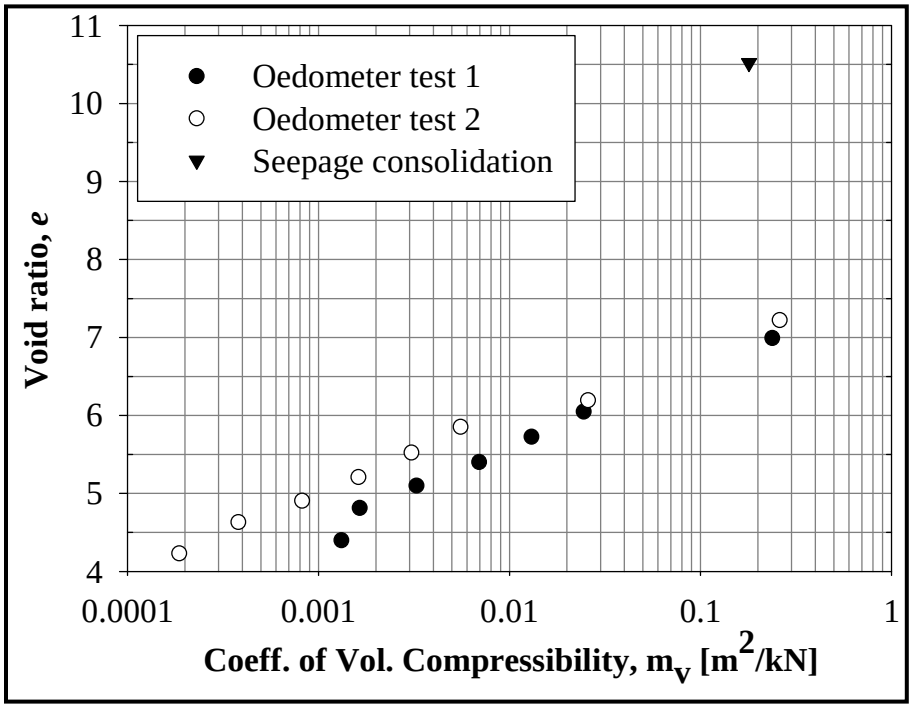

Figure 5.3-18. Variation in coefficient of volumetric compressibility for Cottonwood Bay sediment.

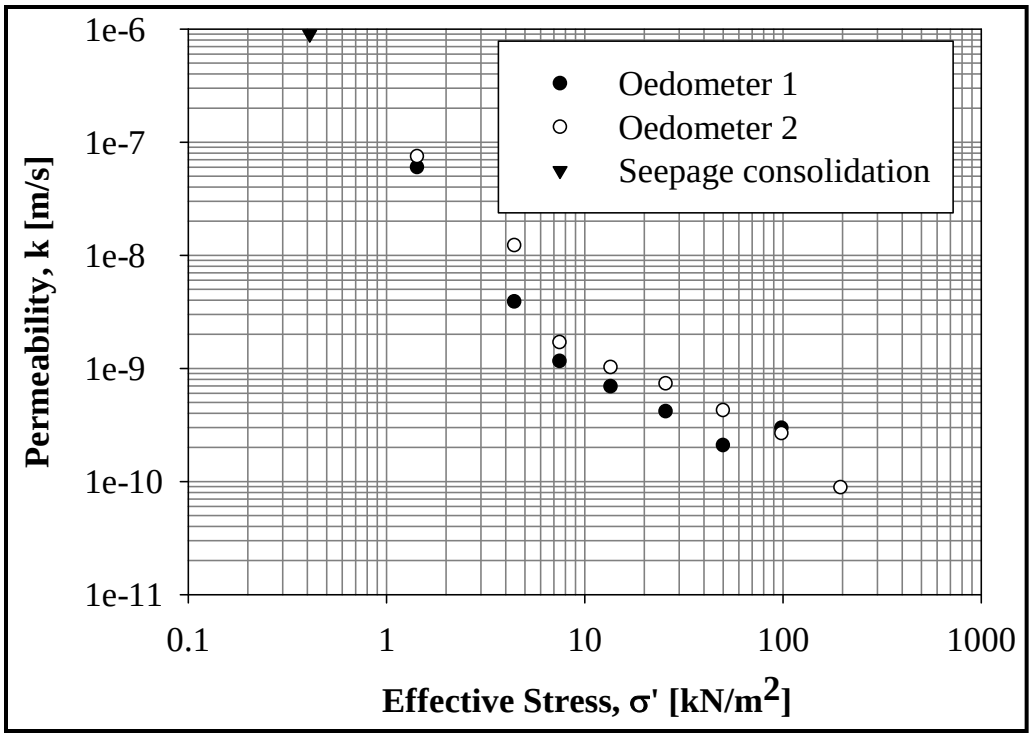

Figure 5.3-19. Permeability versus effective stress for Cottonwood Bay sediment.

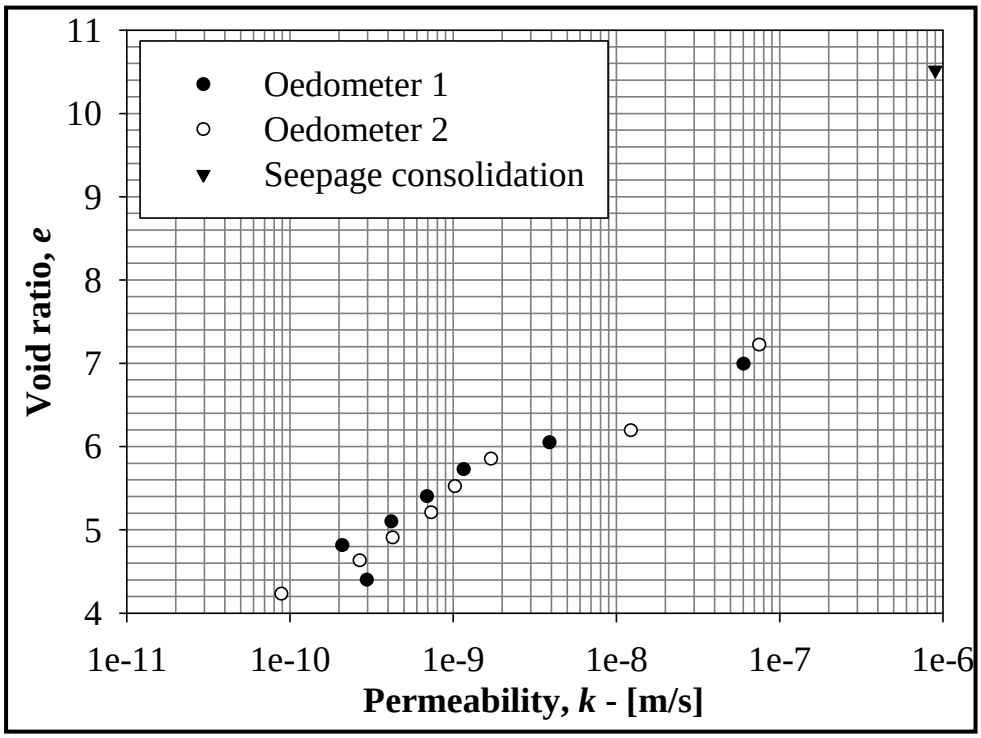

Figure 5.3-20. Void ratio versus permeability for Cottonwood Bay sediment.

5.3.4 Finite Element Analysis

Finite element analyses conducted for this project incorporated various geotextile components to assess increasingly sophisticated deformation and porewater pressure scenarios beyond the basic sand cap investigated in the preliminary models discussed in the First Year Annual Progress Report (NAVFAC 2006). Final results from the various finite element models generated using PLAXIS v8.0 software are presented in the following sub-sections.

Uncoupled Consolidation Model. The uncoupled consolidation model computed the *in situ* stress state of the underlying sediment assuming no steady state or transient groundwater flow. Figure 5.3-21 below shows how the excess pore pressure dissipates with time for this model and that 90% of the consolidation occurs at 400 days, while the 95% consolidation is reached after 600 days.

Confirmation of this curve can be performed by comparing the pressure induced by the mat and the maximum excess pore pressure beneath the sediment through the following equation:

$$ExcessPP = \gamma' \cdot thickness_{mat} = (17 - 9.81)\frac{kN}{m^3} \cdot 0.3m = 2.1\frac{kN}{m^2}$$

The slight difference (2.0 vs. 2.1) is due to stress redistribution.

At the end of consolidation the corresponding displacements can be computed to find the total settlement caused by the potential mat deployment. Figure 5.3-22 below shows the final settlement of the sediment after 600 days and 95% consolidation.

Results indicate that a maximum sediment compression of 9.58 cm occurs beneath the mat. Because the consolidation time estimates are based on a linear stress-strain relationship and assume a constant permeability for the entire model over time, they should be evaluated according to these limitations. Results also show that outside the mat area the maximum displacements of the sediment are nearly 20% and less of the maximum value is caused by the mat deployment.

Figure 5.3-23 shows a horizontal profile of the maximum sediment displacement across the entire uncoupled consolidation model. The maximum settlement occurs directly beneath the mat at nearly 7 m from the mat edge and is constant towards the inside of the mat. The settlement on the sediment surface rapidly decreases beyond the mat edge and reaches a zero displacement at 6.5 m outside the mat limits. The volumetric strain of the sediment serves as an indicator of the area affected by the mat deployment.

Figure 5.3-24 below shows the volumetric strain distribution in the uncoupled model after 95% consolidation. This distribution is similar to the void ratio distribution when the volume of solids is constant. The maximum volumetric strain is 0.98%. These results indicate that the sediment directly below the mat has a final volumetric strain between 100% and 50% of the maximum strain induced by the mat deployment. Due to the soft nature of the material, the uncoupled consolidation model shows that sediment directly beneath the mat is displaced by compressive

effects similar to punching shear effects in foundation design. The pore water displaced by these consolidation effects will occur mainly in the sediment area directly below the mat.

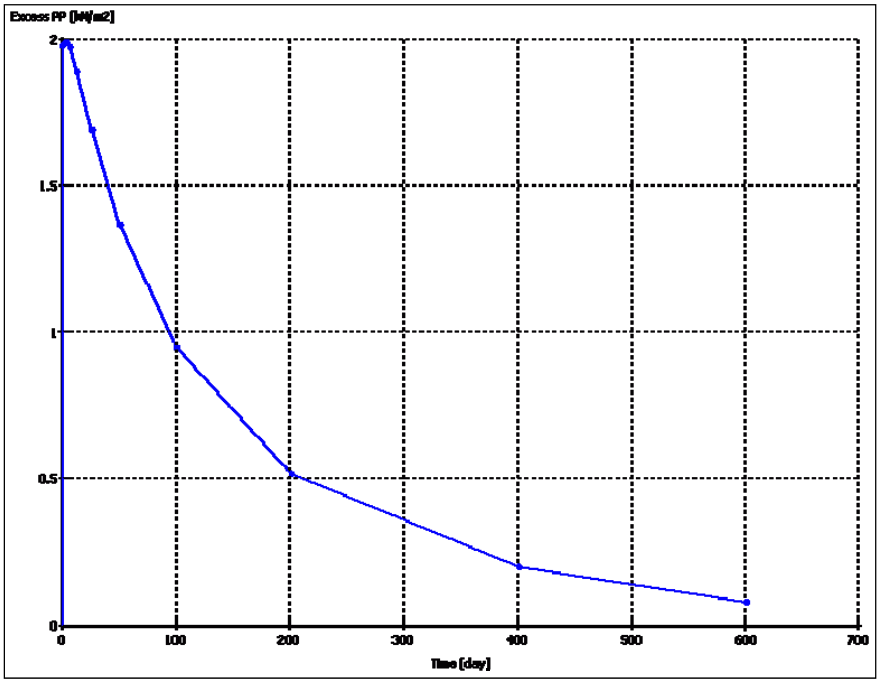

Figure 5.3-21. Excess pore pressure dissipation in the underlying sediment for the uncoupled consolidation finite element model.

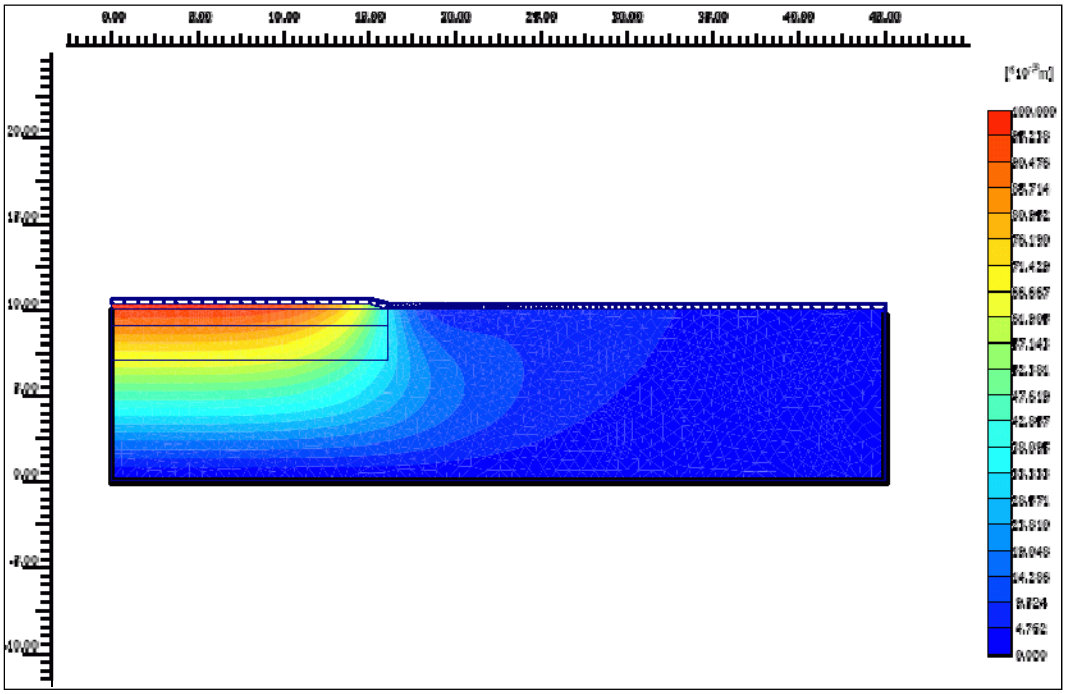

Figure 5.3-22. Settlement due to mat deployment after 95% sediment consolidation under the uncoupled model.

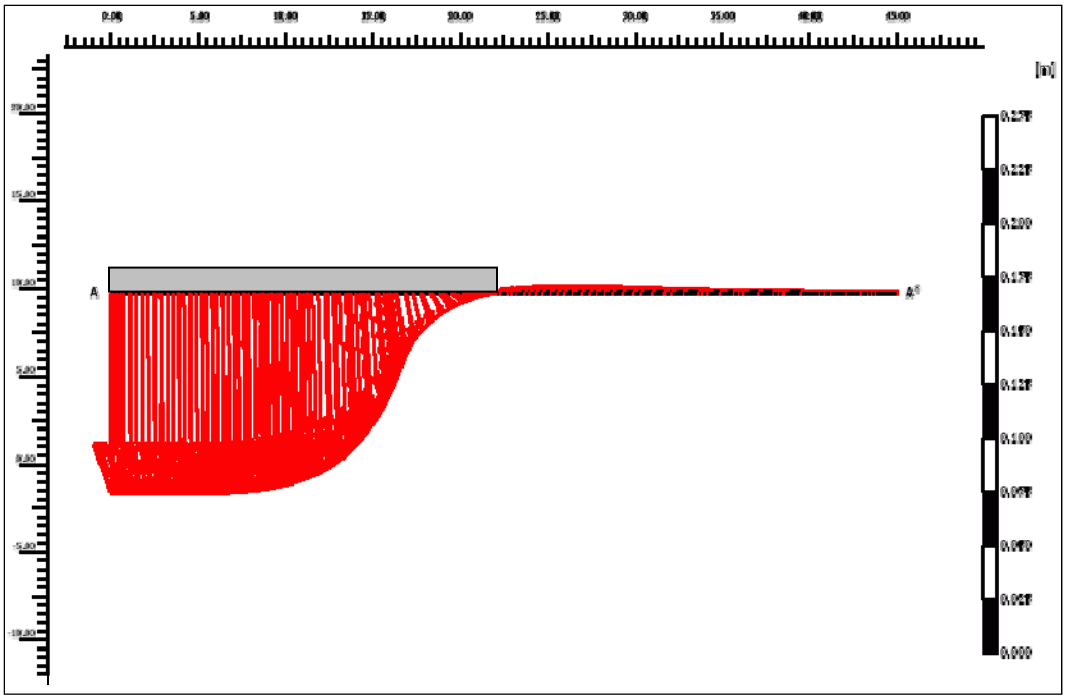

Figure 5.3-23. Horizontal profile of maximum sediment displacement under the uncoupled consolidation model.

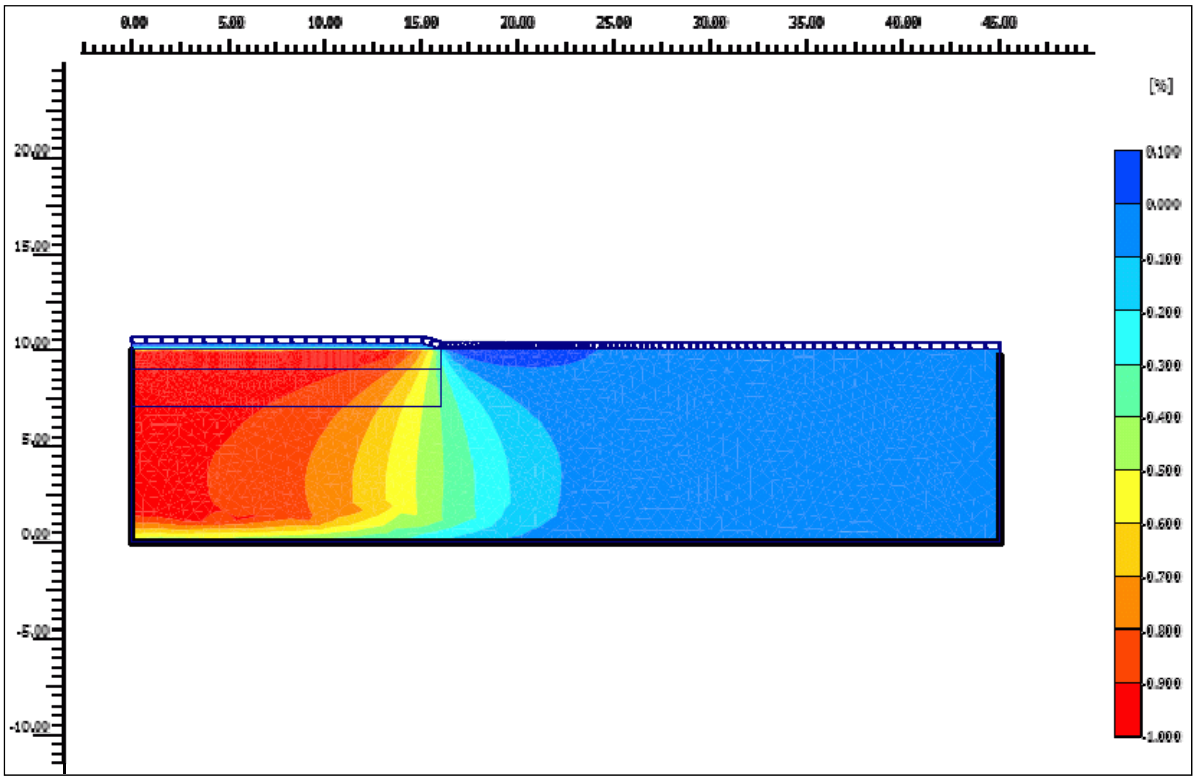

Figure 5.3-24. Volumetric strain after 95% consolidation under the uncoupled consolidation model.

Uncoupled Seepage Model. The uncoupled seepage model assessed potential changes in groundwater flow properties following mat placement for both unclogged and clogged geotextiles. Figure 5.3-25 shows the total water pore pressure distribution for both clogging scenarios. Results indicate that despite having a clogged mat on the second model, the flow of water still moves through the mat albeit at slower rates as shown by the increase in separation between contours from the clogged to the unclogged case. The increase of separation between successive contours indicates lower hydraulic gradient and thus lower seepage velocity. The region near the mat edge shows that the flow is slightly deviated from crossing the mat perpendicularly when the mat is clogged. This result may be of particular interest in selecting the overall extension of the final mat design.

The specific discharge computed for any cross section gives the total water discharge flowing through that section of the model. Figure 5.3-26 shows the specific discharge distribution for both the unclogged and clogged scenarios corresponding to the combined XY direction discharge.

Assuming that 100% of the groundwater flows in the upward direction at the mat deployment site, 35% of the total flow in this model passes through the mat for the unclogged condition. This fraction is slightly reduced to 31% for a clogged mat, thus indicating that ~4% of the groundwater flow was deviated from its original path. It should be noted, however, that the average magnitude of the discharge does not vary significantly from the unclogged to the clogged mat condition and still averages approximately 36-40 m^3/day outside the mat area. The specific discharge distribution varies because the overall boundary conditions change after the mat clogs, but the percentages of groundwater flow moving through and around the mat do not vary significantly.

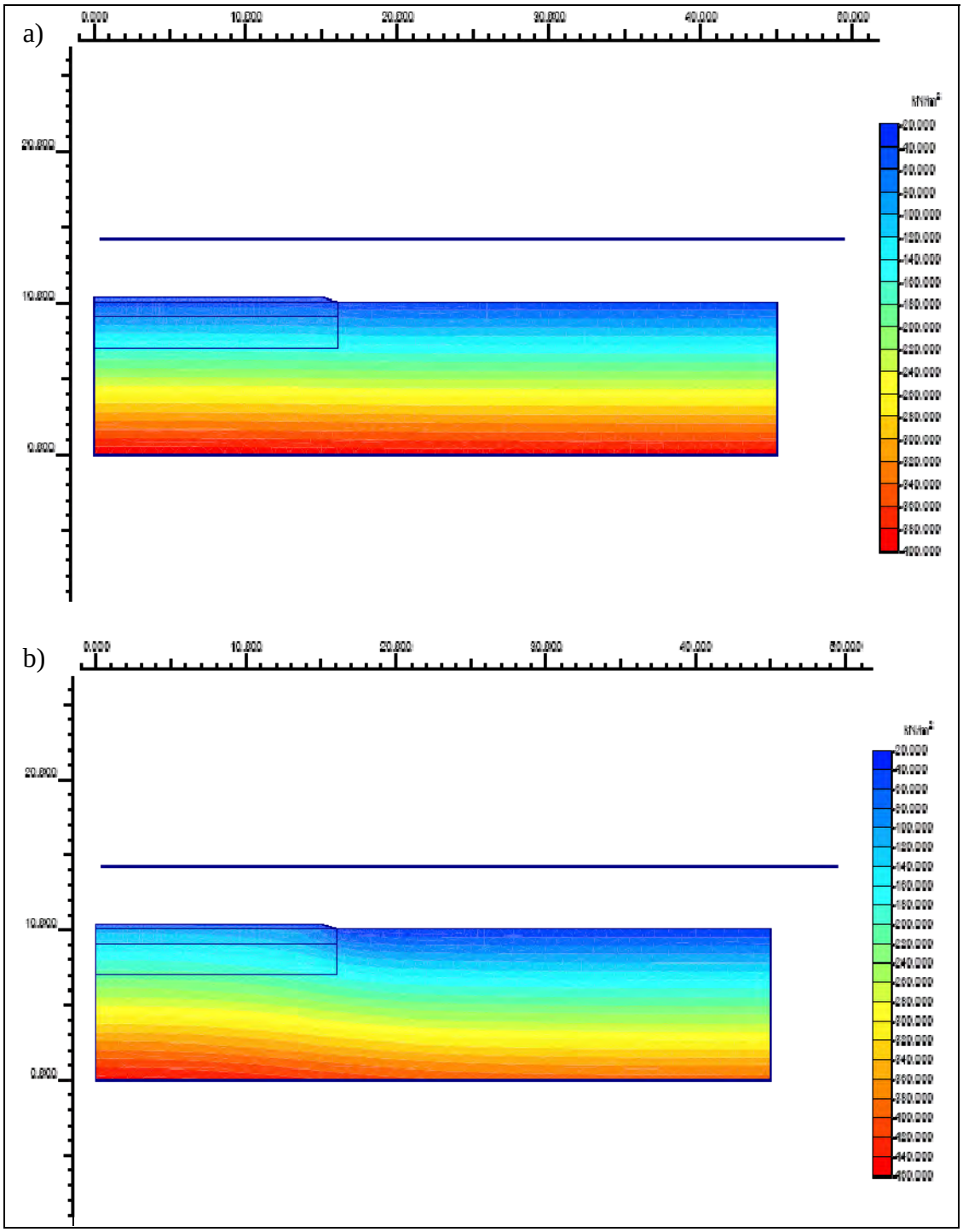

Figure 5.3-25. Total water pore pressure for an unclogged mat (a) and a clogged mat (b) under the uncoupled seepage model.

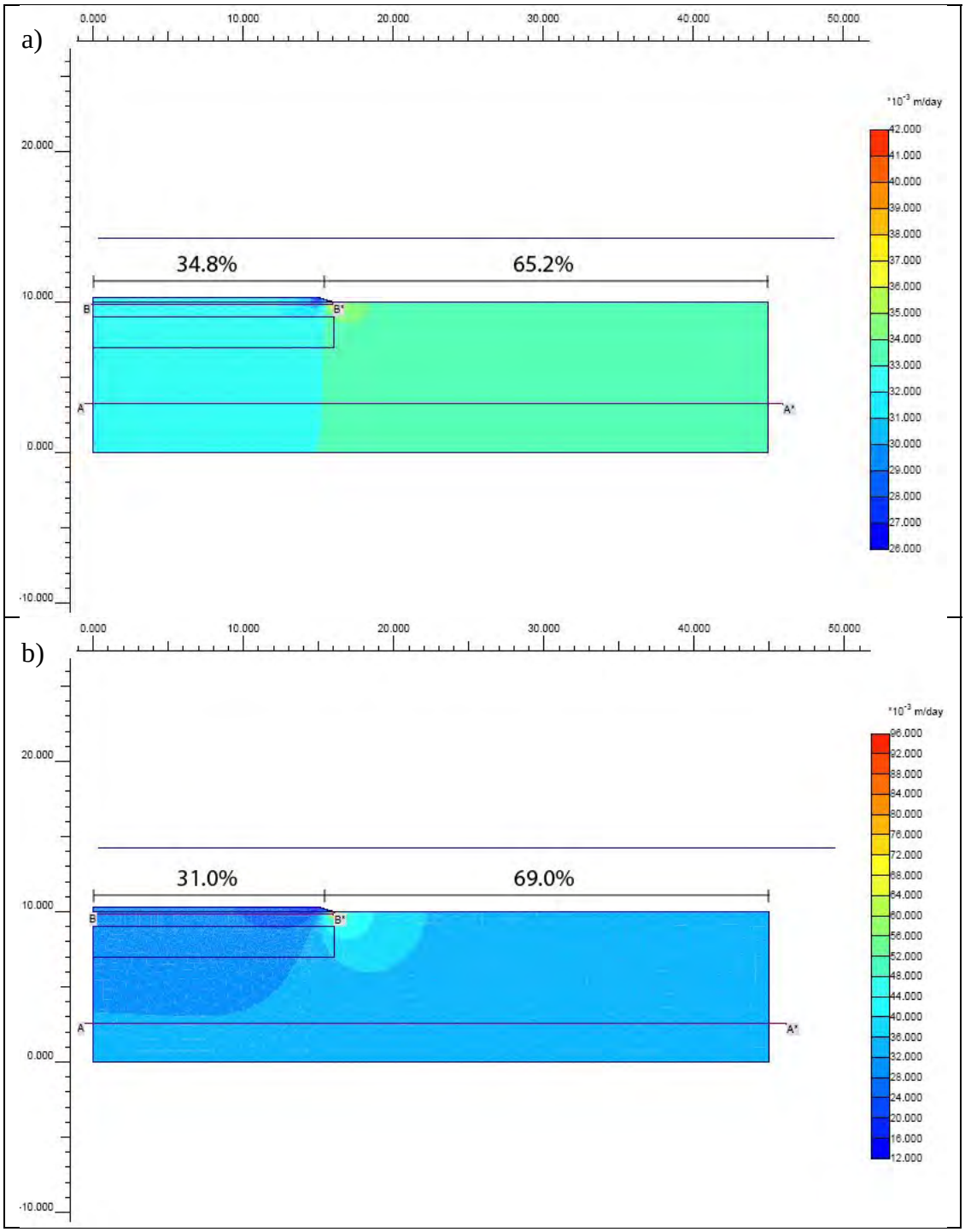

Figure 5.3-26. Specific discharge for an unclogged mat (a) and a clogged mat (b) under the uncoupled seepage model.

Coupled Model. The coupled model merges potential sediment consolidation and groundwater seepage conditions, essentially combining the two uncoupled models, by applying sequential parameters that first define the initial sediment stress caused by mat deployment followed by application of a groundwater flow component that results in a new sediment stress state. Figure 5.3-27 shows the final displacement distribution due to mat deployment under the coupled model.

The maximum displacement for the coupled solution is 9.87 cm, which is close to 9.58 cm obtained without including the groundwater flow in the uncoupled consolidation solution. The 3% increase is the result of the sequential groundwater flow parameter being added following initial sediment consolidation in the coupled solution.

Figure 5.3-28 shows a horizontal profile of the maximum sediment displacement across the entire coupled model. The small increase of the estimated maximum settlement compared to the uncoupled consolidation model and shown in the previous figure does not significantly affect the shape of the settlement profile. The maximum displacement of the mat still occurs 7 m from the edge and remains constant towards the inside of the mat.

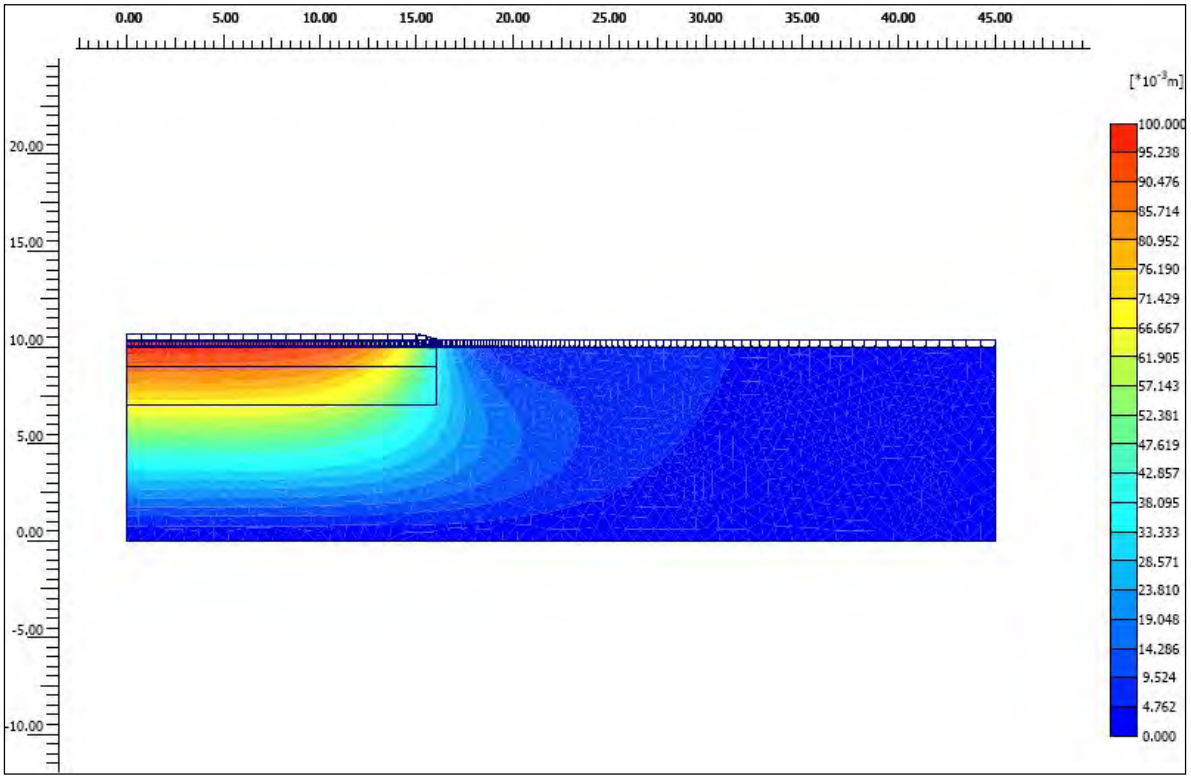

Figure 5.3-27. Sediment settlement due to mat deployment under the coupled model.

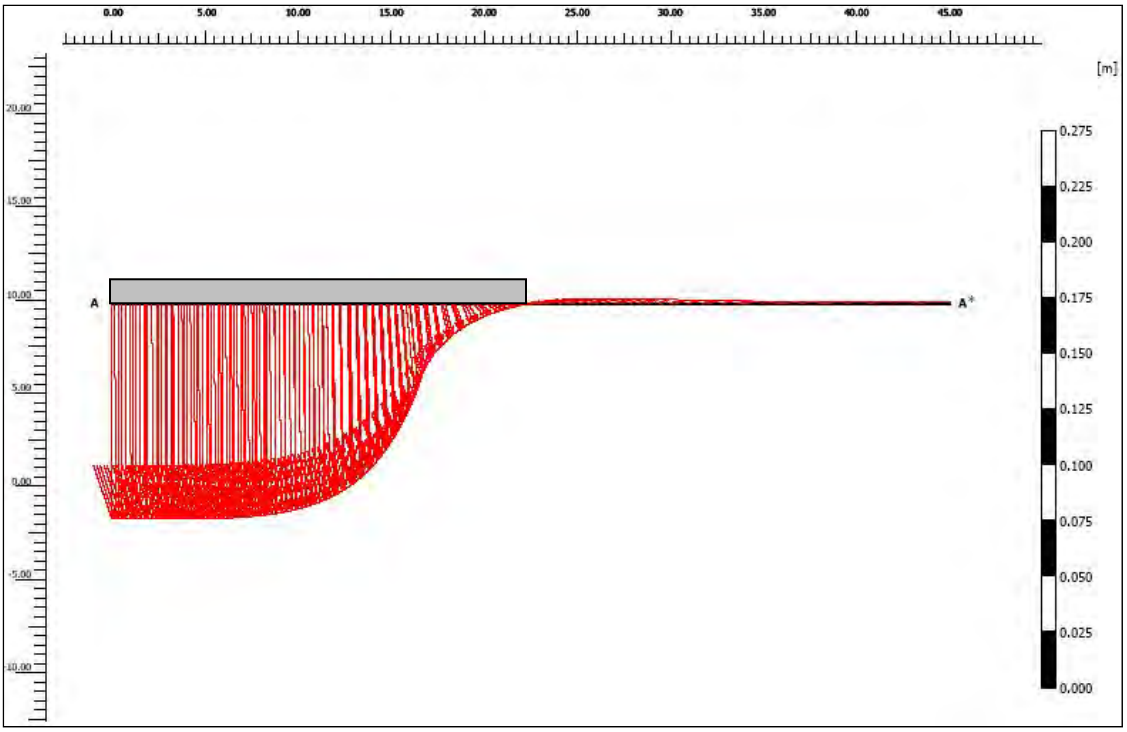

Figure 5.3-28. Horizontal profile of the maximum sediment displacement under the coupled model.

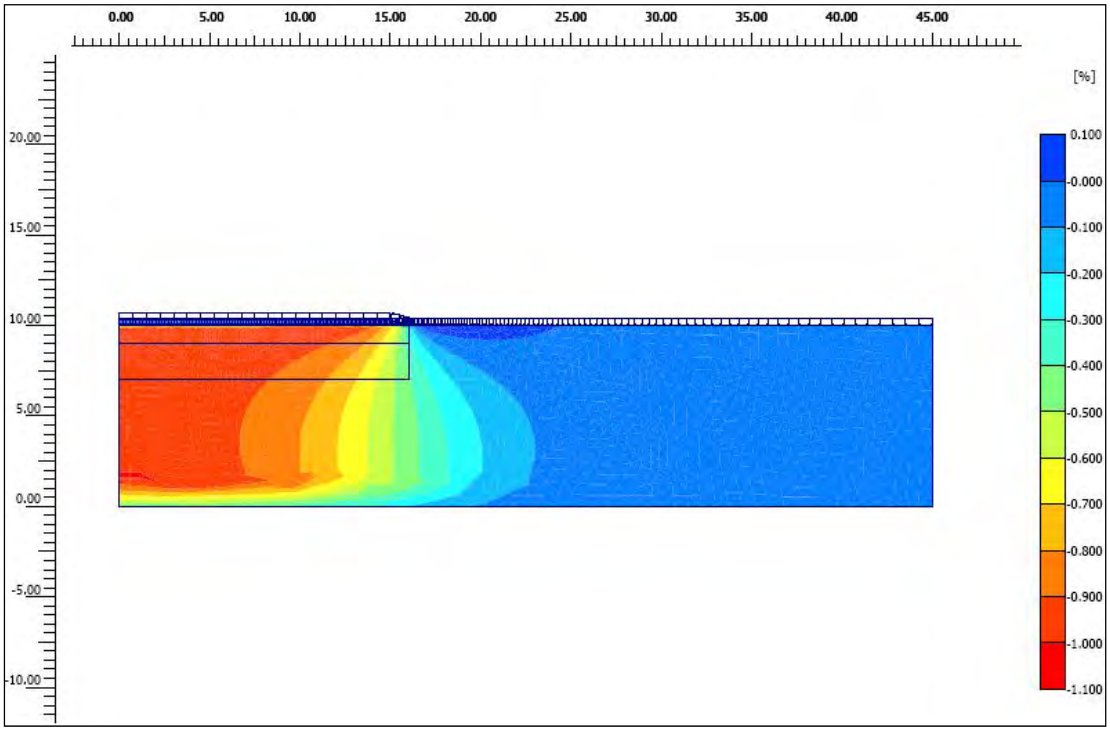

Figure 5.3-29. Volumetric strain under the coupled model.

The volumetric strain distribution for the coupled model is presented in Figure 5.3-29. The maximum volumetric strain was found to be 1.03% for the coupled solution as compared to 0.98% for the uncoupled consolidation solution. The estimated final volumetric strain increases 5% from the uncoupled to the coupled solution. Because the sediment and mat permeabilities as well as the flow rate and water level are constant throughout the coupled solution, there is no change in the amount of flow passing through and around the mat. Similar specific discharge results as the uncoupled seepage model (Figure 5.3-25) are expected for the coupled model when the sediment permeability is varied according to the consolidation tests results.

Summary. Overall results from the FEA process indicate that the soft nature of the underlying sediment will result in significant compression directly beneath the mat following deployment. The porewater displacement caused by this consolidation will be confined mainly to the sediment directly below the mat and a relatively low level of geotextile clogging will not significantly alter groundwater flow patterns. Model results show that a permeability decrease of several orders of magnitude would be required to greatly impact groundwater flow, but this level of clogging is not expected under field conditions based on the results of the gradient ratio testing. Data collected from laboratory tests to be performed on the field weathered small-scale test mats following retrieval will ultimately be used to refine both the uncoupled and coupled finite element models with real permeability data rather than clogging assumptions. The FEA does not favor selection of any particular geotextile at this stage.

Seepage Consolidation Testing. Continued low stress sediment consolidation tests were performed during year three on unweathered geotextiles in order to provide compression curves (e vs. σ') that indicate a reduction of the void ratio as effective stress increases. Nevertheless, permeability tests carried out at each sediment load increment show an inverse behavior, essentially increasing permeability with a decrease in voids. This result indicates seepage along the wall of the cylinder due to radial consolidation. A solution is currently being developed to remedy the seepage problem. A seepage consolidation test has been running for 43 days with favorable results in that wall seepage has not been observed after data reduction.

Consolidation Modeling. Results of the consolidation modeling are provided in Appendix C. Figure C-1 shows the geometry of the 2D model and Table B-1 lists the geotechnical properties used to define the Modified Cam-Clay model. Figure C-2 shows the excess pore pressure profiles during consolidation along the center of the model. The results indicate that 90% of the consolidation process would occur within 120 days of mat deployment.

The settlement of the sediment surface along the mat during consolidation is presented in Figure C-3. The results show uniform settlement of 1.5 cm within the capped area and that most of the sediment distortion occurs within 0.5 m of the border of the mat. The voids within the soil mass are squeezed during the consolidation of the soft sediment.

Figure C-4 shows the rate of water expulsion from the sediment into the water column and along the mat surface during consolidation. The results show that after nearly 10 days of consolidation the magnitude of water flow from the sediment is reduced by two orders of magnitude from its maximum initial value.

Groundwater Flow Modeling. Results of the groundwater flow modeling are also provided in Appendix C; Figure C-5 shows the geometry of the 2D model. The USACE recommends limiting the GR-value of geotextile-soil systems to 3.0 for filtration applications. Replacing GR = 3.0 in the definition of the GR value given by the ASTM standard and using Darcy's law leads to the following definition of clogging in terms of the permeability of the sediment and the sediment-geotextile interface:

$$k_{\text{Sediment}-\text{Geotextile}} = 0.33 \cdot k_{\text{Sediment}}$$

Table B-2 lists the permeability of the soft sediment (measured using the falling head test) and the permeability of the reactive core mat layer used to simulate different degrees of geotextile clogging. The results of the simulations are better represented by the contours of pressure head (meters of water) and the flow paths of water beneath the reactive mat. These results for the five simulations listed are presented in Figure C-6 to C-11.

The results in Figure C-8 show that even a two orders of magnitude reduction of the geotextile permeability does not significantly affect the direction of the flow paths, and the majority of the water still flows through the reactive core mat. A significant deviation of the flow paths is observed in Figure C-9 when the geotextile permeability is three orders of magnitude less than the sediment permeability.

The amount of water actually passing through the mat can be obtained by integrating the water velocities along the mat and assuming a 1 m thickness of the model. The volume of water crossing the reactive core mat for the different clogging scenarios is shown in Figure C-11.

The results shown in Figure C-11 also indicate that the reduction of water flow under USACE clogging conditions (GR = 3.0) is not significant (less than 1%). A 50% reduction of the flow crossing the reactive core mat occurs when the permeability of the geotextile is about 0.004 of the sediment permeability, and a 75% reduction when the mat permeability is 0.001 of the sediment permeability.

In addition to field evaluation, Task 3 also included gradient ratio testing to evaluate geotextile flow properties under laboratory conditions as well as a finite element analysis to evaluate sediment deformation and porewater pressure increases caused by the weight of a potential reactive mat. Preliminary flow-through column experiments were used to evaluate flux for three stock geotextiles and one unweathered organoclay mat by closely mimicking expected processes in the field, thus providing baseline data to which the results of similar testing on the recovered small-scale geotextile mats can be compared.

5.3.5 Gas Permeability Testing

During the course of the geotextile gas permeability testing described in Section 4.3.4, images of the state of the bubble underneath the geotextile were taken daily until the gas bubble had completely disappeared either by flow through the geotextile, by dissipation in the water or by a combination of both mechanisms. Table 5.3-2 below lists the approximate daily volume of the gas bubble during the test and Figure 5.3-30 shows the most detailed images taken at day zero

and day twelve of the experiment. These pictures were taken approximately from the same distance, which allows a rough estimation of the bubble volume over time by comparing the initial dimensions to subsequent observations. Figure 5.3-31 shows a graph of the measured bubble volume during the test with the best exponential fit to the data.

Table 5.3-2. Approximate gas bubble volume over time during the gas permeability test.

Day	Volume of gas bubble [cm^3]
1	1.000
2	0.990
3	0.990
4	0.830
5	0.800
6	0.730
7	0.550
8	0.450
9	0.290
10	0.200
11	0.110
12	0.100
13	0.040
14	0.010
15	0.001

Figure 5.3-30. Biogas bubble flow/dissipation at Day 0 (left) and Day 12 (right) of the gas permeability test.

Gas was flowing/dissipating during this experiment over an area of nearly 2 cm^2 (the initial bubble had a volume of 1 cm^3 and an average thickness of 0.5 cm). The rate of gas flow/dispersion over time per square meter of geotextile was then obtained from the volume versus time fitted curve and normalized to the square meter of geotextile. The rate of gas flow/dispersion over time per square meter of geotextile is shown in Figure 5.3-32.

The rate of gas flow/dissipation was found to vary over time from 3000 to 100 cm^3/day per square centimeter of the fine AOS 170 geotextile. This result indicated that the volume of the gas bubble affects the rate of gas flow through the geotextile and it is possible that the greater buoyant force from the bubble on the geotextile at the beginning of the experiment promotes a greater gas flow rate passing through the geotextile. However, this buoyant force must be compared to the submerged weight of the potential reactive mat to prevent overturning of the system.

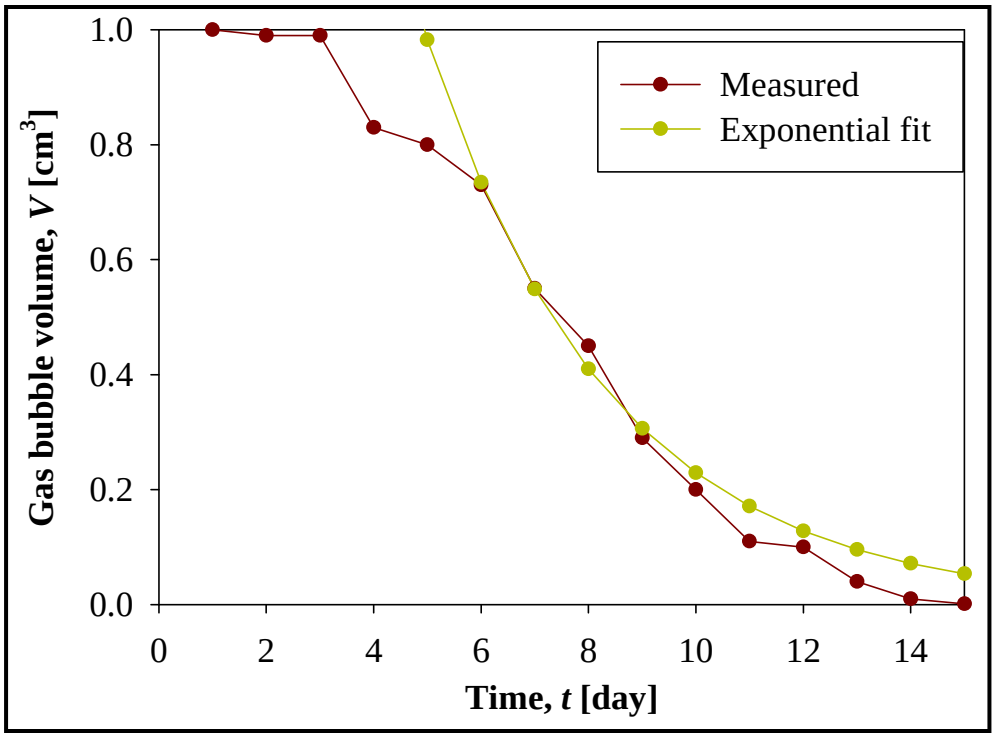

Figure 5.3-31. Volume of the gas bubble beneath the geotextile versus time.

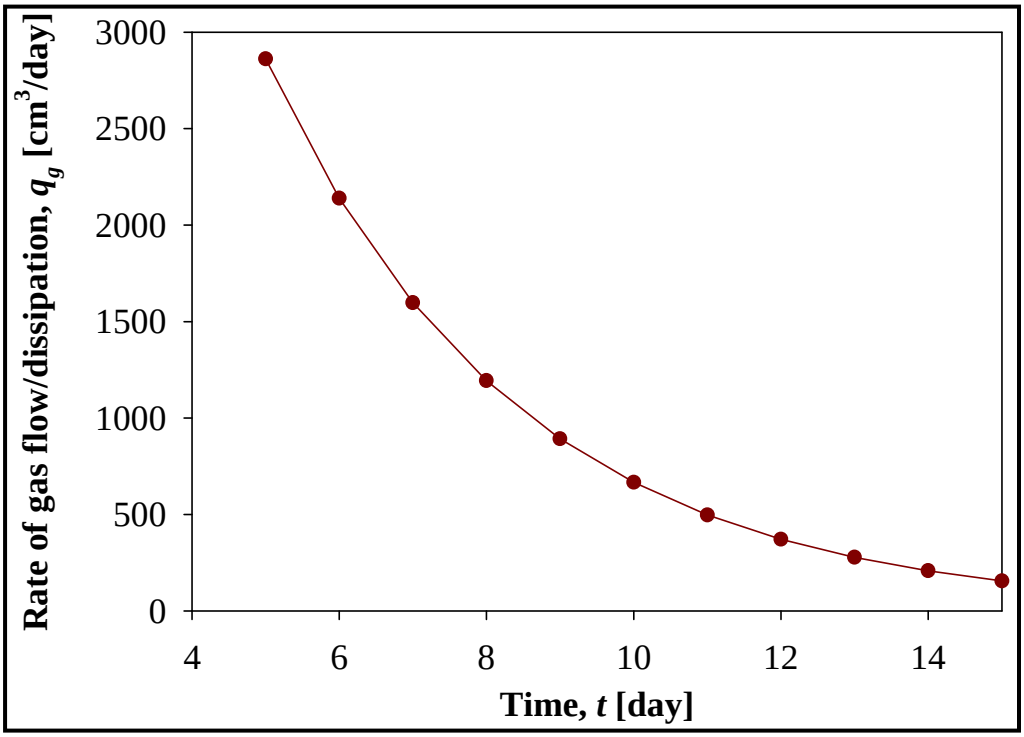

Figure 5.3-32. Flow/dissipation rate of gas versus time per square meter of geotextile.

Comparing the peak gas flow/dissipation rate measured for the heaviest and finest geotextile (AOS 170, 8 oz/yd^2) shown in Figure 5.3-32 (3000 cm^3/day) to the maximum freshwater sediment gas production rates reported in the literature (up to 2640 cm^3/day) (Qingzhong *et al*. 2007) showed that gas accumulation beneath the geotextile is not expected to represent a main hazard to the stability and integrity of a geotextile deployed over sediment under the assumed conditions as long as there is a sand/sediment protective layer providing additional weight to the cap. Reactive core mats used for full-scale implementation are expected to be built using geotextiles with a coarser opening size (AOS 70 to 80), which would transfer gas even faster compared to the geotextile tested in the laboratory gas permeability experiment (AOS 170). Therefore, the rate of gas flow/dissipation in the field is expected to be greater than the values presented above, which would provide an additional margin of safety to the structural integrity of the mat system independent of the weight of a potential sand cap. Regardless, a sand cap component should still be included even with a coarse geotextile to ensure ultimate stability of the system.

In the case of the small test mats deployed in Cottonwood Bay without an overlying sand layer, field observations indicated that the initial buoyant force generated by gas buildup were sufficient to lift the mat, particularly for the finest geotextile (AOS 170). As this gas buildup eventually dispersed over time and further gas production decreased with decreasing temperature, the test mats ultimately returned to the lake floor during the winter months. Similar conditions occurred at the larger prototype mat system, with gas buildup and mat lifting being observed in the summer at the two mat areas without an overlying sand layer (T1 and T3). When compared to these two treatments, the gas buildup and mat lifting at the mat with sand cap area (T2) was found to be negligible, thus confirming the laboratory conclusions stated above.

5.4 Task 4: Prototype Mat Testing

The purpose of Task 4 was to field test a prototype mat system in order to assess *in-situ* chemical sequestration effectiveness and flux properties of various reactive mat/sand cap arrangements.

The final design specifications for the prototype mat system are discussed in Section 4.4.1. This mat system was deployed in April 2008 following the methodology described in Section 4.4.2. Following successful deployment, confirmation and monitoring events in the form of geophysical surveys, passive contaminant sampling (two rounds), groundwater flow surveys, sediment coring and sediment cap sampling were conducted to evaluate the success of the various mat/cap treatments in achieving overall project goals. The analytical results of these individual tasks are provided in the following sub-sections and referenced to the appropriate appendices.

5.4.1 Geophysical Investigation

Final images from the prototype mat system confirmatory geophysical investigation are presented in Appendix D. Raw side-scan sonar, bathymetry and sub-bottom data were processed to provide a pictorial view of the prototype mat system area and the post-cap surfaces.

Side-Scan Sonar. The final side-scan mosaic produced a clear planview image of the prototype mat system layout and identified the acoustic signature unique to this type of geotextile (Appendix D, Figure D-1). The side-scan data also confirmed the horizontal distribution of sand capping material (dark patches with a different reflective signature), thus allowing for an evaluation of the success of sand placement techniques in construction goals. Sand capping material settled in areas T2 and T4 over the desired width of the treatment.

Bathymetry. Bathymetry data for the prototype mat system indicated that water depths ranged from 4.5 ft to 5.8 ft at the time of collection (December 2008), with 5.0 ft deep areas directly over the mats and deeper areas generally to the north (Appendix D, Figure D-2). However, deeper points (5.6-5.8 ft) were also present underneath the mats in areas T1 and T3, which may represent local sediment depressions.

Sub-Bottom Profiling. Sub-bottom profiling data for the prototype mat system indicated that the isopach depth below the sediment-water interface (*i.e.*, thickness) of the uppermost sediment layer ranged from 0.2 ft to 1.25 ft (Appendix D, Figure D-3). Points of decreased sediment layer thickness (0.20-0.25 ft) in areas T1 and T3 may provide evidence of localized variability in depositional history.

Sediment Profile Imaging. Visual analysis of the SPI images taken at the prototype mat system allowed for an evaluation of sediment buildup on the mats, confirming sand capping thickness in appropriate areas, and a description of control area conditions. By definition, the use of the SPI measurement method was limited in areas T1 and T3 because the camera prism could not penetrate the geotextile mats in these mat only treatments. Thus images from these areas depicted only conditions on the mat surfaces at six months. In contrast, images from areas T2, T4 and T5 were able to depict sediment cross-sections above the mats or natural substrate, thus confirming the vertical distribution of sand capping material to confirm what had previously been documented by diver observations.

The SPI images from each mat treatment area included the following notable features after six months of soak time:

- **T1 (Single Mat Only)** – Substantial natural sediment buildup, biofilm formation or capping material overflow deposited on top of the single layer mat in a non-capping area (Appendix D, Figure D-5).
- **T2 (Single Mat with Sand Cap)** – Sand capping thickness >2" over the single layer mat; apparent redox potential discontinuity (RPD) depth (*i.e.*, the depth of oxygen penetration into the sediment indicative of microorganism activity) of approximately 0.23" (Appendix D, Figure D-6).
- **T3 (Double Mat)** – Poor image quality; also likely substantial natural sediment buildup, biofilm formation or capping material overflow deposited on top of the single layer mat in a non-capping area (Appendix D, Figure D-7).
- **T4 (Sand Cap Only)** – Sand capping thickness of approximately 1.85" before mixing of cap material with natural tan and gray soft mud; apparent RPD depth of approximately 0.85" (Appendix D, Figure D-8).

- **T5 (No Treatment/Control)** – Some capping material overflow present above the natural tan and gray soft mud; apparent RPD depth of approximately 0.58" (Appendix D, Figure D-9).

The fact that the apparent RPD depth was two times greater in the T5 control area and four times greater in the T4 capping only area than in the T2 mat capping area indicates slightly diminished microorganism activity in the engineered substrate when placed over a cap as compared to the natural substrate after six months, but colonization was occurring.

Modeling Verification. Geophysical data collected at the prototype mat system were ultimately compared to the laboratory consolidation testing and finite element analysis results to evaluate the success of these modeling exercises in predicting mat performance in a freshwater, soft-sediment environment. The side-scan sonar mosaic was used to identify the specific mat/sand cap locations via their unique acoustic signature within the general target area. Bathymetry data was collected from the treatment deployment areas both before (July 2007) and after (December 2008) mat placement in order to allow an evaluation of any appreciable changes in bottom topography and water depth that might have occurred due to the placement of the capping materials.

Bathymetry data collected in Cottonwood Bay both before and after mat placement are shown concurrently in Figure 5.4-1. The bathymetry data was corrected to the same hydrographic control point to account for yearly fluctuations in lake water levels and then plotted as specific data points along the survey lanes. Results of the July 2007 bathymetry survey conducted prior to mat placement indicated that the study area was relatively flat with a gradual increase in depth from south to north. Less consistent trends were observed after the mats had been in place for 16 months (Dec 2008), suggesting some disturbance and/or deformation in the natural sediment due to mat placement activities.

The 2007 bathymetry survey was designed to cover the entire placement area in Cottonwood Bay, which resulted in robust survey lanes that did not ultimately pass directly over the future mat treatment areas. Thus the comparison of pre-mat to post-mat changes in bathymetry was not possible. However, the December 2008 survey conducted 16 months after mat placement did reflect changes in elevation due to mats as compared to adjacent non-treatment areas. The placement of the half-inch (1.3 cm) thick mat with an additional three-inch (7.6 cm) sand cap in area T2 would be expected to add 3.5 inches (8.9 cm) of total relief to the ambient surface, assuming solid conditions without compression. In soft substrate such as the conditions experienced in Cottonwood Bay, however, the weight of the mat/sand could exceed the load-bearing capacity of the underlying natural sediment causing compression and therefore subsidence of the mat and sand treatments.

Modeling efforts predicted maximum sediment compression of 9.6-9.9 cm due to consolidation (Section 5.3.3). Post-mat bathymetry data collected at the center of area T2 revealed relief of up to 4 cm above the surrounding sediments one year after mat deployment (Figure 5.4.1). When subtracted from the expected 8.9 cm relief to be caused by the thickness of the mat/sand cap, this finding suggests at actual net sediment compression at this location of approximately 5 cm. Compression of this magnitude is within the expected range as predicted by the model. In

comparison, the sand-only treatment (T4) was uniformly level with the surrounding environment, such that potentially greater consolidation occurred in this treatment than T2.

As far as the mat-only treatments, results were highly variable, with areas of noticeable elevation change up to 20 cm observed in some portions of areas T1 and T3. As the bathymetry survey was conducted during the winter when biological activity is at its lowest, this added relief is not believed to have been caused by gas accumulation lifting the mats off the surface. Instead, the changes were attributed to localized irregularities in the mat surface possibly resulting from a fold or crease in the mat geotextile (which seems apparent from the side scan data) or other sources of roughness caused by monitoring activities (*e.g.*, SPI survey, passive sampler deployment, Trident and Ultraseep survey). The SPI images taken on top of the mats showed sediment accumulation ranging from approximately 0-0.5" (~1.27 cm) for the treatments without a sand cap, thus suggesting relatively negligible impacts of sediment deposition on the topography of the overall mat system. In general the geophysical data revealed changes within the range of modeled expectations and exhibited sufficient sensitivity to be a useful tool for monitoring mat conditions.

With regard to the Trident Probe and Ultraseep groundwater flow data (discussed in Section 5.4.3), the control area showed essentially no flow while the various mat/sand treatments showed approximately 0-3 cm/day. This discrepancy is likely due to the nature of clay sublayers in the natural sediment where groundwater escapes through cracks in a non-uniform manner across the area. A lack of consistency observed at the local mat level makes it difficult to compare the field and model groundwater flow results with any certainty.

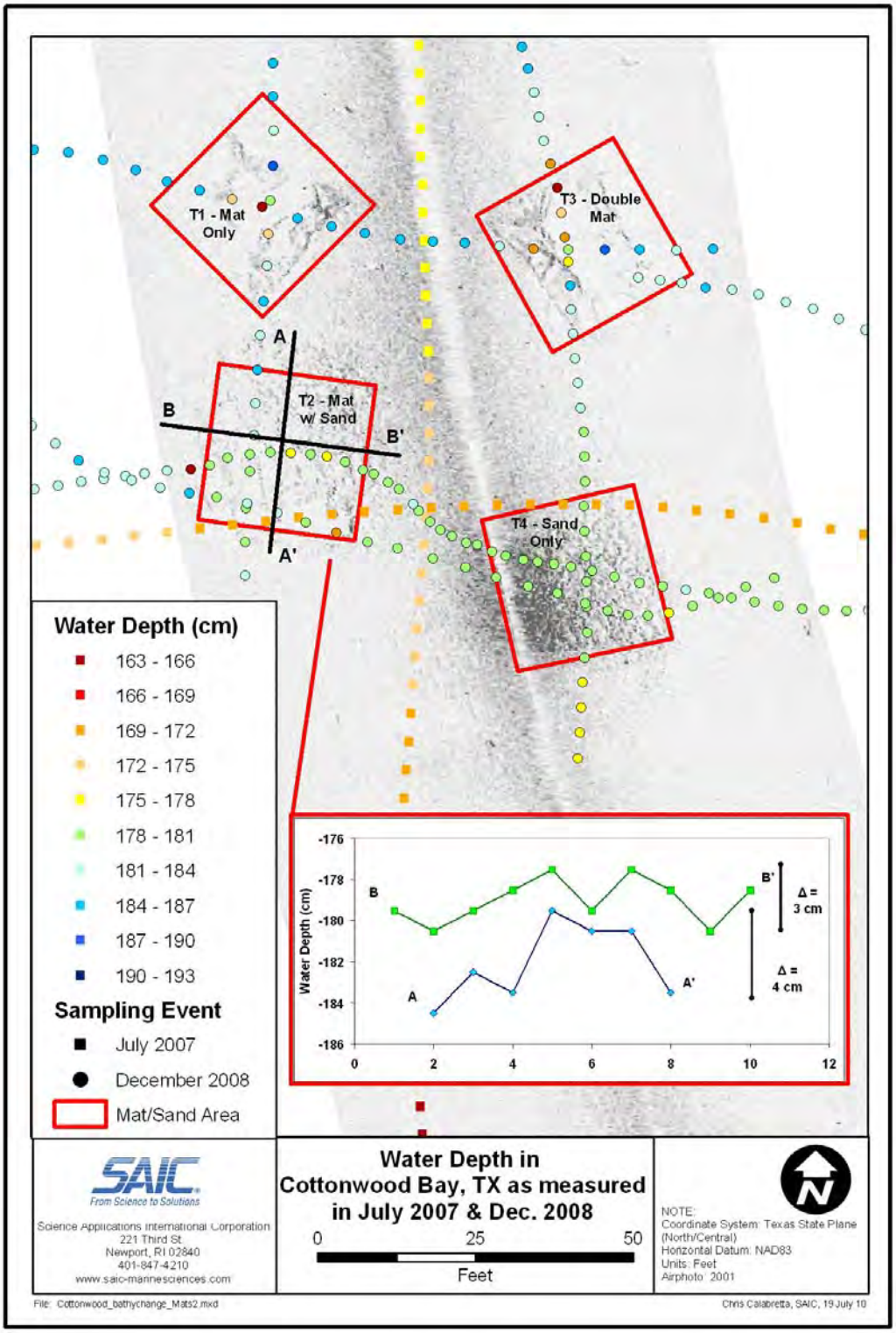

Figure 5.4-1. Water depth comparison in Cottonwood Bay from bathymetry collected both before and after placement of the prototype mat system.

5.4.2 Diffusion Sampling Results

In evaluating the passive sampling data to determine whether the reactive mat technology achieved the project goal of demonstrating significant contaminant reduction across the treatment boundary, a set of conditions was established that must be met for each test parameter in order for the resulting analytical values to be considered relevant and applicable to the effects of the prototype mat system. Data trends that did not meet these conditions were considered artifacts of the test site exhibited independent of the reactive mat influence and the associated analytes were not considered suitable subjects on which to base project conclusions. These test conditions were defined as follows.

- *The analyte must be detected in the below treatment samples*. It is impossible to determine the reduction capabilities of the mat technology on contaminants that are non-detect or otherwise non-existant in the natural sediment environment.
- *The below treatment concentration must be greater than or equal to the above treatment concentration*. In order for sampler data to accurately depict mat effects on contaminant levels at the site based on the known properties of the technology, these data must demonstrate either a contaminant reduction or no change across the treatment boundary. Because the mats themselves, including the reactive core, were constructed from virgin materials, and only clean material was used for the sand cap, the technology did not contribute any contaminants to the test environment. It is therefore impossible for concentrations to increase across the treatment boundary without non-treatment influences, which would then make the resulting gradient irrelevant. Contaminants can either be blocked by the mats (concentrations elevated below treatment, non-detect above), sequestered within the mat amendments (concentrations greater below treatment than above) or flow through the mats unimpeded (concentrations equal below and above).
- *The below treatment concentration must be greater than the ambient surface water concentration*. In order for the below treatment samples to demonstrate true contaminant levels in the natural sediment, these concentrations must be independent of the overlying water column prior to encountering the mat technology. A situation in which ambient surface water concentrations were greater than or equal to below treatment concentrations would suggest contributions from outside sources or contaminant dilution within the sediment. The resulting contaminant gradient would then decrease from the overlying water into the sediment opposite of groundwater flow, which would make an accurate assessment of mat effects on flow concentrations impossible.

Peeper Analytical Results. Raw horizontal and vertical peeper analytical results for the prototype mat system collected during the first round (December 2008) and second round (December 2009) of passive contaminant sampling are presented in Appendix E. Analytical results from the three chambers (*i.e.*, sub-replicates) within each horizontal peeper were averaged to produce a single value for that replicate at a particular horizon within a treatment. These three replicate values were then averaged to produce a single summary value for that particular horizon in the treatment. In contrast, analytical results from the fifteen chambers within each vertical peeper were treated as independent values for each discrete horizon, but three replicate values were still averaged to produce a single summary value for that horizon within a treatment.

Prior to performing any calculations, non-detect results were substituted with one half the method detection limit (MDL) following standard USEPA protocol. A summary of the final Year One and Year Two peeper data showing mean results for all non-lithogenic metals of concern at each treatment is presented in Table 5.4-1.

Table 5.4-1. Summary of first year (top) and second year (bottom) peeper mean analytical results for all metals of concern at the prototype mat system.

Year 1 Peeper Results: Metals

		T1 - Mat Only		T2 - Mat w/ Sand		T3 - Double Mat			T4 - Sand Only		T5 - No Treatment
Analyte	Units	Below Treatment	Above Treatment	Below Treatment	Above Treatment	Below Treatment	Between Treatment	Above Treatment	Below Treatment	Above Treatment	Above Treatment
Arsenic	ug/L	20	29	6.9	6.9	29	6.9	6.9	6.9	6.9	13
Barium	ug/L	110	65	98	67	146	47	52	61	58	54
Cadmium	ug/L	2.4	0.99	0.93	1.9	2.2	0.16	0.16	0.16	0.16	0.55
Chromium	ug/L	7.7	3.0	7.7	10	10	2.0	5.5	0.66	0.71	0.65
Copper	ug/L	5.7	2.2	3.4	7.2	2.2	2.1	3.6	1.6	1.7	0.67
Lead	ug/L	19	3.5	3.5	20	5.9	3.5	3.5	3.5	3.5	3.5
Nickel	ug/L	4.2	2.2	8.9	5.1	5.8	1.3	2.2	1.5	1.5	1.6
Silver	ug/L	0.21	0.21	0.21	0.21	0.21	0.21	0.21	0.21	0.21	0.21
Vanadium	ug/L	8.5	3.5	1.8	9.5	7.3	0.76	2.1	0.49	0.49	0.89
Zinc	ug/L	45	8.2	24	47	33	9.3	5.6	2.4	2.5	2.8

Year 2 Peeper Results: Metals

		T1 - Mat Only		T2 - Mat w/ Sand		T3 - Double Mat			T4 - Sand Only		T5 - No Treatment
Analyte	Units	Below Treatment	Above Treatment	Below Treatment	Above Treatment	Below Treatment	Between Treatment	Above Treatment	Below Treatment	Above Treatment	Above Treatment
Arsenic	ug/L	31	6.9	6.9	6.9	42	6.9	6.9	6.9	6.9	11
Barium	ug/L	122	41	104	71	181	43	41	60	55	49
Cadmium	ug/L	1.5	0.16	0.47	0.16	3.5	0.16	0.16	0.74	0.34	0.97
Chromium	ug/L	3.7	1.6	13	1.0	1.8	1.4	1.2	0.39	0.32	0.32
Copper	ug/L	0.4	1.2	1.6	0.82	0.33	0.6	1.1	0.33	0.33	0.33
Lead	ug/L	3.5	3.5	3.5	3.5	4.0	3.5	3.5	3.5	3.5	3.5
Nickel	ug/L	2.6	1.1	3.6	1.9	3.1	1.0	4.6	0.73	0.73	0.73
Silver	ug/L	0.41	0.21	0.8	0.29	0.68	0.21	0.21	0.41	0.21	0.34
Vanadium	ug/L	4.9	0.96	1.6	0.85	6.6	0.62	0.95	0.49	0.49	0.49
Zinc	ug/L	11	3.2	11	4.3	16	1.5	2.2	2.0	1.2	1.2

In order to provide a quantitative basis for evaluating the efficacy of the different mat treatments, hypothesis testing was performed to compare the below and above datasets for each analyte and determine whether any observed reductions were statistically significant. This hypothesis testing consisted of a simple two-sample t-test conducted at the 95% confidence coefficient (alpha = 0.05). The null hypothesis was defined as the above treatment mean being greater than or equal to the below treatment mean (*i.e.*, no treatment effect on contaminant reduction). In contrast, the alternative hypothesis was defined as the above treatment mean being less than the below treatment mean (*i.e.*, contaminant reduction occurred across treatment). A p-value less than 0.05 would reject the null hypothesis and conclude that statistically significant contaminant reduction occurred at the treatment. A p-value greater than 0.05 would fail to reject the null hypothesis and effective treatment by the mats could not be accurately concluded. Each above/below treatment dataset consisted of three peeper replicates with no data points excluded. All hypothesis testing calculations were performed using USEPA ProUCL software and population variances for each dataset were determined automatically within the context of the t-test application, which in turn determined whether the pooled (equal variance) or Satterthwaite

(unequal variance) was selected. The results for the hypothesis testing of each analyte at each treatment are shown in Table 5.4-2.

Table 5.4-2. Results of hypothesis testing to determine the statistical significance of contaminant reductions across treatment boundaries for all metals of concern at the prototype mat system.

Significance Level: Alpha = 0.05
Null Hypothesis: Above Treatment >= Below Treatment (p-value > 0.05)
Alternative Hypothesis: Above Treatment < Below Treatment (p-value < 0.05)

	T1 - Mat Only				T2 - Mat w/ Sand				T3 - Double Mat (Below to Between)			
Analyte	Replicate Variance (n=3)	p-value	Reject Null? (Above < Below)	Conclusion Explanation	Replicate Variance (n=3)	p-value	Reject Null? (Above < Below)	Conclusion Explanation	Replicate Variance (n=3)	p-value	Reject Null? (Above < Below)	Conclusion Explanation
Year 1 Peeper Results												
Arsenic	EQUAL	0.645	NO	b	EQUAL	N/A	NO	a	UNEQUAL	0.174	NO	c
Barium	EQUAL	0.072	NO	c	EQUAL	0.087	NO	c	UNEQUAL	0.084	NO	c
Cadmium	EQUAL	0.170	NO	c	EQUAL	0.693	NO	b	EQUAL	0.106	NO	c
Chromium	UNEQUAL	0.187	NO	c	EQUAL	0.698	NO	b	UNEQUAL	0.112	NO	c
Copper	UNEQUAL	0.254	NO	c	EQUAL	0.789	NO	b	EQUAL	0.421	NO	c
Lead	EQUAL	0.187	NO	c	EQUAL	0.813	NO	a	EQUAL	0.187	NO	c
Nickel	UNEQUAL	0.236	NO	c	UNEQUAL	0.165	NO	c	EQUAL	0.046	YES	d
Silver	EQUAL	N/A	NO	a	EQUAL	N/A	NO	a	EQUAL	N/A	NO	a
Vanadium	EQUAL	0.189	NO	c	UNEQUAL	0.802	NO	b	UNEQUAL	0.142	NO	c
Zinc	UNEQUAL	0.173	NO	c	UNEQUAL	0.687	NO	b	EQUAL	0.092	NO	c
Year 2 Peeper Results												
Arsenic	UNEQUAL	0.211	NO	c	EQUAL	N/A	NO	a	UNEQUAL	0.211	NO	c
Barium	UNEQUAL	0.134	NO	c	EQUAL	0.086	NO	c	UNEQUAL	0.114	NO	c
Cadmium	EQUAL	0.187	NO	c	EQUAL	0.187	NO	c	EQUAL	0.187	NO	c
Chromium	UNEQUAL	0.211	NO	c	UNEQUAL	0.208	NO	c	EQUAL	0.358	NO	c
Copper	EQUAL	0.999	NO	b	EQUAL	0.269	NO	c	EQUAL	0.813	NO	a
Lead	EQUAL	N/A	NO	a	EQUAL	N/A	NO	a	EQUAL	0.187	NO	c
Nickel	EQUAL	0.117	NO	c	EQUAL	0.067	NO	c	EQUAL	0.027	YES	d
Silver	EQUAL	0.059	NO	c	EQUAL	0.034	YES	d	EQUAL	0.001	YES	d
Vanadium	UNEQUAL	0.210	NO	c	EQUAL	0.045	YES	d	UNEQUAL	0.202	NO	c
Zinc	UNEQUAL	0.146	NO	c	EQUAL	0.061	NO	c	UNEQUAL	0.09	NO	c

	T3 - Double Mat (Below to Above)				T4 - Sand Only			
Analyte	Replicate Variance (n=3)	p-value	Reject Null? (Above < Below)	Conclusion Explanation	Replicate Variance (n=3)	p-value	Reject Null? (Above < Below)	Conclusion Explanation
Year 1 Peeper Results								
Arsenic	UNEQUAL	0.174	NO	c	EQUAL	N/A	NO	a
Barium	UNEQUAL	0.092	NO	c	EQUAL	0.326	NO	c
Cadmium	EQUAL	0.138	NO	c	EQUAL	N/A	NO	a
Chromium	UNEQUAL	0.207	NO	c	EQUAL	0.749	NO	b
Copper	EQUAL	0.986	NO	b	EQUAL	0.565	NO	b
Lead	EQUAL	0.187	NO	c	EQUAL	N/A	NO	a
Nickel	UNEQUAL	0.106	NO	c	EQUAL	0.178	NO	b
Silver	EQUAL	N/A	NO	a	EQUAL	N/A	NO	a
Vanadium	UNEQUAL	0.183	NO	c	EQUAL	N/A	NO	a
Zinc	UNEQUAL	0.094	NO	c	EQUAL	0.707	NO	b
Year 2 Peeper Results								
Arsenic	UNEQUAL	0.211	NO	c	EQUAL	0.211	NO	a
Barium	UNEQUAL	0.112	NO	c	EQUAL	0.379	NO	c
Cadmium	EQUAL	0.187	NO	c	EQUAL	0.099	NO	c
Chromium	UNEQUAL	0.299	NO	c	EQUAL	0.211	NO	c
Copper	EQUAL	1.000	NO	a	EQUAL	N/A	NO	a
Lead	EQUAL	0.187	NO	c	EQUAL	N/A	NO	a
Nickel	EQUAL	0.661	NO	b	EQUAL	N/A	NO	a
Silver	EQUAL	0.001	YES	d	EQUAL	0.015	YES	d
Vanadium	UNEQUAL	0.110	NO	c	EQUAL	N/A	NO	b
Zinc	UNEQUAL	0.095	NO	c	EQUAL	0.211	NO	a

Conclusion Explanation:
a - Analyte not detected in sediment porewater (below treatment); no contamination to be treated.
b - Below treatment mean concentration not greater than above treatment mean concentration; potential non-treatment influences.
c - Below treatment mean concentration greater than above treatment mean concentration but reduction not statistically significant.
d - Below treatment mean concentration greater than above treatment mean concentration and reduction is statistically significant.

Key summary plots showing average concentrations above (yellow), between (red) and below (blue) treatment boundaries for select metals (nickel, zinc, copper) for the first year and second

year peeper sampling efforts are provided in Figure 5.4-2. These specific analytes were chosen as the primary metals of interest for the mat system assessment because they were previously identified as CoCs in the USGS Cottonwood Bay dataset (EnSafe 2001) and produced consistently detected results in the horizontal peeper analysis, suggesting that observed trends are real and not artifacts of variability in non-detect results. Ambient surface water contaminant concentrations determined from the peeper suspended in the water column were also included in the Year Two plots to provide a point of comparison for final reduction data and background values.

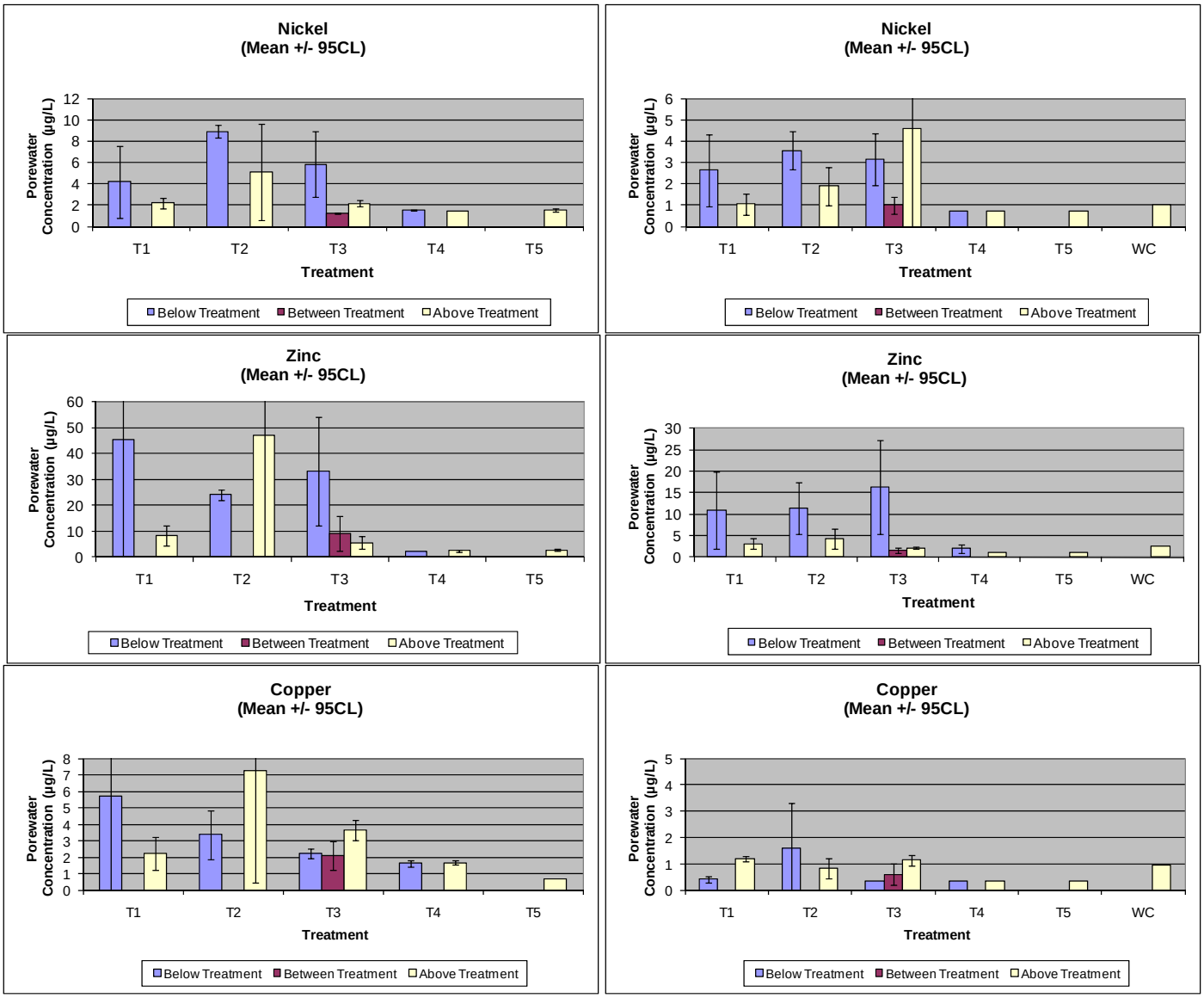

Figure 5.4-2. First year (left column) and second year (right column) peeper analytical results for select metals (nickel, zinc, copper) at the prototype mat system.

Results from the hypothesis testing and summary plots indicated certain trends that were not consistent over the two sampling years and did not appear logical based on the expected

properties of the test site. One notable anomaly was that zinc and copper concentrations below treatment in area T1 were much higher in Year One than Year Two and these values were also substantially greater than the below treatment concentrations in other areas; logic dictates that below treatment concentrations should be relatively consistent in all areas since they all contain the same natural sediment, with some leeway allowed for local variation. A second notable anomaly was that the Year One zinc and copper concentrations above treatment in area T2 and the Year Two nickel concentration above treatment in area T3 were substantially greater than the ambient water column concentration, an illogical result considering the mats could not add contaminants to the environment. Because these anomalies could not be explained through a typical uncertainty analysis, the decision was made to further inspect the entire raw peeper dataset at the most robust level for the presence of potential outliers which, due to the limited number of peeper replicates (n = 3) in each test area, would skew the final treatment data in a manner unrepresentative of true mat behavior and thus erroneously impact final conclusions regarding mat efficacy in sequestering metals. The outlier investigation was performed as an alternative approach to standard regulatory protocol and was not intended to replace the full dataset provided above.

The outlier investigation was conducted by compiling the peeper sub-replicate (*i.e.*, chambers within each peeper) data at each horizon within each treatment into one dataset with nine values (n = 9). Treating all sub-replicate concentrations as independent values in this manner was considered appropriate because increasing sample size would strengthen the power of the outlier test and true large variations would not be expected between different chambers located only centimeters apart within the same sampler. A Dixon's Q-test for detection of a single outlier was then performed on each population using USEPA ProUCL software. This simple test is based on the statistical distribution of "subrange ratios" of ordered data samples drawn from the same normal population and allows one to examine if one (and only one) observation from a small set of replicate observations (typically 3 to 10) can be "legitimately" rejected or not at different significance levels. For the purposes of this investigation, a significance level of 5% was selected as the cutoff point for outlier identification. A list of the suspected outliers identified with this technique along with the maximum significance level (< 5%) of each identification is provided for both Year One and Year Two in Table 5.4-3. The raw sub-replicate data used for this evaluation is provided in Appendix E.

As shown in Table 5.4-3, excluding these sub-replicate outliers from the overall peeper dataset substantially decreases the mean concentrations for the replicates in which they were contained, which would in turn decrease the summary mean for that horizon in that particular treatment. Depending on whether the outlier was identified in a below mat or above mat sample, its presence was explained by either potential particulate contamination within the peeper chamber (below) or non-treatment influences (above).

As an alternative approach to standard regulatory protocol, these outliers were removed from the peeper dataset at the sub-replicate level and the adjusted replicate means were rolled up into the final treatment summary values. The hypothesis testing described above was then re-run with the new replicate means (still n = 3) to provide a more accurate assessment of statistically significant contaminant reductions across the various treatments. The results of this second

round of hypothesis testing are provided in Table 5.4-4; all analytes affected by outlier exclusion are highlighted.

Table 5.4-3. Suspected outliers for metals of concern in the peeper dataset identified at the sub-replicate level.

Statistical Outliers: Metals

Analyte	Treatment	Horizon	Replicate (n=3)	Sub-Replicate (n=9)	Result (ug/L)	Dixon's Test Statistic	Outlier @ 5% Significance?	Max Outlier Significance Level	Replicate Mean w/ Outlier	Replicate Mean w/o Outlier	Outlier Explanation
Year 1 Outliers											
Copper	T1 - Mat Only	Below Mat	Rep 1 (A)	A-3	37	0.911	YES	1%	5.7	1.9	a
Zinc	T1 - Mat Only	Below Mat	Rep 1 (A)	A-3	267	0.938	YES	1%	45	18	a
Copper	T2 - Mat w/ Sand	Above Mat	Rep 3 (L)	L-1	42	0.975	YES	1%	7.2	2.8	b
Nickel	T2 - Mat w/ Sand	Above Mat	Rep 3 (L)	L-1	20	0.840	YES	1%	5.1	1.8	b
Zinc	T2 - Mat w/ Sand	Above Mat	Rep 3 (L)	L-1	251	0.978	YES	1%	47	5.4	b
Year 2 Outliers											
Nickel	T3 - Double Mat	Above Mat	Rep 2 (R)	H2a	25	0.815	YES	1%	4.6	2.2	b

Outlier Explanation:
a - Value 10x greater than colocated sub-replicates; suggesting potential particulate sample contamination.
b - Value 10x greater than colocated below treatment data; suggesting non-treatment influences.
Source:
See Appendix E for full peeper sub-replicate dataset.

Table 5.4-4. Results of hypothesis testing to determine the statistical significance of contaminant reductions across treatment boundaries for all metals of concern at the prototype mat system with the exclusion of sub-replicate outliers.

Significance Level: Alpha = 0.05
Null Hypothesis: Above Treatment >= Below Treatment (p-value > 0.05)
Alternative Hypothesis: Above Treatment < Below Treatment (p-value < 0.05)

	T1 - Mat Only					T2 - Mat w/ Sand					T3 - Double Mat (Below to Between)				
Analyte	Sub-Rep Outliers Removed?	Replicate Variance (n=3)	p-value	Reject Null? (Above < Below)	Conclusion Explanation	Sub-Rep Outliers Removed?	Replicate Variance (n=3)	p-value	Reject Null? (Above < Below)	Conclusion Explanation	Sub-Rep Outliers Removed?	Replicate Variance (n=3)	p-value	Reject Null? (Above < Below)	Conclusion Explanation
Year 1 Peeper Results															
Copper	YES	EQUAL	0.609	NO	b	YES	EQUAL	0.309	NO	c	NO	EQUAL	0.421	NO	c
Nickel	NO	UNEQUAL	0.236	NO	c	YES	EQUAL	0.000	YES	d	NO	EQUAL	0.046	YES	d
Zinc	YES	EQUAL	0.040	YES	d	YES	EQUAL	0.001	YES	d	NO	EQUAL	0.092	NO	c
Year 2 Peeper Results															
Nickel	NO	EQUAL	0.117	NO	c	NO	EQUAL	0.067	NO	c	NO	EQUAL	0.027	YES	d

	T3 - Double Mat (Below to Above)					T4 - Sand Only				
Analyte	Sub-Rep Outliers Removed?	Replicate Variance (n=3)	p-value	Reject Null? (Above < Below)	Conclusion Explanation	Sub-Rep Outliers Removed?	Replicate Variance (n=3)	p-value	Reject Null? (Above < Below)	Conclusion Explanation
Year 1 Peeper Results										
Copper	NO	EQUAL	0.986	NO	b	NO	EQUAL	0.565	NO	b
Nickel	NO	UNEQUAL	0.106	NO	c	NO	EQUAL	0.178	NO	b
Zinc	NO	UNEQUAL	0.094	NO	c	NO	EQUAL	0.707	NO	b
Year 2 Peeper Results										
Nickel	YES	EQUAL	0.226	NO	c	NO	EQUAL	N/A	NO	a

Conclusion Explanation:
a - Analyte not detected in sediment porewater (below treatment); no contamination to be treated.
b - Below treatment mean concentration not greater than above treatment mean concentration; potential non-treatment influences.
c - Below treatment mean concentration greater than above treatment mean concentration but reduction not statistically significant.
d - Below treatment mean concentration greater than above treatment mean concentration and reduction is statistically significant.
Notes:
= Result affected by outlier removal.

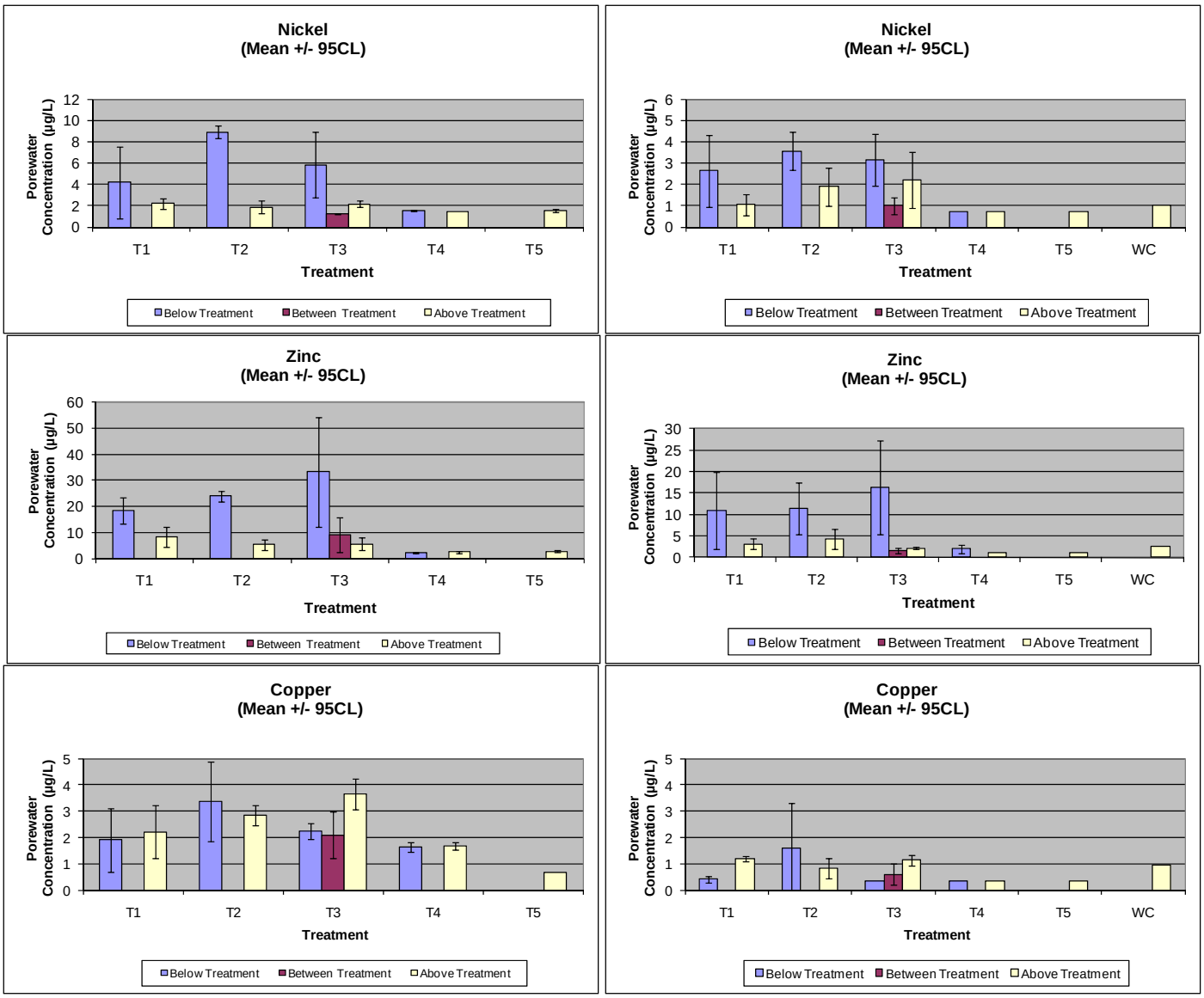

Figure 5.4-3. First year (left column) and second year (right column) peeper analytical results for select metals (nickel, zinc, copper) at the prototype mat system with the exclusion of sub-replicate outliers.

A second set of summary plots for select metals (nickel, zinc, copper) generated with the exclusion of the outliers was also generated for comparison purposes and is shown in Figure 5.4-3. When compared to the previous plots above, it is clear that the outlier removal produces mean zinc and copper concentrations below treatment in area T1 that are more akin to the below treatment concentrations observed in the other areas and the nickel, copper and zinc concentrations above treatment in areas T2 and T3 are more in line with the concentrations observed in the overlying water column. These changes also had the effect of reversing the reduction trends in areas T2 and T3 to be more consistent with expected results based on the nature of the technology (*i.e.*, the mats do not add contaminants to the environment).

Findings from the peeper dataset included the following:

- Hypothesis testing on the full dataset indicated that of all the analytes that satisfied the test conditions described above (*i.e.*, excluding conclusions "a" and "b" in Table 5.4-2), only silver and vanadium in area T2, silver in area T3 and silver in area T4 showed statistically significant concentration reductions across the treatment boundary from below to above (*i.e.*, conclusion "d" in Table 5.4-2). In addition, nickel and silver showed statistically significant reductions in area T3 (double mat) from below the mats to between the mats, suggesting that the double mat array sequesters contaminant contributions emanating from both below and above the treatment. All other analytes satisfying the test conditions showed some reduction of mean concentrations, but replicate data was insufficient to prove that these reductions were significant. However, changing the significance level of the hypothesis test by reducing the confidence coefficient from 95% to 90% (alpha = 0.1) would also demonstrate significant reductions for barium (T1, T2, T3), nickel (T2) and zinc (T3).
- When taking the alternative step of repeating the hypothesis testing with the exclusion of statistically proven sub-replicate outliers from the peeper dataset, zinc in area T1 as well as nickel and zinc in area T2 then also show statistically significant concentration reductions across the treatment boundary (*i.e.*, conclusion "d" in Table 5.4-4). Due to the nature of the sampler design (*i.e.*, multiple sub-replicate chambers within each peeper only centimeters apart), these outliers were considered true anomalous values and excluding them in this manner was deemed an important step in accurate data analysis.
- Nickel. All three mat treatments (T1, T2, T3) had mean nickel and zinc concentrations generally two to four times greater in the natural porewater below the treatment (*i.e.*, reactive mat/sand cap) than in the porewater above the treatment, suggesting effective sequestration by the mat system. Results for area T3 further indicated a general decrease in porewater concentration between the two mat layers while for area T4, concentrations in porewater in sediment below the sand-only cap were not elevated above the cap or water-only control concentrations.
- Zinc. All three mat treatments (T1, T2, and T3) had zinc concentrations generally two to four times greater in the natural porewater below the treatment (*i.e.*, reactive mat/sand cap) than in the porewater above the treatment, suggesting effective sequestration by the mat system. Again, results for area T3 indicate a general decrease in porewater concentration between the mats and in area T4, concentrations in sediment porewater were not elevated above the sand cap porewater or surface water control concentrations.
- Copper. None of the three mat treatments (T1, T2, and T3) showed a decrease in porewater concentrations in sediments below the mat compared to above the mat, thus suggesting that the mat system is less effective at sequestering copper than nickel and zinc. However, measurements between mats of the T3 treatment did indicate a general decrease in porewater concentration, suggesting some sequestration of copper by the mat system is occurring.
- The second year horizontal peeper dataset closely replicated the first year horizontal peeper results, confirming that the findings presented for nickel, zinc and copper are indicative of real trends as opposed to random processes or analytical error.

All peeper data has been presented above in a manner consistent with application in a regulatory environment (*i.e.*, one half MDL substituted for non-detect values, no suspected outliers excluded). In order to evaluate the potential influence of method MDLs on peeper trends, however, an additional alternative evaluation was conducted in which the non-detect values in the "below treatment" samples from the Year Two dataset were removed while the non-detect values in the "above treatment" samples were retained (Table 5.4-5). This adjustment followed the logic that the mat system would not show any tangible reduction effects on ambient contaminant concentrations that are already below MDLs but would be capable of reducing elevated contaminant concentrations to levels below those same detection limits. For the select metals of concern, removing non-detect values significantly increased the "below treatment" concentrations in some areas. It also resulted in the removal of copper from areas T3 and T4 and nickel from area T4 as all replicates were non-detect. Although most of the absolute increases were small, these effects cannot be considered negligible because the overall results were generally very low and small differences in values resulted in appreciable differences in trends across treatments. The presence of non-detect values increases uncertainty in the interpretation of the peeper data because lowering the "below treatment" results in turn decreases the calculated difference from "above treatment" results which is the measure of contaminant sequestration efficacy of the mat treatments.

Table 5.4-5. Comparison of "below treatment" peeper concentrations with and without non-detect values included in the mean calculations.

			T1 - Mat Only		T2 - Mat w/ Sand		T3 - Double Mat		T4 - Sand Only	
Analyte	Units	MDL	Below Treatment (w/o NDs)	Above Treatment (w/ NDs)	Below Treatment (w/o NDs)	Above Treatment (w/ NDs)	Below Treatment (w/o NDs)	Above Treatment (w/ NDs)	Below Treatment (w/o NDs)	Above Treatment (w/ NDs)
Cadmium	ug/L	0.31	4.2	0.16	1.1	0.16	10	0.16	0.74	0.34
Chromium	ug/L	0.64	3.7	1.6	13	1.0	2.5	1.2	0.47	0.32
Copper	ug/L	0.67	0.54	1.2	2.2	0.82	N/A	1.1	N/A	0.33
Nickel	ug/L	1.5	3.6	1.1	3.6	1.9	3.1	1.5	N/A	0.73
Zinc	ug/L	2.3	11	3.2	11	4.3	16	2.2	2.8	1.2

N/A = Data not available; all replicates non-detect

Key vertical summary plots showing average porewater concentrations at different depths in each treatment area for select metals (cadmium, chromium) are provided in Figure 5.4-4. These particular metals were chosen for the vertical plots in place of nickel, zinc and copper because the concentrations of the latter CoCs were entirely non-detect in the Year Two vertical peeper dataset. Discrete data points in the vertical plots correspond to porewater concentrations in each peeper chamber when deployed upright and reflect the fine-scale contaminant concentration differences in the sediment horizons immediately below or within the treatment interface. The results do show overall differences in metals concentrations over depth, confirming that local spatial variation is occurring and would complicate the interpretation of treatment effectiveness.

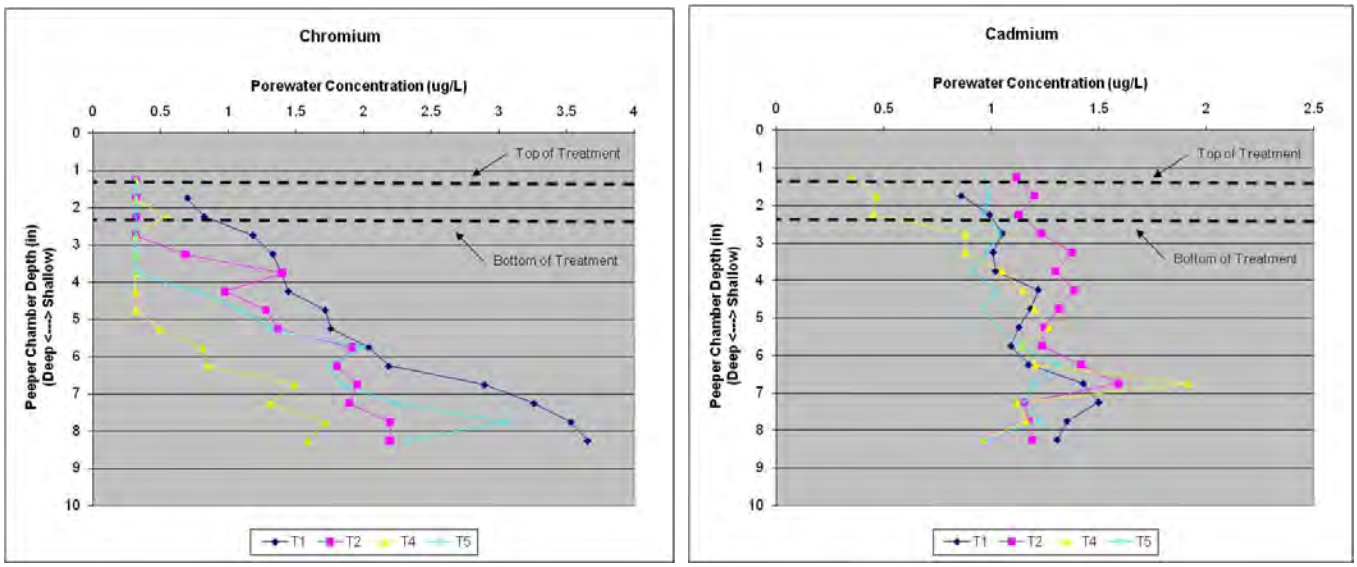

Figure 5.4-4. Second year vertical peeper analytical results for select metals (cadmium, chromium) at the prototype mat system.

SPMD Analytical Results. Raw SPMD analytical results for the prototype mat system collected during the first round (December 2008) and second round (December 2009) of passive contaminant sampling are provided in Appendix F. Similar to the peeper data, non-detect results were substituted with one half the method detection limit (MDL) following standard USEPA protocol. A summary of the final Year One and Year Two SPMD data showing mean results for PAHs at each treatment is presented in Table 5.4-6. Hypothesis testing was conducted in the same manner as for the peeper analysis to determine whether observed reductions across the treatment boundaries were statistically significant. The results for the hypothesis testing of each PAH compound at each treatment are shown in Table 5.4-7.

As stated in Section 4.4.4, seven SPMDs from Year One experienced tearing with measurable water infiltration and/or oil loss during the deployment process, which in turn increased uncertainty in the analytical results. These samplers were heat sealed prior to extraction and extra care was taken during the analytical cleanup process to minimize the effects of oil carryover. Based on communication from the extraction laboratory, the impact of SPMD damage on final Year One analytical results was considered negligible within the scope of the overall dataset, especially since damaged replicates showed similar results when compared to pristine replicates from the same area. No SPMDs from Year Two experienced measurable water infiltration and/or oil loss. Thus potential SPMD damage had no effect on that dataset. The fact that the Year Two data showed similar trends to the Year One data despite significantly less damage further supports the conclusion that the effects of SPMD damage on the Year One dataset were minimal.

Table 5.4-6. Summary of first year (top) and second year (bottom) SPMD mean analytical results for all PAHs at the prototype mat system.

Year 1 SPMD Results: PAHs

		T1 - Mat Only		T2 - Mat w/ Sand		T3 - Double Mat			T4 - Sand Only		T5 - No Treatment
Analyte	Units	Below Treatment	Above Treatment	Below Treatment	Above Treatment	Below Treatment	Between Treatment	Above Treatment	Below Treatment	Above Treatment	Above Treatment
Naphthalene (L)	pg/L	N/A	N/A	N/A	N/A	N/A	N/A	N/A	N/A	N/A	N/A
Acenaphthylene (L)	pg/L	129	129	129	129	602	129	129	129	129	129
Acenaphthene (L)	pg/L	1203	295	6830	206	4890	88	283	543	236	271
Fluorene (L)	pg/L	1743	705	6060	665	5707	417	593	1138	858	1306
Phenanthrene (L)	pg/L	1508	1765	17508	1357	13254	935	2531	1512	1392	1596
Anthracene (L)	pg/L	476	234	2342	151	1452	62	182	224	151	177
Fluoranthene (H)	pg/L	3302	4279	9674	2636	9519	912	4310	2171	2822	3256
Pyrene (H)	pg/L	3725	4732	10562	2928	10902	1046	4627	3059	3294	3634
Benzo(a)anthracene (H)	pg/L	539	589	1915	404	2148	178	507	448	511	630
Chrysene (H)	pg/L	595	923	2263	443	2143	253	1033	470	623	683
Benzo(b)fluoranthene	pg/L	856	1042	1450	817	1950	363	946	829	817	925
Benzo(k)fluoranthene	pg/L	324	553	647	451	847	173	557	424	522	573
Benzo(a)pyrene (H)	pg/L	223	225	549	175	598	72	187	290	427	343
Indeno(1,2,3-c,d)pyrene	pg/L	212	238	287	206	364	97	218	214	194	251
Dibenzo(a,h)anthracene (H)	pg/L	91	84	136	78	267	58	99	64	84	96
Benzo(g,h,i)perylene	pg/L	326	337	470	295	625	126	309	309	281	358
Total LMW PAHs	pg/L	5060	3128	32869	2509	25905	1632	3719	3545	2766	3480
Total HMW PAHs	pg/L	8476	10832	25099	6664	25578	2519	10763	6501	7761	8641
Total LMW+HMW PAHs	pg/L	13536	13961	57968	9173	51483	4151	14482	10046	10527	12121

Year 2 SPMD Results: PAHs

		T1 - Mat Only		T2 - Mat w/ Sand		T3 - Double Mat			T4 - Sand Only		T5 - No Treatment
Analyte	Units	Below Treatment	Above Treatment	Below Treatment	Above Treatment	Below Treatment	Between Treatment	Above Treatment	Below Treatment	Above Treatment	Above Treatment
Naphthalene (L)	pg/L	N/A	N/A	N/A	N/A	N/A	N/A	N/A	N/A	N/A	N/A
Acenaphthylene (L)	pg/L	327	256	404	232	260	129	355	129	129	177
Acenaphthene (L)	pg/L	2862	299	4119	330	1309	87	259	227	325	232
Fluorene (L)	pg/L	2736	495	3483	723	3003	167	464	873	896	715
Phenanthrene (L)	pg/L	6313	2697	8574	1639	4287	761	2697	1314	1473	1590
Anthracene (L)	pg/L	1150	228	1286	208	932	65	218	248	238	279
Fluoranthene (H)	pg/L	8379	7752	9566	4222	8478	1122	8082	3925	4189	5509
Pyrene (H)	pg/L	3922	3171	4589	1863	4172	567	3560	1697	1863	2420
Benzo(a)anthracene (H)	pg/L	1273	619	1379	532	1166	191	776	473	512	607
Chrysene (H)	pg/L	1301	1348	1500	706	1099	220	1383	613	674	897
Benzo(b)fluoranthene	pg/L	997	975	1223	771	1472	305	1454	869	1068	1090
Benzo(k)fluoranthene	pg/L	567	680	655	505	642	193	713	459	451	588
Benzo(a)pyrene (H)	pg/L	355	195	421	182	365	69	219	166	174	336
Indeno(1,2,3-c,d)pyrene	pg/L	112	101	206	137	224	62	193	138	146	172
Dibenzo(a,h)anthracene (H)	pg/L	46	46	92	46	84	46	46	46	46	46
Benzo(g,h,i)perylene	pg/L	228	165	358	235	351	105	269	231	225	269
Total LMW PAHs	pg/L	13387	3975	17866	3132	9790	1208	3992	2790	3061	2993
Total HMW PAHs	pg/L	15276	13129	17548	7552	15364	2215	14066	6921	7459	9815
Total LMW+HMW PAHs	pg/L	28663	17105	35413	10684	25155	3424	18058	9711	10520	12808

N/A = Data not available.

Table 5.4-7. Results of hypothesis testing to determine the statistical significance of contaminant reductions across treatment boundaries for PAHs at the prototype mat system.

Significance Level: Alpha = 0.05
Null Hypothesis: Above Treatment >= Below Treatment (p-value > 0.05)
Alternative Hypothesis: Above Treatment < Below Treatment (p-value < 0.05)

	T1 - Mat Only				T2 - Mat w/ Sand				T3 - Double Mat (Below to Between)			
Analyte	Replicate Variance (n=3)	p-value	Reject Null? (Above < Below)	Conclusion Explanation	Replicate Variance (n=3)	p-value	Reject Null? (Above < Below)	Conclusion Explanation	Replicate Variance (n=3)	p-value	Reject Null? (Above < Below)	Conclusion Explanation
Year 1 Peeper Results												
Naphthalene (L)	EQUAL	N/A	NO	a	EQUAL	N/A	NO	a	EQUAL	N/A	NO	a
Acenaphthylene (L)	EQUAL	N/A	NO	a	EQUAL	N/A	NO	a	EQUAL	0.187	NO	c
Acenaphthene (L)	UNEQUAL	0.225	NO	c	UNEQUAL	0.078	NO	c	EQUAL	0.154	NO	c
Fluorene (L)	EQUAL	0.064	NO	c	UNEQUAL	0.094	NO	c	UNEQUAL	0.102	NO	c
Phenanthrene (L)	UNEQUAL	0.633	NO	b	UNEQUAL	0.103	NO	c	UNEQUAL	0.158	NO	c
Anthracene (L)	EQUAL	0.168	NO	c	UNEQUAL	0.117	NO	c	UNEQUAL	0.162	NO	c
Fluoranthene (H)	EQUAL	0.761	NO	b	UNEQUAL	0.138	NO	c	UNEQUAL	0.142	NO	c
Pyrene (H)	EQUAL	0.736	NO	b	UNEQUAL	0.131	NO	c	UNEQUAL	0.140	NO	c
Benzo(a)anthracene (H)	EQUAL	0.592	NO	b	UNEQUAL	0.148	NO	c	UNEQUAL	0.118	NO	c
Chrysene (H)	EQUAL	0.957	NO	b	EQUAL	0.101	NO	c	UNEQUAL	0.121	NO	c
Benzo(b)fluoranthene	EQUAL	0.726	NO	b	UNEQUAL	0.228	NO	c	EQUAL	0.030	YES	d
Benzo(k)fluoranthene	UNEQUAL	0.870	NO	b	UNEQUAL	0.273	NO	c	EQUAL	0.023	YES	d
Benzo(a)pyrene (H)	EQUAL	0.508	NO	b	UNEQUAL	0.160	NO	c	UNEQUAL	0.125	NO	c
Indeno(1,2,3-c,d)pyrene	EQUAL	0.619	NO	b	UNEQUAL	0.273	NO	c	EQUAL	0.028	YES	d
Dibenzo(a,h)anthracene (H)	EQUAL	0.440	NO	c	EQUAL	0.179	NO	c	EQUAL	0.145	NO	c
Benzo(g,h,i)perylene	EQUAL	0.537	NO	b	UNEQUAL	0.232	NO	c	EQUAL	0.035	YES	d
Total LMW PAHs	EQUAL	0.171	NO	c	UNEQUAL	0.097	NO	c	UNEQUAL	0.152	NO	c
Total HMW PAHs	EQUAL	0.751	NO	b	UNEQUAL	0.135	NO	c	UNEQUAL	0.135	NO	c
Total LMW+HMW PAHs	EQUAL	0.533	NO	b	UNEQUAL	0.112	NO	c	UNEQUAL	0.144	NO	c
Year 2 Peeper Results												
Naphthalene (L)	EQUAL	N/A	NO	a	EQUAL	N/A	NO	a	EQUAL	N/A	NO	a
Acenaphthylene (L)	EQUAL	0.376	NO	c	EQUAL	0.082	NO	c	EQUAL	0.060	NO	c
Acenaphthene (L)	UNEQUAL	0.156	NO	c	UNEQUAL	0.097	NO	c	EQUAL	0.067	NO	c
Fluorene (L)	UNEQUAL	0.122	NO	c	UNEQUAL	0.097	NO	c	UNEQUAL	0.051	NO	c
Phenanthrene (L)	UNEQUAL	0.258	NO	c	UNEQUAL	0.183	NO	c	UNEQUAL	0.071	NO	c
Anthracene (L)	UNEQUAL	0.166	NO	c	UNEQUAL	0.137	NO	c	UNEQUAL	0.048	YES	d
Fluoranthene (H)	UNEQUAL	0.477	NO	c	UNEQUAL	0.139	NO	c	EQUAL	0.015	YES	d
Pyrene (H)	EQUAL	0.366	NO	c	UNEQUAL	0.130	NO	c	UNEQUAL	0.041	YES	d
Benzo(a)anthracene (H)	UNEQUAL	0.232	NO	c	UNEQUAL	0.132	NO	c	EQUAL	0.019	YES	d
Chrysene (H)	UNEQUAL	0.522	NO	b	UNEQUAL	0.183	NO	c	EQUAL	0.501	NO	c
Benzo(b)fluoranthene	EQUAL	0.479	NO	c	EQUAL	0.034	YES	d	EQUAL	0.006	YES	d
Benzo(k)fluoranthene	EQUAL	0.691	NO	b	UNEQUAL	0.180	NO	c	UNEQUAL	0.019	YES	d
Benzo(a)pyrene (H)	UNEQUAL	0.238	NO	c	UNEQUAL	0.117	NO	c	EQUAL	0.006	YES	d
Indeno(1,2,3-c,d)pyrene	EQUAL	0.433	NO	c	EQUAL	0.022	YES	d	EQUAL	0.005	YES	d
Dibenzo(a,h)anthracene (H)	EQUAL	N/A	NO	a	EQUAL	0.063	NO	c	EQUAL	0.065	NO	c
Benzo(g,h,i)perylene	EQUAL	0.291	NO	b	EQUAL	0.031	YES	d	EQUAL	0.007	YES	d
Total LMW PAHs	UNEQUAL	0.199	NO	c	UNEQUAL	0.143	NO	c	UNEQUAL	0.031	YES	d
Total HMW PAHs	UNEQUAL	0.406	NO	c	UNEQUAL	0.139	NO	c	EQUAL	0.016	YES	d
Total LMW+HMW PAHs	UNEQUAL	0.281	NO	c	UNEQUAL	0.141	NO	c	UNEQUAL	0.035	YES	d

Table 5.4.7. Continued.

Analyte	T3 - Double Mat (Below to Above)				T4 - Sand Only			
	Replicate Variance (n=3)	p-value	Reject Null? (Above < Below)	Conclusion Explanation	Replicate Variance (n=3)	p-value	Reject Null? (Above < Below)	Conclusion Explanation
Year 1 Peeper Results								
Naphthalene (L)	EQUAL	N/A	NO	a	EQUAL	N/A	NO	a
Acenaphthylene (L)	EQUAL	0.187	NO	c	EQUAL	N/A	NO	a
Acenaphthene (L)	UNEQUAL	0.190	NO	c	UNEQUAL	0.166	NO	c
Fluorene (L)	UNEQUAL	0.107	NO	c	EQUAL	0.078	NO	c
Phenanthrene (L)	UNEQUAL	0.184	NO	c	EQUAL	0.348	NO	c
Anthracene (L)	UNEQUAL	0.179	NO	c	EQUAL	0.103	NO	c
Fluoranthene (H)	UNEQUAL	0.237	NO	c	EQUAL	0.897	NO	b
Pyrene (H)	UNEQUAL	0.225	NO	c	EQUAL	0.629	NO	b
Benzo(a)anthracene (H)	UNEQUAL	0.149	NO	c	EQUAL	0.735	NO	b
Chrysene (H)	UNEQUAL	0.218	NO	c	EQUAL	0.985	NO	b
Benzo(b)fluoranthene	UNEQUAL	0.114	NO	c	EQUAL	0.476	NO	c
Benzo(k)fluoranthene	UNEQUAL	0.160	NO	c	EQUAL	0.798	NO	b
Benzo(a)pyrene (H)	UNEQUAL	0.169	NO	c	EQUAL	0.790	NO	b
Indeno(1,2,3-c,d)pyrene	EQUAL	0.096	NO	c	EQUAL	0.342	NO	c
Dibenzo(a,h)anthracene (H)	UNEQUAL	0.661	NO	c	EQUAL	0.741	NO	b
Benzo(g,h,i)perylene	UNEQUAL	0.118	NO	c	UNEQUAL	0.334	NO	c
Total LMW PAHs	UNEQUAL	0.168	NO	c	EQUAL	0.143	NO	c
Total HMW PAHs	UNEQUAL	0.217	NO	c	EQUAL	0.839	NO	b
Total LMW+HMW PAHs	UNEQUAL	0.189	NO	c	EQUAL	0.622	NO	b
Year 2 Peeper Results								
Naphthalene (L)	EQUAL	N/A	NO	a	EQUAL	N/A	NO	a
Acenaphthylene (L)	EQUAL	0.874	NO	b	EQUAL	N/A	NO	a
Acenaphthene (L)	UNEQUAL	0.124	NO	c	EQUAL	0.792	NO	b
Fluorene (L)	UNEQUAL	0.061	NO	c	UNEQUAL	0.544	NO	b
Phenanthrene (L)	EQUAL	0.174	NO	c	EQUAL	0.789	NO	b
Anthracene (L)	UNEQUAL	0.068	NO	c	EQUAL	0.411	NO	c
Fluoranthene (H)	UNEQUAL	0.437	NO	c	EQUAL	0.681	NO	b
Pyrene (H)	UNEQUAL	0.322	NO	c	EQUAL	0.717	NO	b
Benzo(a)anthracene (H)	EQUAL	0.144	NO	c	EQUAL	0.739	NO	b
Chrysene (H)	EQUAL	0.834	NO	b	EQUAL	0.745	NO	b
Benzo(b)fluoranthene	EQUAL	0.481	NO	c	EQUAL	0.810	NO	b
Benzo(k)fluoranthene	EQUAL	0.970	NO	b	EQUAL	0.410	NO	c
Benzo(a)pyrene (H)	EQUAL	0.051	NO	c	EQUAL	0.710	NO	b
Indeno(1,2,3-c,d)pyrene	EQUAL	0.196	NO	c	EQUAL	0.685	NO	b
Dibenzo(a,h)anthracene (H)	EQUAL	0.065	NO	c	EQUAL	N/A	NO	a
Benzo(g,h,i)perylene	EQUAL	0.072	NO	c	EQUAL	0.338	NO	c
Total LMW PAHs	UNEQUAL	0.062	NO	c	EQUAL	0.789	NO	b
Total HMW PAHs	UNEQUAL	0.387	NO	c	EQUAL	0.704	NO	b
Total LMW+HMW PAHs	UNEQUAL	0.185	NO	c	EQUAL	0.760	NO	b

Conclusion Explanation:

a - Analyte not detected in sediment porewater (below treatment); no contamination to be treated.

b - Below treatment mean concentration not greater than above treatment mean concentration; potential non-treatment influences.

c - Below treatment mean concentration greater than above treatment mean concentration but reduction not statistically significant.

d - Below treatment mean concentration greater than above treatment mean concentration and reduction is statistically significant.

Key summary plots for one low molecular weight PAH (anthracene) and one high molecular weight PAH (benzo[a]anthracene) showing average concentrations above (yellow), between (red) and below (blue) treatment boundaries are provided in Figure 5.4-5. Findings from the SPMD dataset included the following:

- All above-treatment samples replicated well and indicated contaminant concentrations comparable to the control area.
- Hypothesis testing on the full dataset indicated that of all the analytes that satisfied the test conditions described above (*i.e.*, excluding conclusions "a" and "b" in Table 5.4-7), only benzo[b]fluoranthene, indeno(1,2,3-c,d)pyrene and benzo(g,h,i)perylene in area T2 showed statistically significant concentration reductions across the treatment boundary from below to above (*i.e.*, conclusion "d" in Table 5.4-7). In addition, several PAHs including totals showed statistically significant reductions in area T3 (double mat) from below the mats to between the mats, suggesting that the double mat array sequesters contaminant contributions emanating from both below and above the treatment. All other analytes satisfying the test conditions showed some reduction of mean concentrations, but replicate data was insufficient to prove that these reductions were significant. However, changing the significance level of the hypothesis test by reducing the confidence coefficient from 95% to 90% (alpha = 0.1) would also demonstrate significant reductions for several additional PAHs in areas T2 and T3.
- The single mat with sand cap (T2) and double mat (T3) treatments achieved five to six times greater contaminant sequestration (below vs. above mat concentration).
- Reduced PAH concentrations in the middle layer of the double mat treatment (T3) confirms the efficacy of the mats in reducing flux of chemical from either sediment or surface water sources.
- Treatment effectiveness was comparable for both low and high molecular weight compounds.
- Effectiveness of mat only (T1) and sand only (T4) treatments in sequestering PAHs could not be assessed as below treatment concentrations were not different from surface water.

Overall, the SPMD deployments were fully effective in measuring changes in chemical gradients of PAHs as a function of various test treatments. Conclusions generated from the SPMD data indicated that the deployment configuration of a single layer geotextile mat with sand capping (T2) could be an effective means of reducing PAH exposure in the surface sediments. Patterns observed were generally comparable to metals findings indicating similar groundwater flux processes at each of the treatments.

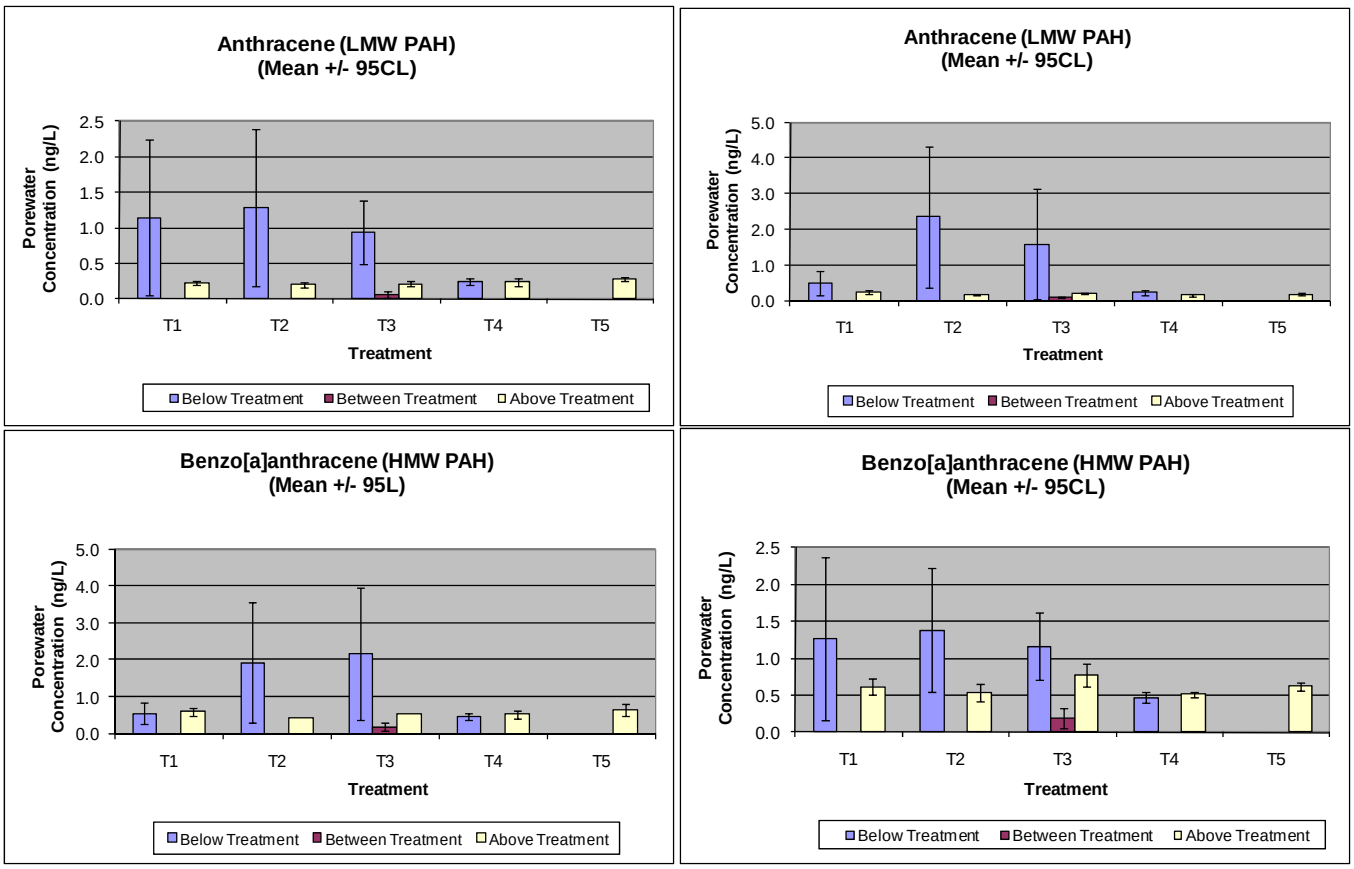

Figure 5.4-5 First year (left column) and second year (right column) SPMD analytical results for select low molecular weight (anthracene), high molecular weight (benzo[a]anthracene) and total PAHs at the prototype mat system.

SPME Analytical Results. Because the entire SPME dataset for the prototype mat system was non-detect (*i.e.*, concentrations < 5 µg/L), no conclusions could be generated from this sampling method regarding the success of the various treatments in sequestering PAH contaminants. The SPME results were not tabulated and are not included in this report. The lack of adequate exposure concentrations for measurable uptake by SPME fibers is consistent with the historical data used in the study design which suggests elevated sediment PAH concentrations (*i.e.*, 2000 ng/g BaP = 0.2 µg/L @ 1% TOC), but at concentrations below SPME detection.

Discussion. Final passive sampler data showed that contaminant sequestering trends, in terms of above versus below treatment concentrations, were generally consistent for metals and PAHs in each of the five treatment areas. Statistically significant retardation of chemical flux for both metals (*e.g.*, nickel, zinc) and PAHs (*e.g.*, anthracene, benzo[a]anthracene) by the mats was indicated by statistically higher (non-overlapping 95% UCL bars) contaminant concentrations maintained immediately beneath the mat than above the mat. These contaminant treatment/sequestration results were particularly relevant for the mat/sand (T2) and double mat (T3) treatments. Additional evidence of mat performance was also revealed by in porewater contaminants observed between mat layers in the double mat treatment (T3), the reductions being significantly ($p = 0.05$) less than background sediment or water column concentrations.

The repeatability of results between sampling years provided additional certainty in reliable performance, at least over the two year duration of the tests.

In general, greater porewater concentration gradients were maintained by mats with a cover (*e.g.*, sand in area T2 or another mat in area T3). This effect was attributed to better bottom contact compared to the other treatments where methane gas releases from the sediment below the treatment was observed to cause gas uplift of a single mat. Such mat uplift likely allowed the advecting porewater chemicals to be diluted by surface water under the floating mat. In contrast to the mats, the sand-only treatment did not exhibit a similar porewater concentration gradient, though this effect may have been due to the thin sand layer applied and/or overall lower porewater concentrations within the sediments being capped (*i.e.*, same as the water column concentration). From these results, it can be concluded that the reactive mat technology, when deployed with sufficient weighting (*e.g.*, sand cover), is an effective technology for sequestering contaminants in sediments.

5.4.3 Volumetric Sampling Results

Volumetric sampling conducted at the prototype mat system included passive flow sampling using Ultraseep technology as well as active draw sampling using the Trident Probe. The concurrent use of these two sampling techniques was designed to provide a comparison between groundwater-mediated contaminant concentrations passing upward through the various mat treatments and contaminant concentrations in porewater at various layers beneath the treatments.

Trident Probe Analytical Results. The ultimate goal of the Trident Probe effort was to collect porewater samples from various target treatment layers (*e.g.*, deep sediment, shallow sediment, mat interface, sand cap, overlying water). Whereas vertical sampling using the vertical peeper arrays was only previously conducted in non-mat areas, the three-pronged Trident Probe was inserted through the mat layers (via surgical cuts made by divers at appropriate locations) to simultaneously collect samples from three depths. Based on the limitations of the Trident Probe hardware, the final sample depths were 2 inches above the treatment interface, 3.5 inches below the treatment interface, 11 inches below the treatment interface and 24 inches below the treatment interface (in select areas only). Similar to the Ultraseep sample analyses, Trident Probe porewater samples were analyzed only for metals because previous SPMD results indicated that organics concentrations would be significantly below detection limits that could be achieved with the volume of water likely to be collected by the sampler.

The Trident Probe data provided synoptic chemical gradients for metals and were used to validate the concentrations previously observed in the peepers. Raw analytical chemistry results from the Trident Probe samples are presented in Appendix H and summarized for metals of concern in Table 5.4-8. Because the Trident Probe base plate rested flat against the mat/sediment surface during sampling, the depths provided in this table represent sample location relative to the treatment-water interface and include the thickness of the mats where applicable (*e.g.*, T1, T2, T3). To determine absolute depth of each sample relative to the mud line, the thickness of a single mat (0.5") is subtracted from the sample depths in areas T1 and T2 and twice the thickness of a single mat (double mat; 1") is subtracted from the sample depths in area T3.

Graphical results for nickel showing porewater concentrations drawn directly from various horizons at each mat system treatment represent the common trends in the Trident Probe data (Figure 5.4-6). Results of the Trident Probe measurements in general revealed substantial reductions in metals concentrations below mats (T1-T3) as well as the sand cover (T4) as compared to the control treatment (Figure 5.4-7). This finding demonstrates that only a thin layer of sand will act as a vertical barrier to porewater advection (10-20X reduction) and allows diffusion to dominate the exchange process, which is the basis for the predicted effectiveness of thin layer capping in low advection environments. However, the addition of mats shows that the reactive materials will sequester the metals to a far greater extent (80-300X reduction) and thus provide a far more effective barrier. This effect was noted in SERDP project ER-1501 and described as the amendment-induced "zone-of-influence" (Knox *et al.* 2011). As a result, porewater containing PAHs (*e.g.*, benzo(a)anthracene) and metals (*e.g.*, zinc) does not readily escape the cap, though perhaps a trend of slightly higher above treatment values is observed relative to the no cap control (Figure 5.4-3). This interpretation is corroborated by further concentration reductions observed in porewater samples taken between mat layers of treatment T3 at which measured levels were typically less than respective background and water column concentrations. Meanwhile, a concentration gradient was not established in the control treatment because the diffusion process allows rapid equilibrium with the overlying surface water. These results also indicate that isolation of the above treatment samples from the surface water is needed to detect the cap sequestration effectiveness, particularly in low concentration, low advection environments. Overall findings from the Trident Probe dataset include the following:

- Large reservoirs of metals existed within the deeper, subsurface sediments (>11") for all treatment locations.
- Concentrations in shallow sediments (< 3") appeared to be depressed in the treatment areas (T1, T2, T3, T4) relative to the control location (T5).
- Trident Probe data were generally corroborated by peeper measurements; nickel occurred at 4-8 µg/L in the treatment areas (0-2" data not available for the control).
- Chemical gradients observed in Trident Probe data indicated reductions in metals concentrations below reactive mats 6-8X higher than the sand cap only treatment. This reduction may be due to a "halo" effect wherein porewater metals (and presumably organics) are sequestered into the amendment cap at depths deeper than the point of physical contact, possibly due to diffusion.

Table 5.4-8. Summary of Trident Probe mean analytical results for all metals of concern at the prototype mat system.

Trident Probe Data: Metals
Treatment Summary - Replicate Averages

Analyte	Units	T1 - Mat Only			T2 - Mat w/ Sand			T3 - Double Mat			
		Below Trtmnt -11 in	Below Trtmnt -3.5 in	Above Trtmnt +2 in	Below Trtmnt -11 in	Below Trtmnt -3.5 in	Above Trtmnt +2 in	Below Trtmnt -11 in	Below Trtmnt -3.5 in	Btwn Trtmnt +0 in	Above Trtmnt +2 in
Arsenic (As)	ug/L	38	6.9	6.9	38	48	6.9	42	6.9	6.9	6.9
Barium (Ba)	ug/L	408	50	42	440	231	40	507	79	68	39
Cadmium (Cd)	ug/L	54	0.156	0.286	65	0.772	0.156	77	0.156	0.489	0.156
Chromium (Cr)	ug/L	1128	2.1	4.2	1608	2.1	2.0	1797	2.2	7.6	3.4
Copper (Cu)	ug/L	212	1.6	2.8	227	1.4	2.0	290	2.2	3.8	3.1
Lead (Pb)	ug/L	290	3.5	3.5	261	3.5	3.5	336	3.5	3.5	3.5
Nickel (Ni)	ug/L	79	1.3	2.1	75	1.6	1.7	111	3.4	2.4	1.9
Silver (Ag)	ug/L	1.5	0.206	0.206	2.0	0.206	0.206	2.3	0.206	0.206	0.206
Vanadium (V)	ug/L	133	1.6	5.2	94	1.3	4.1	146	1.0	5.1	4.8
Zinc (Zn)	ug/L	727	8.2	11	619	10	9.7	856	28	23	18

Analyte	Units	T4 - Sand Only				T5 - No Treatment			
		Below Trtmnt -24 in	Below Trtmnt -11 in	Below Trtmnt -3.5 in	Above Trtmnt +2 in	Below Trtmnt -24 in	Below Trtmnt -11 in	Below Trtmnt -3.5 in	Above Trtmnt +2 in
Arsenic (As)	ug/L	89	25	30	6.9	52	51	78	6.9
Barium (Ba)	ug/L	1118	307	891	38	1073	822	960	38
Cadmium (Cd)	ug/L	475	10.0	0.569	0.156	81	386	59	0.156
Chromium (Cr)	ug/L	50000	232	2.9	2.8	812	7317	902	3.7
Copper (Cu)	ug/L	592	40	1.6	3.3	250	546	397	3.0
Lead (Pb)	ug/L	675	47	3.5	3.5	144	495	471	3.5
Nickel (Ni)	ug/L	139	18	1.6	1.3	117	109	166	2.5
Silver (Ag)	ug/L	4.0	0.575	0.206	0.206	1.1	1.1	0.69	0.206
Vanadium (V)	ug/L	187	25	2.8	4.5	404	116	368	4.4
Zinc (Zn)	ug/L	2700	143	9.4	11	468	1744	1926	7.6

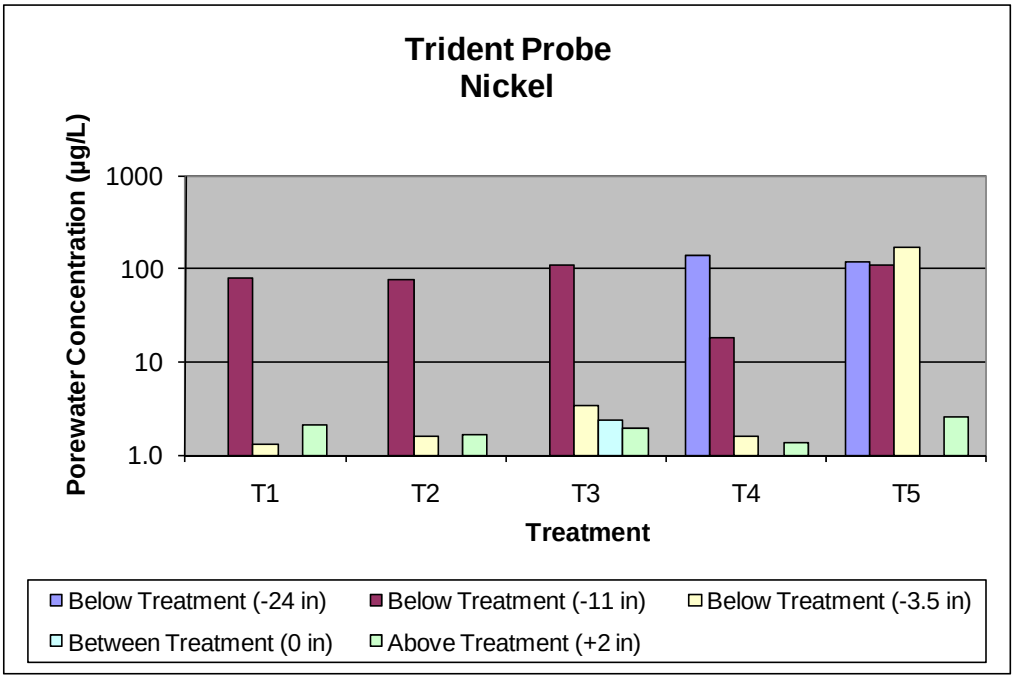

Figure 5.4-6. Trident Probe analytical results for a select metal (nickel) at the prototype mat system relative to the treatment-water interface (thickness of mat included where applicable).

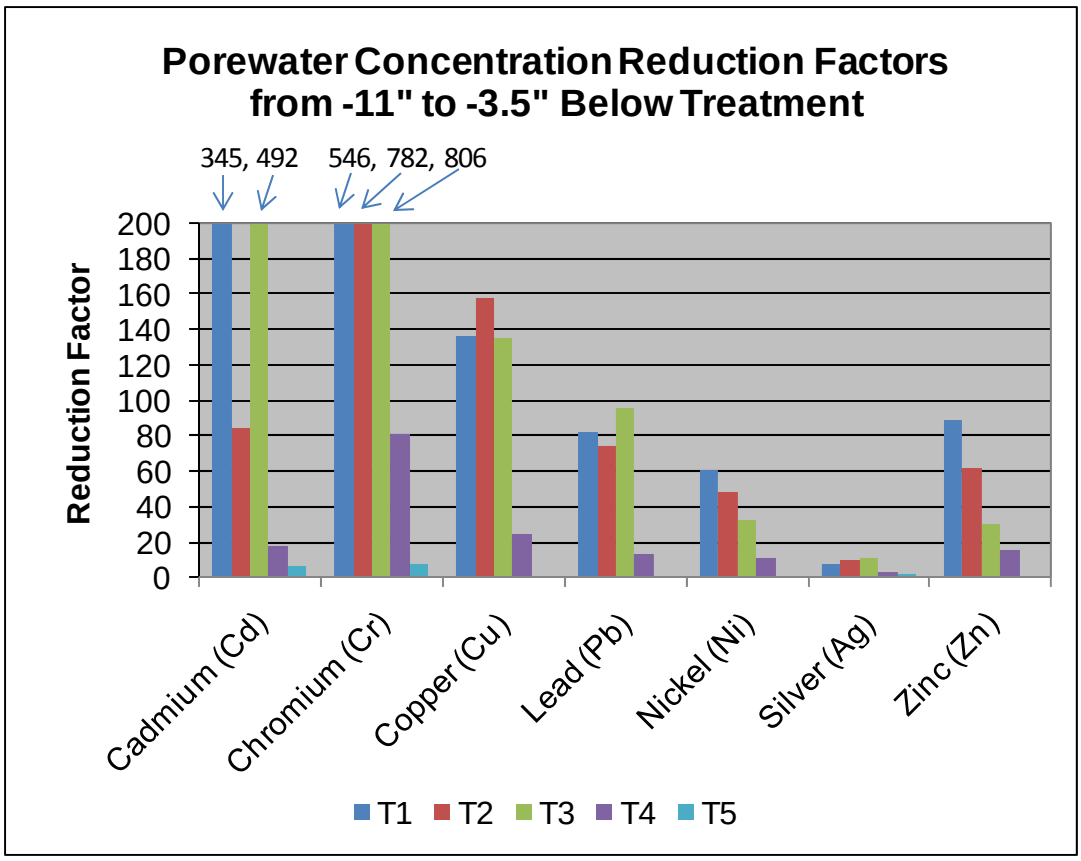

Figure 5.4-7. Reduction factors for deep (-11") versus shallow (-3.5", directly below treatment) porewater concentrations for various metals below the mat system treatments as measured by the Trident Probe.

Ultraseep Analytical Results. The ultimate goal of the Ultraseep measurements was to directly quantify the groundwater-mediated transport of contaminants upward through the various treatments. Because the SPMD approach quantified PAH concentrations at very low concentrations (*i.e.*, pg/L), analyzing Ultraseep groundwater samples for organics was deemed impractical (*i.e.*, a large volume of water, >100 L, would be required to achieve reliable detection limits). Thus the Ultraseep groundwater samples were analyzed only for metals. All electronic groundwater flux data and raw Ultraseep sample analytical results for the prototype mat system collected during the groundwater flow survey (June 2009) are presented in Appendix G. The mean analytical chemistry results for metals of concern at each treatment area are summarized in Table 5.4-9.

All tabulated results presented here for the Ultraseep technology reflect a "discharge fraction" calculation wherein the resulting metals concentrations for that sample are reflective of only the volume of porewater collected while flowing from the treatment (*i.e.*, the discharge; typically 0.1-1.0 L) and not the required volume of deionized water inside the Ultraseep machine (~0.5L) with which the environmental sample is mixed when sampling is initiated (Figure 5.4-8). Findings from the Ultraseep dataset shown in Figure 5.4-5 reveal the following: 1) Nickel: 30-115 µg/L; 2) Zinc: 45-135 µg/L; and 3) Copper: 10-105 µg/L. An inverse relationship

between discharge fraction and overall metal concentration is loosely apparent. As will be discussed below, observed Ultraseep are substantially higher that either peeper or trident data; this uncertainty is discussed in Section 5.4.5, below.

Table 5.4-9. Summary of Ultraseep mean analytical results for all metals of concern at the prototype mat system adjusted to reflect the discharge sample.

Ultraseep Sample Results: Metals
Treatment Summary - Replicate Averages

Analyte	Units	T1 - Mat Only Average	T2 - Mat w/ Sand Average	T3 - Double Mat Average	T4 - Sand Only Average	T5 - No Treatment Average
Arsenic (As)	ug/L	41	111	39	40	70
Barium (Ba)	ug/L	238	485	191	295	373
Cadmium (Cd)	ug/L	0.924	2.5	0.889	0.894	1.6
Chromium (Cr)	ug/L	6.7	22	5.8	4.7	9.2
Copper (Cu)	ug/L	13	107	13	10.0	16
Lead (Pb)	ug/L	21	57	20	20	36
Nickel (Ni)	ug/L	87	115	34	29	42
Silver (Ag)	ug/L	1.2	3.3	1.2	1.2	2.1
Vanadium (V)	ug/L	13	50	15	13	30
Zinc (Zn)	ug/L	114	135	80	47	98

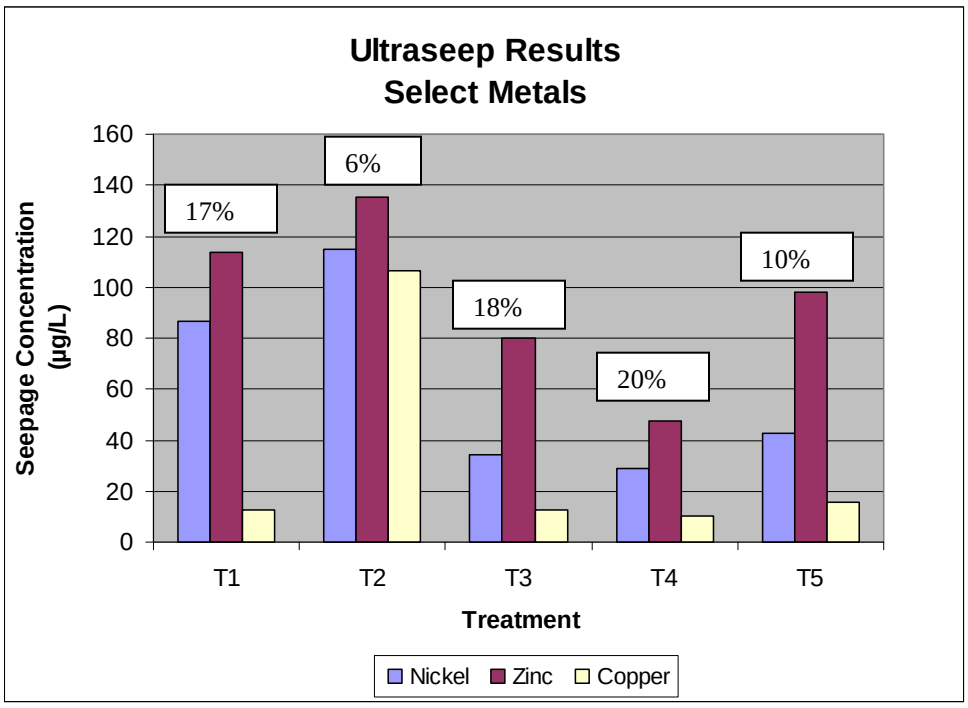

Figure 5.4-8. Ultraseep analytical results for select metals for the prototype mat system treatments. Discharge fraction (%) values indicated in text boxes (see text).

5.4.4 Sediment Coring

Mat System Sediment Data. The goal of the sediment coring effort was to collect sediment cores from each mat system treatment area and analyze the surface (0-4") and subsurface (4-8") intervals for characterization of the natural sediment and confirmation of the potential chemical flux through the various mat/sand layers. The resulting sediment data were also used to calculate the approximate PAH porewater concentrations (via equilibrium-partitioning) and therefore validate the previous SPMD results as well as partly address the data gap left by absence of Ultraseep and Trident Probe organics data. Sediment core locations, photos and raw analytical chemistry data are provided in Appendix I. A summary of the sediment core chemistry results for non-lithogenic metals of concern and PAHs at each treatment is presented in Table 5.4-10.

Table 5.4-10. Summary of sediment core chemistry for all metals of concern and PAHs at the prototype mat system.

Sediment Core Analytical Results

		T1 - Mat Only		T2 - Mat w/ Sand		T3 - Double Mat		T4 - Sand Only		T5 - No Treatment		T0 - Between Treatments	
Analyte	Units	Surface (0-4 in)	Subsurface (4-8 in)	Surface (0-4 in)	Subsurface (4-8 in)	Surface (0-4 in)	Subsurface (4-8 in)	Surface (0-4 in)	Subsurface (4-8 in)	Surface (0-4 in)	Subsurface (4-8 in)	Surface (0-4 in)	Subsurface (4-8 in)
Metals													
Arsenic	mg/kg	11	10	10	9.5	9.5	9.3	4.2	8	10	9.9	8.8	8.4
Barium	mg/kg	120	120	120	110	110	110	57	100	110	120	110	110
Cadmium	mg/kg	4.7	6.2	4.7	5.9	4.2	5.1	1.9	4.7	4.6	5.9	4.2	4.7
Chromium	mg/kg	190	270	180	250	170	210	75	190	190	240	170	190
Copper	mg/kg	38	37	36	38	34	35	16	32	37	39	34	35
Lead	mg/kg	60	72	63	68	56	65	25	58	64	72	54	61
Mercury	mg/kg	0.16	0.2	0.15	0.19	0.16	0.19	0.07	0.17	0.17	0.18	0.14	0.17
Nickel	mg/kg	35	32	32	32	31	31	14	27	33	34	30	30
Silver	mg/kg	3.4	4.5	3.7	4.1	2.8	3.8	1.2	3.3	3.1	4	2.9	3.3
Vanadium	mg/kg	41	36	39	35	35	37	16	29	39	37	33	34
Zinc	mg/kg	220	190	200	200	200	190	91	170	210	220	200	190
Polycyclic Aromatic Hydrocarbons													
Naphthalene (L)	ug/kg	11	9.0	11	8.7	11	9.3	5.8	7.4	11	9.0	10	8.7
Acenaphthylene (L)	ug/kg	11	9.0	11	8.7	11	9.3	5.8	7.4	11	9.0	10	8.7
Acenaphthene (L)	ug/kg	29	29	30	24	23	31	5.8	28	28	26	39	25
Fluorene (L)	ug/kg	23	25	23	18	11	24	5.8	21	11	23	31	19
Phenanthrene (L)	ug/kg	440	430	450	360	390	430	170	400	390	470	550	320
Anthracene (L)	ug/kg	73	51	82	67	81	80	31	73	70	81	110	46
Fluoranthene (H)	ug/kg	0.0	9.0	2300	1800	1500	1700	640	1600	1300	1800	1100	1500
Pyrene (H)	ug/kg	0.0	9.0	1700	1400	1000	1200	400	1100	960	1200	770	1000
Benzo[a]anthracene (H)	ug/kg	690	860	1000	840	710	730	260	680	620	820	490	530
Chrysene (H)	ug/kg	710	930	1100	910	730	880	270	780	660	890	550	540
Benzo[b]fluoranthene	ug/kg	0.0	890	1100	860	820	1000	340	790	790	860	490	710
Benzo[k]fluoranthene	ug/kg	550	880	1100	860	620	590	230	700	630	770	480	520
Benzo[e]pyrene	ug/kg	0.0	9.0	1400	1100	850	1000	350	1000	810	1100	710	860
Benzo[a]pyrene (H)	ug/kg	710	9.0	1000	830	680	740	280	720	690	760	480	590
Indeno[1,2,3-cd]pyrene	ug/kg	570	700	770	630	540	700	220	590	560	670	690	430
Dibenz[a,h]anthracene (H)	ug/kg	180	270	230	190	180	220	68	220	180	240	240	140
Benzo[g,h,i]perylene	ug/kg	550	640	690	560	450	600	190	610	480	630	700	390
2-Methylnaphthalene (L)	ug/kg	11	9.0	11	8.7	11	9.3	5.8	7.4	11	9.0	10	8.7
Total LMW PAHs	ug/kg	598	562	617	495	537	593	230	544	531	627	761	436
Total HMW PAHs	ug/kg	2290	2087	7330	5970	4800	5470	1918	5100	4410	5710	3630	4300
Total LMW+HMW PAHs	ug/kg	2888	2649	7947	6465	5337	6063	2148	5644	4941	6337	4391	4736

Graphical results for select metals (nickel, copper, zinc) and PAHs (anthracene, benzo[a]anthracene) showing sediment concentrations in each horizon for the various treatment areas are provided in Figure 5.4-9. Because zinc concentrations were fundamentally greater than nickel and copper, these values were divided by ten in order to allow all data to be plotted on the same axis. Stand-alone findings from the sediment core dataset included the following:

- Metals (nickel, copper, zinc) and PAHs (anthracene, benzo[a]anthracene) in surface (solid bars) and subsurface (shaded bars) sediments generally showed greater than two times the range in concentration across treatment areas (note T4 surface includes 3" sand cap and 1" of underlying surface sediment) (Figure 5.4-9).
- Concentration gradients were generally not observed in surface versus subsurface sediments, suggesting that the more variable porewater concentrations are likely driven by partitioning dynamics (*e.g.*, TOC concentration) and not bulk chemical concentration.

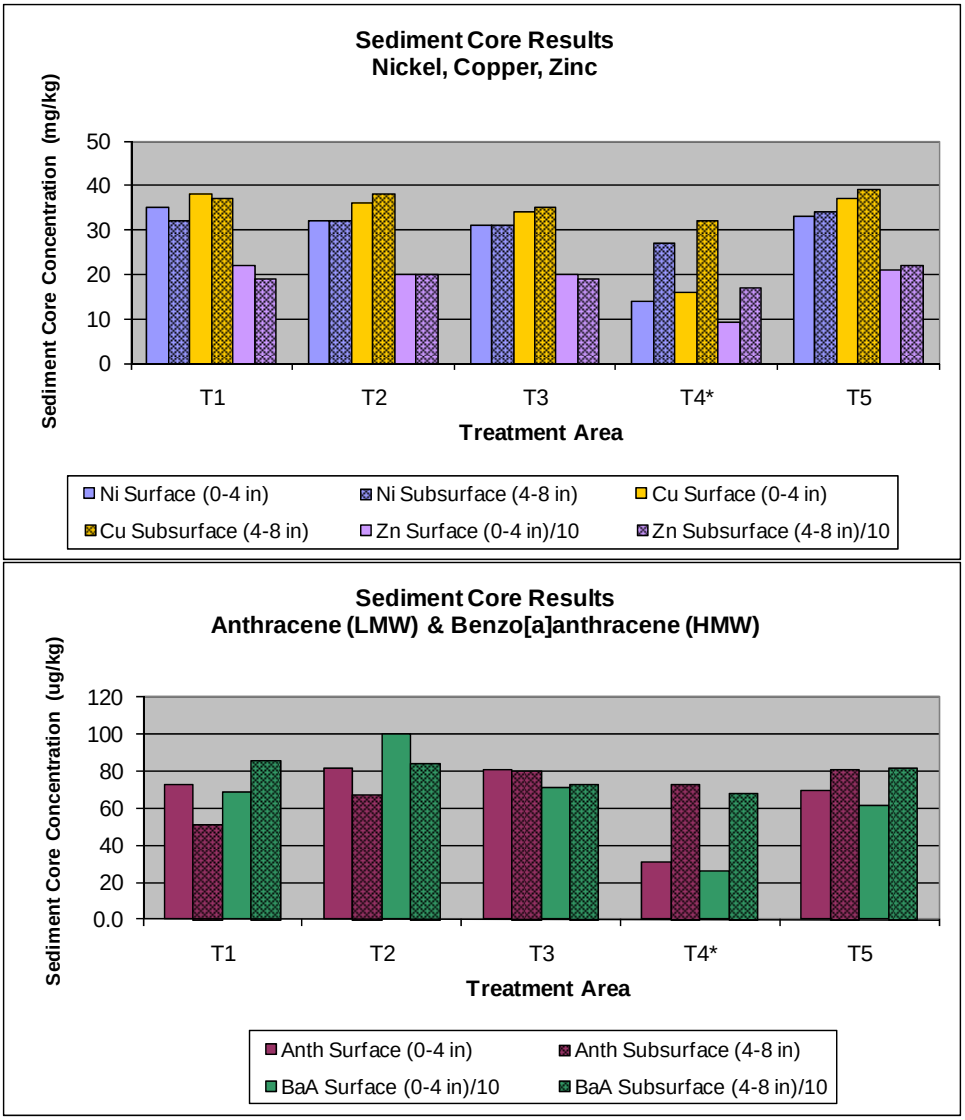

*****_For area T4, the 0-4 in horizon represents predominantly the sand cap material and the 4-8 in horizon represents the natural sediment comparable to the surface horizon in other areas._

Figure 5.4-9. Sediment core analytical results in surface (0-4") and subsurface (4-8") layers for select metals (nickel, copper, zinc) and PAHs (anthracene, benzo[a]anthracene) at various treatments in the prototype mat system.

When jointly considering both the sediment core data and the diffusion sampler data, metals and PAHs in area T4 were found to have relatively lower (2-3X) concentrations in both the below and above treatment diffusion samples as compared to the other test areas (*e.g.*, nickel, zinc, PAHs; Figure 5.4-1). This trend cannot be explained by a lack of contaminant loading or partitioning as comparable surface sediment concentrations and TOC across all treatments were observed. The lack of vertical concentration trends across the cap suggests the thin cap layer did not sequester porewater constituents within the sediments and that equilibration across the cap may be occurring. It is notable that the observed background water column concentrations for nickel and zinc (see WC, Figure 5.4-1) trended higher than the above treatment concentrations, such that the observed patterns appear treatment-related and not due to background influences. Although the cap was constructed of fine-grained material of an appreciable (2-3") thickness, the overall binding capacity of the cap material and/or its porosity may not have been sufficient to provide a discrete buffer between the natural sediment and the overlying water column in the absence of a reactive mat.

5.4.5 Sources of Uncertainty

In order to reach a final evaluation of mat system performance, data from each of the subsequent sampling and monitoring events were integrated and reviewed concurrently to assess sources of uncertainty in the conclusions regarding mat performance. Cross-comparison of different datasets allowed for a valid assessment of the success of each specific mat/cap treatment in achieving contaminant flux and sequestration goals in context with the properties of the native sediment at the selected pilot site and the potential geophysical impacts of the treatment on the surrounding natural conditions.

Historic Sediment Data Comparison. Surface sediment data collected during the Year Two mat system monitoring process were compared to historic bulk surface sediment data for the general prototype mat system area in Cottonwood Bay collected during previous site evaluations in order to assess the consistency of current contaminant concentrations with historic conditions documented for the chosen pilot site. In order to perform this comparison, historic Cottonwood Bay sediment data provided by the USGS as described in First Year Annual Progress Report (NAVFAC 2006) were filtered to only include surface values from 1999 stations (Bay-7) and 1996 stations (M2.3, M2.4, M2.5, M2.7) in the immediate vicinity of the final mat system construction area. The average of these historic concentrations was then plotted against the average of the 2009 surface concentrations at five locations adjacent to the control area and mat system treatments (Figure 5.4-10). Sediment core data collected from area T4 were removed from the 2009 averages because surface subsample data from this point reflected mostly clean sand cap material and not natural sediment conditions.

Results indicated that historical (1996-1999) surface sediment contaminant concentrations in Cottonwood Bay were approximately twice that observed in 2009, suggesting natural attenuation through deposition of cleaner sediment has occurred over the past ten years. Such recent reduction in sediment values likely explain the low-level porewater concentrations observed in surface sediments as well as sharp increases in some metals with depth below. This phenomenon introduces extra sensitivity to the effect that placement/depth of diffusion samplers has on the apparent differences among the treatments.

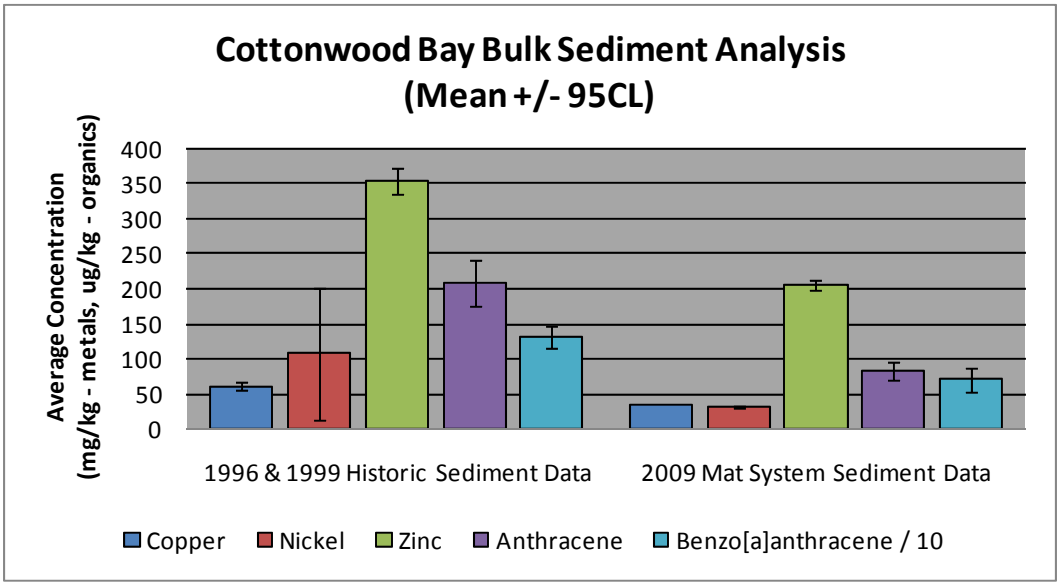

Figure 5.4-10. Historic and recent bulk sediment analytical results for select metals and organics at the prototype mat system area in Cottonwood Bay.

Porewater Monitoring Methodologies. Peeper, Trident Probe and Ultraseep porewater samples collected from the prototype mat system were all analyzed for metals by the same laboratory methodology. Representative results for zinc are tabulated in Table 5.4-11 including the "above treatment" measures for Ultraseep, Trident +2", and Peeper above treatment, as well as the "below treatment" measures consisting of the "peeper below treatment" and trident -3.5" values for comparison. Respective trident and peeper findings for each horizon which exhibited 3X agreement. In contrast, the Ultraseep concentrations were 10X higher than both of the above treatment results. Because this difference included both the sand-only and control areas, the observed trends do not appear to reflect upon mat performance. The explanation for this trend is unclear, but such enrichment could be related to minor amounts of turbidity retained in the samples.

Table 5.4-11. Ultraseep, deep Trident Probe and "below treatment" peeper results for zinc in the prototype mat system.

Analyte	Units	T1 Mat Only	T2 Mat w/ Sand	T3 Double Mat	T4 Sand Only	T5 No Treatment
Zinc						
Ultraseep	ug/L	114	135	80	47	98
Peeper Above Treatment (Year One)	ug/L	7.0	6.6	5.6	2.5	2.8
Trident Probe (+2 in)	ug/L	11	9.7	18	11	7.6
Peeper Below Treatment (Year One)	ug/L	15	24	33	2.4	N/A
Trident Probe (-3.5 in)	ug/L	8.2	10	28	9.4	1926

Low Contaminant Concentrations. Because porewater contaminant concentrations measured in the passive contaminant samplers (peepers for metals, SPMDs for PAHs) were substantially low compared to the expected contaminant concentrations based on historically documented site conditions, there was some uncertainty as to whether the chosen sampling techniques were

accurately quantifying current site contamination before and after treatment. In order to investigate this potential discrepancy, bulk sediment analyses were added to the second year passive contaminant sampling effort as described in Section 5.4.4. Results from these analyses proved that contaminant concentrations during the year two sampling event were significantly less than historic levels (see Figure 5.4-10), likely due to years of deposition on top of previous hotspots, and thus were accurately reflected by the sampler results. Furthermore, the relative contaminant trends observed in the surface sediment samples across treatments closely resembled the relative trends observed in the sampler data for both metals and organics, particularly for an increase in LMW PAHs in area T2 and a predictable contaminant void in the sand capping horizon in area T4. These correlations offers further evidence that passive sampler data were accurately documenting local contaminant conditions for the treatment areas relative to each other even if overall contaminant concentrations were within a range that made precise quantification difficult.

Variability in Contaminant Concentrations. The fact that porewater contaminant concentrations as determined by the various mat system sampling techniques (peepers, SPMDs, Ultraseep, Trident Probe) were relatively low (metals < 30 µg/L in peepers; PAHs < 5 ng/L in SPMDs) compared to what was expected at the Cottonwood Bay pilot site based on available historic data leads to the question of whether these samples reflect true differences in treatment effects or random variation in fine scale values. In order to address this question of true treatment effects versus random variation, passive contaminant sampling with peepers (metals) and SPMDs (PAHs) was repeated after one year to provide a second dataset featuring the same number of replicates designed to strengthen the overall conclusions. Reduction trends for select analytes in the Year Two data showed a strong correlation to trends in the Year One data across treatments (see Section 5.4.2); such replication suggests that the apparent effects of each treatment are true and not an artifact of random sample variation. Additionally, 95% upper confidence limit (UCL) and lower confidence limit (LCL) error bars added to the peeper and SPMD plots are often found to be non-overlapping or nearly so, which implies true statistical differences between treatments. Thus, generally speaking, adequate replication was performed in order to elucidate the treatment effects of interest.

Background Influences on Sample Data. Another point of uncertainty in the mat system sampling dataset was whether the "above treatment" samples were more reflective of the overlying water column (*i.e.*, background conditions) than the concentrations of chemicals in groundwater upwelling through the treatments. In order to test this hypothesis, an additional peeper was suspended in the water column during the second round of passive contaminant sampling and the resulting equilibrium concentrations were compared to the porewater data across the treatment interfaces from the same dataset (Table 5.4-12). Results show that background concentrations were less than or approximately equal to "above treatment" porewater values for the same analytes. For example, data from area T2 (mat with sand cap) showed that the "above treatment" concentrations for nickel and zinc were less than the "below treatment" concentrations but still greater than the water column concentrations, thus suggesting that the sand layer provided a buffer from the overlying water concentrations. A comparable relationship was also present but less evident for areas T1 (mat only) and T3 (double mat only) where the "above treatment" peepers were placed directly on top of the mat with no capping material to serve as a buffer between the treatment and the water column. Thus, influence of

background conditions on "above treatment" passive sampler responses does not appear problematic.

Table 5.4-12. Comparison of Year One and Year Two "above treatment" peeper concentrations with background water column peeper concentrations.

Analyte	Units	T1 - Mat Only		T2 - Mat w/ Sand		T3 - Double Mat		T4 - Sand Only		T5 - No Treatment		Background
		Above Treatment (Year 1)	Above Treatment (Year 2)	Above Treatment (Year 1)	Above Treatment (Year 2)	Above Treatment (Year 1)	Above Treatment (Year 2)	Above Treatment (Year 1)	Above Treatment (Year 2)	Above Treatment (Year 1)	Above Treatment (Year 2)	Water Column
Copper	ug/L	2.2	1.2	3.0	0.82	3.6	1.1	1.7	0.33	0.67	0.33	0.96
Nickel	ug/L	2.0	1.1	2.1	1.9	2.0	1.5	1.5	0.73	1.6	0.73	1.0
Zinc	ug/L	7.0	3.2	6.6	4.3	5.6	2.2	2.5	1.2	2.8	1.2	2.5

6.0 CONCLUSIONS AND IMPLICATIONS FOR FUTURE RESEARCH/IMPLEMENTATION

The overall project goal was to determine the most successful mat arrangement for sequestering contaminants. Based on the findings from these comprehensive studies, the reactive core mat technology has been determined to be effective at sequestering metals and PAH compounds in fine-grained sediments at a quiescent site with low groundwater flow. Therefore, it would be suitable to use the system for full-scale demonstration/validation under similar conditions. The combined results of the laboratory chemical and geotechnical testing, field mini-mat testing and finally mat prototype testing involving different reactive mat arrangements provide a solid foundation to support further expansion of testing in a pilot scale demonstration (*e.g.*, increase mat size tested from 400 ft^2 to 10,000 ft^2). The substantive conclusions are as follows:

1. Laboratory batch and column testing with contaminants and mixtures of dissolved phase natural organic matter (humic and fulvic acids) indicated that the mat amendments should remain effective in adsorption of metals and organics in marine environments of low to moderate dissolved organic matter levels;
2. Geotextile testing and modeling have identified a material and mesh size that are effective in the retention of the amendment material but sufficiently porous to allow the free flow of groundwater through the mats;
3. Repeated testing of field acclimated amendments contained in mini-mat systems deployed over a two year period did not show any reduction in adsorptive capacity, lending confidence to longer term effectiveness of the mat system as presently designed;
4. Field observations revealed that methane accumulations can lift the reactive mats from the sediment surface, but these effects can be mitigated if an overlying sand layer is used to provide additional weight and stability to the system. This expectation was confirmed by gas permeability testing conducted on geotextiles in a controlled laboratory setting, the results of which indicated that a coarse opening geotextile (*e.g.*, AOS 80) should be sufficient in allowing the maximum methane production found in freshwater environments to pass through the mat without experiencing uplift if such additional weighting is in place.
5. Conclusions regarded as relevant in assessment of whether mats did serve as an effective barrier to advection/diffusion were focused on select contaminants that were (1) detected

in the below treatment samples, (2) had a below treatment mean concentration greater than or equal to the above treatment concentration and (3) had a below treatment concentration greater than the ambient surface water concentration. Statistically significant (at 90-95% confidence) below/above reductions were observed in primarily two treatments (mat/sand and double mat) for select metals (nickel, zinc, barium, silver, vanadium) and several PAHs (benzo[b]fluoranthene, indeno[1,2,3-c,d]pyrene, benzo[g,h,i]perylene, anthracene, benzo[a]anthracene), thus demonstrating that contaminant sequestration had occurred. Maintenance of two- to four-fold concentration gradients across the prototype mat boundary for both metals and organics were well replicated over a two year period which suggests that the mats did serve as an effective barrier to diffusion for these contaminants.

6. Chemical gradients observed in Trident Probe data indicated reductions in metals concentrations below reactive mats 6-8X higher than the sand cap only treatment. This reduction may be due to a "halo" effect wherein porewater metals (and presumably organics) are sequestered into the amendment cap at depths deeper than the point of physical contact, possibly due to diffusion.

7. Demonstrated mat performance for other metals of ecological concern (*e.g.*, copper) was less robust because of overall low environmental concentrations relative to detection limits.

In conclusion, the reactive mats were proven to be generally effective in sequestering chemicals in sediment and are significantly thinner than non-reactive caps that may require a thickness of a meter or more as needed to ensure effective cover. This lightweight design did prove somewhat problematic due to uplift caused by methane accumulation beneath the mats, but this situation can be rectified by adding an additional sand layer coating. Conclusive (*i.e.*, statistically significant) results were observed for a small number of contaminants, but these cases were generally limited by the number of positive detections rather than mat effectiveness. More definitive results are expected if a follow-on test site has higher porewater constituent concentrations (*i.e.*, in the ecological risk range) so as to allow for documentation of larger gradients/reductions across the mat boundary.

The findings from this study represent significant evolution in the maturity of amendment technology. A mat with sand cover is expected to be an effective treatment in the majority of cases, although double mats may be applied if extra reduction in contaminant flux is desired. Presently, a mixture of apatite, organoclay and activated carbon in roughly equal proportions will address both metals and non-polar organics (PCBs and PAHs); depending on site contaminants one or more amendments could be replaced with extra amendment of the remaining type to likely boost effectiveness as needed.

Finally, promoting the use of reactive mats as a far more environmentally sustainable remedy relative to traditional dredging would be achieved by a pilot scale demonstration. Reactive mat capping (assuming sand capping alone would be insufficient) when used as a remedy would largely eliminate greenhouse gas (CO-, CO_2) emissions otherwise released during excavation by dredge barge and trucking equipment, and would increase the life expectancy of landfills not otherwise depleted with dredged material. Lastly, the use of reactive mats may also provide a

starting point to monitored natural attenuation (MNA), wherein the initial benthic recolonization made possible by the mats would jump-start further sediment deposition and therefore eventual re-establishment of infaunal communities.

ACKNOWLEDGEMENTS

Ms. Amy L. Hawkins:	Naval Facilities Engineering Service Center Lead Investigator Specialist in Sediment Risk Assessment
Dr. Gregory A. Tracey:	Science Applications International Corporation Specialist in Contaminated Sediment Assessment
Dr. Kevin H. Gardner:	University of New Hampshire Expertise in Laboratory Evaluation of Contaminated Sediments and Reactive Capping Materials
Dr. Jeffrey S. Melton:	University of New Hampshire Expertise in Reactive Cap Design and Performance Evaluation

This page is intentionally left blank.

REFERENCES

Adams, R.G., R. Lohmann, L.A. Fernandez, J.K. MacFarlane, P.M. Gschwend. 2007. Polyethylene Devices: Passive Samplers for Measuring Dissolved Hydrophobic Organic Compounds in Aquatic Environments. *Environ. Sci. Technol*., 2007, 41 (4), pp 1317-1323. January.

Barker, R.A. and C.L. Braun. 2000. Computer-model analysis of ground-water flow and simulated effects of contaminant remediation at Naval Weapons Industrial Reserve Plant, Dallas, Texas. U.S. Geological Survey Water-Resources Investigations Report 00–4197, 44 p.

Chadwick, D.B., J. Groves, C. Smith, and R. Paulsen. 2003. Hardware description and sampling protocols for the Trident Probe and UltraSeep system: Technologies to evaluate contaminant transfer between groundwater and surface water. Technical Report #1902, SSC San Diego, United States Navy.

Colwell, F.S., S. Boyd, M.E. Delwiche, D.W. Reed, T.J. Phelps, and D.T. Newby. 2008. Estimates of Biogenic Methane Production Rates in Deep Marine Sediments at Hydrate Ridge, Cascadia Margin. *Appl. Environ. Microbiol*. Vol. 74, No. 11, pp 3444-3452.

EnSafe/Allen & Hoshall. 1994. Comprehensive long-term environmental action-Navy stabilization work plan. Revision I: Memphis, Tenn. 83 p.

EnSafe/Allen & Hoshall. 1996. Draft RCRA, facility investigation report, Naval Weapons Industrial Reserve Plant, Dallas, Texas. Volume I: Memphis, Tenn.

EnSafe. 2000. Ecological Risk Assessment Screening Level, Mountain Creek Lake, Dallas, Texas. Prepared for SOUTNAVFACENGCOM, Charleston, SC.

EnSafe. 2001. Affected Property Assessment Report, Mountain Creek Lake, Dallas, Texas. Prepared for NAVFAC under contract N62467-89-D-0318, CTO 0025.

Fischer, G.R., A.D. Mare and R.D. Holtz. 1999. Influence of Procedural Variables on the Gradient Ratio Test. *Geotechnical Testing Journal*. Vol. 22, No. 1, pp 22–31.

Groundwater Seepage, Inc. 2007. Final. Data Report. Groundwater Upwelling Survey, Naval Weapons Industrial Reserve Plant, Cottonwood Bay, Dallas, Texas. November.

Iocco, L.E., P. Wilber and R.J. Diaz. 2000. Final Report. Benthic Habitats of Selected Areas of the Hudson River, NY Based on Sediment Profile Imagery. September.

Knox, A.S., M.H. Paller, D.D. Reible, X.Ma, I.G. Petrisor. 2008. Sequestering Agents for Active Caps-Remediation of Metals and Organics. *Soil and Sediment Contamination*, 17 (5) 516-532 (2008).

Knox, A.S., M.H. Paller, K. Dixon, D.D. Reible. 2011. Field Performance of Active Caps – Assessment of Contaminant Immobilization, Erosion Resistance, and Toxicity. SERDP Project ER-1501.

Lafleur, J., J. Mlynarek and A.L. Rollin. 1989. Filtration of Broadly Graded Cohesionless Soils. *Journal of Geotechnical Engineering.* Vol. 115, No. 12, pp 1747-1768.

McDonough, K.M., P. Murphy, J. Olsta, Y. Zhu, D. Reible, G. Lowry. 2007. Development and Placement of a Sorbent-amended Thin Layer Sediment Cap in the Anacostia River. *Journal of Soil and Sediment Remediation*. 16:3, 313-322 (2007).

Qingzhong, Y., K. T. Valsaraj, D.D. Reible and C.S. Willson. 2007. A Laboratory Study of Sediment and Contaminant Release during Gas Ebullition. *Journal of the Air & Waste Management Association (1995).* Vol. 57, No. 9, pp 1103-1111.

Reible, D.D., D. Lampert, W. D. Constant, R.D. Mutch, and Y. Zhu. 2006. Active Capping Demonstration in the Anacostia River, Washington, DC. *Remediation: The Journal of Environmental Cleanup Costs, Technologies and Techniques*. Vol. 17(1).

Melton, J.S., B.S. Crannell, K.H. Gardner, T. Eighmy and D.D. Reible. 2005. Apatite-Based Reactive Barrier Technology in the Anacostia River Study. In: *Remediation of Contaminated Sediments 2005: Finding Achievable Risk Reduction Solutions. Proceedings of the Third International Conference on Remediation of Contaminated Sediments*. R.F. Olfenbuttel and P.J. White, Eds. Battelle Press, Columbus, OH.

NAVFAC. 2006. Annual Progress Report. Reactive Capping Mat Development and Evaluation for Sequestering Contaminants in Sediment. Prepared for SERDP Project Number ER-1493. With Science Applications International Corporation and the University of New Hampshire. December.

NAVFAC. 2007. Second Year Annual Progress Report. Reactive Capping Mat Development and Evaluation for Sequestering Contaminants in Sediment. Prepared for SERDP Project Number ER-1493. With Science Applications International Corporation and the University of New Hampshire. December.

Niederer, C., R.P. Schwarzenbach and K. Goss. 2007. Elucidating Differences in the Sorption Properties of 10 Humic and Fulvic Acids for Polar and Nonpolar Organic Chemicals. *Environ. Sci. Tech*. 2007, 41, 6711 – 6717.

Osterberg, R. and K Mortense. 1992. Fractal dimension of Humic Acids. *European Biophysics Journal*. 1992, 21, 163-167.

Owenby, J.R. and D.S. Ezell. 1992. Climatography of the United States-Monthly station normals of temperature, precipitation, and heating and cooling degree days, 1961–91. Asheville, N.C. National Climatic Data Center no. 81, 65 p.

Petty, J.D., C.E. Orazio, J.N. Huckins, R.W. Gale, J.A. Lebo, J.C. Meadows, K.R. Echols, W.L. Cranor. 2000. Considerations involved with the use of semipermeable membrane devices for monitoring environmental contaminants. *Journ. of Chrom.* A Vol. 879, pp. 83-95.

Pirbazari, M., V. Ravindram, S.P. Wong and M.R. Stevens. 1989. Adsorption of Micropollutants on Activated Carbon. Aquatic Humic Substances – Influence on Fate and Treatment of Pollutants. ACS publishers. 1989, 549-578.

Reible, D. and G. Lotufo. 2008. Lab Demonstration Plan, Summary and Results ER-0624, Demonstration and Evaluation of Solid Phase Microextraction for the Assessment of Bioavailability and Contaminant Mobility. June 5.

Rhoads, D.C. and J.D. Germano. 1982. Characterization of organism-sediment relations using sediment profile imaging: An efficient method of remote ecological monitoring of the seafloor (Remots™ System). *Mar. Ecol. Prog. Ser.* 8: 115-128.

Rhoads, D.C., and J.D. Germano. 1986. Interpreting long-term changes in benthic community structure: A new protocol. *Hydrobiologia.* 142: 291-308.

Saparpakorn, P., J.H. Kim and S. Hannongbua. 2007. Investigation on the Binding of Polycyclic Aromatic Hydrocarbons with Soil Organic Matter: A Theoretical Approach. *Molecules*. 2007, 12, 703-715.

Sharma, B. 2008. Evaluation of Reactive Cap Sorbents for In-Situ Remediation of Contaminated Sediments. Submitted to the University of New Hampshire. September.

VanMetre, P.C., S.A. Jones, J.B. Moring, B.J. Mahler and J.T. Wilson. 2003. Chemical Quality of Water, Sediment, and Fish in Mountain Creek Lake, Dallas, Texas, 1994-97. Geological Survey Water-Resources Investigations Report 03-4082, 69 p.

Wu , F. C., R.D. Evans and P.J. Dillon. 2003. Separation and Characterization of NOM by High-Performance Liquid Chromatography and On-Line Three Dimensional Excitation Emission Matrix Fluorescence Detection. *Environ. Sci. Tech.* 2003, 37, 3687-3693.

Zhao, X., P. Viana, K. Yin, K. Rockne, D. Hey, J. Schuh, R. Lanyon. 2007. Combined Active Capping/Wetland Demonstration in the Chicago River. Paper D-019 in: E.A. Foote and G.S. Durell (Conference Chairs), Remediation of Contaminated Sediments 2007. Proceedings of the Fourth International Conference on Remediation of Contaminated Sediments (Savannah, Georgia; January 2007). Battelle Press, Columbus, OH.

This page is intentionally left blank.

APPENDIX A

"SERDP Project Number ER-1493 First Year Annual Progress Report (December 2006)"

This page is intentionally left blank

1. COVER PAGE

ANNUAL PROGRESS REPORT:

REACTIVE CAPPING MAT DEVELOPMENT AND EVALUATION FOR SEQUESTERING CONTAMINANTS IN SEDIMENTS

Prepared For:

PROJECT NUMBER: ER-1493

Prepared By:

NAVAL FACILITIES ENGINEERING SERVICE CENTER
1100 23RD AVENUE
PORT HUENEME, CA 93043

LEAD INVESTIGATOR: MS. AMY HAWKINS

With:

SCIENCE APPLICATIONS INTERNATIONAL CORPORATION
221 THIRD STREET
NEWPORT, RI 02840

And:

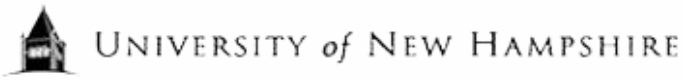

GREGG HALL
DURHAM, NH 03824

01 DECEMBER 2006

This page is intentionally left blank

2. FRONT MATTER

TABLE OF CONTENTS

LIST OF FIGURES

LIST OF FIGURES
(Continued)

LIST OF TABLES

LIST OF ACRONYMS

BERA	Baseline Ecological Risk Assessment
CETCO	Colloid Environmental Technologies Company
CoPCs	Contaminants of Potential Concern
DCE	Dichloroethene
DOC	Dissolved Organic Carbon
EFANE	Engineering Field Activity Northeast
ESTCP	Environmental Security Technology Certification Program
FEA	Finite Element Analysis
FS	Feasibility Study
HA	Humic Acid
NAS	Naval Air Station
NAVFAC	Naval Facilities Engineering Command
NEESA	Naval Energy and Environmental Support Activity
NFESC	Naval Facilities Engineering Service Center
NWIRP	Naval Weapons Industrial Reserve Plant
PAHs	Polycyclic Aromatic Hydrocarbons
PCBs	Polychlorinated Biphenyls
RI	Remedial Investigation
SAIC	Science Application International Corporation
SERDP	Strategic Environmental Research and Development Program
SPI	Sediment Profile Imaging
TCE	Trichloroethene
TNRCC	Texas Natural Resource Conservation Commission
TOC	Total Organic Carbon
TRRP	Texas Risk Reduction Program
UNH	University of New Hampshire
USEPA	United States Environmental Protective Agency
USGS	United States Geological Survey
VC	Vinyl Chloride
VOCs	Volatile Organic Compounds

ACKNOWLEDGEMENTS

Ms. Amy Hawkins:	Naval Facilities Engineering Service Center Lead Investigator Specialist in Sediment Risk Assessment
Dr. Gregory A. Tracey:	Science Applications International Corporation Specialist in Contaminated Sediment Assessment
Dr. Kevin H. Gardner:	University of New Hampshire Expertise in Laboratory Evaluation of Contaminated Sediments and Reactive Capping Materials
Dr. Jeffrey S. Melton:	University of New Hampshire Expertise in Reactive Cap Design and Performance Evaluation

3. EXECUTIVE SUMMARY

U.S. Navy Strategic Environmental Research and Development Program (SERDP) Project Number ER-1493 (Reactive Capping Mat Development and Evaluation for Sequestering Contaminants in Sediments) focuses on developing optimal mixtures of reactive amendments to treat a variety of contaminants at a site and then delivering these mixtures within a geotextile mat to be positioned on top of the sediments of concern. The overall project goal is to develop a chemically effective, mechanically stable, and cost efficient technology that could be deployed in a wide variety of environmental settings to effectively sequester both metal and organic contaminants while simultaneously allowing both groundwater flux and surficial biological colonization. A series of laboratory and limited field experiments were designed to increase understanding of the practical effectiveness and limitations of the reactive capping mat technology. In order to achieve the project objective, four separate tasks were defined. The goal of this Annual Progress Report is to describe the state of these tasks as of November 2006.

Task 1. Composite Material Testing. The purpose of this task is to identify the mixture of amendment materials that most effectively sequesters contaminants by collecting data on adsorption, sequestration and chemical breakthrough properties of the mixed reactive mat system. To accomplish Task 1, the University of New Hampshire (UNH) has conducted batch adsorption experiments to characterize the sorption properties of various reactive amendments for a range of contaminant combinations in terms of absorption kinetics and adsorption isotherms. The effects of humic acid on adsorption properties was also assessed with humic acid being shown to have a significant influence on the performance of certain amendments as reactive cap materials. Finite element models were also prepared to evaluate prospective sediment deformation and pore water pressure increases caused by the weight of a potential reactive cap. Following these procedures, flow-through column experiments will be used to evaluate flux for various sorbent mixtures and sorbent layers by more closely mimicking processes in the field.

Task 2. Pilot Site Establishment. The purpose of this task is to identify a location that can serve as both a pilot site for initial small-scale field tests of geotextile mats (Task 3) and then ultimately as the target location for full-scale testing of the prototype mat system (Task 4). The basic requirements for the site are sediments that contain a mixture of metal and organic contaminants with associated exposure pathways of environmental concern. In order to select sites appropriate for further investigation, data on potential locations were reviewed for compatibility with expected mat performance characteristics. First a “long list” list of prospective Navy sites was compiled and subject to a detailed screening process in terms of various chemical, physical, biological and logistical factors. Two suitable primary sites were then selected out of this list and compared with regard to nature and extent of contamination, groundwater flow, management planning and ongoing remediation. These sites will now be subject to further geophysical testing before a selection of one of them as the final pilot site for geotextile testing and mat deployment is accomplished.

Task 3. Geotextile Testing. The purpose of this task is to test different types of geotextile material at the selected pilot site to assess whether biofouling and biofilm formation will

adversely affect the ability of the fabric to allow water to pass through the mat, whether environmental weathering compromises the ability of the mat to retain the amendment material and whether environmental weathering compromises the reactivity of the sequestration agents. Although initial field deployment cannot proceed until Task 2 is completed and a pilot site has been identified, the materials and combinations for geotextile testing have been selected and several small-scale test mats or varying composition have been fabricated. Once active in the field, these mats will be monitored and evaluated in order to assess how material type, geotextile weight and apparent opening size affect biofouling and sediment clogging.

Task 4. Prototype Mat Testing. The purpose of this task is to field test a prototype full-scale mat system constructed of the most adsorbent amendment (identified in Task 1) and the geotextile most resistant to biofouling and clogging (identified in Task 3) with the goal of assessing in situ chemical sequestration effectiveness and flux properties. Data collected during all previous tasks will be used to select the most effective amendment mixture, geotextile combination and deployment location to be used in the prototype mat test. Once deployed, the prototype mat will be subject to as-built confirmation and monitoring by passive sampling. A groundwater seepage survey will also be conducted to evaluate flux through the mat and cores will be collected for confirmatory chemical analyses. Efforts on Task 4 have not begun.

4. OBJECTIVE

The objective of this project is to develop a mixture of chemically reactive materials suitable for incorporation within an engineered geotextile mat to create a composite active capping system capable of deployment in a wide variety of environmental settings in order to effectively sequester both metal and organic contaminants.

5. BACKGROUND

In situ capping has frequently been used to physically separate contaminated sediments from the aquatic environment above the cap and, in some cases, also acting as an impermeable barrier to groundwater flux. Sequestration based on physical separation alone, however, is not desirable because it does not ensure that dissolved phase contaminant flux is eliminated as a transport pathway either through the cap or around it. More recently, in situ capping with chemically reactive materials has been explored to provide a physical barrier to remobilization of sediment-bound contaminants while at the same time sequestering dissolved contaminants as they out-flux through the cap via groundwater flow. To date, these studies have largely focused on applying one type of reactive material to treat one class of contaminant and have typically been deployed as relatively thick layers of the material (6 to 12 inches) over the bottom. These approaches may not be applied at many sites which have physically challenging site conditions, multiple classes of contaminants, concerns over contaminant remobilization or are prohibitively large relative to the costs of using coarsely applied reactive materials.

At many sites, it may be more practical to sequester sediment contaminants through in situ capping if the cap would prevent physical contact with biota and retard leaching of chemicals into overlying waters while simultaneously allowing natural groundwater flow through the cap.

The mixed reactive capping materials developed in this project will satisfy these requirements. They will be non-intrusive, will simultaneously address multiple contaminant classes, will be easily deployed and will offer greater slope stability, erosion stability, and permeability to natural groundwater flow. These benefits expand the utility of the mixed-reactive mat system to intertidal and sloped environments where normal sand cap or unconstrained reactive materials would be lost. Finally, the reactive mats can be fabricated on land to control mat thickness (0.5 inch) and integrity, thus minimizing the cost of composite material used as compared to the current practice of placement through the water column in thicker but variable layers (2 to 6 inches).

6. MATERIALS AND METHODS

This section provides a detailed description of how scientific questions were approached and addressed for each of the four tasks. Details are provided for the experimental design of the laboratory investigations and proposed field work. Given that the overall goal of the project is to develop a chemically effective, mechanically stable, and cost efficient technology that could be deployed in a wide variety of environmental settings, all laboratory and field studies were designed to increase understanding of the practical effectiveness and limitations of the technology.

6.1. TASK 1: COMPOSITE MATERIAL TESTING

In order to determine the optimal mixture of reactive sequestering materials in the geotextile cap design, many laboratory studies were required to evaluate the empirical chemistry of adsorption. Coconut shell based activated carbon and three different formulations of brand name organoclays shown in Figure 6.1-1 were tested as potential sorbents for organic compounds and apatite was tested with metals. Several common contaminants of interest, including five (5) coplanar and non-coplanar PCBs, three (3) PAHs of different ring structures and water solubilities and two (2) heavy metals were subject to investigation. The batch studies were performed as both single contaminant systems and multi-contaminant competitive systems.

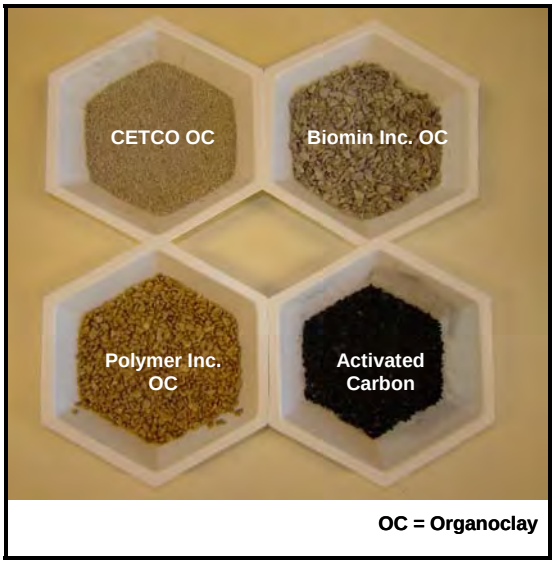

Figure 6.1-1. Reactive capping materials for organic contaminant sequestration.

The absorption capacity of the different sorbents was evaluated by performing batch experimentation (Figure 6.1-2). Initially, kinetics experiments were performed for each contaminant onto each sorbent. The kinetics of the reaction was used to determine the time to reach equilibrium. Kinetics experiments were performed at a single loading rate, typically with the contaminant concentration near the solubility of the compound and a moderate amount of sorbent applied. The experiments were performed with and without dissolved organic carbon in the form of humic acid being present in the system. Humic acid was preloaded onto the sorbent for 48 hours before spiking contaminants. Organic contaminants were prepared by dissolving the solid compound in acetone or methanol at a known concentration and spiking into 125 mL of de-ionized laboratory water. Pure stock laboratory metals standards were used in the apatite studies.

Figure 6.1-2. Batch experiments using activated carbon and organic contaminants.

Isotherms were developed using the established equilibration times. For this process, the experiments were conducted at different loading rates (mg of adsorbate per g of adsorbent) until maximum adsorption capacity was achieved (Table 6.1 1). Determination of the effect of dissolved organic carbon (DOC) at various concentrations on sorption affinity and capacity of sorbents was also established.

Contaminant	Solubility in water	Loading rates	Concentration of contaminant	Mass of contaminant	Mass of sorben added
	(mg/L)	(mg)/ AC(g)	(mg/L)	(mg)	(g)
Monochlorobiphenyl	4*	0.1- 200	0.08 - 160	0.01 - 20	0.1
Tetrachlorobiphenyl	0.26*	0.1 – 10.0	0.008 - 8	0.001 - 1	0.1
Hexahlorobiphenyl	0.038*	0.001 – 2	0.008 - 6	0.001 - 0.2	0.1
Naphthalene	31.69**	0.1-150	0.32-120	0.04-15	0.1-0.4
Phenanthrene	1-1.6**	0.1-500	0.48-400	0.06-50	0.1-0.6
Pyrene	0.129-0.165**	0.01-50	0.04-40	0.005-5	0.1-0.5
Lead	NA	0.05-20	0.3-40	0.03-4	0.15-0.6
Copper	NA	-	-	-	-
* Erickson M.D (1997) ** Fetterolf (1998)					

Table 6.1-1. Loading rates for adsorption experiments.

In order to extract the organic compounds from water, a liquid-liquid extraction was performed (Pirbazari and Weber 1981). Twenty mL of samples and 10 mL of hexane (pesticide grade) were placed in a 40 mL vial. The vials were sealed with Teflon® lined screw cap and shaken vigorously for 30 seconds three times at intervals of 30 seconds each. The top layer of hexane (containing contaminant and extraction surrogate) was then decanted off and filtered through 5 g of sodium sulfate and whatman 41 ashless filter paper. This cleanup step was performed in order to dry the samples and remove residual of humic acid. The samples were then stored at 4ºC prior to GC/MS analysis using USEPA SW-846 Method 8270C.

Experiments using metals and apatite were kept at a pH of 7. Ten mL samples were collected with syringes and filtered through 0.45 µm polypropylene filters. They were then preserved with ultra high purity nitric acid and stored at 4ºC prior to ICP-AES analysis using USEPA SW-846 Method 6010B.

6.2. TASK 2: PILOT SITE SELECTION

The purpose of selecting a pilot site is to identify a location for the small-scale field testing of geotextile mats. This site will also ultimately serve as the location for full-scale prototype mat system deployment.

6.2.1. Strategy Overview

The SAIC-UNH team has worked with EFANE/NFESC sponsors to select sites that will be appropriate for conducting the geotextile field tests. In order to accomplish this task, data on potential sites were reviewed for compatibility with expected mat performance characteristics. The overall site selection process was two-phased, with the first objective being the identification

of the most advantageous locations in terms of addressing the research goals from a "long list" of prospective Navy sites. Phase one is now complete, with two sites having been chosen as potential pilot sites based on the criteria provided in the following section. Descriptions of these two sites are presented in Section 7.2.1 of this report.

The second objective of the site selection process is to further characterize the geophysical properties of the two alternative sites with the ultimate goal of selecting one pilot site for small-scale geotextile testing. Work on the second phase is ongoing with the intent to conduct additional geophysical testing at each site before making a final decision. The availability of transportation venues and shoreside infrastructure will also be evaluated. In addition, one of the locations will be selected and assessed for groundwater seepage and pore water chemistry.

6.2.2. Primary Selection Criteria

As stated above, a series of criteria were generated in order to screen many prospective sites for characteristics that would allow for the most comprehensive understanding of the field dynamics of the reactive mats with the goal of choosing two sites for further geophysical evaluation. These criteria for phase one site selection included an evaluation of chemical, physical, and biological data as well as site management and logistical considerations. Desirable site chemical and physical characteristics used for the screening process are provided in Table 6.2-1. Desirable site biological characteristics are provided in Table 6.2-2. Desirable site management and logistical characteristics are provided in Table 6.2-3.

Chemical/Physical Factors	***Desired Characteristics***
Mixed Contaminants	Organic and metal contaminants at concentrations identified to cause moderate to high ecological or human heath risks.
Contaminant Levels	Contaminants at concentrations identified to cause moderate to high ecological or human heath risks.
Intertidal	Opportunity to demonstrate effectiveness in intertidal zones.
Stability Factors	Opportunity to demonstrate resilience of reactive mat with respect to destabilizers (e.g. slope, erosion, wave action).
Groundwater	Groundwater seepage contributing CoPC sources.
Sediment Oxygen Demand	Known condition and seasonal variability - not extreme.
AVS/Phosphate/Iron/TOC/Humic Acid	Known condition and seasonal variability- not extreme.
Rate/Quality of Sedimentation	Known condition/variability - not extreme. Understanding of ongoing processes and their effect on condition.
Other Sediment Characteristics Affecting Bioavailability	Known Grain size, clay presence and type of soot, humic acid, TOC,- not extreme.
Presence of Other Stressors Which May Confound Interpretation of Results	Remedial benefit must not be masked by ancillary factors (low oxygen, high ammonia, sulfides, thermal stress).
Smooth Surface	Absence of debris that would add logistical steps or compromise trial.

Table 6.2-1. Chemical and physical criteria used for the site selection process.

Biological Factors	***Desired Characteristics***
Previous site investigations conducted; benthic habitat degraded.	Scope for recovery is known and measurable.
Reference site established, representative, and sufficiently different from impaired site.	Ability to characterize change due to reactive mat.
Biofilm Expectation.	Test realistic biofouling to demonstrate degree of flow reduction thru mat.

Table 6.2-2. Biological criteria used for the site selection process.

Site Management and Logistics	***Desired Characteristics***
Previous Site Investigations Conducted	Analytical/habitat investigation completed.
Site Status	RI/FS or similar effort supports need for remediation in 2-5 years.
Site Activity	Absence of activities proximate to the study area that could confound interpretation of the reactive mat study.
Geographic Location	Demonstration sites are located in varying geographic regions.
Transport Access	Truck, vessel access for mat and equipment.
Site Access	Locations accessible or with un-restricted access by sampling personnel (including non-DoD personnel).
Site Facilities	Electricity, running water, facilities for sampling personnel.
Health and Safety	No significant health and safety concerns for field program execution. No UXO or active range concerns on firing range sites.
Client Cooperation	Support from site management.

Table 6.2-3. Management and logistics criteria used for the site selection process.

While these criteria were not quantitatively weighted, priority was given as to potential reactive mat effectiveness in binding bioavailable metal and organic contaminants at the site as well as in maintaining ambient environmental processes such as groundwater flux and surficial biological colonization. Other practical criteria for the phase one site selection process included the chronology and direction of each prospective site's risk assessment remedial management plans. Ideally, the site would be a near-term candidate for remedial dredging or traditional capping where it would be possible to test the hypothesis that the reactive mat would be the more effective, stable and economically advantageous alternative. Additional logistic considerations included accessibility of the site, availability of information to characterize existing conditions and site/program management staff with at least a minimal availability of time to support project planning and execution.

In establishing a suitably challenging environment, the literature describing each prospective site was reviewed to determine if remediation was planned and if contaminants of potential concern (CoPCs) had been established for both metals and organic contaminants. Other site factors that were sought included the absence of major obstructions such as rocks and/or debris that would make laying the mats difficult, and the presence of groundwater seeps to evaluate retention of existing water flow characteristics in the environment. Likewise, sites with energetic environments such as an intertidal or shoal-type habitat where a traditional sand cap would be insufficiently stable to provide a permanent form of remediation were desired.

Other salient characteristics of each prospective site included factors that would affect bioavailability of contaminants and/or reactive capacity of the apatite, organic carbon and organoclay to bind the contaminants. Findings from Task 1 laboratory studies including determinations of binding kinetics of reactive materials were also considered in the evaluation of

site suitability. For instance, sediment organic carbon and humic acids effect bioavailability and should not be present in very high concentrations for an optimal demonstration of reactive mat effectiveness.

6.2.3. Geophysical Surveys

Once two suitable sites were identified using the criteria provided in the preceding section, additional geophysical testing was planned to compare and contrast the properties of each location before ultimately choosing a pilot site for small-scale geotextile testing. This second phase geophysical evaluation will consist of bathymetry surveys, side-scan sonar surveys and sediment profile imaging (SPI) to be performed at each of the two locations. Data from these operations will be used to comprehensively characterize water depth, bottom features and habitat characteristics, respectively. The availability of transportation venues and shoreside infrastructure will also be evaluated in order to assess each site's ability to accommodate mat deployment and monitoring. In addition, one of the locations will be subject to confirmatory groundwater seepage and pore water chemistry testing. Based on the conclusions of the geophysical evaluations, one of the two primary sites will be chosen as the pilot site for small-scale geotextile testing and completion of Task 3 will proceed at that location.

6.3. TASK 3: GEOTEXTILE TESTING

Task 3 includes the construction and deployment of small-scale geotextile test mats of different compositions at one of the primary sites identified in Task 2. Although the final pilot site for mat deployment has yet to be determined, the test mats have been constructed based on the methodology described below. Once these mats are deployed, follow up investigations will include geotextile monitoring and testing as well as overall performance evaluation with the goal of identifying the geotextile most resistant to biofilm accumulation and adverse weathering effects.

Fabrication. Working with the Colloid Environmental Technologies Company (CETCO), UNH and SAIC decided on the construction of a total of 14 mats each measuring 2 m x 2 m. These mats were designed such that the amendment material is bound in a high loft core sandwiched between a woven backing geotextile and a non-woven top geotextile. This choice of geotextiles will enable the principal investigators to assess how material type, geotextile weight and apparent opening size affect biofouling and sediment clogging. In addition, some of the mats will be installed "upside down" to investigate how a woven geotextile behaves at the sediment interface. Twelve of the mats have a mixture of apatite, activated carbon and organoclay in the core. The maximum achievable loading rate was ~0.8 lb/sq ft due to the light density of activated carbon. The core mixture was composed of apatite (0.23 lb/sq ft), activated carbon and organoclay (0.28 lb/sq ft each). Two mats were also made with Ottawa sand in the core as controls. Table 6.3-1 summarizes the design of the mats.

Material	Weight	AOS	Core	Number of Mats
polyester	5	170	Mixed	4
polypropylene	6	70	Mixed	4
polypropylene	8	80	Mixed	4
polypropylene	6	70	Ottawa Sand	2

Table 6.3-1. Material design of small scale geotextile mats.

CETCO had organoclay and activated carbon on site while UNH provided approximately 800 lbs of raw apatite sand which was processed to produce a viable material. The sand was first screened to collect the material with a grain size between the 4 and 16 mesh sizes (4.75 mm and 1.18 mm) in order to remove debris (shells, rocks, sticks, etc.) and non-reactive soil. Particles in this size range also have higher phosphate content the fine material. The screened material was then crushed and re-sieved to obtain material between the 20 and 70 mesh (0.850 mm and 0.212 mm) in order to achieve a fine sand that was suitable for constructing the mats. Approximately 100 pounds of the crushed sand was sent to CETCO, with an additional 50 pounds kept at UNH for laboratory testing.

A geotechnical test system was purchased to measure the clogging potential of the composite mats. The ASTM D 5101 method directly measures the clogging potential of the actual sediment/geotextile system (i.e., an intact column of sediment covered by the reactive mat) so as to provide a realistic estimate of the actual cap performance with regard to clogging and sediment infiltration. Preliminary testing showed that trapped bubbles are a significant problem when using a fine grained material such as sediment. The test procedure is currently being modified to be conducted using upward flow through the sediment and geotextile, which better simulates the actual field conditions where groundwater is present. In addition, experiments are being conducted to determine if sample preparation in a nitrogen atmosphere will help eliminate bubbles. Figure 6.3-1 is a photograph of the current experimental setup.

Figure 6.3-1. Permeability column test setup.

Deployment. Test mats will be shipped directly to the pilot site for field deployment. As biofouling and biofilm growth are site specific, the test mats will be deployed soon after Task 2 is completed and a pilot site is established in order to maximize the time available for selection of the geotextile to be used for prototype full-scale mat construction. The small-scale geotextiles will be deployed with sufficient space between them to reduce any possible interference (e.g., suppression of groundwater flux by nearby mats).

Monitoring and Testing. Following deployment, divers under the direction of SAIC will inspect and collect samples from the geotextiles to document their condition. To evaluate biofouling, push cores of the geotextile mats will be collected with mat surface and overlying water preserved in the core tube. At the UNH lab, cores taken from the field will be analyzed to measure changes in hydraulic conductivity due to biofouling. Observations of relative percent fouling of the geotextile material will be made. Permeability tests will be performed by removing the bottom cap from the core tube, and measuring the time required for static head pressure of the overlying water column to flux through the mat "plug" at the end. The elapsed time will be compared to a control of clean, un-fouled mat. After this test, the fouling layer will be scraped off the mat, dried, and then weighed.

A related issue is the growth of biofilms on the surface of the reactive materials themselves, regardless of specific type of material used in the mat. These colonies may not be sufficient to cause biofouling by clogging the pore spaces, but they may influence the local chemistry at the surface of the amendments, thus influencing contaminant uptake. Samples of biofilm coated materials will be gathered during this task and retested using the same techniques used in Task 1 to quantify how biofilms may enhance or diminish amendment effectiveness. Additional samples of reactive core material will be gathered to determine how the in situ redox conditions influence amendment effectiveness. The samples will again be tested following the techniques used in Task 1, though the samples will be sterilized first to minimize the impact of biofilms.

Performance Evaluation. The relationship between permeability and fouling data from this task will be evaluated in light of initial measurements collected in Task 1 to determine whether surficial fouling is significantly impeding hydraulic conductivity. These data will help select the geotextile offering the best balance between fouling resistance and contaminant of amendment material, and whether a sand cap is needed to protect the mat from biofouling organisms. Based on these results, the mat design may be modified (e.g., alternate type of geotextile, alternate dimension, layering strategy, etc.) prior to construction and deployment of the prototype mats (Task 4). Ancillary information on the effects of biofouling on reactivity will be compared to the laboratory data collected in Task 1 to determine if deployment in an anoxic environment causes any significant change in performance compared to the laboratory tests.

6.4. TASK 4: PROTOTYPE MAT TESTING

The purpose of Task 4 is to field test a prototype mat system constructed of the most effective amendment (identified in Task 1) and the geotextile most resistant to fouling (identified in Task 3) in order to assess in-situ chemical sequestration effectiveness and flux properties. To accomplish this task, full-scale prototype mats will be constructed per exact specifications and deployed at the pilot site identified in Task 2. Task 4 cannot be undertaken until both Task 2 and

Task 3 have been fully completed. Full-scale mats will be fabricated and deployed based on the methodology described below and as-built confirmation and monitoring by passive sampling will also be conducted.

Deployment. For the prototype treatment, two mat rolls (each 15 feet by 25 feet by ½ inch thick) will be laid side-by-side with some overlap, yielding a footprint of approximately 25 feet by 25 feet. This footprint is estimated to be the minimum area required to alleviate "edge effects" such that groundwater should percolate through the mat rather than simply be displaced to the edges. The actual footprint of the deployed mats may vary slightly, however, depending on pilot site conditions.

The mat rolls will be loaded from a wharf at the site onto a deck barge using a crane or fork truck. The barge will be fitted with a spindle or frame fixture that will allow pay-out of the material from the edge of the vessel. Divers will bring the tail edge of the roll to the bottom, securing it in place with sand bags. The barge will then back away, paying out the rolled material over the bottom. The divers will monitor the mat to ensure it rests evenly on the bottom. Once the mat sections are deployed, additional sand bags will be placed at the edges to anchor it in place. Additional anchoring with steel rod or screw-type anchors may be necessary to secure the mat. The mats will be deployed with sufficient space between them to reduce any possible interference (e.g., suppression of groundwater flux by nearby mats).

On the second day of the deployment, one of the mat treatments would receive an additional 3 to 6-inch biological layer of sand/silt mix (up to 28 yd^3) to provide a substrate for recolonization of the benthos while at the same time protecting the mat from bioturbation. Sand capping to typical cap depths (3 to 6 inches up to 28 yd^3) of an equivalent area with no mat will serve as a control. The sand will be spread over the areas by washing it over the side of the deck barge with a large volume hose drawing site water. This provides a gradual deposition of sand on the cap, rather than a potentially damaging mass of sand from a clamshell bucket.

As-Built Confirmation. Divers will visually inspect the mats to ensure they have been properly deployed, and inspect the sand layer to ensure adequate sand coverage has been achieved. They will install settlement rods into the mat to serve as a vertical control against which to make follow-up measures of mat settlement, burial, etc. In addition, a 1-day acoustic (side-scan, sub-bottom) survey of the cap will be done shortly after placement to look for localized cap failure and to evaluate the overall quality of cap deployment. The side-scan images will help confirm that the cap was resting flat on the bottom. Sub-bottom profiles will help confirm that the cap is in contact with the bottom, and that any voids between the cap and substrate are minimal.

Monitoring by Passive Sampling. Five months after deployment, after the mat has had sufficient time to "settle" on the bottom, divers will return to install two types of in situ passive diffusion samplers to measure sequestration of contaminants by the mat. By installing such devices above and below the mat (as accessed at center seams), the effectiveness of the mat in sequestering metal and organic contaminants in the substrate can be evaluated. Passive sampling devices will include both pore water expression samplers ("peepers") and semi-permeable membrane devices (SPMDs). Divers will also inspect the mat for stability, including any

slumping affects due to wave and current action, as well as benthic colonization. Finally, the divers will measure mat height relative to the settlement rods and photo document mat condition. This inspection will be repeated one year post-deployment.

Also at the one year interval, seepage meter measurements will be made to quantify water flux from sediments and through the mats as well as to identify any change in contaminant concentration with respect to source (e.g., groundwater flux out of the mat versus overlying water penetration into the mat). Also at that time, trident probe measurements will be conducted to allow mapping of groundwater flow and to guide sampling locations for pore water measurement. Finally, divers will collect push cores of the mats as well as under and over (naturally-deposited or sand) layers of sediment for chemical analysis. Analytical results will provide information on metals and organics speciation between the substrate and the mat, thus identifying any enhanced ability of the mat to preferentially bind certain contaminants over others.

7. RESULTS AND ACCOMPLISHMENTS

This section provides an explanation of how the project's objectives have been met to date by documenting the technical progress and accomplishments in relation to specific tasks and milestones. Specific figures and tables are provided that highlight the data obtained for each task.

7.1. TASK 1: COMPOSITE MATERIAL TESTING

The purpose of Task 1 is to identify the mixture of amendment materials that would most effectively sequester contaminants as part of a reactive mat. To accomplish this task, UNH conducted laboratory tests to collect data on adsorption, sequestration and chemical breakthrough properties of the potential mixed reactive mat system. Results of these experiments with regard to absorption kinetics, adsorption isotherms and the effects of humic acid on adsorption properties are discussed in the following sub-sections. Finite element models were also prepared to evaluate potential sediment deformation and pore water pressure increases caused by the weight of the reactive cap. Results of the initial modeling process are also provided.

7.1.1. Absorption Kinetics

Kinetics experiments were performed in the laboratory to determine the time needed to reach equilibrium for specific contaminants with the proposed capping materials in the presence and absence of humic acid. Currently, data has been obtained for the kinetics of the adsorption of monochlorobiphenyl (Figure 7.1-1), tetrachlorobiphenyl (Figure 7.1-2), hexachlorobiphenyl (Figure 7.1-3), phenanthrene (Figure 7.1-4) and pyrene (Figure 7.1-5) to activated carbon; and for the adsorption of copper and lead (Figures 7.1-6 and Figure 7.1-7) to apatite. Humic acid was found to reduce the adsorption capacity of most compounds and to slow the time to reach equilibrium in most cases. The kinetics experiments will be repeated for the organic compounds in the future using select organoclays.

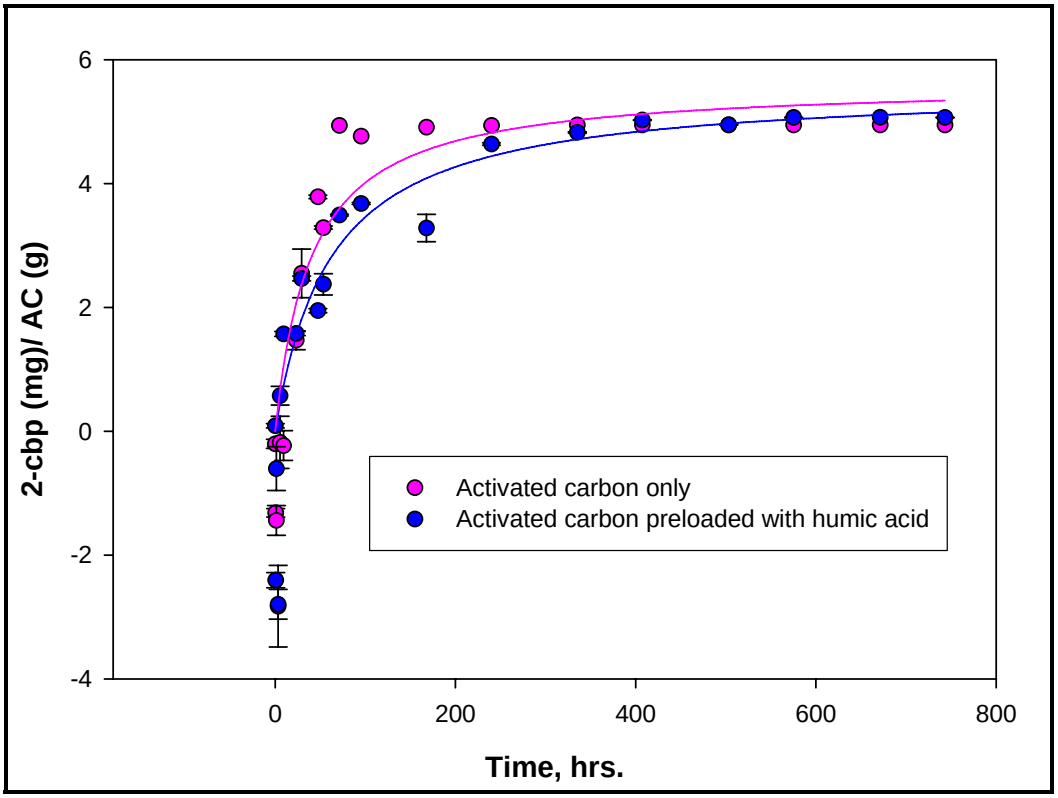

Figure 7.1-1. Kinetics of 2-chlorobiphenyl adsorption on activated carbon.

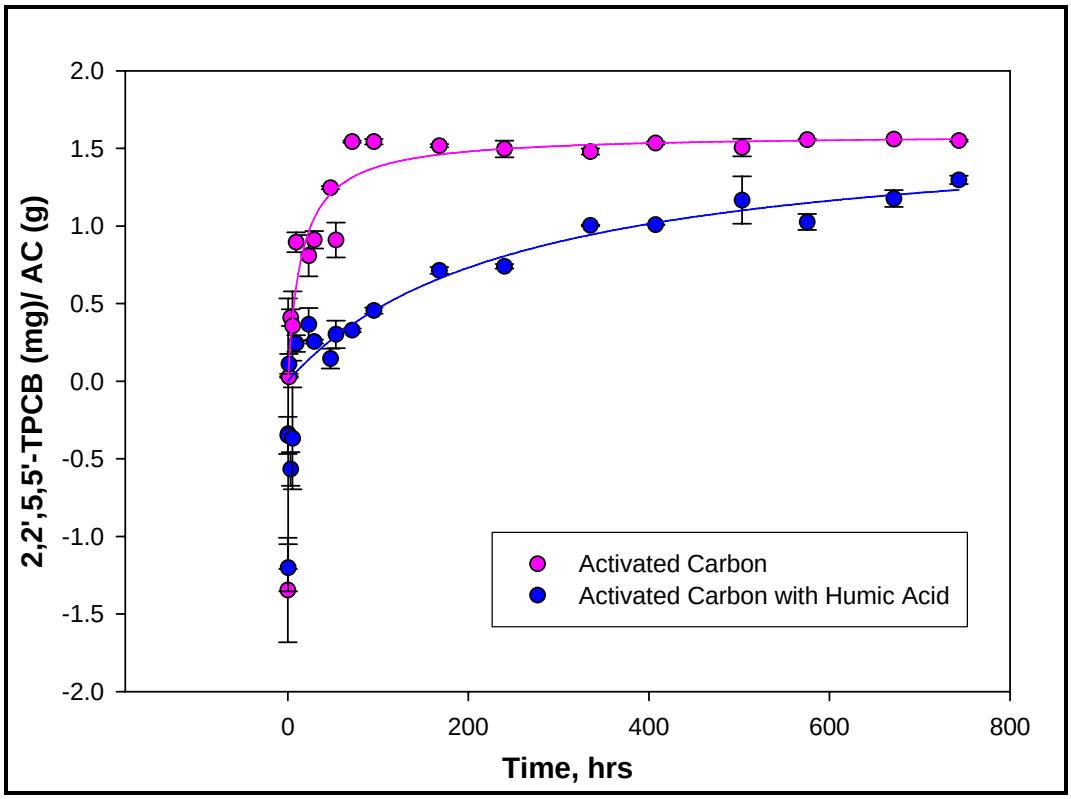

Figure 7.1-2. Kinetics of tetrapolychlorobiphenyl adsorption on activated carbon.

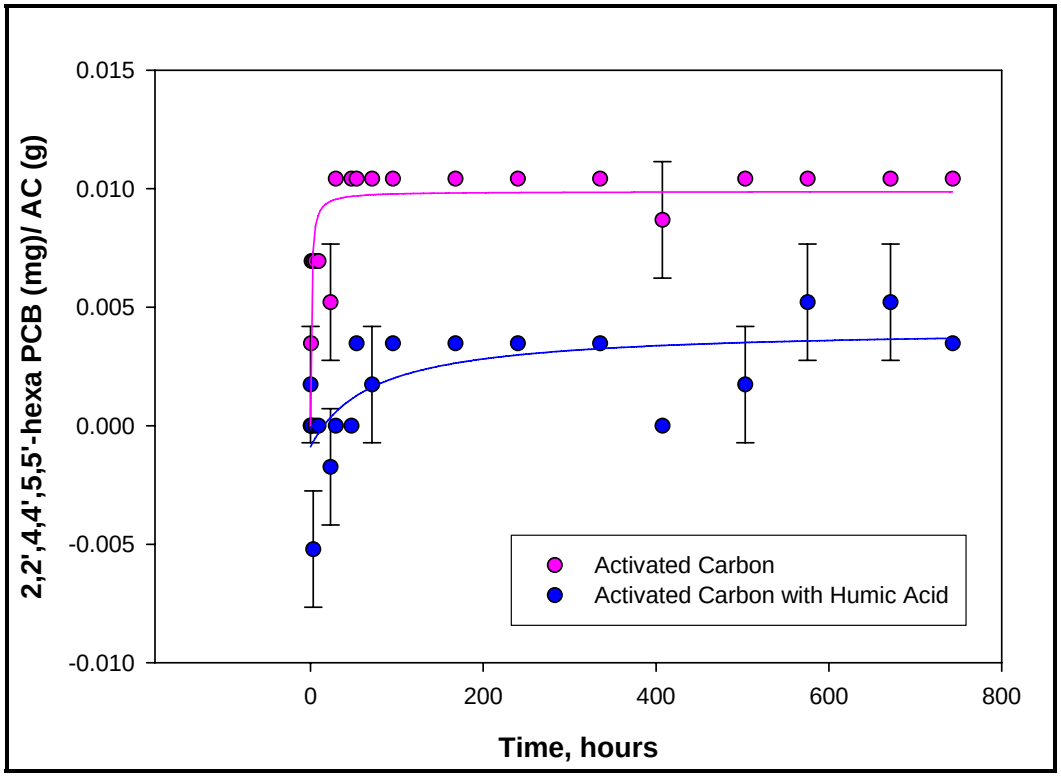

Figure 7.1-3. Kinetics of hexachlorobiphenyl adsorption on activated carbon.

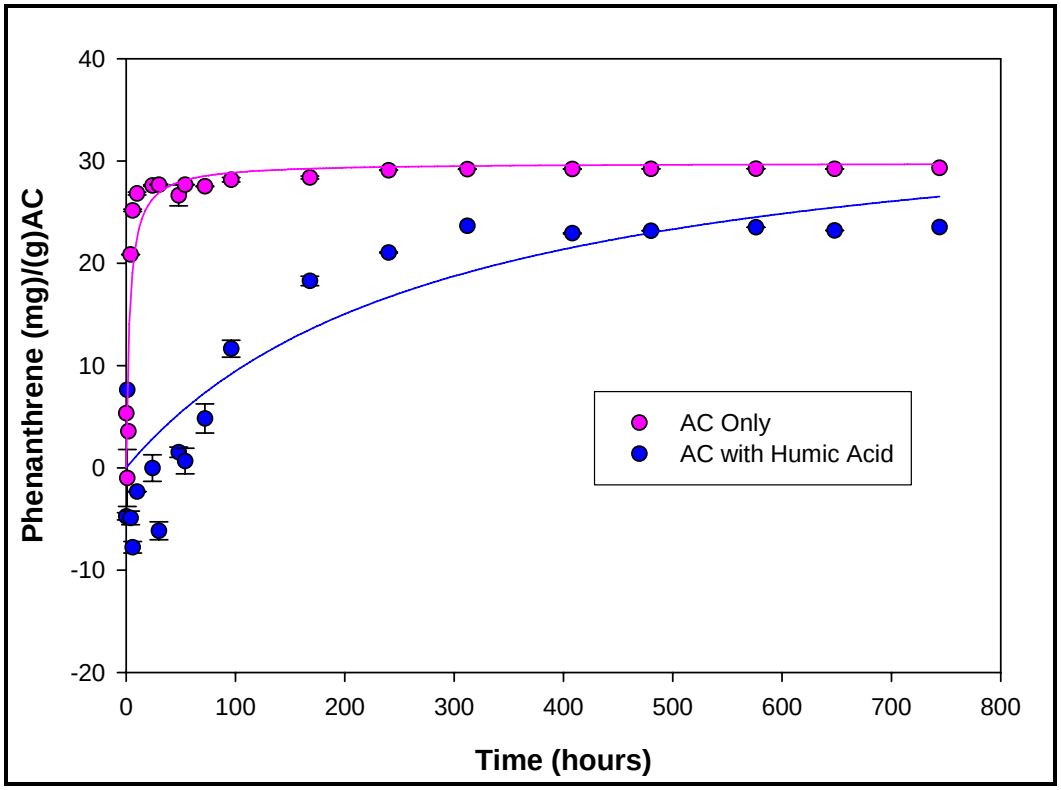

Figure 7.1-4. Kinetics of phenanthrene adsorption on activated carbon.

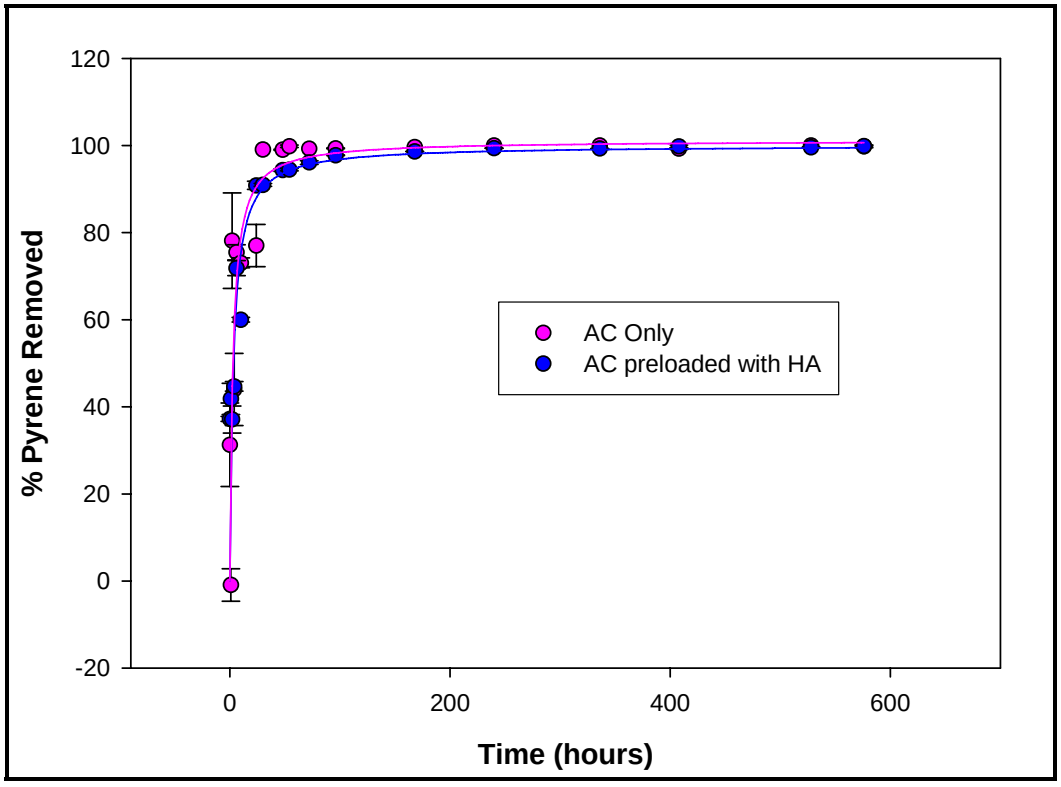

Figure 7.1-5. Kinetics of pyrene adsorption on activated carbon.

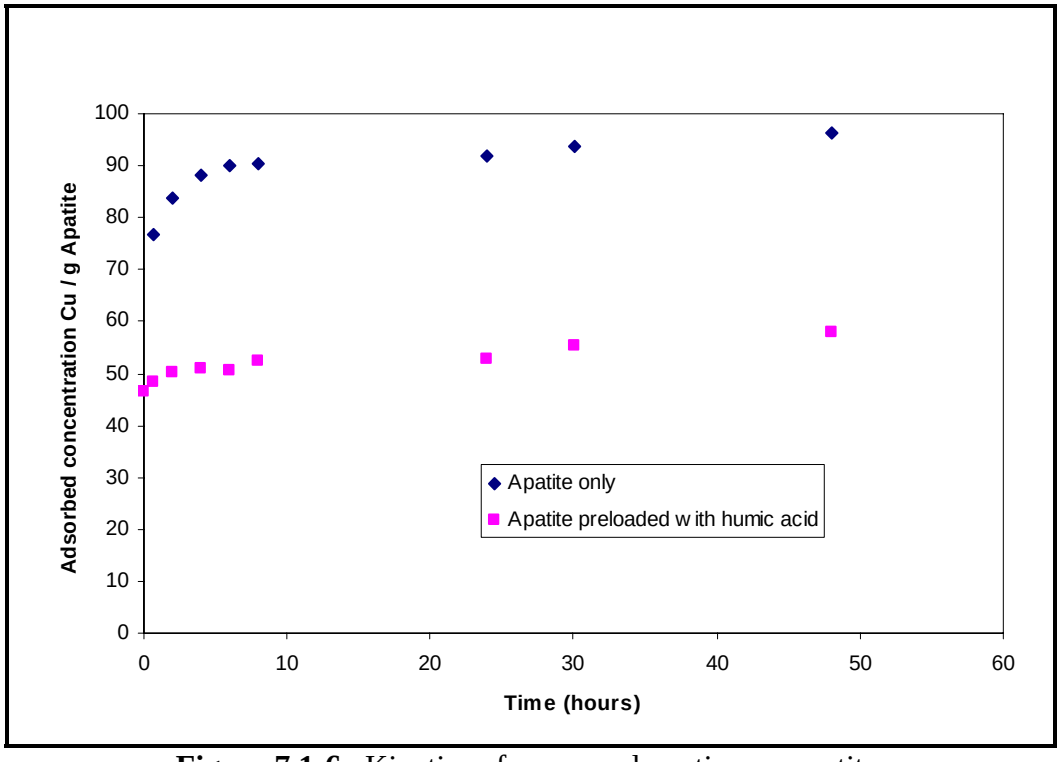

Figure 7.1-6. Kinetics of copper adsorption on apatite.

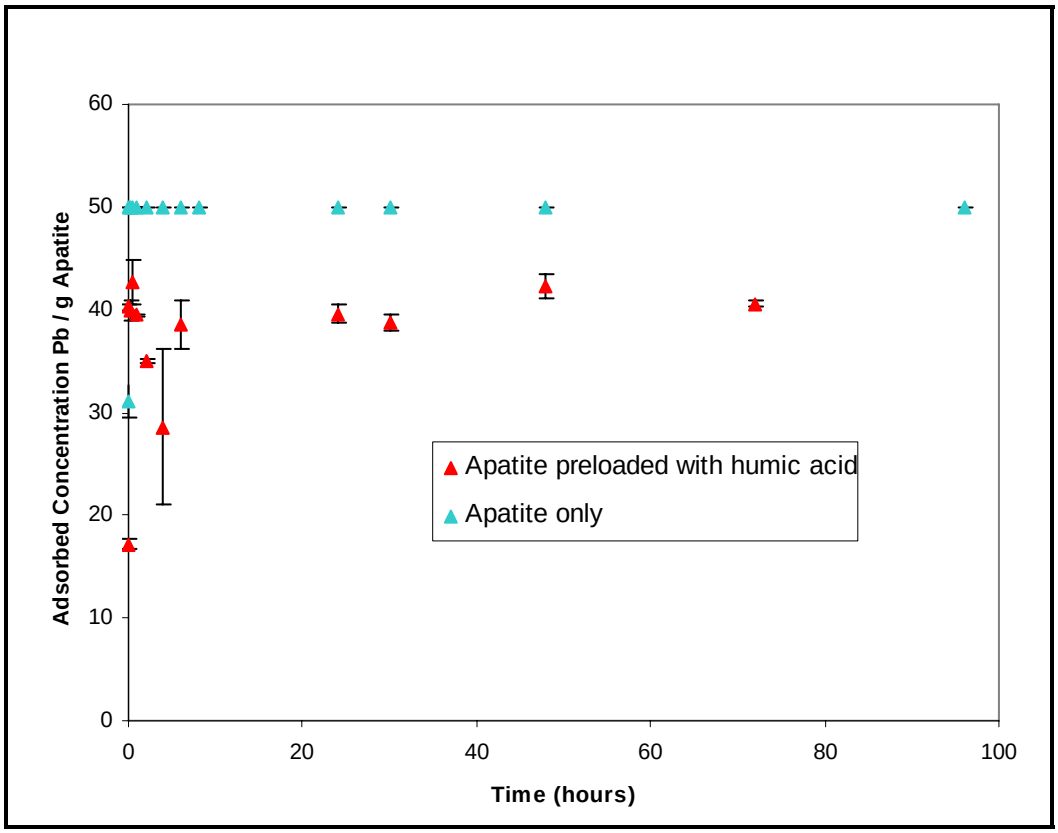

Figure 7.1-7. Kinetics of lead adsorption on apatite.

7.1.2. Adsorption Isotherms

Adsorption isotherm experiments are continuously running in order to determine the effects of humic acids found in sediments on the adsorption of contaminants to the proposed capping materials. Currently, UNH has produced adsorption isotherms at a suite of loading rates for 2-chlorobiphenyl (Figure 7.1-8), 2,2'5,5'-tetrachlorobiphenyl (non-coplanar; Figure 7.1-9 and Figure 7.1-10), 3,3'4,4'-tetrachlorobiphenyl (coplanar; Figure 7.1-11 and Figure 7.1-12), 2,2',4,4',5,5'-hexachlorobiphenyl (Figure 7.1-13), 3,3'4,4',5,5'-hexachlorobiphenyl (Figure 7.1-14), phenanthrene (Figure 7.1-15) and pyrene (Figure 7.1-16) on activated carbon and for lead (Figure 7.1-17) on apatite. Preloading activated carbon with humic acid resulted in reduced sorption in all cases. Spiking humic acid after a contaminant has equilibrated with activated carbon indicated in most cases that humic acid does compete with activated carbon for the sorption of contaminants or that complexation by humic acid in solution causes desorption to occur (these data are referred to as "spiked with HA"). Isotherm experiments to evaluate the adsorption capacity of activated carbon for naphthalene and apatite for copper with and without humic acid are also in progress. Eventually, all experiments will be repeated using organoclays and the same organic contaminants, as well as adsorption studies using various mixtures of contaminants and sorbents to evaluate competition effects. Once completed, a peer-reviewed journal article is expected to be published with these kinetic and adsorption studies for the organic compounds and activated carbon.

In Figure 7.1-8, the reducing effect of preloading of activated carbon with humic acid was found to be very high, which can be attributed to the pore-blockage effect. It can also be seen that once 2-chlorobiphenyl gets adsorbed on activated carbon, subsequent spiking with humic acid causes a negligible amount of desorption.

Figure 7.1-9 represents non-coplanar tetrachlorobiphenyl with the solubility limit of 0.26 mg/L in water. In this plot it can be seen that the effect of preloading humic acid is high but there is negligible desorption. If the data points are extended to concentrations higher than the solubility limit to super-saturated conditions, however, then the desorption effect becomes prominent as shown in Figure 7.1-10.

Figure 7.1-11 is a coplanar tetrachloro-congener with the solubility limit of 0.26 mg/L in water. This plot also shows the effect of preloading activated carbon with humic acid but no desorption effect can be seen when humic acid is spiked after equilibration. If data points are increased to a super-saturated condition (Figure 7.1-12), however, then the trend was found to be different than that of non-coplanar congener. In super-saturated conditions, an unfavorable adsorption pattern was seen in the case of preloaded activated carbon but there was no desorption effect.

Figure 7.1-13 is a non-coplanar hexachloro-congener with the solubility limit of 0.038 mg/L. In this plot it is apparent that the reduction in adsorption capacity of activated carbon is greater in the case of preloading, although there is negligible desorption effect. In the case of a co-planar hexachloro-congener there is negligible effect in both the cases (Figure 7.1-14).

Figure 7.1-15 is an isotherm for the PAH phenanthrene with the solubility limit of 1.2 mg/L. In this plot we can see that the adsorption capacity of activated carbon is greater with humic acid preloading, and there is a slight desorption effect when humic acid is spiked into the solution. In the case of pyrene (solubility 0.12 mg/L), humic acid has an effect on adsorption and the desorption effects are not yet shown (Figure 7.1-16).

Figure 7.1-17 shows the adsorption of lead onto apatite at pH 7 for various loading rates. Preloading apatite with humic acid shows a marked decrease in adsorption efficiency of apatite.

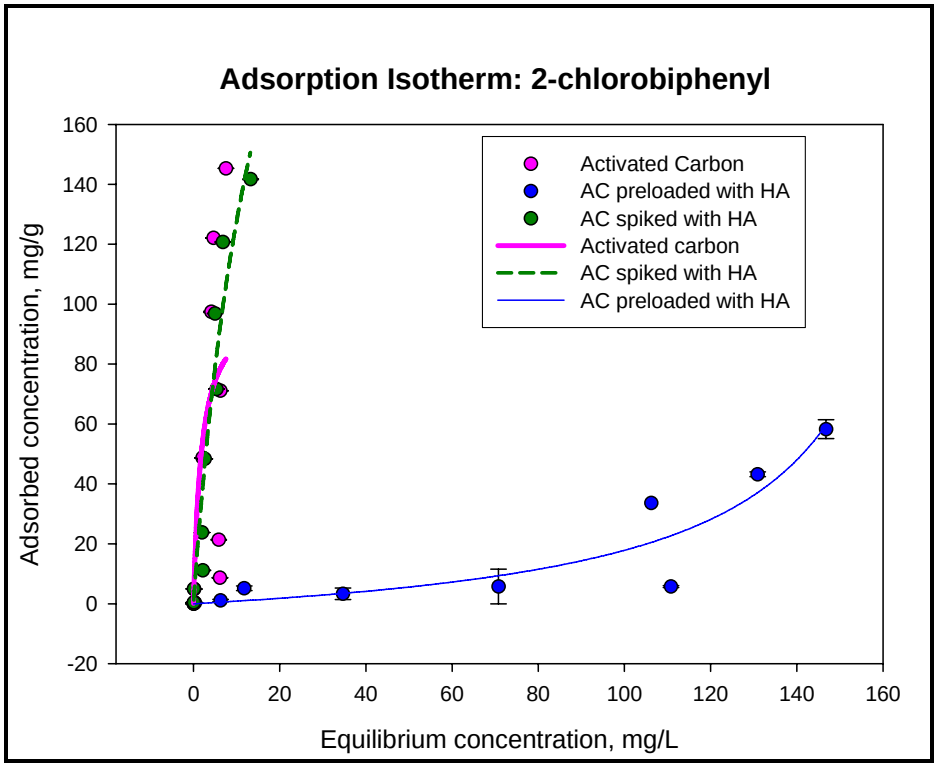

Figure 7.1-8. Adsorption isotherm of 2-chlorobiphenyl onto activated carbon.

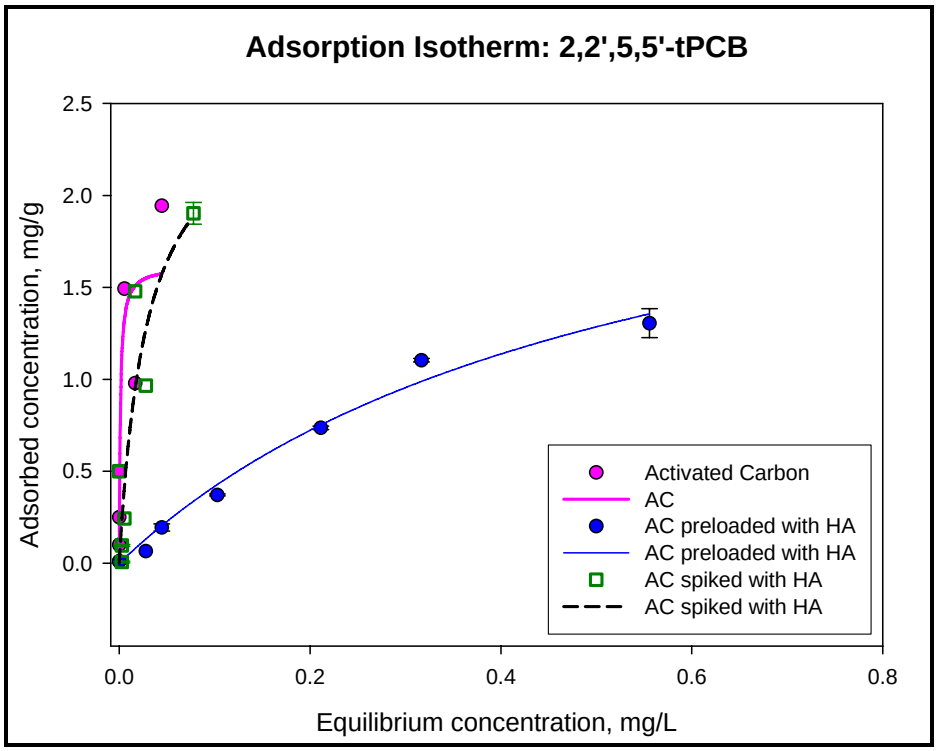

Figure 7.1-9. Adsorption isotherm of 2,2',5,5'-tetrachlorobiphenyl onto activated carbon.

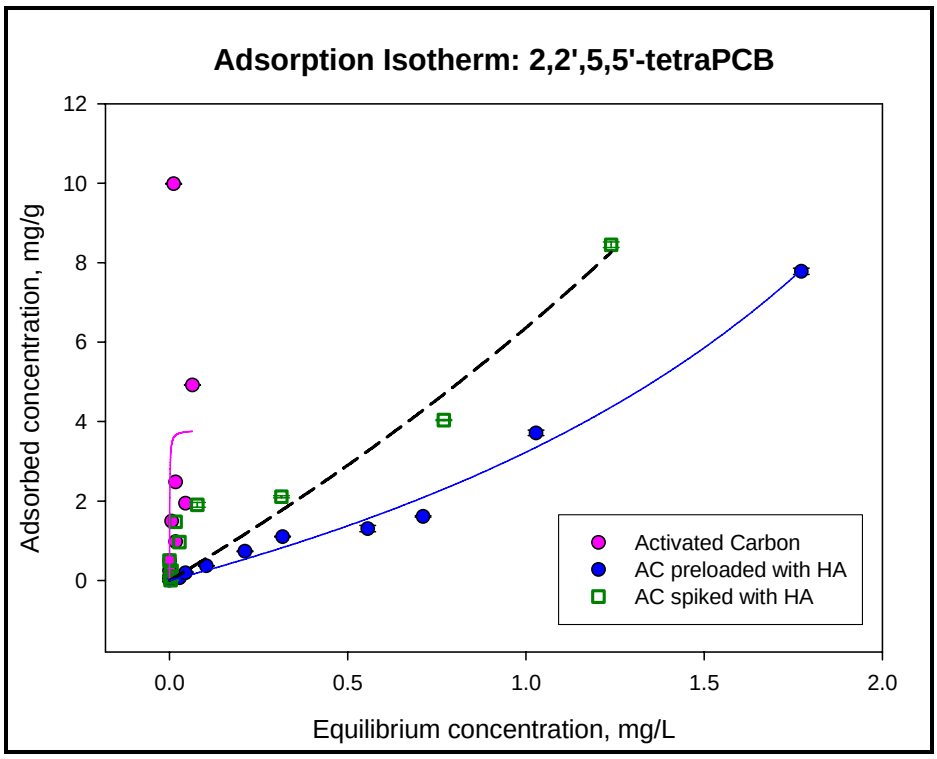

Figure 7.1-10. Extended adsorption isotherm of 2,2',5,5'-tetrachlorobiphenyl onto activated carbon.

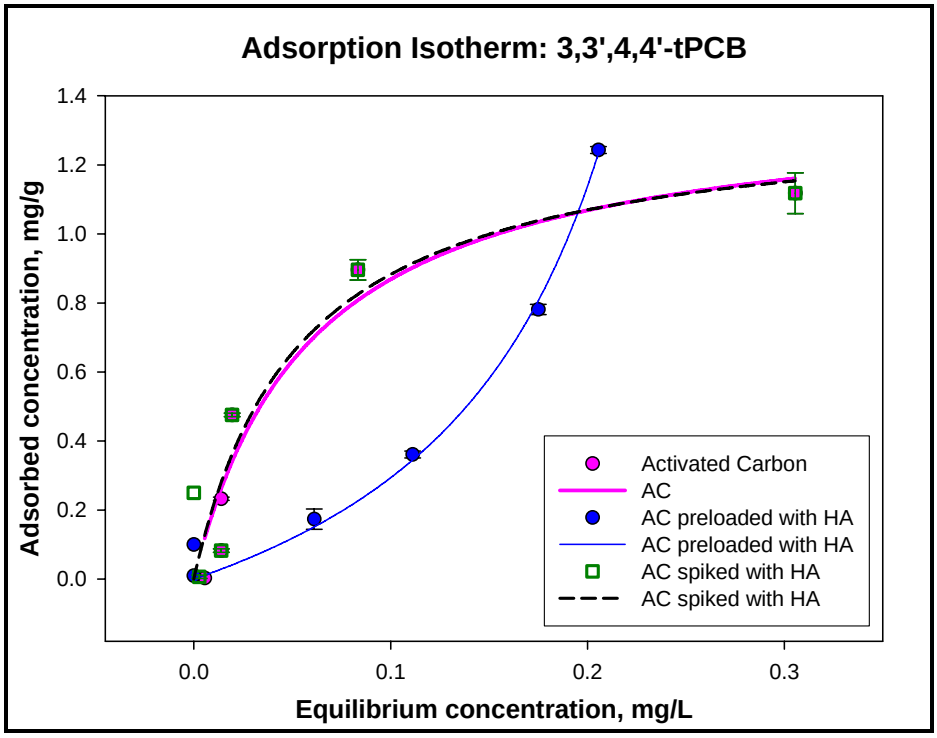

Figure 7.1-11. Adsorption isotherm for 3,3',4,4'-tetrachlorobiphenyl onto activated carbon.

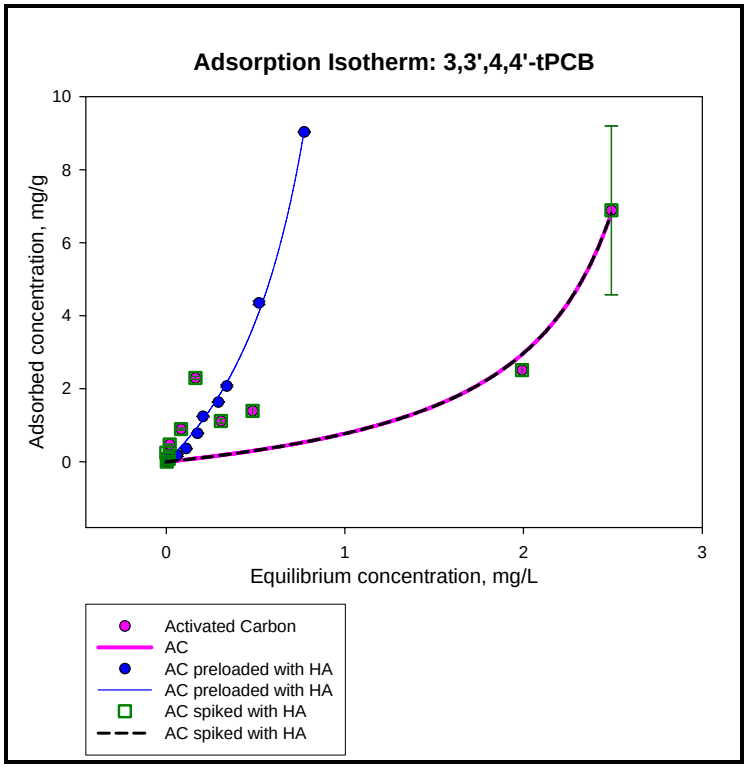

Figure 7.1-12. Extended Adsorption isotherm for 3,3',4,4'-tetrachlorobiphenyl onto activated carbon.

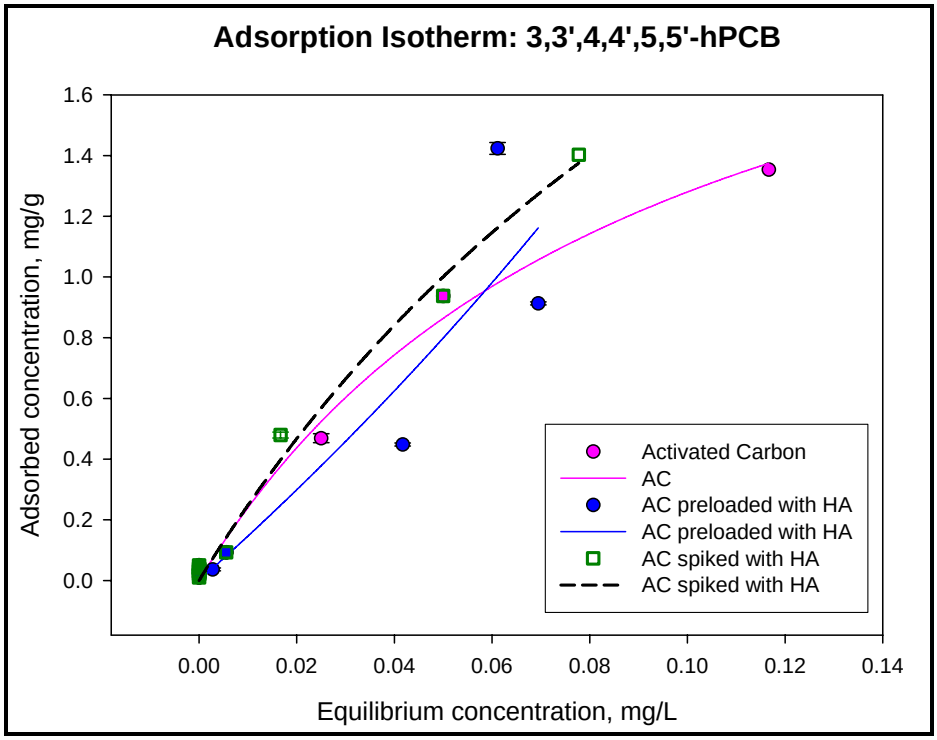

Figure 7.1-13. Adsorption isotherm of non-coplanar 2,2',4,4',5,5'–hexachlorobiphenyl onto activated carbon.

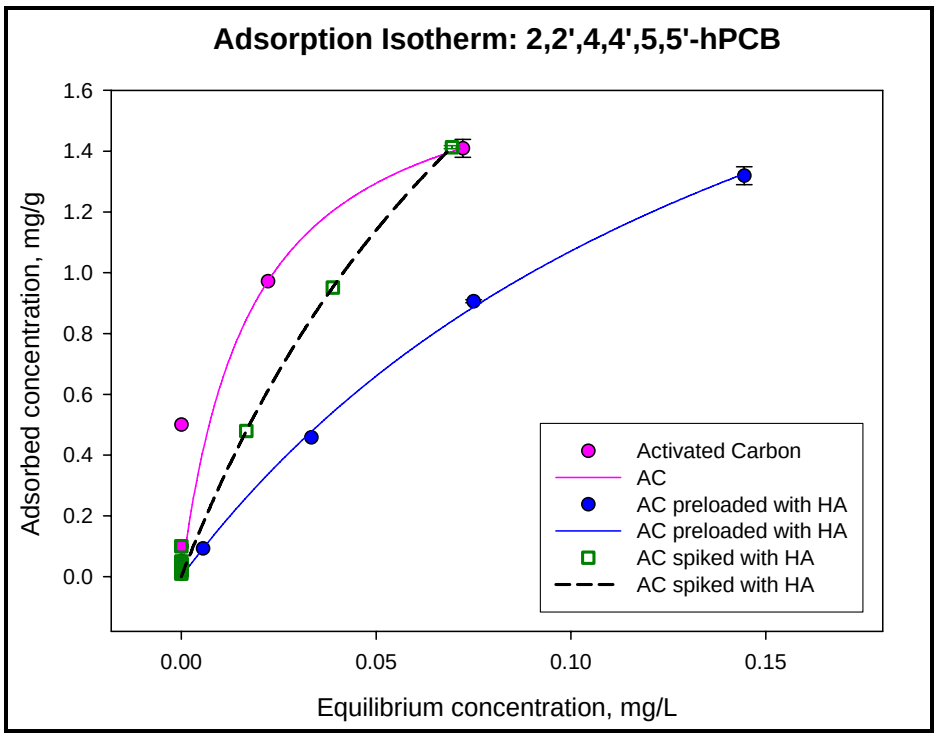

Figure 7.1-14. Adsorption isotherm for co-planar 2,2',4,4'5,5'-hexachlorobiphenyl onto activated carbon.

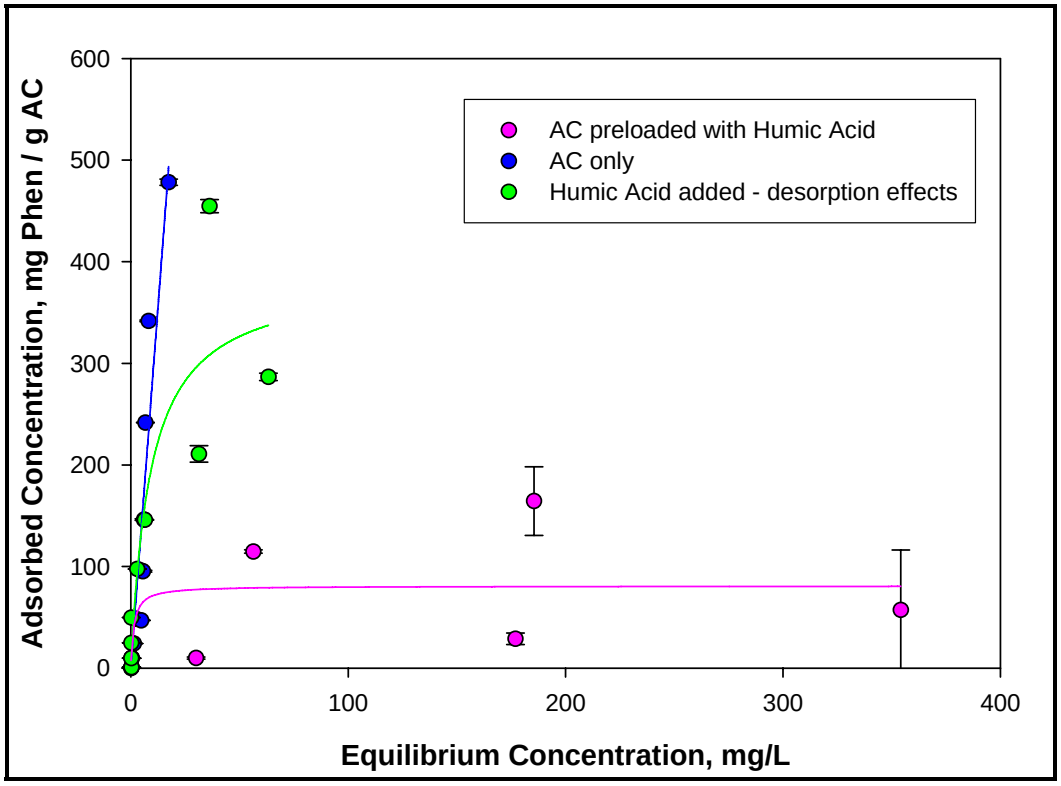

Figure 7.1-15. Adsorption isotherm for phenanthrene onto activated carbon.

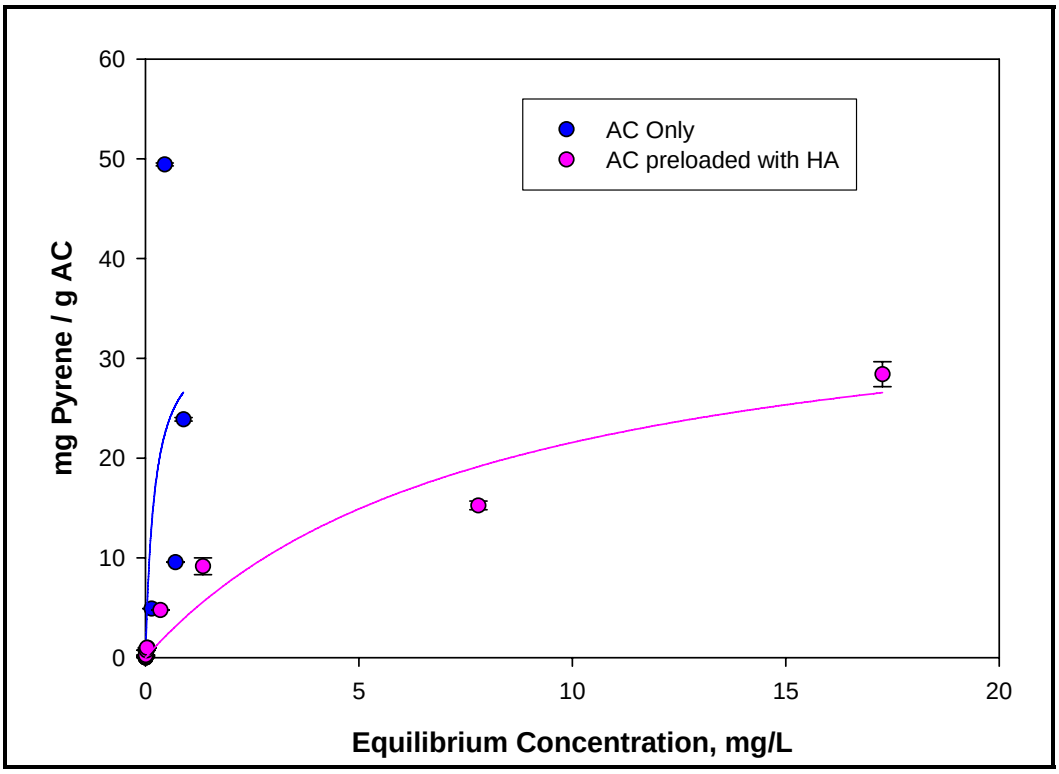

Figure 7.1-16. Adsorption isotherm for pyrene onto activated carbon.

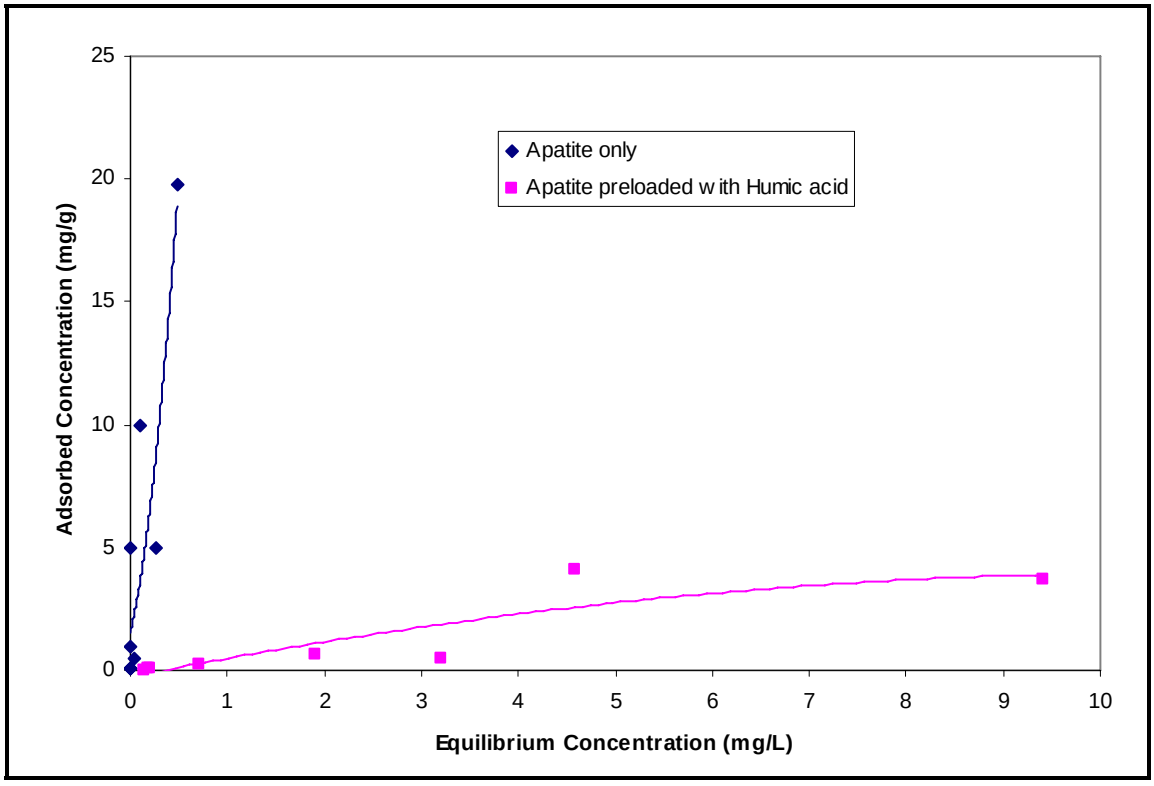

Figure 7.1-17. Adsorption isotherm for lead onto apatite.

7.1.3. Effects of Humic Acid Concentration

In varying the amount of humic acid in solution, adsorption decreased with increasing concentration of humic acid as shown for 3 PCBs and phenanthrene in Figure 7.1-18, Figure 7.1-19, Figure 7.1-20 and Figure 7.1-21, respectively. Phenanthrene shows significant deviations from the behavior of the other compounds studied, with a marked increase in sorption affinity with increased humic acid concentrations. The mechanisms responsible for this observation have not yet been investigated.

In summary, humic acids can have significant influence on the performance of activated carbon and apatite. Even more significantly, for some compounds in the presence of humic acid there is a significant desorption of PAH and PCB that was previously adsorbed. This phenomenon is likely due to the complexation of the aqueous phase of the chemicals which increases the total concentration of the aqueous phase contaminant. In general, these results show that a thin reactive cap will not be sufficient. Humic acid effects do have to be taken into consideration regarding the proper design of a reactive cap as well as an accurate prediction of its long-term performance.

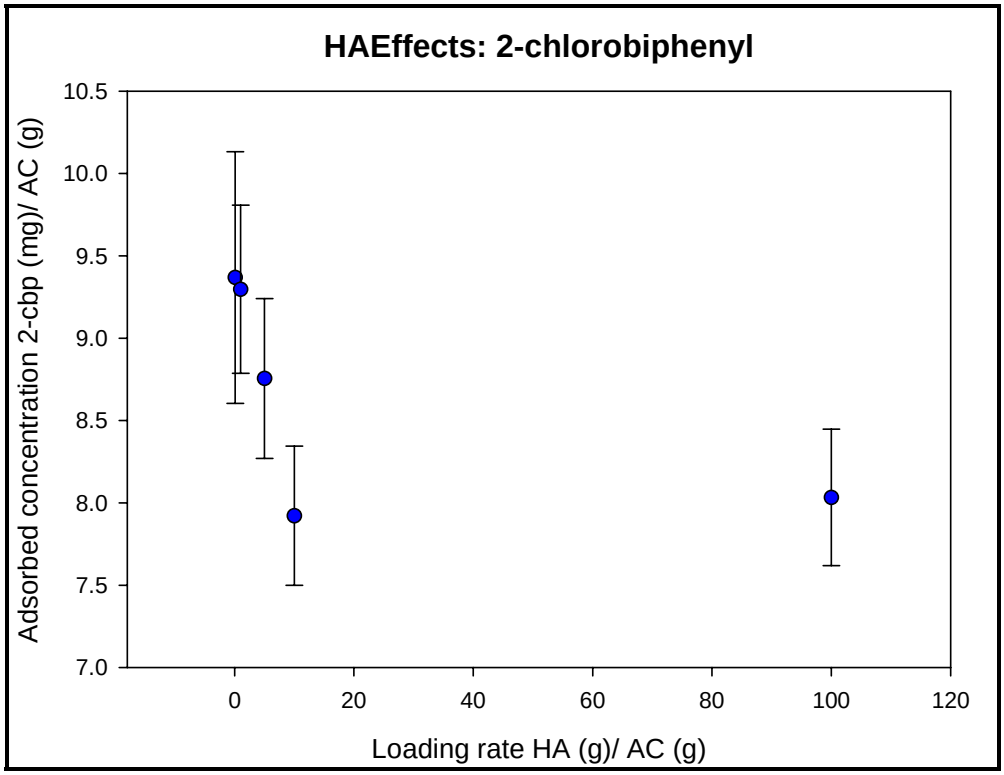

Figure 7.1-18. Humic acid effects on monochlorobiphenyl sorption to activated carbon.

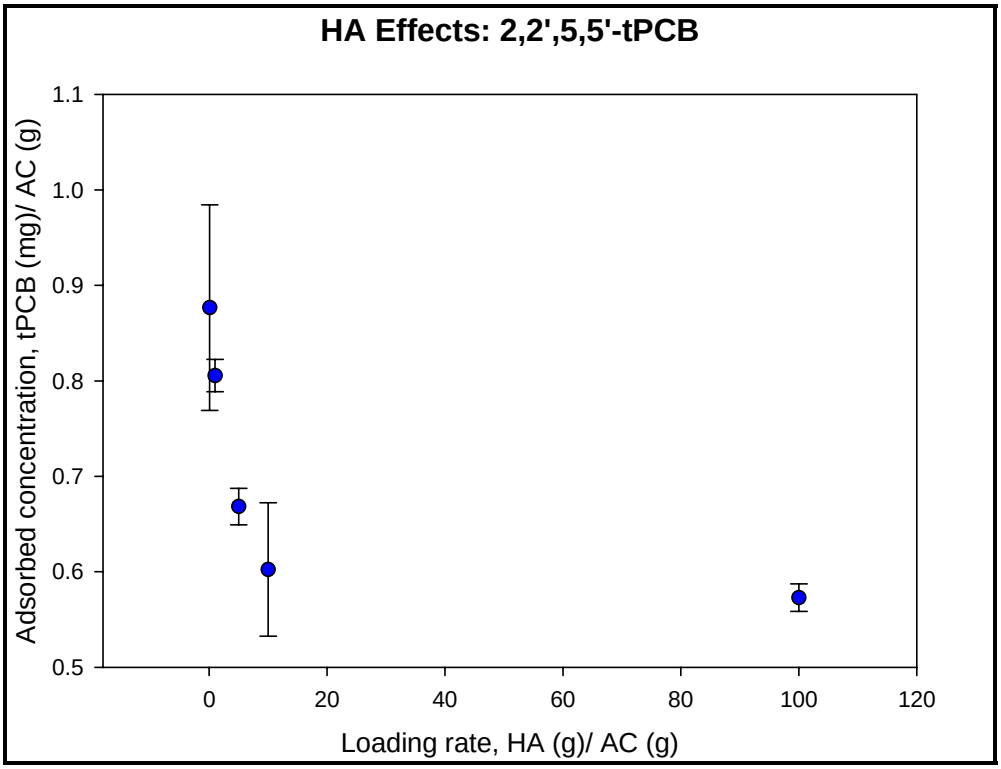

Figure 7.1-19. Humic acid effects on tetrachlorobiphenyl sorption to activated carbon.

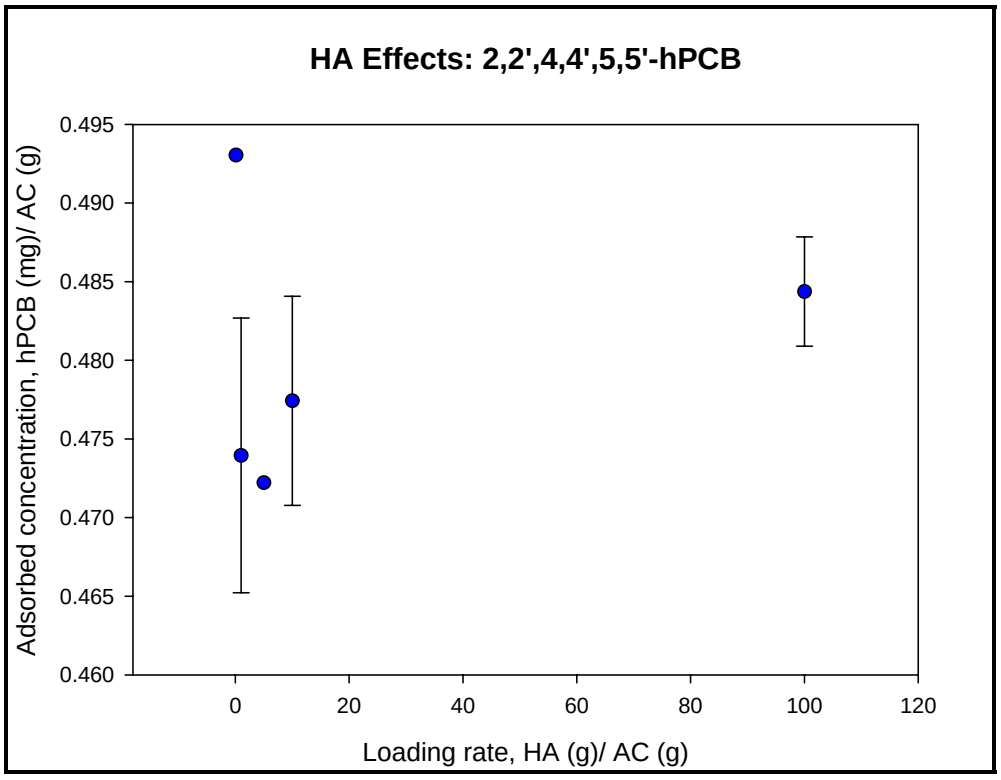

Figure 7.1-20. Humic acid effects on hexachlorobiphenyl sorption to activated carbon.

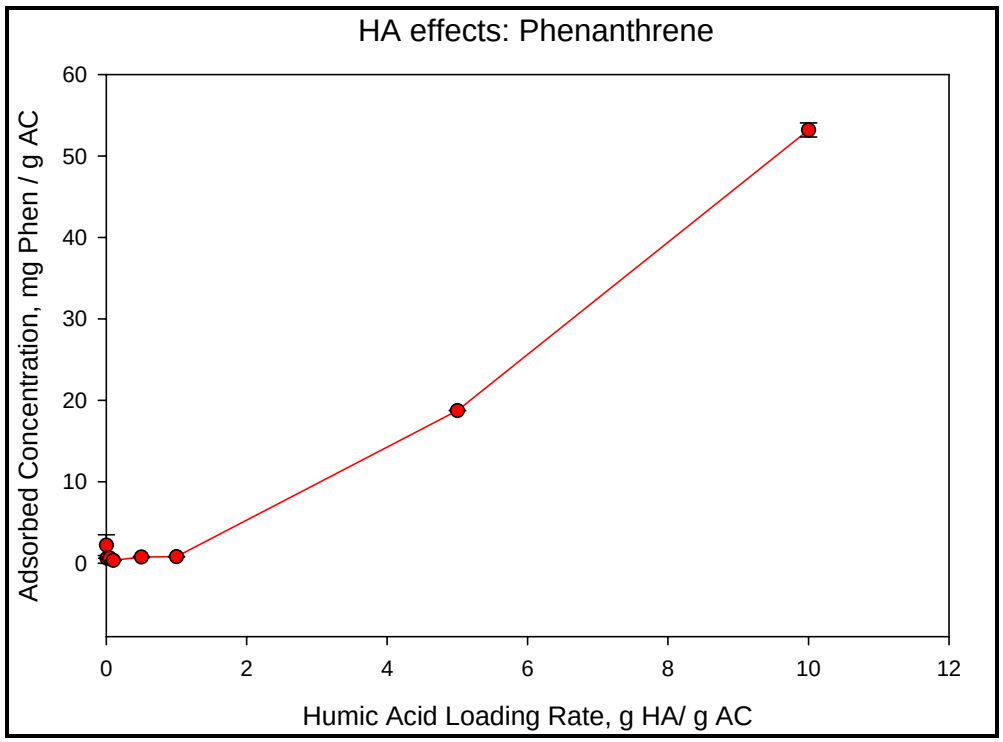

Figure 7.1-21. Humic acid effects on phenanthrene sorption to activated carbon.

7.1.4. Finite Element Modeling

The main goal of the finite element analysis (FEA) is to understand the potential sediment deformation (consolidation) caused by the weight of the cap as well as the subsequent pore water pressure increase and resulting advective transport. The use of FEA allows for an evaluation of 2D transport with regard to flow around the cap edges. A groundwater component will eventually be added to see how this edge flow affects advective transport.

The current finite element model was constructed with Plaxis v. 8.0 using a symmetrical half-sand cap 5 m in length. The model represents a 10 m wide mat but by symmetry only a half portion is actually modeled. To minimize any boundary effects an extended model was also developed. The geometry of the extended model was defined as a total width of 33 m (6 times the mat width) and a depth of sediment of 25 m (5 times the mat width). Figure 7.1-22 presents the geometry of the extended model.

For the current model, the 5 m half-sand cap is placed over sediment that is treated as an elastic-plastic material with no creep. The sand layer (protective layer) has a thickness of 30 cm (1 ft). Because PLAXIS v. 8.0 does not have the ability to model the geotextile cross plane permeability, the geotextile in this model only works as a tension element. Thus the mat was modeled using a double system with the following properties:

- A geotextile element was used to account for the tension supported by the mat. The properties required for this type of element are Young's Modulus and cross section area.
- An additional layer of soil using an equivalent geotextile permittivity was placed on top of the geotextile element.

Figure 7.1-23 presents a detail of the mat geometry and the double system used to model the mat tension strength and cross plane permittivity.

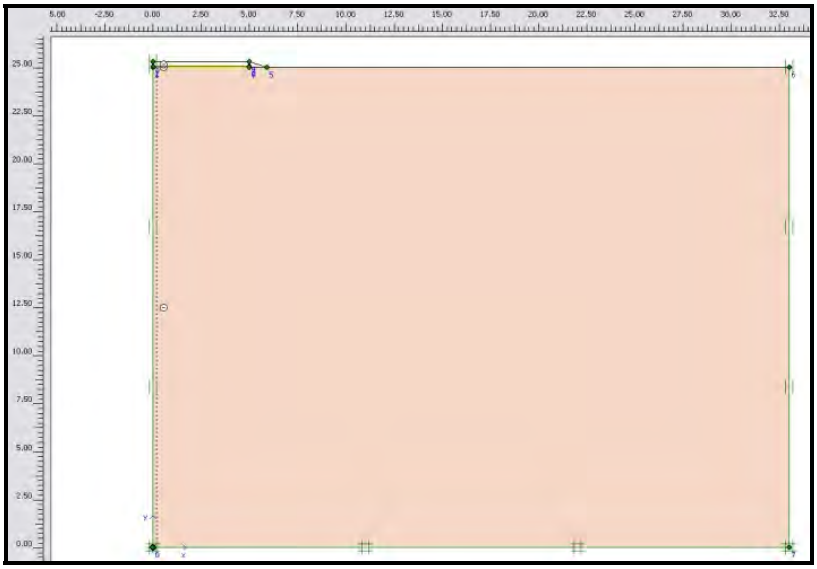

Figure 7.1-22. Geometry of extended finite element model.

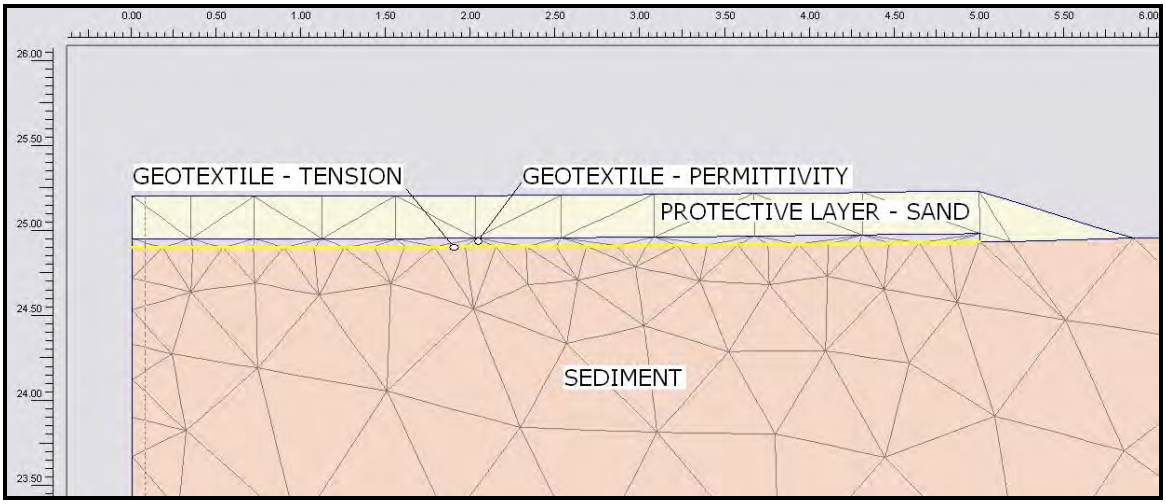

Figure 7.1-23. Detail of mat geometry including the finite element mesh.

Data is currently being collected to evaluate the initial sediment deformation under the current model. Once that goal is accomplished, a more complex sediment model will be generated that considers both consolidation and secondary creep. Ultimately, geotextile mats will be added to the models and increasingly sophisticated scenarios will be assessed. Data for the current model

in terms of deformed mesh, total sediment displacement and excess pore pressure are provided in Figure 7.1-24, Figure 7.1-25 and Figure 7.1-26, respectively.

Figure 7.1-24 shows by comparison the finite element mesh before and after the mat is placed. It does not include the contours of final sediment displacements (displacements scaled 20x) because it is not possible to include such data on this plot. Thus the mesh comparison shows only the maximum displacement value.

Figure 7.1-25 is a contour plot of the total sediment displacements that occur after the mat is placed. It includes the initial finite element mesh. The final displacements are scaled by a factor of 20. The final mesh is not presented because the combination of results and final mesh is not possible using Plaxis.

Figure 7.1-26 is a contour plot of the excess pore water pressure caused when the mat is placed on top of the model. This distribution is plotted on top of the deformed geometry, which is also scaled by a factor 20, and includes the initial finite element mesh. The mat dimension is 10 m, but by symmetry only half of it is modeled. The protective layer of sand is 0.3m thick.

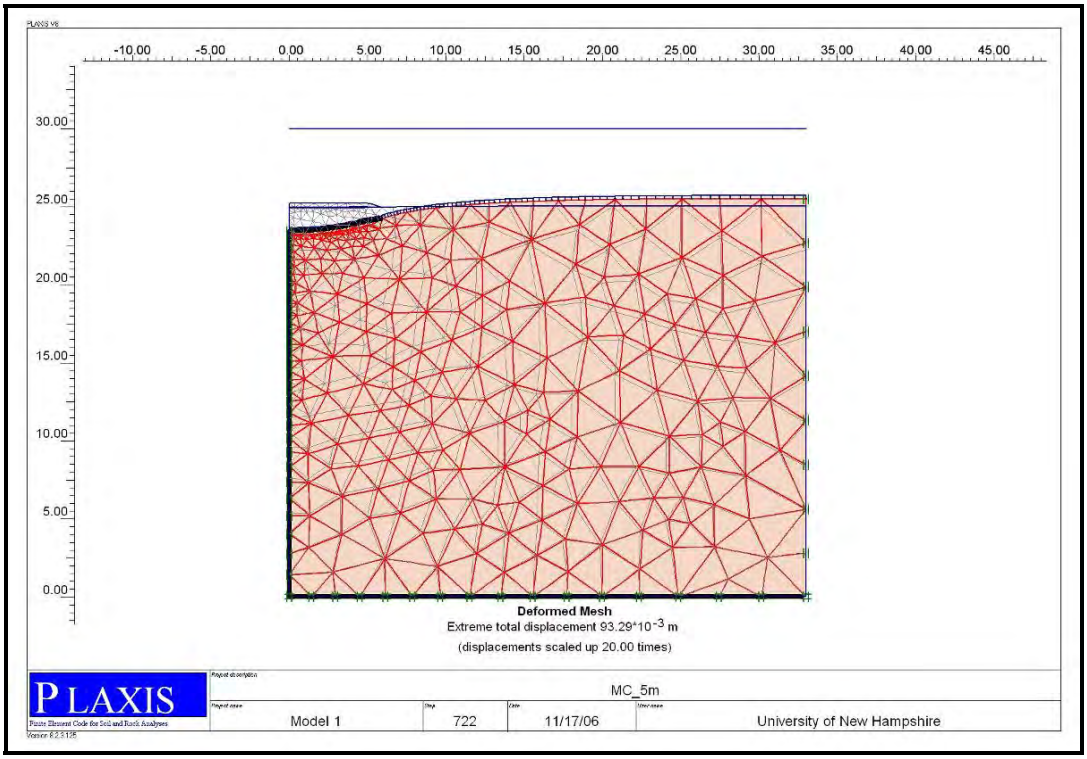

Figure 7.1-24. Finite element model of mesh comparison before and after mat placement (maximum sediment displacement, no shading).

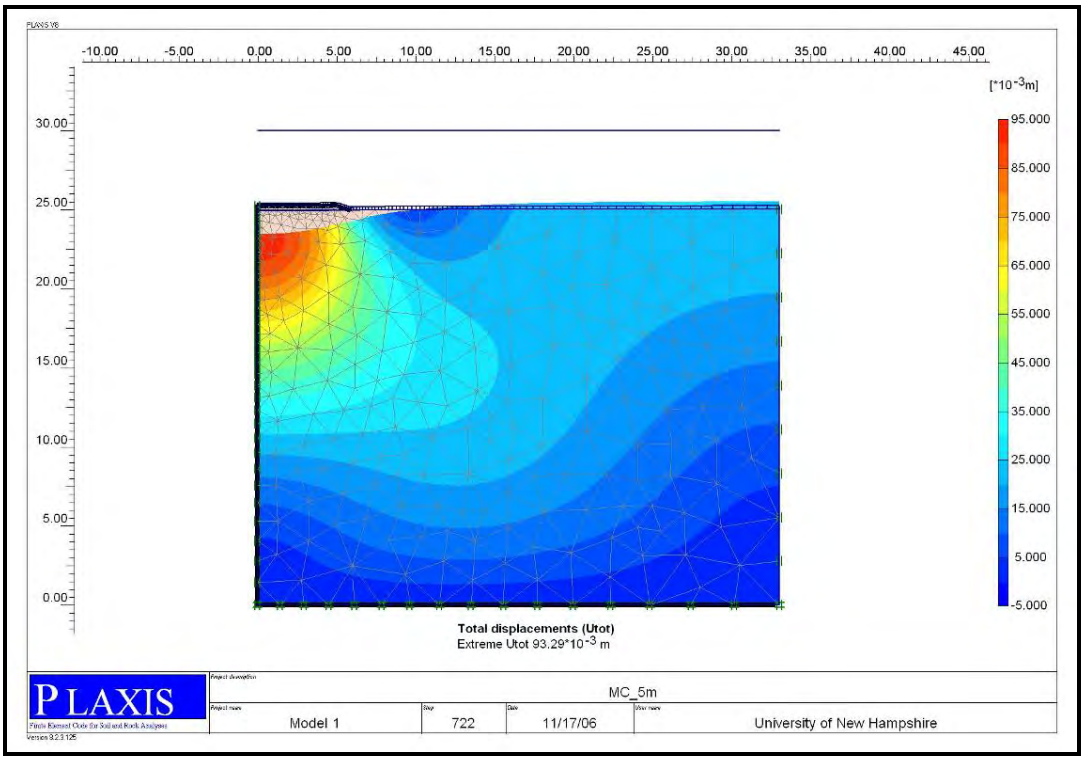

Figure 7.1-25. Finite element model of total sediment displacement after mat placement.

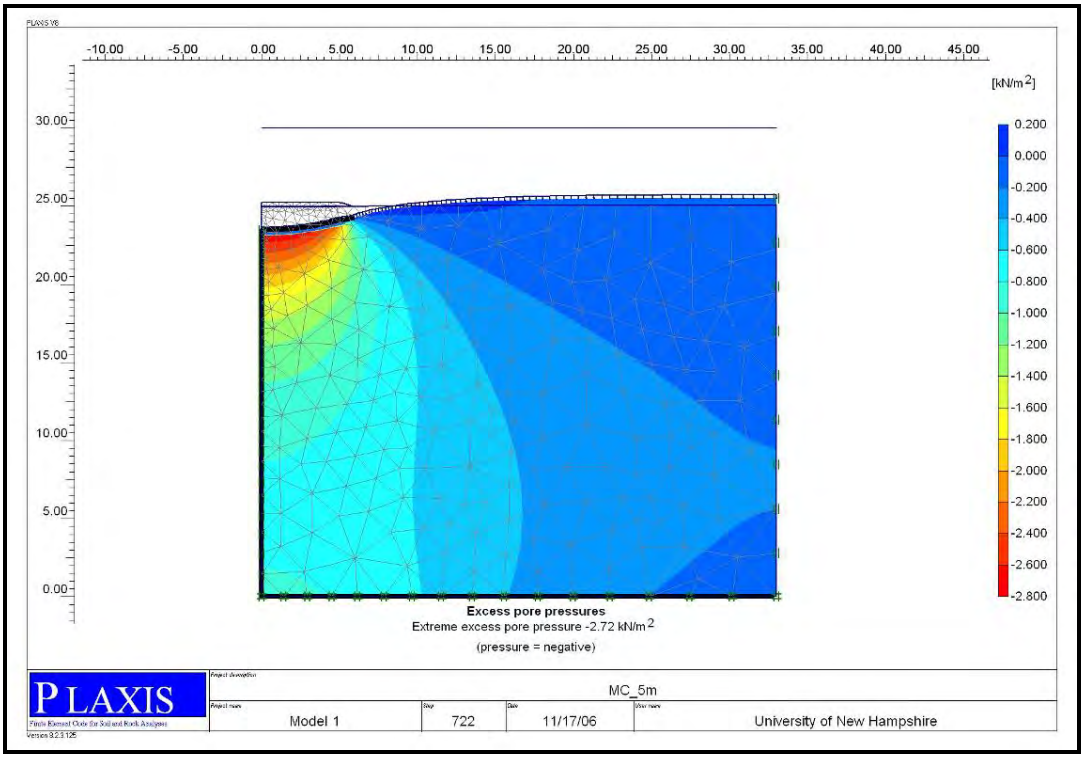

Figure 7.1-26. Finite element model of excess pore water pressure caused by mat placement.

7.2. TASK 2: PILOT SITE SELECTION

The purpose of selecting a pilot site is to identify a location for the small-scale field testing of geotextile mats as well as full-scale deployment of the prototype mat system. As described in Section 6.2.1, the pilot site selection process consists of two phases. Phase one involved the narrowing of several potential Navy sites down to two primary sites based on a series of chemical, physical, biological and logistical factors that would provide a challenging and suitable environment for geotextile field operations. Once the two primary sites were identified, a focused site comparison was performed to evaluate the history, surficial hydrology, hydrogeologic properties, nature and extent of contamination and past remediation efforts for each location. A summary of the accomplishments for phase one is provided in the following sub-sections.

Phase two of the pilot site selection process will involve geophysical testing of the two primary sites to determine which is most appropriate for initial mat deployment. The geophysical investigation will consist of a bathymetry survey, a side-scan sonar survey and sediment profile imaging performed at both sites as well as a groundwater seepage survey and pore water chemistry testing at one of the sites. To date the phase one process has been completed but phase two activities are still in preparation.

7.2.1. Site Selection Overview

Phase One Site Selection. The first step of the site selection process involved generating a "long list" of prospective Navy sites to be considered as possible pilot sites. Knowledgeable NFESC staff and other Navy personnel were contacted for input and a web search was conducted to generate the following list of potential sites:

- Philadelphia Naval Business Center Reserve Basin, Philadelphia, PA;
- Naval Station Newport, Narragansett Bay, Newport, RI;
- Portsmouth Naval Shipyard, Kittery, ME;
- Cottonwood Bay within Mountain Creek Lake, adjacent to the Naval Weapons Industrial Reserve Plant and Naval Air Station Dallas, Dallas, TX;
- Pearl Harbor, adjacent to Honolulu Naval facilities, Honolulu, HI;
- Puget Sound Naval Shipyard, Bremerton, WA;
- Mare Island Navy Yard, North San Pablo Bay, CA;
- Hunters Point Shipyard, San Francisco Bay, CA;

- Washington Naval Shipyard, Anacostia River, Washington, D.C.;
- Indian Head Naval Surface Warfare Center, Mattawoman Creek, Indian Head, MD;
- Naval Air Station, Florida Panhandle, Pensacola, FL;
- Great Lakes Naval Training Station, Pettibone Creek, Chicago, IL;
- Quantico Marine Base, Quantico, VA.

Each of the locations on this list was subject to a detailed evaluation with respect to the site screening parameters outlined in Section 6.2.2. Based on these criteria, two suitable primary sites were identified to serve as the potential pilot site for small-scale geotextile testing as well as the full-scale prototype mat deployment. These primary sites representing the most promising opportunities for field testing include Cottonwood Bay within Mountain Creek Lake adjacent to the Naval Weapons Industrial Reserve Plant (NWIRP) and Naval Air Station (NAS) Dallas in Dallas, Texas and Pearl Harbor adjacent to the Honolulu Naval Facilities in Honolulu, Hawaii. The characteristics leading to the selection of these two sites for further study are provided in Table 7.2-1 and the principal rationales used for the elimination of other prospective sites from primary site consideration are provided in Table 7.2-2. A detailed comparison of the Cottonwood Bay and Pearl Harbor sites is provided in the following sub-section.

Selection Criteria Parameter	Preferred Condition(s)	Cottonwood Bay Dallas, TX	Pearl Harbor Honolulu, HI
CHEMICAL/PHYSICAL PARAMETERS			
Mixed Contaminants/Concentrations	Organic and metal contaminants at concentrations identified to cause moderate to high ecological or human heath risks.	Chromium, Lead, PCBs	Copper, Zinc, PAHs
Contaminant Levels	Contaminants at concentrations identified to cause moderate to high ecological or human heath risks.	Yes but data are 10 years old	Yes
Intertidal	Opportunity to demonstrate effectiveness in intertidal zones.	Freshwater	Yes
Stability factors	Opportunity to demonstrate resilience of reactive mat with respect to destabilizers (e.g., slope, erosion, wave action).	Low energy environment	Range over potential sites within harbor
Groundwater	Demonstrate effectiveness in treating/accommodating groundwater seep; groundwater contributing CoPC sources.	Known groundwater discharge of VOCs	Groundwate study conducted; some seeps identifed
Redox	Known condition and seasonal variability to effectively describe challenge - not extreme.	TBD	TBD
Sediment Oxygen Demand	Known condition and seasonal variability - not extreme	Likely High	TBD
AVS/Phosphate/Iron/TOC	Known condition and seasonal variability- not extreme	TBD	TBD
Rate/Quality of Sedimentation	Known condition/variability - not extreme; Understanding of ongoing processes and their effect on condition.	Characterized for part of cove	TBD
Other Sediment Characteristics Affecting Bioavailability	Known Grain size, clay presence and type of soot, humic acid, TOC,- not extreme	TBD	Range of grain size, TOC
Presence of Other Stressors Which May Confound Interpretation of Results	Remedial benefit must not be masked by ancillary factors (e.g., low oxygen, high ammonia, sulfides, thermal stress).	Low DO	TBD
Smooth Surface	Absence of debris that would add logistical steps or compromise trial.	Cobble in Shallows	Minor Coral
BIOLOGICAL PARAMETERS			
Previous Site Investigations Conducted; Benthic Habitat Degraded	Scope for recovery is known and measurable.	Yes	Yes
Reference Site Established, Representative and Characterized as Sufficiently Different from Impaired Site	Ability to characterize change due to reactive mat.	Yes	Yes
Biofilm Expectation	Test realistic but not high-end biofouling to demonstrate degree of flow reduction through mat.	Probably High	Low
SITE HISTORICAL AND LOGISTICAL PARAMETERS			
Previous Site Investigations Conducted	Analytical/habitat investigation completed.	Yes, but not as BERA or RI/FS	BERA; RI/FS
Site Status	RI/FS or similar effort supports need for remediation.	Source reductions since 1975; Planning to cap w/in 2-3 year time frame	Possible remediation w/in 2-3 yearr time frame
Site Activity	Absence of activities proximate to the study area that could confound interpretation of the reactive mat study.	Restricted Acess-Must Resolve	TBD
Geographic Location	Demonstration sites are located in varying geographic regions.	Warm temperate, accelerates reaction process and fouling	Warm temperate, accelerates reaction process and fouling
Transport Access	Rail, vessel access for mat and equipment.	Probably	Probably
Site Access	Access to sampling crew available within proposed schedule/cost framework; Locations accessible with un-restricted access for sampling personnel (including non-DoD personnel).	Staging area available; moderate distance	Staging area available; greatest distance
Site Facilities	Electricity, running water, facilities for sampling personnel.	Probably	Probably
Health and Safety - Field Study	No significant health and safety concerns for field program execution.	None	None at selected sites
Health and Safety - Ordnance	No UXO or active range concerns on firing range sites.	None	None at selected sites
Receptive Client	Support from site management.	Likely, but staffing low	Likely

TBD = To Be Determined.

Table 7.2-1. Preliminary assessment leading to selection of Cottonwood Bay and Pearl Harbor sites.

Potential Sites	Elimination Rationale(s)
Philadelphia Naval Business Center Reserve Basin, Philadelphia, PA	Ongoing dredging operations likely to interfere; Absence of Navy support staff .
Naval Station Newport, Newport, RI	No remediation planned due to low-level risk
Portsmouth Naval Shipyard, Kittery, ME	No remediation planned due to low-level risk
Puget Sound Naval Shipyard, Bremerton, WA	No remediation planned due to low-level risk
Mare Island Navy Yard, North San PabloBay, CA	Hot spot targeted for remediation likely too small for the current study.
Hunters Point Shipyard, San Francisco Bay, CA	Ongoing management planning is complex and would likely impact timely completion of the study.
Washington Naval Shipyard, Washington, D.C.	Bottom characterized as having excessive debris; Very high organic load and silt content.
Indian Head Naval Surface Warfare Center, Indian Head, MD	Navy support staff could not be identified.
Naval Air Station, Pensacola, FL	No remediation planned due to low-level risk
Great Lakes Naval Training Station, Chicago, IL	Insufficient site support.
Quantico Marine Base, Quantico, VA	Stressors other than contaminants (e.g., low oxygen) and low-level contaminant risks.

Table 7.2-2. Rationales for the elimination of prospective Navy sites from consideration for pilot site selection.

Primary Site Comparison. The primary site review for Cottonwood Bay focused on two reports: *Chemical Quality of Water, Sediment, and Fish in Mountain Creek Lake, Dallas, Texas, 1994-97* (VanMetre *et al*. 2003) provided by the U.S. Geological Survey (USGS) and *Texas Natural Resource Conservation Commission Affected Property Assessment Report* (Ensafe 2001) provided by the Navy as part of the requirements of the Texas Risk Reduction Program (TRRP). Information to evaluate Pearl Harbor was obtained mainly from the *Remedial Investigation Report for Pearl Harbor Sediment* (NAVFAC 2006) and also from the *Baseline Ecological Risk Assessment for Pearl Harbor Sediment Remedial Investigation* (NAVFAC 2006). Correspondence and phone conferences with site managers also contributed to current understanding of the conditions and management at each location as well as logistical considerations that are important for site assessment.

The principal CoPCs at Cottonwood Bay were determined to be chromium, lead, PCBs and PAHs with some incidence of pesticides and VOCs. In contrast, Pearl Harbor presents the need for remediation to reduce copper, zinc, PAHs and PCBs as well as other metals, pesticides and

dioxin/furans in some locations. Both sites have sufficiently elevated concentrations of metals and organics to provide a representative test of reactive mat performance. Contaminant concentrations in historic sediment samples for Cottonwood Bay and Pearl Harbor are provided in Table 7.2-3 and Table 7.2-4, respectively. The locations within each site corresponding to these samples are shown in Figure 7.2-1 and Figure 7.2-2.

		Cottonwood Bay Sediment Sampling Stations					
Parameter	**Units**	**BG1**	**MCL5**	**OF401**	**Bay 11**	**Bay 7**	**Bay 16**
Metals	mg/Kg	Cr = 15 Cu = 16 Zn = 64	Cr = 83 Cu = 33 Zn = 130	Cr = 473 Cu = 71 Zn = 502	Cr = 350 Cu = 53 Zn = 350	Cr = 349 Cu = 55 Zn = 210	Cr = 350 Cu = 52 Zn = 280
Fluoranthene	ug/Kg	960	740	2400	NS	3600	4800
PCBs	ug/Kg	NS	6	4350*	NS	210	190
Dioxins/Furans (e.g., 2,4,5,6,7-PeCDF)	ug/Kg	NS	NS	NS	NS	NS	NS
Gain Size: Fines	%	NA	NA	NA	NA	NA	NA
Total Organic Carbon	%	NA	NA	NA	NA	NA	NA
Depth	m	NA	NA	NA	NA	NA	NA

* = Sum of 3 Arochlors
NS = Not Sampled
NA = Not Available; Information forthcoming.

Table 7.2-3. Select sediment data available from historic Cottonwood Bay studies.

		Pearl Harbor Sediment Sampling Stations[1]					
Parameter	**Units**	**SE Loch/Naval Station Berths 1-Fy**	**SE Loch/SubBase Shipyard 1-Kx**	**SE Loch/Ford Island Runway-Stormdrain 1-Py**	**Bishops Point Hickham AFB 2-Iz**	**Bishops Point Hickham AFB 2-Jx**	**Iroquois Point Shallow Intertidal 2-Kx**
Metals	mg/Kg	Cu = 659 Zn = 720	Cu = 1890 Zn = 854	Cu = 2020 Zn = 145	Cu = 120 Zn = 42	Cu = 17 Zn = 65	Cu = 36 Zn = 84
HPAHs	ug/Kg	21430	52,660	2427	8700	1818	12,159
Fluoranthene	ug/Kg	1100	4800	120	550	200	1700
PCBs	ug/Kg	764	234	17	410	26	6
Dioxins/Furans (e.g., 2,4,5,6,7-PeCDF)	ug/Kg	3	17	2	7	2	2
Grain Size: Fines	%	65	51	35	52	7	87
Total Organic Carbon	%	2.4	3.8	2.7	4.8	8.1	1.5
Depth	m	>10	>10	2-10	2-10	2-10	<2

(1) - Each station (e.g., 1-F) corresponds to three samples (x,y,z); data from one sample provided.

Table 7.2-4. Select sediment data available from historic Pearl Harbor studies.

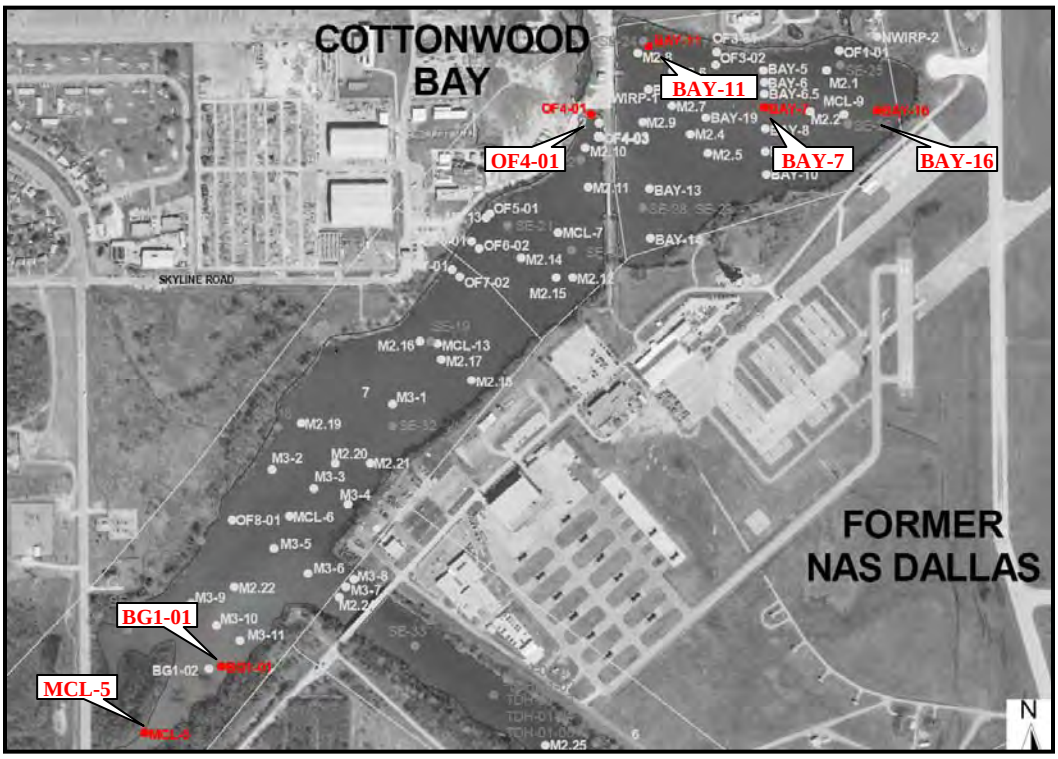

Figure 7.2-1. Cottonwood Bay sampling stations used in the site evaluation process (modified from Ensafe 2001).

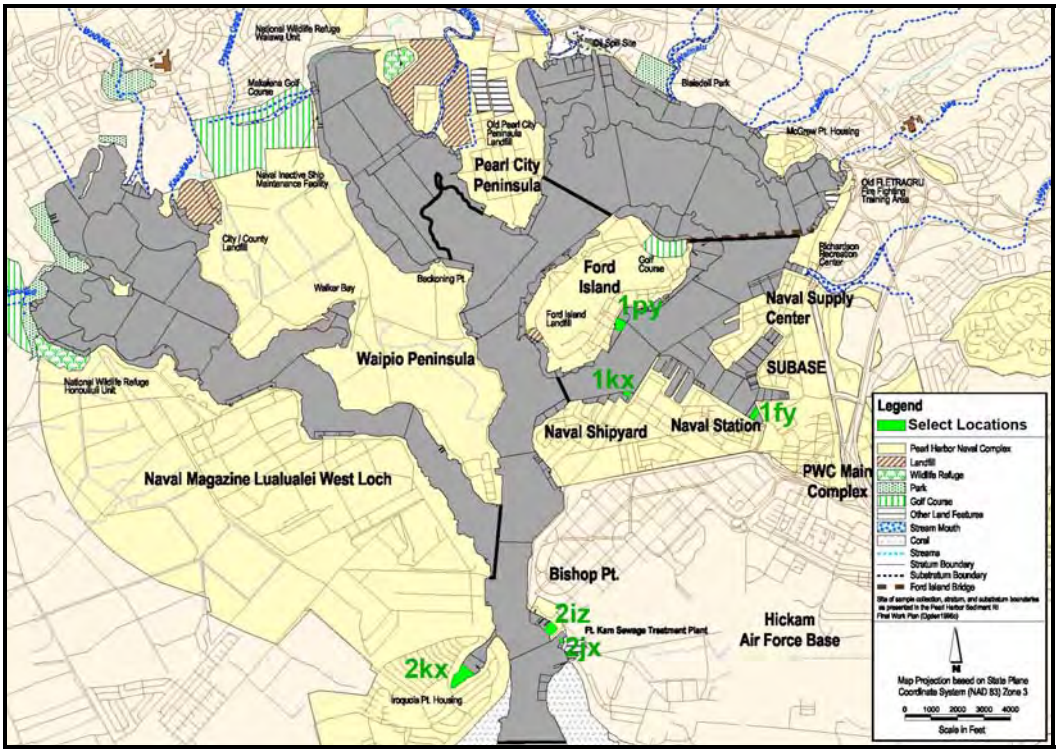

Figure 7.2-2. Pearl Harbor sampling stations used in the site evaluation process (modified from EarthTech 2006).

As shown in Table 7.2-3 and Table 7.2-4, sediments have been more thoroughly and more recently characterized at the Pearl Harbor site relative to Cottonwood Bay, especially for parameters such as grain size and TOC. The Cottonwood Bay data reviewed for the present evaluation were all greater than ten years old, thus lending some uncertainty with regard to current conditions. Additional data for Cottonwood Bay is forthcoming, however, and may fill some of these important data gaps. Based on the available Cottonwood Bay sediment data, concentrations of chromium and PCBs were generally higher at Station OF401 adjacent to the NWIRP while concentrations of PAHs (e.g., fluoranthene) increased with proximity to the NAS. Concentrations of CoPCs were generally lowest in the southwestern area where Cottonwood Creek enters the bay.

Relevant Pearl Harbor sediment sampling stations were selected from areas identified in the BERA (NAVFAC 2006) as presenting relatively high risks to the aquatic community. A further refinement of appropriate locations then resulted from discussions with the Remedial Program Manager and authors of the Pearl Harbor RI report (NAVFAC 2006). Concentrations of CoPCs are generally higher in the southeastern loch as represented by sediment data from stations within sub-areas 1F, 1K and 1P. Sub-area 1F is a berthing area located within the inner harbor that is likely to constitute a relatively low-energy environment. Sub-area 1K is located in a shipyard across from the island landfill and has the highest levels of copper, zinc and PAHs. Sub-area 1P is a shallower storm drain region located directly shoreward from the island landfill. Bishops Point is a berthing area in the harbor channel that has relatively high flow characteristics likely to cause resuspension events. Deploying mats in this area would provide a demonstration of mat efficacy in reducing resuspension of contaminated sediments. Across the channel from Bishops Point is a shallow intertidal inlet known as Iroquois Point which is marked by particularly high levels of PAHs. Sediment grain size is highly variable across the selected Pearl Harbor stations (1F, 1K, 1P, Bishops Point, Iroquois Point) with fine particles representing only 7% in the Bishops Point sample but up to 87% in the Iroquois Point sample. Total organic carbon ranges from a low of 1.5% at the Iroquois Point station to a high of 8.1% at the Bishops Point station. The latter represents an unusual case where low percent fines and high TOC are co-located.

Regarding flow parameters, Cottonwood Bay appears to have more groundwater influence while Pearl Harbor is subject to tidal flow and limited groundwater movement. At both sites there is a likelihood of measurable biofilm, although Cottonwood Bay is likely to have a higher accretion rate relative to Pearl Harbor where turbidity is expected to be lower.

In terms of management planning, both sites have identified needs for remediation. Pearl Harbor has been investigated following USEPA guidance for risk assessment and remedial investigations but a Feasibility Study (FS) has yet to be completed. Cottonwood Bay studies were conducted primarily by the USGS and can be characterized as “nature and extent” evaluations that provided data for a Screening Level Risk Assessment (EnSafe 2000). This report was not finalized when the Affected Property Assessment Report was submitted in 2001, but at that time the Texas Natural Resource Conservation Commission (TNRCC) determined that additional studies would be required. The most recent remedial information for Cottonwood Bay is currently being sought from both NAVFAC Southeast and EnSafe.

Logistically, both Cottonwood Bay and Pearl Harbor are accessible and have infrastructure that will support mobilization and field activities. However, both sites do have security limitations that must be addressed. Access to the east end of Cottonwood Bay is currently restricted for security reasons and entrance into Pearl Harbor stations near the Naval Facility and berthing areas may also be restricted. Site access challenges will ultimately depend on specific areas within each site chosen for field activities, with some regions expected to be more accessible than others. In general, more contaminated zones tend to correspond to more restricted sites areas.

Whereas a comparison of the Cottonwood Bay and Pearl Harbor sites in terms of the potential for further investigation is provided in the previous paragraphs, additional background conditions for both primary sites are presented in the following sub-section.

7.2.2. Focused Site Assessment

Cottonwood Bay and Pearl Harbor were selected as primary sites during phase one of the site selection process. Background conditions for each of these locations are described separately in the following sub-sections. A final determination as to which of the two sites will serve as the pilot site for Task 3 will not be made until after the geophysical testing described in Section 6.2.3 is completed.

7.2.2.1. Cottonwood Bay, Texas

As discussed in Section 7.2.1, the majority of information regarding the background for Cottonwood Bay was obtained from a USGS sampling effort (VanMetre *et al*. 2003) and subsequent groundwater modeling (Barker and Braun 2000). Details about the site that were provided in these documents will be confirmed and refined during the site visit and geophysical survey to be performed during the next phase of Task 2.

Site Description and History. The Cottonwood Bay site is located in northeastern Texas within Dallas County approximately four miles southeast of Grand Prairie between routes I-30 and I-20. The site is adjacent to the Naval Weapons Industrial Reserve Plant (NWIRP) and Naval Air Station Dallas (NAS). Recreational fishing is popular in the connected Mountain Creek Lake, but consumption of catch is banned due to PCB contamination.

Surficial Hydrology. Cottonwood Bay is an artificially constructed stream and groundwater fed freshwater body that is connected to Mountain Creek Lake by a narrow channel (Figure 7.2-3). Cottonwood Creek feeds directly into the bay and, along with surface runoff, constitutes the main surface water input into the bay (Figure 7.2-4). The east and west lagoons to the north of the bay were constructed for stormwater runoff but also receive input from groundwater. Cottonwood Bay and Mountain Creek Lake have relatively consistent water elevations throughout the year.

Hydrogeologic Properties. The source of most groundwater is precipitation, which averages about 36 in/yr (Owenby and Ezell 1992). Precipitation readily infiltrates the porous

higher-altitude areas around the northern limits of the site, while the buildings and impervious surfaces which characterize the lower elevations create runoff instead of infiltration.

The water table slopes toward Cottonwood Bay and Mountain Creek Lake (Figure 7.2-4). An unconfined aquifer, which is composed mostly of silty sand and silty clay, thins to the south and eventually becomes level with site's water bodies (EnSafe 1994). Most of the groundwater discharges to Cottonwood Bay and Mountain Creek Lake which maintains the water levels of those water bodies. The rest of the ground water either discharges to the east and west lagoons, flows out of the site area to the east, or is evapo-transpired back into the atmosphere (Barker and Braun 2000).

The surficial aquifer is comprised of recent soils. While the aquifer is unconfined on the surface, it is confined at depth by the Eagle Ford shale (University of Texas 1987). Directly below the shale is the Woodbine confined aquifer which does not discharge into Cottonwood Bay.

Nature and Extent of Contamination. Sediment concentrations of CoPCs, including three metals (chromium, copper and zinc), PCBs and fluoranthene (representing the highest measured PAH) at Cottonwood Bay are presented in Table 7.2-3. Two of the stations are in the southwestern end of the bay near the terminus of Cottonwood Creek, while four represent stations in the northeastern quadrant in the vicinity of NWIRP and NAS (Figure 7.2-1). The highest metal concentrations are for total chromium while PAHs represent the greatest organic contaminant loads in Cottonwood Bay sediments. Concentrations of metals and organics are generally about a factor of five lower at the southwestern stations. The CoPCs most likely to be driving risks at the site are PAHs. Groundwater intrusion may contribute to lake water and sediment risks, with trichloroethene (TCE), dichloroethene (DCE), vinyl chloride (VC), chromium, lead, and other metallic contaminants measured in the shallow unconfined aquifer underlying the NWIRP (EnSafe 1996).

Remediation Efforts. A series of wells and trenches were installed at the Cottonwood Bay site as early as 1996 (Figure 7.2-5). The purpose of this remedial activity was to remove groundwater from the aquifer before it reaches Cottonwood Bay and then treat the water for VOCs. Modeling indicates that the trench intercepts about 827 ft^3/day of groundwater that otherwise would enter Cottonwood Bay. While the trenches intercept groundwater before it can reach Cottonwood Bay, the wells (when actively pumping) create a depression that reverses the direction of groundwater flow in order to draw contaminated water away from the bay.

Figure 7.2-3. Overview of Cottonwood Bay area.

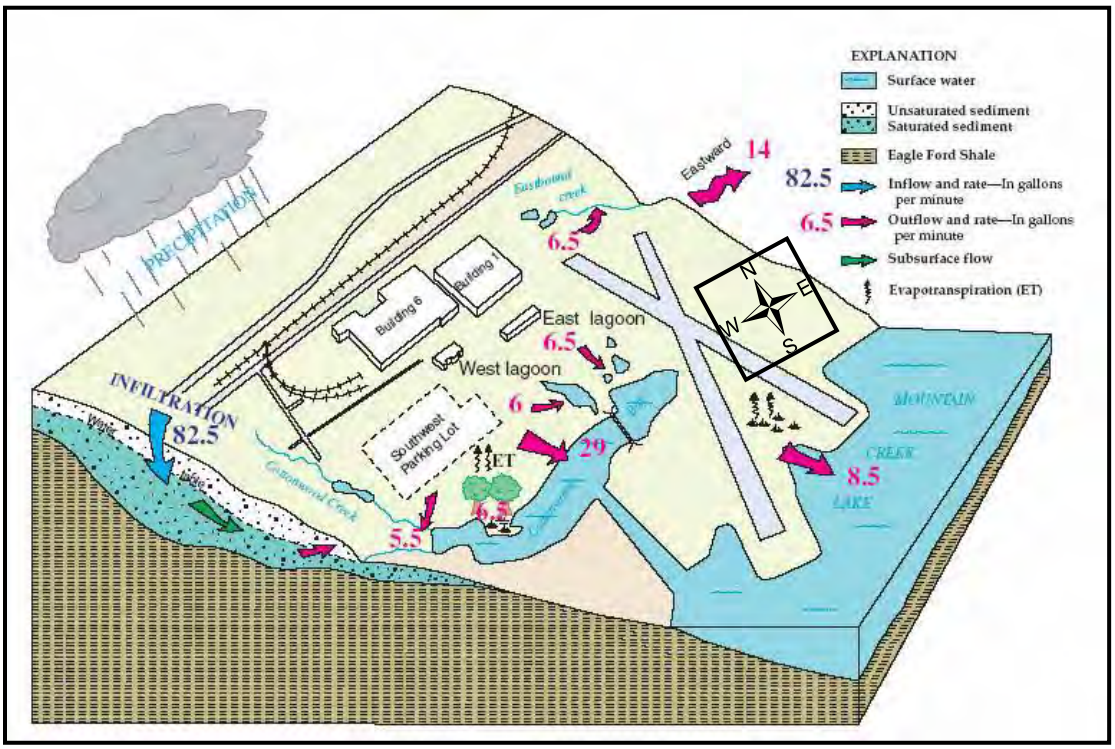

Figure 7.2-4. Conceptual model of hydrogeologic setting of the Cottonwood Bay area (modified from Barker and Braun 2000).

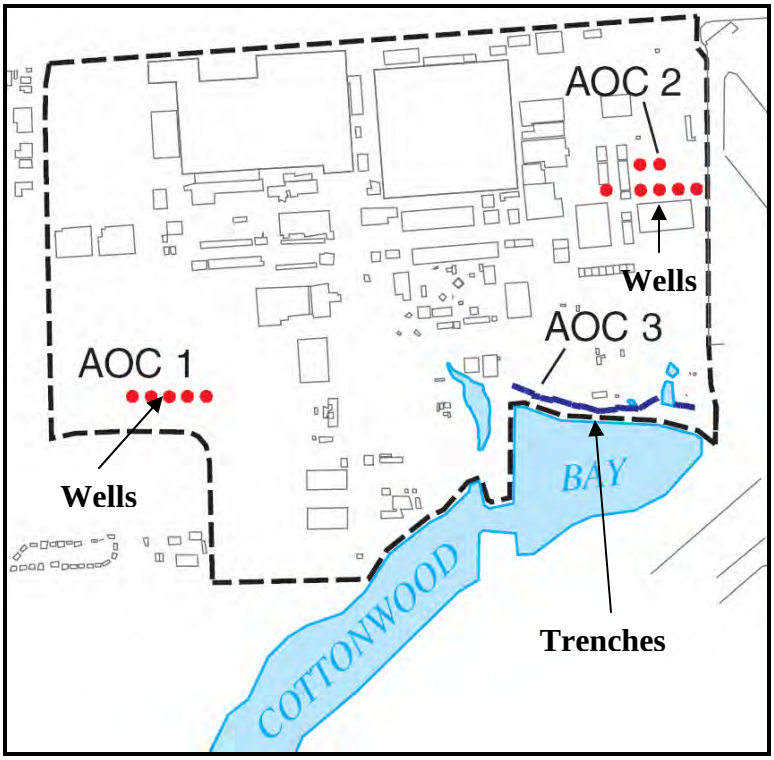

Figure 7.2-5. Locations of remedial wells and trenches at the Cottonwood Bay site (modified from Barker and Braun 2000).

7.2.2.2. Pearl Harbor, Hawaii

The majority of information regarding the background for Pearl Harbor that is presented in the following sections was obtained from a remedial investigation (EarthTech 2006) and other naval studies. Details about the site that were provided in these documents will be confirmed and refined during the site visit and geophysical survey to be performed by during the next phase of Task 2.

Site Description and History. The Pearl Harbor site is located on Oahu, the most heavily populated island of the Hawaiian island chain (Figure 7.2-6). Pearl Harbor is almost entirely encompassed by the Pearl Harbor Naval Complex. A wide variety of direct ordnance disposal, industrial operations, and agricultural activities may have introduced contaminants directly into the harbor. Upland sources transported by streams and groundwater are also viable transport pathways for contamination.

Surficial Hydrology. Pearl Harbor is the largest estuary on Oahu and one of the largest in the state of Hawaii. It contains 21 square kilometers of surface water area with a mean depth of 9.1 m (ESTCP 2000). Tidal flow and circulation are weak and variable with a mean tidal current velocity of 0.15 m/s and a maximum ebb flow of 0.3 m/s in the entrance channel. Salinity in Pearl Harbor ranges from 10 to 37.5 parts per thousand, with a yearly average of 32.8 parts per thousand. Harbor water temperatures annually range from 22.9ºC to 29.4°C and dissolved oxygen values range from 2.8 to 11.0 mg/L.

Pearl Harbor is most appropriately described as a high-nutrient estuary. It represents a drowned river system with bathymetry that is characterized by shallow areas north becoming deeper in the center of each lobe. The depth gradient is steep to the east where dredging has been used to maintain navigation depths (Figure 7.2-7). Pearl Harbor is directly connected to the Pacific Ocean to the south and contains a range of salinity depending on weather conditions and proximity to stream input. The Waikele, Waiawa, and Halawa streams flow into the western, central, and eastern portions of the harbor, respectively.

Hydrogeologic Properties. Sedimentary deposits overlying volcanic rocks control the groundwater movement throughout the harbor area (Youngberg 1973). The surficial aquifer is comprised of coarse soils. While the aquifer is unconfined on the surface, it is confined at depth by impermeable clay. Directly below the shale is a zone of fractured basalts, comprising the Koolau confined aquifer (NEESA 1983). Both aquifers generally follow the land topography and flow toward the ocean, eventually discharging to Pearl Harbor and the Pacific Ocean (Figure 7.2-8). Recharge occurs by infiltration from rainfall, streams and irrigation, but large groundwater withdrawals over the past 100 years have caused water levels in the deep aquifer to decline (Oki 1998).

Nature and Extent of Contamination. Twenty contaminants that pose a human health and/or ecological risk were identified in the remedial investigation (EarthTech 2006). A map summarizing the number of contaminants of concern in each area of Pearl Harbor was prepared for the Remedial Investigation (RI) document and is provided in this section for reference. The risks identified as likely drivers of remediation at the site include copper, PAHs, PCBs and

dioxin/furans. The mix of contaminants varies amongst areas within Pearl Harbor, with the highest copper and PCB concentrations generally occurring in the Southeast Loch. Bishops Point, located in the intertidal zone of the harbor entry channel, and the nearby shallow subtidal Iroquois Point also have high measured concentrations of multiple contaminants and these sites have also been identified as candidates for remediation. Contaminant concentrations for select sediment samples from each area are sited in Table 7.2-4. As displayed in Figure 7.2-2, multiple exceedances of concern do occur within several sub-areas. It is also noteworthy that for each of the stations selected for presentation in Table 7.2-4, toxicity tests conducted with amphipods and echinoderms resulted in at least one occurrence of toxic effects, thus confirming bioavailability of the toxicants.

Remediation Efforts. To date no known remediation efforts have been conducted in the areas of Pearl Harbor being considered for this project. It should be noted, however, that development of an FS is currently ongoing and that sites to be targeted for remedial efforts have been identified.

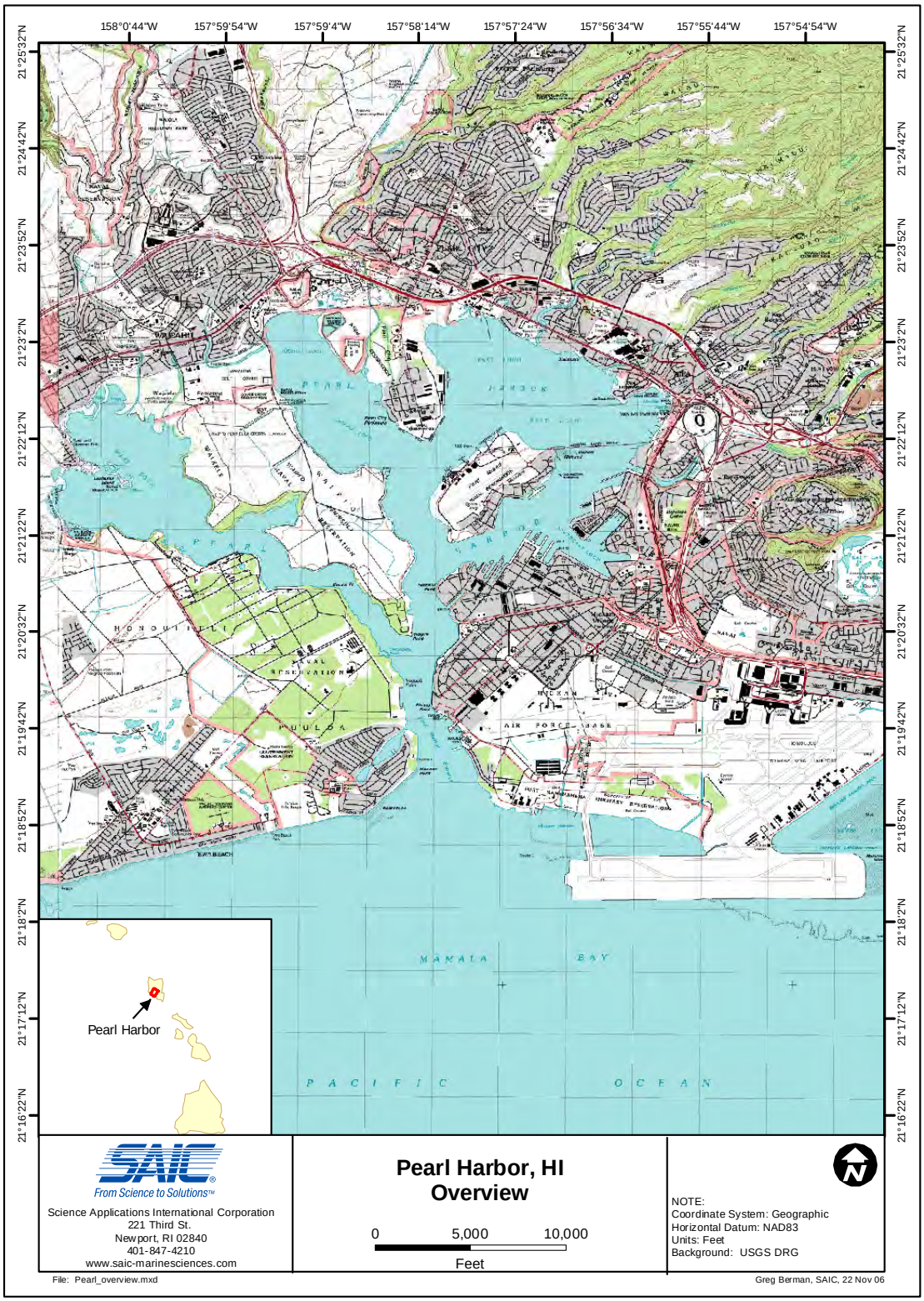

Figure 7.2-6. Overview of Pearl Harbor area.

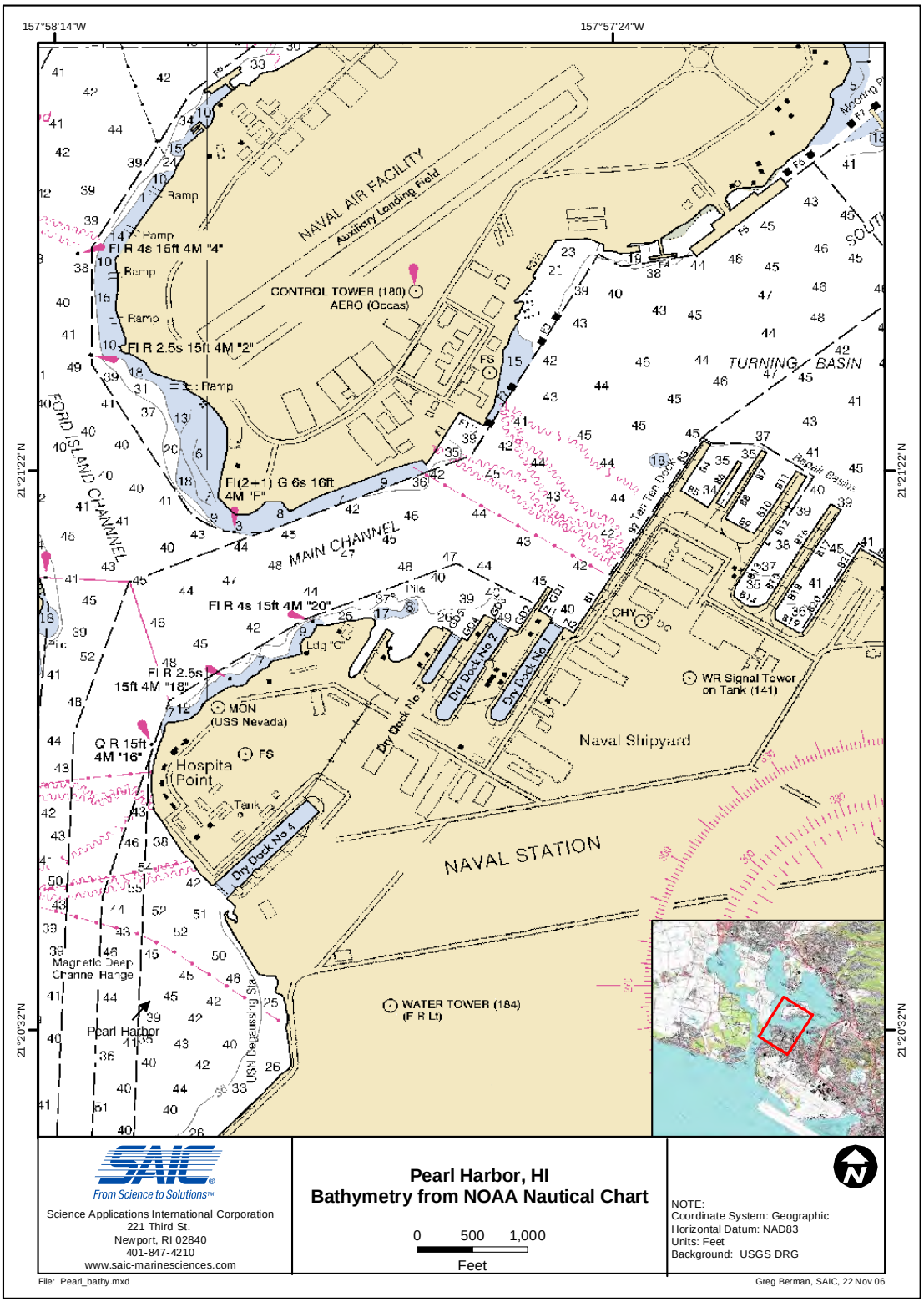

Figure 7.2-7. Nautical chart of Pearl Harbor area showing bathymetry.

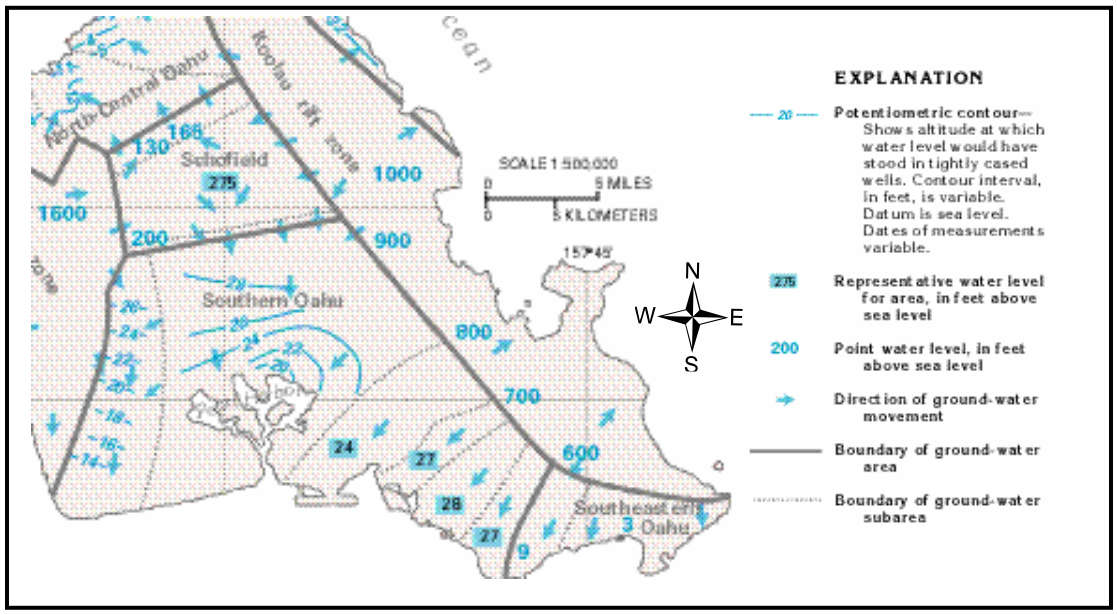

Figure 7.2-8. Water level data showing potentiometric contours for southern Oahu (modified from Nichols et al. 1996).

7.2.3. Geophysical Testing

Now that phase one of Task 2 (primary site selection) is complete with the Cottonwood Bay and Pearl Harbor sites having been chosen for further investigation, phase two (geophysical testing) can proceed. Much of the preliminary preparation for the geophysical testing at each site is completed with preliminary plans for bathymetry, side-scan sonar and sediment profile imaging surveys having already been established. Confirmatory groundwater seepage and pore water chemistry testing will be performed at one of the locations that has yet to be determined. Based on the conclusions of these geophysical evaluations, either Cottonwood Bay or Pear Harbor will be chosen as the pilot site for small-scale geotextile testing to be accomplished in Task 3.

7.3. TASK 3: GEOTEXTILE TESTING

Task 3 includes the construction and deployment of small-scale geotextile test mats at the pilot site that will ultimately be identified in Task 2. Fourteen test mats of various composition have already been constructed based on the methodology described in Section 6.3. Once these mats are deployed, follow up investigations will include geotextile monitoring and testing as well as overall performance evaluation. Operations for Task 3 will proceed according to the timeline strategy shown in Figure 7.3-1.

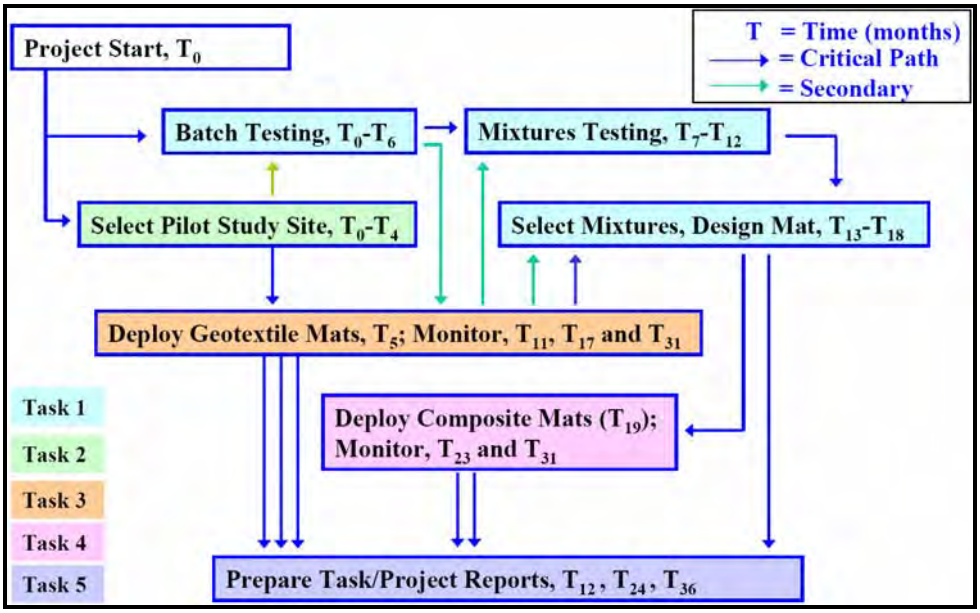

Figure 7.3-1. Timeline strategy showing the interconnectivity of separate tasks.

Laboratory testing of geotextiles has already begun with a geotechnical test system having been purchased to measure the clogging potential of the different geotextiles. Preliminary testing indicates that bubbles can pose a significant problem when using a fine grained material. Thus the test procedure is undergoing modification to use upward flow through the sediment and geotextile in order to better simulates the actual field conditions where groundwater is present. Additionally, nitrogen atmospheres are also being examined to potentially eliminate bubbles. The data collected during this task will help select the best geotextile to be used for full-scale mat deployment in Task 4.

7.4. TASK 4: PROTOTYPE MAT TESTING

Task 4 will test a prototype full-scale mat system constructed of the most effective amendment and the geotextile most resistant to fouling in order to assess in-situ chemical sequestration effectiveness and flux properties. The exact location, composition, and deployment strategy of the prototype mats will be determined by the conclusions drawn from the pilot site establishment and geotextile testing tasks.

8. CONCLUDING SUMMARY

This annual report summarizes progress on SERDP Project Number ER-1493 (Reactive Capping Mat Development and Evaluation for Sequestering Contaminants in Sediments) through November 2006 with regard to tasks presented in the original proposal and subsequent amendments. To meet Task 1 (Composite Material Testing), batch studies have been completed to characterize the absorption kinetics and binding capacities of activated carbon, organoclay and apatite, respectively, including behavior of batches amended with humic acid. The presence of humic acid has been shown to have a significant influence on the sorption properties of activated carbon and apatite, including causing a significant desorption of previously adsorbed PAHs and

PCBs for some compounds. In addition, finite element modeling exercises were conducted with Plaxis v. 8.0 to evaluate 2D transport with regard to permittivity (accounting for the weight of the mat) in order to optimize mat design for limiting flow diversion. The initial model performed well and will be augmented with additional sediment creep and groundwater components to assess how advective transport is affected by the presence of the mat.

Task 2 (Pilot Site Selection) was divided into two phases. The first phase involved development of a series of criteria including chemical, physical, biological and logistical factors to be used in selecting primary sites for further investigation. A long list of prospective Navy sites was compiled with NFESC and Navy personnel assistance and then ultimately narrowed to two primary sites based on the aforementioned criteria. These two primary sites are Cottonwood Bay in Dallas, Texas and Pearl Harbor in Honolulu, Hawaii. A primary site comparison was performed between each of these locations in terms of nature and extent of sediment contamination, groundwater flow parameters, management planning, logistics and ongoing remediation. As part of this comparison, data from existing environmental reports as well as information gained from site managers were used to provide a more detailed analysis of each site with respect to the screening criteria. Select target stations within each site were also identified for potential further investigation. In addition, background information was compiled for each site to provide context for evaluating potential mat performance. Overall, sediment properties have been more thoroughly characterized at Pearl Harbor, but additional data for Cottonwood Bay is in preparation.

Phase two of the pilot site selection process has yet to be completed. This phase will involve additional geophysical testing at both of the primary sites with the ultimate goal of selecting one location to serve as the pilot site for small-scale geotextile testing (Task 3) as well as full-scale prototype reactive mat deployment (Task 4). Planning for phase two testing has already been completed with activities scheduled to commence in early 2007.

The goal of Task 3 (Geotextile Testing) is to deploy small-scale geotextile mats of different composition to assess whether biofouling and biofilm formation adversely affect the ability for water to pass through the mat, whether environmental weathering compromises the ability of the mat to retain the amendment material and whether environmental weathering compromises the reactivity of the sequestration agents. Field mobilization for Task 3 will not begin until both phases of Task 2 have been completed. The fabrication portion of Task 3 has already been accomplished, however, as a series of mat designs for field testing of geotextile behavior have been selected and 14 small-scale test mats have been constructed using various amendment combinations of apatite, activated carbon, organoclay and Ottawa sand. A geotechnical test system was also purchased to measure the clogging potential of these test mats.

Task 4 (Prototype Mat Testing) will consist of deployment of a prototype full-scale mat system constructed of the geotextile most resistant to biofilm formation and adverse weathering effects. This activity will follow Task 3 as the results from the preceding investigation will be needed to guide full-scale mat fabrication. The prototype mat system will ultimately be deployed at the pilot site identified in Task 2. Overall, all tasks are proceeding well and are being executed on or ahead of schedule.

9. APPENDICES

REFERENCES

Barker, R.A. and C.L. Braun. 2000. Computer-model analysis of ground-water flow and simulated effects of contaminant remediation at Naval Weapons Industrial Reserve Plant, Dallas, Texas. U.S. Geological Survey Water-Resources Investigations Report 00–4197, 44 p.

EarthTech. 2006. Remedial Investigation Report Pearl Harbor Sediment. Prepared for NAVFAC under contract N62742-94-D-0048, CTO 0115.

EnSafe/Allen & Hoshall. 1994. Comprehensive long-term environmental action-Navy stabilization work plan. Revision I: Memphis, Tenn. 83 p.

EnSafe/Allen & Hoshall. 1996. Draft RCRA, facility investigation report, Naval Weapons Industrial Reserve Plant, Dallas, Texas. Volume I: Memphis, Tenn.

EnSafe. 2000. Ecological Risk Assessment Screening Level, Mountain Creek Lake, Dallas, Texas. Prepared for SOUTNAVFACENGCOM, Charleston, SC.

EnSafe. 2001. Affected Property Assessment Report, Mountain Creek Lake, Dallas, Texas. Prepared for NAVFAC under contract N62467-89-D-0318, CTO 0025.

Environmental Security Technology Certification Program (ESTCP). 2000. Quantifying In Situ Metal Contaminant Mobility in Marine Sediments, Environmental Security Technology Certificaiton Program: U.S. Department of Defense. November.

Naval Energy and Environmental Support Activity (NEESA). 1983. Initial Assessment Study of Pearl Harbor Naval Base, Oahu, Hawaii. NEESA 13-002. Port Hueneme, CA. October.

NAVFAC. 2006. Baseline Ecological Risk Assessment for Pearl Harbor Sediment Remedial Investigation. Prepared under contract N62742-94-D-0048, CTO 0115.

NAVFAC. 2006. Remedial Investigation Report for Pearl Harbor Sediment. Prepared under contract N62742-94-D-0048, CTO 0115.

Nichols, W.D., P.J. Shade, P.J. and C.D. Hunt, Jr. 1996. Summary of the Oahu, Hawaii, regional aquifer-system analysis. U.S. Geological Survey Professional Paper 1412-A, 61 p.

Oki, D.S. 1998. Geohydrology of the central Oahu, Hawaii, ground-water flow system and numerical simulation of the effects of additional pumping. U.S. Geological Survey Water-Resources Investigations Report 97-4276, 132 p.

Owenby, J.R. and D.S. Ezell. 1992. Climatography of the United States-Monthly station normals of temperature, precipitation, and heating and cooling degree days, 1961–91. Asheville, N.C. National Climatic Data Center no. 81, 65 p.

Pirbazari, M. and W.J. Weber. 1981. Adsorption of Polychlorinated biphenyls from Water by Activated Carbon. Chemistry in Use, Ann Arbor Science, Publishers Inc. The Butterworth Group. 1981, 2, 309-339.

University of Texas, Bureau of Economic Geology. 1987. Geologic atlas of Texas, Dallas Sheet. Austin, Tex. Scale 1:250,000.

VanMetre, P.C., S.A. Jones, J.B. Moring, B.J. Mahler and J.T. Wilson. 2003. Chemical Quality of Water, Sediment, and Fish in Mountain Creek Lake, Dallas, Texas, 1994-97. Geological Survey Water-Resources Investigations Report 03-4082, 69 p.

Youngberg, A.D. 1973. A Study of Sediments and Soil Samples from Pearl Harbor Area. Port Hueneme, CA. Naval Civil Engineering Laboratory.

This page is intentionally left blank

APPENDIX B

"SERDP Project Number ER-1493 Second Year Annual Progress Report (December 2007)"

This page is intentionally left blank

1. COVER PAGE

SECOND YEAR ANNUAL PROGRESS REPORT:

REACTIVE CAPPING MAT DEVELOPMENT AND EVALUATION FOR SEQUESTERING CONTAMINANTS IN SEDIMENT

Prepared For:

PROJECT NUMBER: ER-1493

Prepared By:

NAVAL FACILITIES ENGINEERING SERVICE CENTER
1100 23RD AVENUE
PORT HUENEME, CA 93043

LEAD INVESTIGATOR: MS. AMY HAWKINS

With:

SCIENCE APPLICATIONS INTERNATIONAL CORPORATION
221 THIRD STREET
NEWPORT, RI 02840

And:

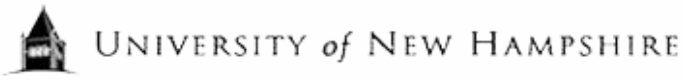

GREGG HALL
DURHAM, NH 03824

01 DECEMBER 2007

This page is intentionally left blank

2. FRONT MATTER

TABLE OF CONTENTS

TABLE OF CONTENTS
(Continued)

Page

LIST OF FIGURES

LIST OF FIGURES
(Continued)

LIST OF FIGURES
(Continued)

LIST OF FIGURES
(Continued)

LIST OF FIGURES
(Continued)

LIST OF TABLES

LIST OF TABLES
(Continued)

LIST OF ACRONYMS

AOS	Apparent Opening Size
ANOVA	Analysis of Variance
BET	Brunauer, Emmett and Teller
CETCO	Colloid Environmental Technologies Company
CoPC	Contaminant of Potential Concern
DGPS	Digital Global Positioning System
DOC	Dissolved Organic Carbon
EFANE	Engineering Field Activity Northeast
FA	Fulvic Acid
FEA	Finite Element Analysis
GC	Gas Chromatograph
GIS	Geographic Information System
GR	Gradient Ratio
HA	Humic Acid
HOC	Halogenated Organic Compound
MS	Mass Spectrometer
NAS	Naval Air Station
NAVFAC	Naval Facilities Engineering Command
NFESC	Naval Facilities Engineering Service Center
NOM	Natural Organic Matter
OSY	Ounce Per Square Yard
PAH	Polycyclic Aromatic Hydrocarbon
PCB	Polychlorinated Biphenyls
SAIC	Science Applications International Corporation
SDI	Specialty Devices, Inc.
SERDP	Strategic Environmental Research and Development Program
SPI	Sediment Profile Imaging
TCMX	Tetrachlorometaxylene
TNRCC	Texas Natural Resource Conservation Commission
TRRP	Texas Risk Reduction Program
USGS	United States Geological Survey

ACKNOWLEDGEMENTS

Ms. Amy Hawkins:	Naval Facilities Engineering Service Center Lead Investigator Specialist in Sediment Risk Assessment
Dr. Gregory A. Tracey:	Science Applications International Corporation Specialist in Contaminated Sediment Assessment
Dr. Kevin H. Gardner:	University of New Hampshire Expertise in Laboratory Evaluation of Contaminated Sediments and Reactive Capping Materials
Dr. Jeffrey S. Melton:	University of New Hampshire Expertise in Reactive Cap Design and Performance Evaluation

This page is intentionally left blank

3. EXECUTIVE SUMMARY

U.S. Navy Strategic Environmental Research and Development Program (SERDP) Project Number ER-1493 (Reactive Capping Mat Development and Evaluation for Sequestering Contaminants in Sediment) focuses on developing optimal mixtures of reactive amendments to treat a variety of contaminants at a site and then delivering these mixtures within a geotextile mat to be positioned on top of the sediments of concern. The overall project goal is to develop a chemically effective, mechanically stable, and cost efficient technology that could be deployed in a wide variety of environmental settings to effectively sequester both metal and organic contaminants while simultaneously allowing both groundwater flux and surficial biological colonization. In order to achieve the project objective, a series of laboratory and focused field experiments were designed to increase understanding of the practical effectiveness and limitations of the proposed reactive capping mat technology. Four separate tasks were defined that provide a logical scientific process for mat construction, pilot site selection and performance evaluation. These tasks were first described in detail in the First Year Annual Progress Report for Project Number ER-1493 prepared in December 2006 (NAVFAC 2006). That document also chronicled all actions that took place in the first year of project funding up to December 2006 as well as explained the proposed activities for all tasks moving forward. The goal of this Second Year Annual Progress Report is to describe the work that has been accomplished for each task from December 2006 to date in terms of methods used and results achieved as well as to outline activities that are still planned for year three.

Task 1. Composite Material Testing. The purpose of this task is to identify the mixture of amendment materials that most effectively sequesters contaminants by collecting data on adsorption, sequestration and chemical breakthrough properties of the mixed reactive mat system. In the first year of project activity, researchers from the University of New Hampshire (UNH) conducted batch adsorption experiments to characterize the sorption properties of various reactive amendments for a range of contaminant combinations in terms of absorption kinetics and adsorption isotherms.

The focus of the year two composite material testing effort was to investigate the interference caused by humic acid on the adsorption of coplanar and non-coplanar PCBs and PAHs onto activated carbons and organoclays, the two types of sorbent material being considered for incorporation into the final reactive mat design. To accomplish this goal, several additional kinetic and isotherm studies were conducted using various formulations of activated carbons and organoclays as sorbents to sequester individual PCB congeners and PAH compounds. These sorbent materials were subjected to humic acid preloading or spiking and resulting effects on the ability to sequester contaminants was evaluated. Results showed that preloading of sorbents with humic acid coupled with the simultaneous adsorption of humic acid and contaminant significantly reduced the adsorption capacity for all selected PCB congeners and PAHs. Experiments conducted without preloading of sorbent surfaces demonstrated that desorption upon subsequent spiking with humic acid (simulating long-term exposure to pore water that contains high humic acid concentrations) was not pronounced and varied with co-planarity of PCBs and number of rings of PAHs. Also, humic acids were found to interfere to a much greater extent with adsorption to activated carbon than with various organoclay formulations.

In addition to these adsorption studies, structural analyses, BET surface area analyses and thermogravimetric analyses were performed to evaluate the physical properties of the activated carbon and organoclay particles. Experiments were also conducted to determine the effects of fulvic acid (FA) and natural organic matter (NOM) on adsorption properties of the amendment materials to mimic the dissolved organic carbon (DOC) that will be present in real site conditions. The results of this work indicated that organic acids, which are quite concentrated in sediment pore water, have a significant impact on the efficacy of reactive mat components and are an essential factor in the design and ultimate performance of this type of in-situ sediment management approach. Based on the overall results of the organoclay characterization process, the preliminary recommendation is to proceed with CETCO organoclay featuring a bentonite base material for construction of the prototype reactive mats to be used during the year three full-scale mat testing effort. As of this report, Task 1 activities are still ongoing.

Task 2. Pilot Site Establishment. The purposes of this task were to first identify a project location (water body) that could be used as a pilot site for initial field testing of small-scale geotextile mats (Task 3) and then ultimately to select a particular area within this water body to serve as the target location for full-scale field testing of a prototype mat system (Task 4) based on specific geophysical and chemical properties. The basic requirement for a potential pilot site was the presence of sediments containing a mixture of metal and organic contaminants with associated exposure pathways of environmental concern based on previous investigations. In year one, a broad review of available environmental reports for compatibility with expected mat performance characteristics was able to produce a "long list" list of prospective Navy sites that could potentially serve as the pilot site for field evaluation. From this list, Cottonwood Bay in Grand Prairie, Texas and Pearl Harbor in Honolulu, Hawaii were selected as the two most suitable primary project sites based on a variety of chemical, physical, biological and logistical factors.

In year two, a more rigorous review of available site documentation was performed to compare the two primary sites in terms of nature and extent of contamination, groundwater flow properties, management planning and ongoing remediation. Cottonwood Bay was ultimately selected as the most appropriate pilot site for mat testing and a decision was made to proceed with future tasks at this location. Following the deployment of small-scale geotextile test mats (Task 3), a series of geophysical surveys were conducted in both the eastern and western portions of Cottonwood Bay in order to characterize site conditions including water depth and lake sediment properties with the goal of selecting a specific location for full-scale mat system deployment (Task 4). This geophysical investigation was performed by Science Applications International Corporation (SAIC) and consisted of bathymetry surveys, sub-bottom profiling, side-scan sonar surveys, sediment profile imaging (SPI) and sediment vibracoring. Concurrent with the SAIC investigation, researchers from UNH collected sediment and groundwater samples from Cottonwood Bay East to characterize contaminant conditions around the area of small-scale test mat deployment. Groundwater Seepage Inc. then conducted a follow-up groundwater seep survey in Cottonwood Bay East with the goal of defining the extent of sub-surface groundwater plumes that may be radiating from adjacent Naval Weapons Industrial Reserve Plant (NWIRP)

property and serving as contaminant transport pathways into the bay as suggested by prior groundwater models.

Based on the combined results of all the geophysical surveys, an area on the western side of Cottonwood Bay East approximately 200 feet from the NWIRP shoreline was chosen as the preferred target location for future full-scale mat system deployment. This area was selected mainly because of its location within a high potential groundwater discharge zone and the presence of elevated contaminant levels, both conditions of which are necessary for evaluating overall mat performance. As of this report, Task 2 activities have been completed.

Task 3. Geotextile Testing. The purpose of this task is to field test different types of geotextile material at the selected pilot site to assess whether biofouling and biofilm formation will adversely affect the ability of the fabric to allow water to pass through the final mat design, whether environmental weathering compromises the ability of the mat to retain the amendment material and whether environmental weathering compromises the reactivity of the sequestration agents. The geotextile most resistant to biofouling as determined from this field test will ultimately be used to construct the prototype mat system for full-scale field testing in Task 4. Although field deployment could not proceed until a pilot site was selected in Task 2, fourteen small-scale test mats (6 ft x 6 ft) of various geotextile composition and featuring different apparent opening sizes (AOS) were fabricated during year one. In year two, these mats were deployed in Cottonwood Bay East and are currently actively soaking in the field. Two retrieval events are planned for year three to coincide with six months and one year of soak time, at which point the entire replicate mats will be removed from the water and shipped to a UNH laboratory for performance evaluation to assess how material type, geotextile weight and apparent opening size affect biofouling and sediment clogging. Retrieval of the first set of replicates is planned for December 2007.

In addition to field evaluation, Task 3 also includes gradient ratio testing to evaluate geotextile flow properties under laboratory conditions as well as a finite element analysis to evaluate prospective sediment deformation and pore water pressure increases caused by the weight of a potential reactive mat. In year two, preliminary flow-through column experiments were used to evaluate flux for various sorbent mixtures and sorbent layers by closely mimicking processes in the field, thus providing baseline data to which the pending small-scale geotextile mat performance evaluation can be compared. As of this report, Task 3 is not yet completed.

Task 4. Prototype Mat Testing. The purpose of this task is to field test a prototype full-scale mat system constructed of the most adsorbent amendment (identified in Task 1) and the geotextile most resistant to biofouling and clogging (identified in Task 3) with the goal of assessing in situ chemical sequestration effectiveness and flux properties. This mat "system" will consist of one single layer geotextile, one double layer geotextile, one single layer geotextile with sand cover, one region of sand cover only and one control region of bare sediment with neither a geotextile nor a sand cover. Data collected from laboratory composite material testing and the retrieval of the first series of small-scale test mats will be used to guide construction of the full-scale reactive mats (25 ft x 25 ft) to be used for these treatments. Data collected from the Cottonwood Bay geophysical surveys (Task 2) conducted in year two were used to select a specific area for deployment of the mat system. Once deployed, the contaminant sequestration effectiveness of

the prototype mat system will be monitored by passive sampling with peepers placed on each treatment as well as the control area after five months of soak time. Deployment of these peepers will coincide with removal of the second set of replicate small-scale test mats. A groundwater seepage survey will then be conducted for each treatment after one year of soak time to evaluate flux through the mat. Construction and deployment of the full-scale prototype mat system is planned for February 2008. As of this report, Task 4 has not yet begun.

4. OBJECTIVE

The objective of SERDP Project Number ER-1493 is to develop a mixture of chemically reactive materials suitable for incorporation within an engineered geotextile mat to create a composite active capping system capable of deployment in a wide variety of environmental settings in order to effectively sequester both metal and organic contaminants.

5. BACKGROUND

In situ capping has frequently been used to physically separate contaminated sediments from the aquatic environment above the cap and, in some cases, to act as an impermeable barrier to groundwater flux. Sequestration based on physical separation alone, however, is not always desirable because it does not ensure that dissolved phase contaminant flux is eliminated as a transport pathway either through the cap or around it. More recently, in situ capping with chemically reactive materials has been explored as an option to provide a physical barrier to remobilization of sediment-bound contaminants while at the same time sequestering dissolved contaminants as they flux through the cap via groundwater flow. To date, studies of these reactive capping methods have largely focused on applying one type of reactive material to treat one particular class of contaminant and have typically involved deploying relatively thick layers of unconsolidated material (6 to 12 inches) over the bottom. This approach may not be effective at many sites with physically challenging conditions, multiple classes of contaminants or concerns over contaminant remobilization and may also be prohibitively large due to the costs of using large amounts coarsely applied reactive materials.

In contrast to thick layers of reactive material, it may be more practical at many sites to sequester sediment contaminants through in situ capping with a reactive geotextile mat if the mat would prevent physical contact with biota and retard leaching of chemicals into overlying waters while simultaneously allowing natural groundwater flow. The mixed reactive capping materials developed in this project will satisfy these requirements when incorporated into a functional mat system. Overall, the reactive mats will be non-intrusive, will simultaneously address multiple contaminant classes, will be easily deployed and will offer greater slope stability, erosion stability, and permeability to natural groundwater flow than a thick layer of unconsolidated reactive material. These benefits expand the utility of the reactive mat system to intertidal and sloped environments where the stability and effectiveness of either a traditional sand cap or unconstrained reactive materials would be diminished due to dynamic conditions. Finally, reactive mats can be fabricated on land to control mat thickness (0.5 inch) and integrity, thus minimizing the amount and cost of composite material as compared to the current practice of placing large amounts of substrate through the water column in thicker but variable layers.

Year one activities for SERDP Project ER-1493 were described in the First Year Annual Progress Report prepared in December 2006 (NAVFAC 2006). These first year actions involved separating the project into four separate tasks and then performing composite material testing as well as identifying a primary pilot site and fabricating small-scale test mats. The following sections of this Second Year Annual Progress Report describe the materials and methods (Section 6) and results (Section 7) for all year two activities including continued composite material testing, final pilot site selection, geophysical surveys, and small-scale test mat deployment. A concluding summary (Section 8) is also provided to review all year two accomplishments as well as to outline continued efforts planned for year three.

6. MATERIALS AND METHODS

This section provides a detailed description of how scientific questions were approached and addressed for each of the four tasks in year two. Details are provided for the experimental design of the laboratory investigations as well as completed and proposed field work. Given that the overall goal of this project is to develop a chemically effective, mechanically stable, and cost efficient technology that could be deployed in a wide variety of environmental settings, all laboratory and field studies were designed to increase understanding of the practical effectiveness and limitations of this technology.

6.1. TASK 1: COMPOSITE MATERIAL TESTING

The purpose of composite material testing for the present project is to determine the optimal mixture of reactive sequestering materials to be incorporated in the final geotextile mat design. To accomplish this goal, many laboratory studies were required to evaluate the empirical chemistry of adsorption of various potential amendments. The first year effort for Task 1 involved testing coconut shell-based activated carbon and three different formulations of brand name organoclays as potential sorbents for organic compounds as well as apatite as a potential sorbent for metals. These sorbent materials were exposed to several common contaminants of interest including five coplanar and non-coplanar polychlorinated biphenyls (PCBs), three polycyclic aromatic hydrocarbons (PAHs) of different ring structures and water solubilities and two heavy metals. Batch studies were performed as both single contaminant systems and multi-contaminant competitive systems. The methods for these initial experiments are discussed in detail in the First Year Annual Progress Report for this project (NAVFAC 2006).

The focus of the year two composite material testing effort was to investigate the interference caused by humic acid on the adsorption of coplanar and non-coplanar PCBs and PAHs onto activated carbons and organoclays, the two types of sorbent materials being considered for incorporation into the final reactive mat design. To accomplish this goal, several additional kinetic and isotherm studies were conducted using various formulations of activated carbons and organoclays.

In addition to these adsorption studies, structural analyses for activated carbon and organoclay were conducted using scanning electron microscopy and x-ray diffractometry, atomic force

microscopy and scanning electron microscopy, respectively, to observe physical differences caused by humic acid on the surfaces of the sorbent material molecules. Brunauer, Emmett and Teller (BET) surface area analyses were also conducted to determine the surface area of activated carbon and organoclay particles. To enhance this investigation, thermogravimetric analyses of organoclays were performed to determine the percent organic content that increases the hydrophobicity, and thus adsorption capacity, of this type of material. Finally, supplemental experiments were conducted to determine the effects of fulvic acid (FA) and natural organic matter (NOM) isolated from sediment pore water. These results supported the understanding of the influence that different fractions of dissolved organic carbon (DOC) would be expected to have under real site conditions on the sorbent properties of potential reactive mat amendments.

6.1.1. Characterization of Activated Carbon

The laboratory methods used to investigate the adsorption of PCBs on coconut shell-derived activated carbon in the presence of humic acid are described in the following sub-sections. The typical physical properties of this activated carbon source as used for these experiments are summarized in Table 6.1-1.

Particle size [ASTM D-2862]*	12 x 40 US Mesh
Ash Content (Base Material)[ASTM D-2866]*	3% w/w
Bulk Density [ASTM D-2854]*	0.50 g/cm^3
Iodine Number [BSC 90-032]*	1050 mg/g
BET Surface Area of Bare Activated Carbon	872.053 m^2/g
*Values obtained from Calgon Carbon Corporation, Pittsburgh, PA, USA	

Table 6.1-1. Typical physical properties of coconut shell activated carbon.

Batch Experiments. Batch adsorption experiments for the characterization of activated carbon were conducted using acetone and deionized water. The acetone was used to prepare a stock solution to serve as a carrier solvent for PCB congeners because of a known lack of significant interference caused by acetone on PCB adsorption by activated carbon. Each experiment was conducted in separate batches of 125 mL stock solution with varying concentrations of PCBs and the sorbent phase.

Preloading of Activated Carbon. The preloading of activated carbon for kinetics and isotherm experiments was done with 1 g/L of humic acid solution prepared in deionized water. A 10% sodium azide solution was added to the humic acid solution and the sorbent samples were equilibrated for 48 hours at 150 rpm on a rotary shaker to ensure thorough mixing.

Kinetic Studies. Batch experiments were conducted for the duration of one month to evaluate the kinetics of adsorption of 2-chlorobiphenyl, 2,2',5,5'-tetrachlorobiphenyl and 2,2',4,4',5,5'-hexachlorobiphenyl on activated carbon in the presence and absence of humic acid. Activated carbon samples were spiked with the PCB solution after preloading with humic acid and then equilibrated for 48 hours. The concentrations of the experimental PCB solutions were 6.6 mg/L for 2-chlorobiphenyl, 5.04 mg/L for 2,2',5'-tetrachlorobiphenyl and 0.08 mg/L for

2,2',4,4',5,5'-hexachlorobiphenyl. The samples were continuously mixed on a rotary shaker at 150 rpm for the duration of the experiment.

Isotherm Studies. Separate batches were prepared at different loading rates of all PCB congeners with bare activated carbon and activated carbon preloaded with humic acid to obtain adsorption isotherms. The preloading time and procedure was the same as performed for the kinetics studies described above. In the preloaded samples, humic acid was present in two forms: (i) humic acid adsorbed on activated carbon due to preloading and (ii) humic acid in dissolved form in a deionized water matrix. These studies were conducted with an adsorption equilibration time of 72 hours which as shown by the kinetics experiments represents a reasonable equilibrium period. Separate isotherm studies were also conducted to evaluate and compare the performance of coal based activated carbon (Calgon F400) regarding the adsorption of 2,2',5,5'-tetrachlorobiphenyl.

Sample Extraction. Once the equilibrium time was reached for each batch experiment, the supernatant of each sample was extracted into hexane by the vial liquid-liquid extraction method using tetrachlorometaxylene (TCMX) as a surrogate standard. Twenty mL of sample and 10 mL of hexane was taken into a 40 mL vial. These vials were then sealed with Teflon®-lined screw caps and shaken vigorously for 30 seconds on three separate occasions. The vials were then stored for 24 hours at 4˚C, at which point the extracts were passed through sodium sulfate to remove any chemically bound water prior to analysis with gas chromatograph columns.

Desorption Studies. Once initial sampling was completed at 72 hours, humic acid was added to the bare activated carbon samples to obtain the same concentration of humic acid as in the preloaded samples. This was done in order to determine the extent of desorption for PCBs already adsorbed on activated carbon. These treatments were again equilibrated by 72 hours of rotary mixing prior to sampling.

Determination of Humic Acid Effects. Batch experiments were conducted to obtain the adsorption behavior of 2-chlorobiphenyl, 2,2',5,5'-tetrachlorobiphenyl and 2,2',4,4',5,5'-hexachlorobiphenyl on activated carbon at different humic acid loading rates. These experiments were conducted at a fixed loading rate of the PCB solutions with varied loading rates of humic acid. The activated carbon was preloaded with humic acid at different rates for 48 hours prior to spiking with the PCB solutions. Separate experiments were also conducted to determine the effect of different humic acid loading rates on coal based activated carbon for the adsorption of 2,2',5,5'-tetrachlorobiphenyl. These experimental mixtures were also allowed to equilibrate for 72 hours.

Gas Chromatographic Analysis. All sample extracts were analyzed for PCB adsorption using a Varian CP3800 Gas Chromatograph (GC)/Saturn 2200 Ion Trap Mass Spectrometer (MS) with a CP8400 Auto Sampler. The GC column used was a DB-5 type capillary column (Varian Factor Four VF-5ms), 30 m long, 0.25 mm internal diameter and 0.5 µm thick. The ion-trap was operated in selected scan mode (MS/MS) for each PCB congener. The column oven temperature was programmed to hold at 40˚C for two minutes followed by a temperature ramp up to 184˚C at the rate of 12˚C per minute and then up again to 280˚ C at the rate of 4˚ C per minute with the final hold time of two minutes.

6.1.2. Characterization of Organoclays

The laboratory methods used to investigate the adsorption of PCBs on three different types of organoclays (CETCO, Polymer Ventures, Biomin, Inc.) in the presence of humic acid are described in the following sub-sections. The parameters and data selected to characterize these three organoclays are summarized in Table 6.1-2; scanning electron micrograph images of surface profiles and cross-section profiles of the three organoclays are shown in Figure 6.1-1 and Figure 6.1-2, respectively.

Organoclay	**CETCO**	**Polymer Ventures**	**Biomin, Inc.**
Base Clay	Bentonite	Attapulgite	Bentonite
BET surface area (m^2/ g)	0.3225	16.7294	0.1872
Percent Organic Matter*	19.10	10.54	26.95
Inorganic Cations (ppm)**			
Calcium (Ca)	967.2	750.8	682.2
Magnesium (Mg)	175.0	230.0	169.0
Potassium (K)	79.0	337.0	46.0
Phosphorus (P)	1.0	12.0	1.0
Estd. CEC ** based on inorganic cations (meq/ 100g)	6.50	6.53	4.94
* Measured by using thermogravimetric analyzer (TGA)			
* *Analyzed by University of New Hampshire Cooperative Extension			

Table 6.1-2. Parameters estimated for characterization of three compositions of organoclay.

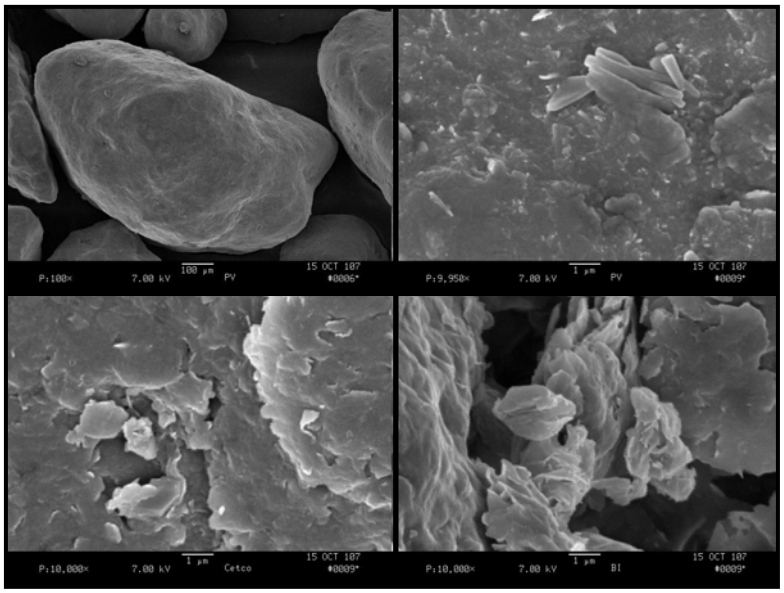

Figure 6.1-1. Scanning electron micrograph surface profiles of three different organoclays: Polymer Ventures (100x magnification - top left and 10K x magnification - top right), CETCO (10K x magnification - bottom left) and Biomin, Inc. (10K x magnification - bottom right).

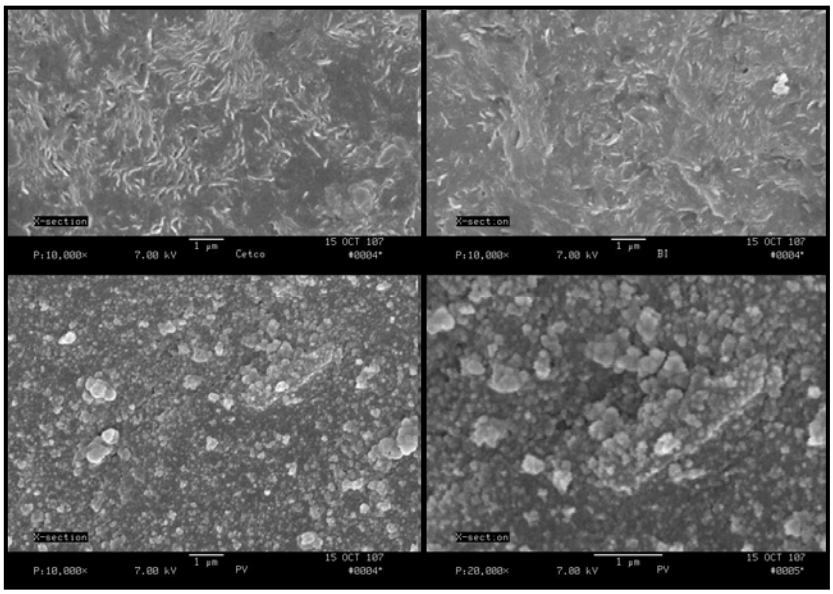

Figure 6.1-2. Scanning electron micrograph cross-section profiles of three different organoclays: CETCO (10K x magnification - top left), Biomin, Inc. (10K x magnification - top right) and Polymer Ventures (10K x magnification – bottom left and 20K x magnification - bottom right).

Batch Experiments. Experiments for the characterization of three different organoclays were conducted in separate batches of 125 mL with varying concentrations of PCBs and the sorbent phase. All the batch experiments were conducted using methanol and deionized water.

Preloading of Organoclays. The preloading of organoclays for kinetics and isotherm experiments was done with 1g/L of humic acid solution prepared in deionized water. A 10% sodium azide solution was added to the humic acid stock solution. The sorbent samples were equilibrated for 48 hours at 150 rpm on a rotary shaker to ensure thorough mixing.

Kinetic Studies. Batch experiments were conducted for the duration of 15 days to evaluate the kinetics of adsorption of 2-chlorobiphenyl on two compositions of organoclay (with different base clays) including CETCO organoclay containing bentonite and Polymer Ventures organoclay containing attapulgite in the presence and absence of humic acid. Samples were spiked with a 4 ppm PCB solution after preloading of the organoclays with humic acid and equilibrated for 48 hours. The samples were continuously mixed on a rotary shaker at 150 rpm for the duration of the experiment.

Isotherm Studies. Batch experiments were carried at different loading rates of all PCB congeners with both bare organoclay and organoclay preloaded with humic acid to obtain adsorption isotherms. The preloading time and procedure was the same as performed for activated carbon and the organoclay kinetics studies described above. The isotherm studies for organoclays were conducted for the equilibration time of 48 hours which represents a reasonable approximation as shown by the kinetics experiments. Sample extraction and gas chromatography analysis were performed the same way for the organoclay experiments as they were for the activated carbon experiments described above.

Desorption Studies. Once sampling was completed at 48 hours as described for activated carbon above, humic acid was added to the bare organoclay samples to obtain the same concentration of humic acid as in preloaded samples in order to determine the extent of desorption for PCBs already adsorbed on organoclay. These samples were again equilibrated for 48 hours of mixing prior to sampling.

6.1.3. Effects of Humic Acid, Fulvic Acid and Natural Organic Matter

Additional studies were conducted to assess the combined effects of humic acid, fulvic acid and NOM on the overall performance of activated carbon and organoclay in sequestering PCBs and PAHs. Laboratory methods for these experiments are described in the following sub-sections.

***Batch Experiments*.** The additional experiments were conducted in 40 ml vials with varying concentrations of 2,2',5,5'-tetrachlorobiphenyl and phenanthrene to obtain adsorption isotherms at equilibration time of 72 hours. All the batch experiments were conducted using and acetone and deionized water as the stock solution for activated carbon and methanol and deionized water as the stock solution for organoclay.

Preloading Process. The preloading of activated carbon and organoclay was done with 1, 100 and 1000 mg/L solutions of humic acid and fulvic acid. The NOM substrate was prepared in deionized water and extracted from Hudson River (NY) sediment and Passaic River (NJ) sediment pore water solutions. A 10% sodium azide was added to the humic acid stock solution. The sorbent samples were equilibrated for 48 hours at 150 rpm on a rotary shaker to ensure thorough mixing.

6.2. TASK 2: PILOT SITE SELECTION

The purpose of selecting a pilot site for this project was to identify a location for the field testing of small-scale geotextile mats. Once a primary pilot site was selected, geophysical surveys were conducted to determine a specific area within this site that will ultimately serve as the location for full-scale prototype mat system deployment.

6.2.1. Strategy Overview

In year one, the SAIC-UNH team worked with Engineering Field Activity Northeast (EFANE) and the Naval Facilities Engineering Service Center (NFESC) to select sites that would be appropriate for conducting geotextile field tests. In order to accomplish this task, data on potential sites were reviewed for compatibility with expected mat performance characteristics. The overall pilot site selection process was two-phased, with the first objective being the identification of the most advantageous location from a "long list" of prospective Navy sites in terms of addressing the research goals and serving as the small-scale geotextile testing site. Phase one was completed during year one activities, with Cottonwood Bay in Grand Prairie, Texas and Pearl Harbor in Honolulu, Hawaii having been chosen as potential pilot sites based on the criteria described in the First Year Annual Progress Report (NAVFAC 2006) and

summarized in the following section. Based on a comprehensive review of chemical, biological and logistical factors, Cottonwood Bay was ultimately chosen as the primary pilot site at which to proceed with small-scale geotextile testing and geophysical investigations.

The second objective of the site selection process was to further characterize the geophysical properties of the primary pilot site (Cottonwood Bay) with the ultimate goal of defining a specific target area for deployment of the prototype full-scale test mat system. These geophysical surveys included groundwater seepage and pore water chemistry analyses. The Cottonwood Bay geophysical investigations were conducted during year two activities. Methods for these surveys are discussed in detail in Section 6.2.3 of this report.

6.2.2. Primary Site Selection Criteria

During the year one effort, a series of criteria were generated in order to screen many prospective sites for characteristics that would allow for the most comprehensive understanding of the field dynamics of the reactive mats with the goal of choosing two sites for further geophysical evaluation. These criteria for phase one site selection included an evaluation of chemical, physical, and biological data as well as site management and logistical considerations. The desirable characteristics for each of these parameters were provided in a series of tables in the First Year Annual Progress Report (NAVFAC 2006).

While these criteria were not quantitatively weighted, priority was given to the presence of both metals and organics in sediment so as to fully assess the potential for the reactive mats to bind bioavailable contaminants as well as to the ability of the mats to maintain ambient environmental processes such as groundwater flux and surficial biological colonization. Other practical criteria for initial screening included the chronology and direction of risk assessment remedial management plans; the ideal primary location should be a near-term candidate for remedial dredging or traditional capping such that it would be possible to evaluate a reactive mat as a more effective, stable and economically advantageous alternative. Additional logistic considerations included accessibility of the site, availability of information to characterize existing conditions and cooperation of site/program management staff with at least some minimal availability of time to support project planning and execution.

Once the two most suitable pilot sites were established (Cottonwood Bay and Pearl Harbor), a comprehensive review of the literature for each location was performed to determine if remediation was planned and if contaminants of potential concern (CoPCs) had been established for both metals and organics. Other site factors that were sought in the literature included the absence of major obstructions such as rocks and/or debris that would make deployment of the mats in direct contact with the sediments difficult, and the presence of groundwater seeps that would require an evaluation of approach to retain existing water flow characteristics in the environment. Additionally, the presence of an energetic environment such as an intertidal zone or a shoaled habitat was also preferred for mat testing because a traditional sand cap would be insufficiently stable to provide a permanent form of remediation in this setting. Other salient characteristics of the prospective pilot site included factors that would affect the bioavailability of contaminants and/or the reactive capacity of the apatite, organic carbon and organoclay to bind the contaminants. Findings from the Task 1 laboratory studies were considered in the

evaluation of pilot site suitability because elevated organic carbon and humic acid in sediments could effect bioavailability and should not be present in very high concentrations for an optimal demonstration of reactive mat effectiveness. Finally, the availability of transportation venues and shoreside infrastructure were also evaluated for each site in order to assess the ability to accommodate mat deployment and monitoring.

The results of this comprehensive review were used during the year two effort to select Cottonwood Bay as the primary pilot site for future activities, a determination which is discussed in detail in Section 7.2 of this report. This water body is situated between routes I-30 and I-20 within Dallas County and is adjacent to the NWIRP and Naval Air Station Dallas (NAS). It is connected to the larger Mountain Creek Lake by a man-made diversion channel that transects NAS property, running underneath the entrance bridge and alongside the former base airstrip. Cottonwood Bay is divided into two main portions (East and West) by a causeway running from NWIRP property to NAS property. These two portions are heretofore referred to as "Cottonwood Bay East" and "Cottonwood Bay West."

6.2.3. Geophysical Surveys

Once Cottonwood Bay in Grand Prairie, Texas was identified from a comprehensive literature review as the primary pilot site for SERDP Project Number ER-1493, an extensive geophysical investigation was conducted in year two to characterize site conditions including water depth, habitat characteristics and lake sediment properties with the goal of selecting a specific location for future full-scale mat system deployment. This phase two evaluation was performed by SAIC and consisted of bathymetry surveys, sub-bottom profiling, side-scan sonar surveys, sediment profile imaging and sediment vibracoring. Groundwater Seepage Inc. then conducted a follow-up groundwater seep survey with the goal of defining the extent of sub-surface groundwater plumes that may be radiating from adjacent NWIRP property and serving as contaminant transport pathways into the bay.

The Cottonwood Bay geophysical surveys were conducted over five days in late July 2007 (7/24, 7/ 25, 7/28, 7/29 and 7/31) and the groundwater seep survey was conducted on 9/6-9/7/07. Weather conditions on these days were hot and humid with air temperatures ranging from 90-100°F. Isolated thunderstorms developed in the area during most afternoons, but these storms did not prohibit field work on any of the days with the exception of 1.5 hours of lost time on July 29. Throughout the course of the Cottonwood Bay investigation, surface water conditions were mostly calm. As determined by daily CTD casts (3 total), the average water temperature in the bay was measured at 86.0°F (30.0°C) with the average speed of sound measured for bathymetric correction purposes was 1508.7 m/s.

All geophysical activities were performed from either a 12-ft dual jon-boat survey craft or a 28-ft pontoon boat equipped with a survey-quality positioning system. Then UNH sampling activities were conducted from a single 12-ft jon-boat. The jon-boats were launched from the shore for activities in Cottonwood Bay East and from a public boat ramp in Mountain Creek Lake for activities in Cottonwood Bay West. The pontoon boat was only used for coring activities in Cottonwood Bay West and was also launched from the public boat ramp in Mountain Creek

Lake. A daily health and safety briefing was conducted each morning by SAIC Site Health and Safety Officer (SHSO) prior to initiating survey activities. Vessels, survey equipment and technical support were provided by Specialty Devices, Inc. (SDI) of Wylie, Texas. The specific methodologies used to complete each of the geophysical testing components are discussed in the following sub-sections and results and final conclusions are discussed in Section 7.2 of this report.

Bathymetry. Bathymetry data were collected from the two portions of Cottonwood Bay using a single-beam echo-sounder interfaced with a BSS+3 survey computer featuring HYPACK v.4.3 and SDIDEPTH software (Figure 6.2-1). The profiler was deployed from an A-frame winch between the dual jon-boats directly below the GPS antenna to produce negligible layback. Bathymetry data were collected from Cottonwood Bay East on 7/25/07 along eleven planned survey lines (7 N-S, 4 E-W) and a shoreline trace. Bathymetry data were then collected from Cottonwood Bay West on Saturday, July 28 along nineteen planned survey lines (15 N-S, 3 E-W). The sixteenth planned survey line in the western portion (the westernmost line closest to the shore) could not be accessed due to shallow water and aquatic vegetation. Data logging was continuous between survey lines in each area to reduce processing time and produce a higher quality dataset.

Figure 6.2-1. Bathymetry and sub-bottom transducer deployed from dual jon-boat survey craft.

The bathymetry surveys at Cottonwood Bay were performed using the water level as a reference with the acoustic survey system measuring the distance between this reference and the water/bottom interface. The distance between the water level and the bottom was calibrated during the survey using a bar check method which compared the acoustically measured depth to a geodetic marker of known elevation. The accuracy of such a bar check is limited by the stability of the water line on the boat and is generally accepted to be within 1-inch. For Cottonwood Bay, the geodetic elevation was a first order geodetic reference marker located near the lake at the intersection of SE 14th Street and Sampsell Street in Grand Prairie (H269 reset marker; PID CS2549), checked with a kinematic digital global positioning system (DGPS). This

measurement was compared to the lake level elevations reported by the U. S. Geological Survey (USGS) and found to match within 2 cm (<1-inch). Overall, the elevation of the water level in Cottonwood Bay and Mountain Creek Lake was measured and reported on the days of bathymetry data acquisition as approximately 457.73 ft (NAVD 88). This value was used as the reference for all hydrographic data collected during the Cottonwood Bay investigation.

Bathymetry data collected by the SDI survey computer (BSS+3) were transferred onto SDI's network computers. Each RAW data file was then processed through the DEPTHPIC program, which graphically displays the acoustic record collected by the SDI bathymetry/sub-bottom transducer and allows the user to change the weighting of each frequency to highlight different sediment characteristics. To identify the water/bottom interface, an SDI survey technician traced the present post-impoundment surface (200 kHz frequency) by digitizing the acoustic data using the computer mouse. The interpreted depths and horizontal positions for this profile were then exported from DEPTHPIC to ASCII files featuring x, y, z values. These files were reviewed by the survey technician and obvious spikes and anomalies were removed. Finally, an SAIC geographic information system (GIS) analyst used the processed files (shapefiles, geotiffs, etc.) to generate bathymetric maps for both portions of Cottonwood Bay. This figure includes an extrapolation component to estimate depths for the entire area between survey lines.

Sub-Bottom Profiling. Sub-bottom profile data were collected from the two portions of Cottonwood Bay concurrently with bathymetry data using the same transducer interfaced with the same BSS+3 survey computer featuring HYPACK v.4.3 and SDIDEPTH software (Figure 6.2-1). Because these two surveys were conducted simultaneously, they followed the same lines and reference level calibration procedure described in the previous sub-section.

Sub-bottom profile data were exported from the SDI survey computer (BSS+3) and processed in the same manner as the bathymetry data. To identify sub-bottom interfaces, an SDI survey technician traced the pre-impoundment surfaces (50 kHz and 24 kHz frequencies) rather than the post-impoundment surface. An SAIC GIS analyst then used the processed sub-bottom data to determine the thickness of the uppermost sediment layer by subtracting the depth of the post-impoundment surface (bathymetry) from the depth of the first pre-impoundment surface.

Side-Scan Sonar. Side-scan sonar data were collected from the two portions of Cottonwood Bay using an IMAGINEX dual frequency digital side-scan sonar transducer ("fish") interfaced with a BSS+3 survey computer featuring HYPACK v.4.3 software (Figure 6.2-2). This transducer functions at 330 kHz to provide wide-area coverage but can also operate at 800 kHz to achieve extremely high resolution for seeing the fine detail required for object identification. Vessel location recorded using DGPS and vertical fish elevation determined with a depth sounder were mapped in the HYPACK software.

Figure 6.2-2. Side-scan sonar transducer ("fish') deployed from dual jon-boat survey craft.

The side-scan transducer was deployed from the A-frame between the dual jon-boats at a point directly below the GPS antenna to produce negligible layback. Side-scan data were collected from Cottonwood Bay East on Wednesday, July 25 along four planned E-W survey lines as well as several supplemental fill lines to increase coverage. The horizontal range of the side-scan transducer was set at 15 m for this portion of the survey. Side-scan data were then collected from Cottonwood Bay West on Saturday, July 28 along three planned E-W survey lines and several supplemental fill lines to ensure full coverage. Several other lines and a shoreline trace were also surveyed in the area where the diversion channel enters the bay beneath the NAS bridge so as to provide special coverage for this area of interest. The horizontal range of the side-scan transducer was set at 100 ft for the western bay. Similar to the bathymetry/sub-bottom surveys, data logging for side-scan was continuous between survey lines in each area to reduce processing time and produce a higher quality dataset.

An initial data review revealed that full coverage was not achieved in Cottonwood Bay East with the attempted side-scan configuration. Thus a second survey was conducted in this area on Tuesday, July 31 using a single jon-boat with the transducer deployed from port side. During this additional side-scan effort, data were collected along 7 N-S survey lines as well as a complete shoreline trace and the horizontal range of the transducer was increased to 100 ft. Data logging was continuous to produce a higher quality dataset and full coverage was ultimately achieved with this configuration.

Similar to the bathymetry/sub-bottom surveys, side-scan sonar data collected by the SDI survey computer (BSS+3) were transferred onto SDI's network computers. This data was then processed in HYPACK by an SDI survey technician to produce a final data product which provides mosaic pictorial views of the two survey areas. An SAIC GIS analyst placed these mosaics on corresponding aerial photographs to generate figures for each portion of the bay that illustrate results of the side-scan sonar survey.

Sediment Profile Imaging. The SPI technology utilizes an underwater still camera-mirror system to take cross-sectional pictures of the sediment-water interface and the upper six inches of sediment, which encompasses most of the biologically active zone of a lake or seafloor. Within the SPI mechanism, the camera is encased in a solid pressure vessel and points straight down into a water-filled prism featuring a sharp cutting edge to penetrate the sediment surface and a mirror tilted at 45° to capture a horizontal reflection of the sediment-water interface. Light for the underwater photographs is provided by a remotely controlled strobe that is programmed to fire in synchronization with camera exposure. An ideal resulting image will feature the sediment-water interface about 3/4 of the way up the frame and show both the overlying water column and several inches of sediment cross-section. Analytical results from SPI pictures provide a reliable reconnaissance tool for assessing the overall condition of a benthic habitat that is less labor intensive than standard benthic community assessment methods using surface grab sampling.

For the Cottonwood Bay investigation, SPI photographs were taken from the dual jon-boat survey craft equipped with an A-frame and manual winch. The handheld camera frame was attached to the A-frame such that it could be lowered between the hulls using the winch (Figure 6.2-3). Preliminary images were collected on Tuesday, July 24 from six stations in Cottonwood Bay East using an analog camera by lowering the frame to the lake floor and allowing the prism to penetrate the sediment surface. Upon developing the film from these preliminary attempts, however, the analog camera was found to produce poor quality images and the SPI effort was forced to proceed with a fully digital camera setup. Using the digital camera, images were then collected from thirteen stations in Cottonwood Bay East. The frame base plate (serving as a penetration stop) was set at six inches for this effort and three image replicates were taken at each station. A field review of the resulting digital photographs indicated poor quality images at several stations due to over-penetration of the camera into the soft sediment. Thus the SPI process was repeated on 7/25/07 at seven stations in Cottonwood Bay East with the frame base plate set at eleven inches to decrease penetration. Following these adjustments, a second field review indicated good quality images at all 13 Cottonwood East stations.

Figure 6.2-3. Digital SPI camera deployed from dual jon-boat survey craft.

On 7/27/07, the SPI data collection was continued with the digital camera at eight stations in Cottonwood Bay West. For this effort the frame base plate was set at either six, nine or twelve inches depending on the firmness of the sediment as tested with a metal rod and three image replicates were taken at each station. In all, images were obtained from another 25 station with the base plate configuration again varying between six, nine and twelve inches. A review of the resulting digital photographs indicated at least one good quality image from all West stations except for W-8, which had low penetration due to unexpected hard bottom near the NAS Bridge. Here the base plate configuration decreased from nine inches to six inches to increase penetration and sampling repeated. Following this adjustment, good quality images were obtained from this station.

The acquisition goal of the Cottonwood Bay SPI investigation was to obtain and analyze one acceptable quality image from each of the 38 total East and West stations. Representative replicates were evaluated for the various parameters defined as follows:

- **Grain Size Major Mode** – The dominant grain size observed within the entire photographed sediment column.
- **Camera Penetration** – The distance (cm) the camera prism was able to penetrate the sediment surface; a relative measure of density or compressive strength bearing capacity of the sediment.
- **Boundary Roughness** – Vertical variations (cm) in the sediment-water interface; a quantification of small-scale surface relief.
- **Benthic Habitat** – A visual classification of habitat in terms of sediment type and relative bottom hardness.

- **Successional Stage** – The relative stage of benthic community present in the surface sediment ranging from opportunistic pioneering species to equilibrium community deposit feeders.
- **Redox-Potential Discontinuity (RPD) Depth** – Thickness (cm) of the surface layer of oxygenated sediments.
- **Methane** – The presence of methane gas bubbles as a product of the anaerobic decomposition of organic matter; indicative of anoxic conditions and may signify a preferential transport pathway for contaminants to surface waters.
- **Organism-Sediment Index (OSI)** – A numerical ranking that describes overall habitat quality as a function of RPD depth, successional stage and the presence of methane; values range from -10 for highly degraded/disturbed conditions to +11 for healthy/undisturbed conditions; used primarily to characterize marine habitats.
- **Benthic Habitat Quality (BHQ) Index** – A numerical ranking that describes overall habitat quality as a function of RPD depth, surface structures (*e.g.*, fecal pellets, tubes, feeding pits) and subsurface structures (*e.g.*, burrows, oxic voids); values range from 0 for the poorest quality habitat to +17 for the highest quality habitat; used primarily to characterize freshwater habitats.

Sediment Vibracoring. Sediment vibracoring for Cottonwood Bay was conducted in the western portion of the bay on 7/29/07 using a 28-ft pontoon boat and the SDI Vibe-Core-D electric coring apparatus with five foot aluminum tubes and no core catchers (Figure 6.2-4). Vibracores were not collected in the eastern portion of the bay due logistical factors preventing access with the coring vessel. The goal for this vibracore effort was to obtain one core suitable for analysis from each of two specific target areas in order to confirm the sediment layers identified in the sub-bottom and SPI surveys.

Cores were obtained by lowering the aluminum tube attached to the electric head to the bottom of the lake with an electric winch and vibrating for 1-2 minutes until a hard layer providing a sediment "plug" was reached. In cases where hard bottom was encountered immediately, additional weight was added to the coring head in order to achieve proper penetration into the sediment surface. Upon retrieval, the aluminum tube was removed from the electric head and the sediment core was extruded onto the boat deck using a rubber push rod. Analyzable cores were photographed and characterized, and documented with paper log entries before all material was ultimately returned to the coring location.

Figure 6.2-4. Vibe-Core-D coring apparatus deployed through moon pool of pontoon boat.

Groundwater Seepage Survey. Groundwater Seepage Inc. conducted a groundwater seepage survey in Cottonwood Bay East over 9/6-9/7/07 based on results of the SAIC geophysical investigation with the objective of identifying groundwater upwelling zones potentially emanating from the adjacent NWIRP property. This survey was accomplished using the 12-ft dual jon-boat survey craft provided by SDI and Trident probe pore water monitoring technology.

The Trident probe is a direct-push, integrated temperature sensor, conductivity sensor, and pore water sampler that was developed to screen sites for areas where groundwater may be discharging to a surface water body based on the principle that upwelling groundwater would have different conductivity and colder temperatures (Chadwick *et al*. 2003). Thus real-time differences in observed conductivity and/or temperature indicate areas where groundwater discharge may be occurring. The integral porewater sampler can also be used to rapidly confirm the presence of freshwater or other chemical constituents by retaining samples for laboratory analysis, but this component was not used during this portion of Cottonwood Bay survey activities. A pole-mounted GPS receiver records the location of each push. Images of the complete Trident probe system are provided in Figure 6.2-5.

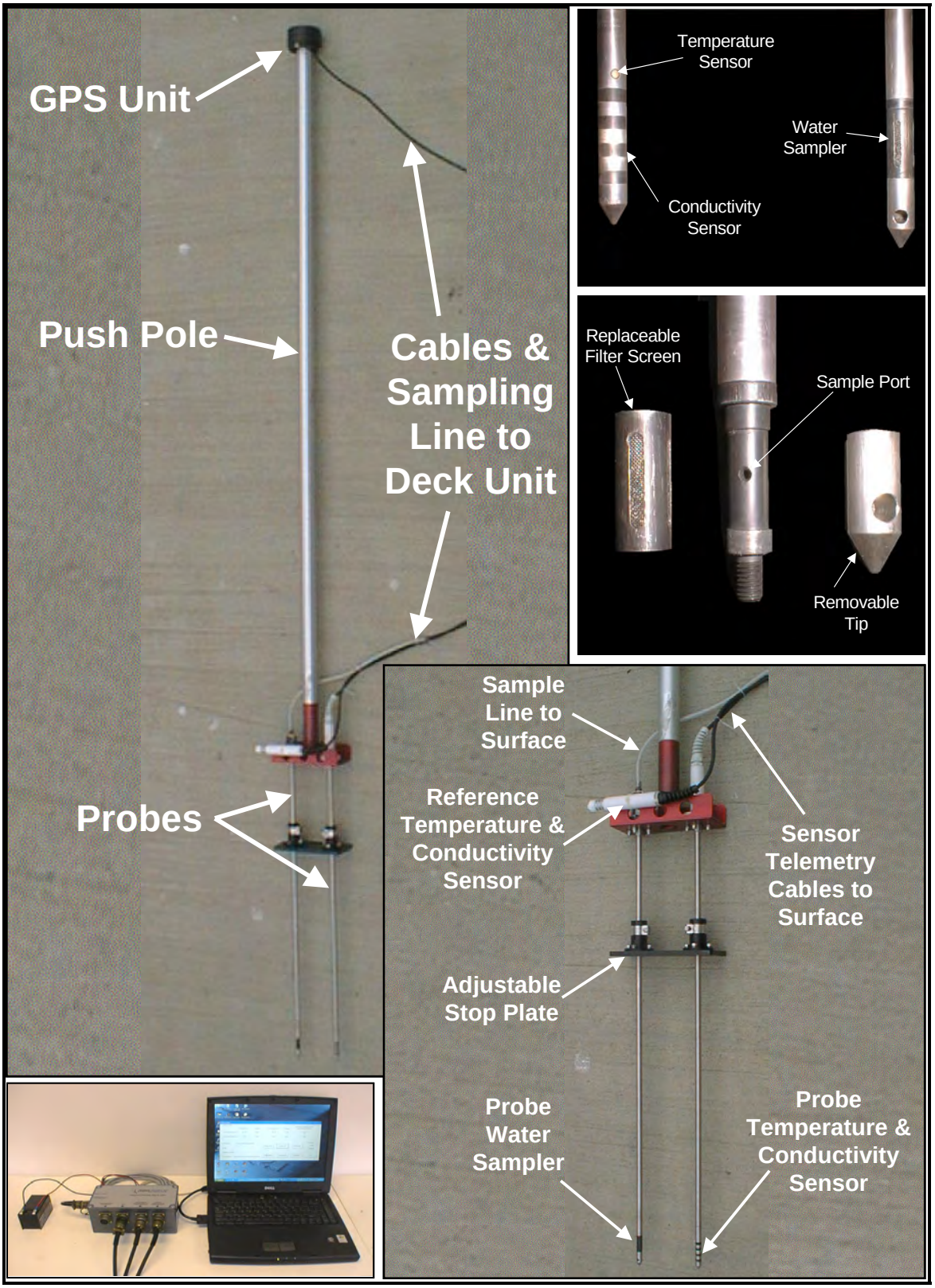

Figure 6.2-5. Complete Trident probe system showing the conductivity and temperature sensor, water sampling probe, push-pole, GPS unit and deck unit.

The experimental design for the Trident survey at Cottonwood Bay focused on identifying potential groundwater discharge zones along the northern shoreline adjacent to the NWIRP property. The sampling grid consisted of five N-S transects containing a total of 41 stations. Data were collected at each of these stations for water depth, surface water temperature, surface water conductivity, subsurface temperature, subsurface conductivity, GPS location and a subjective determination of sediment type. Water depth was determined using a hand held acoustic fathometer. Surface water quality parameters were collected by holding the probe in the water column one foot above the sediment-water interface and subsurface water quality parameters were collected by inserting the probe into the sediment two feet below the sediment-surface water interface. During deployment, real-time data were collected from the conductivity and temperature sensors on the probe as well as the GPS unit by interfacing with TridentTalk software. Once the sensor readings had stabilized, data was recorded by activating the "Log current data" button on the TridentTalk display. Average sensor values for each parameter were calculated automatically from a minimum of nine replicate readings once stabilization had been achieved. The real-time data was then reviewed in numeric format and displayed spatially using the AGIS graphical information system software. The spatial AGIS display provided a capability for rapidly evaluating the most likely areas of groundwater discharge based on temperature and conductivity contrast. The resulting survey data were used to develop spatial maps indicating potential areas of groundwater discharge.

6.3. TASK 3: GEOTEXTILE TESTING

The purpose of the geotextile testing task for this project was to field test different types of geotextile material at the selected pilot site in order to assess: (i) whether biofouling and biofilm formation will adversely affect the ability of the fabric to allow water to pass through the final mat design, (ii) whether environmental weathering compromises the ability of the mat to retain the amendment material and (iii) whether environmental weathering compromises the reactivity of the sequestration agents. The geotextile found to be most resistant to biofouling after a specified soak period as determined from this small-scale field test will ultimately be selected to construct the prototype mat system for full-scale field testing.

The geotextile testing task completed to date includes the construction of small-scale test mats of different compositions as well as the deployment (7/07), initial retrieval (12/07) and laboratory study (1/08-3/08) of these mats in year two. Future monitoring is planned for year three (6/08-8/08). While the test mats were soaking, laboratory gradient ratio testing and finite element analyses were conducted for clean, non-fouled mats to develop initial results regarding stability, clogging potential and prospective sediment deformation leading to excess pore water pressure. These laboratory testing and modeling procedures will continue in year three to incorporate field data from the weathered test mats once they are retrieved. Descriptions of the various components of Task 3 for the year two effort are provided in the following sections.

6.3.1. Field Evaluation

Fabrication. During year one, investigators from UNH and SAIC working with the Colloid Environmental Technologies Company (CETCO) of Arlington Heights, Illinois identified the need for, and fabrication of a total of 14 small-scale test mats of different materials and apparent

opening sizes (AOS), each measuring 6 ft x 6 ft (Figure 6.3-1). These mats were designed and constructed by CETCO such that the amendment material was bound within a high loft core "sandwich" between a woven backing geotextile (silt curtain) and a non-woven top geotextile (fabric). This arrangement was chosen to allow the principal investigators the ability to assess how material type and apparent opening size affect biofouling and sediment clogging. Twelve of the mats contain a mixed core composite consisting of apatite (0.23 lb/sq ft), activated carbon (0.28 lb/sq ft) and organoclay (0.28 lb/sq ft). The maximum achievable loading rate for this mixture was ~0.8 lb/sq ft due to the light density of activated carbon. The remaining two mats contained an Ottawa sand core to serve as a replicated control. Table 6.3-1 below summarizes the design of the small-scale test mats.

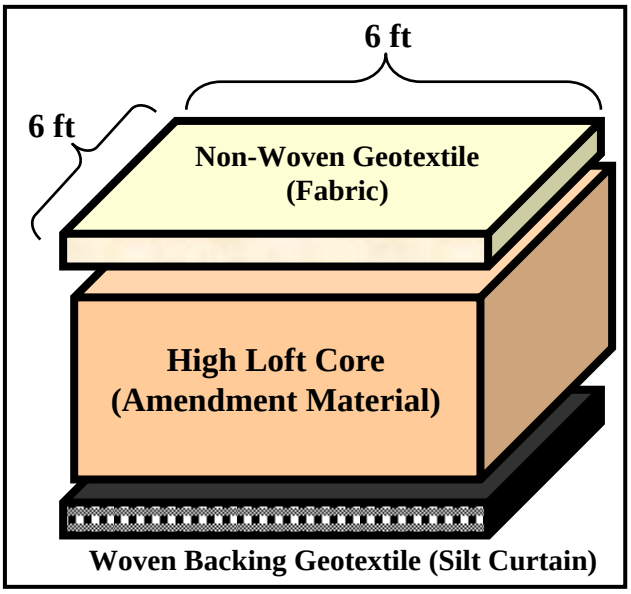

Figure 6.3-1. Construction diagram of small-scale geotextile test mats.

Total of 14 Test Mats Constructed			
Material	**Core / Mass Per Area**	**AOS**	**Quantity**
Polyester	Mixed - 5 oz/sy	170	4
Polypropylene	Mixed - 6 oz/sy	70	4
Polypropylene	Mixed - 8 oz/sy	80	4
Polypropylene	Ottawa Sand - 6 oz/sy	70	2

Table 6.3-1. Material design summary of small-scale geotextile test mats.

Deployment. As discussed in Section 6.2, Cottonwood Bay in Grand Prairie, Texas was selected as the primary pilot site for geotextile testing following a comprehensive literature review conducted during the present project year (year 2). Following construction, the small-scale test mats were shipped directly from the CETCO plant to the SDI warehouse in Texas to await field deployment. Cottonwood Bay East was selected as the target area for mat deployment prior to the geophysical investigation based on sediment and groundwater properties identified in the

existing literature. In June 2007, the 14 small-scale mats were placed in Cottonwood Bay East in two rows of seven near the northern shore of the bay adjacent to the NWIRP property. Each of these rows consisted of two polyester test mats with a 170 apparent opening size and mixed core, two polypropylene test mats with a 70 apparent opening size and mixed core, two polypropylene test mats with an 80 apparent opening size and mixed core and one polypropylene control mat with a 70 apparent opening size and sand core.

All of the test mats contained the same amendment core mixture featuring a combination of apatite, activated carbon and organoclay. For the similar mats in each row, one replicate was deployed with the woven backing geotextile (silt curtain) face down and the other replicate was deployed with the woven backing geotextile face up. This arrangement was selected to investigate how the different geotextiles behave under direct contact with the sediment surface. The control mats were deployed with the woven backing geotextile face down in both rows.

All mats were weighted to the sediment surface with ceramic bricks tethered to each corner with plastic zip ties and the location of the southwest corner of each mat was marked with an aluminum stake. Each mat was also tagged with a colored zip tie to aid in differentiating each replicate during the evaluation process. Approximately five feet of space was left between each mat to reduce any possible interference associated with edge effects (*e.g.*, suppression of groundwater flux by nearby mats). Field photographs of the small-scale test mat deployment process are shown in Figure 6.3-2. A schematic diagram of the final mat arrangements is shown in Figure 6.3-3.

Figure 6.3-2. Small-scale geotextile test mat deployment.

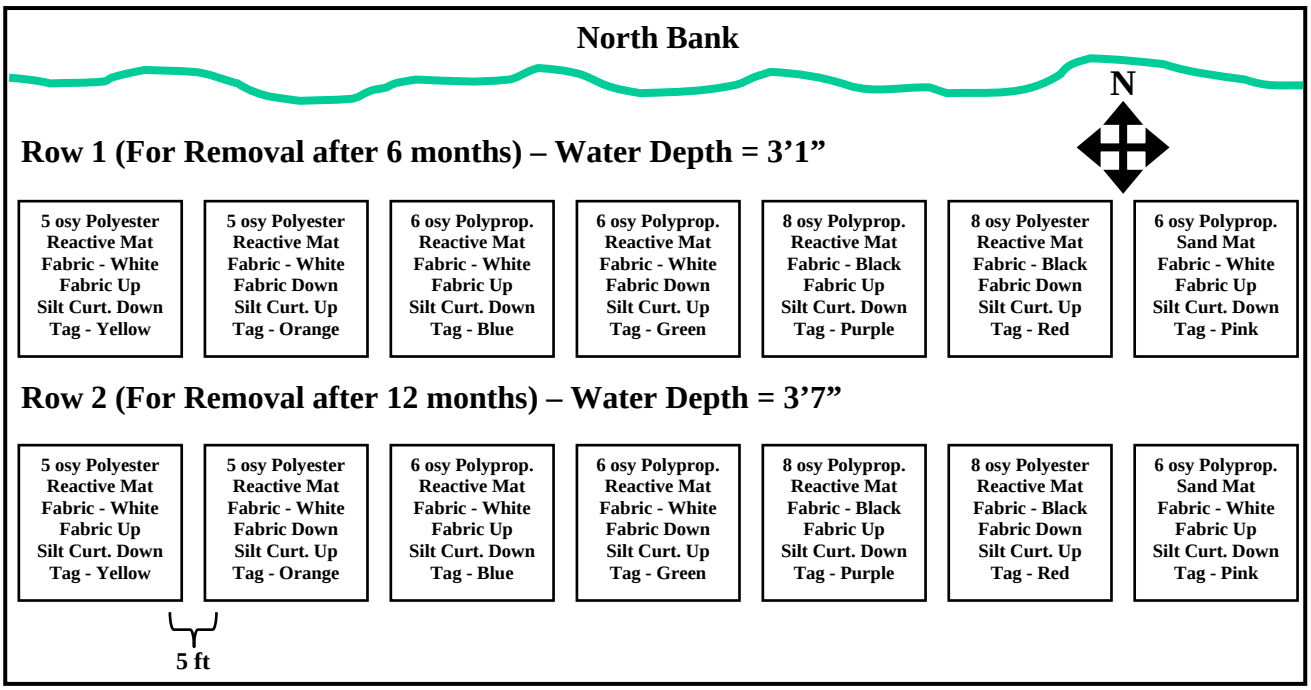

Figure 6.3-3. Schematic diagram of final small-scale geotextile test mat arrangement.

Monitoring and Retrieval. As part of the small-scale geotextile test mat performance evaluation process planned for year three, the row of seven mats closer to the shoreline (Row 1) will be removed in its entirety six months after deployment (12/07) for laboratory testing to assess potential hydraulic conductivity changes due to biofouling and reactivity changes due to biofilm growth. The second row of seven further from the shoreline (Row 2) will then be removed in its entirety one year after deployment (June 2008) for similar testing. During the retrieval process, each replicate mat will be carefully removed from the water so as not to disturb potential biofilm accumulation. Once on shore, the mats will be rolled up, sealed in containers and shipped to the UNH laboratory.

During the Cottonwood Bay East bathymetry survey that took place during the year two geophysical investigation (July 2007), SAIC personnel entered the water with waders for a brief field evaluation of the small-scale mat arrangement approximately one month after initial placement. This evaluation was performed by wading near the mats and observing whether any of them had significantly shifted positions or become subject to any unexpected deterioration. It was noted at this time that Mat 1 in Row 1 (the westernmost mat in the row closer to shore) had accumulated significant gas underneath, apparently from bubbles evolved from the sediment, such that the mat had been floated off the lake floor. Similar conditions were also noted in Mat 2 and Mat 3 in Row 2 (the second and third westernmost mats in the row further from shore). These bubbles are believed to have resulted from a build-up of gas (*e.g.*, methane) either percolating through the sediment surface or being produced by biological activity taking place beneath the mat. Because the westernmost mats in each row featured the smallest apparent opening size (either 5 oz/sy or 6 oz/sy), it was postulated that these gaseous accumulations were not able to pass through the small AOS. Whether the mat was deployed with the woven backing geotextile up or down appeared to make no difference in terms of gas accumulation. Prior to

concluding the field evaluation, SAIC personnel released the bubbles from the mats in question by lightly stepping on them to force all gas accumulation out the side until they were again laying flat on the lake floor.

Concurrent with the Cottonwood Bay East geophysical investigation, researchers from UNH also collected analytical sediment and groundwater samples to characterize contaminant conditions around the area of small-scale test mat deployment. These samples were shipped to a laboratory for chemical testing. Results from these analyses were intended to evaluate whether the specific small-scale test mat location could potentially serve as the site for full-scale mat system deployment based on desired chemical characteristics.

Performance Evaluation. Following each of the two test mat retrieval events, laboratory performance evaluations will investigate the relationship between permeability and biofouling to determine whether surficial material accumulation in the field is significantly impeding hydraulic conductivity. Additional laboratory testing will also assess the effects of biofouling on amendment reactivity to determine if deployment in an anoxic environment causes any significant change in adsorption properties. Laboratory data from the field samples will be compared to initial permeability and reactivity measurements collected during the composite material testing phase (Task 1). The initial (6 month) comparisons will help select the geotextile that offers the best balance between fouling resistance and amendment material effectiveness as well as assess whether a sand cap is needed to protect the mat from extensive biofouling or degradation.

In order to accomplish the proposed performance testing, a geotechnical test column system was purchased to measure the clogging potential of the recovered test mats. A photograph of the experimental setup is shown in Figure 6.3-4. This ASTMD 5101 method directly measures the clogging potential of the actual sediment/geotextile system *(i.e.*, an intact column of sediment covered by the reactive mat) so as to provide a realistic estimate of the actual cap performance with regard to clogging and sediment infiltration.

Figure 6.3-4. Geotextile permeability column experimental setup.

Once the retrieved small-scale test mat segments are received at the UNH laboratory, observations will be made regarding relative percent fouling of the geotextile material. Permeability tests will then be performed using the test system by placing a section of mat sample into the column and measuring the time required for static head pressure of an underlying water column to flux through the mat surface. The elapsed time will then be compared to the flux time of a clean, non-fouled mat. After this test, the fouling layer will be scraped off the mat, dried, and weighed.

Another issue of concern for mat performance is the growth of biofilms on the surface of the reactive materials themselves, regardless of specific type of amendment used in the mat. These colonies may not be sufficient to cause biofouling by clogging geotextile pore spaces, but they may influence the local chemistry at the surface of the amendments and thus impact contaminant uptake. To investigate this situation, samples of biofilm coated materials will be gathered from the recovered mat segments and tested with the same techniques used in Task 1 to quantify how biofilms may enhance or diminish amendment effectiveness. Additional clean samples of reactive core material will also be gathered from the recovered mat segments to determine how in-situ redox conditions have influenced amendment effectiveness. These samples will also be tested with the same laboratory techniques used in Task 1 but will be sterilized first to minimize any potential impact from biofilms.

6.3.2. Gradient Ratio Testing

The purpose of gradient ratio testing is to evaluate the stability and clogging potential of a sediment-geotextile filter system. Different flow rates will be tested to determine whether the geotextile is likely to become impermeable to flow under a range of natural field conditions. Using the geotextile permeability column shown in Figure 6.3-4, water is pushed through the sediment perpendicular to the plane of the geotextile by applying an increasing hydraulic gradient until sediment particles are forced inside the fabric to such an extent that it becomes

clogged, at which point a conclusion can be made as to the amount of hydraulic pressure that would be needed for the mat to fail under field conditions. After running the test, the sediment particles in contact with the geotextile leave a mark on the cross flow area thus allowing each geotextile to be tested only once. The mass of sediment that crosses the geotextile while the filter system is stabilizing, thus causing clogging, is collected and weighed for further analyses. A detailed picture of the permeability column showing geotextile-sediment contact and reactive mat-sediment contact is provided in Figure 6.3-5. Comparative images of a geotextile sample before and after a gradient ratio test are shown in Figure 6.3-6 and accumulated sediment that has passed through the geotextile during a test is shown in Figure 6.3-7.

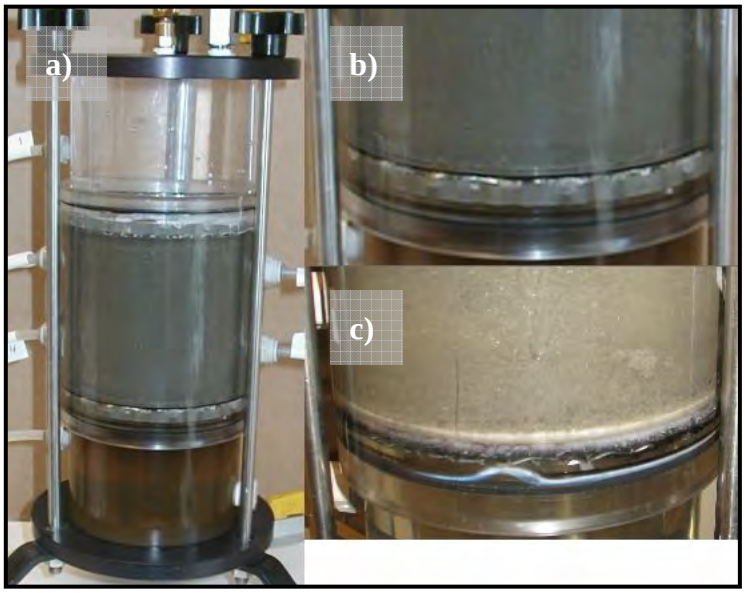

Figure 6.3-5. Detailed photograph of geotextile permeability test column showing (a) permeameter for gradient ratio tests, (b) geotextile-sediment contact and (c) mat-sediment contact.

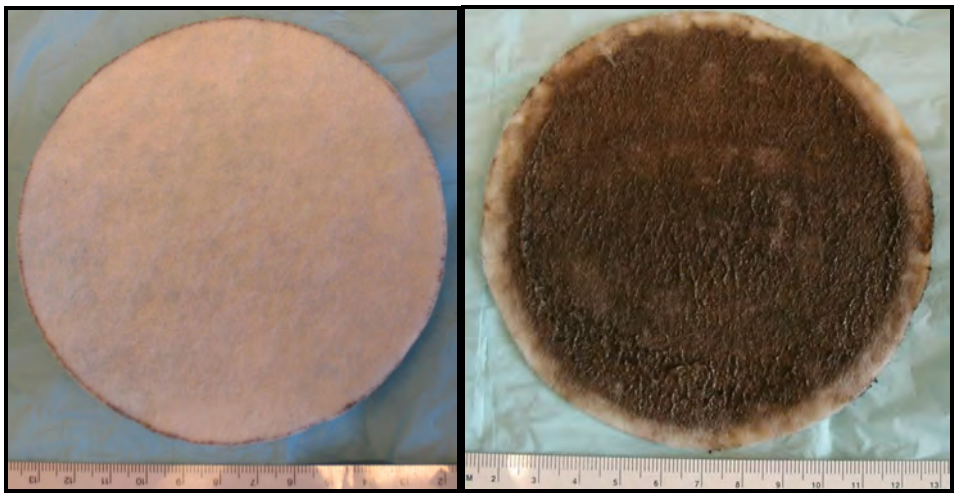

Figure 6.3-6. Comparative images of a geotextile sample before (left) and after (right) a gradient ratio test.

Figure 6.3-7. Sediment that has passed through the geotextile during a gradient ratio test.

The gradient ratio value is defined as the ratio of hydraulic gradient in the soil-geotextile section of the test column to the hydraulic gradient in the soil-only section of the test column as shown in the following equation:

$$GR = \frac{i_{Soil-Geotextile}}{i_{Soil}} \begin{matrix} >1 & \text{Clogging} \\ <1 & \text{Piping} \end{matrix}$$

Values lower than unity (<1) indicate piping conditions conducive to flow, while values larger than unity (>1) indicate clogging of the filter system. Values slightly less than one are generally preferred for a reactive mat system since they show a stable system allowing low flow without clogging. When evaluating the effectiveness of a geotextile, the stability of the gradient ratio value might be as important as the value itself because it denotes a stable filter system without further particle transport.

Preliminary gradient ratio testing conducted on various stock geotextiles during year one showed that trapped bubbles are a significant impediment to groundwater flux through the system in a fine grained matrix such as the sediment expected to be encountered in Cottonwood Bay. Experiments were conducted to determine if sample preparation in a nitrogen atmosphere would help eliminate bubbles, but results indicated that such a process had negligible effects. The bubble trapping problem was ultimately corrected by refining sample preparation techniques to remove bubbles from sediment prior to sealing the test column.

In year two, gradient ratio testing was continued on stock geotextiles as well as on clean, non-fouled mats so as to establish baseline stability and clogging conditions to which results from similar tests on field weathered geotextile mats will ultimately be compared. Vertical upward flow through the sediment-mat interface was first planned for the testing process to provide consistency between the experimental conditions and the natural field conditions, but

hydraulic consolidation occurred due to the effective stress variation with time and a separation between the sediment and the geotextile eventually developed. Thus downward water flow was used for all subsequent tests. Due to the low permeability of the sediment in the test column, it was not possible to measure the flow rate of the entire system according to the ASTM-D 5101 standard. Instead, clogging potential was evaluated using the gradient ratio value only. This procedure will be repeated in year three using segments of the field-weathered small-scale test mats to determine whether biofouling increases the likelihood of clogging under similar hydraulic conditions compared to a clean mat.

The stock geotextiles used in the year two gradient ratio tests were the same three CETCO geotextiles (in terms of material, mass per area and AOS) used to construct the small-scale test mats (Table 6.3-1). These CETCO geotextiles were selected to cover a wide range of AOS and mass per area for practical applications as well as to mimic the arrangements being tested in the field, which is necessary to collect baseline data on the unweathered condition. An additional Typar 3801 geotextile was also planned for gradient ratio testing, but as of this report this material has not yet been evaluated.

In addition to geotextiles, complete reactive mats were also subject to gradient ratio testing for baseline clogging potential evaluation. The characteristics of the clean, non-fouled reactive mats used in these experiments are presented in Table 6.3-2. These representative mats contained various mixtures of the amendment materials that are being considered for the final reactive mat design.

Mass Per Area [kg/m^2]	Thickness [cm]	Reactive Material
4.0	~0.10	Organoclay
4.6	~0.10	Organoclay/Apatite
0.4	~0.10	Activated Carbon

Table 6.3-2. Characteristics of clean representative mats used in gradient ratio experiments.

6.3.3. Finite Element Analysis

The main goal of finite element analysis (FEA) is to understand the potential sediment deformation (consolidation) that will be caused by the weight of the reactive mat as well as the resulting pressure increase that will force porewater out of the underlying sediment, thus potentially altering natural seepage and contamination patterns. The use of FEA allows for an evaluation of 2D transport with regard to flow around the mat edges. A groundwater component is added to see how this edge flow affects advective transport.

Preliminary finite element models were constructed in year one with Plaxis (v. 8.0) software using a simulated symmetrical half-sand cap 5 m in length placed over sediment that was treated as an elastic-plastic material with no creep. This elastic-plastic (or Mohr-Coulomb) model is a simple representation of soil/sediment behavior as it is loaded in which the stress-strain behavior of the sediment is treated as reversible (elastic) until the stress from loading reaches the failure point, at which time the soil cannot support any further load and the deformation is permanent (plastic behavior). The “no creep” condition indicates that the sediment does not undergo any

time dependent deformation in this model. Once initial data was collected under this basic sand cap model, a more complex sediment model that was generated that considered both consolidation and secondary creep.

The simulated sand cap (protective layer) for the elastic-plastic model had a thickness of 30 cm (~1 ft). Because PLAXIS (v. 8.0) does not allow for changes in the permeability of geotextile elements, water was assumed to flow freely through the geotextile by the modeling software. To adjust for this deficiency and allow for the goal of evaluating varying permeability, a thin layer of low weight sand was placed over the geotextile in the model to serve as a tensile load. The permeability of this thin sand layer was then adjusted to in effect change the permeability of the geotextile.

In year two, various geotextile mat components were added to the finite element model runs to assess increasingly sophisticated scenarios. These geotextile inclusive models started with a hypothetical clean mat with the goal of investigating if and how flow patterns would be significantly affected by the level of clogging anticipated to occur under field conditions. In year three, true biofouling data obtained from the small-scale test mats will be used to modify the finite element models with actual permeability values. Specific parameters of the year two finite element analysis are discussed in the following sub-sections.

Geometry and Boundary Conditions. Geometry and boundary conditions were defined to constrain general field conditions and to promote applicability to different circumstances. Field information obtained on a similar cap test area on the Anacostia River in Washington D.C. was used to develop the typical geometry for the current model as shown in Figure 6.3-8.

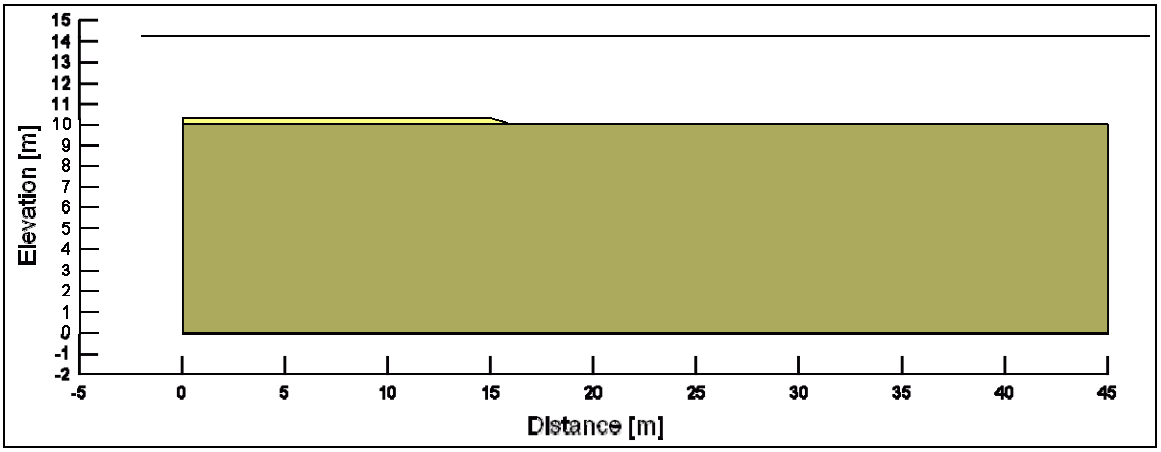

Figure 6.3-8. Geometry of a typical reactive mat application for finite element modeling.

This model was symmetric with respect to the vertical left axis. The sediment region was 45 m long by 10 m deep and the reactive mat was defined as an overlying layer of sandy material 15 m long by 0.3 m thick. The mat permeability was used to simulate its clogged state, while the unit weight was used to simulate the weight of the mat's protective layer. The depth of water was set at 4.21 m, which was equivalent to the average depth observed at the Anacostia River mats.

The boundary conditions for the model included the displacement (flux rate) conditions as shown in Figure 6.3-9. The displacement boundary conditions fix any displacement at the base and the horizontal displacement on both sides of the model. The flux boundary conditions control the pressure head at the top of the sediment-mat regions based on the water level (static or tide variation). Flux was prohibited on both vertical sides of the model. The average flux rate (3.3 cm/day) observed on one of the evaluation mats of the Anacostia River was used to produce the groundwater flow for this seepage analysis. Because all the boundary conditions can only coexist in a fully coupled analysis, they are not all required on each step of the uncoupled solutions.

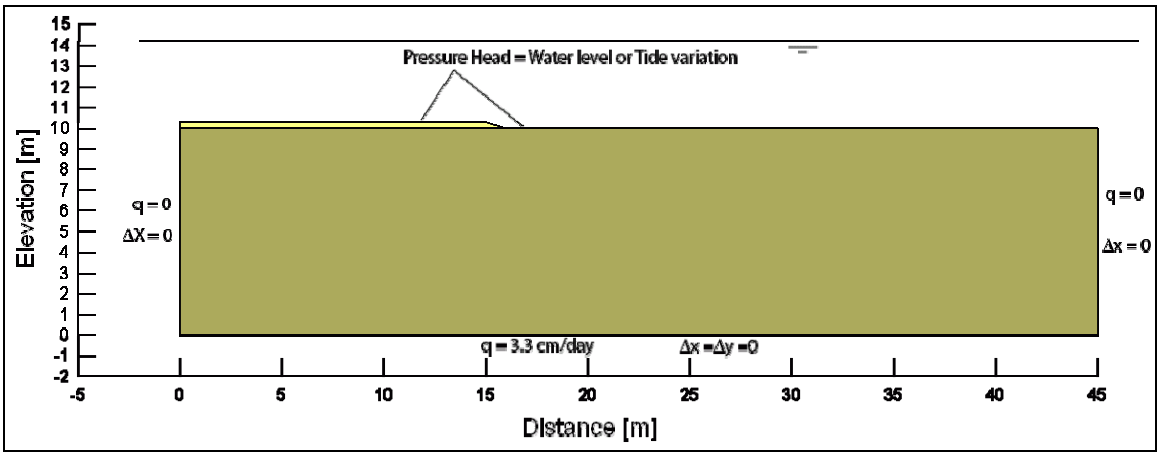

Figure 6.3-9. Summary of the boundary conditions for finite element modeling.

Geotechnical Parameters. The geotechnical properties of soft sediment will be determined mainly by the seepage and oedometer consolidation tests that are currently being developed for incorporation in further analyses. Until these results are available, reliable estimates of these parameters have been obtained and used for qualitative analyses. Table 6.3-3 shows a summary of the geotechnical property estimates.

Property	Sediment	Reactive Mat
Permeability, k [cm/s]	1.5×10^{-5}	1.0×10^{-3}
Initial void ratio, e	1.6	0.7
Unsaturated unit weight, γ_{unsat} [kN/m^3]	11	15
Saturated unit weight, γ_{sat} [kN/m^3]	14	17
Poisson's ratio, ν	0.3	0.25
Young's modulus at 1 m, E_{ref} [kN/m^2]	163.41	10000
Increment of E per meter depth [kN/m^2]	163.41	0

Table 6.3-3. Summary of average geotechnical property estimates for finite element modeling.

The Young's modulus had a constant value from the sediment surface to a depth of 1 m to avoid numerical complications due to small or zero stiffness values. The high Young's modulus of sand was used to avoid numerical complications at the sloped end of the mat. A linear elastic model based was used for a first approximation to the final configuration. Nonlinear constitutive

models will be used based on the results from the consolidation tests on soft sediment and additional test information.

Numerical solutions for the individual analysis of consolidation, seepage, and contaminant transport cases are available in the technical literature. Some finite element software includes these individual solutions but the fully coupled analysis is not available in the literature and is part of ongoing research. Consequently, the uncoupled solutions are employed in the current model since they have been proven to be useful in understanding the individual contributions to the overall final configuration. They can also produce computationally more efficient results similar to those obtained using the coupled solution. The following sub-sections present uncoupled and coupled solutions to the consolidation-seepage problem. The contaminant transport solution is not presented in this report.

Uncoupled Consolidation Model. The uncoupled consolidation model shows potential sediment deformation following mat placement independent of groundwater flow. This model was solved in two stages with the first stage computing the in-situ stress state of the sediment including the pore pressure distribution. The model assumed no steady state or transient groundwater flow and only the hydrostatic pressure was included. The geometry and boundary conditions of the model were the same as those shown in Figure 6.3-8 and Figure 6.3-9 above, but the flux rate at the base was $q = 0\ m^3/s$ to avoid groundwater flow through the sediment.

Consolidation time is the time required to dissipate the excess pore pressure induced by the weight of the mat. For practical purposes, 90-95% of the dissipation was defined as the end point of consolidation. A point was selected at mid-depth of the sediment layer to verify the excess pore pressure dissipation.

Uncoupled Seepage Model. The uncoupled seepage model shows potential changes in pore water properties and groundwater flow following mat placement independent of sediment consolidation. Two models were generated to assess post-mat groundwater seepage. The first model assumed the same permeability for the mat and the sediment. This scenario represented the case of an unclogged mat since the water drains freely from the sediment into the mat and out to the bay. The second model assumed a mat permeability one order of magnitude less than the sediment in order to simulate a clogged mat through which groundwater would not move freely.

Coupled Model. The coupled solution of the consolidation-seepage case is defined in three stages:

- Stage 1. Initial in-situ stress state without groundwater flow.
- Stage 2. Groundwater flow is applied by defining a flux rate at the base of the model and the total head at the sediment surface. A new initial stress state is achieved.
- Stage 3. Mat deployment and consolidation under groundwater flow conditions. Coupled solution.

The stages of the coupled modeling process are solved in sequence to simulate the real field conditions expected following mat deployment. No information is currently available from the consolidation tests to simulate the change of the sediment permeability during consolidation. Therefore, the time required to dissipate the excess pore pressure due to the mat deployment may be higher than the value estimated here. If a longer time is truly required to consolidate the sediment, that means that the lower permeability layer (filter cake) expected to develop beneath the mat will also take longer to develop. Again, a linear stress-strain relationship was used to simulate soil behavior. Field displacements are thus generally overestimated.

6.4. TASK 4: PROTOTYPE MAT TESTING

The purpose of the prototype mat testing task for this project is to field test a prototype mat system constructed of different arrangements of the most effective amendment (identified in Task 1) and the geotextile most resistant to fouling (identified in Task 3) in order to assess in-situ chemical sequestration effectiveness and flux properties. To accomplish this task, full-scale prototype mats will be constructed per proposed specifications and deployed at the most suitable target area within Cottonwood Bay as determined by the previous geophysical investigation (Task 2). The Task 4 effort is planned entirely for year three as mat fabrication cannot commence until results from the first small-scale geotextile test mat retrieval operation (scheduled for December 2007) are available. Construction and deployment of the full-scale mat system is currently scheduled for February-March 2008. Once they are actively soaking under field conditions, the full-scale mat arrangements will be monitored for contaminant adsorption and flux properties by passive sampling and groundwater seepage surveys.

Construction. For assembly of each full-scale prototype test mat arrangement, two 25 ft x 15 ft x 0.5 inch mat panels will be constructed of the non-woven geotextile (fabric) most resistant to fouling and the most adsorbent amendment material. These panels will be laid side-by-side with five feet of overlap to constitute each individual "mat" with a footprint of approximately 25 ft x 25 ft, which is the estimated minimum area required to alleviate "edge effects" such that groundwater will percolate through the mat rather than simply be displaced to the edges. The actual footprint of the deployed mats may vary slightly, however, depending on pilot site conditions. A diagram of the construction and layout for the full-scale mats is provided in Figure 6.4-1.

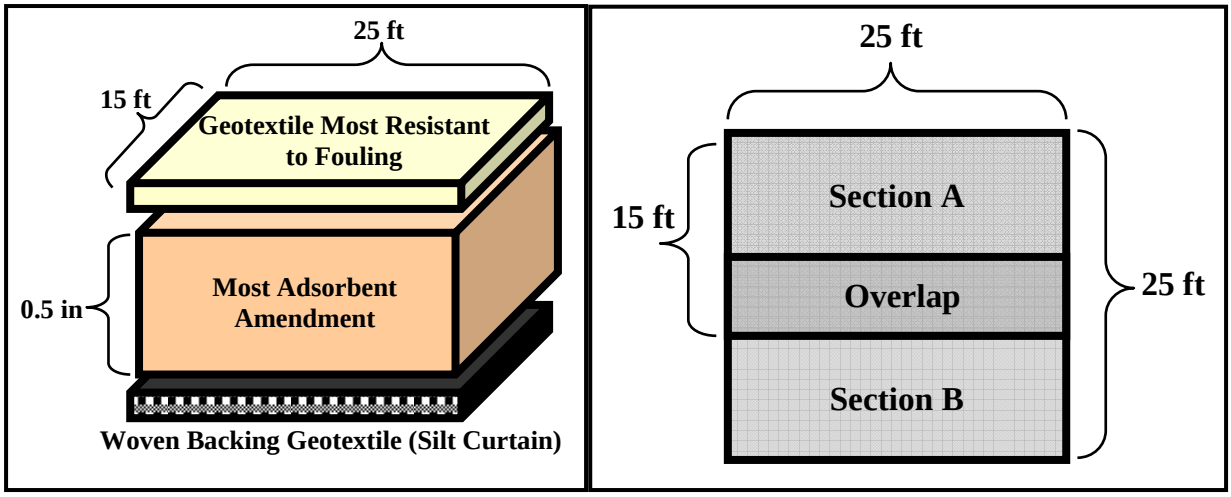

Figure 6.4-1. Construction and layout diagrams of full-scale geotextile test mats.

The overall mat system will include four test arrangements as well as a similar size area of untreated lake floor which will be monitored over the soak time and serve as a control for the test data. The various test arrangements will consist of a single layer geotextile, a double layer geotextile, a single layer geotextile with a sand cover and an area of sand cover only, all of which are shown in Figure 6.4-2. Where applicable, the sand cover will feature a three to six-inch layer of sand/silt mix (up to 28 yd^3) to provide a substrate for recolonization of the benthos while at the same time protecting the mat from bioturbation.

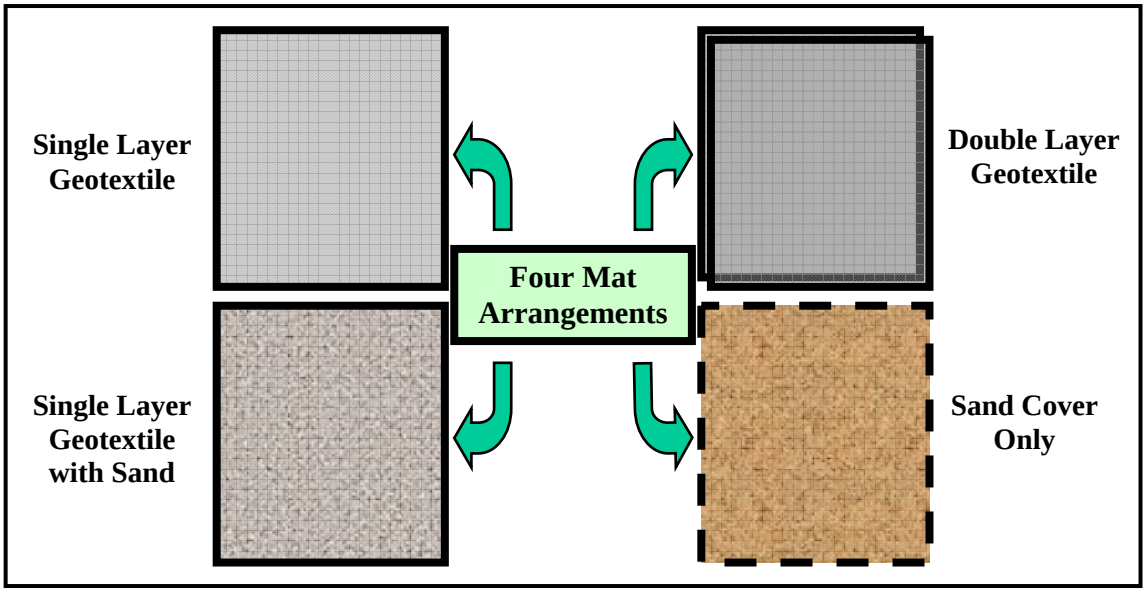

Figure 6.4-2. Various arrangements for full-scale prototype mat system testing.

Deployment. It is expected that full-scale test mats will be loaded onto a vessel from the Cottonwood Bay causeway using a crane or fork truck. The vessel will be fitted with a spindle or frame fixture that will allow pay-out of the geotextile material. Depending on the water depth of the target area, either divers or technicians in waders will bring the leading edge of each mat

to the bottom and secure it in place with ceramic bricks in a process similar to the small-scale mat deployment. The vessel will then pull away to pay out the rest of the material. Field personnel will monitor the final layout to ensure that all mats are resting evenly on the bottom. Due to the size of the various mat sections, additional sand bags, steel rods or screw-type anchors may be necessary to secure the mats in place. The different arrangements will be configured with sufficient space between them to reduce any possible interference. Sand will be spread over designated areas by washing it over the side of the vessel with a large volume hose drawing site water so as to provide a gradual deposition of cover material rather than a potentially damaging mass as would be expected from a clamshell bucket.

As-Built Confirmation. Following deployment, either divers or technicians in waders will visually inspect the various mat arrangements to ensure that they have been properly secured as well as to inspect the sand layers where appropriate to ensure adequate coverage has been achieved. They will install settlement rods into the mat to serve as a vertical control against which to make follow-up measures of changes in mat elevation or potential burial. In addition, a one-day acoustic (bathymetry, sub-bottom profile, side-scan sonar) survey of the cap will be done shortly after placement to look for localized cap failure and to evaluate the overall quality of cap deployment. The side-scan images will help confirm that the cap is resting flat on the bottom. Sub-bottom profiles will help confirm that the cap is in contact with the bottom, and that any voids between the cap and substrate are minimal.

Monitoring. Five months after deployment, after the mat has had sufficient time to "settle" on the bottom, field personnel will return to install two types of in-situ passive diffusion samplers to measure sequestration of contaminants by each mat arrangement. By installing such devices above and below the mat (as accessed at center seams), the effectiveness of the mat in sequestering metal and organic contaminants in the substrate can be evaluated. Passive sampling devices will include both pore water expression samplers ("peepers") and semi-permeable membrane devices (SPMDs). Personnel will also inspect the mat for stability, including any slumping affects due to wave and current action, as well as benthic colonization. Mat heights will also be measured relative to the settlement rods. This initial monitoring effort will coincide with the one-year retrieval of the second row of small-scale test mats.

After one year of soak time for the full-scale mat system, groundwater seepage measurements will be made to quantify water flux through the mats from underlying sediments as well as to identify any changes in contaminant concentration with respect to source (*e.g.*, groundwater flux out of the mat versus overlying water penetration into the mat). Field personnel will also collect samples of the mats as well as both underlying and overlying sediment layers (either naturally deposited or engineered sand cover) for chemical analysis. Analytical results will provide information on metals and organics speciation between the substrate and the mat, thus identifying any enhanced ability of the mat to preferentially bind certain classes of contaminants.

7. RESULTS AND ACCOMPLISHMENTS

This section provides an explanation of how objectives for SERDP Project Number ER-1493 have been met to date by documenting the technical progress and accomplishments in relation to specific tasks for year two. Specific figures and tables are provided that highlight the data obtained for each task.

7.1. TASK 1: COMPOSITE MATERIAL TESTING

The purpose of Task 1 is to identify the mixture of amendment materials that would most effectively sequester contaminants as part of a reactive mat. To accomplish this task, UNH conducted laboratory tests in year two to characterize activated carbon and three different types of organoclays in terms of adsorption and desorption of PCBs in the presence of humic acid. Additional experiments were also conducted to assess the combined effects of humic acid, fulvic acid and NOM on adsorption properties of these materials. Results of these experiments with regard to kinetics, isotherms and statistical analyses are discussed in the following sections.

7.1.1. Characterization of Activated Carbon

Kinetic Studies. Kinetic experiments were conducted to obtain the equilibration time required for adsorption of various PCBs by activated carbon. Figure 7.1-1 shows the kinetics of 2-chlorobiphenyl, 2, 2',5,5'-tetrachlorobiphenyl and 2,2',4,4',5,5'-hexachlorobiphenyl adsorption on both bare activated carbon and activated carbon preloaded with humic acid.

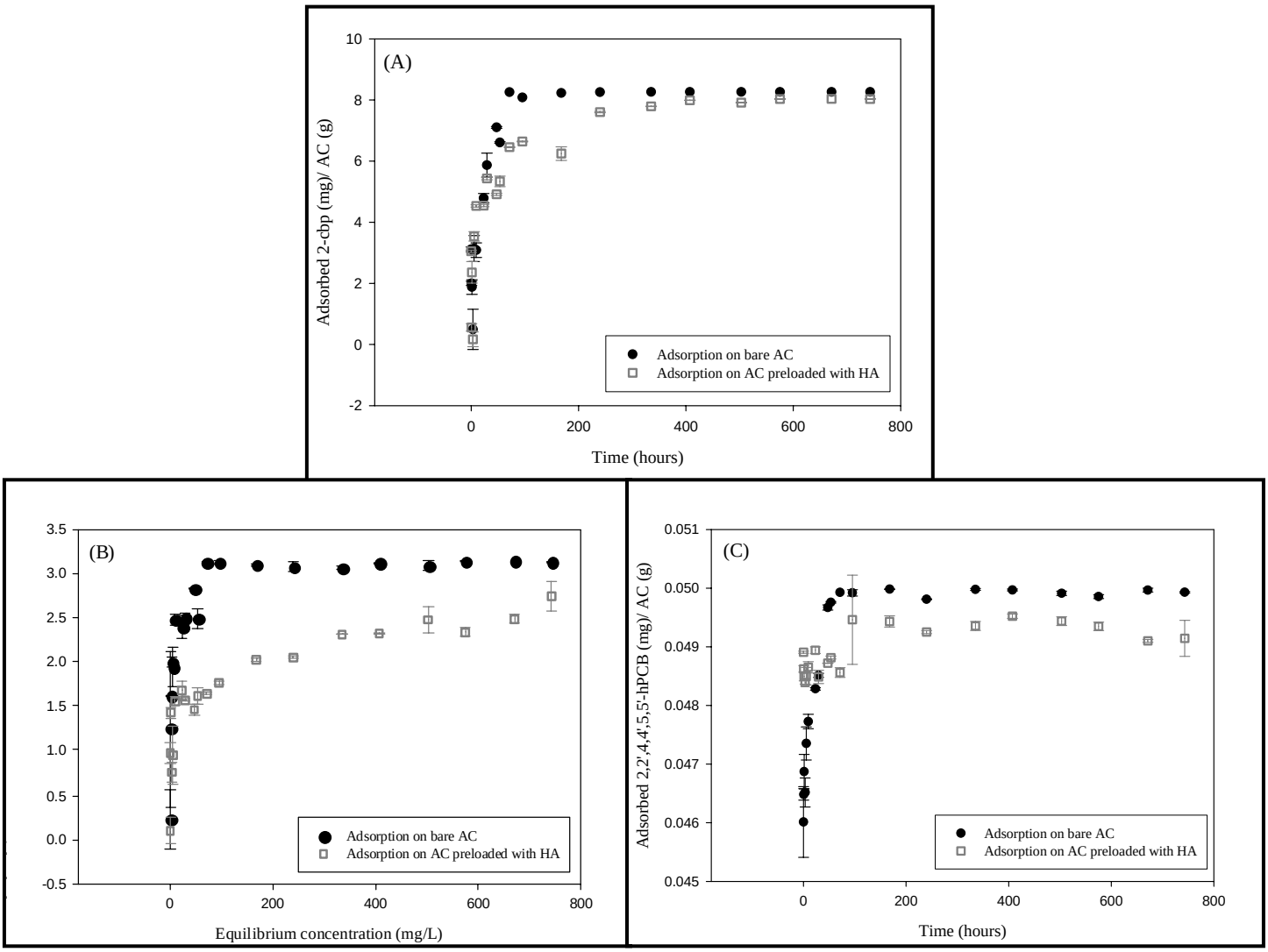

Figure 7.1-1. Kinetics of adsorption of different PCB congeners on coconut shell activated carbon in the presence and absence of humic acid: (A) 2-chlorobiphenyl, (B) 2,2',5,5'-tetrachlorobiphenyl and (C) 2,2',4,4',5,5'-hexachlorobiphenyl.

The kinetics of 2-chlorobiphenyl (A) indicated that adsorption equilibrium was reached at approximately 72 hours on bare activated carbon. Preloading the activated carbon with humic acid appeared to increase the equilibrium time. Because smaller molecular weight compounds like 2-chlorobiphenyl have higher diffusivity as reported by Schaffner *et al*. (1997), they could gradually enter the micropores which sieve the larger humic acid molecules and thereby will be less impacted by preloading as compared to the higher weight chlorinated compounds.

Adsorption equilibrium was reached at approximately 72 hours for 2,2',5,5'-tetrachlorobiphenyl (B) and 50 hours for 2,2',4,4',5,5'-hexachlorobiphenyl (C) on both bare activated carbon and activated carbon preloaded with humic acid. Unlike 2-chlorobiphenyl, the preloading effect for both of these congeners remained significant for the complete duration of experiment due to the pore blockage effect and increased complexation of highly chlorinated congeners to humic acid

as compared to the mono-chlorinated congener. Greater complexation with humic acid is expected from more highly chlorinated congeners as shown by K_{DOC} complexation constants reported in Table 7.1-1 below. The complex formation of humic acid with halogenated organic compounds (HOCs) increases with the increase in hydrophobicity of the compound as shown by these K_{DOC} values (Pirbazari *et al*. 1989).

PCB congener	† Solubility Limit in water (ppm)	† Log K_{OW}	Log K_{DOC}	Isotherm Studies Concentration Range (mg/L)
2-cbp	4.0	4.7	3.63*	0.008 – 6.108
2,2',5,5'- tPCB	0.26	5.9	4.6 **	0.008 – 0.400
3,3',4,4'- tPCB	0.26	5.9	-	0.008 – 0.800
2,2',4,4',5,5'- hPCB	0.038	6.7	5.3**	0.032 – 0.800
3,3',4,4',5,5'- hPCB	0.038	6.7	-	0.024 – 0.800

Table 7.1-1. Solubility limit, log octanol-water partition coefficients and log K_{DOC} values for selected PCB congeners.

Kinetic studies were important to characterize activated carbon not only for subsequent equilibrium isotherm experiments but also for assessing the potential effectiveness of a thin reactive mat. Previous studies conducted at the Anacostia River for demonstration of specific discharge and tidal heights using the UltraSeep technology showed that the average specific discharge rate of sediment pore water to the overlying water column was 5 cm/day (Trident and UltraSeep 2006). This flow rate underscores the significance of understanding adsorption equilibration times, as contaminant residence time in a thin layer reactive mat may be significantly less than 24 hours.

Isotherm Studies. Isotherm studies were conducted to determine the adsorption capacity of activated carbon in the presence and absence of humic acid. Various PCB congeners were selected as the target contaminants for this study to obtain sorption data on a range of chlorination degree and co-planarity. The Freundlich model was used to obtain the isotherms for these studies by applying the following equation:

$$q_e = K_F \ (C_e{}^{(1/n)})$$

where q_e is the amount of adsorbed (mg/g), K_F is the Freundlich isotherm constant, C_e is the equilibrium concentration (mg/L) and $1/n$ is the dimensionless Freundlich exponent.

Figure 7.1-2 shows Freundlich adsorption isotherms for five PCB congeners in the presence and absence of humic acid. The humic acid interferences were obtained as: (i) the preloading effect of humic acid on activated carbon and (ii) the desorption effect in which activated carbon was spiked with humic acid after PCB adsorption to simulate the long term exposure to pore water humic acid concentrations. In a system where activated carbon and humic acid are present, the sorption of PCBs can occur either by adsorption on activated carbon surface or by complexation with adsorbed humic acid.

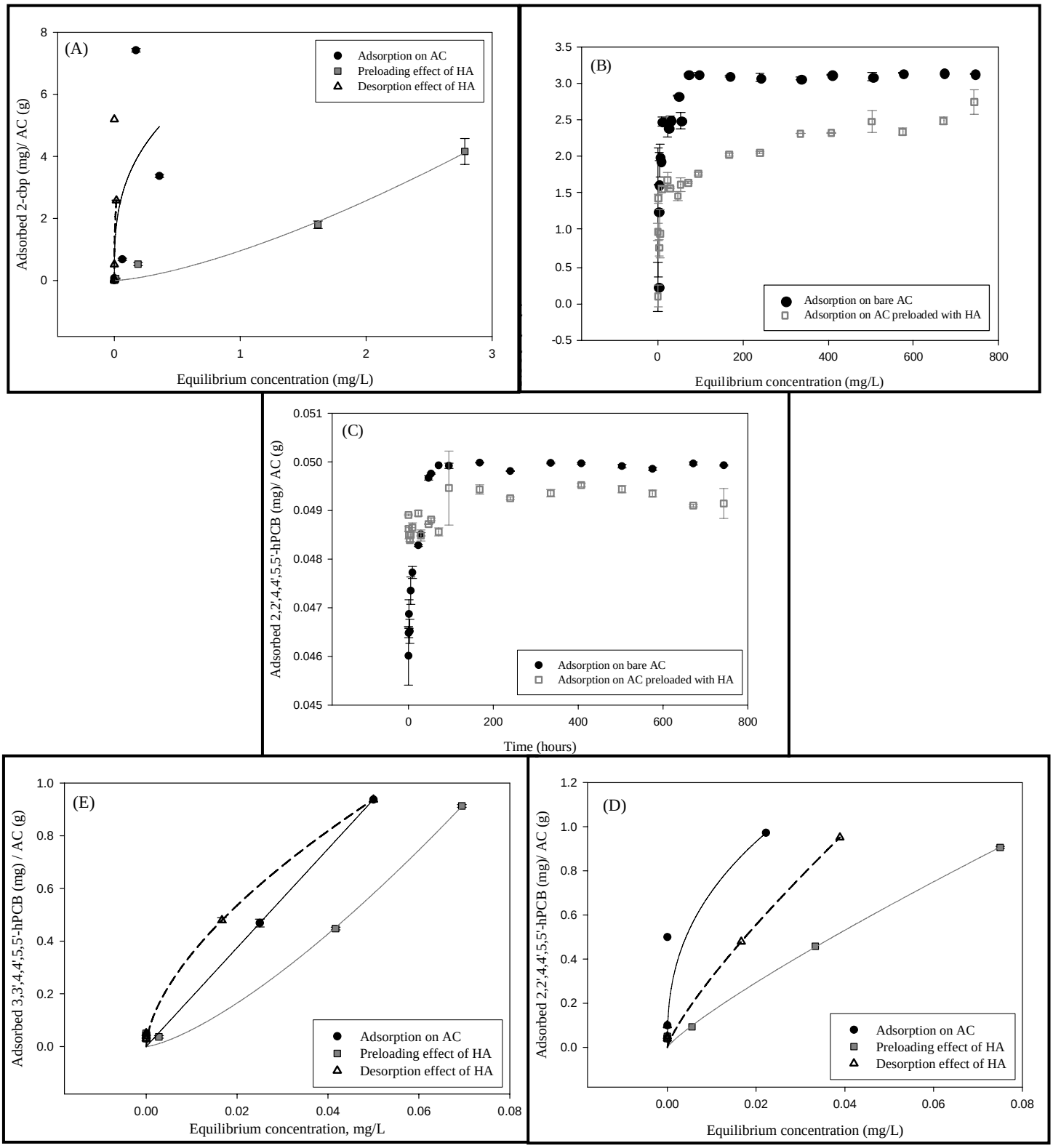

Figure 7.1-2. Freundlich adsorption isotherms for PCBs on bare activated carbon including preloading and desorption effects of humic acid: (A) 2-cbp, (B) 2,2',5,5'-tPCB (C) 3,3',4,4'-tPCB (D) 2,2',4,4',5,5'-hPCB and (E) 3,3',4,4',5,5'-hPCB.

In all of these isotherms, a significant reduction in the adsorption capacity of activated carbon was found in the presence of humic acid. This reduction may be caused by the pore blockage effect resulting from the preloading of activated carbon with humic acid molecules prior to the entry of HOCs into the pores (Pignatello *et al*. 2006 and Li *et al*. 2003) and the hydrophobic partitioning of HOCs to dissolved humic acid (Poerschmann *et al*.). When activated carbon is preloaded with humic acid, the larger humic acid molecules that cannot enter the micropores and mesopores block the pore channels by clump formations (Pignatello *et al*. 2006). These types of formations were observable in scanning electron micrograph images of bare coconut shell activated carbon compared to activated carbon preloaded with 1 g/L of humic acid for a period of 48 hours as shown in Figure 7.1-3.

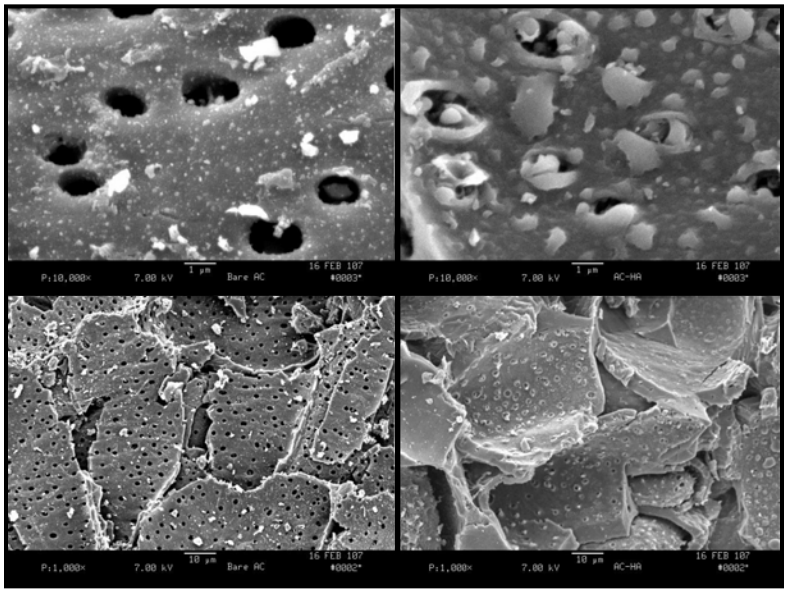

Figure 7.1-3. Scanning electron micrograph image of bare coconut shell activated carbon (upper and lower left) and activated carbon preloaded with humic acid (upper and lower right).

The performance of coconut shell based activated carbon, which has a distinctly different pore structure, was compared with coal based activated carbon for 2,2',5,5'-tetrachlorobiphenyl and the adsorption capacity of coconut shell activated carbon was approximately twice as high as that of coal based activated carbon. However, when both carbon types were preloaded with humic acid, their performance was similar as shown in Figure 7.1-4 below. The difference in the performance of bare coconut shell activated carbon and bare coal based activated carbon can be attributed to the less porous structure of coal based activated carbon which can be seen in the comparative scanning electron micrograph images (Figure 7.1-3).

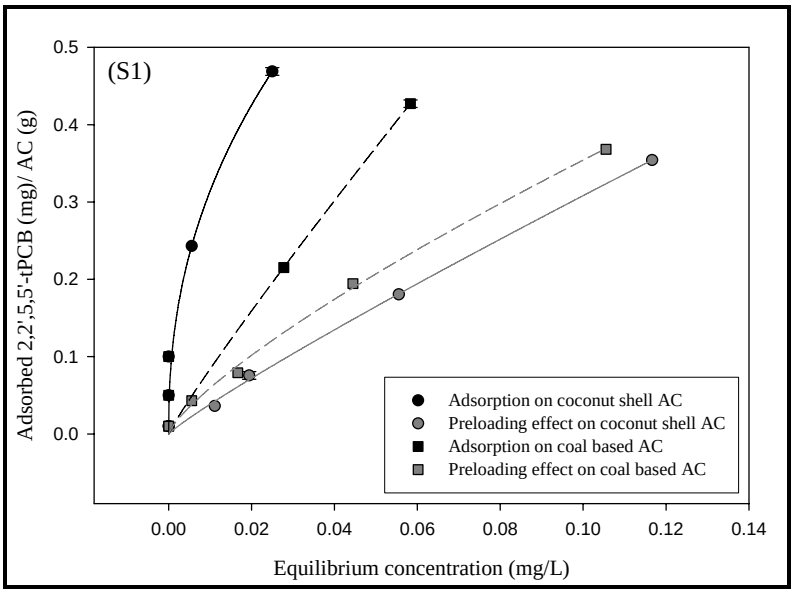

Figure 7.1-4. Comparative adsorption isotherms for coal based and coconut shell based activated carbon for 2,2',5,5'-tetrachlorobiphenyl.

Experiments were conducted to determine the effect of humic acid on the adsorption capacity of activated carbon at different loadings of humic acid and fixed loading of PCBs. The results for all three congeners (mono-chloro, tetra-chloro- and hexa-chloro) showed that the adsorption capacity of activated carbon decreased with the increase in humic acid concentration as shown in Figure 7.1-5 below. These effects were found to be least in case of hexa-chlorobiphenyl followed by mono-chlorobiphenyl and then tetra-chlorobiphenyl. The experiment conducted to measure the effect of humic acid loadings on coal based activated carbon also showed reduction in adsorption capacity of coal based activated carbon with the increase in humic acid loadings (Figure 7.1-6).

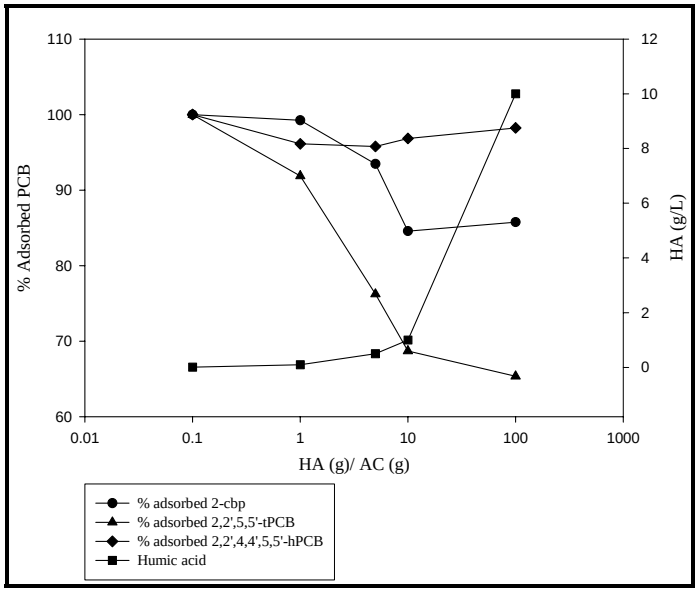

Figure 7.1-5. Effect of different loadings of humic acid on 2-chlorobiphenyl, 2,2',5,5'-tPCB and 2,2',4,4',5,5'-hPCB.

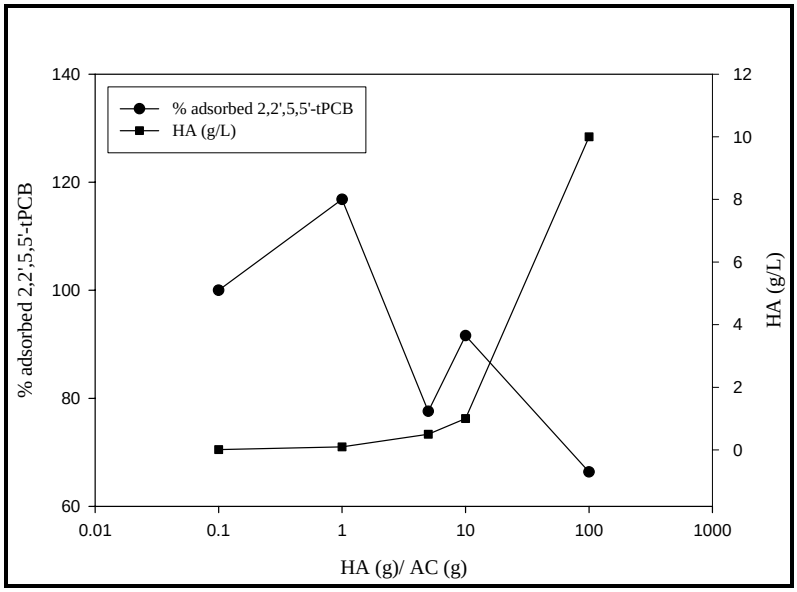

Figure 7.1-6. Effect of different loadings of humic acid on coal based activated carbon.

Desorption Studies. The studies conducted to evaluate the desorption effects of humic acid showed that once PCBs were adsorbed on activated carbon the desorption effect varied with the co-planarity of the congener. Desorption was found to be more pronounced among non-coplanar PCB congeners (Figure 7.1-2B,D) as compared to the mono-chlorinated congener (Figure 7.1-2A) and the co-planar tetra- and hexa-congeners (Figure 7.1-2C,E), all of which did not show any significant desorption. This variation in desorption effects between co-planar and non-coplanar PCBs can be explained by the steric hindrances in the non-coplanar configuration which decrease sorption affinity (Cornelissen *et al*. 2004).

Statistical Analysis. Statistical analysis of activated carbon adsorption data was performed using SAS JMP® (v. 5.1) software. Two models were developed on the fit model platform to evaluate the performance of activated carbon (for tetra- and hexa-chlorobiphenyl) and to compare the performance of both types of activated carbon (coconut shell and coal based).

Model 1 was developed based on the hypothesis that performance of coconut shell-based activated carbon varies both with the degree of chlorination of the congener and the co-planarity of the congener. The three factors considered in this model were: (i) the PCB congener itself, (ii) loading rate and (iii) adsorption density on activated carbon (preloading/desorption effects). The full factorial design was developed with these three factors along with the quadratic term of loading rate. According to analysis of variance (ANOVA) the p-value was < 0.0001, thus indicating the hypothesis of model 1 cannot be rejected: There is a significant effect of the number of chlorine atoms and co-planarity of congeners on adsorption capacity of coconut shell activated carbon. In the Effect test, an F-test was performed on each term (main effects and interaction terms) of the model to determine the significance of the factors based on the p-value < 0.05. The Prediction profiler was used to develop interaction profiles which demonstrated significant interactions among all the factors (PCB congeners, loading rate and treatment). The Student's t value was obtained to compare the adsorption affinities of all PCB congeners at $\alpha = 0.05$ which showed higher adsorption for hexa-chlorobiphenyls as compared to tetra-chlorobiphenyls as outlined in Table 7.1-2. The least square means of all PCB congeners were plotted against the treatment effects (preloading/desorption effect) and it was found that the desorption effect was not significant in the case of co-planar (tetra- and hexa- congeners) and both hexa-chloro-congeners. The preloading effect was found to be less significant in the case of hexa-chloro-congeners compared to tetra-chloro-congeners as shown in Figure 7.1-7.

Alpha = 0.050; t = 2.0639			
PCB congener	**Levels ***		**Least Square Mean**
2,2',4,4',5,5'- hPCB	A		0.2934
3,3',4,4', 5, 5'- tPCB	B		0.2837
3,3',4,4'- hPCB		C	0.2671
2,2',5,5'-tPCB		C	0.2654
* Levels not connected by same letter are significantly different			

Table 7.1-2. Model 1 – Least square mean differenced Student's t statistics for the adsorption of different PCB congeners on coconut shell based activated carbon.

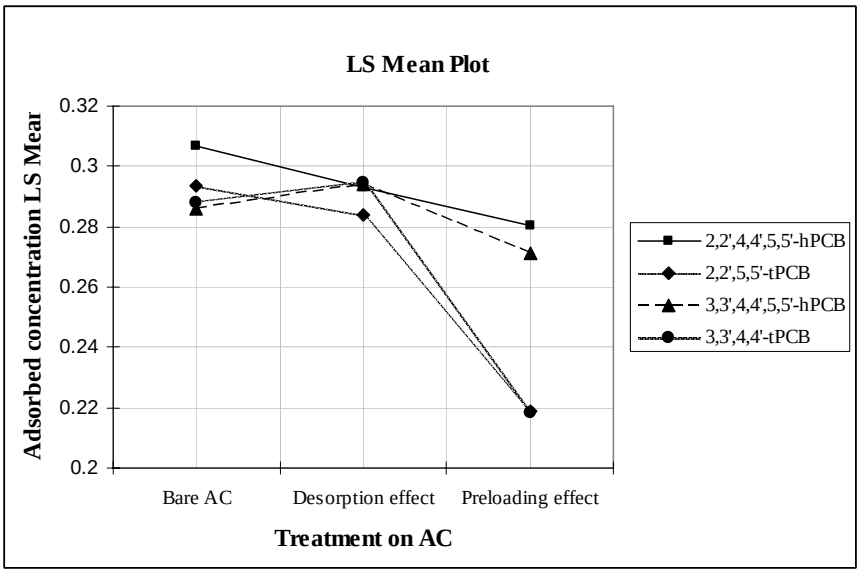

Figure 7.1-7. Least square mean plot to determine the effects of different humic acid treatments on adsorption of various PCB congeners by activated carbon.

Model 2 was developed based on the hypothesis that the performance of coconut shell based activated carbon is better than that of coal based activated carbon for 2,2',5,5'-tetrachlorobiphenyl. In this model the three factors that were taken into consideration included type of activated carbon, treatment on activated carbon and loading rate of this congener. The full factorial design was developed with all three factors considered and the quadratic term for loading rate. According to ANOVA the p-value obtained was < 0.0001, thus indicating that the hypothesis of model 2 can also not be rejected. The Student's t values obtained at $\alpha = 0.05$ to determine the effects of humic acid on performance of both type of carbons showed that the preloading effect was significant for both types, the desorption effect was less pronounced and similar for both types and the performance of coconut shell activated carbon was better than that of coal based activated carbon in the absence of humic acid as outlined in Table 7.1-3.

Alpha = 0.050; t = 2.14479						
Treatment on Activated Carbon	**Levels***					**Least Square Mean**
Bare Coconut shell AC	A					0.178
Coconut shell AC: Desorption effect		B				0.172
Coal based AC: Desorption effect		B	C			0.168
Bare Coal based AC			C			0.164
Coal based AC: Preloading effect				D		0.143
Coconut shell AC: Preloading effect					E	0.135
* Levels not connected by same letter are significantly different						

Table 7.1-3. Model 2 – Least square mean differenced Student's t statistics for the adsorption of 2,2',5,5'-tPCB on different types of activated carbon.

Evaluation of Isotherm Coefficients. The main goal of the composite material testing task is to understand the design parameters for a potential reactive mat that considers the interference and complexation with natural organic acids. In order to compare materials and the sorption affinity for different congeners, adsorption coefficients (K_d) were estimated using a linear fit for all the isotherms shown in the previous figures. These coefficients are presented in Table 7.1-4.

	Adsorption coefficients		**Freundlich Isotherm Constants**			
	Kd values		**K_f**		**1/n**	
Coconut Shell AC	**Adsorption on Bare AC**	**Preloading Effect**	**Adsorption on Bare AC**	**Preloading Effect**	**Adsorption on Bare AC**	**Preloading Effect**
2-cbp	12.625	1.3862	7.002	0.958	0.336	1.425
2,2',5,5'-tPCB	16.501	2.963	2.347	2.469	0.437	0.9038
3,3',4,4'-tPCB	10.485	3.9139	6.575	11.711	0.795	1.558
2,2',4,4',5,5'-hPCB	35.988	11.626	4.442	8.267	0.399	0.853
3,3',4,4',5,5'-hPCB	18.197	12.216	18.750	35.595	1.000	1.374
Coal based AC						
2,2',5,5'-tPCB	6.344	3.352	5.888	2.108	0.923	0.775

Table 7.1-4. Adsorption coefficients and Freundlich isotherm constants obtained for select PCB congeners with different types of activated carbon.

In this study the preloading effect was found to be most significant for 2-chlorobiphenyl with non-coplanar 2, 2',5,5'-tetrachlorobiphenyl with 89% and 82% reductions in adsorption capacity, respectively. The effect was less dominant in the case of co-planar 3,3',4,4'-tetrachlorobiphenyl and non-coplanar 2, 2',4,4',5,5'-hexachlorobiphenyl with 63% and 68% reductions in adsorption capacity, respectively. Effects were least prevalent for co-planar 3,3',4,4',5,5'-hexachlorobiphenyl with only a 33% reduction in adsorption capacity. The measure of non-linearity for isotherms was estimated using the Freundlich isotherm coefficient (1/n). The trend was found to be favorable with $1/n < 1$ for all bare activated carbon isotherms and non-coplanar congeners with preloaded humic acid but in the case of co-planar congeners and 2-chlorobiphenyl with preloading, the value of (1/n) was greater than unity (1) and the trend of the isotherm was unfavorable (Figure 7.1-2).

Summary. The overall characterization of activated carbon showed that adsorption capacity for higher chlorinated congeners was higher than that of lower chlorinated congeners and stronger (with no desorption effect) for higher chlorinated and co-planar congeners than lower chlorinated and non-coplanar congeners. Adsorption affinity and capacity can be significantly affected by the presence of humic acid (preloading effect) which is a factor that should be included in the final design and performance of potential reactive mats under typical site conditions.

7.1.2. Characterization of Organoclays

Kinetic Studies. Kinetic experiments were conducted to obtain the equilibration time required for adsorption of 2-chlorobiphenyl on CETCO organoclay containing bentonite and Polymer Ventures organoclay containing attapulgite in the presence and absence of humic acid. The adsorption kinetic curves for these two different types of organoclay are shown in Figure 7.1-8 below.

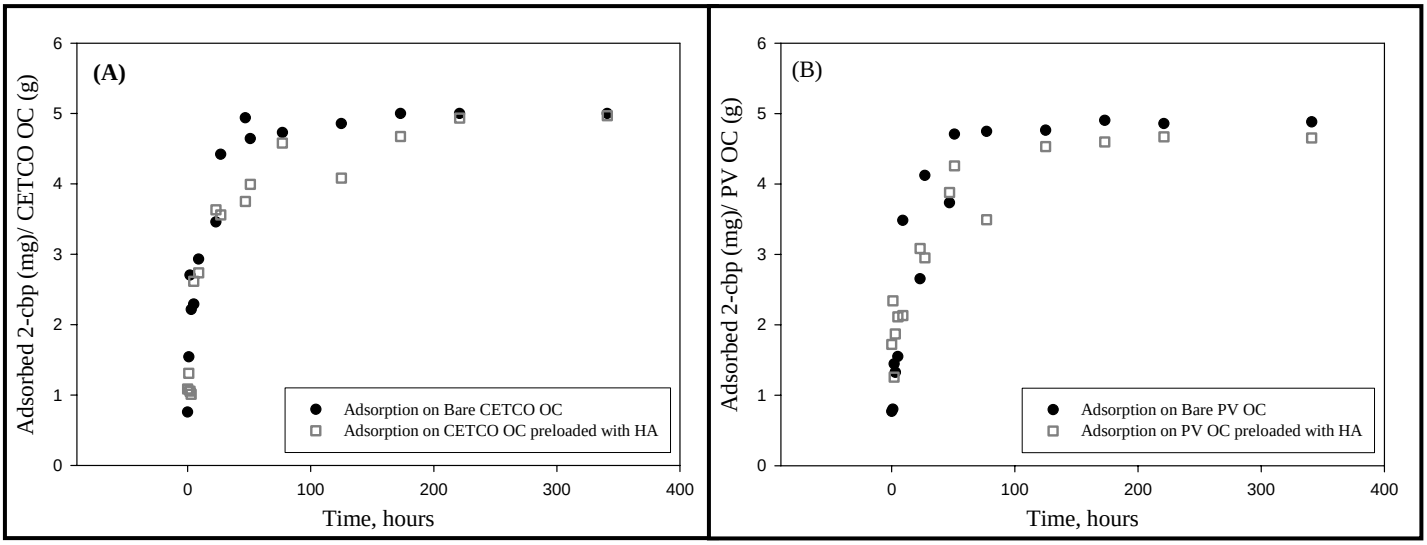

Figure 7.1-8. Kinetics of adsorption of 2-chlorobiphenyl on two different types of organoclay: (A) CETCO organoclay containing bentonite and (B) Polymer Ventures organoclay containing attapulgite.

Isotherm Studies. Isotherm studies were conducted to determine the adsorption capacity of various PCB congeners (2-chlorobiphenyl, 2,2',5,5'-tPCB, 3,3',4,4'-tPCB, 2,2',4,4',5,5'-hPCB, 3,3',4,4',5,5'-hPCB) on three different organoclays (CETCO, Polymer Ventures, Biomin, Inc.) in the presence and absence of humic acid as well as to evaluate the desorption effects caused by prolonged exposure to humic acid following initial adsorption on these organoclay types. Figure 7.1-9 shows Langmuir isotherms for adsorption of five PCB congeners on bare CETCO organoclay along with the preloading and desorption effects of humic acid. Figure 7.1-10 shows Langmuir isotherms for adsorption of two PCB congeners on bare Polymer Ventures organoclay along with the preloading and desorption effects of humic acid. Figure 7.1-11 shows Langmuir isotherms for the adsorption of 2-chlorobiphenyl on bare Biomin, Inc. organoclay along with the preloading and desorption effects of humic acid. Isotherm curves for all five PCB congeners are not available for the Polymer Ventures and Biomin, Inc. organoclays because composite material testing has not been completed in year two and will continue in year three.

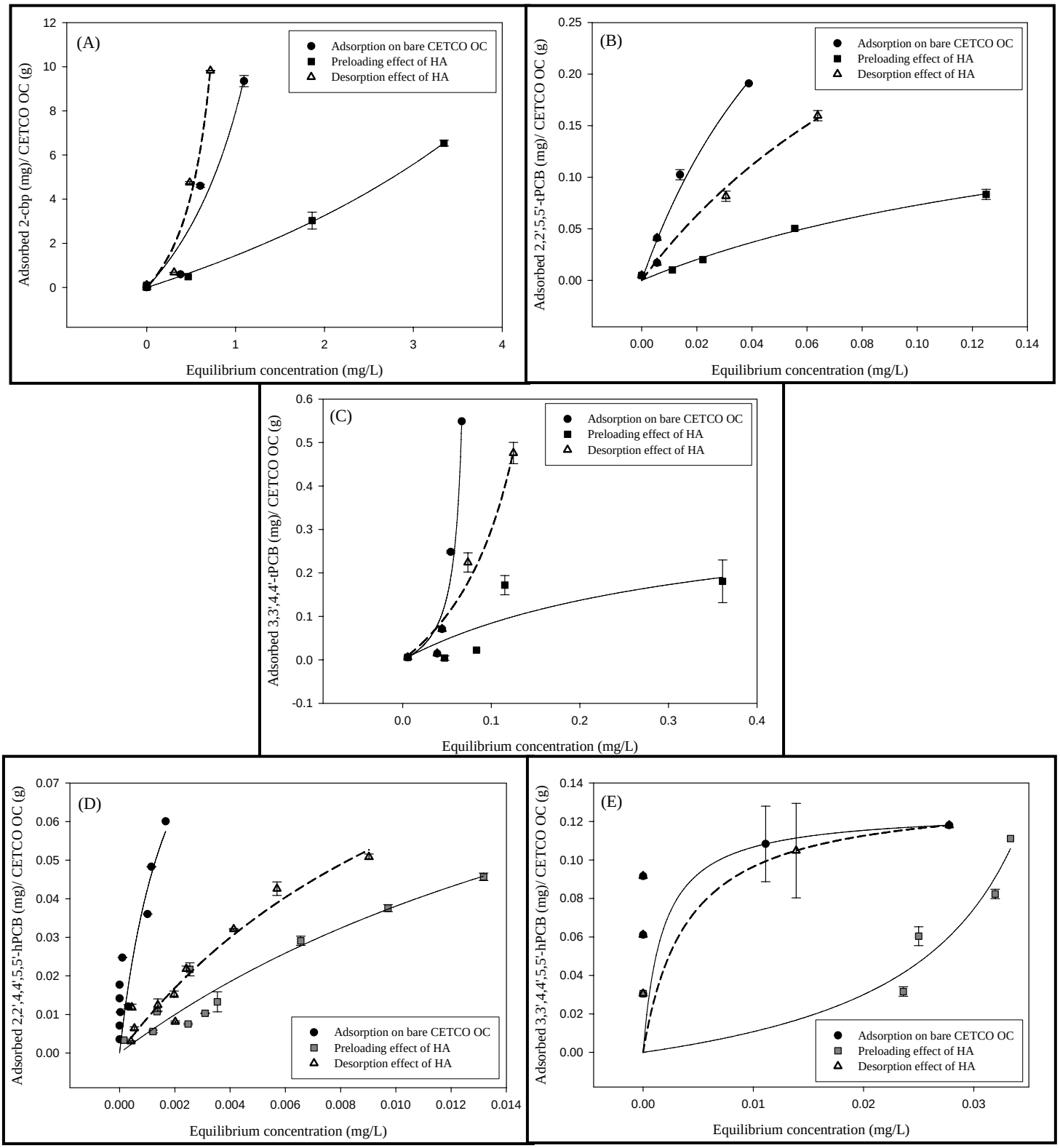

Figure 7.1-9. Langmuir adsorption isotherms for five PCBs on bare CETCO organoclay with preloading and desorption effects of humic acid: (A) 2-cbp, (B) 2,2',5,5'-tPCB, (C) 3,3',4,4'-tPCB, (D) 2,2',4,4',5,5'-hPCB and (E) 3,3',4,4',5,5'-hPCB.

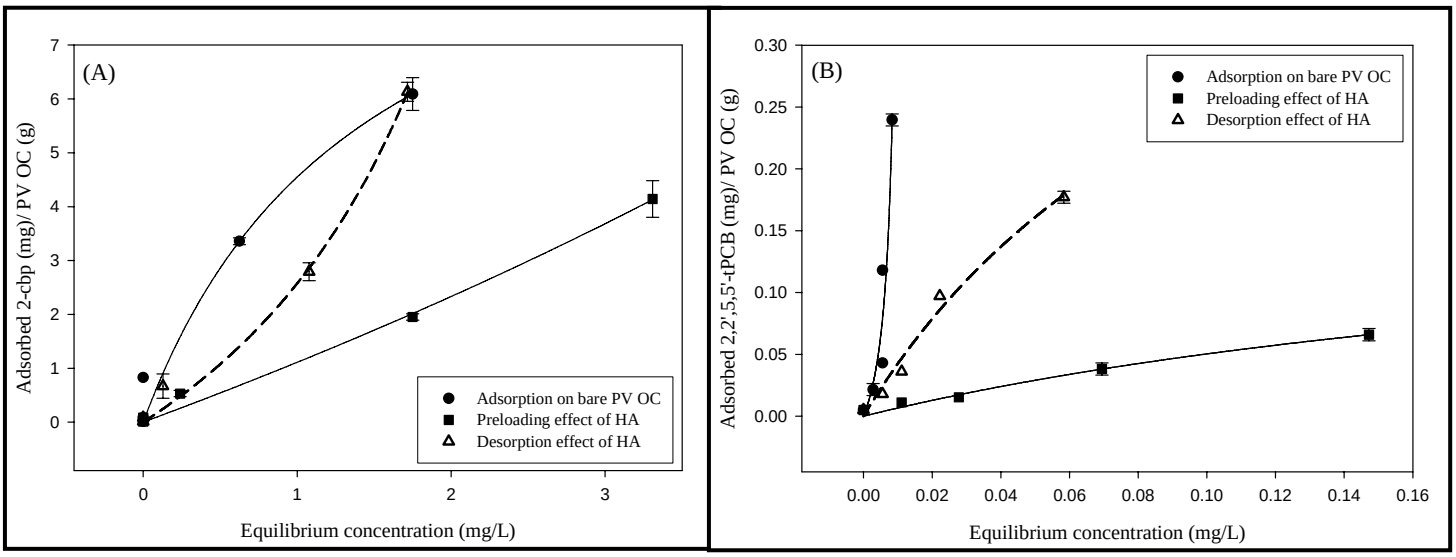

Figure 7.1-10. Langmuir isotherms for adsorption of two selected PCB congeners on bare Polymer Ventures organoclay with preloading and desorption effects of humic acid: (A) 2-chlorobiphenyl and (B) 2,2',5,5'-tPCB.

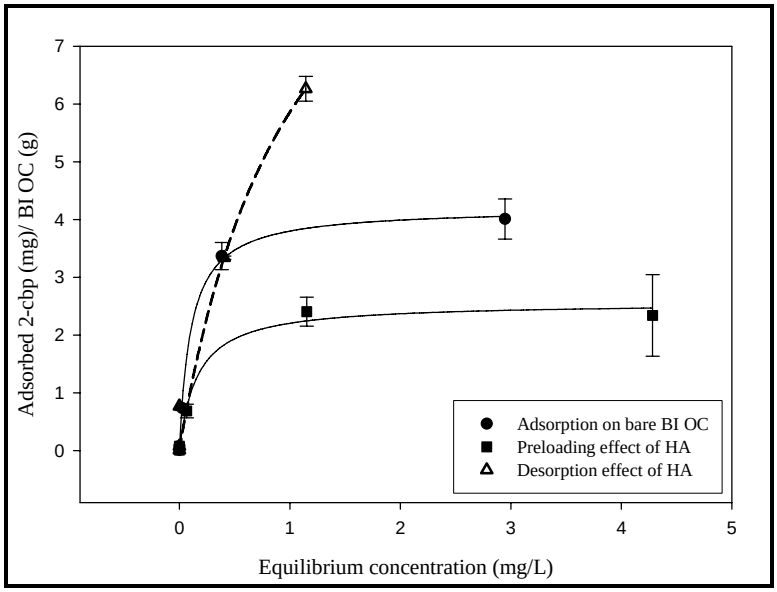

Figure 7.1-11. Langmuir Isotherms for adsorption of 2-chlorobiphenyl on bare Biomin, Inc. organoclay with preloading and desorption effects of humic acid.

***Statistical Analysis*.** Statistical analysis of adsorption data for the three different organoclays was also performed using SAS JMP® (v. 5.1) software. Because the adsorption experiments on the different organoclay amendments were conducted at different loading rates for each of the different contaminant congeners, a least squares fit analysis was done on the results of each experiment as a function of loading rate with the mean of the fit data being used to characterize the response of that amendment to that particular contaminant. This process was repeated for adsorption, desorption and preloading. As shown below, the responses of the three different organoclays were be plotted versus adsorption, desorption and preloading for each contaminant.

Each point on these figures represents the average behavior of that organoclay with respect to loading rate.

Least square mean plots to determine the effects of different humic acid treatments (bare, desorption, preloading) on the adsorption of various PCB congeners by CETCO organoclay are shown in Figure 7.1-12. Least square mean plots to determine the effects of different humic acid treatments on the adsorption of 2-chlorobiphenyl by the three different types of organoclay (CETCO, Polymer Ventures, Biomin, Inc.) are shown in Figure 7.1-13. Finally, least square mean plots to determine the effects of different humic acid treatments on the adsorption of 2,2',5,5'-tetrachlorobiphenyl by two different types of organoclay (CETCO and Polymer Ventures) containing different base clay material (bentonite and attapulgite, respectively) are shown in Figure 7.1-14.

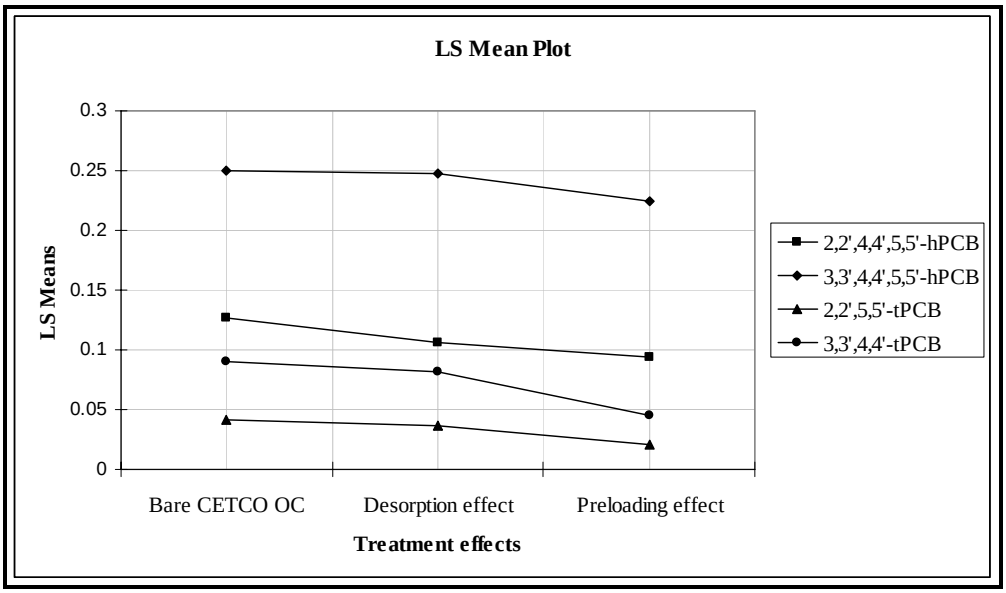

Figure 7.1-12. Least square mean plot to determine the effects of different humic acid treatments on the performance of CETCO organoclay in sequestering tetra- and hexa-chlorobiphenyls.

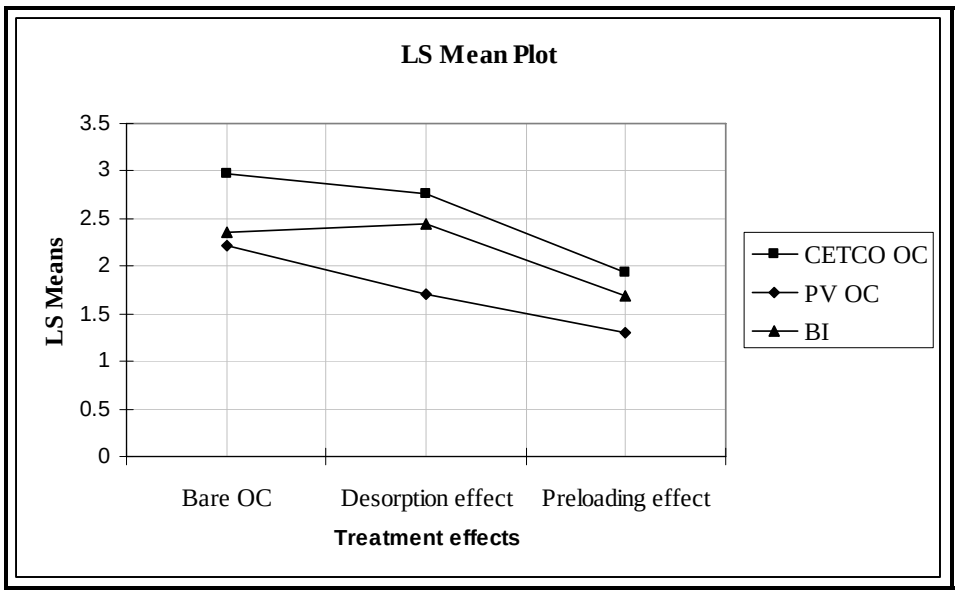

Figure 7.1-13. Least square mean plot to compare the effects of different humic acid treatments on the performance of three different organoclays in sequestering 2-chlorobiphenyl.

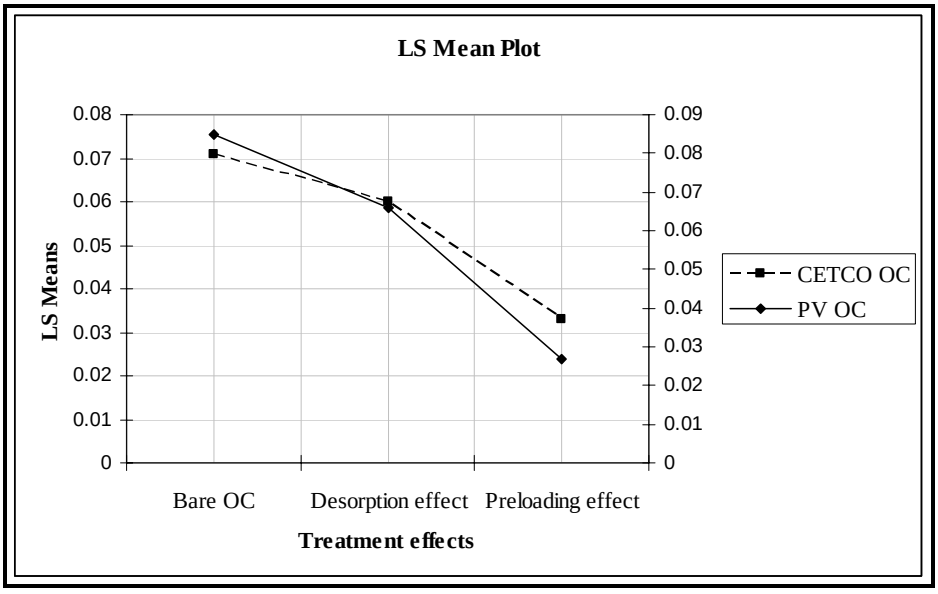

Figure 7.1-14. Least square mean plot to compare the effects of different humic acid treatments on the performance of two organoclays with different base clay materials in sequestering 2,2',5,5'-tetrachlorobiphenyl.

Evaluation of Isotherm Coefficients. In order to compare different organoclays in terms of their sorption affinities for different PCB congeners, adsorption coefficients (K_d) were estimated using a linear fit for all the isotherms shown in the previous figures. Both Freundlich and Langmuir isotherm coefficients for CETCO organoclay, Polymer Ventures organoclay and Biomin, Inc organoclay are shown in Table 7.1-5, Table 7.1-6 and Table 7.1-7, respectively. The K_d values

for each of these organoclays regarding humic acid preloading and desorption effects are shown in Table 7.1-8, Table 7.1-9 and Table 7.1-10, respectively.

PCB congener	Treatment	Freundlich Isotherms Coeff.		Langmuir Isotherm Coeff.	
		Kf	1/n	Nmax	b
2-cbp	Bare OC	8.2	1.6	-9.6	-0.5
	Preloading effect	1.3	1.3	-13.0	-0.1
	Desorption effect	21.0	2.2	-4.7	-0.9
2,2',5,5'- tPCB	Bare OC	2.8	0.8	0.6	13.8
	Preloading effect	0.4	0.8	0.2	5.3
	Desorption effect	1.3	0.8	0.5	7.3
3,3',4,4'-tPCB	Bare OC	126057.6	4.6	-0.1	-13.2
	Preloading effect	0.4	0.7	0.4	3.0
	Desorption effect	19.8	1.8	-0.3	-4.7
2,2',4,4',5,5'-hPCB	Bare OC	1.5	0.5	0.1	517.2
	Preloading effect	1.4	0.8	0.1	41.6
	Desorption effect	1.9	0.8	0.1	72.0
3,3',4,4',5,5'-hPCB	Bare OC	0.2	0.1	0.1	565.7
	Preloading effect	1014.5	2.7	0.0	-22.1
	Desorption effect	0.2	0.2	0.1	250.1

Table 7.1-5. Adsorption isotherm coefficients for CETCO organoclay.

PCB congener	Treatment	Freundlich Isotherms Coeff.		Langmuir Isotherm Coeff.	
		Kf	1/n	Nmax	b
2-cbp	Bare OC	4.4	0.6	11.1	0.7
	Preloading effect	1.2	1.1	-23.2	0.0
	Desorption effect	2.6	1.6	-6.6	-0.3
2,2',5,5'- tPCB	Bare OC	68760.2	2.6	-0.1	-90.3
	Preloading effect	0.3	0.8	0.2	3.6
	Desorption effect	1.9	0.8	0.5	8.6

Table 7.1-6. Adsorption isotherm coefficients for Polymer Ventures organoclay.

PCB congener	Treatment	Freundlich Isotherms Coeff.		Langmuir Isotherm Coeff.	
		Kf	1/n	Nmax	b
2-cbp	Bare OC	3.3	0.2	4.2	9.5
	Preloading effect	1.8	0.2	2.6	6.2
	Desorption effect	5.8	0.6	12.1	0.9

Table 7.1-7. Adsorption isotherm coefficients for Biomin, Inc. organoclay.

PCB Congeners	Bare CETCO OC	Preloading effect	Desorption effect	% Reduction due to preloading
2-cbp	12.7	1.9	8.5	84.9
2,2',5,5'-tPCB	4.9	0.6	2.3	86.7
3,3',4,4'-tPCB	7.9	0.5	4.3	93.5
2,2',4,4',5,5'-hPCB	27.3	2.7	4.7	90.1
3,3'4,4',5,5'-hPCB	2.0	1.9	1.9	5.6

Table 7.1-8. K_d values for adsorption of five PCBs by CETCO organoclay.

	Bare PV OC	Preloading effect	Desorption effect	% Reduction due to preloading
2-cbp	3.4	1.2	3.3	64.4
2,2',5,5'-tPCB	26.2	0.4	3.0	98.4

Table 7.1-9. K_d values for adsorption of two PCBs by Polymer Ventures organoclay.

	Bare BI OC	Preloading effect	Desorption effect	% Reduction due to preloading
2-cbp	5.3	0.5	1.2	90.7

Table 7.1-10. K_d values for adsorption of 2-chlorobiphenyl by Biomin, Inc. organoclay.

Summary. Data presented in the previous sub-sections indicates that adsorption of higher chlorinated PCB congeners was higher than that of lower chlorinated PCB congeners on CETCO organoclay and the desorption effect was less pronounced in co-planar congeners as compared to that of non-coplanar congeners. The humic acid preloading effect was more significant in lower chlorinated congeners as compared to that of higher chlorinated congeners. When performance of three compositions of organoclays was compared for the adsorption of 2-chlorobiphenyl, the maximum adsorption was found to occur on the CETCO organoclay. When performance of CETCO organoclay (bentonite base clay) and Polymer Ventures organoclay (attapulgite base clay) was compared for the adsorption of 2,2',5,5'-tPCB, the adsorption capacity of the Polymer Ventures organoclay was found to be higher than that of the CETCO organoclay but preloading effects were more significant. Desorption effects were similar between the two materials. Based on the overall results of the organoclay characterization process, the preliminary recommendation is to proceed with CETCO organoclay featuring a bentonite base material for construction of the prototype reactive mats to be used during the year three full-scale mat testing effort.

7.1.3. Effects of Humic Acid, Fulvic Acid and Natural Organic Material

Additional studies were conducted to assess the combined effects of humic acid, fulvic acid and NOM on the overall performance of activated carbon and organoclay in sequestering PCBs and PAHs. Pore water samples from the Passaic River in New Jersey and the Hudson River in New York were incorporated into these additional studies to simulate the impacts of ambient field conditions that are expected to occur during final mat deployment.

Kinetic Studies for PCBs. The effects of Passaic River sediment pore water, Hudson River sediment pore water, humic acid, fulvic acid and NOM on the adsorption equilibrium of 2,2',5,5'-tetrachlorobiphenyl for both organoclay and activated carbon are shown in Figure 7.1-15. Least square mean plots to quantify the effects of these parameters on the adsorption of 2,2',5,5'-tetrachlorobiphenyl by organoclay and activated carbon are shown in Figure 7.1-16.

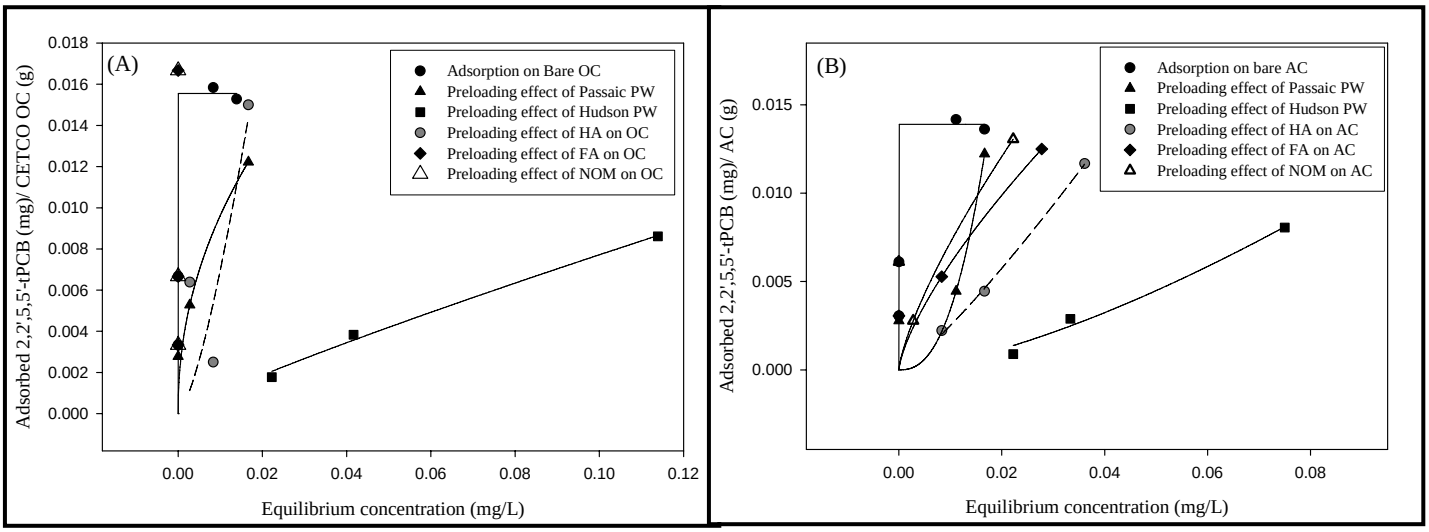

Figure 7.1-15. Effects of Passaic River sediment pore water, Hudson River sediment pore water, humic acid, fulvic acid and natural organic matter on the adsorption kinetics of 2,2',5,5'-tetrachlorobiphenyl by (A) organoclay and (B) activated carbon.

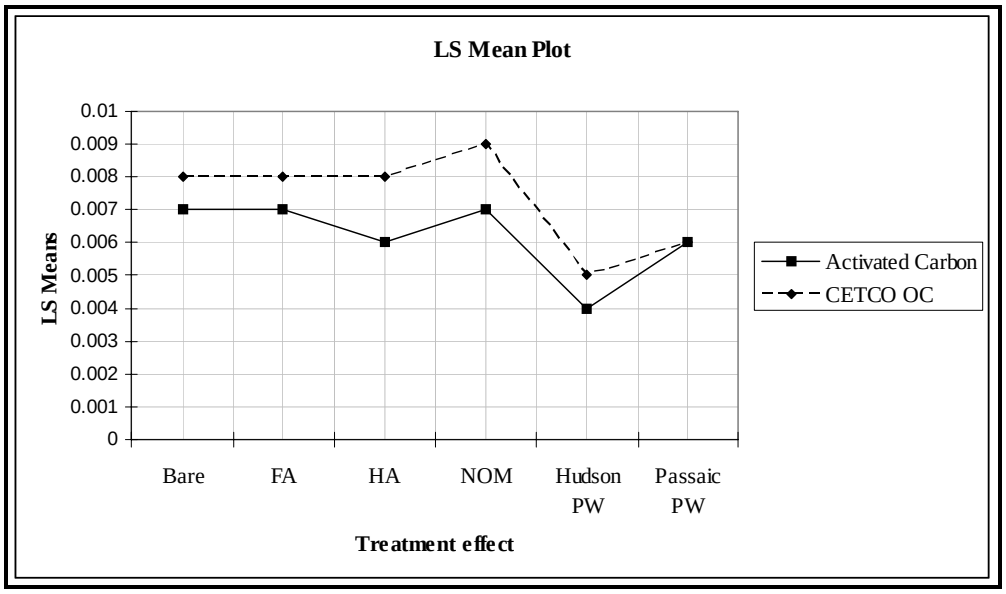

Figure 7.1-16. Least square mean plot to compare the effects of Passaic River sediment pore water, Hudson River sediment pore water, humic acid, fulvic acid and natural organic matter on the adsorption of 2,2',5,5'-tetrachlorobiphenyl by organoclay and activated carbon.

Kinetic Studies for PAHs. The effects of Passaic River sediment pore water, Hudson River sediment pore water, humic acid, fulvic acid and NOM on the adsorption equilibrium of phenanthrene for both CETCO organoclay and activated carbon are shown in Figure 7.1-17. Least square mean plots to quantify the effects of these parameters on the adsorption of phenanthrene by organoclay and activated carbon are shown in Figure 7.1-18. Similarly, the effects of these parameters on the adsorption equilibrium of pyrene for both CETCO organoclay and activated are shown in Figure 7.1-19.

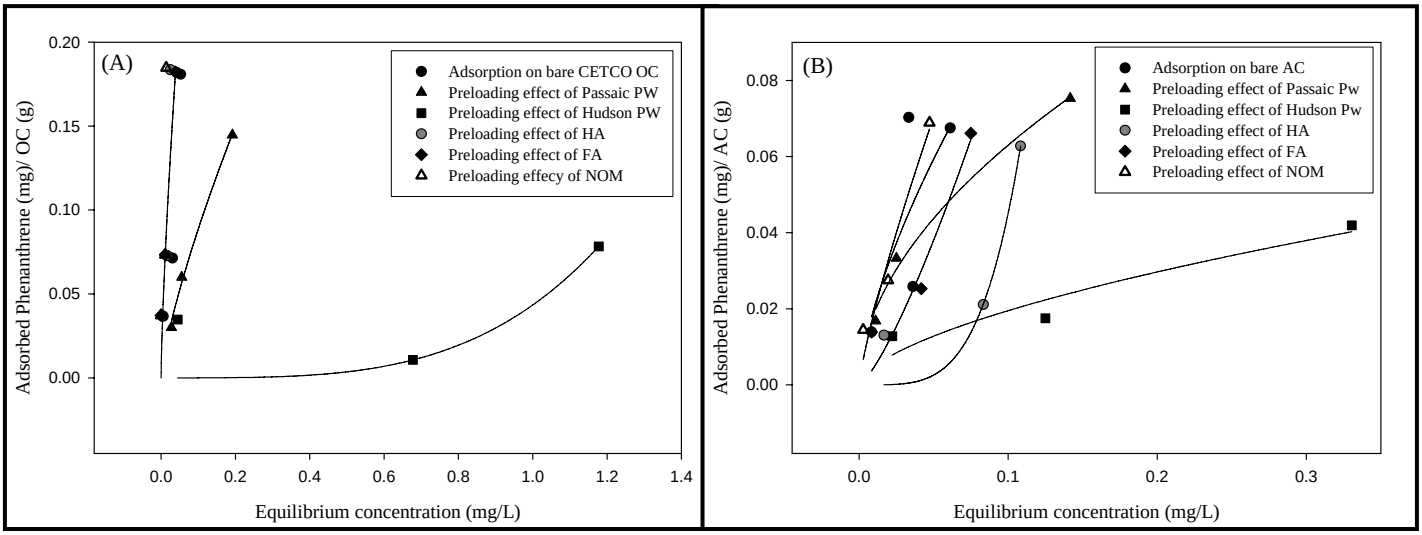

Figure 7.1-17. Effects of Passaic River sediment pore water, Hudson River sediment pore water, humic acid, fulvic acid and natural organic matter on the adsorption kinetics of phenanthrene by (A) organoclay and (B) activated carbon.

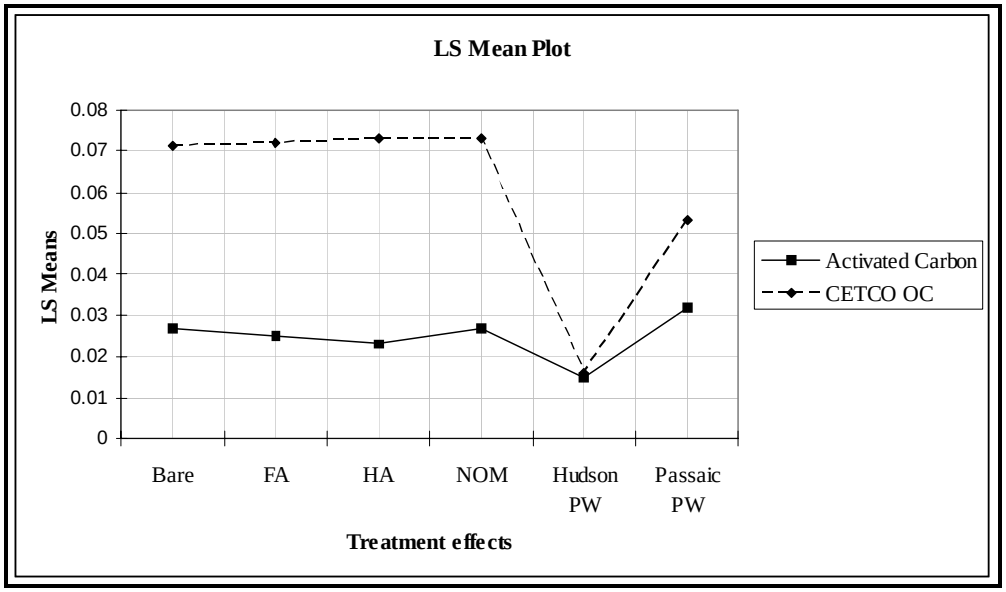

Figure 7.1-18. Least square mean plot to compare the effects of Passaic River sediment pore water, Hudson River sediment pore water, humic acid, fulvic acid and natural organic matter on the adsorption of phenanthrene by organoclay and activated carbon.

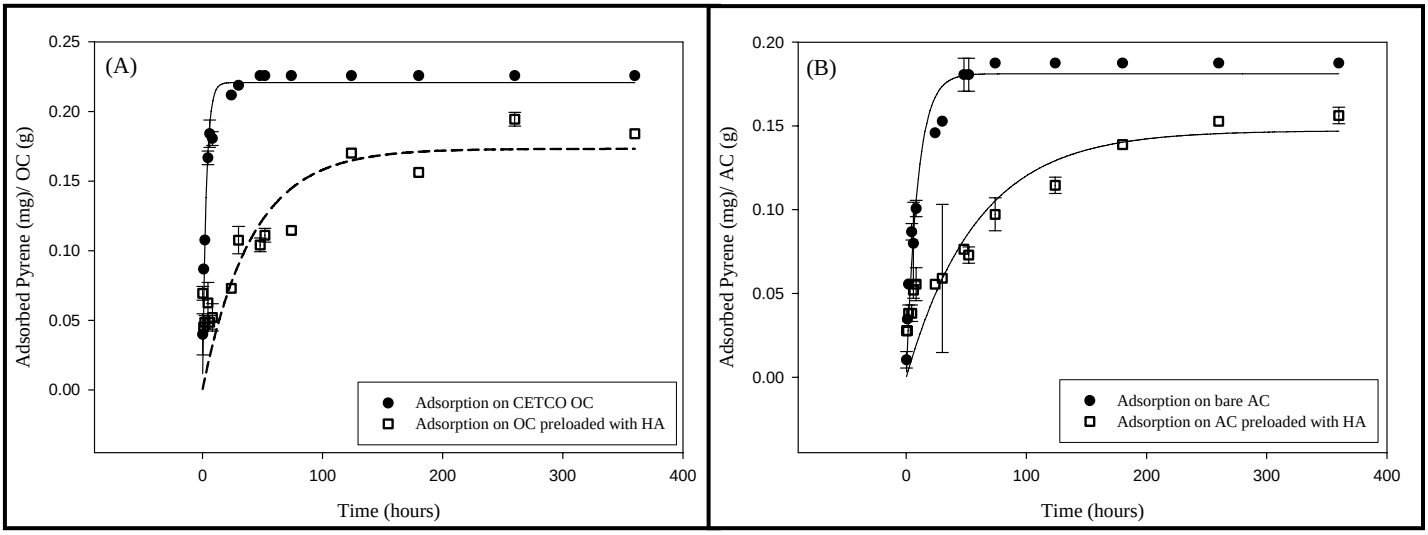

Figure 7.1-19. Effects of Passaic River sediment pore water, Hudson River sediment pore water, humic acid, fulvic acid and natural organic matter on the adsorption kinetics of pyrene by (A) organoclay and (B) activated carbon.

Evaluation of Isotherm Coefficients. In order to compare organoclay and activated carbon in terms of their sorption affinities for PCBs (2,2',5,5'-tetrachlorobiphenyl) and PAHs (phenanthrene) in the presence of Passaic River pore water, Hudson River pore water, humic acid, fulvic acid and NOM, adsorption coefficients (K_d) were estimated using a linear fit for all the isotherms shown in the previous figures. Freundlich isotherm coefficients for both organoclay and activated carbon under these conditions are shown for the adsorption of

2,2',5,5'-tetrachlorobiphenyl and phenanthrene in Table 7.1-11 and Table 7.1-12, respectively. The K_d values for each of these compounds regarding the Passaic River pore water, Hudson River pore water, humic acid, fulvic acid and NOM treatments are shown in Table 7.1-13 and Table 7.1-14, respectively.

2,2',5,5'-tPCB	Treatment	Freundlich Isotherms Coeff.	
		Kf	1/n
OC	Bare OC	0.02	0.42
	PPW	0.08	0.47
	HPW	0.06	0.88
	HA	4.84	1.42
	FA	0.01	1.00
	NOM	0.01	1.00
AC	Bare OC	0.01	0.39
	PPW	333.80	2.49
	HPW	0.35	1.46
	HA	0.62	1.20
	FA	0.16	0.72
	NOM	0.22	0.74

Table 7.1-11. Isotherm coefficients for adsorption of 2,2',5,5'-tetrachlorobiphenyl by organoclay and activated carbon under various exposure treatments.

Phenanthrene	Treatment	Freundlich Isotherms Coeff.	
		Kf	1/n
OC	Bare OC	4.63	1.08
	PPW	0.51	0.76
	HPW	0.04	3.61
	HA	457.49	2.12
	FA	457.49	2.12
	NOM	457.49	2.12
AC	Bare OC	0.44	0.67
	PPW	0.21	0.53
	HPW	0.08	0.61
	HA	608.02	4.13
	FA	1.90	1.31
	NOM	0.81	0.82

Table 7.1-12. Isotherm coefficients for adsorption of phenanthrene by organoclay and activated carbon under various exposure treatments.

	Kd
CETCO OC	0.95
AC	0.67
OC_Passaic PW	0.54
AC_Passaic PW	0.5
OC_Hudson PW	0.07
AC_Hudson PW	0.13
OC_HA	0.68
AC_HA	0.34
OC_FA	2
AC_FA	0.34
OC_NOM	
AC_NOM	0.39

Table 7.1-13. K_d values for adsorption of 2,2',5,5'-tetrachlorobiphenyl by organoclay and activated carbon under various exposure treatments.

	Kd
CETCO OC	3.3
AC	1.22
OC_Passaic PW	0.67
AC_Passaic PW	0.41
OC_Hudson PW	0.03
AC_Hudson PW	0.09
OC_HA	6.18
AC_HA	0.45
OC_FA	3.76
AC_FA	0.78
OC_NOM	8.51
AC_NOM	1.25

Table 7.1-14. K_d values for adsorption of phenanthrene by organoclay and activated carbon under various exposure treatments.

Preloading Effects. Additional kinetic studies were conducted to evaluate the affects of different loading levels of humic acid, fulvic acid and NOM (50, 500, 5000 g material/g sorbent) on the adsorption equilibriums of PCBs (2,2',5,5'-tetrachlorobiphenyl) and PAHs (phenanthrene) for organoclay and activated carbon. Effects on the adsorption of both 2,2',5,5'-tetrachlorobiphenyl and phenanthrene caused by variable loading levels for humic acid, fulvic acid and NOM are shown in Figure 7.1-20, Figure 7.1-21 and Figure 7.1-22, respectively.

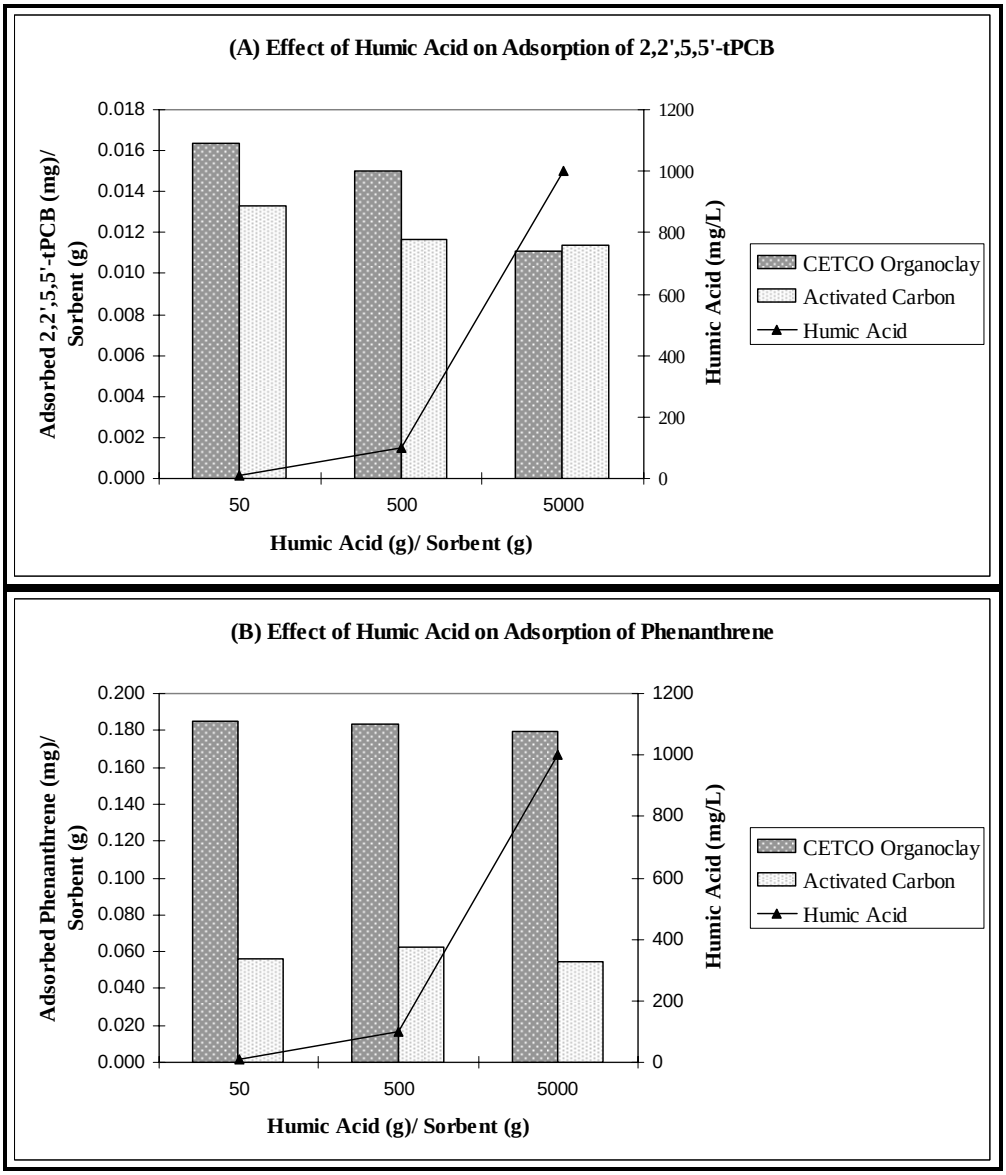

Figure 7.1-20. Effects of different loading levels of humic acid on the adsorption kinetics of organoclay and activated carbon for (A) 2,2',5,5'-tetrachlorobiphenyl and (B) phenanthrene.

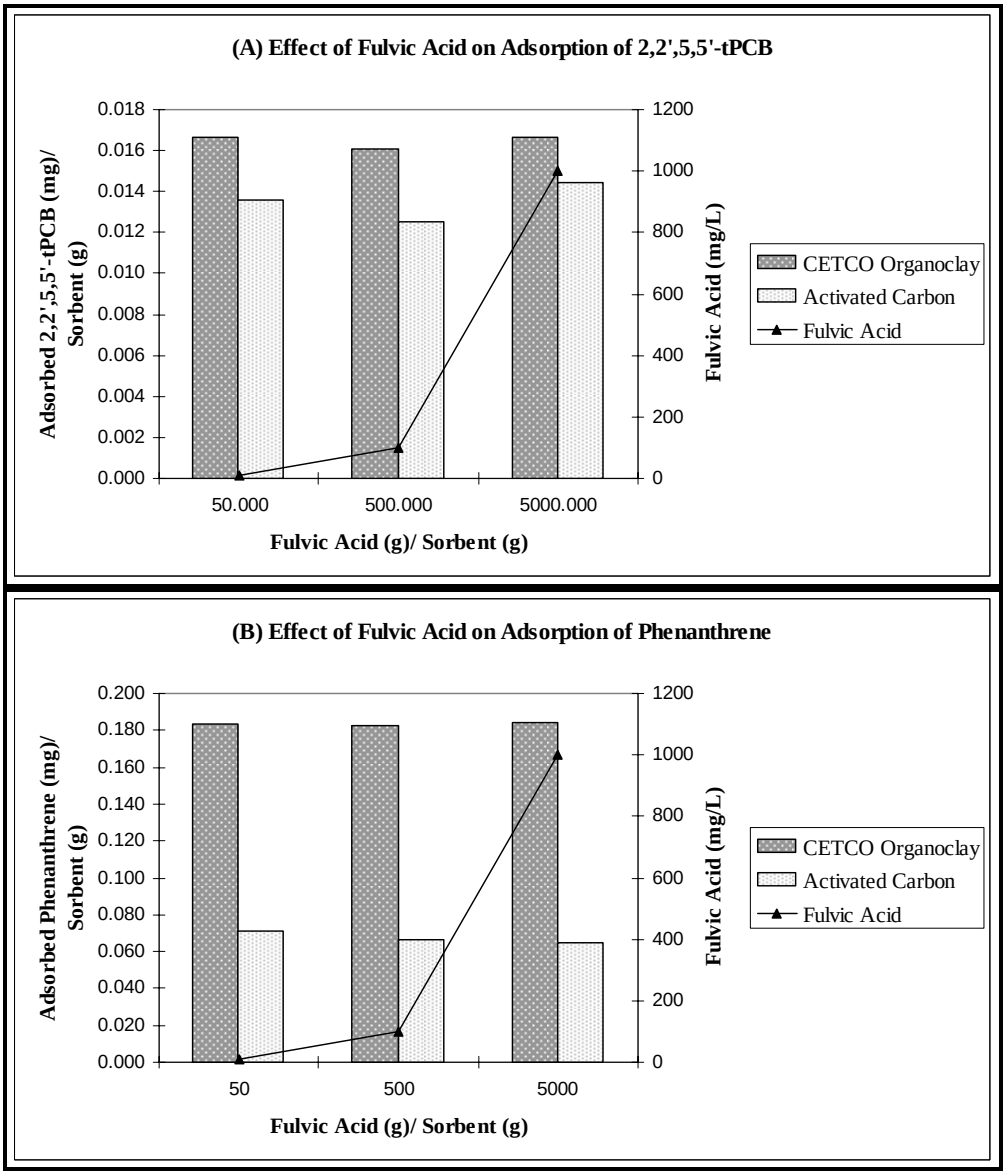

Figure 7.1-21. Effects of different loading levels of fulvic acid on the adsorption kinetics of organoclay and activated carbon for (A) 2,2',5,5'-tetrachlorobiphenyl and (B) phenanthrene.

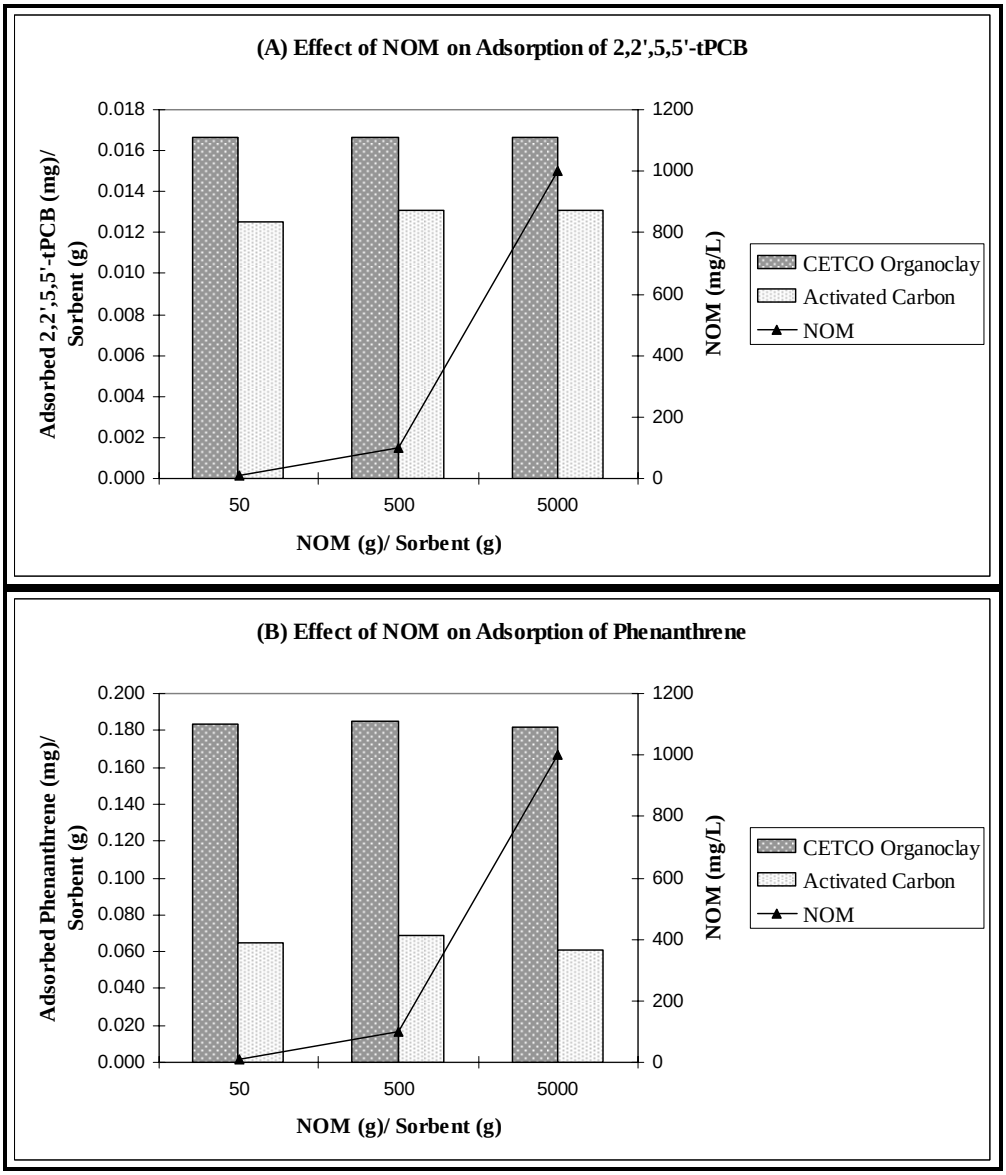

Figure 7.1-22. Effects of different loading levels of natural organic matter on the adsorption kinetics of organoclay and activated carbon for (A) 2,2',5,5'-tetrachlorobiphenyl and (B) phenanthrene.

Summary. These results show that the adsorption capacity of organoclay was consistently higher than that of activated carbon for 2,2',5,5'-tPCB and phenanthrene. The effects of humic acid were more pronounced than the effects of fulvic acid and NOM, the latter of which were both found to have a negligible influence on the adsorption capacity of both sorbents. The preloading effect of extracted Hudson River pore water on adsorption was found to be significant, which may be attributed to the presence of colloidal material that might have blocked the way of target contaminants to the sorbent surface. Similar effects were not dominant for preloading with Passaic River pore water. The results of this work indicate that organic acids, which are quite concentrated in sediment porewater, have a significant impact on the efficacy of

potential reactive mat components and should be an essential factor in the final design and ultimate performance evaluation of the reactive mat technology.

7.2. TASK 2: PILOT SITE SELECTION

The purpose of selecting a pilot site for this project was to identify a suitable location for the small-scale field testing of geotextile mats as well as a specific target area for full-scale deployment of a prototype mat system. As described in Section 6.2.1, the pilot site selection process consisted of two phases that involved first narrowing a "long list" of potential Navy sites down to two primary sites based on a series of chemical, physical, biological and logistical factors that would provide a challenging and suitable environment for geotextile testing and then performing a focused comparison of these two primary sites in terms of history, surficial hydrology, hydrogeologic properties, nature and extent of contamination and past remediation efforts as documented in existing literature. Once a decision was made to proceed with field activities at one of the primary sites (Cottonwood Bay), phase two of the pilot site selection process then involved conducting a geophysical investigation to determine a specific area for full-scale mat system deployment based on bottom topography, habitat characteristics and groundwater seepage properties.

Phase one of the pilot site selection task was completed during the year one effort, as was the focused comparison between the two most suitable primary sites based on existing literature. The decision to proceed with field activities at Cottonwood Bay over Pearl Harbor was made in year two, followed by the phase two comprehensive geophysical investigation. To date the entire pilot site selection process has been completed. A summary of the accomplishments for each phase of this task are provided in the following sections.

7.2.1. Site Selection Overview

Phase One Site Selection. A detailed description of phase one of the pilot site selection process is provided in the First Year Annual Progress Report for Project Number ER-1493 (NAVFAC 2006). In summary, the first step involved generating a "long list" of prospective aquatic Navy sites to be considered as possible geotextile testing locations. Knowledgeable NFESC staff and other Navy personnel were contacted for input and a web search was conducted to generate a list of potential sites that included Cottonwood Bay, Pearl Harbor, the Philadelphia Naval Business Center Reserve Basin, Naval Station Newport, the Portsmouth Naval Shipyard and the Hunters Point Shipyard, among others. Each of these locations was subject to a detailed evaluation with respect to the site screening parameters outlined in Section 6.2.2. Based on these criteria, Cottonwood Bay in Grand Prairie, Texas (adjacent to the NWIRP and NAS Dallas) and Pearl Harbor in Honolulu, Hawaii (adjacent to the Honolulu Naval Facilities) were identified as the most suitable locations for small-scale geotextile testing and full-scale prototype mat deployment. The specific characteristics leading to the selection of these two sites as well as the principal rationales used to eliminate other prospective sites from primary site consideration are provided in a series of tables in the First Year Annual Progress Report (NAVFAC 2006).

Phase Two Primary Site Comparison. The focused literature review for the selected primary sites focused on two reports each for Cottonwood Bay and Pearl Harbor. These documents were

Chemical Quality of Water, Sediment, and Fish in Mountain Creek Lake, Dallas, Texas, 1994-97 (VanMetre *et al*. 2003) provided by the U.S. Geological Survey (USGS), *Texas Natural Resource Conservation Commission Affected Property Assessment Report* (EnSafe 2001) provided by the Navy as part of the requirements of the Texas Risk Reduction Program (TRRP), *Remedial Investigation Report for Pearl Harbor Sediment* (NAVFAC 2006), and *Baseline Ecological Risk Assessment for Pearl Harbor Sediment Remedial Investigation* (NAVFAC 2006). Correspondence and phone conferences with site managers also contributed to the understanding of the conditions and management at each location as well as logistical considerations that would be important for further site assessment.

Detailed results of the focused site comparison between Cottonwood Bay and Pearl Harbor, including several tables and figures, are provided in the First Year Annual Progress Report (NAVFAC 2006). In summary, both sites were found to have sufficiently elevated concentrations of metals and organics to provide a representative test of reactive mat performance, although principle metals of concern at Cottonwood Bay were chromium and lead while principle metals of concern at Pearl Harbor were copper and zinc. At the time of the initial focused comparison, sediments had been more thoroughly and recently characterized at Pearl Harbor. Available data for Cottonwood Bay were all found to be greater than ten years old, thus introducing some uncertainty with regard to current site conditions. More current Cottonwood Bay data was obtained during year two to fill existing data gaps which included the document *Computer-model analysis of ground-water flow and simulated effects of contaminant remediation at Naval Weapons Industrial Reserve Plant, Dallas, Texas* provided by the USGS (Barker and Braun 2000).

Regarding flow parameters, Cottonwood Bay appeared to have significant groundwater influence while Pearl Harbor is subject to tidal flow and limited groundwater movement. At both sites there is a likelihood of measurable biofilm, although Cottonwood Bay was deemed more likely to have a higher accretion rate relative to Pearl Harbor, where turbidity and nutrient loading is expected to be lower. In terms of management planning, both sites have identified needs for remediation and groundwater control measures are currently in place at Cottonwood Bay. Pearl Harbor has been investigated following USEPA guidance for risk assessment and remedial investigations but a Feasibility Study (FS) for remediation alternatives has yet to be completed. Logistically, both Cottonwood Bay and Pearl Harbor were deemed accessible and found to possess the necessary infrastructure to support mobilization and field activities. Security limitations were identified for both sites, however, with access to the eastern portion of Cottonwood Bay restricted by NAS security and entrance into Pearl Harbor near the Naval Facility berthing areas also restricted.

Final Site Selection. Cottonwood Bay was ultimately deemed more suitable for geotextile testing than Pearl Harbor and thus selected as the final pilot site for this project. Although contaminant conditions at both sites are generally similar, Cottonwood Bay was found to have more thorough mixtures of both metals and organics that would correspond well to overall adsorption goals. Cottonwood Bay was also found to have a significantly greater groundwater flow potential, which made it a more attractive location for evaluating potential groundwater flux through the reactive mats. Although an energetic environment such as the intertidal zones within

Pearl Harbor was originally sought in order to provide conditions where a traditional sand cap would be insufficiently stable to provide a permanent form of remediation, the relatively constant conditions and groundwater flow parameter present at Cottonwood Bay were considered more important in evaluating mat performance than a dynamic setting. Logistical and travel considerations also contributed heavily to the selection of Cottonwood Bay since its location within the contiguous United States would make it more cost effective in terms of transporting equipment and field personnel. Finally, the location of Cottonwood Bay within the general Mountain Creek Lake area already scheduled for remediation under the TRRP made it an attractive site for further investigation, with results of the proposed geophysical surveys not only applicable to SERDP goals but also to the overall Mountain Creek Lake remedial investigation and feasibility study. Previously established contacts within NAVFAC and EnSafe, Inc. familiar with the Cottonwood Bay site were also able to assist with site access logistics as well as mitigating security concerns with the relevant NWIRP and NAS parties. A detailed discussion of all background conditions for Cottonwood Bay prior to initiation of the geophysical investigation is provided in the following section.

7.2.2. Selected Site Background Assessment

Cottonwood Bay in Grand Prairie, Texas was selected as the primary site for this project during the site selection process. As discussed in Section 7.2.1, the majority of information regarding the background conditions at Cottonwood Bay was obtained from a USGS sampling effort (VanMetre *et al*. 2003), a TRRP analysis (EnSafe 2001) and subsequent groundwater modeling (Barker and Braun 2000). Details about the site that were provided in these documents and compiled during both the year one and year two efforts are described in the following sub-sections.

Site Description and History. Cottonwood Bay is located in northeastern Texas within Dallas County approximately four miles southeast of Grand Prairie between routes I-30 and I-20. The site is adjacent to the NWIRP and NAS Dallas and is the ultimate product of a landfill event that took place during the original construction of the NAS airstrip. Recreational fishing is popular in the connected Mountain Creek Lake, but consumption of catch is banned due to PCB contamination. An overview of the entire Cottonwood Bay site is provided in Figure 7.2-1.

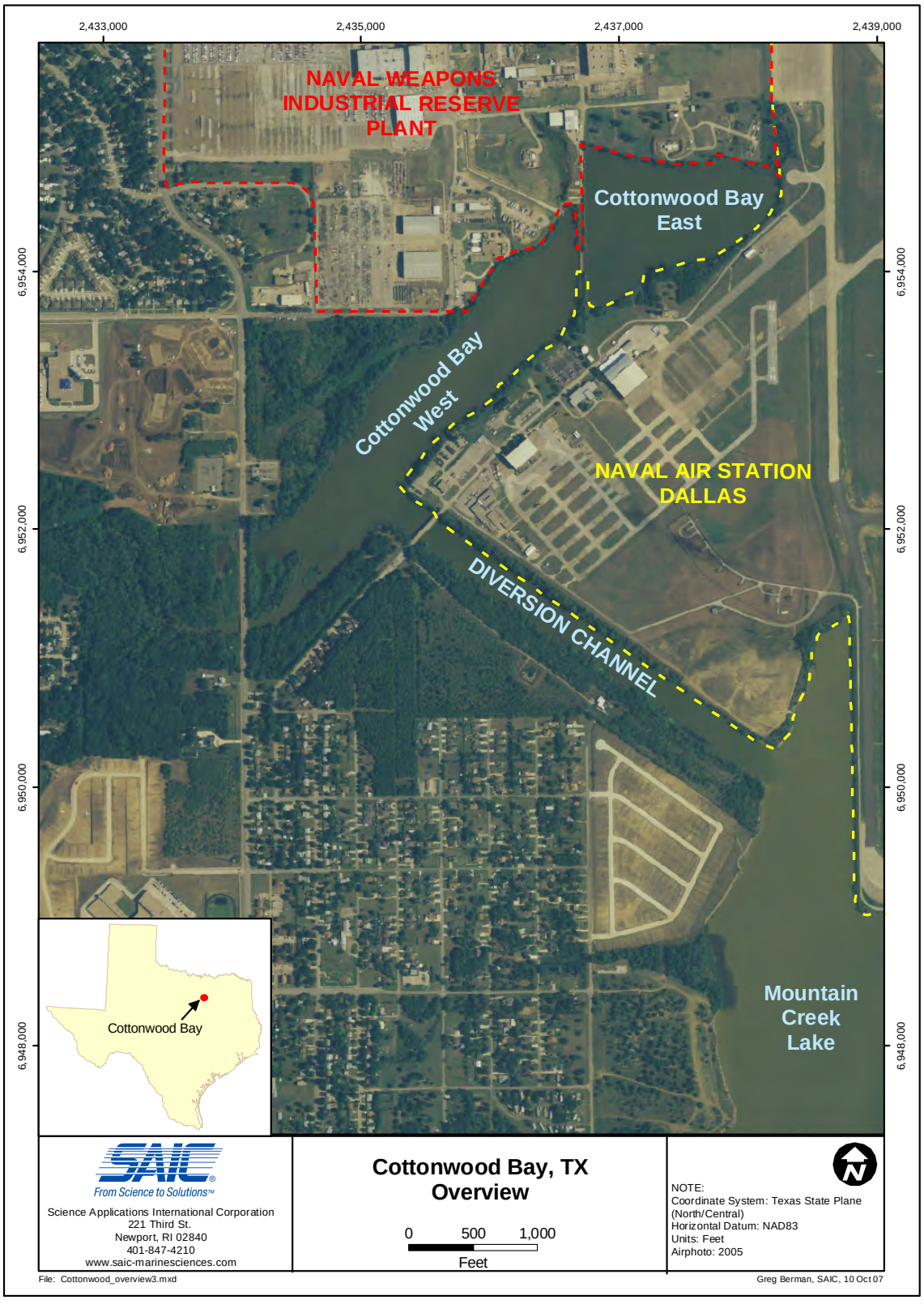

Figure 7.2-1. Overview of the Cottonwood Bay site.

***Surficial Hydrology*.** Cottonwood Bay is an artificially constructed stream and groundwater-fed freshwater body that is connected to Mountain Creek Lake by a narrow channel (Figure 7.2-1). The Cottonwood Creek diversion channel feeds directly into the bay and, along with surface runoff, constitutes the main surface water input into the bay (Figure 7.2-2). The east and west lagoons on NWIRP property to the north of the bay were constructed to contain stormwater runoff but also receive input from groundwater. Cottonwood Bay and Mountain Creek Lake have relatively consistent water elevations throughout the year and are not very dynamic environments.

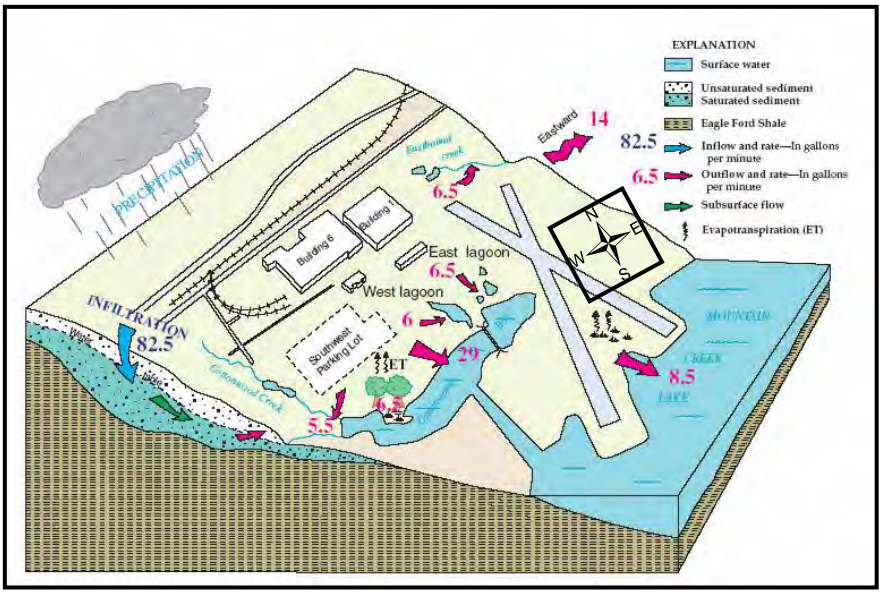

Figure 7.2-2. Conceptual model of the hydrogeologic setting of the Cottonwood Bay site (modified from Barker and Braun 2000).

Hydrogeologic Properties. The source of most groundwater is precipitation which averages about 36 in/yr in Grand Prairie (Owenby and Ezell 1992). Precipitation readily infiltrates the porous higher-altitude areas around the northern limits of the Cottonwood Bay site, while the buildings and impervious surfaces which characterize the lower elevations create runoff instead of infiltration.

As shown in Figure 7.2-2, the water table slopes toward Cottonwood Bay and Mountain Creek Lake. As an unconfined aquifer, which is composed mostly of silty sand and silty clay, it thins to the south and eventually becomes level with the site's water bodies (EnSafe 1994). Most of the groundwater discharges to Cottonwood Bay and Mountain Creek Lake which maintains the surface water levels of both of those water bodies. The rest of the ground water either discharges to the east and west retention lagoons, flows out of the site area to the east, or is evapo-transpired back into the atmosphere (Barker and Braun 2000).

The surficial aquifer at Cottonwood Bay is comprised of relatively recently placed soils. While the aquifer is unconfined on the surface, it is confined at depth by the Eagle Ford shale (University of Texas 1987). Directly below the shale is the Woodbine confined aquifer which does not discharge into Cottonwood Bay.

Nature and Extent of Contamination. The concentrations of select CoPCs in Cottonwood Bay sediments, including three metals (chromium, copper and zinc), PCBs and fluoranthene (representing the highest measured PAH) as determined from previous site investigations are presented in Table 7.2-1. The locations of the historic samples from which these data were generated are shown in Figure 7.2-3. The red markers on this figure indicate previous sampling stations of interest with high concentrations of mixed contaminants that are included in the table below. Two of these stations are in the southwest end of the bay near the terminus of Cottonwood Creek diversion channel, while four represent stations in the northeastern quadrant in the vicinity of NWIRP and NAS.

The highest metals concentrations in the historic Cottonwood Bay sediment samples were found for total chromium while the greatest organic contaminant loads were found for PAHs. Concentrations of chromium and PCBs were generally higher at Station OF401 adjacent to the NWIRP while concentrations of PAHs (*e.g.*, fluoranthene) increased with proximity to the NAS. Concentrations of metals and organics were found to be generally lower by a factor of five at the southwestern stations in Cottonwood Bay West where diversion channel enters the bay as compared to stations in Cottonwood Bay East on the opposite side of the causeway. Groundwater intrusion may also be contributing to lake water and sediment risks since trichloroethene (TCE), dichloroethene (DCE), vinyl chloride (VC), chromium, lead, and other metallic contaminants have been measured in the shallow unconfined aquifer underlying the NWIRP (EnSafe 1996).

		Cottonwood Bay Sediment Sampling Stations					
Parameter	**Units**	**BG1**	**MCL5**	**OF401**	**Bay 11**	**Bay 7**	**Bay 16**
Metals	mg/Kg	Cr = 15 Cu = 16 Zn = 64	Cr = 83 Cu = 33 Zn = 130	Cr = 473 Cu = 71 Zn = 502	Cr = 350 Cu = 53 Zn = 350	Cr = 349 Cu = 55 Zn = 210	Cr = 350 Cu = 52 Zn = 280
Fluoranthene	ug/Kg	960	740	2400	NS	3600	4800
PCBs	ug/Kg	NS	6	4350*	NS	210	190
Dioxins/Furans (e.g., 2,4,5,6,7-PeCDF)	ug/Kg	NS	NS	NS	NS	NS	NS
Gain Size: Fines	%	NA	NA	NA	NA	NA	NA
Total Organic Carbon	%	NA	NA	NA	NA	NA	NA
Depth	m	NA	NA	NA	NA	NA	NA

* = Sum of 3 Arochlors
NS = Not Sampled
NA = Not Available; Information forthcoming.

Table 7.2-1. Select sediment data available from historic Cottonwood Bay samples.

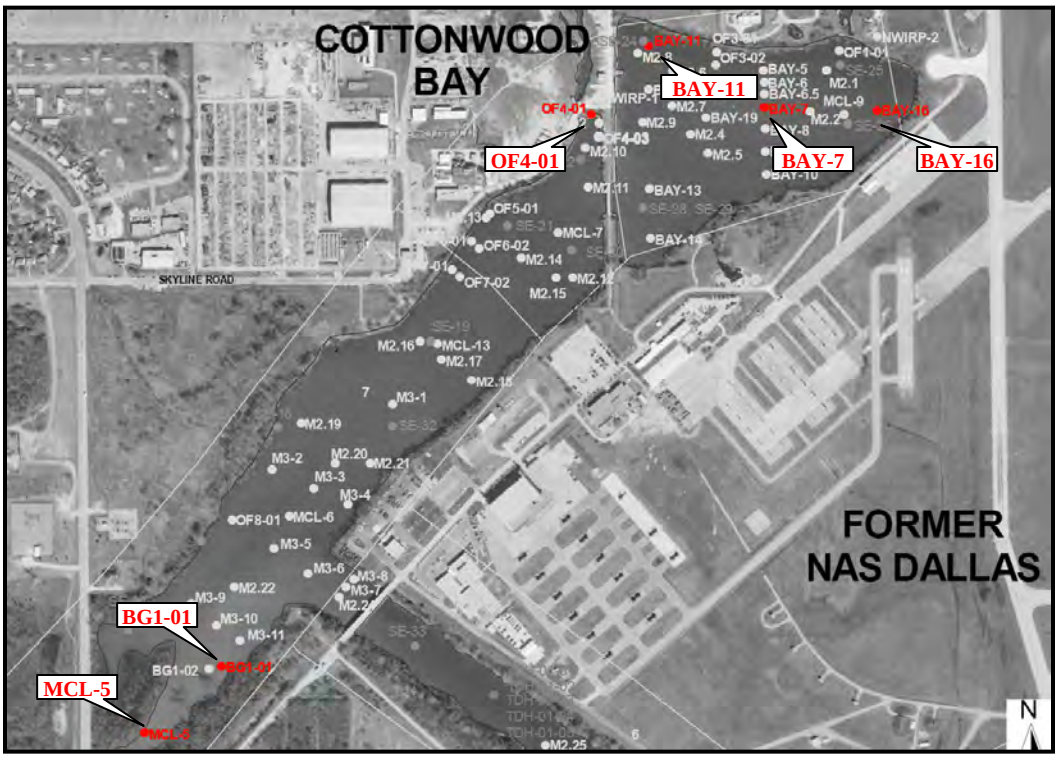

Figure 7.2-3. Historic Cottonwood Bay sampling stations used in the site background assessment (modified from EnSafe 2001).

Remediation Efforts. As shown in Figure 7.2-4, a series of wells and trenches were installed at the Cottonwood Bay site as early as 1996 with the goal of controlling the flow of groundwater and surface runoff on the NWIRP property. The specific purpose of these remedial activities was to remove groundwater from the aquifer before it reaches Cottonwood Bay and then treat the water to mitigate VOC contamination. Modeling indicates that the trenches adjacent to Cottonwood Bay East intercept about 827 ft^3/day of groundwater that otherwise would enter the bay. While the trenches intercept groundwater before it can reach Cottonwood Bay, the wells (when actively pumping) create a depression that reverses the direction of groundwater flow in order to draw contaminated water away from the bay.

Additional Cottonwood Bay remedial studies were conducted primarily by the USGS and can be characterized as "nature and extent" evaluations that provided data for a Screening Level Risk Assessment (EnSafe 2000). This report was not finalized when the Affected Property Assessment Report was submitted in 2001, but at that time the Texas Natural Resource Conservation Commission (TNRCC) determined that additional studies would be required before additional action could take place at the site. A remedial action plan for Cottonwood Bay is currently being prepared by NAVFAC Southeast.

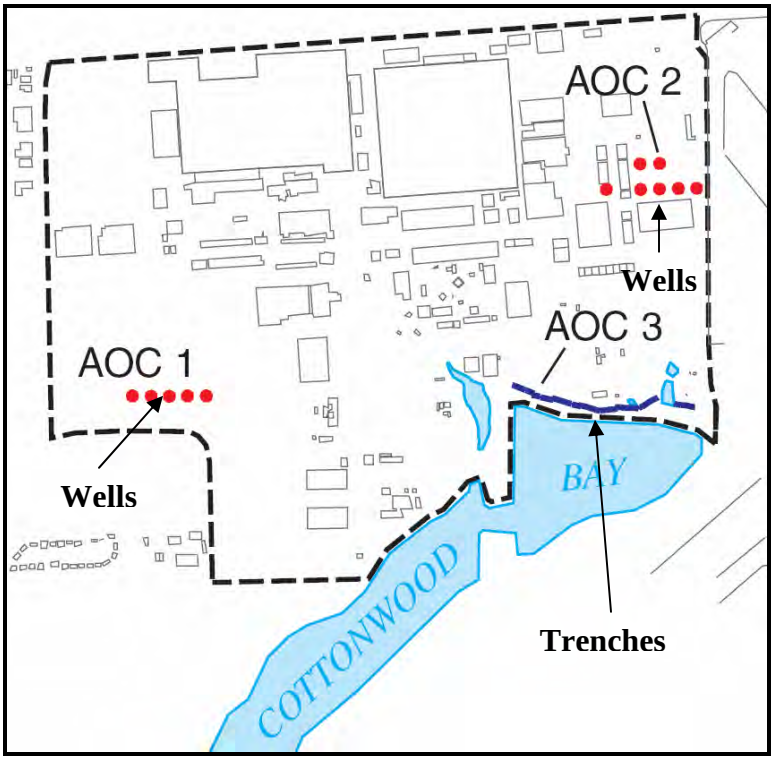

Figure 7.2-4. Locations of remedial wells and trenches at the Cottonwood Bay site (modified from Barker and Braun 2000).

7.2.3. Geophysical Surveys

Once Cottonwood Bay in Grand Prairie, Texas was identified in year two as the primary pilot site for this project an extensive geophysical investigation was conducted to characterize site conditions including water depth, habitat characteristics and lake sediment properties with the goal of selecting a specific location for future full-scale mat system deployment. The methods used to complete this phase two evaluation are provided in Section 6.3 of this report. Geophysical survey results are discussed in the following sub-sections.

Bathymetry. Spatial results from the Cottonwood Bay bathymetry surveys are presented in Figure 7.2-5. Water depths in the eastern portion of the bay ranged from zero along the shorelines to approximately 6.6 ft in the center. Depth increases were found to be relatively steep with a majority of the area constituting the deeper topography. In the western portion of the bay, water depths generally ranged from zero along the shorelines to approximately 3-4 ft in the center. Only two areas with depths greater than 6 ft were observed. These deeper zones are located at the southern end of the study area where the diversion channel enters the bay and at the eastern end of the study area adjacent to the causeway. Overall, water depths and gradients were significantly greater in Cottonwood Bay East. Cottonwood Bay West was observed to have much more aquatic vegetation visible at the water surface, especially in the southwest corner.

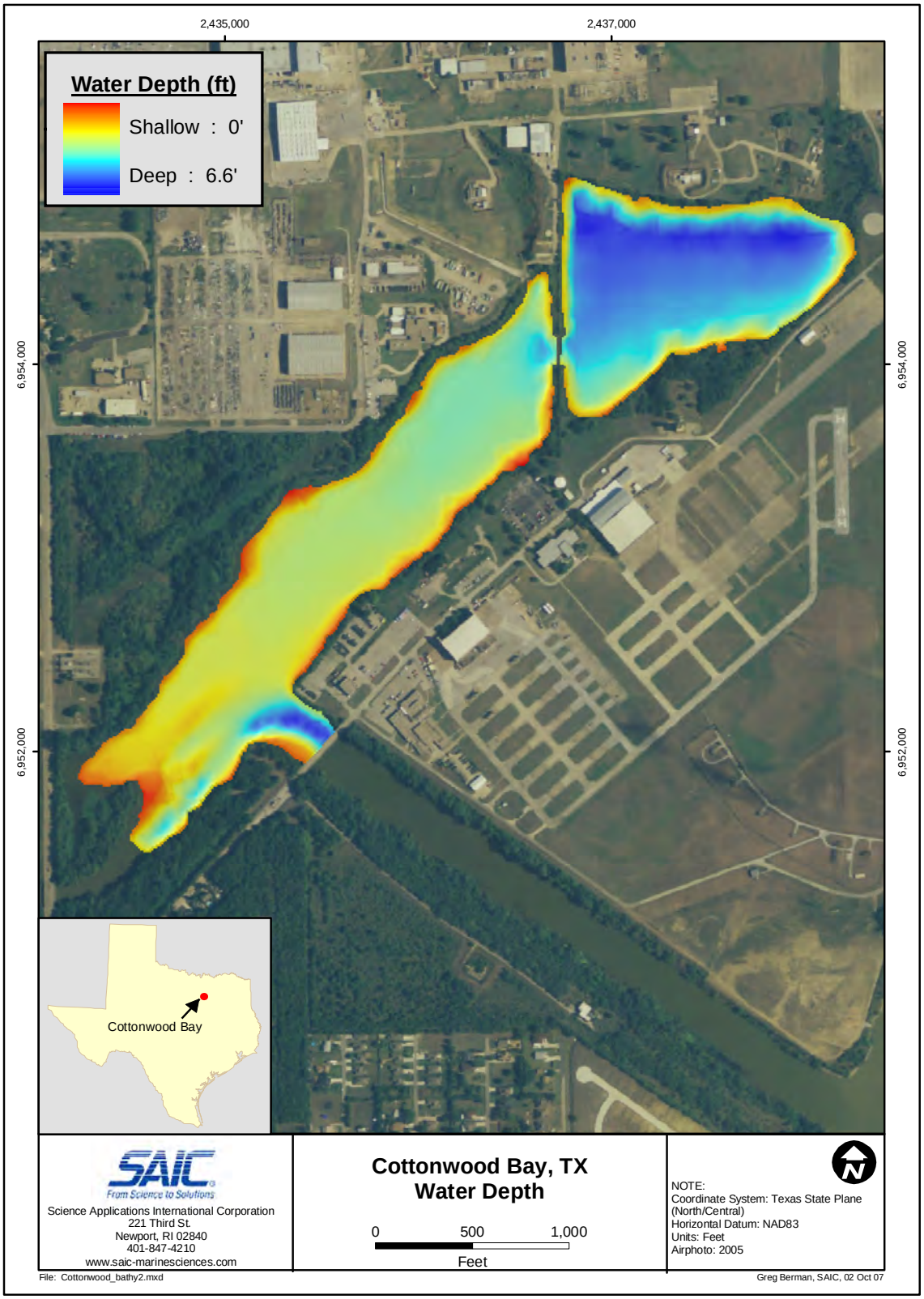

Figure 7.2-5. Bathymetry results for Cottonwood Bay.

Sub-Bottom Profiling. Sediment thickness results generated from sub-bottom profile data for Cottonwood Bay are shown in Figure 7.2-6. This figure depicts the depth from the sediment-water interface to the basement sediment layer identified in the digital data. For the eastern portion of the bay, sediment thickness ranged from zero along the shorelines to approximately 2.5 ft in the center. For the western portion of the bay, sediment thickness generally ranged from zero along the shorelines to approximately 1 ft in the center. Small areas of increased sediment thickness (2-2.5 ft) were observed in both the southwest corner and the point where the diversion channel enters the bay beneath the NAS Bridge.

Seismic profile cross-sections generated from sub-bottom profiling data along two select transects in Cottonwood Bay East are shown in Figure 7.2-7. As shown in these images, a thin lens of material was identified above the main sediment-water interface (red line). The composition of this lens is unknown, however, and may represent either a sediment deposit or a layer of leaf detritus. This lens was not confirmed in the sediment vibracores collected from Cottonwood Bay East to be discussed below.

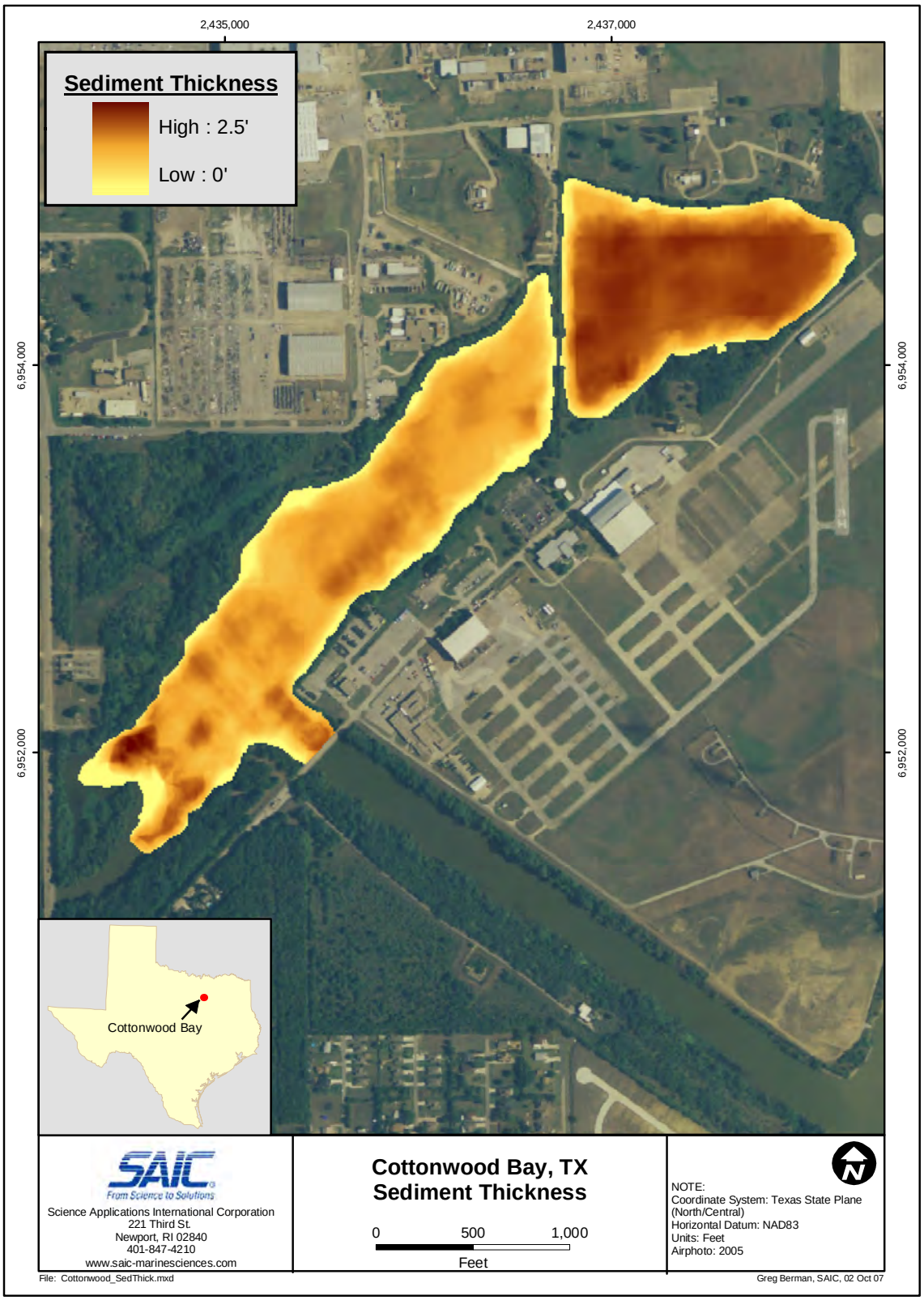

Figure 7.2-6. Sediment thickness results for Cottonwood Bay developed from sub-bottom profile data.

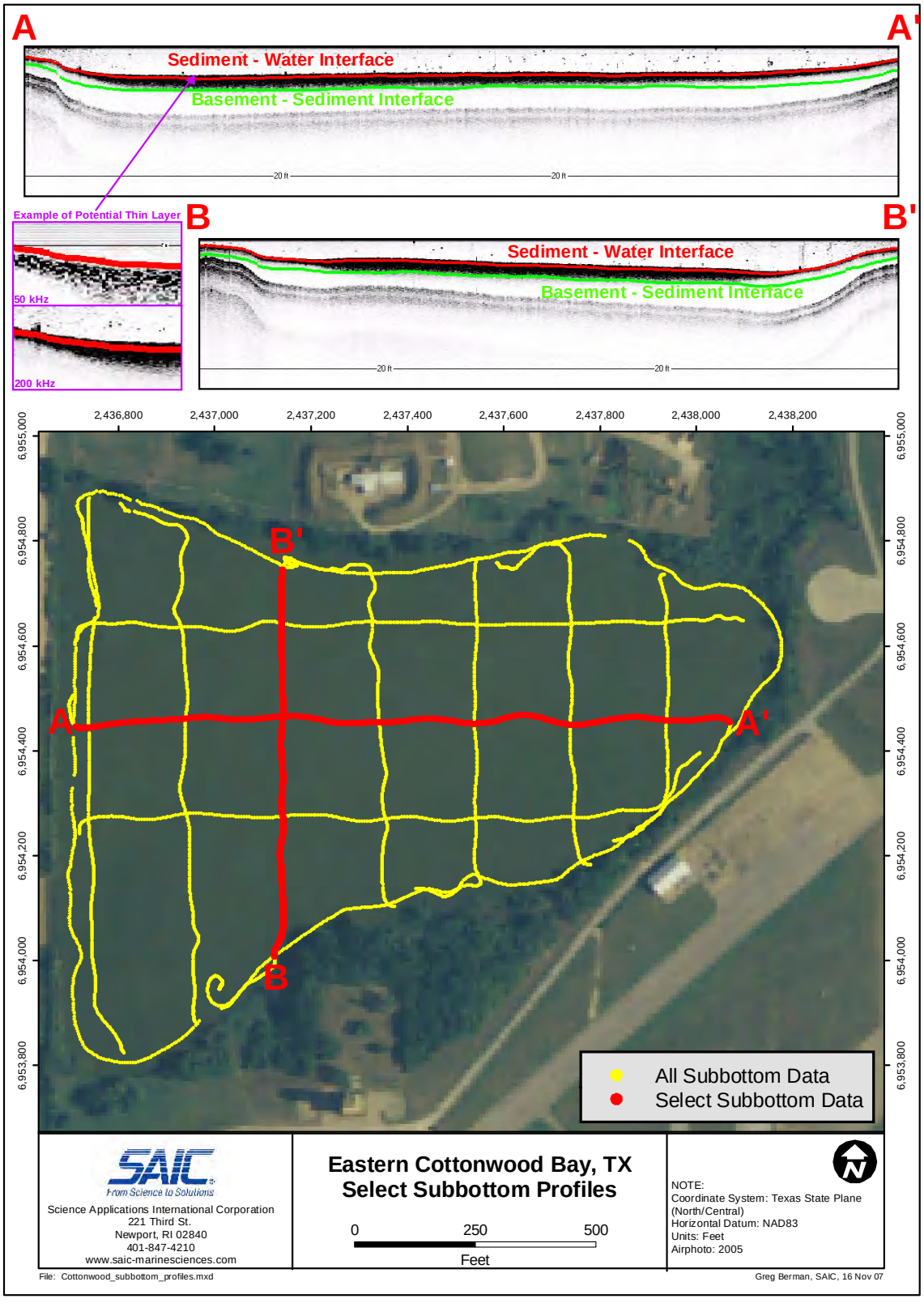

Figure 7.2-7. Select sub-bottom profiling cross-sections for Cottonwood Bay East.

Side-Scan Sonar. Complete spatial results from the Cottonwood Bay side-scan sonar surveys are presented in Figure 7.2-8. Zoomed-in results showing particular features of interest for both Cottonwood Bay East and Cottonwood Bay West are shown in Figure 7.2-9 and Figure 7.2-10, respectively. As shown in the mosaic for Cottonwood Bay East, multiple linear features were identified in the northwest portion of the study area near the NWIRP shoreline. These features may represent logs or man-made debris that could interfere with potential dredging. The mosaic for Cottonwood Bay West shows linear features in the middle of the study area near the NAS shoreline as well as mounded materials at the point where the diversion channel enters the bay. These linear features may correspond to a relic pontoon dock that was observed tied to the shoreline in that general area, a dilapidated fence that was found to be running along that portion of the bay or one of several outfalls that were found to be protruding from NAS property. The mounded materials may have resulted from sediment deposition that occurred as runoff from the deeper diversion channel entering the more shallow bay.

Figure 7.2-8. Complete side-scan sonar results for Cottonwood Bay.

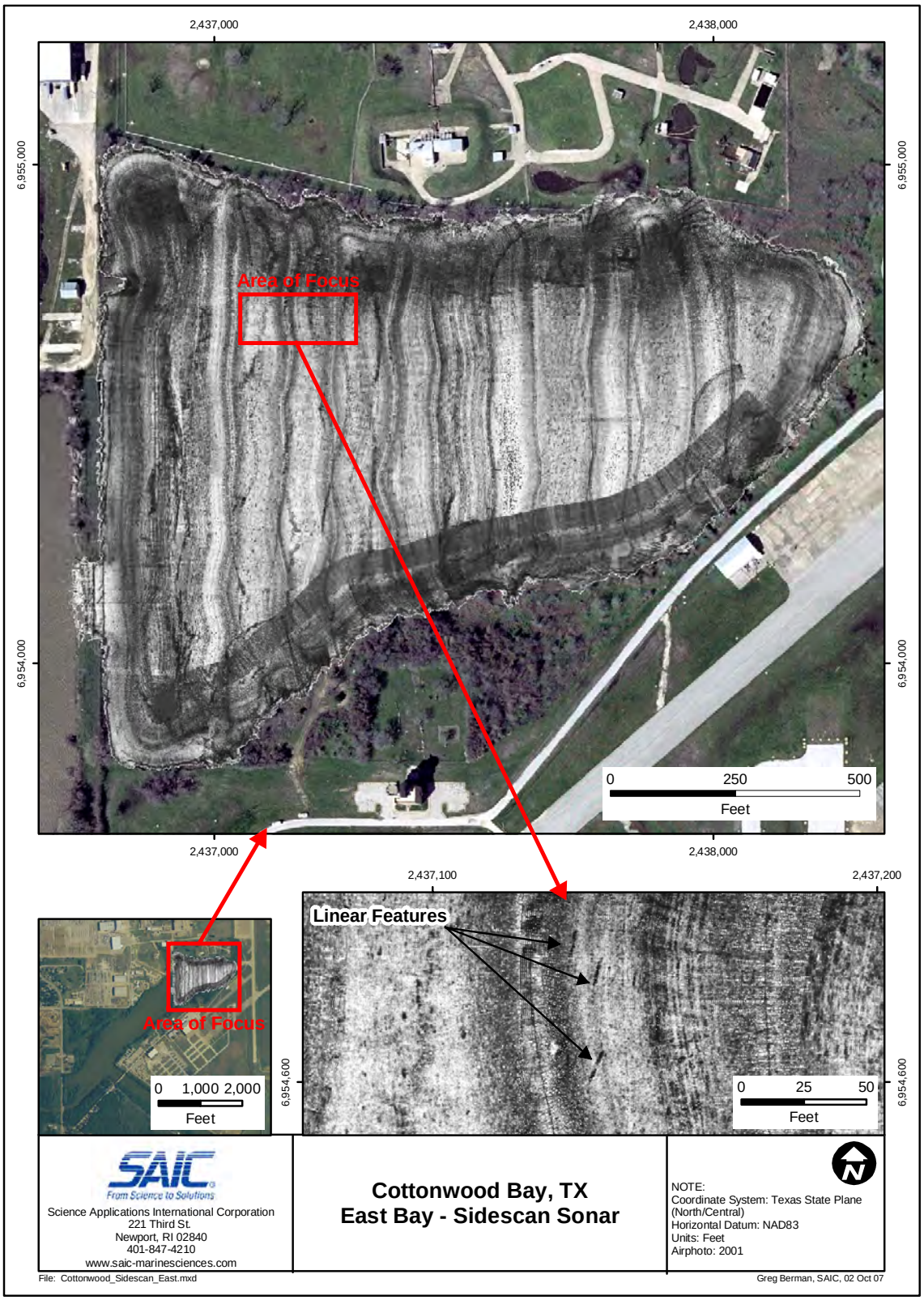

Figure 7.2-9. Side-scan sonar results for Cottonwood Bay East showing features of interest.

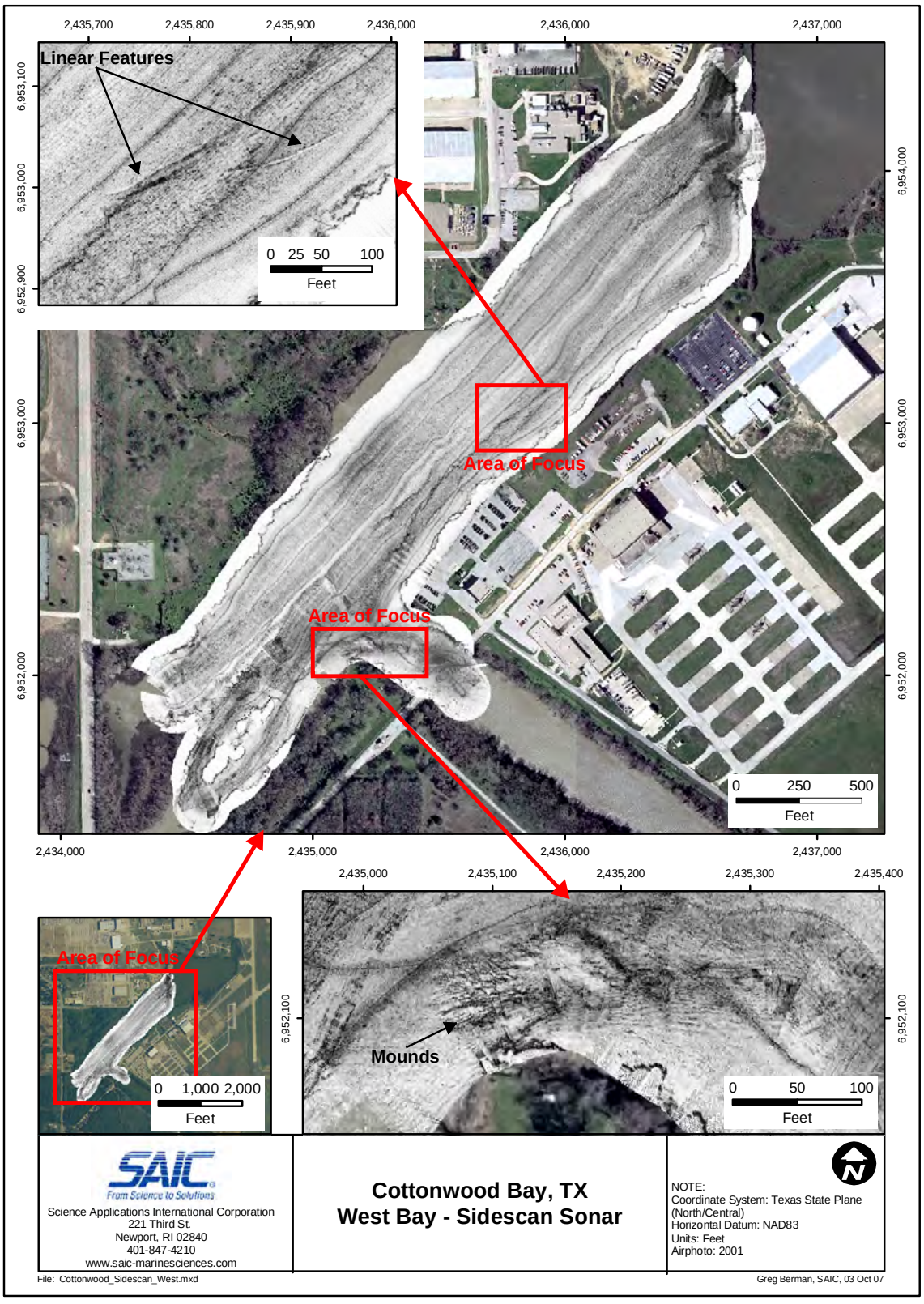

Figure 7.2-10. Side-scan sonar results for Cottonwood Bay West showing features of interest.

In addition to these side-scan observations, visual observations indicated the presence of several stumps (approximately six inches in diameter) sticking out of the water and other submerged natural structures (*e.g.*, fallen trees) in both portions of Cottonwood Bay, especially the central and western areas of Cottonwood Bay West, that were not necessarily evident in the side-scan returns. Rip-rap was also visually observed in Cottonwood Bay West in the northeast corner adjacent to the causeway and an apparent NWIRP loading dock.

Sediment Profile Imaging. A summary of the sediment habitat data collected from the Cottonwood Bay SPI analysis is presented in Table 7.2-2. The location of the final SPI stations for Cottonwood Bay East and West are shown in Figure 7.2-11 and Figure 7.2-12, respectively. Representative SPI photographs from Cottonwood Bay East, the portion of the bay of particular interest for geotextile testing, are provided in Figure 7.2-13.

Table 7.2-2. Summary of sediment profile imaging results for Cottonwood Bay.

Station	Grain Size Major Mode (# replicates)	Camera Penetration Mean (cm)	Boundary Roughness Mean (cm)	Benthic Habitat (# replicates)	Successional Stages Present (# replicates)	RPD Depth Mean (cm)	Methane Present	Bubble Count	OSI Mean	Additional Description	Additional Value
Cottonwood Bay East											
CW-E-1	> 4 phi (1)	8.30	1.92	UN.SF (1)	INDET (1)	2.12	Yes	9	IND	BHQ	4
CW-E-2	> 4 phi (1)	6.79	2.94	UN.SI (1)	INDET (1)	1.40	Yes	0	IND	BHQ	3
CW-E-3	> 4 phi (1)	13.23	1.43	UN.SI (1)	INDET (1)	2.46	Yes	14	IND	BHQ	4
CW-E-4	> 4 phi (1)	7.39	1.31	UN.SI (1)	INDET (1)	2.12	Yes	8	IND	BHQ	4
CW-E-5	> 4 phi (1)	17.97	1.42	UN.SF (1)	INDET (1)	2.22	Yes	3	IND	BHQ	3
CW-E-6	> 4 phi (1)	18.88	1.78	UN.SF (1)	INDET (1)	2.56	Yes	32	IND	BHQ	3
CW-E-7	> 4 phi (1)	10.18	2.90	UN.SI (1)	INDET (1)	3.04	Yes	10	IND	BHQ	3
CW-E-8	> 4 phi (1)	12.30	0.85	UN.SI (1)	ST I (1)	2.16	Yes	23	2.00	BHQ	4
CW-E-9	> 4 phi (1)	13.03	1.66	UN.SI (1)	ST I (1)	2.29	Yes	22	3.00	BHQ	4
CW-E-10	> 4 phi (1)	12.85	2.64	UN.SI (1)	ST I (1)	2.54	Yes	41	3.00	BHQ	4
CW-E-11	> 4 phi (1)	18.90	1.97	UN.SF (1)	INDET (1)	IND	Yes	6	IND	BHQ	IND
CW-E-12	> 4 phi (1)	0.00	0.00	INDET	INDET (1)	IND	No	0	IND	BHQ	IND
CW-E-13	> 4 phi (1)	18.86	1.09	UN.SF (1)	INDET (1)	2.81	Yes	31	IND	BHQ	3
AVG	-	12.21	1.69	-	-	2.34	-	15	2.67	-	3.55
MIN	-	0.00	0.00	-	-	1.40	-	0	2.00	-	3.00
MAX	-	18.90	2.94	-	-	3.04	-	41	3.00	-	4.00
Cottonwood Bay West											
CW-W-1	> 4 phi (1)	11.59	0.99	UN.SI (1)	INDET (1)	1.55	Yes	19	IND	BHQ	2
CW-W-2	> 4 phi (1)	9.04	0.90	UN.SI (1)	INDET (1)	2.15	Yes	26	IND	BHQ	3
CW-W-3	> 4 phi (1)	14.54	0.54	UN.SF (1)	INDET (1)	1.91	Yes	42	IND	BHQ	2
CW-W-4	> 4 phi (1)	10.00	0.87	UN.SI (1)	INDET (1)	2.03	Yes	27	IND	BHQ	3
CW-W-5	> 4 phi (1)	15.89	0.95	UN.SF (1)	INDET (1)	1.84	Yes	34	IND	BHQ	2
CW-W-6	> 4 phi (1)	9.16	2.61	UN.SI (1)	INDET (1)	2.20	Yes	35	IND	BHQ	3
CW-W-7	> 4 phi (1)	13.94	2.07	UN.SF (1)	INDET (1)	2.08	Yes	28	IND	BHQ	3
CW-W-8	> 4 phi (1)	13.30	2.13	UN.SF (1)	INDET (1)	1.74	Yes	74	IND	BHQ	2
CW-W-9	> 4 phi (1)	8.07	3.32	UN.SI (1)	INDET (1)	3.04	Yes	7	IND	BHQ	4
CW-W-10	> 4 phi (1)	6.86	0.95	UN.SI (1)	INDET (1)	1.84	Yes	9	IND	BHQ	2
CW-W-11	> 4 phi (1)	4.65	1.04	UN.SI (1)	INDET (1)	1.77	Yes	2	IND	BHQ	2
CW-W-12	> 4 phi (1)	12.38	0.36	UN.SF (1)	INDET (1)	2.45	Yes	9	IND	BHQ	3
CW-W-13	> 4 phi (1)	5.85	1.19	UN.SI (1)	INDET (1)	1.64	Yes	14	IND	BHQ	2
CW-W-14	> 4 phi (1)	12.12	1.68	UN.SI (1)	INDET (1)	2.20	Yes	17	IND	BHQ	2
CW-W-15	> 4 phi (1)	12.10	0.93	UN.SI (1)	ST I (1)	2.04	Yes	49	2.00	BHQ	3
CW-W-16	> 4 phi (1)	13.18	1.53	UN.SI (1)	INDET (1)	2.25	Yes	18	IND	BHQ	3
CW-W-17	> 4 phi (1)	14.43	2.00	UN.SI (1)	INDET (1)	2.27	Yes	16	IND	BHQ	3
CW-W-18	> 4 phi (1)	13.66	0.56	UN.SI (1)	INDET (1)	2.34	Yes	12	IND	BHQ	3
CW-W-19	> 4 phi (1)	1.35	2.69	HR (1)	INDET (1)	1.37	No	0	IND	BHQ	3
CW-W-20	> 4 phi (1)	13.72	0.95	UN.SF (1)	INDET (1)	1.99	Yes	57	IND	BHQ	2
CW-W-21	> 4 phi (1)	6.76	2.37	UN.SF (1)	INDET (1)	IND	Yes	11	IND	BHQ	IND
CW-W-22	> 4 phi (1)	16.77	1.40	UN.SF (1)	INDET (1)	1.99	Yes	37	IND	BHQ	2
CW-W-23	> 4 phi (1)	13.23	2.96	UN.SF (1)	INDET (1)	1.91	Yes	21	IND	BHQ	3
CW-W-24	> 4 phi (1)	10.73	2.32	UN.SI (1)	INDET (1)	1.97	Yes	18	1.00	BHQ	2
CW-W-25	> 4 phi (1)	18.55	2.02	UN.SF (1)	INDET (1)	2.02	Yes	27	IND	BHQ	3
AVG	-	11.27	1.57	-	-	2.02	-	24	1.50	-	2.58
MIN	-	1.35	0.36	-	-	1.37	-	0	1.00	-	2.00
MAX	-	18.55	3.32	-	-	3.04	-	74	2.00	-	4.00

Habitat Classifications: UN.SI - Unconsolidated Soft Bottom Silt; UN.SF - Unconsolidated Soft Bottom Very Soft Mud; HR - Hard Bottom/Hard Clay

Successional Stages: INDET - Indeterminate; ST I - Successional Stage I (opportunistic pioneering species)

Other: RPD - Redox Potential Discontinuity; OSI - Organism Sediment Index (marine); BHQ - Benthic Habitat Quality Index (freshwater)

Figure 7.2-11. Location of SPI stations for Cottonwood Bay East.

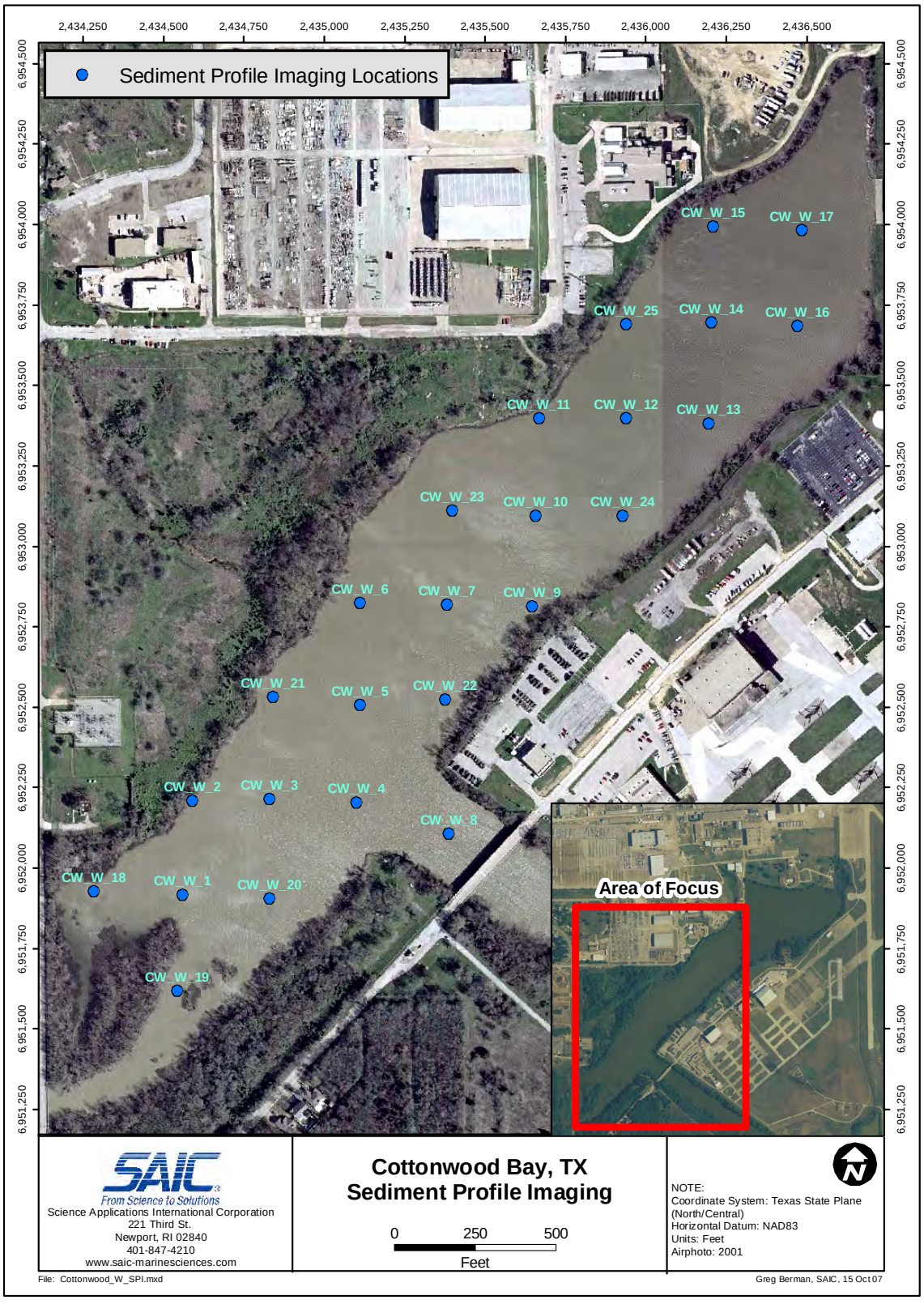

Figure 7.2-12. Location of SPI stations for Cottonwood Bay West.

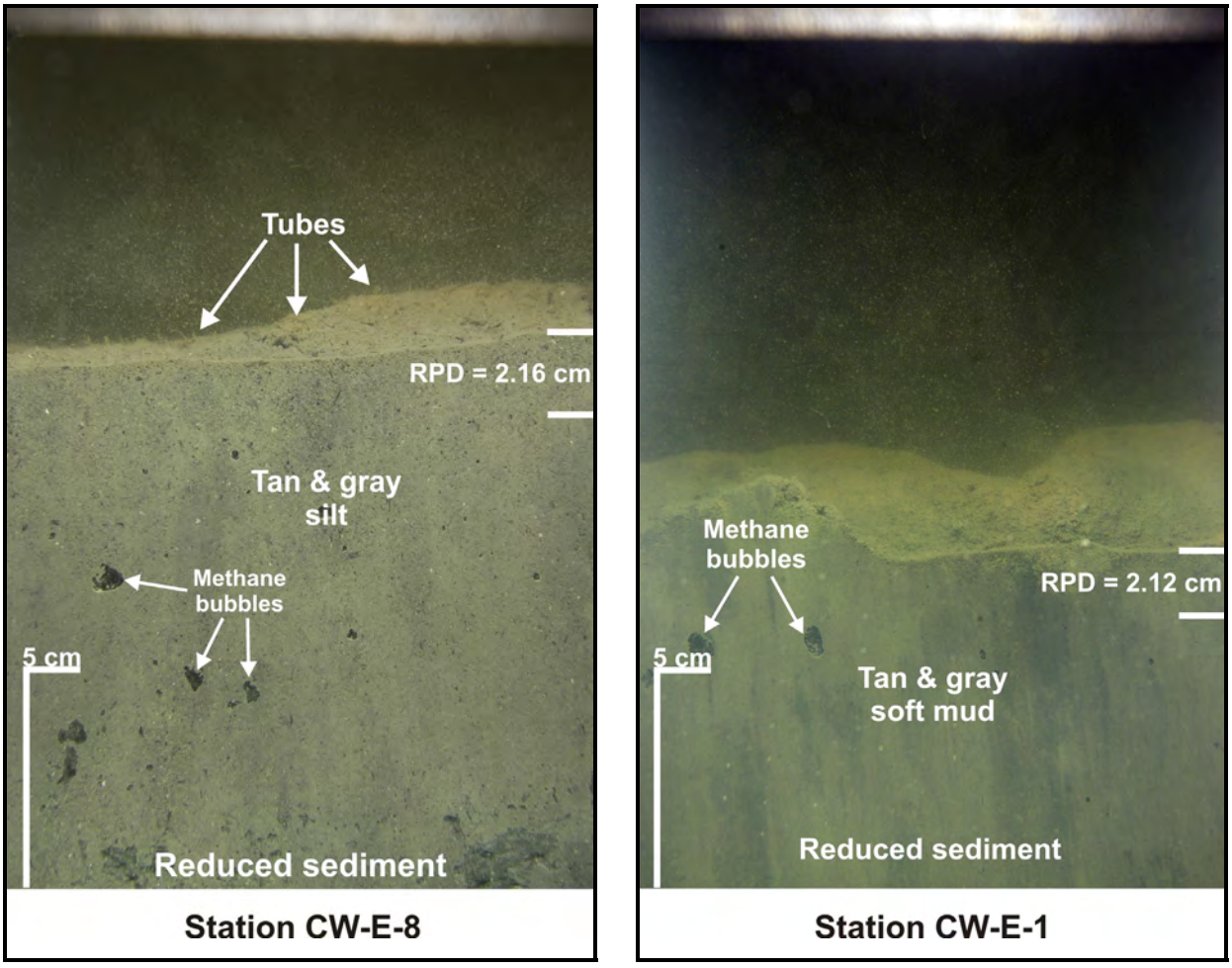

Figure 7.2-13. Representative SPI photographs for Cottonwood Bay East showing unconsolidated soft mud (UN.SF) and unconsolidated silty sand (UN.SI) benthic habitats with reduced sediment at depth and methane bubbles.

The grain size major mode for all images from both portions of the bay was consistent at >4 phi, which indicates predominantly fine-grained material such as silt or clay according to the Udden-Wentworth size class scale.

For Cottonwood Bay East, the mean camera penetration ranged from 0.00 cm (no penetration) to 18.90 cm, indicating a wide range of bottom compressive strengths. The average penetration mean for the East was relatively high at 12.21 cm, thus indicating a trend towards softer sediments. The minimum penetration value of 0.00 cm was encountered at station CW-E-12 at which penetration is believed to have been obstructed by natural debris (*e.g.*, tree branches) present on the lake floor. For Cottonwood Bay West, the mean camera penetration ranged from 1.35 cm to 18.55 cm, thus also indicating a wide range of bottom compressive strengths. The average penetration mean for the West was relatively high at 11.27 cm, again showing a trend towards softer sediments.

Mean boundary roughness in Cottonwood Bay East ranged from 0.00 cm (no boundary visible) to 2.94 cm, which signifies an uneven surface at some stations. Similar results were encountered in Cottonwood Bay West with boundary roughness values ranging from 0.36 cm to 3.32 cm.

For benthic habitat, all but one of the 13 stations in Cottonwood Bay East were classified as "Unconsolidated Soft Bottom" (UN). These soft bottom stations were then further classified as either "Silty" (UN.SI) or "Very Soft Mud" (UN.SF). The one station that was not classified as unconsolidated soft bottom (CW-E-12) was considered indeterminate due to low camera penetration caused by the presence of debris. Likewise, the benthic habitats in all but one of the 25 stations in Cottonwood Bay West were characterized as either "Silty" (UN.SI) or "Very Soft Mud" (UN.SF) unconsolidated bottom. The lone western station that was not characterized as unconsolidated soft bottom (CW-W-19) was otherwise considered "Hard Bottom/Hard Clay" (HR). This station was located at the extreme western corner of the study area adjacent to a region of dense aquatic vegetation.

Successional stage could only be determined at three stations in Cottonwood Bay East (CW-E-8, CW-E-9, CW-E-10) and one station in Cottonwood Bay West (CW-W-15). Each of these areas was considered a "Stage I" (ST I) infaunal habitat, which often feature the presence of opportunistic, pioneering species with rapid population growth rates that quickly colonize a site following disturbance and generally include smaller species that inhabit the uppermost portion of the substrate, feeding on surface sediments or from the water column (Rhoads and Germano 1982, 1986). Mean RPD depth in Cottonwood Bay ranged from 1.40 cm to 3.04 cm in the east and from 1.37 cm to 3.04 cm in west. These values are generally indicative of moderately well-oxygenated surface sediments. The presence of methane bubbles was observed in images from all stations in both portions of the bay with the exception of CW-E-12 and CW-W-19 (low penetration stations), thus signifying anoxic conditions at depth across the entire study area. Bubble counts per image reached a maximum of 41 (Station CW-E-10) for the images from Cottonwood Bay East and a maximum of 74 (Station CW-W-8) for the images from Cottonwood Bay West.

Due to indeterminate data for some of the other parameters, the mean OSI value could only be calculated for three stations in Cottonwood Bay East (CW-E-8, CW-E-9, CW-E-10) and two stations in Cottonwood Bay West (CW-W-15, CW-W-24). These values ranged from +1.00 to +3.00. In a marine environment, index values in this range would indicate highly degraded or disturbed overall habitat conditions. Because Cottonwood Bay is a freshwater habitat, however, OSI values are uncertain because the organic enrichment and disturbance paradigms used to assign benthic successional stage, which are included in the OSI calculations, are not well known (Iocco *et al*. 2000). Thus a more applicable BHQ index based on a combination of surface and subsurface biogenic features was calculated. This parameter could be determined for 11 of 13 stations in Cottonwood Bay East and 24 of 25 stations in Cottonwood Bay West and values ranged from +2.00 to +4.00. Index values in this range are typically associated with pioneering communities in moderately stressed habitats (Iocco *et al*. 2000).

Overall, the SPI photographs collected from Cottonwood Bay revealed a generally consistent soft bottom with degraded habitat conditions. There was some variability between stations in

terms of sediment color and amount of methane bubbles present, but this variability was not as significant as in the adjacent Mountain Creek Lake where a similar SPI survey revealed soft bottom at some stations and shell bottom at other stations within the same cove. The fact that bottom conditions were consistent in Cottonwood Bay put less emphasis on SPI results in determining a specific target area for full-scale geotextile testing as compared to other survey parameters.

Sediment Vibracoring. The locations of the Cottonwood Bay West vibracore stations corresponded to previously occupied SPI stations CW-8 and CW-17 and are shown with the yellow markers in Figure 7.2-14. Station CW-8 was targeted due to its location in the mouth of the diversion channel, thus making it likely to show historic sedimentation patterns due to potential influx into the bay. At station CW-8, the sediment proved harder than expected with regard to achieving proper penetration and only a few inches of extremely hard clay could be retrieved on the first two attempts. After moving the coring vessel approximately 125 ft closer to the shoreline from the exact target area, a suitable 38-inch intact sediment core was obtained on the third attempt (C) to be photographed and characterized. The surface water was approximately 28 inches deep at this location.

Station CW-17 was targeted due to its proximity to the causeway, thus making it more likely to be representative of conditions in Cottonwood Bay East where vibracoring was not attempted due to logistical concerns. At station CW-17, the sediment proved softer than station CW-8 and without a core catcher all material was lost from the tube during the first attempt. The second attempt (B) yielded a 28-inch intact sediment core, but this sample was not deemed acceptable for full analysis because it was believed that some material was lost during the extrusion process. Nevertheless, this replicate was photographed. Finally, a suitable 36-inch intact sediment core was obtained on the third attempt (C) to be photographed and characterized. The surface water was approximately 54 inches deep at this location.

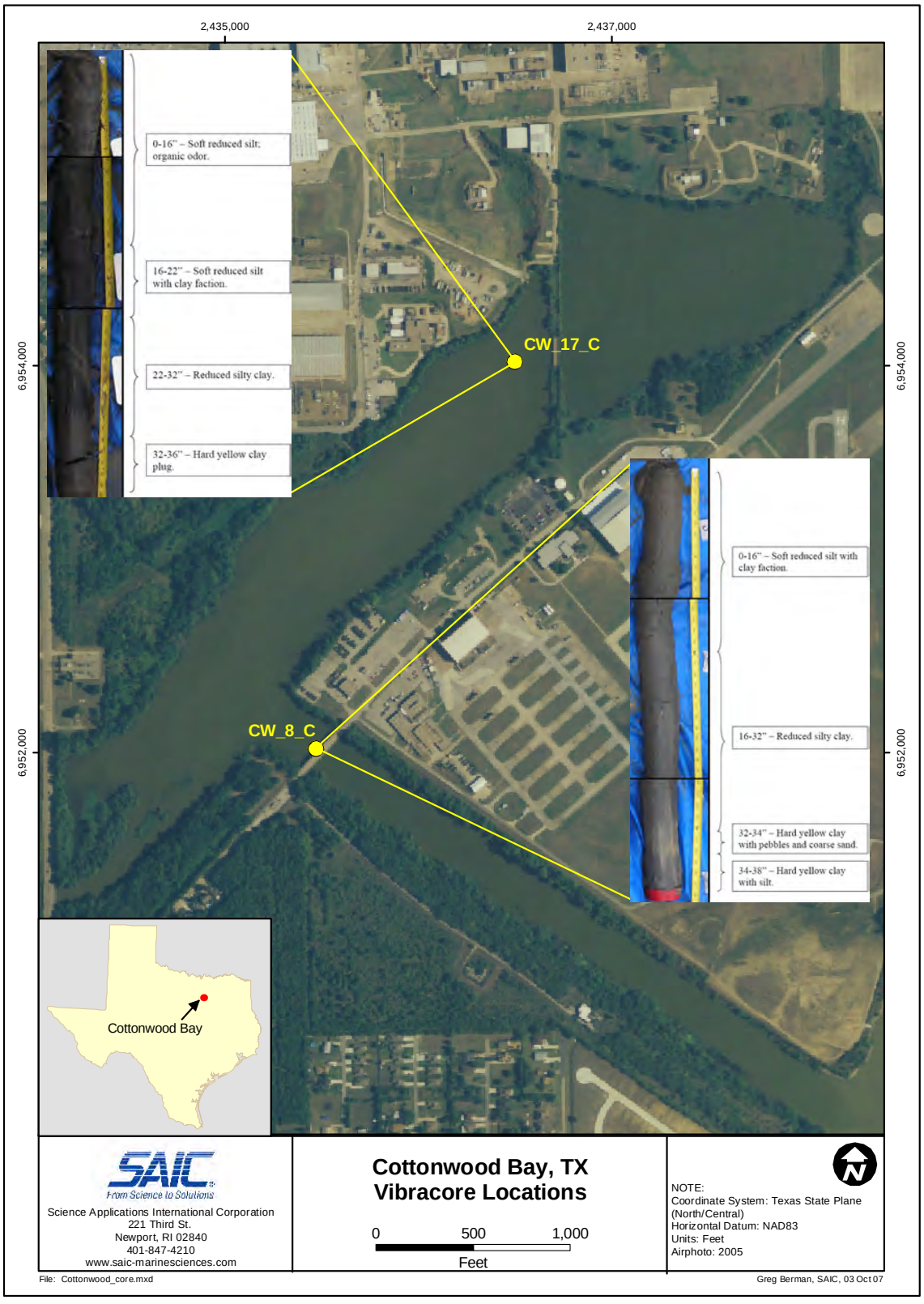

Figure 7.2-14. Locations and field photographs of the sediment vibracores collected from Cottonwood Bay West (Station CW-8 and Station CW-17).

Photographic mosaics of the sediment vibracores retained from stations CW-8 and CW-17 in Cottonwood Bay West are also provided in Figure 7.2-14.

Core CW-8-C was characterized as follows:

- Station – CW-8
- Total length – 38 inches.
- 0-16" – Soft reduced silt with clay faction.
- 16-32" – Reduced silty clay.
- 32-34" – Hard yellow clay with pebbles and coarse sand.
- 34-38" – Hard yellow clay with silt.

Core CW-17-C was characterized as follows:

- Station – CW-17
- Total length – 36 inches.
- 0-16" – Soft reduced silt; organic odor.
- 16-22" – Soft reduced silt with clay faction.
- 22-32" – Reduced silty clay.
- 32-36" – Hard yellow clay plug.

These characterizations were ultimately used to calibrate and confirm the sub-bottom profiling dataset for Cottonwood Bay. Sediment thickness results from the vibracores were consistent with the soft surface and hard underlying layers identified in the sub-bottom survey. In addition, the vibracore characterizations were also used to confirm the grain size and habitat conditions identified in the SPI photographs.

Groundwater Seepage Survey. Results for the Cottonwood Bay groundwater seepage survey were provided to SAIC in the *Draft Data Report, Groundwater Upwelling Survey, Naval Weapons Industrial Reserve Plant, Cottonwood Bay, Dallas, Texas* (Groundwater Seepage, Inc. 2007). In this report, horizontal mapping of conductivity and temperature data obtained with the Trident probe system at the groundwater-surface water interface were used to identify likely areas of groundwater discharge along various N-S transects. Final Trident probe stations for the Cottonwood Bay groundwater seepage survey are shown in Figure 7.2-15.

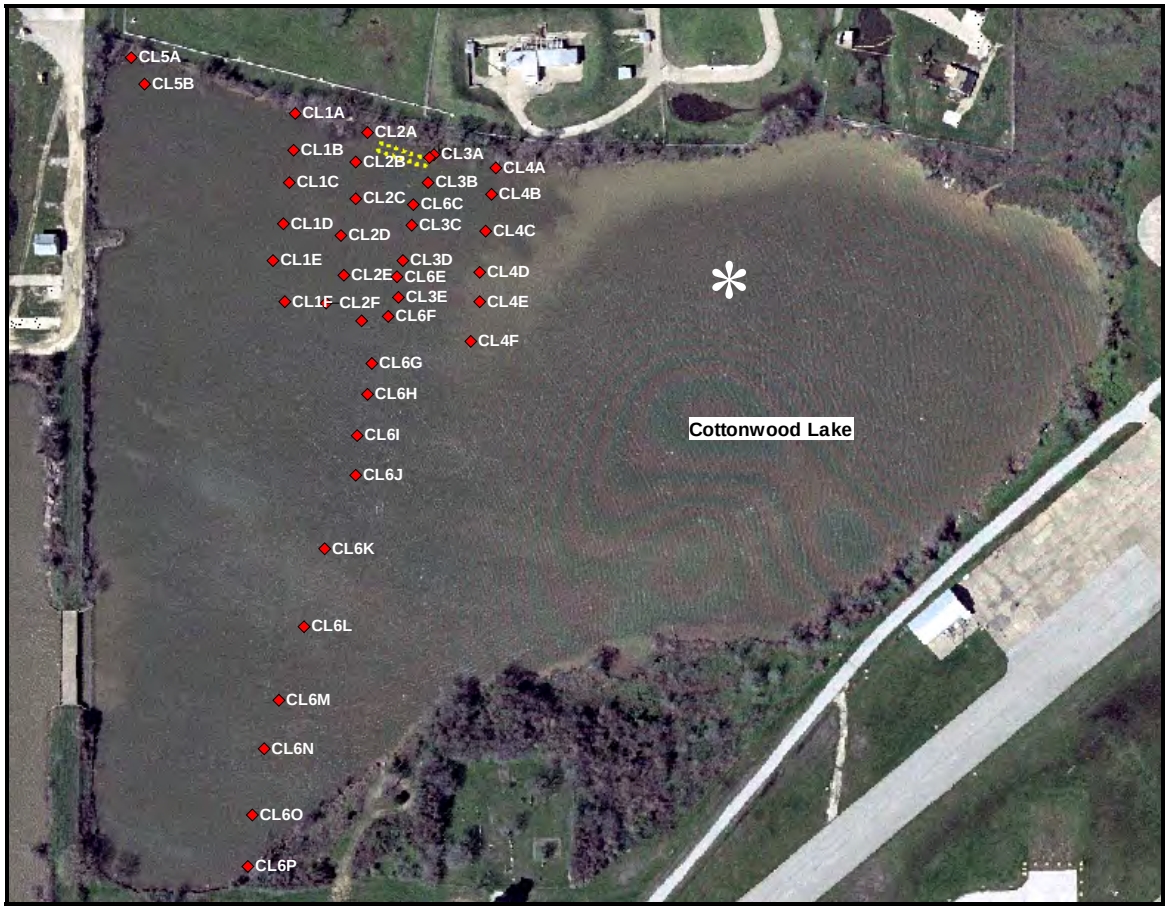

Figure 7.2-15. Trident probe stations for the Cottonwood Bay groundwater seepage survey.

During the summer when the Cottonwood Bay seepage survey was conducted, groundwater in this region was expected to be cooler than the surface water. Groundwater temperatures in an upland monitoring well averaged 23°C during the course of the survey while Cottonwood Bay surface water temperatures as determined with the Trident probe ranged from 27.8°C to 29.8°C and averaged 28.5°C across stations. Subsurface temperatures as determined by the Trident probe ranged from 24.8°C to 28.2°C and averaged 26.9°C across stations. All areas with subsurface water temperatures less than the surface water minimum were considered to represent zones of potential groundwater upwelling.

Surface water conductivity as determined with the Trident probe ranged from 0 mS/cm to 0.5 mS/cm and averaged 0.39 mS/cm across stations. Subsurface water conductivity as determined with the Trident probe ranged from 0 mS/cm to 3.1 mS/cm and averaged 1.09 mS/cm across stations. In contrast to the temperature differences, all areas with subsurface conductivity measurements greater than the surface water maximum were considered to represent zones of potential groundwater upwelling. The increase in conductivity in Cottonwood Bay groundwater could be caused by increased contaminant loads being transported from upland properties. Complete Trident probe temperature and conductivity statistics for Cottonwood Bay are summarized in Table 7.2-3 below.

	Probe temperature C	Probe cond. mS/cm	Reference temperature C	Reference cond. mS/cm
Minimum	24.818	0.600	27.805	0.381
Maximum	28.226	2.100	29.839	0.500
Average	26.876	1.093	28.485	0.393
Stdev	1.148	0.386	0.509	0.022

Table 7.2-3. Trident probe temperature and conductivity statistics for Cottonwood Bay.

In general, cooler subsurface temperatures were observed in association with higher subsurface conductivity for several of the outer transect stations. The majority of these areas were found to be located approximately 200 feet from the northern shoreline, but similar conditions were also observed in one area near the southern shoreline. Spatial results from the relative subsurface temperature and conductivity mapping process were used to define three zones of increasing groundwater discharge potential as shown in Figure 7.2-16 below. The zone with the highest potential for groundwater seepage (blue) begins approximately 200 feet offshore. Lithology of an upland monitoring well coupled with observed resistance to Trident probe penetration at some of the inshore stations seemed to indicate the presence of a clay layer deflecting terrestrial groundwater flow further offshore.

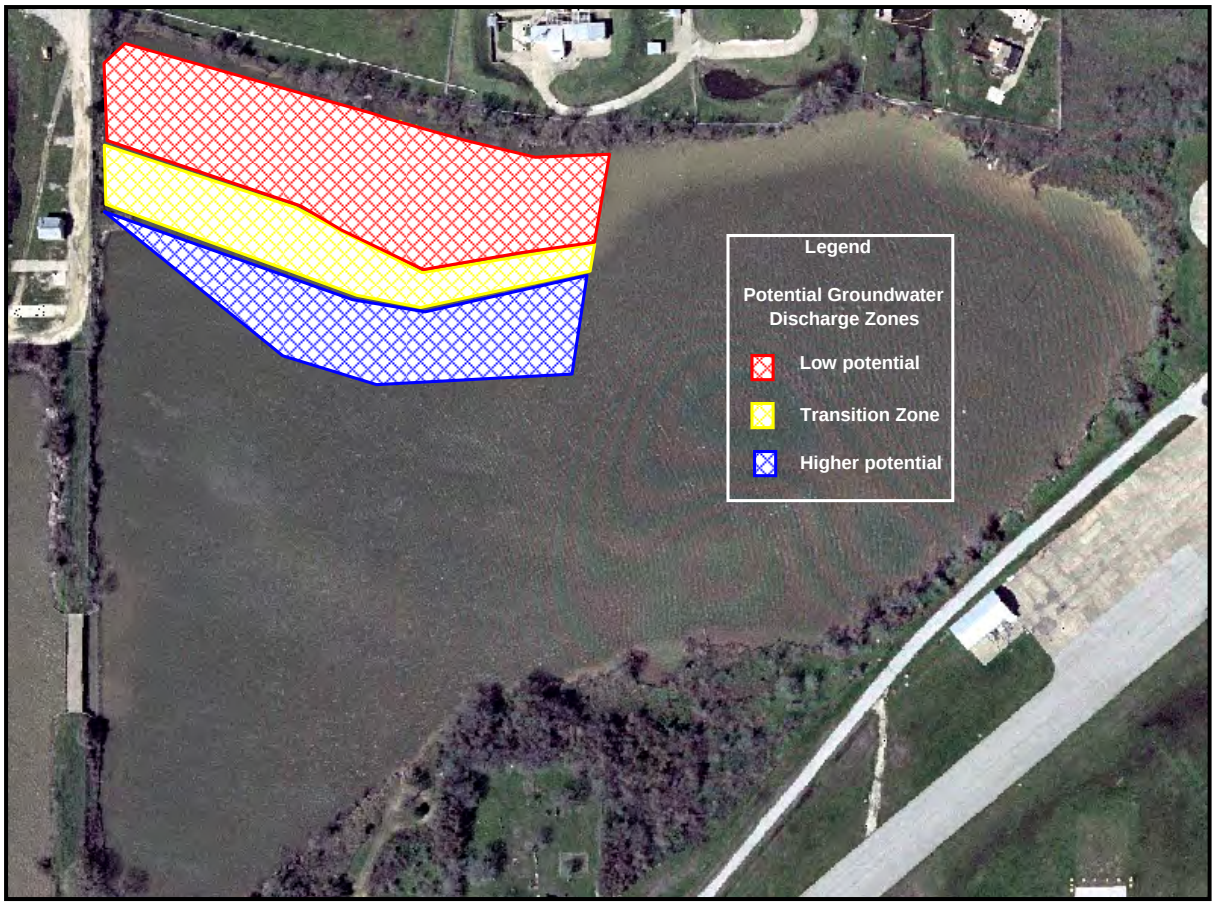

Figure 7.2-16. Potential groundwater discharge zones for Cottonwood Bay.

7.2.4. Target Area Establishment

Based on the overall results of the Cottonwood Bay geophysical investigation, the eastern portion of the bay was selected as the general area of focus for further full-scale geotextile testing due to greater water depths, increased sediment layer thickness, consistent bottom characteristics and the presence of confirmed groundwater plumes that will allow for accurate assessment of flux through the various test mat arrangements. These parameters were then considered both individually and in combination to select a specific target area within Cottonwood Bay East to serve as the deployment location for the full-scale prototype mat system featuring four different 25 x 25 ft test arrangements and one 25 x 25 ft control area to be constructed for Task 4 during the year three effort. Because the side-scan sonar survey did not identify any major obstacles in Cottonwood Bay East and the SPI photographs showed a consistently unconsolidated soft bottom environment with generally degraded habitat conditions, these two parameters could not be used to select any preferred areas. They did, however, indicate that no areas should be eliminated from consideration due to logistically unfavorable conditions such as an abnormally hard bottom or debris that could potentially impede mat placement. Instead, groundwater seepage results and sediment chemistry data from previous sampling events were given the most weight in selecting a target area compatible with project goals.

The preferred target area for future full-scale prototype mat testing is shown in Figure 7.2-17. This area is located in the western portion of Cottonwood Bay East approximately 200 feet south of the NWIRP shoreline and corresponds to the region of high potential groundwater discharge shown in Figure 7.2-16 above. Chemistry results for this area indicate consistently elevated levels of lead and benzo[a]pyrene and the relatively high density of available groundwater seepage and sediment chemistry data lead to low potential variability and decreased uncertainty. Sub-bottom profiling and SPI results did not show any major obstructions that could impede groundwater flow or contaminant transport in this area, but the side-scan survey did indicate some linear features of note nearby. Water depths in this zone are approximately six feet which could negatively impact mat deployment and ultimate retrieval as well as the placement of passive sampling devices by precluding the use of waders by field personnel. The location of this target area in the middle of the bay may also provide logistical complications in deploying the sand cap for the various full-scale mat treatments from either the southern shoreline or the causeway. If the preferred target area is ultimately deemed inaccessible, a second area of high potential groundwater seepage and suitable contamination is also shown in Figure 7.2-17 closer to the southern shoreline.

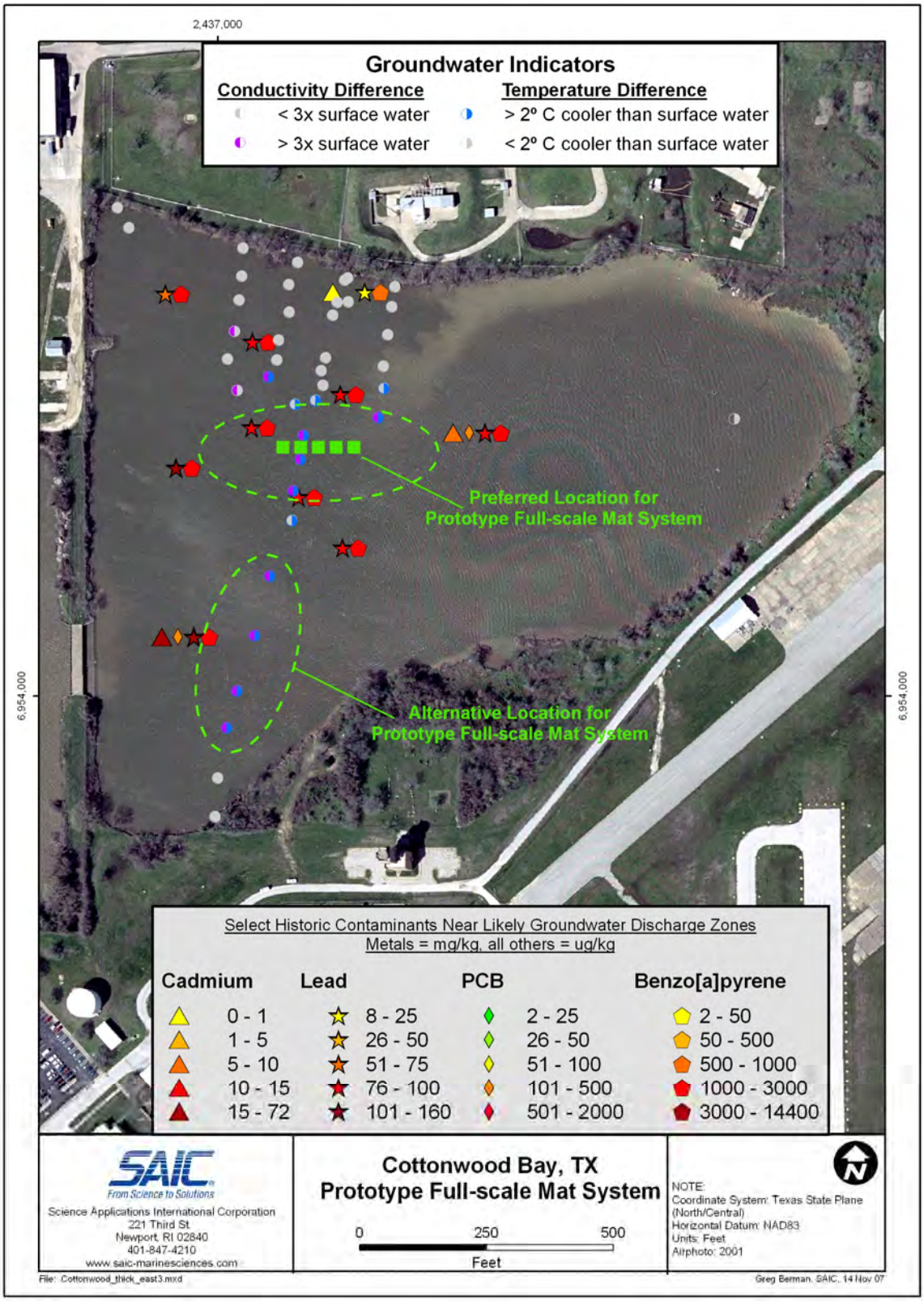

Figure 7.2-17. Preferred target areas for future full-scale prototype mat system deployment based on the results of the Cottonwood Bay geophysical surveys.

7.3. TASK 3: GEOTEXTILE TESTING

The purpose of the geotextile testing task for this project is to field test different types of geotextile material at the selected pilot site to assess whether biofouling and biofilm formation will adversely affect the ability of the fabric to allow water to pass through the final mat design, whether environmental weathering compromises the ability of the mat to retain the amendment material and whether environmental weathering compromises the reactivity of the sequestration agents. This task also included laboratory gradient ratio testing and finite element analysis to assess stability, clogging potential and prospective sediment deformation for clean, non-fouled mats before the weathered test mats are retrieved. To date the entire geotextile testing task has not been completed. A summary of the year two accomplishments for each component of this task are provided in the following sections.

7.3.1. Field Evaluation

Fourteen test mats of various compositions were deployed for field testing in Cottonwood Bay East in June 2007 as described in Section 6.3. Retrieval events for the two rows of replicates are planned for December 2007 and July 2007, respectively. Once these retrieval events occur, replicates of the various mats will be shipped to the UNH laboratory for performance testing with a geotechnical test column system via the ASTMD 5101 method. Until these laboratory tests are conducted in year three, no new geotextile field testing results will be available.

7.3.2. Gradient Ratio Testing

Preliminary laboratory gradient ratio testing conducted during year one showed that trapped bubbles are a significant impediment to groundwater flux through a fine grained matrix and that sample preparation in a nitrogen atmosphere may be successful in eliminating these bubbles.

Similar testing was conducted in year two using three stock geotextiles (CETCO 1, CETCO 2, and CETCO 3) and a clean organoclay mat following the methods described in Section 6.3.2. The gradient ratio value over time obtained for the CETCO 1 geotextile is shown in Figure 7.3-1.

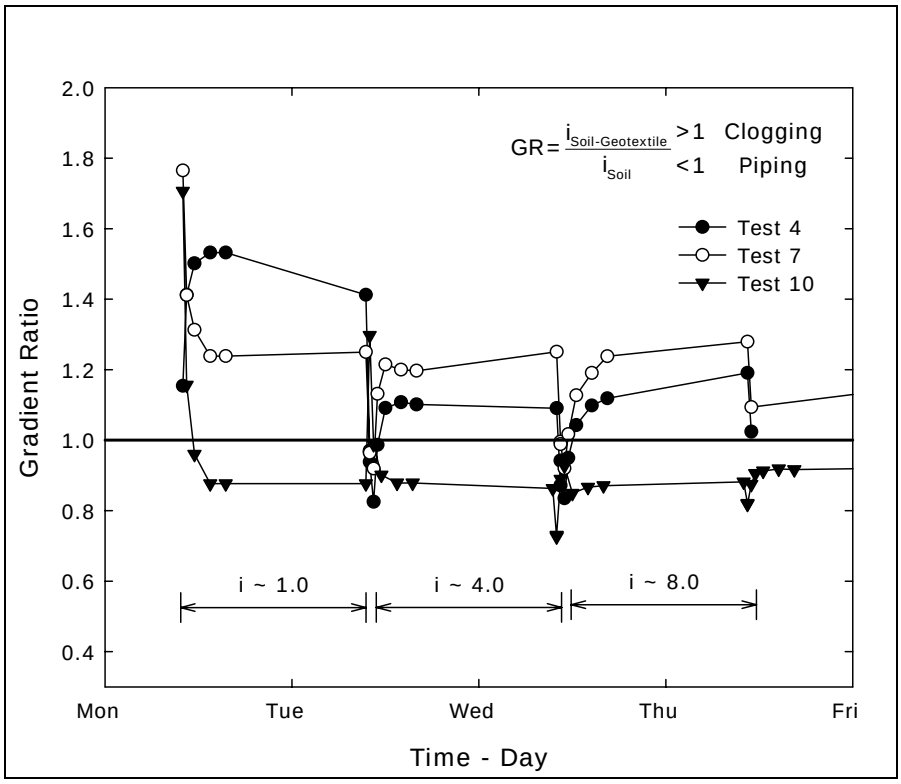

Figure 7.3-1. Gradient ratio value vs. time for the CETCO 1 geotextile.

A stable system was achieved throughout the experiments for the CETCO 1 geotextile. The first two tests show a stable system on the clogging side of the gradient ratio value, except for high hydraulic gradients which are not expected under typical field applications due to the homogeneity of the sediments near the surface. The third test shows a stable system on the piping side of the gradient ratio scale during the low to mid range of hydraulic gradients. For hydraulic gradients of eight and up, a slowly increasing trend towards the clogging side is observed. This trend can be attributed in part to the increasing consolidation of the sediment lower section (downward flow) and the forced movement of particles near the contact surface between the geotextile and the sediment.

The gradient ratio value over time obtained for the CETCO 2 geotextile is shown in Figure 7.3-2.

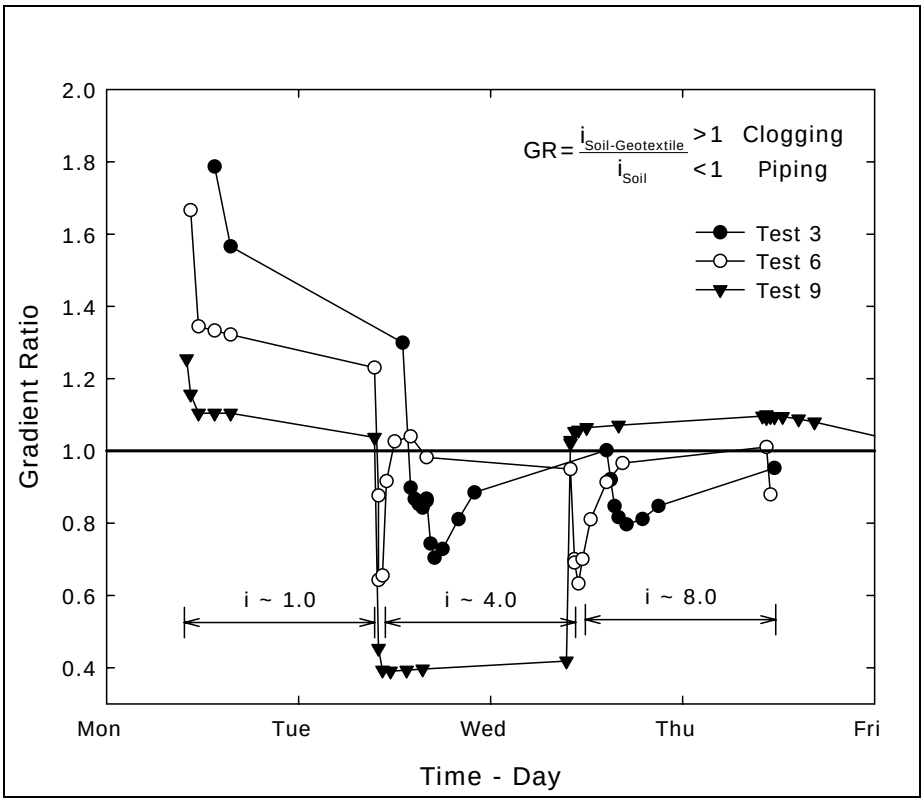

Figure 7.3-2. Gradient ratio value vs. time for the CETCO 2 geotextile.

At low hydraulic gradient the gradient ratio value for the CETCO 2 geotextile moves consistently towards stabilization near the GR=1 value, on the clogging side of the scale. However, this value seems to stabilize rapidly at higher hydraulic gradients (i>4). Test 9 shows a very low gradient ratio value (~0.4) at i=4, and increases to GR=1.05 immediately on the next hydraulic gradient stage (i=6). This particular behavior is attributed to experimental causes rather than real filter effects. At high hydraulic gradient (i>8) the system is stable but shows the gradient ratio value moving steadily to the clogging side of the scale.

The gradient ratio value over time obtained for the CETCO 3 geotextile is shown in Figure 7.3-3.

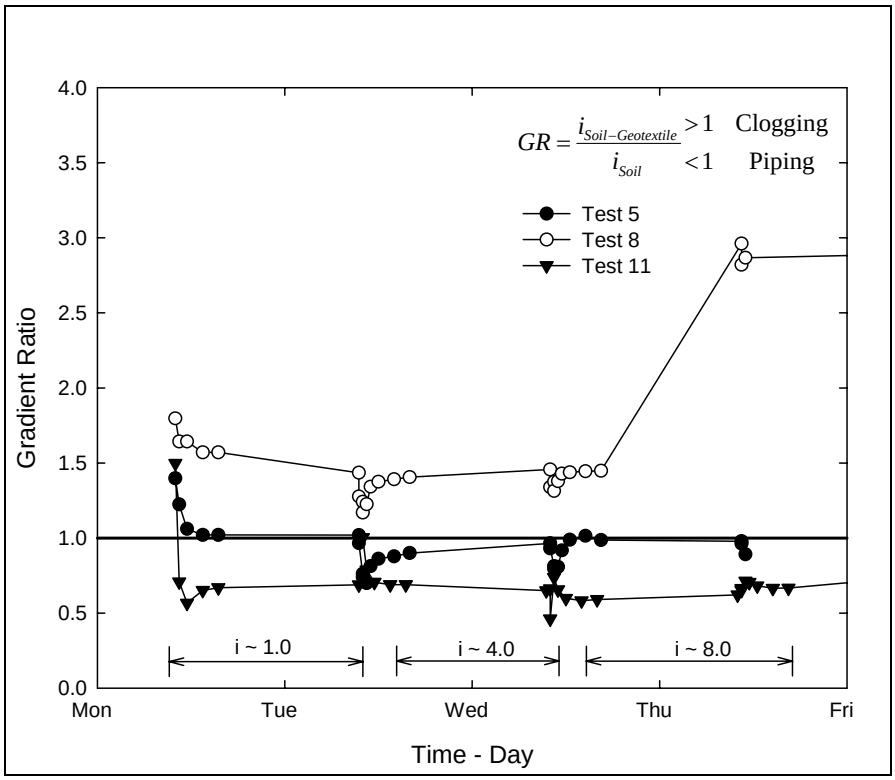

Figure 7.3-3. Gradient ratio value vs. time for the CETCO 3 geotextile.

The result from Test 8 for the CETCO 3 geotextile appear to be abnormally high with an abrupt step on the *i*=8 region. This abnormal behavior might be attributed to small wall seepage flow that was undetected during the experiment. The average trend of the gradient ratio value for the tests is very close to the piping-clogging border, and slightly lower than GR=1. Moreover, the system shows a nearly steady condition at the end of each hydraulic gradient stage, thus indicating that the system is in a stable condition without further clogging or piping development. Even under high hydraulic gradient (*i*=8) the system appears to be in a nearly steady state condition, which was not the case for other geotextiles tested.

The same gradient ratio test carried out on the three stock geotextiles is also planned for clean reactive mats containing different amendments, but to date these tests have only been completed for a single mat containing organoclay. The gradient ratio value over time obtained for a clean organoclay mat is shown in Figure 7.3-4.

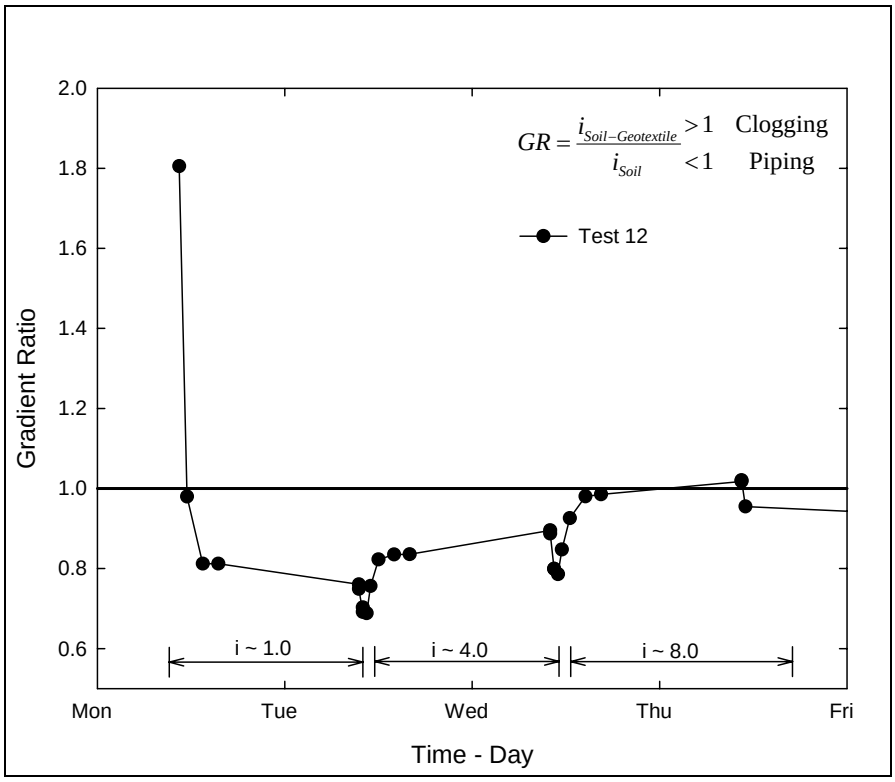

Figure 7.3-4. Gradient ratio value vs. time for the clean organoclay mat.

The results from the organoclay mat gradient ratio test indicate that the filter system is stable under low hydraulic gradient (*i*~1) as would be expected to occur in field applications. For hydraulic gradients between 4 and 8 the gradient ratio value shows a trend towards the clogging side of the scale and with clear indications of stabilization by reaching a constant value. This behavior may be due to particle reaccommodation (*i.e.*, particles rearranging themselves from a more loosely packed configuration to a more tightly packed arrangement) caused by the increasing effective stress acting on the system.

The quantity of sediment particles passing trough the geotextiles during each gradient ratio test was determined as an indicator of flow path tortuosity, or the measure of how much the path of a particle twists and curves as it passes through the material. For a given geotextile, the greater the tortuosity, the more difficult it is for a particle to pass through. The weight of passing material versus mesh size versus mass per area of geotextile is shown in Figure 7.3-5.

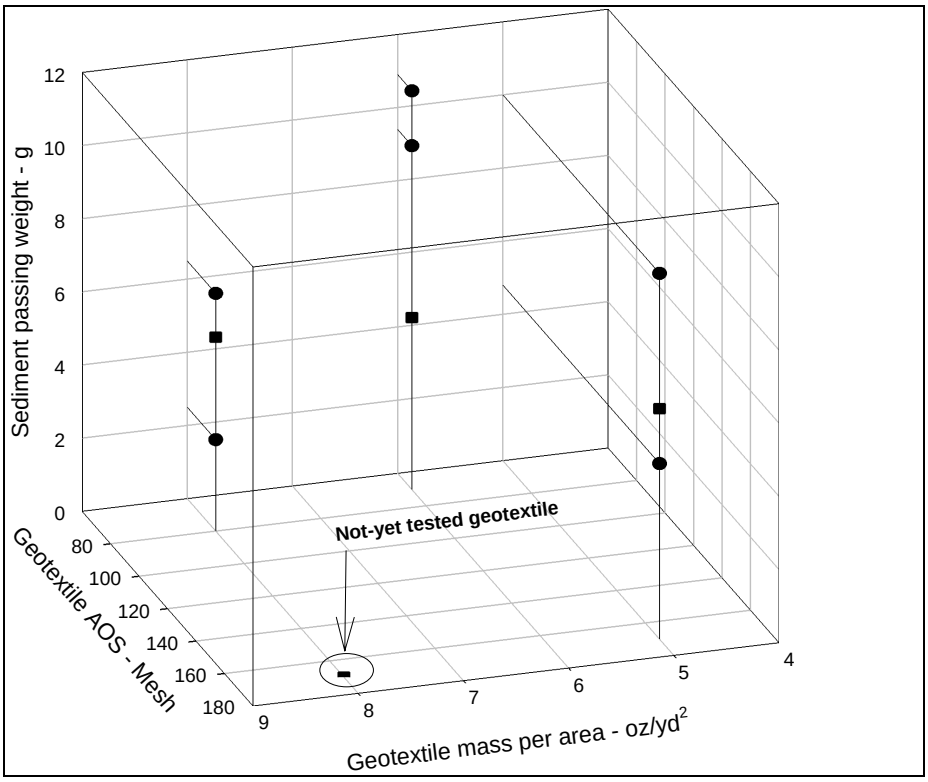

Figure 7.3-5. Weight of sediment passing through each geotextile during the gradient ratio tests.

These results show that the amount of sediment passing through the geotextile is highly dependant on both the mesh size and the mass per area of the geotextile. There is a combined effect in which more weight of sediment passes trough the geotextile for larger mesh size and/or lower geotextile mass per area (tortuosity). It should be noted, however, that conclusion is based on the mass of sediment crossing the geotextile rather than the particle size. Further grain size distribution tests of the sediment samples will provide information regarding the relationship between sediment particle size, tortuosity and geotextile AOS. The location of a fourth geotextile (Typar 3801) is shown in Figure 7.3-5, but this material has not yet been included in a gradient ratio test. Testing will be conducted for this geotextile for completeness of the study, but results will not be considered in reactive mat construction.

A similar sediment passage evaluation will be conducted on the weathered small-scale mats when they are subjected to gradient ratio testing following retrieval. Preliminary results on the clean organoclay mat indicate that 3.8 grams of sediment crossed the material during the gradient ratio test. This result shows that the increase in tortuosity when a complete mat is used compared to a single layer geotextile strongly reduces the weight of particles passing through the system. Preliminary results on the individual stock geotextiles indicate that the different arrangements behave remarkably similar regardless of material, mass per area or AOS. The amount of sediment passing through the weathered small-scale test mats is expected to be fabric dependent based on the amount of biofouling, but the limited range of fabrics under consideration may indicate that geotextile type is not a very significant variable in final mat construction.

7.3.3. Finite Element Analysis

Finite element analyses conducted for this project in year two incorporated various geotextile components to assess increasingly sophisticated deformation and porewater pressure scenarios beyond the basic sand cap investigated in the preliminary models. Year two results from the various finite element models generated using PLAXIS v. 8.0 software are presented in the following sub-sections.

Uncoupled Consolidation Model. The uncoupled consolidation model computed the *in situ* stress state of the underlying sediment assuming no steady state or transient groundwater flow. Figure 7.3-6 below shows how the excess pore pressure dissipates with time for this model and that 90% of the consolidation occurs at 400 days, while the 95% consolidation is reached after 600 days.

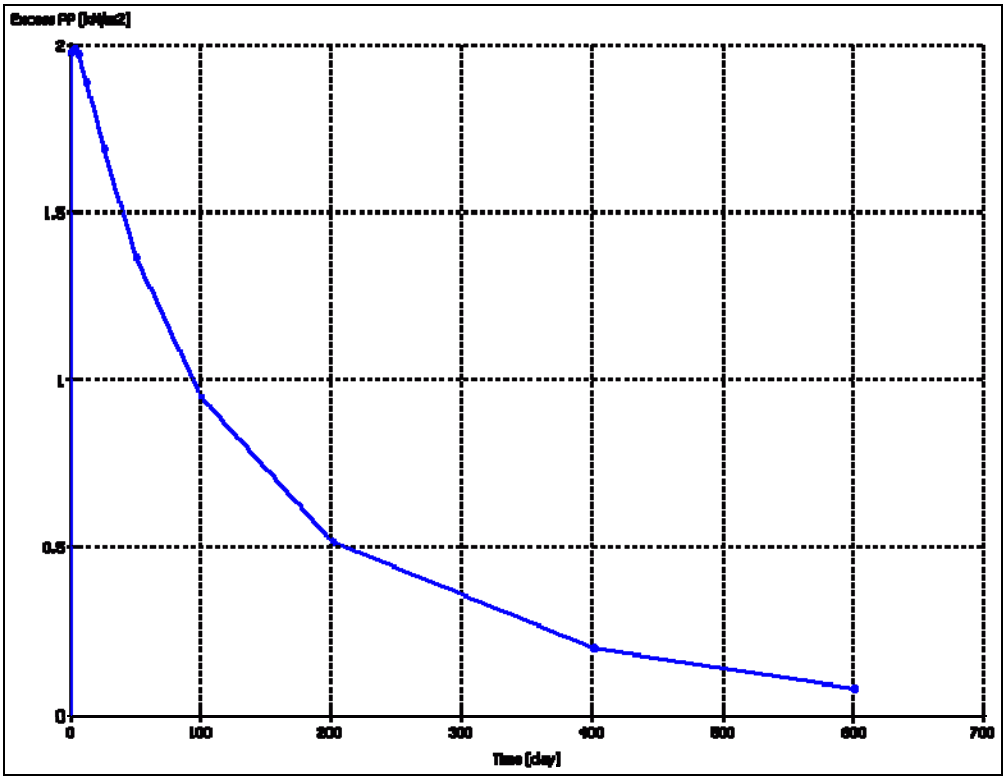

Figure 7.3-6. Excess pore pressure dissipation in the underlying sediment for the uncoupled consolidation finite element model.

Confirmation of this curve can be performed by comparing the pressure induced by the mat and the maximum excess pore pressure beneath the sediment through the following equation:

$$ExcessPP = \gamma' \cdot thickness_{mat} = (17 - 9.81)\frac{kN}{m^3} \cdot 0.3m = 2.1\frac{kN}{m^2}$$

The slight difference (2.0 vs. 2.1) is due to stress redistribution.

At the end of consolidation the corresponding displacements can be computed to find the total settlement caused by the potential mat deployment. Figure 7.3-7 below shows the final settlement of the sediment after 600 days and 95% consolidation.

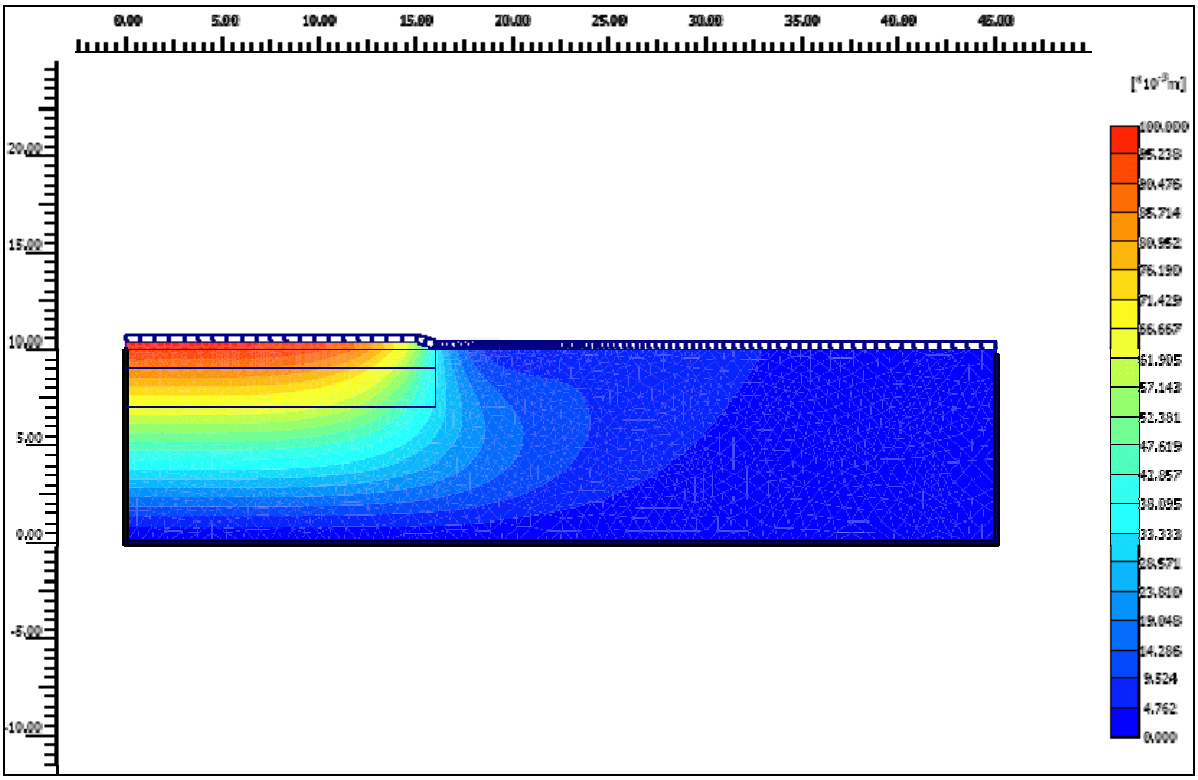

Figure 7.3-7. Settlement due to mat deployment after 95% sediment consolidation under the uncoupled model.

Results indicate that a maximum sediment compression of 9.58 cm occurs beneath the mat. Because the consolidation time estimates are based on a linear stress-strain relationship and assume a constant permeability for the entire model over time, they should be evaluated according to these limitations. Results also show that outside the mat area the maximum displacements of the sediment are nearly 20% and less of the maximum value is caused by the mat deployment.

Figure 7.3-8 shows a horizontal profile of the maximum sediment displacement across the entire uncoupled consolidation model. The maximum settlement occurs directly beneath the mat at nearly 7 m from the mat edge and is constant towards the inside of the mat. The settlement on the sediment surface rapidly decreases beyond the mat edge and reaches a zero displacement at 6.5 m outside the mat limits. The volumetric strain of the sediment serves as an indicator of the area affected by the mat deployment.

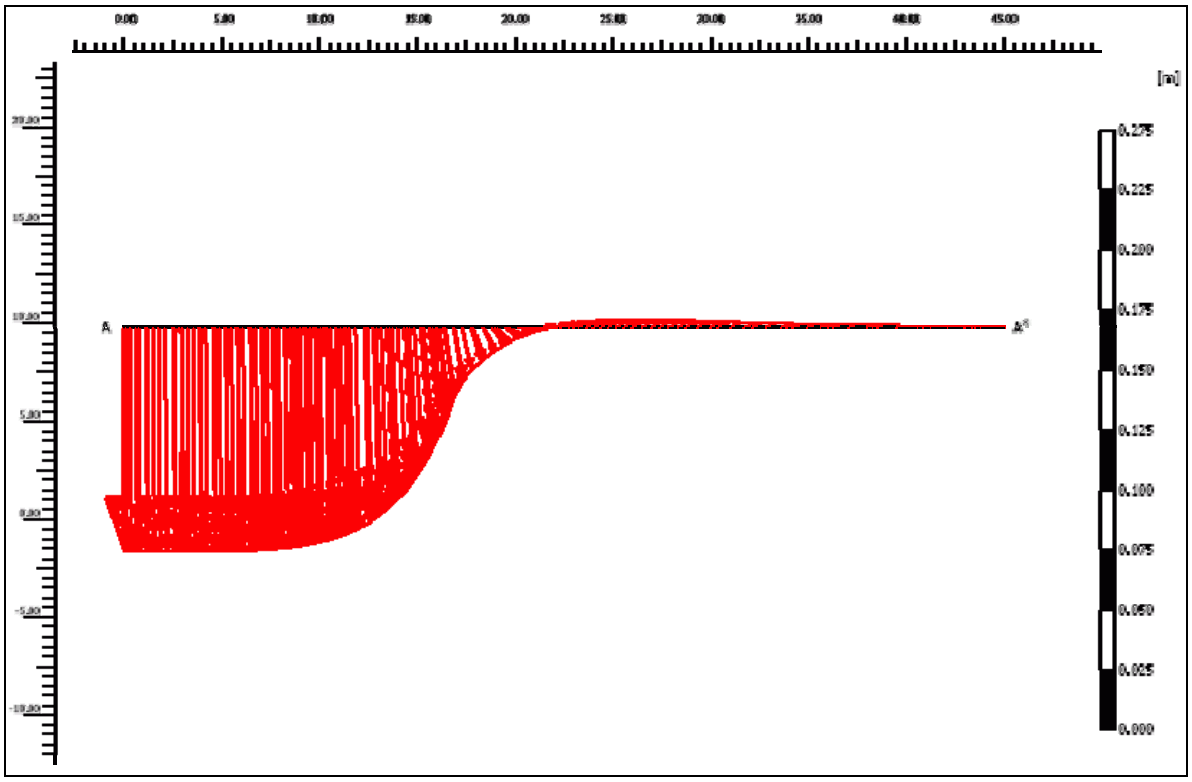

Figure 7.3-8. Horizontal profile of maximum sediment displacement under the uncoupled consolidation model.

Figure 7.3-9 below shows the volumetric strain distribution in the uncoupled model after 95% consolidation. This distribution is similar to the void ratio distribution when the volume of solids is constant. The maximum volumetric strain is 0.98%. These results indicate that the sediment directly below the mat has a final volumetric strain between 100% and 50% of the maximum strain induced by the mat deployment. Due to the soft nature of the material, the uncoupled consolidation model shows that sediment directly beneath the mat is displaced by compressive effects similar to punching shear effects in foundation design. The pore water displaced by these consolidation effects will occur mainly in the sediment area directly below the mat.

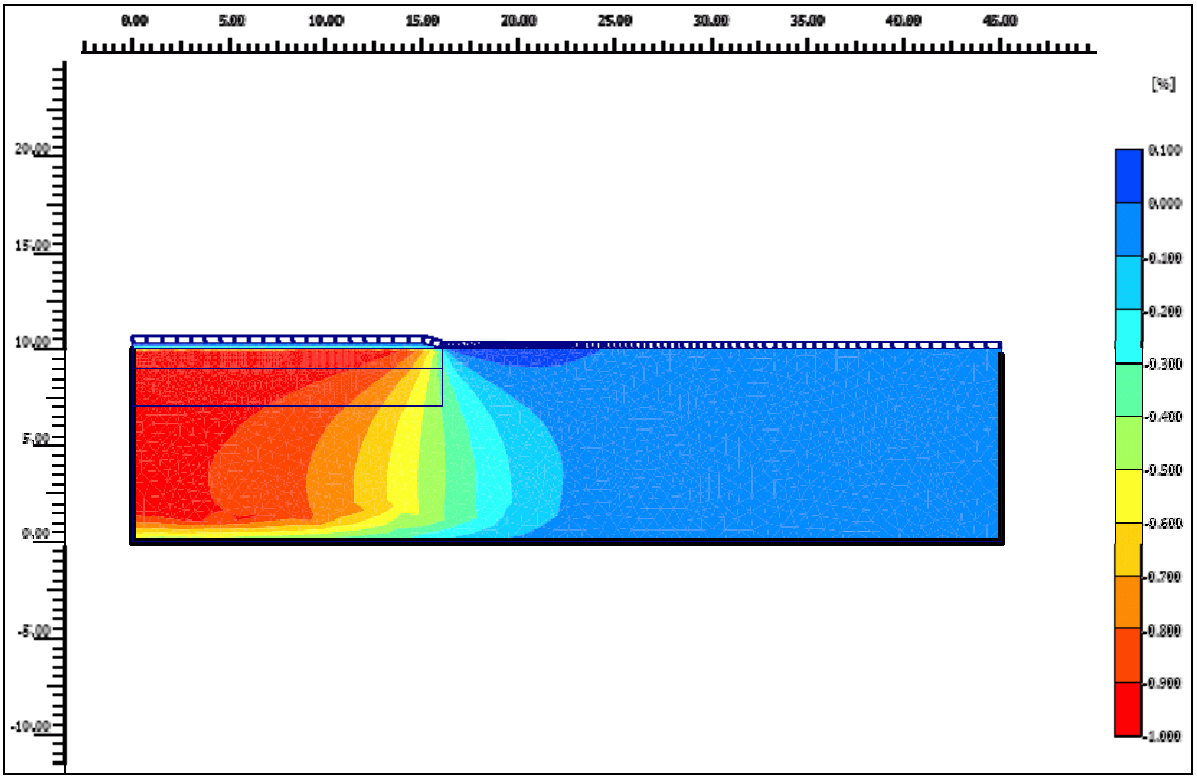

Figure 7.3-9. Volumetric strain after 95% consolidation under the uncoupled consolidation model.

Uncoupled Seepage Model. The uncoupled seepage model assessed potential changes in groundwater flow properties following mat placement for both unclogged and clogged geotextiles. Figure 7.3-10 shows the total water pore pressure distribution for both clogging scenarios. Results indicate that despite having a clogged mat on the second model, the flow of water still moves through the mat albeit at slower rate as shown by the increase in separation between contours from the clogged to the unclogged case. The increase of separation between successive contours indicates lower hydraulic gradient and thus lower seepage velocity. The region near the mat edge shows that the flow is slightly deviated from crossing the mat perpendicularly when the mat is clogged. This result may be of particular interest in selecting the overall extension of the final mat design.

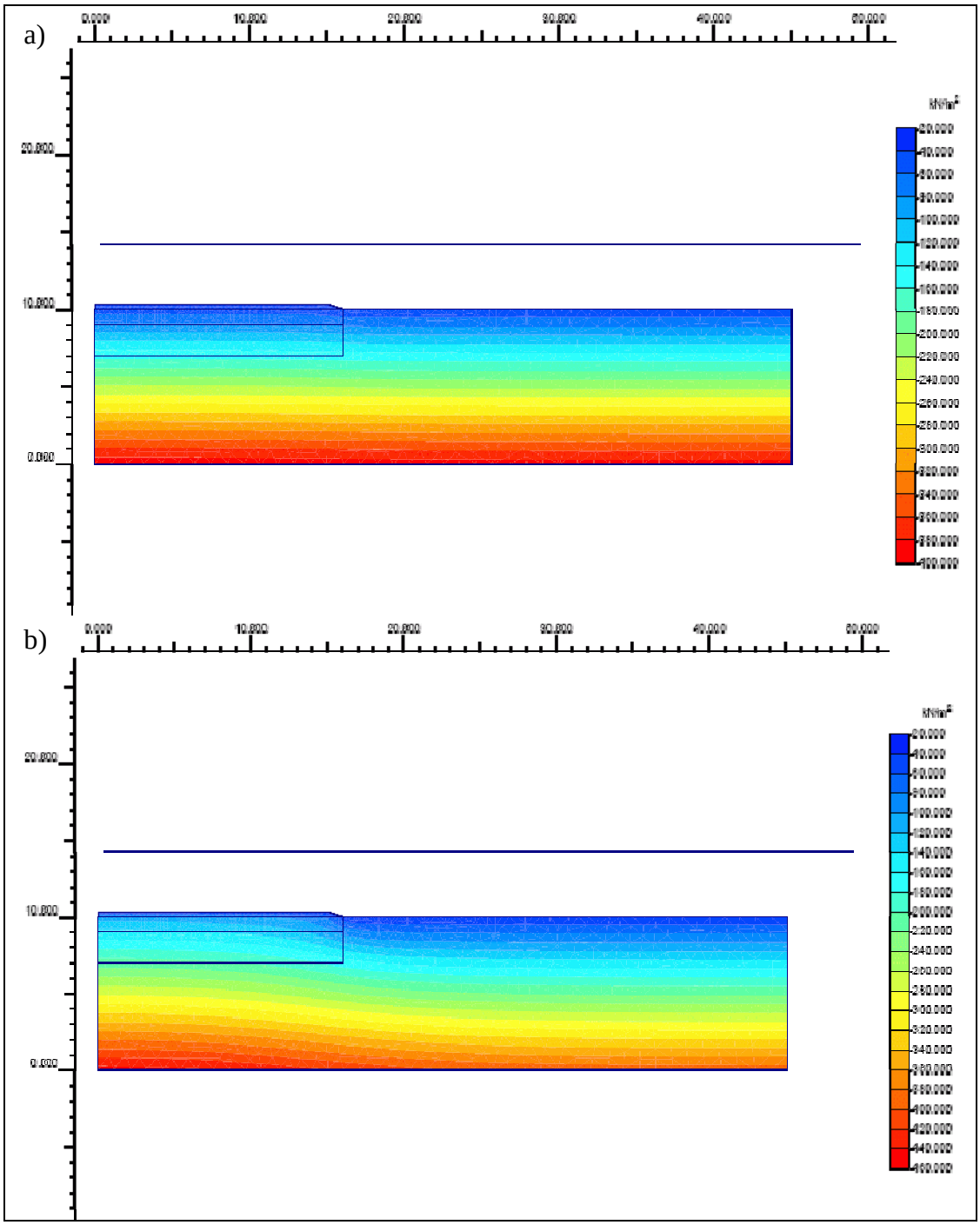

Figure 7.3-10. Total water pore pressure for an unclogged mat (a) and a clogged mat (b) under the uncoupled seepage model.

The specific discharge computed for any cross section gives the total water discharge flowing through that section of the model. Figure 7.3-11 shows the specific discharge distribution for both the unclogged and clogged scenarios corresponding to the combined XY direction discharge.

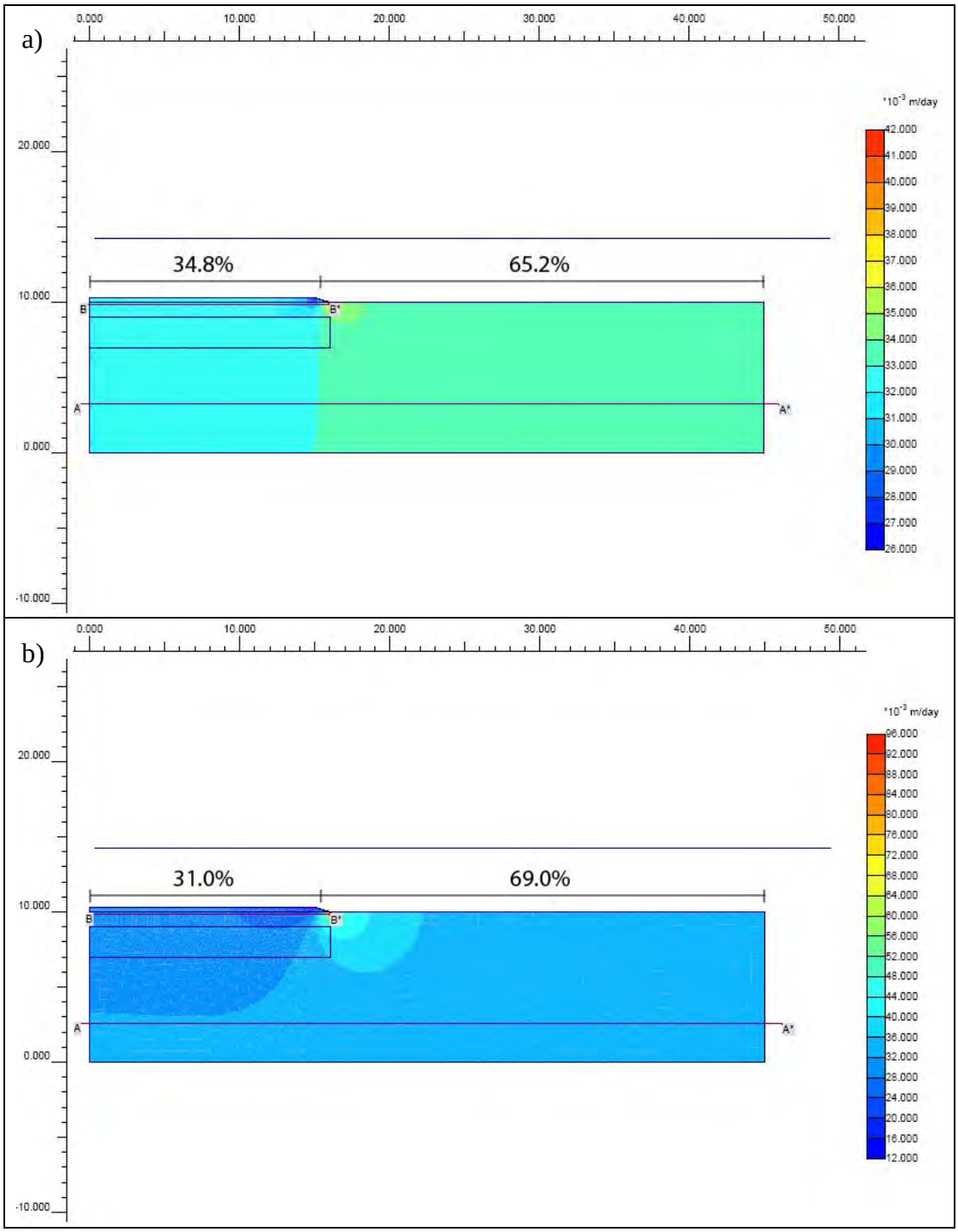

Figure 7.3-11. Specific discharge for an unclogged mat (a) and a clogged mat (b) under the uncoupled seepage model.

Assuming that 100% of the groundwater flows in the upward direction at the mat deployment site, 34.8% of the total flow in this model passes through the mat for the unclogged condition. This fraction is slightly reduced to 31.0% for a clogged mat, thus indicating that 3.3% of the groundwater flow was deviated form its original path. It should be noted, however, that the

average magnitude of the discharge does not vary significantly from the unclogged to the clogged mat condition and still averages approximately 36-40 m^3/day outside the mat area. The specific discharge distribution varies because the overall boundary conditions change after the mat clogs, but the percentages of groundwater flow moving through and around the mat do not vary significantly.

Coupled Model. The coupled model merges potential sediment consolidation and groundwater seepage conditions, essentially combining the two uncoupled models, by applying sequential parameters that first define the initial sediment stress caused by mat deployment followed by application of a groundwater flow component that results in a new sediment stress state. Figure 7.3-12 shows the final displacement distribution due to mat deployment under the coupled model.

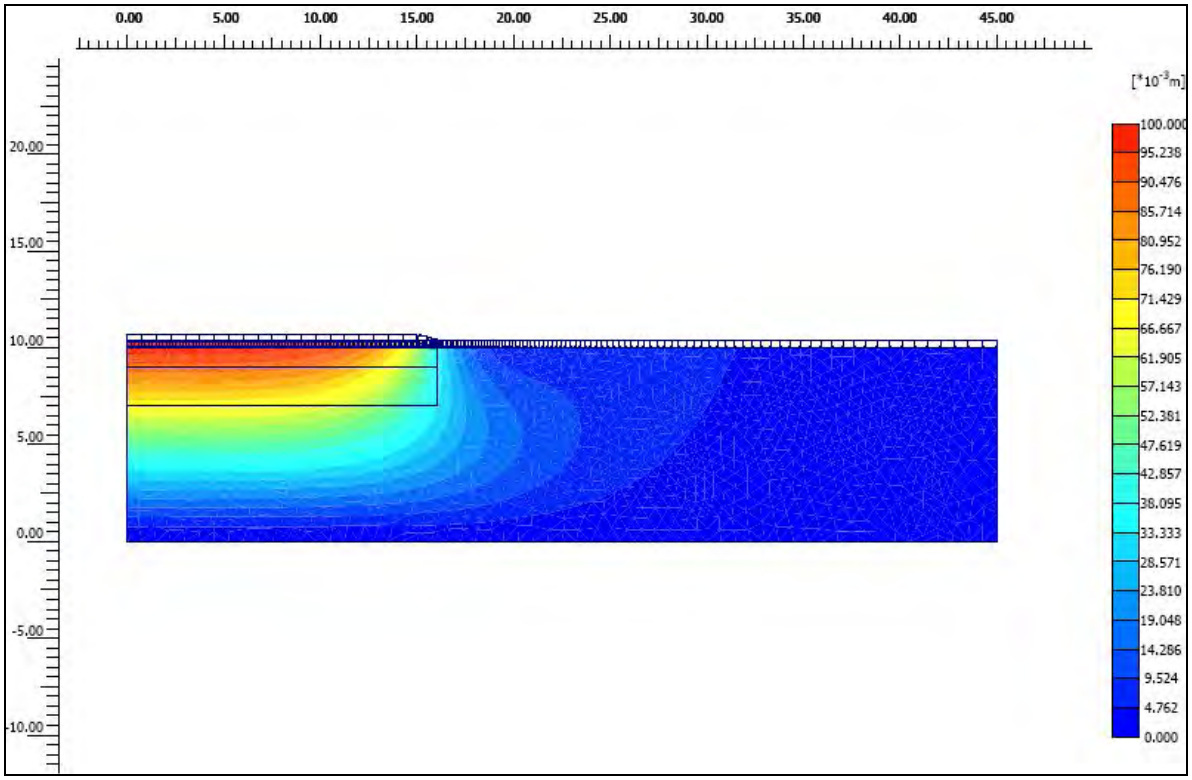

Figure 7.3-12. Sediment settlement due to mat deployment under the coupled model.

The maximum displacement for the coupled solution is 9.87 cm, which is close to 9.58 cm obtained without including the groundwater flow in the uncoupled consolidation solution. The 3% increase is the result of the sequential groundwater flow parameter being added following initial sediment consolidation in the coupled solution.

Figure 7.3-13 shows a horizontal profile of the maximum sediment displacement across the entire coupled model.

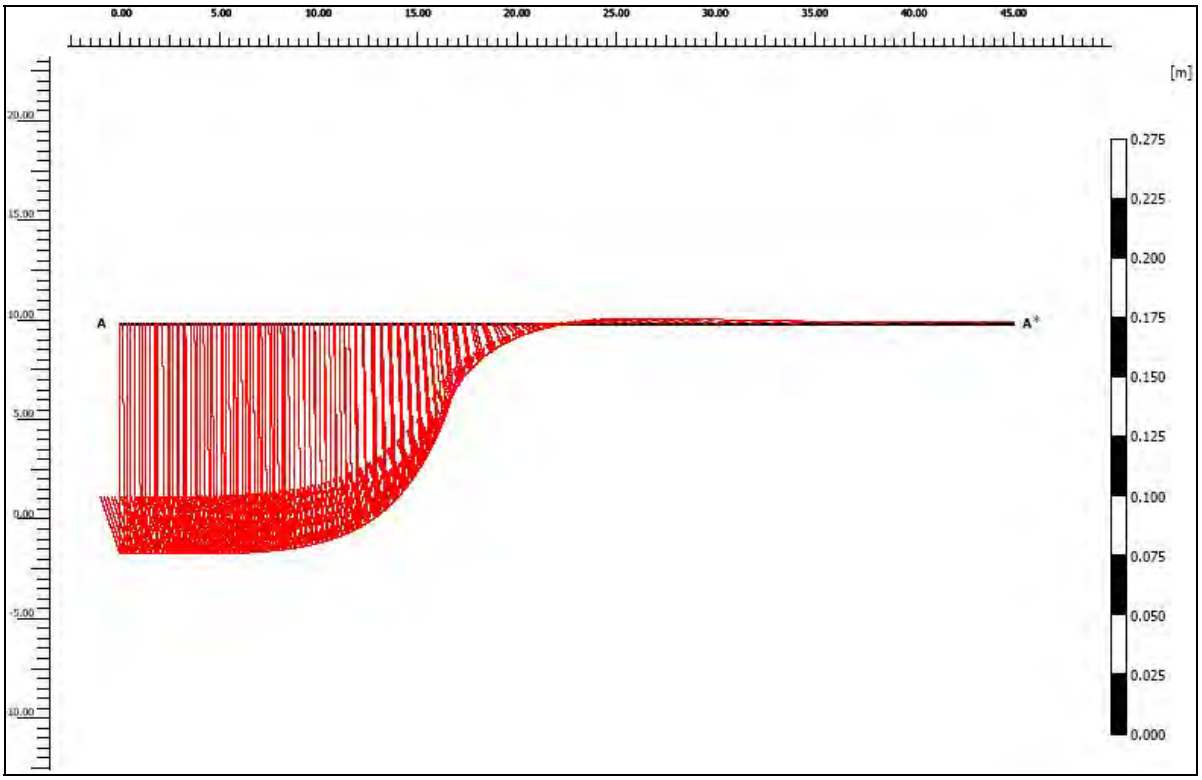

Figure 7.3-13. Horizontal profile of the maximum sediment displacement under the coupled model.

The small increase of the estimated maximum settlement compared to the uncoupled consolidation model and shown in the previous figure does not significantly affect the shape of the settlement profile. The maximum displacement of the mat still occurs 7 m from the edge and remains constant towards the inside of the mat.

The volumetric strain distribution for the coupled model is presented in Figure 7.3-14. The maximum volumetric strain was found to be 1.03% for the coupled solution as compared to 0.98% for the uncoupled consolidation solution. The estimated final volumetric strain increases 5% from the uncoupled to the coupled solution. Because both the sediment and mat permeabilities, as well as the flow rate and water level, are constant throughout the coupled solution, there is no change in the amount of flow passing through and around the mat. Similar specific discharge results as the uncoupled seepage model (Figure 7.3-11) are expected for the coupled model when the sediment permeability is varied according to the consolidation tests results.

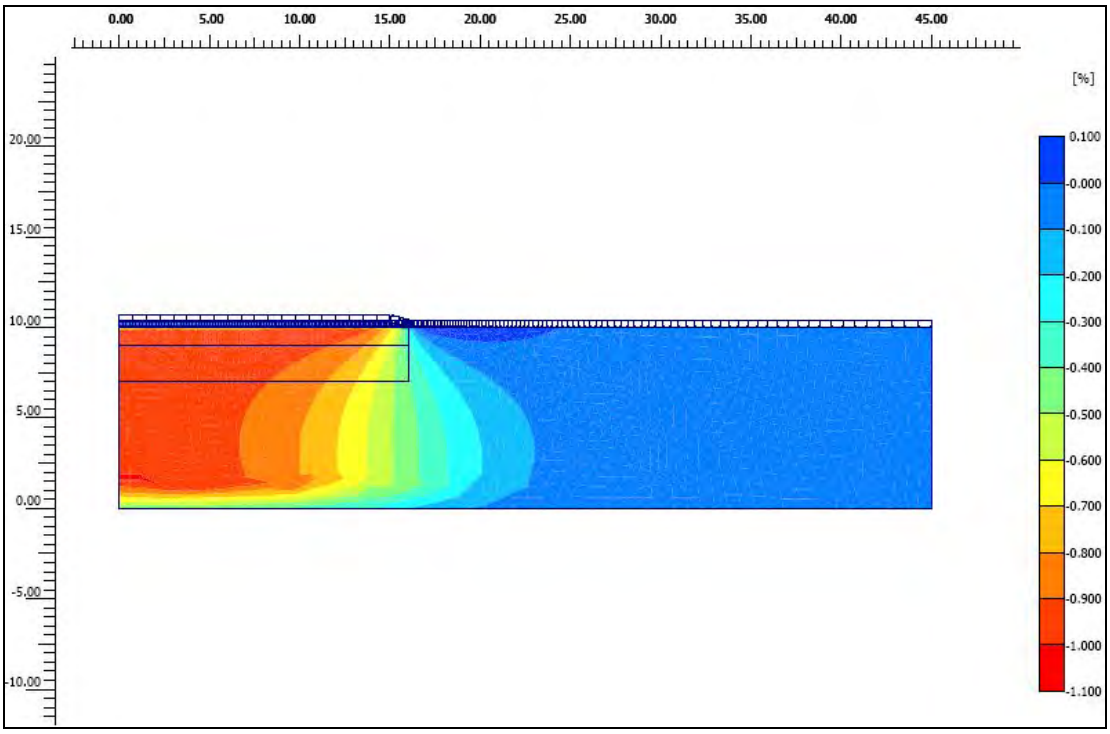

Figure 7.3-14. Volumetric strain under the coupled model.

Summary. Overall results from the FEA process indicate that the soft nature of the underlying sediment will result in significant compression directly beneath the mat following deployment. The porewater displacement caused by this consolidation will be confined mainly to the sediment directly below the mat and a relatively low level of geotextile clogging will not significantly alter groundwater flow patterns. Model results show that a permeability decrease of several orders of magnitude would be required to greatly impact groundwater flow, but this level of clogging is not expected under field conditions based on the results of the gradient ratio testing. Data collected from laboratory tests to be performed on the field weathered small-scale test mats following retrieval will ultimately be used to refine both the uncoupled and coupled finite element models with real permeability data rather than clogging assumptions. The finite FEA does not favor selection of any particular geotextile at this stage.

7.4. TASK 4: PROTOTYPE MAT TESTING

The purpose of Task 4 is to field test a prototype mat system featuring various mat arrangements constructed of the most effective amendment and the geotextile most resistant to clogging/biofouling in order to assess in-situ chemical sequestration effectiveness and flux properties. The exact target location where this mat system will be deployed was determined in year two by the results of the Cottonwood Bay geophysical investigation as described in Section 7.2.4 of this report. The composition of the prototype mats will be determined by the results of previous composite material testing and the performance evaluation of the small-scale test mats that will occur in year three. Because Task 4 has yet to commence, no year two results are available at this time. A schedule of all completed and future tasks for this project is provided in Figure 7.4-1.

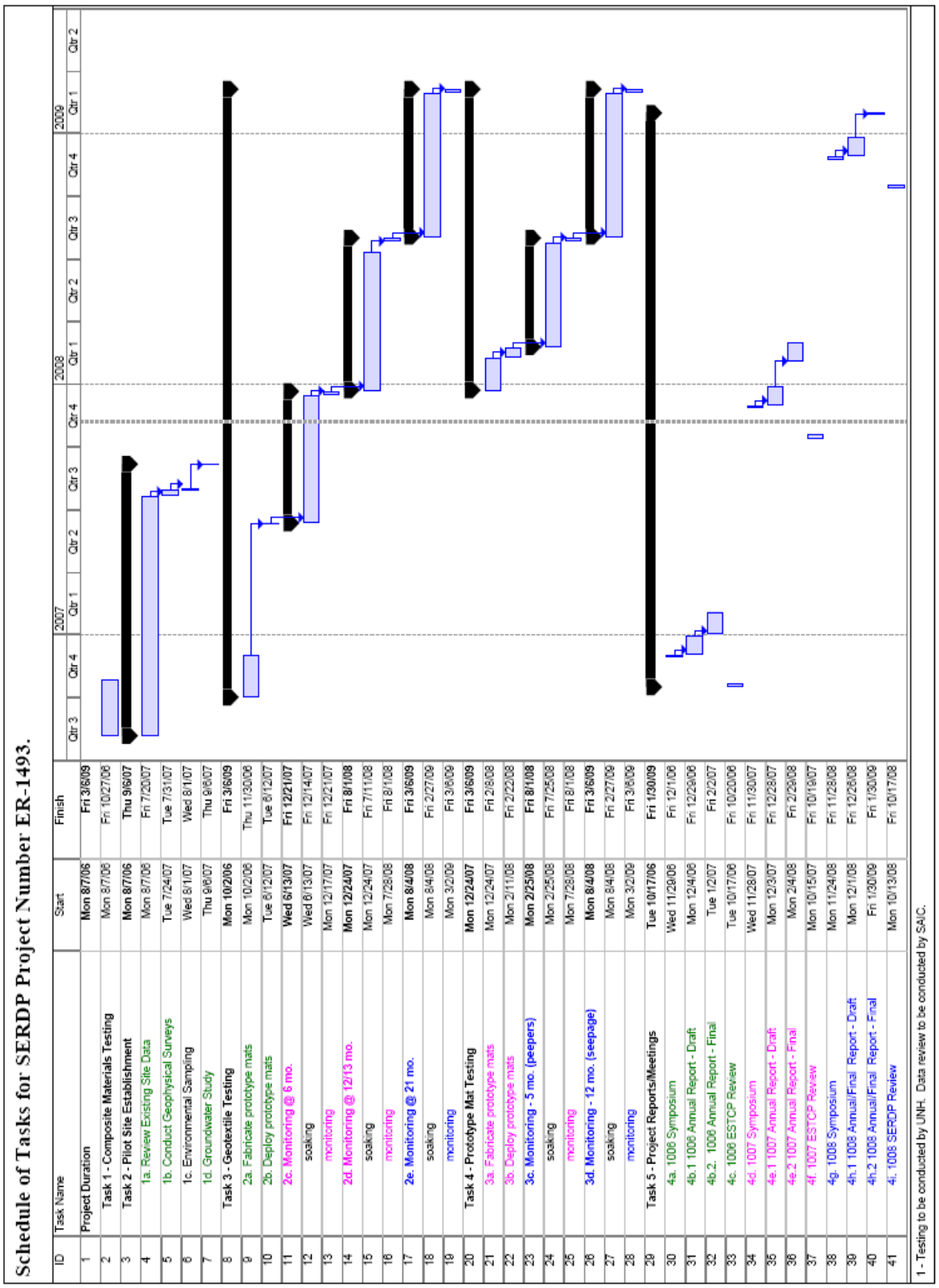

Figure 7.4-1. Schedule of all completed and future tasks for SERDP Project Number ER-1493.

8. CONCLUDING SUMMARY

This annual report summarizes year two progress on SERDP Project Number ER-1493 (Reactive Capping Mat Development and Evaluation for Sequestering Contaminants in Sediments) through December 2007 with regard to tasks presented in the original proposal. To meet Task 1 (Composite Material Testing) objectives, the UNH laboratory conducted batch kinetic studies to evaluate adsorption equilibrium times and batch isotherm studies to evaluate PCB adsorption concentrations for two types of activated carbon (coconut shell based and coal based) and three types of organoclays (CETCO, Polymer Ventures and Biomin, Inc.) with the goal of characterizing the effectiveness of each material as a potential reactive amendment to be included in the final geotextile mat design. The overall characterization of activated carbon showed that the adsorption capacity was greater for higher chlorinated PCB congeners and that adsorption affinity and capacity can be significantly affected by the preloading of humic acid. There was also less of a desorption effect for higher chlorinated and co-planar PCB congeners resulting from prolonged exposure to humic acid. The overall characterization of different organoclays indicated that adsorption of higher chlorinated PCB congeners was greater than that of lower chlorinated PCB congeners on CETCO organoclay but the humic acid preloading effect was more significant for lower chlorinated congeners. Similar to activated carbon, the desorption effect due to chronic humic acid exposure was less pronounced for co-planar PCB congeners as compared to non-coplanar PCB congeners. Additional testing involving exposure of activated carbon and organoclay to humic acid, fulvic acid, NOM, Passaic River porewater and Hudson River pore water showed preloading effects were more pronounced for humic acid than other compounds and that organic acids in sediment pore water have a significant impact on the effectiveness of potential reactive mat amendments in sequestering contaminants.

To meet Task 2 (Pilot Site Selection) objectives, a rigorous review of available site documentation was performed to compare Cottonwood Bay in Grand Prairie, Texas and Pearl Harbor in Honolulu, Hawaii in terms of nature and extent of contamination, groundwater flow properties, management planning and ongoing remediation. Cottonwood Bay was ultimately selected as the most appropriate pilot site for mat testing and a management decision was made to proceed with future tasks at this location. A series of geophysical surveys were conducted in both the eastern and western portions of Cottonwood Bay to characterize site conditions with the goal of selecting a specific location for future full-scale mat system deployment. This geophysical investigation consisted of bathymetry surveys, sub-bottom profiling, side-scan sonar surveys, SPI photography, sediment vibracoring and a follow-up groundwater seepage survey. Results indicated that water depths and sediment thickness were generally greater in Cottonwood Bay East and that there were no major obstacles on the sediment surface throughout the project area.

Bottom characteristics as observed in the SPI photographs revealed a consistently unconsolidated soft bottom environment with generally degraded habitat conditions. A region of high groundwater upwelling potential was identified approximately 200 ft from the NWIRP shoreline in Cottonwood Bay East. Based on the combined results of all the geophysical surveys, an area on the western side of Cottonwood Bay East approximately 200 feet from the NWIRP shoreline was chosen as the preferred target location for future full-scale mat system deployment. This

area was selected mainly because of its location within a high potential groundwater discharge zone and the presence of elevated contaminant levels, both conditions of which are necessary for evaluating overall mat performance.

To meet Task 3 (Geotextile Testing) objectives, fourteen small-scale geotextile test mats (6 ft x 6 ft) were constructed of different compositions and different AOS to assess which arrangement would be least affected by biofouling and biofilm formation. These mats were deployed in Cottonwood Bay East in June 2007 in two rows of replicates which are currently soaking in the field. Two retrieval events are planned to coincide with six months and one year of soak time, at which point the entire replicate mats will be removed from the water and shipped to a UNH laboratory for performance evaluation to assess how material type, geotextile weight and AOS affect biofouling and sediment clogging. In addition to field evaluation, Task 3 also included gradient ratio testing to evaluate geotextile flow properties under laboratory conditions as well as a finite element analysis to evaluate sediment deformation and pore water pressure increases caused by the weight of a potential reactive mat. Preliminary flow-through column experiments were used to evaluate flux for three stock geotextiles and one unweathered organoclay mat by closely mimicking expected processes in the field, thus providing baseline data to which the results of similar testing on the recovered small-scale geotextile mats can be compared.

Gradient ratio testing results indicated that a significant hydraulic head would be required to force sediment particles into any of the test geotextiles to the extent that they would become clogged and thus impermeable to groundwater flow. Because such drastic hydraulic conditions are not expected to occur in the field, the use of geotextiles as planned to contain reactive material should be appropriate for achieving project goals. Overall results from the finite element modeling process indicated that soft underlying sediment will undergo some compression directly beneath a reactive mat following deployment, but this compression will not extend greatly beyond the mat edges. Pore water displacement caused by this consolidation will be confined mainly to the sediment directly below the mat. When using a fully permeable geotextile as the starting point for the models, results indicated that a permeability decrease of several orders of magnitude would be required to greatly impact groundwater flow around a reactive mat. This level of clogging is not expected to occur under field conditions based on the results of the gradient ratio testing. Biofouling data from the recovered small-scale test mats will ultimately be used to refine the finite element models with actual permeability values.

Task 4 (Prototype Mat Testing) has yet to begin and thus no year two conclusions are available at this time. The year three effort for this task will consist of construction and deployment of a prototype full-scale mat system featuring for different reactive mat arrangements constructed of the geotextile most resistant to biofouling as well as one control area featuring no mat or sand cap. These mat arrangements will be constructed of the most effective amendment and the geotextile most resistant to biofouling as identified in the other tasks and then monitored in the field to assess in-situ chemical sequestration effectiveness and flux properties. The preferred target location at which this mat system will be deployed was determined by the results of the Cottonwood Bay geophysical investigation and is located in Cottonwood Bay East in a zone of high groundwater upwelling potential. Construction and deployment of the full-scale mat system

is currently planned for February 2008. Overall, all tasks have proceeded well and are being executed on schedule.

9. APPENDICES

REFERENCES

Barker, R.A. and C.L. Braun. 2000. Computer-model analysis of ground-water flow and simulated effects of contaminant remediation at Naval Weapons Industrial Reserve Plant, Dallas, Texas. U.S. Geological Survey Water-Resources Investigations Report 00–4197, 44 p.

Chadwick, D.B., J. Groves, C. Smith, and R. Paulsen. 2003. Hardware description and sampling protocols for the Trident Probe and UltraSeep system: Technologies to evaluate contaminant transfer between groundwater and surface water. Technical Report #1902, SSC San Diego, United States Navy.

Cornelissen, G., M. Elmquist; I. Groth and O. Gustafsson. 2004. Effect of Sorbate Planarity on Environmental Black Carbon Sorption. *Environmental Science and Technology*. 2004, 38, 3574-3580.

EnSafe/Allen & Hoshall. 1996. Draft RCRA, facility investigation report, Naval Weapons Industrial Reserve Plant, Dallas, Texas. Volume I: Memphis, Tenn.

EnSafe. 2000. Ecological Risk Assessment Screening Level, Mountain Creek Lake, Dallas, Texas. Prepared for SOUTNAVFACENGCOM, Charleston, SC.

EnSafe. 2001. Affected Property Assessment Report, Mountain Creek Lake, Dallas, Texas. Prepared for NAVFAC under contract N62467-89-D-0318, CTO 0025.

Groundwater Seepage, Inc. 2007. Draft Data Report. Groundwater Upwelling Survey, Naval Weapons Industrial Reserve Plant, Cottonwood Bay, Dallas, Texas. November.

Iocco, L.E., P. Wilber and R.J. Diaz. 2000. Final Report. Benthic Habitats of Selected Areas of the Hudson River, NY Based on Sediment Profile Imagery. September.

Li, Qilin, V.L. Snoeyink, B.J. Marinas and C Campos. 2003. Pore Blockage Effect of NOM on Atrazine Adsorption Kinetics of PAC: The Roles of PAC Pore Size Distribution and NOM Molecular Weight. *Water Research.* 2003, 37, 4863-4872.

NAVFAC. 2006. Baseline Ecological Risk Assessment for Pearl Harbor Sediment Remedial Investigation. Prepared under contract N62742-94-D-0048, CTO 0115.

NAVFAC. 2006. Remedial Investigation Report for Pearl Harbor Sediment. Prepared under contract N62742-94-D-0048, CTO 0115.

NAVFAC. 2006. Annual Progress Report. Reactive Capping Mat Development and Evaluation for Sequestering Contaminants in Sediment. Prepared for SERDP Project Number ER-1493. With Science Applications International Corporation and the University of New Hampshire. December.

Owenby, J.R. and D.S. Ezell. 1992. Climatography of the United States-Monthly station normals of temperature, precipitation, and heating and cooling degree days, 1961–91. Asheville, N.C. National Climatic Data Center no. 81, 65 p.

Pignatello, J. J., S. Kwon and Y. Lu. 2006. Effect of Natural Organic Substances on the Surface and Adsorptiive Properties of Envrionmental Black Carbon (Char): Attenuation of Surface Activity by Humic and Fulvic Acids. *Environ. Sci. Tech*. 2006, 40, 7757-7763.

Pirbazari, M., V. Ravindram, S.P. Wong and M.R. Stevens. 1989. Adsorption of Micropollutants on Activated Carbon. *Aquatic Humic Substances – Infuence on Fate and Treatment of Pollutants*. ACS Publishers, 1989, 549-578.

Poerschmann, J., F.D. Kopinke, J. Plugge and A. Georgi. Interaction of Organic Chemicals (PAHs, PCB, Triazines, Nitroaromatics and Organotin Compounds) with Dissolved Humic Organic Matter. *Interaction of Organic Chemicals with Dissolved Humic Organic Matter*. 223-240.

Rhoads, D.C. and J.D. Germano. 1982. Characterization of organism-sediment relations using sediment profile imaging: An efficient method of remote ecological monitoring of the seafloor (Remots™ System). *Mar. Ecol. Prog. Ser.* 8: 115-128.

Rhoads, D.C., and J.D. Germano. 1986. Interpreting long-term changes in benthic community structure: A new protocol. *Hydrobiologia* 142: 291-308.

Schaffner, L.C., R.M. Dickhut, S. Mitra, P.W. Lay and C. Brouwer-Riel. 1997. Effects of Physical Chemistry and Bioturbation by Estuarine Macrofauna on the Transport of Hydrophobic Organic Contaminants in the Benthos. *Environmental Science and Technology*. 1997, 31, 3120-3125.

Trident and UltraSeep. 2006. Draft Data Report. Month 30 Post – Capping Evaluation for the Apatite Cap Test Area on the Anacostia River, Washington, D.C. Submitted to Environmental Research Group, University of New Hampshire, Durham, NH by Coastal Monitoring Associates, San Diego, CA. December.

University of Texas, Bureau of Economic Geology. 1987. Geologic atlas of Texas, Dallas Sheet. Austin, Tex. Scale 1:250,000.

VanMetre, P.C., S.A. Jones, J.B. Moring, B.J. Mahler and J.T. Wilson. 2003. Chemical Quality of Water, Sediment, and Fish in Mountain Creek Lake, Dallas, Texas, 1994-97. Geological Survey Water-Resources Investigations Report 03-4082, 69 p.

APPENDIX C

"Mat System Consolidation and Groundwater Flow Modeling Results"

This page is intentionally left blank

Figure C-1. Geometry of a generic reactive cap site for consolidation modeling (not to scale).

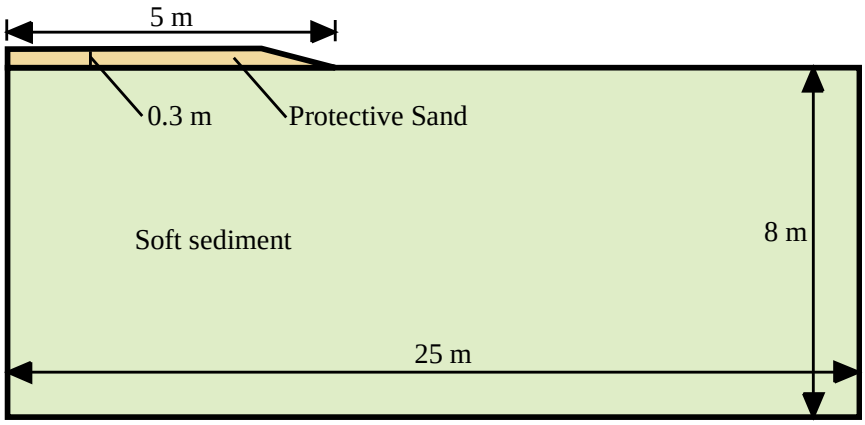

Table C-1. Parameters for the Modified Cam-Clay constitutive model.

Parameter	Units	Value
Unit weight, γ	kN/m^3	16.5
Poisson's ratio, ν		0.25
Initial void ratio, *e*		1.75
Over Consolidation Ratio		1
Lambda, λ		0.04863
Kappa, κ		0.0102
Effective friction angle, ϕ'	°	40
Volumetric water content	m^3/m^3	0.624

Figure C-2. Excess pore pressure dissipation profiles

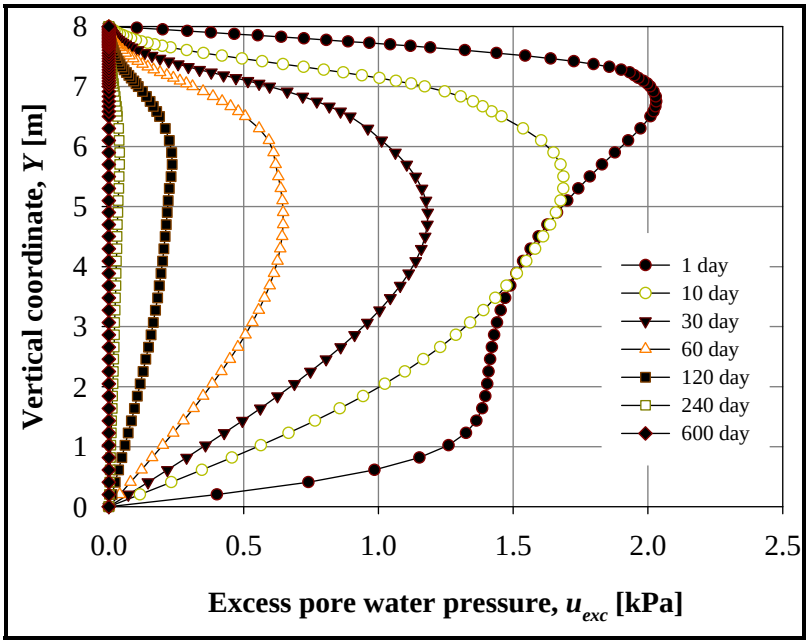

Figure C-3. Surface settlement.

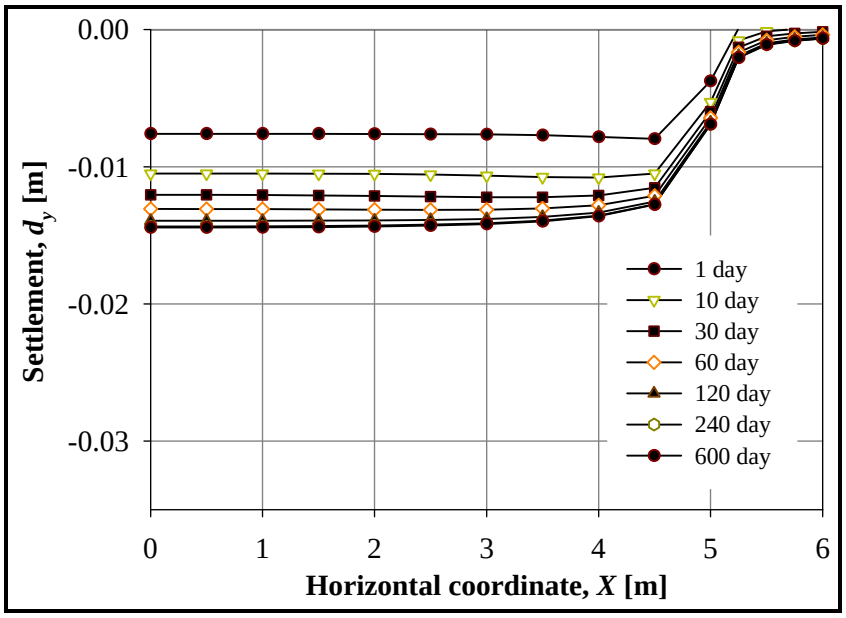

Figure C-4. Advective flow during consolidation.

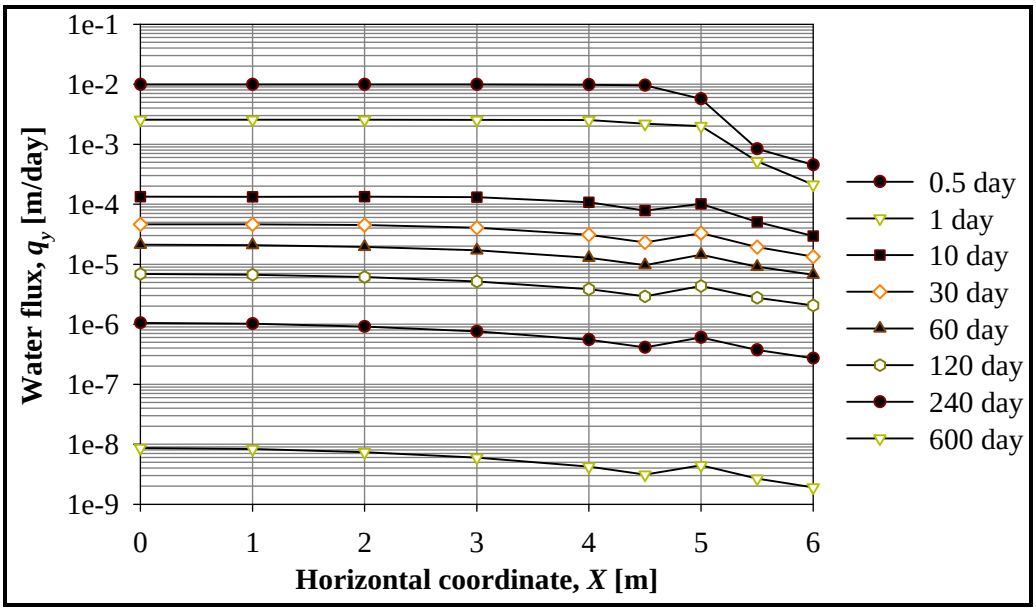

Figure C-5. Geometry of a generic reactive cap site for groundwater flow modeling (not to scale).

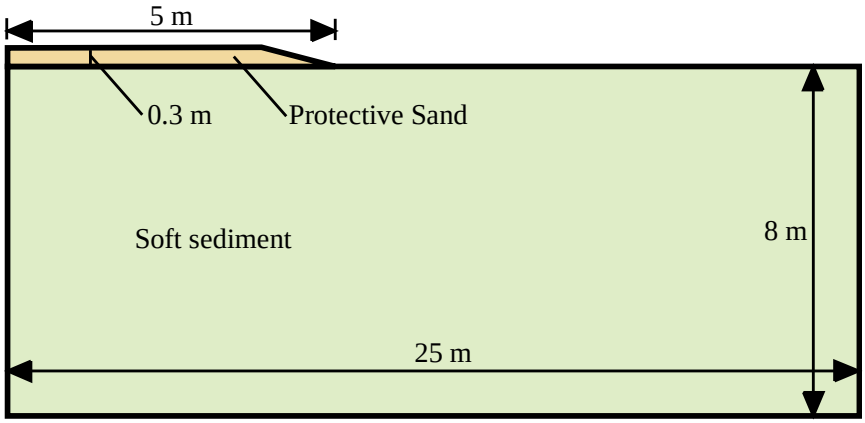

Table C-2. Permeability of the sediment and geotextile for different clogged scenarios

Degree of mat clogging	Sediment permeability [m/s]	Geotextile permeability [m/s]
$k_{Soil-Geotextile} = 1 \times k_{Soil}$	1 x 10-7	1 x 10-7
$k_{Soil-Geotextile} = 0.1 \times k_{Soil}$	1 x 10-7	1 x 10-8
$k_{Soil-Geotextile} = 0.01 \times k_{Soil}$	1 x 10-7	1 x 10-9
$k_{Soil-Geotextile} = 0.001 \times k_{Soil}$	1 x 10-7	1 x 10-10
$k_{Soil-Geotextile} = 0.0001 \times k_{Soil}$	1 x 10-7	1 x 10-11

Figure C-6. Pressure head contours (m) and flow paths (k_{GT} = 1 x k_{SED}).

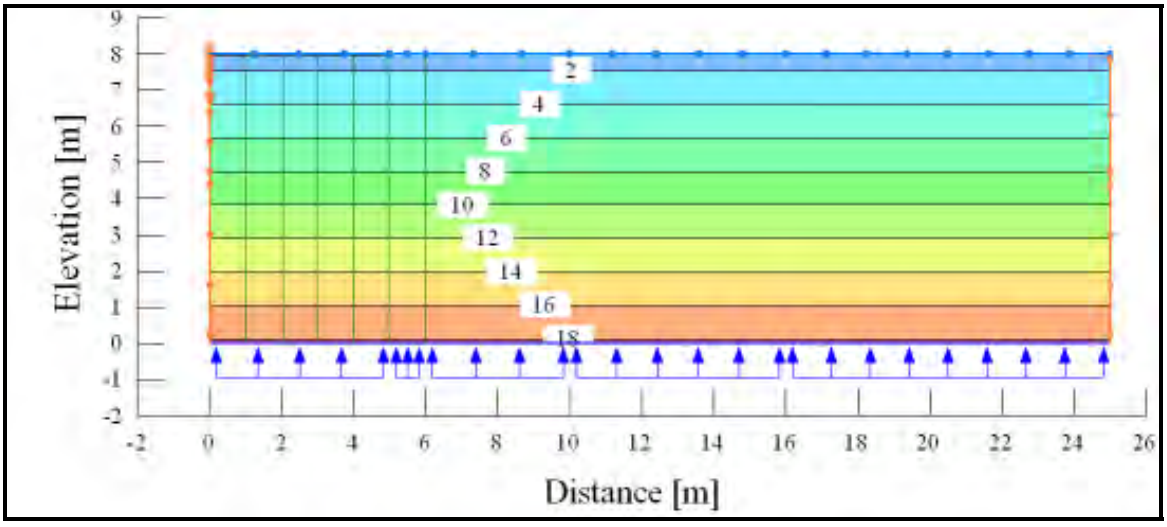

Figure C-7. Pressure head contours (m) and flow paths (k_{GT} = 0.1 x k_{SED}).

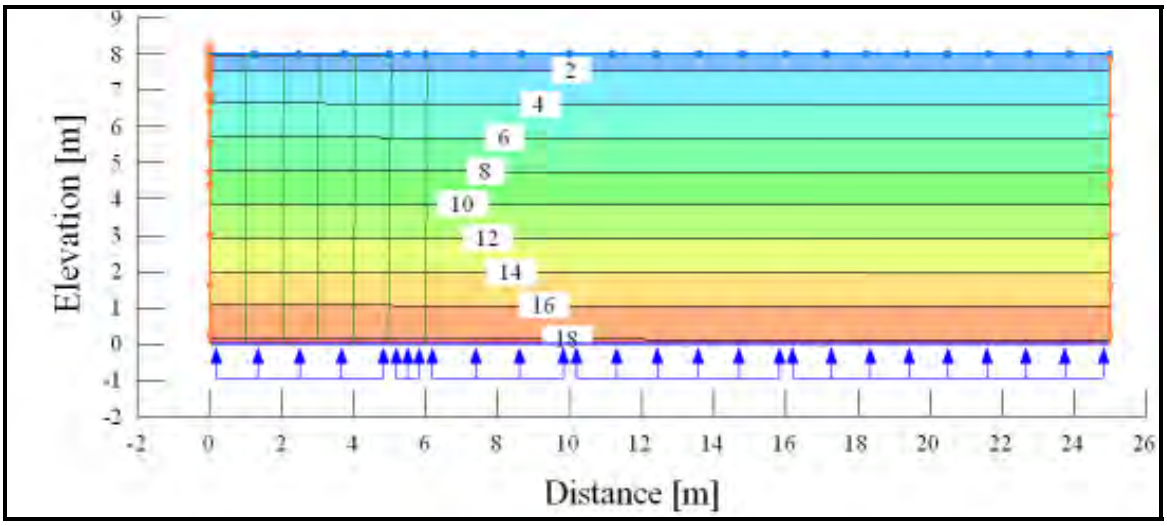

Figure C-8. Pressure head contours (m) and flow paths (k_{GT} = 0.01 x k_{SED}).

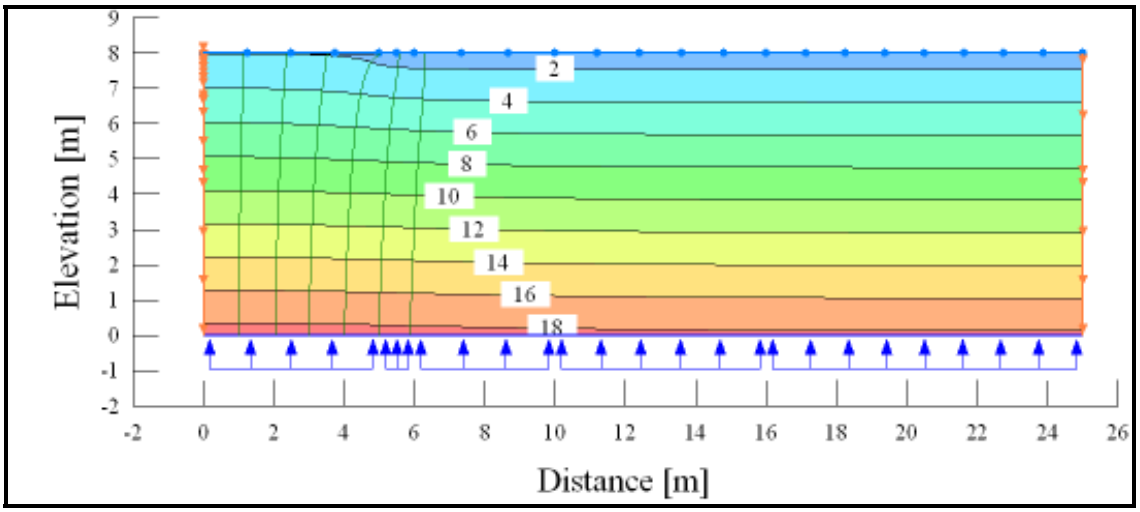

Figure C-9. Pressure head contours (m) and flow paths (k_{GT} = 0.001 x k_{SED}).

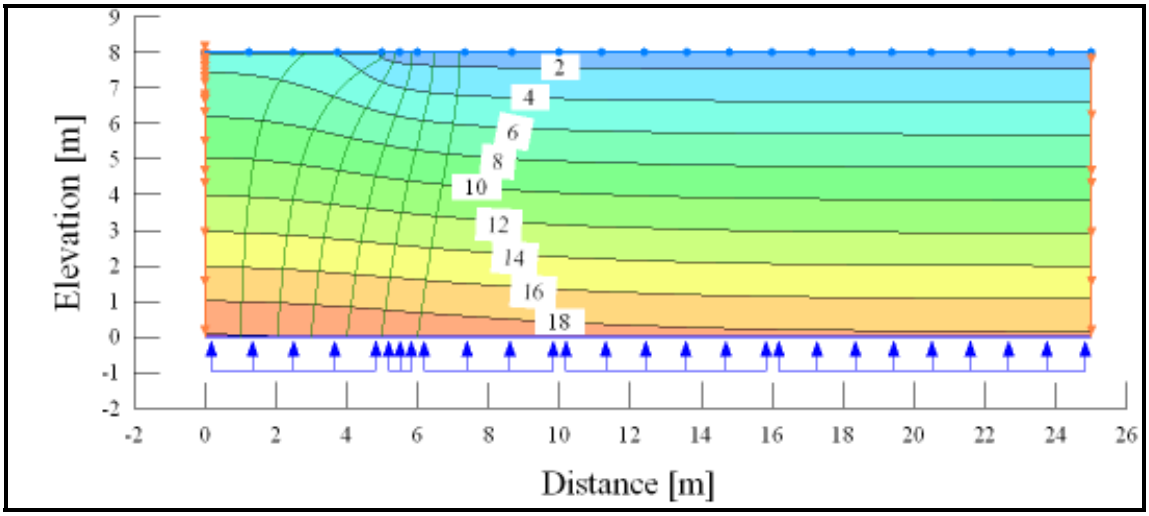

Figure C-10. Pressure head contours (m) and flow paths (k_{GT} = 0.0001 x k_{SED})

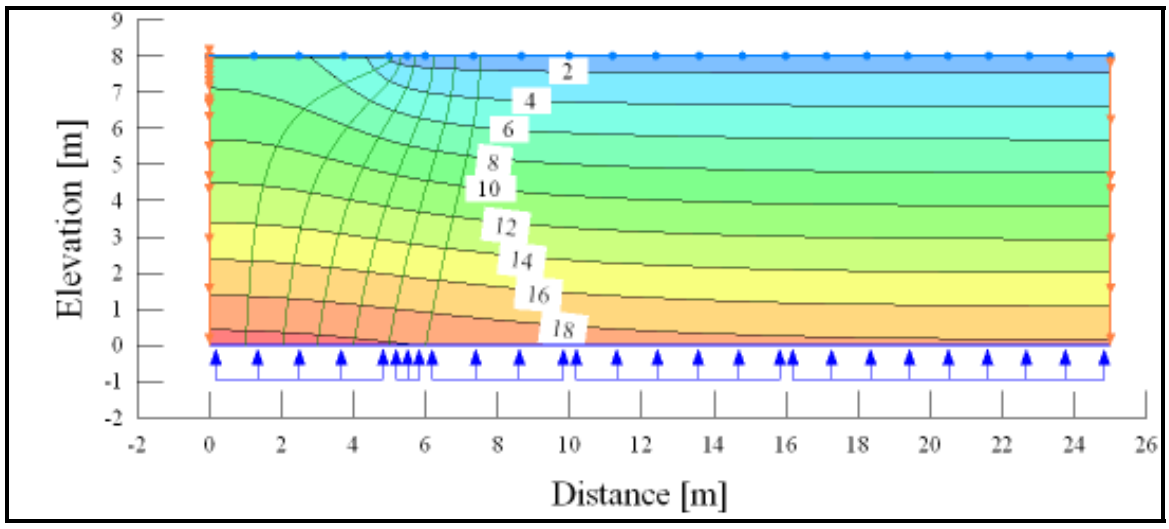

Figure C-11. Water flow through the cap for different clogging scenarios.

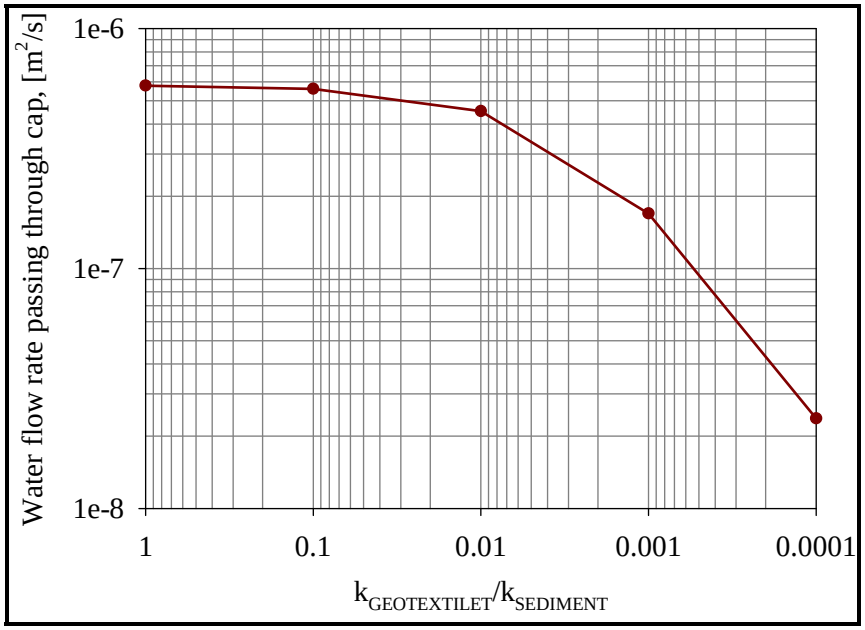

APPENDIX D

“Prototype Mat System Geophysical Results (December 2008)”

This page is intentionally left blank

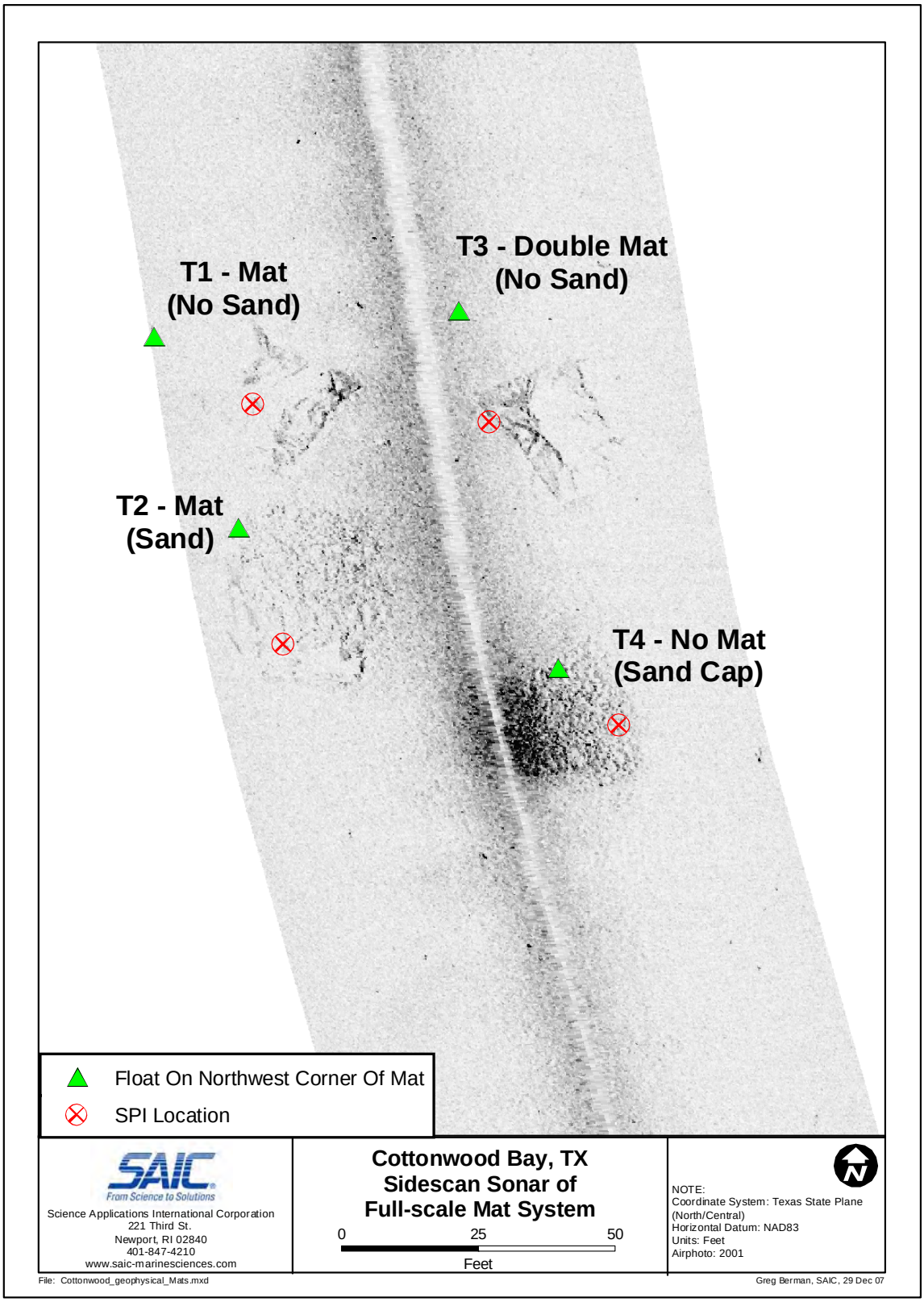

Figure D-1. Side-scan sonar mosaic of the prototype mat system after six months of soak time.

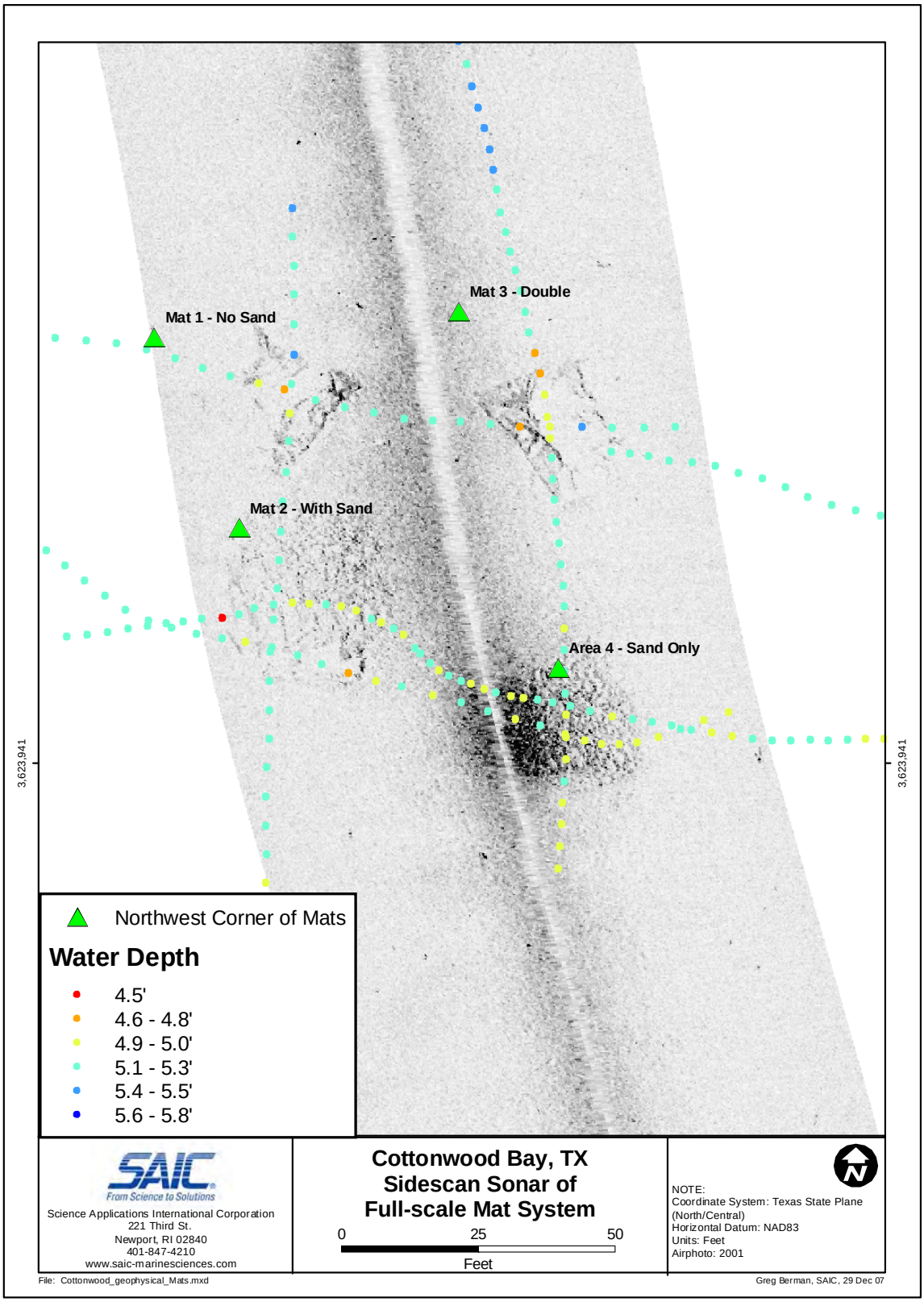

Figure D-2. Side-scan sonar mosaic of the prototype mat system with bathymetry.

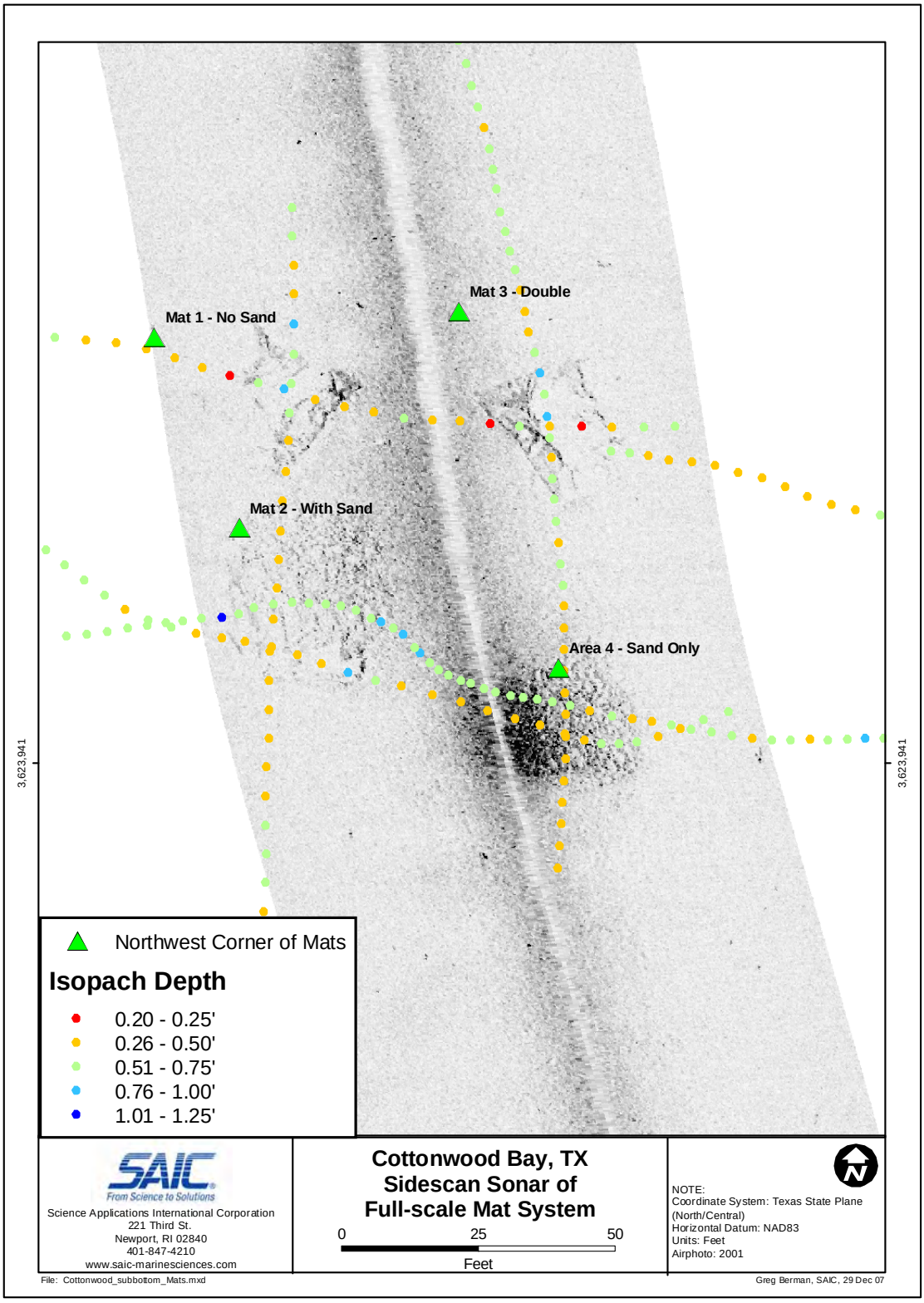

Figure D-3. Side-scan sonar mosaic of the prototype mat system with the sub-bottom isopach depth below the sediment-water interface of the uppermost sediment layer.

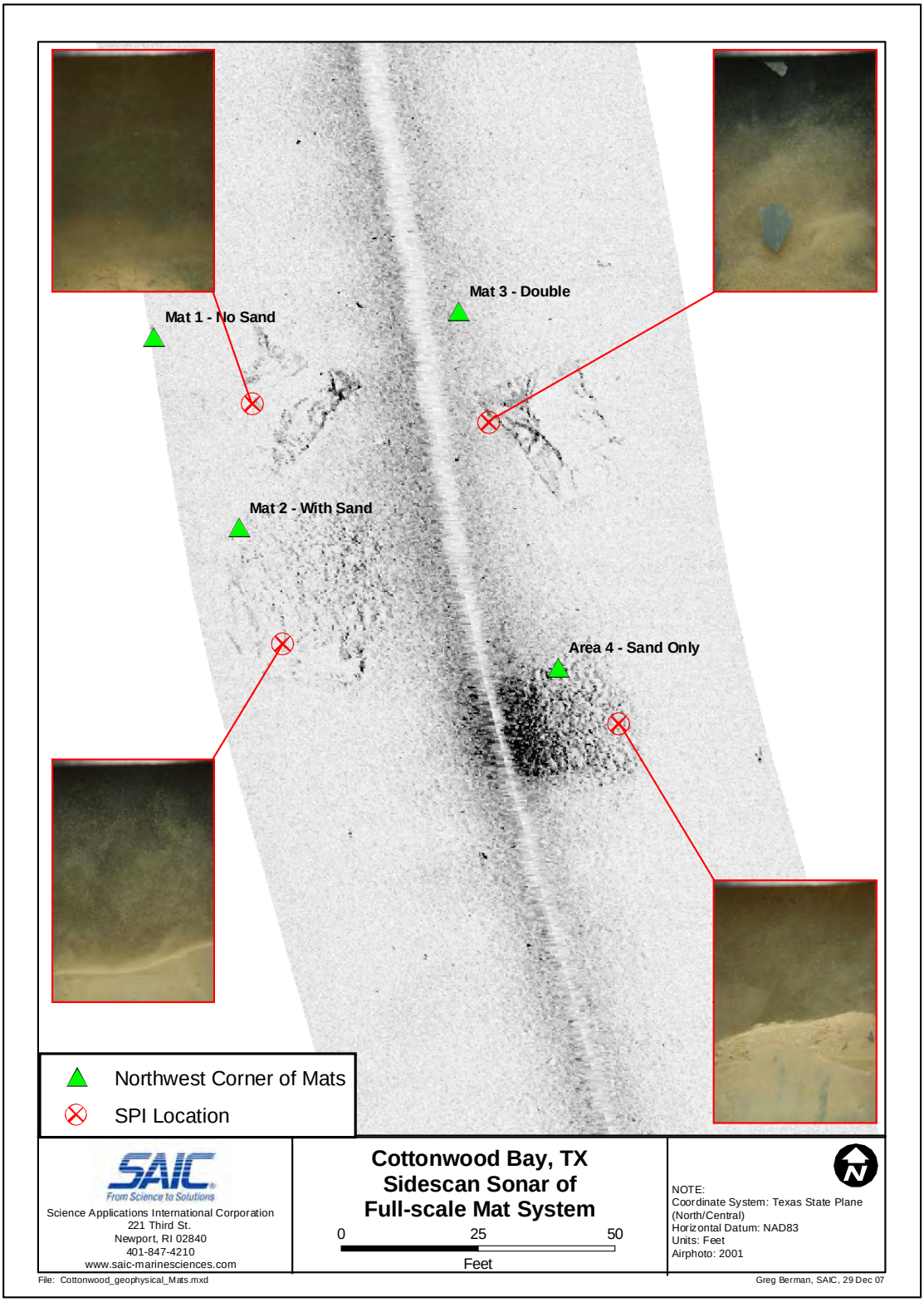

Figure D-4. Side-scan sonar mosaic of the prototype mat system with representative sediment profile images of each treatment area.

Figure D-5. Sediment profile image of prototype mat system area T1 (single mat only) taken on top of geotextile.

Figure D-6. Sediment profile image of prototype mat system area T2 (single mat with sand cap) taken in capping material.

Figure D-7. Sediment profile image of prototype mat system area T3 (double mat) taken on top of geotextile.

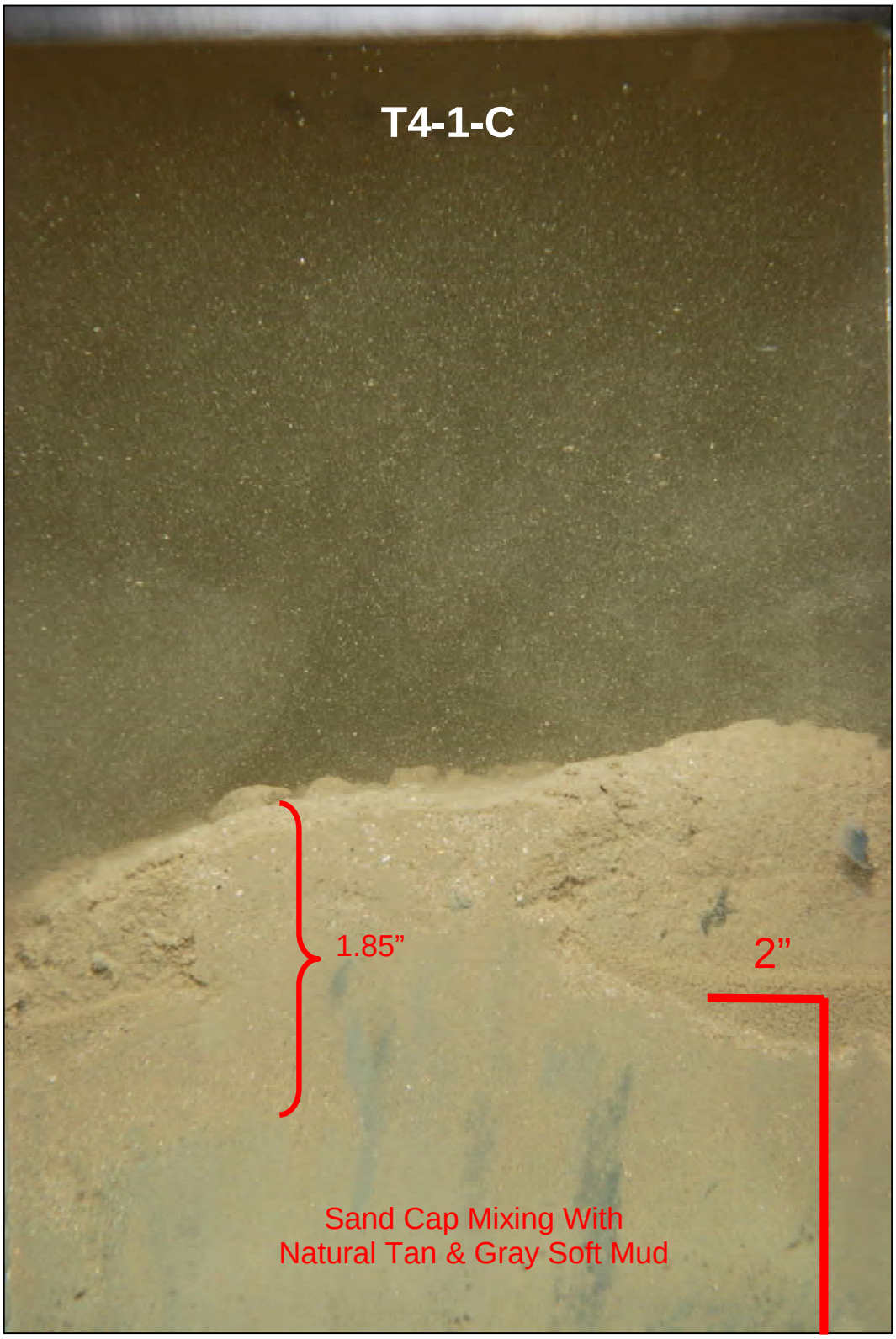

Figure D-8. Sediment profile image of prototype mat system area T4 (sand cap only) taken in capping material.

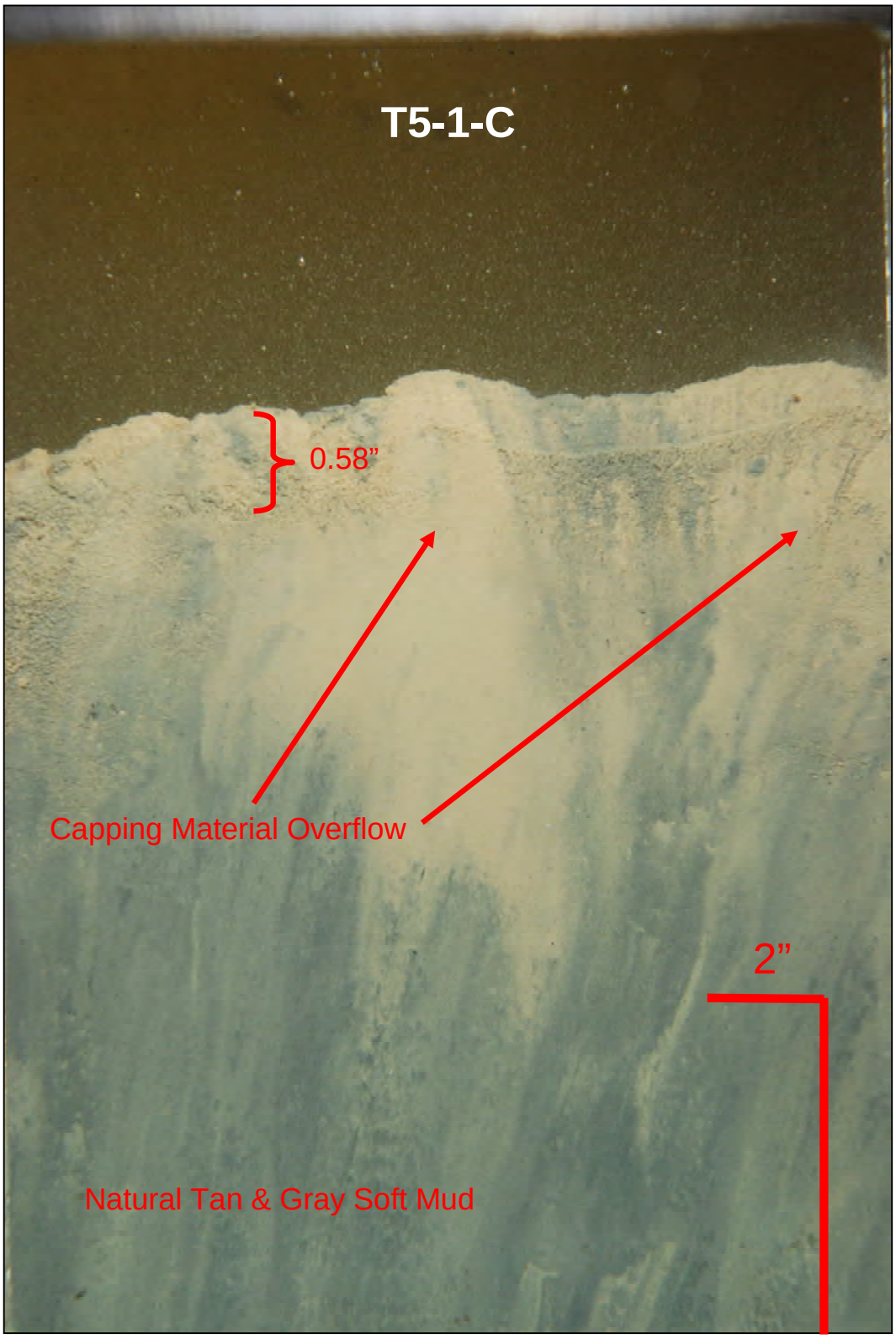

Figure D-9. Sediment profile image of prototype mat system area T5 (no treatment) taken in the natural substrate.

This page is intentionally left blank

APPENDIX E

"First and Second Year Peeper Analytical Results (December 2008 & December 2009)"

This page is intentionally left blank

Table E-1. Year One horizontal peeper raw sub-replicate analytical results for Cottonwood Bay.

	A-1 (ug/L)	A-2 (ug/L)	A-3 (ug/L)	B-1 (ug/L)	B-2 (ug/L)	B-3 (ug/L)	C-2 (ug/L)	C-3 (ug/L)	D-1 (ug/L)
Ag 328.068	0.21	0.21	0.21	0.21	0.21	0.21	0.21	0.21	0.21
Al 308.215	262	275	2684	41	33	36	40	200	34
As 193.696	6.9	26	6.9	129	19	6.9	6.9	6.9	6.9
Ba 455.403	82	122	188	171	60	54	70	73	44
Be 313.107	0.04	0.04	0.95	0.04	0.01	0.01	0.01	0.01	0.01
Ca 317.933	-	-	-	-	-	-	-	-	-
Cd 226.502	1.1	2.4	6.3	6.8	0.87	0.32	0.16	0.47	0.16
Co 228.615	0.72	0.72	6.1	0.72	0.72	0.72	0.72	0.72	0.72
Cr 267.716	5.8	5.4	35	2.9	0.32	0.32	3.2	10	2.1
Cu 324.754	3.2	2.5	37	0.33	0.92	0.97	1.4	3.6	2.6
Fe 259.837	9488	26779	13696	-	9823	4700	272	1477	41
K 766.491	5670	5797	6601	5363	5131	5170	5808	5891	5585
Mg 279.800	4675	4659	5204	4038	4241	3938	4438	4525	2845
Mn 257.610	1650	1807	2193	2027	1965	1624	2330	1955	16
Na 588.995	32887	33475	35867	28589	29263	28590	31737	32088	25374
Ni 231.604	3.2	3.0	19	3.5	1.9	0.73	3.0	3.8	0.73
Pb 220.353	3.5	3.5	49	3.5	3.5	3.5	3.5	3.5	3.5
Sb 206.834	4.6	4.6	4.6	4.6	4.6	4.6	4.6	4.6	4.6
Se 196.026	18	18	18	18	18	18	18	18	18
Tl 190.794	8.2	8.2	8.2	8.2	8.2	8.2	8.2	8.2	8.2
V 292.401	3.7	6.9	43	11	1.1	0.49	0.49	1.8	0.49
Zn 213.857	22	28	267	18	5.6	1.2	12	20	1.2

= Non-Detect (1/2 MDL substituted)

Table E-1. Year One horizontal peeper raw sub-replicate analytical results for Cottonwood Bay.

	D-2 (ug/L)	D-3 (ug/L)	E-1 (ug/L)	E-2 (ug/L)	E-3 (ug/L)	F-1 (ug/L)	F-2 (ug/L)	G-1 (ug/L)	G-2 (ug/L)
Ag 328.068	0.21	0.21	0.21	0.21	0.21	0.21	0.21	0.21	0.21
Al 308.215	35	39	37	38	41	42	262	70	49
As 193.696	6.9	6.9	24	24	33	6.9	6.9	6.9	6.9
Ba 455.403	46	45	122	114	148	54	56	93	103
Be 313.107	0.01	0.01	0.04	0.03	0.06	0.01	0.03	0.01	0.01
Ca 317.933	-	-	-	-	-	-	-	-	-
Cd 226.502	0.16	0.16	3.0	2.9	4.3	0.16	0.16	0.56	0.63
Co 228.615	0.72	0.72	0.72	0.72	0.72	0.72	0.72	0.72	0.72
Cr 267.716	2.8	4.2	0.95	0.66	1.4	1.2	4.9	8.8	8.6
Cu 324.754	2.5	2.9	0.33	0.33	0.33	1.8	4.2	2.7	2.5
Fe 259.837	49	97	38813	33543	-	385	778	404	2548
K 766.491	5567	5438	5513	5583	5578	5418	5519	7701	7720
Mg 279.800	2869	2843	4224	4253	4312	3368	3212	7709	7715
Mn 257.610	42	56	2568	2585	2683	898	457	1381	1355
Na 588.995	25444	24229	31643	31855	32389	26470	26143	54568	54178
Ni 231.604	0.73	1.6	0.73	0.73	0.73	2.1	2.4	8.4	8.2
Pb 220.353	3.5	3.5	3.5	3.5	3.5	3.5	3.5	3.5	3.5
Sb 206.834	4.6	4.6	4.6	4.6	4.6	4.6	4.6	4.6	4.6
Se 196.026	18	18	18	18	18	18	18	18	18
Tl 190.794	8.2	8.2	8.2	8.2	8.2	8.2	8.2	8.2	8.2
V 292.401	1.8	1.8	5.8	4.0	7.3	0.49	2.7	1.2	1.5
Zn 213.857	1.2	3.3	15	10	18	3.3	16	24	22

= Non-Detect (1/2 MDL substituted)

Table E-1. Year One horizontal peeper raw sub-replicate analytical results for Cottonwood Bay.

	G-3 (ug/L)	H-1 (ug/L)	H-2 (ug/L)	H-3 (ug/L)	I-1 (ug/L)	I-2 (ug/L)	I-3 (ug/L)	J-1 (ug/L)	J-2 (ug/L)
Ag 328.068	0.21	0.21	0.21	0.21	0.21	0.21	0.21	0.21	0.21
Al 308.215	47	111	40	40	39	40	112	36	37
As 193.696	6.9	6.9	6.9	6.9	6.9	6.9	6.9	6.9	6.9
Ba 455.403	120	51	50	50	96	90	93	46	48
Be 313.107	0.01	0.01	0.01	0.01	0.01	0.01	0.01	0.01	0.01
Ca 317.933	-	-	-	-	-	-	-	-	-
Cd 226.502	0.81	0.16	0.16	0.16	0.66	0.16	2.7	0.16	0.16
Co 228.615	0.72	0.72	0.72	0.72	2.5	1.7	1.8	0.72	0.72
Cr 267.716	6.3	9.6	6.3	5.2	3.9	3.8	22	4.2	5.2
Cu 324.754	2.2	3.4	2.5	2.6	2.2	8.2	5.5	3.5	2.9
Fe 259.837	4878	819	448	326	437	334	266	376	639
K 766.491	7738	5548	5393	5531	7900	7950	7957	5637	5637
Mg 279.800	7735	2968	3100	3052	7709	7659	7775	2908	2906
Mn 257.610	1363	22	16	4.7	992	944	914	65	101
Na 588.995	-	25685	25600	25609	-	-	-	25583	25627
Ni 231.604	9.2	1.8	3.9	1.5	11	8.0	9.9	1.8	0.73
Pb 220.353	3.5	3.5	3.5	3.5	3.5	3.5	3.5	3.5	3.5
Sb 206.834	4.6	4.6	4.6	4.6	4.6	4.6	4.6	4.6	4.6
Se 196.026	18	18	18	18	18	18	18	18	18
Tl 190.794	8.2	8.2	8.2	8.2	8.2	8.2	8.2	8.2	8.2
V 292.401	2.2	3.5	1.8	1.4	1.6	0.49	2.0	1.8	2.7
Zn 213.857	26	9.2	4.3	4.3	28	18	35	5.1	7.4

= Non-Detect (1/2 MDL substituted)

Table E-1. Year One horizontal peeper raw sub-replicate analytical results for Cottonwood Bay.

	J-3 (ug/L)	K-1 (ug/L)	K-2 (ug/L)	K-3 (ug/L)	L-1 (ug/L)	L-2 (ug/L)	L-3 (ug/L)	M-1 (ug/L)	M-2 (ug/L)
Ag 328.068	0.21	0.21	0.21	0.21	0.21	0.21	0.21	0.21	0.21
Al 308.215	37	39	51	47	3944	108	43	79	61
As 193.696	6.9	6.9	6.9	6.9	6.9	6.9	6.9	6.9	6.9
Ba 455.403	50	93	102	93	209	52	50	88	94
Be 313.107	0.01	0.01	0.01	0.01	1.1	0.01	0.01	0.01	0.01
Ca 317.933	-	-	-	-	-	-	-	-	-
Cd 226.502	0.16	0.16	0.41	0.16	5.4	0.16	0.16	0.46	0.34
Co 228.615	0.72	1.9	0.72	1.7	9.9	0.72	0.72	2.0	2.2
Cr 267.716	6.5	3.4	7.8	4.7	52	1.5	0.86	11	8.0
Cu 324.754	3.3	2.2	2.5	2.2	42	2.7	2.2	3.0	2.6
Fe 259.837	734	801	2483	1345	10190	199	62	1107	2128
K 766.491	5700	7906	8073	7762	6653	5638	5577	8295	8229
Mg 279.800	2954	7735	7791	7616	3826	2974	2918	7409	7302
Mn 257.610	157	1264	1337	1282	1634	43	17	1184	1195
Na 588.995	25917	-	-	-	27707	25867	25603	-	-
Ni 231.604	2.0	9.2	8.7	7.4	20	1.6	0.73	10	9.1
Pb 220.353	3.5	3.5	3.5	3.5	52	3.5	3.5	3.5	3.5
Sb 206.834	4.6	4.6	4.6	4.6	4.6	4.6	4.6	4.6	4.6
Se 196.026	18	18	18	18	18	18	18	18	18
Tl 190.794	8.2	8.2	8.2	8.2	8.2	8.2	8.2	8.2	8.2
V 292.401	2.8	1.7	2.1	1.9	46	1.1	0.49	1.4	1.4
Zn 213.857	9.6	22	24	18	251	4.6	1.2	21	18

= Non-Detect (1/2 MDL substituted)

Table E-1. Year One horizontal peeper raw sub-replicate analytical results for Cottonwood Bay.

	M-3 (ug/L)	N-2 (ug/L)	N-3 (ug/L)	O-1 (ug/L)	O-2 (ug/L)	O-3 (ug/L)	P-1 (ug/L)	P-2 (ug/L)	P-3 (ug/L)
Ag 328.068	0.21	0.21	0.21	0.21	0.21	0.21	0.21	0.21	0.21
Al 308.215	51	138	3.3	35	40	36	127	45	110
As 193.696	6.9	6.9	6.9	6.9	6.9	6.9	6.9	6.9	15
Ba 455.403	88	51	25	48	51	48	97	95	135
Be 313.107	0.01	0.01	0.03	0.01	0.01	0.01	0.01	0.01	0.03
Ca 317.933	-	-	-	-	-	-	-	-	-
Cd 226.502	0.16	0.16	0.16	0.16	0.16	0.16	0.16	0.16	1.3
Co 228.615	2.1	0.72	0.72	0.72	0.72	0.72	0.72	0.72	0.72
Cr 267.716	6.6	1.8	2.0	5.6	5.7	5.4	4.0	1.0	4.9
Cu 324.754	2.1	3.3	0.33	2.8	3.2	2.9	2.6	1.4	2.8
Fe 259.837	1111	253	140	337	390	297	1225	872	13083
K 766.491	8268	5528	2748	5639	5580	5688	7149	7234	7225
Mg 279.800	7384	2858	1455	2904	2847	2897	6321	6338	6528
Mn 257.610	1205	51	11	21	91	40	2166	2193	1877
Na 588.995	-	25214	12320	25963	25638	26018	51172	51114	51447
Ni 231.604	9.9	2.3	0.73	0.73	3.7	1.7	3.1	2.5	3.1
Pb 220.353	3.5	3.5	3.5	3.5	3.5	3.5	3.5	3.5	3.5
Sb 206.834	4.6	4.6	4.6	4.6	4.6	4.6	4.6	4.6	4.6
Se 196.026	40	18	18	18	18	18	18	38	18
Tl 190.794	8.2	8.2	8.2	8.2	8.2	8.2	8.2	8.2	8.2
V 292.401	1.3	1.3	0.49	1.7	2.4	1.6	1.2	0.49	7.4
Zn 213.857	18	7.3	1.2	2.7	4.2	2.7	18	10	30

= Non-Detect (1/2 MDL substituted)

Table E-1. Year One horizontal peeper raw sub-replicate analytical results for Cottonwood Bay.

	Q-1 (ug/L)	Q-2 (ug/L)	Q-3 (ug/L)	R-1 (ug/L)	R-2 (ug/L)	S-1 (ug/L)	S-2 (ug/L)	S-3 (ug/L)	T-1 (ug/L)
Ag 328.068	0.21	0.21	0.21	0.21	0.21	0.21	0.21	0.21	0.21
Al 308.215	36	33	36	126	98	76	137	101	37
As 193.696	6.9	6.9	6.9	6.9	6.9	103	56	34	6.9
Ba 455.403	52	51	51	51	48	332	227	161	52
Be 313.107	0.01	0.01	0.01	0.01	0.01	0.06	0.03	0.01	0.01
Ca 317.933	-	-	-	-	-	-	-	-	-
Cd 226.502	0.16	0.16	0.16	0.16	0.16	7.2	4.2	3.2	0.16
Co 228.615	0.72	0.72	0.72	0.72	0.72	0.72	0.72	0.72	0.72
Cr 267.716	1.1	2.9	1.8	6.8	6.2	19	25	14	0.9
Cu 324.754	1.5	1.6	1.5	3.9	3.4	0.83	2.7	2.2	1.4
Fe 259.837	778	429	412	328	278	-	43770	21601	1001
K 766.491	5709	5830	5778	5706	5650	7409	7481	7311	5618
Mg 279.800	3858	3906	3918	2963	2916	7133	7308	7277	3321
Mn 257.610	982	847	878	40	42	1860	1826	1731	607
Na 588.995	28569	28886	28651	25886	25885	53158	54087	53306	26970
Ni 231.604	0.73	0.73	0.73	1.9	0.73	5.4	4.9	4.4	0.73
Pb 220.353	3.5	3.5	3.5	3.5	3.5	11	3.5	3.5	3.5
Sb 206.834	4.6	4.6	4.6	4.6	4.6	4.6	4.6	4.6	4.6
Se 196.026	18	18	18	18	18	18	18	18	18
Tl 190.794	8.2	8.2	8.2	8.2	8.2	8.2	8.2	8.2	8.2
V 292.401	0.49	0.49	0.49	2.1	2.2	23	15	10	0.49
Zn 213.857	14	19	20	10	6.8	78	63	43	1.2

= Non-Detect (1/2 MDL substituted)

Table E-1. Year One horizontal peeper raw sub-replicate analytical results for Cottonwood Bay.

	T-2 (ug/L)	T-3 (ug/L)	U-1 (ug/L)	U-2 (ug/L)	U-3 (ug/L)
Ag 328.068	0.21	0.21	0.21	0.21	0.21
Al 308.215	32	36	44	44	36
As 193.696	6.9	6.9	6.9	6.9	6.9
Ba 455.403	52	51	56	54	63
Be 313.107	0.01	0.01	0.01	0.01	0.01
Ca 317.933	-	-	-	-	-
Cd 226.502	0.16	0.16	0.16	0.16	0.16
Co 228.615	0.72	0.72	0.72	0.72	0.72
Cr 267.716	1.6	3.9	3.4	6.4	3.5
Cu 324.754	1.5	1.5	3.6	4.5	4.9
Fe 259.837	988	1059	351	1274	785
K 766.491	5638	5513	5619	5643	5795
Mg 279.800	3312	3271	2923	2897	3000
Mn 257.610	603	607	181	170	379
Na 588.995	26970	26430	25819	25758	26259
Ni 231.604	0.73	0.73	2.1	1.9	1.8
Pb 220.353	3.5	3.5	3.5	3.5	3.5
Sb 206.834	4.6	4.6	4.6	4.6	4.6
Se 196.026	18	18	18	18	18
Tl 190.794	8.2	8.2	8.2	8.2	8.2
V 292.401	0.49	0.49	1.5	2.8	2.0
Zn 213.857	2.6	3.1	4.1	5.8	5.4

= Non-Detect (1/2 MDL substituted)

Table E-2. Year One vertical peeper raw sub-replicate analytical results for area T4 (sand cap only).

	AA-1 (ug/L)	AA-2 (ug/L)	AA-3 (ug/L)	AA-4 (ug/L)	AA-5 (ug/L)	AA-6 (ug/L)	AA-7 (ug/L)	AA-8 (ug/L)	AA-9 (ug/L)	AA-10 (ug/L)	AA-11 (ug/L)	AA-12 (ug/L)	AA-13 (ug/L)	AA-14 (ug/L)	AA-15 (ug/L)
Ag 328.068	0.21	0.21	0.21	0.21	0.21	0.21	0.21	0.21	0.21	0.21	0.21	-	0.21	0.21	0.21
Al 308.215	34	31	31	33	32	31	33	32	34	35	34	-	34	37	29
As 193.696	6.9	6.9	6.9	6.9	6.9	6.9	6.9	6.9	6.9	6.9	14	-	6.9	15	6.9
Ba 455.403	56	60	57	54	51	50	45	50	59	71	74	-	83	109	97
Be 313.107	0.01	0.01	0.01	0.01	0.01	0.01	0.01	0.01	0.01	0.01	0.01	-	0.01	0.01	0.01
Ca 317.933	-	-	-	-	-	-	-	-	-	-	-	-	-	-	-
Cd 226.502	0.16	0.16	0.16	0.16	0.16	0.16	0.16	0.42	0.68	0.67	0.7	-	0.8	1.8	1.3
Co 228.615	0.72	0.72	0.72	0.72	0.72	0.72	0.72	0.72	0.72	0.72	0.72	-	0.72	0.72	1.5
Cr 267.716	0.32	0.32	0.32	0.32	0.32	0.32	0.32	0.71	0.32	0.82	0.32	-	0.69	1.5	1.2
Cu 324.754	1.4	1.6	1.2	1.3	1.7	1.7	1.9	0.95	0.75	0.33	0.69	-	0.8	0.33	0.33
Fe 259.837	463	515	782	633	395	314	2309	5002	6904	7850	6951	-	8080	18650	11859
K 766.491	4974	4898	4756	4780	4792	4755	4588	4565	4871	5396	-	-	-	-	-
Mg 279.800	2928	2899	2841	2815	2849	2933	2978	3436	4169	5480	6656	-	7251	7730	8339
Mn 257.610	143	129	382	260	96	186	635	1247	1727	2353	2753	-	2862	2972	2932
Na 588.995	24640	24503	24557	24553	24536	24475	24796	25614	27092	29215	31376	-	33038	34873	37134
Ni 231.604	0.73	0.73	0.73	0.73	0.73	0.73	0.73	0.73	0.73	0.73	0.73	-	0.73	0.73	0.73
Pb 220.353	3.5	3.5	3.5	3.5	3.5	3.5	3.5	3.5	3.5	3.5	3.5	-	3.5	3.5	3.5
Sb 206.834	4.6	4.6	4.6	4.6	4.6	4.6	4.6	4.6	4.6	4.6	4.6	-	4.6	4.6	4.6
Se 196.026	18	18	18	18	18	18	18	18	18	18	18	-	18	18	18
Tl 190.794	8.2	8.2	8.2	8.2	8.2	8.2	8.2	8.2	8.2	8.2	8.2	-	8.2	8.2	8.2
V 292.401	0.49	0.49	0.49	0.49	0.49	0.49	0.49	0.49	0.49	0.49	0.49	-	0.49	1.9	1.1
Zn 213.857	1.2	1.2	1.2	1.2	1.2	1.2	1.2	1.2	1.2	1.2	1.2	-	1.2	3.9	1.2

Table E-2. Year One vertical peeper raw sub-replicate analytical results for area T4 (sand cap only).

	W-1 (ug/L)	W-2 (ug/L)	W-3 (ug/L)	W-4 (ug/L)	W-5 (ug/L)	W-6 (ug/L)	W-7 (ug/L)	W-8 (ug/L)	W-9 (ug/L)	W-10 (ug/L)	W-11 (ug/L)	W-12 (ug/L)	W-13 (ug/L)	W-14 (ug/L)	W-15 (ug/L)
Ag 328.068	0.21	0.21	0.21	0.21	0.21	0.21	0.21	0.21	0.21	0.21	0.21	0.21	0.21	0.21	0.21
Al 308.215	28	27	29	30	31	32	33	30	30	30	27	29	32	32	34
As 193.696	6.9	6.9	6.9	6.9	6.9	6.9	6.9	6.9	6.9	6.9	6.9	6.9	6.9	6.9	6.9
Ba 455.403	55	56	55	49	49	55	51	42	46	49	53	61	71	71	86
Be 313.107	0.01	0.01	0.01	0.01	0.01	0.01	0.01	0.01	0.01	0.01	0.01	0.01	0.01	0.01	0.01
Ca 317.933	-	-	-	-	-	-	-	-	-	-	-	-	-	-	-
Cd 226.502	0.16	0.16	0.16	0.16	0.16	0.16	0.16	0.16	0.16	0.34	0.39	0.67	1.1	0.84	1.5
Co 228.615	0.72	0.72	0.72	0.72	0.72	0.72	0.72	0.72	0.72	0.72	0.72	0.72	0.72	0.72	0.72
Cr 267.716	0.65	0.32	0.32	0.32	0.32	0.32	0.64	0.77	0.32	0.32	0.32	0.32	0.78	1.0	1.5
Cu 324.754	1.6	1.4	1.2	2.3	1.9	1.3	1.3	1.1	0.97	0.88	0.91	0.33	0.33	0.33	0.33
Fe 259.837	127	396	1387	1109	760	2848	1996	2001	2378	3478	5169	7398	9944	8743	14712
K 766.491	4981	4980	4871	4851	4860	4684	4612	4275	4288	4405	4460	4773	5102	5416	-
Mg 279.800	2972	2988	2946	2946	2850	2825	2844	2820	2865	3107	3507	4331	5113	5984	6621
Mn 257.610	11	92	226	208	100	282	310	661	616	819	1154	1638	1977	2226	2389
Na 588.995	24806	24950	24870	24768	24751	24583	24737	24201	24548	25205	25757	27930	29708	31783	33380
Ni 231.604	0.73	0.73	0.73	1.7	0.73	0.73	0.73	0.73	0.73	0.73	0.73	0.73	0.73	0.73	0.73
Pb 220.353	3.5	3.5	3.5	3.5	3.5	3.5	3.5	3.5	3.5	3.5	3.5	3.5	3.5	3.5	3.5
Sb 206.834	4.6	4.6	4.6	4.6	4.6	4.6	4.6	4.6	4.6	4.6	4.6	4.6	4.6	4.6	4.6
Se 196.026	18	18	18	18	18	18	18	18	18	18	18	18	18	18	18
Tl 190.794	8.2	8.2	8.2	8.2	8.2	8.2	8.2	8.2	8.2	8.2	8.2	8.2	8.2	8.2	8.2
V 292.401	0.49	0.49	0.49	0.49	0.49	1.7	0.49	0.49	0.49	0.49	0.49	0.49	1.1	1.3	1.4
Zn 213.857	2.4	1.2	1.2	2.3	1.2	2.6	2.6	1.2	1.2	1.2	1.2	1.2	1.2	2.4	3.3

Table E-2. Year One vertical peeper raw sub-replicate analytical results for area T4 (sand cap only).

	Y-1 (ug/L)	Y-2 (ug/L)	Y-3 (ug/L)	Y-4 (ug/L)	Y-5 (ug/L)	Y-6 (ug/L)	Y-7 (ug/L)	Y-8 (ug/L)	Y-9 (ug/L)	Y-10 (ug/L)	Y-11 (ug/L)	Y-12 (ug/L)	Y-13 (ug/L)	Y-14 (ug/L)	Y-15 (ug/L)
Ag 328.068	0.21	0.21	0.21	0.21	0.21	0.21	0.21	0.21	0.21	0.21	0.21	0.21	0.21	0.21	0.21
Al 308.215	41	35	28	32	39	32	30	32	35	33	39	33	38	57	34
As 193.696	6.9	6.9	6.9	6.9	6.9	6.9	14	15	6.9	18	6.9	18	22	23	18
Ba 455.403	66	69	67	70	63	58	58	67	79	93	105	123	128	138	146
Be 313.107	0.01	0.01	0.01	0.01	0.01	0.01	0.01	0.01	0.01	0.01	0.01	0.01	0.01	0.01	0.01
Ca 317.933	-	-	-	-	-	-	-	-	-	-	-	-	-	-	-
Cd 226.502	0.16	0.16	0.16	0.16	0.16	0.34	0.39	0.86	1.1	1.3	1.5	1.8	1.9	2.1	1.8
Co 228.615	0.72	0.72	0.72	0.72	0.72	0.72	0.72	0.72	0.72	0.72	0.72	0.72	0.72	0.72	0.72
Cr 267.716	0.9	0.65	0.32	0.85	0.32	0.76	0.98	0.74	2.7	1.3	2.5	0.98	0.97	1.7	1.1
Cu 324.754	1.7	1.5	1.9	1.5	1.2	1.0	0.7	0.33	0.33	0.73	0.67	0.33	0.33	0.33	0.81
Fe 259.837	381	526	431	962	1116	3814	5813	9326	11544	14138	15997	18948	19756	20475	19816
K 766.491	4959	4941	4981	4807	4678	4350	4205	4444	4934	5288	-	-	-	-	-
Mg 279.800	3073	3086	2998	2926	2868	2906	3180	3877	4665	5524	6213	7109	7621	7831	8026
Mn 257.610	128	201	114	363	386	1046	1442	2012	2375	2767	2998	3418	3488	3466	3367
Na 588.995	24786	24678	24543	24493	24605	24836	25039	26243	27385	28463	29393	30680	31958	32534	33254
Ni 231.604	0.73	1.9	1.7	0.73	0.73	0.73	0.73	0.73	0.73	0.73	0.73	0.73	0.73	0.73	0.73
Pb 220.353	3.5	3.5	3.5	3.5	3.5	3.5	3.5	3.5	3.5	3.5	3.5	3.5	3.5	3.5	3.5
Sb 206.834	4.6	4.6	4.6	4.6	4.6	4.6	4.6	4.6	4.6	4.6	4.6	4.6	4.6	4.6	4.6
Se 196.026	18	18	18	18	18	18	18	18	18	18	18	18	18	44	18
Tl 190.794	8.2	8.2	8.2	8.2	8.2	8.2	8.2	8.2	8.2	8.2	8.2	8.2	8.2	8.2	8.2
V 292.401	0.49	0.49	0.49	0.49	0.49	0.49	1.1	1.7	1.7	2.0	2.3	1.8	2.3	1.9	2.3
Zn 213.857	3.1	2.6	1.2	1.2	1.2	1.2	1.2	2.7	3.9	3.0	3.3	4.1	3.8	5.0	3.5

Table E-2. Year One vertical peeper raw sub-replicate analytical results for area T4 (sand cap only).

	Z-1 (ug/L)	Z-2 (ug/L)	Z-3 (ug/L)	Z-4 (ug/L)	Z-5 (ug/L)	Z-6 (ug/L)	Z-7 (ug/L)	Z-8 (ug/L)	Z-9 (ug/L)	Z-10 (ug/L)	Z-11 (ug/L)	Z-12 (ug/L)	Z-13 (ug/L)	Z-14 (ug/L)	Z-15 (ug/L)
Ag 328.068	0.21	0.21	0.21	0.21	0.21	0.21	0.21	0.21	0.21	0.21	0.21	0.21	0.21	0.21	0.21
Al 308.215	33	33	33	33	33	33	33	33	33	33	33	33	33	33	33
As 193.696	6.9	6.9	6.9	6.9	6.9	6.9	6.9	6.9	6.9	6.9	6.9	6.9	6.9	6.9	6.9
Ba 455.403	57	57	57	57	57	57	57	57	57	57	57	57	57	57	57
Be 313.107	0.01	0.01	0.01	0.01	0.01	0.01	0.01	0.01	0.01	0.01	0.01	0.01	0.01	0.01	0.01
Ca 317.933	-	-	-	-	-	-	-	-	-	-	-	-	-	-	-
Cd 226.502	0.16	0.16	0.16	0.16	0.16	0.16	0.16	0.16	0.16	0.16	0.16	0.16	0.16	0.16	0.16
Co 228.615	0.72	0.72	0.72	0.72	0.72	0.72	0.72	0.72	0.72	0.72	0.72	0.72	0.72	0.72	0.72
Cr 267.716	0.32	0.32	0.32	0.32	0.32	0.32	0.32	0.32	0.32	0.32	0.32	0.32	0.32	0.32	0.32
Cu 324.754	1.9	1.9	1.9	1.9	1.9	1.9	1.9	1.9	1.9	1.9	1.9	1.9	1.9	1.9	1.9
Fe 259.837	92	92	92	92	92	92	92	92	92	92	92	92	92	92	92
K 766.491	5062	5062	5062	5062	5062	5062	5062	5062	5062	5062	5062	5062	5062	5062	5062
Mg 279.800	3019	3019	3019	3019	3019	3019	3019	3019	3019	3019	3019	3019	3019	3019	3019
Mn 257.610	20	20	20	20	20	20	20	20	20	20	20	20	20	20	20
Na 588.995	24691	24691	24691	24691	24691	24691	24691	24691	24691	24691	24691	24691	24691	24691	24691
Ni 231.604	0.73	0.73	0.73	0.73	0.73	0.73	0.73	0.73	0.73	0.73	0.73	0.73	0.73	0.73	0.73
Pb 220.353	3.5	3.5	3.5	3.5	3.5	3.5	3.5	3.5	3.5	3.5	3.5	3.5	3.5	3.5	3.5
Sb 206.834	4.6	4.6	4.6	4.6	4.6	4.6	4.6	4.6	4.6	4.6	4.6	4.6	4.6	4.6	4.6
Se 196.026	18	18	18	18	18	18	18	18	18	18	18	18	18	18	18
Tl 190.794	8.2	8.2	8.2	8.2	8.2	8.2	8.2	8.2	8.2	8.2	8.2	8.2	8.2	8.2	8.2
V 292.401	0.49	0.49	0.49	0.49	0.49	0.49	0.49	0.49	0.49	0.49	0.49	0.49	0.49	0.49	0.49
Zn 213.857	1.2	1.2	1.2	1.2	1.2	1.2	1.2	1.2	1.2	1.2	1.2	1.2	1.2	1.2	1.2

= Non-Detect (1/2 MDL substituted)
Chamber depth increases from left to right; each chamber 0.5" apart.

Table E-3. Year One vertical peeper raw sub-replicate analytical results for area T5 (no treatment/control).

	AB-1 (ug/L)	AB-2 (ug/L)	AB-3 (ug/L)	AB-4 (ug/L)	AB-5 (ug/L)	AB-6 (ug/L)	AB-7 (ug/L)	AB-8 (ug/L)	AB-9 (ug/L)	AB-10 (ug/L)	AB-11 (ug/L)	AB-12 (ug/L)	AB-13 (ug/L)	AB-14 (ug/L)	AB-15 (ug/L)
Ag 328.068	0.21	0.21	0.21	0.21	0.21	0.21	0.21	0.21	0.21	0.21	0.21	0.21	0.21	0.21	0.21
Al 308.215	18	17	20	23	32	48	13	20	20	20	20	14	19	22	58
As 193.696	17	19	17	16	19	14	6.9	18	6.9	17	6.9	6.9	6.9	6.9	6.9
Ba 455.403	60	68	72	73	77	77	70	78	76	80	79	73	83	82	84
Be 313.107	0.01	0.01	0.01	0.01	0.01	0.01	0.01	0.01	0.01	0.01	0.01	0.01	0.01	0.01	0.01
Ca 317.933	-	-	-	-	-	-	-	-	-	-	-	-	-	-	-
Cd 226.502	0.78	0.92	0.97	0.92	1.3	0.97	0.85	1.2	1.1	1.1	1.2	0.86	1.2	1.3	1.4
Co 228.615	0.72	0.72	0.72	0.72	0.72	0.72	0.72	0.72	0.72	0.72	0.72	0.72	0.72	0.72	0.72
Cr 267.716	0.32	0.32	0.32	0.32	1.6	0.32	0.32	0.89	0.74	1.1	1.4	1.7	2.1	2.5	5.1
Cu 324.754	0.33	0.33	0.75	0.33	0.33	0.33	0.33	0.33	0.33	0.33	0.33	0.33	0.33	0.33	0.33
Fe 259.837	8557	10016	11357	11675	12719	12317	8826	12788	10971	12357	12118	9971	12287	13518	14379
K 766.491	5606	5624	5718	5678	5647	5721	6061	5794	5779	5787	5857	6189	5946	6018	5959
Mg 279.800	5853	6029	5964	5923	5896	6024	6441	6020	5940	5976	6150	6848	6437	6412	6632
Mn 257.610	2469	2596	2614	2567	2557	2505	2504	2385	2259	2184	2137	2133	2037	1950	1923
Na 588.995	31372	31985	32291	32262	32155	32494	34313	32560	32163	32057	32570	35020	33607	33869	34603
Ni 231.604	0.73	0.73	0.73	0.73	0.73	0.73	1.5	0.73	0.73	0.73	0.73	1.5	0.73	1.7	0.73
Pb 220.353	3.5	3.5	3.5	3.5	3.5	3.5	3.5	3.5	3.5	3.5	3.5	3.5	3.5	3.5	3.5
Sb 206.834	4.6	4.6	4.6	4.6	4.6	4.6	4.6	4.6	4.6	4.6	4.6	4.6	4.6	4.6	4.6
Se 196.026	18	18	18	18	18	18	18	18	18	18	18	18	18	18	18
Tl 190.794	8.2	8.2	8.2	8.2	8.2	8.2	8.2	8.2	8.2	8.2	8.2	8.2	8.2	8.2	8.2
V 292.401	1.3	1.7	1.4	1.6	1.6	1.7	0.49	1.7	1.5	1.8	1.5	1.2	1.3	1.5	1.9
Zn 213.857	3.2	2.6	2.9	3.3	4.2	2.6	1.2	2.7	2.8	2.8	3.1	1.2	2.9	2.8	4.9

Table E-3. Year One vertical peeper raw sub-replicate analytical results for area T5 (no treatment/control).

	AC-1 (ug/L)	AC-2 (ug/L)	AC-3 (ug/L)	AC-4 (ug/L)	AC-5 (ug/L)	AC-6 (ug/L)	AC-7 (ug/L)	AC-8 (ug/L)	AC-9 (ug/L)	AC-10 (ug/L)	AC-11 (ug/L)	AC-12 (ug/L)	AC-13 (ug/L)	AC-14 (ug/L)
Ag 328.068	0.21	0.21	0.21	0.21	0.21	0.21	0.21	0.21	0.21	0.21	0.21	0.21	0.21	0.21
Al 308.215	18	18	20	20	21	16	19	20	22	19	18	19	19	20
As 193.696	6.9	18	15	14	6.9	15	6.9	6.9	6.9	6.9	6.9	6.9	6.9	6.9
Ba 455.403	53	63	65	64	67	66	67	68	70	71	72	75	76	77
Be 313.107	0.01	0.01	0.01	0.01	0.01	0.01	0.01	0.01	0.01	0.01	0.01	0.01	0.01	0.01
Ca 317.933	-	-	-	-	-	-	-	-	-	-	-	-	-	-
Cd 226.502	0.4	0.85	0.76	0.78	0.83	0.73	0.74	0.72	0.9	0.92	1.0	1.0	1.3	1.2
Co 228.615	0.72	0.72	0.72	0.72	0.72	0.72	0.72	0.72	0.72	0.72	0.72	0.72	0.72	0.72
Cr 267.716	0.32	0.32	0.32	0.32	0.32	0.32	0.32	0.85	0.86	0.94	1.4	1.6	1.9	2.1
Cu 324.754	0.33	0.33	0.33	0.33	0.33	0.33	0.33	0.33	0.33	0.33	0.33	0.33	0.33	0.33
Fe 259.837	5323	8733	8818	8608	9183	7855	8686	9773	10143	10759	11392	12598	13664	13616
K 766.491	5657	5661	5681	5662	5642	5624	5643	5641	5707	5690	5678	5689	5724	5747
Mg 279.800	5591	5579	5429	5335	5256	5194	5209	5279	5290	5382	5405	5509	5591	5718
Mn 257.610	2294	2346	2297	2254	2166	2085	2036	2005	1943	1932	1911	1918	1917	1916
Na 588.995	32288	32451	32532	32476	32381	32128	32114	32122	32314	32363	32393	32673	32911	33206
Ni 231.604	0.73	0.73	0.73	0.73	0.73	0.73	0.73	0.73	0.73	0.73	0.73	0.73	0.73	0.73
Pb 220.353	3.5	3.5	3.5	3.5	3.5	3.5	3.5	3.5	3.5	3.5	3.5	3.5	3.5	3.5
Sb 206.834	4.6	4.6	4.6	4.6	4.6	4.6	4.6	4.6	4.6	4.6	4.6	4.6	4.6	4.6
Se 196.026	18	18	18	18	18	18	18	18	18	18	18	18	18	18
Tl 190.794	8.2	8.2	8.2	8.2	8.2	8.2	8.2	8.2	8.2	8.2	8.2	8.2	8.2	8.2
V 292.401	0.49	1.3	1.5	1.6	1.6	1.3	1.2	1.3	1.4	1.3	1.6	1.7	1.8	1.8
Zn 213.857	1.2	1.2	3.4	2.9	1.2	1.2	5.0	2.8	3.5	2.6	2.8	3.6	3.1	3.0

Table E-3. Year One vertical peeper raw sub-replicate analytical results for area T5 (no treatment/control).

	AD-1 (ug/L)	AD-2 (ug/L)	AD-3 (ug/L)	AD-4 (ug/L)	AD-5 (ug/L)	AD-6 (ug/L)	AD-7 (ug/L)	AD-8 (ug/L)	AD-9 (ug/L)	AD-10 (ug/L)	AD-11 (ug/L)	AD-12 (ug/L)	AD-13 (ug/L)	AD-14 (ug/L)	AD-15 (ug/L)
Ag 328.068	0.21	0.21	0.21	0.21	0.21	0.21	0.21	0.21	0.21	0.21	0.21	0.21	0.21	0.21	0.21
Al 308.215	20	19	19	20	20	18	19	22	17	15	15	21	20	19	16
As 193.696	6.9	6.9	6.9	6.9	15	6.9	6.9	6.9	6.9	6.9	6.9	6.9	6.9	6.9	6.9
Ba 455.403	51	56	60	65	67	66	75	72	74	74	77	80	83	81	79
Be 313.107	0.01	0.01	0.01	0.01	0.01	0.01	0.01	0.01	0.01	0.01	0.01	0.01	0.01	0.01	0.01
Ca 317.933	-	-	-	-	-	-	-	-	-	-	-	-	-	-	-
Cd 226.502	0.41	0.66	0.78	0.9	0.92	0.62	0.93	0.86	0.84	0.85	1.1	1.1	1.3	1.3	1.2
Co 228.615	0.72	0.72	0.72	0.72	0.72	0.72	0.72	0.72	0.72	0.72	0.72	0.72	0.72	0.72	0.72
Cr 267.716	0.32	0.32	0.32	0.32	0.32	0.32	0.32	0.69	0.76	1.1	1.5	2.0	2.2	2.5	2.4
Cu 324.754	0.33	0.33	0.33	0.33	0.33	0.33	0.33	0.33	0.33	0.33	0.33	0.33	0.33	0.33	0.33
Fe 259.837	5471	7162	8553	9446	9794	8711	10841	9592	10127	9067	12591	13417	14216	14400	12625
K 766.491	5278	5386	5439	5508	5588	5556	5614	5663	5673	5690	5729	5836	5892	5924	5959
Mg 279.800	5307	5302	5377	5713	5617	5554	5662	5759	5799	5862	5972	6131	6242	6343	6424
Mn 257.610	2173	2289	2397	2492	2473	2427	2425	2345	2263	2164	2108	2034	1986	1954	1915
Na 588.995	30868	31251	31780	32577	32370	31971	32072	32209	32294	32402	32843	33544	34343	34544	34984
Ni 231.604	0.73	0.73	0.73	0.73	0.73	0.73	0.73	0.73	0.73	0.73	0.73	0.73	0.73	0.73	0.73
Pb 220.353	3.5	3.5	3.5	3.5	3.5	3.5	3.5	3.5	3.5	3.5	3.5	3.5	3.5	3.5	3.5
Sb 206.834	4.6	4.6	4.6	4.6	4.6	4.6	4.6	4.6	4.6	4.6	4.6	4.6	4.6	4.6	4.6
Se 196.026	18	18	18	18	18	18	18	18	18	18	18	18	18	18	18
Tl 190.794	8.2	8.2	8.2	8.2	8.2	8.2	8.2	8.2	8.2	8.2	8.2	8.2	8.2	8.2	8.2
V 292.401	0.49	0.49	0.49	1.2	1.1	0.49	1.3	1.1	1.2	1.1	1.7	0.99	1.2	1.9	1.3
Zn 213.857	2.8	1.2	2.5	3.1	2.5	1.2	2.5	2.6	2.5	1.2	3.6	3.8	2.9	3.0	2.4

Table E-3. Year One vertical peeper raw sub-replicate analytical results for area T5 (no treatment/control).

	T5-1 (ug/L)	T5-2 (ug/L)	T5-3 (ug/L)	T5-4 (ug/L)	T5-5 (ug/L)	T5-6 (ug/L)	T5-7 (ug/L)	T5-8 (ug/L)	T5-9 (ug/L)	T5-10 (ug/L)	T5-11 (ug/L)	T5-12 (ug/L)	T5-13 (ug/L)	T5-14 (ug/L)
Ag 328.068	0.21	0.21	0.21	0.21	0.21	0.21	0.21	0.21	0.21	0.21	0.21	0.21	0.21	0.21
Al 308.215	22	31	21	20	26	27	31	21	25	20	22	24	25	22
As 193.696	22	20	22	22	23	23	14	16	6.9	6.9	6.9	6.9	6.9	6.9
Ba 455.403	51	59	62	64	68	70	74	75	76	78	80	80	80	81
Be 313.107	0.01	0.01	0.01	0.01	0.01	0.01	0.01	0.01	0.01	0.01	0.01	0.01	0.01	0.01
Ca 317.933	-	-	-	-	-	-	-	-	-	-	-	-	-	-
Cd 226.502	0.59	0.84	1.0	1.0	1.0	1.0	1.1	1.4	1.3	1.2	1.2	1.3	1.2	1.3
Co 228.615	0.72	0.72	0.72	0.72	0.72	0.72	0.72	0.72	0.72	0.72	0.72	0.72	0.72	0.72
Cr 267.716	0.7	0.85	0.73	0.32	0.68	0.83	0.75	0.32	0.73	0.75	1.1	1.1	1.6	1.7
Cu 324.754	0.33	0.33	0.33	0.33	0.33	0.33	0.33	0.33	0.33	0.33	0.33	0.33	0.33	0.33
Fe 259.837	7343	8968	9802	10779	11509	12353	13162	13250	12937	13095	13493	13817	14344	14471
K 766.491	5066	5239	5328	5335	5420	5469	5467	5562	5591	5669	5751	5807	5860	5900
Mg 279.800	5161	5386	5548	5586	5531	5534	5618	5684	5684	5804	5900	6005	6116	6127
Mn 257.610	2109	2302	2459	2584	2632	2696	2737	2677	2549	2456	2348	2255	2183	2118
Na 588.995	29365	30209	30758	30875	31435	32005	32154	32530	32506	32863	33329	33809	34242	34748
Ni 231.604	1.9	0.73	0.73	0.73	0.73	0.73	0.73	0.73	0.73	0.73	0.73	0.73	2.7	0.73
Pb 220.353	3.5	3.5	3.5	3.5	3.5	3.5	3.5	3.5	3.5	3.5	3.5	3.5	3.5	3.5
Sb 206.834	4.6	4.6	4.6	4.6	4.6	4.6	4.6	4.6	4.6	4.6	4.6	4.6	4.6	4.6
Se 196.026	18	18	18	18	18	18	18	18	18	18	18	18	18	18
Tl 190.794	8.2	8.2	8.2	8.2	8.2	8.2	8.2	8.2	8.2	8.2	8.2	8.2	8.2	8.2
V 292.401	1.3	2.1	2.4	2.0	1.7	2.0	1.9	2.0	1.9	1.9	1.7	1.9	2.0	1.3
Zn 213.857	2.9	3.4	2.6	2.9	3.3	3.9	3.6	3.4	4.1	3.3	15	3.9	4.1	3.4

= Non-Detect (1/2 MDL substituted)
Chamber depth increases from left to right; each chamber 0.5" apart.

Table E-4. Year One horizontal peeper replicate analytical results for Cottonwood Bay.

Analyte	Detection Limit	Units	T1-HP-SDM-NW A		T1-HP-MW-NW B		T1-HP-SDM-SW C		T1-HP-MW-SW D		T1-HP-SDM-NE E	
Aluminum	2.3	ug/L	1074		37		120		36		39	
Antimony	9.2	ug/L	4.6	U	4.6	U	4.6	U	4.6	U	4.6	U
Arsenic	14	ug/L	26		74		6.9	U	6.9	U	27	
Barium	0.05	ug/L	131		95		71		45		128	
Beryllium	0.03	ug/L	0.34		0.04		0.01	U	0.01	U	0.04	
Cadmium	0.31	ug/L	3.3		2.7		0.47		0.16	U	3.4	
Calcium	0.87	ug/L	0.44	U	0.44	U	0.44	U	0.44	U	0.44	U
Chromium	0.64	ug/L	15		2.9		6.8		3.0		1.0	
Cobalt	1.4	ug/L	6.1		0.72	U	0.72	U	0.72	U	0.72	U
Copper	0.67	ug/L	14		0.94		2.5		2.7		0.33	U
Iron	1.2	ug/L	16654		7261		875		62		36178	
Lead	7.1	ug/L	49		3.5		3.5	U	3.5	U	3.5	U
Magnesium	4.2	ug/L	4846		4072		4482		2852		4263	
Manganese	0.08	ug/L	1883		1872		2143		38		2612	
Nickel	1.5	ug/L	8.4		2.7		3.4		1.6		0.73	U
Potassium	1.6	ug/L	6023		5221		5850		5530		5558	
Selenium	36	ug/L	18	U	18	U	18	U	18	U	18	U
Silver	0.41	ug/L	0.21	U	0.21	U	0.21	U	0.21	U	0.21	U
Sodium	10	ug/L	34077		28814		31913		25016		31962	
Thallium	16	ug/L	8.2	U	8.2	U	8.2	U	8.2	U	8.2	U
Vanadium	0.99	ug/L	18		6.0		1.8		1.8		5.7	
Zinc	2.3	ug/L	106		12		16		3.3		14	

U = Concentration below detection limit in all sub-replicates; 1/2 detection limit used instead.

N/A = Data not available.

Table E-4. Year One horizontal peeper replicate analytical results for Cottonwood Bay.

Analyte	Detection Limit	Units	T1-HP-MW-NEF		T2-HP-SDM-NWG		T2-HP-MSN-NWH		T2-HP-SDM-SWI		T2-HP-MSN-SWJ	
Aluminum	2.3	ug/L	152		56		64		64		37	
Antimony	9.2	ug/L	4.6	U	4.6	U	4.6	U	4.6	U	4.6	U
Arsenic	14	ug/L	6.9	U	6.9	U	6.9	U	6.9	U	6.9	U
Barium	0.05	ug/L	55		106		50		93		48	
Beryllium	0.03	ug/L	0.03		0.01	U	0.01	U	0.01	U	0.01	U
Cadmium	0.31	ug/L	0.16	U	0.67		0.16	U	1.7		0.16	U
Calcium	0.87	ug/L	0.44	U	0.44	U	0.44	U	0.44	U	0.44	U
Chromium	0.64	ug/L	3.1		7.9		7.0		10		5.3	
Cobalt	1.4	ug/L	0.72	U	0.72	U	0.72	U	2.0		0.72	U
Copper	0.67	ug/L	3.0		2.5		2.8		5.3		3.2	
Iron	1.2	ug/L	582		2610		531		346		583	
Lead	7.1	ug/L	3.5	U	3.5	U	3.5	U	3.5	U	3.5	U
Magnesium	4.2	ug/L	3290		7720		3040		7714		2923	
Manganese	0.08	ug/L	677		1366		14		950		108	
Nickel	1.5	ug/L	2.3		8.6		2.4		9.6		1.9	
Potassium	1.6	ug/L	5469		7720		5491		7936		5658	
Selenium	36	ug/L	18	U	18	U	18	U	18	U	18	U
Silver	0.41	ug/L	0.21	U	0.21	U	0.21	U	0.21	U	0.21	U
Sodium	10	ug/L	26307		54373		25631		5.1	U	25709	
Thallium	16	ug/L	8.2	U	8.2	U	8.2	U	8.2	U	8.2	U
Vanadium	0.99	ug/L	2.7		1.7		2.2		1.8		2.4	
Zinc	2.3	ug/L	9.7		24		5.9		27		7.3	

Table E-4. Year One horizontal peeper replicate analytical results for Cottonwood Bay.

Analyte	Detection Limit	Units	T2-HP-SDM-NEK		T2-SD-MSN-NEL		T3-SD-SDM-NWM		T3-HP-MM-NWN		T3-SD-MW-NWO	
Aluminum	2.3	ug/L	46		1365		64		71		37	
Antimony	9.2	ug/L	4.6	U	4.6	U	4.6	U	4.6	U	4.6	U
Arsenic	14	ug/L	6.9	U	6.9	U	6.9	U	6.9	U	6.9	U
Barium	0.05	ug/L	96		104		90		38		49	
Beryllium	0.03	ug/L	0.01	U	1.1		0.01	U	0.03		0.01	U
Cadmium	0.31	ug/L	0.41		5.4		0.4		0.16	U	0.16	U
Calcium	0.87	ug/L	0.44	U	0.44	U	0.44	U	0.44	U	0.44	U
Chromium	0.64	ug/L	5.3		18		8.4		1.9		5.5	
Cobalt	1.4	ug/L	1.8		9.9		2.1		0.72	U	0.72	U
Copper	0.67	ug/L	2.3		16		2.5		3.3		3.0	
Iron	1.2	ug/L	1543		3484		1448		196		341	
Lead	7.1	ug/L	3.5	U	52		3.5	U	3.5	U	3.5	U
Magnesium	4.2	ug/L	7714		3239		7365		2157		2883	
Manganese	0.08	ug/L	1294		564		1195		31		51	
Nickel	1.5	ug/L	8.4		11		9.7		2.3		2.7	
Potassium	1.6	ug/L	7914		5956		8264		4138		5635	
Selenium	36	ug/L	18	U	18	U	40		18	U	18	U
Silver	0.41	ug/L	0.21	U	0.21	U	0.21	U	0.21	U	0.21	U
Sodium	10	ug/L	5.1	U	26393		5.1	U	18767		25873	
Thallium	16	ug/L	8.2	U	8.2	U	8.2	U	8.2	U	8.2	U
Vanadium	0.99	ug/L	1.9		24		1.4		1.3		1.9	
Zinc	2.3	ug/L	21		128		19		7.3		3.2	

Table E-4. Year One horizontal peeper replicate analytical results for Cottonwood Bay.

Analyte	Detection Limit	Units	T3-HP-SDM-NE P		T3-HP-MM-NE Q		T3-HP-MW-NE R		T3-HP-SDM-SE S		T3-HP-MM-SE T	
Aluminum	2.3	ug/L	94		35		112		105		35	
Antimony	9.2	ug/L	4.6	U	4.6	U	4.6	U	4.6	U	4.6	U
Arsenic	14	ug/L	15		6.9	U	6.9	U	64		6.9	U
Barium	0.05	ug/L	109		51		50		240		52	
Beryllium	0.03	ug/L	0.03		0.01	U	0.01	U	0.05		0.01	U
Cadmium	0.31	ug/L	1.3		0.16	U	0.16	U	4.9		0.16	U
Calcium	0.87	ug/L	0.44	U	0.44	U	0.44	U	0.44	U	0.44	U
Chromium	0.64	ug/L	3.3		1.9		6.5		20		2.1	
Cobalt	1.4	ug/L	0.72	U	0.72	U	0.72	U	0.72	U	0.72	U
Copper	0.67	ug/L	2.3		1.5		3.6		1.9		1.5	
Iron	1.2	ug/L	5060		540		303		32685		1016	
Lead	7.1	ug/L	3.5	U	3.5	U	3.5	U	11		3.5	U
Magnesium	4.2	ug/L	6396		3894		2939		7239		3301	
Manganese	0.08	ug/L	2079		902		41		1806		606	
Nickel	1.5	ug/L	2.9		0.73	U	1.9		4.9		0.73	U
Potassium	1.6	ug/L	7203		5773		5678		7400		5590	
Selenium	36	ug/L	38		18	U	18	U	18	U	18	U
Silver	0.41	ug/L	0.21	U	0.21	U	0.21	U	0.21	U	0.21	U
Sodium	10	ug/L	51244		28702		25886		53517		26790	
Thallium	16	ug/L	8.2	U	8.2	U	8.2	U	8.2	U	8.2	U
Vanadium	0.99	ug/L	4.3		0.49	U	2.2		16		0.49	U
Zinc	2.3	ug/L	19		18		8.5		61		2.9	

Table E-4. Year One horizontal peeper replicate analytical results for Cottonwood Bay.

Analyte	Detection Limit	Units	T3-HP-MW-SE U	
Aluminum	2.3	ug/L	42	
Antimony	9.2	ug/L	4.6	U
Arsenic	14	ug/L	6.9	U
Barium	0.05	ug/L	58	
Beryllium	0.03	ug/L	0.01	U
Cadmium	0.31	ug/L	0.16	U
Calcium	0.87	ug/L	0.44	U
Chromium	0.64	ug/L	4.5	
Cobalt	1.4	ug/L	0.72	U
Copper	0.67	ug/L	4.3	
Iron	1.2	ug/L	803	
Lead	7.1	ug/L	3.5	U
Magnesium	4.2	ug/L	2940	
Manganese	0.08	ug/L	243	
Nickel	1.5	ug/L	2.0	
Potassium	1.6	ug/L	5686	
Selenium	36	ug/L	18	U
Silver	0.41	ug/L	0.21	U
Sodium	10	ug/L	25945	
Thallium	16	ug/L	8.2	U
Vanadium	0.99	ug/L	2.1	
Zinc	2.3	ug/L	5.1	

Table E-5. Year One horizontal peeper replicate analytical results for area T1 (single mat only).

T1 - Single Mat Only

Analyte	Units	Rep 1		Rep 2		Rep 3		Rep Average	
		Below Mat (A)	Above Mat (B)	Below Mat (C)	Above Mat (D)	Below Mat (E)	Above Mat (F)	Below Mat	Above Mat
Aluminum	ug/L	1074	37	120	36	39	152	411	75
Antimony	ug/L	4.6	4.6	4.6	4.6	4.6	4.6	4.6	4.6
Arsenic	ug/L	26	74	6.9	6.9	27	6.9	20	29
Barium	ug/L	131	95	71	45	128	55	110	65
Beryllium	ug/L	0.34	0.04	0.01	0.01	0.04	0.03	0.13	0.03
Cadmium	ug/L	3.3	2.7	0.47	0.16	3.4	0.16	2.4	0.99
Calcium	ug/L	0.44	0.44	0.44	0.44	0.44	0.44	0.44	0.44
Chromium	ug/L	15	2.9	6.8	3.0	1.0	3.1	7.7	3.0
Cobalt	ug/L	6.1	0.72	0.72	0.72	0.72	0.72	2.5	0.72
Copper	ug/L	14	0.94	2.5	2.7	0.33	3.0	5.7	2.2
Iron	ug/L	16654	7261	875	62	36178	582	17902	2635
Lead	ug/L	49	3.5	3.5	3.5	3.5	3.5	19	3.5
Magnesium	ug/L	4846	4072	4482	2852	4263	3290	4530	3405
Manganese	ug/L	1883	1872	2143	38	2612	677	2213	862
Nickel	ug/L	8.4	2.7	3.4	1.6	0.73	2.3	4.2	2.2
Potassium	ug/L	6023	5221	5850	5530	5558	5469	5810	5407
Selenium	ug/L	18	18	18	18	18	18	18	18
Silver	ug/L	0.21	0.21	0.21	0.21	0.21	0.21	0.21	0.21
Sodium	ug/L	34077	28814	31913	25016	31962	26307	32650	26712
Thallium	ug/L	8.2	8.2	8.2	8.2	8.2	8.2	8.2	8.2
Vanadium	ug/L	18	6.0	1.8	1.8	5.7	2.7	8.5	3.5
Zinc	ug/L	106	12	16	3.3	14	9.7	45	8.2

Analyte	Units	Rep 1		Rep 2		Rep 3		Rep Average	
		Below Mat (A)	Above Mat (B)	Below Mat (C)	Above Mat (D)	Below Mat (E)	Above Mat (F)	Below Mat	Above Mat
Percent Reduction									
Aluminum	%	-	96.6	-	70.0	-	-291.0	-	81.8
Antimony	%	-	0.0	-	0.0	-	0.0	-	0.0
Arsenic	%	-	-186.2	-	0.0	-	74.2	-	-47.2
Barium	%	-	27.6	-	36.7	-	57.1	-	41.0
Beryllium	%	-	88.7	-	0.0	-	39.9	-	80.7
Cadmium	%	-	18.7	-	66.9	-	95.4	-	58.3
Calcium	%	-	0.0	-	0.0	-	0.0	-	0.0
Chromium	%	-	81.2	-	54.9	-	-203.8	-	61.1
Cobalt	%	-	88.2	-	0.0	-	0.0	-	71.3
Copper	%	-	93.4	-	-6.3	-	-805.5	-	61.3
Iron	%	-	56.4	-	92.9	-	98.4	-	85.3
Lead	%	-	92.9	-	0.0	-	0.0	-	81.2
Magnesium	%	-	16.0	-	36.4	-	22.8	-	24.8
Manganese	%	-	0.6	-	98.2	-	74.1	-	61.0
Nickel	%	-	68.0	-	51.5	-	-208.2	-	47.3
Potassium	%	-	13.3	-	5.5	-	1.6	-	6.9
Selenium	%		0.0	-	0.0	-	0.0	-	0.0
Silver	%	-	0.0	-	0.0	-	0.0	-	0.0
Sodium	%	-	15.4	-	21.6	-	17.7	-	18.2
Thallium	%	-	0.0	-	0.0	-	0.0	-	0.0
Vanadium	%	-	66.7	-	-0.3	-	53.2	-	59.0
Zinc	%	-	88.9	-	79.5	-	32.0	-	81.8

Table E-6. Year One horizontal peeper replicate analytical results for area T2 (single mat with sand cap).

T2 - Single Mat With Sand Cap

Analyte	Units	Rep 1		Rep 2		Rep 3		Rep Average	
		Below Mat (G)	Above Mat (H)	Below Mat (I)	Above Mat (J)	Below Mat (K)	Above Mat (L)	Below Mat	Above Mat
Aluminum	ug/L	56	64	64	37	46	1365	55	489
Antimony	ug/L	4.6	4.6	4.6	4.6	4.6	4.6	4.6	4.6
Arsenic	ug/L	6.9	6.9	6.9	6.9	6.9	6.9	6.9	6.9
Barium	ug/L	106	50	93	48	96	104	98	67
Beryllium	ug/L	0.01	0.01	0.01	0.01	0.01	1.1	0.01	0.36
Cadmium	ug/L	0.67	0.16	1.7	0.16	0.41	5.4	0.93	1.9
Calcium	ug/L	0.44	0.44	0.44	0.44	0.44	0.44	0.44	0.44
Chromium	ug/L	7.9	7.0	10	5.3	5.3	18	7.7	10
Cobalt	ug/L	0.72	0.72	2.0	0.72	1.8	9.9	1.5	3.8
Copper	ug/L	2.5	2.8	5.3	3.2	2.3	16	3.4	7.2
Iron	ug/L	2610	531	346	583	1543	3484	1500	1532
Lead	ug/L	3.5	3.5	3.5	3.5	3.5	52	3.5	20
Magnesium	ug/L	7720	3040	7714	2923	7714	3239	7716	3067
Manganese	ug/L	1366	14	950	108	1294	564	1203	229
Nickel	ug/L	8.6	2.4	9.6	1.9	8.4	11	8.9	5.1
Potassium	ug/L	7720	5491	7936	5658	7914	5956	7856	5701
Selenium	ug/L	18	18	18	18	18	18	18	18
Silver	ug/L	0.21	0.21	0.21	0.21	0.21	0.21	0.21	0.21
Sodium	ug/L	54373	25631	5.1	25709	5.1	26393	18128	25911
Thallium	ug/L	8.2	8.2	8.2	8.2	8.2	8.2	8.2	8.2
Vanadium	ug/L	1.7	2.2	1.8	2.4	1.9	24	1.8	9.5
Zinc	ug/L	24	5.9	27	7.3	21	128	24	47

Analyte	Units	Rep 1		Rep 2		Rep 3		Rep Average	
		Below Mat (A)	Above Mat (B)	Below Mat (C)	Above Mat (D)	Below Mat (E)	Above Mat (F)	Below Mat	Above Mat
Percent Reduction									
Aluminum	%	-	-15.4	-	42.2	-	-2875.1	-	-787.7
Antimony	%	-	0.0	-	0.0	-	0.0	-	0.0
Arsenic	%	-	0.0	-	0.0	-	0.0	-	0.0
Barium	%	-	52.3	-	48.0	-	-8.1	-	31.3
Beryllium	%	-	0.0	-	0.0	-	-8304.1	-	-2768.0
Cadmium	%	-	76.6	-	90.9	-	-1234.7	-	-106.7
Calcium	%	-	0.0	-	0.0	-	0.0	-	0.0
Chromium	%	-	10.9	-	47.2	-	-239.8	-	-30.8
Cobalt	%	-	0.0	-	63.3	-	-454.9	-	-153.0
Copper	%	-	-14.6	-	39.3	-	-585.6	-	-115.6
Iron	%	-	79.7	-	-68.6	-	-125.8	-	-2.2
Lead	%	-	0.0	-	0.0	-	-1372.7	-	-457.6
Magnesium	%	-	60.6	-	62.1	-	58.0	-	60.2
Manganese	%	-	99.0	-	88.7	-	56.4	-	81.0
Nickel	%	-	72.0	-	80.0	-	-30.8	-	42.4
Potassium	%	-	28.9	-	28.7	-	24.7	-	27.4
Selenium	%	-	0.0	-	0.0	-	0.0	-	0.0
Silver	%	-	0.0	-	0.0	-	0.0	-	0.0
Sodium	%	-	52.9	-	-505770.9	-	-519221.4	-	-42.9
Thallium	%	-	0.0	-	0.0	-	0.0	-	0.0
Vanadium	%	-	-35.5	-	-35.2	-	-1180.5	-	-436.1
Zinc	%	-	75.5	-	72.7	-	-501.1	-	-95.4

Table E-7. Year One horizontal peeper replicate analytical results for area T3 (double mat).

T3 - Double Mat

Analyte	Units	Rep 1			Rep 2		
		Below Mats (M)	Between Mats (N)	Above Mats (O)	Below Mats (P)	Between Mats (Q)	Above Mats (R)
Aluminum	ug/L	64	71	37	94	35	112
Antimony	ug/L	4.6	4.6	4.6	4.6	4.6	4.6
Arsenic	ug/L	6.9	6.9	6.9	15	6.9	6.9
Barium	ug/L	90	38	49	109	51	50
Berylium	ug/L	0.01	0.03	0.01	0.03	0.01	0.01
Cadmium	ug/L	0.4	0.16	0.16	1.3	0.16	0.16
Calcium	ug/L	0.44	0.44	0.44	0.44	0.44	0.44
Chromium	ug/L	8.4	1.9	5.5	3.3	1.9	6.5
Cobalt	ug/L	2.1	0.72	0.72	0.72	0.72	0.72
Copper	ug/L	2.5	3.3	3.0	2.3	1.5	3.6
Iron	ug/L	1448	196	341	5060	540	303
Lead	ug/L	3.5	3.5	3.5	3.5	3.5	3.5
Magnesium	ug/L	7365	2157	2883	6396	3894	2939
Manganese	ug/L	1195	31	51	2079	902	41
Nickel	ug/L	9.7	2.3	2.7	2.9	0.73	1.9
Potassium	ug/L	8264	4138	5635	7203	5773	5678
Selenium	ug/L	40	18	18	38	18	18
Silver	ug/L	0.21	0.21	0.21	0.21	0.21	0.21
Sodium	ug/L	5.1	18767	25873	51244	28702	25886
Thalium	ug/L	8.2	8.2	8.2	8.2	8.2	8.2
Vanadium	ug/L	1.4	1.3	1.9	4.3	0.49	2.2
Zinc	ug/L	19	7.3	3.2	19	18	8.5

Analyte	Units	Rep 1			Rep 2		
		Below Mats (M)	Between Mats (N)	Above Mats (O)	Below Mats (P)	Between Mats (Q)	Above Mats (R)
Percent Reduction							
Aluminum	%	-	-11.0	48.0	-	62.5	-219.0
Antimony	%	-	0.0	0.0	-	0.0	0.0
Arsenic	%	-	0.0	0.0	-	55.0	0.0
Barium	%	-	57.7	-29.5	-	53.2	3.0
Beryllium	%	-	-150.4	60.1	-	58.9	0.0
Cadmium	%	-	61.1	0.0	-	88.2	0.0
Calcium	%	-	0.0	0.0	-	0.0	0.0
Chromium	%	-	77.4	-191.7	-	42.2	-243.4
Cobalt	%	-	65.3	0.0	-	0.0	0.0
Copper	%	-	-28.7	9.7	-	32.8	-139.5
Iron	%	-	86.4	-73.8	-	89.3	43.8
Lead	%	-	0.0	0.0	-	0.0	0.0
Magnesium	%	-	70.7	-33.7	-	39.1	24.5
Manganese	%	-	97.4	-63.1	-	56.6	95.5
Nickel	%	-	76.3	-15.5	-	74.8	-155.5
Potassium	%	-	49.9	-36.2	-	19.9	1.6
Selenium	%	-	54.7	0.0	-	52.0	0.0
Silver	%	-	0.0	0.0	-	0.0	0.0
Sodium	%	-	-369172.6	-37.9	-	44.0	9.8
Thallium	%	-	0.0	0.0	-	0.0	0.0
Vanadium	%	-	7.9	-50.6	-	88.6	-341.7
Zinc	%	-	61.6	55.8	-	8.5	52.0

Table E-7. Year One horizontal peeper replicate analytical results for area T3 (double mat).

T3 - Double Mat

Analyte	Units	Rep 3			Rep Average		
		Below Mats (S)	Between Mats (T)	Above Mats (U)	Below Mats	Between Mats	Above Mat
Aluminum	ug/L	105	35	42	87	47	64
Antimony	ug/L	4.6	4.6	4.6	4.6	4.6	4.6
Arsenic	ug/L	64	6.9	6.9	29	6.9	6.9
Barium	ug/L	240	52	58	146	47	52
Berylium	ug/L	0.05	0.01	0.01	0.03	0.02	0.01
Cadmium	ug/L	4.9	0.16	0.16	2.2	0.16	0.16
Calcium	ug/L	0.44	0.44	0.44	0.44	0.44	0.44
Chromium	ug/L	20	2.1	4.5	10	2.0	5.5
Cobalt	ug/L	0.72	0.72	0.72	1.2	0.72	0.72
Copper	ug/L	1.9	1.5	4.3	2.2	2.1	3.6
Iron	ug/L	32685	1016	803	13065	584	482
Lead	ug/L	11	3.5	3.5	5.9	3.5	3.5
Magnesium	ug/L	7239	3301	2940	7000	3117	2921
Manganese	ug/L	1806	606	243	1693	513	111
Nickel	ug/L	4.9	0.73	2.0	5.8	1.3	2.2
Potassium	ug/L	7400	5590	5686	7622	5167	5666
Selenium	ug/L	18	18	18	32	18	18
Silver	ug/L	0.21	0.21	0.21	0.21	0.21	0.21
Sodium	ug/L	53517	26790	25945	34922	24753	25901
Thalium	ug/L	8.2	8.2	8.2	8.2	8.2	8.2
Vanadium	ug/L	16	0.49	2.1	7.3	0.76	2.1
Zinc	ug/L	61	2.9	5.1	33	9.3	5.6

Analyte	Units	Rep 3			Rep Average		
		Below Mats (S)	Between Mats (T)	Above Mats (U)	Below Mats	Between Mats	Above Mat
Percent Reduction							
Aluminum	%	-	66.5	-18.8	-	46.2	-35.2
Antimony	%	-	0.0	0.0	-	0.0	0.0
Arsenic	%	-	89.2	0.0	-	76.0	0.0
Barium	%	-	78.4	-11.4	-	67.9	-11.1
Beryllium	%	-	73.3	0.0	-	37.2	33.4
Cadmium	%	-	96.8	0.0	-	92.9	0.0
Calcium	%	-	0.0	0.0	-	0.0	0.0
Chromium	%	-	89.0	-107.6	-	80.9	-177.9
Cobalt	%	-	0.0	0.0	-	38.6	0.0
Copper	%	-	21.5	-190.8	-	6.3	-73.9
Iron	%	-	96.9	21.0	-	95.5	17.4
Lead	%	-	66.4	0.0	-	39.7	0.0
Magnesium	%	-	54.4	10.9	-	55.5	6.3
Manganese	%	-	66.5	59.9	-	69.7	78.3
Nickel	%	-	85.1	-165.5	-	78.5	-72.1
Potassium	%	-	24.5	-1.7	-	32.2	-9.7
Selenium	%	-	0.0	0.0	-	43.3	0.0
Silver	%	-	0.0	0.0	-	0.0	0.0
Sodium	%	-	49.9	3.2	-	29.1	-4.6
Thallium	%	-	0.0	0.0	-	0.0	0.0
Vanadium	%	-	97.0	-327.1	-	89.7	-174.2
Zinc	%	-	95.3	-77.3	-	72.0	39.6

Table E-7. Year One horizontal peeper replicate analytical results for area T3 (double mat).

T3 - Double Mat

Analyte	Units	Rep 1			Rep 2		
		Below Mats (M)	Between Mats (N)	Above Mats (O)	Below Mats (P)	Between Mats (Q)	Above Mats (R)
Percent Reduction							
Aluminum	%	-	-	42.3	-	-	-19.5
Antimony	%	-	-	0.0	-	-	0.0
Arsenic	%	-	-	0.0	-	-	55.0
Barium	%	-	-	45.2	-	-	54.6
Beryllium	%	-	-	0.0	-	-	58.9
Cadmium	%	-	-	61.1	-	-	88.2
Calcium	%	-	-	0.0	-	-	0.0
Chromium	%	-	-	33.9	-	-	-98.5
Cobalt	%	-	-	65.3	-	-	0.0
Copper	%	-	-	-16.3	-	-	-60.8
Iron	%	-	-	76.4	-	-	94.0
Lead	%	-	-	0.0	-	-	0.0
Magnesium	%	-	-	60.9	-	-	54.0
Manganese	%	-	-	95.8	-	-	98.0
Nickel	%	-	-	72.6	-	-	35.7
Potassium	%	-	-	31.8	-	-	21.2
Selenium	%	-	-	54.7	-	-	52.0
Silver	%	-	-	0.0	-	-	0.0
Sodium	%	-	-	-508994.0	-	-	49.5
Thallium	%	-	-	0.0	-	-	0.0
Vanadium	%	-	-	-38.8	-	-	49.5
Zinc	%	-	-	83.0	-	-	56.1

Table E-7. Year One horizontal peeper replicate analytical results for area T3 (double mat).

T3 - Double Mat

Analyte	Units	Rep 3			Rep Average		
		Below Mats (S)	Between Mats (T)	Above Mats (U)	Below Mats	Between Mats	Above Mat
Percent Reduction							
Aluminum	%	-	-	60.2	-	-	27.3
Antimony	%	-	-	0.0	-	-	0.0
Arsenic	%	-	-	89.2	-	-	76.0
Barium	%	-	-	75.9	-	-	64.3
Beryllium	%	-	-	73.3	-	-	58.2
Cadmium	%	-	-	96.8	-	-	92.9
Calcium	%	-	-	0.0	-	-	0.0
Chromium	%	-	-	77.2	-	-	47.1
Cobalt	%	-	-	0.0	-	-	38.6
Copper	%	-	-	-128.2	-	-	-63.0
Iron	%	-	-	97.5	-	-	96.3
Lead	%	-	-	66.4	-	-	39.7
Magnesium	%	-	-	59.4	-	-	58.3
Manganese	%	-	-	86.5	-	-	93.4
Nickel	%	-	-	60.3	-	-	63.0
Potassium	%	-	-	23.2	-	-	25.7
Selenium	%	-	-	0.0	-	-	43.3
Silver	%	-	-	0.0	-	-	0.0
Sodium	%	-	-	51.5	-	-	25.8
Thallium	%	-	-	0.0	-	-	0.0
Vanadium	%	-	-	87.0	-	-	71.7
Zinc	%	-	-	91.7	-	-	83.1

Table E-8. Year One vertical peeper replicate analytical results for area T4 (sand cap only).

T4 - Sand Cap Only

Analyte	Units	Rep 1		Rep 2		Rep 3	
		Below Sand (AA-3-5)	Above Sand (AA-1)	Below Sand (W-3-5)	Above Sand (W-1)	Below Sand (Y-3-5)	Above Sand (Y-1)
Aluminum	ug/L	32	34	30	28	33	41
Antimony	ug/L	4.6	4.6	4.6	4.6	4.6	4.6
Arsenic	ug/L	6.9	6.9	6.9	6.9	6.9	6.9
Barium	ug/L	54	56	51	55	67	66
Beryllium	ug/L	0.01	0.01	0.01	0.01	0.01	0.01
Cadmium	ug/L	0.16	0.16	0.16	0.16	0.16	0.16
Calcium	ug/L	N/A	N/A	N/A	N/A	N/A	N/A
Chromium	ug/L	0.64	0.64	0.64	0.65	0.71	0.9
Cobalt	ug/L	0.72	0.72	0.72	0.72	0.72	0.72
Copper	ug/L	1.4	1.4	1.8	1.6	1.5	1.7
Iron	ug/L	603	463	1085	127	836	381
Lead	ug/L	3.5	3.5	3.5	3.5	3.5	3.5
Magnesium	ug/L	2835	2928	2914	2972	2931	3073
Manganese	ug/L	246	143	178	11	288	128
Nickel	ug/L	1.5	1.5	1.5	1.5	1.5	1.5
Potassium	ug/L	4776	4974	4861	4981	4822	4959
Selenium	ug/L	18	18	18	18	18	18
Silver	ug/L	0.21	0.21	0.21	0.21	0.21	0.21
Sodium	ug/L	24548	24640	24796	24806	24547	24786
Thallium	ug/L	8.2	8.2	8.2	8.2	8.2	8.2
Vanadium	ug/L	0.49	0.49	0.49	0.49	0.49	0.49
Zinc	ug/L	2.3	2.3	2.3	2.4	2.3	3.1

Analyte	Units	Rep 1		Rep 2		Rep 3	
		Below Sand (AA-3-5)	Above Sand (AA-1)	Below Sand (W-3-5)	Above Sand (W-1)	Below Sand (Y-3-5)	Above Sand (Y-1)
Percent Reduction							
Aluminum	%	-	-6.8	-	7.0	-	-24.5
Antimony	%	-	0.0	-	0.0	-	0.0
Arsenic	%	-	0.0	-	0.0	-	0.0
Barium	%	-	-3.8	-	-6.9	-	1.3
Beryllium	%	-	0.0	-	0.0	-	0.0
Cadmium	%	-	0.0	-	0.0	-	0.0
Calcium	%	-	N/A	-	N/A	-	N/A
Chromium	%	-	0.0	-	-2.1	-	-26.3
Cobalt	%	-	0.0	-	0.0	-	0.0
Copper	%	-	-4.5	-	8.6	-	-7.6
Iron	%	-	23.3	-	88.3	-	54.5
Lead	%	-	0.0	-	0.0	-	0.0
Magnesium	%	-	-3.3	-	-2.0	-	-4.9
Manganese	%	-	41.9	-	94.0	-	55.4
Nickel	%	-	0.0	-	5.1	-	5.1
Potassium	%	-	-4.2	-	-2.5	-	-2.8
Selenium	%	-	0.0	-	0.0	-	0.0
Silver	%	-	0.0	-	0.0	-	0.0
Sodium	%	-	-0.4	-	0.0	-	-1.0
Thalium	%	-	0.0	-	0.0	-	0.0
Vanadium	%	-	0.0	-	0.0	-	0.0
Zinc	%	-	0.0	-	-1.6	-	-34.2

N/A = Data not available.

Table E-8. Year One vertical peeper replicate analytical results for area T4 (sand cap only).

T4 - Sand Cap Only

Analyte	Units	Rep 4		Rep Average	
		Below Sand (Z-3-5)	Above Sand (Z-1)	Below Sand	Above Sand
Aluminum	ug/L	33	33	32	34
Antimony	ug/L	4.6	4.6	4.6	4.6
Arsenic	ug/L	6.9	6.9	6.9	6.9
Barium	ug/L	73	57	61	58
Beryllium	ug/L	0.01	0.01	0.01	0.01
Cadmium	ug/L	0.16	0.16	0.16	0.16
Calcium	ug/L	N/A	N/A	N/A	N/A
Chromium	ug/L	0.65	0.64	0.66	0.71
Cobalt	ug/L	0.72	0.72	0.72	0.72
Copper	ug/L	1.8	1.9	1.6	1.7
Iron	ug/L	136	92	665	265
Lead	ug/L	3.5	3.5	3.5	3.5
Magnesium	ug/L	2992	3019	2918	2998
Manganese	ug/L	32	20	186	75
Nickel	ug/L	1.6	1.5	1.5	1.5
Potassium	ug/L	5086	5062	4886	4994
Selenium	ug/L	18	18	18	18
Silver	ug/L	0.21	0.21	0.21	0.21
Sodium	ug/L	24712	24691	24651	24731
Thallium	ug/L	8.2	8.2	8.2	8.2
Vanadium	ug/L	0.49	0.49	0.49	0.49
Zinc	ug/L	2.7	2.3	2.4	2.5

Analyte	Units	Rep 4		Rep Average	
		Below Sand (Z-3-5)	Above Sand (Z-1)	Below Sand	Above Sand
Percent Reduction					
Aluminum	%	-	-0.5	-	-6.4
Antimony	%	-	0.0	-	0.0
Arsenic	%	-	0.0	-	0.0
Barium	%	-	21.7	-	4.5
Beryllium	%	-	0.0	-	0.0
Cadmium	%	-	0.0	-	0.0
Calcium	%	-	N/A	-	N/A
Chromium	%	-	1.7	-	-7.2
Cobalt	%	-	0.0	-	0.0
Copper	%	-	-9.2	-	-2.9
Iron	%	-	32.9	-	60.1
Lead	%	-	0.0	-	0.0
Magnesium	%	-	-0.9	-	-2.7
Manganese	%	-	37.7	-	59.4
Nickel	%	-	6.3	-	4.2
Potassium	%	-	0.5	-	-2.2
Selenium	%	-	0.0	-	0.0
Silver	%	-	0.0	-	0.0
Sodium	%	-	0.1	-	-0.3
Thalium	%	-	0.0	-	0.0
Vanadium	%	-	0.0	-	0.0
Zinc	%	-	13.1	-	-5.0

N/A = Data not available.

Table E-9. Year One vertical peeper replicate analytical results for area T5 (no treatment/control).

T5 - No Treatment (Control)

Analyte	Units	Rep 1 Above Sed (AB-1)	Rep 2 Above Sed (AC-1)	Rep 3 Above Sed (AD-1)	Rep 4 Above Sed (T5-1)	Rep Average Above Sed
Aluminum	ug/L	18	18	20	22	19
Antimony	ug/L	4.6	4.6	4.6	4.6	4.6
Arsenic	ug/L	17	6.9	6.9	22	13
Barium	ug/L	60	53	51	51	54
Beryllium	ug/L	0.01	0.01	0.01	0.01	0.01
Cadmium	ug/L	0.78	0.4	0.41	0.59	0.55
Calcium	ug/L	N/A	N/A	N/A	N/A	N/A
Chromium	ug/L	0.64	0.64	0.64	0.7	0.65
Cobalt	ug/L	0.72	0.72	0.72	0.72	0.72
Copper	ug/L	0.67	0.67	0.67	0.67	0.67
Iron	ug/L	8557	5323	5471	7343	6674
Lead	ug/L	3.5	3.5	3.5	3.5	3.5
Magnesium	ug/L	5853	5591	5307	5161	5478
Manganese	ug/L	2469	2294	2173	2109	2261
Nickel	ug/L	1.5	1.5	1.5	1.9	1.6
Potassium	ug/L	5606	5657	5278	5066	5402
Selenium	ug/L	18	18	18	18	18
Silver	ug/L	0.21	0.21	0.21	0.21	0.21
Sodium	ug/L	31372	32288	30868	29365	30973
Thallium	ug/L	8.2	8.2	8.2	8.2	8.2
Vanadium	ug/L	1.3	0.49	0.49	1.3	0.89
Zinc	ug/L	3.2	2.3	2.8	2.9	2.8

N/A = Data not available.

Table E-10. Summary of Year One peeper analytical results for the Cottonwood Bay prototype mat system.

Treatment Summary - Replicate Averages

Analyte	Units	T1 - Mat Only			T2 - Mat w/ Sand		
		Below Treatment	Between Treatment	Above Treatment	Below Treatment	Between Treatment	Above Treatment
Aluminum	ug/L	411	-	75	55	-	489
Antimony	ug/L	4.6	-	4.6	4.6	-	4.6
Arsenic	ug/L	20	-	29	6.9	-	6.9
Barium	ug/L	110	-	65	98	-	67
Beryllium	ug/L	0.13	-	0.03	0.01	-	0.36
Cadmium	ug/L	2.4	-	0.99	0.93	-	1.9
Calcium	ug/L	0.44	-	0.44	0.44	-	0.44
Chromium	ug/L	7.7	-	3.0	7.7	-	10
Cobalt	ug/L	2.5	-	0.72	1.5	-	3.8
Copper	ug/L	5.7	-	2.2	3.4	-	7.2
Iron	ug/L	17902	-	2635	1500	-	1532
Lead	ug/L	19	-	3.5	3.5	-	20
Magnesium	ug/L	4530	-	3405	7716	-	3067
Manganese	ug/L	2213	-	862	1203	-	229
Nickel	ug/L	4.2	-	2.2	8.9	-	5.1
Potassium	ug/L	5810	-	5407	7856	-	5701
Selenium	ug/L	18	-	18	18	-	18
Silver	ug/L	0.21	-	0.21	0.21	-	0.21
Sodium	ug/L	32650	-	26712	18128	-	25911
Thallium	ug/L	8.2	-	8.2	8.2	-	8.2
Vanadium	ug/L	8.5	-	3.5	1.8	-	9.5
Zinc	ug/L	45	-	8.2	24	-	47

N/A = Data not available.

Table E-10. Summary of Year One peeper analytical results for the Cottonwood Bay prototype mat system.

Treatment Summary - Replic

Analyte	Units	T3 - Double Mat			T4 - Sand Only		
		Below Treatment	Between Treatment	Above Treatment	Below Treatment	Between Treatment	Above Treatment
Aluminum	ug/L	87	47	64	32	-	34
Antimony	ug/L	4.6	4.6	4.6	4.6	-	4.6
Arsenic	ug/L	29	6.9	6.9	6.9	-	6.9
Barium	ug/L	146	47	52	61	-	58
Beryllium	ug/L	0.03	0.02	0.01	0.01	-	0.01
Cadmium	ug/L	2.2	0.16	0.16	0.16	-	0.16
Calcium	ug/L	0.44	0.44	0.44	N/A	-	N/A
Chromium	ug/L	10	2.0	5.5	0.66	-	0.71
Cobalt	ug/L	1.2	0.72	0.72	0.72	-	0.72
Copper	ug/L	2.2	2.1	3.6	1.6	-	1.7
Iron	ug/L	13065	584	482	665	-	265
Lead	ug/L	5.9	3.5	3.5	3.5	-	3.5
Magnesium	ug/L	7000	3117	2921	2918	-	2998
Manganese	ug/L	1693	513	111	186	-	75
Nickel	ug/L	5.8	1.3	2.2	1.5	-	1.5
Potassium	ug/L	7622	5167	5666	4886	-	4994
Selenium	ug/L	32	18	18	18	-	18
Silver	ug/L	0.21	0.21	0.21	0.21	-	0.21
Sodium	ug/L	34922	24753	25901	24651	-	24731
Thallium	ug/L	8.2	8.2	8.2	8.2	-	8.2
Vanadium	ug/L	7.3	0.76	2.1	0.49	-	0.49
Zinc	ug/L	33	9.3	5.6	2.4	-	2.5

N/A = Data not available.

Table E-10. Summary of Year One peeper analytical results for the Cottonwood Bay prototype mat system.

Treatment Summary - Replic

Analyte	Units	T5 - No Treatment		
		Below Treatment	Between Treatment	Above Treatment
Aluminum	ug/L	-	-	19
Antimony	ug/L	-	-	4.6
Arsenic	ug/L	-	-	13
Barium	ug/L	-	-	54
Beryllium	ug/L	-	-	0.01
Cadmium	ug/L	-	-	0.55
Calcium	ug/L	-	-	N/A
Chromium	ug/L	-	-	0.65
Cobalt	ug/L	-	-	0.72
Copper	ug/L	-	-	0.67
Iron	ug/L	-	-	6674
Lead	ug/L	-	-	3.5
Magnesium	ug/L	-	-	5478
Manganese	ug/L	-	-	2261
Nickel	ug/L	-	-	1.6
Potassium	ug/L	-	-	5402
Selenium	ug/L	-	-	18
Silver	ug/L	-	-	0.21
Sodium	ug/L	-	-	30973
Thallium	ug/L	-	-	8.2
Vanadium	ug/L	-	-	0.89
Zinc	ug/L	-	-	2.8

N/A = Data not available.

Table E-11. Year Two horizontal peeper raw sub-replicate analytical results for Cottonwood Bay.

	T1-Bot-H1a *(ug/L)*	T1-Bot-H1b *(ug/L)*	T1-Bot-H1c *(ug/L)*	T1-Bot-H2a *(ug/L)*	T1-Bot-H2b *(ug/L)*	T1-Bot-H2c *(ug/L)*	T1-Bot-H3a *(ug/L)*	T1-Bot-H3b *(ug/L)*
Ag 328.068	0.21	0.21	0.21	0.8	0.21	0.48	0.44	0.5
Al 308.215	63	71	1.1	60	1.1	1.1	87	1.1
As 193.696	6.9	6.9	6.9	61	95	78	6.9	6.9
Ba 455.403	48	50	53	200	233	245	89	89
Be 313.107	0.01	0.01	0.01	0.01	0.01	0.01	0.01	0.01
Ca 317.933	-	-	-	-	-	-	-	-
Cd 226.502	0.16	0.16	0.16	3.6	4.3	4.7	0.16	0.16
Co 228.615	0.72	0.72	0.72	0.72	2.0	1.6	0.72	0.72
Cr 267.716	0.8	1.6	0.32	12	6.0	5.6	4.2	1.7
Cu 324.754	0.33	0.33	0.33	0.33	0.33	0.33	0.97	0.33
Fe 259.837	300	383	215	38657	-	-	1879	1201
K 766.491	4171	4162	4150	10401	10412	10653	6807	7214
Mg 279.800	3173	3169	3199	7262	7178	7883	4974	5330
Mn 257.610	870	999	1032	1481	1552	1555	2074	2273
Na 588.995	21860	21560	21926	89905	89075	95481	32805	34973
Ni 231.604	0.73	0.73	0.73	4.2	4.6	4.7	3.0	3.0
Pb 220.353	3.5	3.5	3.5	3.5	3.5	3.5	3.5	3.5
Sb 206.834	4.6	4.6	4.6	4.6	4.6	4.6	4.6	4.6
Se 196.026	18	18	18	18	18	18	18	18
Tl 190.794	8.2	8.2	8.2	8.2	8.2	8.2	8.2	8.2
V 292.401	0.49	0.49	0.49	12	13	13	2.7	1.4
Zn 213.857	3.2	3.5	2.6	22	20	23	11	7.2

= Non-Detect (1/2 MDL Substituted)

Table E-11. Year Two horizontal peeper raw sub-replicate analytical results for Cottonwood Bay.

	T1-Bot-H3c *(ug/L)*	T1-Top-H1a *(ug/L)*	T1-Top-H1b *(ug/L)*	T1-Top-H1c *(ug/L)*	T1-Top-H2a *(ug/L)*	T1-Top-H2b *(ug/L)*	T1-Top-H2c *(ug/L)*	T1-Top-H3a *(ug/L)*
Ag 328.068	0.68	0.21	0.21	0.21	0.21	0.21	0.21	0.21
Al 308.215	1.1	1.1	1.1	1.1	129	1.1	1.1	1.1
As 193.696	6.9	6.9	6.9	6.9	6.9	6.9	6.9	6.9
Ba 455.403	90	42	41	41	42	40	40	41
Be 313.107	0.01	0.01	0.01	0.01	0.01	0.01	0.01	0.01
Ca 317.933	-	-	-	-	-	-	-	-
Cd 226.502	0.16	0.16	0.16	0.16	0.16	0.16	0.16	0.16
Co 228.615	0.72	0.72	0.72	0.72	0.72	0.72	0.72	0.72
Cr 267.716	0.9	1.9	1.1	1.1	3.0	1.4	1.5	1.5
Cu 324.754	0.33	1.1	1.0	1.0	1.7	1.3	0.99	1.2
Fe 259.837	600	46	29	22	307	78	34	78
K 766.491	7246	4134	4113	4111	4134	4116	4108	4103
Mg 279.800	5453	2594	2573	2577	2583	2575	2561	2575
Mn 257.610	2204	33	14	12	27	8.0	4.3	12
Na 588.995	36717	20529	20463	20484	20606	20462	20375	20444
Ni 231.604	2.0	0.73	0.73	0.73	2.1	0.73	2.3	0.73
Pb 220.353	3.5	3.5	3.5	3.5	3.5	3.5	3.5	3.5
Sb 206.834	4.6	4.6	4.6	4.6	4.6	4.6	4.6	4.6
Se 196.026	18	18	18	18	18	18	18	18
Tl 190.794	8.2	8.2	8.2	8.2	8.2	8.2	8.2	8.2
V 292.401	0.49	1.6	1.3	0.49	1.7	0.49	0.49	1.0
Zn 213.857	6.5	2.9	1.2	1.2	7.1	4.2	2.6	3.8

= Non-Detect (1/2 MDL Substituted)

Table E-11. Year Two horizontal peeper raw sub-replicate analytical results for Cottonwood Bay.

	T1-Top-H3b *(ug/L)*	T1-Top-H3c *(ug/L)*	T2-Bot-H1a *(ug/L)*	T2-Bot-H1b *(ug/L)*	T2-Bot-H2a *(ug/L)*	T2-Bot-H2b *(ug/L)*	T2-Bot-H2c *(ug/L)*	T2-Bot-H3a *(ug/L)*
Ag 328.068	0.21	0.21	0.95	1.1	0.92	1.0	0.92	0.43
Al 308.215	61	1.1	190	256	55	1.1	1.1	1.1
As 193.696	6.9	6.9	6.9	6.9	6.9	6.9	6.9	6.9
Ba 455.403	41	40	102	104	132	129	130	76
Be 313.107	0.01	0.01	0.01	0.01	0.01	0.01	0.01	0.01
Ca 317.933	-	-	-	-	-	-	-	-
Cd 226.502	0.16	0.16	0.43	1.7	0.16	0.16	0.16	0.16
Co 228.615	0.72	0.72	0.72	0.72	0.72	0.72	0.72	0.72
Cr 267.716	1.6	1.2	16	57	1.4	0.32	0.32	1.6
Cu 324.754	1.3	0.93	2.2	5.4	0.33	0.33	0.33	0.33
Fe 259.837	118	13	949	1284	1667	677	2126	582
K 766.491	4101	4096	10386	10645	9488	9563	9312	6023
Mg 279.800	2571	2570	8607	8704	8454	8214	7893	4551
Mn 257.610	32	3.8	1342	1342	2855	2880	2799	1996
Na 588.995	20312	20386	59314	60655	44493	43514	43225	25476
Ni 231.604	0.73	0.73	4.5	5.1	3.2	3.7	3.0	2.3
Pb 220.353	3.5	3.5	3.5	3.5	3.5	3.5	3.5	3.5
Sb 206.834	4.6	4.6	4.6	4.6	4.6	4.6	4.6	4.6
Se 196.026	18	18	18	18	18	18	18	18
Tl 190.794	8.2	8.2	8.2	8.2	8.2	8.2	8.2	8.2
V 292.401	1.1	0.49	2.1	2.0	1.5	0.49	1.5	0.49
Zn 213.857	4.3	1.2	17	20	10	8.3	9.4	5.8

= Non-Detect (1/2 MDL Substituted)

Table E-11. Year Two horizontal peeper raw sub-replicate analytical results for Cottonwood Bay.

	T2-Bot-H3b *(ug/L)*	T2-Bot-H3c *(ug/L)*	T2-Top-H1a *(ug/L)*	T2-Top-H1b *(ug/L)*	T2-Top-H1c *(ug/L)*	T2-Top-H2a *(ug/L)*	T2-Top-H2b *(ug/L)*	T2-Top-H2c *(ug/L)*
Ag 328.068	0.21	0.64	0.45	0.5	0.42	0.21	0.21	0.21
Al 308.215	1.1	1.1	1.1	1.1	231	1.1	1.1	1.1
As 193.696	6.9	6.9	6.9	6.9	6.9	6.9	6.9	6.9
Ba 455.403	83	79	88	91	94	69	77	82
Be 313.107	0.01	0.01	0.01	0.01	0.01	0.01	0.01	0.01
Ca 317.933	-	-	-	-	-	-	-	-
Cd 226.502	0.16	0.16	0.16	0.16	0.16	0.16	0.16	0.16
Co 228.615	0.72	0.72	0.72	0.72	0.72	0.72	0.72	0.72
Cr 267.716	2.2	1.7	1.1	0.32	5.5	0.32	0.32	0.81
Cu 324.754	0.33	1.3	0.33	0.33	1.9	0.33	0.33	0.33
Fe 259.837	3630	925	335	166	925	384	46	398
K 766.491	6155	6096	4268	4298	4344	4236	4483	4529
Mg 279.800	4681	4653	3773	3921	4208	3466	3574	3636
Mn 257.610	2168	2091	1908	2107	2308	1108	1235	1617
Na 588.995	25474	25651	20991	20977	21339	20468	20501	20413
Ni 231.604	2.8	2.7	2.0	1.9	3.0	0.73	0.73	0.73
Pb 220.353	3.5	3.5	3.5	3.5	3.5	3.5	3.5	3.5
Sb 206.834	4.6	4.6	4.6	4.6	4.6	4.6	4.6	4.6
Se 196.026	18	18	18	18	18	18	18	18
Tl 190.794	8.2	8.2	8.2	8.2	8.2	8.2	8.2	8.2
V 292.401	2.7	1.2	0.49	0.49	2.6	1.1	0.49	1.0
Zn 213.857	7.8	7.6	4.1	4.0	14	3.9	1.2	3.1

= Non-Detect (1/2 MDL Substituted)

Table E-11. Year Two horizontal peeper raw sub-replicate analytical results for Cottonwood Bay.

	T2-Top-H3a *(ug/L)*	T2-Top-H3b *(ug/L)*	T3-Bot-H1a *(ug/L)*	T3-Bot-H1b *(ug/L)*	T3-Bot-H1c *(ug/L)*	T3-Bot-H2a *(ug/L)*	T3-Bot-H2b *(ug/L)*	T3-Bot-H2c *(ug/L)*
Ag 328.068	0.21	0.21	0.7	0.59	0.86	0.55	0.5	0.62
Al 308.215	1.1	1.1	1.1	1.1	1.1	1.1	1.1	1.1
As 193.696	6.9	6.9	70	112	156	6.9	6.9	6.9
Ba 455.403	47	46	242	331	449	93	93	96
Be 313.107	0.01	0.01	0.03	0.07	0.11	0.01	0.01	0.01
Ca 317.933	-	-	-	-	-	-	-	-
Cd 226.502	0.16	0.16	6.7	9.3	14	0.16	0.16	0.16
Co 228.615	0.72	0.72	2.1	2.8	2.9	0.72	0.72	0.72
Cr 267.716	0.32	0.32	1.9	3.2	5.7	1.8	0.32	2.3
Cu 324.754	1.5	1.0	0.33	0.33	0.33	0.33	0.33	0.33
Fe 259.837	1035	811	#VALUE!	#VALUE!	#VALUE!	678	94	1138
K 766.491	3829	3792	7155	7324	7433	6991	7265	7093
Mg 279.800	3000	2957	5558	5567	5601	5028	5098	4938
Mn 257.610	1189	1426	2346	2527	2634	2126	2163	1999
Na 588.995	20441	20428	47351	48013	49397	33107	33069	33008
Ni 231.604	2.8	2.6	3.3	4.2	6.2	2.5	0.73	2.7
Pb 220.353	3.5	3.5	3.5	3.5	7.9	3.5	3.5	3.5
Sb 206.834	4.6	4.6	4.6	4.6	4.6	4.6	4.6	4.6
Se 196.026	18	18	18	18	18	18	18	18
Tl 190.794	8.2	8.2	8.2	8.2	8.2	8.2	8.2	8.2
V 292.401	0.49	0.49	13	15	26	1.3	0.49	2.3
Zn 213.857	3.1	2.6	23	27	42	9.1	7.1	9.4

= Non-Detect (1/2 MDL Substituted)

Table E-11. Year Two horizontal peeper raw sub-replicate analytical results for Cottonwood Bay.

	T3-Bot-H3a *(ug/L)*	T3-Bot-H3b *(ug/L)*	T3-Bot-H3c *(ug/L)*	T3-Med-H1a *(ug/L)*	T3-Med-H1b *(ug/L)*	T3-Med-H1c *(ug/L)*	T3-Med-H2a *(ug/L)*	T3-Med-H2b *(ug/L)*
Ag 328.068	0.65	0.82	0.86	0.21	0.21	0.21	0.21	0.21
Al 308.215	1.1	1.1	1.1	1.1	1.1	50	1.1	1.1
As 193.696	6.9	6.9	6.9	6.9	6.9	6.9	6.9	6.9
Ba 455.403	107	107	107	39	40	40	42	42
Be 313.107	0.01	0.01	0.01	0.01	0.01	0.01	0.01	0.01
Ca 317.933	-	-	-	-	-	-	-	-
Cd 226.502	0.16	0.16	0.16	0.16	0.16	0.16	0.16	0.16
Co 228.615	0.72	0.72	0.72	0.72	0.72	0.72	0.72	0.72
Cr 267.716	0.32	0.32	0.32	0.32	0.88	2.3	0.32	0.32
Cu 324.754	0.33	0.33	0.33	0.33	0.33	0.33	0.33	0.33
Fe 259.837	270	42	78	18	161	232	368	450
K 766.491	9545	9693	9697	4151	4107	4090	4166	4168
Mg 279.800	6678	6765	7059	2591	2558	2572	2623	2601
Mn 257.610	1724	1783	1786	25	58	66	78	69
Na 588.995	59849	60253	62638	20786	20686	20589	21150	21084
Ni 231.604	3.3	2.6	2.6	0.73	0.73	0.73	0.73	0.73
Pb 220.353	3.5	3.5	3.5	3.5	3.5	3.5	3.5	3.5
Sb 206.834	4.6	4.6	4.6	4.6	4.6	4.6	4.6	4.6
Se 196.026	18	18	18	18	18	18	18	18
Tl 190.794	8.2	8.2	8.2	8.2	8.2	8.2	8.2	8.2
V 292.401	0.49	0.49	0.49	0.49	0.49	0.49	0.49	0.49
Zn 213.857	11	9.7	8.3	1.2	2.7	3.1	1.2	1.2

= Non-Detect (1/2 MDL Substituted)

Table E-11. Year Two horizontal peeper raw sub-replicate analytical results for Cottonwood Bay.

	T3-Med-H2c *(ug/L)*	T3-Med-H3a *(ug/L)*	T3-Med-H3b *(ug/L)*	T3-Med-H3c *(ug/L)*	T3-Top-H1a *(ug/L)*	T3-Top-H1b *(ug/L)*	T3-Top-H1c *(ug/L)*	T3-Top-H2a *(ug/L)*
Ag 328.068	0.21	0.21	0.21	0.21	0.21	0.21	0.21	0.21
Al 308.215	1.1	1.1	65	1.1	1.1	1.1	1.1	1.1
As 193.696	6.9	6.9	6.9	6.9	6.9	6.9	6.9	6.9
Ba 455.403	42	46	48	48	41	41	41	41
Be 313.107	0.01	0.01	0.01	0.01	0.01	0.01	0.01	0.01
Ca 317.933	-	-	-	-	-	-	-	-
Cd 226.502	0.16	0.16	0.16	0.16	0.16	0.16	0.16	0.16
Co 228.615	0.72	0.72	0.72	0.72	0.72	0.72	0.72	0.72
Cr 267.716	0.96	1.9	1.6	3.9	0.74	1.2	0.81	1.3
Cu 324.754	0.33	0.33	2.7	0.33	0.95	1.1	1.0	1.3
Fe 259.837	401	910	1341	1267	14	76	33	21
K 766.491	4151	4142	4115	4144	4179	4184	4128	4151
Mg 279.800	2605	2869	2877	2911	2590	2577	2584	2585
Mn 257.610	25	476	480	481	2.8	8.8	3.8	27
Na 588.995	20535	20990	20903	21111	20704	20711	20951	20744
Ni 231.604	3.1	0.73	0.73	0.73	0.73	0.73	0.73	25
Pb 220.353	3.5	3.5	3.5	3.5	3.5	3.5	3.5	3.5
Sb 206.834	4.6	4.6	4.6	4.6	4.6	4.6	4.6	4.6
Se 196.026	18	18	18	18	18	18	18	18
Tl 190.794	8.2	8.2	8.2	8.2	8.2	8.2	8.2	8.2
V 292.401	0.49	1.1	0.49	1.0	0.49	1.2	0.49	1.1
Zn 213.857	1.2	1.2	1.2	1.2	2.4	2.7	2.3	2.8

= Non-Detect (1/2 MDL Substituted)

Table E-11. Year Two horizontal peeper raw sub-replicate analytical results for Cottonwood Bay.

	T3-Top-H2b *(ug/L)*	T3-Top-H2c *(ug/L)*	T3-Top-H3a *(ug/L)*	T3-Top-H3b *(ug/L)*	T3-Top-H3c *(ug/L)*
Ag 328.068	0.21	0.21	0.21	0.21	0.21
Al 308.215	1.1	1.1	1.1	1.1	1.1
As 193.696	6.9	6.9	6.9	6.9	6.9
Ba 455.403	41	44	41	41	41
Be 313.107	0.01	0.01	0.01	0.01	0.01
Ca 317.933	-	-	-	-	-
Cd 226.502	0.16	0.16	0.16	0.16	0.16
Co 228.615	0.72	0.72	0.72	0.72	0.72
Cr 267.716	1.2	1.7	1.3	1.3	1.1
Cu 324.754	1.0	1.5	1.1	1.2	1.1
Fe 259.837	32	64	18	39	13
K 766.491	4112	4195	4253	4236	4250
Mg 279.800	2571	2635	2599	2582	2588
Mn 257.610	8.4	60	6.4	20	4.3
Na 588.995	20566	21385	21148	21040	21179
Ni 231.604	2.0	5.3	1.6	1.9	3.2
Pb 220.353	3.5	3.5	3.5	3.5	3.5
Sb 206.834	4.6	4.6	4.6	4.6	4.6
Se 196.026	18	18	18	18	18
Tl 190.794	8.2	8.2	8.2	8.2	8.2
V 292.401	0.99	2.8	0.49	0.49	0.49
Zn 213.857	1.2	3.0	1.2	2.8	1.2

= Non-Detect (1/2 MDL Substituted)

Table E-12. Year Two vertical peeper raw sub-replicate analytical results for areas T1 (single mat), T2 (mat with sand), T4 (sand cap only) and T5 (control/no treatment).

	T1-Va-1 *(ug/L)*	*T1-Va-2* *(ug/L)*	*T1-Va-3* *(ug/L)*	*T1-Va-4* *(ug/L)*	*T1-Va-5* *(ug/L)*	*T1-Va-6* *(ug/L)*	*T1-Va-7* *(ug/L)*	*T1-Va-8* *(ug/L)*	*T1-Va-9* *(ug/L)*	*T1-Va-10* *(ug/L)*	*T1-Va-11* *(ug/L)*	*T1-Va-12* *(ug/L)*	*T1-Va-13* *(ug/L)*	*T1-Va-14* *(ug/L)*
Ag 328.068	0.5	0.63	0.51	0.6	0.55	0.45	0.53	0.57	0.58	0.41	0.56	0.58	0.48	0.45
Al 308.215	25	25	25	25	25	25	25	25	25	25	25	25	25	25
As 193.696	6.9	6.9	6.9	6.9	6.9	6.9	6.9	6.9	6.9	6.9	6.9	6.9	6.9	6.9
Ba 455.403	78	80	77	71	64	60	58	60	59	60	60	60	59	58
Be 313.107	0.01	0.01	0.01	0.01	0.01	0.01	0.01	0.01	0.01	0.01	0.01	0.01	0.01	0.01
Ca 317.933	110000	110000	110000	110000	110000	110000	110000	110000	110000	110000	110000	110000	110000	110000
Cd 226.502	1.3	1.4	1.5	1.4	1.2	1.1	1.1	1.2	1.2	1.0	1.0	1.1	0.99	0.86
Co 228.615	1.5	0.72	0.72	0.72	0.72	0.72	0.72	0.72	0.72	0.72	0.72	0.72	0.72	1.5
Cr 267.716	3.7	3.5	3.3	2.9	2.2	2.0	1.8	1.7	1.4	1.4	1.3	1.2	0.82	0.7
Cu 324.754	0.33	0.33	0.33	0.33	0.33	0.33	0.33	0.33	0.33	0.33	0.33	0.33	0.33	0.33
Fe 259.837	16196	16938	16950	17026	16229	15304	14587	14852	14161	13745	13105	13435	12801	12378
K 766.491	8104	7945	7814	7767	7616	7577	7489	7406	7317	7316	7175	7121	7053	6909
Mg 279.800	7351	7158	7065	7064	6978	6810	6684	6699	6553	6427	6297	6374	6183	6042
Mn 257.610	1891	1910	1904	1941	1952	1958	1968	2019	2057	2094	2131	2213	2230	2241
Na 588.995	84319	81228	77967	74912	73881	71618	68985	66894	63825	63364	59477	58400	56189	54073
Ni 231.604	0.73	0.73	0.73	0.73	0.73	0.73	0.73	2.5	0.73	0.73	0.73	0.73	0.73	0.73
Pb 220.353	3.5	3.5	3.5	3.5	3.5	3.5	3.5	3.5	3.5	3.5	3.5	3.5	3.5	3.5
Sb 206.834	4.6	4.6	4.6	4.6	4.6	4.6	4.6	4.6	4.6	4.6	4.6	4.6	4.6	4.6
Se 196.026	18	18	18	18	18	18	18	18	18	18	18	18	18	18
Tl 190.794	8.2	8.2	8.2	8.2	8.2	8.2	8.2	8.2	8.2	8.2	8.2	8.2	8.2	8.2
V 292.401	1.2	1.6	1.2	1.0	0.49	1.0	0.49	0.49	0.49	0.49	0.49	0.49	0.49	0.49
Zn 213.857	1.2	1.2	1.2	1.2	1.2	2.3	1.2	1.2	1.2	1.2	1.2	1.2	1.2	1.2

	T2-Va-1 *(ug/L)*	*T2-Va-2* *(ug/L)*	*T2-Va-3* *(ug/L)*	*T2-Va-4* *(ug/L)*	*T2-Va-5* *(ug/L)*	*T2-Va-6* *(ug/L)*	*T2-Va-7* *(ug/L)*	*T2-Va-8* *(ug/L)*	*T2-Va-9* *(ug/L)*	*T2-Va-10* *(ug/L)*	*T2-Va-11* *(ug/L)*	*T2-Va-12* *(ug/L)*	*T2-Va-13* *(ug/L)*	*T2-Va-14* *(ug/L)*	*T2-Va-15* *(ug/L)*
Ag 328.068	0.76	0.78	0.74	0.65	0.68	0.77	0.67	0.74	0.71	0.68	0.66	0.56	0.72	0.68	0.66
Al 308.215	25	25	25	25	25	25	25	25	25	25	25	25	25	25	25
As 193.696	6.9	6.9	6.9	6.9	6.9	6.9	6.9	6.9	6.9	6.9	6.9	6.9	6.9	6.9	6.9
Ba 455.403	70	70	69	71	70	72	71	74	73	72	72	74	70	72	69
Be 313.107	0.01	0.01	0.01	0.01	0.01	0.01	0.01	0.01	0.01	0.01	0.01	0.01	0.01	0.01	0.01
Ca 317.933	110000	110000	110000	110000	110000	110000	110000	110000	110000	110000	110000	110000	110000	110000	-
Cd 226.502	1.2	1.2	1.2	1.6	1.4	1.2	1.2	1.3	1.4	1.3	1.4	1.2	1.1	1.2	1.1
Co 228.615	0.72	0.72	0.72	0.72	0.72	0.72	0.72	0.72	0.72	0.72	0.72	0.72	0.72	1.6	0.72
Cr 267.716	2.2	2.2	1.9	2.0	1.8	1.9	1.4	1.3	0.98	1.4	0.68	0.32	0.32	0.32	0.32
Cu 324.754	0.33	0.33	0.33	0.33	0.33	0.33	0.33	0.33	0.33	0.33	0.33	0.33	0.33	0.33	0.33
Fe 259.837	15657	17176	17143	17966	17054	17215	16410	16955	16708	16625	16237	16427	15397	15564	14434
K 766.491	7686	7549	7494	7467	7459	7440	7471	7446	7601	7425	7491	7415	7407	7461	7417
Mg 279.800	7934	7673	7464	7338	7324	7260	7200	7179	7210	7018	7048	6972	6958	6940	6974
Mn 257.610	2135	2204	2252	2306	2341	2387	2433	2515	2625	2663	2734	2810	2891	2991	3143
Na 588.995	51849	51009	49323	48144	47053	46372	45586	43493	44408	41745	41419	40316	39553	39022	39459
Ni 231.604	0.73	0.73	0.73	0.73	0.73	0.73	0.73	0.73	0.73	0.73	0.73	0.73	0.73	0.73	0.73
Pb 220.353	3.5	3.5	3.5	3.5	3.5	3.5	3.5	3.5	3.5	3.5	3.5	3.5	3.5	3.5	3.5
Sb 206.834	4.6	4.6	4.6	4.6	4.6	4.6	4.6	4.6	4.6	4.6	4.6	4.6	4.6	4.6	4.6
Se 196.026	18	18	18	18	18	18	18	18	18	18	18	18	18	18	18
Tl 190.794	8.2	8.2	8.2	8.2	8.2	8.2	8.2	8.2	8.2	8.2	8.2	8.2	8.2	8.2	8.2
V 292.401	1.2	0.49	1.2	1.1	0.49	1.0	0.49	1.0	0.49	0.49	0.49	1.0	0.49	0.49	0.49
Zn 213.857	2.7	1.2	2.4	1.2	2.6	1.2	1.2	1.2	1.2	1.2	1.2	1.2	1.2	1.2	1.2

Table E-12. Year Two vertical peeper raw sub-replicate analytical results for areas T1 (single mat), T2 (mat with sand), T4 (sand cap only) and T5 (control/no treatment).

	T4-Va-1 (ug/L)	*T4-Va-2* (ug/L)	*T4-Va-3* (ug/L)	*T4-Va-4* (ug/L)	*T4-Va-5* (ug/L)	*T4-Va-6* (ug/L)	*T4-Va-7* (ug/L)	*T4-Va-8* (ug/L)	*T4-Va-9* (ug/L)	*T4-Va-10* (ug/L)	*T4-Va-11* (ug/L)	*T4-Va-12* (ug/L)	*T4-Va-13* (ug/L)	*T4-Va-14* (ug/L)	*T4-Va-15* (ug/L)
Ag 328.068	0.66	0.59	0.61	0.63	0.74	0.64	0.7	0.74	0.7	0.57	0.58	0.53	0.21	0.21	0.21
Al 308.215	25	25	25	25	25	25	25	25	25	25	25	25	61	25	25
As 193.696	6.9	6.9	6.9	6.9	6.9	6.9	6.9	6.9	6.9	6.9	6.9	6.9	6.9	6.9	6.9
Ba 455.403	73	75	73	74	73	74	83	76	75	72	72	67	60	62	66
Be 313.107	0.01	0.01	0.01	0.01	0.01	0.01	0.01	0.01	0.01	0.01	0.01	0.01	0.01	0.01	0.01
Ca 317.933	110000	110000	110000	110000	110000	110000	110000	110000	110000	110000	110000	110000	110000	110000	-
Cd 226.502	1.1	1.3	1.2	1.3	1.3	1.2	1.3	1.1	1.2	1.1	1.1	1.0	0.74	0.51	0.33
Co 228.615	0.72	0.72	0.72	0.72	0.72	0.72	0.72	0.72	0.72	0.72	0.72	0.72	0.72	0.72	0.72
Cr 267.716	1.6	1.8	1.3	1.1	0.71	0.81	0.67	0.32	0.32	0.32	0.32	0.32	0.76	0.32	0.32
Cu 324.754	0.33	0.33	0.33	0.33	0.33	0.33	0.33	0.33	0.33	0.33	0.33	0.33	0.33	0.33	0.33
Fe 259.837	13894	16552	16123	15841	15641	15860	17434	15790	15474	14716	13766	13063	8639	8229	5585
K 766.491	7214	7199	7154	7091	7131	7032	6948	6866	6854	6701	6591	6236	5498	5125	4901
Mg 279.800	7496	7252	7165	7121	7196	6833	6794	6842	6689	6524	6383	5971	5266	4776	4587
Mn 257.610	2227	2284	2361	2419	2516	2570	2689	2817	2895	2933	2913	2779	2020	2240	2261
Na 588.995	42586	41422	41519	39416	40112	38570	37724	36927	36102	35026	33847	32030	28767	26420	25525
Ni 231.604	0.73	0.73	0.73	0.73	0.73	0.73	0.73	0.73	0.73	0.73	0.73	0.73	0.73	0.73	0.73
Pb 220.353	3.5	3.5	3.5	3.5	3.5	3.5	3.5	3.5	3.5	3.5	3.5	3.5	3.5	3.5	3.5
Sb 206.834	4.6	4.6	4.6	4.6	4.6	4.6	4.6	4.6	4.6	4.6	4.6	4.6	4.6	4.6	4.6
Se 196.026	18	18	18	18	18	18	18	18	18	18	18	18	18	18	18
Tl 190.794	8.2	8.2	8.2	8.2	8.2	8.2	8.2	8.2	8.2	8.2	8.2	8.2	8.2	8.2	8.2
V 292.401	0.49	1.0	0.49	1.1	0.49	0.49	1.2	0.49	0.49	0.49	0.49	0.49	0.49	0.49	0.49
Zn 213.857	1.2	1.2	1.2	1.2	1.2	1.2	1.2	1.2	1.2	1.2	1.2	1.2	6.2	1.2	1.2

	T4-Vb-1 (ug/L)	*T4-Vb-2* (ug/L)	*T4-Vb-3* (ug/L)	*T4-Vb-4* (ug/L)	*T4-Vb-5* (ug/L)	*T4-Vb-6* (ug/L)	*T4-Vb-7* (ug/L)	*T4-Vb-8* (ug/L)	*T4-Vb-9* (ug/L)	*T4-Vb-10* (ug/L)	*T4-Vb-11* (ug/L)	*T4-Vb-12* (ug/L)	*T4-Vb-13* (ug/L)	*T4-Vb-14* (ug/L)	*T4-Vb-15* (ug/L)
Ag 328.068	0.51	0.54	0.55	0.57	0.65	0.46	0.52	0.44	0.43	0.21	0.49	0.43	0.21	0.21	0.21
Al 308.215	25	25	25	25	25	25	25	25	25	25	25	25	25	25	25
As 193.696	6.9	6.9	15	27	6.9	6.9	6.9	6.9	6.9	6.9	6.9	6.9	6.9	6.9	6.9
Ba 455.403	68	62	63	118	65	65	66	73	63	62	58	55	47	45	44
Be 313.107	0.01	0.01	0.01	0.01	0.01	0.01	0.01	0.01	0.01	0.01	0.01	0.01	0.01	0.01	0.01
Ca 317.933	110000	110000	110000	110000	110000	110000	110000	110000	110000	110000	110000	110000	110000	110000	90854
Cd 226.502	0.87	1.0	0.98	2.5	1.1	1.1	1.2	1.3	1.1	0.97	0.68	0.75	0.16	0.42	0.36
Co 228.615	1.4	0.72	0.72	1.7	0.72	0.72	1.5	0.72	0.72	0.72	0.72	0.72	0.72	0.72	0.72
Cr 267.716	1.6	1.6	1.3	1.9	0.99	0.82	0.32	0.32	0.32	0.32	0.32	0.32	0.32	0.32	0.32
Cu 324.754	0.33	0.33	0.33	0.33	0.33	0.33	0.33	0.33	0.33	0.33	0.33	0.33	0.33	0.33	0.33
Fe 259.837	13135	14003	14058	33034	14503	14303	13920	15427	11862	11361	10637	9793	5737	6248	4815
K 766.491	6997	6910	6809	6759	6775	6676	6642	6579	6348	6231	6043	5612	4796	4557	4336
Mg 279.800	7098	6891	6780	6806	6677	6514	6461	6452	6001	5927	5678	5208	3931	4021	3911
Mn 257.610	2031	2055	2157	2331	2342	2388	2455	2499	2412	2403	2369	2213	1205	1677	1801
Na 588.995	43240	41926	41577	40612	39739	38289	37496	36472	34261	33135	31749	28681	24484	23847	23205
Ni 231.604	0.73	0.73	0.73	0.73	0.73	0.73	0.73	0.73	0.73	0.73	0.73	0.73	0.73	0.73	0.73
Pb 220.353	3.5	3.5	3.5	3.5	3.5	3.5	3.5	3.5	3.5	3.5	3.5	3.5	3.5	3.5	3.5
Sb 206.834	4.6	4.6	4.6	4.6	4.6	4.6	4.6	4.6	4.6	4.6	4.6	4.6	4.6	4.6	4.6
Se 196.026	18	18	18	18	18	18	18	18	18	18	18	18	18	18	18
Tl 190.794	8.2	8.2	8.2	8.2	8.2	8.2	8.2	8.2	8.2	8.2	8.2	8.2	8.2	8.2	8.2
V 292.401	0.49	0.49	0.49	3.0	0.49	0.49	0.49	0.49	0.49	0.49	0.49	0.49	0.49	0.49	0.49
Zn 213.857	1.2	1.2	1.2	5.3	3.3	1.2	1.2	1.2	1.2	1.2	1.2	1.2	1.2	4.3	1.2

Table E-12. Year Two vertical peeper raw sub-replicate analytical results for areas T1 (single mat), T2 (mat with sand), T4 (sand cap only) and T5 (control/no treatment).

	T5-Va-1 (ug/L)	*T5-Va-2* (ug/L)	*T5-Va-3* (ug/L)	*T5-Va-4* (ug/L)	*T5-Va-5* (ug/L)	*T5-Va-6* (ug/L)	*T5-Va-7* (ug/L)	*T5-Va-8* (ug/L)	*T5-Va-9* (ug/L)	*T5-Va-10* (ug/L)	*T5-Va-11* (ug/L)	*T5-Va-12* (ug/L)	*T5-Va-13* (ug/L)	*T5-Va-14* (ug/L)	*T5-Va-15* (ug/L)
Ag 328.068	0.46	0.5	0.44	0.53	0.51	0.43	0.42	0.21	0.46	0.21	0.48	0.21	0.21	0.21	0.21
Al 308.215	25	52	25	25	25	64	25	25	25	25	25	25	25	25	25
As 193.696	6.9	6.9	6.9	6.9	6.9	6.9	6.9	6.9	6.9	6.9	6.9	6.9	6.9	6.9	6.9
Ba 455.403	49	52	50	48	48	48	48	49	50	49	53	47	45	45	44
Be 313.107	0.01	0.01	0.01	0.01	0.01	0.01	0.01	0.01	0.01	0.01	0.01	0.01	0.01	0.01	0.01
Ca 317.933	110000	110000	110000	110000	110000	110000	110000	110000	110000	110000	110000	110000	110000	110000	-
Cd 226.502	0.73	1.0	1.0	1.1	1.2	0.92	0.89	0.81	1.0	0.72	0.89	0.78	0.72	0.71	0.83
Co 228.615	1.5	0.72	0.72	0.72	0.72	0.72	0.72	0.72	0.72	0.72	0.72	0.72	0.72	0.72	0.72
Cr 267.716	2.0	3.0	2.2	1.7	1.7	2.5	1.3	1.1	0.8	0.32	0.32	0.32	0.32	0.32	0.32
Cu 324.754	0.33	0.33	0.33	0.33	0.33	0.33	0.33	0.33	0.33	0.33	0.33	0.33	0.33	0.33	0.33
Fe 259.837	10818	13538	13338	12912	12630	12266	11485	10757	10501	10154	11990	10070	10261	10326	11078
K 766.491	6619	6406	6531	6186	6309	6027	6022	6032	5945	5928	5834	5721	5664	5544	5348
Mg 279.800	6378	5917	6540	5811	6378	5606	5609	5765	5457	5393	5316	5254	5185	5082	4982
Mn 257.610	1647	1692	1774	1751	1825	1785	1830	1842	1868	1915	1986	2073	2161	2266	2326
Na 588.995	44293	41394	42645	38417	39321	35616	34748	34297	32594	30720	29738	28604	27751	26757	25566
Ni 231.604	4.2	0.73	5.4	3.0	0.73	0.73	0.73	0.73	0.73	3.1	0.73	0.73	0.73	0.73	0.73
Pb 220.353	3.5	3.5	3.5	3.5	3.5	3.5	3.5	3.5	3.5	3.5	3.5	3.5	3.5	3.5	3.5
Sb 206.834	4.6	4.6	4.6	4.6	4.6	4.6	4.6	4.6	4.6	4.6	4.6	4.6	4.6	4.6	4.6
Se 196.026	18	18	18	18	18	18	18	18	18	18	18	18	18	18	18
Tl 190.794	8.2	8.2	8.2	8.2	8.2	8.2	8.2	8.2	8.2	8.2	8.2	8.2	8.2	8.2	8.2
V 292.401	0.49	1.3	1.2	0.49	0.49	1.3	0.49	0.49	0.49	0.49	0.49	0.49	0.49	0.49	0.49
Zn 213.857	1.2	3.1	4.1	1.2	1.2	3.3	1.2	1.2	1.2	1.2	1.2	1.2	1.2	1.2	1.2

	T5-Vb-1 (ug/L)	*T5-Vb-2* (ug/L)	*T5-Vb-3* (ug/L)	*T5-Vb-4* (ug/L)	*T5-Vb-5* (ug/L)	*T5-Vb-6* (ug/L)	*T5-Vb-7* (ug/L)	*T5-Vb-8* (ug/L)	*T5-Vb-9* (ug/L)	*T5-Vb-10* (ug/L)	*T5-Vb-11* (ug/L)	*T5-Vb-12* (ug/L)	*T5-Vb-13* (ug/L)	*T5-Vb-14* (ug/L)	*T5-Vb-15* (ug/L)
Ag 328.068	0.57	0.58	0.47	0.47	0.57	0.59	0.48	0.55	0.5	0.54	0.6	0.49	0.54	0.48	0.48
Al 308.215	25	25	25	25	25	25	25	25	25	25	25	25	25	25	25
As 193.696	6.9	6.9	6.9	6.9	16	6.9	6.9	6.9	6.9	6.9	6.9	6.9	6.9	15	15
Ba 455.403	57	65	64	60	61	60	60	58	59	59	57	56	55	55	54
Be 313.107	0.01	0.01	0.01	0.01	0.01	0.01	0.01	0.01	0.01	0.01	0.01	0.01	0.01	0.01	0.01
Ca 317.933	110000	110000	110000	110000	110000	110000	110000	110000	110000	110000	110000	110000	110000	110000	-
Cd 226.502	1.2	1.4	1.3	1.3	1.4	1.3	1.2	1.1	1.0	1.1	1.1	1.3	1.2	1.3	1.1
Co 228.615	0.72	0.72	0.72	0.72	0.72	0.72	0.72	0.72	0.72	0.72	0.72	0.72	0.72	0.72	0.72
Cr 267.716	2.6	3.1	2.3	1.9	1.8	1.5	1.3	1.1	0.74	0.32	0.32	0.32	0.32	0.32	0.32
Cu 324.754	0.33	0.33	0.33	0.33	0.98	0.33	0.33	0.33	0.33	0.33	0.33	0.33	0.33	0.33	0.33
Fe 259.837	14944	16778	16437	16402	16313	15623	14714	14151	13939	14036	14330	14761	14604	14745	13299
K 766.491	6802	6641	6574	6559	6751	6591	6533	6435	6462	6417	6317	6383	6387	6177	6040
Mg 279.800	6731	6566	6426	6474	7042	6559	6407	6146	6072	5990	5878	5991	6179	5922	5983
Mn 257.610	1805	1855	1898	1975	2065	2096	2154	2241	2376	2508	2618	2823	3007	3109	3276
Na 588.995	38855	37169	36126	35446	36384	34242	32363	31137	30455	29803	28625	28286	28128	26916	26403
Ni 231.604	0.73	3.4	1.8	0.73	0.73	0.73	6.2	0.73	0.73	0.73	0.73	0.73	0.73	0.73	0.73
Pb 220.353	3.5	3.5	3.5	3.5	3.5	3.5	3.5	3.5	3.5	3.5	3.5	3.5	3.5	3.5	3.5
Sb 206.834	4.6	4.6	4.6	4.6	4.6	4.6	4.6	4.6	4.6	4.6	4.6	4.6	4.6	4.6	4.6
Se 196.026	18	18	18	18	18	18	18	18	18	18	18	18	18	18	18
Tl 190.794	8.2	8.2	8.2	8.2	8.2	8.2	8.2	8.2	8.2	8.2	8.2	8.2	8.2	8.2	8.2
V 292.401	1.1	1.7	1.7	1.4	1.3	1.3	1.2	1.0	1.0	1.1	1.1	1.1	1.1	1.4	0.49
Zn 213.857	1.2	1.2	1.2	1.2	5.1	1.2	1.2	1.2	1.2	1.2	1.2	1.2	1.2	1.2	1.2

= Non-Detect (1/2 MDL substituted)
Chamber depth increases from left to right; each chamber 0.5" apart.

Table E-13. Year Two horizontal peeper raw sub-replicate analytical results for the Cottonwood Bay prototype mat system.

Analyte	Detection Limit	Units	T1-HP-SDM-NW A		T1-HP-MW-NW B		T1-HP-SDM-SW C		T1-HP-MW-SW D		T1-HP-SDM-NE E	
Aluminum	2.3	ug/L	45		1.1	U	30		21		21	
Antimony	9.2	ug/L	4.6	U	4.6	U	4.6	U	4.6	U	4.6	U
Arsenic	14	ug/L	6.9	U	6.9	U	6.9	U	6.9	U	78	
Barium	0.05	ug/L	50		41		89		41		226	
Beryllium	0.03	ug/L	0.01	U	0.01	U	0.01	U	0.01	U	0.01	U
Cadmium	0.31	ug/L	0.16	U	0.16	U	0.16	U	0.16	U	4.2	
Calcium	0.87	ug/L	N/A	U	N/A	U	N/A	U	N/A	U	N/A	U
Chromium	0.64	ug/L	0.91		1.3		2.3		1.4		7.9	
Cobalt	1.4	ug/L	0.72	U	0.72	U	0.72	U	0.72	U	1.4	
Copper	0.67	ug/L	0.33	U	1.1		0.54		1.1		0.33	U
Iron	1.2	ug/L	300		32		1227		70		38657	
Lead	7.1	ug/L	3.5	U	3.5	U	3.5	U	3.5	U	3.5	U
Magnesium	4.2	ug/L	3180		2581		5253		2572		7441	
Manganese	0.08	ug/L	967		20		2183		16		1529	
Nickel	1.5	ug/L	0.73	U	0.73	U	2.7		0.73	U	4.5	
Potassium	1.6	ug/L	4161		4119		7089		4100		10489	
Selenium	36	ug/L	18	U	18	U	18	U	18	U	18	U
Silver	0.41	ug/L	0.21	U	0.21	U	0.54		0.21	U	0.49	
Sodium	10	ug/L	21782		20492		34832		20381		91487	
Thalium	16	ug/L	8.2	U	8.2	U	8.2	U	8.2	U	8.2	U
Vanadium	0.99	ug/L	0.49	U	1.1		1.5		0.88		13	
Zinc	2.3	ug/L	3.1		1.7		8.2		3.1		22	

U = Concentration below detection limit in all sub-replicates; 1/2 detection limit used instead.

N/A = Data not available.

Table E-13. Year Two horizontal peeper raw sub-replicate analytical results for the Cottonwood Bay prototype mat system.

Analyte	Detection Limit	Units	T1-HP-MW-NE F		T2-HP-SDM-NW G		T2-HP-MSN-NW H		T2-HP-SDM-SW I		T2-HP-MSN-SW J	
Aluminum	2.3	ug/L	44		223		78		1.1	U	1.1	U
Antimony	9.2	ug/L	4.6	U	4.6	U	4.6	U	4.6	U	4.6	U
Arsenic	14	ug/L	6.9	U	6.9	U	6.9	U	6.9	U	6.9	U
Barium	0.05	ug/L	40		103		91		79		47	
Beryllium	0.03	ug/L	0.01	U	0.01	U	0.01	U	0.01	U	0.01	U
Cadmium	0.31	ug/L	0.16	U	1.1		0.16	U	0.16	U	0.16	U
Calcium	0.87	ug/L	N/A	U	N/A	U	N/A	U	N/A	U	N/A	U
Chromium	0.64	ug/L	2.0		37		2.3		1.8		0.32	U
Cobalt	1.4	ug/L	0.72	U	0.72	U	0.72	U	0.72	U	0.72	U
Copper	0.67	ug/L	1.3		3.8		0.86		0.66		1.3	
Iron	1.2	ug/L	140		1117		475		1712		923	
Lead	7.1	ug/L	3.5	U	3.5	U	3.5	U	3.5	U	3.5	U
Magnesium	4.2	ug/L	2573		8655		3967		4628		2978	
Manganese	0.08	ug/L	13		1342		2108		2085		1308	
Nickel	1.5	ug/L	1.7		4.8		2.3		2.6		2.7	
Potassium	1.6	ug/L	4119		10515		4303		6091		3810	
Selenium	36	ug/L	18	U	18	U	18	U	18	U	18	U
Silver	0.41	ug/L	0.21	U	1.0		0.46		0.43		0.21	U
Sodium	10	ug/L	20481		59985		21102		25534		20435	
Thalium	16	ug/L	8.2	U	8.2	U	8.2	U	8.2	U	8.2	U
Vanadium	0.99	ug/L	0.9		2.1		1.2		1.5		0.49	U
Zinc	2.3	ug/L	4.6		18		7.4		7.1		2.8	

Table E-13. Year Two horizontal peeper raw sub-replicate analytical results for the Cottonwood Bay prototype mat system.

Analyte	Detection Limit	Units	T2-HP-SDM-NE K		T2-SD-MSN-NE L		T3-SD-SDM-NW M		T3-HP-MM-NW N		T3-SD-MW-NW O	
Aluminum	2.3	ug/L	19		1.1	U	1.1	U	18		1.1	U
Antimony	9.2	ug/L	4.6	U	4.6	U	4.6	U	4.6	U	4.6	U
Arsenic	14	ug/L	6.9	U	6.9	U	113		6.9	U	6.9	U
Barium	0.05	ug/L	131		76		341		39		41	
Beryllium	0.03	ug/L	0.01	U	0.01	U	0.07		0.01	U	0.01	U
Cadmium	0.31	ug/L	0.16	U	0.16	U	10		0.16	U	0.16	U
Calcium	0.87	ug/L	N/A	U	N/A	U	N/A	U	N/A	U	N/A	U
Chromium	0.64	ug/L	0.68		0.48		3.6		1.2		0.93	
Cobalt	1.4	ug/L	0.72	U	0.72	U	2.6		0.72	U	0.72	U
Copper	0.67	ug/L	0.33	U	0.33	U	0.33	U	0.33	U	1.0	
Iron	1.2	ug/L	1490		276		N/A	U	137		41	
Lead	7.1	ug/L	3.5	U	3.5	U	5.0		3.5	U	3.5	U
Magnesium	4.2	ug/L	8187		3559		5575		2574		2584	
Manganese	0.08	ug/L	2845		1320		2502		50		5.1	
Nickel	1.5	ug/L	3.3		0.73	U	4.6		0.73	U	0.73	U
Potassium	1.6	ug/L	9454		4416		7304		4116		4164	
Selenium	36	ug/L	18	U	18	U	18	U	18	U	18	U
Silver	0.41	ug/L	0.96		0.21	U	0.72		0.21	U	0.21	U
Sodium	10	ug/L	43744		20460		48254		20687		20789	
Thalium	16	ug/L	8.2	U	8.2	U	8.2	U	8.2	U	8.2	U
Vanadium	0.99	ug/L	1.2		0.88		18		0.49	U	0.73	
Zinc	2.3	ug/L	9.3		2.7		31		2.3		2.5	

Table E-13. Year Two horizontal peeper raw sub-replicate analytical results for the Cottonwood Bay prototype mat system.

Analyte	Detection Limit	Units	T3-HP-SDM-SE P		T3-HP-MM-SE Q		T3-HP-MW-SE R		T3-HP-SDM-NE S		T3-HP-MM-NE T	
Aluminum	2.3	ug/L	1.1	U	1.1	U	1.1	U	1.1	U	23	
Antimony	9.2	ug/L	4.6	U	4.6	U	4.6	U	4.6	U	4.6	U
Arsenic	14	ug/L	6.9	U	6.9	U	6.9	U	6.9	U	6.9	U
Barium	0.05	ug/L	94		42		42		107		47	
Beryllium	0.03	ug/L	0.01	U	0.01	U	0.01	U	0.01	U	0.01	U
Cadmium	0.31	ug/L	0.16	U	0.16	U	0.16	U	0.16	U	0.16	U
Calcium	0.87	ug/L	N/A	U	N/A	U	N/A	U	N/A	U	N/A	U
Chromium	0.64	ug/L	1.5		0.53		1.4		0.32	U	2.4	
Cobalt	1.4	ug/L	0.72	U	0.72	U	0.72	U	0.72	U	0.72	U
Copper	0.67	ug/L	0.33	U	0.33	U	1.3		0.33	U	1.1	
Iron	1.2	ug/L	637		406		39		130		1173	
Lead	7.1	ug/L	3.5	U	3.5	U	3.5	U	3.5	U	3.5	U
Magnesium	4.2	ug/L	5021		2610		2597		6834		2886	
Manganese	0.08	ug/L	2096		58		32		1764		479	
Nickel	1.5	ug/L	2.0		1.5		11		2.9		0.73	U
Potassium	1.6	ug/L	7116		4161		4153		9645		4134	
Selenium	36	ug/L	18	U	18	U	18	U	18	U	18	U
Silver	0.41	ug/L	0.56		0.21	U	0.21	U	0.78		0.21	U
Sodium	10	ug/L	33061		20923		20898		60913		21001	
Thalium	16	ug/L	8.2	U	8.2	U	8.2	U	8.2	U	8.2	U
Vanadium	0.99	ug/L	1.3		0.49	U	1.6		0.49	U	0.88	
Zinc	2.3	ug/L	8.6		1.2	U	2.3		9.6		1.2	U

Table E-13. Year Two horizontal peeper raw sub-replicate analytical results for the Cottonwood Bay prototype mat system.

Analyte	Detection Limit	Units	T3-HP-MW-NE	U
Aluminum	2.3	ug/L	1.1	U
Antimony	9.2	ug/L	4.6	U
Arsenic	14	ug/L	6.9	U
Barium	0.05	ug/L	41	
Beryllium	0.03	ug/L	0.01	U
Cadmium	0.31	ug/L	0.16	U
Calcium	0.87	ug/L	N/A	U
Chromium	0.64	ug/L	1.3	
Cobalt	1.4	ug/L	0.72	U
Copper	0.67	ug/L	1.1	
Iron	1.2	ug/L	23	
Lead	7.1	ug/L	3.5	U
Magnesium	4.2	ug/L	2590	
Manganese	0.08	ug/L	10	
Nickel	1.5	ug/L	2.2	
Potassium	1.6	ug/L	4246	
Selenium	36	ug/L	18	U
Silver	0.41	ug/L	0.21	U
Sodium	10	ug/L	21122	
Thalium	16	ug/L	8.2	U
Vanadium	0.99	ug/L	0.49	U
Zinc	2.3	ug/L	1.7	

Table E-14. Year Two horizontal peeper replicate analytical results for area T1 (single mat only).

T1 - Single Mat Only

Analyte	Units	Rep 1		Rep 2		Rep 3		Rep Average	
		Below Mat (A)	Above Mat (B)	Below Mat (C)	Above Mat (D)	Below Mat (E)	Above Mat (F)	Below Mat	Above Mat
Aluminum	ug/L	45	1.1	30	21	21	44	32	22
Antimony	ug/L	4.6	4.6	4.6	4.6	4.6	4.6	4.6	4.6
Arsenic	ug/L	6.9	6.9	6.9	6.9	78	6.9	31	6.9
Barium	ug/L	50	41	89	41	226	40	122	41
Berylium	ug/L	0.01	0.01	0.01	0.01	0.01	0.01	0.01	0.01
Cadmium	ug/L	0.16	0.16	0.16	0.16	4.2	0.16	1.5	0.16
Calcium	ug/L	N/A	N/A	N/A	N/A	N/A	N/A	N/A	N/A
Chromium	ug/L	0.91	1.3	2.3	1.4	7.9	2.0	3.7	1.6
Cobalt	ug/L	0.72	0.72	0.72	0.72	1.4	0.72	0.96	0.72
Copper	ug/L	0.33	1.1	0.54	1.1	0.33	1.3	0.4	1.2
Iron	ug/L	300	32	1227	70	38657	140	13394	81
Lead	ug/L	3.5	3.5	3.5	3.5	3.5	3.5	3.5	3.5
Magnesium	ug/L	3180	2581	5253	2572	7441	2573	5291	2575
Manganese	ug/L	967	20	2183	16	1529	13	1560	16
Nickel	ug/L	0.73	0.73	2.7	0.73	4.5	1.7	2.6	1.1
Potassium	ug/L	4161	4119	7089	4100	10489	4119	7246	4113
Selenium	ug/L	18	18	18	18	18	18	18	18
Silver	ug/L	0.21	0.21	0.54	0.21	0.49	0.21	0.41	0.21
Sodium	ug/L	21782	20492	34832	20381	91487	20481	49367	20451
Thalium	ug/L	8.2	8.2	8.2	8.2	8.2	8.2	8.2	8.2
Vanadium	ug/L	0.49	1.1	1.5	0.88	13	0.9	4.9	0.96
Zinc	ug/L	3.1	1.7	8.2	3.1	22	4.6	11	3.2

Analyte	Units	Rep 1		Rep 2		Rep 3		Rep Average	
		Below Mat (A)	Above Mat (B)	Below Mat (C)	Above Mat (D)	Below Mat (E)	Above Mat (F)	Below Mat	Above Mat
Percent Reduction									
Aluminum	%	-	97.5	-	29.5	-	-110.3	-	31.1
Antimony	%	-	0.0	-	0.0	-	0.0	-	0.0
Arsenic	%	-	0.0	-	0.0	-	91.2	-	77.5
Barium	%	-	17.7	-	54.5	-	82.1	-	66.5
Berylium	%	-	0.0	-	0.0	-	0.0	-	0.0
Cadmium	%	-	0.0	-	0.0	-	96.3	-	89.6
Calcium	%	-	N/A	-	N/A	-	N/A	-	N/A
Chromium	%	-	-47.9	-	36.2	-	75.1	-	57.1
Cobalt	%	-	0.0	-	0.0	-	49.9	-	24.9
Copper	%	-	-220.6	-	-106.5	-	-298.0	-	-190.6
Iron	%	-	89.3	-	94.3	-	99.6	-	99.4
Lead	%	-	0.0	-	0.0	-	0.0	-	0.0
Magnesium	%	-	18.8	-	51.0	-	65.4	-	51.3
Manganese	%	-	98.0	-	99.3	-	99.2	-	99.0
Nickel	%	-	0.0	-	72.4	-	61.9	-	59.7
Potassium	%	-	1.0	-	42.2	-	60.7	-	43.2
Selenium	%		0.0	-	0.0	-	0.0	-	0.0
Silver	%	-	0.0	-	61.7	-	58.1	-	50.0
Sodium	%	-	5.9	-	41.5	-	77.6	-	58.6
Thalium	%	-	0.0	-	0.0	-	0.0	-	0.0
Vanadium	%	-	-124.9	-	42.9	-	92.9	-	80.2
Zinc	%	-	43.4	-	61.9	-	78.8	-	71.3

N/A = Data not available.

Table E-15. Year Two horizontal peeper replicate analytical results for area T2 (single mat with sand cap).

T2 - Single Mat With Sand Cap

Analyte	Units	Rep 1		Rep 2		Rep 3		Rep Average	
		Below Mat (G)	Above Mat (H)	Below Mat (I)	Above Mat (J)	Below Mat (K)	Above Mat (L)	Below Mat	Above Mat
Aluminum	ug/L	223	78	1.1	1.1	19	1.1	81	27
Antimony	ug/L	4.6	4.6	4.6	4.6	4.6	4.6	4.6	4.6
Arsenic	ug/L	6.9	6.9	6.9	6.9	6.9	6.9	6.9	6.9
Barium	ug/L	103	91	79	47	131	76	104	71
Berylium	ug/L	0.01	0.01	0.01	0.01	0.01	0.01	0.01	0.01
Cadmium	ug/L	1.1	0.16	0.16	0.16	0.16	0.16	0.47	0.16
Calcium	ug/L	N/A	N/A	N/A	N/A	N/A	N/A	N/A	N/A
Chromium	ug/L	37	2.3	1.8	0.32	0.68	0.48	13	1.0
Cobalt	ug/L	0.72	0.72	0.72	0.72	0.72	0.72	0.72	0.72
Copper	ug/L	3.8	0.86	0.66	1.3	0.33	0.33	1.6	0.82
Iron	ug/L	1117	475	1712	923	1490	276	1440	558
Lead	ug/L	3.5	3.5	3.5	3.5	3.5	3.5	3.5	3.5
Magnesium	ug/L	8655	3967	4628	2978	8187	3559	7157	3501
Manganese	ug/L	1342	2108	2085	1308	2845	1320	2091	1579
Nickel	ug/L	4.8	2.3	2.6	2.7	3.3	0.73	3.6	1.9
Potassium	ug/L	10515	4303	6091	3810	9454	4416	8687	4177
Selenium	ug/L	18	18	18	18	18	18	18	18
Silver	ug/L	1.0	0.46	0.43	0.21	0.96	0.21	0.8	0.29
Sodium	ug/L	59985	21102	25534	20435	43744	20460	43087	20666
Thalium	ug/L	8.2	8.2	8.2	8.2	8.2	8.2	8.2	8.2
Vanadium	ug/L	2.1	1.2	1.5	0.49	1.2	0.88	1.6	0.85
Zinc	ug/L	18	7.4	7.1	2.8	9.3	2.7	11	4.3

Analyte	Units	Rep 1		Rep 2		Rep 3		Rep Average	
		Below Mat (A)	Above Mat (B)	Below Mat (C)	Above Mat (D)	Below Mat (E)	Above Mat (F)	Below Mat	Above Mat
Percent Reduction									
Aluminum	%	-	65.2	-	0.0	-	94.0	-	67.2
Antimony	%	-	0.0	-	0.0	-	0.0	-	0.0
Arsenic	%	-	0.0	-	0.0	-	0.0	-	0.0
Barium	%	-	11.4	-	40.8	-	42.0	-	31.7
Berylium	%	-	0.0	-	0.0	-	0.0	-	0.0
Cadmium	%	-	85.7	-	0.0	-	0.0	-	66.6
Calcium	%	-	N/A	-	N/A	-	N/A	-	N/A
Chromium	%	-	93.7	-	82.5	-	28.6	-	92.0
Cobalt	%	-	0.0	-	0.0	-	0.0	-	0.0
Copper	%	-	77.4	-	-90.7	-	0.0	-	48.7
Iron	%	-	57.4	-	46.1	-	81.5	-	61.2
Lead	%	-	0.0	-	0.0	-	0.0	-	0.0
Magnesium	%	-	54.2	-	35.7	-	56.5	-	51.1
Manganese	%	-	-57.1	-	37.3	-	53.6	-	24.5
Nickel	%	-	52.2	-	-3.4	-	77.9	-	46.7
Potassium	%	-	59.1	-	37.4	-	53.3	-	51.9
Selenium	%	-	0.0	-	0.0	-	0.0	-	0.0
Silver	%	-	55.4	-	51.6	-	78.5	-	63.9
Sodium	%	-	64.8	-	20.0	-	53.2	-	52.0
Thalium	%	-	0.0	-	0.0	-	0.0	-	0.0
Vanadium	%	-	42.2	-	66.1	-	25.1	-	45.4
Zinc	%	-	58.9	-	59.9	-	70.9	-	62.4

N/A = Data not available.

Table E-16. Year Two horizontal peeper replicate analytical results for area T3 (double mat).

T3 - Double Mat

Analyte	Units	Rep 1			Rep 2		
		Below Mats (M)	Between Mats (N)	Above Mats (O)	Below Mats (P)	Between Mats (Q)	Above Mats (R)
Aluminum	ug/L	1.1	18	1.1	1.1	1.1	1.1
Antimony	ug/L	4.6	4.6	4.6	4.6	4.6	4.6
Arsenic	ug/L	113	6.9	6.9	6.9	6.9	6.9
Barium	ug/L	341	39	41	94	42	42
Berylium	ug/L	0.07	0.01	0.01	0.01	0.01	0.01
Cadmium	ug/L	10	0.16	0.16	0.16	0.16	0.16
Calcium	ug/L	N/A	N/A	N/A	N/A	N/A	N/A
Chromium	ug/L	3.6	1.2	0.93	1.5	0.53	1.4
Cobalt	ug/L	2.6	0.72	0.72	0.72	0.72	0.72
Copper	ug/L	0.33	0.33	1.0	0.33	0.33	1.3
Iron	ug/L	N/A	137	41	637	406	39
Lead	ug/L	5.0	3.5	3.5	3.5	3.5	3.5
Magnesium	ug/L	5575	2574	2584	5021	2610	2597
Manganese	ug/L	2502	50	5.1	2096	58	32
Nickel	ug/L	4.6	0.73	0.73	2.0	1.5	11
Potassium	ug/L	7304	4116	4164	7116	4161	4153
Selenium	ug/L	18	18	18	18	18	18
Silver	ug/L	0.72	0.21	0.21	0.56	0.21	0.21
Sodium	ug/L	48254	20687	20789	33061	20923	20898
Thalium	ug/L	8.2	8.2	8.2	8.2	8.2	8.2
Vanadium	ug/L	18	0.49	0.73	1.3	0.49	1.6
Zinc	ug/L	31	2.3	2.5	8.6	1.2	2.3

Analyte	Units	Rep 1			Rep 2		
		Below Mats (M)	Between Mats (N)	Above Mats (O)	Below Mats (P)	Between Mats (Q)	Above Mats (R)
Percent Reduction							
Aluminum	%	-	-1431.8	93.5	-	0.0	0.0
Antimony	%	-	0.0	0.0	-	0.0	0.0
Arsenic	%	-	93.9	0.0	-	0.0	0.0
Barium	%	-	88.4	-3.6	-	55.1	0.6
Berylium	%	-	82.7	0.0	-	0.0	0.0
Cadmium	%	-	98.5	0.0	-	0.0	0.0
Calcium	%	-	N/A	N/A	-	N/A	N/A
Chromium	%	-	67.6	20.1	-	64.4	-161.9
Cobalt	%	-	71.8	0.0	-	0.0	0.0
Copper	%	-	0.0	-205.7	-	0.0	-282.8
Iron	%	-	N/A	70.0	-	36.2	90.4
Lead	%	-	29.1	0.0	-	0.0	0.0
Magnesium	%	-	53.8	-0.4	-	48.0	0.5
Manganese	%	-	98.0	89.6	-	97.3	45.0
Nickel	%	-	84.0	0.0	-	22.5	-605.3
Potassium	%	-	43.6	-1.2	-	41.5	0.2
Selenium	%	-	0.0	0.0	-	0.0	0.0
Silver	%	-	71.2	0.0	-	63.0	0.0
Sodium	%	-	57.1	-0.5	-	36.7	0.1
Thalium	%	-	0.0	0.0	-	0.0	0.0
Vanadium	%	-	97.3	-46.9	-	63.1	-230.8
Zinc	%	-	92.5	-6.2	-	86.5	-100.9

Table E-16. Year Two horizontal peeper replicate analytical results for area T3 (double mat).

T3 - Double Mat

Analyte	Units	Rep 3			Rep Average		
		Below Mats (S)	Between Mats (T)	Above Mats (U)	Below Mats	Between Mats	Above Mat
Aluminum	ug/L	1.1	23	1.1	1.1	14	1.1
Antimony	ug/L	4.6	4.6	4.6	4.6	4.6	4.6
Arsenic	ug/L	6.9	6.9	6.9	42	6.9	6.9
Barium	ug/L	107	47	41	181	43	41
Berylium	ug/L	0.01	0.01	0.01	0.03	0.01	0.01
Cadmium	ug/L	0.16	0.16	0.16	3.5	0.16	0.16
Calcium	ug/L	N/A	N/A	N/A	N/A	N/A	N/A
Chromium	ug/L	0.32	2.4	1.3	1.8	1.4	1.2
Cobalt	ug/L	0.72	0.72	0.72	1.3	0.72	0.72
Copper	ug/L	0.33	1.1	1.1	0.33	0.6	1.1
Iron	ug/L	130	1173	23	383	572	35
Lead	ug/L	3.5	3.5	3.5	4.0	3.5	3.5
Magnesium	ug/L	6834	2886	2590	5810	2690	2590
Manganese	ug/L	1764	479	10	2121	195	16
Nickel	ug/L	2.9	0.73	2.2	3.1	1.0	4.6
Potassium	ug/L	9645	4134	4246	8022	4137	4188
Selenium	ug/L	18	18	18	18	18	18
Silver	ug/L	0.78	0.21	0.21	0.68	0.21	0.21
Sodium	ug/L	60913	21001	21122	47409	20870	20937
Thalium	ug/L	8.2	8.2	8.2	8.2	8.2	8.2
Vanadium	ug/L	0.49	0.88	0.49	6.6	0.62	0.95
Zinc	ug/L	9.6	1.2	1.7	16	1.5	2.2

Analyte	Units	Rep 3			Rep Average		
		Below Mats (S)	Between Mats (T)	Above Mats (U)	Below Mats	Between Mats	Above Mat
Percent Reduction							
Aluminum	%	-	-1875.8	94.9	-	-1102.5	91.7
Antimony	%	-	0.0	0.0	-	0.0	0.0
Arsenic	%	-	0.0	0.0	-	83.6	0.0
Barium	%	-	55.7	13.5	-	76.2	4.1
Berylium	%	-	0.0	0.0	-	61.4	0.0
Cadmium	%	-	0.0	0.0	-	95.5	0.0
Calcium	%	-	N/A	N/A	-	N/A	N/A
Chromium	%	-	-664.0	48.7	-	23.4	13.6
Cobalt	%	-	0.0	0.0	-	45.9	0.0
Copper	%	-	-238.2	0.4	-	-79.4	-90.5
Iron	%	-	-803.5	98.0	-	-49.3	94.0
Lead	%	-	0.0	0.0	-	12.0	0.0
Magnesium	%	-	57.8	10.3	-	53.7	3.7
Manganese	%	-	72.9	97.9	-	90.8	92.0
Nickel	%	-	74.3	-200.5	-	68.2	-358.4
Potassium	%	-	57.1	-2.7	-	48.4	-1.2
Selenium	%	-	0.0	0.0	-	0.0	0.0
Silver	%	-	73.4	0.0	-	69.8	0.0
Sodium	%	-	65.5	-0.6	-	56.0	-0.3
Thalium	%	-	0.0	0.0	-	0.0	0.0
Vanadium	%	-	-77.4	43.6	-	90.6	-53.1
Zinc	%	-	87.9	-47.0	-	90.5	-40.0

Table E-16. Year Two horizontal peeper replicate analytical results for area T3 (double mat).

T3 - Double Mat

Analyte	Units	Rep 1			Rep 2		
		Below Mats (M)	Between Mats (N)	Above Mats (O)	Below Mats (P)	Between Mats (Q)	Above Mats (R)
Percent Reduction							
Aluminum	%	-	-	0.0	-	-	0.0
Antimony	%	-	-	0.0	-	-	0.0
Arsenic	%	-	-	93.9	-	-	0.0
Barium	%	-	-	88.0	-	-	55.4
Berylium	%	-	-	82.7	-	-	0.0
Cadmium	%	-	-	98.5	-	-	0.0
Calcium	%	-	-	N/A	-	-	N/A
Chromium	%	-	-	74.1	-	-	6.8
Cobalt	%	-	-	71.8	-	-	0.0
Copper	%	-	-	-205.7	-	-	-282.8
Iron	%	-	-	N/A	-	-	93.9
Lead	%	-	-	29.1	-	-	0.0
Magnesium	%	-	-	53.7	-	-	48.3
Manganese	%	-	-	99.8	-	-	98.5
Nickel	%	-	-	84.0	-	-	-446.3
Potassium	%	-	-	43.0	-	-	41.6
Selenium	%	-	-	0.0	-	-	0.0
Silver	%	-	-	71.2	-	-	63.0
Sodium	%	-	-	56.9	-	-	36.8
Thalium	%	-	-	0.0	-	-	0.0
Vanadium	%	-	-	96.0	-	-	-22.0
Zinc	%	-	-	92.0	-	-	72.9

N/A = Data not available.

Table E-16. Year Two horizontal peeper replicate analytical results for area T3 (double mat).

T3 - Double Mat

Analyte	Units	Rep 3			Rep Average		
		Below Mats (S)	Between Mats (T)	Above Mats (U)	Below Mats	Between Mats	Above Mat
Percent Reduction							
Aluminum	%	-	-	0.0	-	-	0.0
Antimony	%	-	-	0.0	-	-	0.0
Arsenic	%	-	-	0.0	-	-	83.6
Barium	%	-	-	61.7	-	-	77.1
Berylium	%	-	-	0.0	-	-	61.4
Cadmium	%	-	-	0.0	-	-	95.5
Calcium	%	-	-	N/A	-	-	N/A
Chromium	%	-	-	-291.7	-	-	33.8
Cobalt	%	-	-	0.0	-	-	45.9
Copper	%	-	-	-236.9	-	-	-241.8
Iron	%	-	-	81.9	-	-	91.0
Lead	%	-	-	0.0	-	-	12.0
Magnesium	%	-	-	62.1	-	-	55.4
Manganese	%	-	-	99.4	-	-	99.3
Nickel	%	-	-	22.9	-	-	-45.8
Potassium	%	-	-	56.0	-	-	47.8
Selenium	%	-	-	0.0	-	-	0.0
Silver	%	-	-	73.4	-	-	69.8
Sodium	%	-	-	65.3	-	-	55.8
Thalium	%	-	-	0.0	-	-	0.0
Vanadium	%	-	-	0.0	-	-	85.6
Zinc	%	-	-	82.3	-	-	86.8

Table E-17. Year Two vertical peeper replicate analytical results for area T4 (sand cap only).

T4 - Sand Cap Only

Analyte	Units	Rep 1		Rep 2		Rep Average	
		Below Sand (AA-3-5)	Above Sand (AA-1)	Below Sand (Y-3-5)	Above Sand (Y-1)	Below Sand	Above Sand
Aluminum	ug/L	25	25	37	25	31	25
Antimony	ug/L	4.6	4.6	4.6	4.6	4.6	4.6
Arsenic	ug/L	6.9	6.9	6.9	6.9	6.9	6.9
Barium	ug/L	53	44	66	66	60	55
Beryllium	ug/L	0.01	0.01	0.01	0.01	0.01	0.01
Cadmium	ug/L	0.53	0.36	0.94	0.33	0.74	0.34
Calcium	ug/L	N/A	N/A	N/A	N/A	N/A	N/A
Chromium	ug/L	0.32	0.32	0.47	0.32	0.39	0.32
Cobalt	ug/L	0.72	0.72	0.72	0.72	0.72	0.72
Copper	ug/L	0.33	0.33	0.33	0.33	0.33	0.33
Iron	ug/L	8722	4815	11823	5585	10273	5200
Lead	ug/L	3.5	3.5	3.5	3.5	3.5	3.5
Magnesium	ug/L	4939	3911	5873	4587	5406	4249
Manganese	ug/L	1929	1801	2571	2261	2250	2031
Nickel	ug/L	0.73	0.73	0.73	0.73	0.73	0.73
Potassium	ug/L	5484	4336	6108	4901	5796	4618
Selenium	ug/L	18	18	18	18	18	18
Silver	ug/L	0.37	0.21	0.44	0.21	0.41	0.21
Sodium	ug/L	28305	23205	31548	25525	29926	24365
Thallium	ug/L	8.2	8.2	8.2	8.2	8.2	8.2
Vanadium	ug/L	0.49	0.49	0.49	0.49	0.49	0.49
Zinc	ug/L	1.2	1.2	2.8	1.2	2.0	1.2

Analyte	Units	Rep 1		Rep 2		Rep Average	
		Below Sand (AA-3-5)	Above Sand (AA-1)	Below Sand (Y-3-5)	Above Sand (Y-1)	Below Sand	Above Sand
Percent Reduction							
Aluminum	%	-	0.0	-	32.4	-	19.3
Antimony	%	-	0.0	-	0.0	-	0.0
Arsenic	%	-	0.0	-	0.0	-	0.0
Barium	%	-	17.3	-	1.3	-	8.4
Beryllium	%	-	0.0	-	0.0	-	0.0
Cadmium	%	-	32.3	-	64.7	-	53.1
Calcium	%	-	N/A	-	N/A	-	N/A
Chromium	%	-	0.0	-	31.8	-	18.9
Cobalt	%	-	0.0	-	0.0	-	0.0
Copper	%	-	0.0	-	0.0	-	0.0
Iron	%	-	44.8	-	52.8	-	49.4
Lead	%	-	0.0	-	0.0	-	0.0
Magnesium	%	-	20.8	-	21.9	-	21.4
Manganese	%	-	6.7	-	12.0	-	9.7
Nickel	%	-	0.0	-	0.0	-	0.0
Potassium	%	-	20.9	-	19.8	-	20.3
Selenium	%	-	0.0	-	0.0	-	0.0
Silver	%	-	44.6	-	52.8	-	49.1
Sodium	%	-	18.0	-	19.1	-	18.6
Thallium	%	-	0.0	-	0.0	-	0.0
Vanadium	%	-	0.0	-	0.0	-	0.0
Zinc	%	-	0.0	-	59.3	-	42.1

N/A = Data not available.

Table E-18. Year Two vertical peeper replicate analytical results for area T5 (no treatment/control).

T5 - No Treatment (Control)

Analyte	Units	Rep 1 Above Sed (AD-1)	Rep 2 Above Sed (AC-1)	Rep Average Above Sed
Aluminum	ug/L	25	25	25
Antimony	ug/L	4.6	4.6	4.6
Arsenic	ug/L	6.9	15	11
Barium	ug/L	44	54	49
Berylium	ug/L	0.01	0.01	0.01
Cadmium	ug/L	0.83	1.1	0.97
Calcium	ug/L	N/A	N/A	N/A
Chromium	ug/L	0.32	0.32	0.32
Cobalt	ug/L	0.72	0.72	0.72
Copper	ug/L	0.33	0.33	0.33
Iron	ug/L	11078	13299	12189
Lead	ug/L	3.5	3.5	3.5
Magnesium	ug/L	4982	5983	5482
Manganese	ug/L	2326	3276	2801
Nickel	ug/L	0.73	0.73	0.73
Potassium	ug/L	5348	6040	5694
Selenium	ug/L	18	18	18
Silver	ug/L	0.21	0.48	0.34
Sodium	ug/L	25566	26403	25985
Thalium	ug/L	8.2	8.2	8.2
Vanadium	ug/L	0.49	0.49	0.49
Zinc	ug/L	1.2	1.2	1.2

N/A = Data not available.

Table E-19. Summary of the Year Two peeper analytical results for the Cottonwood Bay prototype mat system.

Treatment Summary - Replicate Averages

Analyte	Units	T1 - Mat Only			T2 - Mat w/ Sand		
		Below Treatment	Between Treatment	Above Treatment	Below Treatment	Between Treatment	Above Treatment
Aluminum	ug/L	32	-	22	81	-	27
Antimony	ug/L	4.6	-	4.6	4.6	-	4.6
Arsenic	ug/L	31	-	6.9	6.9	-	6.9
Barium	ug/L	122	-	41	104	-	71
Beryllium	ug/L	0.01	-	0.01	0.01	-	0.01
Cadmium	ug/L	1.5	-	0.16	0.47	-	0.16
Calcium	ug/L	N/A	-	N/A	N/A	-	N/A
Chromium	ug/L	3.7	-	1.6	13	-	1.0
Cobalt	ug/L	0.96	-	0.72	0.72	-	0.72
Copper	ug/L	0.4	-	1.2	1.6	-	0.82
Iron	ug/L	13394	-	81	1440	-	558
Lead	ug/L	3.5	-	3.5	3.5	-	3.5
Magnesium	ug/L	5291	-	2575	7157	-	3501
Manganese	ug/L	1560	-	16	2091	-	1579
Nickel	ug/L	2.6	-	1.1	3.6	-	1.9
Potassium	ug/L	7246	-	4113	8687	-	4177
Selenium	ug/L	18	-	18	18	-	18
Silver	ug/L	0.41	-	0.21	0.8	-	0.29
Sodium	ug/L	49367	-	20451	43087	-	20666
Thallium	ug/L	8.2	-	8.2	8.2	-	8.2
Vanadium	ug/L	4.9	-	0.96	1.6	-	0.85
Zinc	ug/L	11	-	3.2	11	-	4.3

N/A = Data not available.

Table E-19. Summary of the Year Two peeper analytical results for the Cottonwood Bay prototype mat system.

Treatment Summary - Replicate

Analyte	Units	T3 - Double Mat			T4 - Sand Only		
		Below Treatment	Between Treatment	Above Treatment	Below Treatment	Between Treatment	Above Treatment
Aluminum	ug/L	1.1	14	1.1	31	-	25
Antimony	ug/L	4.6	4.6	4.6	4.6	-	4.6
Arsenic	ug/L	42	6.9	6.9	6.9	-	6.9
Barium	ug/L	181	43	41	60	-	55
Beryllium	ug/L	0.03	0.01	0.01	0.01	-	0.01
Cadmium	ug/L	3.5	0.16	0.16	0.74	-	0.34
Calcium	ug/L	N/A	N/A	N/A	N/A	-	N/A
Chromium	ug/L	1.8	1.4	1.2	0.39	-	0.32
Cobalt	ug/L	1.3	0.72	0.72	0.72	-	0.72
Copper	ug/L	0.33	0.6	1.1	0.33	-	0.33
Iron	ug/L	383	572	35	10273	-	5200
Lead	ug/L	4.0	3.5	3.5	3.5	-	3.5
Magnesium	ug/L	5810	2690	2590	5406	-	4249
Manganese	ug/L	2121	195	16	2250	-	2031
Nickel	ug/L	3.1	1.0	4.6	0.73	-	0.73
Potassium	ug/L	8022	4137	4188	5796	-	4618
Selenium	ug/L	18	18	18	18	-	18
Silver	ug/L	0.68	0.21	0.21	0.41	-	0.21
Sodium	ug/L	47409	20870	20937	29926	-	24365
Thallium	ug/L	8.2	8.2	8.2	8.2	-	8.2
Vanadium	ug/L	6.6	0.62	0.95	0.49	-	0.49
Zinc	ug/L	16	1.5	2.2	2.0	-	1.2

N/A = Data not available.

Table E-19. Summary of the Year Two peeper analytical results for the Cottonwood Bay prototype mat system.

Treatment Summary - Replicate

Analyte	Units	T5 - No Treatment			Background
		Below Treatment	Between Treatment	Above Treatment	Water Column
Aluminum	ug/L	-	-	25	19
Antimony	ug/L	-	-	4.6	4.6
Arsenic	ug/L	-	-	11	6.9
Barium	ug/L	-	-	49	46
Beryllium	ug/L	-	-	0.01	0.01
Cadmium	ug/L	-	-	0.97	0.16
Calcium	ug/L	-	-	N/A	N/A
Chromium	ug/L	-	-	0.32	0.94
Cobalt	ug/L	-	-	0.72	0.72
Copper	ug/L	-	-	0.33	0.96
Iron	ug/L	-	-	12189	47
Lead	ug/L	-	-	3.5	3.5
Magnesium	ug/L	-	-	5482	2570
Manganese	ug/L	-	-	2801	11
Nickel	ug/L	-	-	0.73	1.0
Potassium	ug/L	-	-	5694	4132
Selenium	ug/L	-	-	18	18
Silver	ug/L	-	-	0.34	0.21
Sodium	ug/L	-	-	25985	20491
Thallium	ug/L	-	-	8.2	8.2
Vanadium	ug/L	-	-	0.49	0.7
Zinc	ug/L	-	-	1.2	2.5

N/A = Data not available.

This page is intentionally left blank

APPENDIX F

"First and Second Year Semi-Permeable Membrane Device (SPMD) Analytical Results (December 2008 & December 2009)"

This page is intentionally left blank

Table F-1. Year One raw semi-permeable membrane device results for the Cottonwood Bay prototype mat system.

Analyte	Units	18227-001 T1-SD-SDM-NW A	18227-002 T1-SD-MW-NW B	18227-003 T1-SD-MW-SW D	18227-004 T1-SD-SDM-NE E	18227-005 T1-SD-MW-NE F
Naphthalene (L)	pg/L	N/A	N/A	N/A	N/A	N/A
Acenaphthylene (L)	pg/L	129 U	129 U	129 U	129 U	129 U
Acenaphthene (L)	pg/L	1982	354	177	425	354
Fluorene (L)	pg/L	2356	842	409	1130	866
Phenanthrene (L)	pg/L	2088	1751	1666	928	1877
Anthracene (L)	pg/L	750	312	156	203	234
Fluoranthene (H)	pg/L	4744	5023	3535	1860	4279
Pyrene (H)	pg/L	5412	5569	3843	2039	4784
Benzo(a)anthracene (H)	pg/L	767	700	444	311	622
Chrysene (H)	pg/L	750	970	830	440	970
Benzo(b)fluoranthene	pg/L	1113	1225	738	600	1163
Benzo(k)fluoranthene	pg/L	424	541	565	224	553
Benzo(a)pyrene (H)	pg/L	309	274	171	137	229
Indeno(1,2,3-c,d)pyrene	pg/L	303	291	182	121	242
Dibenzo(a,h)anthracene (H)	pg/L	139	104	43 U	43 U	104
Benzo(g,h,i)perylene	pg/L	442	400	253	211	358
Total LMW PAHs	pg/L	7305	3388	2537	2815	3460
Total HMW PAHs	pg/L	12120	12641	8867	4831	10989
Total LMW+HMW PAHs	pg/L	19426	16028	11405	7646	14449

MDL = 5 ng/mL in hexane.

U = Concentration below detection limit; 1/2 detection limit used for conversion.

E = Reported value taken from diluted sample.

N/A = Data not available.

Table F-1. Year One raw semi-permeable membrane device results for the Cottonwood Bay prototype mat system.

Analyte	Units	18227-006 T2-SD-SDM-NW G		18227-007 T2-SD-MSN-NW H		18227-008 T2-SD-SDM-SW I		18227-009 T2-SD-MSN-SW J		18227-010 T2-SD-SDM-NE K	
Naphthalene (L)	pg/L	N/A		N/A		N/A		N/A		N/A	
Acenaphthylene (L)	pg/L	129	U	129	U	129	U	129	U	129	U
Acenaphthene (L)	pg/L	6724		248		12032		88	U	1734	
Fluorene (L)	pg/L	5531		697		11061		409		1587	
Phenanthrene (L)	pg/L	14977		1350		33750	E	1266		3797	
Anthracene (L)	pg/L	1718		156		4841		125		468	
Fluoranthene (H)	pg/L	7907		2605		18605	E	2512		2512	
Pyrene (H)	pg/L	9412		2902		19608	E	2745		2667	
Benzo(a)anthracene (H)	pg/L	1333		400		4000		400		411	
Chrysene (H)	pg/L	1800		630		4500		650		490	
Benzo(b)fluoranthene	pg/L	1213		800		2750		813		388	
Benzo(k)fluoranthene	pg/L	647		482		1118		435		176	
Benzo(a)pyrene (H)	pg/L	446		183		1086		171		114	
Indeno(1,2,3-c,d)pyrene	pg/L	303		218		473		206		85	
Dibenzo(a,h)anthracene (H)	pg/L	139		104		226		43	U	43	U
Benzo(g,h,i)perylene	pg/L	484		316		800		274		126	
Total LMW PAHs	pg/L	29078		2580		61813		2017		7716	
Total HMW PAHs	pg/L	21037		6824		48024		6522		6237	
Total LMW+HMW PAHs	pg/L	50115		9404		109838		8539		13953	

Table F-1. Year One raw semi-permeable membrane device results for the Cottonwood Bay prototype mat system.

Analyte	Units	18227-011 T2-SD-MSN-NE L		18227-012 T3-SD-SDM-NW M		18227-013 T3-SD-MM-NW N		18227-014 T3-SD-MW-NW O		18227-015 T3-SD-SDM-NE P	
Naphthalene (L)	pg/L	N/A		N/A		N/A		N/A		N/A	
Acenaphthylene (L)	pg/L	129	U	1549		129	U	129	U	129	U
Acenaphthene (L)	pg/L	283		13094		88	U	248		1486	
Fluorene (L)	pg/L	890		11301		529		505		1972	
Phenanthrene (L)	pg/L	1455		31641	E	907		2320		1582	
Anthracene (L)	pg/L	172		3591		109		172		375	
Fluoranthene (H)	pg/L	2791		21395	E	1767		4186		2977	
Pyrene (H)	pg/L	3137		24314	E	2039		4314	E	3451	
Benzo(a)anthracene (H)	pg/L	411		4444		333		500		556	
Chrysene (H)	pg/L	50	U	4400	E	480		1000		630	
Benzo(b)fluoranthene	pg/L	838		3000		713		963		975	
Benzo(k)fluoranthene	pg/L	435		1176		329		529		424	
Benzo(a)pyrene (H)	pg/L	171		1257		160		183		251	
Indeno(1,2,3-c,d)pyrene	pg/L	194		545		170		218		242	
Dibenzo(a,h)anthracene (H)	pg/L	87		226		87		87		139	
Benzo(g,h,i)perylene	pg/L	295		989		274		295		358	
Total LMW PAHs	pg/L	2929		61177		1763		3374		5544	
Total HMW PAHs	pg/L	6647		56037		4867		10270		8004	
Total LMW+HMW PAHs	pg/L	9577		117214		6630		13643		13548	

Table F-1. Year One raw semi-permeable membrane device results for the Cottonwood Bay prototype mat system.

Analyte	Units	18227-016 T3-SD-MM-NE Q		18227-017 T3-SD-MW-NE R		18227-018 T3-SD-SDM-SE S		18227-019 T3-SD-MM-SE T		18227-020 T3-SD-MW-SE U	
Naphthalene (L)	pg/L	N/A		N/A		N/A		N/A		N/A	
Acenaphthylene (L)	pg/L	129	U	129	U	129	U	129	U	129	U
Acenaphthene (L)	pg/L	88	U	283		88	U	88	U	319	
Fluorene (L)	pg/L	361		577		3847		361		697	
Phenanthrene (L)	pg/L	949		2320		6539		949		2953	
Anthracene (L)	pg/L	39	U	172		390	U	39	U	203	
Fluoranthene (H)	pg/L	484		4186		4186		484		4558	
Pyrene (H)	pg/L	549		4471		4941		549		5098	
Benzo(a)anthracene (H)	pg/L	100		500		1444		100		522	
Chrysene (H)	pg/L	140		1000		1400		140		1100	
Benzo(b)fluoranthene	pg/L	188		988		1875		188		888	
Benzo(k)fluoranthene	pg/L	94		541		941		94		600	
Benzo(a)pyrene (H)	pg/L	29	U	194		286	U	29	U	183	
Indeno(1,2,3-c,d)pyrene	pg/L	61		218		303	U	61		218	
Dibenzo(a,h)anthracene (H)	pg/L	43	U	104		435	U	43	U	104	
Benzo(g,h,i)perylene	pg/L	53	U	316		526	U	53	U	316	
Total LMW PAHs	pg/L	1567		3481		10994		1567		4301	
Total HMW PAHs	pg/L	1345		10455		12692		1345		11566	
Total LMW+HMW PAHs	pg/L	2911		13937		23687		2911		15867	

Table F-1. Year One raw semi-permeable membrane device results for the Cottonwood Bay prototype mat system.

Analyte	Units	18227-021 T4-SD-SDSN-NE V	18227-022 T4-SD-SNW-NE W	18227-023 T4-SD-SDSN-SE X	18227-024 T4-SD-SNW-SE Y	18227-025 T4-SD-SDSN-SW Z
Naphthalene (L)	pg/L	N/A	N/A	N/A	N/A	N/A
Acenaphthylene (L)	pg/L	129 U	129 U	129 U	129 U	129 U
Acenaphthene (L)	pg/L	319	248	1026	248	283
Fluorene (L)	pg/L	1058	818	1443	914	914
Phenanthrene (L)	pg/L	1603	1814	1751	1329	1181
Anthracene (L)	pg/L	187	187	312	125	172
Fluoranthene (H)	pg/L	1860	3628	2326	2419	2326
Pyrene (H)	pg/L	4078	4078	2510	3216	2588
Benzo(a)anthracene (H)	pg/L	556	633	433	511	356
Chrysene (H)	pg/L	460	700	430	590	520
Benzo(b)fluoranthene	pg/L	1175	900	563	688	750
Benzo(k)fluoranthene	pg/L	529	682	365	518	376
Benzo(a)pyrene (H)	pg/L	320	640	389	469	160
Indeno(1,2,3-c,d)pyrene	pg/L	303	170	170	218	170
Dibenzo(a,h)anthracene (H)	pg/L	104	43 U	43 U	104	43 U
Benzo(g,h,i)perylene	pg/L	421	274	253	274	253
Total LMW PAHs	pg/L	3296	3196	4661	2744	2679
Total HMW PAHs	pg/L	7379	9723	6131	7308	5993
Total LMW+HMW PAHs	pg/L	10675	12919	10792	10053	8672

Table F-1. Year One raw semi-permeable membrane device results for the Cottonwood Bay prototype mat system.

Analyte	Units	18227-026 T4-SD-SNW-SW AA		18227-027 T5-SD-SDW-NE AB		18227-028 T5-SD-SDW-SE AC		18227-029 T5-SD-SDW-SW AD	
Naphthalene (L)	pg/L	N/A		N/A		N/A		N/A	
Acenaphthylene (L)	pg/L	129	U	129	U	129	U	129	U
Acenaphthene (L)	pg/L	212		283		248		283	
Fluorene (L)	pg/L	842		1154		986		1779	
Phenanthrene (L)	pg/L	1034		1835		1877		1076	
Anthracene (L)	pg/L	141		187		125		219	
Fluoranthene (H)	pg/L	2419		4000		3442		2326	
Pyrene (H)	pg/L	2588		4314	E	3922		2667	
Benzo(a)anthracene (H)	pg/L	389		822		611		456	
Chrysene (H)	pg/L	580		810		660		580	
Benzo(b)fluoranthene	pg/L	863		1163		825		788	
Benzo(k)fluoranthene	pg/L	365		729		529		459	
Benzo(a)pyrene (H)	pg/L	171		674		160		194	
Indeno(1,2,3-c,d)pyrene	pg/L	194		352		206		194	
Dibenzo(a,h)anthracene (H)	pg/L	104		122		43	U	122	
Benzo(g,h,i)perylene	pg/L	295		484		295		295	
Total LMW PAHs	pg/L	2357		3589		3365		3486	
Total HMW PAHs	pg/L	6252		10742		8838		6344	
Total LMW+HMW PAHs	pg/L	8609		14331		12203		9830	

Table F-2. Year One semi-permeable membrane device results for area T1 (single mat only).

T1 - Single Mat Only

Analyte	Units	Rep 1		Rep 2		Rep 3		Rep Average	
		Below Mat (A)	Above Mat (B)	Below Mat (C)	Above Mat (D)	Below Mat (E)	Above Mat (F)	Below Mat	Above Mat
Naphthalene (L)	pg/L	N/A	N/A	-	N/A	N/A	N/A	N/A	N/A
Acenaphthylene (L)	pg/L	129	129	-	129	129	129	129	129
Acenaphthene (L)	pg/L	1982	354	-	177	425	354	1203	295
Fluorene (L)	pg/L	2356	842	-	409	1130	866	1743	705
Phenanthrene (L)	pg/L	2088	1751	-	1666	928	1877	1508	1765
Anthracene (L)	pg/L	750	312	-	156	203	234	476	234
Fluoranthene (H)	pg/L	4744	5023	-	3535	1860	4279	3302	4279
Pyrene (H)	pg/L	5412	5569	-	3843	2039	4784	3725	4732
Benzo(a)anthracene (H)	pg/L	767	700	-	444	311	622	539	589
Chrysene (H)	pg/L	750	970	-	830	440	970	595	923
Benzo(b)fluoranthene	pg/L	1113	1225	-	738	600	1163	856	1042
Benzo(k)fluoranthene	pg/L	424	541	-	565	224	553	324	553
Benzo(a)pyrene (H)	pg/L	309	274	-	171	137	229	223	225
Indeno(1,2,3-c,d)pyrene	pg/L	303	291	-	182	121	242	212	238
Dibenzo(a,h)anthracene (H)	pg/L	139	104	-	43	43	104	91	84
Benzo(g,h,i)perylene	pg/L	442	400	-	253	211	358	326	337
Total LMW PAHs	pg/L	7305	3388	-	2537	2815	3460	5060	3128
Total HMW PAHs	pg/L	12120	12641	-	8867	4831	10989	8476	10832
Total LMW+HMW PAHs	pg/L	19426	16028	-	11405	7646	14449	13536	13961

Analyte	Units	Rep 1		Rep 2		Rep 3		Rep Average	
		Below Mat (A)	Above Mat (B)	Below Mat (C)	Above Mat (D)	Below Mat (E)	Above Mat (F)	Below Mat	Above Mat
Percent Reduction									
Naphthalene (L)	%	-	N/A	-	-	-	N/A	-	N/A
Acenaphthylene (L)	%	-	0.0	-	-	-	0.0	-	0.0
Acenaphthene (L)	%	-	82	-	-	-	17	-	75
Fluorene (L)	%	-	64	-	-	-	23	-	60
Phenanthrene (L)	%	-	16	-	-	-	-102.27	-	-17.02
Anthracene (L)	%	-	58	-	-	-	-15.38	-	51
Fluoranthene (H)	%	-	-5.88	-	-	-	-130.0	-	-29.58
Pyrene (H)	%	-	-2.9	-	-	-	-134.62	-	-27.02
Benzo(a)anthracene (H)	%	-	8.7	-	-	-	-100.0	-	-9.28
Chrysene (H)	%	-	-29.33	-	-	-	-120.45	-	-55.18
Benzo(b)fluoranthene	%	-	-10.11	-	-	-	-93.75	-	-21.65
Benzo(k)fluoranthene	%	-	-27.78	-	-	-	-147.37	-	-70.91
Benzo(a)pyrene (H)	%	-	11	-	-	-	-66.67	-	-0.85
Indeno(1,2,3-c,d)pyrene	%	-	4.0	-	-	-	-100.0	-	-12.38
Dibenzo(a,h)anthracene (H)	%	-	25	-	-	-	-140.0	-	7.9
Benzo(g,h,i)perylene	%	-	9.5	-	-	-	-70.0	-	-3.23
Total LMW PAHs	%	-	54	-	-	-	-22.92	-	38
Total HMW PAHs	%	-	-4.29	-	-	-	-127.44	-	-27.8
Total LMW+HMW PAHs	%	-	17	-	-	-	-88.96	-	-3.14

N/A = Data not available.

Table F-3. Year One semi-permeable membrane device results for area T2 (single mat with sand cap).

T2 - Single Mat With Sand Cap

Analyte	Units	Rep 1		Rep 2		Rep 3		Rep Average	
		Below Mat (G)	Above Mat (H)	Below Mat (I)	Above Mat (J)	Below Mat (K)	Above Mat (L)	Below Mat	Above Mat
Naphthalene (L)	pg/L	N/A	N/A	N/A	N/A	N/A	N/A	N/A	N/A
Acenaphthylene (L)	pg/L	129	129	129	129	129	129	129	129
Acenaphthene (L)	pg/L	6724	248	12032	88	1734	283	6830	206
Fluorene (L)	pg/L	5531	697	11061	409	1587	890	6060	665
Phenanthrene (L)	pg/L	14977	1350	33750	1266	3797	1455	17508	1357
Anthracene (L)	pg/L	1718	156	4841	125	468	172	2342	151
Fluoranthene (H)	pg/L	7907	2605	18605	2512	2512	2791	9674	2636
Pyrene (H)	pg/L	9412	2902	19608	2745	2667	3137	10562	2928
Benzo(a)anthracene (H)	pg/L	1333	400	4000	400	411	411	1915	404
Chrysene (H)	pg/L	1800	630	4500	650	490	50	2263	443
Benzo(b)fluoranthene	pg/L	1213	800	2750	813	388	838	1450	817
Benzo(k)fluoranthene	pg/L	647	482	1118	435	176	435	647	451
Benzo(a)pyrene (H)	pg/L	446	183	1086	171	114	171	549	175
Indeno(1,2,3-c,d)pyrene	pg/L	303	218	473	206	85	194	287	206
Dibenzo(a,h)anthracene (H)	pg/L	139	104	226	43	43	87	136	78
Benzo(g,h,i)perylene	pg/L	484	316	800	274	126	295	470	295
Total LMW PAHs	pg/L	29078	2580	61813	2017	7716	2929	32869	2509
Total HMW PAHs	pg/L	21037	6824	48024	6522	6237	6647	25099	6664
Total LMW+HMW PAHs	pg/L	50115	9404	109838	8539	13953	9577	57968	9173

Analyte	Units	Rep 1		Rep 2		Rep 3		Rep Average	
		Below Mat (A)	Above Mat (B)	Below Mat (C)	Above Mat (D)	Below Mat (E)	Above Mat (F)	Below Mat	Above Mat
Percent Reduction									
Naphthalene (L)	%	-	N/A	-	N/A	-	N/A	-	N/A
Acenaphthylene (L)	%	-	0.0	-	0.0	-	0.0	-	0.0
Acenaphthene (L)	%	-	96	-	99	-	84	-	97
Fluorene (L)	%	-	87	-	96	-	44	-	89
Phenanthrene (L)	%	-	91	-	96	-	62	-	92
Anthracene (L)	%	-	91	-	97	-	63	-	94
Fluoranthene (H)	%	-	67	-	87	-	-11.11	-	73
Pyrene (H)	%	-	69	-	86	-	-17.65	-	72
Benzo(a)anthracene (H)	%	-	70	-	90	-	0.0	-	79
Chrysene (H)	%	-	65	-	86	-	90	-	80
Benzo(b)fluoranthene	%	-	34	-	70	-	-116.13	-	44
Benzo(k)fluoranthene	%	-	25	-	61	-	-146.67	-	30
Benzo(a)pyrene (H)	%	-	59	-	84	-	-50.0	-	68
Indeno(1,2,3-c,d)pyrene	%	-	28	-	56	-	-128.57	-	28
Dibenzo(a,h)anthracene (H)	%	-	25	-	81	-	-100.0	-	43
Benzo(g,h,i)perylene	%	-	35	-	66	-	-133.33	-	37
Total LMW PAHs	%	-	91	-	97	-	62	-	92
Total HMW PAHs	%	-	68	-	86	-	-6.58	-	73
Total LMW+HMW PAHs	%	-	81	-	92	-	31	-	84

N/A = Data not available.

Table F-4. Year One Semi-permeable membrane device results for area T3 (double mat).

T3 - Double Mat

Analyte	Units	Rep 1			Rep 2		
		Below Mats (M)	Between Mats (N)	Above Mats (O)	Below Mats (P)	Between Mats (Q)	Above Mats (R)
Naphthalene (L)	pg/L	N/A	N/A	N/A	N/A	N/A	N/A
Acenaphthylene (L)	pg/L	1549	129	129	129	129	129
Acenaphthene (L)	pg/L	13094	88	248	1486	88	283
Fluorene (L)	pg/L	11301	529	505	1972	361	577
Phenanthrene (L)	pg/L	31641	907	2320	1582	949	2320
Anthracene (L)	pg/L	3591	109	172	375	39	172
Fluoranthene (H)	pg/L	21395	1767	4186	2977	484	4186
Pyrene (H)	pg/L	24314	2039	4314	3451	549	4471
Benzo(a)anthracene (H)	pg/L	4444	333	500	556	100	500
Chrysene (H)	pg/L	4400	480	1000	630	140	1000
Benzo(b)fluoranthene	pg/L	3000	713	963	975	188	988
Benzo(k)fluoranthene	pg/L	1176	329	529	424	94	541
Benzo(a)pyrene (H)	pg/L	1257	160	183	251	29	194
Indeno(1,2,3-c,d)pyrene	pg/L	545	170	218	242	61	218
Dibenzo(a,h)anthracene (H)	pg/L	226	87	87	139	43	104
Benzo(g,h,i)perylene	pg/L	989	274	295	358	53	316
Total LMW PAHs	pg/L	61177	1763	3374	5544	1567	3481
Total HMW PAHs	pg/L	56037	4867	10270	8004	1345	10455
Total LMW+HMW PAHs	pg/L	117214	6630	13643	13548	2911	13937

Analyte	Units	Rep 1			Rep 2		
		Below Mats (M)	Between Mats (N)	Above Mats (O)	Below Mats (P)	Between Mats (Q)	Above Mats (R)
Percent Reduction							
Naphthalene (L)	%	-	N/A	N/A	-	N/A	N/A
Acenaphthylene (L)	%	-	92	0.0	-	0.0	0.0
Acenaphthene (L)	%	-	99	-180.0	-	94	-220.0
Fluorene (L)	%	-	95	4.5	-	82	-60.0
Phenanthrene (L)	%	-	97	-155.81	-	40	-144.44
Anthracene (L)	%	-	97	-57.14	-	90	-340.0
Fluoranthene (H)	%	-	N/A	-136.84	-	84	-765.38
Pyrene (H)	%	-	N/A	-111.54	-	84	-714.29
Benzo(a)anthracene (H)	%	-	93	-50.0	-	82	-400.0
Chrysene (H)	%	-	89	-108.33	-	78	-614.29
Benzo(b)fluoranthene	%	-	76	-35.09	-	81	-426.67
Benzo(k)fluoranthene	%	-	72	-60.71	-	78	-475.0
Benzo(a)pyrene (H)	%	-	N/A	-14.29	-	89	-580.0
Indeno(1,2,3-c,d)pyrene	%	-	69	-28.57	-	75	-260.0
Dibenzo(a,h)anthracene (H)	%	-	62	0.0	-	69	-140.0
Benzo(g,h,i)perylene	%	-	72	-7.69	-	85	-500.0
Total LMW PAHs	%	-	97	-91.38	-	72	-122.24
Total HMW PAHs	%	-	N/A	-111.01	-	83	-677.46
Total LMW+HMW PAHs	%	-	N/A	-105.79	-	79	-378.71

Table F-4. Year One Semi-permeable membrane device results for area T3 (double mat).

T3 - Double Mat

Analyte	Units	Rep 3			Rep Average		
		Below Mats (S)	Between Mats (T)	Above Mats (U)	Below Mats	Between Mats	Above Mat
Naphthalene (L)	pg/L	N/A	N/A	N/A	N/A	N/A	N/A
Acenaphthylene (L)	pg/L	129	129	129	602	129	129
Acenaphthene (L)	pg/L	88	88	319	4890	88	283
Fluorene (L)	pg/L	3847	361	697	5707	417	593
Phenanthrene (L)	pg/L	6539	949	2953	13254	935	2531
Anthracene (L)	pg/L	390	39	203	1452	62	182
Fluoranthene (H)	pg/L	4186	484	4558	9519	912	4310
Pyrene (H)	pg/L	4941	549	5098	10902	1046	4627
Benzo(a)anthracene (H)	pg/L	1444	100	522	2148	178	507
Chrysene (H)	pg/L	1400	140	1100	2143	253	1033
Benzo(b)fluoranthene	pg/L	1875	188	888	1950	363	946
Benzo(k)fluoranthene	pg/L	941	94	600	847	173	557
Benzo(a)pyrene (H)	pg/L	286	29	183	598	72	187
Indeno(1,2,3-c,d)pyrene	pg/L	303	61	218	364	97	218
Dibenzo(a,h)anthracene (H)	pg/L	435	43	104	267	58	99
Benzo(g,h,i)perylene	pg/L	526	53	316	625	126	309
Total LMW PAHs	pg/L	10994	1567	4301	25905	1632	3719
Total HMW PAHs	pg/L	12692	1345	11566	25578	2519	10763
Total LMW+HMW PAHs	pg/L	23687	2911	15867	51483	4151	14482

Analyte	Units	Rep 3			Rep Average		
		Below Mats (S)	Between Mats (T)	Above Mats (U)	Below Mats	Between Mats	Above Mat
Percent Reduction							
Naphthalene (L)	%	-	N/A	N/A	-	N/A	N/A
Acenaphthylene (L)	%	-	0.0	0.0	-	79	0.0
Acenaphthene (L)	%	-	0.0	-260.0	-	98	-220.0
Fluorene (L)	%	-	91	-93.33	-	93	-42.31
Phenanthrene (L)	%	-	85	-211.11	-	93	-170.68
Anthracene (L)	%	-	90	-420.0	-	96	-191.67
Fluoranthene (H)	%	-	88	-842.31	-	90	-372.79
Pyrene (H)	%	-	89	-828.57	-	90	-342.5
Benzo(a)anthracene (H)	%	-	93	-422.22	-	92	-185.42
Chrysene (H)	%	-	90	-685.71	-	88	-307.89
Benzo(b)fluoranthene	%	-	90	-373.33	-	81	-160.92
Benzo(k)fluoranthene	%	-	90	-537.5	-	80	-222.73
Benzo(a)pyrene (H)	%	-	90	-540.0	-	88	-157.89
Indeno(1,2,3-c,d)pyrene	%	-	80	-260.0	-	73	-125.0
Dibenzo(a,h)anthracene (H)	%	-	90	-140.0	-	78	-70.0
Benzo(g,h,i)perylene	%	-	90	-500.0	-	80	-144.44
Total LMW PAHs	%	-	86	-174.56	-	94	-127.87
Total HMW PAHs	%	-	89	-760.03	-	90	-327.32
Total LMW+HMW PAHs	%	-	88	-445.0	-	92	-248.9

Table F-4. Year One Semi-permeable membrane device results for area T3 (double mat).

T3 - Double Mat

Analyte	Units	Rep 1			Rep 2		
		Below Mats (M)	Between Mats (N)	Above Mats (O)	Below Mats (P)	Between Mats (Q)	Above Mats (R)
Percent Reduction							
Naphthalene (L)	%	-	-	N/A	-	-	N/A
Acenaphthylene (L)	%	-	-	92	-	-	0.0
Acenaphthene (L)	%	-	-	98	-	-	81
Fluorene (L)	%	-	-	96	-	-	71
Phenanthrene (L)	%	-	-	93	-	-	-46.67
Anthracene (L)	%	-	-	95	-	-	54
Fluoranthene (H)	%	-	-	N/A	-	-	-40.63
Pyrene (H)	%	-	-	N/A	-	-	-29.55
Benzo(a)anthracene (H)	%	-	-	89	-	-	10.0
Chrysene (H)	%	-	-	77	-	-	-58.73
Benzo(b)fluoranthene	%	-	-	68	-	-	-1.28
Benzo(k)fluoranthene	%	-	-	55	-	-	-27.78
Benzo(a)pyrene (H)	%	-	-	N/A	-	-	23
Indeno(1,2,3-c,d)pyrene	%	-	-	60	-	-	10
Dibenzo(a,h)anthracene (H)	%	-	-	62	-	-	25
Benzo(g,h,i)perylene	%	-	-	70	-	-	12
Total LMW PAHs	%	-	-	94	-	-	37
Total HMW PAHs	%	-	-	N/A	-	-	-30.63
Total LMW+HMW PAHs	%	-	-	N/A	-	-	-2.87

N/A = Data not available.

Table F-4. Year One Semi-permeable membrane device results for area T3 (double mat).

T3 - Double Mat

Analyte	Units	Rep 3			Rep Average		
		Below Mats (S)	Between Mats (T)	Above Mats (U)	Below Mats	Between Mats	Above Mat
Percent Reduction							
Naphthalene (L)	%	-	-	N/A	-	-	N/A
Acenaphthylene (L)	%	-	-	0.0	-	-	79
Acenaphthene (L)	%	-	-	-260.0	-	-	94
Fluorene (L)	%	-	-	82	-	-	90
Phenanthrene (L)	%	-	-	55	-	-	81
Anthracene (L)	%	-	-	48	-	-	87
Fluoranthene (H)	%	-	-	-8.89	-	-	55
Pyrene (H)	%	-	-	-3.17	-	-	58
Benzo(a)anthracene (H)	%	-	-	64	-	-	76
Chrysene (H)	%	-	-	21	-	-	52
Benzo(b)fluoranthene	%	-	-	53	-	-	51
Benzo(k)fluoranthene	%	-	-	36	-	-	34
Benzo(a)pyrene (H)	%	-	-	36	-	-	69
Indeno(1,2,3-c,d)pyrene	%	-	-	28	-	-	40
Dibenzo(a,h)anthracene (H)	%	-	-	76	-	-	63
Benzo(g,h,i)perylene	%	-	-	40	-	-	51
Total LMW PAHs	%	-	-	61	-	-	86
Total HMW PAHs	%	-	-	8.9	-	-	58
Total LMW+HMW PAHs	%	-	-	33	-	-	72

Table F-5. Year One semi-permeable membrane device results for area T4 (sand cap only).

T4 - Sand Cap Only

Analyte	Units	Rep 1		Rep 2		Rep 3		Rep Average	
		Below Sand (V)	Above Sand (W)	Below Sand (X)	Above Sand (Y)	Below Sand (Z)	Above Sand (AA)	Below Sand	Above Sand
Naphthalene (L)	pg/L	N/A	N/A	N/A	N/A	N/A	N/A	N/A	N/A
Acenaphthylene (L)	pg/L	129	129	129	129	129	129	129	129
Acenaphthene (L)	pg/L	319	248	1026	248	283	212	543	236
Fluorene (L)	pg/L	1058	818	1443	914	914	842	1138	858
Phenanthrene (L)	pg/L	1603	1814	1751	1329	1181	1034	1512	1392
Anthracene (L)	pg/L	187	187	312	125	172	141	224	151
Fluoranthene (H)	pg/L	1860	3628	2326	2419	2326	2419	2171	2822
Pyrene (H)	pg/L	4078	4078	2510	3216	2588	2588	3059	3294
Benzo(a)anthracene (H)	pg/L	556	633	433	511	356	389	448	511
Chrysene (H)	pg/L	460	700	430	590	520	580	470	623
Benzo(b)fluoranthene	pg/L	1175	900	563	688	750	863	829	817
Benzo(k)fluoranthene	pg/L	529	682	365	518	376	365	424	522
Benzo(a)pyrene (H)	pg/L	320	640	389	469	160	171	290	427
Indeno(1,2,3-c,d)pyrene	pg/L	303	170	170	218	170	194	214	194
Dibenzo(a,h)anthracene (H)	pg/L	104	43	43	104	43	104	64	84
Benzo(g,h,i)perylene	pg/L	421	274	253	274	253	295	309	281
Total LMW PAHs	pg/L	3296	3196	4661	2744	2679	2357	3545	2766
Total HMW PAHs	pg/L	7379	9723	6131	7308	5993	6252	6501	7761
Total LMW+HMW PAHs	pg/L	10675	12919	10792	10053	8672	8609	10046	10527

Analyte	Units	Rep 1		Rep 2		Rep 3		Rep Average	
		Below Sand (V)	Above Sand (W)	Below Sand (X)	Above Sand (Y)	Below Sand (Z)	Above Sand (AA)	Below Sand	Above Sand
Percent Reduction									
Naphthalene (L)	%	-	N/A	-	N/A	-	N/A	-	N/A
Acenaphthylene (L)	%	-	0.0	-	0.0	-	0.0	-	0.0
Acenaphthene (L)	%	-	22	-	76	-	25	-	57
Fluorene (L)	%	-	23	-	37	-	7.9	-	25
Phenanthrene (L)	%	-	-13.16	-	24	-	13	-	7.9
Anthracene (L)	%	-	0.0	-	60	-	18	-	33
Fluoranthene (H)	%	-	-95.0	-	-4.0	-	-4.0	-	-30.0
Pyrene (H)	%	-	0.0	-	-28.13	-	0.0	-	-7.69
Benzo(a)anthracene (H)	%	-	-14.0	-	-17.95	-	-9.38	-	-14.05
Chrysene (H)	%	-	-52.17	-	-37.21	-	-11.54	-	-32.62
Benzo(b)fluoranthene	%	-	23	-	-22.22	-	-15.0	-	1.5
Benzo(k)fluoranthene	%	-	-28.89	-	-41.94	-	3.1	-	-23.15
Benzo(a)pyrene (H)	%	-	-100.0	-	-20.59	-	-7.14	-	-47.37
Indeno(1,2,3-c,d)pyrene	%	-	44	-	-28.57	-	-14.29	-	9.4
Dibenzo(a,h)anthracene (H)	%	-	58	-	-140.0	-	-140.0	-	-31.82
Benzo(g,h,i)perylene	%	-	35	-	-8.33	-	-16.67	-	9.1
Total LMW PAHs	%	-	3.0	-	41	-	12	-	22
Total HMW PAHs	%	-	-31.77	-	-19.21	-	-4.32	-	-19.39
Total LMW+HMW PAHs	%	-	-21.02	-	6.9	-	0.73	-	-4.78

N/A = Data not available.

Table F-6. Year One semi-permeable membrane device results for area T5 (no treatment/control).

T5 - No Treatment (Control)

Analyte	Units	Rep 1 Above Sed (AB)	Rep 2 Above Sed (AC)	Rep 3 Above Sed (AD)	Rep Average Above Sed
Naphthalene (L)	pg/L	N/A	N/A	N/A	N/A
Acenaphthylene (L)	pg/L	129	129	129	129
Acenaphthene (L)	pg/L	283	248	283	271
Fluorene (L)	pg/L	1154	986	1779	1306
Phenanthrene (L)	pg/L	1835	1877	1076	1596
Anthracene (L)	pg/L	187	125	219	177
Fluoranthene (H)	pg/L	4000	3442	2326	3256
Pyrene (H)	pg/L	4314	3922	2667	3634
Benzo(a)anthracene (H)	pg/L	822	611	456	630
Chrysene (H)	pg/L	810	660	580	683
Benzo(b)fluoranthene	pg/L	1163	825	788	925
Benzo(k)fluoranthene	pg/L	729	529	459	573
Benzo(a)pyrene (H)	pg/L	674	160	194	343
Indeno(1,2,3-c,d)pyrene	pg/L	352	206	194	251
Dibenzo(a,h)anthracene (H)	pg/L	122	43	122	96
Benzo(g,h,i)perylene	pg/L	484	295	295	358
Total LMW PAHs	pg/L	3589	3365	3486	3480
Total HMW PAHs	pg/L	10742	8838	6344	8641
Total LMW+HMW PAHs	pg/L	14331	12203	9830	12121

N/A = Data not available.

Table F-7. Summary of Year One semi-permeable membrane device results for the Cottonwood Bay prototype mat system..

Treatment Summary - Replicate Averages

Analyte	Units	T1 - Mat Only			T2 - Mat w/ Sand		
		Below Treatment	Between Treatment	Above Treatment	Below Treatment	Between Treatment	Above Treatment
Naphthalene (L)	pg/L	N/A	-	N/A	N/A	-	N/A
Acenaphthylene (L)	pg/L	129	-	129	129	-	129
Acenaphthene (L)	pg/L	1203	-	295	6830	-	206
Fluorene (L)	pg/L	1743	-	705	6060	-	665
Phenanthrene (L)	pg/L	1508	-	1765	17508	-	1357
Anthracene (L)	pg/L	476	-	234	2342	-	151
Fluoranthene (H)	pg/L	3302	-	4279	9674	-	2636
Pyrene (H)	pg/L	3725	-	4732	10562	-	2928
Benzo(a)anthracene (H)	pg/L	539	-	589	1915	-	404
Chrysene (H)	pg/L	595	-	923	2263	-	443
Benzo(b)fluoranthene	pg/L	856	-	1042	1450	-	817
Benzo(k)fluoranthene	pg/L	324	-	553	647	-	451
Benzo(a)pyrene (H)	pg/L	223	-	225	549	-	175
Indeno(1,2,3-c,d)pyrene	pg/L	212	-	238	287	-	206
Dibenzo(a,h)anthracene (H)	pg/L	91	-	84	136	-	78
Benzo(g,h,i)perylene	pg/L	326	-	337	470	-	295
Total LMW PAHs	pg/L	5060	-	3128	32869	-	2509
Total HMW PAHs	pg/L	8476	-	10832	25099	-	6664
Total LMW+HMW PAHs	pg/L	13536	-	13961	57968	-	9173

N/A = Data not available.

Table F-7. Summary of Year One semi-permeable membrane device results for the Cottonwood Bay prototype mat system..

Treatment Summary - Replicate Averages

Analyte	Units	T3 - Double Mat			T4 - Sand Only		
		Below Treatment	Between Treatment	Above Treatment	Below Treatment	Between Treatment	Above Treatment
Naphthalene (L)	pg/L	N/A	N/A	N/A	N/A	-	N/A
Acenaphthylene (L)	pg/L	602	129	129	129	-	129
Acenaphthene (L)	pg/L	4890	88	283	543	-	236
Fluorene (L)	pg/L	5707	417	593	1138	-	858
Phenanthrene (L)	pg/L	13254	935	2531	1512	-	1392
Anthracene (L)	pg/L	1452	62	182	224	-	151
Fluoranthene (H)	pg/L	9519	912	4310	2171	-	2822
Pyrene (H)	pg/L	10902	1046	4627	3059	-	3294
Benzo(a)anthracene (H)	pg/L	2148	178	507	448	-	511
Chrysene (H)	pg/L	2143	253	1033	470	-	623
Benzo(b)fluoranthene	pg/L	1950	363	946	829	-	817
Benzo(k)fluoranthene	pg/L	847	173	557	424	-	522
Benzo(a)pyrene (H)	pg/L	598	72	187	290	-	427
Indeno(1,2,3-c,d)pyrene	pg/L	364	97	218	214	-	194
Dibenzo(a,h)anthracene (H)	pg/L	267	58	99	64	-	84
Benzo(g,h,i)perylene	pg/L	625	126	309	309	-	281
Total LMW PAHs	pg/L	25905	1632	3719	3545	-	2766
Total HMW PAHs	pg/L	25578	2519	10763	6501	-	7761
Total LMW+HMW PAHs	pg/L	51483	4151	14482	10046	-	10527

N/A = Data not available.

Table F-7. Summary of Year One semi-permeable membrane device results for the Cottonwood Bay prototype mat system..

Treatment Summary - Replicate Averages

Analyte	Units	T5 - No Treatment		
		Below Treatment	Between Treatment	Above Treatment
Naphthalene (L)	pg/L	-	-	N/A
Acenaphthylene (L)	pg/L	-	-	129
Acenaphthene (L)	pg/L	-	-	271
Fluorene (L)	pg/L	-	-	1306
Phenanthrene (L)	pg/L	-	-	1596
Anthracene (L)	pg/L	-	-	177
Fluoranthene (H)	pg/L	-	-	3256
Pyrene (H)	pg/L	-	-	3634
Benzo(a)anthracene (H)	pg/L	-	-	630
Chrysene (H)	pg/L	-	-	683
Benzo(b)fluoranthene	pg/L	-	-	925
Benzo(k)fluoranthene	pg/L	-	-	573
Benzo(a)pyrene (H)	pg/L	-	-	343
Indeno(1,2,3-c,d)pyrene	pg/L	-	-	251
Dibenzo(a,h)anthracene (H)	pg/L	-	-	96
Benzo(g,h,i)perylene	pg/L	-	-	358
Total LMW PAHs	pg/L	-	-	3480
Total HMW PAHs	pg/L	-	-	8641
Total LMW+HMW PAHs	pg/L	-	-	12121

N/A = Data not available.

Table F-8. Year Two raw semi-permeable membrane device results for the Cottonwood Bay prototype mat system.

Analyte	Units	19293-001 T1-SD-SDM-NW A		19292-002 T1-SD-MW-NW B		19293-003 T1-SD-SDM-SW C		19293-004 T1-SD-MW-SW D		19293-005 T1-SD-SDM-NE E	
Naphthalene (L)	pg/L	N/A		N/A		N/A		N/A		N/A	
Acenaphthylene (L)	pg/L	129	U	330		723		129	U	129	U
Acenaphthene (L)	pg/L	419		318		6632		300		1536	
Fluorene (L)	pg/L	896		542		5424		495		1887	
Phenanthrene (L)	pg/L	1099		2904		15557		2697		2282	
Anthracene (L)	pg/L	228		243		2583		258		638	
Fluoranthene (H)	pg/L	3068		8808		16823		7620		5245	
Pyrene (H)	pg/L	1585		3755		7927		3171		2253	
Benzo(a)anthracene (H)	pg/L	426		768		2719		544		674	
Chrysene (H)	pg/L	436		1489		2766		1170		702	
Benzo(b)fluoranthene	pg/L	479		1184		1729		891		785	
Benzo(k)fluoranthene	pg/L	275		801		939		688		488	
Benzo(a)pyrene (H)	pg/L	117		231		717		158		231	
Indeno(1,2,3-c,d)pyrene	pg/L	32	U	32	U	193		155		110	
Dibenzo(a,h)anthracene (H)	pg/L	46	U	46	U	46	U	46	U	46	U
Benzo(g,h,i)perylene	pg/L	56	U	56	U	358		224		269	
Total LMW PAHs	pg/L	2771		4338		30918		3879		6471	
Total HMW PAHs	pg/L	5678		15097		30998		12709		9151	
Total LMW+HMW PAHs	pg/L	8449		19435		61917		16588		15622	

MDL = 5 ng/mL in hexane.

U = Concentration below detection limit; 1/2 detection limit used for conversion.

N/A = Data not available.

Table F-8. Year Two raw semi-permeable membrane device results for the Cottonwood Bay prototype mat system.

Analyte	Units	19293-006 T1-SD-MW-NE F	19293-007 T2-SD-SDM-NW G	19293-008 T2-SD-MSN-NW H	19293-009 T2-SD-SDM-SW I	19293-010 T2-SD-MSN-SW J
Naphthalene (L)	pg/L	N/A	N/A	N/A	N/A	N/A
Acenaphthylene (L)	pg/L	310	568	129 U	269	284
Acenaphthene (L)	pg/L	279	8028	213	1780	255
Fluorene (L)	pg/L	448	6368	495	1910	613
Phenanthrene (L)	pg/L	2489	20535	1369	2489	1473
Anthracene (L)	pg/L	182	2735	182	532	182
Fluoranthene (H)	pg/L	6828	16823	3662	5740	4453
Pyrene (H)	pg/L	2587	8093	1418	2753	2086
Benzo(a)anthracene (H)	pg/L	544	2482	378	768	603
Chrysene (H)	pg/L	1383	2872	660	809	734
Benzo(b)fluoranthene	pg/L	851	1463	559	997	771
Benzo(k)fluoranthene	pg/L	551	901	501	588	538
Benzo(a)pyrene (H)	pg/L	195	705	170	255	170
Indeno(1,2,3-c,d)pyrene	pg/L	116	193	101	219	181
Dibenzo(a,h)anthracene (H)	pg/L	46 U	104	46 U	126	46 U
Benzo(g,h,i)perylene	pg/L	215	448	213	314	269
Total LMW PAHs	pg/L	3709	38233	2389	6980	2807
Total HMW PAHs	pg/L	11582	31080	6334	10451	8093
Total LMW+HMW PAHs	pg/L	15291	69313	8723	17431	10900

Table F-8. Year Two raw semi-permeable membrane device results for the Cottonwood Bay prototype mat system.

Analyte	Units	19293-011 T2-SD-SDM-NE K	19293-012 T2-SD-MSN-NE L	19293-013 T3-SD-SDM-NW M	19293-014 T3-SD-MM-NW N	19293-015 T3-SD-MW-NW O
Naphthalene (L)	pg/L	N/A	N/A	N/A	N/A	N/A
Acenaphthylene (L)	pg/L	377	284	305	129 U	336
Acenaphthene (L)	pg/L	2548	524	2304	87 U	258
Fluorene (L)	pg/L	2170	1061	2217	151	448
Phenanthrene (L)	pg/L	2697	2074	3111	933	2697
Anthracene (L)	pg/L	593	258	638	38 U	198
Fluoranthene (H)	pg/L	6136	4552	6630	910	8313
Pyrene (H)	pg/L	2920	2086	3254	459	3504
Benzo(a)anthracene (H)	pg/L	887	615	910	66	745
Chrysene (H)	pg/L	819	723	894	149	1383
Benzo(b)fluoranthene	pg/L	1210	984	1463	132	1290
Benzo(k)fluoranthene	pg/L	476	476	638	79	688
Benzo(a)pyrene (H)	pg/L	304	207	304	30 U	219
Indeno(1,2,3-c,d)pyrene	pg/L	206	129	206	32 U	168
Dibenzo(a,h)anthracene (H)	pg/L	46 U	46 U	93	46 U	46 U
Benzo(g,h,i)perylene	pg/L	314	224	381	56 U	224
Total LMW PAHs	pg/L	8384	4201	8575	1339	3936
Total HMW PAHs	pg/L	11112	8229	12085	1661	14210
Total LMW+HMW PAHs	pg/L	19495	12430	20659	3000	18146

Table F-8. Year Two raw semi-permeable membrane device results for the Cottonwood Bay prototype mat system.

Analyte	Units	19293-016 T3-SD-SDM-SE P		19293-017 T3-SD-MM-SE Q		19293-018 T3-SD-MW-SE R		19293-019 T3-SD-SDM-NE S		19293-020 T3-SD-MM-NE T	
Naphthalene (L)	pg/L	N/A		N/A		N/A		N/A		N/A	
Acenaphthylene (L)	pg/L	129	U	129	U	325		346		129	U
Acenaphthene (L)	pg/L	1536		87	U	241		87	U	87	U
Fluorene (L)	pg/L	1840		226		472		4953		123	
Phenanthrene (L)	pg/L	2489		788		2697		7260		560	
Anthracene (L)	pg/L	638		119		258		1519		38	U
Fluoranthene (H)	pg/L	5938		1880		7818		12865		574	
Pyrene (H)	pg/L	2837		918		3338		6425		325	
Benzo(a)anthracene (H)	pg/L	816		378		626		1773		130	
Chrysene (H)	pg/L	809		383		1277		1596		128	
Benzo(b)fluoranthene	pg/L	1090		572		1077		1862		213	
Benzo(k)fluoranthene	pg/L	626		375		688		663		125	
Benzo(a)pyrene (H)	pg/L	316		146		146		474		30	U
Indeno(1,2,3-c,d)pyrene	pg/L	206		121		168		258		32	U
Dibenzo(a,h)anthracene (H)	pg/L	46	U	46	U	46	U	115		46	U
Benzo(g,h,i)perylene	pg/L	291		204		246		381		56	U
Total LMW PAHs	pg/L	6632		1349		3993		14165		937	
Total HMW PAHs	pg/L	10761		3751		13251		23247		1234	
Total LMW+HMW PAHs	pg/L	17393		5101		17243		37412		2171	

Table F-8. Year Two raw semi-permeable membrane device results for the Cottonwood Bay prototype mat system.

Analyte	Units	19293-021 T3-SD-MW-NE U	19293-022 T4-SD-SDSN-NE V	19293-023 T4-SD-SNW-NE W	19293-024 T4-SD-SDSN-SE X	19293-025 T4-SD-SNW-SE Y
Naphthalene (L)	pg/L	N/A	N/A	N/A	N/A	N/A
Acenaphthylene (L)	pg/L	403	129 U	129 U	129 U	129 U
Acenaphthene (L)	pg/L	279	286	489	307	237
Fluorene (L)	pg/L	472	896	1250	825	825
Phenanthrene (L)	pg/L	2697	1597	1390	1265	1369
Anthracene (L)	pg/L	198	198	273	289	273
Fluoranthene (H)	pg/L	8115	4651	3761	3958	4057
Pyrene (H)	pg/L	3838	2086	1752	1752	1752
Benzo(a)anthracene (H)	pg/L	957	556	485	485	496
Chrysene (H)	pg/L	1489	691	564	628	660
Benzo(b)fluoranthene	pg/L	1995	1117	1316	918	931
Benzo(k)fluoranthene	pg/L	763	526	463	426	426
Benzo(a)pyrene (H)	pg/L	292	182	182	170	158
Indeno(1,2,3-c,d)pyrene	pg/L	245	155	129	142	168
Dibenzo(a,h)anthracene (H)	pg/L	46 U	46 U	46 U	46 U	46 U
Benzo(g,h,i)perylene	pg/L	336	224	208	246	246
Total LMW PAHs	pg/L	4048	3106	3531	2816	2834
Total HMW PAHs	pg/L	14738	8213	6790	7039	7170
Total LMW+HMW PAHs	pg/L	18785	11319	10321	9855	10004

Table F-8. Year Two raw semi-permeable membrane device results for the Cottonwood Bay prototype mat system.

Analyte	Units	19293-026 T4-SD-SDSN-SW Z		19293-027 T4-SD-SNW-SW AA		19293-028 T5-SD-SDW-SW AB		19293-029 T5-SD-SDW-NW AC		19293-030 T5-SD-SDW-SE AD	
Naphthalene (L)	pg/L	N/A		N/A		N/A		N/A		N/A	
Acenaphthylene (L)	pg/L	129	U	129	U	274		129	U	129	U
Acenaphthene (L)	pg/L	87	U	248		223		206		265	
Fluorene (L)	pg/L	896		613		613		660		873	
Phenanthrene (L)	pg/L	1079		1659		1805		1618		1348	
Anthracene (L)	pg/L	258		167		289		304		243	
Fluoranthene (H)	pg/L	3167		4750		6333		5344		4849	
Pyrene (H)	pg/L	1252		2086		2753		2420		2086	
Benzo(a)anthracene (H)	pg/L	378		556		674		603		544	
Chrysene (H)	pg/L	521		798		1064		862		766	
Benzo(b)fluoranthene	pg/L	572		957		1290		1051		931	
Benzo(k)fluoranthene	pg/L	426		463		651		601		513	
Benzo(a)pyrene (H)	pg/L	146		182		219		644		146	
Indeno(1,2,3-c,d)pyrene	pg/L	117		142		193		181		142	
Dibenzo(a,h)anthracene (H)	pg/L	46	U	46	U	46	U	46	U	46	U
Benzo(g,h,i)perylene	pg/L	224		222		246		336		224	
Total LMW PAHs	pg/L	2449		2817		3203		2917		2858	
Total HMW PAHs	pg/L	5510		8418		11090		9919		8437	
Total LMW+HMW PAHs	pg/L	7959		11235		14293		12836		11295	

Table F-9. Year Two semi-permeable membrane device results for area T1 (single mat only).

T1 - Single Mat Only

Analyte	Units	Rep 1		Rep 2		Rep 3		Rep Average	
		Below Mat (A)	Above Mat (B)	Below Mat (C)	Above Mat (D)	Below Mat (E)	Above Mat (F)	Below Mat	Above Mat
Naphthalene (L)	pg/L	N/A	N/A	N/A	N/A	N/A	N/A	N/A	N/A
Acenaphthylene (L)	pg/L	129	330	723	129	129	310	327	256
Acenaphthene (L)	pg/L	419	318	6632	300	1536	279	2862	299
Fluorene (L)	pg/L	896	542	5424	495	1887	448	2736	495
Phenanthrene (L)	pg/L	1099	2904	15557	2697	2282	2489	6313	2697
Anthracene (L)	pg/L	228	243	2583	258	638	182	1150	228
Fluoranthene (H)	pg/L	3068	8808	16823	7620	5245	6828	8379	7752
Pyrene (H)	pg/L	1585	3755	7927	3171	2253	2587	3922	3171
Benzo(a)anthracene (H)	pg/L	426	768	2719	544	674	544	1273	619
Chrysene (H)	pg/L	436	1489	2766	1170	702	1383	1301	1348
Benzo(b)fluoranthene	pg/L	479	1184	1729	891	785	851	997	975
Benzo(k)fluoranthene	pg/L	275	801	939	688	488	551	567	680
Benzo(a)pyrene (H)	pg/L	117	231	717	158	231	195	355	195
Indeno(1,2,3-c,d)pyrene	pg/L	32	32	193	155	110	116	112	101
Dibenzo(a,h)anthracene (H)	pg/L	46	46	46	46	46	46	46	46
Benzo(g,h,i)perylene	pg/L	56	56	358	224	269	215	228	165
Total LMW PAHs	pg/L	2771	4338	30918	3879	6471	3709	13387	3975
Total HMW PAHs	pg/L	5678	15097	30998	12709	9151	11582	15276	13129
Total LMW+HMW PAHs	pg/L	8449	19435	61917	16588	15622	15291	28663	17105

Analyte	Units	Rep 1		Rep 2		Rep 3		Rep Average	
		Below Mat (A)	Above Mat (B)	Below Mat (C)	Above Mat (D)	Below Mat (E)	Above Mat (F)	Below Mat	Above Mat
Percent Reduction									
Naphthalene (L)	%	-	N/A	-	N/A	-	N/A	-	N/A
Acenaphthylene (L)	%	-	-156.0	-	82	-	-140.0	-	22
Acenaphthene (L)	%	-	24	-	95	-	82	-	90
Fluorene (L)	%	-	39	-	91	-	76	-	82
Phenanthrene (L)	%	-	-164.15	-	83	-	-9.09	-	57
Anthracene (L)	%	-	-6.67	-	90	-	71	-	80
Fluoranthene (H)	%	-	-187.1	-	55	-	-30.19	-	7.5
Pyrene (H)	%	-	-136.84	-	60	-	-14.81	-	19
Benzo(a)anthracene (H)	%	-	-80.56	-	80	-	19	-	51
Chrysene (H)	%	-	-241.46	-	58	-	-96.97	-	-3.54
Benzo(b)fluoranthene	%	-	-147.22	-	48	-	-8.47	-	2.2
Benzo(k)fluoranthene	%	-	-190.91	-	27	-	-12.82	-	-19.85
Benzo(a)pyrene (H)	%	-	-97.92	-	78	-	16	-	45
Indeno(1,2,3-c,d)pyrene	%	-	0.0	-	20	-	-5.88	-	9.6
Dibenzo(a,h)anthracene (H)	%	-	0.0	-	0.0	-	0.0	-	0.0
Benzo(g,h,i)perylene	%	-	0.0	-	38	-	20	-	28
Total LMW PAHs	%	-	-56.51	-	87	-	43	-	70
Total HMW PAHs	%	-	-165.9	-	59	-	-26.57	-	14
Total LMW+HMW PAHs	%	-	-130.02	-	73	-	2.1	-	40

N/A = Data not available.

Table F-10. Year Two semi-permeable membrane device results for area T2 (single mat with sand cap).

T2 - Single Mat With Sand Cap

Analyte	Units	Rep 1		Rep 2		Rep 3		Rep Average	
		Below Mat (G)	Above Mat (H)	Below Mat (I)	Above Mat (J)	Below Mat (K)	Above Mat (L)	Below Mat	Above Mat
Naphthalene (L)	pg/L	N/A	N/A	N/A	N/A	N/A	N/A	N/A	N/A
Acenaphthylene (L)	pg/L	568	129	269	284	377	284	404	232
Acenaphthene (L)	pg/L	8028	213	1780	255	2548	524	4119	330
Fluorene (L)	pg/L	6368	495	1910	613	2170	1061	3483	723
Phenanthrene (L)	pg/L	20535	1369	2489	1473	2697	2074	8574	1639
Anthracene (L)	pg/L	2735	182	532	182	593	258	1286	208
Fluoranthene (H)	pg/L	16823	3662	5740	4453	6136	4552	9566	4222
Pyrene (H)	pg/L	8093	1418	2753	2086	2920	2086	4589	1863
Benzo(a)anthracene (H)	pg/L	2482	378	768	603	887	615	1379	532
Chrysene (H)	pg/L	2872	660	809	734	819	723	1500	706
Benzo(b)fluoranthene	pg/L	1463	559	997	771	1210	984	1223	771
Benzo(k)fluoranthene	pg/L	901	501	588	538	476	476	655	505
Benzo(a)pyrene (H)	pg/L	705	170	255	170	304	207	421	182
Indeno(1,2,3-c,d)pyrene	pg/L	193	101	219	181	206	129	206	137
Dibenzo(a,h)anthracene (H)	pg/L	104	46	126	46	46	46	92	46
Benzo(g,h,i)perylene	pg/L	448	213	314	269	314	224	358	235
Total LMW PAHs	pg/L	38233	2389	6980	2807	8384	4201	17866	3132
Total HMW PAHs	pg/L	31080	6334	10451	8093	11112	8229	17548	7552
Total LMW+HMW PAHs	pg/L	69313	8723	17431	10900	19495	12430	35413	10684

Analyte	Units	Rep 1		Rep 2		Rep 3		Rep Average	
		Below Mat (A)	Above Mat (B)	Below Mat (C)	Above Mat (D)	Below Mat (E)	Above Mat (F)	Below Mat	Above Mat
Percent Reduction									
Naphthalene (L)	%	-	N/A	-	N/A	-	N/A	-	N/A
Acenaphthylene (L)	%	-	77	-	-5.77	-	25	-	43
Acenaphthene (L)	%	-	97	-	86	-	79	-	92
Fluorene (L)	%	-	92	-	68	-	51	-	79
Phenanthrene (L)	%	-	93	-	41	-	23	-	81
Anthracene (L)	%	-	93	-	66	-	56	-	84
Fluoranthene (H)	%	-	78	-	22	-	26	-	56
Pyrene (H)	%	-	82	-	24	-	29	-	59
Benzo(a)anthracene (H)	%	-	85	-	22	-	31	-	61
Chrysene (H)	%	-	77	-	9.2	-	12	-	53
Benzo(b)fluoranthene	%	-	62	-	23	-	19	-	37
Benzo(k)fluoranthene	%	-	44	-	8.5	-	0.0	-	23
Benzo(a)pyrene (H)	%	-	76	-	33	-	32	-	57
Indeno(1,2,3-c,d)pyrene	%	-	48	-	18	-	38	-	34
Dibenzo(a,h)anthracene (H)	%	-	55	-	63	-	0.0	-	50
Benzo(g,h,i)perylene	%	-	53	-	14	-	29	-	34
Total LMW PAHs	%	-	94	-	60	-	50	-	82
Total HMW PAHs	%	-	80	-	23	-	26	-	57
Total LMW+HMW PAHs	%	-	87	-	37	-	36	-	70

N/A = Data not available.

Table F-11. Year Two semi-permeable membrane device results for area T3 (double mat).

T3 - Double Mat

Analyte	Units	Rep 1			Rep 2		
		Below Mats (M)	Between Mats (N)	Above Mats (O)	Below Mats (P)	Between Mats (Q)	Above Mats (R)
Naphthalene (L)	pg/L	N/A	N/A	N/A	N/A	N/A	N/A
Acenaphthylene (L)	pg/L	305	129	336	129	129	325
Acenaphthene (L)	pg/L	2304	87	258	1536	87	241
Fluorene (L)	pg/L	2217	151	448	1840	226	472
Phenanthrene (L)	pg/L	3111	933	2697	2489	788	2697
Anthracene (L)	pg/L	638	38	198	638	119	258
Fluoranthene (H)	pg/L	6630	910	8313	5938	1880	7818
Pyrene (H)	pg/L	3254	459	3504	2837	918	3338
Benzo(a)anthracene (H)	pg/L	910	66	745	816	378	626
Chrysene (H)	pg/L	894	149	1383	809	383	1277
Benzo(b)fluoranthene	pg/L	1463	132	1290	1090	572	1077
Benzo(k)fluoranthene	pg/L	638	79	688	626	375	688
Benzo(a)pyrene (H)	pg/L	304	30	219	316	146	146
Indeno(1,2,3-c,d)pyrene	pg/L	206	32	168	206	121	168
Dibenzo(a,h)anthracene (H)	pg/L	93	46	46	46	46	46
Benzo(g,h,i)perylene	pg/L	381	56	224	291	204	246
Total LMW PAHs	pg/L	8575	1339	3936	6632	1349	3993
Total HMW PAHs	pg/L	12085	1661	14210	10761	3751	13251
Total LMW+HMW PAHs	pg/L	20659	3000	18146	17393	5101	17243

Analyte	Units	Rep 1			Rep 2		
		Below Mats (M)	Between Mats (N)	Above Mats (O)	Below Mats (P)	Between Mats (Q)	Above Mats (R)
Percent Reduction							
Naphthalene (L)	%	-	N/A	N/A	-	N/A	N/A
Acenaphthylene (L)	%	-	58	-160.0	-	0.0	-152.0
Acenaphthene (L)	%	-	96	-196.0	-	94	-176.0
Fluorene (L)	%	-	93	-196.88	-	88	-108.33
Phenanthrene (L)	%	-	70	-188.89	-	68	-242.11
Anthracene (L)	%	-	94	-420.0	-	81	-117.95
Fluoranthene (H)	%	-	86	-813.04	-	68	-315.79
Pyrene (H)	%	-	86	-663.64	-	68	-263.64
Benzo(a)anthracene (H)	%	-	93	-1025.0	-	54	-65.63
Chrysene (H)	%	-	83	-828.57	-	53	-233.33
Benzo(b)fluoranthene	%	-	91	-879.8	-	48	-88.37
Benzo(k)fluoranthene	%	-	88	-773.02	-	40	-83.33
Benzo(a)pyrene (H)	%	-	90	-620.0	-	54	0.0
Indeno(1,2,3-c,d)pyrene	%	-	84	-420.0	-	41	-38.3
Dibenzo(a,h)anthracene (H)	%	-	50	0.0	-	0.0	0.0
Benzo(g,h,i)perylene	%	-	85	-300.0	-	30	-20.88
Total LMW PAHs	%	-	84	-194.02	-	80	-195.87
Total HMW PAHs	%	-	86	-755.44	-	65	-253.21
Total LMW+HMW PAHs	%	-	85	-504.9	-	71	-238.04

Table F-11. Year Two semi-permeable membrane device results for area T3 (double mat).

T3 - Double Mat

Analyte	Units	Rep 3			Rep Average		
		Below Mats (S)	Between Mats (T)	Above Mats (U)	Below Mats	Between Mats	Above Mat
Naphthalene (L)	pg/L	N/A	N/A	N/A	N/A	N/A	N/A
Acenaphthylene (L)	pg/L	346	129	403	260	129	355
Acenaphthene (L)	pg/L	87	87	279	1309	87	259
Fluorene (L)	pg/L	4953	123	472	3003	167	464
Phenanthrene (L)	pg/L	7260	560	2697	4287	761	2697
Anthracene (L)	pg/L	1519	38	198	932	65	218
Fluoranthene (H)	pg/L	12865	574	8115	8478	1122	8082
Pyrene (H)	pg/L	6425	325	3838	4172	567	3560
Benzo(a)anthracene (H)	pg/L	1773	130	957	1166	191	776
Chrysene (H)	pg/L	1596	128	1489	1099	220	1383
Benzo(b)fluoranthene	pg/L	1862	213	1995	1472	305	1454
Benzo(k)fluoranthene	pg/L	663	125	763	642	193	713
Benzo(a)pyrene (H)	pg/L	474	30	292	365	69	219
Indeno(1,2,3-c,d)pyrene	pg/L	258	32	245	224	62	193
Dibenzo(a,h)anthracene (H)	pg/L	115	46	46	84	46	46
Benzo(g,h,i)perylene	pg/L	381	56	336	351	105	269
Total LMW PAHs	pg/L	14165	937	4048	9790	1208	3992
Total HMW PAHs	pg/L	23247	1234	14738	15364	2215	14066
Total LMW+HMW PAHs	pg/L	37412	2171	18785	25155	3424	18058

Analyte	Units	Rep 3			Rep Average		
		Below Mats (S)	Between Mats (T)	Above Mats (U)	Below Mats	Between Mats	Above Mat
Percent Reduction							
Naphthalene (L)	%	-	N/A	N/A	-	N/A	N/A
Acenaphthylene (L)	%	-	63	-212.0	-	50	-174.67
Acenaphthene (L)	%	-	0.0	-220.0	-	93	-197.33
Fluorene (L)	%	-	98	-284.62	-	94	-178.3
Phenanthrene (L)	%	-	92	-381.48	-	82	-254.55
Anthracene (L)	%	-	98	-420.0	-	93	-235.94
Fluoranthene (H)	%	-	96	-1313.79	-	87	-620.59
Pyrene (H)	%	-	95	-1079.49	-	86	-527.45
Benzo(a)anthracene (H)	%	-	93	-636.36	-	84	-305.35
Chrysene (H)	%	-	92	-1066.67	-	80	-529.03
Benzo(b)fluoranthene	%	-	89	-837.5	-	79	-376.05
Benzo(k)fluoranthene	%	-	81	-510.0	-	70	-269.33
Benzo(a)pyrene (H)	%	-	94	-860.0	-	81	-217.65
Indeno(1,2,3-c,d)pyrene	%	-	88	-660.0	-	72	-212.5
Dibenzo(a,h)anthracene (H)	%	-	60	0.0	-	45	0.0
Benzo(g,h,i)perylene	%	-	85	-500.0	-	70	-155.32
Total LMW PAHs	%	-	93	-331.98	-	88	-230.37
Total HMW PAHs	%	-	95	-1094.59	-	86	-534.91
Total LMW+HMW PAHs	%	-	94	-765.4	-	86	-427.43

Table F-11. Year Two semi-permeable membrane device results for area T3 (double mat).

T3 - Double Mat

Analyte	Units	Rep 1			Rep 2		
		Below Mats (M)	Between Mats (N)	Above Mats (O)	Below Mats (P)	Between Mats (Q)	Above Mats (R)
Percent Reduction							
Naphthalene (L)	%	-	-	N/A	-	-	N/A
Acenaphthylene (L)	%	-	-	-10.17	-	-	-152.0
Acenaphthene (L)	%	-	-	89	-	-	84
Fluorene (L)	%	-	-	80	-	-	74
Phenanthrene (L)	%	-	-	13	-	-	-8.33
Anthracene (L)	%	-	-	69	-	-	60
Fluoranthene (H)	%	-	-	-25.37	-	-	-31.67
Pyrene (H)	%	-	-	-7.69	-	-	-17.65
Benzo(a)anthracene (H)	%	-	-	18	-	-	23
Chrysene (H)	%	-	-	-54.76	-	-	-57.89
Benzo(b)fluoranthene	%	-	-	12	-	-	1.2
Benzo(k)fluoranthene	%	-	-	-7.84	-	-	-10.0
Benzo(a)pyrene (H)	%	-	-	28	-	-	54
Indeno(1,2,3-c,d)pyrene	%	-	-	19	-	-	19
Dibenzo(a,h)anthracene (H)	%	-	-	50	-	-	0.0
Benzo(g,h,i)perylene	%	-	-	41	-	-	15
Total LMW PAHs	%	-	-	54	-	-	40
Total HMW PAHs	%	-	-	-17.59	-	-	-23.14
Total LMW+HMW PAHs	%	-	-	12	-	-	0.86

N/A = Data not available.

Table F-11. Year Two semi-permeable membrane device results for area T3 (double mat).

T3 - Double Mat

Analyte	Units	Rep 3			Rep Average		
		Below Mats (S)	Between Mats (T)	Above Mats (U)	Below Mats	Between Mats	Above Mat
Percent Reduction							
Naphthalene (L)	%	-	-	N/A	-	-	N/A
Acenaphthylene (L)	%	-	-	-16.42	-	-	-36.42
Acenaphthene (L)	%	-	-	-220.0	-	-	80
Fluorene (L)	%	-	-	90	-	-	85
Phenanthrene (L)	%	-	-	63	-	-	37
Anthracene (L)	%	-	-	87	-	-	77
Fluoranthene (H)	%	-	-	37	-	-	4.7
Pyrene (H)	%	-	-	40	-	-	15
Benzo(a)anthracene (H)	%	-	-	46	-	-	33
Chrysene (H)	%	-	-	6.7	-	-	-25.81
Benzo(b)fluoranthene	%	-	-	-7.14	-	-	1.2
Benzo(k)fluoranthene	%	-	-	-15.09	-	-	-11.04
Benzo(a)pyrene (H)	%	-	-	38	-	-	40
Indeno(1,2,3-c,d)pyrene	%	-	-	5.0	-	-	13
Dibenzo(a,h)anthracene (H)	%	-	-	60	-	-	45
Benzo(g,h,i)perylene	%	-	-	12	-	-	23
Total LMW PAHs	%	-	-	71	-	-	59
Total HMW PAHs	%	-	-	37	-	-	8.4
Total LMW+HMW PAHs	%	-	-	50	-	-	28

Table F-12. Year Two semi-permeable membrane device results for area T4 (sand cap only).

T4 - Sand Cap Only

Analyte	Units	Rep 1		Rep 2		Rep 3		Rep Average	
		Below Sand (V)	Above Sand (W)	Below Sand (X)	Above Sand (Y)	Below Sand (Z)	Above Sand (AA)	Below Sand	Above Sand
Naphthalene (L)	pg/L	N/A	N/A	N/A	N/A	N/A	N/A	N/A	N/A
Acenaphthylene (L)	pg/L	129	129	129	129	129	129	129	129
Acenaphthene (L)	pg/L	286	489	307	237	87	248	227	325
Fluorene (L)	pg/L	896	1250	825	825	896	613	873	896
Phenanthrene (L)	pg/L	1597	1390	1265	1369	1079	1659	1314	1473
Anthracene (L)	pg/L	198	273	289	273	258	167	248	238
Fluoranthene (H)	pg/L	4651	3761	3958	4057	3167	4750	3925	4189
Pyrene (H)	pg/L	2086	1752	1752	1752	1252	2086	1697	1863
Benzo(a)anthracene (H)	pg/L	556	485	485	496	378	556	473	512
Chrysene (H)	pg/L	691	564	628	660	521	798	613	674
Benzo(b)fluoranthene	pg/L	1117	1316	918	931	572	957	869	1068
Benzo(k)fluoranthene	pg/L	526	463	426	426	426	463	459	451
Benzo(a)pyrene (H)	pg/L	182	182	170	158	146	182	166	174
Indeno(1,2,3-c,d)pyrene	pg/L	155	129	142	168	117	142	138	146
Dibenzo(a,h)anthracene (H)	pg/L	46	46	46	46	46	46	46	46
Benzo(g,h,i)perylene	pg/L	224	208	246	246	224	222	231	225
Total LMW PAHs	pg/L	3106	3531	2816	2834	2449	2817	2790	3061
Total HMW PAHs	pg/L	8213	6790	7039	7170	5510	8418	6921	7459
Total LMW+HMW PAHs	pg/L	11319	10321	9855	10004	7959	11235	9711	10520

Analyte	Units	Rep 1		Rep 2		Rep 3		Rep Average	
		Below Sand (V)	Above Sand (W)	Below Sand (X)	Above Sand (Y)	Below Sand (Z)	Above Sand (AA)	Below Sand	Above Sand
Percent Reduction									
Naphthalene (L)	%	-	N/A	-	N/A	-	N/A	-	N/A
Acenaphthylene (L)	%	-	0.0	-	0.0	-	0.0	-	0.0
Acenaphthene (L)	%	-	-70.73	-	23	-	-184.0	-	-43.08
Fluorene (L)	%	-	-39.47	-	0.0	-	32	-	-2.7
Phenanthrene (L)	%	-	13	-	-8.2	-	-53.85	-	-12.11
Anthracene (L)	%	-	-38.46	-	5.3	-	35	-	4.1
Fluoranthene (H)	%	-	19	-	-2.5	-	-50.0	-	-6.72
Pyrene (H)	%	-	16	-	0.0	-	-66.67	-	-9.84
Benzo(a)anthracene (H)	%	-	13	-	-2.44	-	-46.88	-	-8.33
Chrysene (H)	%	-	18	-	-5.08	-	-53.06	-	-9.83
Benzo(b)fluoranthene	%	-	-17.86	-	-1.45	-	-67.44	-	-22.96
Benzo(k)fluoranthene	%	-	12	-	0.0	-	-8.82	-	1.8
Benzo(a)pyrene (H)	%	-	0.0	-	7.1	-	-25.0	-	-4.88
Indeno(1,2,3-c,d)pyrene	%	-	17	-	-18.18	-	-20.88	-	-5.92
Dibenzo(a,h)anthracene (H)	%	-	0.0	-	0.0	-	0.0	-	0.0
Benzo(g,h,i)perylene	%	-	7.0	-	0.0	-	1.0	-	2.6
Total LMW PAHs	%	-	-13.67	-	-0.66	-	-14.99	-	-9.68
Total HMW PAHs	%	-	17	-	-1.85	-	-52.78	-	-7.78
Total LMW+HMW PAHs	%	-	8.8	-	-1.51	-	-41.15	-	-8.33

N/A = Data not available.

Table F-13. Year Two semi-permeable membrane device results for area T5 (no treatment/control).

T5 - No Treatment (Control)

Analyte	Units	Rep 1 Above Sed (AB)	Rep 2 Above Sed (AC)	Rep 3 Above Sed (AD)	Rep Average Above Sed
Naphthalene (L)	pg/L	N/A	N/A	N/A	N/A
Acenaphthylene (L)	pg/L	274	129	129	177
Acenaphthene (L)	pg/L	223	206	265	232
Fluorene (L)	pg/L	613	660	873	715
Phenanthrene (L)	pg/L	1805	1618	1348	1590
Anthracene (L)	pg/L	289	304	243	279
Fluoranthene (H)	pg/L	6333	5344	4849	5509
Pyrene (H)	pg/L	2753	2420	2086	2420
Benzo(a)anthracene (H)	pg/L	674	603	544	607
Chrysene (H)	pg/L	1064	862	766	897
Benzo(b)fluoranthene	pg/L	1290	1051	931	1090
Benzo(k)fluoranthene	pg/L	651	601	513	588
Benzo(a)pyrene (H)	pg/L	219	644	146	336
Indeno(1,2,3-c,d)pyrene	pg/L	193	181	142	172
Dibenzo(a,h)anthracene (H)	pg/L	46	46	46	46
Benzo(g,h,i)perylene	pg/L	246	336	224	269
Total LMW PAHs	pg/L	3203	2917	2858	2993
Total HMW PAHs	pg/L	11090	9919	8437	9815
Total LMW+HMW PAHs	pg/L	14293	12836	11295	12808

N/A = Data not available.

Table F-14. Summary of Year Two semi-permeable membrane device results for the Cottonwood Bay prototype mat system.

Treatment Summary - Replicate Averages

Analyte	Units	T1 - Mat Only			T2 - Mat w/ Sand		
		Below Treatment	Between Treatment	Above Treatment	Below Treatment	Between Treatment	Above Treatment
Naphthalene (L)	pg/L	N/A	-	N/A	N/A	-	N/A
Acenaphthylene (L)	pg/L	327	-	256	404	-	232
Acenaphthene (L)	pg/L	2862	-	299	4119	-	330
Fluorene (L)	pg/L	2736	-	495	3483	-	723
Phenanthrene (L)	pg/L	6313	-	2697	8574	-	1639
Anthracene (L)	pg/L	1150	-	228	1286	-	208
Fluoranthene (H)	pg/L	8379	-	7752	9566	-	4222
Pyrene (H)	pg/L	3922	-	3171	4589	-	1863
Benzo(a)anthracene (H)	pg/L	1273	-	619	1379	-	532
Chrysene (H)	pg/L	1301	-	1348	1500	-	706
Benzo(b)fluoranthene	pg/L	997	-	975	1223	-	771
Benzo(k)fluoranthene	pg/L	567	-	680	655	-	505
Benzo(a)pyrene (H)	pg/L	355	-	195	421	-	182
Indeno(1,2,3-c,d)pyrene	pg/L	112	-	101	206	-	137
Dibenzo(a,h)anthracene (H)	pg/L	46	-	46	92	-	46
Benzo(g,h,i)perylene	pg/L	228	-	165	358	-	235
Total LMW PAHs	pg/L	13387	-	3975	17866	-	3132
Total HMW PAHs	pg/L	15276	-	13129	17548	-	7552
Total LMW+HMW PAHs	pg/L	28663	-	17105	35413	-	10684

N/A = Data not available.

Table F-14. Summary of Year Two semi-permeable membrane device results for the Cottonwood Bay prototype mat system.

Treatment Summary - Replicate Averages

Analyte	Units	T3 - Double Mat			T4 - Sand Only		
		Below Treatment	Between Treatment	Above Treatment	Below Treatment	Between Treatment	Above Treatment
Naphthalene (L)	pg/L	N/A	N/A	N/A	N/A	-	N/A
Acenaphthylene (L)	pg/L	260	129	355	129	-	129
Acenaphthene (L)	pg/L	1309	87	259	227	-	325
Fluorene (L)	pg/L	3003	167	464	873	-	896
Phenanthrene (L)	pg/L	4287	761	2697	1314	-	1473
Anthracene (L)	pg/L	932	65	218	248	-	238
Fluoranthene (H)	pg/L	8478	1122	8082	3925	-	4189
Pyrene (H)	pg/L	4172	567	3560	1697	-	1863
Benzo(a)anthracene (H)	pg/L	1166	191	776	473	-	512
Chrysene (H)	pg/L	1099	220	1383	613	-	674
Benzo(b)fluoranthene	pg/L	1472	305	1454	869	-	1068
Benzo(k)fluoranthene	pg/L	642	193	713	459	-	451
Benzo(a)pyrene (H)	pg/L	365	69	219	166	-	174
Indeno(1,2,3-c,d)pyrene	pg/L	224	62	193	138	-	146
Dibenzo(a,h)anthracene (H)	pg/L	84	46	46	46	-	46
Benzo(g,h,i)perylene	pg/L	351	105	269	231	-	225
Total LMW PAHs	pg/L	9790	1208	3992	2790	-	3061
Total HMW PAHs	pg/L	15364	2215	14066	6921	-	7459
Total LMW+HMW PAHs	pg/L	25155	3424	18058	9711	-	10520

N/A = Data not available.

Table F-14. Summary of Year Two semi-permeable membrane device results for the Cottonwood Bay prototype mat system.

Treatment Summary - Replicate Averages

Analyte	Units	T5 - No Treatment		
		Below Treatment	Between Treatment	Above Treatment
Naphthalene (L)	pg/L	-	-	N/A
Acenaphthylene (L)	pg/L	-	-	177
Acenaphthene (L)	pg/L	-	-	232
Fluorene (L)	pg/L	-	-	715
Phenanthrene (L)	pg/L	-	-	1590
Anthracene (L)	pg/L	-	-	279
Fluoranthene (H)	pg/L	-	-	5509
Pyrene (H)	pg/L	-	-	2420
Benzo(a)anthracene (H)	pg/L	-	-	607
Chrysene (H)	pg/L	-	-	897
Benzo(b)fluoranthene	pg/L	-	-	1090
Benzo(k)fluoranthene	pg/L	-	-	588
Benzo(a)pyrene (H)	pg/L	-	-	336
Indeno(1,2,3-c,d)pyrene	pg/L	-	-	172
Dibenzo(a,h)anthracene (H)	pg/L	-	-	46
Benzo(g,h,i)perylene	pg/L	-	-	269
Total LMW PAHs	pg/L	-	-	2993
Total HMW PAHs	pg/L	-	-	9815
Total LMW+HMW PAHs	pg/L	-	-	12808

N/A = Data not available.

APPENDIX G

“Prototype Mat System Ultraseep Flow and Analytical Data (June 2009)”

This page is intentionally left blank

T1- Mat (No Sand)

Specific Disharge T1 (Deployment 1)

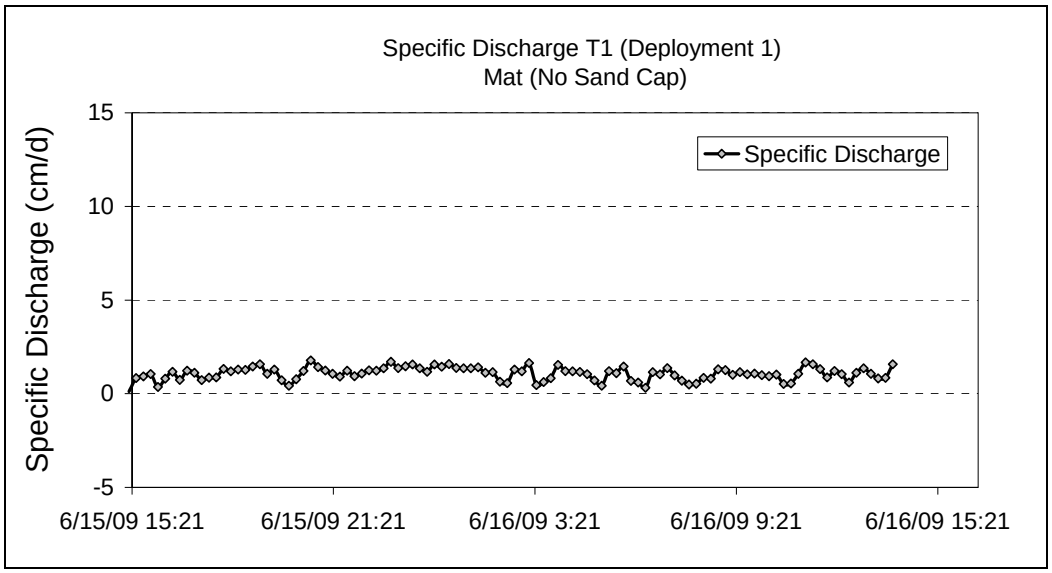

Dilution Results T1 (Deployment 1)

Sample	Total Sample (ml)	Total Discharge Water In Sample	Discharge Fraction	Surface Water Fraction
Composite	671	113.06033	17%	83%

Ultraseep Temperature/Conductivity Results T1 (Deployment 1)

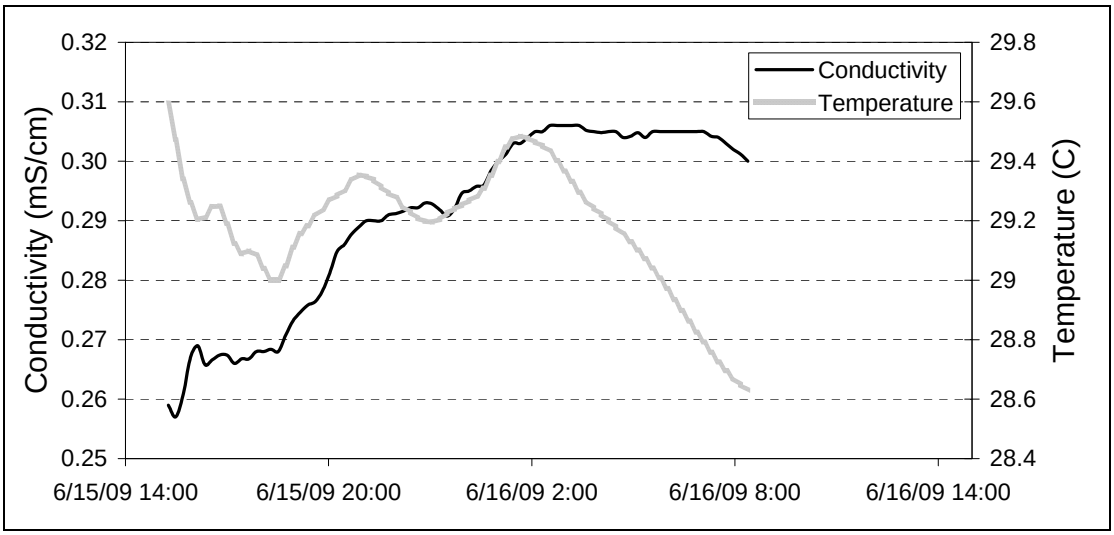

T2 - (Mat w/Sand Cap)

Specific Discharge T2 (Deployment 1)

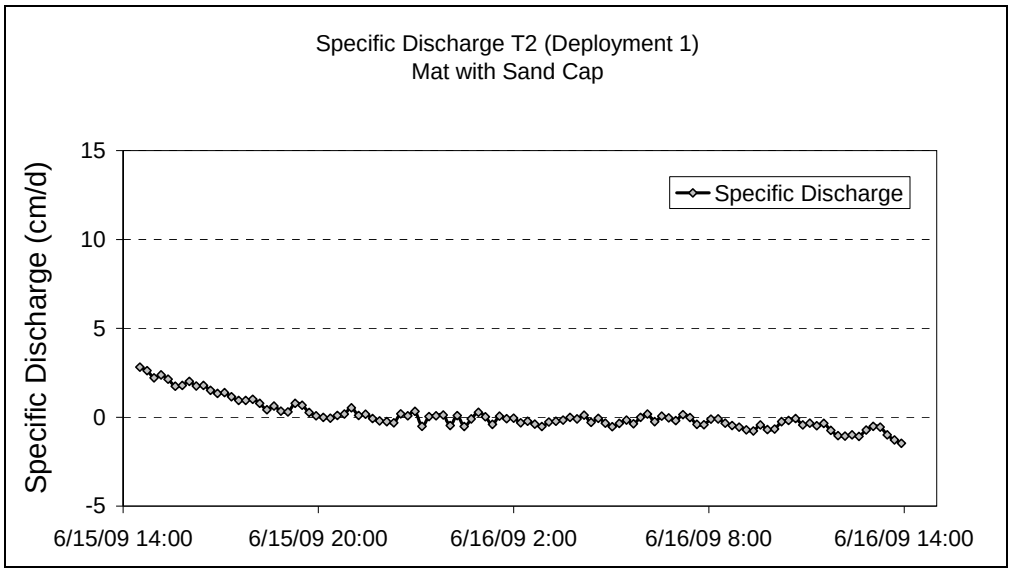

Dilution Results T2 (Deployment 1)

Sample	Total Sample (ml)	Total Discharge Water In Sample	Discharge Fraction	Surface Water Fraction
Composite	215	13.385602	6%	94%

Ultraseep Temperature/Conductivity Results T2 (Deployment 1)

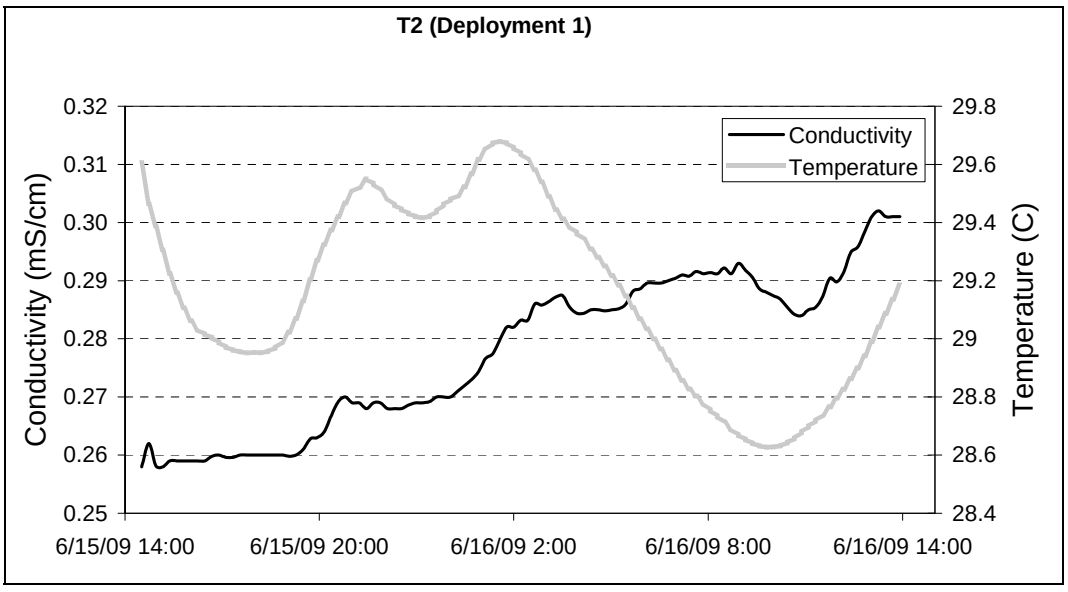

T3 - Double Mat (No Sand)

Specific Disharge T3 (Deployment 2)

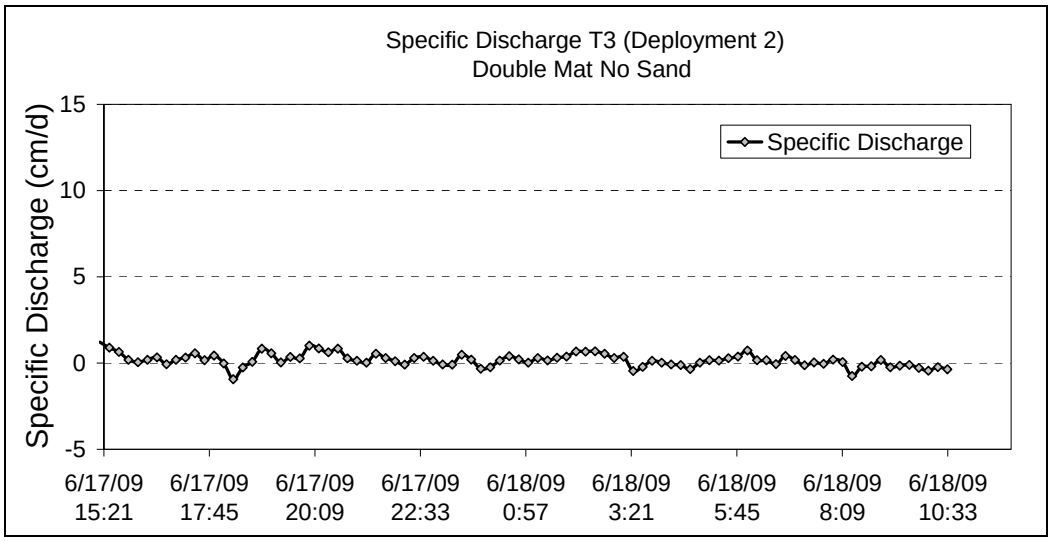

Ultraseep Temperature/Conductivity Results T3 (Deployment 2)

Sample	Total Sample (ml)	Total Discharge Water In Sample	Discharge Fraction	Surface Water Fraction
Composite	103	18.04442	18%	82%

T4 - Sand Cap Only

Specific Discharge T4 (Deployment 1)

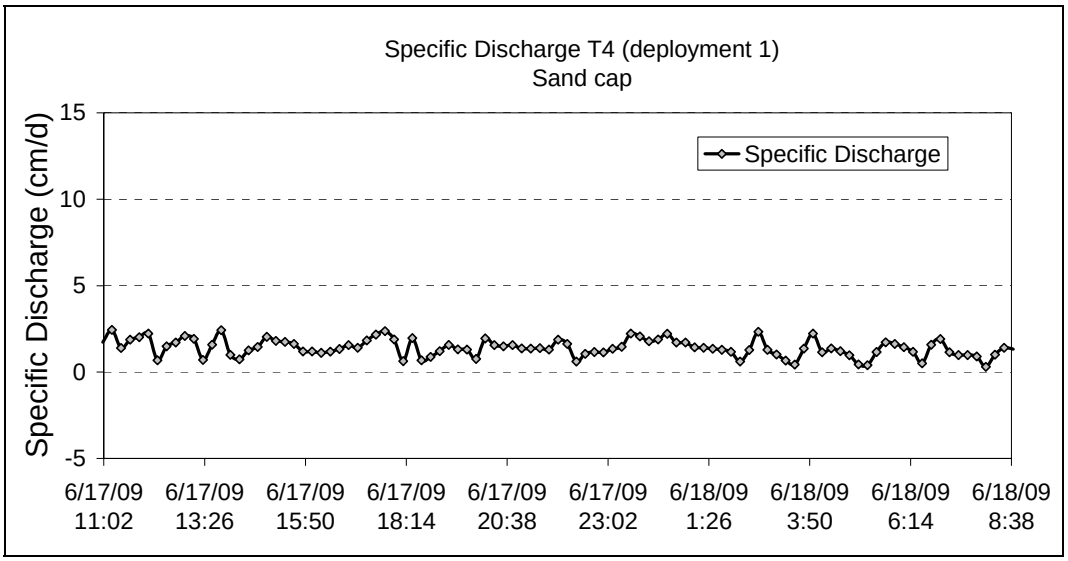

Dilution Results T4 (Deployment 1)

Sample	Total Sample (ml)	Total Discharge Water In Sample	Discharge Fraction	Surface Water Fraction
Composite	868	172.64953	20%	80%

Ultraseep Temperature/Conductivity Results T4 (Deployment 1)

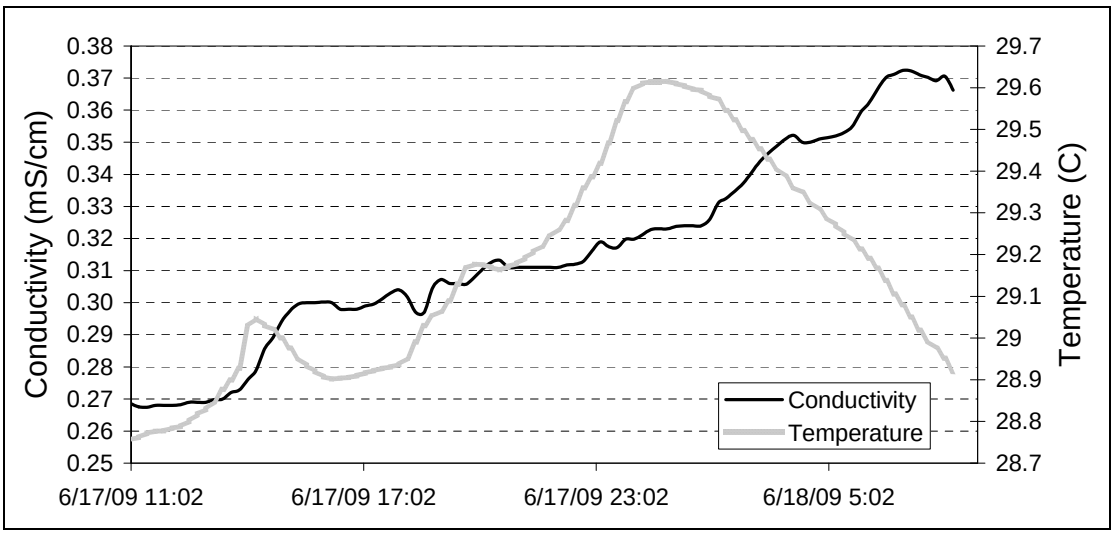

T4 - Sand Cap Only

Specific Discharge T4 (Deployment 2)

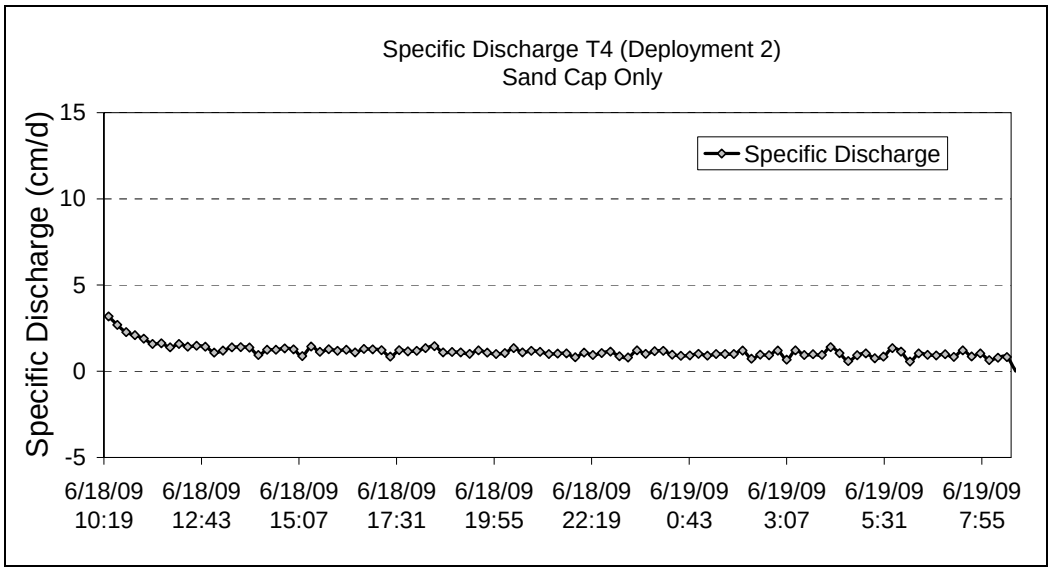

Dilution Results T4 (Deployment 2)

Sample	Total Sample (ml)	Total Discharge Water In Sample	Discharge Fraction	Surface Water Fraction
Composite	722	111.85128	15%	85%

Ultraseep Temperature/Conductivity Results T4 (Deployment 2)

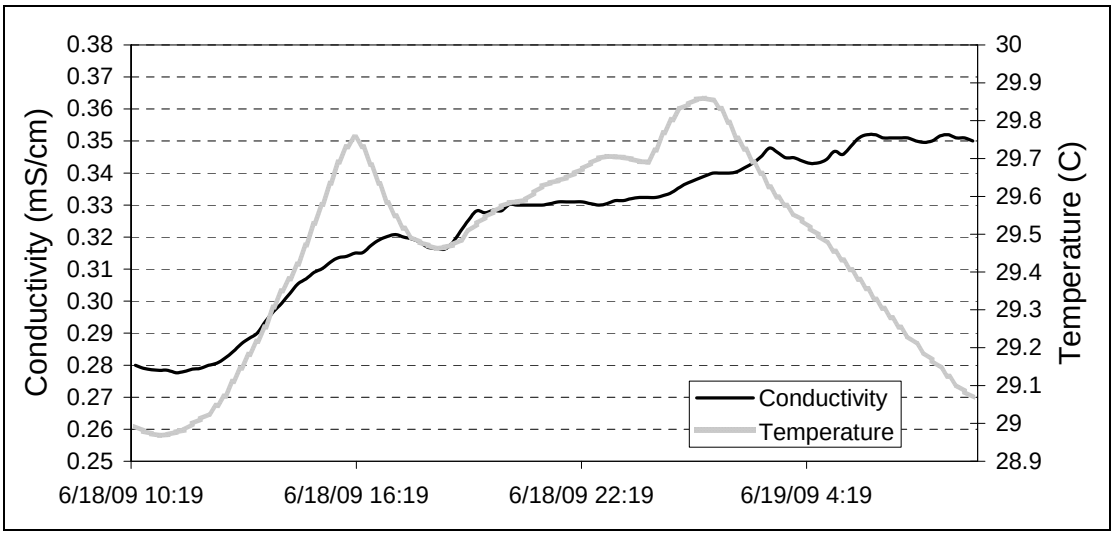

T5 - Control (No Treatment)

Specific Discharge T5 (Deployment 1)

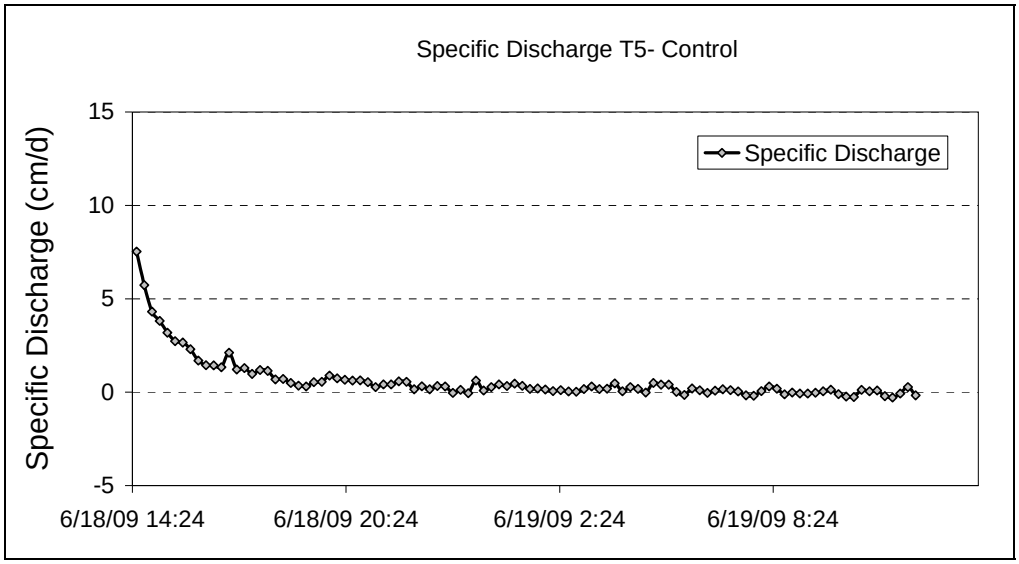

Dilution Results T5 (Deployment 1)

Sample	Total Sample (ml)	Total Discharge Water In Sample	Discharge Fraction	Surface Water Fraction
Composite	344	34.087793	10%	90%

Table G-1. Ultraseep raw analytical results for the prototype mat system adjusted to reflect the discharge sample.

Analyte	Units	Detection Limit	T1-US-MW-1 Surface A		T2-US-SNW-1 Surface I		T3-US-MW-2 Surface T		T4-US-SNW-1 Surface CC		T4-US-SNW-2 Surface DD		T5-US-SDW-1 Surface KK	
Aluminum (Al)	ug/L	2.3	421		1516		345		390		555		739	
Antimony (Sb)	ug/L	9.2	27	U	74	U	26	U	23	U	30	U	46	U
Arsenic (As)	ug/L	14	41	U	111	U	39	U	35	U	45	U	70	U
Barium (Ba)	ug/L	0.05	238		485		191		264		326		373	
Beryllium (Be)	ug/L	0.03	0.074	U	0.201	U	0.072	U	0.063	U	0.081	U	0.127	U
Cadmium (Cd)	ug/L	0.31	0.924	U	2.5	U	0.889	U	0.783	U	1.0	U	1.6	U
Calcium (Ca)	ug/L	0.87	259892		514713		201605		216105		291679		396899	
Chromium (Cr)	ug/L	0.64	6.7		22		5.8		3.6		5.8		9.2	
Cobalt (Co)	ug/L	1.4	4.3	U	12	U	4.1	U	3.6	U	4.7	U	7.3	U
Copper (Cu)	ug/L	0.67	13		107		13		9.2		11		16	
Iron (Fe)	ug/L	1.2	2397		4378		475		1866		1801		3177	
Lead (Pb)	ug/L	7.1	21	U	57	U	20	U	18	U	23	U	36	U
Magnesium (Mg)	ug/L	4.2	12751		35677		10719		10889		14436		20772	
Manganese (Mn)	ug/L	0.08	2705		956		128		2244		1998		1925	
Nickel (Ni)	ug/L	1.5	87		115		34		26		32		42	
Potassium (K)	ug/L	1.6	27647		75163		25072		24084		32900		48951	
Selenium (Se)	ug/L	36	107	U	290	U	103	U	91	U	116	U	182	U
Silver (Ag)	ug/L	0.41	1.2	U	3.3	U	1.2	U	1.0	U	1.3	U	2.1	U
Sodium (Na)	ug/L	10	92367		295061		81780		79589		108007		156719	
Thallium (Tl)	ug/L	16	49	U	132	U	47	U	41	U	53	U	83	U
Vanadium (V)	ug/L	0.99	13		50		15		11		15		30	
Zinc (Zn)	ug/L	2.3	114		135		80		47		48		98	

U = Concentration below detection limit; 1/2 detection limit used instead.

**Concentrations calculated from analytical results and Ultraseep internal dilution values.

Table G-2. Summary of Ultraseep analytical results for the prototype mat system adjusted to reflect the discharge sample.

Full-Scale Mat System

Analyte	Units	T1 - Mat Only			T2 - Mat w/ Sand		
		Rep 1 (A)	Rep 2 (B)*	Average	Rep 1 (I)	Rep 2 (J)	Average
Aluminum (Al)	ug/L	421	-	421	1516	-	1516
Antimony (Sb)	ug/L	27	-	27	74	-	74
Arsenic (As)	ug/L	41	-	41	111	-	111
Barium (Ba)	ug/L	238	-	238	485	-	485
Beryllium (Be)	ug/L	0.074	-	0.074	0.201	-	0.201
Cadmium (Cd)	ug/L	0.924	-	0.924	2.5	-	2.5
Calcium (Ca)	ug/L	259892	-	259892	514713	-	514713
Chromium (Cr)	ug/L	6.7	-	6.7	22	-	22
Cobalt (Co)	ug/L	4.3	-	4.3	12	-	12
Copper (Cu)	ug/L	13	-	13	107	-	107
Iron (Fe)	ug/L	2397	-	2397	4378	-	4378
Lead (Pb)	ug/L	21	-	21	57	-	57
Magnesium (Mg)	ug/L	12751	-	12751	35677	-	35677
Manganese (Mn)	ug/L	2705	-	2705	956	-	956
Nickel (Ni)	ug/L	87	-	87	115	-	115
Potassium (K)	ug/L	27647	-	27647	75163	-	75163
Selenium (Se)	ug/L	107	-	107	290	-	290
Silver (Ag)	ug/L	1.2	-	1.2	3.3	-	3.3
Sodium (Na)	ug/L	92367	-	92367	295061	-	295061
Thallium (Tl)	ug/L	49	-	49	132	-	132
Vanadium (V)	ug/L	13	-	13	50	-	50
Zinc (Zn)	ug/L	114	-	114	135	-	135

*Ultraseep attempted but no sample collected.

Table G-2. Summary of Ultraseep analytical results for the prototype mat system adjusted to reflect the discharge sample.

Full-Scale Mat System

Analyte	Units	T3 - Double Mat			T4 - Sand Only		
		Rep 1 (S)	Rep 2 (T)	Average	Rep 1 (CC)	Rep 2 (DD)	Average
Aluminum (Al)	ug/L	-	345	345	390	555	473
Antimony (Sb)	ug/L	-	26	26	23	30	26
Arsenic (As)	ug/L	-	39	39	35	45	40
Barium (Ba)	ug/L	-	191	191	264	326	295
Beryllium (Be)	ug/L	-	0.072	0.072	0.063	0.081	0.072
Cadmium (Cd)	ug/L	-	0.889	0.889	0.783	1.0	0.894
Calcium (Ca)	ug/L	-	201605	201605	216105	291679	253892
Chromium (Cr)	ug/L	-	5.8	5.8	3.6	5.8	4.7
Cobalt (Co)	ug/L	-	4.1	4.1	3.6	4.7	4.2
Copper (Cu)	ug/L	-	13	13	9.2	11	10.0
Iron (Fe)	ug/L	-	475	475	1866	1801	1833
Lead (Pb)	ug/L	-	20	20	18	23	20
Magnesium (Mg)	ug/L	-	10719	10719	10889	14436	12663
Manganese (Mn)	ug/L	-	128	128	2244	1998	2121
Nickel (Ni)	ug/L	-	34	34	26	32	29
Potassium (K)	ug/L	-	25072	25072	24084	32900	28492
Selenium (Se)	ug/L	-	103	103	91	116	104
Silver (Ag)	ug/L	-	1.2	1.2	1.0	1.3	1.2
Sodium (Na)	ug/L	-	81780	81780	79589	108007	93798
Thallium (Tl)	ug/L	-	47	47	41	53	47
Vanadium (V)	ug/L	-	15	15	11	15	13
Zinc (Zn)	ug/L	-	80	80	47	48	47

Table G-2. Summary of Ultraseep analytical results for the prototype mat system adjusted to reflect the discharge sample.

Full-Scale Mat System

Analyte	Units	T5 - No Treatment	
		Rep 1 (KK)	Average
Aluminum (Al)	ug/L	739	739
Antimony (Sb)	ug/L	46	46
Arsenic (As)	ug/L	70	70
Barium (Ba)	ug/L	373	373
Beryllium (Be)	ug/L	0.127	0.127
Cadmium (Cd)	ug/L	1.6	1.6
Calcium (Ca)	ug/L	396899	396899
Chromium (Cr)	ug/L	9.2	9.2
Cobalt (Co)	ug/L	7.3	7.3
Copper (Cu)	ug/L	16	16
Iron (Fe)	ug/L	3177	3177
Lead (Pb)	ug/L	36	36
Magnesium (Mg)	ug/L	20772	20772
Manganese (Mn)	ug/L	1925	1925
Nickel (Ni)	ug/L	42	42
Potassium (K)	ug/L	48951	48951
Selenium (Se)	ug/L	182	182
Silver (Ag)	ug/L	2.1	2.1
Sodium (Na)	ug/L	156719	156719
Thallium (Tl)	ug/L	83	83
Vanadium (V)	ug/L	30	30
Zinc (Zn)	ug/L	98	98

APPENDIX H

"Prototype Mat System Trident Probe Analytical Results (June 2009)"

This page is intentionally left blank

Table H-1. Trident Probe raw analytical results for the Cottonwood Bay prototype mat system.

Analyte	Units	Detection Limit	T1-TP-MW-1 +2 in C		T1-TP-SDM-1 -3.5 in D		T1-TP-SUB-1 -11 in E*		T1-TP-MW-2 +2 in F		T1-TP-SDM-2 -3.5 in G		T1-TP-SUB-2 -11 in H	
Aluminum (Al)	ug/L	2.3	326		126		10639		155		113		12548	
Antimony (Sb)	ug/L	9.2	4.6	U	4.6	U	4.6	U	4.6	U	4.6	U	4.6	U
Arsenic (As)	ug/L	14	6.9	U	6.9	U	36		6.9	U	6.9	U	40	
Barium (Ba)	ug/L	0.05	44		54		384		40		47		433	
Beryllium (Be)	ug/L	0.03	0.075		0.013	U	2.2		0.013	U	0.013	U	3.0	
Cadmium (Cd)	ug/L	0.31	0.417		0.156	U	51		0.156	U	0.156	U	56	
Calcium (Ca)	ug/L	0.87	49691		50000		50000		43002		49959		50000	
Chromium (Cr)	ug/L	0.64	6.4		2.5		1259		2.1		1.6		998	
Cobalt (Co)	ug/L	1.4	0.725	U	0.725	U	16		0.725	U	0.725	U	19	
Copper (Cu)	ug/L	0.67	3.8		1.8		199		1.8		1.3		226	
Iron (Fe)	ug/L	1.2	982		593		41032		409		708		49601	
Lead (Pb)	ug/L	7.1	3.5	U	3.5	U	247		3.5	U	3.5	U	333	
Magnesium (Mg)	ug/L	4.2	2035		2859		7787		2064		2278		8524	
Manganese (Mn)	ug/L	0.08	113		704		2462		57		426		2937	
Nickel (Ni)	ug/L	1.5	2.2		0.735	U	74		1.9		1.9		83	
Potassium (K)	ug/L	1.6	4867		5630		13175		4999		5106		14377	
Selenium (Se)	ug/L	36	18	U	18	U	18	U	18	U	18	U	18	U
Silver (Ag)	ug/L	0.41	0.206	U	0.206	U	2.3		0.206	U	0.206	U	0.761	
Sodium (Na)	ug/L	10	15289		21660		50000		15708		17607		50000	
Thallium (Tl)	ug/L	16	8.2	U	8.2	U	8.2	U	8.2	U	8.2	U	8.2	U
Vanadium (V)	ug/L	0.99	6.3		1.1		112		4.1		2.0		154	
Zinc (Zn)	ug/L	2.3	18		9.8		615		4.7		6.6		839	

* Sample had visable sediment suspended in water.

U = Concentration below detection limit; 1/2 detection limit used instead.

Table H-1. Trident Probe raw analytical results for the Cottonwood Bay prototype mat system.

Analyte	Units	T2-TP-SNW-1 +2 in K		T2-TP-SDM-1 -3.5 in M		T2-TP-SUB-1 -11 in N*		T2-TP-SNW-2 +2 in O		T2-TP-SDM-2 -3.5 in Q		T2-TP-SUB-2 -11 in R*		T3-TP-MW-1 +2 in U	
Aluminum (Al)	ug/L	156		182		16035		161		43		3532		136	
Antimony (Sb)	ug/L	4.6	U	4.6	U	4.6	U	4.6	U	4.6	U	4.6	U	4.6	U
Arsenic (As)	ug/L	6.9	U	71		53		6.9	U	25		23		6.9	U
Barium (Ba)	ug/L	38		101		614		41		361		266		35	
Beryllium (Be)	ug/L	0.013	U	0.013	U	3.3		0.013	U	0.013	U	0.745		0.013	U
Cadmium (Cd)	ug/L	0.156	U	0.881		118		0.156	U	0.663		12		0.156	U
Calcium (Ca)	ug/L	40403		50000		50000		42589		50000		50000		36922	
Chromium (Cr)	ug/L	2.2		3.8		3051		1.9		0.319	U	164		2.5	
Cobalt (Co)	ug/L	0.725	U	0.725	U	23		0.725	U	0.725	U	6.4		0.725	U
Copper (Cu)	ug/L	2.0		2.5		400		2.1		0.333	U	54		3.0	
Iron (Fe)	ug/L	398		10372		50000		444		10427		19199		348	
Lead (Pb)	ug/L	3.5	U	3.5	U	445		3.5	U	3.5	U	77		3.5	U
Magnesium (Mg)	ug/L	2008		5703		8895		2072		6468		7805		1911	
Manganese (Mn)	ug/L	65		2898		2945		53		2427		2252		73	
Nickel (Ni)	ug/L	1.5		2.4		125		1.8		0.735	U	25		1.7	
Potassium (K)	ug/L	4893		8134		14535		5083		9447		11697		4638	
Selenium (Se)	ug/L	18	U	18	U	18	U	18	U	18	U	18	U	18	U
Silver (Ag)	ug/L	0.206	U	0.206	U	3.4		0.206	U	0.206	U	0.60		0.206	U
Sodium (Na)	ug/L	15334		30033		50000		15983		34424		52985		14659	
Thallium (Tl)	ug/L	8.2	U	8.2	U	8.2	U	8.2	U	8.2	U	8.2	U	8.2	U
Vanadium (V)	ug/L	4.2		2.2		150		4.1		0.494	U	38		4.3	
Zinc (Zn)	ug/L	6.7		16		996		13		3.7		241		23	

Table H-1. Trident Probe raw analytical results for the Cottonwood Bay prototype mat system.

Analyte	Units	T3-TP-MM-1 - V		T3-TP-SDM-1 -3.5 in W		T3-TP-SUB-1 -11 in X		T3-TP-MW-2 +2 in Y		T3-TP-MM-2 - Z		T3-TP-SDM-2 3.5 in AA		T3-TP-SUB-2 -11 in BB*	
Aluminum (Al)	ug/L	195		185		18813		256		602		48		9558	
Antimony (Sb)	ug/L	4.6	U	4.6	U	4.6	U	4.6	U	4.6	U	4.6	U	4.6	U
Arsenic (As)	ug/L	6.9	U	6.9	U	53		6.9	U	6.9	U	6.9	U	31	
Barium (Ba)	ug/L	77		74		670		43		58		85		345	
Beryllium (Be)	ug/L	0.013	U	0.013	U	3.9		0.027		0.108		0.013	U	2.1	
Cadmium (Cd)	ug/L	0.156	U	0.156	U	128		0.156	U	0.822		0.156	U	25	
Calcium (Ca)	ug/L	50000		50000		50000		48410		50000		50000		50000	
Chromium (Cr)	ug/L	3.0		3.5		3115		4.2		12		0.999		478	
Cobalt (Co)	ug/L	0.725	U	0.725	U	26		0.725	U	0.725	U	0.725	U	14	
Copper (Cu)	ug/L	2.0		3.6		452		3.2		5.6		0.672		129	
Iron (Fe)	ug/L	1172		1743		50000		759		2068		2535		42498	
Lead (Pb)	ug/L	3.5	U	3.5	U	509		3.5	U	3.5	U	3.5	U	163	
Magnesium (Mg)	ug/L	3236		3476		10502		2083		2139		4575		8870	
Manganese (Mn)	ug/L	1103		1034		3356		96		361		1073		3328	
Nickel (Ni)	ug/L	0.735	U	6.1		170		2.1		4.0		0.735	U	53	
Potassium (K)	ug/L	5780		6409		16043		4972		5195		6937		13725	
Selenium (Se)	ug/L	18	U	18	U	18	U	18	U	18	U	18	U	18	U
Silver (Ag)	ug/L	0.206	U	0.206	U	2.8		0.206	U	0.206	U	0.206	U	1.8	
Sodium (Na)	ug/L	21752		25961		50000		15635		16082		28302		50000	
Thallium (Tl)	ug/L	8.2	U	8.2	U	8.2	U	8.2	U	8.2	U	8.2	U	8.2	U
Vanadium (V)	ug/L	1.4		1.5		180		5.2		8.8		0.494	U	111	
Zinc (Zn)	ug/L	13		53		1165		12		34		4.0		547	

Table H-1. Trident Probe raw analytical results for the Cottonwood Bay prototype mat system.

Analyte	Units	T4-TP-SNW-1 +2 in EE		T4-TP-SDSN-1 -3.5 in FF		T4-TP-SUB-1 -11 in GG		T4-TP-SNW-2 +2 in HH		T4-TP-SDSN-2 -3.5 in II		T4-TP-SUB-2 -11 in JJ		T5-TP-SDW-1 +2 in MM	
Aluminum (Al)	ug/L	205		37		499		150		256		4219		210	
Antimony (Sb)	ug/L	4.6	U	4.6	U	4.6	U	4.6	U	4.6	U	4.6	U	4.6	U
Arsenic (As)	ug/L	6.9	U	42		34		6.9	U	17		16		6.9	
Barium (Ba)	ug/L	39		1726		424		38		55		189		38	
Beryllium (Be)	ug/L	0.013	U	0.013	U	0.08		0.013	U	0.013	U	0.826		0.013	U
Cadmium (Cd)	ug/L	0.156	U	0.982		2.0		0.156	U	0.156	U	18		0.156	U
Calcium (Ca)	ug/L	41834		50000		50000		40383		50000		50000		39888	
Chromium (Cr)	ug/L	3.5		0.319	U	17		2.0		5.4		446		3.7	
Cobalt (Co)	ug/L	0.725	U	0.725	U	2.1		0.725	U	0.725	U	6.9		0.725	U
Copper (Cu)	ug/L	4.9		0.333	U	5.7		1.8		2.9		74		3.0	
Iron (Fe)	ug/L	547		14606		17067		372		1638		14040		616	
Lead (Pb)	ug/L	3.5	U	3.5	U	3.5	U	3.5	U	3.5	U	91		3.5	U
Magnesium (Mg)	ug/L	1978		6766		7173		2014		2463		6763		1940	
Manganese (Mn)	ug/L	88		2373		3292		58		503		2073		97	
Nickel (Ni)	ug/L	2.0		0.735	U	5.9		0.735	U	2.4		30		2.5	
Potassium (K)	ug/L	4762		9451		10088		4904		5463		10569		4780	
Selenium (Se)	ug/L	18	U	18	U	18	U	18	U	18	U	18	U	18	U
Silver (Ag)	ug/L	0.206	U	0.206	U	0.206	U	0.206	U	0.206	U	0.944		0.206	U
Sodium (Na)	ug/L	14973		34022		36063		15354		18236		49054		15028	
Thallium (Tl)	ug/L	8.2	U	8.2	U	8.2	U	8.2	U	8.2	U	8.2	U	8.2	U
Vanadium (V)	ug/L	4.8		1.4		6.7		4.2		4.3		43		4.4	
Zinc (Zn)	ug/L	15		5.3		38		7.5		14		247		7.6	

Table H-1. Trident Probe raw analytical results for the Cottonwood Bay prototype mat system.

Analyte	Units	T5-TP-SUB-1 -3.5 in NN*		T5-TP-SUB2-1 -11 in OO*		T5-TP-SUB3-1 -24 in TT*		T4-TP-SUB2-1 -24 in UU*	
Aluminum (Al)	ug/L	32443		12555		41240		23311	
Antimony (Sb)	ug/L	4.6	U	18		4.6	U	27	
Arsenic (As)	ug/L	78		51		52		89	
Barium (Ba)	ug/L	960		822		1073		1118	
Beryllium (Be)	ug/L	7.0		2.7		7.3		4.2	
Cadmium (Cd)	ug/L	59		386		81		475	
Calcium (Ca)	ug/L	50000		50000		50000		50000	
Chromium (Cr)	ug/L	902		7317		812		50000	
Cobalt (Co)	ug/L	53		21		27		29	
Copper (Cu)	ug/L	397		546		250		592	
Iron (Fe)	ug/L	50000		50000		50000		50000	
Lead (Pb)	ug/L	471		495		144		675	
Magnesium (Mg)	ug/L	10936		11417		12837		11987	
Manganese (Mn)	ug/L	5888		2517		50000		2884	
Nickel (Ni)	ug/L	166		109		117		139	
Potassium (K)	ug/L	19962		14434		18203		16006	
Selenium (Se)	ug/L	18	U	18	U	18	U	18	U
Silver (Ag)	ug/L	0.69		1.1		1.1		4.0	
Sodium (Na)	ug/L	48144		50000		50000		50000	
Thallium (Tl)	ug/L	8.2	U	8.2	U	8.2	U	8.2	U
Vanadium (V)	ug/L	368		116		404		187	
Zinc (Zn)	ug/L	1926		1744		468		2700	

Table H-2. Trident Probe analytical results for area T1 (single mat only).

T1 - Single Mat Only

Analyte	Units	Rep 1			Rep 2			Rep Average		
		Below Mat -11 in (E)	Below Mat -3.5 in (D)	Above Mat +2 in (C)	Below Mat -11 in (H)	Below Mat -3.5 in (G)	Above Mat +2 in (F)	Below Mat -11 in	Below Mat -3.5 in	Above Mat +2 in
Aluminum (Al)	ug/L	10639	126	326	12548	113	155	11594	120	241
Antimony (Sb)	ug/L	4.6	4.6	4.6	4.6	4.6	4.6	4.6	4.6	4.6
Arsenic (As)	ug/L	36	6.9	6.9	40	6.9	6.9	38	6.9	6.9
Barium (Ba)	ug/L	384	54	44	433	47	40	408	50	42
Beryllium (Be)	ug/L	2.2	0.013	0.075	3.0	0.013	0.013	2.6	0.013	0.044
Cadmium (Cd)	ug/L	51	0.156	0.417	56	0.156	0.156	54	0.156	0.286
Calcium (Ca)	ug/L	50000	50000	49691	50000	49959	43002	50000	49979	46346
Chromium (Cr)	ug/L	1259	2.5	6.4	998	1.6	2.1	1128	2.1	4.2
Cobalt (Co)	ug/L	16	0.725	0.725	19	0.725	0.725	17	0.725	0.725
Copper (Cu)	ug/L	199	1.8	3.8	226	1.3	1.8	212	1.6	2.8
Iron (Fe)	ug/L	41032	593	982	49601	708	409	45317	651	695
Lead (Pb)	ug/L	247	3.5	3.5	333	3.5	3.5	290	3.5	3.5
Magnesium (Mg)	ug/L	7787	2859	2035	8524	2278	2064	8156	2569	2050
Manganese (Mn)	ug/L	2462	704	113	2937	426	57	2699	565	85
Nickel (Ni)	ug/L	74	0.735	2.2	83	1.9	1.9	79	1.3	2.1
Potassium (K)	ug/L	13175	5630	4867	14377	5106	4999	13776	5368	4933
Selenium (Se)	ug/L	18	18	18	18	18	18	18	18	18
Silver (Ag)	ug/L	2.3	0.206	0.206	0.761	0.206	0.206	1.5	0.206	0.206
Sodium (Na)	ug/L	50000	21660	15289	50000	17607	15708	50000	19633	15499
Thallium (Tl)	ug/L	8.2	8.2	8.2	8.2	8.2	8.2	8.2	8.2	8.2
Vanadium (V)	ug/L	112	1.1	6.3	154	2.0	4.1	133	1.6	5.2
Zinc (Zn)	ug/L	615	9.8	18	839	6.6	4.7	727	8.2	11

Table H-3. Trident Probe analytical results for area T2 (single mat with sand cap).

T2 - Single Mat With Sand Cap

Analyte	Units	Rep 1			Rep 2			Rep Average		
		Below Mat -11 in (N)	Below Mat -3.5 in (M)	Above Mat +2 in (K)	Below Mat -11 in (R)	Below Mat -3.5 in (Q)	Above Mat +2 in (O)	Below Mat -11 in	Below Mat -3.5 in	Above Mat +2 in
Aluminum (Al)	ug/L	16035	182	156	3532	43	161	9784	113	159
Antimony (Sb)	ug/L	4.6	4.6	4.6	4.6	4.6	4.6	4.6	4.6	4.6
Arsenic (As)	ug/L	53	71	6.9	23	25	6.9	38	48	6.9
Barium (Ba)	ug/L	614	101	38	266	361	41	440	231	40
Beryllium (Be)	ug/L	3.3	0.013	0.013	0.745	0.013	0.013	2.0	0.013	0.013
Cadmium (Cd)	ug/L	118	0.881	0.156	12	0.663	0.156	65	0.772	0.156
Calcium (Ca)	ug/L	50000	50000	40403	50000	50000	42589	50000	50000	41496
Chromium (Cr)	ug/L	3051	3.8	2.2	164	0.319	1.9	1608	2.1	2.0
Cobalt (Co)	ug/L	23	0.725	0.725	6.4	0.725	0.725	14	0.725	0.725
Copper (Cu)	ug/L	400	2.5	2.0	54	0.333	2.1	227	1.4	2.0
Iron (Fe)	ug/L	50000	10372	398	19199	10427	444	34599	10399	421
Lead (Pb)	ug/L	445	3.5	3.5	77	3.5	3.5	261	3.5	3.5
Magnesium (Mg)	ug/L	8895	5703	2008	7805	6468	2072	8350	6086	2040
Manganese (Mn)	ug/L	2945	2898	65	2252	2427	53	2599	2662	59
Nickel (Ni)	ug/L	125	2.4	1.5	25	0.735	1.8	75	1.6	1.7
Potassium (K)	ug/L	14535	8134	4893	11697	9447	5083	13116	8790	4988
Selenium (Se)	ug/L	18	18	18	18	18	18	18	18	18
Silver (Ag)	ug/L	3.4	0.206	0.206	0.60	0.206	0.206	2.0	0.206	0.206
Sodium (Na)	ug/L	50000	30033	15334	52985	34424	15983	51492	32229	15659
Thallium (Tl)	ug/L	8.2	8.2	8.2	8.2	8.2	8.2	8.2	8.2	8.2
Vanadium (V)	ug/L	150	2.2	4.2	38	0.494	4.1	94	1.3	4.1
Zinc (Zn)	ug/L	996	16	6.7	241	3.7	13	619	10	9.7

Table H-4. Trident Probe analytical results for area T3 (double mat).

T3 - Double Mat

Analyte	Units	Rep 1				Rep 2				Rep Average			
		Below Mats -11 in (X)	Below Mats -3.5 in (W)	Btwn Mats +0 in (V)	Above Mats +2 in (U)	Below Mats -11 in (BB)	Below Mats -3.5 in (AA)	Btwn Mats +0 in (Z)	Above Mats +2 in (Y)	Below Mats -11 in	Below Mats -3.5 in	Btwn Mats +0 in	Above Mats +2 in
Aluminum (Al)	ug/L	18813	185	195	136	9558	48	602	256	14186	117	399	196
Antimony (Sb)	ug/L	4.6	4.6	4.6	4.6	4.6	4.6	4.6	4.6	4.6	4.6	4.6	4.6
Arsenic (As)	ug/L	53	6.9	6.9	6.9	31	6.9	6.9	6.9	42	6.9	6.9	6.9
Barium (Ba)	ug/L	670	74	77	35	345	85	58	43	507	79	68	39
Beryllium (Be)	ug/L	3.9	0.013	0.013	0.013	2.1	0.013	0.108	0.027	3.0	0.013	0.06	0.02
Cadmium (Cd)	ug/L	128	0.156	0.156	0.156	25	0.156	0.822	0.156	77	0.156	0.489	0.156
Calcium (Ca)	ug/L	50000	50000	50000	36922	50000	50000	50000	48410	50000	50000	50000	42666
Chromium (Cr)	ug/L	3115	3.5	3.0	2.5	478	0.999	12	4.2	1797	2.2	7.6	3.4
Cobalt (Co)	ug/L	26	0.725	0.725	0.725	14	0.725	0.725	0.725	20	0.725	0.725	0.725
Copper (Cu)	ug/L	452	3.6	2.0	3.0	129	0.672	5.6	3.2	290	2.2	3.8	3.1
Iron (Fe)	ug/L	50000	1743	1172	348	42498	2535	2068	759	46249	2139	1620	553
Lead (Pb)	ug/L	509	3.5	3.5	3.5	163	3.5	3.5	3.5	336	3.5	3.5	3.5
Magnesium (Mg)	ug/L	10502	3476	3236	1911	8870	4575	2139	2083	9686	4026	2687	1997
Manganese (Mn)	ug/L	3356	1034	1103	73	3328	1073	361	96	3342	1053	732	85
Nickel (Ni)	ug/L	170	6.1	0.735	1.7	53	0.735	4.0	2.1	111	3.4	2.4	1.9
Potassium (K)	ug/L	16043	6409	5780	4638	13725	6937	5195	4972	14884	6673	5487	4805
Selenium (Se)	ug/L	18	18	18	18	18	18	18	18	18	18	18	18
Silver (Ag)	ug/L	2.8	0.206	0.206	0.206	1.8	0.206	0.206	0.206	2.3	0.206	0.206	0.206
Sodium (Na)	ug/L	50000	25961	21752	14659	50000	28302	16082	15635	50000	27131	18917	15147
Thallium (Tl)	ug/L	8.2	8.2	8.2	8.2	8.2	8.2	8.2	8.2	8.2	8.2	8.2	8.2
Vanadium (V)	ug/L	180	1.5	1.4	4.3	111	0.494	8.8	5.2	146	1.0	5.1	4.8
Zinc (Zn)	ug/L	1165	53	13	23	547	4.0	34	12	856	28	23	18

Table H-5. Trident Probe analytical results for area T4 (sand cap only).

T4 - Sand Cap Only

Analyte	Units	Rep 1				Rep 2				Rep Average			
		Below Sand -24 in (UU)	Below Sand -11 in (GG)	Below Sand -3.5 in (FF)	Above Sand +2 in (EE)	Below Sand -24 in (-)	Below Sand -11 in (JJ)	Below Sand -3.5 in (II)	Above Sand +2 in (HH)	Below Sand -24 in	Below Sand -11 in	Below Sand -3.5 in	Above Sand +2 in
Aluminum (Al)	ug/L	23311	499	37	205	-	4219	256	150	23311	2359	147	178
Antimony (Sb)	ug/L	27	4.6	4.6	4.6	-	4.6	4.6	4.6	27	4.6	4.6	4.6
Arsenic (As)	ug/L	89	34	42	6.9	-	16	17	6.9	89	25	30	6.9
Barium (Ba)	ug/L	1118	424	1726	39	-	189	55	38	1118	307	891	38
Beryllium (Be)	ug/L	4.2	0.08	0.013	0.013	-	0.826	0.013	0.013	4.2	0.453	0.013	0.013
Cadmium (Cd)	ug/L	475	2.0	0.982	0.156	-	18	0.156	0.156	475	10.0	0.569	0.156
Calcium (Ca)	ug/L	50000	50000	50000	41834	-	50000	50000	40383	50000	50000	50000	41109
Chromium (Cr)	ug/L	50000	17	0.319	3.5	-	446	5.4	2.0	50000	232	2.9	2.8
Cobalt (Co)	ug/L	29	2.1	0.725	0.725	-	6.9	0.725	0.725	29	4.5	0.725	0.725
Copper (Cu)	ug/L	592	5.7	0.333	4.9	-	74	2.9	1.8	592	40	1.6	3.3
Iron (Fe)	ug/L	50000	17067	14606	547	-	14040	1638	372	50000	15554	8122	460
Lead (Pb)	ug/L	675	3.5	3.5	3.5	-	91	3.5	3.5	675	47	3.5	3.5
Magnesium (Mg)	ug/L	11987	7173	6766	1978	-	6763	2463	2014	11987	6968	4614	1996
Manganese (Mn)	ug/L	2884	3292	2373	88	-	2073	503	58	2884	2683	1438	73
Nickel (Ni)	ug/L	139	5.9	0.735	2.0	-	30	2.4	0.735	139	18	1.6	1.3
Potassium (K)	ug/L	16006	10088	9451	4762	-	10569	5463	4904	16006	10329	7457	4833
Selenium (Se)	ug/L	18	18	18	18	-	18	18	18	18	18	18	18
Silver (Ag)	ug/L	4.0	0.206	0.206	0.206	-	0.944	0.206	0.206	4.0	0.575	0.206	0.206
Sodium (Na)	ug/L	50000	36063	34022	14973	-	49054	18236	15354	50000	42559	26129	15164
Thallium (Tl)	ug/L	8.2	8.2	8.2	8.2	-	8.2	8.2	8.2	8.2	8.2	8.2	8.2
Vanadium (V)	ug/L	187	6.7	1.4	4.8	-	43	4.3	4.2	187	25	2.8	4.5
Zinc (Zn)	ug/L	2700	38	5.3	15	-	247	14	7.5	2700	143	9.4	11

Table H-6. Trident Probe analytical results for area T5 (no treatment - control).

T5 - No Treatment (Control)

Analyte	Units	Rep 1				Rep Average			
		Below Sed -24 in (TT)	Below Sed -11 in (OO)	Below Sed -3.5 in (NN)	Above Sed +2 in (MM)	Below Sed -24 in	Below Sed -11 in	Below Sed -3.5 in	Above Sed +2 in
Aluminum (Al)	ug/L	41240	12555	32443	210	41240	12555	32443	210
Antimony (Sb)	ug/L	4.6	18	4.6	4.6	4.6	18	4.6	4.6
Arsenic (As)	ug/L	52	51	78	6.9	52	51	78	6.9
Barium (Ba)	ug/L	1073	822	960	38	1073	822	960	38
Beryllium (Be)	ug/L	7.3	2.7	7.0	0.013	7.3	2.7	7.0	0.013
Cadmium (Cd)	ug/L	81	386	59	0.156	81	386	59	0.156
Calcium (Ca)	ug/L	50000	50000	50000	39888	50000	50000	50000	39888
Chromium (Cr)	ug/L	812	7317	902	3.7	812	7317	902	3.7
Cobalt (Co)	ug/L	27	21	53	0.725	27	21	53	0.725
Copper (Cu)	ug/L	250	546	397	3.0	250	546	397	3.0
Iron (Fe)	ug/L	50000	50000	50000	616	50000	50000	50000	616
Lead (Pb)	ug/L	144	495	471	3.5	144	495	471	3.5
Magnesium (Mg)	ug/L	12837	11417	10936	1940	12837	11417	10936	1940
Manganese (Mn)	ug/L	50000	2517	5888	97	50000	2517	5888	97
Nickel (Ni)	ug/L	117	109	166	2.5	117	109	166	2.5
Potassium (K)	ug/L	18203	14434	19962	4780	18203	14434	19962	4780
Selenium (Se)	ug/L	18	18	18	18	18	18	18	18
Silver (Ag)	ug/L	1.1	1.1	0.69	0.206	1.1	1.1	0.69	0.206
Sodium (Na)	ug/L	50000	50000	48144	15028	50000	50000	48144	15028
Thallium (Tl)	ug/L	8.2	8.2	8.2	8.2	8.2	8.2	8.2	8.2
Vanadium (V)	ug/L	404	116	368	4.4	404	116	368	4.4
Zinc (Zn)	ug/L	468	1744	1926	7.6	468	1744	1926	7.6

Table H-7. Summary of Trident Probe analytical results for the prototype mat system.

Treatment Summary - Replicate Averages

Analyte	Units	T1 - Mat Only					T2 - Mat w/ Sand				
		Below Trtmnt -24 in	Below Trtmnt -11 in	Below Trtmnt -3.5 in	Btwn Trtmnt +0 in	Above Trtmnt +2 in	Below Trtmnt -24 in	Below Trtmnt -11 in	Below Trtmnt -3.5 in	Btwn Trtmnt +0 in	Above Trtmnt +2 in
Aluminum (Al)	ug/L	-	11594	120	-	241	-	9784	113	-	159
Antimony (Sb)	ug/L	-	4.6	4.6	-	4.6	-	4.6	4.6	-	4.6
Arsenic (As)	ug/L	-	38	6.9	-	6.9	-	38	48	-	6.9
Barium (Ba)	ug/L	-	408	50	-	42	-	440	231	-	40
Beryllium (Be)	ug/L	-	2.6	0.013	-	0.044	-	2.0	0.013	-	0.013
Cadmium (Cd)	ug/L	-	54	0.156	-	0.286	-	65	0.772	-	0.156
Calcium (Ca)	ug/L	-	50000	49979	-	46346	-	50000	50000	-	41496
Chromium (Cr)	ug/L	-	1128	2.1	-	4.2	-	1608	2.1	-	2.0
Cobalt (Co)	ug/L	-	17	0.725	-	0.725	-	14	0.725	-	0.725
Copper (Cu)	ug/L	-	212	1.6	-	2.8	-	227	1.4	-	2.0
Iron (Fe)	ug/L	-	45317	651	-	695	-	34599	10399	-	421
Lead (Pb)	ug/L	-	290	3.5	-	3.5	-	261	3.5	-	3.5
Magnesium (Mg)	ug/L	-	8156	2569	-	2050	-	8350	6086	-	2040
Manganese (Mn)	ug/L	-	2699	565	-	85	-	2599	2662	-	59
Nickel (Ni)	ug/L	-	79	1.3	-	2.1	-	75	1.6	-	1.7
Potassium (K)	ug/L	-	13776	5368	-	4933	-	13116	8790	-	4988
Selenium (Se)	ug/L	-	18	18	-	18	-	18	18	-	18
Silver (Ag)	ug/L	-	1.5	0.206	-	0.206	-	2.0	0.206	-	0.206
Sodium (Na)	ug/L	-	50000	19633	-	15499	-	51492	32229	-	15659
Thallium (Tl)	ug/L	-	8.2	8.2	-	8.2	-	8.2	8.2	-	8.2
Vanadium (V)	ug/L	-	133	1.6	-	5.2	-	94	1.3	-	4.1
Zinc (Zn)	ug/L	-	727	8.2	-	11	-	619	10	-	9.7

Table H-7. Summary of Trident Probe analytical results for the prototype mat system.

Treatment Summary - Replica

Analyte	Units	T3 - Double Mat					T4 - Sand Only				
		Below Trtmnt -24 in	Below Trtmnt -11 in	Below Trtmnt -3.5 in	Btwn Trtmnt +0 in	Above Trtmnt +2 in	Below Trtmnt -24 in	Below Trtmnt -11 in	Below Trtmnt -3.5 in	Btwn Trtmnt +0 in	Above Trtmnt +2 in
Aluminum (Al)	ug/L	-	14186	117	399	196	23311	2359	147	-	178
Antimony (Sb)	ug/L	-	4.6	4.6	4.6	4.6	27	4.6	4.6	-	4.6
Arsenic (As)	ug/L	-	42	6.9	6.9	6.9	89	25	30	-	6.9
Barium (Ba)	ug/L	-	507	79	68	39	1118	307	891	-	38
Beryllium (Be)	ug/L	-	3.0	0.013	0.06	0.02	4.2	0.453	0.013	-	0.013
Cadmium (Cd)	ug/L	-	77	0.156	0.489	0.156	475	10.0	0.569	-	0.156
Calcium (Ca)	ug/L	-	50000	50000	50000	42666	50000	50000	50000	-	41109
Chromium (Cr)	ug/L	-	1797	2.2	7.6	3.4	50000	232	2.9	-	2.8
Cobalt (Co)	ug/L	-	20	0.725	0.725	0.725	29	4.5	0.725	-	0.725
Copper (Cu)	ug/L	-	290	2.2	3.8	3.1	592	40	1.6	-	3.3
Iron (Fe)	ug/L	-	46249	2139	1620	553	50000	15554	8122	-	460
Lead (Pb)	ug/L	-	336	3.5	3.5	3.5	675	47	3.5	-	3.5
Magnesium (Mg)	ug/L	-	9686	4026	2687	1997	11987	6968	4614	-	1996
Manganese (Mn)	ug/L	-	3342	1053	732	85	2884	2683	1438	-	73
Nickel (Ni)	ug/L	-	111	3.4	2.4	1.9	139	18	1.6	-	1.3
Potassium (K)	ug/L	-	14884	6673	5487	4805	16006	10329	7457	-	4833
Selenium (Se)	ug/L	-	18	18	18	18	18	18	18	-	18
Silver (Ag)	ug/L	-	2.3	0.206	0.206	0.206	4.0	0.575	0.206	-	0.206
Sodium (Na)	ug/L	-	50000	27131	18917	15147	50000	42559	26129	-	15164
Thallium (Tl)	ug/L	-	8.2	8.2	8.2	8.2	8.2	8.2	8.2	-	8.2
Vanadium (V)	ug/L	-	146	1.0	5.1	4.8	187	25	2.8	-	4.5
Zinc (Zn)	ug/L	-	856	28	23	18	2700	143	9.4	-	11

Table H-7. Summary of Trident Probe analytical results for the prototype mat system.

Treatment Summary - Replic

Analyte	Units	T5 - No Treatment				
		Below Trtmnt -24 in	Below Trtmnt -11 in	Below Trtmnt -3.5 in	Btwn Trtmnt +0 in	Above Trtmnt +2 in
Aluminum (Al)	ug/L	41240	12555	32443	-	210
Antimony (Sb)	ug/L	4.6	18	4.6	-	4.6
Arsenic (As)	ug/L	52	51	78	-	6.9
Barium (Ba)	ug/L	1073	822	960	-	38
Beryllium (Be)	ug/L	7.3	2.7	7.0	-	0.013
Cadmium (Cd)	ug/L	81	386	59	-	0.156
Calcium (Ca)	ug/L	50000	50000	50000	-	39888
Chromium (Cr)	ug/L	812	7317	902	-	3.7
Cobalt (Co)	ug/L	27	21	53	-	0.725
Copper (Cu)	ug/L	250	546	397	-	3.0
Iron (Fe)	ug/L	50000	50000	50000	-	616
Lead (Pb)	ug/L	144	495	471	-	3.5
Magnesium (Mg)	ug/L	12837	11417	10936	-	1940
Manganese (Mn)	ug/L	50000	2517	5888	-	97
Nickel (Ni)	ug/L	117	109	166	-	2.5
Potassium (K)	ug/L	18203	14434	19962	-	4780
Selenium (Se)	ug/L	18	18	18	-	18
Silver (Ag)	ug/L	1.1	1.1	0.69	-	0.206
Sodium (Na)	ug/L	50000	50000	48144	-	15028
Thallium (Tl)	ug/L	8.2	8.2	8.2	-	8.2
Vanadium (V)	ug/L	404	116	368	-	4.4
Zinc (Zn)	ug/L	468	1744	1926	-	7.6

This page is intentionally left blank

APPENDIX I

“Prototype Mat System Sediment Core Results (October 2009)”

This page is intentionally left blank

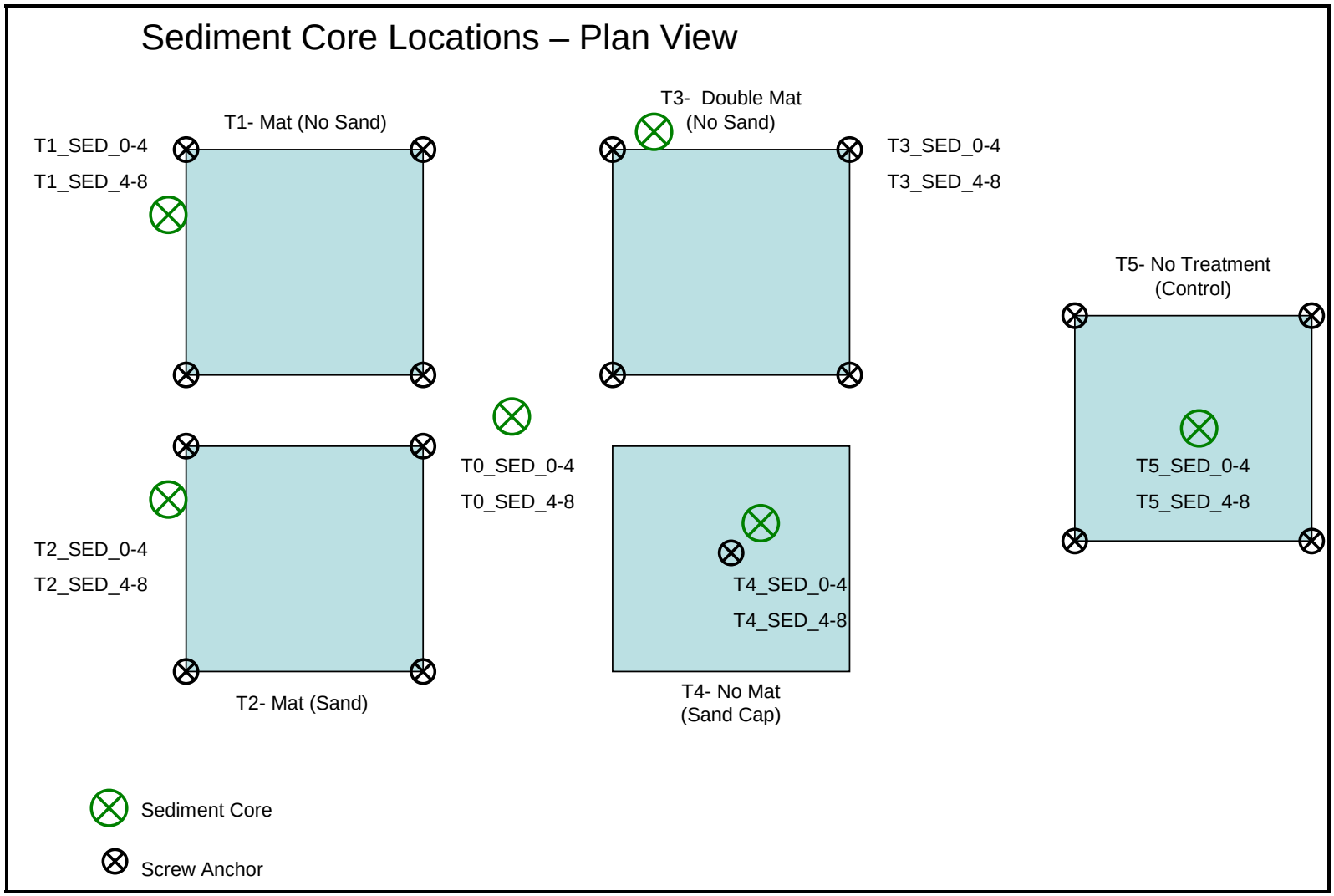

Figure I-1. Locations of sediment cores collected at the prototype mat system.

Figure I-2. Sediment core collected from treatment area T1 (mat only).

Figure I-3. Sediment core collected from treatment area T2 (mat with sand cap).

Figure I-4. Sediment core collected at treatment area T3 (double mat).

Figure I-5. Sediment core collected at treatment area T4 (sand cap only).

Figure I-6. Sediment core collected at control area T5 (no treatment).

Figure I-7. Sediment core collected at area T0 (between all treatments).

Table I-1. Raw analytical chemsitry results for sediment cores collected at the full-scale mat system.

Analyte	Units	T1 - Mat Only		T2 - Mat w/ Sand	
		Surface (0-4 in)	Subsurface (4-8 in)	Surface (0-4 in)	Subsurface (4-8 in)
Metals					
Aluminum	mg/kg	16000	14000	14000	13000
Antimony	mg/kg	N/A J5	N/A	N/A	N/A
Arsenic	mg/kg	11 E	10	10	9.5
Barium	mg/kg	120 E	120	120	110
Beryllium	mg/kg	1.2	1.1	1.2	1.1
Cadmium	mg/kg	4.7	6.2	4.7	5.9
Calcium	mg/kg	77000	79000	78000	81000
Chromium	mg/kg	190	270	180	250
Cobalt	mg/kg	9.7	8.7	9.2	8.8
Copper	mg/kg	38 E	37	36	38
Iron	mg/kg	21000 E	18000	19000	16000
Lead	mg/kg	60 E	72	63	68
Magnesium	mg/kg	2600 J5,J7	2300	2300	2200
Manganese	mg/kg	640	490	590	490
Mercury	mg/kg	0.16 J5	0.2	0.15	0.19
Nickel	mg/kg	35	32	32	32
Potassium	mg/kg	2200 J5,J7	2000	1900	1800
Selenium	mg/kg	N/A	N/A	N/A	N/A
Silver	mg/kg	3.4 E	4.5	3.7	4.1
Sodium	mg/kg	550	370	350	490
Thallium	mg/kg	N/A	N/A	N/A	N/A
Vanadium	mg/kg	41	36	39	35
Zinc	mg/kg	220 E	190	200	200

Table I-1. Raw analytical chemsitry results for sediment cores collected at the full-scale mat system.

Analyte	Units	T3 - Double Mat		T4 - Sand Only	
		Surface (0-4 in)	Subsurface (4-8 in)	Surface (0-4 in)	Subsurface (4-8 in)
Metals					
Aluminum	mg/kg	12000	12000	5100	11000
Antimony	mg/kg	N/A	N/A	N/A	N/A
Arsenic	mg/kg	9.5	9.3	4.2	8
Barium	mg/kg	110	110	57	100
Beryllium	mg/kg	1.1	1.1	N/A	N/A
Cadmium	mg/kg	4.2	5.1	1.9	4.7
Calcium	mg/kg	71000	77000	44000	73000
Chromium	mg/kg	170	210	75	190
Cobalt	mg/kg	8.8	8.7	4.2	7.4
Copper	mg/kg	34	35	16	32
Iron	mg/kg	18000	18000	8300	15000
Lead	mg/kg	56	65	25	58
Magnesium	mg/kg	2100	2000	1200	1900
Manganese	mg/kg	590	490	320	430
Mercury	mg/kg	0.16	0.19	0.07	0.17
Nickel	mg/kg	31	31	14	27
Potassium	mg/kg	1700	1700	730	1500
Selenium	mg/kg	N/A	N/A	N/A	N/A
Silver	mg/kg	2.8	3.8	1.2	3.3
Sodium	mg/kg	340	360	N/A	480
Thallium	mg/kg	N/A	N/A	N/A	N/A
Vanadium	mg/kg	35	37	16	29
Zinc	mg/kg	200	190	91	170

Table I-1. Raw analytical chemsitry results for sediment cores collected at the full-scale mat system.

Analyte	Units	T5 - No Treatment		T0 - Between Treatments	
		Surface (0-4 in)	Subsurface (4-8 in)	Surface (0-4 in)	Subsurface (4-8 in)
Metals					
Aluminum	mg/kg	13000	13000	11000	10000
Antimony	mg/kg	N/A	N/A	N/A	N/A
Arsenic	mg/kg	10	9.9	8.8	8.4
Barium	mg/kg	110	120	110	110
Beryllium	mg/kg	1.1	1.1	1	1
Cadmium	mg/kg	4.6	5.9	4.2	4.7
Calcium	mg/kg	78000	84000	74000	77000
Chromium	mg/kg	190	240	170	190
Cobalt	mg/kg	9.6	9.6	8.8	8.6
Copper	mg/kg	37	39	34	35
Iron	mg/kg	21000	20000	18000	17000
Lead	mg/kg	64	72	54	61
Magnesium	mg/kg	2100	2200	2000	1900
Manganese	mg/kg	630	550	600	500
Mercury	mg/kg	0.17	0.18	0.14	0.17
Nickel	mg/kg	33	34	30	30
Potassium	mg/kg	1800	1800	1600	1500
Selenium	mg/kg	N/A	N/A	N/A	N/A
Silver	mg/kg	3.1	4	2.9	3.3
Sodium	mg/kg	360	390	340	320
Thallium	mg/kg	N/A	N/A	N/A	N/A
Vanadium	mg/kg	39	37	33	34
Zinc	mg/kg	210	220	200	190

Table I-1. Raw analytical chemsitry results for sediment cores collected at the full-scale mat system.

Analyte	Units	T1 - Mat Only		T2 - Mat w/ Sand	
		Surface (0-4 in)	Subsurface (4-8 in)	Surface (0-4 in)	Subsurface (4-8 in)
Polycyclic Aromatic Hydrocarbons					
Naphthalene (L)	ug/kg	11 U	9.0 U	11 U	8.7 U
Biphenyl	ug/kg	11 U	9.0 U	11 U	8.7 U
Acenaphthylene (L)	ug/kg	11 U	9.0 U	11 U	8.7 U
Acenaphthene (L)	ug/kg	29	29	30	24
Fluorene (L)	ug/kg	23	25	23	18
Dibenzothiophene	ug/kg	11 U	9.0 U	11 U	8.7 U
Phenanthrene (L)	ug/kg	440	430	450	360
Anthracene (L)	ug/kg	73	51	82	67
Fluoranthene (H)	ug/kg	0.0 U	9.0 U	2300 D (10)	1800 D (10)
Pyrene (H)	ug/kg	0.0 U	9.0 U	1700 D (10)	1400 D (10)
Benzo[a]anthracene (H)	ug/kg	690	860 D (10)	1000 D (10)	840 D (10)
Chrysene (H)	ug/kg	710	930 D (10)	1100 D (10)	910 D (10)
Benzo[b]fluoranthene	ug/kg	0.0 U	890 D (10)	1100 D (10)	860 D (10)
Benzo[k]fluoranthene	ug/kg	550	880 D (10)	1100 D (10)	860 D (10)
Benzo[e]pyrene	ug/kg	0.0 U	9.0 U	1400 D (10)	1100 D (10)
Benzo[a]pyrene (H)	ug/kg	710	9.0 U	1000 D (10)	830 D (10)
Perylene	ug/kg	520	9.0 U	660	540
Indeno[1,2,3-cd]pyrene	ug/kg	570	700 D (10)	770	630
Dibenz[a,h]anthracene (H)	ug/kg	180	270	230	190
Benzo[g,h,i]perylene	ug/kg	550	640	690	560
1-Methylnaphthalene	ug/kg	11 U	9.0 U	11 U	8.7 U
2-Methylnaphthalene (L)	ug/kg	11 U	9.0 U	11 U	8.7 U
2,6-Dimethylnaphthalene	ug/kg	77	9.0 U	62	51
2,3,5-Trimethylnaphthalene	ug/kg	11 U	9.0 U	11 U	8.7 U
2-Fluorobiphenyl	ug/kg	55	59	46	46
o-Terphenyl	ug/kg	75	76	69	69
Total LMW PAHs	ug/kg	598	562	617	495
Total HMW PAHs	ug/kg	2290	2087	7330	5970
Total LMW+HMW PAHs	ug/kg	2888	2649	7947	6465

Table I-1. Raw analytical chemsitry results for sediment cores collected at the full-scale mat system.

Analyte	Units	T3 - Double Mat		T4 - Sand Only	
		Surface (0-4 in)	Subsurface (4-8 in)	Surface (0-4 in)	Subsurface (4-8 in)
Polycyclic Aromatic Hydrocarbons					
Naphthalene (L)	ug/kg	11 U	9.3 U	5.8 U	7.4 U
Biphenyl	ug/kg	11 U	9.3 U	5.8 U	7.4 U
Acenaphthylene (L)	ug/kg	11 U	9.3 U	5.8 U	7.4 U
Acenaphthene (L)	ug/kg	23	31	5.8 U	28
Fluorene (L)	ug/kg	11 U	24	5.8 U	21
Dibenzothiophene	ug/kg	11 U	9.3 U	5.8 U	7.4 U
Phenanthrene (L)	ug/kg	390	430	170	400
Anthracene (L)	ug/kg	81	80	31	73
Fluoranthene (H)	ug/kg	1500 D (10)	1700 D (10)	640 D (10)	1600 D (10)
Pyrene (H)	ug/kg	1000 D (10)	1200 D (10)	400	1100 D (10)
Benzo[a]anthracene (H)	ug/kg	710	730 D (10)	260	680 D (10)
Chrysene (H)	ug/kg	730	880 D (10)	270	780 D (10)
Benzo[b]fluoranthene	ug/kg	820	1000 D (10)	340	790 D (10)
Benzo[k]fluoranthene	ug/kg	620	590 D (10)	230	700 D (10)
Benzo[e]pyrene	ug/kg	850 D (10)	1000 D (10)	350	1000 D (10)
Benzo[a]pyrene (H)	ug/kg	680	740 D (10)	280	720 D (10)
Perylene	ug/kg	460	620	180	580
Indeno[1,2,3-cd]pyrene	ug/kg	540	700	220	590 D (10)
Dibenz[a,h]anthracene (H)	ug/kg	180	220	68	220
Benzo[g,h,i]perylene	ug/kg	450	600	190	610 D (10)
1-Methylnaphthalene	ug/kg	11 U	9.3 U	5.8 U	7.4 U
2-Methylnaphthalene (L)	ug/kg	11 U	9.3 U	5.8 U	7.4 U
2,6-Dimethylnaphthalene	ug/kg	62	67	27	57
2,3,5-Trimethylnaphthalene	ug/kg	11 U	9.3 U	5.8 U	7.4 U
2-Fluorobiphenyl	ug/kg	43	56	50	59
o-Terphenyl	ug/kg	68	78	63	90
Total LMW PAHs	ug/kg	537	593	230	544
Total HMW PAHs	ug/kg	4800	5470	1918	5100
Total LMW+HMW PAHs	ug/kg	5337	6063	2148	5644

Table I-1. Raw analytical chemsitry results for sediment cores collected at the full-scale mat system.

Analyte	Units	T5 - No Treatment		T0 - Between Treatments	
		Surface (0-4 in)	Subsurface (4-8 in)	Surface (0-4 in)	Subsurface (4-8 in)
Polycyclic Aromatic Hydrocarbons					
Naphthalene (L)	ug/kg	11 U	9.0 U	10 U	8.7 U
Biphenyl	ug/kg	11 U	9.0 U	10 U	8.7 U
Acenaphthylene (L)	ug/kg	11 U	9.0 U	10 U	8.7 U
Acenaphthene (L)	ug/kg	28	26	39	25
Fluorene (L)	ug/kg	11 U	23	31	19
Dibenzothiophene	ug/kg	11 U	9.0 U	10 U	8.7 U
Phenanthrene (L)	ug/kg	390	470	550	320
Anthracene (L)	ug/kg	70	81	110	46
Fluoranthene (H)	ug/kg	1300 D (10)	1800 D (10)	1100 D (10)	1500 D (10)
Pyrene (H)	ug/kg	960 D (10)	1200 D (10)	770 D (10)	1000 D (10)
Benzo[a]anthracene (H)	ug/kg	620	820 D (10)	490 D (10)	530
Chrysene (H)	ug/kg	660	890 D (10)	550 D (10)	540
Benzo[b]fluoranthene	ug/kg	790	860 D (10)	490 D (10)	710 D (10)
Benzo[k]fluoranthene	ug/kg	630	770 D (10)	480 D (10)	520
Benzo[e]pyrene	ug/kg	810 D (10)	1100 D (10)	710 D (10)	860 D (10)
Benzo[a]pyrene (H)	ug/kg	690	760 D (10)	480 D (10)	590
Perylene	ug/kg	460	620	600	390
Indeno[1,2,3-cd]pyrene	ug/kg	560	670	690	430
Dibenz[a,h]anthracene (H)	ug/kg	180	240	240	140
Benzo[g,h,i]perylene	ug/kg	480	630	700	390
1-Methylnaphthalene	ug/kg	11 U	9.0 U	10 U	8.7 U
2-Methylnaphthalene (L)	ug/kg	11 U	9.0 U	10 U	8.7 U
2,6-Dimethylnaphthalene	ug/kg	77	64	80	64
2,3,5-Trimethylnaphthalene	ug/kg	11 U	9.0 U	10 U	8.7 U
2-Fluorobiphenyl	ug/kg	51	51	54	61
o-Terphenyl	ug/kg	66	90	75	76
Total LMW PAHs	ug/kg	531	627	761	436
Total HMW PAHs	ug/kg	4410	5710	3630	4300
Total LMW+HMW PAHs	ug/kg	4941	6337	4391	4736

Table I-1. Raw analytical chemsitry results for sediment cores collected at the full-scale mat system.

Analyte	Units	T1 - Mat Only		T2 - Mat w/ Sand	
		Surface (0-4 in)	Subsurface (4-8 in)	Surface (0-4 in)	Subsurface (4-8 in)
Alkyl Aromatic Hydrocarbons					
C1-Naphthalenes	ug/kg	N/A	9.0 U	11 U	8.7 U
C2-Naphthalenes	ug/kg	11 U	9.0 U	11 U	8.7 U
C3-Naphthalenes	ug/kg	22	28	34	27
C4-Naphthalenes	ug/kg	11 U	9.0 U	11 U	8.7 U
C1-Fluorenes	ug/kg	11 U	18	36	29
C2-Fluorenes	ug/kg	11 U	30	11 U	8.7 U
C3-Fluorenes	ug/kg	11 U	19	43	35
C1-Phenanthrenes/anthracenes	ug/kg	260	4100 D (10)	270	220
C2-Phenanthrenes/anthracenes	ug/kg	220	260	310	260
C3-Phenanthrenes/anthracenes	ug/kg	81	130	170	130
C4-Phenanthrenes/anthracenes	ug/kg	11 U	36	11 U	8.7 U
C1-Fluoranthenes/pyrenes	ug/kg	570	610	830	670
C1-Chrysenes/benzo[a]anthracenes	ug/kg	530	1500	810	650
C2-Chrysenes/benzo[a]anthracenes	ug/kg	170	91	350	280
C3-Chrysenes/benzo[a]anthracenes	ug/kg	110	74	190	150
C4-chrysenes/benzo[a]anthracenes	ug/kg	N/A	62	27	22
Total Organic Carbon					
TOC Rep 1	%	2.9	2.8	3.3	2.3
TOC Rep 2	%	2.7	2.8	2.8	2.3
Average TOC	%	2.8	2.8	3.0	2.3

U = Concentration below detection limit; 1/2 detection limit used instead.

D = Analyte value taken from dilution in parenthesis.

E = Serial dilution RPD above limit of 10%

J = Estimated; MS/MSD recovery below limit.

N/A = Data not available.

Table I-1. Raw analytical chemsitry results for sediment cores collected at the full-scale mat system.

Analyte	Units	T3 - Double Mat		T4 - Sand Only	
		Surface (0-4 in)	Subsurface (4-8 in)	Surface (0-4 in)	Subsurface (4-8 in)
Alkyl Aromatic Hydrocarbons					
C1-Naphthalenes	ug/kg	11 U	9.3 U	5.8 U	7.4 U
C2-Naphthalenes	ug/kg	11 U	9.3 U	5.8 U	7.4 U
C3-Naphthalenes	ug/kg	24	26	5.8 U	29
C4-Naphthalenes	ug/kg	11 U	9.3 U	5.8 U	7.4 U
C1-Fluorenes	ug/kg	27	41	12	37
C2-Fluorenes	ug/kg	11 U	9.3 U	15	7.4 U
C3-Fluorenes	ug/kg	28	29	5.8 U	43
C1-Phenanthrenes/anthracenes	ug/kg	250	220	110	290
C2-Phenanthrenes/anthracenes	ug/kg	220	270	87	310
C3-Phenanthrenes/anthracenes	ug/kg	94	120	38	120
C4-Phenanthrenes/anthracenes	ug/kg	11 U	9.3 U	5.8 U	7.4 U
C1-Fluoranthenes/pyrenes	ug/kg	590	720	220	690
C1-Chrysenes/benzo[a]anthracenes	ug/kg	580	740	220	620
C2-Chrysenes/benzo[a]anthracenes	ug/kg	160	290	56	280
C3-Chrysenes/benzo[a]anthracenes	ug/kg	120	91	36	150
C4-chrysenes/benzo[a]anthracenes	ug/kg	11 U	26	5.8 U	29
Total Organic Carbon					
TOC Rep 1	%	2.6	2.9	1.5	2.6
TOC Rep 2	%	3.0	3.1	1.5	2.5
Average TOC	%	2.8	3.0	1.5	2.6

Table I-1. Raw analytical chemsitry results for sediment cores collected at the full-scale mat system.

Analyte	Units	T5 - No Treatment		T0 - Between Treatments	
		Surface (0-4 in)	Subsurface (4-8 in)	Surface (0-4 in)	Subsurface (4-8 in)
Alkyl Aromatic Hydrocarbons					
C1-Naphthalenes	ug/kg	11 U	9.0 U	10 U	8.7 U
C2-Naphthalenes	ug/kg	11 U	9.0 U	10 U	8.7 U
C3-Naphthalenes	ug/kg	26	23	22	22
C4-Naphthalenes	ug/kg	11 U	9.0 U	10 U	8.7 U
C1-Fluorenes	ug/kg	30	35	68	29
C2-Fluorenes	ug/kg	30	40	42	23
C3-Fluorenes	ug/kg	27	38	50	28
C1-Phenanthrenes/anthracenes	ug/kg	250	290	310	210
C2-Phenanthrenes/anthracenes	ug/kg	210	310	360	190
C3-Phenanthrenes/anthracenes	ug/kg	88	140	130	75
C4-Phenanthrenes/anthracenes	ug/kg	11 U	40	10 U	8.7 U
C1-Fluoranthenes/pyrenes	ug/kg	540	770	840	450
C1-Chrysenes/benzo[a]anthracenes	ug/kg	520	710	750	450
C2-Chrysenes/benzo[a]anthracenes	ug/kg	220	280	290	140
C3-Chrysenes/benzo[a]anthracenes	ug/kg	100	210	210	100
C4-chrysenes/benzo[a]anthracenes	ug/kg	23	34	29	28
Total Organic Carbon					
TOC Rep 1	%	3.2	2.9	2.3	2.4
TOC Rep 2	%	2.9	2.4	2.2	2.6
Average TOC	%	3.0	2.7	2.3	2.5

ATTACHMENT 1

"Evaluation of Reactive Cap Sorbents for In Situ Remediation of Contaminated Sediments"

Bhawana Sharma

Submitted to the University of New Hampshire

September 2008

This page is intentionally left blank

EVALUATION OF REACTIVE CAP SORBENTS FOR *in-situ* REMEDIATION OF CONTAMINATED SEDIMENTS

BY

BHAWANA SHARMA
M.S., University of Rajasthan, 2001
M.Tech., Indian Institute of Technology, Kanpur, 2004

DISSERTATION

Submitted to the University of New Hampshire
In Partial Fulfillment of
the Requirements for the Degree of

Doctor of Philosophy
In
Civil Engineering

September 2008

This dissertation has been examined and approved.

_____

Dissertation Director, Kevin H. Gardner,
Associate Professor of Civil Engineering

_____

Jeffrey S. Melton,
Research Assistant Professor of Civil Engineering

_____

M. Robin Collins,
Professor of Civil Engineering

_____

Philip J. Ramsey,
Adjunct and Visiting Faculty of Statistics

_____

Jenna Jambeck,
Research Assistant Professor of Civil Engineering

DEDICATION

In memory of

Shri Bihari Lal Sharma

(December 21, 1918 – February 29, 2008)

This dissertation is dedicated to my Grand pa. You will always be my inspiration and will always be remembered.

ACKNOWLEDGMENT

“A teacher affects eternity; he can never tell where his influence stops”

Henry Adams

This is how my PhD career and my life have been influenced by great teachings of my thesis advisor Dr. Kevin H. Gardner. I thank you for being such a great advisor and providing me immense support and continuous encouragement during my research life. I am really thankful to you for giving me an opportunity to work on this project that I really enjoyed. Word of thanks to Strategic Environmental Research and Development Program (SERDP) for funding my research.

I thank my committee members who have always helped me in my research work with their valuable suggestions. I thank Dr. Jeffrey Melton for his erudite discussions that helped me with my queries about project details and helping me with my experimental set up. I thank Dr. Jenna Jambeck for her help during my PhD career and her great involvement in shaping my career afterwards. I thank Dr. M. Robin Collins for his timely and valuable suggestions. I thank Dr. Phil Ramsey for his great advises on statistical element of my research.

Thanks to Dr. James Malley and Dr. Nancy Kinner for allowing me to use instruments in their labs. It was great to work in the vicinity of Environmental Research Group (ERG) with great professors, staff and students. Thanks to all Professors from whom I learned not only in class but through general interactions as well. Thanks to Dr. Thomas Ballestero for providing me help in developing my interest in water resources. I am really thankful to the entire member of Environmental Research Group for being a part of my life and helping me grow in so many ways. My special thanks to Maddy for being so generous and helpful.

Thanks to Deana, Scott, Sandy, Ashley, Don, Rafael and Hud for their great help in accomplishing my lab. work. Thanks to Emese for being such a great friend with whom I have shared all the stressful as well as joyful moments of my PhD life. All the great moments that I have shared with Ketaki at work or otherwise deserve mention. Thanks to Birdie, Irina, Linda, Carolina, Alison, Vaso, Whitney, Shannon and Cyndy for being great friends and making our working niche really enjoyable.

Words cannot express how grateful I am for having a great family which is the biggest asset and support of my life. I thank my *mummy* Mrs. Pushpa Sharma and *papa* Dr. Satya Prakash Sharma for being a constant source of my inspiration and a great support in my life. Thanks to *mummyji* for her prayers and blessings that helped me a lot. I am thankful to my parents-in-law Shri S. N. Singh and Smt. Krishna Devi for their encouragement and great understanding. My *bhaiya* Dr. Rajesh Sharma and Dr. Sanjeev Sharma, *bhabhi* Dr. Chanchal Sharma and Dr. Prerna Sharma, *didi* Dr. Nikita Sharma, *jiju* Dr. Harish Sharma have always encouraged to me work hard and excel in life. Getting a glance of my little sweethearts (Gungun, Pihu, Ishaan, Rish and of course new addition Tiya) was always relaxing in stressful days. Thanks to all my family members for their love and support.

I thank my husband Shrawan Singh who plays a vital role in every aspect of my life. I thank you for being so loving and caring during all good and bad times and for encouraging me to overcome every obstacle in life to come out with flying colors.

Last but not least I would like to thank all my great friends from UNH and IITK for being such a great support and making my life enjoyable. All the convivial moments we have shared left a deep impression in my life with indelible memories.

TABLE OF CONTENTS

LIST OF TABLES

LIST OF FIGURES

ABSTRACT

EVALUATION OF REACTIVE CAP SORBENTS FOR *in-situ* REMEDIATION OF CONTAMINATED SEDIMENTS

By

Bhawana Sharma

University of New Hampshire, September 2008

Contaminated sediments can be treated using in-situ treatment methods that aim to either degrade or sequester contaminants, reducing their bioavailability. The main purpose of this research was to develop and evaluate a reactive capping mat that can be used for in-situ remediation of contaminated sediments. This study investigated the interferences caused by humic acid on the adsorption of co-planar and non-co-planar polychlorinated biphenyls (PCBs) including 2-chlorobiphenyl, 2, 2', 5, 5'-tetrachlorobiphenyl, 3, 3', 4, 4'- tetrachlorobiphenyl, 2, 2', 4, 4', 5, 5'- hexachlorobiphenyl and 3, 3', 4, 4', 5, 5'- hexachlorobiphenyl and polycyclic aromatic hydrocarbons (PAHs) including naphthalene, phenanthrene and pyrene on two types of sorbents being evaluated for use in a mat: activated carbon and organoclays. Several kinetic and isotherm studies have been conducted using several formulations of activated carbons and organoclays as sorbents to treat individual PCB congeners and PAHs. The results

showed that preloading of sorbents with humic acid, and simultaneous adsorption of humic acid and contaminant, significantly reduced the adsorption capacity for all selected PCB congeners and PAHs. Experiments conducted without preloading of sorbent surfaces demonstrated that desorption upon subsequent spiking with humic acid, to simulate the long-term exposure to porewater that contains high humic acid concentrations, was not pronounced and varied with co-planarity of PCBs and number of rings of PAHs. Also, humic acids were found to interfere to a much greater extent with adsorption to activated carbon than with organoclay formulations evaluated in this work.

Experiments were also conducted to determine the effects of Suwannee River fulvic acid (FA), humic acid (HA) and natural organic matter (NOM) obtained from International Humic Substance Society (IHSS) and pore water isolated from sediment of the Hudson River and the Passaic River to understand the influence of different fractions of dissolve organic carbon that will be present in real site conditions. The results demonstrated enhancement in adsorption of PCB and PAH in presence of fulvic acid on both type of sorbents including activated carbon and organoclay but the effect of humic acid and NOM varied with contaminant. The humic acid had more reducing effect on PCB adsorption as compared to NOM and NOM had more reducing effects on PAH adsorption.

A structural analysis using Scanning Electron Microscopy for activated carbon and X-Ray Diffractometry, Atomic Force Microscopy and Scanning Electron Microscopy for organoclay were conducted to observe differences caused by humic acid on the surfaces of the sorbents. BET surface area analysis has also been conducted to determine the surface area of activated carbon and organoclays. Thermo gravimetric analysis of organoclays was done to determine the % organic content which increases the hydrophobicity and thereby adsorption capacity of organoclays. This research indicate that organic acids, which are quite concentrated in sediment porewater, have a significant impact on the efficacy of reactive cap components and are an essential factor in the design and ultimate performance of this type of in-situ sediment management approach.

CHAPTER 1

INTRODUCTION

Objectives

In the1990s, the extent and severity of sediment contamination was brought into consideration and the USEPA planned to take actions to reduce the risk posed by contaminated sediments to fish as well as to humans and wildlife. In 1997, the EPA estimated about 10% of sediments (top 5 cm that represents biologically active zone) under national water surfaces to be contaminated with toxic chemicals (USEPA, 1997). This estimate fostered the requirement to set up goals and objectives for remediation of contaminated sediments. According to the EPA the assessment and subsequent actions needed to be based on “sound science” and “site specifications” (USEPA, 1998). Based on the hierarchical approach for the evaluation of treatment methods, first of all source control should be assessed followed by in-situ remediation such as natural recovery or capping technology and finally ex-situ treatment methods such as dredging (wet) or dry excavation (Cushing, 1999).

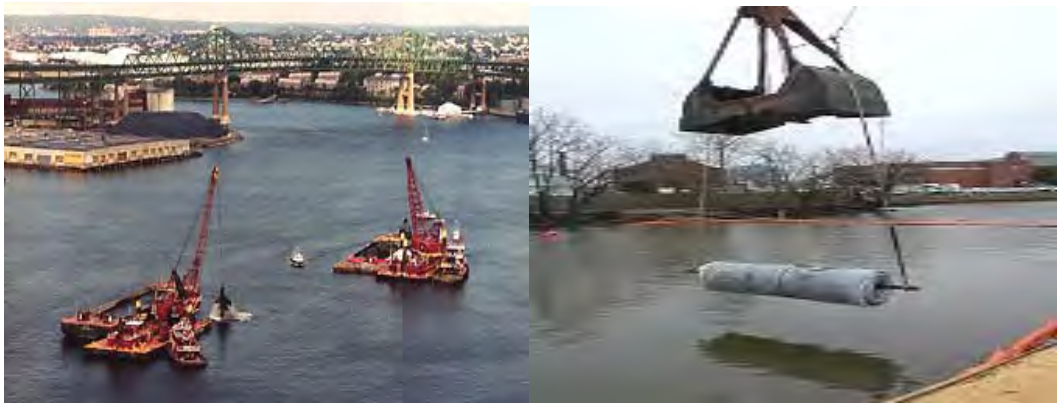

Dredging Reactive Core Mat

In dredging technology, sediments are removed from the given site followed by treatment and disposal. Contaminated sediments should not be removed from a site if it is more harmful compared with leaving them in place or using alternative management strategies such as in-situ remediation using capping technology.

Figure 1.1 shows the concentration profile in Cottonwood Bay (Mountain Creek Lake, Dallas, Texas, 1994-97) the field site selected for the deployment of the reactive capping mats deployed in this study. In this figure it is shown that the concentration of contaminants first increases with the increase in depth and then decreases with further increase in depth. Also, it was also observed in the M2.40 core that the concentration of cesium-137 was highest around 45 cm, for DDT the first peak was observed from 30 – 50 cm and second DDT peak was observed around 65 cm and for Dieldrin first peak around 50 cm and second around 65 cm. In the MCL-4 core the concentration of DDT was found to be high from 20-80 cm depth.

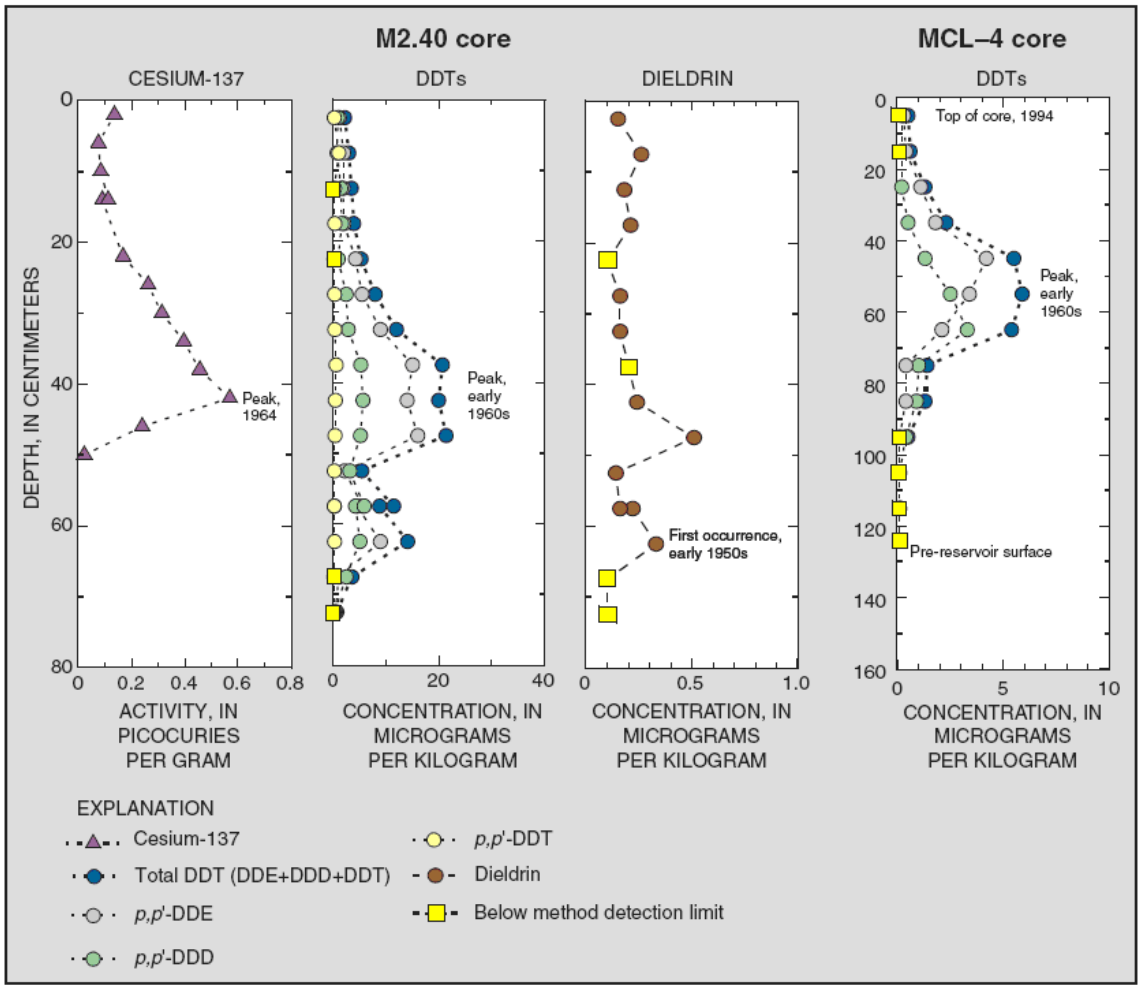

Figure 1.1 Contaminant Concentration Profile in Study Field Site

(Source: USGS, Water-Resource Investigations Report 03-4082)

This shows that the concentration profile of different contaminants can vary with depth. Therefore, dredging of the top layer might expose the higher concentrations of the contaminant present at that depth in the sediments. These types of sites should be either dredged deep enough to remove high concentrations of all contaminants of concern, which can be very expensive, or alternative technology should be used such as reactive capping technology.

The contaminant flux from sediments to overlying water is governed by various processes including bioturbation, mechanical scouring, uprooting of macrophytes in addition to the pore water flux by diffusion and advection. Therefore, the goal of this research is focused on development of a reactive capping mat, containing sorbent amendment mixture, which can be deployed over a contaminated sediment bed for sequestration of contaminants as well as isolation of contaminated sediments from the overlying water body. The action of a reactive cap is to reduce or eliminate mechanisms responsible for contaminant transport (bioturbation, scouring, uprooting) and to provide reactivity to reduce contaminant flux associated with diffusive and advective mechanisms.

The in-situ remediation process for contaminated sediments requires understanding of the influence of high concentrations of background natural organic acids, like humic acids, that influence the efficacy of treatment and fate of organic contaminants. To get a better understanding of the entirety of the process and improved quality of the reactive capping mat, six sigma analyses which includes DMAIC (i.e. Define, Measure, Improve, Analyze and Control), was used as a helpful tool. When the project was at the definition phase the SIPOC model (i.e. Suppliers, Inputs, Process, Outputs, and Customers) was developed to achieve the goal of defining quality, characteristics and identification of factors or variables which may impact the process (Figure 1.2). During experimentation the random factors such as presence of natural organic matter were considered to be a major factor of the design in order to estimate the actual performance of the sorbents that could be observed after deployment of the reactive caps in the real site conditions.

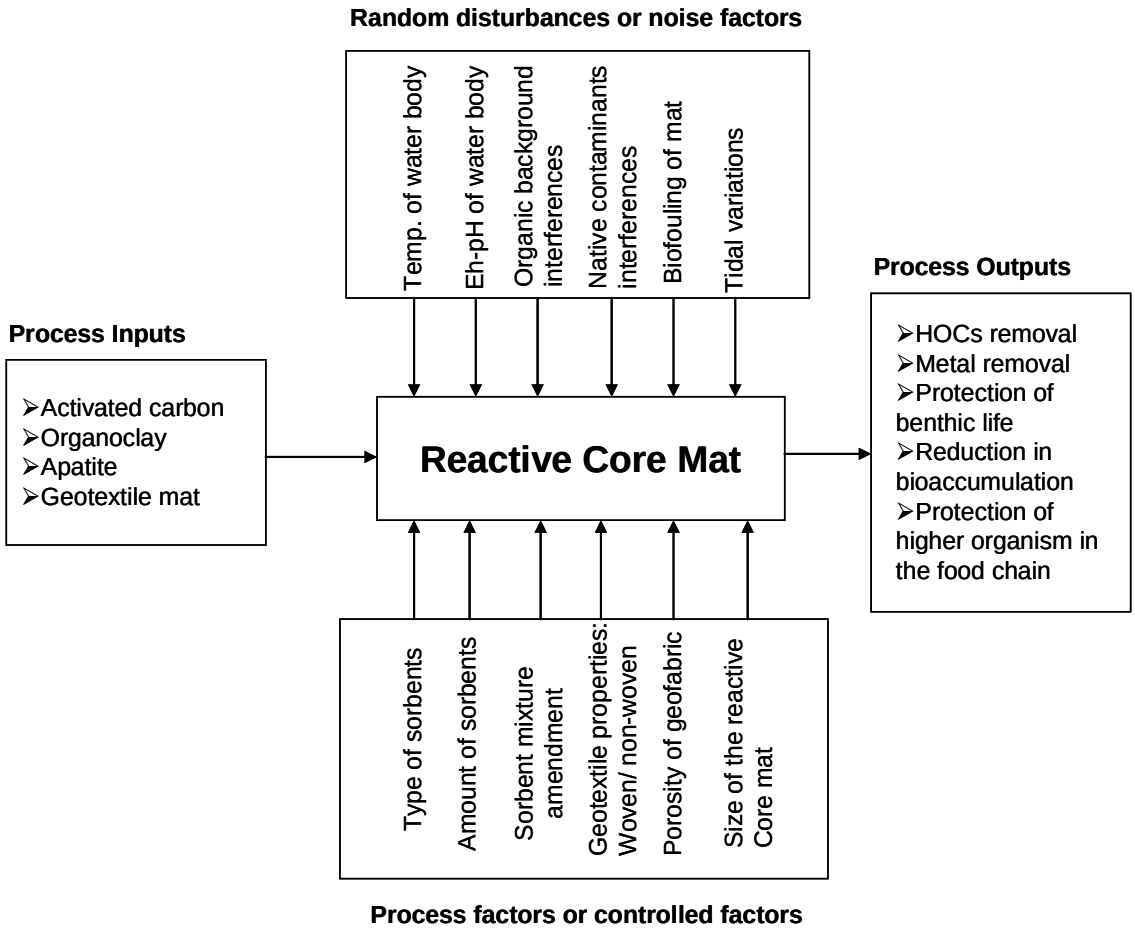

Figure 1.2: SIPOC Model for Reactive Core Mat

In this study the performance of different formulations of activated carbon and organoclay were evaluated in the presence and absence of natural organic matter for sequestration of persistent hydrophobic organic contaminants. The effect of natural organic matter, which is ubiquitous in nature and is important in governing the fate and transport of hydrophobic organic contaminants, on the efficacy of the sorbents was immensely studied in the form of various fractions such as humic acid and fulvic acid and natural organic matter (as a whole) in the colloidal and non-colloidal form.

Dissertation Organization

This dissertation has been organized in the form of a compilation of papers. The effect of humic acid on the performance of activated carbon for PCB sequestration (chapter 2), different formulations of organoclay on PCB sequestration (chapter 3), PAH adsorption on activated carbon and organoclay (chapter 4) and the effect of different fractions of natural organic matter on activated carbon and organoclay (chapter 5) have been discussed in detail.

Chapter 2 focuses on the interferences caused by humic acid on the adsorption capacity of coconut shell and coal based activated carbon for co-planar and non-coplanar PCBs. In this chapter results have been produced from kinetics studies to demonstrate the effects of humic acid on the adsorption kinetics of PCBs and isotherm studies to show the effect on the adsorption capacity of activated carbon due to preloading with humic acid. Scanning electron micrographs were produced to show the differences in the porous structure of coal based and coconut shell based activated carbon and to show the pore blockage effect caused by preloading activated carbon with high concentrations of humic acid.

Findings: The results showed that preloading of activated carbon with humic acid significantly reduced the adsorption capacity for all selected PCB congeners. Experiments conducted without preloading of activated carbon demonstrated that desorption upon subsequent spiking with humic acid was not found to be statistically

significant and varied with co-planarity of PCBs. Slight desorption was found for non-coplanar tetrachlorobiphenyl as compared to the mono-chloro-congener and the co-planar tetra-and hexa-congeners which did not show any observable desorption. Desorption was found to be observable in the case of non-coplanar hexachlorobiphenyl but the phenomenon was found to be insignificant statistically.

Chapter 3 discusses the performance of three different formulations of organoclays, which have different base clay and organic cations, for adsorption of co-planar and non-coplanar PCBs in the presence and absence of humic acid. This chapter was focused on adsorption of organic contaminants on organoclay and the effect of humic acid on the adsorption of PCBs onto organoclay. Chapter 3 demonstrates the kinetics of adsorption of PCB on two different formulations of organoclay and isotherm studies to show effect of humic acid on adsorption capacity of organoclays for PCB congeners.

Findings: Studies showed a significant reduction in the performance of organoclays due to preloading with high concentrations of humic acid for all selected PCB congeners. The reduction in sorption affinity due to preloading ranged from 46 % to 96% depending on the congener and the composition of organoclay. Desorption studies that were conducted to simulate the long-term exposure to high humic acid concentrations in the sediment pore water (in typical site conditions) also showed effects that were less pronounced compared to preloading effect and varied with the composition of organoclay and PCB congener. No desorption was noticed in case of 2-

chlorobiphenyl adsorption on CETCO and Biomin Inc. organoclay but significant desorption was observed in the case of Polymer Ventures organoclay that had different base clay as compared to CETCO and Biomin Inc. that had same base clays. Desorption effect on adsorption of 2, 2', 5, 5'-tPCB was found to be similar for CETCO and Polymer Ventures organoclay. The statistical analysis done to evaluate the performance of CETCO organoclay for tetra- and hexa- chlorobiphenyl showed preloading effect to be more pronounced in case of co-planar congeners compared to their non-coplanar isomers and desorption effects were not substantial in any case.

Chapter 4 compares the performance of activated carbon and organoclay for PAH adsorption in the presence and absence of humic acid. This chapter illustrates the effect of humic acid on adsorption of small ringed PAHs that are readily transported in sediment pore water. Chapter 4 explains the effect of humic acid on the kinetics of PAH adsorption on activated carbon and organoclay and shows the effect of preloading the sorbent with high concentration of humic acid on selected PAHs.

Findings: The performance of bare organoclay was found to be better for naphthalene and pyrene compared to activated carbon. The preloading effect was found to be significant for both the sorbents for phenanthrene and pyrene though there was negligible effect on naphthalene adsorption. Desorption effects were not found to be significant for naphthalene for both the sorbents but it was statistically significant for phenanthrene and pyrene adsorption on organoclay. This shows that if these sorbents are exposed to very high concentrations of natural organics such as 1g L^{-1} (as in the

case of this study) then it can affect the performance of the reactive core mat. Also, long term exposure of organoclay to natural organic matter might affect the performance by desorption depending on the sorption pattern of target compounds and their partition coefficients for humic acid.

Chapter 5 illustrates the effect of different fractions of natural organic matter (that plays a significant role in fate and transport of hydrophobic organic contaminants) on the adsorption of PCB and PAH on activated carbon and organoclay. This chapter also demonstrates the effect of colloidal and non-colloidal pore water on the performance of sorbents. Chapter 5 also discusses the effect of natural organic matter present in Cottonwood Bay, Texas (study field site) on the performance of the sorbent mixture that was present in the reactive core mats deployed in the field for six months.

Findings: Results showed a significant effect of Aldrich humic acid on 2, 2', 5', 5'-tetrachlorobiphenyl adsorption on both the sorbents. There was a slight enhancement of the adsorption capacity of organoclay for 2, 2', 5', 5'-tetrachlorobiphenyl in the presence of Suwannee River fulvic acid but no effect was observed for activated carbon. There was no effect of Suwannee River NOM on 2, 2', 5', 5'-tetrachlorobiphenyl adsorption on both the sorbents. In the case of phenanthrene adsorption, no effect of any fraction of natural organics was noticed for organoclay. In the case of activated carbon the effects of Aldrich humic acid, Suwannee River humic acid, Suwannee River fulvic acid and Suwannee River NOM were found to have similar reducing effect. A significant effect of Hudson River porewater (high aquatic humics) was observed on the performance of

both the sorbents for both the contaminants, although only a small effect was found for the Passaic porewater (which was low in humics).

References

B. S. Cushing. State of Current Contaminated Sediment Management Practices. Applied Environmental Management, Inc. Fall 1999.

USEPA. September 1997. The Incidence and Severity of Sediment Contamination in Surface Waters of the U. S. Vol. 1. EPA 823-R-97-006.

USEPA. April 1998. EPA's Contaminated Sediment Management Strategy. EPA 823-R-98-001.

USGS, Water –Resources Investigations Report 03-4082. Chemical Quality of Water, Sediment, and Fish in Mountain Creek Lake, Dallas, Texas, 1994-97. In cooperation with the Southern Divison Naval Facilities Engineering Command.

CHAPTER 2

EVALUATION OF COCONUT SHELL ACTIVATED CARBON AS A REACTIVE CAP SORBENT FOR SEQUESTRATION OF PCBS IN PRESENCE OF HUMIC ACID

Abstract

This study investigated the interferences caused by humic acid on the adsorption of co-planar and non-coplanar polychlorinated biphenyls on activated carbon. Kinetic and equilibrium studies were conducted using activated carbon as a sorbent for individual PCB congeners including 2-chlorobiphenyl, 2, 2', 5, 5'-tetrachlorobiphenyl, 3, 3', 4, 4'- tetrachlorobiphenyl, 2, 2', 4, 4', 5, 5'- hexachlorobiphenyl and 3, 3', 4, 4', 5, 5'-hexachlorobiphenyl (BZ 1, 52, 77, 153 and 169 respectively) in the presence and absence of humic acid. The results showed that preloading of activated carbon with humic acid significantly reduced the adsorption capacity for all selected PCB congeners. Experiments conducted without preloading of activated carbon demonstrated that desorption upon subsequent spiking with humic acid (simulating long-term exposure to pore water that contains high humic acid concentrations) was not found to be statistically significant and varied with co-planarity of PCBs. Analysis of surface properties using Scanning Electron Microscopy demonstrated observable pore blockage caused by humic acid on the surfaces of the activated carbon.

Introduction

Sediments that are contaminated with hydrophobic organic contaminants (HOCs) that are toxic, bioaccumulative and persistent are of major concern both from the perspective of human health and the health of aquatic ecosystems. These sediments can be treated using ex-situ treatment methods following environmental dredging or in-situ treatment methods such as monitored natural attenuation and capping technologies. To date monitored natural attenuation and sand caps have been used as an in-situ treatment method and now reactive capping is gaining attention for its potential effective use. Reactive capping can be accomplished both by mixing reactive material into a sediment bed (Zimmerman et al. 2004; Werner et al. 2005) or by binding the reactive material into a geotextile and deploying it over a contaminated sediment bed (Mc Donough et al. 2008). There is substantial information available for adsorption of aromatic compounds (Zimmerman et al. 2004; Walters et al. 1984; and Cornelissen et al. 2006) and chlorinated compounds (Sotelo et al. 2002; and Karanfil et al. 1999) on activated carbon. Zimmerman et al. (2004) have shown a 92% reduction in polychlorinated biphenyl (PCBs) aqueous concentration and 84% reduction in polycyclic aromatic hydrocarbon (PAHs) aqueous concentrations and up to 89% reduction in PCB flux to overlying water with addition of 3.4 wt. % of activated carbon to sediments. Cornelissen et al. (2006) have shown significant reduction in pore water concentrations of PAH by addition of 2 wt. % of activated carbon to sediments. The studies have also shown an increase in effectiveness with the increase in contact time from one month to six months (Werner et al. 2005; and Millward et al. 2005).

Significant research has investigated activated carbon as a sorbent for organic pollutants but the remediation process for contaminated sediments requires understanding the influence of high concentrations of background natural organic acids, like humic acids, that influence the efficacy of treatment and fate of organic contaminants. The adsorption efficiency of activated carbon can be reduced in the presence of ubiquitous humic and other substances that occur naturally (Pirbazari et al. 1989; and Matsui et al. 2003). The objective of this study was to evaluate the adsorption capacity of coconut shell activated carbon for PCBs in the presence of humic acid in order to understand its potential use in reactive capping for in-situ remediation of contaminated sediments. In the present study, several kinetic and isotherm experiments have been conducted to determine the sorption behavior of these contaminants on activated carbon in the presence of humic acid, which can occur at very high concentrations in sediment pore water. The concentration of dissolved organic carbon (DOC) in sediment pore water has been reported to be as high as 200 -2500 μM (0.6 g/L to 7.5 g/L) for the upper ~ 20-30 cm of sediments (Burgie et al. 2001).

The reduction in adsorption capacity of activated carbon by humic substances can be attributed to two mechanisms: pore blockage caused by humic acid or competition of HOCs with humic acid for adsorption sites. The adsorption system in the presence of humic acid is complex and consists of freely dissolved HOCs and humic acid, dissolved HOC- humic acid complexes, adsorbed HOC and humic acid, and adsorbed complexes. To control the competition between humic acid molecules and HOCs for adsorption sites, understanding the relationship between the optimum pore

size region for adsorption of target HOC and pore size region for DOC adsorption is important (Karanfil et al. 2006). Large humic molecules cannot enter the micropore network and can block access to the large internal pore structure of activated carbon (Pignatello et al. 2006). For effective adsorption of HOCs the size distribution of micropores in activated carbon should be about twice the kinetic diameter of the contaminant, which has been reported to reduce the pore blockage caused by DOC (Quinlivan et al. 2005). The molecular weight of DOC also plays an important role as microporous carbon can be affected by low molecular weight DOC and mesoporous carbon by high molecular weight DOC (Li et al. 2003; and Newcombe et al. 2002). Therefore, the pore blockage effect of DOC has been reported to be reduced by using activated carbon with large micropores and mesopores (Li et al. 2003). Besides pore structure, surface chemistry can also significantly affect the adsorption of organic compounds on activated carbon. Some studies showed that hydrophobic carbon surfaces, which are present with coconut-shell based activated carbon or coal based activated carbon, can be more effective for adsorption of organic compounds compared to hydrophilic carbon surfaces, like some of the chemically modified activated carbon, due to interference of water adsorption with HOC adsorption (Quinlivan et al. 2005; Newcombe et al. 2002; and Newcombe et al. 1997). Taking this into consideration, coconut shell activated carbon was selected for this study. McDonough et al. (2008) have studied the performance of coal based activated carbon in the presence of simulated pore water at very low concentration of dissolved organic matter. In this research coconut shell activated carbon, which is more porous than coal based activated carbon, has been evaluated at very high concentrations of humic acid.

Contaminant flux from sediments to overlying waters has been ascribed to various processes including bioturbation by epibenthic and infaunal organisms, mechanical scouring, uprooting of macrophytes in addition to the pore water flux by diffusion and advection (Butcher et al. 2004). Therefore, the goal of this research is focused on development of reactive capping mat (containing a sorbent amendment mixture) or in general a thin layer cap that can be deployed over a contaminated sediment bed for sequestration of contaminants as well as isolation of contaminated sediments from the overlying water body. The action of a reactive cap is to reduce or eliminate mechanisms responsible for contaminant transport (bioturbation, scouring, uprooting) and to provide reactivity to reduce contaminant flux associated with diffusive and advective mechanisms. The fate and transport of contaminants in this type of system requires knowledge of how complexation with and interference from natural organic acids influences partitioning to the solid surface of a sorbent that can be used in the reactive cap. Therefore, it is important to evaluate the performance of a sorbent in the presence of natural organic acids such as humic acid that can be found in high concentrations under typical site conditions.

Materials and Methods

Chemicals

Ultra high purity chemicals and GC-grade solvents including hexane, methanol and acetone were used for all experiments and were obtained from Fischer Scientific

(Agawam, MA, USA). The five PCB congeners were selected for this research on the basis of number of chlorine atoms and co-planarity to represent a wide range of hydrophobicity. The PCB congeners used were 2-chlorobiphenyl, 2, 2', 5, 5'-tetrachlorobiphenyl, 3, 3', 4, 4'-tetrachlorobiphenyl, 2, 2', 4, 4', 5, 5'-hexachlorobiphenyl and 3, 3', 4, 4', 5, 5'-hexachlorobiphenyl (BZ 1, 52, 77, 153 and 169 respectively). 2, 4, 6-trichlorobiphenyl (BZ 30) was used as an internal standard because of no overlapping with peaks of other selected PCB congeners and 2, 4, 5, 6-tetrachloro-m-xylene (TCMX) was used as surrogate standard. These PCB congeners and TCMX were purchased (Ultra scientific, North Kingstown, RI, USA) either in neat form or dissolved in hexane. Humic acid sodium salt (Sigma-Aldrich, St. Louis, MO, USA) was used as a representative natural organic matter. Aldrich humic acid was used in this study in order to attain worst case analysis by obtaining very high concentration of humic acid solution which could not be achieved otherwise by using sediment pore water. Sodium azide (EMD Chemicals Inc., San Diego, CA, USA) was used as bactericide to avoid biological growth in the experiments and sodium sulfate anhydrous (Fisher Scientific, Morris Plains, NJ, USA) was used in preparatory step for GC analysis of samples.

Activated carbon: The sorbent used in this study was coconut shell activated carbon, OLC 12 x 40 (Calgon Carbon Corporation, Pittsburg, PA, USA). This material was selected because it is widely used for removal of trace organic compounds and it has high microporosity (Figure 2.1). Table 2.1 shows the properties of the material. Coal based Calgon F400 was also used for some of the studies to compare the performance of these two activated carbons.

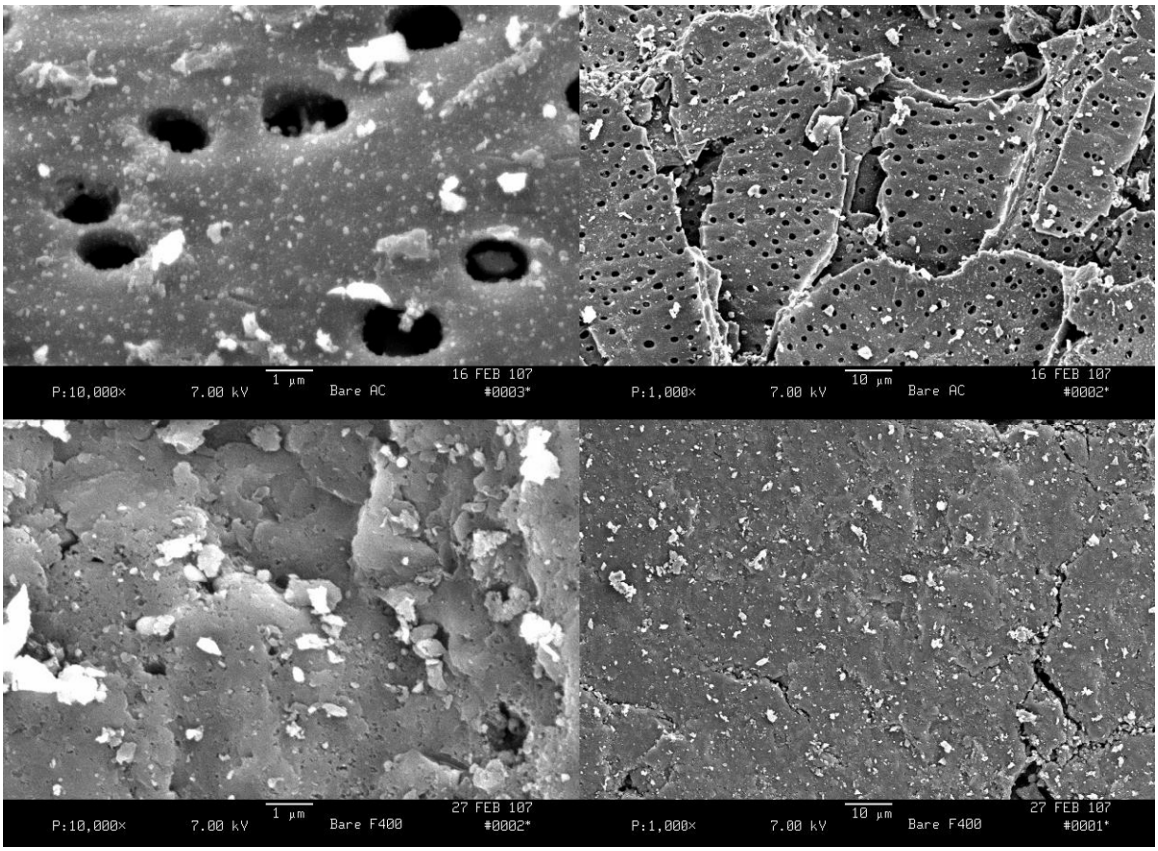

Figure 2.1: Comparative SEM image for coconut shell AC (top two images) and coal based AC (bottom two images).

Table 2.1 shows the properties of the material. Coal based Calgon F400 was also used for some of the studies to compare the performance of these two activated carbons.

Table2.1. Typical Properties of Coconut Shell Activated Carbon:

Particle size [ASTM D-2862]*	12 x 40 US Mesh
Ash Content (Base Material)[ASTM D-2866]*	3% w/w
Bulk Density [ASTM D-2854]*	0.50 g/ cm^3
Iodine Number [BSC 90-032]*	1050 mg/g
BET Surface Area of Bare AC	872.05 m^2/ g

Batch Experiments

Batch experimentation method was used to determine the kinetics of PCB adsorption on activated carbon and to determine the adsorption capacity of activated carbon for PCBs in the presence and absence of humic acid. All the experiments were conducted in separate batches of 125 ml deionized (DI) water using acetone as a carrier solvent for PCB congeners. Acetone was used to prepare the stock solution because of a lack of significant interference of acetone on PCB adsorption on activated carbon (Pirbazari et al. 1981). For quality assurance purpose duplicates were prepared in all the experiments (error bars in each plot represent standard deviation between duplicates) and controls were used to account for any kind of PCB loss other than adsorption on activated carbon. The effect of humic acid was determined in two ways: Preloading effect and Desorption effect.

Preloading of Activated Carbon: The preloading of activated carbon for kinetics and isotherm experiments was done with 1g/L of humic acid solution prepared in de-ionized (DI) water. A 10% sodium azide was added to the humic acid stock solution to avoid biological growth. All the samples were equilibrated for 48 hours at 150 rpm on a rotary shaker to ensure thorough mixing. Preloaded samples having activated carbon

preloaded with humic acid along with the humic acid solution were used as such for further experimentation to mimic site conditions with very high concentrations of humic acid.

SEM sample preparation: Scanning electron micrographs were obtained for bare activated carbon and activated carbon preloaded with humic acid. The preloaded samples were prepared with 0.1 and 1 g/L humic acid solution containing 10% sodium azide. In case of the lower loading of humic acid no effect was found as compared to the higher (1g/L) loading of humic acid (Figure 2.2). This also confirmed that in case of 1 g/L humic acid pores are blocked not due to sodium azide but due to high concentration of humic acid (Figure 2.2).

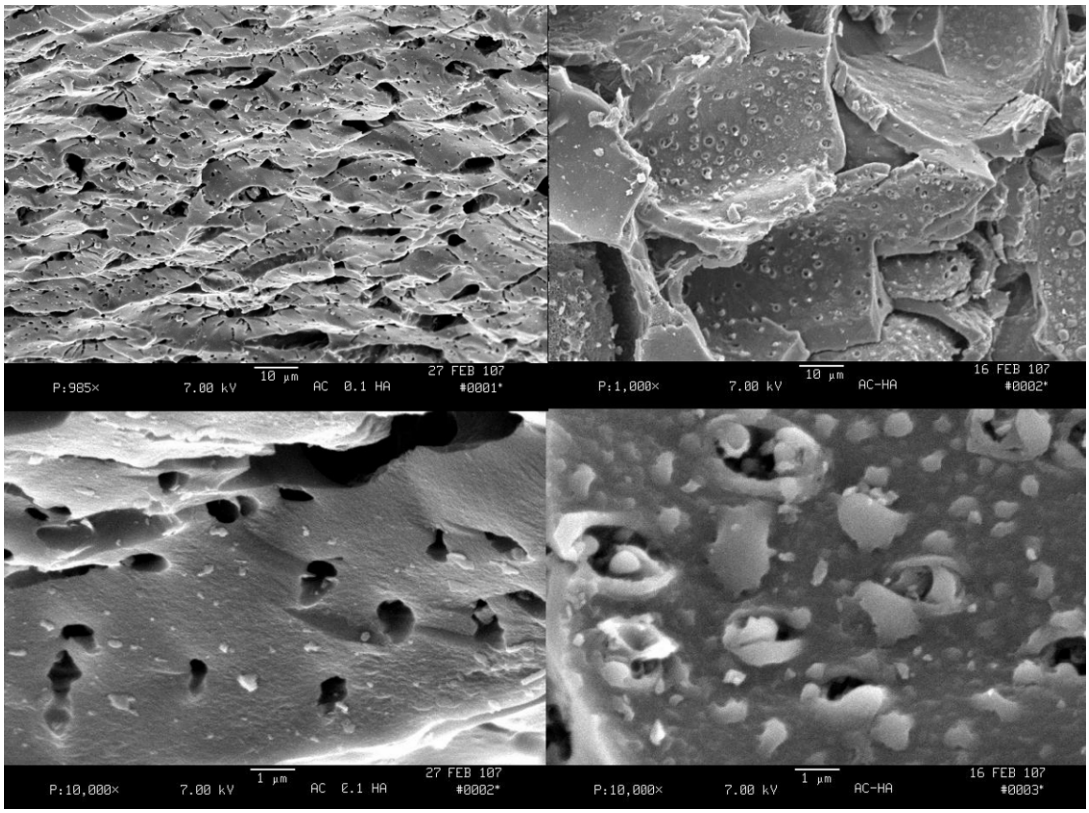

Figure 2.2: Comparative SEM image for coconut shell AC preloaded with 0.1 g/L humic acid solution (upper and bottom left) and coconut shell AC preloaded with 1 g/L (upper and bottom right).

Kinetic Studies

Batch experiments were conducted for the duration of one month to evaluate the kinetics of adsorption of PCBs and to determine the effect of humic acid on adsorption process. PCBs selected for this study were 2-chlorobiphenyl, 2, 2', 5, 5'-tetrachlorobiphenyl and 2, 2', 4, 4', 5, 5'-hexachlorobiphenyl. The effect of humic acid was determined by preloading of activated carbon as mentioned in the previous section. Separate batches were prepared for samples with bare activated carbon in DI water and preloaded activated carbon which remained in humic acid solution as used for preloading. Experiments for all three PCB congeners were conducted separately to avoid interferences in the performance of activated carbon due to competition among congeners for adsorption sites. The concentrations of PCBs used were different for each congener: 6 mg L^{-1} for 2-chlorobiphenyl, 5 mg L^{-1} for 2, 2', 5, 5'-tetrachlorobiphneyl and 0.08 mg L^{-1} for 2, 2', 4, 4', 5, 5'-hexachlorobiphenyl. The samples were continuously mixed on a rotary shaker at 150 rpm for the duration of the experiment.

Isotherm Studies

Separate batches were prepared at different loading rates of all PCB congeners with bare activated carbon (table 2.2) and activated carbon preloaded with humic acid to obtain adsorption isotherms. The preloading time and procedure was the same as performed for the kinetics studies (above). As mentioned earlier in preloaded samples humic acid was present in two forms (i) humic acid adsorbed on activated carbon due to

preloading (ii) humic acid in dissolved form in DI water matrix. These studies were conducted for the equilibration time of 72 hours which represents a reasonable approximation of equilibrium as shown by the kinetics experiments for bare activated carbon. The preliminary studies were also conducted to evaluate and compare the performance of coal based activated carbon, Calgon F400, for adsorption of 2, 2', 5, 5'-tetrachlorobiphenyl in the presence of humic acid.

Table 2.2: Solubility limit, Log Octanol-water partition coefficients and Log K_{DOC} values of selected PCB congeners

PCB congener	† Solubility Limit in water (ppm)	† Log K_{OW}	Log K_{DOC}	Isotherm Studies Concentration Range (mg/L)
2-cbp	4.0	4.7	3.63*	0.008 – 6.108
2,2',5,5'- tPCB	0.26	5.9	4.6 **	0.008 – 0.400
3,3',4,4'- tPCB	0.26	5.9	-	0.008 – 0.800
2,2',4,4',5,5'- hPCB	0.038	6.7	5.3**	0.032 – 0.800
3,3',4,4',5,5'- hPCB	0.038	6.7	-	0.024 – 0.800

* Butcher et al. 2004; ** Poerschmann et al. 1999; † Erickson, 1997

Desorption studies: These studies were conducted to simulate the long term exposure of reactive cap sorbents to natural organic matter that can occur in site conditions. Once sampling was completed at 72 hours, humic acid was added to the bare activated carbon samples to obtain the same concentration of humic acid as in preloaded samples to determine the extent of desorption for PCBs already adsorbed on activated carbon. These samples were again equilibrated for 72 hours of mixing prior to the sampling.

Determination of HA Effects

Batch experiments were conducted to obtain the adsorption behavior of 2-chlorobiphenyl, 2, 2', 5, 5'-tetrachlorobiphenyl and 2, 2', 4, 4', 5, 5'-hexachlorobiphenyl at different loadings of humic acid. These experiments were conducted at fixed loading of PCB with varied loading rates of humic acid with respect to activated carbon. The activated carbon was preloaded with different loading rates of humic acid for 48 hours prior to the spiking of PCB. These experiments were also allowed to equilibrate for 72 hours. Experiments were also conducted to determine the effect of different loadings of humic acid on coal based activated carbon for adsorption of 2, 2', 5, 5'-tetrachlorobiphenyl.

Sample Extraction and Analysis

The supernatant of each sample was extracted into hexane using TCMX as a surrogate standard by vial liquid-liquid extraction method. Twenty ml of sample and ten ml of hexane was taken into a 40 ml vial. The vials were sealed with Teflon® lined screw caps and shaken vigorously for 30 seconds three times at intervals of 30 seconds

each. The vials were then stored for at least for 24 hours at 4˚ C. The surrogate recoveries by using this extraction method were found to be in the range of 70-130%. The extracts were then passed through sodium sulfate to remove any chemically bound water prior to running on GC columns. The GC vials were prepared using these filtered solvents and an internal standard.

Gas Chromatography/ Mass Spectrometry Analysis

Internal standard method was used for analysis of all the samples. All extracts were analyzed using a Varian CP3800 Gas Chromatograph (GC)/ Saturn 2200 Ion Trap Mass Spectrometer (MS) with a CP8400 Auto Sampler. The GC column used was a DB-5 type capillary column (Varian Factor Four VF-5ms), 30 m long, 0.25 mm ID and 0.5 µm thick. The ion-trap was operated in selected scan mode (MS/MS) for each PCB congener. The column oven temperature was programmed at 40˚ C with hold time of 2 min followed by a temperature ramp up to 184˚ C at the rate of 12˚ C/ min. and then to 280˚ C at the rate of 4˚ C/ min with the final held time of 2 minutes.

Results and discussions

Kinetic studies:

Experiments were conducted to obtain the equilibration time required for adsorption of PCBs on activated carbon. Figure 2.3 shows the kinetics of 2-chlorobiphenyl, 2, 2', 5, 5'-tetrachlorobiphenyl and 2, 2', 4, 4', 5, 5'-hexachlorobiphenyl adsorption on bare activated carbon and activated carbon preloaded with humic acid.

The kinetics of 2-chlorobiphenyl (Figure 2.3-A) indicated equilibrium was reached at approximately 72 hours for adsorption on bare activated carbon. The equilibrium for preloaded activated carbon was found to be delayed and the impact of preloading was found to be decreased with time. Smaller compounds like 2-chlorobiphenyl that have higher diffusivity (Schaffner et al., 1997) can more rapidly enter micropores which sieve the larger humic acid molecules. Equilibrium was reached at approximately 72 hours for 2, 2', 5, 5'-tetrachlorobiphenyl and 50 hours for 2, 2', 4, 4', 5, 5'-hexachlorobiphenyl adsorption on bare activated carbon and activated carbon preloaded with humic acid (Fig. 2.3 B-C). The preloading effect was significant for tetrachlorobiphenyl and was found to gradually decrease with time but remained significant for the duration of the experiment.

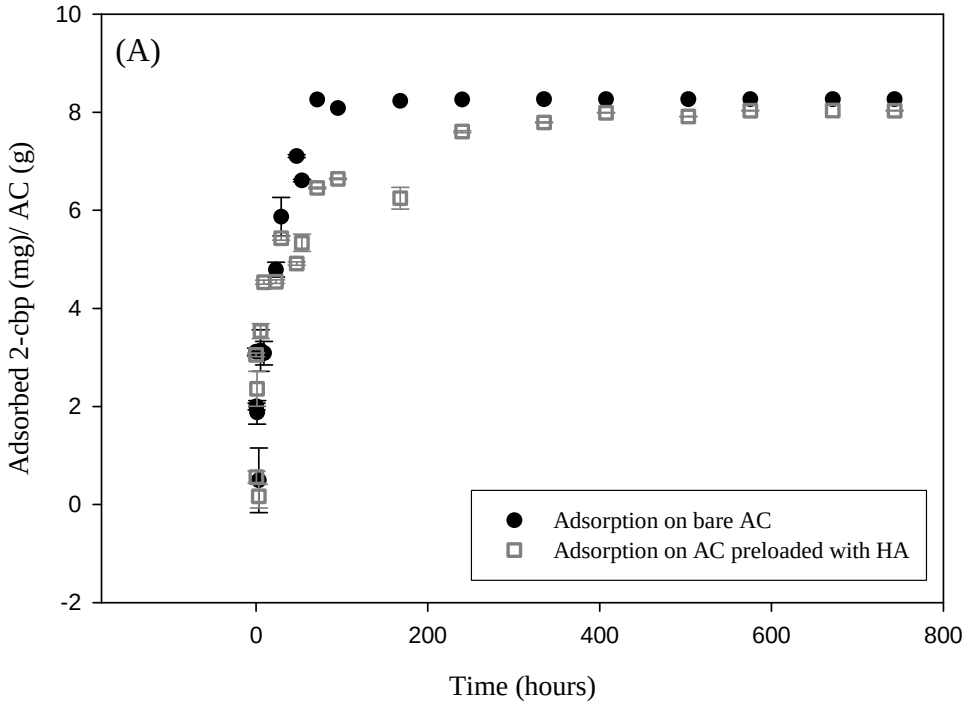

Figure 2.3 A: Kinetics of adsorption of PCB congeners on coconut shell AC in presence and absence of HA: 2-chlorobiphenyl

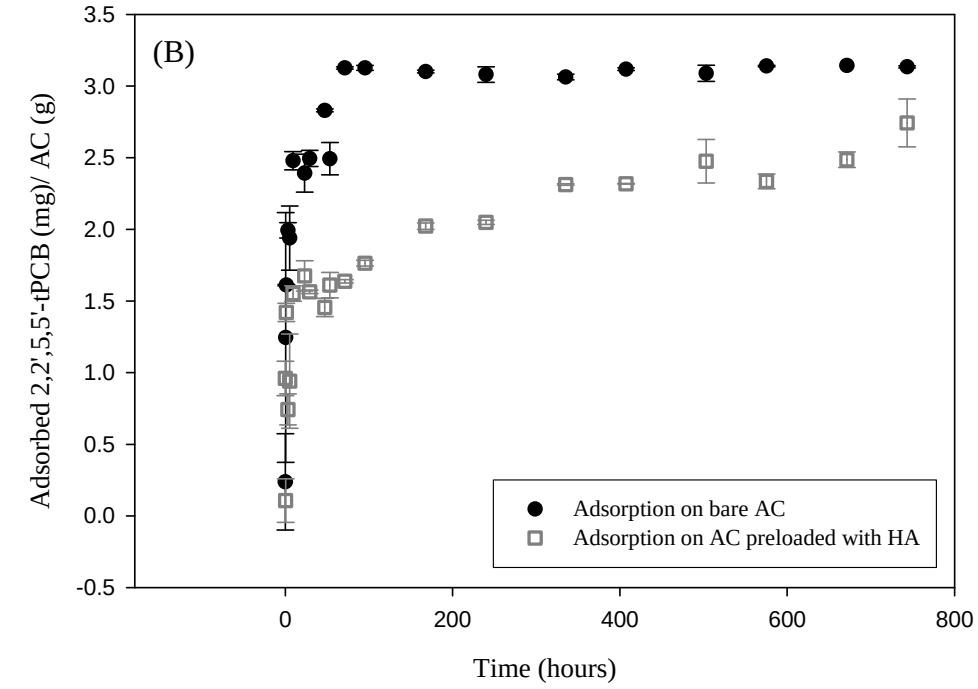

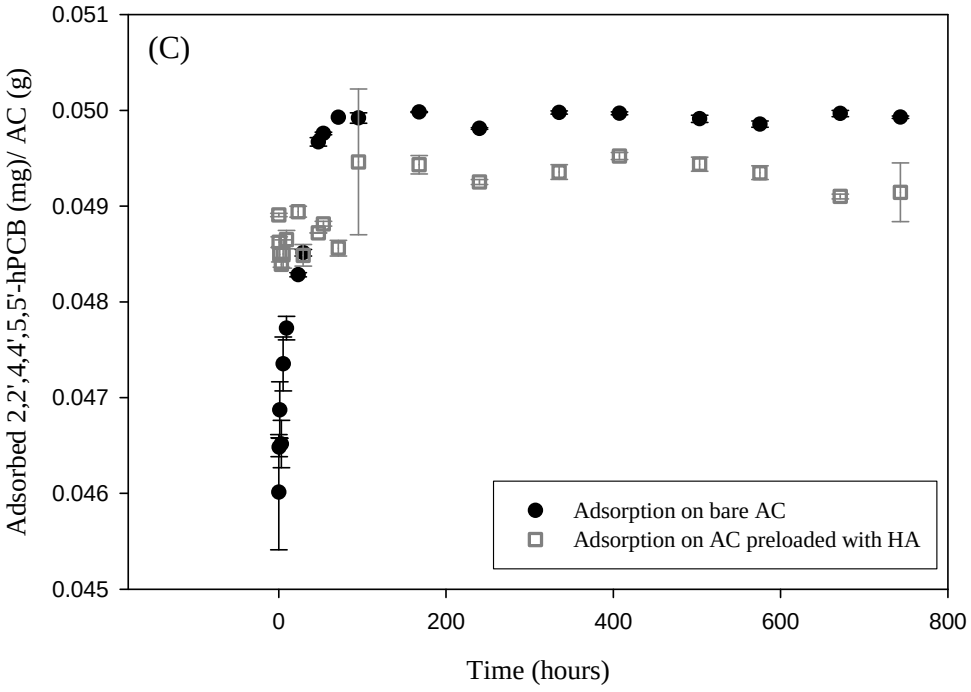

Figure 2.3: Kinetics of adsorption of PCB congeners on coconut shell AC in presence and absence of HA: (B) 2, 2', 5, 5'-tetrachlorobiphenyl and (C) 2, 2', 4, 4', 5, 5'-hexachlorobiphenyl.

The effect of preloading on hexachlorobiphenyl was found to be very low (due to very low concentration of hexa-chloro biphenyl used in the experiment) and remained consistent with time. This study showed that preloading of activated carbon with humic acid appeared to increase the time required to reach equilibrium. These retardation effects could be due to the pore blockage effect and more complexation of highly chlorinated congeners to humic acid as compared to mono-chloro-congener. Greater complexation with humic acid is expected from more highly chlorinated congeners as shown by K_{DOC} complexation constants reported in table 2.2, which increase with the increase in hydrophobicity of the compound (Pirbazari et al. 1989).

Kinetics was important to characterize not only for the conduct of equilibrium isotherm experiments but also for the application of a thin reactive cap; studies conducted at Anacostia River for demonstration of specific discharge and tidal heights showed the average specific discharge of sediment pore water to the overlying water column of 5 cm/ day (Draft data report, 2006). This underscores the significance of understanding adsorption equilibration times, as residence time in a thin layer cap may be significantly less that 24 hours.

Isotherm studies:

Isotherm studies were conducted to determine the adsorption capacity of activated carbon in the presence and absence of humic acid. The selection of PCBs for this study was designed to obtain a range in the degree of chlorination and co-planarity

to obtain an idea of sorption behavior for a range of PCB congeners. The Freundlich model was used to obtain the isotherms using the equation:

$$q_e = K_F\ (C_e^{\ (1/n)})$$

where, q_e is the amount of adsorbed (mg g^{-1}), K_F is the Freundlich Isotherm constant, C_e is the equilibrium concentration (mg L^{-1}) and *1/n* is the dimensionless Freundlich exponent. Figure 2.4 shows data and Freundlich adsorption isotherms for all above mentioned PCB congeners in the presence and absence of humic acid. The humic acid interferences were obtained as: (i) preloading effect of humic acid on activated carbon and (ii) desorption effect in which activated carbon was spiked with humic acid after PCB adsorption to simulate the long term exposure to pore water humic acid concentrations.

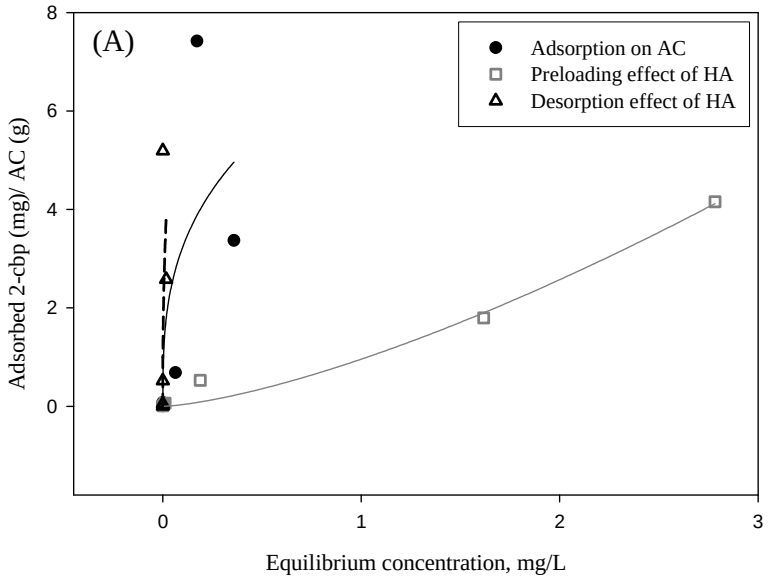

Figure2.4 A. Freundlich Adsorption Isotherms for selected PCB congeners with bare AC and preloading and desorption effect of HA: 2-chlorobiphenyl

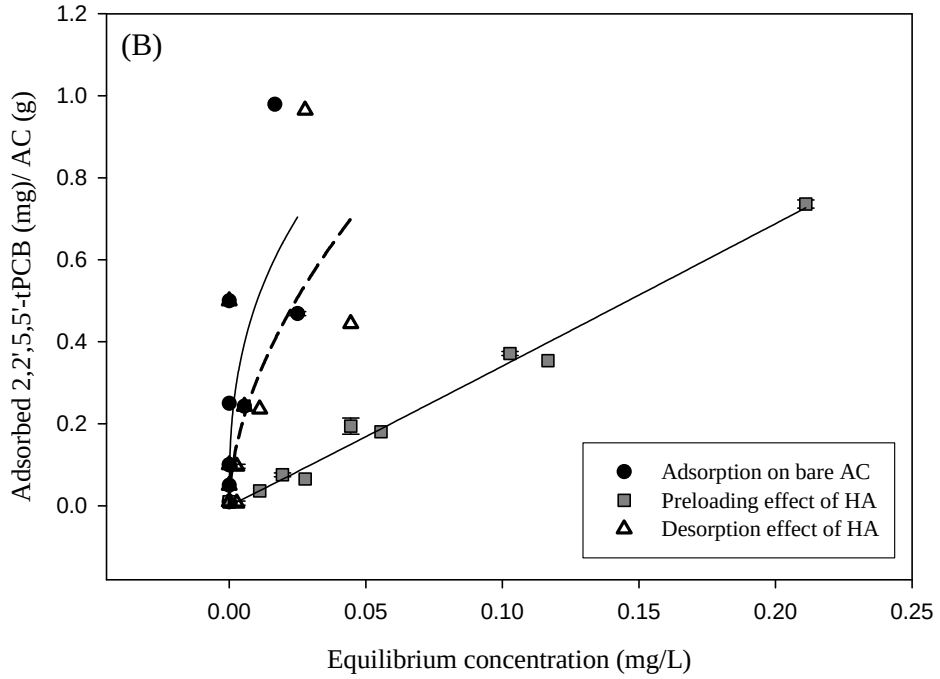

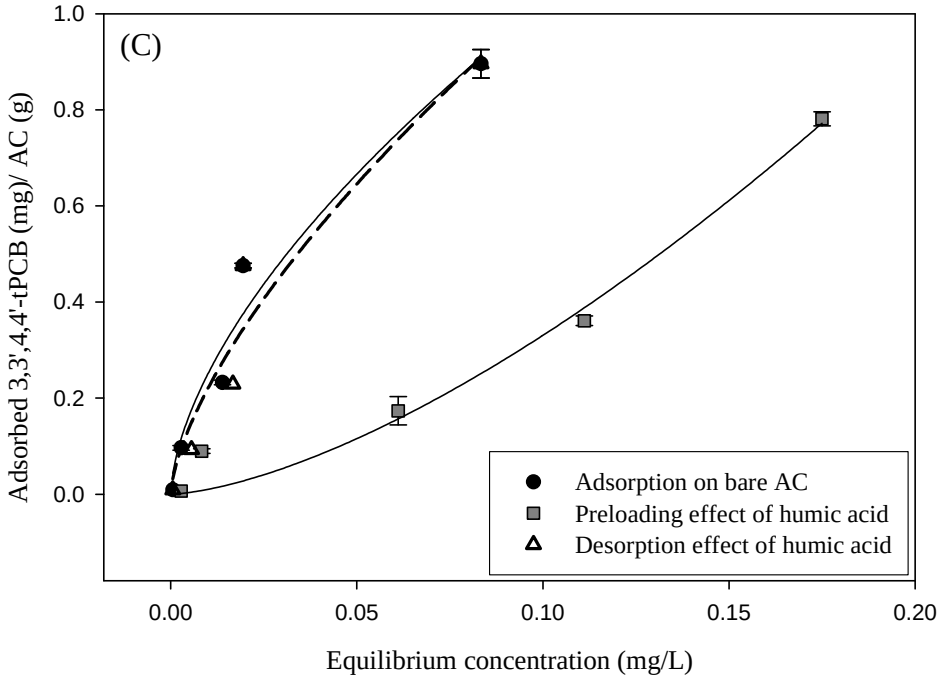

Figure 2.4 B - C. Freundlich Adsorption Isotherms for selected PCB congeners with bare AC and preloading and desorption effect of HA: (B) 2, 2', 5, 5'-tPCB (C) 3, 3', 4, 4'-tPCB

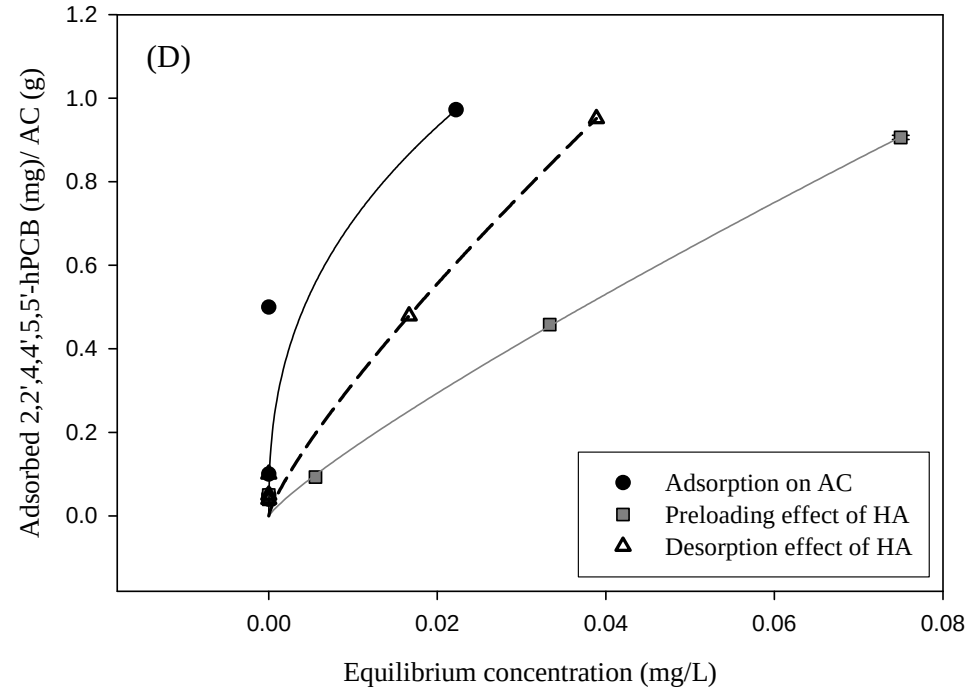

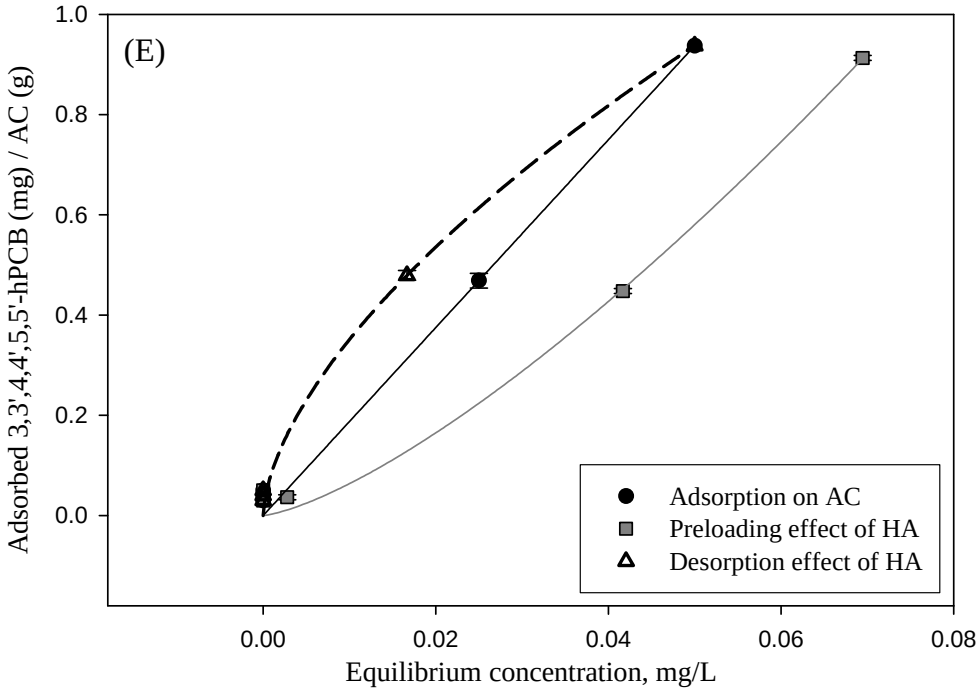

Figure 2.4 D - E. Freundlich Adsorption Isotherms for selected PCB congeners with bare AC and preloading and desorption effect of HA: (D) 2,2',4,4',5,5'-hPCB (E) 3,3',4,4',5,5'-hPCB

In all of the isotherms, a significant reduction in adsorption capacity of activated carbon was found in the presence of humic acid as shown in figure 2.4. This reduction may be due to the pore blockage effect caused by the preloading of activated carbon with humic acid molecules prior to the entry of HOCs into the pores (Pignatello et al. 2006; and Li et al. 2003) and the hydrophobic partitioning of HOCs to dissolved humic acid (Poerschmann et al. 1999). When activated carbon is preloaded with humic acid, the larger humic acid molecules that cannot enter the micro- and mesopores block the pore channels by clump formations (Pignatello et al. 2006). These types of formations due to preloading of activated carbon by humic acid molecules were observable in scanning electron micrographs (SEM) as shown in figure 2.2. The studies conducted to evaluate desorption effects of humic acid showed that once PCBs were adsorbed on activated carbon there is negligible desorption that varied with the co-planarity of the congener. Slight desorption was found for non-coplanar tetrachlorobiphenyl (Figure 2.4 B) as compared to the mono-chloro-congener (Figure 2.4A) and the co-planar tetra-and hexa-congeners (Fig. 2.4 C & E) which did not show any observable desorption. Desorption was found to be observable in the case of non-coplanar hexachlorobiphenyl in figure 2.4 D but the phenomenon was found to be insignificant statistically (Figure 2.5). This slight variation in desorption effect between co-planar and non-coplanar PCBs can be explained by the steric hindrances in the non-coplanar configuration which decrease sorption affinity (Cornelissen et al. 2004).

The data obtained from the isotherm studies was analyzed statistically using software JMP® 7. A model was developed on the Fit model platform to evaluate the

performance of activated carbon for tetra- and hexa-chlorobiphenyls. The model 1 was developed based on the hypothesis that performance of coconut shell activated carbon varies with the degree of chlorination of the congener and the co-planarity of the congeners in the presence of humic acid (table 2.3). The three factors considered in this model were: PCB congener, loading rate and treatment (preloading/desorption effects). The full factorial design was developed with these three factors along with the quadratic term of loading rate.

Table 2.3: Specifications for Statistical Model 1

Model 1 specification
PCB congener
Loading Rate
Treatment on AC
PCB congener*Treatment on AC
PCB congener* Loading Rate
Treatment on AC* Loading Rate
PCB congener*Treatment on AC* Loading Rate
Loading I* Loading Rate
Loading I* Loading Rate *PCB congener
Loading I* Loading Rate *Treatment on AC
Loading I* Loading Rate *Treatment on AC*PCB congener

According to analysis of variance (ANOVA) the p-value was < 0.0001, therefore, the model is significant and there is a significant effect of the number of chlorine atoms and co-planarity of congeners on adsorption capacity of coconut shell activated carbon in presence of humic acid (details in additional information). F-test was performed on each term (main effects and interaction terms) of the model to determine the significance of the factors based on the p-value < 0.05. The Student's t was obtained to compare the adsorption affinities of all PCB congeners at $\alpha = 0.05$ and showed higher adsorption for hexa-chlorobiphenyls compared to tetra-chlorobiphenyls (table 2.4).

Table 2.4: LS Means Differences Student's t

Alpha = 0.050 t = 2.0639			
PCB congener	Levels *		Least Square Means
2,2',4,4',5,5'- hPCB	A		0.2934
3,3',4,4', 5, 5'- hPCB	B		0.2837
2, 2', 5, 5' - tPCB		C	0.2654
3,3',4,4'-tPCB		C	0.2653

* Levels not connected by same letter are significantly different

The least square means of all PCB congeners were plotted against the treatment effects (preloading/ desorption effect) and it was found that the desorption effect of humic acid was not significant in the case of co-planar (tetra- and hexa- congeners) and both hexa-chloro-congeners. The preloading effect of humic acid was found to be significant for all the congeners (Figure 2.5).

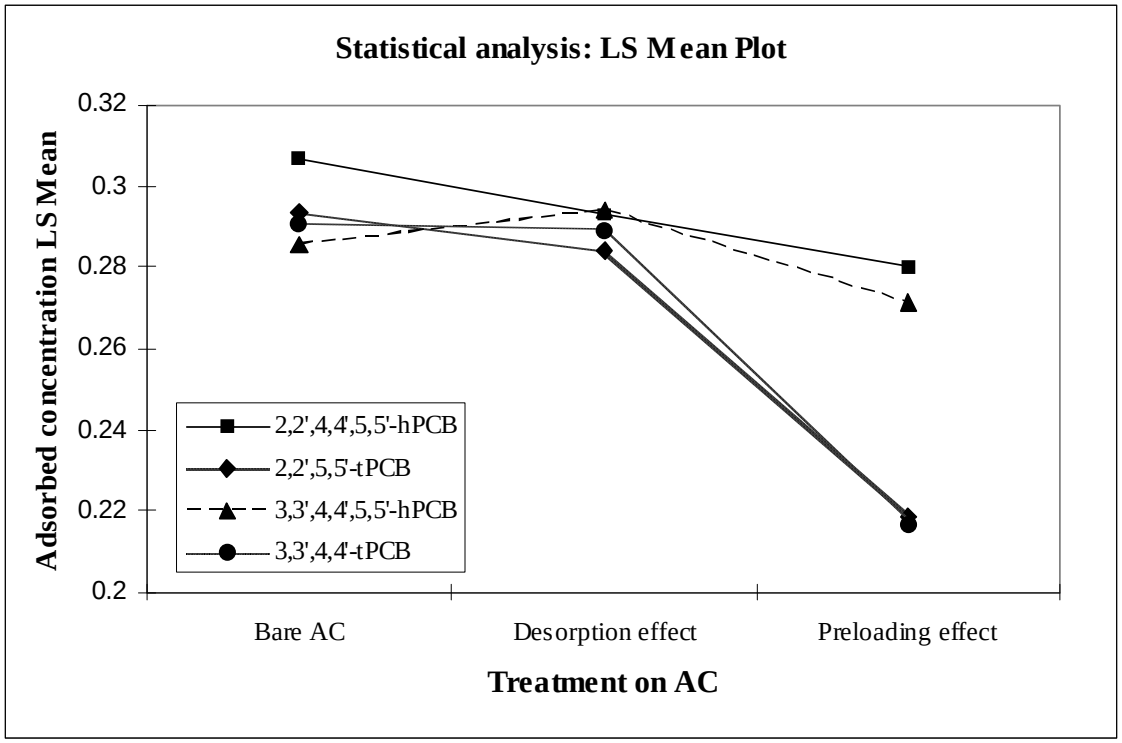

Figure 2.5: LS Mean Plot to determine the effects of AC treatments on PCB adsorption

The coconut shell based activated carbon has a distinctly different pore structure than the coal based activated carbon. The coal based activated carbon has a less porous structure compared to that of coconut shell activated carbon which can be seen in comparative SEM images for both types of activated carbon (Figure 2.1). However, when both carbon types were preloaded with humic acid, their performance was found to be similar (Figure 2.6). Model 2 was developed on JMP ® 7 to determine the performance of both types of carbon in presence of humic acid (table 2.5). The statistical analysis of data also confirmed that humic acid has similar effects on both types of carbons (Figure 2.7).

Table 2.5: Specifications for Statistical Model 2

Model 2 specification:
Type of AC
Treatment
Type of AC*Treatment
Loading rate
Type of AC*Loading rate
Treatment*Loading rate
Type of AC*Treatment*Loading rate
Loading rate*Loading rate

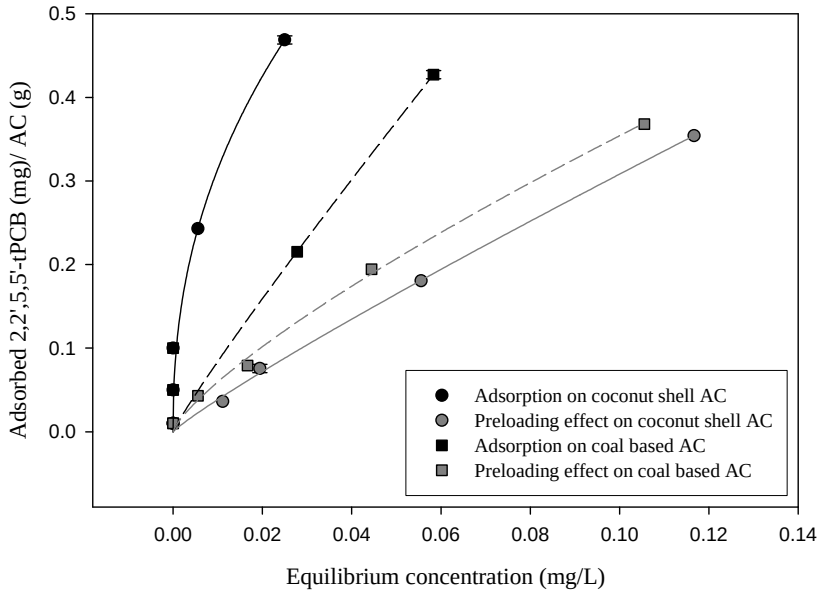

Figure 2.6: Comparative Isotherms for Coal Based and Coconut Shell based AC for 2, 2', 5, 5'- tetrachlorobiphenyl

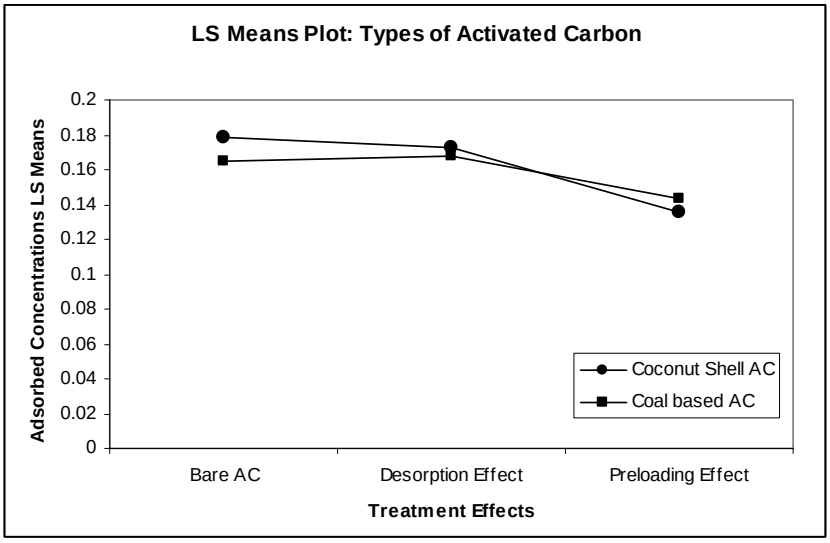

Figure 2.7: Least Square Means plot: Preloading effect of humic acid on coconut shell activated carbon and coal based activated carbon

Experiments were also conducted to determine the effect of humic acid on the adsorption capacity of both types of activated carbon at different loadings of humic acid and fixed loading of PCBs. The results for all three congeners (mono-chloro, tetra-

chloro- and hexa-chloro) showed that the adsorption capacity of coconut shell activated carbon decreased with the increase in humic acid concentration (Figure 2.8).

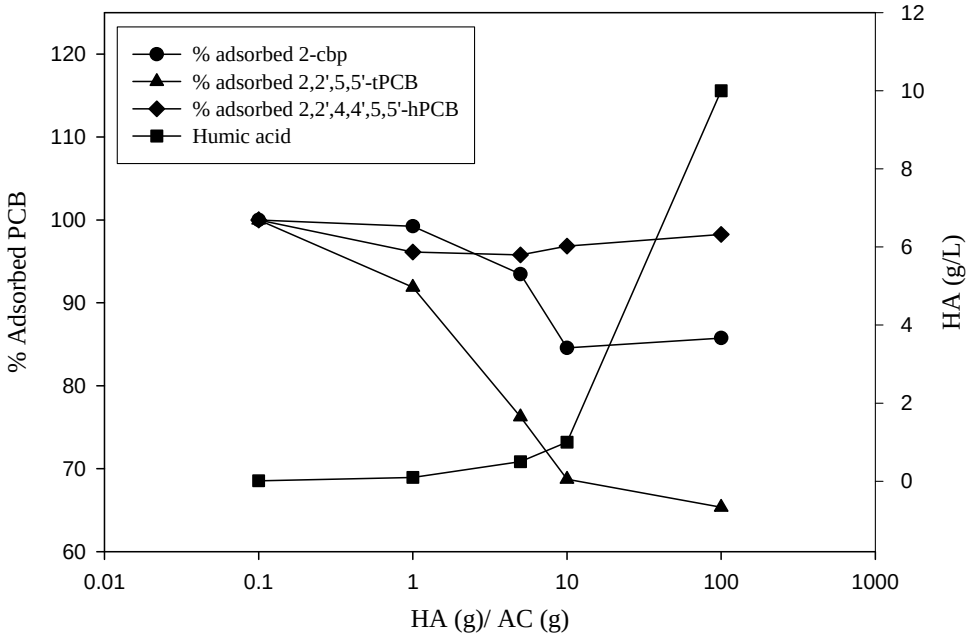

Figure 2.8: Effect of different loadings of HA on adsorption of 2-chlorobiphenyl; 2, 2', 5, 5'-tPCB and 2, 2', 4, 4', 5, 5'-hPCB

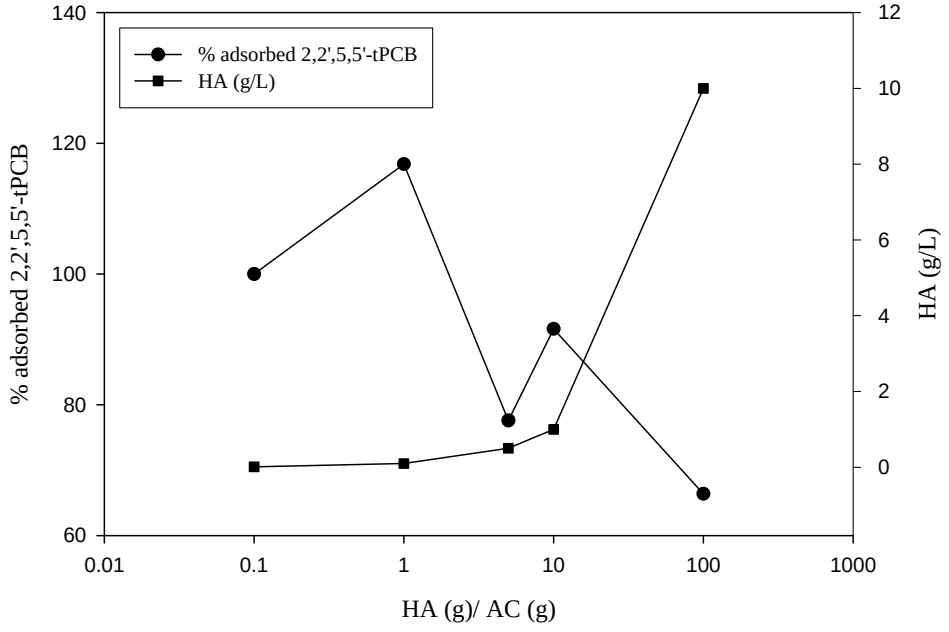

Figure 2.9: Effect of different loadings of HA on coal based activated carbon

The effects were found to be least in case of hexa-chlorobiphenyl followed by mono-chlorobiphenyl and then tetra-chlorobiphenyl. The experiment conducted to measure the effect of humic acid loadings on coal based activated carbon also showed reduction in adsorption capacity of coal based activated carbon with the increase in humic acid loadings (Figure 2.9).

All the isotherms obtained using coconut shell and coal based activated carbon were also evaluated by performing bivariate analysis on JMP® 7.1 to obtain the log-linear form of Freundlich model.

$$log\ qe = log\ Kf + n^{-1} log\ Ce$$

To perform this set of data analysis all the values were converted to nano gram level and then log values were obtained for equilibrium concentration (ng L^{-1}) and adsorbed concentration (ng kg^{-1}). The linear fit was obtained by using Fit Y by X platform and for each log Kf ($ng^{(1-(1/n))}\ L^{(1/n)}\ kg^{-1}$) and n^{-1} values confidence intervals were also obtained (as mentioned in table 2.6).

Evaluation of isotherm coefficients:

As mentioned earlier, the main aim of this research is to more completely understand the design parameters for a reactive sediment cap that considers the interference for and complexation with natural organic acids. In order to compare materials and the sorption affinity for different congeners, adsorption coefficients (K_d) were also estimated using a linear fit for all the isotherms (Table 2.6).

	Adsorption coefficients		*Freundlich Isotherm Constants*							
			Non-linear form ($q_e = K_f C_e^{(1/n)}$)				Linear form ($\log q_e = \log K_f + n^{-1} \log C_e$)			
			K_f ($mg^{(1-(1/n))} L^{(1/n)} g^{-1}$)		1/n		Log K_f ($ng^{(1-(1/n))} L^{(1/n)} kg^{-1}$)		1/n	
Coconut Shell AC	Kd (L/g)									
	Bare AC	Preloading effect	Bare AC	Preloading effect	Bare AC	Preloading effect	Bare AC	Preloading effect	Bare AC	Preloading effect
2-cbp	12.63	1.39	7.00	0.96	0.34	1.43	7.41	6.76	0.39	0.39
2,2',5,5'-tPCB	16.50	2.96	2.35	2.47	0.44	0.90	7.52	6.86	0.25	0.27
3,3',4,4'-tPCB	9.99	4.12	4.11	10.83	0.61	1.52	4.67	3.72	0.90	0.97
2,2',4,4',5,5'-hPCB	35.99	11.63	4.44	8.27	0.40	0.85	8.00	7.60	0.23	0.22
3,3',4,4',5,5'-hPCB	17.85	12.22	18.75	35.60	1.00	1.37	7.59	7.49	0.27	0.22
Coal based AC										
2,2',5,5'-tPCB	6.34	3.35	5.89	2.11	0.92	0.78	7.56	6.90	0.20	0.28

Table 2.6: Adsorption Coefficients and Freundlich Isotherm Constants obtained for Selected PCB congeners

In this study, based on K_d values, the preloading effect was found to be most significant for 2-chlorobiphenyl with 89% and non-coplanar 2, 2', 5, 5'-tetrachlorobiphenyl with 82% reduction in adsorption affinity. The effect was less dominant in the case of co-planar 3, 3', 4, 4'-tetrachlorobiphenyl with 59 % and non-coplanar 2, 2', 4, 4', 5, 5'-hexachlorobiphenyl with 68% reduction and was least in case of co-planar 3, 3', 4, 4', 5, 5'-hexachlorobiphenyl with 32% reduction. The measure of non-linearity for isotherms was estimated using the Freundlich isotherm coefficient (1/n). Using the non-linear form of Freundlich coefficients, the trend was found to be favorable with $1/n < 1$ (table 2.6 – non-linear) for all bare activated carbon isotherms and non-coplanar congeners with preloaded humic acid but in the case of co-planar congeners and 2-chlorobiphenyl with preloading, the value of (1/n) was greater than 1 and the trend of the isotherm was unfavorable as shown in figure 2.4. Using the linear form of Freundlich coefficients when log Kf values were compared for bare activated carbon with that of preloaded activated carbon, the difference in magnitude ranged from 0.101 to 0.954 again indicating significant affect of preloading with humic acid (table 2.6 - linear).

Summary

This study demonstrated the preloading and desorption effect of humic acid on adsorption capacity of coconut shell activated for co-planar and non-coplanar PCBs. The adsorption affinity of bare activated carbon was found to be greater with no desorption effect for highly chlorinated and co-planar congeners compared to lower chlorinated and non-coplanar congeners. Adsorption affinity and capacity of coconut

shell activated carbon was found to be significantly affected by preloading with high concentrations of humic acid. The presence of humic acid is a major factor in the design and performance of reactive caps under typical site conditions. The reactive capping mat that will be deployed over the sediment bed will come across high concentrations of natural organic matter. Therefore, it is important to evaluate the performance of sorbents that will be used in the mat in the presence of high organic acid concentrations. This study showed that sorbent material exposure to humic acid prior to the sorption of contaminants effect performance significantly.

Additional Information

Model 1 Details:

Actual by Predicted Plot

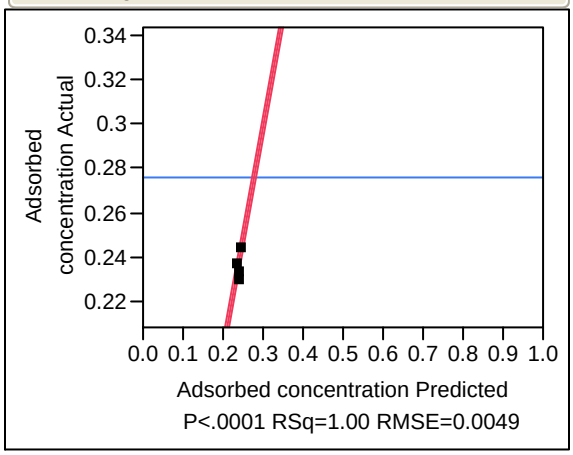

Analysis of Variance

Source	DF	Sum of Squares	Mean Square	F Ratio
Model	35	5.7685679	0.164816	6822.730
Error	24	0.0005798	0.000024	**Prob > F**
C. Total	59	5.7691476		<.0001*

Effect Tests

Source	Nparm	DF	Sum of Squares	F Ratio	Prob > F
PCB congener	3	3	0.0029605	40.8507	<.0001*
LR	1	1	1.5138861	62668.81	<.0001*
Treatment on AC	2	2	0.0087793	181.7149	<.0001*
PCB congener*Treatment on AC	6	6	0.0033484	23.1017	<.0001*
PCB congener*LR	3	3	0.0042246	58.2939	<.0001*
Treatment on AC*LR	2	2	0.0074106	153.3839	<.0001*
PCB congener*Treatment on AC*LR	6	6	0.0028585	19.7220	<.0001*
LR*LR	1	1	0.0002215	9.1712	0.0058*
LR*LR*PCB congener	3	3	0.0001772	2.4450	0.0885
LR*LR*Treatment on AC	2	2	0.0002977	6.1611	0.0069*
LR*LR*Treatment on AC*PCB congener	6	6	0.0007645	5.2744	0.0014*

Model 2 details:

Variability Chart for Adsorption

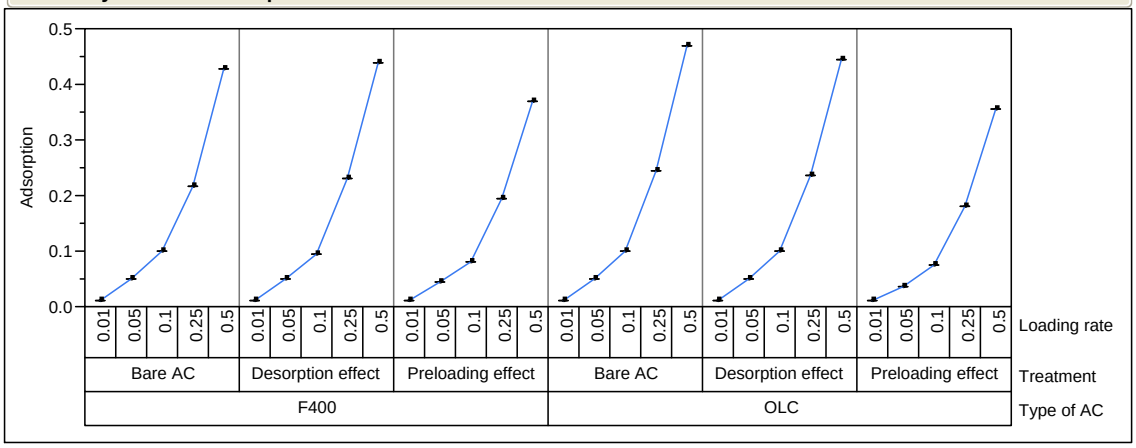

Analysis of Variance

Source	DF	Sum of Squares	Mean Square	F Ratio
Model	12	0.66843353	0.055703	5233.994
Error	17	0.00018092	0.000011	**Prob > F**
C. Total	29	0.66861446		<.0001*

Effect Tests

Source	Nparm	DF	Sum of Squares	F Ratio	Prob > F
Type of AC	1	1	0.00009042	8.4964	0.0097*
Treatment	2	2	0.00666554	313.1567	<.0001*
Type of AC*Treatment	2	2	0.00058111	27.3016	<.0001*
Loading rate	1	1	0.28056137	26362.35	<.0001*
Type of AC*Loading rate	1	1	0.00017908	16.8266	0.0007*
Treatment*Loading rate	2	2	0.00583070	273.9347	<.0001*
Type of AC*Treatment*Loading rate	2	2	0.00060769	28.5500	<.0001*
Loading rate*Loading rate	1	1	0.00026159	24.5794	0.0001*

SEM images of activated carbon at different magnifications

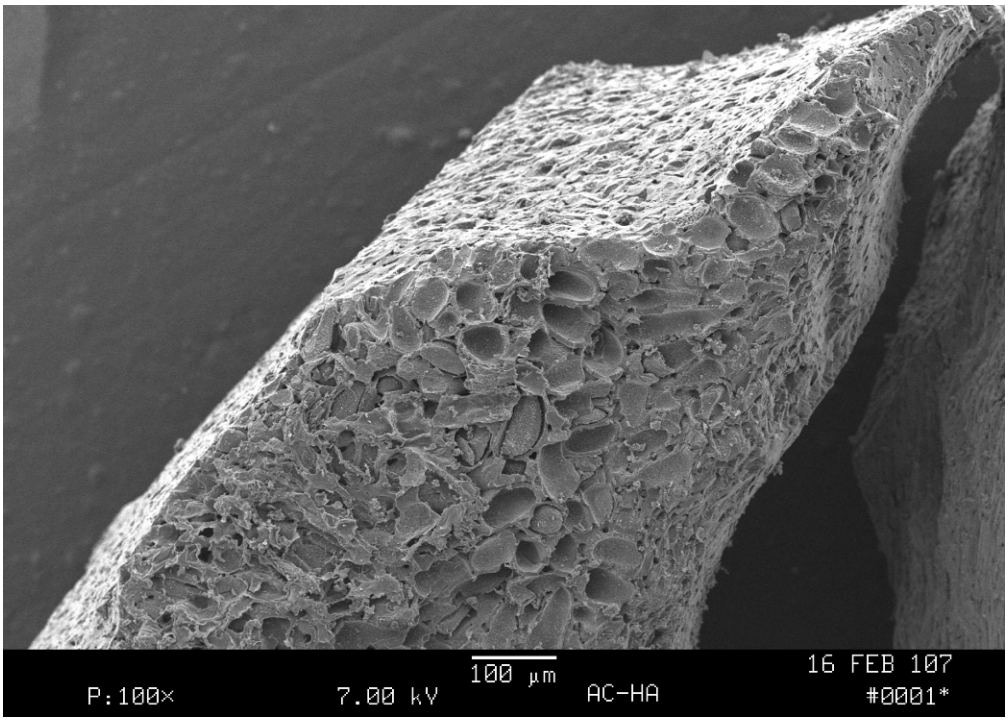

Coconut shell activated carbon: 100 x magnifications

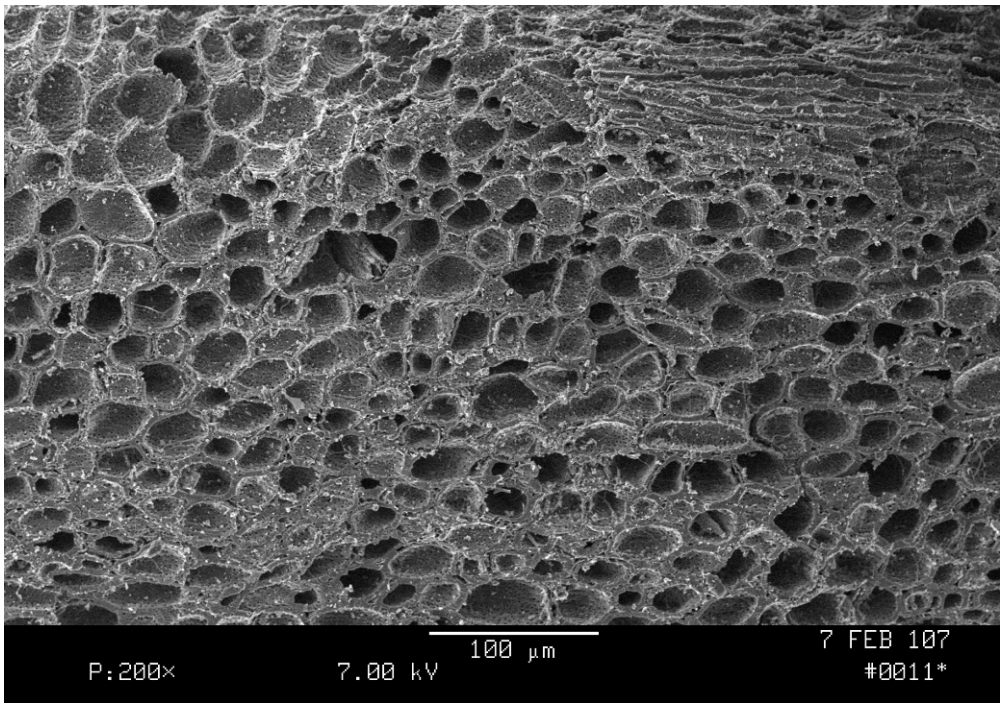

Coconut shell activated carbon: 200 x magnifications

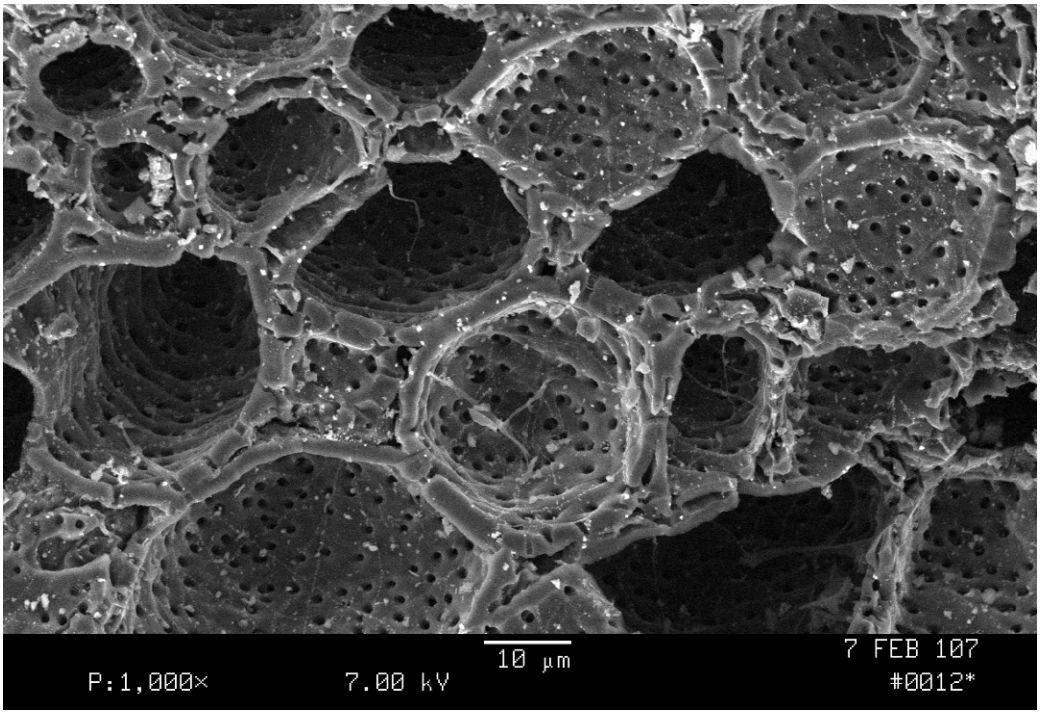

Coconut shell activated carbon: 1000 x magnifications

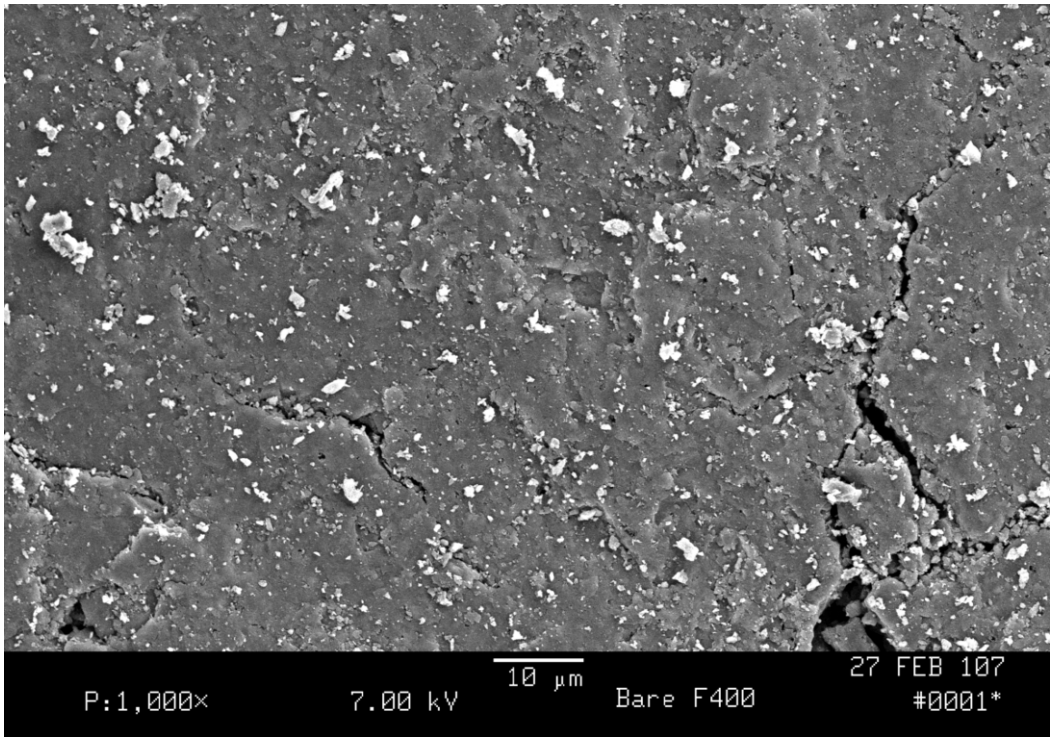

Coal based activated carbon: 1000 x magnifications

Preliminary studies: 24 hours study

Some preliminary studies were conducted to determine the performance of activated carbon for adsorption of mono- and tetra- chlorobiphenyl in the presence and absence of humic acid. These experiments were conducted for 24 hours equilibration time.

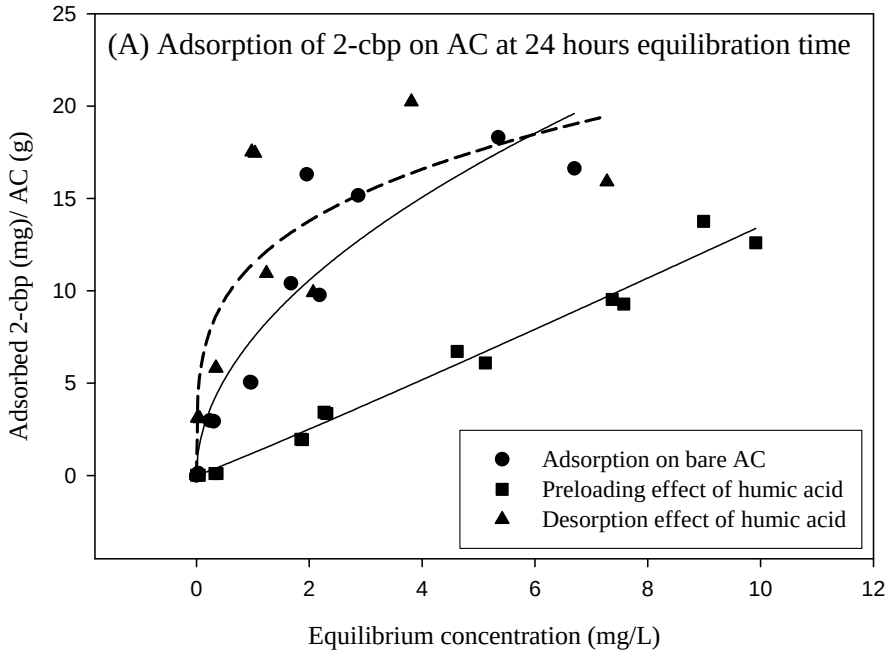

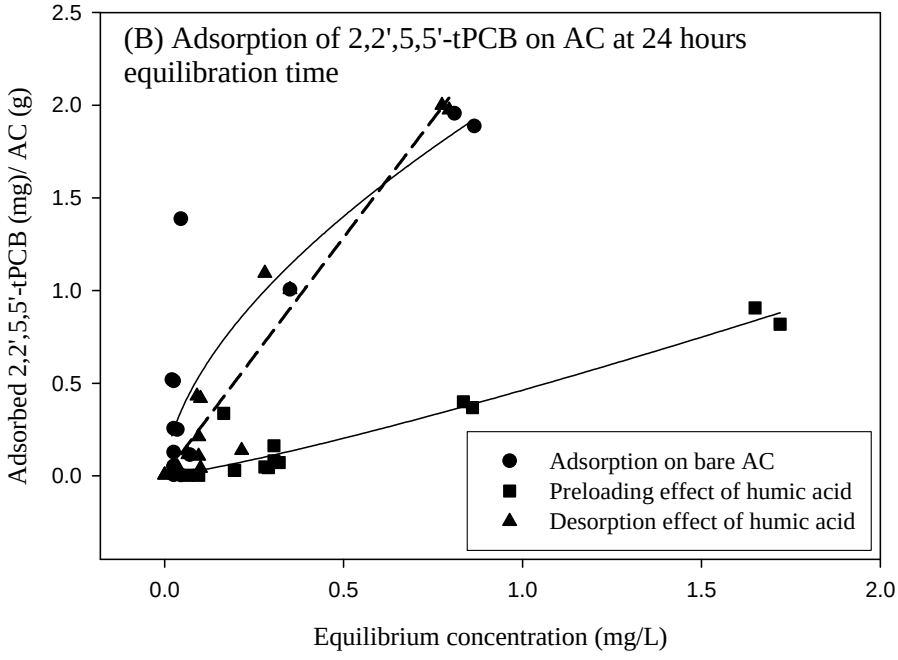

Adsorption coefficients for adsorption of selected PCB congeners on coconut shell activated carbon in 24 hours:

	Adsorption coefficients		Freundlich Isotherm Constants			
Coconut Shell AC	Kd (L/g)		K_f ($mg^{(1-(1/n))}$ $L^{(1/n)}$ g^{-1})		1/n	
	Bare AC	Preloading effect	Bare AC	Preloading effect	Bare AC	Preloading effect
2-cbp	2.901	1.360	7.423	1.218	0.570	1.044
2,2',5,5'-tPCB	2.026	0.519	2.092	0.426	0.579	1.187

Results showed significant reducing effects on adsorption capacity of activated carbon in the presence of humic acid. Negligible desorption effects were noticed.

References

Burgie, D. J. Dissolved organic matter in Chesapeake Bay sediment pore waters. *Organic Geochemistry*, 2001, 32, 487-505.

Butcher, J.B.; and Garvey, E. A. PCB Loading from Sediment in the Hudson River: Congener Signature Analysis of Pathways. *Environmental Science and Technology*, 2004, 38, 3232-3238.

Cornelissen, G.; Elmquist; M.; Groth, I.; and Gustafsson, O. Effect of Sorbate Planarity on Environmental Black Carbon Sorption. *Environmental Science and Technology*, 2004, 38, 3574-3580.

Cornelissen, G.; Breedveld, G.D.; Kalaitzidis, S.; Christanis, K.; Kibsgaard, A.; Oen, A. MP. Strong Sorption of Native PAHs to Pyrogenic and Unburned Carbonaceous Geosorbents in Sediments. *Environmental Science and Technology*, 2006, 40, 1197-1203.

Draft Data Report. Trident and UltraSeep Month 30 Post – Capping Evaluation for the Apatite Cap Test Area on the Anacostia River, Washington, D.C. December 2006, submitted to Environmental Research Group, University of New Hampshire, Durham, NH by Coastal Monitoring Associates, San Diego, CA.

Erickson, M.D. *Analytical Chemistry of PCBs. Second Edition.* Lewis Publishers, 1997.

Karanfil, T. and Kilduff, J. E. Role of Granular Activated Carbon Surface Chemistry on the Adsorption of Organic Compounds. 1. Priority Pollutants. *Environmental Science and Technology*, 1999, 33, 3217-3224.

Karanfil, T.; Dastgheib, S.A. and Mauldin, D. Exploring Molecular Sieve Capabilities of Activated Carbon Fibers to Reduce the Impact of NOM Preloading on Trichloroethylene Adsroption *Environmental Science and Technology*, 2006, 40, 1321-1327.

Li, Qilin; Snoeyink, V.L.; Marinas, B.J.; Campos, C. Pore Blockage Effect of NOM on Atrazine Adsorption Kinetics of PAC: The Roles of PAC Pore Size Distribution and NOM Molecular Weight. *Water Research.* 2003, 37, 4863-4872.

Matsui, Y.; Fukuda, Y.; Inoue, T.; Matsushita, T. Effect of Natural Organic Matter on Powdered Activated Carbon Adsorption of Trace Contaminants: Characteristics and Mechanism of Competitive Adsorption. *Water Research*. 2003**,** 37, 4413-4424.

McDonough, K. M.; Fairey, J. L.; Lowry, G. V. Adsorption of Polychlorinated biphenyls to Activated Carbon : Equilibrium Isotherms and a Preliminary Assessment of the Effect of Dissolved Organic Matter and Biofilm Loadings. *Water Research*, 2008, 42, 575-584.

Millward, R. N.; Bridges, T. S.; Ghosh, U.; Zimmerman, J.R.; Luthy, R.G. Addition of Activated Carbon to Sediments to Reduce PCB Bioaccumulation by a polychaete (Neanthes *arenaceodentata*) and an Amphipod (Leptocheirus *plumulosus*). *Environ. Sci. Tech*. 2005, 39, 2880-2887.

Newcombe, G.; Drikas, M. and Hayes, R. Influence of Characterized Natural Organic Material on Activated Carbon Adsorption: II. Effect on Pore Volume Distribution and Adsorption of 2-Methylisoborneol. *Water Research*, 1997, 31, 1065-1073.

Newcombe, G., Morrison, J., Hepplewhite, C., Knappe, D. R. U. Simultaneous Adsorption of MIB and NOM onto activated carbon: II. Competitive effects. *Carbon*, 2002, 40, 2147-2156.

Pignatello, J. J.; Kwon, S.; Lu, Y. Effect of Natural Organic Substances on the Surface and Adsorptiive Properties of Envrionmental Black Carbon (Char): Attenuation of Surface Activity by Humic and Fulvic Acids. *Environ. Sci. Tech*. 2006, 40, 7757-7763.

Pirbazari, M. and Weber, W. J. Adsorption of Polychlorinated Biphenyls from Water by Activated Carbon. Chemistry in Water Reuse Volume 2. *Ann Arbor Science,* 1981, 309-39.

Pirbazari, M.; Ravindram, V.; Wong, Sau-Pong and Stevens, M.R. Adsorption of Micropollutants on Activated Carbon. *Aquatic Humic Substances – Infuence on Fate and Treatment of Pollutants*, ACS publishers, 1989, 549-578.

Poerschmann, J.; Kopinke, Frank-Dieter; Plugge, J.; Georgi, A. Interaction of Organic Chemicals (PAHs, PCB, Triazines, Nitroaromatics and Organotin Compounds) with Dissolved Humic Organic Matter. *Special Pubilcation – Royal Society of Chemistry*, 247 (Understanding Humic Substances), 1999, 223-240. Publisher: Royal Society of Chemistry.

Quinlivan, P. A., Li, L., Knappe, D. R. U. Effects of Activated Carbon Characteristics on the Simultaneous Adsorption of Aqueous Organic Micropollutants and Natural Organic Matter. *Water Research*, 2005, 39, 1663-1673.

Schaffner, L.C; Dickhut, R.M.; Mitra, S.; Lay, P.W.; and Brouwer-Riel, C. Effects of Physical Chemistry and Bioturbation by Estuarine Macrofauna on the Transport of Hydrophobic Organic Contaminants in the Benthos. *Environmental Science and Technology*, 1997, 31, 3120-3125.

Sotelo, J.L.; Ovejero, G.; Delgedo, J.A.; Martinez, I. Comparison of adsorption equilibrium and kinetics of four chlorinated organics from water onto GAC. *Water Research* 2002, 36, 599-608.

Walters, W. R.; Luthy, R. G. Equilibrium Adsorption of Polycyclic Aromatic Hydrocarbons from Water onto Activated Carbon. *Environ. Sci. Tech*. 1984, 18, 395-403.

Werner, D.; Higgins, C. P.; Luthy, R. G. The sequestration of PCBs in Lake Hartwell Sediment with Activated Carbon. *Water Research*, 2005, 39, 2105-2113.

Zimmerman, J.R.; Ghosh, U.; Luthy, R. G.; Bridges, T. S.; Millward, R. N. Addition of Carbon Sorbents to Reduce PCB and PAH Bioavailability in Marine Sediments: Physicochemical Tests. *Environ. Sci. Tech*. 2004, 38, 5458 – 5464.

CHAPTER 3

EFFECT OF HUMIC ACID ON ADSORPTION OF POLYCHLORINATED BIPHENYLS ONTO ORGANOCLAY

Abstract

Organoclay was evaluated as a reactive cap sorbent that can be used for in-situ remediation of contaminated sediments. With this aim, sorption of co-planar and non-coplanar polychlorinated biphenyls including 2-chlorobiphenyl (BZ # 1), 2, 2', 5, 5'-tetrachlorobiphenyl (BZ # 52), 3, 3', 4, 4'- tetrachlorobiphenyl (BZ # 77), 2, 2', 4, 4', 5, 5'-hexachlorobiphenyl (BZ # 153) and 3, 3', 4, 4', 5, 5'- hexachlorobiphenyl (BZ # 169) on organoclays was studied. Three commercially available organoclays were characterized and used for kinetic and equilibrium studies for selected PCB congeners. Kinetic studies were conducted to obtain equilibration time of adsorption of PCBs on organoclay and to determine the effect of humic acid on the kinetics of adsorption. Isotherm studies were conducted to determine the adsorption capacity of organoclays in the presence and absence of humic acid. Studies showed a significant reduction in the performance of organoclays due to preloading with high concentrations of humic acid for all selected PCB congeners. The reduction in sorption capacity due to preloading ranged from 46 % to 96% depending on the congener and the composition of organoclay. Desorption studies that were conducted to simulate the long-term exposure to high humic acid

concentrations in the sediment pore water in typical site conditions also showed reducing effects that were less pronounced compared to preloading effects and varied with the composition of organoclay and PCB congener.

Introduction

Hydrophobic organic contaminants (HOCs) such as polychlorinated biphenyls (PCBs) are of great concern in riverine and marine environments due to their eventual settlement with sediments. PCBs, which are group of 209 congeners, are listed at number five in the CERCLA 2005 priority list of hazardous substances. This listing is based not only on the toxicity of the compounds but also on their frequency of occurrence in national priority list (NPL) sites and their potential of exposure to human beings. The major problem of these contaminants is their continued persistence due to strong sorption on sediments and slow degradation. Highly PCB contaminated sites in riverine and estuarine environments present environmental, economic and technical challenges to meet the clean up goals. Currently, dredging, monitored natural recovery, and in-situ capping are the remediation options for contaminated sediments. Reactive capping, which consists of a geotextile mat impregnated with sorbents, is the subject of this research as an alternative to dredging for in-situ management of contaminated sites.

One of the sorbents that can be used in reactive caps to sequester HOCs effectively is activated carbon. Therefore, in our previous studies the performance of

activated carbon was evaluated in the presence and absence of humic acid. Results showed significant reduction in the adsorption capacity of activated carbon due to the pore blockage effect caused by preloading the activated carbon with humic acid. The reduction of adsorption affinity and capacity has significant implications for the design and performance of the reactive mats, and for this reason it was desirable to evaluate additional sorptive media that may perform better in the presence of natural organic matter. Some studies have discussed that sorbents such as organoclays have better performance in the presence of natural organics that can be found in sediments (Zhao and Vance, 1998). Therefore, three commercially available organoclays were selected for this study in order to evaluate PCB sorption and the interference from humic acid.

Natural clays that have electrically charged and hydrophilic surfaces are ineffective in sequestration of HOCs from water (Dental et al., 1998). In natural clays inorganic cations are strongly hydrated in the presence of water and results in hydrophilic surfaces which are ineffective for sequestration of HOCs (Jayens and Boyd, 1991). If the exchangeable inorganic cations from the interlayer space of these clays are replaced by organic cations such as quaternary ammonium compounds, this can significantly improve their capability to remove HOCs (Carmondy at al, 2007; Dental et al., 1998). Due to intercalation of organic cations the interlayer spacing between the silica sheets increases to create an organophilic zone for adsorption of HOCs. These organophilic surfaces created by alkyl chains provide surfactant properties to the clay and these modified clays are known as organoclays. The size of organophilic zone and the hydrophobicity can be measured by determining the dimensions and the structure of

organic cation as well as cation exchange capacity (CEC) and geometry of the base clay (Dental et al., 1998). The hydrophobic characteristics can be altered by changing the properties of organic cation such as increasing the length of alkyl chain or varying the number or branches of the alkyl group (Pernyeszi et al., 2006). The lower the amount of organic cation, the greater the compatibility of organoclay with soil and bacteria and the cost of material is also low (Pernyeszi et al., 2006). Also, with higher amounts there can be a concern of desorption of these organic cations which are used to enhance adsorption capacity of clay for organic contaminants. Studies have shown that organic cations are adsorbed by ion-exchange mechanism with organic cation loading up to 70 % of cation exchange capacity (CEC) of clay and hydrophobic sorption starts to occur with ion-exchange when loading is equal or greater to CEC (Sheng et al., 1998). The organic cations that get adsorbed by ion-exchange mechanism are resistant to desorption where as those which are adsorbed by hydrophobic interaction are less resistant to desorption (Sheng et al., 1998).

Organoclays have been studied for soil remediation, groundwater purification, industrial waste water treatment and oil spill remediation using batch systems (Zhao et al., 1998; Dental et al., 1998; Carmondy et al., 2007; Pernyeszi et al., 2006; Ake et al., 2003; Wiles et al., 2005). There are limitations for direct use of organoclay in column systems and flow systems due to their low permeability and wettability (Pernyeszi et al., 2006). Therefore, studies have been conducted by adhering organoclays to sand and activated carbon in order to increase their hydraulic permeability for their use in column systems (Ake et al., 2003; Wiles et al., 2005). Studies have shown good adsorption

capacity of organoclays for chlorinated compounds such as trichloroethylene and poly-chlorophenols (Zhao et al., 1998; Dental et al., 1998; Carmondy et al., 2007; Pernyeszi et al., 2006; Ake et al., 2003; Wiles et al., 2005). There remains a need to determine the sorption capacity of organoclays for PCBs which are persistent organic contaminant of major environmental concern.

Studies have shown that humic substances that are formed by decomposition of plant detritus and microbial degradation are ubiquitous and are distributed throughout the hydro- and lithosphere (Wandruszka, 2000). The affect of humic acid on the sorption capacity depends on the type of clay and organic cations used in preparing the organoclay (Zhao et al., 1998). Therefore, it necessitates determining the interferences that can be caused by humic acids on the adsorption capacity of organoclays that can be used as a reactive cap sorbent for in-situ remediation of contaminated sediments. The two main objectives of this study were to determine the sorption capacity of organoclays for PCBs and to determine the affect of humic acid on the sorption capacity of organoclays for its applicability in contaminated sediment remediation.

Chemicals and materials

For all the experiments ultra high purity chemicals and GC-grade solvents obtained from Fischer Scientific (Agawam, MA, USA) were used. The PCB congeners 2-chlorobiphenyl, 2, 2’, 5, 5’-tetrachlorobiphenyl, 3, 3’, 4, 4’-tetrachlorobiphenyl, 2, 2’, 4, 4’, 5, 5’-hexachlorobiphenyl and 3, 3’, 4, 4’, 5, 5’-hexachlorobiphenyl; internal standard

2, 4, 6-trichlorobiphenyl and surrogate standard 2, 4, 5, 6-tetrachloro-m-xylene (TCMX) were purchased from Ultra scientific (North Kingstown, RI, USA) either in neat form or dissolved in hexane. Humic acid sodium salt was obtained from Sigma-Aldrich (St. Louis, MO, USA). Sodium azide that was used to avoid biological growth in the experiments was obtained from EMD Chemicals Inc. (San Diego, CA, USA) and sodium sulfate anhydrous from Fisher Scientific (Morris Plains, NJ, USA)

Organoclays: Three types of organoclays used in this study were obtained as PM 199 from CETCO; PS 86 from Polymer Ventures and Colorsorb 16 x 40 from Biomin Inc. The base clay used in CETCO and Biomin Inc. organoclays was bentonite whereas in Polymer Ventures organoclay attapulgite was used as base clay (Figure 3.1.1 and 3.1.2).

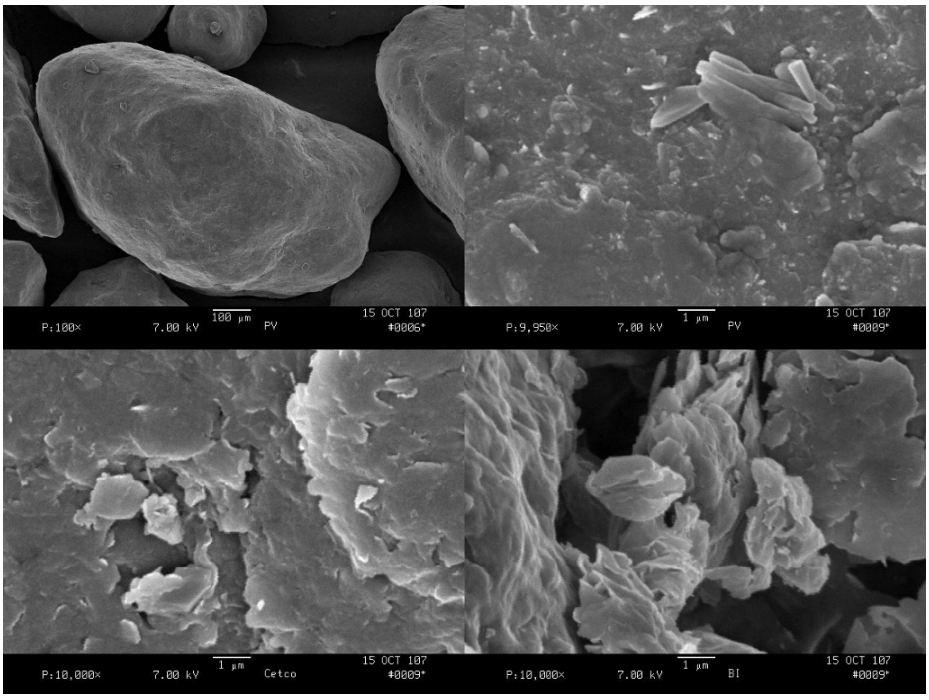

Figure3.1.1: Surface profiles of organoclays: Polymer Ventures (100 x magnification – top left and 10 K x magnification - top right); CETCO (10K x magnification - bottom left) and Biomin Inc. (10K x magnification - bottom right)

Base clay: Bentonite
CETCO organoclay

Base clay: Attapulgite
Polymer Ventures organoclay

Base clay: Bentonite
Biomin Inc. organoclay

Figure3.1.2: Three formulations of organoclay

Characterization of organoclays

X-ray diffraction (XRD): XRD patterns were obtained on small angle X-Ray scattering (SAXS) 2m – 2D area detector using CuK α radiation with a wavelength of 1.5418 A° at the Institute of Technology Characterization Facility, University of Minnesota (Figure 3.1.3). The instrument was operated at 44 KV and 60 mA between 1.3 degree 2θ and 9 degree 2θ at a step size of 0.01 degree 2θ to obtain the interlayer d-spacing of organoclays (table 3.1).

Thermogravimetric analysis (TGA): Differential thermal analysis (DTA) was performed on TA Instruments, model SDTQ600 to obtain % organic content of all three organoclays (table 3.1). Nitrogen flow was maintained at 100 mL min^{-1} with oxygen supply at 242 mL min^{-1} from 28°C to 1000°C with a heating rate of 10°C min^{-1}.

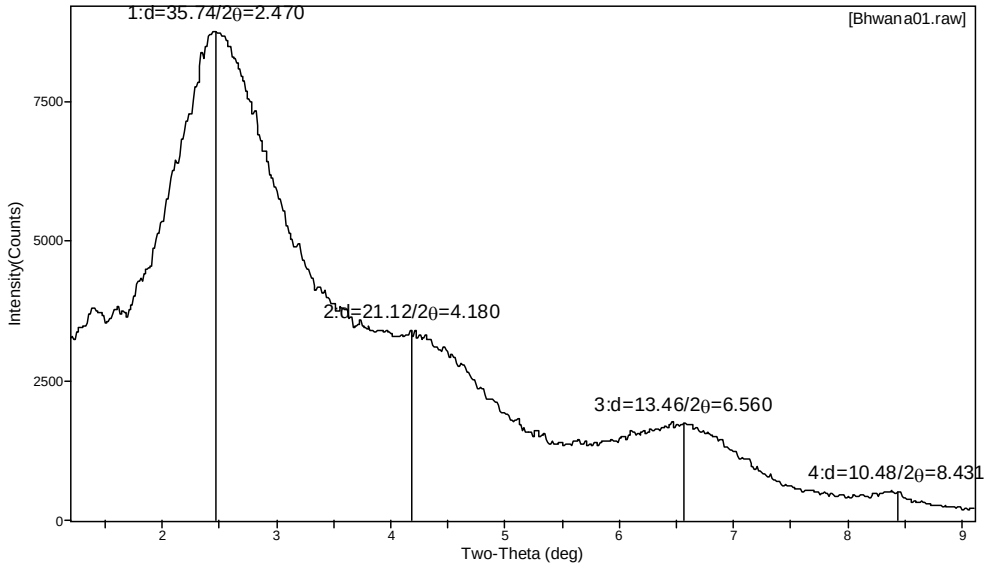

Figure 3.1.3: 2d SAXS scan for determination of d-spacing

Table3.1: Characteristics of Organoclays

	CETCO Organoclay	Polymer Ventures Organoclay	Biomin Inc. Organoclay
Base Clay	Bentonite	Attapulgite	Bentonite
BET surface area (m^2/ g)	0.3225	16.7294	0.1872
Interlayer spacing (d_{001} spacing A°)	35.74 (2θ = 2.47)	35.85 (2θ = 2.46)	37.89 (2θ = 2.33)
% Organic Matter	19.10	10.54	26.95
Inorganic Cations* (ppm)			
Calcium (Ca)	967.2	750.8	682.2
Magnesium (Mg)	175.0	230.0	169.0
Potassium (K)	79.0	337.0	46.0
Phosphorus (P)	1.0	12.0	1.0
Estd. CEC * (meq/ 100g) based on inorganic cations	6.50	6.53	4.94

Overview of experimental protocol

Batch equilibration method was used to for kinetics and isotherm studies of 2-chlorobiphenyl, 2, 2', 5, 5'-tetrachlorobiphenyl, 3, 3', 4, 4'-tetrachlorobiphenyl, 2, 2', 4, 4', 5, 5'-hexachlorobiphenyl and 3, 3', 4, 4', 5, 5'-hexachlorobiphenyl. Experiments were conducted in separate batches of 125 ml of either deionized (DI) water or humic acid solution (prepared in DI water) for pure system and humic acid system, respectively. PCBs were spiked in the system at fixed concentration for kinetics experiment and at different concentration for isotherm studies depending on the loading rate. For spiking, stock solution of PCBs was prepared in ultra-high purity methanol because it has been shown to have no measurable effect on sorption capacity of organoclay (Lee et al.,

2005). Organoclays were either used as obtained from companies or preloaded with humic acid for the system in which effect of humic acid was determined.

Preloading of organoclay with humic acid: For preloading of organoclays, stock solution of 1g L^{-1} humic acid was prepared using de-ionized (DI) water and sodium salt of humic acid as obtained from Sigma Aldrich. To avoid biological growth in the system 10% sodium azide was added to the stock solution. Separate batches were prepared with fixed amount of organoclay and 125 ml of humic acid stock solution in Erlenmeyer flask. All the samples were thoroughly mixed at 150 rpm on a rotary shaker for 48 hours and were used as such for the experiments.

In summary, two types of systems were used for all experiments in 125 ml batches were: a pure system having bare organoclay and PCBs spiked in DI water and a humic acid system having organoclay preloaded with humic acid and PCBs spiked in the humic acid solution. All the methods used for preparing stock solution of PCBs and humic acid, preloading of organoclays and preparation of each batch for pure system and humic acid system were consistent throughout the complete experimentation to maintain the accuracy of the results. All the glassware used was of pyrex to avoid any loss of PCBs on the walls of the flask. The controls were also prepared with each set of experiment to account any loss of PCBs other than sorption on organoclays.

Kinetic experiments

The kinetics of 2-chlorobiphenyl sorption on organoclays was obtained using CETCO (organo-bentonite) and Polymer Ventures (organo-attapulgite) organoclay. Experiments were conducted with 4 mg L^{-1} concentration of 2-chlorobiphenyl for the duration of 15 days in the presence and absence of humic acid. For each kinetic study, the numbers of samples with pure system were equal to that of humic acid system and were sampled at the same time. All the samples were continuously mixed for the length of the experiment prior to sampling at 150 rpm on a rotary shaker.

Sorption Isotherms

Sorption isotherms for all selected PCB congeners were obtained at the equilibration time of 48 hours. The equilibration time was selected on the basis of sorption kinetics of bare organoclay while also considering the retention time of contaminants in a thin reactive cap. Experiments were conducted in the presence and absence of humic acid to determine the effect of humic acid on sorption capacity of organoclays. In all the batches the amount of organoclay was constant with varying concentrations of PCBs depending on the loading rates (table 3.2). The loading rates ranged from concentrations less than and equal to water solubility of each compound and the highest loading was slightly higher than the solubility limit. The second highest loading was equal to the solubility limit of compound in water and was duplicated to check the accuracy of the complete experiment. The effect of humic acid was determined by preloading with humic acid and desorption upon spiking with humic acid. The preloading effect was determined by preloading the organoclays prior to the

sorption of PCBs as mentioned previously. Desorption effects were determined by adding humic acid to the pure system after PCB adsorption for 48 hours. The concentration of humic acid to determine desorption effects was kept the same (1g L^{-1}) as it was in humic acid system to determine the preloading effect. Desorption studies were also conducted for the equilibration time of 48 hours similar to the studies conducted to determine the sorption capacity of organoclay and preloading effect of humic acid.

Table 3.2: Details of selected PCB congeners used in the study

PCB congener	† Solubility Limit in water (ppm)	† Log K_{OW}	Log K_{DOC}	Isotherm Studies Concentration Range (mg/L)
2-cbp	4.0	4.7	3.63*	0.01 – 8
2,2',5,5'- tPCB	0.26	5.9	4.6 **	0.008 – 0.4
3,3',4,4'- tPCB	0.26	5.9	-	0.008 – 0.5
2,2',4,4',5,5'- hPCB	0.038	6.7	5.3**	0.008 – 0.04
3,3',4,4',5,5'- hPCB	0.038	6.7	-	0.008 – 0.04

* Butcher et al., 2004, ** Poerschmann et al., 1999, † Erickson, 1997

Sample analysis

Sample extraction: The vial liquid-liquid extraction method was used for the extraction of supernatant of each sample into hexane with TCMX as a surrogate standard. Ten ml of surrogate solvent (prepared in hexane) with twenty ml of sample was taken into a 40 ml vial sealed with Teflon® lined screw caps. All the samples were extracted in duplicates to determine the variation in extraction procedure. The vials were shaken vigorously for 30 seconds three times at intervals of 30 seconds each and then stored for at least for 24 hours at 4° C to allow proper extraction. The extracts were

passed through sodium sulfate to remove any chemically bound water to avoid any contamination in GC columns. GC vials were then prepared with filtered extracts and addition of 2, 4, 6-trichlorobiphenyl as an internal standard.

Gas Chromatography/ Mass Spectrometry: All the extracts were analyzed using internal standard method on Varian CP3800 Gas Chromatograph (GC)/ Saturn 2200 Ion Trap Mass Spectrometer (MS) with a CP8400 Auto Sampler. The GC column used was a DB-5 type capillary column (Varian Factor Four VF-5ms), 30 m long, 0.25 mm ID and 0.5 µm thick. The ion-trap was operated in selected scan mode (MS/MS) for each PCB congener. The column oven temperature was programmed at 40˚ C with hold time of 2 min followed by a temperature ramp up to 184˚ C at the rate of 12˚ C/ min. and then to 280˚ C at the rate of 4˚ C/ min with the final held time of 2 minutes. The surrogate recoveries were achieved to be in the range of 70 – 120% using this internal standard method.

Results and discussions

Kinetics:

The kinetics experiments were conducted to estimate the equilibration time for adsorption of 2-chlorobiphenyl on two compositions of organoclays having different base clays (CETCO and Polymer Ventures organoclays). The result showed approximately the same time was required to reach equilibrium for both types of organoclays (Figure 3.2). The sorption kinetics of 2-chlorobiphenyl was obtained in the presence and absence of humic acid. For this purpose both types of organoclays were preloaded with humic acid prior to the spiking of 2-chlorobiphenyl in the system.

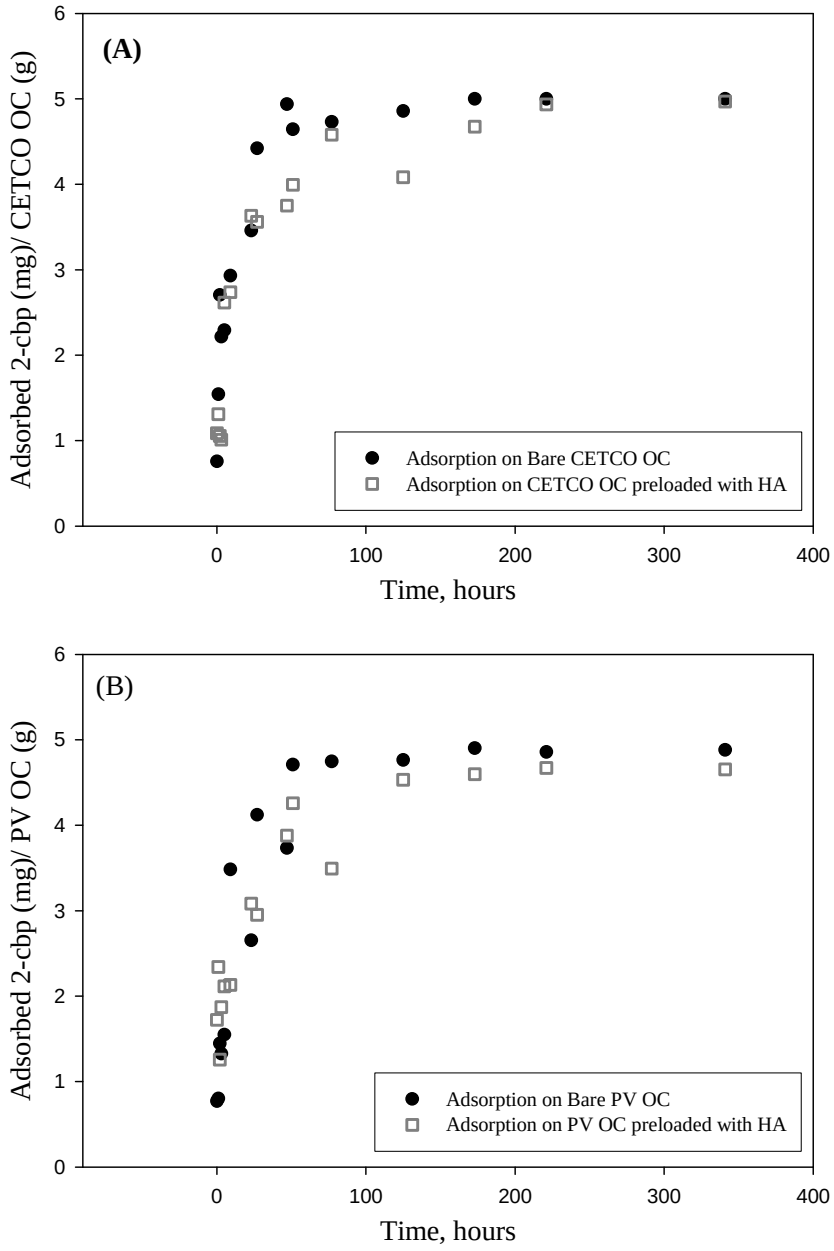

Figure 3.2: Kinetics of sorption of 2-chlorobiphenyl on organoclays: (A) CETCO organoclay (B) Polymer Ventures organoclay

The equilibrium was reached at around 48 hours for bare organoclays, but the presence of humic acid has been found to slow the sorption kinetics. This may be due to the slow diffusivity of 2-chlorobiphenyl into the interlayer spacing of organoclays in

the presence of humic acid molecules that can block the path of the contaminants due to hydrophobic interactions with organophilic outer layers of organoclays.

Isotherms:

The sorption capacity of all the three organoclays was evaluated in the presence and absence of humic acid. PCBs selected for this study were 2-chlorobiphenyl, 2, 2', 5, 5'-tetrachlorobiphenyl, 3, 3', 4, 4'-tetrachlorobiphenyl, 2, 2', 4, 4', 5, 5'-hexachlorobiphenyl and 3, 3', 4, 4', 5, 5'-hexachlorobiphenyl. The selection was done on the basis of their co-planarity to represent the whole range of congeners from lower chlorinated to highly chlorinated ones with different hydrophobicities. The effect of humic acid was evaluated by preloading organoclay with humic acid prior to PCB spiking and desorption effect by spiking humic acid in the system after PCB adsorption on organoclay. Preloading effect was estimated to simulate the typical site conditions where sorbents might come across very high concentrations of natural organics that can affect the sorption capacity of sorbents for target organic contaminants. Desorption studies simulated the long term exposure of these sorbents to organic acids after adsorption of contaminants as well as to determine the reversibility of the system.

Adsorption capacity of the sorbents was evaluated by using linear fit and Freundlich fit for the data (table 3.3). The linear fit was used to obtain the partition coefficient (K_d) to estimate the sorption affinities of organoclays. The Freundlich model used is described as:

$$q_e = K_F\ (C_e^{\ (1/n)})$$

where, q_e is the amount of contaminant adsorbed on the sorbent (mg/g), K_F is the Freundlich isotherm constant, C_e is the equilibrium concentration (mg/L) and *1/n* is the dimensionless Freundlich exponent. The value of the Freundlich exponent was used to understand the nature of adsorption of PCBs on organoclays. The non-linearity of isotherms was estimated based on (1/n) values; the trend is considered to be favorable for (1/n) < 1 and unfavorable for (1/n) > 1 (Figure 3.3 – 3.7).

Sorption of 2-chlorobiphenyl was evaluated for all the three organoclays including CETCO organoclay, Polymer Ventures organoclay and Biomin Inc. organoclay (Figure 3.3 A-C). Figure 3.3 shows significant reduction effect of preloading with humic acid on all the three organoclays for sorption of 2-chlorobiphenyl where as no desorption was noticed for CETCO and Biomin Inc. organoclay and slight desorption was noticed in the case of Polymer Ventures organoclay, when humic acid was introduced in the system once 2-chlorobiphenyl was adsorbed. The adsorption coefficients (K_d) based on a linear fit of the data showed greater affinity in the case of bare CETCO organoclay as compared to the other two compositions, but the sorption capacity of all organoclays for 2-chlorobiphenyl was found to be less as compared to coconut shell activated carbon as evaluated in the previous studies (table 3.3). About 78% reduction in the sorption capacity (Kd values) of CETCO organoclay was noticed due to preloading with humic acid (table 3.3). The reduction was noticed to be about 60% for Polymer Ventures organoclay and about 45% in the case of Biomin Inc. organoclay for 2-chlorobiphenyl sorption.

	Adsorption Isotherm Constants		Freundlich Isotherm Constants			
	Kd (L g^{-1})		K_f ($mg^{[1-(1/n)]}$ $L^{(1/n)}$ g^{-1})		1/n	
CETCO OC	Adsorption on bare OC	Preloading effect	Adsorption on bare OC	Preloading effect	Adsorption on bare OC	Preloading effect
2-cbp	7.8	1.7	7.6	1.2	1.6	1.3
2,2',5,5'-tPCB	11.5	2.7	7	2.1	0.8	0.9
3,3',4,4'-tPCB	7.9	0.5	126057.6	0.4	4.6	0.7
2,2',4,4',5,5'-hPCB	228.2	30.5	20.2	7.3	0.6	0.6
3,3',4,4',5,5'-hPCB	150	9.2	1.3	880	0.3	2.2
PV OC						
2-cbp	4.3	1.7	5.6	1.7	0.6	1
2,2',5,5'-tPCB	53.7	2.1	107604.9	1.8	2.6	0.9
BI OC						
2-cbp	1.9	1	4.9	3	0.3	0.3
Coconut shell AC						
2-cbp	12.6	1.4	7	1	0.3	1.4
2,2',5,5'-tPCB	16.5	3	2.3	2.5	0.4	0.9
3,3',4,4'-tPCB	10.5	3.9	6.6	11.7	0.8	1.6
2,2',4,4',5,5'-hPCB	36	11.6	4.4	8.3	0.4	0.9
3,3',4,4',5,5'-hPCB	18.2	12.2	18.8	35.6	1	1.4
Coal based AC						
2,2',5,5'-tPCB	6.3	3.4	5.9	2.1	0.9	0.8

Table 3.3: Adsorption Isotherm Coefficients (K_d) and Freundlich Isotherm Constants (K_f and 1/n) for different types of sorbents for selected PCB congeners

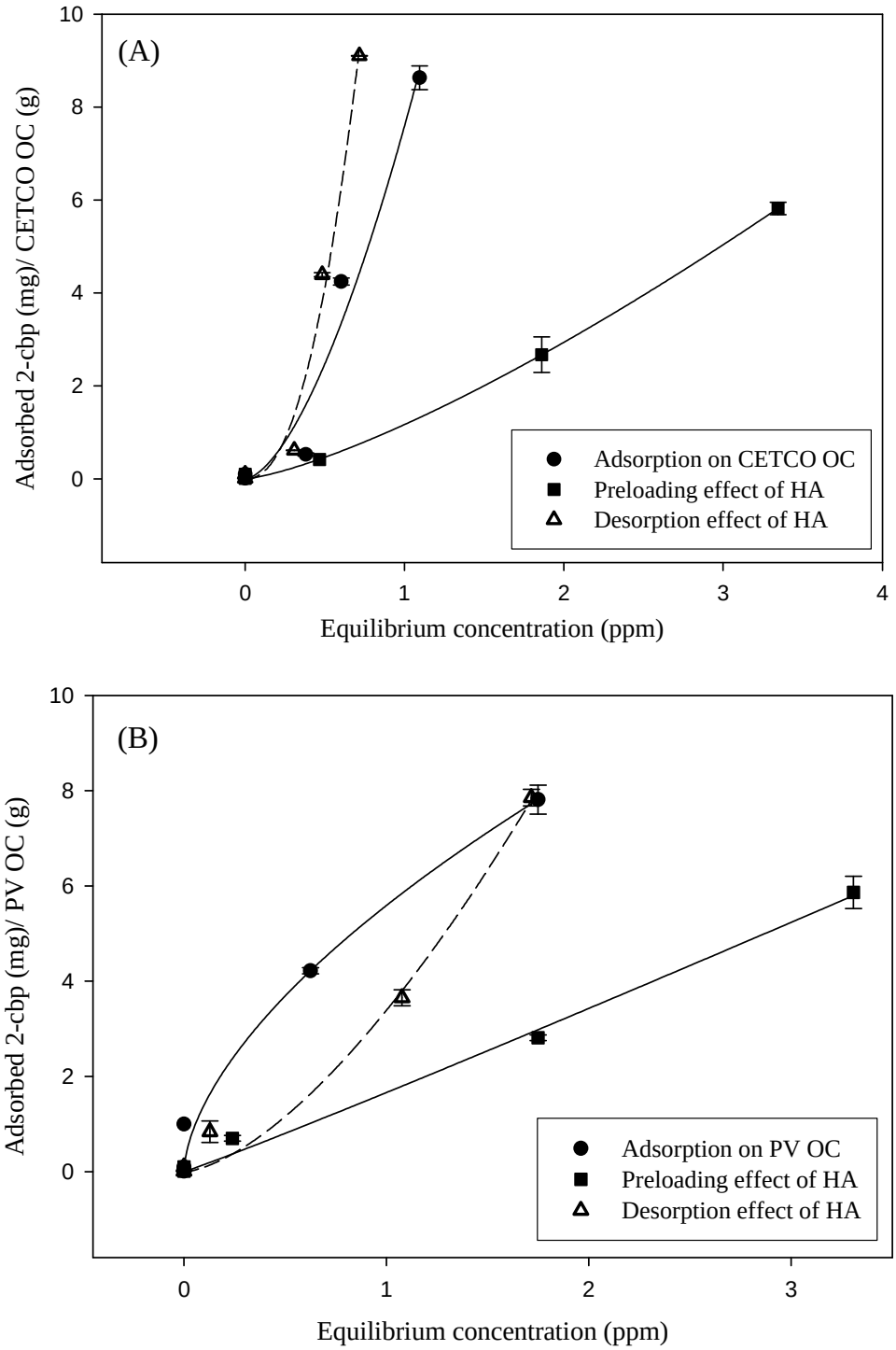

Figure 3.3 A-B: Freundlich adsorption isotherms for 2-chlorobiphenyl in presence and of humic acid (A) CETCO organoclay (B) Polymer Ventures organoclay

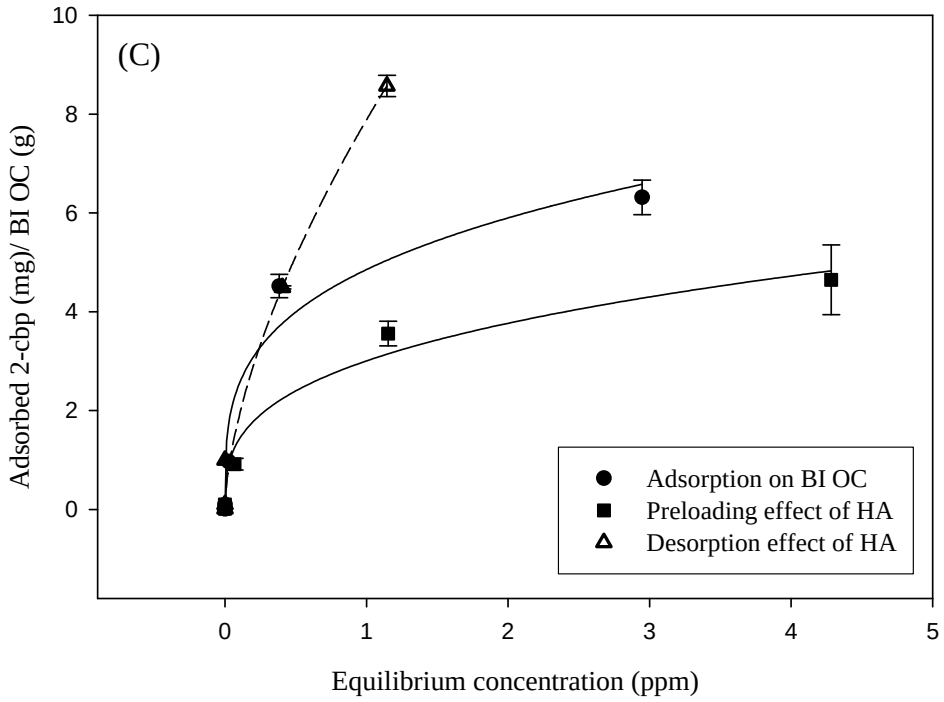

Figure 3.3C: Freundlich adsorption isotherms for 2-chlorobiphenyl in presence and of humic acid: Biomin Inc. organoclay

The statistical analysis was done to evaluate the performance of the three compositions of organoclays for sorption of 2-chlorobiphenyl. The model 1 was developed on the Fit model platform using software JMP® 7 (table 3.4). The hypothesis of this model was that there was difference in the performance of three organoclays for 2-chlorobiphenyl sorption in the presence and absence of humic acid. The three factors considered in this model were: type of organoclay, loading rate of 2-chlorobiphenyl and treatment effects (preloading/ desorption) on organoclay. The regression analysis was done using full factorial design with these three factors.

Table 3.4: Specifications for Statistical Model 1

Model 1 specifications:
Type of OC
Treatment on OC
Type of OC *Treatment on OC
Loading rate
Type of OC *Loading rate
Treatment on OC*Loading rate
Type of OC *Treatment on OC*Loading rate

According to analysis of variance (ANOVA) the p-value was < 0.0001, therefore, the hypothesis of the model was found to be significant (details in additional information). The F-test was performed on each term including main effects and interaction terms of the model to determine the significance of the factors based on the p-value < 0.05. The least square means of adsorbed concentration of 2-chlorobiphenyl on all organoclays were plotted against the treatment effects (preloading/ desorption effect) (Figure 3.4). There was no substantial difference in the performance of bare CETCO and Polymer Ventures organoclays but the sorption capacity of Biomin Inc. organoclay was less. The preloading of organoclays with humic acid significantly reduced their sorption capacity (Figure 3.4). No desorption was found in case of CETCO and Biomin Inc. organoclay but significant desorption was observed in the case of Polymer Ventures organoclay that had different base clay as compared to CETCO and Biomin Inc. that had same base clays (Figure 3.4).

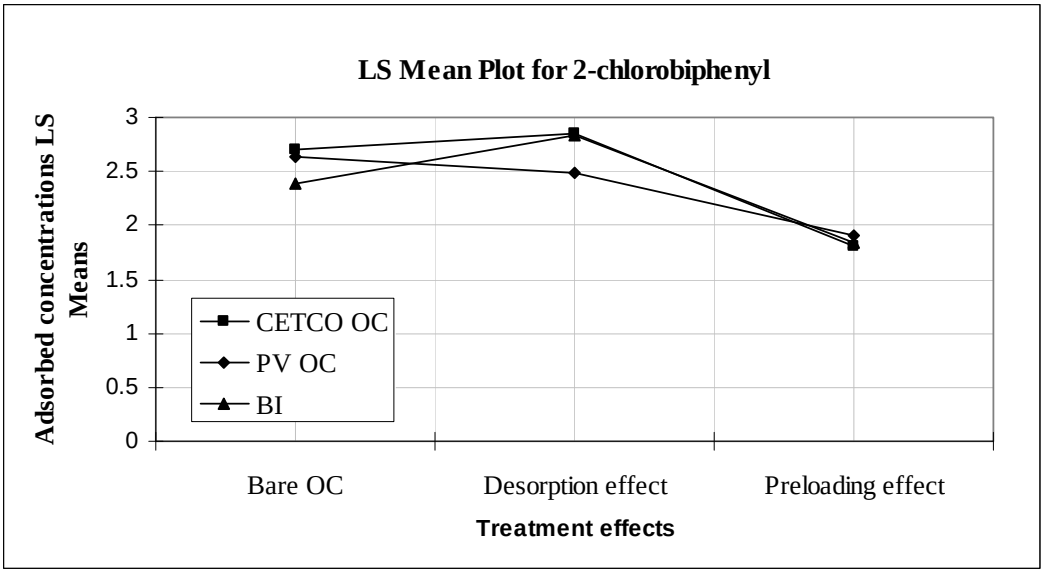

Figure 3.4: Least square means plot for adsorption of 2-chlorobiphenyl on all the three organoclays

For 2, 2', 5, 5'-tetrachlorobiphenyl sorption isotherms were obtained using CETCO and Polymer Ventures organoclay (Figure 3.5 A-B). Based on the Kd values (table 3.3) it was noticed that the sorption capacity of Polymer Ventures organoclay was higher than CETCO organoclay but preloading with humic acid significantly reduced the sorption capacity of both types of organoclays.

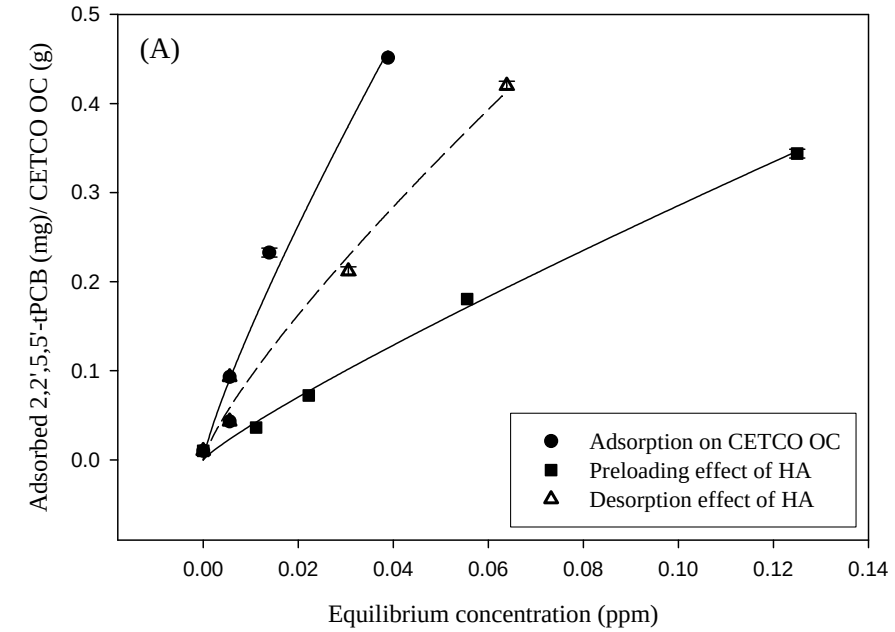

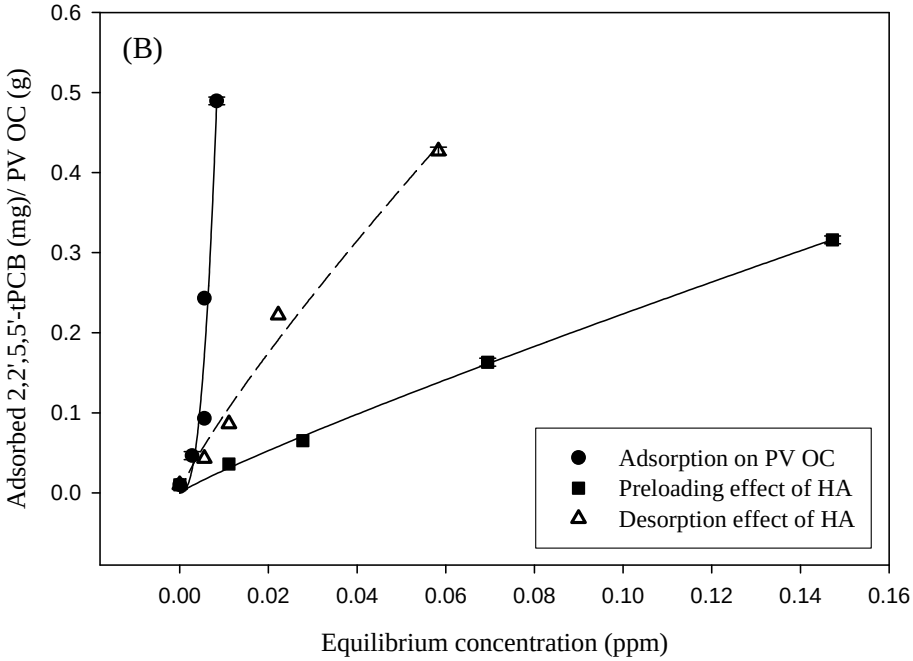

Figure 3.5 A-B: Freundlich adsorption isotherms for adsorption of tetrachlorobiphenyl in presence and absence of humic acid (A) 2, 2', 5, 5'- tPCB adsorption on CETCO organoclay (B) 2, 2', 5, 5'- tPCB adsorption on Polymer ventures organoclay

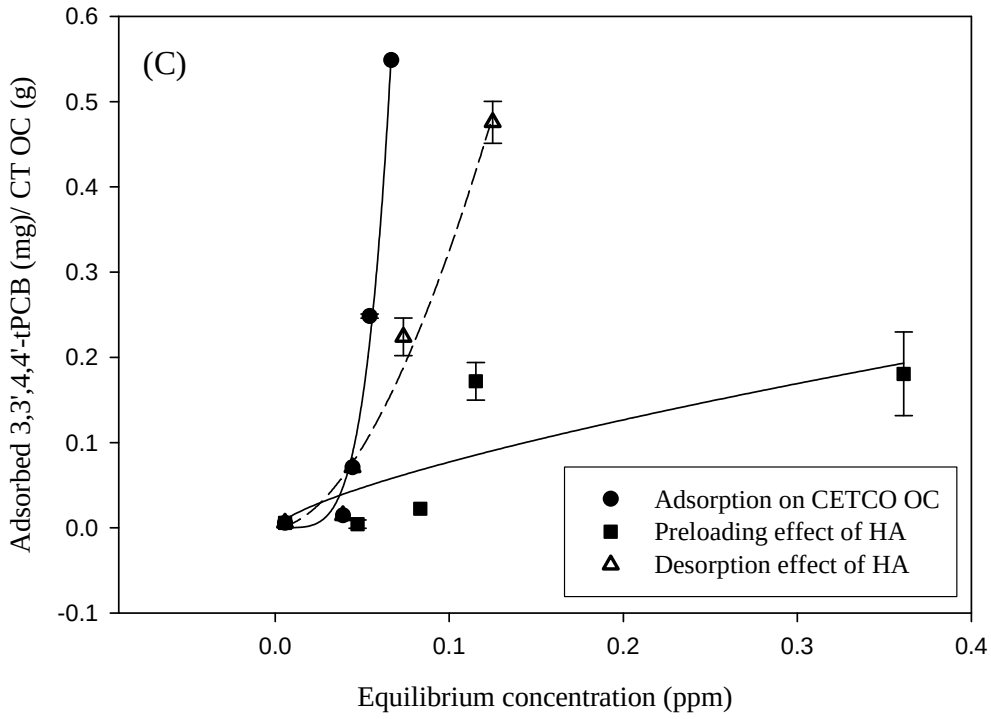

Figure 3.5C: Freundlich adsorption isotherms for adsorption of tetrachlorobiphenyl in presence and absence of humic acid: 3, 3', 4, 4'- tPCB adsorption on CETCO organoclay

The reduction was found to be about 76% for CETCO organoclay and about 96% in the case of Polymer Ventures organoclay (table 3.3). The performance of these two organoclays for sorption of 2, 2', 5, 5'-tetrachlorobipheny was also analyzed statistically using a Fit model platform in JMP® 7. The model 2 was developed based on the hypothesis that the performance of CETCO and Polymer Ventures organoclays are different for 2, 2', 5, 5'-tetrachlorobiphenyl sorption (table 3.5). In this model three factors taken into consideration were: type of organoclay, treatment on organoclay and loading rate of 2, 2', 5, 5'-tetrachlorobiphenyl. The full factorial design was developed with all the three factors and the quadratic term for loading rate.

Table 3.5: Specifications for Statistical Model 2

Model 2 specifications:
Type of OC
Treatment on OC
Type of OC*Treatment on OC
Loading rate
Type of OC*Loading rate
Treatment on OC*Loading rate
Type of OC*Treatment on OC*Loading rate
Loading rate*Loading rate
Loading rate*Loading rate*Type of OC

According to ANOVA the p-value obtained was < 0.0001, therefore, the hypothesis of the model was found to be significant (details in additional information). The Student's t obtained at $\alpha = 0.05$ to determine the effects of humic acid on performance of both type of organoclays showed the performance of bare Polymer Ventures organoclay to be better than that of CETCO organoclay. The preloading effect of humic acid was found to be more significant in the case of Polymer Ventures organoclay but desorption effects were found to be similar in both the cases (table 3.6). This shows CETCO organoclay performed better than Polymer Ventures organoclay in the presence of humic acid.

Table 3.6: LS Means Differences Student's t at α = 0.050 and t = 2.11991 for comparing performance of CETCO and Polymer Ventures organoclays in presence of humic acid

Level*						Least Sq Mean
PV, Bare OC	A					0.177
CETCO, Bare OC		B				0.168
PV, Desorption effect			C			0.158
CETCO, Desorption effect			C			0.158
CETCO, Preloading effect				D		0.131
PV, Preloading effect					E	0.119

The sorption capacity of CETCO organoclay was further evaluated for co-planar 3, 3', 4, 4'- tetrachlorobiphenyl and two of the hexa-chloro-congeners. The performance of CETCO organoclay was compared for non-coplanar and co-planar tetra- and hexa-chlorobiphenyls (Figure 3.5A, 3.5C and 3.6). Adsorption coefficients (Kd) of non-coplanar congener were found to be higher compared to their co-planar isomers for both tetra- and hexa- chlorobiphenyls (table 3.3).

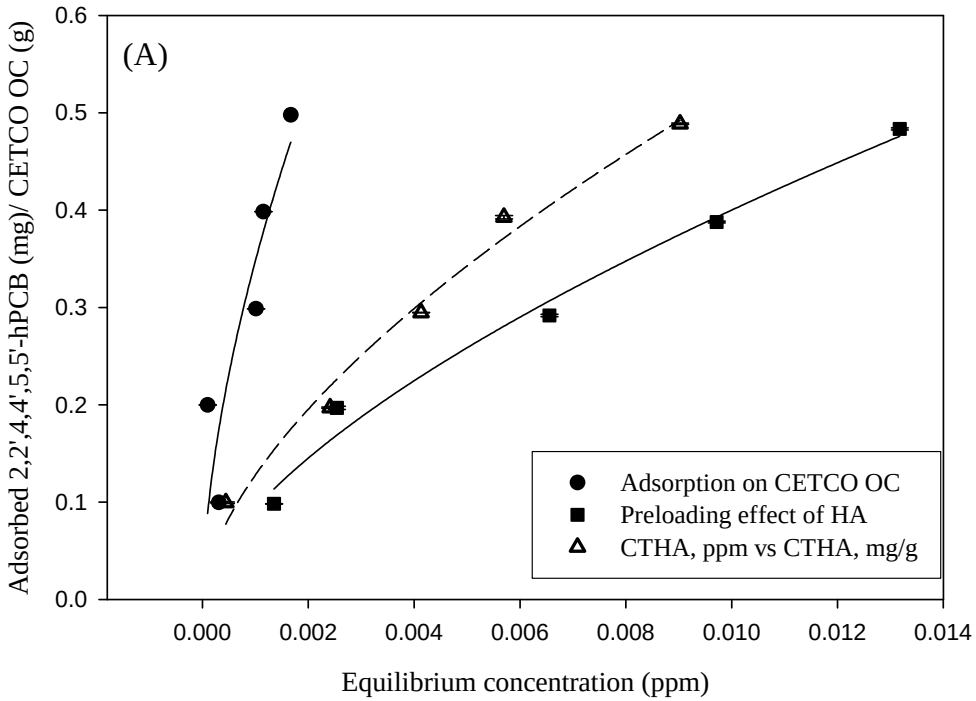

Figure 3.6 A: Freundlich adsorption isotherms for adsorption of hexachlorobiphenyl on CETCO organoclay in presence and absence of humic acid: 2, 2', 4, 4', 5, 5'-hPCB

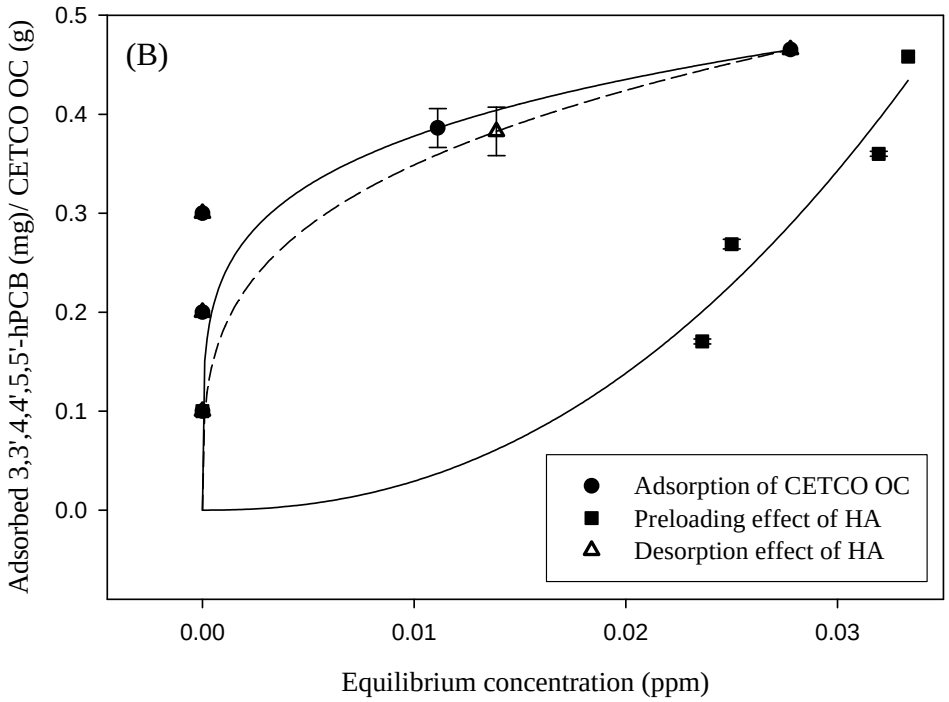

Figure 3.6B: Freundlich adsorption isotherms for adsorption of hexachlorobiphenyl on CETCO organoclay in presence and absence of humic acid: 3, 3', 4, 4', 5, 5'-hPCB

The reduction effect of preloading was found to be more pronounced for co-planar congener but desorption was found to be almost same for both non-coplanar and co-planar congeners. There was about 93% reduction in performance of CETCO organoclay for 3, 3', 4, 4'-tetrachlorobiphenyl, 86% for 2, 2', 4, 4', 5, 5'-hexachlorobiphenyl and 93% for 3, 3', 4, 4', 5, 5'-hexachlorobiphenyl. It is interesting to note that in previous studies, the reduction in performance of activated carbon was noticed to be more for non-coplanar congeners where as in case of CETCO organoclay it has been observed for co-planar congeners. The sorption capacity of CETCO organoclay was also found to be highest for highly chlorinated congeners and the order was: hexa-chlorobiphenyl > tetra-chlorobiphenyl ≥ mono-chlorobiphenyl, which is similar to activated carbon (table 3.3).

The statistical analysis was done on JMP® 7 and a model 3 was developed to evaluate the performance of CETCO organoclay for tetra- and hexa- chlorobiphenyl based on the number of chlorine atoms as well as co-planarity of the congeners in presence and absence of humic acid (table 3.7). The hypothesis of this model was that number of chlorine atoms in PCBs and their co-planarity affect the sorption capacity of CETCO organoclay. The full factorial design was developed for regression analysis of the model with the entire three factors and the quadratic term for loading rate.

Table 3.7: Specifications for Statistical Model 3

Model 3 specification:
PCB congener
Treatment on OC
PCB congener*Treatment on OC
Loading Rate
PCB congener*Loading Rate
Treatment on OC*Loading Rate
PCB congener*Treatment on OC*Loading Rate
Loading Rate*Loading Rate
Loading Rate*Loading Rate*Treatment on OC

The p-value obtained was < 0.0001 in ANOVA, therefore, the hypothesis of this model was significant (details in additional information). The least square means plot was obtained by plotting least square means of adsorbed concentration of all PCB congeners against the treatment effects (preloading/ desorption effect) on CETCO organoclay (Figure 3.7). The preloading effect was found to more pronounced in case of co-planar congeners as compared to their non-coplanar isomers and desorption effects were not substantial in any case (table 3.8). It was also observed that the adsorption

affinity of CETCO organoclay was higher for hexa-chlorobiphenyls than for tetra-chlorobiphenyls for all the treatment effects.

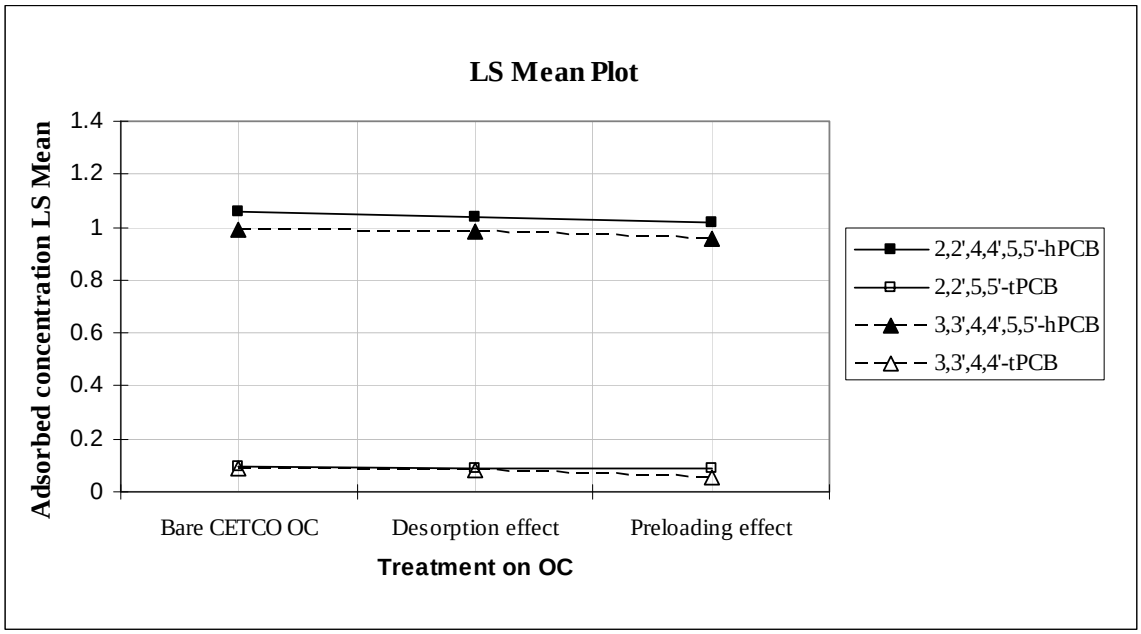

Figure 3.7: Least square means plot for adsorption of tetra- and hexa- chlorinated congeners on CETCO organoclay

Table 3.8: LSMeans Differences Student's t at α=0.050 and t=2.03 for performance of CETCO organoclay for tetra- and hexa- chlorobiphenyl

Level					Least Sq Mean
2,2',4,4',5,5'-hPCB,Bare AC	A				1.056
2,2',4,4',5,5'-hPCB,Desorption effect	A	B			1.036
2,2',4,4',5,5'-hPCB,Preloading effect	A	B			1.019
3,3',4,4',5,5'-hPCB,Bare AC	A	B			0.988
3,3',4,4',5,5'-hPCB,Desorption effect	A	B			0.984
3,3',4,4',5,5'-hPCB,Preloading effect		B			0.957
2,2',5,5'-tPCB,Bare AC			C		0.095
2,2',5,5'-tPCB,Desorption effect			C		0.091
3,3',4,4'-tPCB,Bare AC			C		0.088
2,2',5,5'-tPCB,Preloading effect			C		0.085
3,3',4,4'-tPCB,Desorption effect			C		0.082
3,3',4,4'-tPCB,Preloading effect				D	0.054

The mechanism of sorption of organic contaminants onto organoclay can be explained on the basis of surfactant behavior of the organic cations. The organic contaminants are adsorbed on the oleophilic surface of organoclays due to hydrophobic interactions. The organic cations that are placed in between silica layers of the clay are capable of making micelles and thereby holding organic contaminants in that zone. If humic acid is present in the system then it competes with the target organic contaminant for available sites. Thurman et al. (1982) have reported the radius of gyration of aquatic humic substance to be 4.7- 33 Å corresponding to their molecular weight of 500 to > 10,000. Studies have also shown that depending on pH of the system the building units of humic acid of radial size ≤ 25 Å can be aggregated to make clusters with average radius of 400-500 Å (Oesterberg et al., 1992). While preloading, the larger humic acid molecules that come in contact with the surface of organoclays first get adsorbed to it by hydrophobic interaction with organic cations in the oleophilic zone.

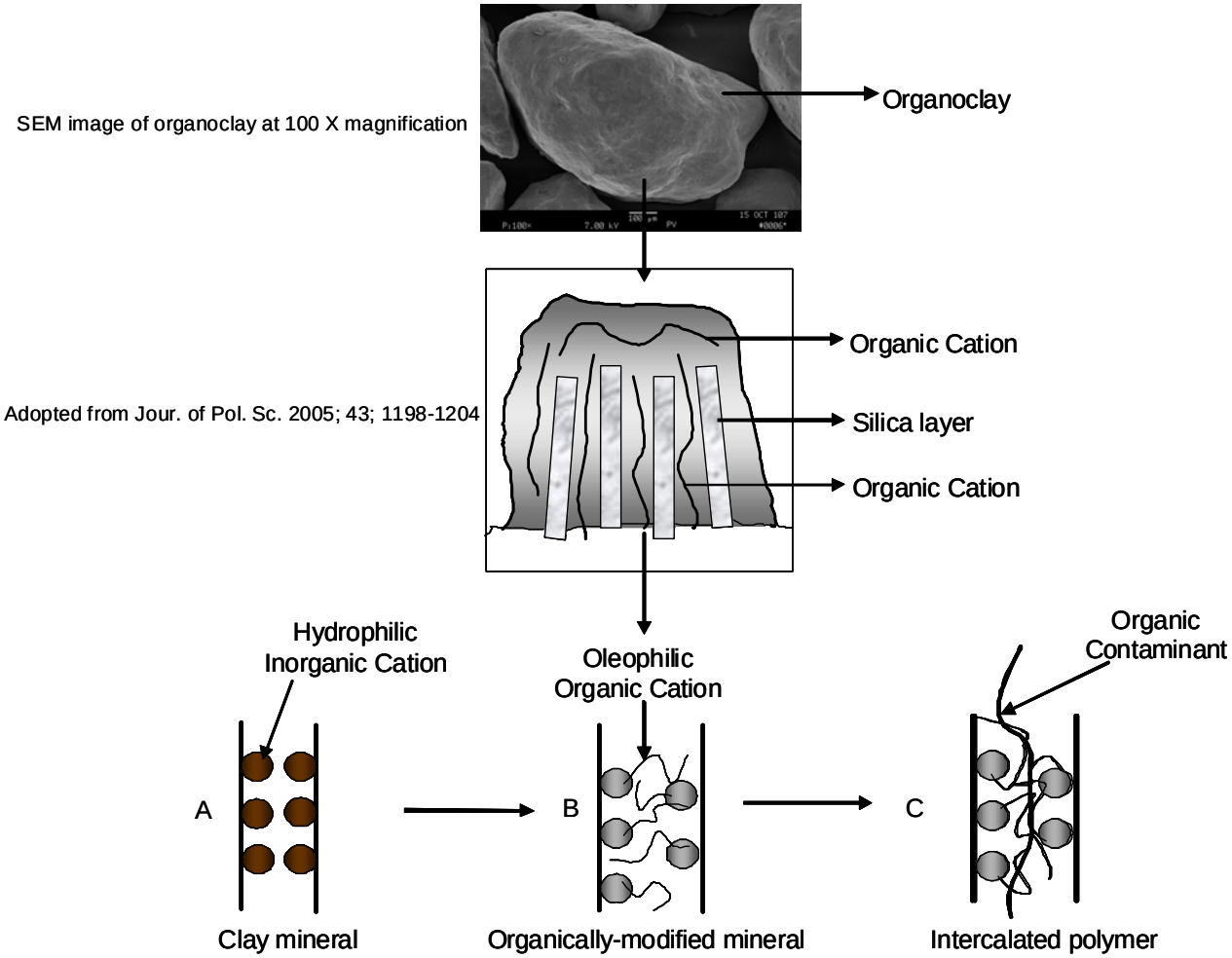

Figure 3.8: Mechanism of sorption of organoclay

These giant humic acid molecules and their aggregates then interfere with the sorption of PCBs by blocking their way to the surfactant moieties. These PCB molecules can adsorb to the humic acid molecules that are already attached to the organoclay surface depending on their partition coefficients (K_{DOC}) as mentioned in table 3.2. In desorption studies 2-chlorobiphenyl did not show any affect from humic acid added in the system after its adsorption but there was some effect in the case of tetra- and hexa-

chlorinated congeners. This fact can be supported by lower K_{DOC} of 2-chlorobiphenyl as compared to that of higher chlorinated congeners that allows its preferable sorption onto organoclay surface.

Additional Information

Model 1 detail:

Actual by Predicted Plot

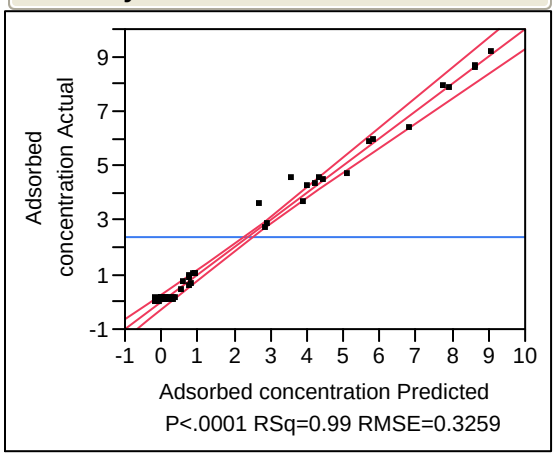

Analysis of Variance

Source	DF	Sum of Squares	Mean Square	F Ratio
Model	17	367.85563	21.6386	203.7433
Error	27	2.86754	0.1062	**Prob > F**
C. Total	44	370.72317		<.0001*

Effect Tests

Source	Nparm	DF	Sum of Squares	F Ratio	Prob > F
OC	2	2	0.10911	0.5137	0.6040
Treatment on OC	2	2	6.54440	30.8102	<.0001*
OC*Treatment on OC	4	4	0.59693	1.4051	0.2589
Loading rate	1	1	346.56433	3263.163	<.0001*
OC*Loading rate	2	2	1.79056	8.4297	0.0014*
Treatment on OC*Loading rate	2	2	11.03097	51.9324	<.0001*
OC*Treatment on OC*Loading rate	4	4	1.21933	2.8702	0.0421*

Model 2 detail:

Actual by Predicted Plot

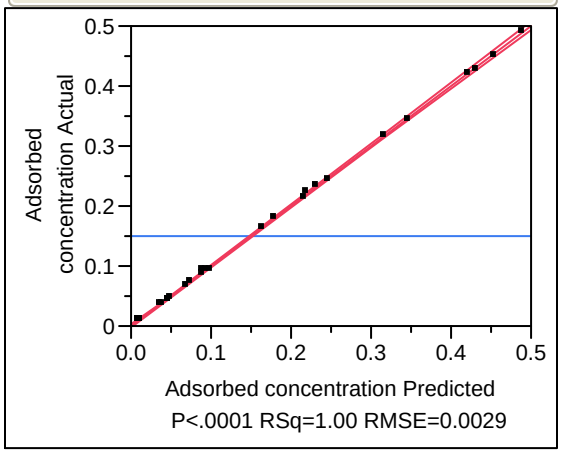

Analysis of Variance

Source	DF	Sum of Squares	Mean Square	F Ratio
Model	13	0.66207551	0.050929	5981.288
Error	16	0.00013624	8.515e-6	**Prob > F**
C. Total	29	0.66221174		<.0001*

Effect Tests

Source	Nparm	DF	Sum of Squares	F Ratio	Prob > F
Type of OC	1	1	0.00000255	0.2992	0.5920
Treatment on OC	2	2	0.01206597	708.5376	<.0001*
Type of OC*Treatment on OC	2	2	0.00054977	32.2835	<.0001*
Loading rate	1	1	0.26588132	31226.15	<.0001*
Type of OC*Loading rate	1	1	0.00000273	0.3203	0.5793
Treatment on OC*Loading rate	2	2	0.01374250	806.9868	<.0001*
Type of OC*Treatment on OC*Loading rate	2	2	0.00075619	44.4048	<.0001*
Loading rate*Loading rate	1	1	0.00006313	7.4141	0.0150*
Loading rate*Loading rate*Type of OC	1	1	0.00001106	1.2992	0.2711

Model 3 detail:

Actual by Predicted Plot

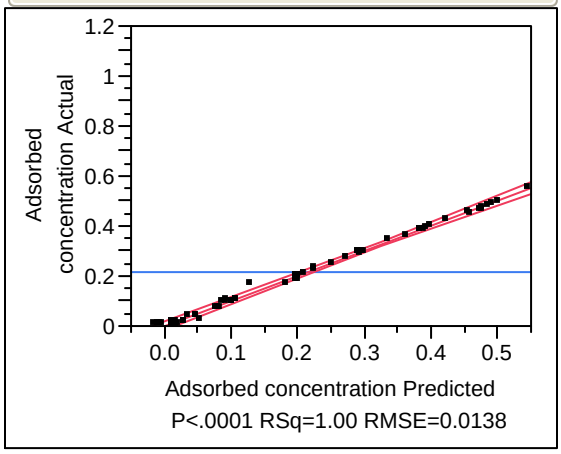

Analysis of Variance

Source	DF	Sum of Squares	Mean Square	F Ratio
Model	26	1.6004990	0.061558	324.7787
Error	33	0.0062547	0.000190	**Prob > F**
C. Total	59	1.6067538		<.0001*

Effect Tests

Source	Nparm	DF	Sum of Squares	F Ratio	Prob > F
PCB congener	3	3	0.80704529	1419.326	<.0001*
Treatment on OC	2	2	0.00052366	1.3814	0.2654
PCB congener*Treatment on OC	6	6	0.00078664	0.6917	0.6578
Loading Rate	1	1	0.62613166	3303.476	<.0001*
PCB congener*Loading Rate	3	3	0.40555736	713.2413	<.0001*
Treatment on OC*Loading Rate	2	2	0.00033598	0.8863	0.4218
PCB congener*Treatment on OC*Loading Rate	6	6	0.01206138	10.6060	<.0001*
Loading Rate*Loading Rate	1	1	0.00025379	1.3390	0.2555
Loading Rate*Loading Rate*Treatment on OC	2	2	0.00188635	4.9762	0.0129*

Atomic Force Micrographs produced to demonstrate the topography of organoclays

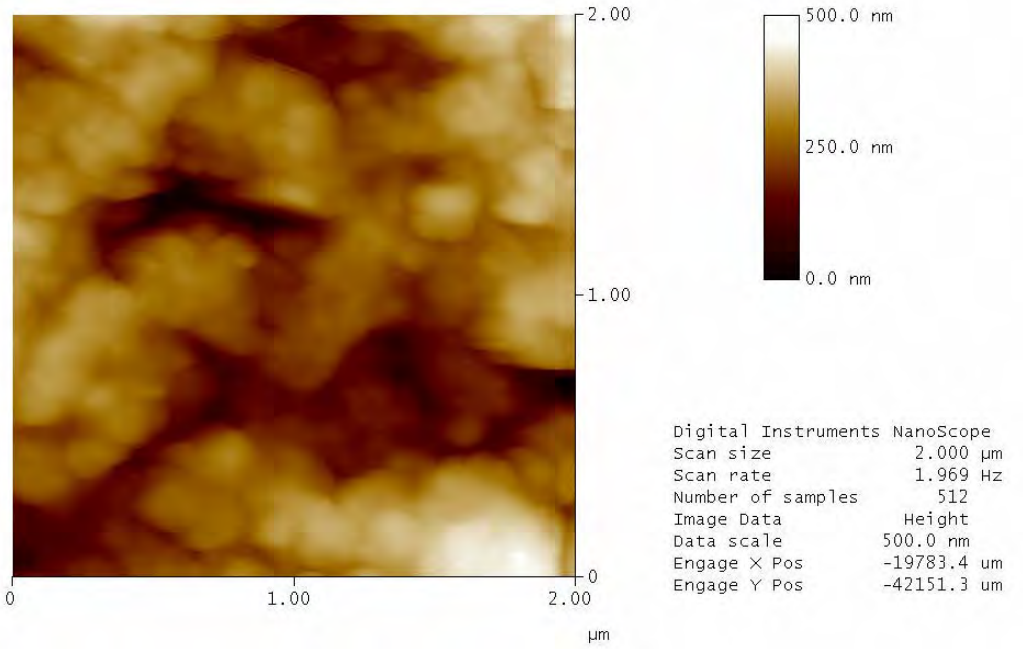

AFM image of CETCO organoclay

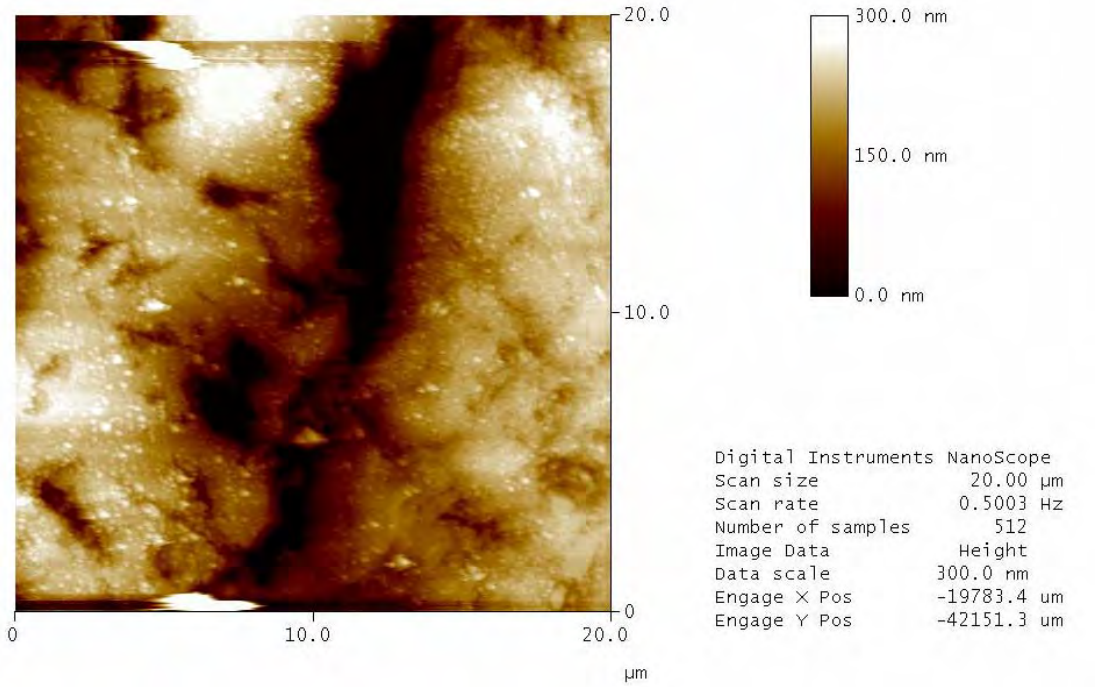

AFM image of Polymer Ventures organoclay

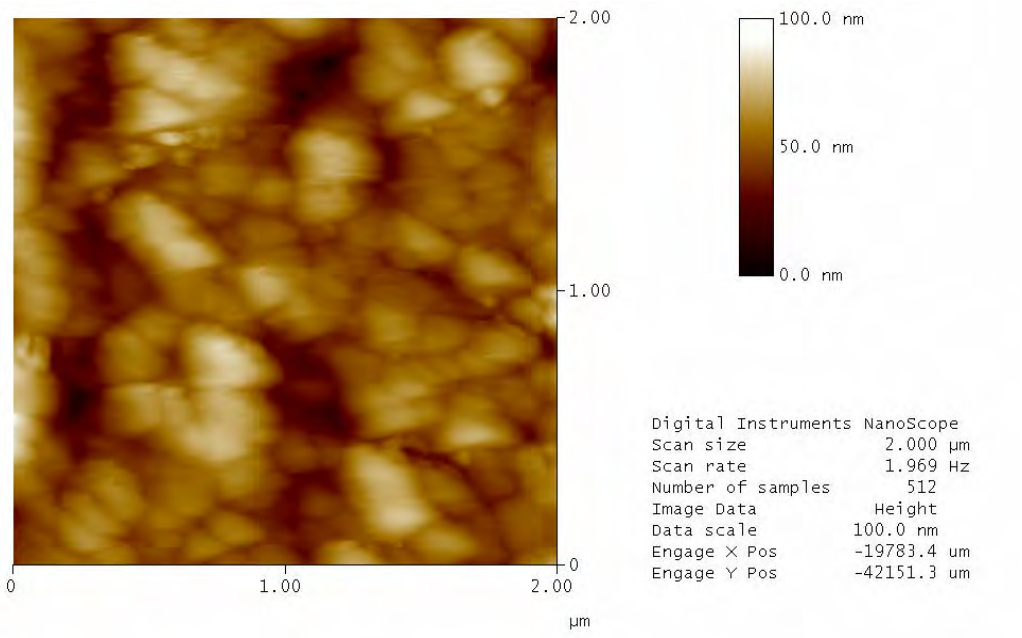

AFM image of Biomin Inc. organoclay

This part of analysis was done in Mechanical Engineering with help of Dr. Todd Gross, Professor and Chair, Dept. of Mechanical Engineering, University of New Hampshire.

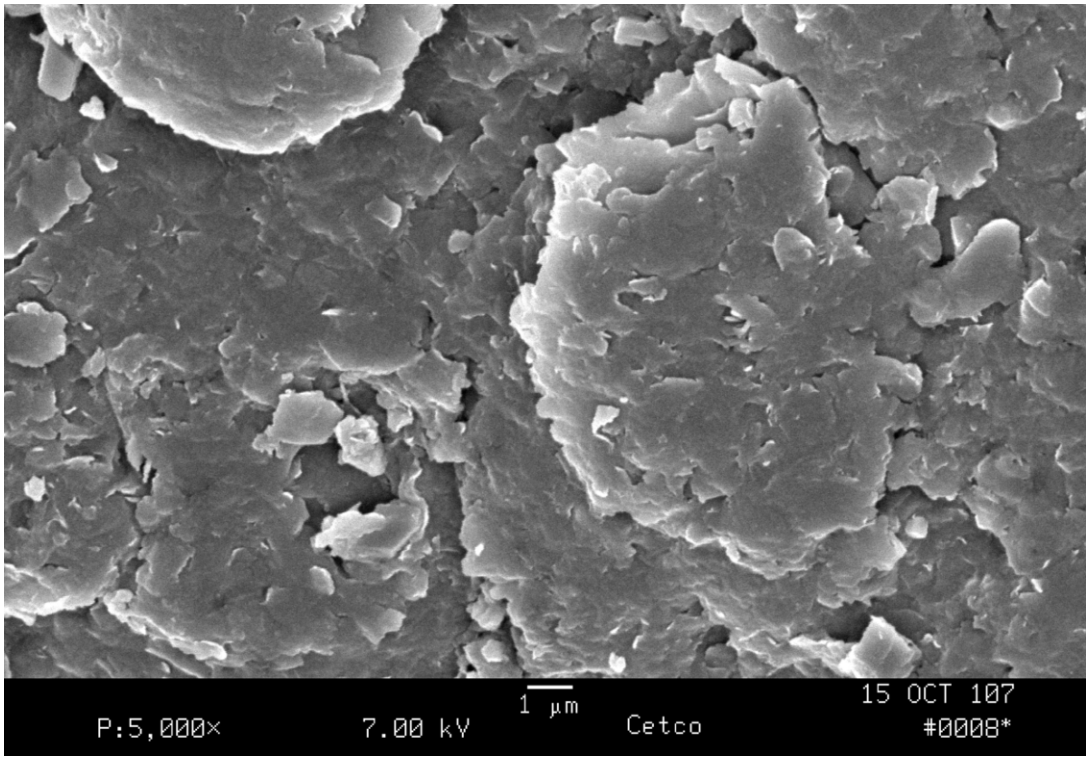

SEM of bare CETCO organoclay

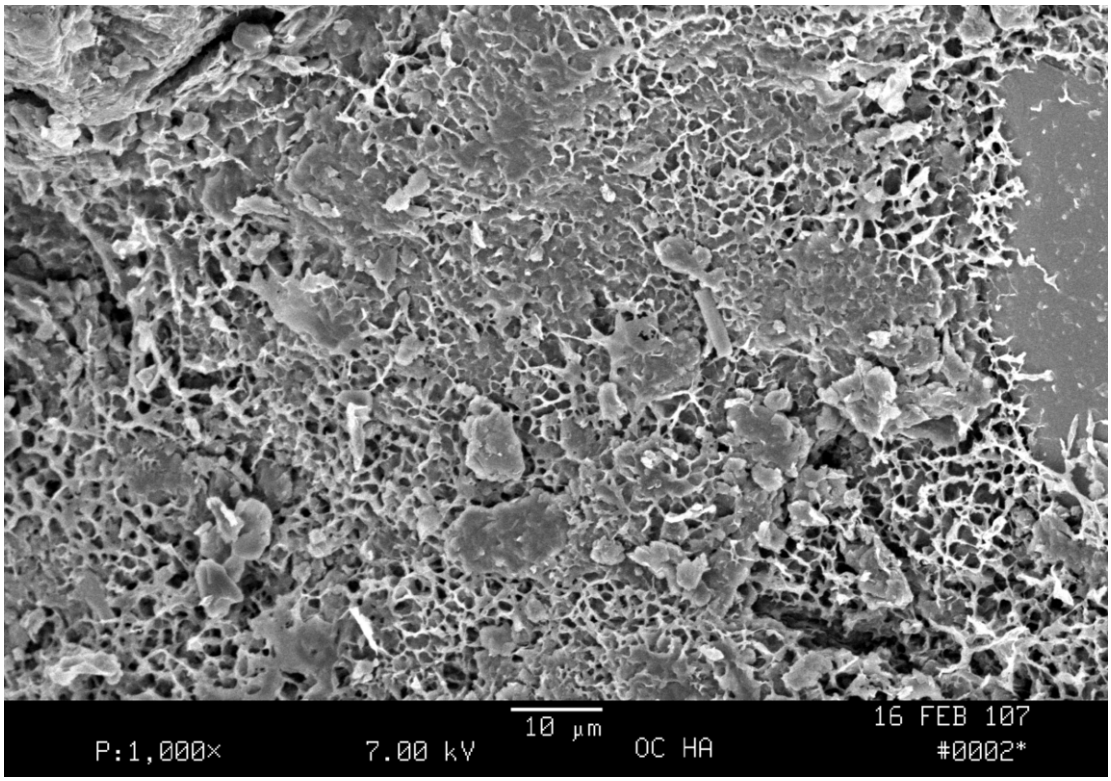

SEM of CETCO organoclay preloaded with 1g/L humic acid solution

References

Ake, C. L.; Wiles, M.C.; Huebner, H. J.; McDonald, T. J.; Cosgriff, D.; Richardson, M.B.; Donnelly, K. C. and Phillips, T. D. Porous organoclay composites for the sorption of polycyclic aromatic hydrocarbons and pentachlorophenol from groundwater. *Chemosphere*, 2003, 51, 835-844.

Arnarson, T. S. and Keil, R. G. Mechanism of pore water organic matter adsorption to montmorillonite. *Marine Chemistry*, 2000, 71, 309- 320.

Butcher, J.B.; and Garvey, E. A. PCB Loading from Sediment in the Hudson River: Congener Signature Analysis of Pathways. *Environmental Science and Technology*, 2004, 38, 3232-3238.

Carmody, O.; Frost, R.; Xi, Y. and Kokot, S. Adsorption of Hydrocarbons on Organo-clays – Implications for Oil Spill Remediation. *Jour. of Colloid and Interface Science*, 2007, 305, 17-24.

Dental, S. K.; Jamarah, A. I. and Sparks D. L. Sorption and Cosorption of 1, 2, 4-Trichlorobenzene and Tannic Acid by Organo-clays. *Water Research*, 1998, 32, 3689-3697.

Erickson, M.D. *Analytical Chemistry of PCBs. Second Edition.* Lewis Publishers, 1997.

Jayens, W. F. and Boyd, S. A. Clay Mineral Type and Organic Compound Sorption by Hexadecyltrimethyammonium – Exchanges Clays. Soil Science Society of American Journal, 1991, 55, 43-48.

Lee, S. Y.; Kim, S. J.; Chung, S. Y. and Jeong, C. H. Sorption of hydrophobic organic compounds onto organoclays. *Chemosphere*, 2005, 55, 781-785.

NRC. *A Risk-Management Strategy for PCB-Contaminated sediments*; National Research Council Report; National Academy Press: Washington, DC, 2001.

Oesterberg, R.; Mortensen, K. Fractal Dimensions of Humic Acids. A Small Angle Neutron Scattering Study. European Biophysics Journal, 1992, 21, 163-7.

Pernyeszi, T.; Kasteel, R.; Witthuhn, B.; Klahre, P.; Vereecken, H. and Klumpp, E. Organoclays for Soil Remediation: Adsorption of 2,4-dichlorobiphenyl on organoclay/ aquifer material mixtures studied under static and flow conditions. *Applied Clay Sciences*, 2006, 32, 179-189.

Poerschmann, J.; Kopinke, Frank-Dieter; Plugge, J.; Georgi, A. Interaction of Organic Chemicals (PAHs, PCB, Triazines, Nitroaromatics and Organotin Compounds) with Dissolved Humic Organic Matter. *Understanding Humic Substances.* Royal Society of Chemistry, 1999, 223-240.

Sheng, G.; Wang, X.; Wu, S. and Boyd, S. A. Enhanced Sorption of Organic Contaminants by Smectitic Soils Modified with a Cationic Surfactant. Journal of Environmental Quality, 1998, 27, 806-814.

Thurman, E. M.; Wershaw, R. L.; Malcolm, R. L.; Pinckney, D. J. Molecular Size of Aquatic Humic Substances. Organic Geochemistry, 1982, 4, 27-35.

Wandruszka, R. V. Humic acids: Their detergent qualities and potential uses in pollution remediation. Geochemical Transactions, 2000, 2.

Wiles, M.C.; Huebner, H.J.; McDonald, T. J.; Donnelly, K. C. and Phillips, T. D. Matrix-immobilized organoclay for the sorption of polycyclic aromatic hydrocarbons and pentachlorophenol from groundwater. *Chemosphere*, 2005, 59, 1455-1465.

Zhao, H. and Vance, G. F. Sorption of Trichloroethylene by Organoclays in the Presence of Humic Substances. *Water Research*, 1998, 32, 3710-3716.

Zimmerman, J.R.; Ghosh, U.; Luthy, R. G.; Bridges, T. S.; Millward, R. N. Addition of Carbon Sorbents to Reduce PCB and PAH Bioavailability in Marine Sediments: Physicochemical Tests. *Environ. Sci. Tech*. 2004, 38, 5458 – 5464.

CHAPTER 4

COMPARISON OF PERFORMANCE OF ACTIVATED CARBON AND ORGANOCLAY AS REACTIVE CAP SORBENTS FOR ADSORPTION OF PAH IN PRESENCE OF HUMIC ACID

Abstract

Coconut shell activated carbon and bentonite based organoclay were compared as reactive cap sorbents that can be used for sequestration of Polycyclic Aromatic Hydrocarbon (PAH) in riverine and marine environment. The presence of natural organic matter (NOM) plays an important role in the fate and transport of organic contaminants in sediments. Therefore, research was conducted to determine the adsorption capacities of sorbents in the presence and absence of humic acid that constitutes an important fraction of NOM. PAHs selected for this study were naphthalene, phenanthrene and pyrene that are readily diffusible in sediment pore waters. Kinetic experiments were conducted to determine the equilibration time required for adsorption of pyrene and phenanthrene onto selected sorbents and to estimate the effects of humic acid. Based on the equilibration time isotherm studies were conducted to determine the adsorption capacities of sorbents for naphthalene, phenanthrene and pyrene. Effect of humic acid was determined in two ways: (i) by preloading the sorbents with humic acid prior to the spiking of PAHs and (ii) desorption caused by humic acid on already adsorbed PAHs. Preloading effects were used to simulate the typical site

conditions and desorption to simulate the long term exposure to NOM present in the system.

Introduction

Polycyclic Aromatic Hydrocarbons (PAHs) are a class of ubiquitous, non-polar organic contaminants that are of major environmental concern because of their toxicity and potential carcinogenity. The concentrations of PAHs in soil and sediments have been found to be increasing with increasing urbanization in the last 20-40 years (Van Metre et al. 2000). The sorption of PAHs to soil and sediment is highly controlled by the presence of organic matter that plays an important role in the fate and transport of PAHs (Means et al. 1980; Liang et al. 2006). The tendency of PAHs to interact with soil and sediment causes slow release of these contaminants into sediment pore water (McGroddy et al. 1995; Maruya et al. 1996). This partitioning behavior of PAHs to solid matrices and their reduced availability to the pore water depend on the presence of organic carbon matrices (such as soot particles) that enhance binding and source of PAHs (pyrogenic/ surface run off) (Maruya et al. 1996). The availability of PAHs in pore water is reliant not only on the solid matrices of sediments but also on the size of the PAH molecules. PAH molecules larger than 10 Å or adsorbed on suspended particles are not easily available for uptake as compared to the small ringed PAHs (including naphthalene, phenanthrene and pyrene) that can diffuse easily in sediment pore water (Williamson et al. 2002). Therefore, this study is focused on adsorption of easily diffusible PAHs including naphthalene, phenanthrene and pyrene on to activated carbon and organoclay in the presence of humic acid. Humic acid, which is complex,

heterogeneous and refractory in nature, constitutes a major part of soil and sediment organic matter (Liang et al. 2006).

Sediments contaminated with hydrophobic organic contaminants (HOCs) such as PAHs can be treated using ex-situ treatment methods such as dredging and disposal or by in-situ treatment methods such as monitored natural recovery (MNR) or capping (reactive/ non-reactive) technology. The most common and in-use technologies are dredging followed by treatment and disposal and MNR. In-situ treatment methods such as reactive capping technologies are under intense research for their effective potential use. Reactive capping can be established by direct mixing of reactive material in the sediments by placement of loose granular material or by introducing reactive core mat consisting of a geotextile impregnated with reactive material in the riverine or marine environment. This research is mainly focused on evaluating sorbents that can be used in the reactive core mat for in-situ management of contaminated sediments.

Studies conducted by Zimmerman et al. (2004) added 3.4 wt % coal - based activated carbon to sediments as in-situ treatment method and showed 84% reduction in aqueous concentration of PAHs. Cornelissen et al. (2006) evaluated the effectiveness of activated carbon amendments and found that 2 wt % of activated carbon can significantly reduce the pore water concentrations of PAHs in strongly sorbing sediments that are rich in carbonaceous geosorbents. However, there can be reduction in the performance of activated carbon in the presence of natural organics such as humic and fulvic acids. The building unit of a humic acid molecules can be ≤ 25 Å and

can form aggregates of average radii of 400-500 Å (Osterberg et al. 1992). These humic molecules that are larger than a target organic contaminants cannot enter the pore structure of activated carbon and may block the way of the target organic contaminants to the internal pore structure (Li et al. 2003; Quinlivan et al. 2005; Pignatello et al. 2006). Besides porosity another factor that plays an important role in adsorption of HOCs is surface chemistry of activated carbon. Based on these two properties (high porosity and hydrophobic surfaces) coconut shell activated carbon was selected for this research.

Another sorbent that was evaluated in this study is bentonite based organoclay. Organoclays are organically modified clays in which inorganic cationic counter ions are replaced by organic cations by an ion exchange process (Jayens and Boyd, 1991). These organic cations increase the interlayer spacing between the silica plates as well as create an oleophilic zone for sorption of organic contaminants (Carmondy at al, 2007; Dental et al., 1998). These organic cations behave like a surfactant and trap organic contaminants into their miceller structure. Studies conducted to use organoclay in soil remediation, groundwater purification, industrial waste water treatment and oil spills have shown good adsorption capacity of organoclays for chlorinated compounds and aromatic hydrocarbons (Zhao et al., 1998; Dental et al., 1998; Carmondy et al., 2007; Pernyeszi et al., 2006; Ake et al., 2003; Wiles et al., 2005). Zhao et al. (1998) have shown that organoclay can perform better than activated carbon in the presence of humic acids depending on its composition. Therefore, in this research organoclay was selected as an alternative or amendment to be used alone or in combination with

activated carbon for reactive capping of sediments. For its applicability in treatment of sediment porewater it was necessary to evaluate its performance in the presence of natural organics such as humic acids. Therefore, the sorption capacity of organoclay was evaluated for PAHs in the presence and absence of humic acid.

With the main objective of developing a reactive capping mat that contains a sorbent amendment mixture capable of sequestering persistent organic contaminants, this research is focused on evaluation of sorbents that can be used in this mat for its effective implementation. For this purpose the sorption affinity and capacity of coconut shell activated carbon was compared with that of bentonite based organoclay for PAHs in the presence and absence of humic acid.

Materials and Methods

Chemicals

PAHs selected for this study were naphthalene, obtained from Accustandard Inc. (New Haven, CT, USA), phenanthrene and pyrene, both of which were obtained from Ultra Scientific (North Kingstown, RI, USA) in neat form or dissolved in methylene chloride. Acenaphthene d-10 used as internal standard and 2-fluorobiphenyl used as surrogate standard were also purchased from Ultra scientific (North Kingstown, RI, USA). Humic acid was obtained from Sigma-Aldrich (St. Louis, MO, USA) in the form of sodium salt. Sodium azide used in the experiments to avoid biological contamination

was purchased from EMD Chemicals Inc. (San Diego, CA, USA). Sodium sulfate anhydrous used in sample preparation to remove chemically bound water prior to GC/ MS analysis was obtained from Fisher Scientific (Morris Plains, NJ, USA). Ultra high purity chemicals and GC-grade solvents used throughout experimentation were obtained from Fischer Scientific (Agawam, MA, USA).

Sorbent material

Activated carbon: OLC 12 x 40 a coconut shell based activated carbon used in this research, was obtained from Calgon Carbon Corporation (Pittsburg, PA, USA). Coconut shell activated carbon was selected because of its high microporosity and wider use in trace organics removal.

Organoclay: PM 199 bentonite based organically modified clay was obtained from CETCO (Arlington Heights, IL, USA). Hydrogenated tallow based quaternary amines have been used to increase the inter-layer spacing of bentonite clay which was found to be about 35.74 Å with about 19% organic content. Because of its high hydrophobicity, PM 199 was used in the experiments as obtained from CETCO with no modification.

Experimental Procedures

All the experiments including kinetic and isotherm studies were conducted in separate batches of 125 ml in the presence and absence of humic acid. The stock solutions of naphthalene, phenanthrene and pyrene were prepared separately in

methanol because there is no measurable effect of methanol on sorption capacity of organoclay (Lee et al., 2005) and activated carbon (Dowaidar et al., 2007). This stock solution was used for spiking the samples prepared with deionized (DI) water or humic acid solution. In kinetic experiments humic acid interferences were determined by preloading the sorbents with humic acid. In isotherm studies the effect of humic acid was determined by preloading the sorbents with humic acid prior to the spiking of PAHs and desorption of contaminants (once adsorbed) was determined by spiking the humic acid in the system after PAHs were allowed to adsorb on sorbent for selected equilibration time.

Preloading sorbents: The preloading of sorbents including organoclay and activated carbon was done by 1g L^{-1} humic acid stock solution having 10% sodium azide to avoid biological growth. The preloading was done in separate batches having 0.1 g of sorbent in 125 ml flask. Sorbents were soaked in the humic acid solution and kept on continuous mixing for 48 hours on rotary shaker at 150 rpm. After preloading the same flask containing preloaded sorbent and humic acid solution was used as such for further experimentation.

Kinetics experiments:

The kinetic studies were conducted to estimate the equilibration time required for adsorption of phenanthrene and pyrene onto activated carbon and organoclay in the presence and absence of humic acid. The experiments were conducted with bare sorbents in de-ionized water and preloaded samples in humic acid solution for 15 days.

The concentration used for phenanthrene was 1.6 mg L^{-1} and 0.16 mg L^{-1} for pyrene. The amount of sorbent was kept constant at 0.1 g. Separate batches were prepared for phenanthrene and pyrene for bare sorbents (organoclay and activated carbon) and preloaded sorbents. All the samples were kept on continuous mixing at 150 rpm until sampling was done.

Isotherm experiments:

Isotherm experiments were conducted at different loadings of selected PAHs including naphthalene, phenanthrene and pyrene for organoclay and activated carbon in the presence and absence of humic acid. These experiments were conducted separately for each PAH for both the sorbents for equilibration time as obtained from pyrene kinetics with continuous mixing at 150 rpm on rotary shaker. Pyrene was the biggest (4-ringed structure) compound among three selected PAHs and had a longer equilibration time than phenanthrene in the presence of humic acid therefore equilibration time was selected on the basis of pyrene kinetics in the presence of humic acid. The effect of humic acid was determined by preloading the sorbents or by spiking humic acid after adsorption of PAHs. For determination of sorbent adsorption capacities, experiments were conducted with bare sorbents in de-ionized water spiked with different concentrations of PAHs (table 4.1). To determine the effect of preloading sorbents were preloaded with humic acid prior to the spiking of PAHs and were kept in the same humic acid solution used for preloading. After equilibration sampling was done for both bare sorbents and preloaded sorbent samples. After sampling, bare sorbent samples were spiked with humic acid to obtain the same concentration of humic acid as

used for preloading (1 g L^{-1}) to determine the desorption effects. The samples were again kept for continuous mixing for the same equilibration time.

Isotherm studies for bare activated carbon: Due to very high adsorption capacity of activated carbon for all selected PAHs it was difficult to determine the actual behavior of activated carbon at low concentrations of PAHs while maintaining the spiked concentrations below the water solubility limits. To estimate the adsorption capacity of activated carbon it was necessary to load the activated carbon with sufficiently high concentrations of PAHs. Therefore, separate systems were prepared having 0.1 g bare activated carbon in de-ionized water and spiked with five different concentrations of PAHs within the solubility limit as done before. These experiments were also conducted separately for each PAH (naphthalene, phenanthrene and pyrene) but spiking was done three times at every 72 hours duration using same concentrations each time in order to obtain the final spike concentration to be thrice as used in the first set of isotherm studies (table 4.1). After third spiking all the samples were kept on continuous mixing on rotary shaker at 150 rpm for equilibration time of 10 days.

Sample Extraction and Analysis:

All the samples were extracted with surrogate solvent having 2-fbp as surrogate standard in methylene chloride. The ratio of sample volume to surrogate solvent (1:2) was kept the same for all the samples. From each batch two sub-samples were extracted in order to estimate any kind of deviation in the extraction method. All the samples were mixed thoroughly with surrogate solvent for 30 seconds three times at

duration of 30 seconds each and then stored at 4˚ C for at least 24 hours. The surrogate recoveries obtained were high in the range of 70 – 130% using this extraction method. The extracted samples solvent was then restored and passed through sodium sulfate prior to GC vial preparation to avoid presence of water in any form. The filtered samples were then taken into GC vials and mixed with internal standard Acenaphthene-d10 followed by GC/MS analysis.

GC/ MS analysis: All the extracted samples were analyzed using internal standard method on Varian CP3800 Gas Chromatograph (GC)/ Saturn 2200 Ion Trap Mass Spectrometer (MS) with a CP8400 Auto Sampler. The GC column used was a DB-5 type capillary column (Varian Factor Four VF-5ms), 30 m long, 0.25 mm ID and 0.5 µm thick. The ion-trap was operated in selected scan mode (MS/MS) for each selected PAH. The column temperature was programmed at 80˚ C with hold time of 2 min followed by a temperature ramp up to 315 ˚ C at the rate of 15˚ C - 30˚ C with final held time of 2 minutes depending on the PAH.

Results and Discussions

Kinetic studies:

Figure 4.1 shows the adsorption kinetics of phenanthrene and pyrene adsorption on organoclay and activated carbon in the presence and absence of humic acid. Figure 4.1A-B represents the kinetics of phenanthrene adsorption on organoclay and activated carbon, respectively. In the case of organoclay the effect of humic acid was found to be

less significant and reduced with time as compared to that of activated carbon. For both type of sorbents equilibration time for phenanthrene adsorption was found to be around 72 hours which was approximately the same for organoclay preloaded with humic acid but it was approximately 120 hours for activated carbon preloaded with humic acid.

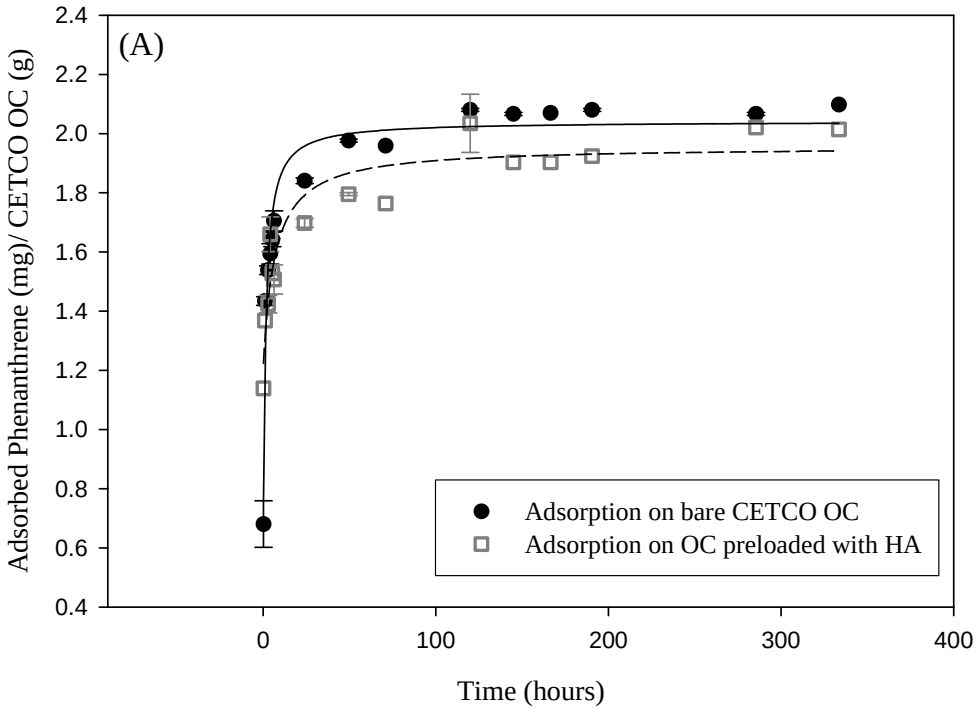

Figure4.1A: Kinetics: Phenanthrene adsorption on organoclay

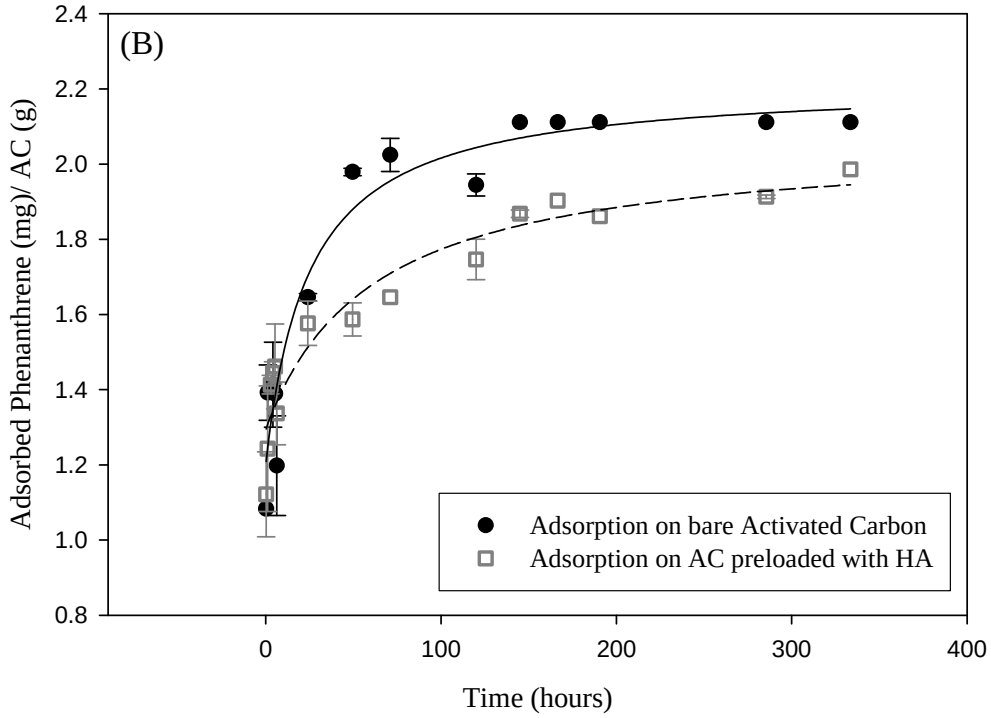

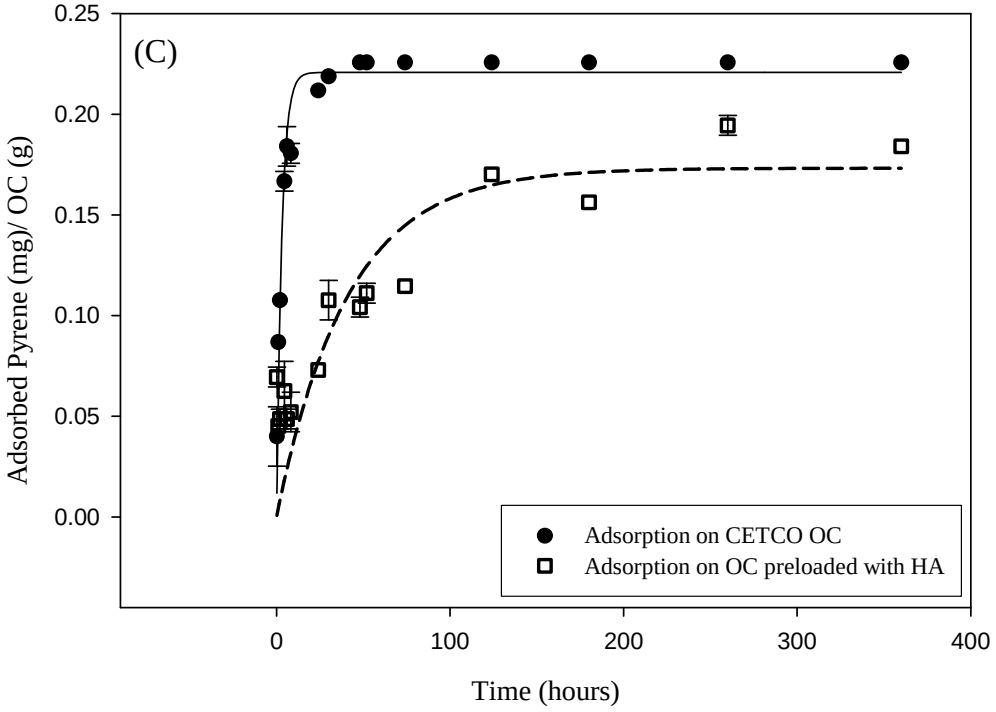

Figure4.1B-C: Kinetics of adsorption: (B) Phenanthrene adsorption on activated carbon (C) Pyrene adsorption on organoclay

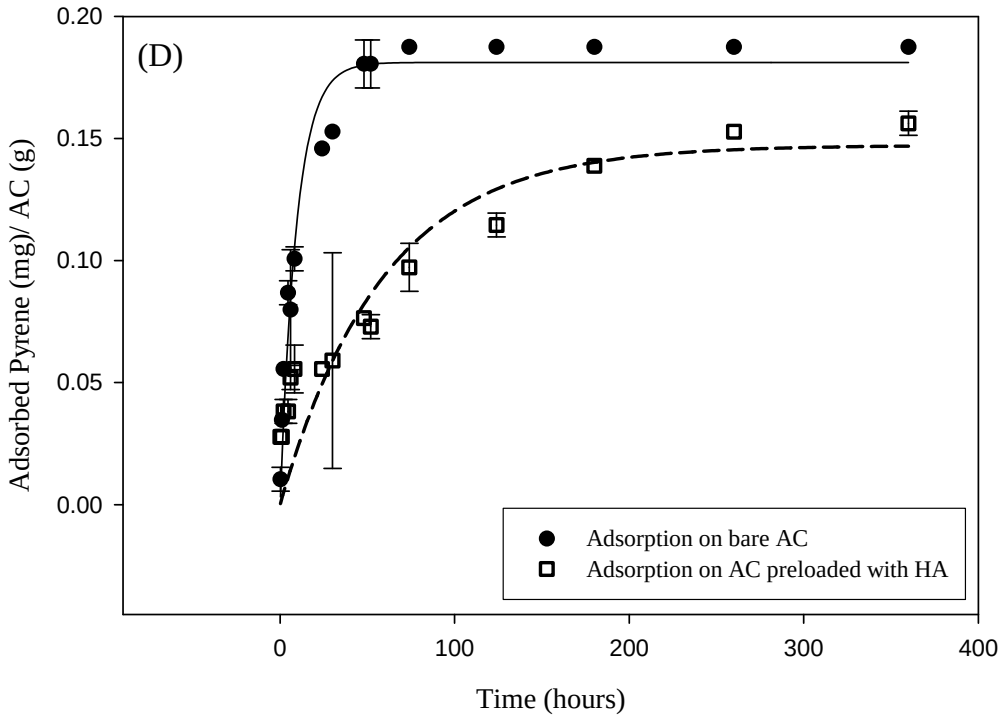

Figure4.1 D: Kinetics: Pyrene adsorption on activated carbon

Figure 4.1 C-D shows kinetics of pyrene adsorption on organoclay and activated carbon, respectively. In the case of pyrene adsorption capacity of organoclay was found to be higher than that of activated carbon and the effect of preloading was also found to be significant in the case of activated carbon. In the case of pyrene also, equilibrium for bare sorbents was achieved around 72 hours but in the presence of humic acid equilibration time was found to be around 100 hours for organoclay and around 200 hours for activated carbon. Therefore, an equilibration time of 5 days was selected for isotherm studies of organoclay for all selected PAHs and 9 days for activated carbon. The delaying effect of preloading the sorbents with humic acid can be attributed to the pore blockage effect on activated carbon and blocking of interlayer spacing of organoclay due to the high loading of humic acid. The humic acid molecule that are ≤ 25

Å and are capable of making bigger aggregates of about 400 – 500 Å (Osterberg et al. 1992) can block porous structure of activated carbon (<4-250 Å given by Henning and Schafer) and 35.74 Å interlayer spacing between the silica layers of organoclay making internal pore structure of activated carbon and hydrophobic zone of organoclay less available to the target compounds. The target compounds then diffuse slowly through a reduced pore area into the available adsorption sites depending on their diffusivity, availability of sites and partition coefficients for humic acid (table 4.1).

PAH	† Minimal box dimension (A°)			††Molecular Diffusion Coefficient 10^5 D/(cm2 s-1) at 40° C	†††Log K_{OW}	††† Log K_{DOC} for humic acid	Isotherm Studies Concentration Range After Single Spiking (mg L^{-1})	Concentration Range After Triple Spiking (mg L^{-1})
	Length (L)	Breadth (B)	Depth (D)					
Naphthalene	8.9	7.2	3.1	1.06	3.3	3.05	0.8 - 40	2.4 - 120
Phenanthrene	11.5	7.7	3.1	0.495	4.44	3.85	0.08 - 2	0.24 - 6
Pyrene	11.4	9.5	3.1	0.49	5.19	4.46	0.008 – 0.2	0.024 – 0.6

† Williamson et al. (2002); †† Gustafson et al. (1994); ††† Poerschmann et al. (1999)

Table 4.1: Details and Concentration of PAH compounds used in the study

Isotherm studies:

The adsorption capacity of activated carbon and organoclay for naphthalene, phenanthrene and pyrene was determined in the presence and absence of humic acid. The effect of humic acid was determined as preloading effect and desorption effect. As mentioned earlier, in the case of preloading both the sorbents were exposed to the high loadings of humic acid prior to the selected PAH adsorption. In the desorption study the selected PAHs were allowed to adsorb on sorbent surfaces followed by introduction of humic acid in the system to determine if PAHs, once adsorbed on sorbent surfaces, are prone to desorption. The adsorption capacities of both the sorbents and the preloading effect of humic acid on the adsorption capacities of both the sorbents were evaluated on the basis of K_d values (table 4.2) that were obtained as slopes by plotting aqueous equilibrium concentration on x-axis against adsorbed concentration on Y-axis. The adsorption capacities of the sorbents were also determined by using the Freundlich model in its non-linear form:

$$q_e = K_f (C_e^{1/n})$$

Here, *qe* is adsorbed concentration (mg g^{-1}), *Kf* is Freundlich Isotherm constant, *Ce* is equilibrium concentration (mg L^{-1}) and 1/n is the Freundlich exponent which is dimensionless. Figure 4.2 shows Freundlich isotherms and actual trends of the adsorption isotherm curves for naphthalene, phenanthrene and pyrene adsorption on activated carbon and organoclay. In the case of activated carbon (Figure 4.2A, 4.2C and 4.2E) the data points obtained from both the isotherm studies were merged to

obtain the trend of isotherm behavior for bare activated carbon over a wide range of concentrations.

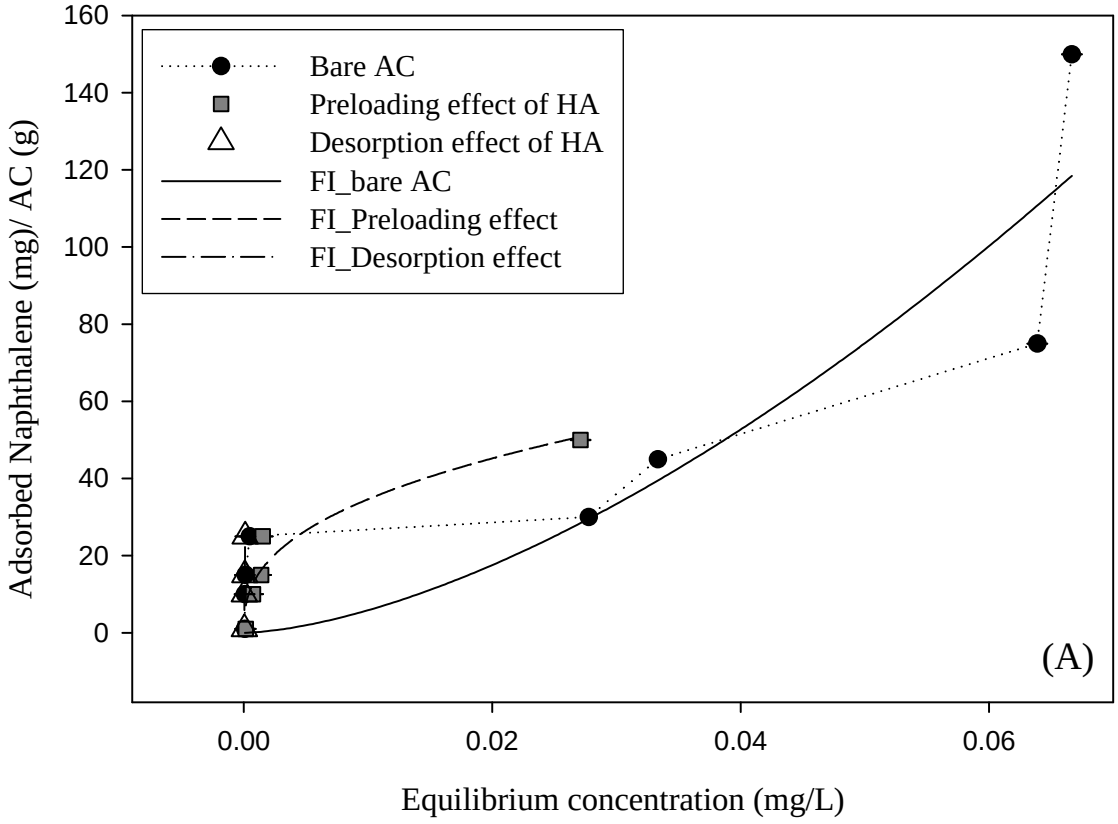

Figure 4.2 A: Freundlich Isotherms and actual trend of curves for adsorption on bare sorbents and preloading and desorption effect of humic acid: Naphthalene adsorption on activated carbon

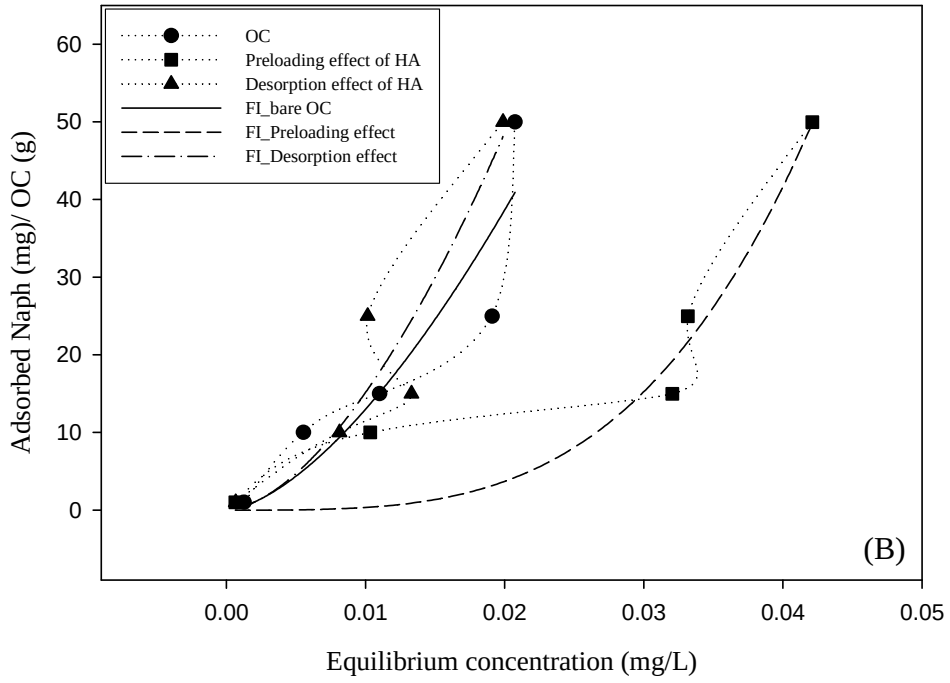

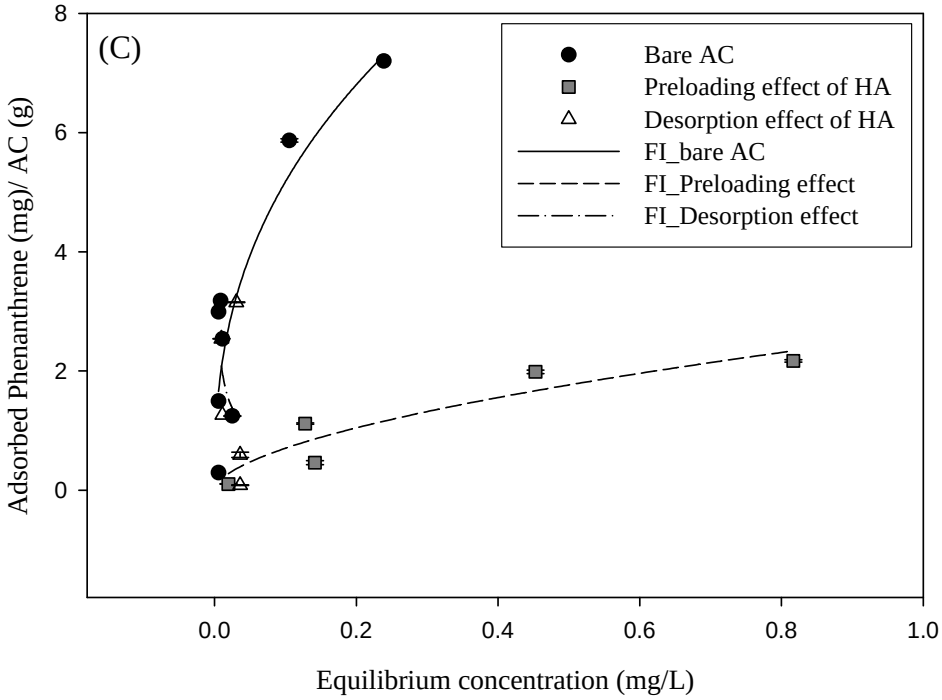

Figure 4.2 B-C: Freundlich Isotherms and actual trend of curves for adsorption on bare sorbents and preloading and desorption effect of humic acid: (b) Naphthalene adsorption on organoclay (c) Phenanthrene adsorption on activated carbon

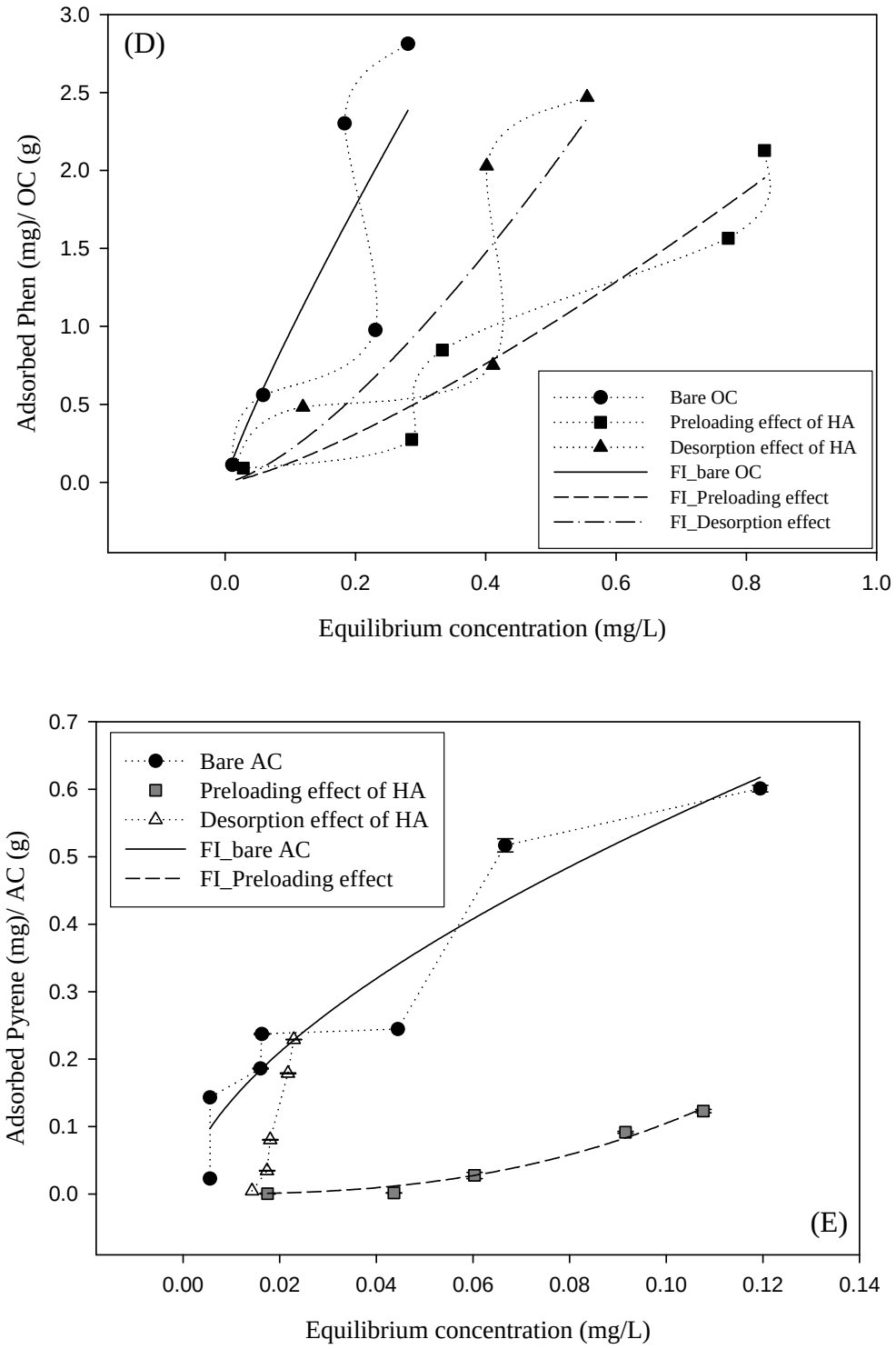

Figure 4.2 D-E: Freundlich Isotherms and actual trend of curves for adsorption on bare sorbents and preloading and desorption effect of humic acid: (d) Phenanthrene adsorption on organoclay (e) Pyrene adsorption on activated carbon

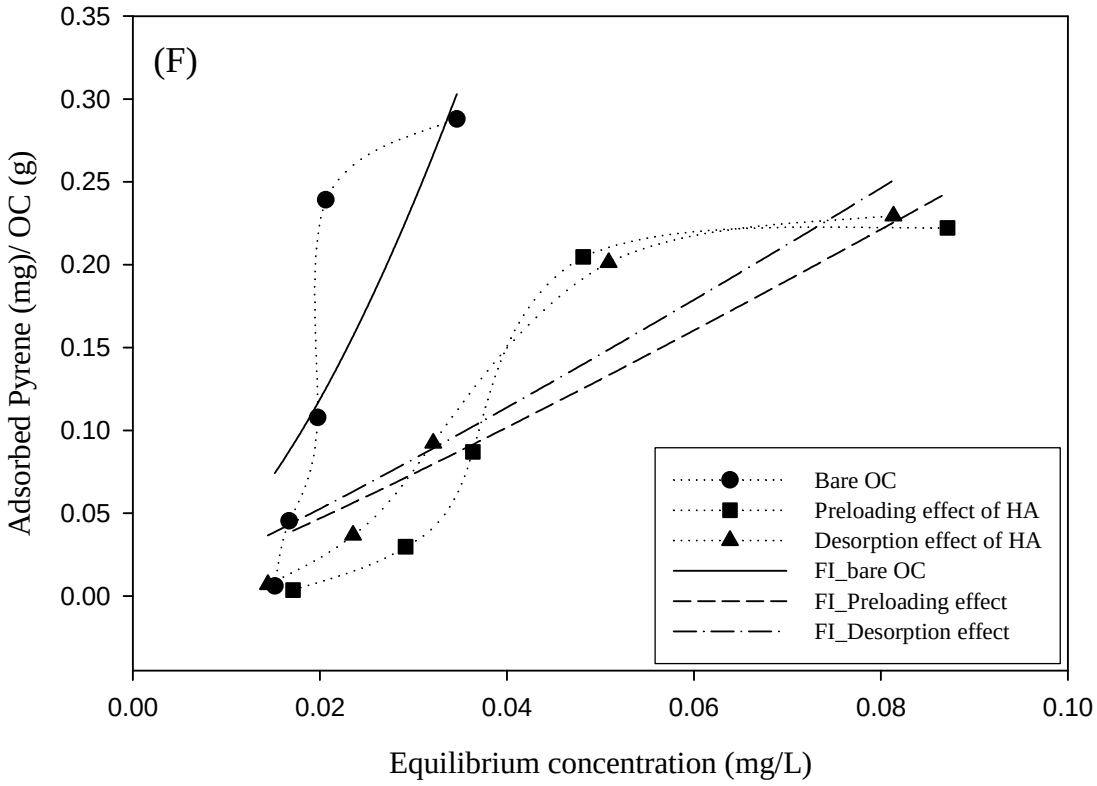

Figure 4.2 F: Pyrene adsorption on organoclay

The adsorption capacity of both the sorbents was found to be very high for naphthalene (table 4.2). The desorption effect of humic acid was not significant for both the sorbents but preloading effect was significant for organoclay (Figure 4.2 A-B). The preloading effect was not found to be as significant for naphthalene adsorption on activated carbon with only 3.4% reduction in comparison to organoclay that had 52.1% reduction in adsorption affinity.

	Adsorption Isotherm Constants		Freundlich Isotherm Constants			
	Kd (L g^{-1})		K_f ($mg^{[1-(1/n)]}$ $L^{(1/n)}$ g^{-1})		1/n	
CETCO OC	Adsorption on bare OC/ AC	Preloading effect	Adsorption on bare OC/ AC	Preloading effect	Adsorption on bare OC/ AC	Preloading effect
Naphthalene	2015.10	964.50	18230.11	3178855.65	1.57	3.49
Phenanthrene	10.58	2.43	7.26	2.49	0.88	1.30
Pyrene	13.42	3.29	93.98	3.75	1.71	1.12
Coconut shell AC						
Naphthalene	1503.30	1452.00	8691.36	203.68	1.59	0.38
Phenanthrene	24.59	2.51	12.84	2.62	0.39	0.57
Pyrene	4.59	1.46	2.22	44.53	0.60	2.63

Table 4.2: Adsorption Isotherm and Freundlich Isotherm Constants for adsorption of Naphthalene, Phenanthrene and Pyrene on Organoclay and Activated Carbon

Based on the K_d values the adsorption capacity was found to be higher for organoclay but the performance of both the sorbents was also compared statistically using JMP® 7 software. The variability chart was developed to indicate the trend of isotherms (linear/ non-linear) to select the factors for the model (details in additional information). The experimental factors considered in the model were the type of sorbent, treatment of sorbent (Bare Sorbent; Preloading and Desorption effects) and the loading rate (table 4.3). Due to the non-linear behavior of the isotherm curves in the variability chart, the quadratic term of loading rate was also included in the model.

Table 4.3: Specifications for statistical model 1

Model 1 specification:
Sorbent
Treatment
Sorbent*Treatment
Loading Rate
Sorbent*Loading Rate
Treatment*Loading Rate
Sorbent*Treatment*Loading Rate
Loading Rate*Loading Rate

The p-value in analysis of variance (ANOVA) was obtained to be < 0.0001 that indicated the selected model was significant (details in additional information). The F-test was also performed to determine the significance of each term selected in the model. The least square means plots of adsorbed concentrations were obtained to determine the difference in adsorption capacities of both sorbents and to determine the preloading and desorption effects on their performance. Statistically, the adsorption capacity of organoclay was found to be slightly higher than that of activated carbon. No desorption was noticed for both the sorbents but reduction in adsorption capacity of organoclay was noticed due to preloading with humic acid (figure 4.3A).

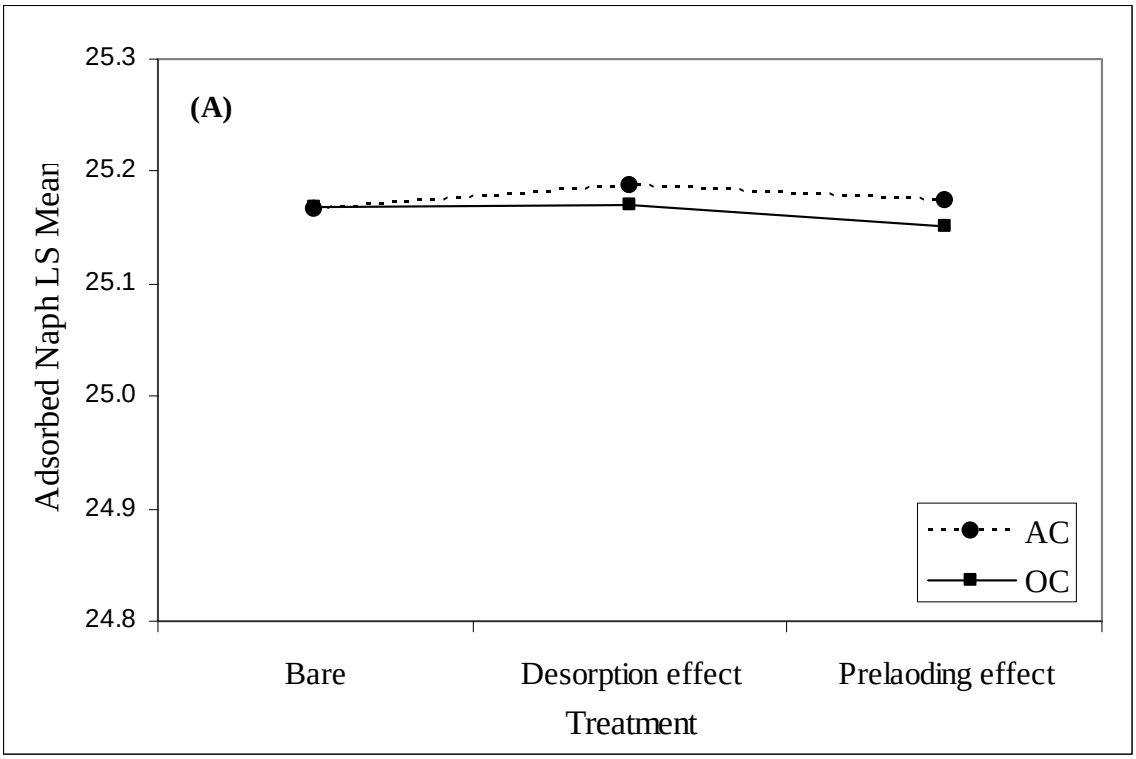

Figure 4.3 A: Least square means plot for comparison of performance of organoclay and activated carbon for adsorption of naphthalene

Figure 4.2C-D shows phenanthrene adsorption on activated carbon and organoclay respectively in the presence and absence of humic acid. The adsorption capacity of activated carbon was found to be higher than that of organoclay based on K_d values (table 4.2). The effect of preloading the sorbents with humic acid was significant for both activated carbon and organoclay. There was a 90 % reduction in adsorption capacity of activated carbon due to preloading with humic acid and a 77 % reduction for organoclay. There was no desorption in the case of activated carbon but slight desorption was noticed in the case of organoclay. The statistical analysis was also done to compare the performance of both the sorbents for phenanthrene adsorption. The

model 2 was developed for phenanthrene as shown in table 4.4 (details in additional information).

Table 4.4: Specifications for statistical model 2

Model 2 specification:
Sorbent
Treatment
Sorbent*Treatment
Loading rate
Sorbent* Loading rate
Treatment* Loading rate
Sorbent*Treatment* Loading rate
Loading rate * Loading rate

The results showed higher adsorption capacity of activated carbon for phenanthrene as compared to that of organoclay (figure4.3B). The preloading effect of humic acid was found to be significant for both the sorbents. There was no desorption in the case of activated carbon but slight desorption was noticed in the case of organoclay.

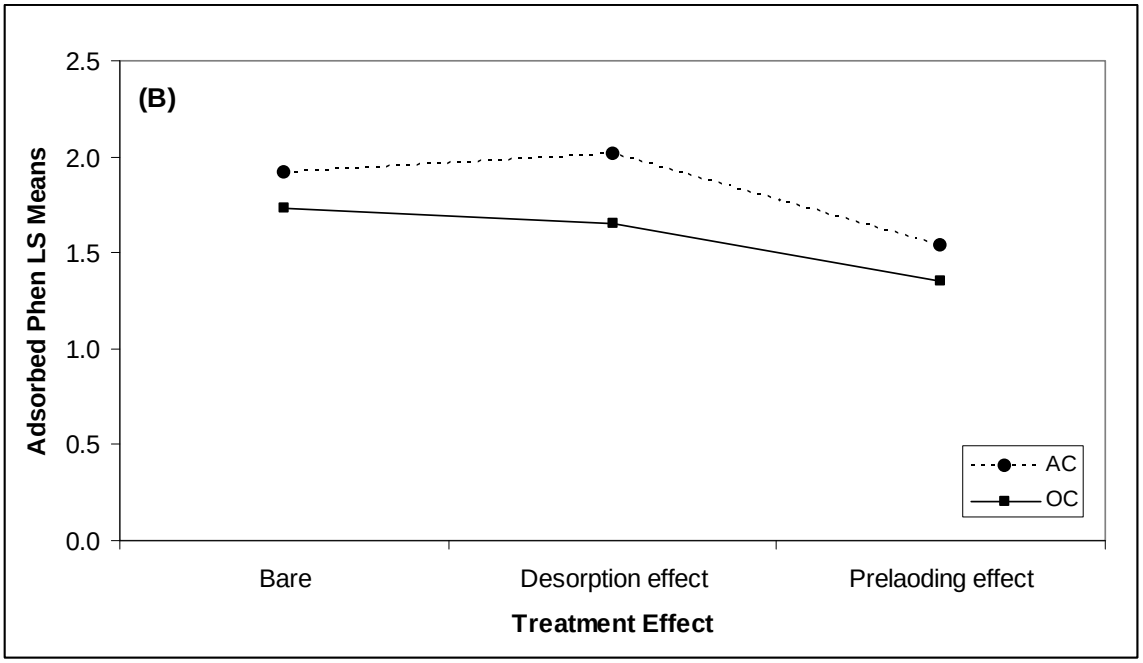

Figure 4.3 B: Least square means plot for comparison of performance of organoclay and activated carbon for adsorption of phenanthrene

Figure 4.2 E-F shows results for pyrene adsorption on activated carbon and organoclay with preloading and desorption effect of humic acid. The adsorption capacity of organoclay was found to be higher than that of activated carbon for pyrene based on the K_d values (table 4.2). The preloading effect was found to be significant for both the sorbents with 76% reduction in adsorption capacity of organoclay and 68% reduction in the adsorption capacity of activated carbon. The desorption effect was found to less in case of activated carbon as compared to organoclay. These results were also analyzed statistically (in the same way as for naphthalene and pyrene) by developing a full factorial model with main factors: the type of sorbent, treatment of sorbent (Bare Sorbent; Preloading and Desorption effects) and the loading rate (table 4.5). Due to non-linear trend of isotherms, quadratic term of loading rate was also considered in the model.

Table 4.5: Specifications for statistical model 3

Model 3 specifications:
Sorbent
Treatment
Sorbent*Treatment
Loading rate
Sorbent* Loading rate
Treatment* Loading rate
Sorbent*Treatment* Loading rate
Loading rate * Loading rate

The adsorption capacity of organoclay was found to be higher than that of activated carbon (figure 4.3C). The preloading effect was found to be significant for both the sorbents and the desorption effect was not significant for activated carbon as it was for organoclay.

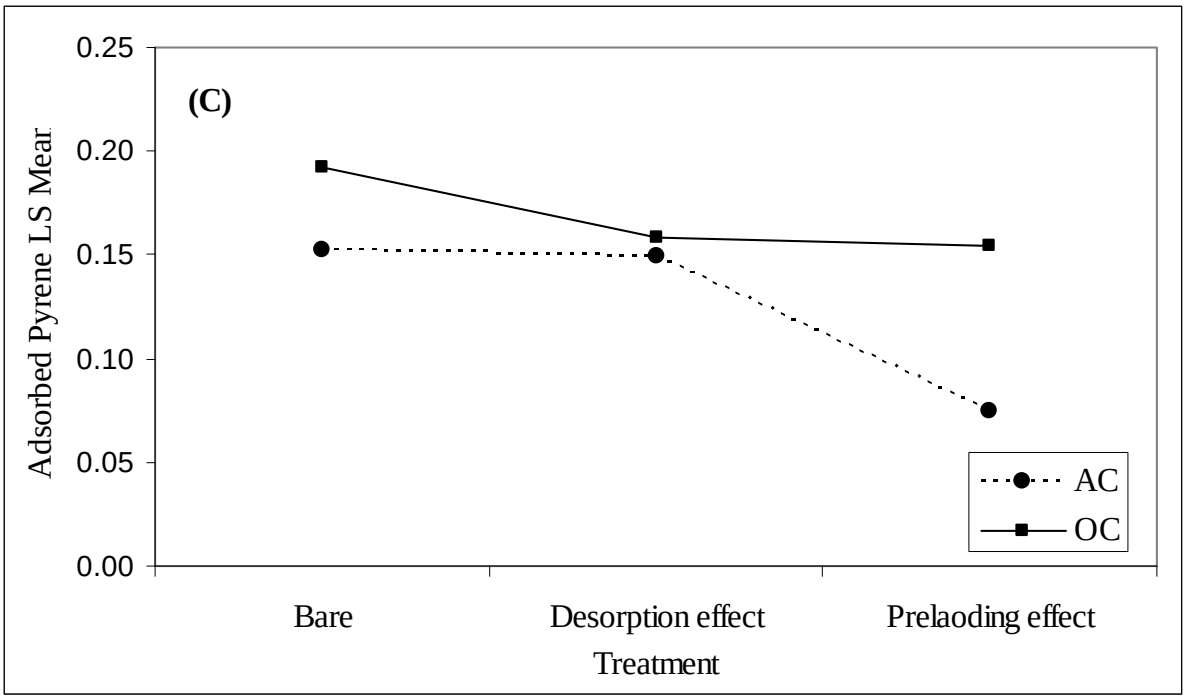

Figure 4.3 C: Least square means plot for comparison of performance of organoclay and activated carbon for adsorption: Pyrene

In isotherm studies, the adsorption capacity of activated carbon was greatest for naphthalene followed by phenanthrene and then for pyrene. For organoclay the maximum adsorption was found for naphthalene but it was very similar for phenanthrene and pyrene (table 4.2). Williamson et al. (2002) reported the minimal box dimensions (table 4.1) for all three PAHs used in this study showed that the length and breadth of naphthalene was smaller than that of phenanthrene and pyrene (which have similar length and slightly different breadth). This shows that highest adsorption of naphthalene on both the sorbents can be attributed to its smaller structure compared to phenanthrene and pyrene.

In the case of organoclay, the S-shape of the curve was apparent (figure 4.2B, D and F). According to El Nahhal et al (2004) S-shape of the isotherms shows low affinity for PAH at lower concentration and more adsorption at higher concentration. Initially, adsorption occurs for single molecular unit of PAH and then, due to intermolecular interaction, PAH molecules vertically stack together. This is followed by competition between molecules present in the solution for adsorption sites giving the characteristic S-shape to the curve.

Humic Acid Effects: The effect of preloading the sorbent with humic acid significantly reduced the adsorption of phenanthrene and pyrene on activated carbon and reduced adsorption of all the three PAHs on organoclay. This reduction in adsorption can be attributed to the pore blockage of activated carbon and blocking of interlayer spacing of organoclay. In desorption studies, it was noticed that the desorption was negligible for naphthalene adsorption on both the sorbents but it was higher for phenanthrene and highest in case of pyrene adsorption on organoclay corresponding to the increase in K_{DOC} values for humic acid. The negligible desorption of naphthalene can be attributed to the highest affinity of both the sorbents and lowest K_{DOC} for naphthalene. The desorption pattern that was observable for phenanthrene and pyrene can be explained on the basis of the nature of adsorption of these compounds on sorbents (especially on organoclay) and their partition coefficients for humic acid. The molecules of phenanthrene and pyrene that stack together due to intermolecular interaction on the organoclay surface at higher concentrations are prone

to migrate back to the humic acid solution due to high partition coefficients for humic acid (K_{DOC} values as reported by Poerschmann et al., 1999) (table4.1).

Conclusion

The adsorption capacity of activated carbon was found to be the highest for naphthalene followed by phenanthrene and pyrene. For organoclay also, the maximum adsorption was seen for naphthalene but it was almost identical for phenanthrene and pyrene that have a slight difference in their box dimensions and have similar diffusivity. The performance of bare organoclay was found to be better for naphthalene and pyrene compared to activated carbon. The preloading effect was found to be significant for both the sorbents for phenanthrene and pyrene though there was negligible effect on naphthalene adsorption. Desorption effects were not found to be significant for naphthalene for both the sorbents but it was statistically significant for phenanthrene and pyrene adsorption on organoclay. This shows that if these sorbents are exposed to very high concentrations of natural organics such as 1g L^{-1} (as in the case of this study) then it can affect the performance of the reactive core mat. Also, long term exposure of organoclay to natural organic matter might affect the performance by desorption depending on the sorption pattern of target compounds and their partition coefficients for humic acid.

Additional Information

Model 1: Naphthalene

Variability Chart for Adsorption

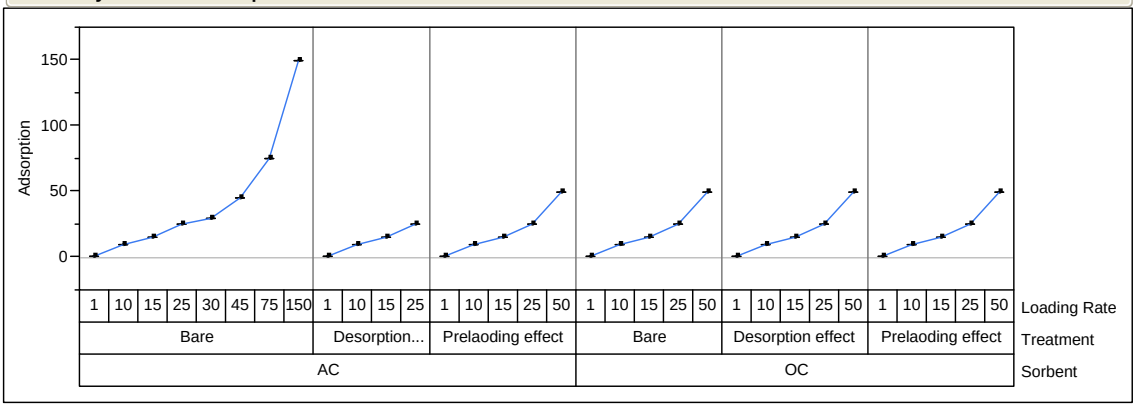

Analysis of Variance

Source	DF	Sum of Squares	Mean Square	F Ratio
Model	12	26419.956	2201.66	27560975
Error	19	0.00151778	7.988e-5	**Prob > F**
C. Total	31	26419.957		<.0001*

Effect Tests

Source	Nparm	DF	Sum of Squares	F Ratio	Prob > F
Sorbent	1	1	0.00083846	10.4961	0.0043*
Treatment	2	2	0.00076508	4.7887	0.0207*
Sorbent*Treatment	2	2	0.00085911	5.3773	0.0141*
Loading Rate	1	1	5544.6311	69409096	<.0001*
Sorbent*Loading Rate	1	1	2.32853e-6	0.0291	0.8662
Treatment*Loading Rate	2	2	0.00046325	2.8995	0.0796
Sorbent*Treatment*Loading Rate	2	2	0.00059497	3.7240	0.0432*
Loading Rate*Loading Rate	1	1	0.0012	14.5595	0.0012*

Model 2: Phenanthrene

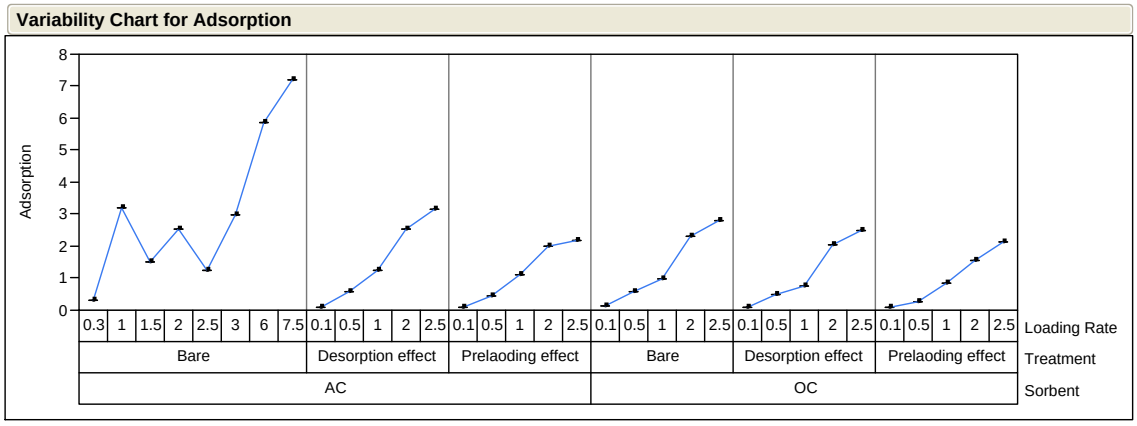

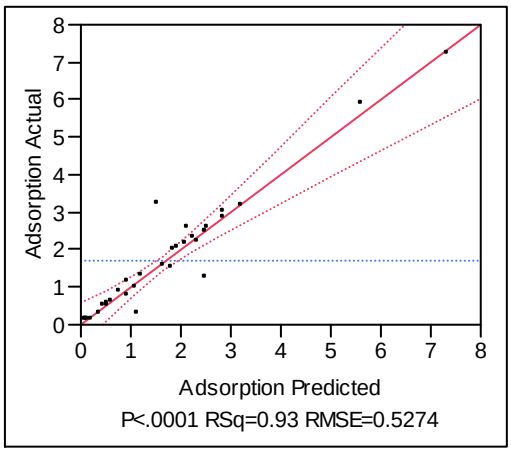

Analysis of Variance

Source	DF	Sum of Squares	Mean Square	F Ratio
Model	12	77.553175	6.46276	23.2332
Error	20	5.563385	0.27817	Prob > F
C. Total	32	83.116560		<.0001*

Effect Tests

Source	Nparm	DF	Sum of Squares	F Ratio	Prob > F
Sorbent	1	1	0.433281	1.5576	0.2264
Treatment	2	2	0.993129	1.7851	0.1935
Sorbent*Treatment	2	2	0.164848	0.2963	0.7468
Loading Rate	1	1	28.253551	101.5696	<.0001*
Sorbent*Loading Rate	1	1	0.036112	0.1298	0.7224
Treatment*Loading Rate	2	2	0.417283	0.7501	0.4852
Sorbent*Treatment*Loading Rate	2	2	0.762388	1.3704	0.2769
Loading Rate*Loading Rate	1	1	0.390341	1.4033	0.2501

Model 3: Pyrene

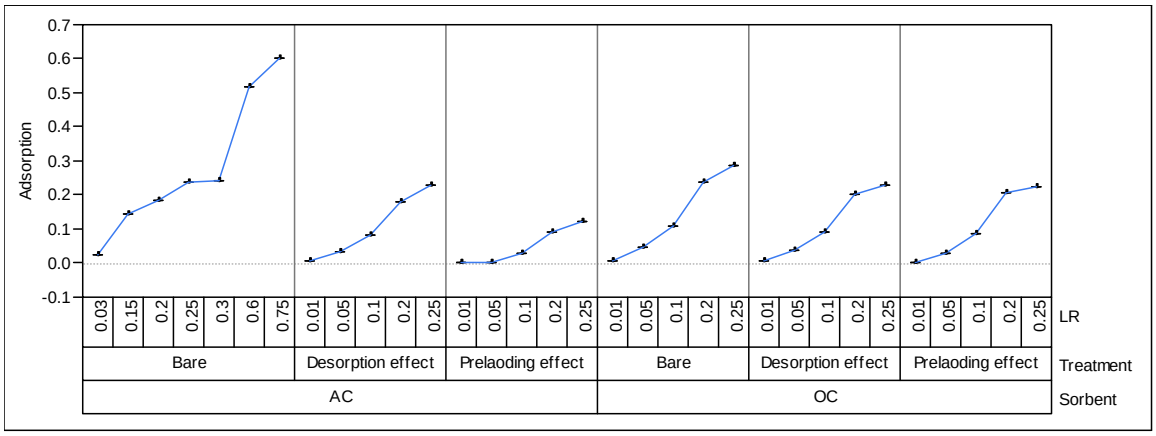

Actual by Predicted Plot

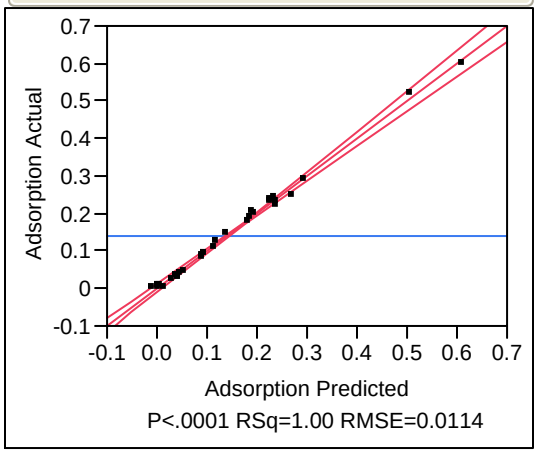

Analysis of Variance

Source	DF	Sum of Squares	Mean Square	F Ratio
Model	12	0.63052876	0.052544	407.5217
Error	19	0.00244978	0.000129	**Prob > F**
C. Total	31	0.63297854		<.0001*

Effect Tests

Source	Nparm	DF	Sum of Squares	F Ratio	Prob > F
Sorbent	1	1	0.01152574	89.3914	<.0001*
Treatment	2	2	0.01448755	56.1813	<.0001*
Sorbent*Treatment	2	2	0.00510109	19.7815	<.0001*
LR	1	1	0.23735722	1840.897	<.0001*
Sorbent*LR	1	1	0.00405245	31.4301	<.0001*
Treatment*LR	2	2	0.00377659	14.6452	0.0001*
Sorbent*Treatment*LR	2	2	0.00178366	6.9169	0.0055*
LR*LR	1	1	0.00059024	4.5778	0.0456*

Preliminary Study

Some preliminary studies were conducted to determine the performance of activated carbon and organoclays for adsorption of naphthalene (representative PAH). These experiments were conducted for the duration of 24 hours. Results showed maximum adsorption capacity of activated carbon for naphthalene followed by CETCO organoclay, Polymer Ventures Organoclay and Biomin Inc. Organoclay.

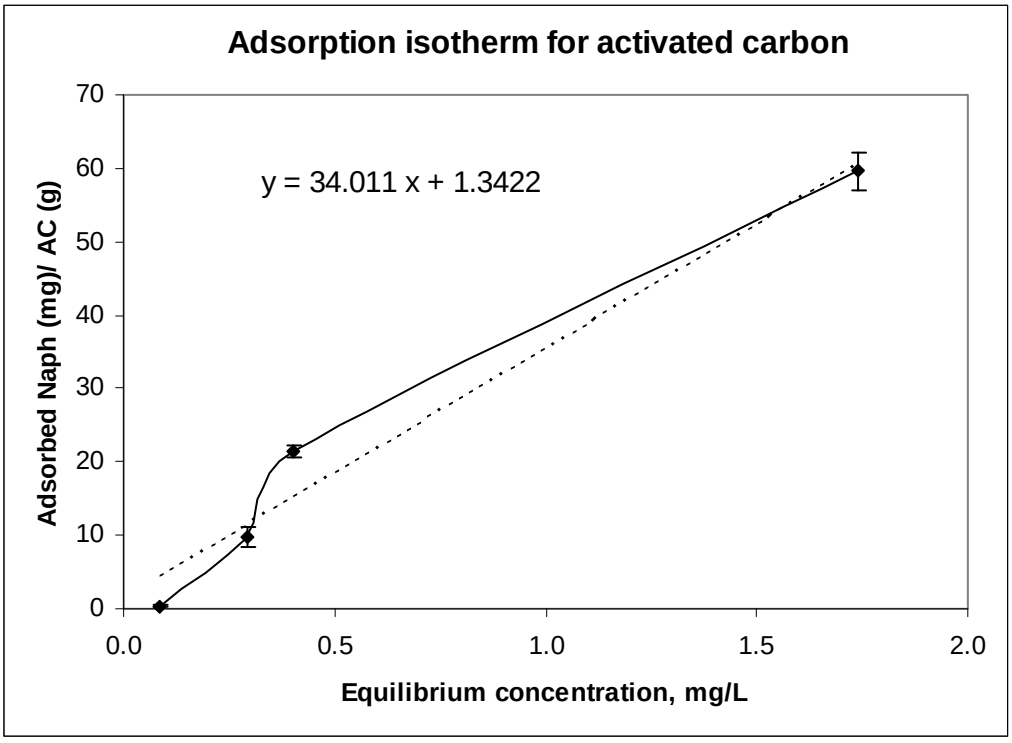

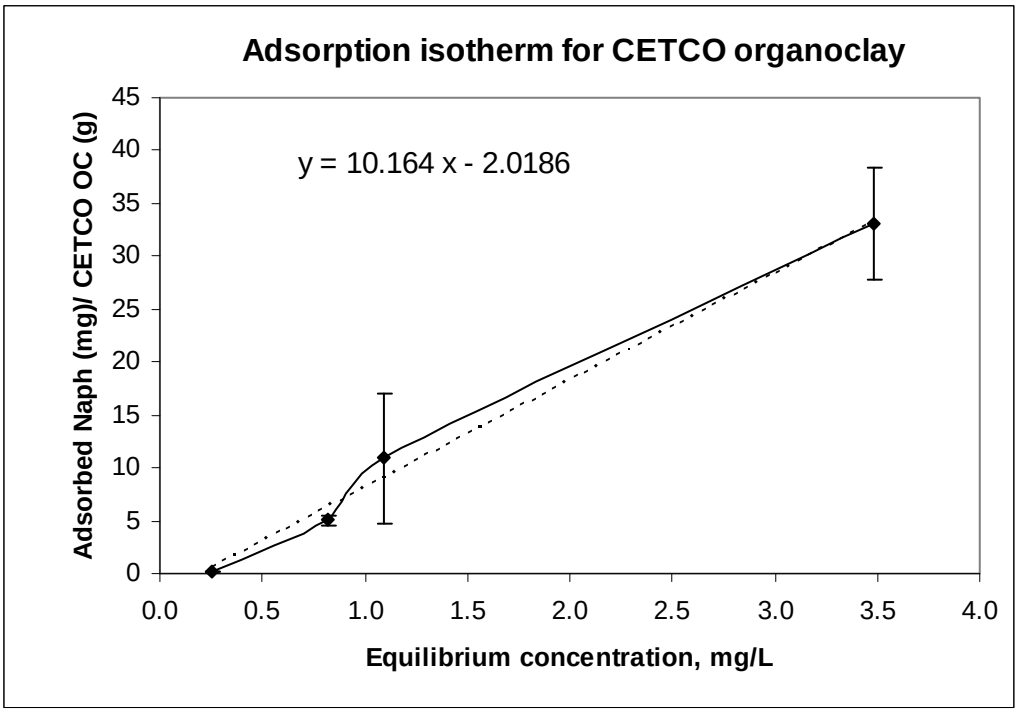
Adsorption isotherm for CETCO organoclay
y = 10.164 x - 2.0186
Adsorbed Naph (mg)/ CETCO OC (g)
Equilibrium concentration, mg/L
0
5
10
15
20
25
30
35
40
45
0.0
0.5
1.0
1.5
2.0
2.5
3.0
3.5
4.0

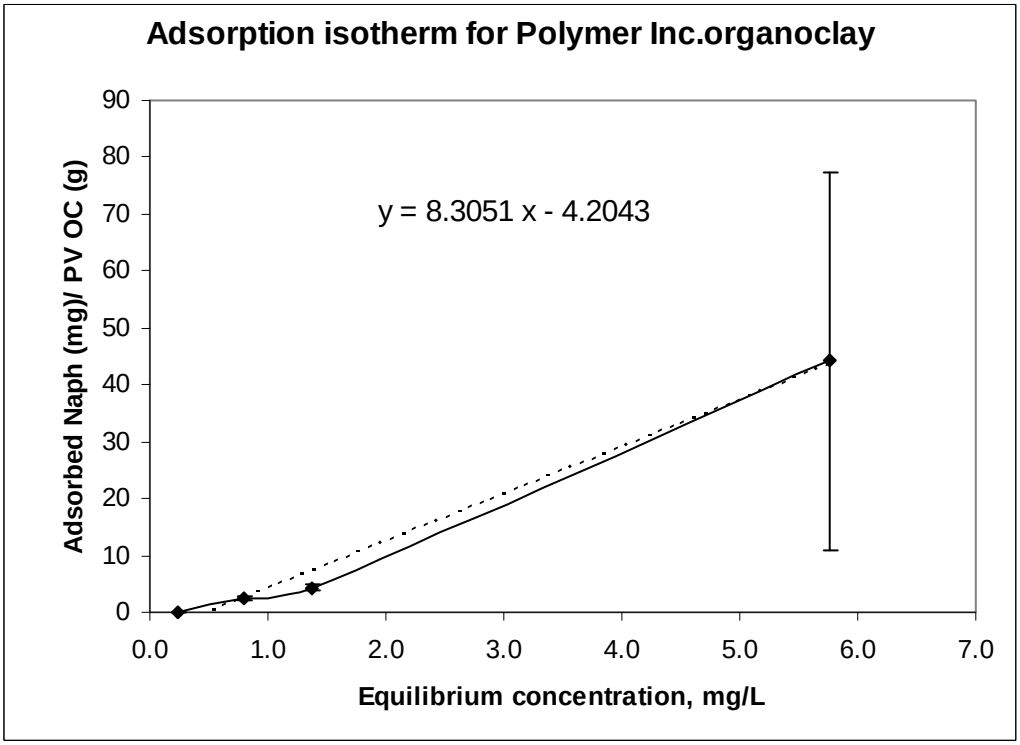
Adsorption isotherm for Polymer Inc.organoclay
y = 8.3051 x - 4.2043
Adsorbed Naph (mg)/ PV OC (g)
Equilibrium concentration, mg/L
0
10
20
30
40
50
60
70
80
90
0.0
1.0
2.0
3.0
4.0
5.0
6.0
7.0

Triple vs. Single Spike experiments:

Experiments conducted to compare triple spiking vs. single spiking of PAHs

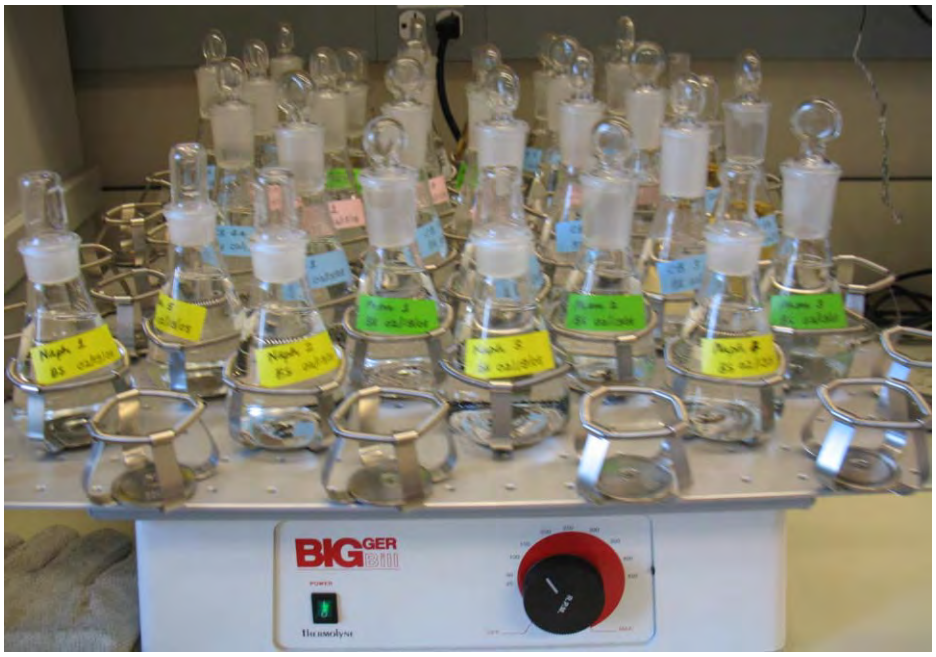

Triple Spike Experiment Set up

Single Spike Experiment Set up

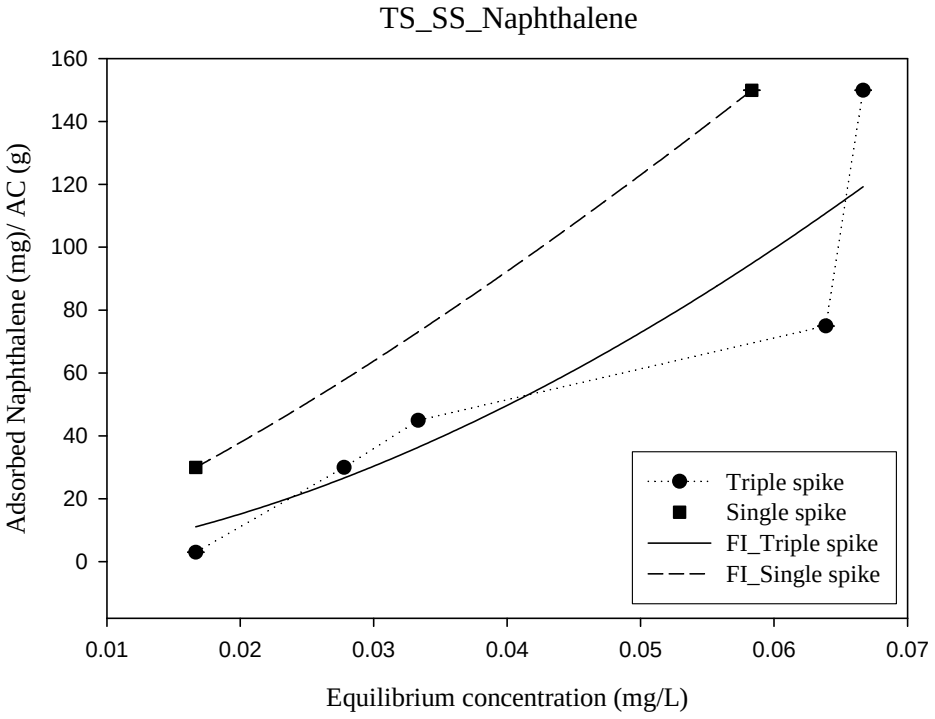
TS_SS_Naphthalene
Adsorbed Naphthalene (mg)/ AC (g)
160
140
120
100
80
60
40
20
0
0.01
0.02
0.03
0.04
0.05
0.06
0.07
Equilibrium concentration (mg/L)
Triple spike
Single spike
FI_Triple spike
FI_Single spike

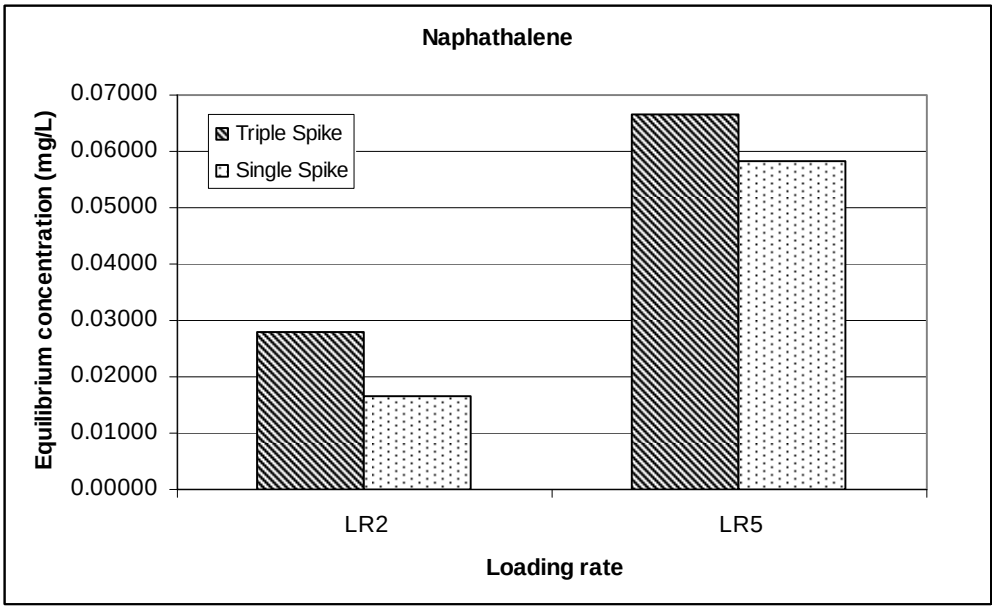
Naphthalene
Equilibrium concentration (mg/L)
0.07000
0.06000
0.05000
0.04000
0.03000
0.02000
0.01000
0.00000
Triple Spike
Single Spike
LR2
LR5
Loading rate

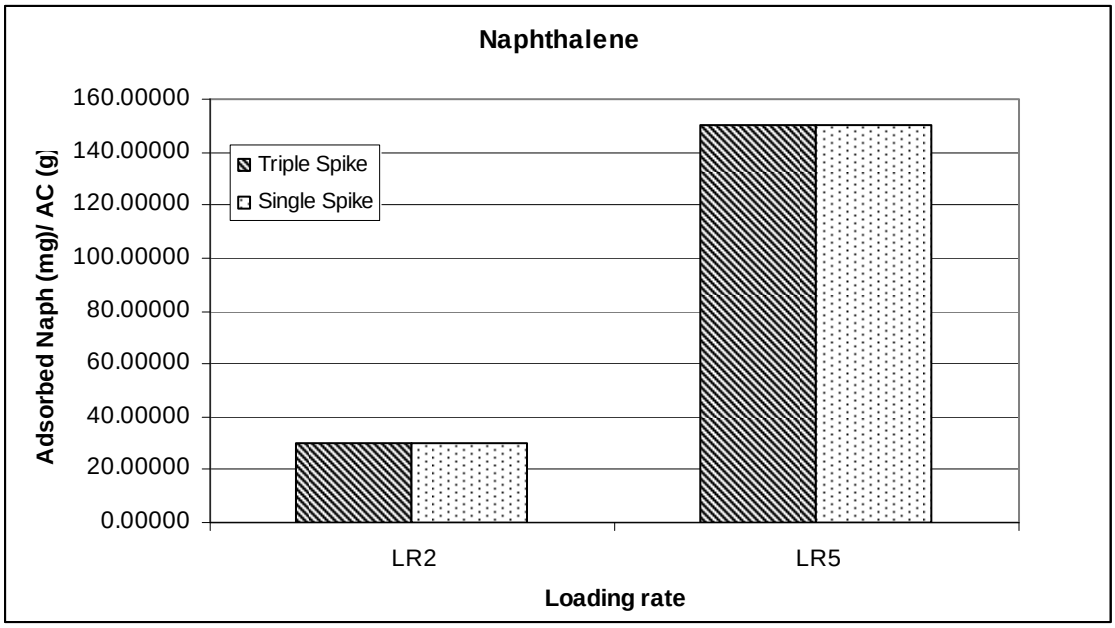
Naphthalene
160.00000
140.00000
120.00000
100.00000
80.00000
60.00000
40.00000
20.00000
0.00000
Adsorbed Naph (mg)/ AC (g)
Triple Spike
Single Spike
LR2
LR5
Loading rate

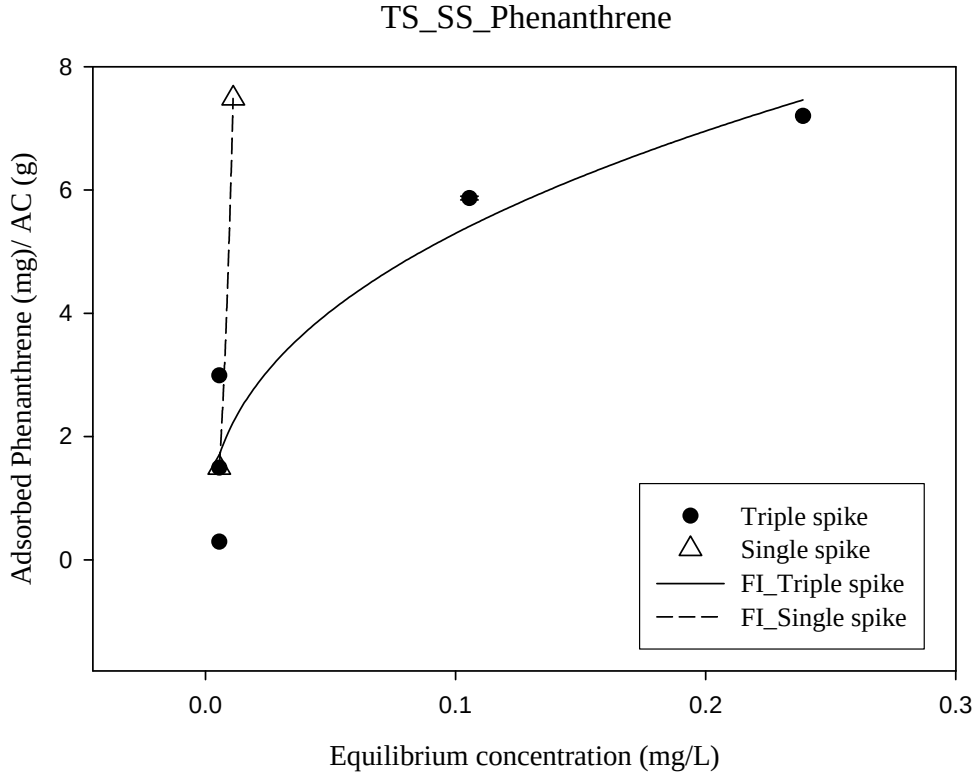
TS_SS_Phenanthrene
8
6
4
2
0
Adsorbed Phenanthrene (mg)/ AC (g)
0.0
0.1
0.2
0.3
Equilibrium concentration (mg/L)
Triple spike
Single spike
FI_Triple spike
FI_Single spike

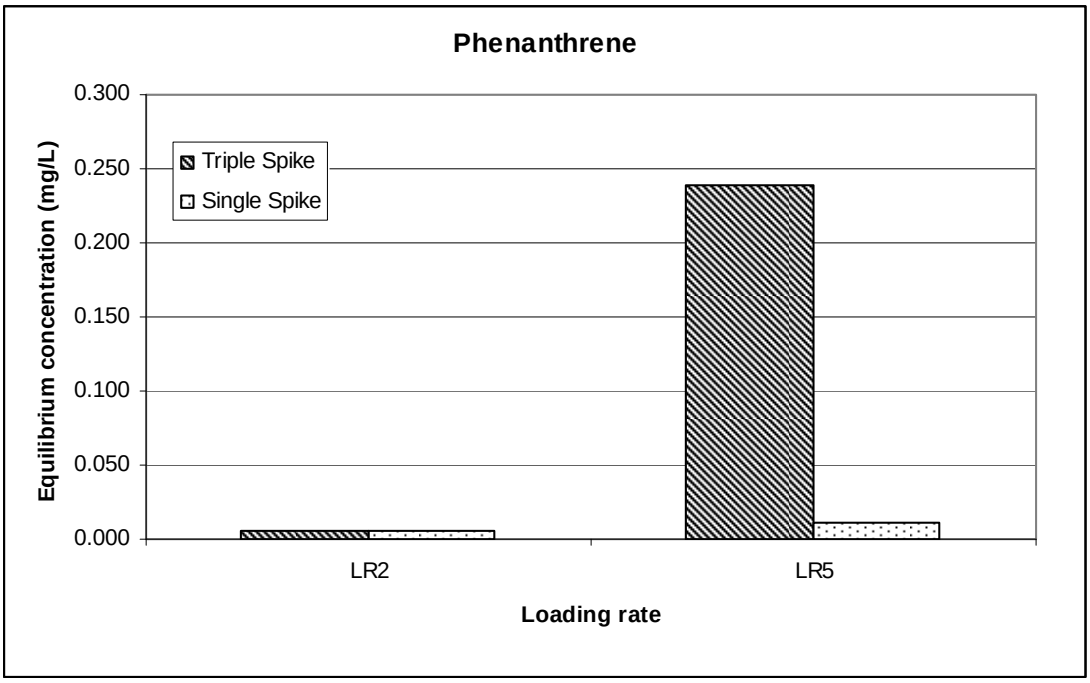
Phenanthrene
0.300
0.250
0.200
0.150
0.100
0.050
0.000
Equilibrium concentration (mg/L)
Triple Spike
Single Spike
LR2
LR5
Loading rate

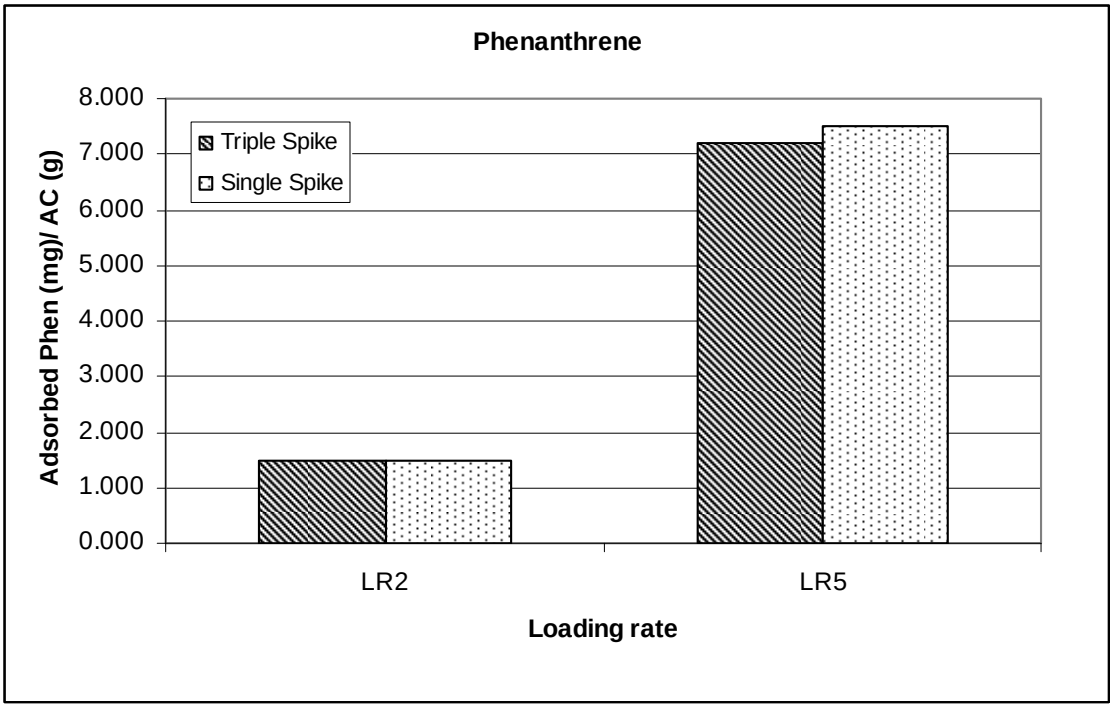
Phenanthrene
8.000
7.000
6.000
5.000
4.000
3.000
2.000
1.000
0.000
Adsorbed Phen (mg)/ AC (g)
Triple Spike
Single Spike
LR2
LR5
Loading rate

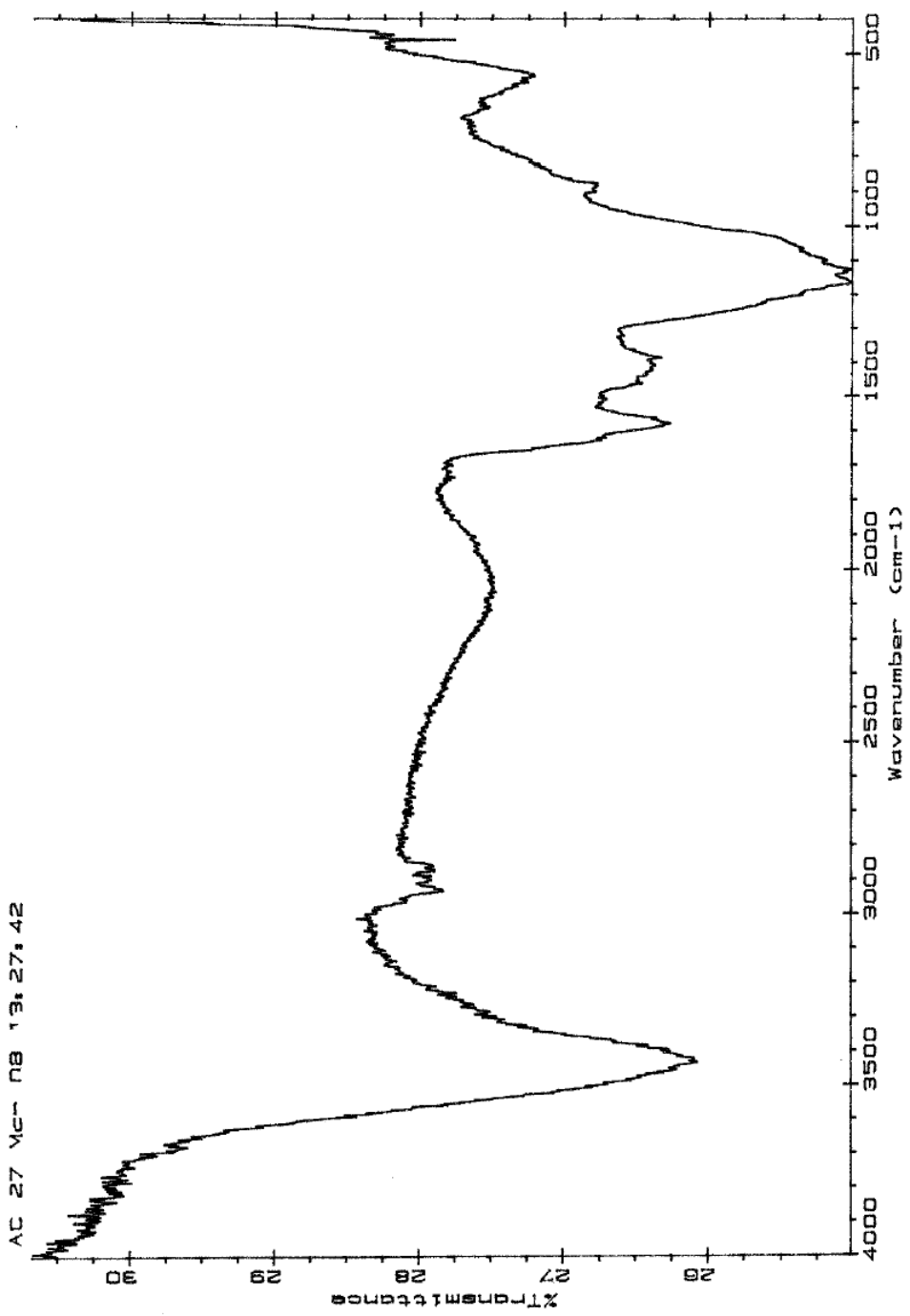

FTIR of bare coconut shell activated carbon

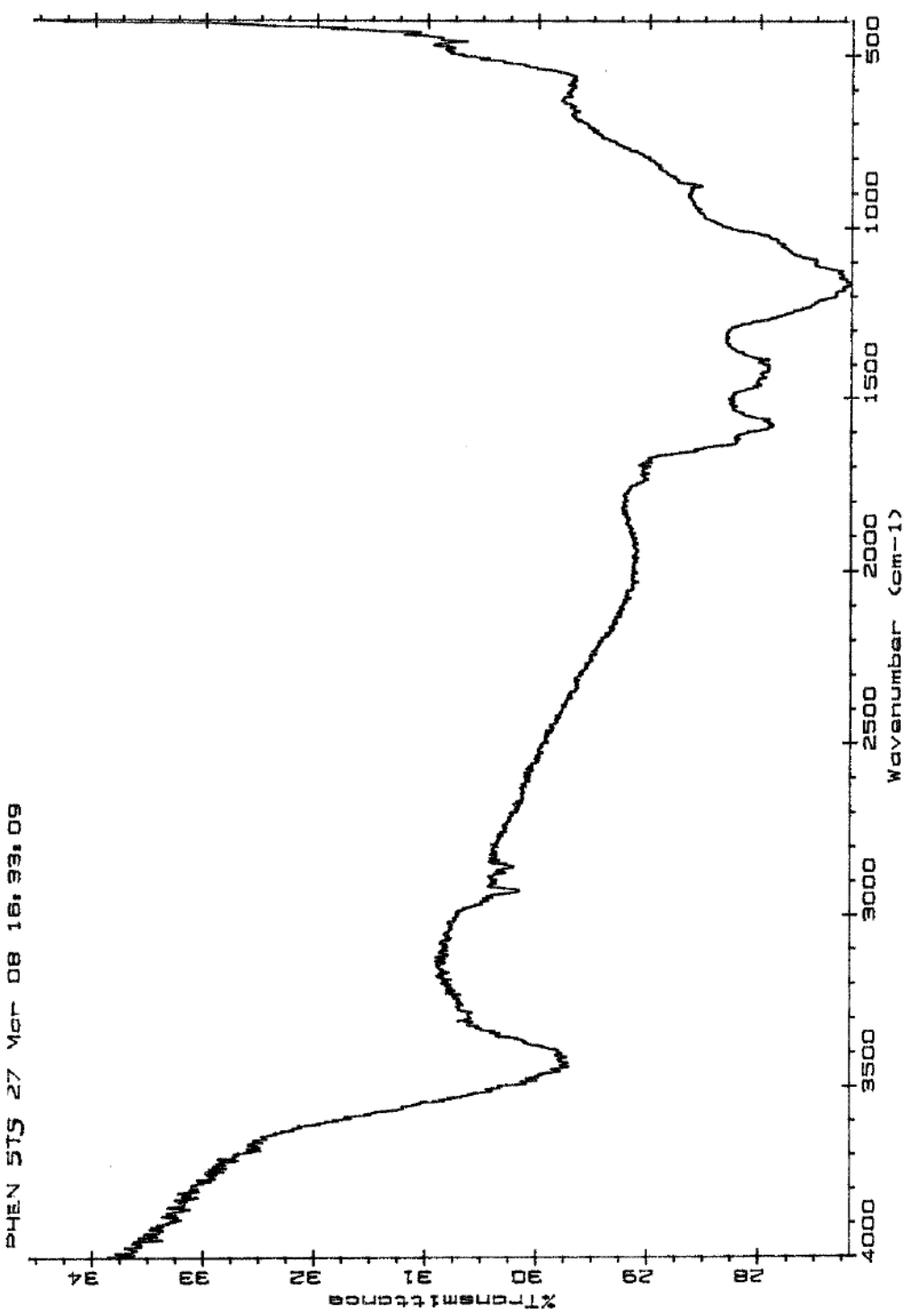

FTIR of coconut shell activated carbon after triple spiking of phenanthrene

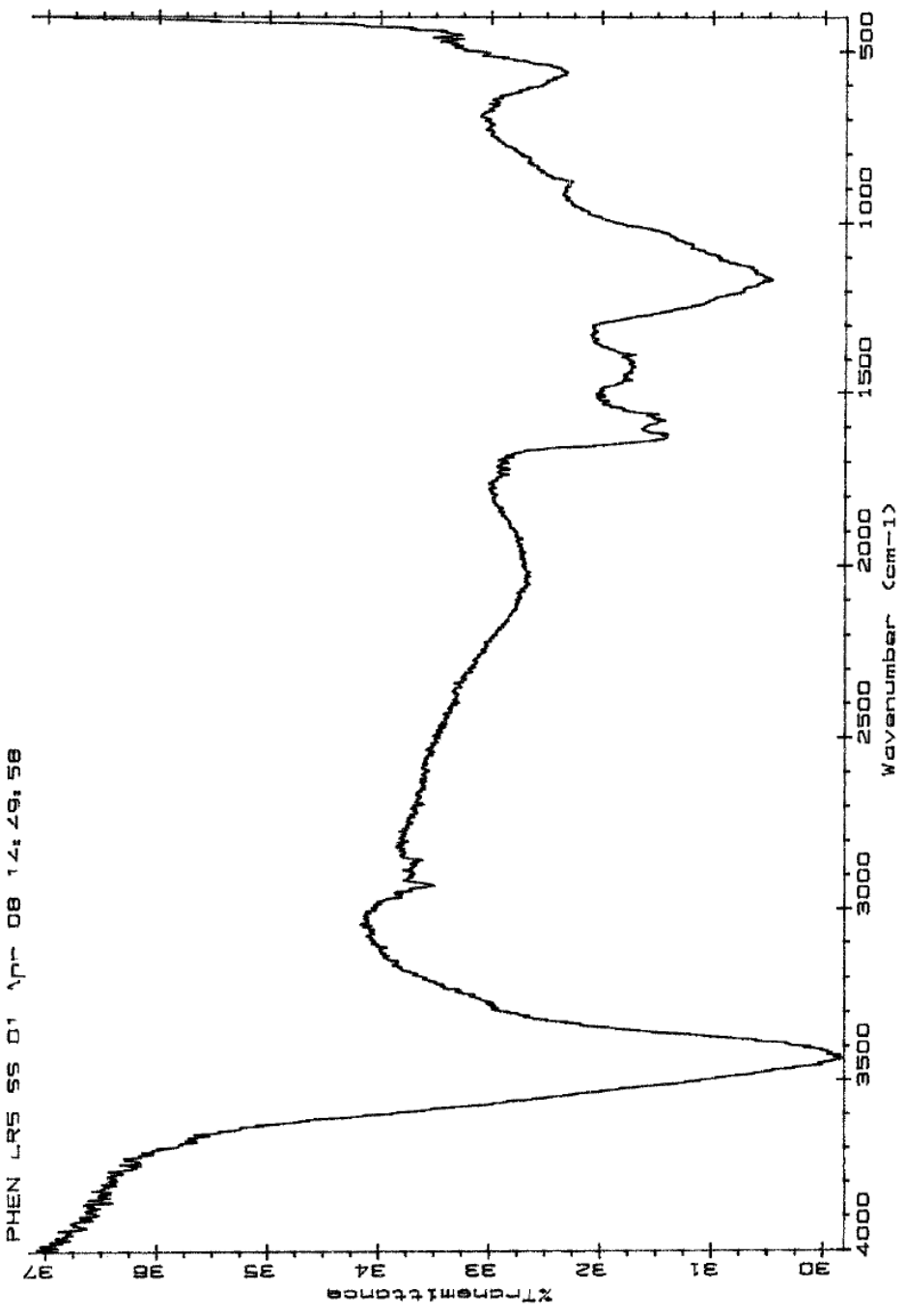

FTIR of coconut shell activated carbon after single spiking of phenanthrene

Infrared Spectroscopy Correlation Table

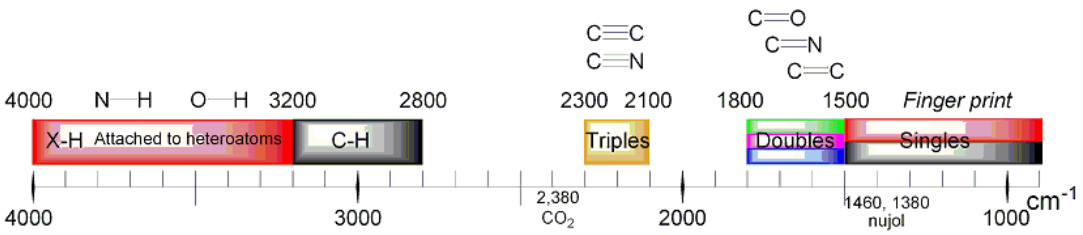

Wavenumbers listed in the table in cm^{-1}.

FTIR of samples were obtained with the help of Dr. Patricia Wilkinson, Parsons Hall, Instrumentation Center, University of New Hampshire.

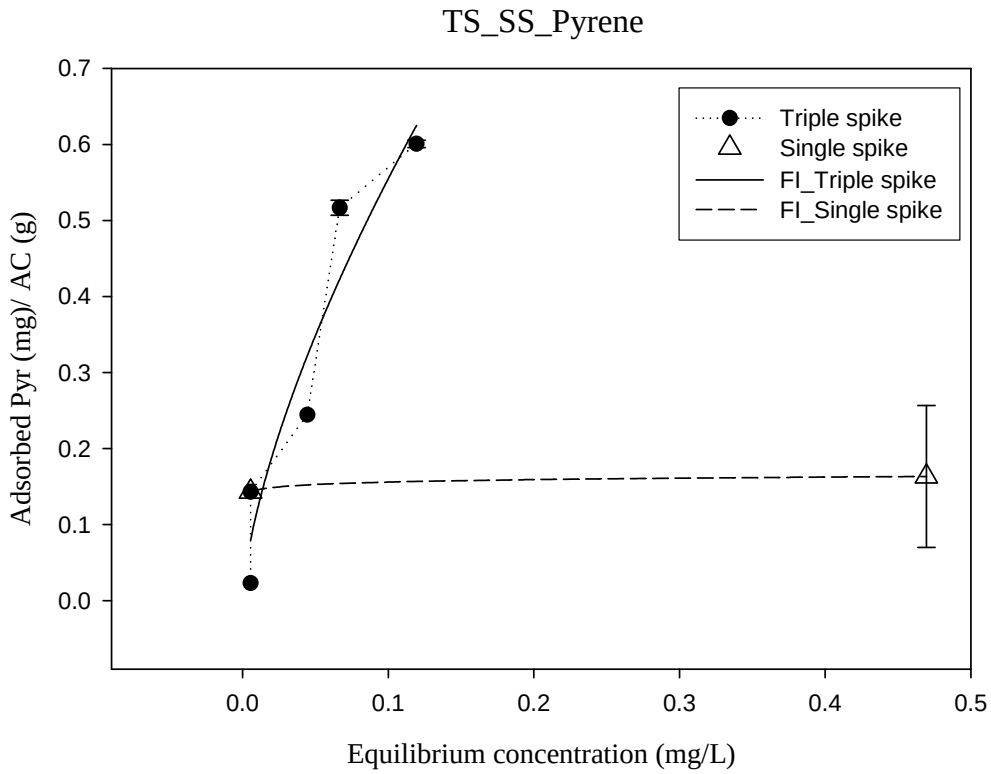

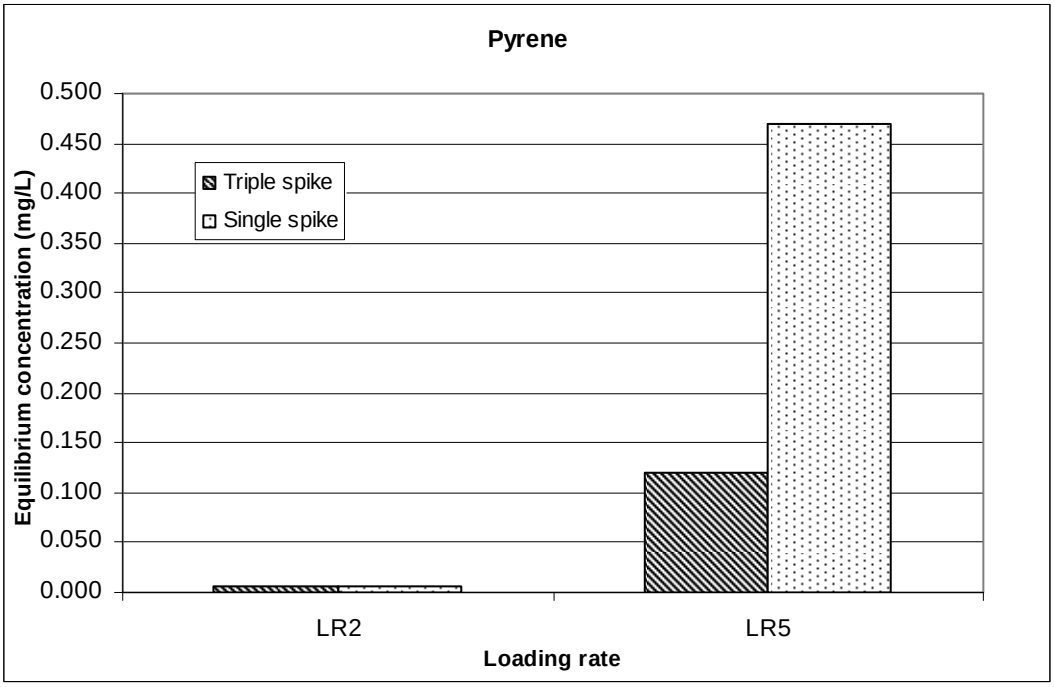
Pyrene
0.500
0.450
0.400
0.350
0.300
0.250
0.200
0.150
0.100
0.050
0.000
Triple spike
Single spike
Equilibrium concentration (mg/L)
LR2
LR5
Loading rate

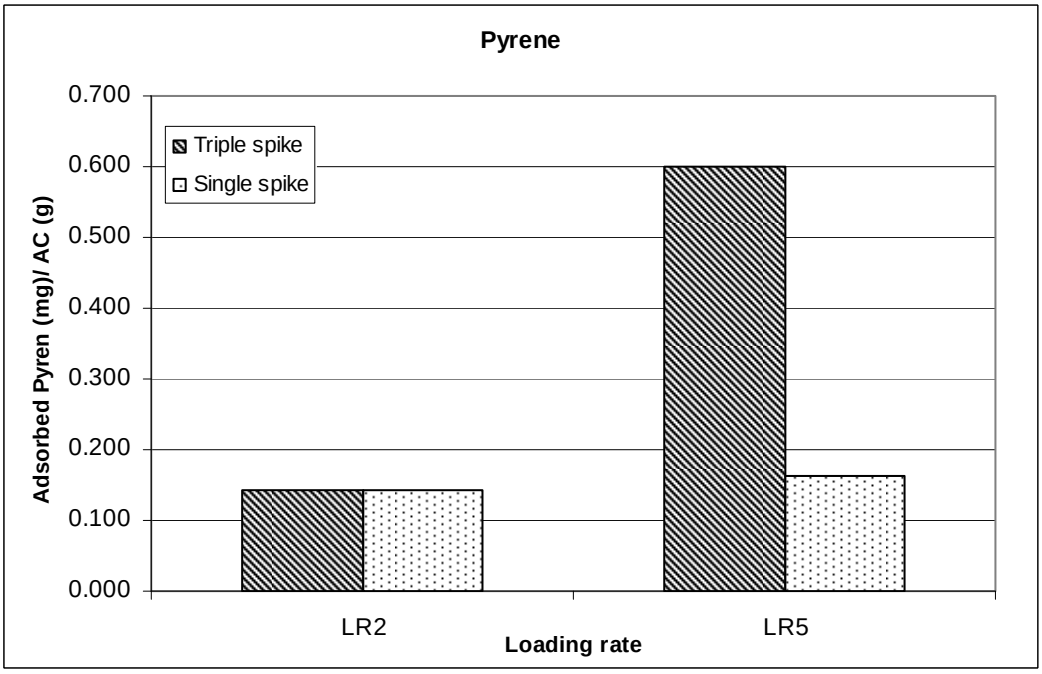
Pyrene
0.700
0.600
0.500
0.400
0.300
0.200
0.100
0.000
Triple spike
Single spike
Adsorbed Pyren (mg)/ AC (g)
LR2
LR5
Loading rate

References

Ake, C. L.; Wiles, M.C.; Huebner, H. J.; McDonald, T. J.; Cosgriff, D.; Richardson, M.B.; Donnelly, K. C. and Phillips, T. D. Porous organoclay composites for the sorption of polycyclic aromatic hydrocarbons and pentachlorophenol from groundwater. *Chemosphere*, 2003, 51, 835-844.

Carmody, O.; Frost, R.; Xi, Y. and Kokot, S. Adsorption of Hydrocarbons on Organo-clays – Implications for Oil Spill Remediation. *Jour. of Colloid and Interface Science*, 2007, 305, 17-24.

Cornelissen, G.; Breedveld, G.D.; Kalaitzidis, S.; Christanis, K.; Kibsgaard, A.; Oen, A. MP. Strong Sorption of Native PAHs to Pyrogenic and Unburned Carbonaceous Geosorbents in Sediments. *Environmental Science and Technology*, 2006, 40, 1197-1203.

Dental, S. K.; Jamarah, A. I. and Sparks D. L. Sorption and Cosorption of 1, 2, 4-Trichlorobenzene and Tannic Acid by Organo-clays. *Water Research*, 1998, 32, 3689-3697.

Dowaidar, A.M.; El-Shahawi, M.S.; Ashour, I. Adsorption of Polycyclic Aromatic Hydrocarbons onto Activated Carbon from Non-Aqueous Media: 1. The Influence of the Organic Solvent Polarity. *Separation Science and Technology*, 2007, 42, 3609-3622.

El Nahhal, Y. Z.; Safi, J. M. Adsorption of Phenanthrene on Organoclays from Distilled and Saline Water. *Journal of Colloid And Interface Science*, 2004, 269, 265-273.

Gustafson, K.E. and Dickhut, R. M. Molecular Diffusivity of Polycyclic Aromatic Hydrocarbons in Aqueous Solution. *Journal of Chemical EngineerinImpregg Data*, 1994, 39, 281-285.

Henning, K.D. and Schafer, S. Impregnated Activated Carbon for Environmental Protection. CarboTech-Aktivkohien GMbH, Franz-Fischer-Weg 61, D-45307 Essen, Germany.

Jayens, W. F. and Boyd, S. A. Clay Mineral Type and Organic Compound Sorption by Hexadecyltrimethyammonium – Exchanges Clays. Soil Science Society of American Journal, 1991, 55, 43-48.

Karanfil, T.; Dastgheib, S.A. and Mauldin, D. Exploring Molecular Sieve Capabilities of Activated Carbon Fibers to Reduce the Impact of NOM Preloading on Trichloroethylene Adsroption *Environmental Science and Technology*, 2006, 40, 1321-1327.

Lee, S. Y.; Kim, S. J.; Chung, S. Y. and Jeong, C. H. Sorption of hydrophobic organic compounds onto organoclays. *Chemosphere*, 2005, 55, 781-785.

Liang, C.; Dang, G.; Xiao, B.;Huang, W. and Liu, C. Equilibrium Sorption of Phenanthrene by Soil Humic Acids. *Chemosphere*, 2006, 63, 1961-1968.

Li, Qilin; Snoeyink, V.L.; Marinas, B.J.; Campos, C. Pore Blockage Effect of NOM on Atrazine Adsorption Kinetics of PAC: The Roles of PAC Pore Size Distribution and NOM Molecular Weight. *Water Research.* 2003, 37, 4863-4872.

Maruya, K.A.; Risebrough, R.W.; Horne, A. J. Partitioning of Polynuclear Aromatic Hydrocarbons between Sediments from San Francisco Bay and Their Porewaters. *Environ. Sci. Tech*. 1996, 30, 2942 – 2947.

McGroddy, S.E. and Farrington, J. W. Sediment Porewater Partitioning of Polycyclic Aromatic Hydrocarbons in Three Cores from Boston Harbor, Massachusetts. *Environ. Sci. Tech*. 1995, 29, 1542 – 1550.

Means, J.C.; Wood, S.G.; Hassett, J.J. and Banwart, W.L. Sorption of Polynuclear Aromatic Hydrocarbons by Sediments and Soils. *Environ. Sci. Tech*. 1980, 14, 1524-1528.

Osterberg, R. and Mortensen K. Fractal dimension of Humic Acids. *European Biophysics Journal*, 1992, 21, 163-167.

Pernyeszi, T.; Kasteel, R.; Witthuhn, B.; Klahre, P.; Vereecken, H. and Klumpp, E. Organoclays for Soil Remediation: Adsorption of 2,4-dichlorobiphenyl on organoclay/ aquifer material mixtures studied under static and flow conditions. *Applied Clay Sciences*, 2006, 32, 179-189.

Pignatello, J. J.; Kwon, S.; Lu, Y. Effect of Natural Organic Substances on the Surface and Adsorptiive Properties of Envrionmental Black Carbon (Char): Attenuation of Surface Activity by Humic and Fulvic Acids. *Environ. Sci. Tech*. 2006, 40, 7757-7763.

Poerschmann, J.; Kopinke, Frank-Dieter; Plugge, J.; Georgi, A. Interaction of Organic Chemicals (PAHs, PCB, Triazines, Nitroaromatics and Organotin Compounds) with Dissolved Humic Organic Matter. *Special Pubilcation – Royal Society of Chemistry*, 247 (Understanding Humic Substances), 1999, 223-240. Publisher: Royal Society of Chemistry.

Quinlivan, P. A., Li, L., Knappe, D. R. U. Effects of Activated Carbon Characteristics on the Simultaneous Adsorption of Aqueous Organic Micropollutants and Natural Organic Matter. *Water Research*, 2005, 39, 1663-1673.

Van Metre, P.C.; Mahler, B.J.; and Furlong, E.T. Urban Sprawl Leaves its PAH Signature. *Environ. Sci. Tech*. 2000, 34, 4064-4070.

Wiles, M.C.; Huebner, H.J.; McDonald, T. J.; Donnelly, K. C. and Phillips, T. D. Matrix-immobilized organoclay for the sorption of polycyclic aromatic hydrocarbons and pentachlorophenol from groundwater. *Chemosphere*, 2005, 59, 1455-1465.

Williamson, K.S.; Petty, J.D.; Huckins, J.N.; Lebo, J.A. and Kaiser, E.M. Sequestration of Priority Pollutant PAHs from Sediment Pore Water Employing Semipermeable Membrane Devices. *Chemosphere*, 2002, 49, 717-729.

Zhao, H. and Vance, G. F. Sorption of Trichloroethylene by Organoclays in the Presence of Humic Substances. *Water Research*, 1998, 32, 3710-3716.

Zimmerman, J.R.; Ghosh, U.; Luthy, R. G.; Bridges, T. S.; Millward, R. N. Addition of Carbon Sorbents to Reduce PCB and PAH Bioavailability in Marine Sediments: Physicochemical Tests. *Environ. Sci. Tech*. 2004, 38, 5458 – 5464.

CHAPTER 5

INTERFERENCES CAUSED BY HUMIC ACID, FULVIC ACID AND NOM PRESENT IN PORE WATER ON PERFORMANCE OF ACTIVATED CARBON AND ORGANOCLAY FOR SEQUESTRATION OF ORGANIC CONTAMINANTS

Abstract

The performances of activated carbon and organoclay were evaluated as reactive cap sorbents that can be used to sequester organic contaminants in the presence of natural organics that are present in sediment porewaters. Experiments were conducted to determine the effect of Aldrich humic acid, Suwannee River humic acid, fulvic acid, natural organic matter and pore water extracted from sediments of the Passaic and Hudson Rivers. Studies were also conducted with a sorbent mixture (containing 35% organoclay, 35% activated carbon and 30% apatite) that was retrieved from reactive core mats deployed in the field for six months to determine the effect of natural organic matter present in the field. The influence of these natural organic materials was determined on the adsorption of 2, 2', 5', 5'-tetrachlorobiphenyl and phenanthrene. Results showed significant effect of Aldrich humic acid on 2, 2', 5', 5'-tetrachlorobiphenyl adsorption on both the sorbents. There was slight enhancement in the adsorption capacity of organoclay for 2, 2', 5', 5'-tetrachlorobiphenyl in the presence of fulvic acid but no effect was observed for activated carbon. There was no effect of

NOM on 2, 2', 5', 5'-tetrachlorobiphenyl adsorption on both the sorbents. In case of phenanthrene adsorption, no effect of any fraction of natural organics was noticed for organoclay. In the case of activated carbon the effects of Aldrich humic acid, Suwannee River humic acid, Suwannee River fulvic acid and Suwannee River NOM were found to have similar reducing effect on phenanthrene adsorption. A significant effect of Hudson River porewater (high humics) was observed on the performance of both the sorbents for both the contaminants, although only small effect was found for the Passaic porewater (which was low in humics).

Introduction

Sediments that provide shelter to a variety of aquatic life are also a major source and sink for hydrophobic organic contaminants (HOCs) such as Polychlorinated Biphenyls (PCBs) and Polycyclic Aromatic Hydrocarbons (PAHs) which are persistent and bioaccumulative in nature. These contaminated sediments can be toxic to benthic organisms that occupy an important position in the food chain and the uptake of HOCs poses a risk to higher tiers of the food chain. The contaminated sediment remediation technologies that are currently in practice are dredging followed by treatment and disposal and monitored natural recovery. For in-situ remediation of riverine or marine sediments, reactive capping technology can be a potential treatment method that may be effective and which is being evaluated in the research reported here. Capping technology includes deployment of reactive caps/ non-reactive sand caps over sediment bed that isolates the contaminated sediments from water body. The reactive caps can

be made by direct mixing of reactive material into the sediment (Werner et al., 2005; Zimmerman et al., 2004) or by covering the sediment using geotextile or loose granular reactive material (McDonough et al., 2008). Reactive caps that consist of geotextile mat impregnated with the reactive materials, also known as reactive core mats, are still under research. Using reactive material bound within a geotextile mat is one of the methods for deploying a reactive cap that may reduce the chances of scouring and ensure uniform coverage.

In this research the reactive core mats are being evaluated to understand the effectiveness of combinations of sorbent amendment mixtures and types of geotextiles. These reactive caps are intended to be multi-symptom remedies that will sequester both organic contaminants such as PCBs and PAHs as well as metals. Pilot scale studies have been conducted by deploying 6’ x 6’ reactive core mats with a sorbent amendment mixture of apatite (a mineral), organoclay and activated carbon in Cottonwood Bay, Texas for six months. Laboratory analysis is being done to determine the effect of biofouling, natural organic matter and clogging of the mats. In this paper results will be discussed for the performance of coconut shell activated carbon and organoclay in the presence of different fractions of ubiquitous natural organic material as well as to determine the effect of natural organic matter (NOM) present in the Cottonwood Bay field site on the performance of sorbent amendment mixture for sequestration of organic contaminants.

Contaminants in sediments can be present either in dissolved phase in pore water or adsorbed to the particulate matrix of sediments, depending on the characteristics of the sediments and the contaminants (Akkanen et al., 2005). In the dissolved phase, HOCs are partitioned between water and dissolved natural organics present in the system. Therefore, it is necessary to understand the complexation behavior of HOCs with NOM including humic acid and fulvic acid that are present in the pore water in addition to understanding the competition of NOM for sorption sites. The pore water can be isolated from the solid phase by means of different techniques depending on whether it is an in-situ or ex-situ extraction method. The most commonly used laboratory scale method for pore water extraction is centrifugation followed by filtration (Akkanen et al., 2005). But filtration can create many problems such as changing the suction pressure leading to change in nature of particulate organic matter or clogging of filters which might not allow colloidal or particulate matter to pass through 0.45 µm filter. By definition, the material that passes through the 0.45 µm is known as dissolved organic material that consist of micro- and macromolecules that are the most important and mobile fraction of natural organic matter. Due to filtration the macromolecules, if associated with each other, are not allowed to pass through the membrane. Brownawell et al.(1985) who studied the biogeochemistry of PCBs in interstitial waters of New Bedford Harbor (NBH) concluded that a high percentage of PCBs in pore water are sorbed to organic colloids and partitioning of HOCs to organic colloids is necessary to evaluate the mobility and bioavailability in sediments. Therefore, only the centrifugation method was used in this study to extract pore water so that all

the fractions of NOM, including colloids, could be taken into account to understand their affect on treatment processes of HOCs.

NOM present in the pore water can be fractionated into humic acid, fulvic acid and humin, which may affect the solubility, transport and bioavailability of HOCs in different ways. The fulvic acid, which has lower molecular weight components, is more hydrophilic compared to humic acid that consists of high molecular weight components and is more hydrophobic (Wu et al. 2003). Fulvic acid consist of naphthalene rings substituted with hydroxyl, carboxyl and short aliphatic chains whereas humic acid consists of phenolic groups and quinone structures in addition to carboxylic groups substituted on large aromatic rings (Saparpakorn et al. 2007). NOM is heterogeneous and consists of humic acids, fulvic acids, proteins and peptides having both hydrophilic and hydrophobic properties (Wu et al. 2003). The chemical properties of these NOM fractions, including acid/ base properties, elemental composition and aromaticity, depend on their origin and is different for freshwater, marine or terrestrial environments (Niederer et al., 2007). Therefore, in this study pore water from five different sites was characterized and humic acid, fulvic acid, NOM and pore water from different origins were used to obtain a range of effects that may be encountered under different site conditions. Sorbent amendment mixture obtained from the reactive core mats deployed in a non-contaminated area of the study field site were also evaluated to determine the effect of longer term exposure to NOM concentrations that are present at a study field site. The main objective of this study is to quantify the effects of different fractions of

NOM from different origins on the performance of activated carbon, organoclay and an amendment mixture for sequestration of organic contaminants.

Materials and Methods

Chemicals

Contaminants of concern used in this study were 2, 2', 5, 5'-tetrachlorobiphenyl, and phenanthrene that were obtained from Ultra Scientific (North Kingstown, RI, USA) either in neat form or dissolved in hexane/ methylene chloride respectively. Internal standards 2, 4, 6-trichlorobiphenyl and Acenaphthene d-10 and surrogate standards 2, 4, 5, 6-tetrachloro-m-xylene (TCMX) and 2-fluorobiphenyl were also purchased from Ultra scientific (North Kingstown, RI, USA). Humic acid sodium salt (Ald-HA) was obtained from Sigma-Aldrich (St. Louis, MO, USA), Suwannee River humic acid (2S101H) (SRHA), Suwannee River fulvic acid (2S101F) (SRFA) and Suwannee River Natural Organic Matter (1R101N) (SRNOM) were obtained from International Humic Substance Society (St. Paul, MN, USA). Sodium azide used to avoid biological contamination in the experiments was obtained from EMD Chemicals Inc. (San Diego, CA, USA) and sodium sulfate anhydrous used to remove chemically bound water from extracted samples was obtained from Fisher Scientific (Morris Plains, NJ, USA). All ultra high purity chemicals and GC-grade solvents were used in the study and obtained from Fischer Scientific (Agawam, MA, USA) were used. DAX-8 resin that was used for fractionation of NOM was purchased from Sigma Aldrich (St. Louis, MO, USA).Hydrochloric acid and Sodium hydroxide that were used to maintain pH were obtained from Fisher Scientific (Fair Lawn, NJ, USA).

Sorbents:

Activated carbon: Coconut shell activated carbon, OLC 12 x 40 obtained from Calgon Carbon Corporation (Pittsburg, PA, USA) was used. This material was selected because it is widely used for removal of trace organic compounds and it has high microporosity.

Organoclay: Organoclay was obtained from CETCO (Arlington Heights, IL, USA) as PM 199 which is organically modified bentonite clay. In PM 199, hydrogenated tallow based quaternary amines were used to increase the inter-layer spacing of bentonite clay. Interlayer (d_{001} spacing) of PM 199 was found to be 35.74 A˚ and organic content to be about 19%.

Amendment mixture: The amendment mixture consisted of 35% activated carbon, 35% organoclay and 30% apatite by weight. Apatite used in this study was obtained from PCS Phosphate Mines (Aurora, NC, USA). Apatite can be used for metal sequestration and is in the mixture for this reason: this paper is focused only on organic contaminants removal. The bare amendment mixture was prepared from the sorbents as obtained from vendors mixed in given proportions to determine the adsorption capacity of the sorbent mixture. The amendment mixture was also obtained from the reactive core mats that were deployed in the study field site for six months to determine the preloading effects of NOM present in the study site. For this purpose 6’ x 6’ mats that were retrieved from the field were cut into 2’ x 2’ pieces and each section was dried

at room temperature for 3 days. The mixture material was then separated from the geotextiles and was collected in a beaker and stored.

Experiment Protocols

Pore Water Extraction and Characterization:

Pore water was extracted from the sediments of six different sites including Hudson River, Passaic River, New Bedford Harbor (NBH), Cocheco River and Gowanas Canal. Centrifugation method (Beckman Coulter J2-HS centrifuge) was used for laboratory scale isolation of porewater from the solid matrix of sediments. The samples were extracted at 20˚ C at 7000 rpm for 30 minutes. The supernatant was then separated and collected into glass vials for further analysis including pH, oxidation-reduction potential (ORP), total organic carbon (TOC), dissolved organic carbon (DOC) (Shimadzu TOC-5000A TOC Analyzer) and ultraviolet (UV) absorbance. Humic acid was isolated from the porewater by precipitation after lowering the pH to 1 using HCl. HA fraction was dissolved by using sufficient 0.1 M NaOH. The pH of supernatent fulvic acid fraction was brought to 2.0 with NaOH and passed through DAX-8 resin (Kim et al., 1990; Thurman et al., 1981). The column was then washed with one void volume of distilled water to remove the salt followed by reverse flow of 0.1 M NaOH to elute the column to obtain FA fraction (Thurman et al., 1981). Both HA and FA fraction were analyzed further for DOC (mg C/ L) and TKN (mg N/ L).

Isotherms studies

Isotherm studies were conducted to determine the preloading effect of different fractions of natural organics and extracted sediment pore water on adsorption capacities of activated carbon and organoclay for 2, 2', 5, 5'- tetrachlorobiphenyl (PCB) and phenanthrene (PAH). The studies to determine the preloading effect of Ald-HA, SRHA, SRFA and SRNOM were conducted in 125 ml flasks at five loadings of both selected contaminants (concentration range given in table 5.1). The studies were conducted separately for PCB and PAH adsorption on activated carbon and organoclay to avoid any interference of contaminants in the performance of sorbents at fixed loading of Ald-HA/ SRHA/ SRFA/ SRNOM. Experiments were also conducted to determine the effect of extracted pore water from sediments of Hudson River (HPW) and Passaic River (PPW) on adsorption capacity of activated carbon and organoclay for selected PCB and PAH molecules. Due to the limited availability of extracted pore water these experiments were conducted at three loadings of contaminants in 40 ml vials. This set of experiments was also conducted separately for PCB and PAH. Spiking of PCB and PAH was done to obtain the required concentration of contaminants in extracted pore waters due to absence of any prior PCB/ PAH concentrations in the sediments (Figure 5.1). All the isotherm studies were conducted for an equilibration time of 72 hours.

Effect of different concentrations of Ald-HA/ SRFA/ SRNOM: Studies were also conducted to determine the effect of varied concentration of Ald-HA, SRFA and SRNOM

that can be found in different site conditions. For this purpose experiments were conducted in 40 ml vials at fixed loading of selected contaminants (based on the solubility limit in water) including 2, 2', 5, 5'-tPCB and phenanthrene (separately for PCB and PAH) at three different loadings of Ald-HA, SRFA and SRNOM.

Preloading of sorbents: For isotherm studies; 0.1 g of sorbent (activated carbon/ organoclay) was preloaded with 100 mg L^{-1} Ald-HA/ SRHA/ SRFA/ SRNOM solution in separate 125 ml flasks. The stock solution of 100 mg $L^{-1}$was prepared for each Aldrich HA, SRHA, SRFA and SRNOM. The initial pH of SRHA, SRFA and SRNOM were found to in the range of 4 and were adjusted to pH 7 using sodium hydroxide solution (table 5.3). To determine the effect of different loadings of Ald-HA/ SRFA/ SRNOM, 0.2 g of sorbent was preloaded with 20 ml of each HA/ FA/ NOM in separate vials at three loadings (10 mg L^{-1}, 100 mg L^{-1} and 1000 mg L^{-1}) of each. These experiments were conducted without any pH adjustment of stock solutions of Ald-HA/ SRFA/ SRNOM solutions which were in found to be 7.21, 4.02 and 4.12 respectively. The stock solutions for preloading were prepared with the highest concentrations of HA/ FA/ NOM with 10 % sodium azide to avoid any biological contamination followed by required dilutions for lower loadings. Sorbents were also preloaded with 20 ml of extracted pore waters with 10% sodium azide (HPW and PPW). The amount of sorbent was 0.2 g and preloading was done in 40 ml vials. Preloading of all the samples was done for 48 hours and samples were kept on rotary shaker at 150 rpm for continuous mixing.

Contaminants	† Log K_{OW}	†Log K_{DOC}		Organic Contaminant Concentration Range for HA/ FA/ NOM effects (mg/L)	Organic Contaminant Concentration Range for extracted pore water effects (mg/L)	Organic Contaminant Concentration Range for sorbent mixture studies (mg/L)
		HA	FA			
Phenanthrene	4.44	3.85	3.26	0.16 – 2.0	0.1 – 2.0	0.08 – 2.0
2,2',5,5'- tPCB	5.9	4.6	-	0.016 – 0.8	0.050 – 0.250	0.008 – 0.4

† Poerschmann et al. 1999

Table 5.1: Log KOW, Log KDOC values and concentration range of phenanthrene and 2, 2', 5, 5'-tPCB

Sorbent amendment mixture performance

Sorbent amendment mixture analysis: Studies were conducted to determine the effect of natural organic matter present in Cottonwood Bay, Texas (table 5.2) on sorbent mixture present in the reactive core mat. For this purpose, experiments were conducted with virgin Sorbent mixture, the sorbent mixture obtained from reactive core mat that was deployed in Cottonwood Bay for six months and virgin sorbent mixture in Cottonwood Bay sediment pore water. These experiments were conducted at five loadings of a contaminant mixture having 2, 2', 5, 5'-tPCB and phenanthrene. Separate batches were prepared with 0.1 g of sorbent mixture (virgin/ Cottonwood Bay) in 125 ml flasks having DI water spiked with contaminant mixture of 2, 2', 5, 5'-tPCB and phenanthrene depending on the loading rate (table 5.1). After spiking samples were kept on rotary shaker for one week at 150 rpm.

Samples/ sorbents extractions and analysis

Sample extraction: Two sub-samples from each vial/ flask were collected and extracted using a surrogate-spiked solvent. For PCB extraction TCMX in hexane was used as a surrogate standard and for PAH extraction 2-fluorobiphenyl in methylene chloride was used. Solvent vials were shaken vigorously three times at an interval of 30 seconds each. The vials were then stored for at least 24 hours at 4° C. The extracted solvents were passed through sodium sulfate to remove any chemically bound water. The filtered samples were then mixed with internal standards in GC vials followed by GC/MS analysis using internal standard method. For PCB 2, 4, 6,-trichlorobiphenyl was used as an internal standard because there was no overlap in the peaks of 2, 4, 6,-

trichlorobiphenyl and 2, 2', 5, 5'-tPCB and for PAH Acenaphthene d10 was used as an internal standard.

Gas Chromatography/ Mass Spectrometry: All the extracts were analyzed using internal standard method on Varian CP3800 Gas Chromatograph (GC)/ Saturn 2200 Ion Trap Mass Spectrometer (MS) with a CP8400 Auto Sampler. The GC column used was a DB-5 type capillary column (Varian Factor Four VF-5ms), 30 m long, 0.25 mm ID and 0.5 µm thick. The ion-trap was operated in selected scan mode (MS/MS) for both PCB and PAH. For PCB the column oven temperature was programmed at 40˚ C with hold time of 2 min followed by a temperature ramp up to 184˚ C at the rate of 12˚ C/ min. and then to 280˚ C at the rate of 4˚ C/ min with the final held time of 2 minutes. For PAH column temperature was programmed at 80˚ C with hold time of 2 min followed by a temperature ramp up to 315 ˚ C at the rate of 25˚ C with final held time of 2 minutes.

Quality Assurance: All the chemicals used in the experiments were of ultra high purity. Experiments were either conducted in Teflon® lined screw cap glass vials or 125 ml glass flasks with the glass stoppers to ensure that there is no volatilization loss. The pyrex glassware was used which was solvent/ soapy water washed and properly rinsed with RO water followed by drying in Muffle furnace at 500˚ C programmed for 8 hours. Experiments were run in duplicates and from each sample vial/ flask 2 sub-samples were extracted to check if there is any deviation in % surrogate recovery. The surrogate recoveries were in the range of 70-120%. For GC/MS analysis internal standard method

was used and in each GC run one read back and one blank was run after every eighth sample. In blanks the concentration of PCB/ PAH was non-detectable.

Results and Discussions

Pore water from aged sediments of six different sites including Hudson River, New Bedford Harbor (NBH), Cocheco River, Passaic River, Gowanus Canal and Cottonwood Bay was extracted and characterized (table 5.2 A-B). The pH of all the six sediments ranged from 7.45 – 7.9. The oxidation-reduction potential of Hudson River sediment pore water was found to be the highest. The TOC values of Hudson River and Passaic River pore water were found to be higher than that of other sediments, therefore, these two sediments pore water were selected for the studies conducted to determine the effect of natural organics present in the extracted pore water on adsorption capacity of sorbents. DOC and TDN analysis was performed to determine the carbon and nitrogen content in humic and fulvic fractions of the extracted pore waters (table 5.2 B).

Table 5.2A: Characteristics of extracted sediment porewater

Sediment samples	pH	ORP(mv)	TOC (mg L-1)	DOC (mg L-1)	UV_{254} (mg L-1)
Hudson River	7.71	175	141.58	24.63	2.919
New Bedford Harbor	7.45	29.3	96.26	93.74	1.387
Cocheco River	7.73	80.5	59.16	57.68	1.257
Passaic River	7.93	70.3	178.86	46.67	0.971
Gowanus Canal	7.94	57.6	85.54	43.3	1.441

Table 5.2B: DOC and TDN in humic and fulvic fraction of extracted sediment porewater

Samples	DOC (mg C/L)	TDN (mg N/L)
Hudson FA	92.7	0.9
Hudson HA	80.2	2.5
NBH FA	52.5	2.1
NBH HA	122.8	1.3
Cocheco FA	94.8	2.3
Cocheco HA	58.7	3.5
Passaic FA	71.8	1.1
Passaic HA	43.6	0.8
Gowanus Canal FA	50.4	1.8
Gowanus Canal HA	50.7	1.2

Results showed high DOC in humic fractions of NBH and Hudson River pore water while the Passaic River pore water showed lowest DOC in humic fraction of porewater. Hudson River porewater with high DOC in the fulvic and humic fractions represents high humic content and Passaic River porewater with high DOC in fulvic fraction and low in HA fraction represents low humic content. Using these two sediment pore waters in the isotherm studies provided a range of effects from high humic content pore water to a mixture of humic and non-humic content of pore water.

Isotherm studies were conducted to evaluate the effect of different fractions of natural organic matter (Ald-HA/ SRHA/ SRFA/ SRNOM) as well as mixture of natural organics present in the extracted pore water on the performance of activated carbon and organoclay for PCB and PAH adsorption. Ald-HA, SRHA, SRFA and SRNOM represented the different fractions that can be present at any given site. The characteristics of these materials are presented in table 5.3. The concentrations of

target organic contaminants were achieved by spiking the required doses of PCB and PAH as described in the experimental procedure section (Figure 5.1). Besides evaluating the individual sorbent performance, the adsorption capacity of the sorbent mixture (virgin or aged in Cottonwood bay) for mixture of contaminants was also evaluated.

Sample	pH of solution	C (%)	H (%)	O (%)	N (%)	S (%)	P (%)	Ash (%)
Aldrich HA†	7.21	69.4	5	39.3	0.75	4.25	0.15	31
Suwannee River HA††	7.17	52.34	4.36	42.98	0.67	0.46	0.004	0.58
Suwannee River FA††	7.11	53.04	4.36	43.91	0.75	0.46	< 0.01	0.98
Suwannee River NOM††	7.24	52.47	4.19	42.69	1.1	0.65	0.02	7

† Zhao et al. (1998); †† International Humic Substance Society

Table 5.3: Elemental composition of humic acid, fulvic acid and NOM and pH of the solutions used in this study

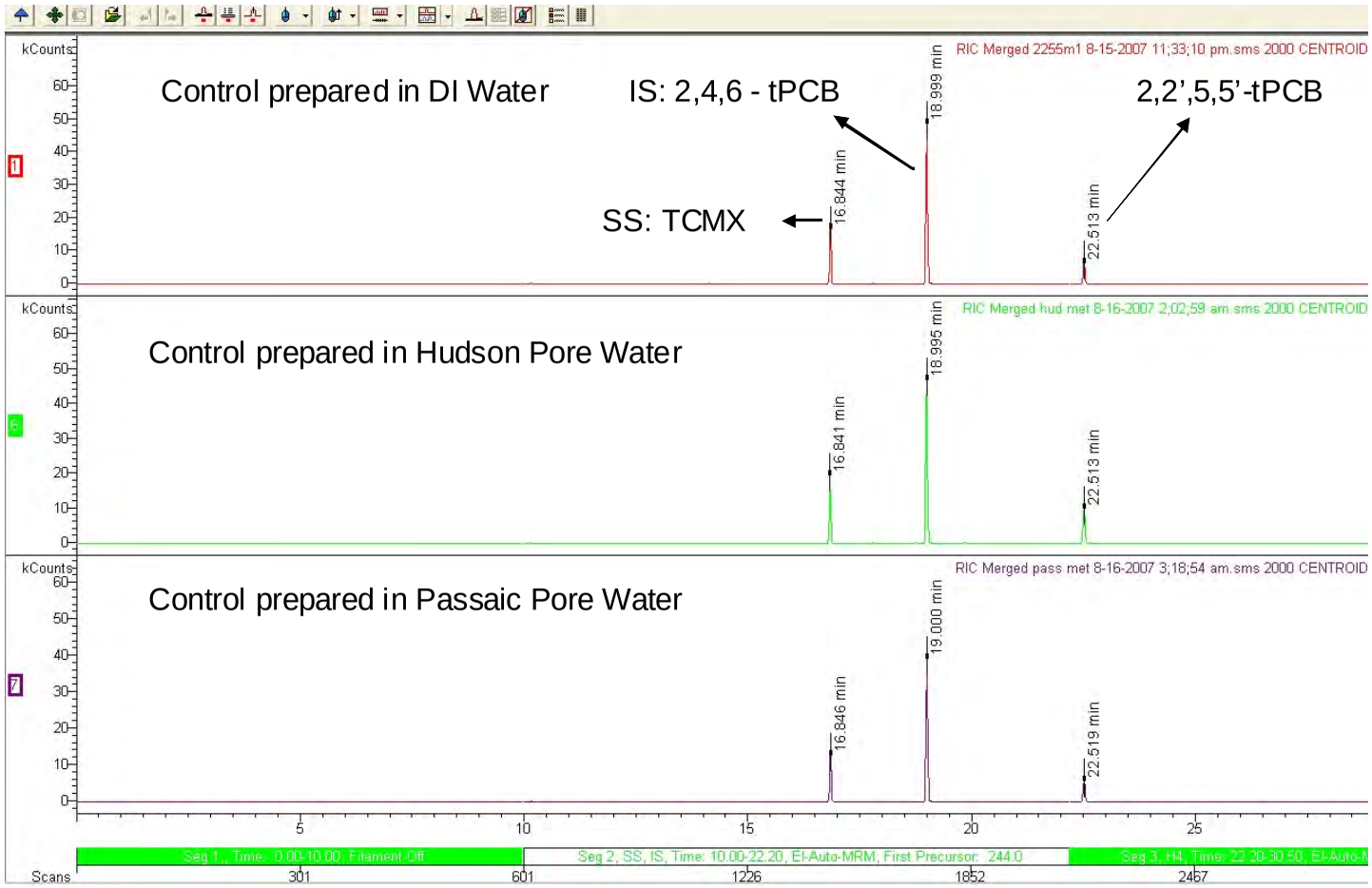

Figure 5.1 A: GC Chromatograms showing peaks of selected contaminants in presence of DI water; Passaic River Pore Water and Hudson River Pore Water: 2, 2', 5, 5'-tPCB

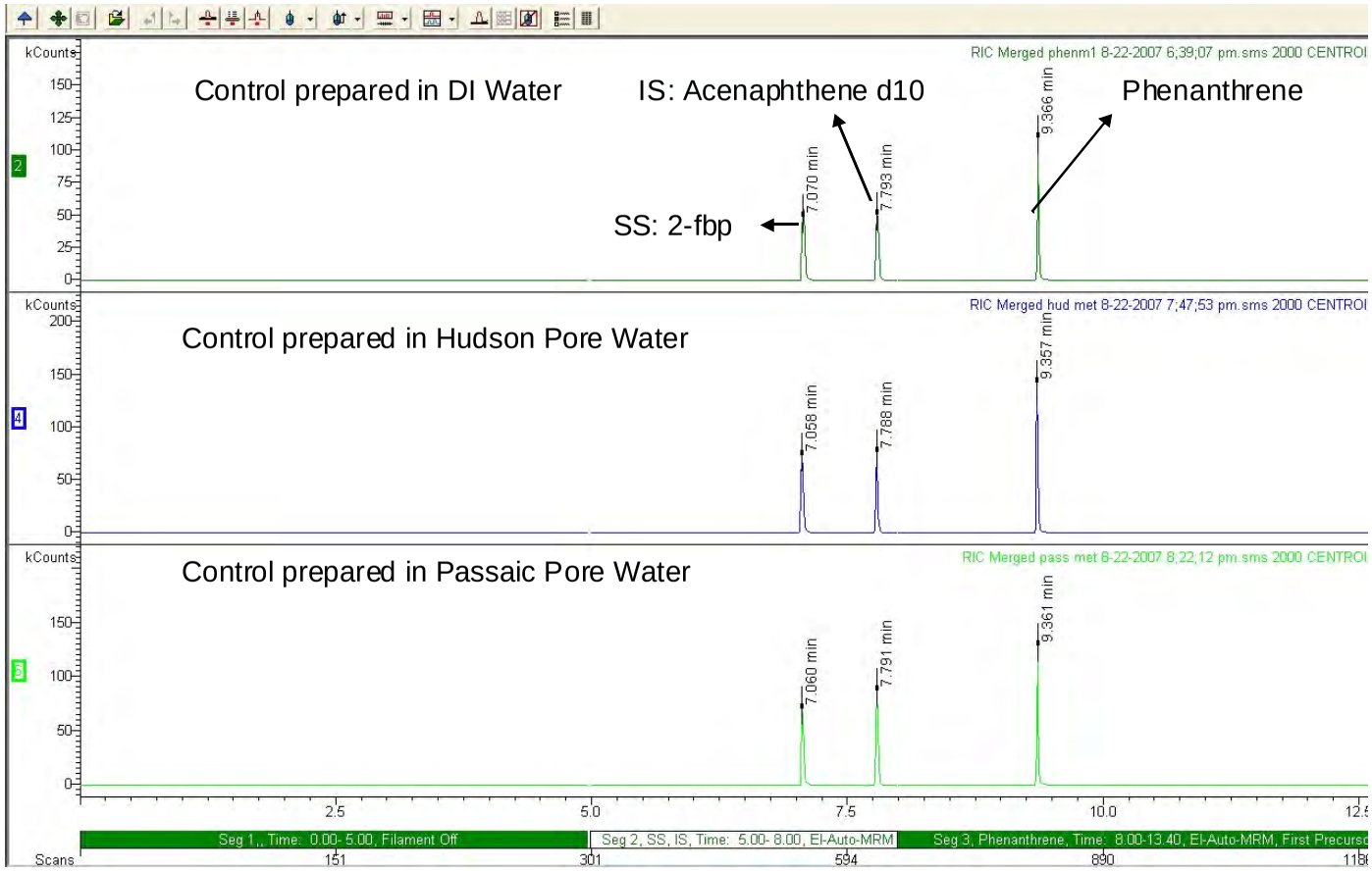

Figure 5.1 B: GC Chromatograms showing peaks of selected contaminants in presence of DI water; Passaic River Pore Water and Hudson River Pore Water: Phenanthrene

The adsorption capacities of the sorbents and sorbent mixture were determined by using a linear partition model (K_d values) developed from the isotherms and the Freundlich isotherm model. The Freundlich isotherm model was used in its non-linear form as:

$$q_e = K_f \ (C_e^{\ (1/n)})$$

where q_e is the mass of adsorbate adsorbed per mass of sorbent (mg/g), C_e is the equilibrium concentration of solute in the aqueous solution after adsorption (mg L^{-1}), K_f is the Freundlich capacity factor and 1/n is the linearity factor.

Preloading effect of Ald-HA/ SRHA/ SRFA/ SRNOM:

Figure 5.2 shows Freundlich isotherms for adsorption of 2, 2', 5, 5'-tPCB and phenanthrene on organoclay and activated carbon in the presence of Ald-HA, SRHA, SRFA and SRNOM. Figure 5.2 A and B represents adsorption of 2, 2', 5, 5'-tPCB on organoclay and activated carbon respectively. The adsorption capacity of both the sorbents for PCB was found to be reduced in the presence of Ald-HA (table 5.4). In the presence of fulvic acid slight enhancement was noticed in the case of organoclay but there was no effect of fulvic acid on adsorption on activated carbon. The presence of NOM had no effect on the adsorption of 2, 2', 5, 5'-tPCB on both activated carbon and organoclay. In case of organoclay the effect of preloading with AldHA/ SRHA/ SRFA/ SRNOM on adsorption capacity was found to be in the following order: AldHA> SRHA> NOM > FA.

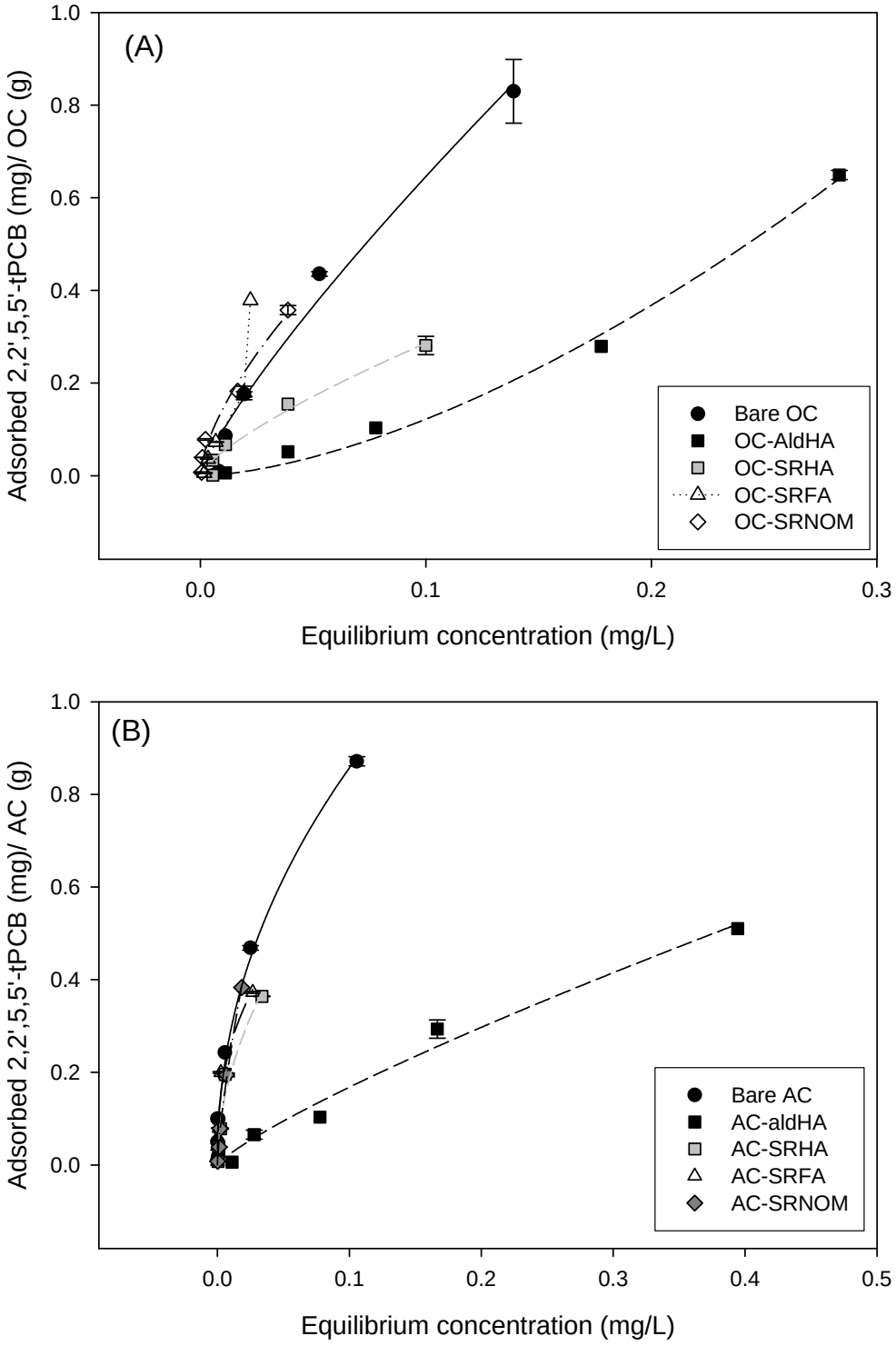

Figure 5.2 A-B: Adsorption of contaminants in presence of different fractions of natural organic matter (A) 2, 2', 5, 5'-tPCB adsorption on OC (B) 2, 2', 5, 5'-tPCB adsorption on AC (OC = Organoclay; AC = Activated Carbon; HA = Humic Acid; FA = Fulvic Acid and NOM = Natural Organic Matter)

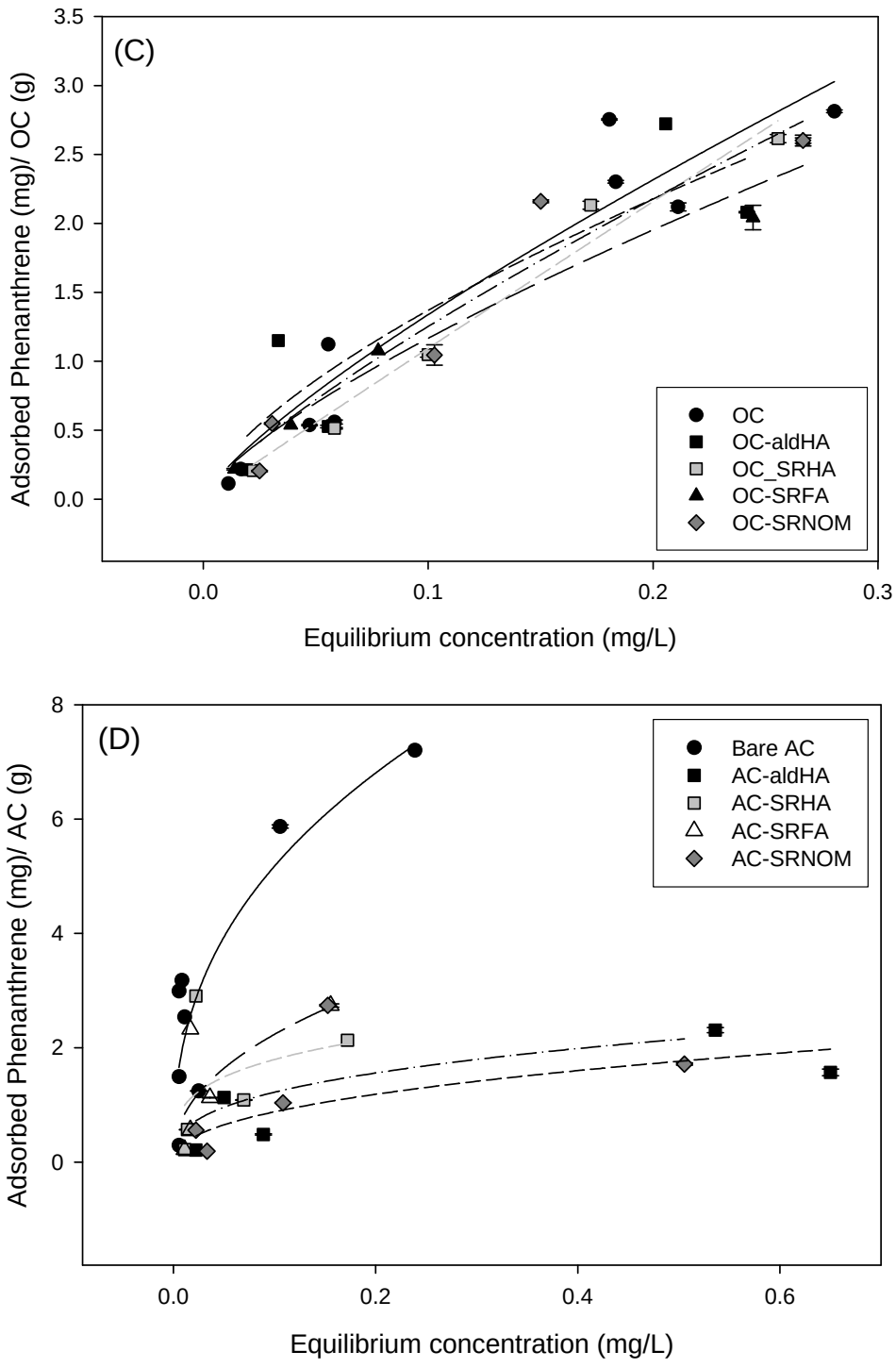

Figure 5.2 C-D: Adsorption of contaminants in presence of different fractions of natural organic matter (C) Phenanthrene adsorption on OC (D) Phenanthrene adsorption on AC (OC = Organoclay; AC = Activated Carbon; HA = Humic Acid; FA = Fulvic Acid and NOM = Natural Organic Matter)

This trend can be supported by the studies conducted by Kohl et al. (1998) who studied the binding of organic contaminants to different fractions of soil organic matter and showed the binding affinity of HA > Humin > FA with 2, 2', 5, 5'-tPCB.

Figure 5.2 C and D represents the adsorption of phenanthrene on organoclay and activated carbon, respectively. The phenanthrene adsorption on organoclay showed no effect of Ald-HA, SRHA, SRFA and SRNOM. In case of activated carbon a significant effect of Ald-HA was noticed (figure 5.2 D). The effect of SRNOM (similar to Ald-HA) was slightly higher than that of SRHA followed by SRFA. This trend can be attributed to the binding affinity of Humin (present in NOM) > HA > FA for phenanthrene as reported by Kohl et al. (1998). Saparpakorn et al. (2007) has also shown that PAHs partition to NOM more strongly as compared to HA and FA due to lower docked energies of NOM (docking is the method to predict orientation of molecule to another to form a stable complex and docked energy is the energy of the overall system with optimized confrontation). The π-π interaction and hydrogen bonding is involved in FA, HA and NOM interactions with PAH in addition to hydrogen bonding with proteinaceous moieties of NOM. Therefore, in the case of phenanthrene, the lowest adsorption was seen in the presence of NOM.

	Adsorption Isotherm Constants		Freundlich Isotherm Constants			
	Kd (L g^{-1})		K_f ($mg^{[1-(1/n)]}$ $L^{(1/n)}$ g^{-1})		1/n	
2,2',5,5'-tPCB	Activated Carbon	Organoclay	Activated Carbon	Organoclay	Activated Carbon	Organoclay
Bare Sorbent	7.69	6.00	2.53	3.51	0.47	0.72
Aldrich HA	1.30	2.30	1.12	4.77	0.82	1.59
SRHA	9.59	2.73	2.23	1.58	0.53	0.74
SRFA	11.73	14.91	1.55	-	0.39	-
SRNOM	20.19	8.49	7.64	2.92	0.75	0.65
Phenanthrene						
Bare Sorbent	24.59	10.67	12.84	8.28	0.39	0.79
Aldrich HA	2.31	8.98	2.38	6.39	0.43	0.67
SRHA	6.35	10.96	3.34	10.46	0.27	0.98
SRFA	12.50	8.34	6.23	6.46	0.45	0.74
SRNOM	2.48	9.91	2.74	7.88	0.35	0.80

Table 5.4: Adsorption coefficients for Isotherm Studies to determine effect of Ald-HA/ SRHA/ SRFA and SRNOM

The isotherm data was analyzed using statistical software JMP® 7 to compare the performance of activated carbon and organoclay for 2, 2', 5, 5'-tPCB and phenanthrene adsorption in presence of Ald-HA/ SRHA/ SRFA and SRNOM (table 5.5 A-B). The full factorial models were developed using type of sorbent, treatment and loading rate as the factors. Due to the non-linear form of the isotherms a quadratic term of loading rate was also used.

Table 5.5 A: Specifications of statistical model 1

Model 1 specification: for 2, 2', 5, 5'-tPCB
Sorbent
Treatment
Sorbent*Treatment
Loading Rate
Sorbent*Loading Rate
Treatment*Loading Rate
Sorbent*Treatment*Loading Rate
Loading Rate*Loading Rate

Table 5.5 B: Specifications of statistical model 2

Model 2 specification: for Phenanthrene
Sorbent
Treatment
Sorbent*Treatment
Loading rate
Sorbent*Loading rate
Treatment*Loading rate
Sorbent*Treatment*Loading rate
Loading rate*Loading rate

The p-value was obtained to be < 0.0001 in analysis of variance (ANOVA) (details in additional information). The F-test was performed on each term used in the model to check the significance. The LS Means student's t- table was obtained for adsorbed concentration and treatment based on the type of sorbents (table 5.6). Results showed slightly higher adsorption capacity of activated carbon for 2, 2', 5, 5'-

tPCB than organoclay. The adsorption was found to be increased in presence of FA but significant reduction was noticed in presence of humic acid for both the sorbents. There was no effect of NOM on adsorption of 2, 2', 5, 5'-tPCB on both the sorbents. Table 5.6 B showed effect of Ald-HA/ SRHA/ SRFA/ SRNOM on performance of sorbents for phenanthrene adsorption. There was no effect of any of the natural organics on the adsorption capacity of organoclay. The performance of activated carbon was found to be different than that of organoclay in the presence of Ald-HA but statistically no difference was noticed in performance of activated carbon in the presence of Ald-HA/ SRHA/ SRFA/ SRNOM.

Table 5.6 A: LS Means Student's t table for performance of activated carbon and organoclay in presence of Ald-HA/ SRHA/ SRFA/ SRNOM for 2, 2', 5, 5'-tPCB
t at α=0.050 and t=2.04523

Level					Least Sq Mean
AC,SRNOM	A				0.223
AC,SRFA	A				0.220
OC,SRFA	A	B			0.215
AC,SRHA	A	B			0.215
OC,SRNOM	A	B			0.209
AC,Bare	A	B			0.208
OC,Bare		B			0.199
OC,SRHA			C		0.168
OC,Ald-HA				D	0.133
AC,Ald-HA				D	0.129

Levels not connected by same letter are significantly different

Table 5.6 B: LS Means Student's t table for performance of activated carbon and organoclay in presence of Ald-HA/ SRHA/ SRFA/ SRNOM for phenanthrene adsorption at α=0.050 and t=2.06866

Level			Least Sq Mean
OC,SRFA	A		1.254
OC,SRHA	A		1.241
OC,Ald-HA	A	B	1.196
AC,SRNOM	A	B	1.169
AC,SRHA	A	B	1.161
AC,SRFA	A	B	1.152
OC,SRNOM	A	B	1.107
AC,Ald-HA		B	0.999

Levels not connected by same letter are significantly different

Preloading effect of extracted pore water:

Figure 5.3 represented the adsorption of 2, 2', 5, 5'-tPCB and phenanthrene on activated carbon and organoclay in the presence of extracted pore water from Hudson River and Passaic River sediments. The Hudson River sediment pore water was more colloidal and the Passaic River Pore Water was clear, though both had high TOC values (table 5.2). The significant reduction in the performance of both the sorbents for adsorption of both the contaminants was noticed in the presence of Hudson River pore water (figure 5.3A-D). This reduction in adsorption of both the contaminants in the presence of Hudson River pore water can be attributed to the partitioning of contaminants towards high humics present in the porewater. The Passaic River pore water which was low in humics did not have as much reduction effect on the performance of both the sorbents as that of Hudson River pore water. The TOC value of Passaic River pore water was higher than that of Hudson River pore water but the

reduction in adsorption was more in case of Hudson River porewater which can be explained on the basis of high aquatic humics present in the Hudson River pore water. The reducing effect of Passaic pore water was very less in case of 2, 2', 5, 5'-tPCB for both the sorbents but it was slightly higher in the case of phenanthrene adsorption (table 5.9).

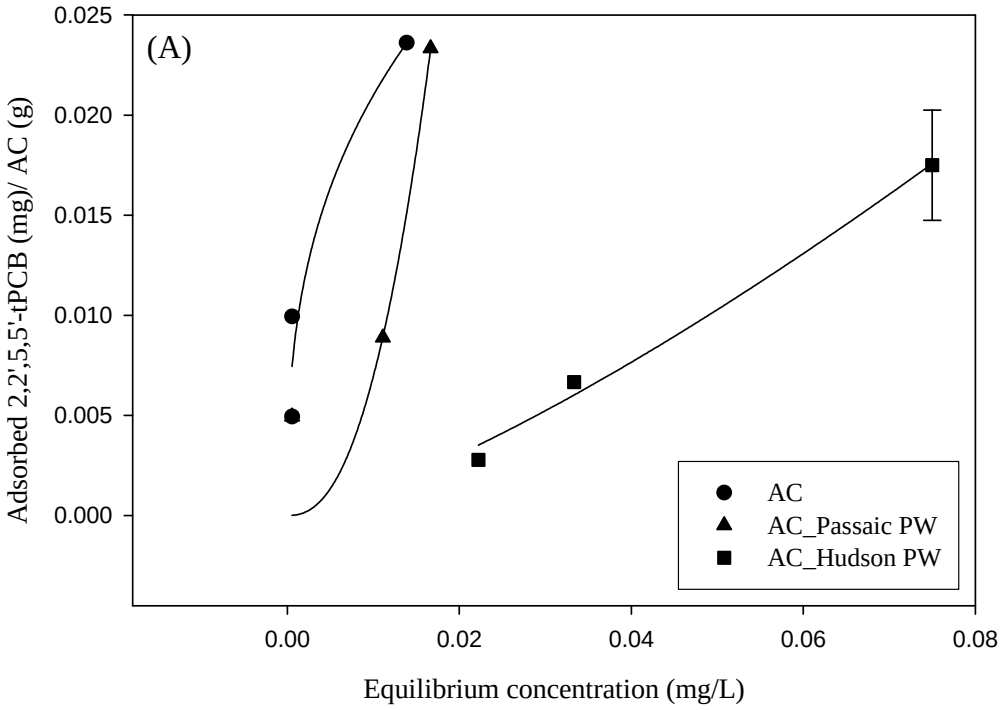

Figure 5.3 A: Adsorption contaminants in presence of extracted pore water: 2, 2', 5, 5'-tPCB adsorption on AC (AC = Activated Carbon and PW = Pore water)

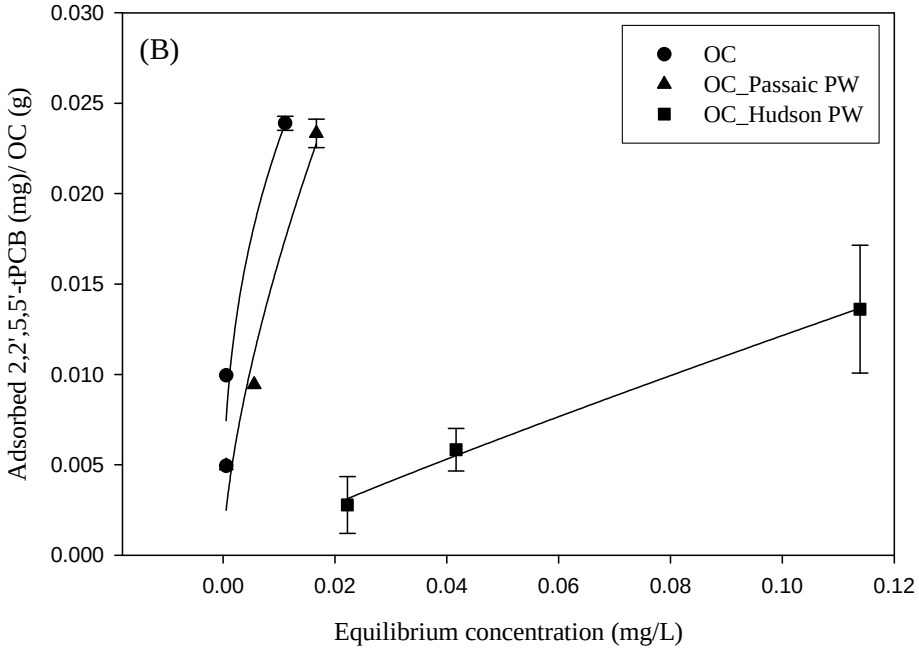

Figure 5.3 B: Adsorption contaminants in presence of extracted pore water: 2, 2', 5, 5'-tPCB adsorption on OC (OC = Organoclay and PW = Pore water)

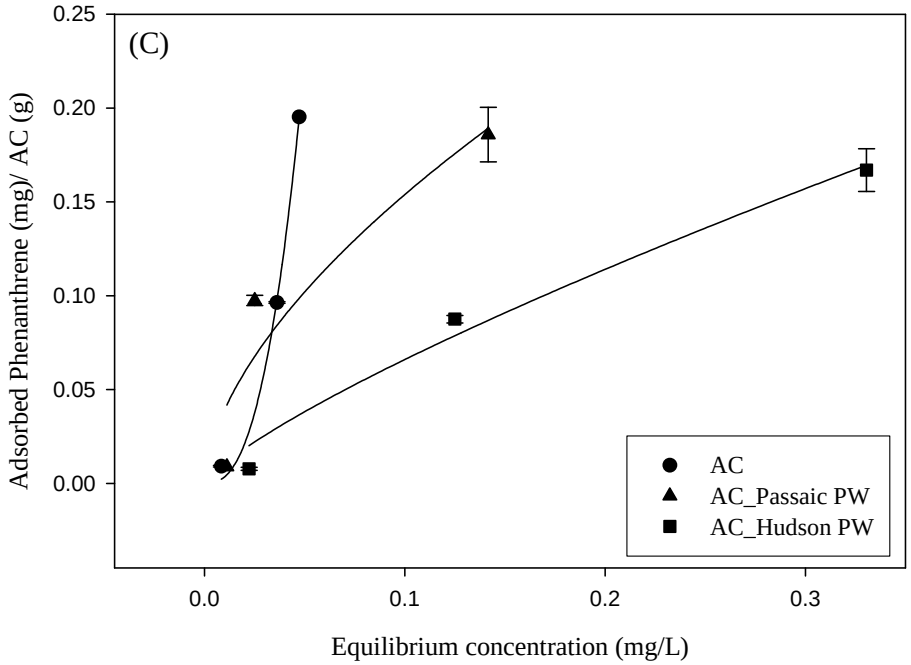

Figure 5.3 C: Adsorption contaminants in presence of extracted pore water: Phenanthrene adsorption on AC (AC = Activated Carbon and PW = Pore water)

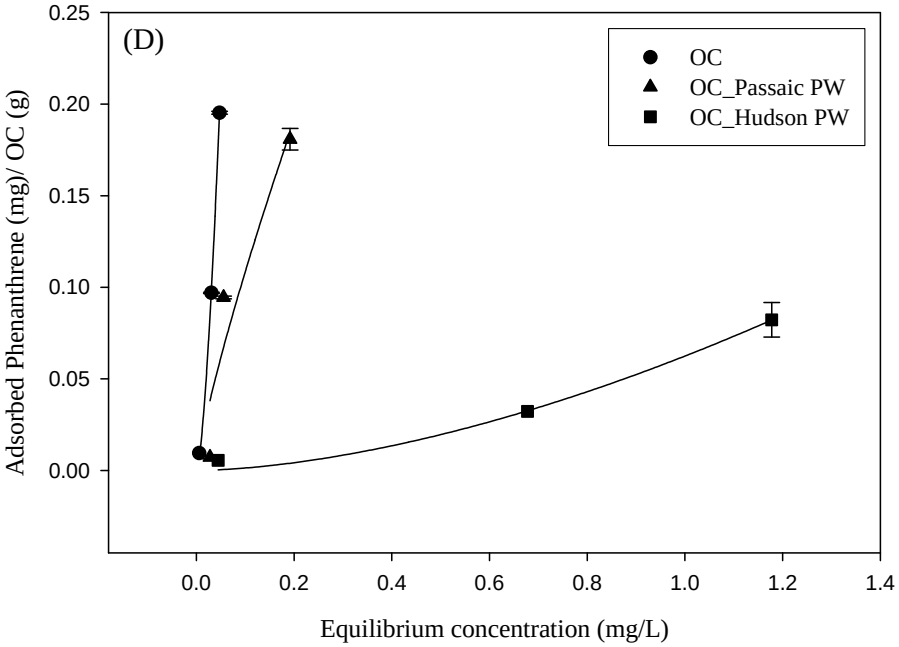

Figure 5.3 D: Adsorption contaminants in presence of extracted pore water (C) Phenanthrene adsorption on AC: Phenanthrene adsorption on OC (OC = Organoclay and PW = Pore water)

The statistical analysis of data was performed to compare the performance of activated carbon and organoclay for 2, 2', 5, 5'-tPCB (model 3) and phenanthrene (model 4) adsorption in presence of extracted pore water (table 5.7).

Table 5.7: Specifications of statistical models 3 and 4

Model 3 and 4 specification:
Sorbent
Treatment
Sorbent*Treatment
Loading Rate
Treatment*Loading Rate
Loading Rate*Loading Rate

The performance of both the sorbents was found to be reduced in the presence of Hudson River pore water (Figure 5.4 A-B). The reducing effect of Hudson River pore water was more pronounced for both the contaminants for both the sorbents but was very high for phenanthrene adsorption on organoclay (table 5.8 A-B).

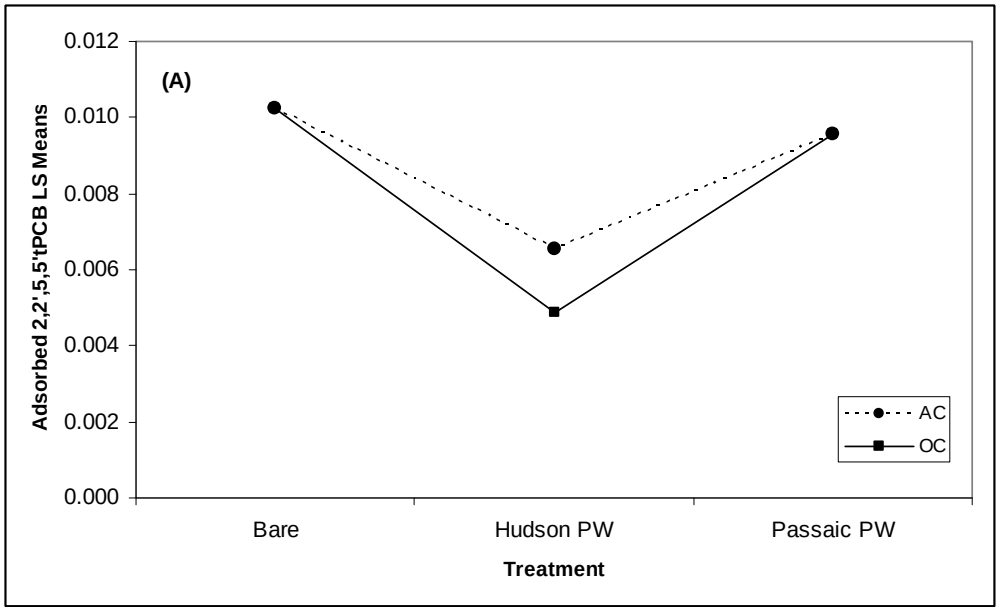

Figure 5.4A: Statistical analysis of performance of sorbents: 2, 2', 5, 5'-tPCB adsorption on AC and OC in presence of extracted pore water (AC = activated carbon; OC = organoclay)

Table 5.8 A: LS Means Student's t table for performance of activated carbon and organoclay in presence of Hudson River and Passaic River porewater for 2, 2', 5, 5'-tPCB adsorption at α=0.050 and t=2.306

Level			Least Sq Mean
AC,Bare	A		0.010
OC,Bare	A		0.010
AC,Passaic PW	A		0.010
OC,Passaic PW	A		0.010
AC,Hudson PW		B	0.007
OC,Hudson PW		B	0.005

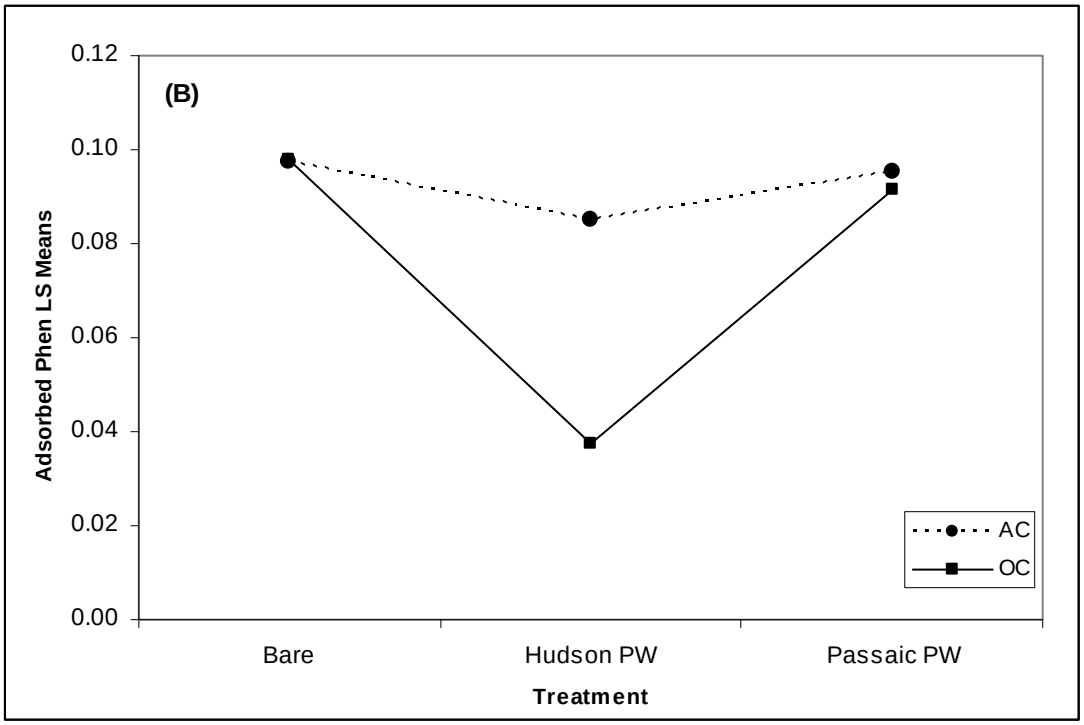

Figure 5.4B: Statistical analysis of performance of sorbents: phenanthrene adsorption on AC and OC in presence of extracted pore water (AC = activated carbon; OC = organoclay)

Table 5.8 B: LS Means Student's t table for performance of activated carbon and organoclay in presence of Hudson River and Passaic River porewater for phenanthrene adsorption at α=0.050 and t=2.570

Level				Least Sq Mean
OC,Bare	A			0.098
AC,Bare	A			0.098
AC,Passaic PW	A			0.095
OC,Passaic PW	A	B		0.092
AC,Hudson PW		B		0.085
OC,Hudson PW			C	0.038

	Adsorption Isotherm Constants		Freundlich Isotherm Constants			
	Kd (L g^{-1})		K_f ($mg^{[1-(1/n)]}$ $L^{(1/n)}$ g^{-1})		1/n	
2,2',5,5'-tPCB	Activated Carbon	Organoclay	Activated Carbon	Organoclay	Activated Carbon	Organoclay
Bare Sorbent	1.13	1.56	0.11	0.14	0.36	0.39
HPW	0.27	0.12	381.12	0.33	2.37	0.65
PPW	1.04	1.16	0.54	0.10	1.32	0.90
Phenanthrene						
Bare Sorbent	4.47	4.38	520.39	24.40	2.58	1.58
HPW	0.50	0.07	0.60	0.71	0.59	0.82
PPW	1.23	0.92	0.41	0.06	0.79	1.67

Table 5.9 Adsorption coefficients for Isotherm Studies to determine effect of extracted porewater

Performance of sorbent amendment mixtures:

In figure 5.5 the performance of virgin sorbent mixture was compared to that of sorbent mixture obtained from Cottonwood Bay and sorbent mixture in presence of Cottonwood Bay porewater for adsorption of 2, 2', 5, 5'-tPCB and phenanthrene.

Table 5.10: Characteristics of Cottonwood Bay porewater

Sediment sample	pH	ORP(mv)	TOC (mg L^{-1})	DOC (mg L^{-1})	UV_{254} (cm^{-1})
Cottonwood Bay	7.59	-32.7	5.715	6.1	0.106

The sorbent mixture that was obtained from the mats represented the realistic scenario having sorbents in the geotextile being deployed over the sediment bed for six months. There was negligible effect of natural organics present in the site on adsorption of 2, 2', 5, 5'-tPCB and the slight reducing effect on phenanthrene adsorption was also found to be statistically negligible. In figure 5.5 the actual trend of isotherms was presented using a dotted line that shows slight S-shaped behavior of the sorbent mixture.

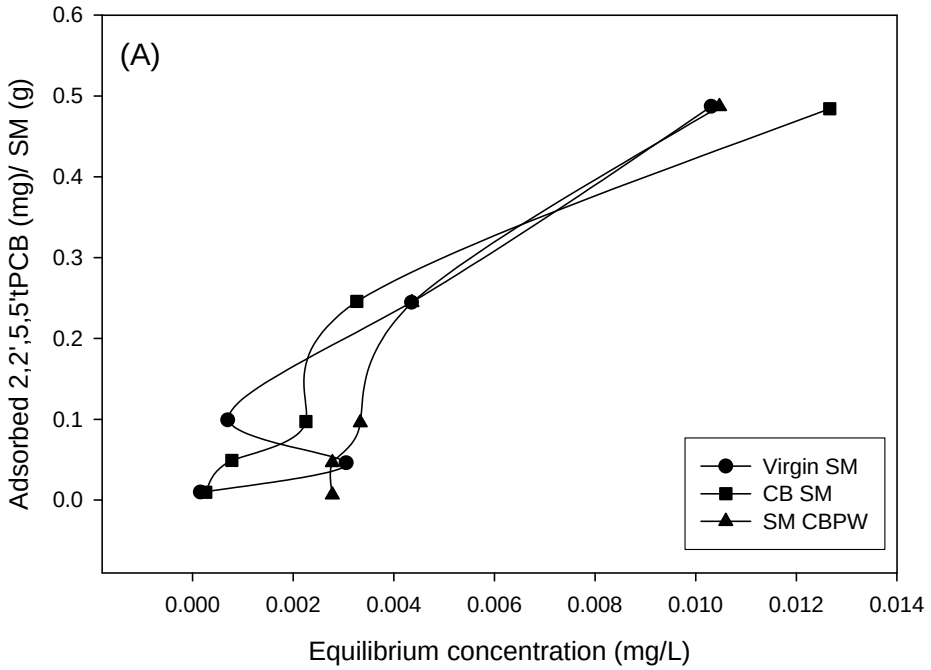

Figure 5.5 A: Comparison of bare sorbent mixture with the sorbent mixture obtained from reactive core mats deployed in Cottonwood Bay for 6 months: 2, 2', 5, 5'-tPCB adsorption(SM = Sorbent mixture; CB = Cottonwood Bay; and PW = Porewater)

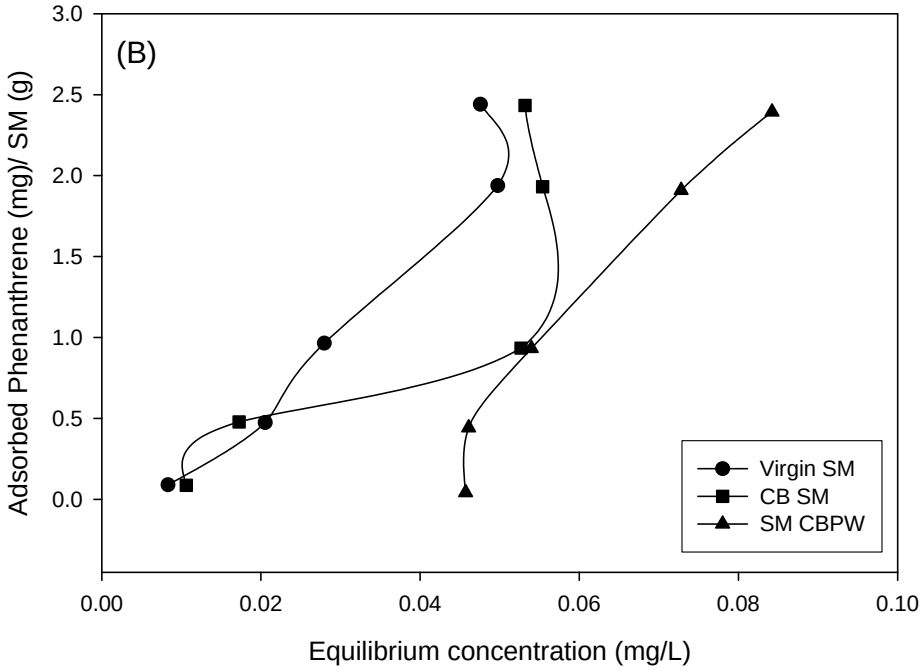

Figure 5.6B: Comparison of bare sorbent mixture with the sorbent mixture obtained from reactive core mats deployed in Cottonwood Bay for 6 months: Phenanthrene adsorption (SM = Sorbent mixture; CB = Cottonwood Bay; and PW = porewater)

The performance of both the sorbent mixtures was also analyzed statistically for adsorption of 2, 2', 5, 5'-tPCB (model 5) and phenanthrene (model 6) (table 5.11). The models were developed on the basis of treatment on sorbent mixture (virgin/ Cottonwood Bay/Porewater) and loading rate (details in additional information).

Table 5.11: Specifications for statistical model 5 and model 6

Model 5 and 6 specification:
Treatment
Loading Rate
Treatment*Loading Rate

LS Mean's plots were obtained to determine the effect of natural organic matter present in Cottonwood Bay (Figure 5.6). The results showed no difference in the performance of virgin sorbent mixture, sorbent mixture obtained from mats and sorbent mixture in Cottonwood Bay porewater (table 5.12 A-B).

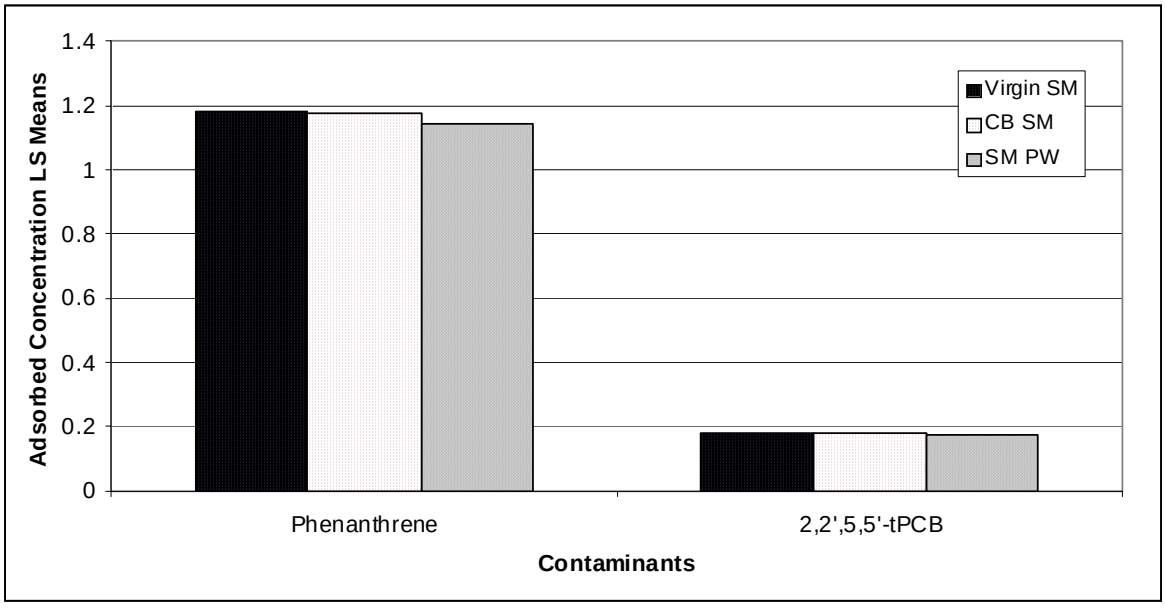

Figure 5.6: Statistical analysis of performance of sorbents: 2, 2', 5, 5'-tPCB and phenanthrene adsorption on SM and CB SM (SM = Sorbent Mixture, CB = Cottonwood Bay and PW = Porewater)

Table 5.12 A-B: LS Means Student's t table for performance of sorbent mixture for 2, 2', 5, 5'-tPCB and phenanthrene adsorption at α=0.050 and t = 2.306

A: 2, 2', 5, 5'-tPCB adsorption

Level		Least Sq Mean
SM	A	0.106
CBSM	A	0.105
SM PW	A	0.104

B: Phenanthrene adsorption

Level		Least Sq Mean
SM	A	1.080
CBSM	A	1.071
SM PW	A	1.042

Levels not connected by same letter are significantly different.

Contaminants	Adsorption Isotherm Constants			Freundlich Isotherm Constants					
	Kd (L g^{-1})			K_f ($mg^{[1-(1/n)]}$ $L^{(1/n)}$ g^{-1})			1/n		
	Virgin Sorbent Mixture	Cottonwood Bay Sorbent Mixture	Sorbent mixture in PW	Virgin Sorbent Mixture	Cottonwood Bay Sorbent Mixture	Sorbent mixture in PW	Bare Sorbent Mixture	Cottonwood Bay Sorbent Mixture	Sorbent mixture in PW
2, 2', 5, 5'-tPCB	45.46	36.82	57.53	65.83	11.78	256.43	1.07	0.73	1.37
Phenanthrene	53.90	37.84	56.54	243.21	106.64	2587.33	1.56	1.40	2.80

Table 5.13: Adsorption coefficients for Isotherm Studies for sorbent mixture evaluation

Effect of different loadings of HA/ FA/ NOM:

Studies were also conducted at three loadings of HA/ FA and NOM to determine the effect of different loadings on adsorption of 2, 2', 5, 5'-tPCB and phenanthrene on activated carbon and organoclay (Figure 5.7). Figure 5.7A-C showed results for 2, 2', 5, 5'-tPCB adsorption and figure 5.7 D – F represents results for phenanthrene adsorption.

In figure 5.7A and D it can be noticed that with the increase in concentration of humic acid the performance of sorbents decreases. The effect of FA and NOM did not show much variation in the effect at different loadings on 2, 2', 5, 5'-tPCB but the trend was slightly decreasing for phenanthrene adsorption on activated carbon. The middle loading of HA/ FA and NOM corresponded to the concentration used in preloading the sorbents for isotherm studies.

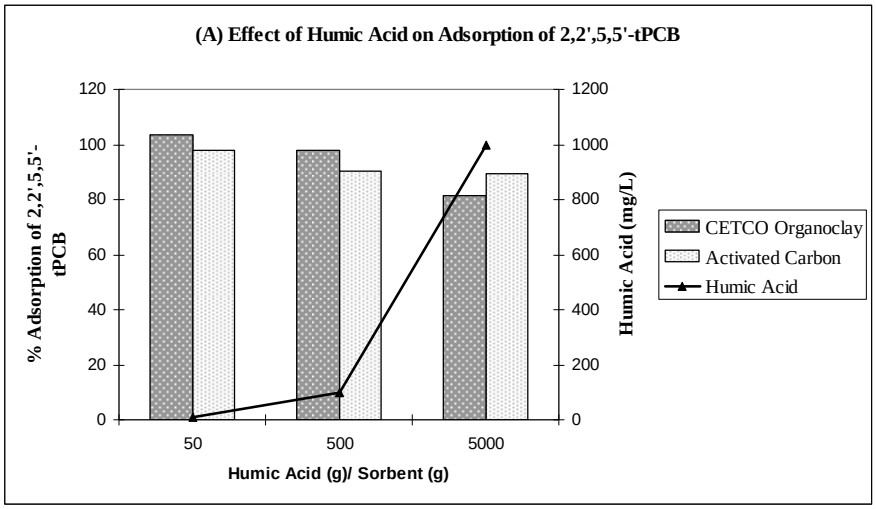

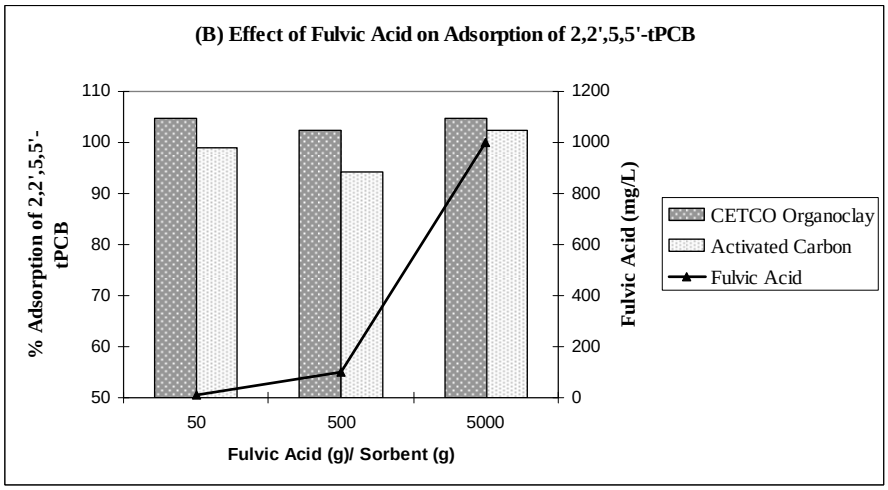

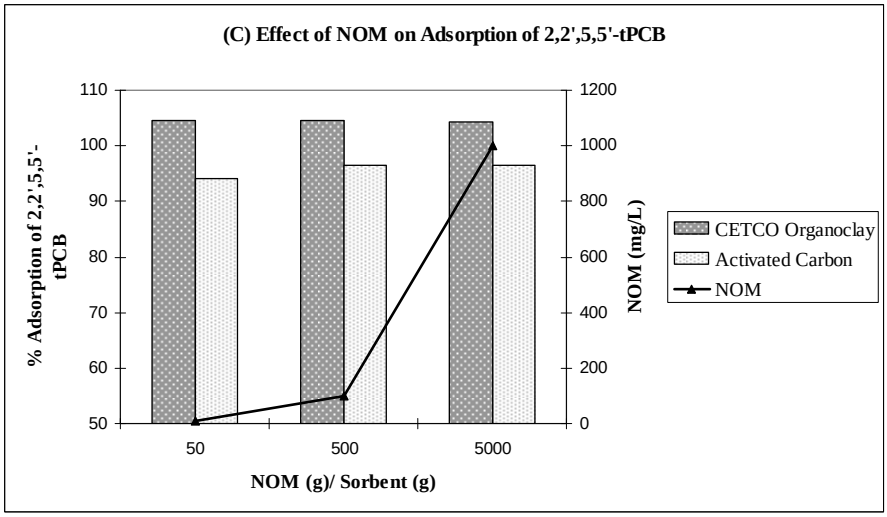

Figure 5.7A-C: Comparison of performance of organoclay and activated carbon for adsorption of 2, 2', 5, 5'-tPCB in the presence of humic acid, fulvic acid and natural organic matter normalized to adsorption on bare materials.

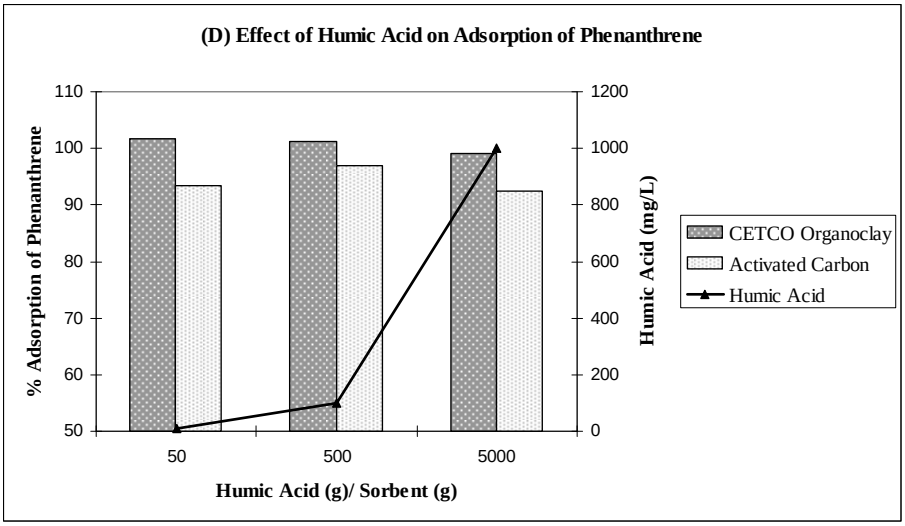

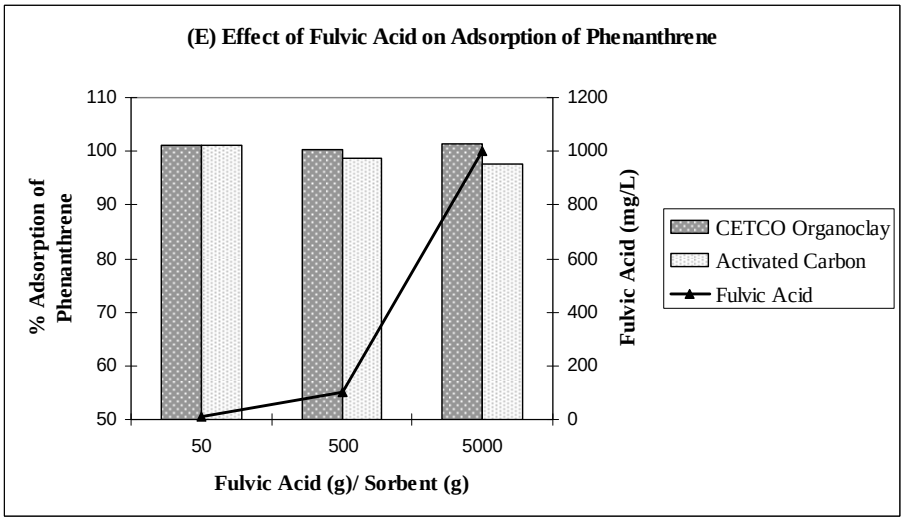

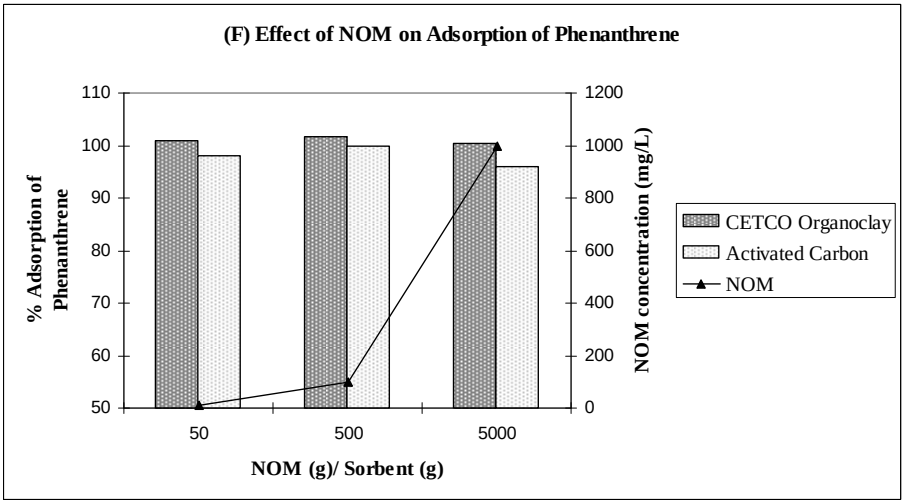

Figure 5.7D-F: Comparison of performance of organoclay and activated carbon for adsorption of phenanthrene in the presence of humic acid, fulvic acid and natural organic matter normalized to adsorption on bare materials.

Summary

This study has been conducted to evaluate the performance of activated carbon and organoclay for 2, 2', 5, 5'-tPCB and phenanthrene adsorption in the presence of different fractions of natural organic matter and extracted pore water to simulate the actual site conditions. Besides evaluating the different sorbents, the sorbent mixture having a combination of different materials was also analyzed and its performance was compared with the sorbent mixture obtained from the reactive capping mat that was deployed in the study field site (Cottonwood Bay) for six months. The results showed significant effect of AldHA on the adsorption of 2, 2', 5, 5'-tPCB on both the sorbents. The effect of SRHA was more pronounced in case of adsorption of 2, 2', 5, 5'-tPCB on organoclay compared to activated carbon. There was slight enhancement on 2, 2', 5, 5'-tPCB adsorption on organoclay in the presence of SRFA but there was no effect on activated carbon. There was no effect of SRNOM on 2, 2', 5, 5'-tPCB adsorption on both the sorbents. In case of phenanthrene, no effect was noticed in presence of any of the natural organics on organoclay. The reducing effects of AldHA/ SRHA/ SRFA and SRNOM were found to be similar on activated carbon. Besides Ald-HA/ SRHA/ SRFA and SRNOM, extracted pore water was also used to evaluate the performance of sorbents. A significant reducing effect was noticed on the performance of both the sorbents for both the contaminants in case of Hudson River sediment pore water which was high in humics compared to Passaic River sediment porewater that had mixture of humic and non-humic contents. The performance of virgin sorbent mixture was also compared with sorbent mixture obtained from the mat that was deployed in the field for six months and with the effect of Cottonwood Bay pore water on virgin sorbent mixture

but negligible effect of natural organic matter that was presented in the field was found. The Ald-HA/ SRFA and SRNOM effects were also determined at different loadings on both the sorbents. The adsorption capacity of both the sorbent was found to be decreased with the increase in Ald-HA concentration. The fulvic acid and natural organic matter did not affect the 2, 2', 5, 5'-tPCB adsorption on both the sorbents but slight reduction was noticed on phenanthrene adsorption on activated carbon.

Additional Information

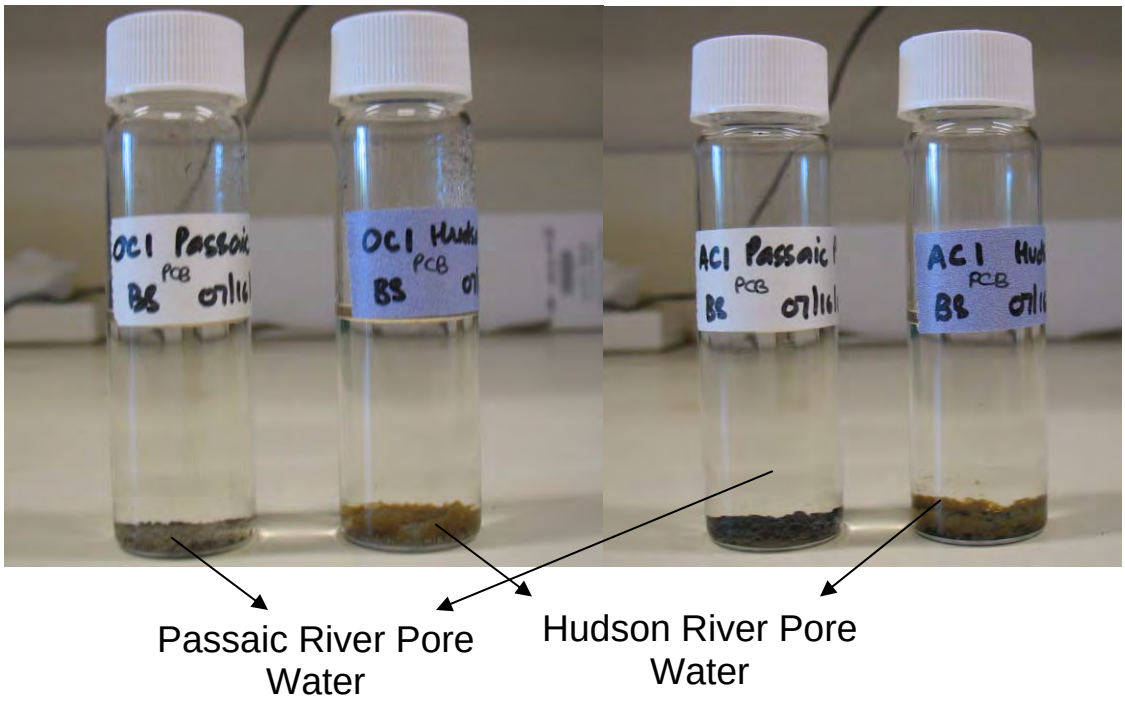

Reactive core mats drying at room temperature prior to sorbent separation

Left: Sorbent mixture obtained from reactive core mat (deployed in the field for 6 months); Right: Virgin sorbent mixture

Model 1 detail: for 2, 2', 5, 5'–tPCB adsorption in presence of Ald-HA/ SRHA/ SRFA/ SRNOM

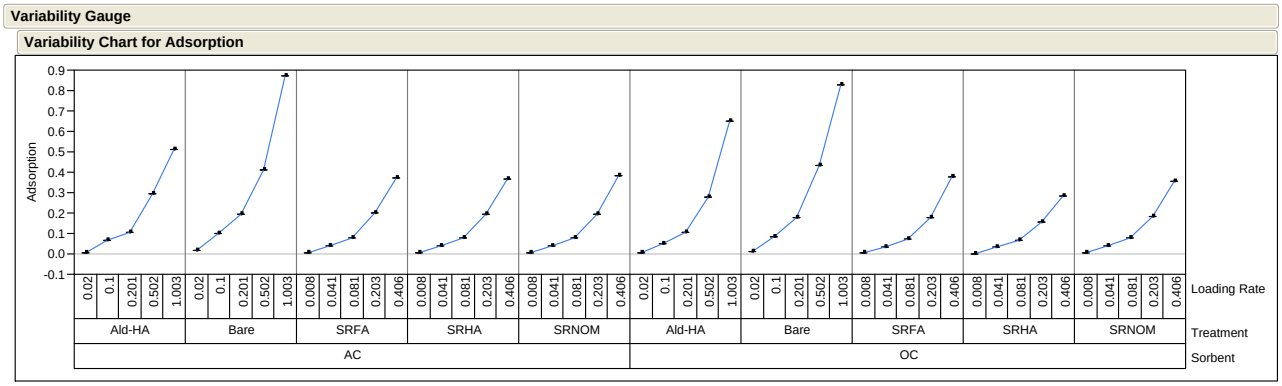

Actual by Predicted Plot

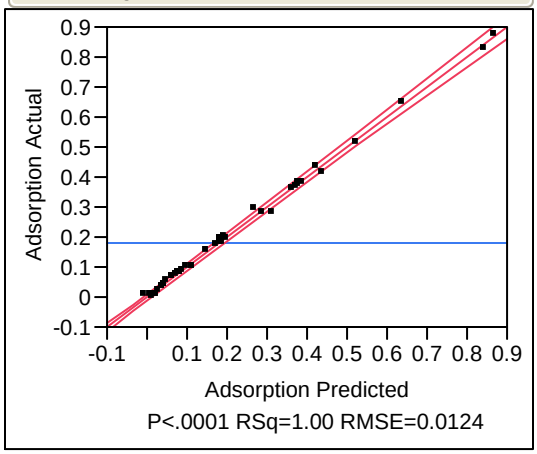

Analysis of Variance

Source	DF	Sum of Squares	Mean Square	F Ratio
Model	20	2.1011635	0.105058	688.4599
Error	29	0.0044254	0.000153	**Prob > F**
C. Total	49	2.1055889		<.0001*

Effect Tests

Source	Nparm	DF	Sum of Squares	F Ratio	Prob > F
Sorbent	1	1	0.00193851	12.7033	0.0013*
Treatment	4	4	0.04126649	67.6062	<.0001*
Sorbent*Treatment	4	4	0.00293094	4.8017	0.0043*
Loading Rate	1	1	0.76939337	5041.935	<.0001*
Sorbent*Loading Rate	1	1	0.00030393	1.9917	0.1688
Treatment*Loading Rate	4	4	0.05156139	84.4721	<.0001*
Sorbent*Treatment*Loading Rate	4	4	0.00821990	13.4665	<.0001*
Loading Rate*Loading Rate	1	1	0.00000233	0.0153	0.9025

Model 2 detail: for phenanthrene adsorption in presence of Ald-HA/ SRHA/ SRFA/ SRNOM

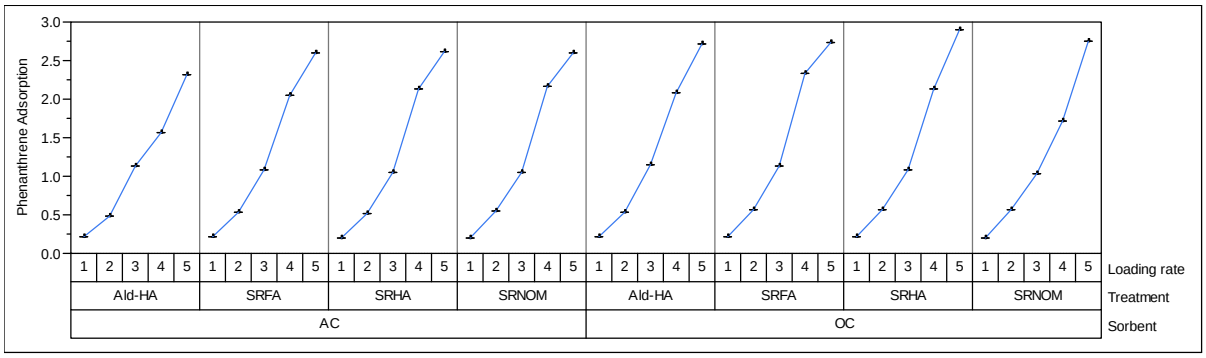

Actual by Predicted Plot

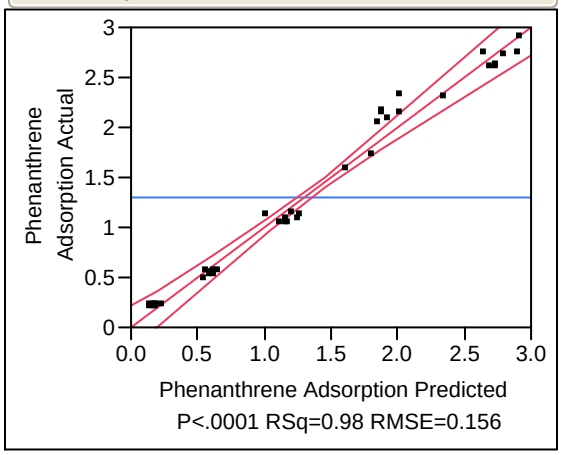

Analysis of Variance

Source	DF	Sum of Squares	Mean Square	F Ratio
Model	16	33.424202	2.08901	85.8206
Error	23	0.559858	0.02434	**Prob > F**
C. Total	39	33.984060		<.0001*

Effect Tests

Source	Nparm	DF	Sum of Squares	F Ratio	Prob > F
Sorbent	1	1	0.062647	2.5737	0.1223
Treatment	3	3	0.079162	1.0840	0.3756
Sorbent*Treatment	3	3	0.086122	1.1794	0.3393
Loading rate	1	1	32.452603	1333.214	<.0001*
Sorbent*Loading rate	1	1	0.058482	2.4026	0.1348
Treatment*Loading rate	3	3	0.064736	0.8865	0.4628
Sorbent*Treatment*Loading rate	3	3	0.052018	0.7123	0.5546
Loading rate*Loading rate	1	1	0.568433	23.3523	<.0001*

Model 3: 2, 2', 5, 5'-tPCB adsorption in presence of extracted porewater

Actual by Predicted Plot

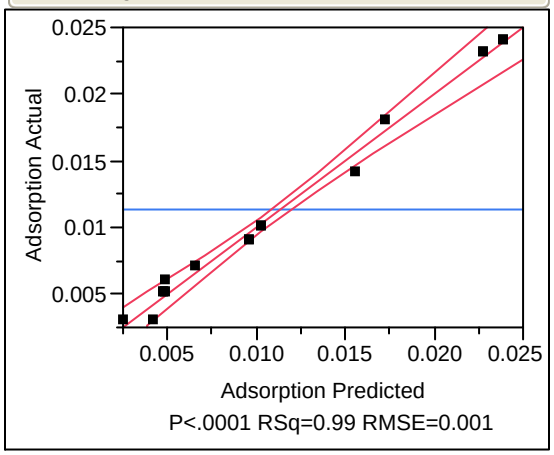

Analysis of Variance

Source	DF	Sum of Squares	Mean Square	F Ratio
Model	9	0.00099839	0.000111	122.8786
Error	8	0.00000722	9.028e-7	**Prob > F**
C. Total	17	0.00100561		<.0001*

Effect Tests

Source	Nparm	DF	Sum of Squares	F Ratio	Prob > F
Sorbent	1	1	0.00000139	1.5385	0.2500
Treatment	2	2	0.00007078	39.2000	<.0001*
Sorbent*Treatment	2	2	0.00000278	1.5385	0.2721
Loading Rate	1	1	0.00083333	923.0769	<.0001*
Treatment*Loading Rate	2	2	0.00002067	11.4462	0.0045*
Loading Rate*Loading Rate	1	1	0.00006944	76.9231	<.0001*

Model 4: Phenanthrene adsorption in presence of extracted porewater

Analysis of Variance

Source	DF	Sum of Squares	Mean Square	F Ratio
Model	12	0.08913506	0.007428	446.2703
Error	5	0.00008322	0.000017	**Prob > F**
C. Total	17	0.08921828		<.0001*

Effect Tests

Source	Nparm	DF	Sum of Squares	F Ratio	Prob > F
Sorbent	1	1	0.00130050	78.1342	0.0003*
Treatment	2	2	0.00472578	141.9626	<.0001*
Sorbent*Treatment	2	2	0.00212800	63.9252	0.0003*
Loading Rate	1	1	0.07648033	4594.947	<.0001*
Sorbent*Loading Rate	1	1	0.00061633	37.0294	0.0017*
Treatment*Loading Rate	2	2	0.00272217	81.7740	0.0002*
Sorbent*Treatment*Loading Rate	2	2	0.00110817	33.2894	0.0013*
Loading Rate*Loading Rate	1	1	0.00005378	3.2310	0.1322

Model 5: Performance of sorbent mixture for 2, 2', 5, 5'-tPCB adsorption

Variability Chart for 2255 PCB Adsorption

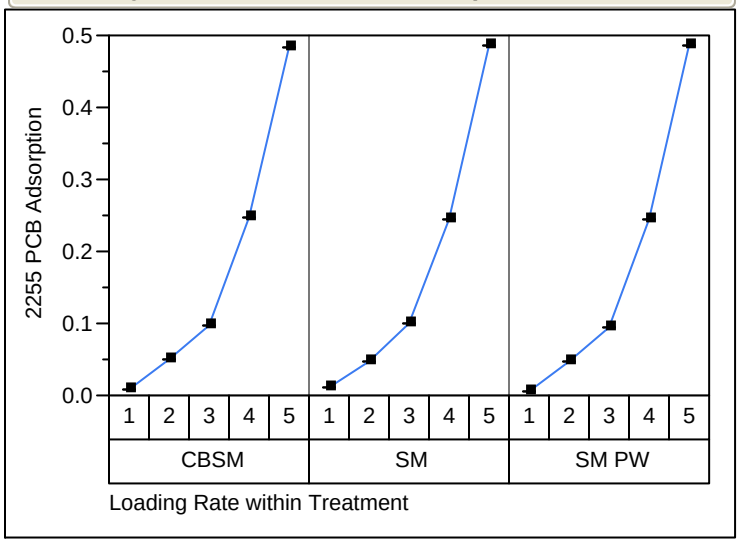

Actual by Predicted Plot

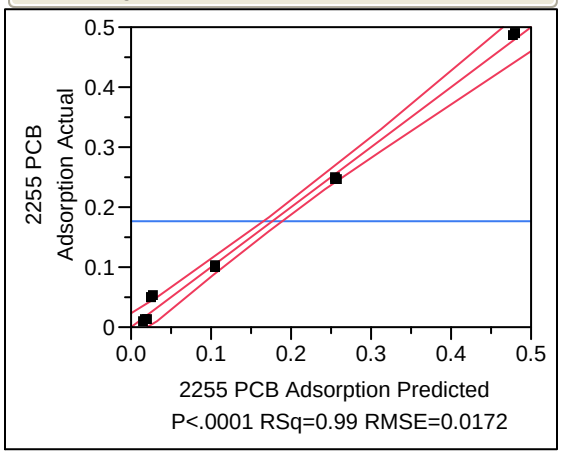

Analysis of Variance

Source	DF	Sum of Squares	Mean Square	F Ratio
Model	6	0.45264500	0.075441	254.8702
Error	8	0.00236798	0.000296	**Prob > F**
C. Total	14	0.45501297		<.0001*

Effect Tests

Source	Nparm	DF	Sum of Squares	F Ratio	Prob > F
Treatment	2	2	0.00000519	0.0088	0.9913
Loading Rate	1	1	0.39852298	1346.375	<.0001*
Treatment*Loading Rate	2	2	0.00000835	0.0141	0.9860
Loading Rate*Loading Rate	1	1	0.05410848	182.8007	<.0001*

Model 6: Performance of sorbent mixture for phenanthrene adsorption

Variability Chart for Phenanthrene Adsorption

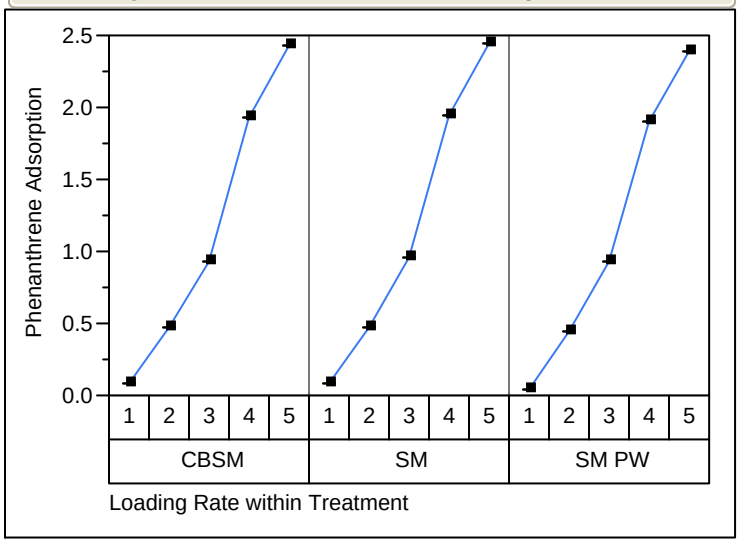

Actual by Predicted Plot

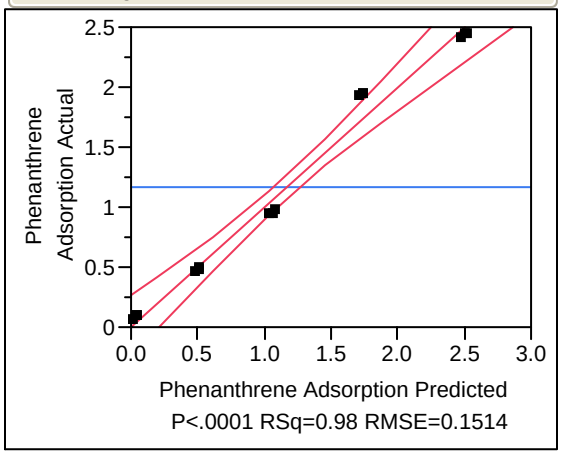

Analysis of Variance

Source	DF	Sum of Squares	Mean Square	F Ratio
Model	6	11.498476	1.91641	83.6549
Error	8	0.183268	0.02291	**Prob > F**
C. Total	14	11.681744		<.0001*

Effect Tests

Source	Nparm	DF	Sum of Squares	F Ratio	Prob > F
Treatment	2	2	0.003774	0.0824	0.9217
Loading Rate	1	1	11.385651	497.0045	<.0001*
Treatment*Loading Rate	2	2	0.000033	0.0007	0.9993
Loading Rate*Loading Rate	1	1	0.109018	4.7588	0.0607

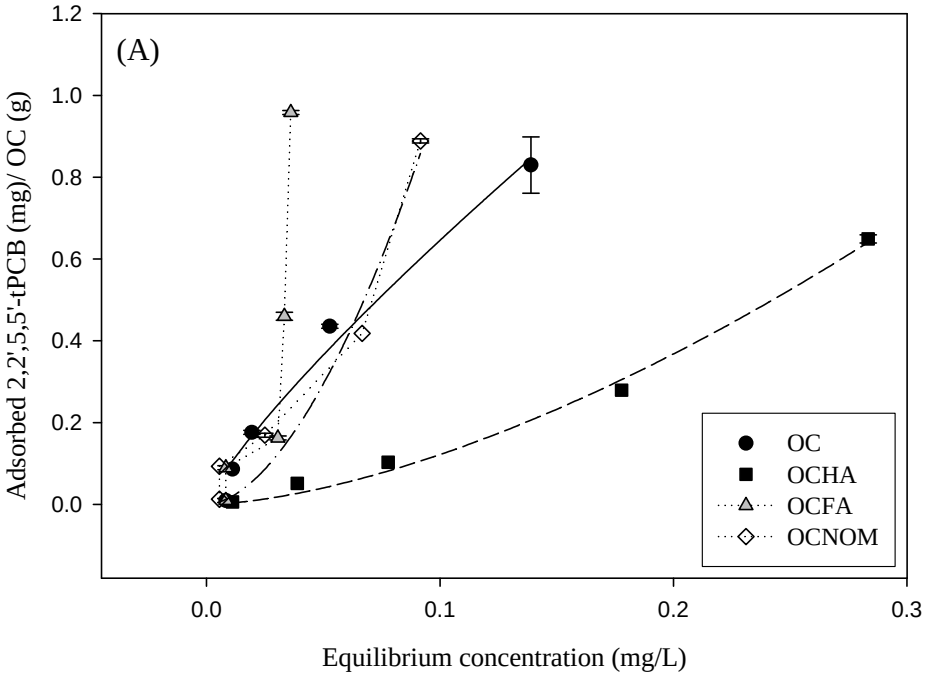
(A)
Adsorbed 2,2',5,5'-tPCB (mg)/ OC (g)
Equilibrium concentration (mg/L)
OC
OCHA
OCFA
OCNOM

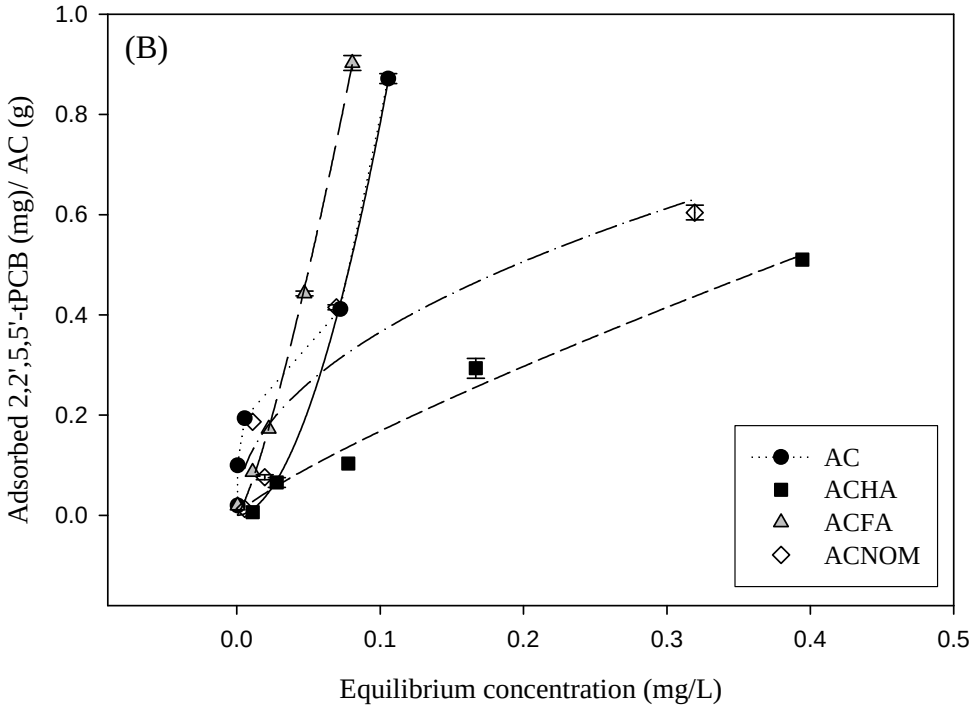
(B)
Adsorbed 2,2',5,5'-tPCB (mg)/ AC (g)
Equilibrium concentration (mg/L)
AC
ACHA
ACFA
ACNOM

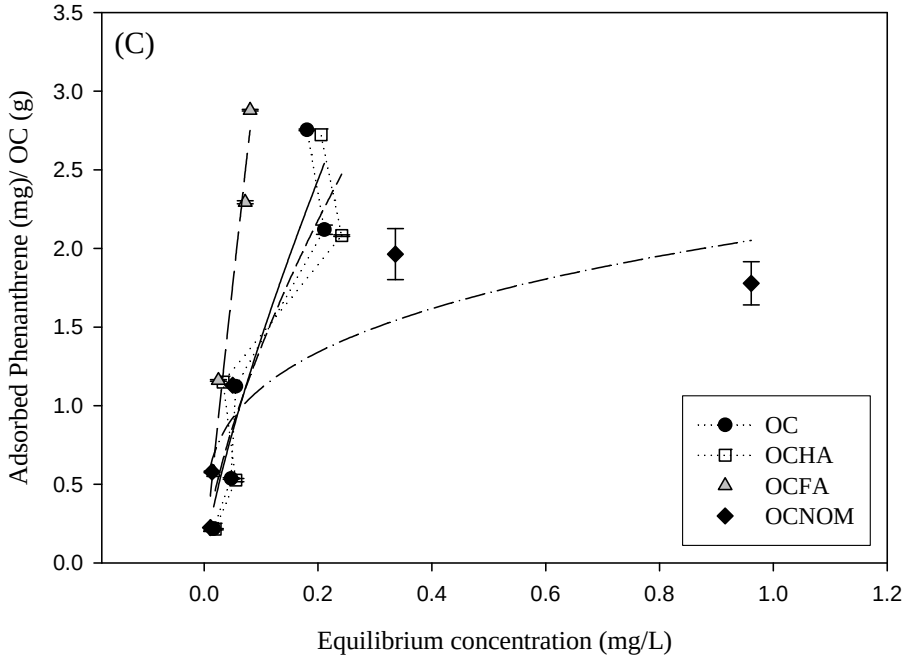

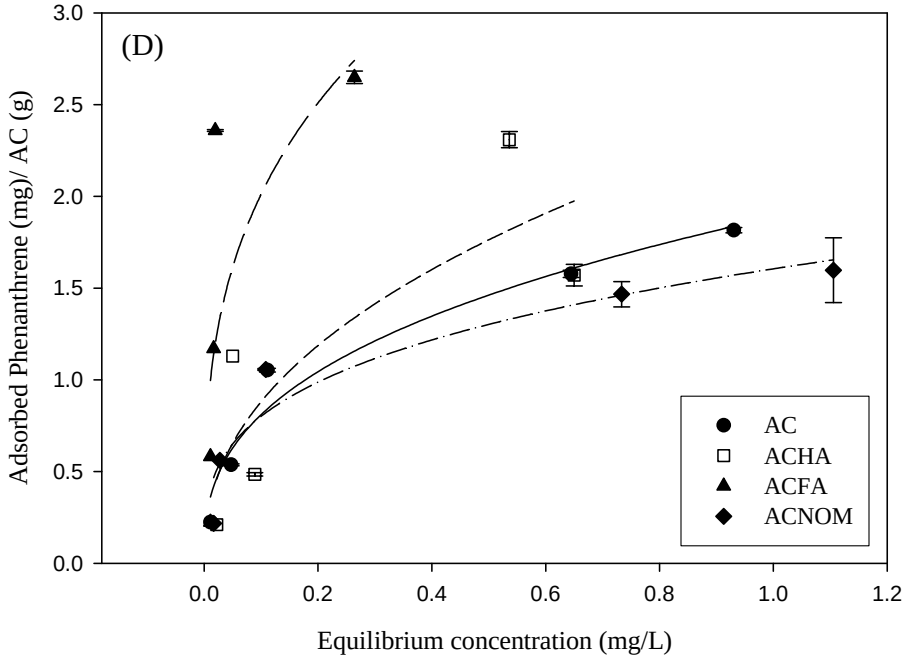

Adsorption of contaminants in presence of different fractions of natural organic matter (A) 2,2',5,5'-tPCB adsorption on OC (B) 2,2',5,5'-tPCB adsorption on AC (C) Phenanthrene adsorption on OC (D) Phenanthrene adsorption on AC (OC = Organoclay; AC = Activated Carbon; HA = Aldrich Humic Acid (pH 7.21); FA = Fulvic Acid (pH 4.02) and NOM = Natural Organic Matter (pH 4.12)

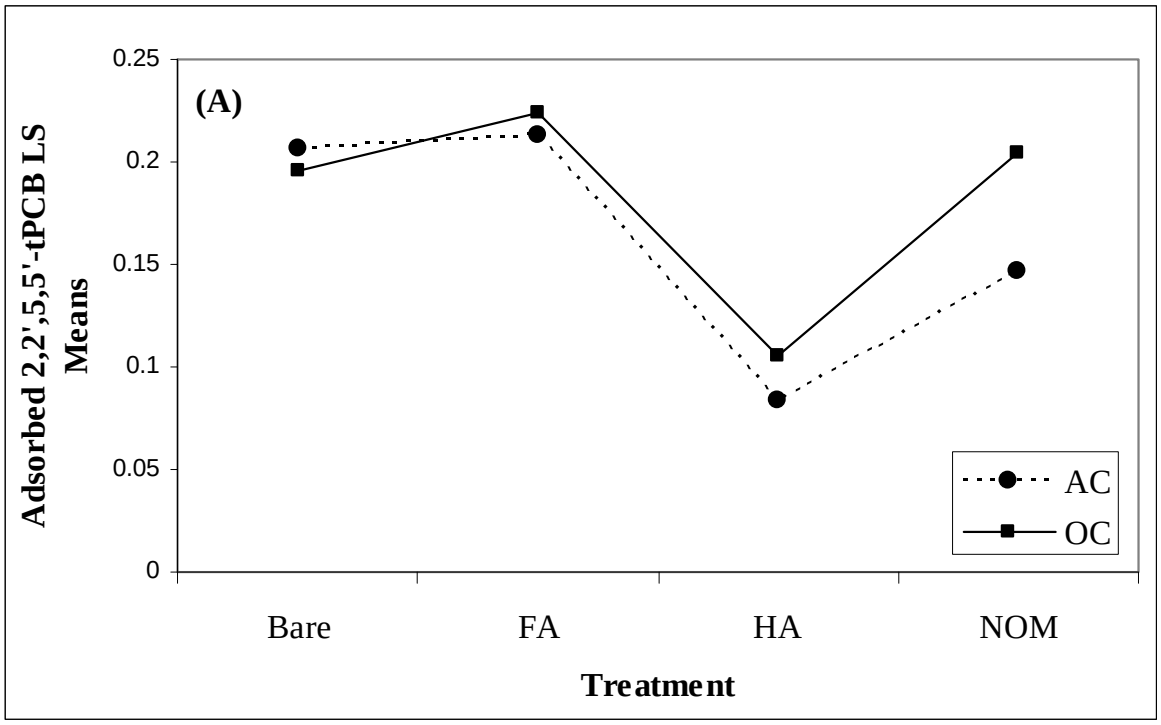

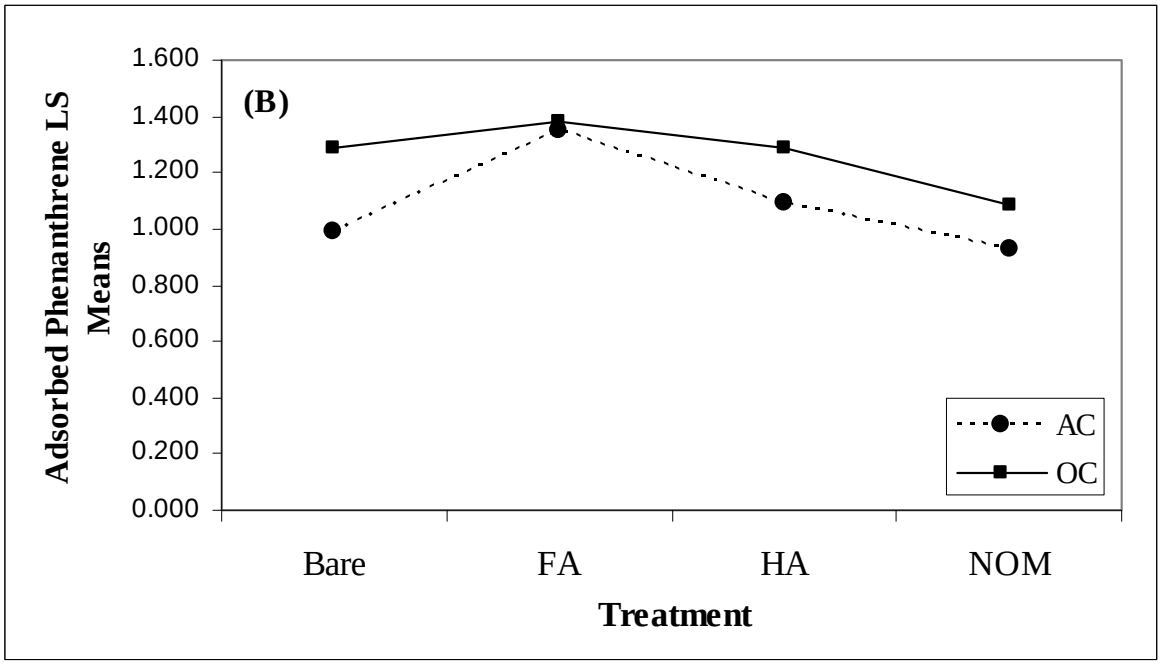

Statistical analysis of performance of sorbents (A) 2, 2', 5, 5'-tPCB adsorption on AC and OC in presence of HA/ FA/ NOM (B) Phenanthrene adsorption on AC and OC in presence of HA/ FA/ NOM (AC = activated carbon; OC = organoclay)

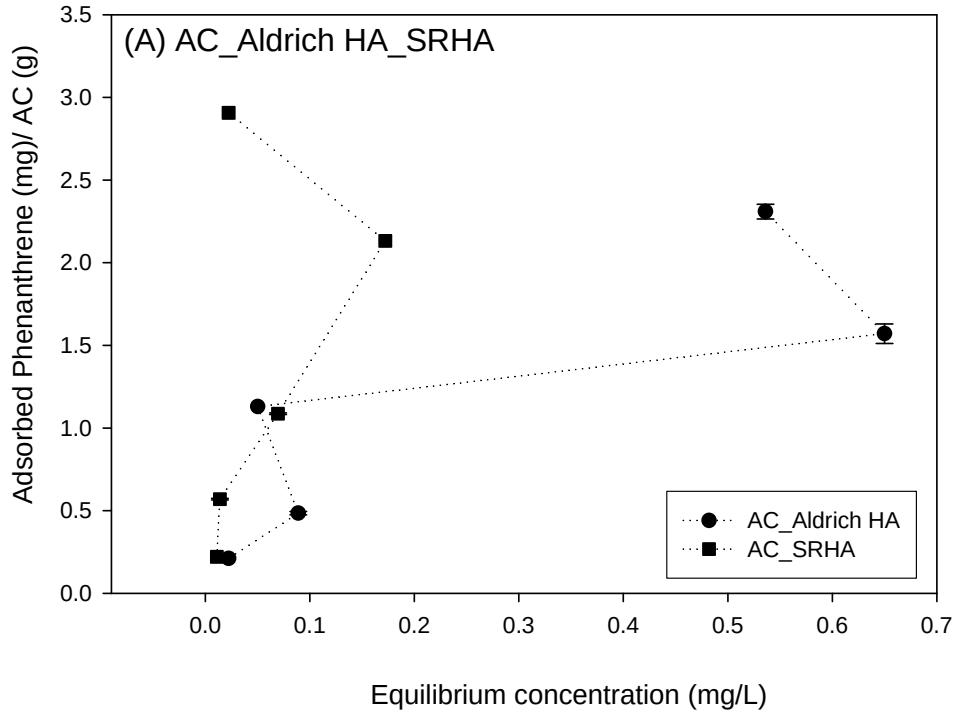

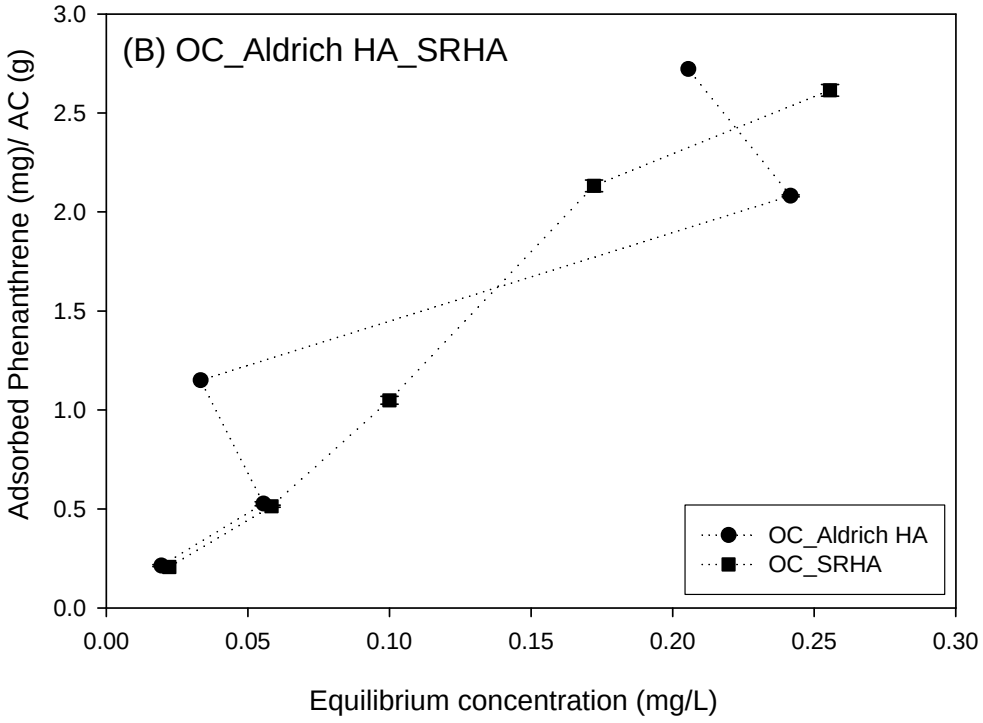

Adsorption of phenanthrene in presence of Aldrich HA and Suwannee River HA (A) Activated carbon (B) Organoclay

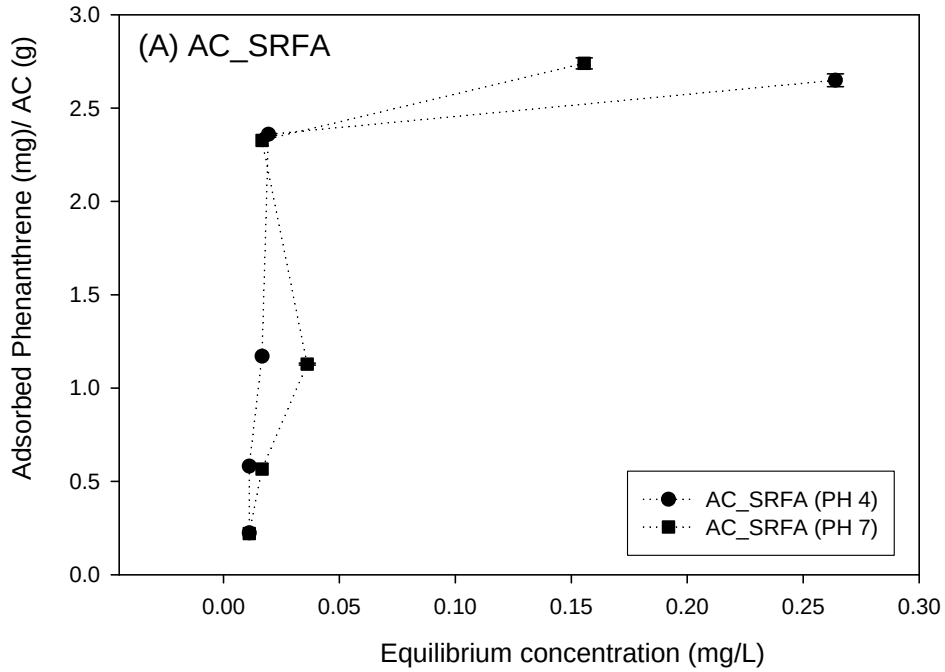

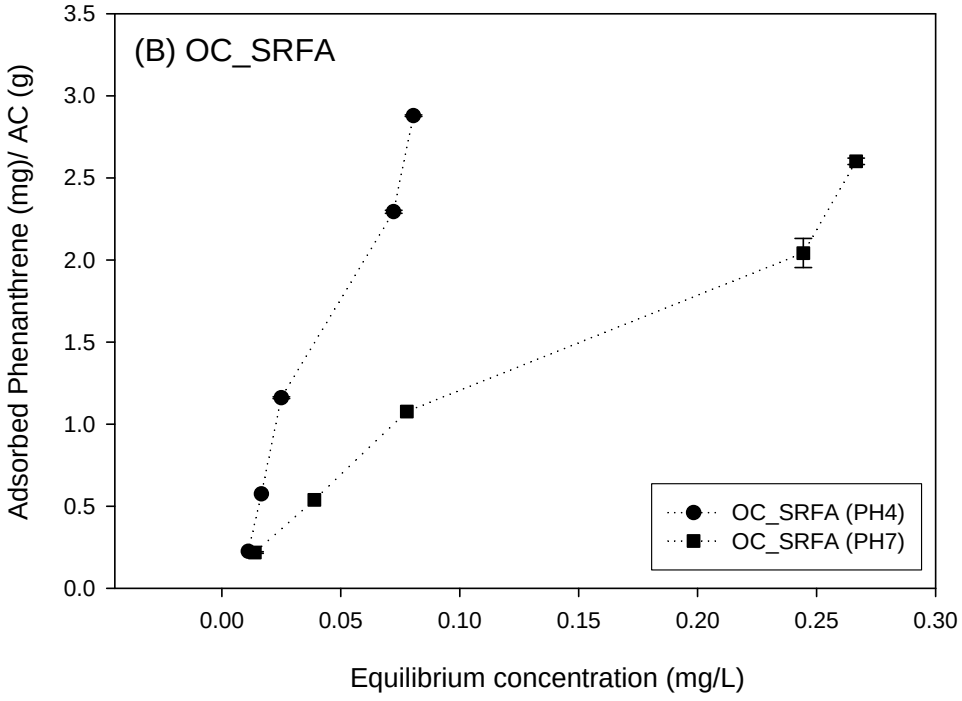

Adsorption of phenanthrene in presence of Suwannee River FA at pH 4 and 7 (A) Activated carbon (B) Organoclay

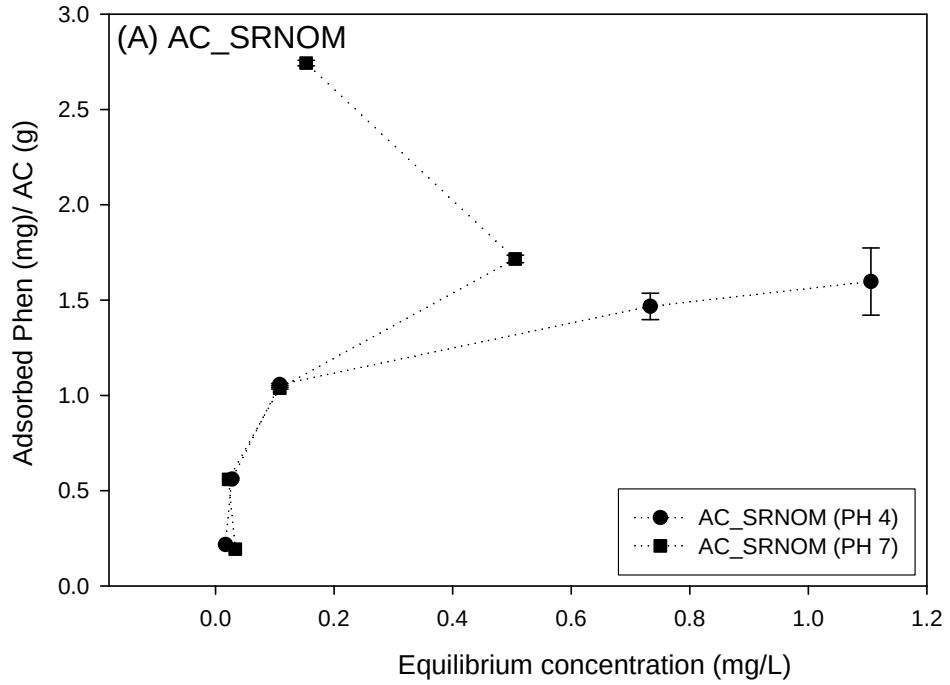

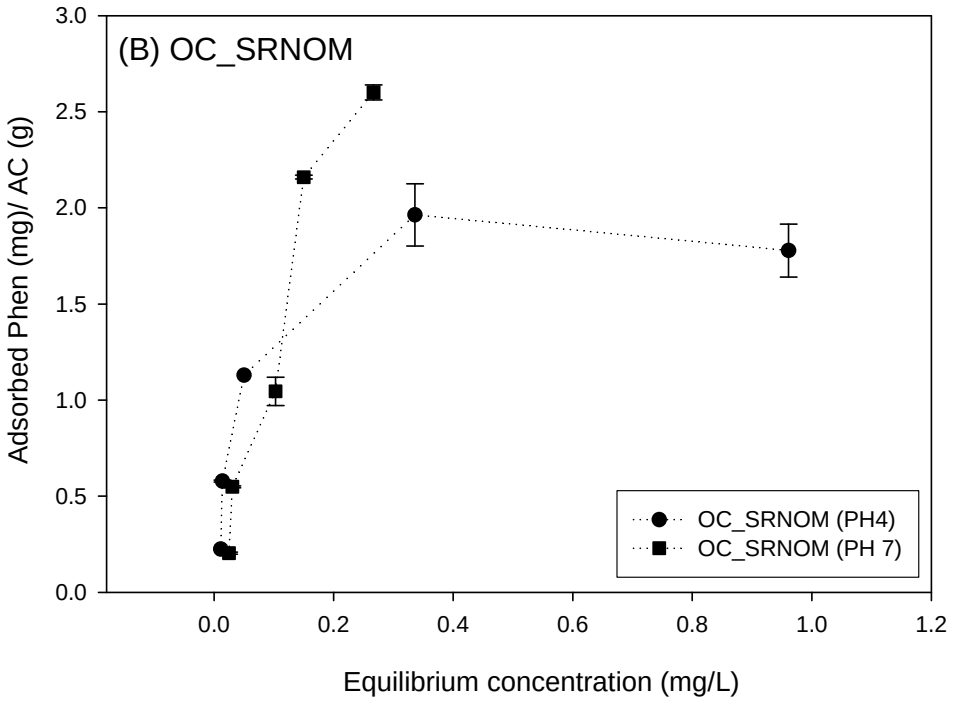

Adsorption of phenanthrene in presence of Suwannee River NOM at pH 4 and 7 (A) Activated carbon (B) Organoclay

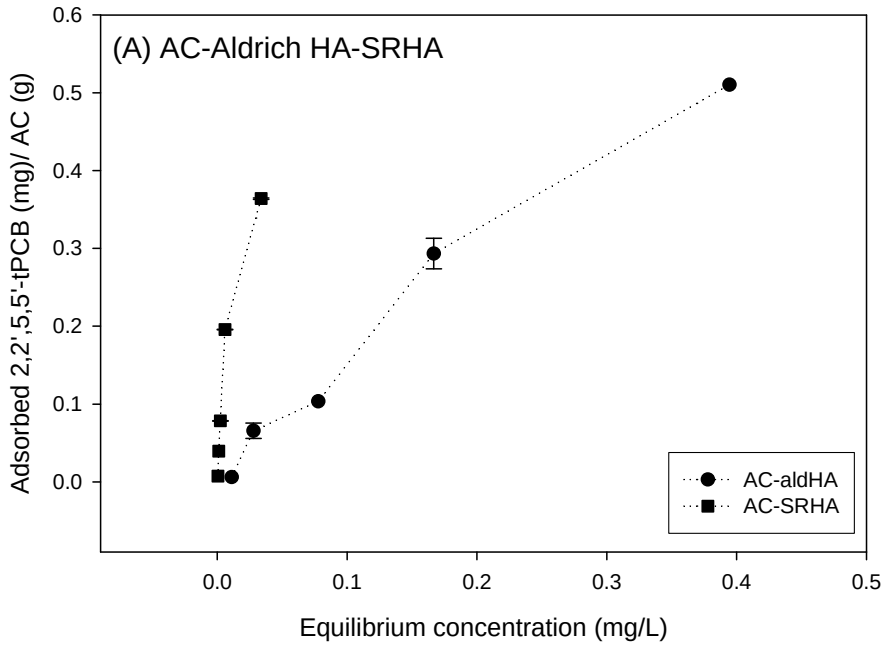

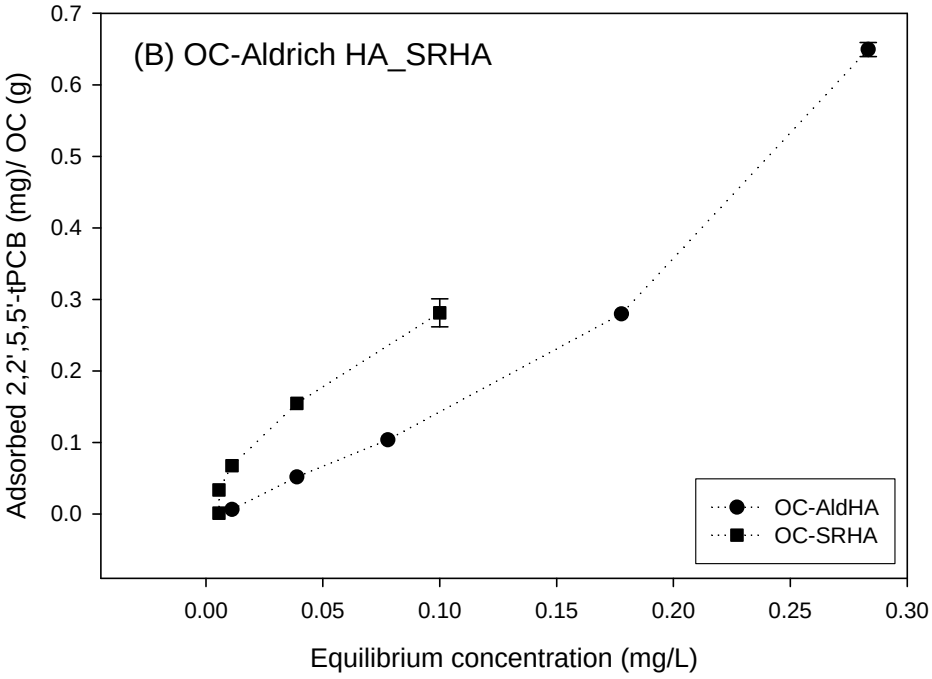

Adsorption of 2, 2', 5, 5'-tPCB in presence of Aldrich HA and Suwannee River HA (A) Activated carbon (B) Organoclay

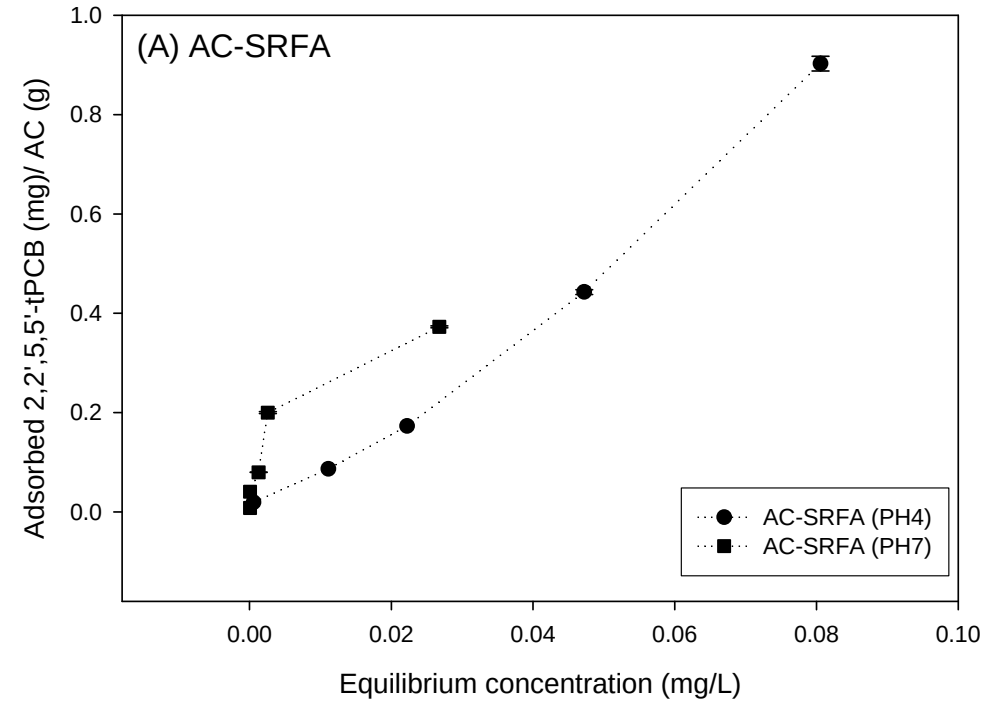

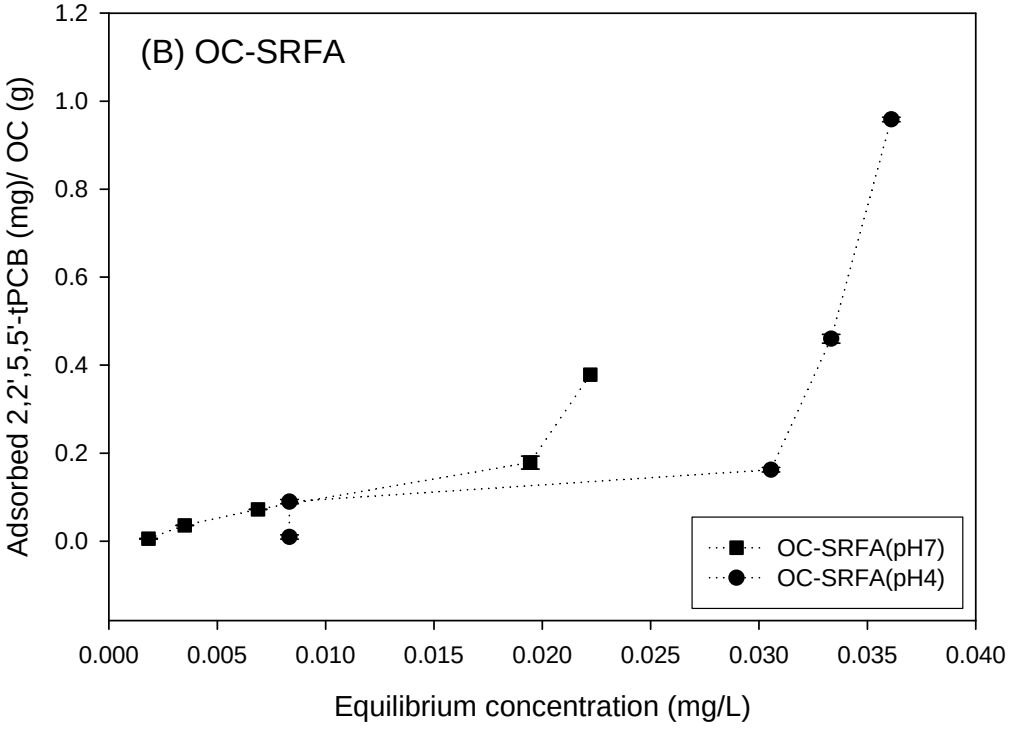

Adsorption of 2, 2', 5, 5'-tPCB in presence of Suwannee River FA at pH 4 and 7 (A) Activated carbon (B) Organoclay

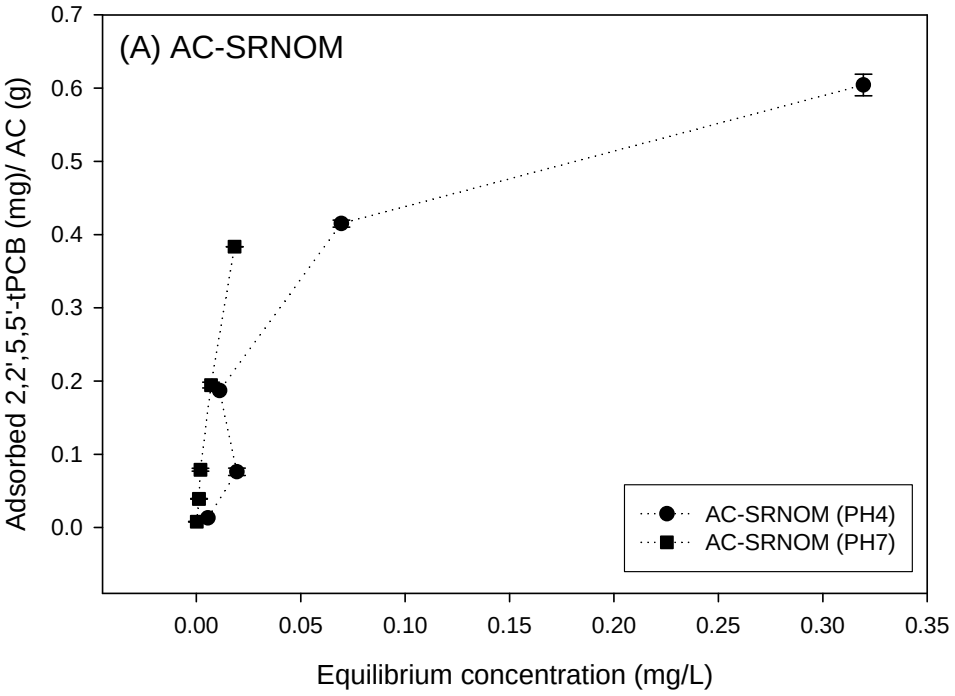

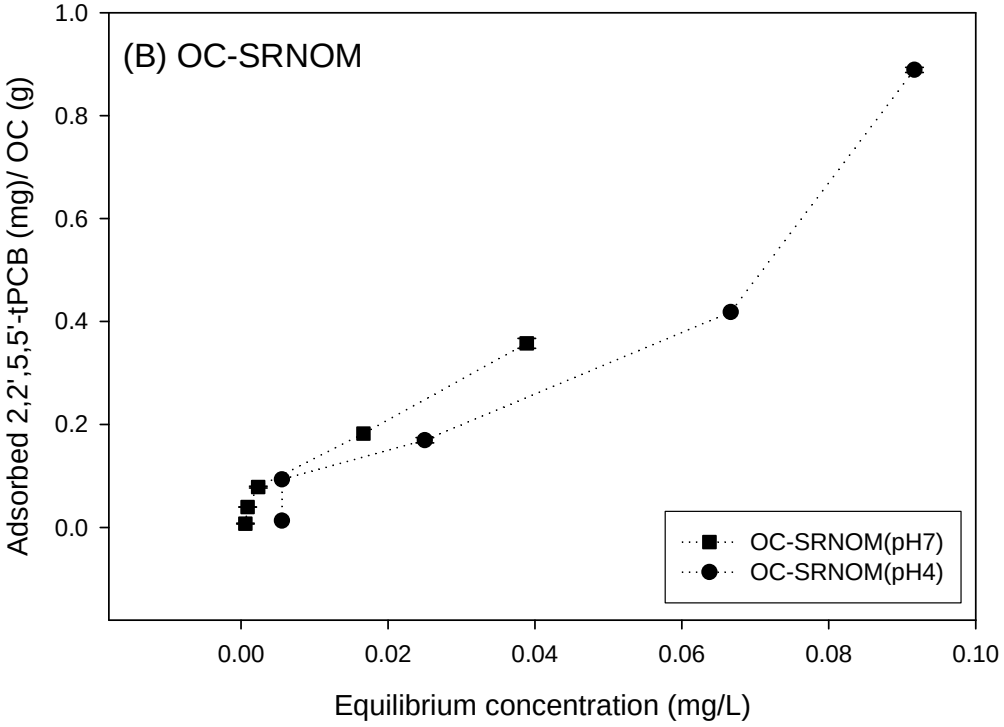

Adsorption of phenanthrene in presence of Suwannee River NOM at pH 4 and 7 (A) Activated carbon (B) Organoclay

References

Akkanen, J.; Lyytikainen, M.; Tuikka, A.; Kukkonen, J.V.K. Dissolved Organic Matter in Pore Water of Freshwater Sediments: Effects of Separation Procedure on Quantity, Quality and Functionality. *Chemosphere*, 2005, 60, 1608-1615.

Brownawell, B.J.; Farrington, J.W. Biogeochemistry of PCBs in Interstitial Waters of Coastal Marine Sediment. *Geochimica et Cosmochimica Acta*, 1985, 50, 157-169.

Chiou, C. T.; Malcolm, R. L.; Brinton, T. I.; Kile, D. E. Water Solubility Enhancement of Some Organic Pollutants and Pesticides by Dissolved Humic and Fulvic Acids. *Environmental Science and Technology*, 1986, 20, 502-508.

Dental, S. K.; Jamarah, A. I. and Sparks D. L. Sorption and Cosorption of 1, 2, 4-Trichlorobenzene and Tannic Acid by Organo-clays. *Water Research*, 1998, 32, 3689-3697.

Edzwald, J.K. and Tobiason, J.E. Enhanced Coagulation: US Requirements and a Broader View. *Water Science and Technology*, 1999, 40, 63-70.

El Nahhal, Y. Z.; Safi, J. M. Adsorption of Phenanthrene on Organoclays from Distilled and Saline Water. *Journal of Colloid And Interface Science*, 2004, 269, 265-273.

Feng X.; Simpson, A. J.; Simpson, M. J. Investigating the Role of Mineral Bound Humic Acid in Phenanthrene Sorption. *Environmental Science and Technology*, 2006, 40, 3260-3266.

Kim, J.I., Buckau, G., Duschner, H. and Psarros, N. Characterization of humic and fulvic acids from Gorleben groundwater. *Fresenius Journal of Analytical Chemistry*, 1990, 338, 245-252.

Kohl, S. D.; and Rice, J. A. The Binding of Contaminants to Humin: A Mass Balance. *Chemosphere*, 1998, 36, 251-261.

McDonough, K. M.; Fairey, J. L.; Lowry, G. V. Adsorption of Polychlorinated biphenyls to Activated Carbon : Equilibrium Isotherms and a Preliminary Assessment of the Effect of Dissolved Organic Matter and Biofilm Loadings. *Water Research*, 2008, 42, 575-584.

Murphy, E. M.; Zachara, J. M.; Smith, S. C. Influence of Mineral Bound Humic Substances on the Sorption of Hydrophobic Organic Contaminants. *Environmental Science and Technology*, 1990, 24, 1507-1516.

Niederer, C.; Schwarzenbach, R.P.; Goss, K. Elucidating Differences in the Sorption Properties of 10 Humic and Fulvic Acids for Polar and Nonpolar Organic Chemicals. *Environ. Sci. Tech*. 2007, 41, 6711 – 6717.

Paolis, F. D.; Kukkonen, J. Binding of Organic Pollutants to Humic and Fulvic Acids: Influence of pH and The Structure of Humic Material. *Chemosphere*, 1997, 34, 1693-1704

Saparpakorn, P.; Kim, J. H.; Hannongbua, S. Investigation on the Binding of Polycyclic Aromatic hydrocarbons with Soil Organic Matter: A Theoretical Approach. *Molecules*, 2007, 12, 703-715.

Thurman, E. M. and Malcolm, R. L. Preparative Isolation of Aquatic Humic Substances. *Environ. Sci. Tech*. 1981, 15, 463-466.

Werner, D.; Higgins, C. P.; Luthy, R. G. The sequestration of PCBs in Lake Hartwell Sediment with Activated Carbon. *Water Research*, 2005, 39, 2105-2113.

Wu , F. C.; Evans, R. D.; and Dillon, P. J. Separation and Characterization of NOM by High-Performance Liquid Chromatography and On-Line Three Dimensional Excitation Emission Matrix Fluorescence Detection. *Environmental Science and Technology*, 2003, 37, 3687-3693.

Zhao, H. and Vance, G. F. Sorption of Trichloroethylene by Organoclays in the Presence of Humic Substances. *Water Research*, 1998, 32, 3710-3716.

Zimmerman, J.R.; Ghosh, U.; Luthy, R. G.; Bridges, T. S.; Millward, R. N. Addition of Carbon Sorbents to Reduce PCB and PAH Bioavailability in Marine Sediments: Physicochemical Tests. *Environ. Sci. Tech*. 2004, 38, 5458 – 5464.